

INTERNATIONAL CONFERENCE ON
POLYMER SCIENCE AND TECHNOLOGY

8-11 JANUARY 2017

PROCEEDINGS-MACRO2017

ORGANISED BY
SOCIETY FOR POLYMER SCIENCE, INDIA
THIRUVANANTHAPURAM CHAPTER

Proceedings of the International Conference on Polymer Science and Technology
Copyright © MACRO2017 and SPSI, Thiruvananthapuram Chapter
Year published: 2017
No part of this publication shall be reproduced in any form without prior permission from the MACRO2017 Organizing Committee/SPSI Thiruvananthapuram Chapter.
Copyright of the original papers remains with the authors.
For copies, please contact Honorary Secretary,
Society for Polymer Science, India, Thiruvananthapuram Chapter
C/o Vikram Sarabhai Space Centre, Thiruvananthapuram-695022, India
E-mail: rsrajeev@gmail.com
Printed and published by the Editorial Committee, MACRO2017
Original text of authors retained as received in print ready format
Single bound volume
Compilation in searchable PDF version
Layout and design: Dr. Santhosh Kumar K.S. /Dr. Gouri C. / Dr. C.P. Reghunadhan Nair

CONTENTS

Focus area: Polymer Synthesis and Characterisation (PSC)

Sl. NO.	MACRO ID	PAPER TITLE	FIRST AUTHOR	PAGE NO.
1.	MACRO 109	Synthesis, Characterization and Application of Water Based Pressure Sensitive Adhesive	Borole Dinesh	1
2.	MACRO 116	Facile Synthesis of Dendrigraft Polymer Having Polyepichlorohydrin Core and Investigation of Their Structure Perfection	Smitha George	8
3.	MACRO 127	Synthesis and antimicrobial activities of dendrimers with indazole as surface units and melamine, S-BINOL core units	Mani Jayanthi	12
4.	MACRO 153	Alkaline Earth Metal Complexes Of Bis-phosphiiminoselenoid Ligand As Highly Iso- selective And Active Catalysts For Ring-Opening Polymerization Of rac-Lactide.	Bhattacharjee Jayeeta	18
5.	MACRO 170	Synthesis and Characterisation of Bio-Surfactant Assisted Conducting Polypyrrole	Adhikari	21
6.	MACRO 176	Design and synthesis of new organic electronic materials based on hetero doped organic polymers	Dr. Anirban Pradhan	23
7.	MACRO 197	Synthesis, Electrolyte and pH Responsive properties of Poly(4-vinylpyridine) Star Polymers	A.Gopinath	24
8.	MACRO 215	Synthesis and Characterization of Flexible/ Stretchable Polyimides containing Long/Bulky Aromatic Side Chains	Tharakan Simi Annie	28
9.	MACRO 216	Applications of Poly(ionic liquids) in Organic Synthesis	Kari Vijayakrishna	29
10.	MACRO 219	Synthesis and Diversified Applications of Water soluble Polythiophene based 'Smart' Graft Copolymers	Chatterjee D. P	30
11.	MACRO 222	Synthesis and applications of achiral & chiral poly(ionic liquids)	Nellepalli Pothanagandhi	36
12.	MACRO 226	Synthesis Of PVDF Based Graft Copolymer For Affinity Chromatography Applications.	Majumdar, S	37
13.	MACRO 228	Controlled Synthesis of End-Functionalized Mannose-6-phosphate Glycopolypeptides for Lysosome Targeting	Das	43
14.	MACRO 231	Strategic Catalyst Designing for Insertion Copolymerization of Polar Olefins with ethylene	Deshmukh Satej S	44

15.	MACRO 240	Synthesis of amino phosphonate grafted resin and their extraction behaviour towards Actinides	Dhrubajyoti Das	45
16.	MACRO 249	Synthesis, Characterization and property investigation of PVDF/rGO Nanocomposites for Energy Harvesting application	Chandan Kumar	46
17.	MACRO 250	Water Soluble Polyperoxides	Mete	50
18.	MACRO 259	Synthesis of Polyaniline & Polypyrrole Nanofibers via Continuous flow and Microfluidic Droplet generator method	Bajpai Rishab	51
19.	MACRO 260	Synthesis of 'Living' Poly(Dimethylaminoethyl Methacrylate) Using CuCl.PMDETA Complex in Environmentally Benign Conditions	Basak, U	54
20.	MACRO 272	Novel L-Menthol-Based Initiators for Atom Transfer Radical Polymerization (ATRP)	Vishwakarma Sambhav	59
21.	MACRO 273	Synthesis of amphiphilic block copolymers through RAFT polymerization and their application as surf-RAFT agent for the miniemulsion polymerization of styrene	Kishor Pawar	61
22.	MACRO 281	Arm First Approach Towards the Synthesis of Core Cross-Linked Star Polymer with Hydrophobic Corona via Click Chemistry	Samanta, Pousali	62
23.	MACRO 284	Synthesis of PEG and NIPA Containing Cationic Block Copolymers with Different Architectures and their Interaction with DNA	Sahoo	63
24.	MACRO 285	Modified Dendritic Amine Grafted on Mesoporous Silica: A Highly Effective Reusable Catalyst for One-Pot Synthesis of Conjugated Nitroalkenes and Nitroaldols	K.A. Jisha	64
25.	MACRO 290	Synthesis and Photovoltaics Applications of Novel Fluorene based Donor-Acceptor Cross-Conjugated Polymers	Bhavna Sharma	65
26.	MACRO 291	Synthesis and Third-order Nonlinear Optical Properties of Phenothiazine-Triazine Copolymer	S. Narayanan	66
27.	MACRO 292	Synthesis of N-Vinyl Pyrrolidone Based Smart Polymers and their Application as Self- Immolative Polyprodrug and Targeted Delivery Vehicles	Maiti	73
28.	MACRO 295	Synthesis of Lectin Binding Glycopolymer Coated Silica Nanoparticles using Grafting from RAFT Polymerization	S N Raju Kutcherlapati	74

29.	MACRO 303	Synthesis and Characterization of Blue Emitting Materials for Organic Light Emitting Diode Applications	Kaur Banpreet	81
30.	MACRO 313	Synthesis and Characterization Of β-CD Induced Block Copolymers via ARGET-ATRP of Vinyl and Acrylate monomers	Karkare P	82
31.	MACRO 314	Synthesis and Aggregation Behavior of Poly(2-oxazoline)-Based Light- and Thermo-responsive Block and Random Copolymers	Jana Somdeb	84
32.	MACRO 319	Poly(vinylidenefluoride)(PVDF) graft Copolymer in Alcohol-Water Environment	Kuila, A	85
33.	MACRO 323	Synthesis of Fluorescent Water-Soluble Amphiphilic Peptide-Polymer Bioconjugate: for Cell Imaging and RNA Binding	Dule	86
34.	MACRO 326	Synthesis of Superporous PolyHIPE Hydrogels as a Scaffold Material for Tissue Engineering Application	Nalawade A. C	87
35.	MACRO 327	Thermo-, pH-, and Anion-Responsive Phosphonium and Imidazolium Poly(ionic liquid)s	Biswas	94
36.	MACRO 340	A Simple Approach For Synthesis Of Externally Initiated Regioregular Poly(3-Hexylthiophene)	Khawas Koomkoom	95
37.	MACRO 341	Designing of Multi-Responsive Amino Acid-Based Zwitterionic Polymers	Maji	97
38.	MACRO 343	Synthesis and composition dependent optical, electronic properties of poly (3-hexyl thiophene)-b-poly(N-isopropyl acrylamide)	Pallavi Kumari	98
39.	MACRO 344	Amphiphilic, thermoresponsive conjugated block copolymer of poly(3-hexyl thiophene)	Kuila Biplab K	104
40.	MACRO 351	BUF Resins Synthesis: An Experimental Study & Characterization of Resins by Changing Bu/U Mole Ratio	Amin	109
41.	MACRO 358	Poly (methylated pyridinium benzimidazolium): A new class of anion exchange membrane	Balakondareddy Sana	116
42.	MACRO 372	Synthesis and Characterization of Stereo-Di-Block Polylactides with Varying Block Length Compositions	Mili	117
43.	MACRO 392	Synthesis and Characterization of New Semifluorinated Sulfonated Polyimides for Proton Exchange Membrane Application	Singh Asheesh	119

44.	MACRO 395	Synthesis and Characterization of Perfluorochain Bearing Crosslinked System via Hydrosilylation Reaction.	Sandeep P.B	120
45.	MACRO 415	Styrene based Comb Copolymers by Click Chemistry and Free Radical Polymerization	Sunitha K	127
46.	MACRO 417	Phenolic resin based organic-inorganic hybrid polymer networks: Synthesis and properties	Satheesh Chandran M	128
47.	MACRO 426	Hyperbranched Polymers as Scaffolds for Supported Catalysis	Perala Suresh Kumar	129
48.	MACRO 427	Organic - inorganic hybrid polytriazoles; Synthesis and shape memory properties	Ragin Ramdas M	131
49.	MACRO 429	Electrically Conductive Oligomeric Conjugated Aromatic Schiff Base- Synthesis and Characterization	Apparao Thota	132
50.	MACRO 430	Cross-stitching Folded Polymeric Systems	Sujoy Bej	133
51.	MACRO 443	Synthesis of Amphiphilic Block Copolymers Using New method of Catalysing Thiol-Ene Reaction	Hafeez Sumbul	135
52.	MACRO 444	Defect-Free Regioregular Poly(3-hexylthiophene) via Nickel Zero Catalyzed Kumada Catalyst-Transfer Polymerization	Tarange Dattatray	136
53.	MACRO 455	GT-g-P (DADMAC): Synthesis, Characterization and Evaluation of Its Cationic Properties as Flocculant for Model Aqueous Suspensions	Pal	137
54.	MACRO 466	Synthesis and Chemical Modification of Polyesters Containing Allyloxy functional Groups by “Click Chemistry” Approach	Dr. Verma Savita	139
55.	MACRO 475	Synthesis and characterization of PMMA/PEDOT and graphene based hybrid materials for conductive transparent thin films	P. A. Saeed	141
56.	MACRO 483	Surface initiated ATRP from GO: Precision Synthesis and Control of Nanocomposite properties	Kattimuttathu I	142
57.	MACRO 488	Fluorene Based Cardo Semifluorinated Poly(Ether Imide)S: Synthesis, Characterization and Gas Transport Properties	Chatterjee	143
58.	MACRO 489	Synthesis and optoelectronic properties of hybrid rr-Poly-3-hexylthiophene (P3HT) GO nanocomposites.	M. Jakeer Hussain	144
59.	MACRO 495	Synthesis of Surface Modified Poly (amidoamine) Dendrimer Functionalized Arginine for Solubility Enhancement of fat soluble Vitamin	E. Murugan	145

60.	MACRO 501	Click Chemistry Route to Covalently Link PVA and Cellulose	Kousar Jahan	146
61.	MACRO 529	Cyclophane as a conformationally twisted monomer in high performance polymers	Shyambo Chatterjee	147
62.	MACRO 530	Synthesis of aliphatic polyesters from a bio derived AB monomer	Y.R. Nevare	153
63.	MACRO 535	Syntheses and characterization of block copolymers of methacrylates bearing POSS as well as fluoro alkyl group	Siva Ponnupandian	160
64.	MACRO 536	Synthesis and Characterisation of Polyamides containing thiazolidine unit	V.P. Ubale	160
65.	MACRO 537	Synthesis and Gas sensing studies of polyazomethines polymers	Y. S. Patil	174
66.	MACRO 545	Synthesis and chemical characterization of high molar mass star-shape poly(L-lactides) (PLLA's).	Adam Michalski	191
67.	MACRO 546	Triblock poly(trimethylene carbonate) and polylactide copolyesters: synthesis, properties and stereocomplex formation	M. Socka	195
68.	MACRO 551	High Performance Liquid Crystalline Polymers from 2,5-furandicarboxylic acid; Synthesis, Characterization and Properties	Wilsens, C.H.R.M	201
69.	MACRO 553	Synthesis and Characterization of Polystyrene Using Modified Graphene oxide based Polymeric Nano-Surfactant via Emulsion Polymerization	Rajender Nutenki	203
70.	MACRO 558	Synthesis and Characterization of Novel Poly(vinyl alcohol-co-styrenesulfonic acid) for Membrane Applications	R.R. Choudhury	210
71.	MACRO 559	Functional Intrinsic Microporous Polymers for Energy Applications: Synthesis and Characterization	A. K. Palai	211

Focus area: Polymers for Energy and Sensing applications (PES)

SI. No.	MACRO ID	PAPER TITLE	FIRST AUTHOR	PAGE NO.
72.	MACRO 111	Fabrication of A Polyaniline Transduced Imidazole Based Conductometric Sensor for Rapid Detection of Cyanide	Paul Anirban	212

73.	MACRO 114	Strain Rate Sensitivity Of Epoxy Composites Toughened With 2D Molybdenum Disulphide	Parthsarthy	214
74.	MACRO 140	Preparation and Characterization of Terpolymer Based Cation Exchange Membrane for Water Desalination by Electrodialysis	Bhadja Vaibhavee	215
75.	MACRO 141	Modulation of Protein Adsorption and Cell Proliferation on Polyethylene Immobilized Graphene Oxide Reinforced HDPE Bionanocomposites	Upadhyay Rahul	217
76.	MACRO 144	Preparation and Characterization of Crosslinked Anion Exchange Membrane for Water Desalination by Electrodialysis	Chatterjee Uma	223
77.	MACRO 146	Thermally and pH Responsive Poly(dimethyl aminoethyl)methacrylate-*b*-Poly(N-isopropyl acrylamide)/Polycaprolactone Amphiphilic Conetwork Gels	Jewrajka Suresh Kumar	225
78.	MACRO 147	Tailoring pyrazoline–aromatic donor based luminescent polymers for organic-electronics	T.Vandana	227
79.	MACRO 155	Planar Heterojunction Perovskite Solar Cell with Poly(3-thiophene acetic acid) as Hole Transporting Layer under Ambient Condition	Arnab Shit	233
80.	MACRO 156	A Potential polyaniline and Perylene Diimide Based Acceptor Material for Highly Efficient Dye sensitized solar cell with 4.32% Efficiency	Pousali chal	234
81.	MACRO 158	Development of Electrochemical Sensor for the Detection of Creatinine with Silane Functionalized Graphene Oxide Based Molecularly Imprinted Polymer film	Anirudhan T S	235
82.	MACRO 164	Fabrication of Graphene Quantum Dot-Doped Polyaniline Nanostructure and Its Opto-electronic and Photovoltaic Properties	Maity	237
83.	MACRO 169	Safe and Non-toxic Carbohydrate Polymer Based Pollutant Sensor Gold Nanoparticles having Fluorescence Quenching Ability	Pattanayak	238
84.	MACRO 182	All-polymer Solar Cell Performance Of N-type Napthalenediimide/ Perylenediimide - Bithiophene Copolymer	Sharma Sandeep	239
85.	MACRO 183	Glutamic Acid Appended Water-Soluble Conjugated Polymer for Fluorescence Sensing and Imaging of Fe2+ Ions in Live Cells	Nikam, Shrikant B	240

86.	MACRO 184	Highly Efficient Supercapacitor Performance of Iodine Doped Reduced Graphene oxide Produced via Mild Reaction Condition	Mandal Debashish	241
87.	MACRO 188	A New class of Polymeric Network as an Efficient Water Toxicant Remover	Rajan Kumar	242
88.	MACRO 191	A New Class Of Norbornene Based Dyes For In-field Rapid As(III) Sensing	Tapendu Samanta	247
89.	MACRO 195	Fluorene Based Triazine Framework as Chemosensor for Selective Sensing of Nitroaromatic Explosives	Saumya Krishnan	251
90.	MACRO 200	Fluorene based Polymers and Copolymers as Sensors	Malik Sudip	257
91.	MACRO 202	Fluorescent Polystyrene Nanobeads for Biosensing and Imaging	Sarabjot Kaur	258
92.	MACRO 205	Synthesis and characterization of partially fluorinated, quaternized anion exchange membrane for alkaline water electrolyser applications	A. Kalaiyarasi	259
93.	MACRO 212	Surfactant Triggered Fluorescence Turn “on/off” Behavior of a Polythiophene – graft – Polyampholyte	Ghosh Radhakanta	264
94.	MACRO 230	Carbamoylmethylphosphine Oxide (CMPO) Derived Cross-Linked Polymers for Uptake of Uranium (VI) From Nitric Acid Media	Suresh Annam	265
95.	MACRO 235	Luminescence Study of Pyrene-tagged Poly-(N-Vinyl-2-pyrrolidone)	Mitra Kheyanath	271
96.	MACRO 242	Design and synthesis of new organic electronic materials based on hetero doped organic polymers	X-Yu Cao	272
97.	MACRO 246	Flexible Micro-Supercapacitors using Silk and Cotton Substrates	Chayanika Das	276
98.	MACRO 248	BODIPY based Polymers for Organic Field Effect Transistors	Singh Saumya	282
99.	MACRO 251	Highly Acid/Oxidative Resistant Cation-Exchange for Membrane Electrolysis	Arindam Kumar Das	283
100.	MACRO 268	HDPE - Sillimanite Mineral Based Composites For Electronic Applications	I.J. Induja	284
101.	MACRO 274	Porous Benzimidazole linked Aryl-imide polymers in The Application of Gas Storage Capacity	Roy Arkapal	285

102.	MACRO 301	Nano-porous Coordination Framework for Electro-sensing of Atropine Sulphate	Vinita	286
103.	MACRO 304	Polypyrrole Coated Fabrics for EMI Shielding Application	Gahlout Pragati	287
104.	MACRO 308	Nitrogen-Enriched Porous Carbon Derived From Polymer of Sucrose and Urea with High CO2 Capture Performance	Deepthi L. Sivadas	288
105.	MACRO 309	Microwave Assisted Synthesis of Poly (indole-5-carboxylic acid) for Sensing Application	Tiwari, P	294
106.	MACRO 311	Thin Film Composite Membranes Containing Functionalized Carbon Nanotubes for Low Pressure Desalination Process	Km Nikita	295
107.	MACRO 324	Redox polymers for electro-kinetic flow-in-a cell	Selvam Mathi	296
108.	MACRO 355	Gas Separation Membranes Made From Tröger's Base-based Polyamide	Bisoi	302
109.	MACRO 366	Fe-N integrated metal organic gel- melamine formaldehyde derived porous carbon structures- a novel catalyst system for alkaline fuel cells	N.S. Sumitha	303
110.	MACRO 369	Polyamine phosphate ester blends with oxypolybezimidazole to improve the properties of proton exchange membrane	K Rambabu	308
111.	MACRO 376	Fabrication of Poly(vinyl chloride)-Chitosan-Cellulose Nanocrystals based Solid Electrolyte Membrane for Direct methanol Fuel Cells: A Sustainable Approach	Gaur, Surendra Singh	309
112.	MACRO 387	Tunable Photoluminescence of Carbazole Based Quinoline Conjugated Polymer by Doping Cds Quantum dot and Poly(vinyl alcohol)	S. Karpagam	310
113.	MACRO 389	Förster's Resonance Energy Transfer (FRET) as a Technique to Monitor the Aggregation Phenomenon of Amphiphilic Polymer	Rajdev, Priya	311
114.	MACRO 391	Ambient dried carbon aerogel as an anode material for lithium ion cells	Ancy Smitha Alex	312
115.	MACRO 393	Electromagnetic Interference Shielding of Nickel Electroplated Fabrics	K.S.Dijith	317
116.	MACRO 408	Renewable Resource Based Ionic Liquid Crystals for Safe and Sustainable Energy Storage	Renjith Sasi	318

117.	MACRO 413	Liquid Crystalline Template Driven Conductive PEDOT Transducer for Nicotine Sensor	Neethu K. S.	320
118.	MACRO 439	Polyaniline salt catalyzed synthesis of hyper branched polyester and its use as dopant in polyaniline salt for coating, fluorescence and supercapacitor electrode	Sangam Naidu Karri	321
119.	MACRO 442	Polybenzimidazole – Polydimethylsiloxane composite films: morphology and mechanical properties	Satheesh Kumar B	322
120.	MACRO 447	Air stable n-type diketopyrrolopyrrole based oligomers for high performance field-effect transistors	Tushita Mukhopadhyay	324
121.	MACRO 451	Indolo[3,2-b]carbazole-based Poly(arylene ethynylene)s: Modulation of Their Optoelectronic Properties by Changing Monomers	M. Vintu	325
122.	MACRO 467	Synthesis and Characterization of Carboxylic Acid Funtionalised Sulfonated Polytriazoles for Proton Exchange Membrane	Saha, Sayantani	331
123.	MACRO 469	Novel Gel Polymer Electrolyte films: Preparation and characterization	Nisha Balachandran	332
124.	MACRO 472	Multifunctional Porous Organic Polymers	Bandyopadhyay Sujoy	338
125.	MACRO 481	Novel process for coating of polyaniline salt on stainless steel electrode: Flexible electrode for High performance supercapacitor	Gopi Chintada	339
126.	MACRO 482	Fabrication and electrical performance of PEDOT:PSS/graphene nanocomposites	R.Aiswaryaa	340
127.	MACRO 484	Poly(aniline-co-pyrrole) - Nanocomposite for Room Temperature Sensing of Carbonmonoxide	Khadeeja Sherin P. R.	341
128.	MACRO 492	Thermoreversible gelation of cycloaliphatic poly (urethane acylsemicarbazides) in DMSO and selective adsorption and separation of dyes from waste water by using xerogels	Sravan Baddi	342
129.	MACRO 500	Molecular interactions in lithium ion batteries: Identification of lithium species in non-aqueous propylene carbonate electrolyte by NMR	Vikas Kumar	348
130.	MACRO 504	Interesting Results Shown By Perovskite-Polymer Hybrid Solar Cell with Enlarged Absorption Spectra and Greater External Quantum Efficiency	Bavane Swapnil Ravindrakumar	354

131.	MACRO 515	Polymerizations with Elemental Sulfur: a Route to Improved Next Generation Batteries	Jeffrey Pyun	355
132.	MACRO 543	Copolymers of waste raw materials: sulphur and naturally occurring phenol derivatives for Lithium Sulphur battery	Swapnil Shukla	357
133.	MACRO 560	Synthesis and characterisation of zinc sulphide quantum dots encapsulated zeolitic imidazolate frame works-8	A. Asif	364

Focus area: Green Sustainable and Biopolymers (GSB)

SL. NO.	MACRO ID	PAPER TITLE	FIRST AUTHOR	PAGE NO.
134.	MACRO 113	Metal organic frameworks as accelerators for ring opening polymerisation of bio-based benzoxazines	Sharma Pratibha	371
135.	MACRO 112	Mesoporous and Hollow Polymers Nanostructure for Drug Delivery	Paik Pradip	377
136.	MACRO 126	Galactitol Based Polyesters for Biomedical Applications	Janeni Natarjan	379
137.	MACRO 137	Electrospun Matrices from Advanced Emulsion Electrospinning Approach	Archana Samanta	380
138.	MACRO 145	Amphiphilic Co-network Gels of Agarose Graft Copolymer and Polycaprolactone-*b*-Polyethylene glycol-*b*-Polycaprolactone for Biomedical Application	Chandel	386
139.	MACRO 157	Water Soluble Poly(ethylene glycol) Methyl Ether Acrylate Containing Polysulfide Polymers *via* Interfacial Polycondensation	Kapil Dev Sayala	388
140.	MACRO 159	Adsorption and Photocatalytic Degradation Studies of Enrofloxacin using Polyacrylic Acid- grafted-Carboxylic Graphene/Titanium Nanotube Composite	Anirudhan T S	389
141.	MACRO 160	Fabrication of solvent responsive transdermal device for the efficient treatment of skin cancer	Anirudhan T S	392
142.	MACRO 163	Preparation and Characterization of Novel Dual Drug Loaded Hydrogel for Combination Therapy	T. S. Anirudhan	399
143.	MACRO 166	Prodrug immobilized nanoparticles of Human Serum Albumin and PLGA for Treatment of Colorectal Cancer	Patel Pratikshkumar R	406
144.	MACRO 167	Biodegradable copolymer for stimuli responsive sustained release of doxorubicin	Sayantani Bhattacharya	409

145.	MACRO 172	Polymer-Chlorambucil Drug Conjugates: A Dynamic Platform of Anticancer Drug Delivery	Saha Biswajit	415
146.	MACRO 173	PEGylated Polymeric Nanogel For Theranostic Applications	Vineeth M Vijayan	416
147.	MACRO 175	Injectable, Elastic and Conducting Hydrogel for Tissue Engineering Applications	Komeri Remya	418
148.	MACRO 178	Synthesis, characterization and *in-vitro* studies of folic acid decorated graphene oxide/chitosan nanocomposites for cancer drug delivery	Ananya Deb	421
149.	MACRO 179	Synthesis and Characterization of Sodium Alginate / Gelatin /Hydroxyapatite Green Nanocomposites	Mohanan A	422
150.	MACRO 187	Microwave assisted polymerization of water soluble monomers	Poorvi M. Purohit	423
151.	MACRO 190	Designing Double Network Hydrogels for Biomedical Applications	Sanoop B. Nair	428
152.	MACRO 192	Polycarbonate-based biodegradable copolymers for stimuli responsive targeted drug delivery	P. Kumar	435
153.	MACRO 198	Norbornene Based Copolymer for Site-specific Theranostic Application	S. Mukherjee	441
154.	MACRO 199	A New Class of Fe(III) Containing Norbornene Copolymer: Very Efficient Theranostic Agent for Cancer Therapy	Patra D	446
155.	MACRO 204	Synthesis and Characterization of N-Vinyl-2-Pyrrolidone based Graft copolymers for Delivery of levofloxacin	Kumar Ashok	447
156.	MACRO 206	Modulation of Protein Adsorption and Cell Proliferation on Polyethylene Immobilized Graphene Oxide Reinforced HDPE Bionano- composites	Upadhyay Rahul	448
157.	MACRO 223	Novel *Borassus* fiber-reinforced polylactic acid composites: processing and mechanical properties	Y. N. Marathe	450
158.	MACRO 233	Enhanced Drug Release by Selective Cleavage of Crosslinks in a Double Crosslinked Hydrogel	Neha Tiwari	457
159.	MACRO 236	Study of swelling characteristics and mechanical properties of 2-Acrylamido-2-Methylpropane Sulphonic Acid (AMPS) based hydrogels	Chaurasia Siddhant	463
160.	MACRO 238	Modification and Hydrogel preparation of Chitosan for Controlled Drug Delivery and Tissue Engineering	Arun Kumar Mahanta	470

161.	MACRO 239	Nanostructure Regulated In Vitro – In Vivo Controlled Delivery of Hydrophobic Anticancer Drug	Sudipta Senapati	482
162.	MACRO 241	Mechanically Tunable Curcumin Incorporated Polyurethane Hydrogels as Potential Biomaterials	V.D. Anumon	487
163.	MACRO 244	Nano-curcumin Encapsulates for Targeted Cancer Therapy	Amarnath Singam	494
164.	MACRO 253	Effect of Different Cross – Linkers on Structure andStability of Polyacrylamide Hydrogels	Khandai Santripti	500
165.	MACRO 255	Synthesis, characterization and application of dextrin grafted polyurethane co polymers.	Shukla A	502
166.	MACRO 256	Highly Regioselective Isomerizing-Hydro formylation of Plant Oils to Monomers and Sustainable Polymers	Pandey Swechchha	509
167.	MACRO 258	Self Assembled Nanostructures from Amphiphilic Mannose 6-phosphate Glycopoly peptides for Lysosome Targeting	Pandey Bhawana	511
168.	MACRO 266	Copolymerization Studies of Allyl Glycidyl Ether with Different Hydrophobic Methacrylates: Lipase Immobilization Study	Rajdeo Kishor	512
169.	MACRO 270	Novel Silk Fibroin b3ased Coatings for PDMS Breast Implants	Shete Abhijit	513
170.	MACRO 271	Modified Silk Fibroin based 3D Scaffolds for Bone Tissue Engineering	Parekh Nimisha	519
171.	MACRO 275	Synthesis of Photo Responsive Polymers and their Applications in Photoresponsive Surfaces and Drug Delivery	Biswas Gargi	525
172.	MACRO 276	Thermal and pH Responsive Polymer-Grafted Magnetic Nanoparticles for Targeted Delivery of Anti-Cancer Drug	Bera, Sharmita	526
173.	MACRO 277	Temperature, pH and Redox Responsive Carbohydrate based Hydrogels for Protein Delivery	Dutta, Sujan	527
174.	MACRO 278	Synthesis of Glycerol Based Dendrimers for Dual Targeted Drug Delivery Applications	Killi Naresh	527
175.	MACRO 282	L-Amino acid Based Enzyme and pH Dual Responsive Nano-carrier for Multi-drug Delivery to Cancer Cells	Saxena, Sonashree	529
176.	MACRO 283	π-Conjugated Fluorophore-*block*-Biodegradable Polymer Nano-carrier for Cellular Imaging and Drug Delivery	Kulkarni Bhagyashree	530

177.	MACRO 286	Polysaccharide-Cisplatin Vesicular Nano-scaffold for Combination Therapy in Cancer	Deshpande, Nilesh U.	531
178.	MACRO 287	Dynamic Self Assembly of Polyarginine based Polypeptides for Biomedical Applications	Korra, Praveen	533
179.	MACRO 288	Random and Block Copolymer Polycapro- lactone Nano-assemblies for Drug Delivery	Malhotra, Mehak	533
180.	MACRO 300	Synthesis and design ofCurcumin Based Gels	MettaLokanadham	535
181.	MACRO 312	Rheological behavior of the biocomposites based on Poly(lactic acid)/jute fibers	Mohammad Tahir Zafar	541
182.	MACRO 329	Templated Synthesis of pH Triggered Hydrolytically Cleavable Polylactic Acid Hollow Spheres Using Self-Assembled Layered Silicate Polystyrene Hybrid	Asha Susan Chacko	543
183.	MACRO 332	Biodegradable Nanoparticles for better Encapsulation of Hydrophilic Anticancer Drug Gemcitabine	Sachin S. Surwase	544
184.	MACRO 336	Synthesis and Characterization of Surface functionalized and Quaternised Dendrimers for Bio Medical Applications.	E. Murugan	551
185.	MACRO 339	Green polymer nanocomposites of self-assembled polysaccharide hydrogels	Prasad V S	552
186.	MACRO 364	Tapioca Starch Grafted Polyacrylamide Application in Water Treatment	Kranthikumar Tungala	553
187.	MACRO 370	Thermal Degradation and Mechanistic Study of Guar Gum, Xanthan Gum and Gum Arabic using Hyphenated TGA-FTIR Analysis: A Comparative Study	Monika	555
188.	MACRO 373	Effect of Hydrolytic Degradation on the Wettability Behaviour of Bio-filler Reinforced Poly (lactic acid) Extruded Bionanocomposites.	Kalita, Kumar	556
189.	MACRO 375	Melt Extruded Poly Lactic Acid/Chitosan-*grafted*-Oligo L-Lactic Acid Bionano composite Films for High Gas Barrier Applications	Pal, Akhilesh Kumar	558
190.	MACRO 379	An investigation of the viscoelastic and thermal behavior of silk nanoparticles/polylactic acid nanocomposites	P. Rahul	561
191.	MACRO 381	Poly lactic acid (PLA) based conductive biomaterial for the detection of Alcohols	Gourhari Chakraborty	568

192.	MACRO 384	Bioactive and non-cytotoxic magnesium incorporated inorganic-organic hybrid resin for biomedical applications.	C Vibha	569
193.	MACRO 404	Green one step morphosynthesis of silver nanoparticles and their antibacterial and anticancerous activity	Maity, Dipanwita	570
194.	MACRO 405	Antibacterial and DNA degradation potential of silver nanoparticles-polysaccharide composite synthesized via green route.	Manna, Dilip Kumar	571
195.	MACRO 407	A Study on Acid and Enzymatic Hydrolysis of Millet Bran, Strain Screening and Effect of Neutralizing Agents on Fermentative Production of D-Lactic Acid	Rengesh Balakrishna	572
196.	MACRO 416	Osteogenic Drug–Layered Magnesiosilicate Complex and its Composite Scaffold for Bone Tissue Engineering Applications	S. Megha	574
197.	MACRO 419	Graphene Oxide immobilized Polyolefin membranes for Antibacterial surface properties	Prasanna Kumar S	580
198.	MACRO 423	Covalently Cross-linked Multifunctional Polycaprolactone / Graphene Composites for Bone Tissue Regeneration Applications	Padmavathy Nagarajan	580
199.	MACRO 431	Interpenetrating Photopolymers for Intraocular Lens Application	Shaik Syed Hussain	581
200.	MACRO 433	Copper Decorated Reduced Graphene Oxide nanoparticle Embedded Polycaprolactone Nanocomposite for Blood Vessel Tissue Engineering	L.R. Jaidev	582
201.	MACRO 448	Guar Gum Based Super Absorbent Hydrogels for Agricultural Applications	Thombare, Nandkishore	583
202.	MACRO 453	Protein Induced Disassembly and Release of Guest Molecules from a Biodegradable Nanocontainer	Molla, Mijanur	584
203.	MACRO 454	Development of polysaccharide derived carbon blocks for the removal of perchlorate from water	R. Radhika	586
204.	MACRO 458	Effect of Hydroxyapatite Loading on Polylactic acid/Hydroxyapatite Composites on its Mechanical, Thermal and Degradation Properties	Prasad Arbind	593
205.	MACRO 477	Self Cross-linkable Anionic waterborne polyurethane-silanol dispersions from Cottonseed oil-based phosphorylated polyol as ionic soft segment	Sashivinay kumar Gaddam	597
206.	MACRO 478	Improved Haemocompatibility of Surface Modified Polycarbonate Urethane	Sudhin Thampi	604

207.	MACRO 485	8-Hydroxypyrene-1,3,6-trisulfonic acid trisodium salt (HPTS) Based High Fluorescent Waterborne Polyurethane Dispersion Coating	Kumar Rajnish	610
208.	MACRO 487	Cellulose Nanomaterials: A Natural Biopolymer as Sustainable Materialfor Future	Chandravati	611
209.	MACRO 490	Dual responsive alginate/poly(N-isopropyl acrylamide)/graphene oxide composite gels for controlled release studies of anti-cancer drug	K. Sudhakar	613
210.	MACRO 491	Phosphorous and sulphur containing bio-based polyurethanes from non-edible renewable resource: Their thermal, mechanical and anti-corrosive properties	Somisetti Varaprasad	614
211.	MACRO 508	Silver and ZnO nanoparticles incorporated agarbiodegradable compositesfor Antibacterial Applications	Rathore, Kalpana	615
212.	MACRO 509	Click -Inspired Chemistry for (Bio) Conjugation in Macromolecular and Polymer Science	Mane, Shivshankar	616
213.	MACRO 539	Synthesis and Characterization of Green Polyester Films	Sidhharth Sirohi	617
214.	MACRO 549	Thermally curable 2-Oxazoline coatings from bio-based building blocks	Roy M.	622
215.	MACRO 550	Small scale screening of novel bio-based polyesters	Noordzij, G.	623
216.	MACRO 556	Engineering Protein Based Bio-polymer Coated Functional Nanomaterials for Bio-application	Chakrabortty, Sabyasachi	624
217.	MACRO 555	Synthesis and characterization ofFlutamideloaded Carbopol/Poly(vinyl pyrrolidone) blend microspheres: In-vitro release studies	P. Kumara Babu	625

Focus area: Nano structures, Self-assembly and Supramolecular polymers (NSP)

SL. NO.	MACRO ID	PAPER TITLE	FIRST AUTHOR	PAGE NO.
218.	MACRO 112	Supramolecular Approches Towards Novel Applications.	Tejas S Bhosale	627
219.	MACRO 120	Molecularly imprinted polymers	Kalsang Tharpa	628

220.	MACRO 121	Amphiphilic and pH Responsive Functionalized Hyperbranched Copolymer: Self Assembling from Polymersomes to Aggregates and Waste Water Treatment through Host-Guest Applications	Das Tamalika	634
221.	MACRO 125	Synthesis and Characterization of HMDA-PCNSL Modified Kaolin (PBT-H) as a Reinforcing Filler in Rubber/Clay Nanocomposites	R. V Sreelekshmi	636
222.	MACRO 128	Au@SiO_2@PSS Hybrid Nanostructures Prepared via Block Copolymer Template Approach: Catalytic Studies	Aruni Shajkumar	642
223.	MACRO 130	Environmentally Friendly Approaches to the Synthesis of Silver Nanoparticles (Ag-NPs) Using Polymeric Materials Extracted From Plants	Songca SP	643
224.	MACRO 133	Triggered Supramolecular Polymerization	Pal, D. S.	644
225.	MACRO 135	Fractionated Crystallization Behaviour of Semicrystalline Polymers Under Confinement in Electrospun Nanofibers of Polymer Blends	Samanta Pratick	645
226.	MACRO 136	Chirality Issues in Supramolecular Polymerization using 1,3-Dihydroxyl Synthon	Ghosh G	650
227.	MACRO 138	Functional Poly(disulfide)s: Synthesis, Aggregation and Triggered Disassembly	Raju Bej	651
228.	MACRO 139	Multi-functional Microgels as Building Blocks for Nanostructured Materials	Agrawal, Garima	658
229.	MACRO 148	Antifouling Thin Film Composite Polyamide Nanofiltration Membranes for the Removal of Heavy Metals from Ground Water	Bera Anupam	659
230.	MACRO 181	Preparation and properties of Hyperbranched polymides/MWCNT nanocomposites	M. Fathima Rigana	661
231.	MACRO 193	POSS And Graphene Oxide Based Polymeric Nanocomposites For High Performance Applications	M.Sarojadevi	662
232.	MACRO 201	Dopant-Assisted Hierarchical Electrical Conducting Folic acid/Polyaniline/ silver-nanoparticles hydrogel with Enhancement of Photoresponse and Energy storage.	Das, Sujoy	664
233.	MACRO 203	Synthesis and Characterization of pH responsive Self-healing Hydrogel	Swati Sharma	665

234.	MACRO 211	Reduced Graphene-Polyaniline Nanofibres Hybrid as Peroxidase Mimetic Material: Exploited for H_2O_2 and Cholesterol Recognition	Singh Shikha	666
235.	MACRO 218	Fluorescent Polymer Films of Carbon Dots-PMMA Nanocomposites	Suchithra C	668
236.	MACRO 221	Superhydrophobic and pH tolerant Silica Surface Decorated with Oligomers; Self-assembled Micro-flower Bunches and Nanofolds	Ramakrishna S	674
237.	MACRO 225	Influence of the diamine modified graphene on polyurethane properties and its biological applications	Patel Dinesh	675
238.	MACRO 227	Size-Dependent Interaction between PIL Stabilized Silver Nanoparticles and DNA: A Spectroscopic Investigation	Kasina Manojkumar	675
239.	MACRO 232	An Approach For Controlled Grafting of PANI Chains From Fluorescent Carbon Nano Dots	Ghosh, T	676
240.	MACRO 234	*In situ* Fabrication of Catalytic Platinum Nanoparticles Embedded Poly(Vinyl alcohol) and Fluorescent Gold Nanocluster Embedded Poly(methyl methacrylate) Films	Madhuri, U. D	682
241.	MACRO 237	Synthesis And Application of Carbon Quantum Dot Grafted Stimuli Responsive Polymer Systems.	Ball, R.	684
242.	MACRO 247	Formation of functional super-helical assemblies by constrained single heptad repeat	Sudipta Mondal	686
243.	MACRO 264	Fabrication of Anisotropic Self-assembled liquid Crystalline Poly (3, 3''' dialkyl quarterthiophene) Films over Liquid Surface	Pandey, R. K	687
244.	MACRO 293	Change in Energy Transfer between Donor-Acceptor Molecules on Stimuli-Induced Disintegration/Transition of Nanostructured Assemblies Prepared from Amphiphilic Block Copolymers	Maiti, Chiranjit	688
245.	MACRO 305	Polypeptide-Based Thermoresponsive Graft Copolymer and Their Self-Aggregation Behaviour in Solution	Bose Avijit	689

246.	MACRO 306	Preparation and Characterization of Shear Thickening Fluids with Surface Modified Silica Nanoparticles	Swarna	691
247.	MACRO 318	Preparation and characterization of PMMA/Cu-Cr LDH nanocomposites via melt intercalation method	Kumar Manish	692
248.	MACRO 321	Thermally Stable Poly(ether-ketone)/MWCNT Composites As An Efficient Electro-magnetic Shielding Material With Improved Mechanical Properties	Sampat Singh Chauhan	693
249.	MACRO 325	Development of Methylcellulose Based Nanocomposites and their Application Possibilities	Pramanik	694
250.	MACRO 331	Polymer Supported Large Area Periodic Silver Nanostructures as an Efficient SERS Platform	V. Raji	695
251.	MACRO 334	Supramolecular Synthons in Designing Gelators Derived from Multiple Drugs	Roy, R.	696
252.	MACRO 337	Nano-sized Coordination Polymers for Cell Imaging and Heterogeneous Catalysis	Sarkar, K	698
253.	MACRO 342	Production of Multiwalled Carbon Nanotubes from PongamiaOil Using Chemical Vapour Deposition Method and Preparation of Polymer Nanocomposites By Using CNTs	Bagotia N.	699
254.	MACRO 352	Mechanically Strong Self-healing Acrylic Copolymers	MirchandaniGirish	700
255.	MACRO 354	Effect of Functionalised Graphene on Sulfonated poly(ether ether ketone) Membrane	Ghosh Priyanka	701
256.	MACRO 357	Ferrocene Functionalized HTPB based Segmented Polyurethanes through Supramolecular Interactions.	Billa Narasimha Rao	703
257.	MACRO 374	Surface Wettability Behaviour of Functionalized-Gum Arabic Dispersed Poly (lactic acid) Bionanocomposite Foams	Borkotoky	705
258.	MACRO 377	PHBV Blends: Comparative Studies of Films and Nanofibers	Bhagyashri S.	706

259.	MACRO 383	Electrospun Nanofibers of PLA composite with Silk Nanoparticles (SNP): Thermal, Mechanical and Wetting properties	S Narendren	708
260.	MACRO 397	Salt-Induced Deposition of Thermoresponsive PNIPAM Coated Metal Nanoparticles on Solid Substrates	Maji, S	709
261.	MACRO 401	Delaminated Layered Double Hydroxide Nanosheets as Multifunctional Nanofillers for Semicrystalline Polymers	Nagendra, Baku	711
262.	MACRO 402	Influence of Additives on the Formation of Block Copolymer-based Supramolecular Thin Films and their Microdomain Control	Deepthi Krishnan	712
263.	MACRO 403	Water soluble polysaccharide from hybrid mushroom and its application in nanoparticle synthesis	Maity, Kankan Kumar	714
264.	MACRO 409	Nanostructured Semiconducting Polymer-Inorganic Composites for Opto-Electronic Applications	Sudha J. Devaki	715
265.	MACRO 412	Carbon Nanoparticles Induced Shape-Recovery Behavior in a Hyperbranched Polymer Composite	Pilla Srinivasarao	716
266.	MACRO 420	Tailored Interface Resulting In Improvement In Mechanical Properties Of Epoxy Composites Containing Poly (ether ether ketone) Grafted Multiwall Carbon Nanotubes	Katti, Prajakta Prathamkumar	717
267.	MACRO 421	Fabrication and Tuning the Nanoporous Channel in Nanoporous Membranes derived using Crystallization Induced Phase Separation in Polymeric Blends	Bose Suryasarathi	718
268.	MACRO 422	Layer-by-Layer Assembly of Engineering Nanostructured Polymer Blends to Screen Electromagnetic Radiation	Biswas Sourav	719
269.	MACRO 425	Janus Folded Structures Based on Alternating Periodically Grafted Polymers	Ramkrishna Sarkar	720
270.	MACRO 432	Effect of Cerium addition on Corrosion Characteristics of Smart Polystyrene MMT Clay Nano Composite coatings on Aluminum Alloys	Rajan, Ramya	722
271.	MACRO 440	Studies on polyurethane nanoclay composite as a barrier coating system	Srirangam Siripothu	723

272.	MACRO 445	Formation of Shish-Kebab structure in poly(vinylidene fluoride)/ionic liquid modified clay nanocomposite	Eapen Thomas	730
273.	MACRO 452	Effect of copolymer functionalized graphene oxide at low loading on interfacial, thermo-mechanical and wear properties epoxy nanocomposites	Rohini Rani	737
274.	MACRO 470	Enhancement of β-crystal polymorph formation in poly(vinylidene fluoride)- zinc oxide nanocomposite films	Parvathy C	738
275.	MACRO 476	Investigations on Thermoreversible Gelation of Self-assembling Amphiphilic Organogelators With PEG Core	M. Himabindu	745
276.	MACRO 486	Graphene Modified Polymeric Surfactant: Synthesis, Characterization and Application for Narrow Disperse Polystyrene Nanoparticles	Rajender Nutenki	746
277.	MACRO 494	TiO_2/Poly(thiourethane-urethane)-urea Nanocomposites Using Sulfur Rich Hyperbranched Polymers: as NIR reflective, High Refractive Index and Anticorrosion Materials	Ireni, Nagaraj Goud	748
278.	MACRO 502	Reversible Shape Switching Phenomena In Linear Thermoplastic Polyurethane Through Molecular Flipping: Potential Application As Smart Gripper	Arpan Biswas	749
279.	MACRO 506	UV based Photocatalytic treatment of Methyl Tertiary-Butyl Ether (MTBE) contaminated water using TiO2–Reduced Graphene Oxide nanocomposites as a photocatalyst	Ojha Ankita	774
280.	MACRO 512	Synergistic Effect of Nano Reinforcement and Cross-linking Towards Polyvinyl alcohol (PVA) Properties	Amit Kumar Sonker	775
281.	MACRO 513	Clay/Graphene nanohybrid incorporated Poly Vinyl Alcohol : An Efficient Flame Retardant	Stanly Sona	776
282.	MACRO 528	Polyethylenimine Grafted GO as a Novel Multi-functional Reinforcing Agent for Epoxy System	Raneesh Konnola	783
283.	MACRO 538	Graphene reinforced self-healing nano composites	S. Rana	784
284.	MACRO 542	Development and rheological study of the polymer blended viscoelastic medium for finishing of microholes	Sachin Singh	788

285.	MACRO 547	Cryo EM characterization of Self assembled Giant Bottlebrush Block Copolymer Surfactants	Marc Schmutz	795

Focus area: Elastomers, Polymer physics and Modelling (EPM)

SL. NO.	MACRO ID	PAPER TITLE	FIRST AUTHOR	PAGE NO.
286.	MACRO 105	Molecular Dynamics simulations of hydrolyzed PVAc - PFO based anti-stain self-clean coatings	Sushanta K Sethi	799
287.	MACRO 117	Influence of Long Chain Branching on Necking Behaviour in Melt Extruded Cast Polyethylene Films	Rokade, Dhammaraj	805
288.	MACRO 119	Large Scale Production of Nylon Nanofibers through Electrospinning and their use in Structural Composites	Anand, Anoop	807
289.	MACRO 129	Dynamic Viscoelasticity and Thermo-Mechanical Characteristics of TPV Composites: Theoretical and Morphological Approaches	Dey, P	810
290.	MACRO 149	Segmental motions in PDLLA at the Glass transition temperature, probed using Solid-state NMR	Kavalakal MathaiEldho	812
291.	MACRO 151	Effect Of Increasing Soft Segments On Properties Of Polyurea for blast mitigating applications	Iqbal Nahid	824
292.	MACRO 165	A Kinetics Study of Light-Induced E–Z Isomerization in Sol, Gel, Xerogel, and Powder States of an Anthracene-Based Organogelator: Fiber to Crystal Transformation	Mondal Sanjoy	828
293.	MACRO 171	Development of New Thermoplastic Elastomeric Polyamide Blends by Electron-Induced Reactive Processing	Shib Shankar Banerjee	829
294.	MACRO 194	Nylon: Past, Present and Future Perspectives	Anuj Mittal	830
295.	MACRO 209	Oriented Crystallization Templated in Aligned Multi-walled Carbon Nanotubes Arrays	Das, N. C	831
296.	MACRO 252	Reversible Shape Switching Phenomena In Linear Thermoplastic Polyurethane Through Molecular Flipping: Potential Application As Smart Gripper	Arpan Biswas	836

297.	MACRO 254	Crystallization Kinetics, Fold Surface Free Energy in Immiscible Polymer Blend PVDF/ABS in Presence of Functionalized Multiwall Carbon Nanotubes	Goutam Prasanna Kar	837
298.	MACRO 262	Electro-spinning of Non-ionic Cellulose Ethers and Characterization by Atomic Force Microscopy, Scanning Electron Microscopy and Contact Angle Measurements	A. C. Wali	841
299.	MACRO 263	Effect of Sepiolite on Non-isothermal Crystallization Kinetics of Polypropylene	Bindu Manchanda	846
300.	MACRO 269	Novel Super TPV: A New Generation Thermoplastic Elastomer	Kinsuk Naskar	847
301.	MACRO 280	Mechanical & Electrical Properties of sPS/P3HT Composites	Samanta Ketaki	848
302.	MACRO 297	Biomimetic crystallization of polylactide and the development of polymeric brick-and-mortar semi-crystalline microstructure	S. Sabapathy	849
303.	MACRO 298	Effect of Chain Length on Properties Predicted by Molecular Dynamics Simulations	Nityanshu Kumar[a]	853
304.	MACRO 307	Rheology and Foamability of Styrene-Ethylene/Butylene-Styrene (SEBS)/ Polystyrene Blends	Ritima Banerjee	860
305.	MACRO 317	Effect of Compatibiliser on Morphology and Melt Extensional Properties of Halloysite Nanotubes -Filled High Density Polyethylene	V. P. Singh	864
306.	MACRO 320	Design and Development of acrylonitrile (AN) and methylmethacrylate (MMA) copolymers for improving the scratch and mar properties of Polymethylmethacrylate (PMMA)	Rai, Roopali	865
307.	MACRO 330	Synergistic Effect of Nucleation / Stereo complexation with Plasticizer on Crystallization of Poly(lactic acid)	Susheela B. Idage	870
308.	MACRO 345	Processing and nanoclay induced piezoelectricity in poly(vinylidene fluoride-*co*-hexafluoro propylene) nanohybrid for device application	Anupama Gaur	877
309.	MACRO 346	Optimization of PMMA Microcapsules using Taguchi Approach to Improve Self-Healing Performance of Polymer Composites.	Sharma, Shilpi	885
310.	MACRO 348	Solvent-Free, Photocurable Mussel-Inspired Polyester Adhesive from Renewable Resources for Underwater Adhesion	Amal Narayanan	886

311.	MACRO 349	Novel Polysiloxanes with Inherent Flame Retardancy: Synthesis and characterisation	K. Indulekha	886
312.	MACRO 350	Dual Functional HQ-Resins: Promising One Shot Tool for both Reinforcement and Crosslinking in Transparent Silicone Polymers	P.S. Drishya	891
313.	MACRO 356	Dielectric Evaluation of Polymer Matrix Composites for Stealth Applications	Jayalakshmi C. G	896
314.	MACRO 359	Investigation on Toughening of Epoxy Resin with addition curable PEEK	Leena K	904
315.	MACRO 360	Space Durable Siloxane Based Thermal Control Coatings With Tailored Optical Properties For Spacecraft Structures	Archana T.S	909
316.	MACRO 362	Tetrazole Functionalized Hydroxyl Terminated Polybutadiene polyurethane	Moumita Dhara	910
317.	MACRO 363	Mechanical characterisation and sorption studies of aromatic solvents through acrylonitrile-butadiene rubber-chitosan biocomposites	Meril Shelly	911
318.	MACRO 367	Room temperature processable heat resistant epoxy-oxazolidone based syntactic foams	Soorya Nair	921
319.	MACRO 378	Coconut Oil Plasticized Poly (lactic acid): Influence of Coconut Oil on Morphological, Rheological and Gas Barrier Properties	Bhasney Siddharth	927
320.	MACRO 382	Tuning base polymer molecular weight and filler composition for optimum cure, mechanical, rheological and dielectric properties of PDMS based one part RTV adhesive	Smitha C Sukumaran	929
321.	MACRO 385	Recyclable Polylactic Acid grafted Cellulose Nanocrystal Films through Reactive Extrusion Approach	Dhar Prodyut	931
322.	MACRO 386	Early prediction of polymer degradation due to weathering	A.K. Sikder	933
323.	MACRO 390	Investigations On Low Density Insulation Materials For Solid Rocket Motors	Ajith kumar H	940
324.	MACRO 399	Structural and Dielectric Properties of Syndiotactic Polystyrene in Bulk and Aerogels	Joseph A.M	945
325.	MACRO 400	Polymer-based Flexible Ferroelectric Nano composites	Anupriya Vijayakumar	946

326.	MACRO 406	Solvent-Induced Crystallization and Phase Transitions of Poly(L-lactide) (PLLA)	Shaiju, P	949
327.	MACRO 410	Fully "Face-on" *vs* Fully "Edge-on": Rational Functionalization of Thiophene Oligomers for Control over Film-State Packing	Ghosh, Tanwistha	950
328.	MACRO 414	Understanding the Interactions of Poly(propylene Glycol) with Thermoplastic Polymers	Muthukrishnan. Sharmila	951
329.	MACRO 424	Malachite Green based Photo-decross-linkable Systems	Orodepo Gabriel O.	956
330.	MACRO 428	Studies on Novel Blend Membranes from Chemically Modified Natural Rubber Latex and Poly(vinyl alcohol)	Janisha Jayadevan[a]	957
331.	MACRO 436	Electrochemical Behavior and Corrosion Inhibiting Effects of Green Nanosilver Modified Epoxy Coatings	Ulaeto, Sarah B	964
332.	MACRO 438	Understanding the Dynamics of Multicomponent BTA Nanofibers in Aqueous Solutions	Bala. N. S. Thota	965
333.	MACRO 441	A Rheokinetic Approach to Cure Optimization of Polyurethane Binders in Composite Solid Propellant	G. Santhosh	967
334.	MACRO 456	Studies on the Influence of Free Volume on Transport Properties of Millable Polyurethane/Natural Rubber Blends	Renu Jose	979
335.	MACRO 457	Autonomic Healing of Polymers with Embedded Microcapsules	Rajasekaran Divya	981
336.	MACRO 461	Rheological and Thermal Studies of Poly Lactic acid/Hydroxyapatite Composites	Prasad Arbind	989
337.	MACRO 462	Effect of Process Parameters and Cure Catalysis on the HTPB-IPDI Based Solid Propellant Behavior	CH Devi Vara Prasad	992
338.	MACRO 468	Catalytic Action of CTAB/ KBr/ C_9OH Micellar Media on the Basic Hydrolysis of Crystal Violet	Karayil, Jasila	999
339.	MACRO 473	New Physical Insights into Shear History Dependent Polymorphism in Poly(vinylidene fluoride)	Amanuel Gebrekrstos	1000
340.	MACRO 474	Translocation of polymer through nanopore under end pulling force	Bappa Ghosh	1001
341.	MACRO 497	Role of size of fillers on the development of an electrically conductive rtv silicone single part adhesive for space applications	Prasanta Kumar Behera	1007

342.	MACRO 498	Effect of particle shape of BN in enhancing thermal conductivity of thermal interface materials	N.Neeraj	1014
343.	MACRO 499	Intermolecular Ene Reaction For High Temperature Curable Polybutadiene Systems	Gayathri S	1021
344.	MACRO 505	Effect of maleic anhydride grafting on MA-g-ABS/EVA miscible blend for high impact strength materials	O. Manaf	1022
345.	MACRO 507	Thermo-mechanical evaluation of organically modified clay filled Polymethylsilsesquioxane	Ancy Smitha Alex	1028
346.	MACRO 511	Studies on Polysiloxane Derived Porous SiOC/ SiO2 Ceramics via Sacrificial Filler Route	Shikha K.T	1035
347.	MACRO 514	A Comparative Study on the Piezoelectric Generation in PANI/ZnO/rGO and PANI/ZnO/f-MWCNT Ternary Nanocomposites	T.P.Nisha	1044
348.	MACRO 517	Kinetics And Regioselectvity Of Phenol-Formaldehyde Reaction; New Insights	Praveen Kumar Solasa	1050
349.	MACRO 518	Electrospun polyurethane fibres reinforced resorcinol-formaldehyde composites	S. Kiran	1057
350.	MACRO 520	A combined theoretical and experimental investigation on the effect of microphase separation on shape memory behavior of polyurethane	E. Swathi	1062
351.	MACRO 521	Influence of Catalyst and Alternate Polyamidoamine Hardener on the Chemical and Physical Properties of 4-Component Epoxy System Used in Solid Rocket Motor	Pradhan S K	1069
352.	MACRO 522	Experiments on Filled and Unfilled HTPB based elastomeric materials for potential applications in solid rocket motors	Ravishankar.P M	1075
353.	MACRO 523	Effect of Graphene Oxide (GO) on Properties of Thermoplastic Polymer Composites	Shashikant Supare	1080
354.	MACRO 524	Kinetic studies of Phenol-Formaldehyde Resins using NMR spectroscopy	SrinivasChinthalapalli	1082
355.	MACRO 525	Scale Up Of Processing Of Resole Type Phenolic Resin For Silica Phenolic Throat Inserts For Liquid Engines	Praveen Kumar Solasa	1085
356.	MACRO 526	Development of High Performance In-Situ Polymer/Polymer Microfibrillar Composites Based on PP/Nylon 6 Blend System: Effect of Draw Ratio and Nano Fillers	Deeraj B.D.S	1091
357.	MACRO 527	Transparent and Electrically Conductive Polyimide Composites for Space Applications	KPP Najiya	1091

358.	MACRO 531	A theoretical investigation to evaluate structural and conformational effects of ligands in transition metal complexes useful for the preparation of ultra-high molecular weight poly(ethylene)s	K. Patel	1092
359.	MACRO 533	Studies on the effect of catalyst and reaction kinetics of Polyether Based PUIR Foam	Remya Balakrishnan	1099
360.	MACRO 534	Flexible Polyurethane Elastomer bearing Ionic Liquid Crosslinks	Prasanta Kumar Behera	1106
361.	MACRO 541	Role of sample preparation techniques for analysis of trace metals in polymers	A.D. Rosa	1107
362.	MACRO 544	A Promising approach to design and develop UV/ Thermal dual cure acrylate binder from renewable resources	Ozlem Kubra AKDOGAN	1111
363.	MACRO 548	Fiber based poly(lactic acid) materials for self-reinforced composites	de Kort, G.W	1112
364.	MACRO 552	Cure Characteristics and Physico-Mechanical Properties of a Conventional Sulphur-Cured Natural Rubber with a Novel Anti-Reversion Agent	G.S Shibulal	1114
365.	MACRO 554	Molecular design of high performing polymers for 3D FDM printing	Srinivas, V	1123
366.	MACRO 557	Fracture mechanics of natural rubber and blends using Finite element analysis	Anand Poomuthu	1125
367.	MACRO 561	Effect of epoxy content and blend composition on the phase morphology and physico-mechanical properties of polyvinyl chloride/epoxidized liquid natural rubber (PVC/ELNR) blends	P. K. Biju	1126
368.	MACRO 562	Novel High Temperature Resistant Materials Based on Polycyclic Silicones for Space Applications	Indulekha K	1127



FOCUS AREA

POLYMER SYNTHESIS AND CHARACTERISATION

MACRO 109

Synthesis, Characterization and Application of Water Based Pressure Sensitive Adhesive

Borole Dinesh* and Digar Mohanlal

Pidilite Industries Ltd,
Mumbai- 400 059, (M.S.) India.
Telephone: (91) 022 - 33087450 Fax: (91) 022 – 28216007
E- mail: dinesh.borole@pidilite.com

Abstract

The pressure sensitive adhesive market includes a number of polymeric raw materials. There are used Natural Rubber, Hot Melt (Synthetic Rubber), Acrylics (Solvent and Water Borne), UV Curable and Silicones. Here we are focusing on Acrylic PSA which includes chemistry such as Acrylic and VAM Acrylic monomer by emulsion polymerization route. This experimentation is characterized by three properties which are useful in characterizing the nature of pressure-sensitive adhesives are tack, peel (adhesion) and shear (cohesion). The first measures the adhesive's ability to adhere quickly, the second its ability to resist removal by peeling, and the third its ability to hold in position when shearing forces are exerted. Generally speaking the first two are directly related to each other but are inversely related to the third. Comparative data of tack, peel strength on various substrate and shear resistance is measured. Pressure sensitive adhesives used in different forms in various applications such as Labels, Medical Dressing, Graphic Films, Tapes and Specialty Applications such as Electronics. Here we are focusing for labels application.

Keywords: *Emulsion Polymer, Acrylics, Tack, Peel and Shear*

Introduction

The term pressure sensitive or sometimes self adhesive is also used to designate special class of adhesive. PSAs are materials that adhere strongly to solid surfaces upon application of light contact pressure for short contact time. PSAs are aggressively and permanently tacky in their dry form, solvent free at room temperature and firmly adhere to

variety of substrate. PSAs are classified according to the physical form in which the adhesive is supplied or according to the chemical composition.

Pressure-sensitive adhesives offer numerous advantages. Application can be easily automated and usually requires no elaborate equipment. When used in assembly, PSAs save time compared to liquid adhesives because they don't require any setup or long curing times. In addition, adhesion is immediate, allowing manufacturing procedures to continue uninterrupted, which results in significant time and labor savings. Pressure-sensitive adhesives eliminate the need for screws, rivets, clips or drilling holes, thus preventing cracks and corrosion and improving the integrity and appearance of the final product. PSAs also provide an insulating seal, as well as sound and vibration control.

Various type of PSAs like hot melt, solvent based and water based are used in various applications. Acrylates chemistry is mainly explored for PSA due to their unique property like high optical clarity, oxidation and ultra violet resistance, migration resistance, low toxicity and low cost[1]. Acrylic emulsion PSAs shows very good adhesive property with polar substrates such as steel, aluminum, tin and wood.

Water-soluble polyacrylate pressure-sensitive adhesives are used primarily in the production of industrial single-sided, double-sided and transfer adhesive tapes[2,3], which are being increasingly used in the paper industry to splice paper webs during manual and flying reel changing. A special area of use re-sides in the manufacture of water-soluble labels. The latest application is in the field of medical products, where neutral electrodes and adhesive tapes for securing operating theatre sheets are of special importance[4].

Emulsion polymerization is one of the most widely used methods of manufacturing acrylic, vinyl polymers, which involves formation of a stable emulsion of monomer in water using emulsifier or protective colloid. In this paper we are higlight on sysnthesis of arylic and vinyl acrylic emulsion synthesis by surfactnat as well as protective colloid and their effect on physical parameters such as solids content, free monomer, viscosity, particle size, molecular weigh etc. and on performance properties such as tack, peel strength on glass, plastic, tin plate and shear strength.

Experimental procedure for Semi Batch Emulsion Polymerization

A four necked glass reactor equipped with a reflux condenser, dropping funnel, nitrogen

assess nozzle and UDF stirrer used. Tmepertaure of polymerization is 80-820C and time of addition of monomer and initiater is 5 hr. Total reaction time is 12 hr. Solid content of finished product is 55 to 57%.

Experimentation

We designed 4 slots of experiments. Each slot consists of 8 experiments. For each slots we consist of 6 factors such as monomer concentration ratio, crosslinking monomer ratio, different plasitisizer and tackifier concentration to prepare 8 experiments.

First slots contains following ingredients

Butyl Acrylate, 2-Ethyl Hexyl Acrylate, Methyl Methacrylate, Methacrylic Acid-Anionic and Non ionic Surfactant and Potasium Per sulphate Initiater and Plastisizer

Second slots contains following ingredients

Butyl Acrylate, 2-Ethyl Hexyl Acrylate, Methyl Methacrylate, Methacrylic Acid-Anionic and Non ionic Surfactant and Potasium Per sulphate Initiater, Rosin based Tackifier and Plastisizer

Third slots contains following ingredients

Vinyl Acetate, 2-Ethyl Hexyl Acrylate, Crosslinking Monomer, Protective colloid, Potasium Per sulphate Initiater and Plastisizer

Fourth slots contains following ingredients

Vinyl Acetate, 2-Ethyl Hexyl Acrylate, Crosslinking Monomer, Protective colloid, Potasium Per sulphate Initiater, Rosin based Tackifier and Plastisizer

Characterization

Three properties which are useful in characterizing the nature of pressure-sensitive adhesives are tack, peel (adhesion) and shear (cohesion). The first measures the adhesive's ability to adhere quickly, the second its ability to resist removal by peeling, and the third its ability to hold in position when shearing forces are exerted. Generally the first two are directly related to each other but are inversely related to the third.

Tack Measurment Method

The tack test methods which are dominant in modern PSA technology are the rolling ball tack test (ASTM D3121-94).

A stainless stell ball is rolled down an inclined ramp on a strip of PSA. The distance that the ball travels before stopping is defined as rolling ball tack. Shorter the distance higher is the tack.

The rolling ball tack test is one measure of the capacity of the adhesive to form a bond with the surface of another material upon brief contact under virtually no pressure. The rolling ball tack test is one method of attempting to quantify the ability of an adhesive to adhere quickly to another surface.

Peel Strength Measurment Method

Peel strength is the average load per unit width of bond line required to separate bonded materials and its unit is N/m.

Generally 180^{o} angle peel test method is used (ASTM D3300)

The values obtained using a peel test is strongly influenced by the physical characteristics of the carrier as well as the thickness of the carrier and the adhesive layer.

Shear Strength Measurment Method

ASTM definitions of cohesion include "The propensity of a single substance to adhere to itself, the internal attraction of molecules towards each other; the ability to resist partition from the mass; internal adhesion; the force holding a single substance together" The standard method (ASTM D3654) to determine shear resistance is to measure the time required to pull a defined are of a PSA from a test panel under a constant load.

Results and Discussion

Table 1: Results of First slot of experiments

Sr. No.	Polymer Properties	Expt-1	Expt-2	Expt-3	Expt-4	Expt-5	Expt-6	Expt-7	Expt-8
1	Solid content (%)	56.2	56.4	55.9	55.7	56.4	56.0	56.1	56.2
2	pH	7.5	7.4	7.2	7.3	7.4	7.5	7.6	7.6
3	Viscosity (ps)	12	13	11	10	14	12	12	13
4	Particle size	360	370	350	360	370	380	350	390
5	%Free monomer	0.05	0.04	0.05	0.04	0.05	0.05	0.05	0.04
6	Molecular weight (lakh)	3.50	3.70	3.40	3.80	4.10	3.90	4.00	4.00
7	Falling ball (tack) (cm)	10	9	8	10	7	8	8	8
8	Peel strength on tin plate (gm/inch)	1000	950	900	1000	950	900	900	900
9	Peel strength on plastic plate (gm/inch)	300	250	240	300	280	250	250	250
10	Peel strength on glass plate (gm/inch)	240	200	200	220	250	200	200	200
11	Shear Resistance (min)	220	210	200	210	220	200	210	210

Table 2: Results of Second slot of experiments

Sr. No.	Polymer Properties	Expt-1	Expt-2	Expt-3	Expt-4	Expt-5	Expt-6	Expt-7	Expt-8
1	Solid content (%)	56.1	55.8	56.2	56.2	56.3	55.5	55.9	56.1
2	pH	7.2	7.4	7.3	7.3	7.5	7.1	7.7	7.5

3	Viscosity (ps)	11	13	12	12	13	11	13	12
4	Particle size	370	360	360	350	380	370	370	350
5	%Free monomer	0.03	0.04	0.04	0.05	0.05	0.04	0.05	0.03
6	Molecular weight (lakh)	3.50	3.80	4.10	4.00	4.20	4.00	3.60	3.70
7	Falling ball (tack) (cm)	10	8	9	8	7	9	8	9
8	Peel strength on tin plate (gm/inch)	1000	900	900	950	960	940	900	880
9	Peel strength on plastic plate (gm/inch)	400	350	320	340	380	340	360	340
10	Peel strength on glass plate (gm/inch)	300	220	300	250	300	240	220	240
11	Shear Resistance (min)	360	320	320	340	360	320	320	300

Table 3: Results of Third slot of experiments

Sr. No.	Polymer Properties	Expt-1	Expt-2	Expt-3	Expt-4	Expt-5	Expt-6	Expt-7	Expt-8
1	Solid content (%)	55.8	55.9	56.1	56.0	56.0	55.5	55.8	55.9
2	pH	4.9	5.1	5.1	5.1	5.0	5.0	5.1	5.2
3	Viscosity (ps)	50	55	45	50	55	52	54	50
4	Particle size	880	900	920	880	910	900	910	870
5	%Free monomer	0.15	0.17	0.19	0.15	0.15	0.14	0.16	0.15
6	Molecular weight (lakh)	2.75	2.55	2.70	2.80	2.80	2.70	2.60	2.50
7	Falling ball (tack) (cm)	12	10	10	10	8	9	10	9
8	Peel strength on tin plate (gm/inch)	1000	900	940	920	980	900	910	950
9	Peel strength on plastic plate (gm/inch)	100	90	80	90	100	90	90	80
10	Peel strength on glass plate (gm/inch)	120	80	120	100	120	100	100	110
11	Shear Resistance (min)	200	220	210	180	220	220	210	210

Table 4: Results of Fourth slot of experiments

Sr. No.	Polymer Properties	Expt-1	Expt-2	Expt-3	Expt-4	Expt-5	Expt-6	Expt-7	Expt-8
1	Solid content (%)	55.8	56.2	56.0	56.4	55.9	55.7	55.8	55.9
2	pH	5.4	5.4	5.5	5.4	5.6	5.5	5.6	5.5
3	Viscosity (ps)	45	55	45	55	55	50	56	53
4	Particle size	820	930	840	840	900	880	870	920
5	%Free monomer	0.15	0.12	0.17	0.14	0.16	0.14	0.12	0.15
6	Molecular weight (lakh)	2.75	2.50	2.60	2.90	2.90	2.80	2.50	2.80
7	Falling ball (tack) (cm)	11	11	10	10	8	10	9	10
8	Peel strength on tin plate (gm/inch)	900	940	950	960	980	900	940	900
9	Peel strength on plastic plate (gm/inch)	200	180	180	190	220	200	190	200
10	Peel strength on glass plate (gm/inch)	280	200	240	240	280	260	250	260
11	Shear Resistance (min)	300	320	340	330	350	300	320	330

First and second slots specification

Solid- 55 to 57%, pH- 7 to 8, Viscosity- 10 to 15 ps

Third and fourth slots specification

Solid- 55 to 57%, pH- 4 to 6, Viscosity- 40 to 60 ps,

Experimentals results are shown in Table 1 to 4.

All the experimentation performed in indetical manner to get comapartive data. We observed that monomer ratio, croosslinking monomer quantity, plastisizer and tackifier plays an important role for wet tack, peel strength and shear resistance. Experiment 5 in each slot of experiment shows uniform results for all characterization. In this experiments molecular weight is higher because of more quantity of crossinking monomer which is key parameter for good results.

Conclusion

Following conclusion can be drawn from present study

1. Acrylic emulsion with and without tackifier shows excellent tack and peel strength with good shear strength

2. Acrylic emulsion with tackfier shows more peel strength on plastic and glass surface. At the same time shear strength also increased by tackifier.

3. VAM Acrylic emulsion with and without tackifier shows excellent tack and peel strength with good shear strength

4. VAM Acrylic emulsion with tackfier shows more peel strength on plastic and glass surface. At the same time shear strength also increased by tackifier.

5. For industrial application Acrylic emulsion with low viscosity useful for high speed machine. 6. For industrial application VAM Acrylic emulsion with high viscosity useful for medium speed machine.

Acknowledgements

This work is supported and done in Pidilite Industries Ltd, Mumbai.

References

1. S. M. Taghizadeh, D. Ghasemi, *IranianPoly.J.*, 19, 343, 2010

2. J. Sakdapipanich, N. thananusont, N. Pukkate, *J.AppliedPoly.Sci.*, 100, 413,2006

3. H. Ismail, Z. Ahmad, F. W. Yew, *J. Physical Sciences*, 22, 51, 2011

4. Z. Czech, *Polimery*, 22, 41, 1996

MACRO 116

Facile Synthesis of Dendrigraft Polymer Having Polyepichlorohydrin Core and Investigation of Their Structure Perfection

Smitha George, K.Sreekumar,[a]

[a] *Department of Applied Chemistry, Cochin University of Science & Technology, Kochi-22, India*
e-mail id: smithaprince80@gmail.com

Abstract

We have functionalized Merrifield resin support with polyepichlorohydrin and dendrons are grown on it up to second generation using a "graft from" approach. The estimation of amine functionality was done and found to be 25 mmolg-^{1} which was 70 % of the theoretical value. Photolytic cleavage of dendrigraft polymer from the support resulted in brown water soluble viscous liquid. The molecular weight of 3966 shows that out of the 9 G1 dendritic substituent's, 5 of them got converted to G2. AFM imaging of G2 polymer shows inhomogeneous worm like appearance.

Keywords: *dendrigraft polymer; SPOS; Photolytic cleavage*

Introduction

Recently, great attention has been directed towards the synthesis of Dendrigraft or Dendronized polymers.[1,2] Most of the reported Dendronized polymers were synthesized from linear polymeric core.[3,4] Dendronized polymers synthesized from cyclic or branched polymeric core are only few.[5,6] This has emerged as a new concept in macromolecular design and materials science due to their unique structures which are seldom achieved by dendrimers and linear polymers. Modification of linear polymers with dendritic reagents is one of the most popular approaches for the synthesis of dendronized linear polymers. The design and synthesis of linear polymers bearing appropriate functional groups to introduce dendritic substituents is important. However, synthesis of these polymers is practically difficult due to the lengthy purification procedure after every stage. So we have tried to synthesize Dendrigraft or Dendronized polymer having branches and also linear polymeric core on a solid resin support using Merrifield's solid phase synthesis concept.[7,8]

Experimental

Photolytic cleavage

Resin (500 mg) was suspended in methanol (50 mL) in the reaction chamber of an immersion type photo reactor. The suspension was degassed for 1h with dry nitrogen and irradiated with Philips HP 125W medium pressure Hg lamp at 340-350 nm for 24 h with constant stirring. A solution of CuSO4 was circulated through the outer jacket of the reactor to filter off light waves below 320 nm. After photolysis, resin beads were filtered and washed with methanol.

Combined filtrate and washings were evaporated under vacuum.

Results and discussion

The pentaerythritol initiated polyepichlorohydrin centred dendritic polymer is synthesised on a solid support using reported procedure.[9] After the solid phase synthesis, it was cleaved photolytically to study the solution properties. The resultant G0 polymer was a brown viscous liquid, soluble in DMSO and methanol. The Chem Bio 3D image of G0 polymer cleaved from the support is shown in the Figure1 .

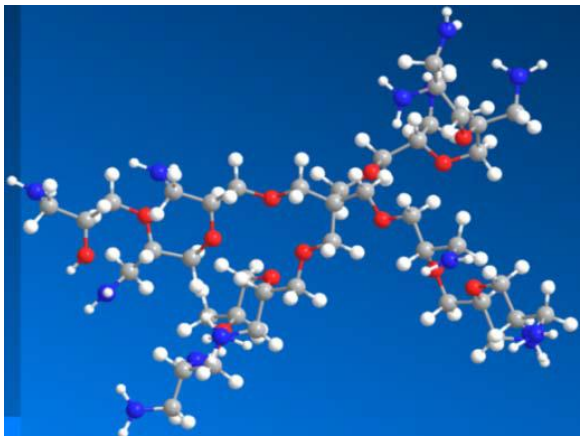


Figure.1 Chem Bio 3D image of G0 Dendrigraft Polymer

The 1H NMR spectrum shows that the polymeric arms are somewhat similar. The appearance of peaks in the range 3.2-3.9 ppm in the 1H NMR spectrum is due to the CH2-O, CH-O and NH2 protons of the polymer. The observed behaviour suggests that growth is regulated by a feedback mechanism due to confinement imposed by the support. From MALDI TOF MS analysis, the molecular weight of the polymer was found to be 884, which was agreeable with the theoretical value. Resin loaded G1 polymer on photolytic cleavage gives a brown viscous liquid. One issue that needs to be addressed is the solubility of Dendronized polymers (DP). It has been known that, in general, DPs containing large number of free peripheral amine groups have low solubility in most commonly used solvents. The lower solubility of the branched chains was attributed to their high propensity to crystallization. Inspection of the 1HNMR spectrum of the G1 DP cleaved from the resin clearly indicates the appearance of amide proton at 7.9 ppm which was absent in G0 DP. To determine the exact number of dendritic substituents introduced, MALDI-TOF MS analysis was performed (matrix: dihydroxybenzoic acid) with the dendronized PEN-G1 polymer. But polymers with polydispersity index greater than 1.2 are difficult to be characterized with MALDI MS due to the signal intensity discrimination against higher mass oligomers. The MALDI-TOF MS of PEN-G1 exhibited several peaks. Focus may be given to two major peaks. The peak at 2857.55 Da is derived from nine dendritic substituents on a pentaerythritol initiated polyether chain. The base peak at 1664.39 Da is derived from four dendritic substituents on a pentaerythritol initiated polyether chain. These results indicate that the G0 polymer was modified to ~70 % with dendron substituents on the polyether backbone.

Generally, in order to minimize defects or cyclisation and to ensure complete reaction, as we go from lower to higher generation, large molar excess of the reagents have to be

taken. The 1H NMR spectrum can provide general information, such as repeating unit or uniformity of branches but cannot confirm the absolute purity of the macromolecules, particularly the identity and number of end groups. This is in large part because, any signal that originates from the small proportion of end groups is overwhelmed by that of the numerous repeating units. As a result 1H NMR spectrum provides little utility in elucidating polymer end groups, either qualitatively or quantitatively.[10] The 1H NMR spectrum of PEN-G2 Dendronized polymer shows broadening of peaks in comparison with PEN-G1 DP. The highest molecular weight of the PEN-G2 polymer from MALDI MS analysis was found to be 3966.02 with a base peak at 1225.41 and another major peak at 1662.72. The molecular weight at 3966.02 shows that out of the 9 G1 dendritic substituents, only 5 of them got converted to G2. The peak at 1662.72 corresponds to the formation of one G2 dendron unit. The peak at 1225.41 is due to cleavage of G2 dendritic unit from the polymeric backbone. The highest mass of 3966 shows that only 30% of dendron substituents are incorporated. The lower experimental mass compared to theoretical mass can be due to missing branches. The difference in experimental and theoretical masses can partially be attributed to structural defects, because, errors can also be due to the polydisperse nature of the polymer. Also, the lower mass may be due to the thermal decomposition of the high generation polymer in comparison with lower generation dendrigraft polymers.



Figure 2 AFM image of G2 polymer

The shape of dendronized polymer in the case of PEN-G2 was analyzed by atomic force microscopy (AFM) as in the case of PEN-G1. In AFM, the film uniformity is mostly determined by the concentration of the dendritic solution regardless of generation. The AFM image of the G2 polymer from lower concentration (0.01 wt%) at a scan width of 15 μm around 10 nm shows a small elongated worm or string like appearance (Figure 2). Since polyether backbone is only having approximately 10-13 units, the length of the worm that we observed is agreeable with the length of the polyether oligomer. Despite the approximate nature owing to uncertainties associated with the AFM technique (tip convolution), it was clear that the average worm length corresponds to the length of the parent polyether, whereas the height of the polymer chain depends upon the dendron generation.

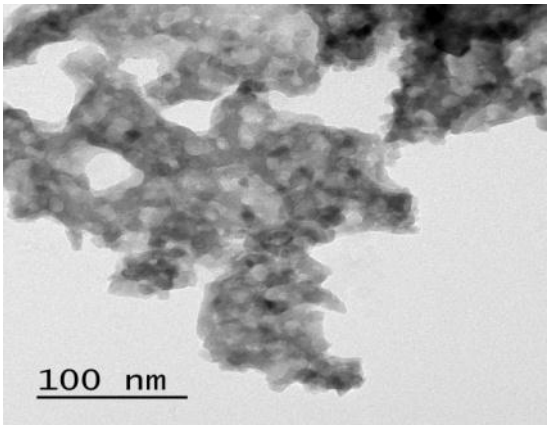


Figure 3 TEM image of PEN G2 polymer

The TEM micrograph of the PEN-G2 polymer in methanolic solution shows polygon shape with low molecular weight polymers aggregate inside the polygon. The polygon shape with longest-extension diameter of up to 13.7 nm may be due to the clustering of polymeric arms in solution (Figure 3). Reports regarding dendrigraft polymers say that they are elongated due to linear polymeric core with dendritic arms. But in solution they remain as spherical.

Conclusions

Polyepichlorohydrin was coupled to Merrifield resin in order to increase the loading capacity. Novel families of dendrigraft G0, G1 and G2 amine polymer having pentaerythritol, glycerol and ethylene glycol initiated polyepichlorohydrin as core have been synthesized and characterized. Characterization of dendrigraft amidoamine polymer having pentaerythritol initiated polyepichlorohydrin as core has been done after photolytic cleavage of the same from the support.

Acknowledgements

We would like to thank STIC, CUSAT for assistance with various analysis. One of the authors (G.S.) thanks the CSIR, Govt. Of India for financial assistance in the form of fellowship. Also thank Thermax, India for providing the gift sample of Merrifield resin.

References

1. J. Yan, W. Li., A. Zhang, *Chem. Comm.*, 50, 12221, 2014.
2. 2. H. J. Sun, S. Zhang, V. Percec, *Chem. Soc.* Rev., 44, 3900, 2015.
3. H. Yu, A. D. Schlueter, B. Zhang, Macromolecules, 47, 4127, 2014
4. E. H. Kang, I.S. Lee, T.L.Choi, J. Am.Chem. Soc., 133, 11904, 2011.
5. B. A. Laurent, S. M. Grayson, J. Am. Chem. Soc., 133, 13421, 2011.
6. Feng X., Taton D., Ibarboure E., Chaikof E. L., Gnanou Y., J. Am. Chem., 130, 11662, 2008.
7. P. Bharathi, J. S. Moore, J. Am. Chem. Soc., 119, 3391, 1997.
8. S. M. Lu, H. Alper, J. Am. Chem. Soc., 125, 13126, 2003.
9. G. Smitha, K. Sreekumar, RSC Adv., 6, 18141, 2016.
10. N. J. Wells, A. Basso, M. Bradley, Biopolymers, 47, 381, 1998.

MACRO 127

Synthesis and antimicrobial activities of dendrimers with indazole as surface units and melamine, *S*-BINOL core units

Mani Jayanthi,[a] Perumal Rajakumar*[a]

[a] *Department of Organic Chemistry, University of Madras,Chennai – 600 025, TamilNadu, India*

** e-mail id: perumalrajakumar@gmail.com*

Abstract

Dendrimers with indazole as surface units and melamine and S-BINOL as core unit has been synthesized in good yield. The antimicrobial studies of the synthesized dendrimers were carried out by well diffusion method[1].

Keywords: *Dendrimer, indazole, O-alkylation, melamine, S-BINOL*

Introduction

The rare heterocyclic compound in nature[2] viz., indazole, possesses broad spectrum of potent pharmacological activities. Since only three natural products which contains indazole unit were isolated,[3-4] the indazole ring system is of much current interest as it happens to be the partial structure of vast number of pharmaceutical compounds. Dendrimers based on melamine can reduce the organ toxicity of solubilized cancer drugs administered by intraperitoneal injection. The solubility of FDA approved hepatotoxins such as methotrexate and 6-mercaptopurine can be increased by mixing them with a dendrimer based on melamine. As Chirality being a characteristic features of many biological systems that plays an important role in the interplay of structure and function, synthesis of large molecules with chirality offers not only a synthetic challenge for organic chemists but also access to a large spectrum of new molecules. Chiral dendrimers which belongs to a class of compounds which offer the possibility to investigate the impact of chirality in macromolecular systems. The influence of chiral units on supramolecular structures and applications of such structures in areas such as catalysis, biosensor research, optical devices etc., are quite challenging. Hence in the present investigation, we report herein the synthesis of dendrimers **1-6** with pharmaceutically important indazole surface group and melamine as well as chiral *S*-(-) BINOL core unit.

Experimental

General: All chemicals and solvents were purchased commercially and used as such without further purification. All melting points of those synthesized compounds are uncorrected and the ^{1}H NMR and ^{13}C NMR spectra were recorded on Bruker 300-MHz instrument in $CDCl_3$ and DMSO-d_6 solvent with tetramethylsilane (TMS) as an internal

reference. Column chromatography was performed on silica gel (ACME, 100–200 mesh). Routine monitoring of the reaction was made using thin-layer chromatography (TLC) developed on 0.25 mm glass plates coated with silica gel-G (ACME**)** 0.25mm thick and visualized with iodine.

Results and discussion

3-(Bromomethyl)-1H-indazole was obtained in good yield from indazole[5] by Vilsmeier Haack formylation followed by reduction with sodium borohydride and then by the reaction of the resulting alcohol with PBr_3 in $CHCl_3$. 3-(Bromomethyl)-1H-indazole thus obtained was further reacted with 4-hydroxy ethylbenzoate in dry DMF in the presence of K_2CO_3 at RT for 24 h to afford the corresponding ester compound **7** in good yield (**Scheme 1**).

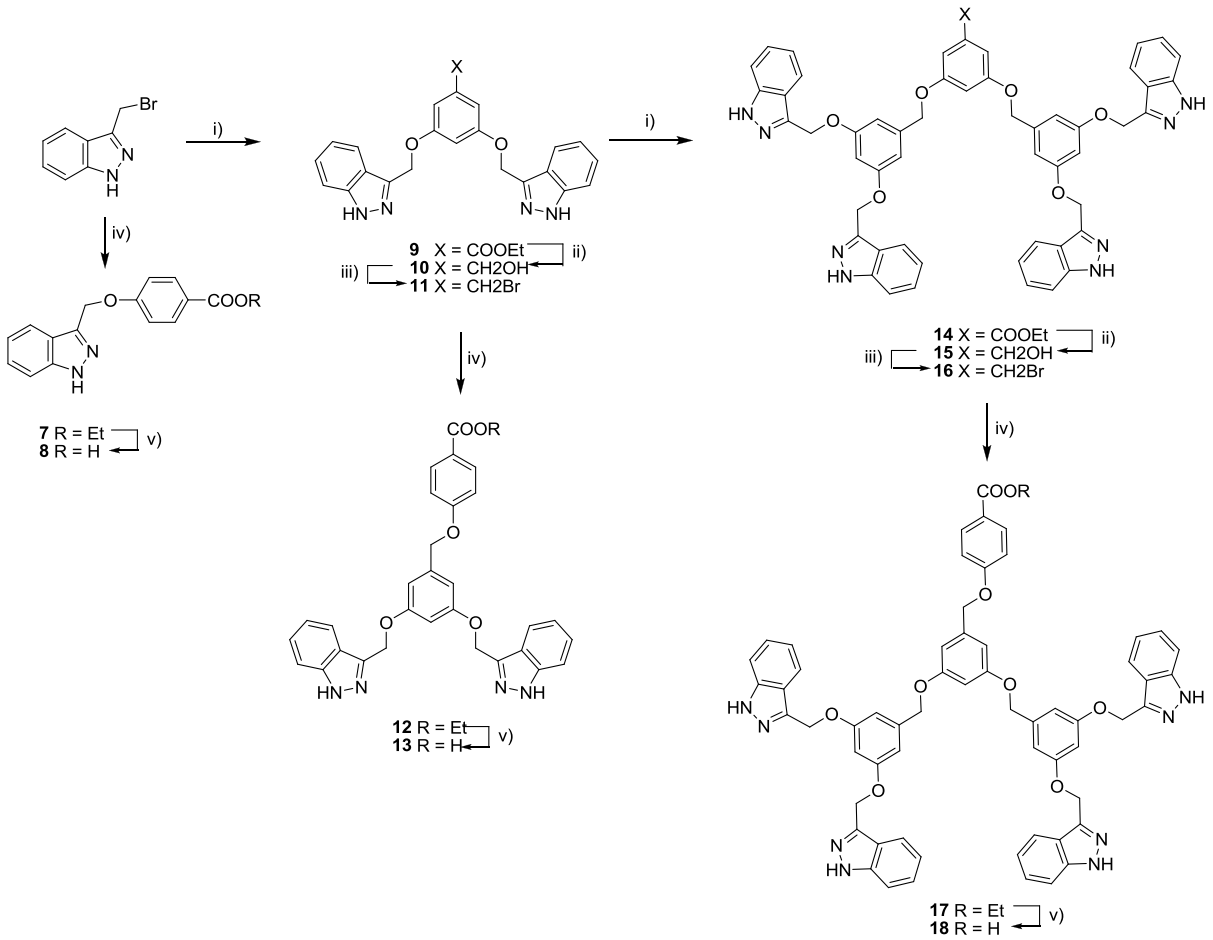
The ester **7** was then hydrolyzed with 1 N HCl in methanol at reflux for 4 h to afford the corresponding carboxylic acid **8** in good yield (**Scheme 1**). In order to synthesize higher generation carboxylic acid dendritic wedge, two equivalents of 3-(bromomethyl)-1H-indazole was treated with one equivalent of ethyl 3,5-dihydroxy benzoate in dry DMF in the presence of K_2CO_3 (**Scheme 1**). The G1-ester **9** was then reduced with LAH in dry THF at 50 ^oC to afford the corresponding hydroxyl compound (G1-CH_2OH) **7** followed by bromination with PBr_3 to afford the first generation dendritic bromide (G1-CH_2Br) **11** (**Scheme 1**).

The first generation dendritic carboxylic ester wedge **12** was obtained by reacting equimolar mixture of 4-hydroxy ethylbenzoate and the bromo compound **11** in dry DMF in the presence of K_2CO_3 (**Scheme 1**) to afford the corresponding O-alkylated compound **12** in good yield. The first generation dendritic carboxylic acid wedge **13** was obtained by hydrolyzing **12** in 1N HCl at reflux for 4 h.

In a similar manner the second generation dendritic bromide **16** was synthesized by repeating similar reaction sequence (**Scheme 1**). The second generation dendritic carboxylic ester wedge **17** was obtaining by reacting equimolar mixture of 4-hydroxy ethylbenzoate and the bromo compound **16** in dry DMF in the presence of K_2CO_3 (**Scheme 1**) to afford the corresponding O-alkylated compound **17** in good yield. The second generation dendritic carboxylic acid wedge **18** was obtained by hydrolyzing **17** in 1N HCl at reflux for 4 h.

General Procedure for Amide formation

To a solution of carboxylic acid (3.0 equiv) in DCM (100 mL) was added EDCI.

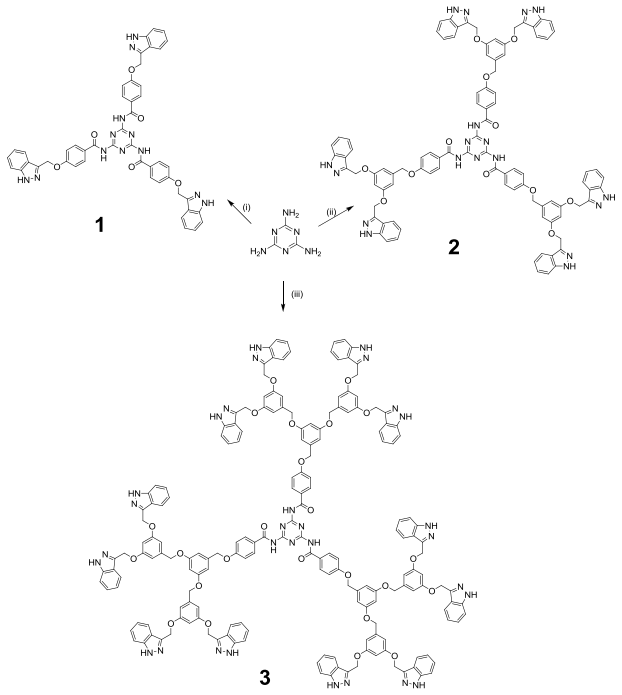


Scheme 1 Reagents and conditions: (i) Ethyl 3,5-dihydroxy benzoate, K_2CO_3, dry DMF, RT, 24 h, **9** (81 %), **14** (80 %) (ii) LAH, THF, 50 ºC, 18 h, **10** (76 %), **15** (77 %) (iii) PBr_3, $CHCl_3$, 0 ºC to RT, 12 h, **11** (74 %), **16** (71 %) (iv) 4-Hydroxy ethylbenzoate, K_2CO_3, dry DMF, RT, 24 h, **7** (85 %), **12** (83 %), **17** (83 %) (v) 1N HCl, Methanol, reflux, 4 h, **8** (80 %), **13** (78 %), **18** (75 %)

HCl/DMAP (4.5 equiv) followed by the addition of amine (1.0 equiv) and stirred at RT for 24 h. The reaction mixture was extracted with $CHCl_3$ (3 x 150 mL), washed with brine solution (100 mL), dried over anhydrous Na_2SO_4. The organic layer was evaporated to dryness and the residue obtained was purified by column chromatography on silica gel (100-200 mesh) by using EtOAc/hexane (1:19) as eluent.

Dendrimer **1**

Yield : 78 %; ^{1}H NMR (300 MHz, $CDCl_3$): δ_H 5.23 (s, 6H); 7.01 (d, J = 7.8 Hz, 6H); 7.26-7.32 (m, 8H), 7.39-7.43 (m, 4H); 7.52-7.55 (m, 3H); 8.03 (dd, J_1 = 1.8 Hz, J_2 = 7.2 Hz, 6H); ^{13}C NMR (75 MHz, $CDCl_3$): δ_C



Scheme 2: Reagents and conditions: (i) **8** (3.0 equiv), EDCI.HCl/DMAP, DCM, RT, 18 h, **1** (78 %) (ii) **13** (3.0 equiv), EDCI.HCl/DMAP, DCM, RT, 18 h, **2** (75 %) (iii) **18** (3.0 equiv), EDCI.HCl/DMAP, DCM, RT, 18 h, **3** (73 %)

67.2, 114.4, 114.5, 123.5, 127.1, 128.8, 129.2, 129.5, 131.6, 131.7, 132.7, 134.1, 162.1, 166.3

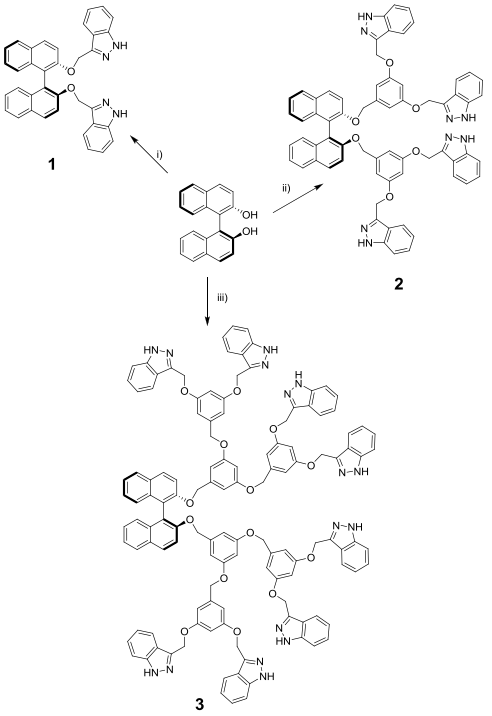
Dendrimer **2**

Yield : 75 %; ^{1}H NMR (300 MHz, $CDCl_3$): δ_H 5.06 (s, 6H); 5.15 (s, 12H); 6.60-6.61 (m, 3H); 6.68-6.69 (m, 6H), 6.95-6.98 (m, 6H); 7.26-7.28 (m, 11H); 7.37-7.40 (m, 7H); 7.51-7.53 (m, 6H); 7.96-7.99 (m, 6H); ^{13}C NMR (75 MHz, $CDCl_3$): δ_C 67.3, 69.9, 101.7, 106.5, 114.5, 122.9, 127.0, 128.9, 129.1, 129.4, 131.6, 132.7, 134.4, 138.9, 160.0, 162.3, 166.8

Dendrimer **3**

Yield : 73 %; ^{1}H NMR (300 MHz, $CDCl_3$): δ_H 5.13 (s, 18H); 5.15 (s, 24H); 6.55-6.57 (m, 7H); 6.64-6.66 (m, 13H), 7.24-7.29 (m, 33H); 7.38 (s, 18H); 7.53 (m, 16H); ^{13}C NMR (75 MHz, $CDCl_3$): δ_C 65.3, 67.2, 70.6, 105.9, 108.6, 115.7, 127.0, 128.9, 129.1, 129.4, 134.8, 137.1, 140.1, 141.3, 143.1, 145.1, 153.9, 159.8

General Procedure for O-alkylation reaction



Scheme 3: Reagents and conditions: (i) 3-(Bromomethyl)-1H-indazole, dry DMF, K_2CO_3, RT, 24 h, **4** (80 %) (ii) **11**, dry DMF, K_2CO_3, RT, 24 h, **5** (78 %) (iii) **16**, dry DMF, K_2CO_3, RT, 24 h, **6** (72 %)

A solution containing the *S*-BINOL (1.0 equiv) and the bromocompound (2.1 equiv) was stirred with K_2CO_3 (10.1 equiv) in dry DMF at 50 ^oC for 24 h after which the reaction mixture was stirred with water and then extracted with $CHCl_3$ (3 x 150 mL), dried over Na_2SO_4, evaporated to dryness to give the O-alkylated compounds. The crude thus obtained was then purified by column chromatography using hexane: $CHCl_3$ (2:3) as eluent.

Dendrimer **4**

Yield: 80 %; ^{1}H NMR: (300 MHz, $CDCl_3$) δ_H 5.13 (s, 4H), 6.82 (d, *J*=4.2 Hz, 4H), 7.04-7.08 (m, 3H), 7.20-7.24 (m, 5H), 7.31-7.36 (m, 3H), 7.40 (d, *J*= 9.0 Hz, 3H), 7.82 (d, *J*= 7.8 Hz, 2H), 7.96 (d, *J*= 9.0 Hz, 2H); ^{13}C NMR: (75 MHz, $CDCl_3$) δ_C 68.0, 115.4, 120.4, 123.8, 125.5, 126.5, 126.6, 127.9, 128.0, 128.2, 128.8, 129.5, 131.5, 134.2, 135.2, 153.8; anal. calcd for $C_{36}H_{26}N_4O_2$: C, 79.10; H, 4.79; found: C, 78.72; H, 4.34; m/z: 547 [M+1]

Dendrimer **5**

Yield: 78 %; ^{1}H NMR: (300 MHz, $CDCl_3$) δ_H 4.73 (s, 8H), 4.99 (s, 4H), 6.24 (s, 4H), 6.35 (s, 2H), 7.20-7.29 (m, 14H), 7.31-7.45 (m, 14H), 7.73-7.75 (m, 2H), 7.87 (d, *J* = 9.0 Hz, 2H); ^{13}C NMR: (75 MHz, $CDCl_3$) δ_C 67.1, 71.0, 101.4, 105.6, 115.8, 120.8, 123.9, 125.5, 126.6, 127.0, 127.8,

128.0, 128.6, 129.1, 129.3, 129.4, 129.5, 129.6, 132.9, 134.2, 134.6, 140.1, 154.0, 159.6; anal. calcd for $C_{66}H_{50}N_8O_6$: C, 75.41; H, 4.79; found: C, 75.12; H, 4.28; m/z: 1051 [M+1]

Dendrimer **6**

Yield: 72 %; ^{1}H NMR: (300 MHz, $CDCl_3$) δ_H 4.73 (s, 16H), 5.14 (s, 12H), 6.24 (s, 13H), 6.35 (s, 5H), 7.23-7.25 (m, 24H), 7.35-7.47 (m, 13H), 7.73-7.76 (m, 3H); 7.86-7.89 (m, 4H); ^{13}C NMR: (75 MHz, $CDCl_3$) δ_C 67.1, 71.0, 101.4, 105.5, 115.8, 120.7, 123.9, 125.5, 126.5, 126.9, 128.0, 129.1, 129.2, 129.3, 129.4, 132.9, 134.2, 134.6, 140.1, 154.0, 159.6; anal. calcd for $C_{126}H_{98}N_{16}O_{14}$: C, 73.46; H, 4.79; found: C, 73.16; H, 4.34

Inhibitory effect of melamine dendrimers 1-3 and chiral dendrimers 4-6 on the growth of human pathogens

The anti-bacterial studies were carried out aseptically under *in vitro* conditions by "cup plate method".[21] All the synthesized dendrimers exhibited different levels of antibacterial activity against the four tested human pathogenic bacteria and fungi with DMSO as control. The antimicrobial activities of six different newly synthesized dendrimers **1-6** were evaluated against four human pathogenic bacteria such as, *Escherichia coli*, *Staphylococcus aureus*, *Pseudomonas aeruginosa*, *Bacillus subtilis* and *Candida albican*s. The biological screening results of dendrimers **1-6** with 10 % DMSO as control with commercial antibiotic viz., tetracycline are tabulated in the form of percentage of zone of inhibition. All the six denedrimers **1-6** shows better activity against all the four human pathogenic bacteria such as, *E. coli*, *S. aureus*, *P. aerugenosa*, *B. subtilis* and one fungi *C. albicans.*

Conclusions

Melamine and chiral core dendrimers with indazole as surface units has been synthesized in good yields. The antimicrobial studies of these synthesized dendrimers **1-6** shows better activity against the human pathogenic bacteria viz., *E. coli, B.subtilis* and the fungi *C. albicans* compared to the standard.

Acknowledgements

The authors thank DST-FIST, New Delhi for NMR spectral facility to the department and DST-PURSE for financial assistance. .

References

1. (a) J. V. Bennet, J.L. Brodie, J.L. Benner, W.M.M. Kirby, *Applied Microbiology*, 14, 2170–2177, 1966. (b) M.A. Janssen, J.J.C. Scheffer, A.B. Svendsen, *Pharmaceutische Weekblad* (Scientific Edition), 9, 193-197, 1987. (c) S. Magaldi, Mata-Essayag S Hartung C, C. Perez, M.T. Colella, C. Olaizola, Y. Ontiveros, *Int. J. Infect. Dis.*, 8, 39-45, 2004.
2. Z. Ali, D. Ferreira, P. Carvalho, M.A. Avery, I.A. Khan, *J Nat Prod* ,71, 1111–1112, 2008.
3. E.L. Elliott, S.M. Bushell, M. Cavero, B. Tolan, T.R. Kelly, *Org.Lett.*, 7, 2449-2451, 2005.

4. K. Inamoto, M. Katsuno, T. Yoshino, Y. Arai, K. Hiroya, T. Sakamoto, *Tetrahedron*, 63, 2695-2711, 2007.
5. K. Lukin, M.C. Hsu, D. Fernando, M.R. Leanna, *J. Org. Chem*., 71, 8166-8172, 2006.

MACRO 153

Alkaline Earth Metal Complexes Of Bis-phosphiiminoselenoid Ligand As Highly Iso-selective And Active Catalysts For Ring-Opening Polymerization Of *rac*-Lactide.

Bhattacharjee Jayeeta, Panda Tarun K.*

Department of Chemistry, Indian Institute of Technology, Hyderabad, Kandi – 502 285, Sangareddy, Telangana, India.

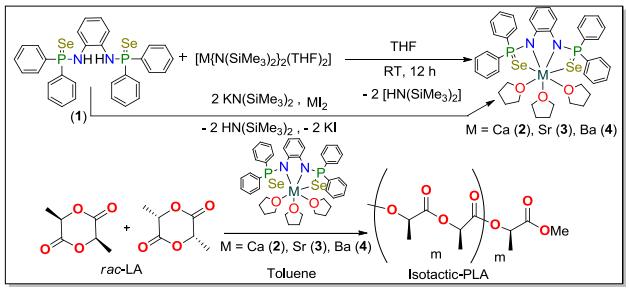
Email-tpanda@iith.ac.in

Various research endeavor are currently receiving ample attention worldwide to explore efficient catalysts to achieve biodegradable polyesters such as polylactide (PLA) for use in medical applications such as sutures, dental devices, orthopedic fixation devices, drug delivery systems, and tissue engineering.[1] In particular, the main focus is to develop a distinct well-defined single site catalyst that can control the stereochemistry of lactide polymerization where it is possible to tune their mechanical properties and degradation profile and escalation their thermal stability and crystallinity to produce a well-regulated molecular weight (M_n) and low polydispersity (PDI) polymer. The isotactic PLAs obtained via ring-opening polymerization (ROP) of the enantiopure L-LA and D-LA have higher melting points (Tm) and modulus than the atactic PLAs, whilst the isotactic stereoblock or stereo-complex PLAs arising via the ROP of rac-LA possess even more superior mechanical properties such as higher Tm and crystallinity than optically pure poly (L-LA) [2] both have become promising biodegradable materials anticipated to replace partly the olefinic plastics as daily commodities. Therefore the stereo-regulated ROP of *rac*-LA has been a hot research topic in the field of polymer chemistry. Numerous initiators, including metal complexes of aluminum,[3] zinc,[3] lanthanides,[4] indium,[5] and magnesium,[3] have been reported. Compared to heterotactic-selective systems, highly iso-selective initiators have rarely been reported. Among these initiators, only aluminum, indium, lanthanides, and zinc complexes have been extensively investigated because of their outstanding isotactic selectivity's. For example, highly active yttrium phosphasalen alkoxide complexes having isoselectivity of P_m = 0.84 and a chiral zinc amidooxazolinate complex with a P_m = 0.91 were recently reported.[4] Nevertheless, it is still rewarding to achieve highly active and highly isoselective catalysts for the ROP of *rac*-lactide. As the metal residues are difficult to remove from the synthesized polymer, nontoxic metal catalysts are encouraged to be an active catalyst for ROP of *rac*-LA. Alkaline earth (Ae) metals Ca, Sr are innocuous, abundant elements in the human body and are suitable for the catalytic synthesis of polylactides for use in medical-related fields, thus exploring Ae metal complexes as catalysts for ring-opening polymerization of lactide is very useful. Even fewer reports of Na and K complexes as pre-catalysts are recently realized,[6] the use of nontoxic alkaline earth metal catalysts are very rare. The scarcity about the synthesis, stability, and reactivity such complexes in the literature are often addressed by the kinetic lability with Schlenk-type equilibria in solution of heavier group 2 complexes which often proved severe detrimental and challenging task to accomplish the compounds.[7]

Herein we demonstrate the Ae metal complexes supported by bis-phosphinaminoselenoid ligand show an unparalleled association of site selectivity, high activity, and controlled polymerization at high molecular weights for the ring opening polymerization of *rac*-LA. The alkaline earth metal complexes with general molecular formula [{$Ph_2P(Se)N\}_2C_6H_4$]M$(THF)_3$ [M = Ca (**2**), Sr (**3**), Ba (**4**)] can be synthesized by two distinct synthetic approaches. In the first method, the well-established [$(THF)_2Ca\{N(SiMe_3)_2\}_2$] compound was made to react with ligand **1** in a 1:1 molar ratio in THF at room temperature to afford the complex **2** via the elimination of volatile hexamethyldisilazane (Scheme 1). However, the most convenient approach for obtaining Complexes is a one-pot reaction, in which the ligand **1** was reacted with anhydrous $KN(SiMe_3)_2$ in a (1:2) molar ratio in THF followed by the addition of anhydrous Ae diiodide into the reaction mixture (Scheme 1). The new complexes **2**-**4** were well characterized using standard analytical and spectroscopic techniques, and the solid-state structures of all three alkaline earth metal complexes were confirmed by single crystal X-ray diffraction analysis.

Compounds **2**–**4** were tested as initiators for the ROP of *rac*-LA. Reaction of **2** or **3** (1 mM) with 100 equivalents of *rac*-LA (25ºC) results in 99% conversion in 2 hours respectively in toluene whereas in case of complex **4** as initiator the reaction is very fast and 99% conversion was achieved within 3 minutes only. Based on the time required to achieve the complete conversion of *rac*-LA into PLA, the order of activity decreased: Ba>Sr~Ca. To quantify these observations, the polymerization kinetics were monitored. Solution studies in $CDCl_3$ demonstrated the polymerization reaction is first order in [monomer] and [catalyst], with k = 19.9 $M^{-1}h^{-1}$ and 21.9 $M^{-1}h^{-1}$ in case of **2** and **3**, whereas k = 500.0 $M^{-1}m^{-1}$ for **4** (Fig-1) at ambient temperature. It was also found that the ROP of *rac*-LA using catalyst **4** is a lower energy process than that of catalyst **2**, **3** as revealed by its activation parameters from *Erying* plot (Table 2).We observed that the ROP of *rac*-LA using our catalyst was a living process, with a linear increase of M_n values and low molecular weight distributions for monomer: initiator (M/I) ratios up to 500 (Table 1). The ^1H and decoupled ^1H NMR spectra of the methine region of PLA derived from *Bernoullian* statistics mode shows that the best isotacticity (P_m) achieved was 0.86 using complex **2**, which is the highest iso-selectivity reported till date in case of an alkali earth-metal complex as a catalyst for *rac*- LA polymerization till now. In

addition, these polymers had a high T_m of 182 °C and T_g of 490°C (From DSC plot in Fig-2 and TGA plot), which is significantly higher than that of the optically pure poly(L-LA) and agree well with the highly isotactic polymeric microstructure.



Scheme 1. Synthesis of initiators followed by synthesis of isotactic PLA.

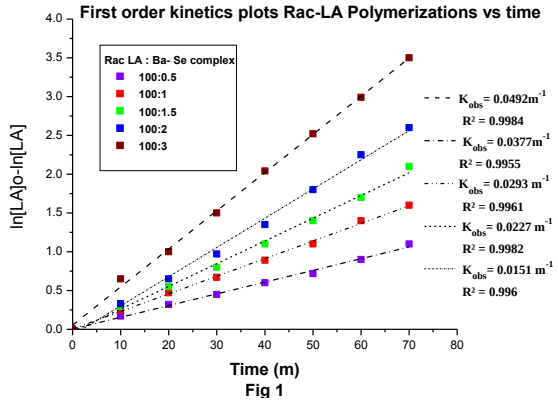


Figure 1: First order kinetics plots for Rec LA polymerizations with time in $CDCl_3$ (1 ML) with different concentration of catalyst 4.

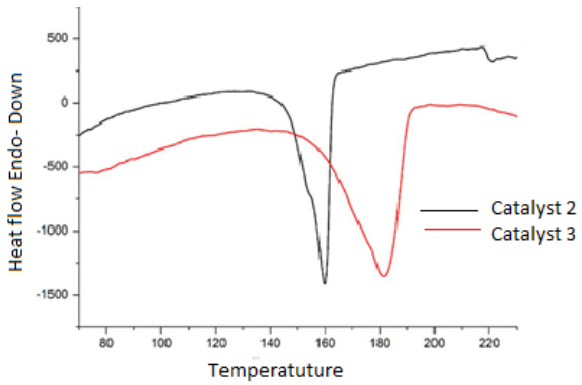


Figure 2: DSC thermograms of the second heating cycles of the poly(rac-LA) catalysed by complex (2,3).

Table 1: Polymerization results – GPC Analysis.

Entry	Catalyst[a]	M:1	Time (h:m)	Conversion (%)	M_{ntheo} (g/mol)	M_{exp} (g/mol)	PDI
1	2	100	00:03	99	14256	15917	1.53
2	2	200	00:03	99	28512	28785	1.50
3	2	300	00:05	99	42768	42337	1.87
4	2	400	00:08	99	57024	54601	1.44
5	2	500	00:10	99	71280	77959	1.64
6	3	100	00:15	99	14256	22107	1.65
7	3	200	00.30	99	28512	33165	1.67
8	3	300	00.30	95	41040	40607	1.58
9	3	400	01.00	95	54720	56416	1.80
10	3	500	01.30	97	69840	68152	1.52
11	4	100	00.50	99	14256	16739	1.21
12	4	200	01.00	99	28512	28992	1.61
13	4	300	01.00	95	41040	40296	1.60
14	4	400	01.30	90	51840	50325	1.82
15	4	500	02.00	93	66960	70860	1.78

Table 2: Activation parameters for polymerization rac-LA with (2, 3, 4) as a catalysis.

S. No	Catalyst	ΔHq kJ/mol)	ΔSq kJ/mol)	ΔGq kJ/mol)
1	$[\{Ph_2P(Se)N\}_2C_6H_4]Ca(THF)_3$	22.27	-172.76	73.7
2	$[\{Ph_2P(Se)N\}_2C_6H_4]Sr(THF)_3$	13.23	-200.65	73
3	$[\{Ph_2P(Se)N\}_2C_6H_4]Ba(THF)_3$	17.58	-182.07	71.8

References

[1] Slomkowski, S.; Penczek, S.; Duda, A. *Polym. Adv. Technol*, 25 (2014) 436.
[2] Zhang, X. C.; Goosen, M. F. A.; Wyss, U. P.; Pichora, D. *J. Macromol. Sci. ReV. Macromol. Chem. Phys., C33* (1993) 81-102.
[3] Bian, S.; Abbina, S.; Lu, Z.; Kolodka, E.; Du, G. *Organometallics*, 33 (2014) 2489.
[4] Bakewell, C.; White, A. J. P.; Long, N. J.; Williams, C. K. *Angew. Chem.*, 53 (2014) 9226.
[5] Normand, M.; Dorcet, V.; Kirillov, E.; Carpentier, J.-F. *Organometallics*, 32 (2013) 1694.
[6] Zhang, J.; Xiong, J.; Sun, Y.; Tang, N.; Wu, J. *Macromolecules*, 47 (2014) 7789−7796.
[7]Buchanan,W. D.; Allis, D. G.; Ruhlandt-Senge, K. *Chem. Commun*., 46 (2010) 4449–446.

MACRO 170

Synthesis and Characterisation of Bio-Surfactant Assisted Conducting Polypyrrole

Adhikari, Arpita[a], Dutta, Koushik[a], Chakraborty, Mukut[b], Chattopadhyay, Dipankar[a]*

[a]*Department of Polymer Sc. & Tech., University of Calcutta, 92, A.P.C. Road, Kolkata 700009, India*
[b] *Department of Chemistry, West Bengal University, Barasat, 700126, India State*

**dipankar.chattopadhyay@gmail.com*

In recent years, conducting polymers have been attracted much importance as advanced materials for bio-sensors, gas-sensors, chemical sensors etc due to their room temperature operation, low fabrication cost, ease of deposition on a variety of substrates [1]. Nanostructured conducting polymers with high surface area, small dimensions and unique physical properties have been used to fabricate various sensor devices. Various morphologies of conducting polymers like nanofibers, nanowires, nanotubes, nanorod etc. have been well reported [2].

In our work, we have presented synthesized conducting polypyrrole having rodlike morphology by using bio-surfactant, ferric chloride and hydrochloric acid which would be effective material for sensor applications. The concentration of the surfactant was kept above its CMC value. Here the bio-surfactant causes the micelle formation which directs the shape and size of the growing polypyrrole. The ratio of the monomer to oxidant was kept at 1:1. The polymerisation was carried out at 0^{o}-5^{o}C for approximately 5 hrs. The as synthesized polypyrrole was characterized using FTIR, UV, XRD, SEM, TEM, TGA etc. The conductivity of polypyrrole has been measured.

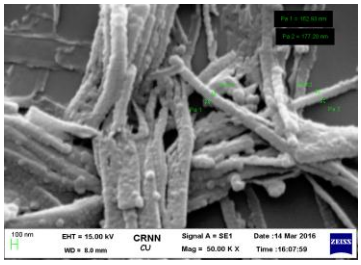


Figure 1.Rodlike polypyrrole synthesized above CMC

Table 1. Morphology dependent conductivity

Concentration of Surfactant	Morphology	Percentage of crystallinity	conductivity
Above CMC	Rodlike	27.23%	186.180 mS cm^{-1}
Below CMC	Spherical	27.04%	132.77 mS cm^{-1}

References:

[1] Bai Hua and Shi Gaoquan* Gas Sensors Based on Conducting Polymers, Sensors 2007, 7, 267-307

[2]Zhang Xue*, †,‡, Zhang Jin ,*† Song Wenhui, ‡ Liu Zhongfan,† Controllable Synthesis of Conducting Polypyrrole Nanostructures, J. Phys. Chem. B 2006, 110, 1158-1165

MACRO 176

Design and synthesis of new organic electronic materials based on hetero doped organic polymers.

Dr. Anirban Pradhan *

DST Inspire Faculty, Department of Materials Science
Indian association for the cultivation of Science(IACS), Jadavpur, Kolkata-32
Telephone- +91 33 2473 4971 (Ext 1453), Email- msap5@iacs.res.in

In the last quarter century, research on polycyclic arenes (PAs) [1] has seen a remarkable renaissance in the literature as compound accessibility and characterization have been made easier with the advent of modern synthetic methods and instrumentation, respectively. [2] One key motivation for this resurgence lies with the unique optical and electronic properties that PAs possess due to their inherently high levels of π-conjugation and delocalization. [3] These
attributes make PAs useful for a varietyof materials applications such as organic lightemitting diodes (OLEDs), field-effect transistors (OFETs), and photovoltaics (OPVs). [4]

Devices such as OLEDs and OPVs are constructed around a donor-acceptor interface between an organic donor layer and an organic acceptor layer. Generally, acene-type molecules such as pentacene and anthradithiophene behave as organic p-type (electron donating) compounds and there are considerably fewer organic n-type (electron accepting) structures in the literature. Thus, there is a pressing need for new molecular frameworks that can transport electrons.

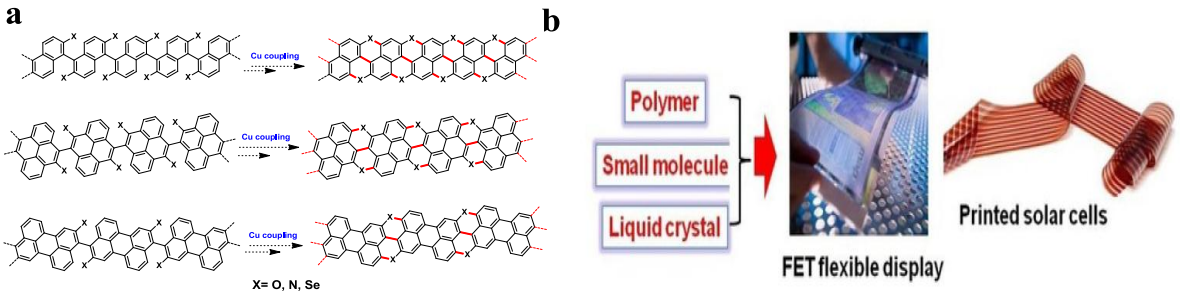


Figure 1. (a) Heterodoped graphene nanoribbons sythesis (b) Applications in printed solar cells

Top down techniques give giant ribbons, bottom-up organic syntheses may lead to exactly designed graphene nanoribbons of controlled geometries. The Scholl reaction is a precious, yet not fully understood, chemical tool for that purpose since it yields efficiently to the graphitization of long and flexible polyphenylene precursors. Even highly twisted structures may be obtained preferentially in spite of the possibility to form less crowded isomers. After discovering this unexpected regioselectivity, we used it on purpose to form polyhelicenic species [5].

References

[1] Harvey, R. G. *Wiley-VCH:* New York, NY 1997.
[2] (a) Haley, M. M.; Tykwinski, R. R., *Eds.; Wiley-VCH: Weinheim*, Germany, 2006. (b) Müllen, K.; Scherf, U., *Eds.; Wiley-VCH: Weinheim*, Germany, 2006.
[3] (a) Bendikov, M.; Wudl, F.; Perepichka, D. F. *Chem. Rev*. 2004, 104, 4891. (b) Anthony, J. E.; Facchetti, A.; Heeney, M.; Marder, S. R.; Zhan, X. *Adv. Mater*. 2010, 22, 3876-3892.
[4] Last Di, C.-A.; Liu, Y.; Yu, G.; Zhu, D. *Acc. Chem. Res*. 2009, 42, 1573-1583.
[5] (a) Pradhan, A.; Dechambenoit, P.; Bock, H.; Durola, F. *Angew. Chem. Int. Ed.* 2011, 50, 12582-12585. (b) Pradhan, A.; Dechambenoit, P.; Bock, H.; Durola, F. *J. Org. Chem.* 2013, 78**,** 2266-2274**.** (c) Bock, H.; Subervie, D.; Mathey, P.; Pradhan, A.; Sarkar, P.; Hillard, E.; Dechambenoit, P.; Durola, F.; *Org. Lett.* 2014, 16, 1546-1549.

MACRO 197

Synthesis, Electrolyte and pH Responsive properties of Poly(4-vinylpyridine) Star Polymers

A.Gopinath, and A.Sultan Nasar*

Department of Polymer Science, University of Madras, Guindy Campus, Chennai 25, India
**e-mail id: drasultannasar@yahoo.com*

Abstract

Star poly(4-vinypyridine)s with six and twelve number of arms were prepared through synthesis of novel dendritic ATRP initiators. The synthesized initiators and polymers were characterized using FT-IR, ^{1}H-NMR, HR-MS and SEC-MALLS techniques. The polymers were used as electrolytes for dye sensitized solar cell (DSSC) and one of the DSSCs showed 3.55% energy conversion efficiency (η). The pH sensitivity of one of these polymers was also determined and found that the polymer was insoluble above the pH=5 and become soluble below the pH=4.

Keywords: Star polymer, Star poly(4-vinypyridine)s, Solar cell, pH responsive material.

Introduction

Star polymers are usually prepared via (i) "core first" method (ii) "coupling onto" method and (iii) "arm first" method. Among these methods, the first two methods invariably require a multifunctional core molecule which may be a dendrimer, a

hyperbranched polymer, an inorganic nanoparticle or an organic molecule. In the "core first" method, polymerization can be performed via anionic, ATRP, NMP, RAFT and ROP method. In the second method, star polymer can be achieved through suitable organic reactions. In this work, our interest is to prepare dendrtic-linear hybrid star polymer via "core first method" using dendrimers as core-cum ATRP initiators. Dendrimers are ultimate choice to be used as core molecules for synthesis of multiarm star polymers, because they can be functionalized for large number of functional groups and with variety of functionality. Among the variety of dendritic molecules, polyurethane dendrimers are more attractive because of they can be functionalized easily at their surface.

Several reports are available on the controlled synthesis of star polymers via ATRP.[1-15] The core molecules used include ATRP reagents of organic, organic-inorganic hybrid materials containing functionalities 2 – 12,[1-4] ATRP reagents of β-cyclo dextrin[5] and glucose.[6] Dendrimers and hyperbranched polymers functionalized with ATRP reagents have also been used as core molecules for the synthesis of multi-arm star polymers that include dendritic-linear block copolymers,[9,10] amphiphilic star polymers,[11,12] organic nanoparticles[13,14] and star polymer electrolyte.[15]

Although poly(4-vinylpyridine) has been reported as its copolymers with many blokcs like polystyrene,[16-18] poly(ε-caprolalone)[19] and poly(N,N-dimethylacrylamide),[20] its star homo polymer is not reported. The reason lies under the fact that the star poly(4-vinylpyridine) homo polymer suffers with separation and purification owing to the limited choice of selection in the solvent-non solvent combination. Whereas, the choice of solvent-non solvent combination is wide for copolymers of poly(4-vinylpyridine), thus, they could be separated and purified easily. As for as poly(4-vinylpyridine) concerned, this material is attractive to be used as polymer electrolyte for DSSC as it has loan pair of electrons on nitrogen atom of each repeat unit that can readily interact with metal cation added and hence will increase the performance of the cell. Considering the star counterpart of poly(4-vinylpyridine), in addition to the structural criteria, topological feature of the polymer will also enhance the efficiency of the DSSC. Herein we report the synthesis of six- and twelve-arm star poly(4-vinylpyridine)s through the synthesis of novel dendritic ATRP initiators and their performance in DSSC and also their pH responsive property.

Results and discussion

Six- and twelve-arm star poly(4-vinylpyridine)s were prepared via "core first" method as shown in Scheme 1. To synthesize star polymers, G1 polyurethane dendrimer functionalized with single and dual functional ATRP initiators, G1-6ATRP Ini and G1-12ATRP Ini respectively, were used as core-cum initiators. Both the initiators have resulted highly narrow dispersed star polymers and the molecular weight obtained was in the order of 10^5.

Both of the polymers were doped with KI/I_2 along with N3-dye to work as efficient polymer electrolytes for dye sensitized solar cell (DSSC). Doped star polymer electrolytes based on G1-12ATRP Ini and G1-6ATRP Ini showed $1x10^2$ and $3.8x10^2$ times higher ionic conductivity respectively compared to the electrolyte prepared without the polymer. This result indicates that the dissociation of the dopant salt occurred effectively and the cations are coordinated with the electron donor atoms (i.e. nitrogen atoms) present in the polymer through Lewis acid–base type of interaction.

The DSSC fabricated with polymer prepared using G1-6ATRP Ini and I^-/I_3^- redox couple yielded 3.55% energy conversion efficiency (η) which is significantly high compared to 0.87% obtained for DSSC fabricated without polymer.

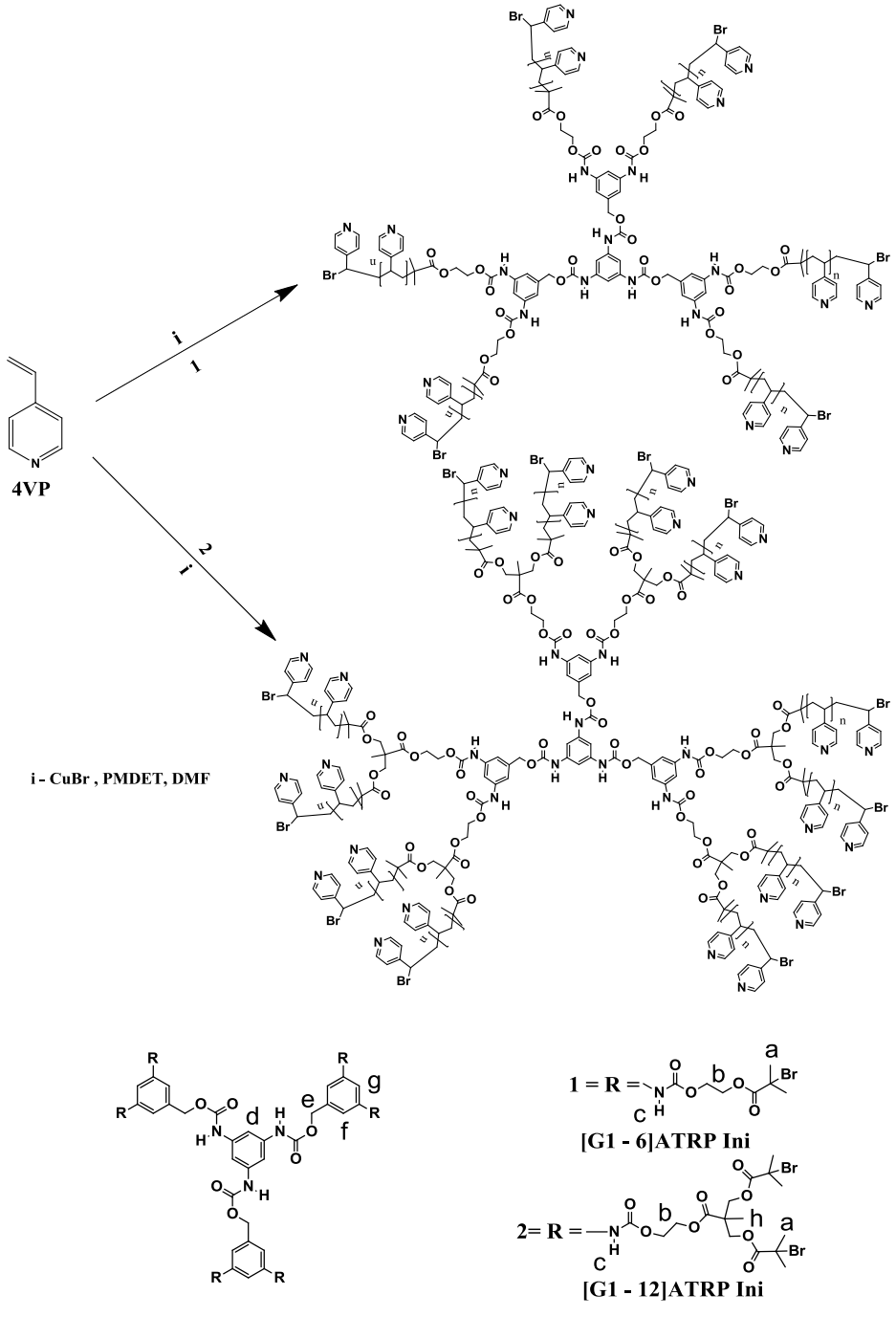
The star polymer prepared with six poly(4-vinylpyridine) arm was tested for its pH-sensitivity and found that this polymer was soluble at pH < 4 and insoluble at pH > 5. This observation is consistent with the reported work.[21,22]

Conclusions

Six- and twelve-arm star poly(4-vinylpyridine)s were prepared with an intention to use as polymer electrolyte for dye sensitized solar cell (DSSC) application.

Scheme 1

Synthesis of six-and twelve-arm star poly(4-vinyl pyridine)s using polyurethane dendritic ATRP initiator



The ionic conductivity and energy conversion efficiency (η) of polymer electrolyte prepared with six-arm star poly(4-vinylpyrine) and I^-/I_3^- redox system were found to be remarkably high compared to the electrolyte prepared without polymer. The pH sensitivity of this polymer was also determined and found that the polymer was insoluble above the pH=5 and become soluble below the pH=4.

Acknowledgements

The authors gratefully acknowledge CSIR, India, for financial support under a Scheme No. 02(0100)/12/EMR-II. Dt. 31-10-2012. One of the authors (A.G) thanks CSIR, India, for awarding Junior Research Fellowship.

References

1. Haifeng Gao, Ke Min and Krzysztof Matyjaszewski, *Macromol. Chem. Phys*. **2006**, 207, 1709-1717.
2. Krzysztof Matyjaszewski, Peter J. Miller, Jeffrey Pyun, Guido Kickelbick and Stephen Diamanti, *Macromolecules*, **1999**, 32, 6526-6535.
3. Dehui Han, Xia Tong and Yue Zhao, *J polym..Sci. Part A: Polym. Chem*., 2**012**, 50, 4198-4205.
4. Bo Chen, Derek G. van der Poll, Katherine Jerger, William C. Floyd, Jean M. J. Frechet, and Francis C. Szoka, *Bioconjugate Chem*. **2011**, 22, 617-624.
5. Micelles, Xinchang Pang, Lei Zhao, Mufit Akinc, Jin Kon Kim, and Zhiqun Lin, *Macromolecules* **2011**, 44, 3746-3752.
6. Vivek Mishra and Rajesh Kumar, *Carbohydrate Polymers*, **2011**, 83, 1534-1540.
7. Andreas Heise, Steve Diamanti, James L. Hedrick, Curtis W. Frank, and Robert D. Miller, *Macromolecules* **2001**, 34, 3798-3801.
8. You-Liang Zhao, Qing Cai, Jing Jiang, Xin-Tao Shuai, Jian-Zhong Bei, Chuan-Fu Chen and Fu Xi, *Polymer*, **2002**, 43, 5819-5825.
9. Youliang Zhao, Xintao Shuai, Chuanfu Chen, and Fu Xi, *Macromolecules* **2004**, 37, 8854-8862.
10. Youliang Zhao, Yongming Chen, Chuanfu Chen and Fu Xi, *Polymer*, **2005**, 46, 5808-5819.
11. Meizhen Yin, Roland Bauer, Markus Klapper and Klaus Mullen, *Macromol. Chem. Phys.* **2007**, 208, 1646-1656.
12. Young Hie Kim, Warren T. Ford, Thomas and H. Mourey, *J Polym. Sci.: Part A: Polym. Chem.*, **2007**, 45, 4623-4634.
13. Guobin Sun and Zhibin Guan, *Macromolecules* **2010**, 43, 9668-9673.
14. Lieven M. Van Renterghem, Mieke Lammens, Bart Dervaux, Pascal Viville, Roberto Lazzaroni, and Filip E. Du Prez, *J. Am. Chem. Soc*. **2008**, 130, 10802-10811.
15. Zhong Shen, Yu Chen, Emilie Barriau and Holger Frey, *Macromol. Chem. Phys*. **2006**, 207, 57-64.

16. Pengfei Shi, Quanlong Li, Xin He, Shentong Li, Pingchuan Sun and Wangqing Zhang, *Macromolecules,* **2014**, 47, 7442-7452.
17. Chu-Hua Lu, Jui-Hsu Wang, Feng-Chin Chang and Shiao-Wei Kuo, *Macromol. Chem. Phys.* **2010**, 211, 1339-1347.
18. Yozo Miura and Hiroyuki Dote, *J Polym. Sci.: Part A: Polym. Chem*., **2005**, 43, 3689-3700.
19. Wan-Chum Chen, Shiao-Wei Kuo, Chu-Hua Lu, U-Ser Jeng and Feng-Chih Chang, *Macromolecules*, **2009**, 42, 3580-3590.
20. Fei Huo, Shentong Li, Quanlong Li, Yaqing Qu and Wangqing Zhang, *Macromolecules*, **2014**, 47, 2340-2349.
21. F. Liu, and A. Eisenberg, *J. Am. Chem. Soc*. **2003,** 125, 15059-15064.
22. P. Shi, Q. Li, X. He, S. Li, P. Sun, and W. Zhang, *Macromolecules*, **2014**, 47, 7442-7452.

MACRO 215

Synthesis and Characterization of Flexible/Stretchable Polyimides Containing Long/Bulky Aromatic Side Chains

Tharakan Simi Annie [a], Muthusamy Sarojadevi [a,*]

[a]Department of Chemistry, Anna University, Chennai-25, India.

E-mail: msrde2000@yahoo.com

Abstract:

To prepare process-able polyimides without sacrificing desired properties, flexible bridging units as well as bulky groups are incorporated into their rigid backbone. The majority of polyetherimides are non-crystalline and their Glass transition temperatures ranges from 200 to 280°C. At the same time there is a continuing need for elastomers capable of withstanding elevated temperatures. In defense industry, specific needs are associated with aircraft fuel tank sealants and O-rings and gaskets in missile structures and engines. Silicone, the commonly used elastomeric material in these applications has some performance limitations. The polyetherimides containing multiple alkyl side chains show much higher elongations but lower tensile strengths and moduli than the commercial Ultem_1000.

In my work I tried to impart elastomeric properties in polyimides without sacrificing their excellent thermal and mechanical properties. One diamine containing long and bulky single pendent group and another one with multiple pendent groups were prepared and their structures were characterized by FT-IR, ^{1}H-NMR etc. Polyimides were synthesized by reacting newly prepared diamines with dianhydride BTDA by two-step method and were characterized using NMR and FT-IR spectroscopy. Silicon-dioxide nano particles were incorporated in polyimide with weight 0.5 and 1 percentages and analyzed by scanning electron microscopy. Properties of polyimides and nanocomposites were studied using DSC, TGA, SEM, XRD, UTM etc. TGA show that resultant polyimide has excellent thermal stability. The fact that Tg is well below the decomposition temperature makes this polymers attractive for the commercial purpose. As the percentage of SiO_2 in the PI increases the thermal stability also increases in PI/SiO_2 hybrids.

References

[1] Eastmond, C.; Paprotny, J. *J Mater Chem*), 7 (1997) 589.

[2] Wang, D H; Shen, Zhihao; Cheng Stephen Z.D; Harris F W. *Polymer,* 48 (2007) 2572-2584.

[3] Wang, D H; Shen, Zhihao; Guo,Mingming; Cheng Stephen Z.D; Harris F W. *Macromolecules,* 40 (2007) 889-900.

MACRO 216

Applications of Poly(ionic liquids) in Organic Synthesis

Kari Vijayakrishna*

Department of Chemistry, School of Advanced Sciences, VIT University, Vellore-632014, Tamil Nadu, India

**Corresponding author: Kari Vijayakrishna e-mail: vijayakrishnakari@gmail.com*

Poly(ionic liquids) well known as PILs or polymerized ionic liquids are getting great attention due to their stand out properties. Their potential applications involve in energy devises, CO2 absorbing materials etc [1].

We have used RAFT polymerization technique to prepare imidazolium based chiral/achiral polymers. These chiral PILs were used as organocatalysts for polymer assisted solution phase Diels Alder reactions, asymmetric Baylis Hillman reaction, Michael Addition reaction etc [2]

We have also used these PILs as stabilizers for making stable Ag, Au, Ni and ZnO nanoparticles [3]. Among these nanoparticles PIL-Ni-NPs possess good catalytic activity towards transfer hydrogenation (TH) reactions of carbonyl compounds in the absence of any additional base. This catalyst system PIL-Ni-NPs chemoselectively reduces only the carbonyl group of α, β unsaturated carbonyl compounds. The magnetically separable PIL-Ni-NPs were recycled and reused for further TH reactions [4]. PILs also utilized as flocculants for water purification [5].

We have demonstrated that Imidazolium based ILs and PILs possess good Vermicidal activity [6]. These synthesized PILs were further used to studies their interaction with ctDNA. UV-Visible absorption, fluorescence quenching studies, gel electrophoresis, CD and FTIR studies has confirmed the electrostatic interaction/binding of polyelectrolytes with DNA [7]. Some of these results will be discussed during the presentation.

References

1. Yuan, J;Mecerreyes, J; Antonietti, M. *Prog Polym Sci* 38 (2013) 1009.
2. Pothanagandhi, N; Vijayakrishna, K. from submitted Manuscripts.
3. (a). Prabhu Charan, KT; Pothanagandhi, N; Vijayakrishna, K; Sivaramakrishna, A; Mecerreyes, D; Sreedhar, B. *Eur. Polym. J.*, 60 (2014) 114. (b). Gracia, R; Vijayakrishna, R; Mecerreyes. D. React Funct Polym, 2014, 79, 54-58. (c). Manojkumar, K; Sivaramakrishna, A; Vijayakrishna, K. *J Nanopart Res* 18 (2016) 1-22.
4. Vijayakrishna, K; Prabhu Charan, KT; Manojkumar, K; Venkatesh, S; Pothanagandhi, N; Sivaramakrishna, A; Mayuri, P; Kumar, AS; Sreedhar, B. *ChemCatChem* 8 (2016) 1139.

5. Isik, M; Fernandes, AMC; Vijayakrishna, K; Paulis, M; Mecerreyes, D. Polymer Chemistry, 7(2016) 1668.
6. (a) Prabhu Charan, KT; Ranjan, P; Manojkumar, K; Pothanagandhi, N; Jha, PC; Khedkar, VM; Sivaramakrishna, A; Vijayakrishna, K. *RSC Adv*. 5 (2015) 75415.(b). Prabhu Charan, KT; Pothanagandhi, N; Manojkumar, K; Ranjan, P; Vijayakrishna, K; Sivaramakrishna, A; Koteswaraiah, P. *J Indian Chem Soc* 92 (2015) 573.
7. Manojkumar, K; Prabhu Charan, KT; Sivaramakrishna, A; Jha, P C; Khedkar, VM; Siva, R; Jayaraman, G; Vijayakrishna, K. *Biomacromolecules*, 16 (2015) 894.

MACRO 219

Synthesis and Diversified Applications of Water soluble Polythiophene based 'Smart' Graft Copolymers

Chatterjee D. P.[a]*; Ghosh, Radhakanta[b]; Das, Sandip[b]; . and Nandi, Arun. K[b].
[a]*Dept. of Chemistry, Presidency University, Kolkata-700 073*
[b]*Polymer Science Unit, Indian Association for the Cultivation of Science, Jadavpur, Kolkata-700 032, INDIA*
**For correspondence: D. P. Chatterjee, Email:dhruba.chem@presiuniv.ac.in*

Abstract

Polythiophene has received considerable attention in polymer research because of its multifarious applications ranging from the field of electronics to bio-materials. Polythiophene shows fascinating optoelectronic properties in the solution phase depending upon the external stimulants like temperature (thermochromism), solvents (solvatochromism), surfactants (surfactochromism) etc. Further exploration of optical properties of polythiophene systems may open up new horizons of applications in the field of sensors, molecular thermometers, ph meter or molecular switches for applications in biomedical fields. However these would require aqueous solubility of polythiophene which is normally water insoluble and hydrophobic.
The present contribution reports synthesis and characterization of polythiophene grafted water soluble stimuli responsive polymers. The synthesized graft copolymers are having promise for being applied as multi functional materials covering a wide range of applications, some exploration of their applications are also reported here.

Keywords: *polymer; NMR; stimuli responsive: graft copolymer; ATRP: molecular device*

Introduction

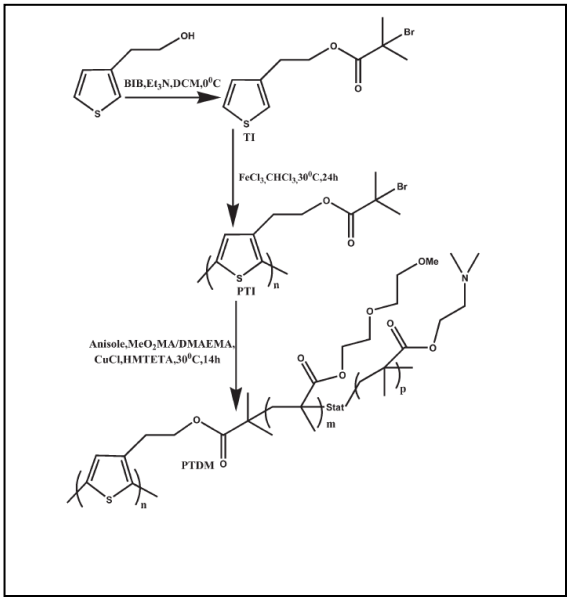
The water soluble stimuli responsive materials have received significant attention as sensors or delivery vehicles. A considerable research effort is focussed in the development of water soluble smart materials which may find applications as chemical and biological sensors,[1] molecular thermometers,[2] molecular logic gates, etc.[3] The process of sensing becomes very much convenient

when optical signals are chosen as the output and it is not at all surprising that most of the reports dealing with molecular sensing have used fluorescence as output signals. A careful literature survey shows that most of the molecular devices have used small molecular fluorophores[4] and there are fewer similar polymer based molecular devices. In most of these cases the idea is to attach a small fluorophore moiety on the polymer (or block copolymer) backbone and then to exploit the intrinsic properties of the backbone polymer to induce a change in the micro environmental conditions surrounding the fluorophore moiety, and thereafter to follow its fluorescence behaviour. An alternative strategy adopted is to synthesize block copolymers having a fluorescent polymer in one of the constituting blocks derived from a monomer having a pendent fluorophore moiety. There are also some other reports in which fluorescent properties of conjugated polymers are used, exploiting the intrinsic properties of conjugated polymers. One major limitation of such CP based molecular devices is their insolubility and poor processability in common solvents, particularly in water. Aqueous solubility of such molecular device systems is very much desirable for a broad range of applications. Accordingly, significant effort has started to develop water soluble stimuli responsive CP based molecular systems.[5] Notably, polymeric fluorescent sensors may be superior to small molecular sensors in respect of stability, easy handling, reusability, signal amplification, etc.

Conjugated polymers like polythiophene (PT), which is having fluorescent properties at the same time, is a very much interesting candidate in this field and most used so far. The fluorescence signal position and intensity of polythiophene shows significant dependence on the micro environmental polarity. As the polarity in the vicinity of the PT domains is decreased, the hydrophobic polymer chains are relaxed, which is reflected by difference in UV absorption position and due to loss of (π-π) stacking or moving away of excimer deactivating water molecules from the vicinity of the fluorophoric PT domains, emission intensity increases significantly. Accordingly, a good number of reports have demonstrated preparation of stimuli responsive polythiophene based graft copolymers by controlled grafting of PNiPAM, PDMAEMA or random/block copolymers of $PMeO_2MA$/OEGMA which have shown stimuli responsive association-dissociation equilibrium in water associated with changes in optical properties of polythiophene chromophore.[5]

In this work we report the synthesis and characterization of PT-g-(PMeO2MA-co-PDMAEMA) (PTDM) graft copolymers using the 'grafting from' approach from a PT backbone by the ATRP technique. The graft copolymeric system shows appreciable aqueous solubility with remarkable thermo and pH responsiveness. The system exhibits significant change in fluorescence emission (output) with variation in temperature and pH (as inputs) following the principle of the AND logic gate. Quaternization of $-NMe_2$ groups of DMAEMA with MeI forms polycationic chains (PQDMAEMA) on PT backbone. Polycations derived from quaternization of pendant tertiary amine groups of PDMAEMA are effective as antibacterial or antimicrobial agents or in gene transfection. Therefore, quaternization of grafted PDMAEMA chains from PT backbone in the stimuli responsive polymer matrix containing fluorophoric backbone PT chains may trigger

fascinating applications as nucleic acid carriers, signalling systems or as the antimicrobial coating agents using the π-network of polythiophene.



Scheme-1: Synthesis of PTDM

Experimental

The monomer (3-thiophene ethanol), diethylene glycolmethylether methacrylate (MeO_2MA) and N,N-dimethyl aminoethyl methacrylate (DMAEMA) were purchased from Aldrich Chemicals, USA. The monomers MeO_2MA and DMAEMA were

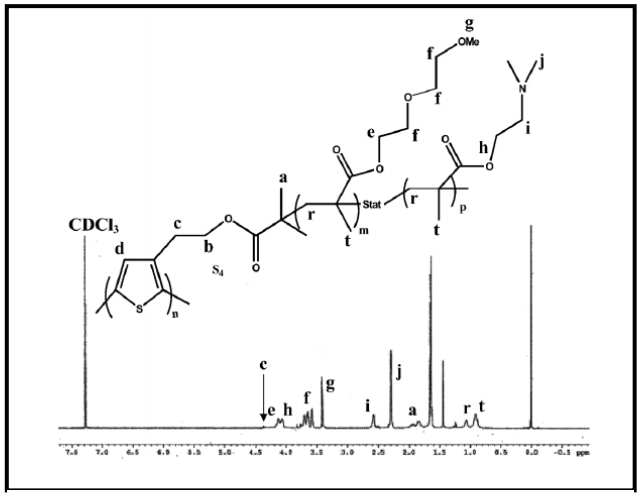
purified by passing through a neutral alumina and basic alumina column, respectively. The ligand 1,1,4,7,10,10-hexamethyl triethylene tetramine (HMTETA; Aldrich, USA) was used as received. The catalyst CuCl (Loba Chemicals, Mumbai) was purified by a reported method.[6] The detailed synthesis of the graft copolymer systems are reported elsewhere[6].

Results and discussion

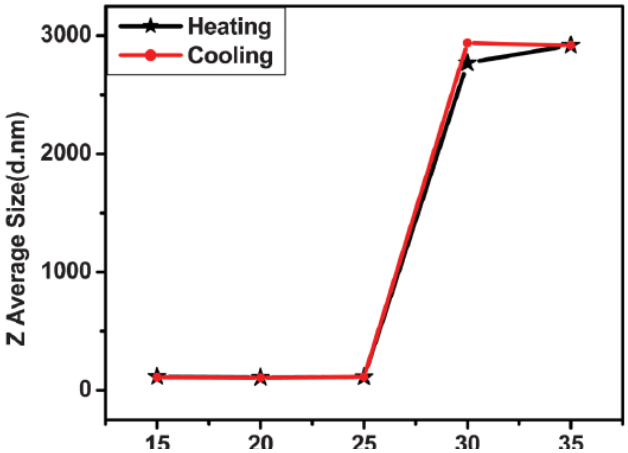
Synthesis of the polythiophene based graft copolymers conducted at first attaching the model ATRP initiator on 3-thiopheneethanol by coupling of 2-bromoisobutyryl bromide (BIBB) and then oxidative polymerization of thiophene catalysed by $FeCl_3$ (Scheme-1).

The polythiophene derivative having pendant ATRP initiating sites is then used as macroinitiator for random or block copolymerization (where applicable) of monomers like DMAEMA or MeO_2MA in anisole medium with CuCl/HMTETA complex at 30^0C.

The ^{1}H-NMR spectrum of the synthesized PT-g-P(DMAEMA-alt-MeO_2MA) graft copolymer shows signals corresponding to the characteristic signals of the grafted polymethacrylate components (PDMAEMA and $PMeO_2MA$) as shown in the signal assignments. However it may be noted here that, the proton 'd' corresponding to the thiophene ring proton is not visible. This has been attributed to suppression of signal intensities of the thiophene ring protons with respect to the huge number of protons present in the grafted high molecular weight polymethacrylate chains. The mole ration of DMAEMA and MeO_2MA units present in the grafted chains has been determined from the ratio of protons 'j' and 'g' as shown in the Figure 1. The number average molecular



(Figure 1): ^{1}H-NMR spectrum of graft copolymer in $CDCl_3$ along with the signal assignments

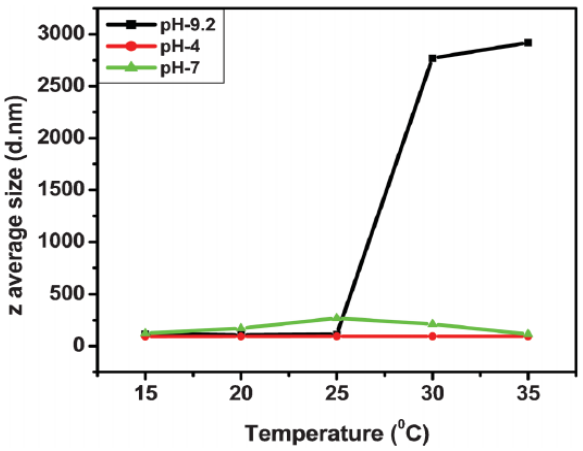


(Figure 2): Temperature dependent DLS analysis of PTDM

weight (M_n) of PTI system has been found to be 38000 from the GPC analysis in THF eluent taking polystyrene as reference. Now, literature reports have shown very nice agreement of GPC molecular weight in the above conditions with the absolutely determined values.[6] Therefore, considering the molecular weight of backbone polystyrene to be 38000 (PDI = 2.8), calculation of the total molar mass of the graft copolymer has been done. Analysis of mole ratios of DMAEMA and MeO_2MA from ^{1}H-NMR spectroscopy has shown nice agreement of their mole ratio present in the graft copolymer with the monomer feed ratios. The M_n of PTDM determined as above shows a value of 4,42,000.

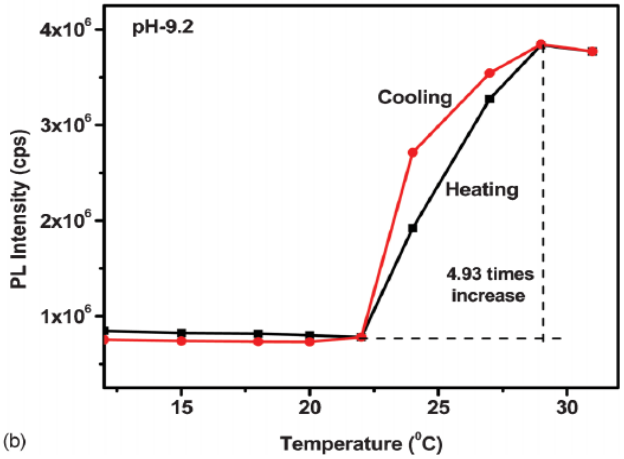
Therefore, the synthesized polymers show appreciable solubility in water. However, the aqueous solution of this graft copolymer shows development of turbidity upon heating when the medium pH is kept at 9.3. DLS analysis of the dilute aqueous solution of PTDM at pH 9.3 shows sudden rise of particle sizes when heated above 25^0C. The size increase occurs up to 29^0C, further heating even up to 50^0C does not show any increase in particle size. In the reverse mode, when the same solution is cooled up to 15^0C, the particle sizes decrease by keeping complete reversibility as is observed from Figure 2.

This is further notable here that the aqueous solution of PTDM when is kept at pH 7 or pH 4, no size increase is observed upon heating as shown in Figure 3.



(Figure 3): Temperature dependent DLS analysis at different pH values

The increase in particle sizes above 25^{0}C as observed from DLS analysis when the pH of the solution is at 9.3 is attributed to the LCST of $PMeO_2MA$ which is reportedly at 21^{0}C in aqueous solution of the homo polymer. Now, in the aqueous solution of PTDM, the PT backbone being insoluble in water, formation of aggregated structure occurs right from the beginning. Now, when the temperature is increased above LCST of $PMeO_2MA$, precipitation of $PMeO_2MA$ chains occur which triggers increase in particle sizes. Therefore, the $PMeO_2MA$ chains undergo coiling upon heating by expulsion of water molecules. However, this transition of $PMeO_2MA$ chains from uncoiled state to coiled and the reverse as a function of temperature occurs by keeping complete reversibility. Another very much interesting observation is similar increase in particle sizes or visual detection of



(Figure 4): Temperature dependent PL analysis of the aqueous solution of PTDM at pH 9.3

Entry	Input$_1$ (T/°C)	Input$_2$ (pH)	Output (PL intensity × 10^5)
I	0 (22)	0 (4 or 7)	0 (9.6 or 8.4)
II	1 (29)	0 (4 or 7)	0 (9.3 or 7.9)
III	0 (22)	1 (9.2)	0 (7.7)
IV	1 (29)	1 (9.2)	1 (38.3)

(Table 1): Truth table for "AND' logic gate operation.

development of turbidity is not found when the medium pH is kept at 7 or 4. This is explained by the fact that, the pK_a of -NMe_2 groups in PDMAEMA being 7.5, at the above said pH values the -NMe_2 groups remain either partially or completely protonated. This develops high degree of hydration and therefore even when the temperature of the solution is increased over 25^0C, dehydration becomes difficult. Precipitation of $PMeO_2MA$ chains is restricted due to repulsion between the positive charges formed on radomly distributed DMAEMA units. At pH 9.3, no such protonation is possible and therefore the reversible aggregation and disaggregation phenomenon due to precipitation of $PMeO_2MA$ chains is nicely observed.

The precipitation of $PMeO_2MA$ chains occur due to dehydration of the diethyleneglycol side chains with increasing temperature. Therefore, this dehydration should decrease the micro environmental polarity of the fluorescent PT backbone. This shows an appreciable increase in fluorescence intensity of the PT chromophore when the temperature of the solution is increased over 25^0C at pH 9.3. Interestingly, this occurs very much by keeping reversibility as is observed from Figure 4. It is notable here that in concurrence with the DLS analysis, here also increasing temperature at neutral or acidic pH values has no effect on the fluorescence emission intensity as under these conditions, increasing temperature does not induce precipitation of $PMeO_2MA$ chains. The optical response of PT chromophore in PTDM as observed from its PL emission spectrum subject to the changes of medium pH and temperature may be fabricated as 'AND' logic gate with the PL emission signal intensity as output and pH, temperature as inputs. The corresponding truth table is given in Table 1.

Conclusion:

The synthesis of polythiophene grafted system with polymethacrylate chain having dual stimuli response is synthesized by ATRP technique. The mole ratio of the different repeating units in the grafted chains are in nice agreement with the monomer feed ratio. The system has shown appreciable reversibility in its response as observed from DLS and PL emission studies and follows nicely the principle of 'AND' logic gate. The system reserves further promises for being applied as multi functional materials.

Acknowledgement:

We thank Presidency University and IACS, Kolkata for providing the financial, instrumental facilities and Chatterjee D.P. also thanks UGC, India for providing the financial support through UGC, Start Up Grant No. F.30-92/2015 (BSR) dated March, 2015.

References

11. McQuade D.T., Pullen A.E., Swager T.M. *Chem. Rev. 100*, 2537, 2000.
12. Uchiyama S., Matsumura Y., de Silva A.P., Iwai K., *Anal. Chem. 75*, 5926, 2003.
13. Uchiyama S., Kawai M., de Silva A.P., Kawai K., *J.Am.Chem.Soc. 126*, 3032, 2004.
14. Chandrasekharan N., Kelly L.A. *J.Am.Chem.Soc. 123*, 9898, 2001.
15. Balamurugan S.S., Bantchev G.B., Yang, Y., McCarley L. *Angew.Chem.Int.Ed. 44*, 4872, 2005.
16. Das S., Chatterjee D.P., Samanta S., Nandi A.K. *RSC Adv. 3*, 17540, 2013.

MACRO 222

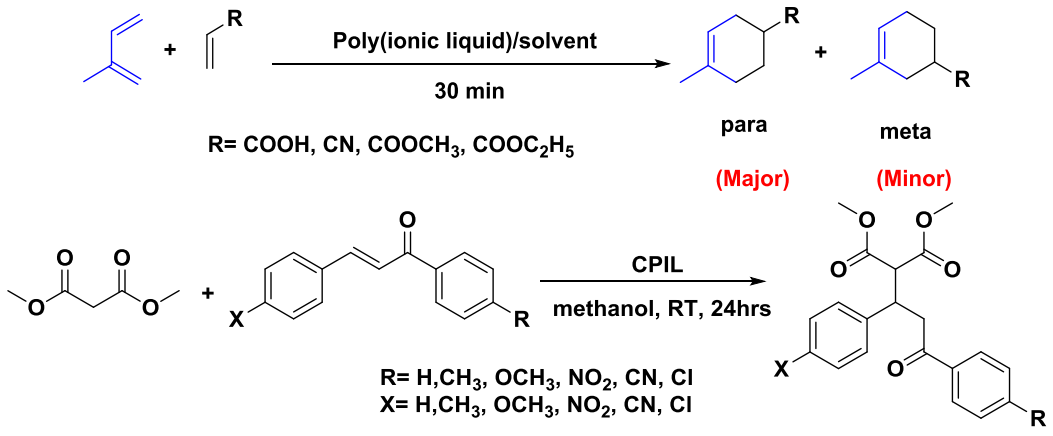
SYNTHESIS AND APPLICATIONS OF ACHIRAL & CHIRAL POLY(IONIC LIQUIDS)

Nellepalli Pothanagandhi and Kari Vijayakrishna*

Department of Chemistry, School of Advanced Sciences,
VIT University, Vellore 632014, Tamil Nadu, India

**Corresponding author: Kari Vijayakrishna, vijayakrishnakari@gmail.com*

We have synthesized different vinylimidazolium based achiral & chiral poly ionic liquids through RAFT polymerization technique [1]. The synthesized PILs were used as catalysts for Diels-Alder reactions between isoprene and different dienophiles like acrylic acid, acrylonitrile, methyl acrylate and ethyl acrylate [2]. These PILs catalyzed the DA reactions observed with quantitative yields with good para/meta ratios. We used Proline based chiral PILs as catalysts for Michael addition reaction between dimethyl malonate and substituted chalcones. In our studies we observed that CPILs showed better catalytic activity than proline, (up to 90% yield) with moderate ee. These results will be discussed during the presentation.



References
[1] Pothanagandhi, N. Vijayakrishna, K. (Unpublished results, 2016).
[2] Bae, HW; Han, J-S; Jung, S; Cheong, M; Kim, HS; Lee, JS. *Appl. Catal., A* 331 (2007)

MACRO 226

Synthesis Of PVDF Based Graft Copolymer For Affinity Chromatography Applications.

Majumdar, S.,[a] Basak, U.,[b] Ghosh, T.,[b] Ball, R.,[c] Chatterjee, D.P.*,[b]

[a]*Department of Chemistry, Indian Institute of Technology*

Kharagpur- 721302, India

[b] *Department of Chemistry, Presidency University, Kolkata- 700073, India*

[c] *Department of Chemistry, Indian Institute of Technology Bombay, Powai, Mumbai-400076, India*

** e-mail id: dhruba.chem@presiuniv.ac.in*

Abstract

Suitable chemical modification of membrane forming materials may result in novel affinity chromatography membrane materials. Poly-vinyledene fluoride (PVDF) is one such commercially available, excellent membrane forming material**.** In this report our aim is to prepare PVDF based graft copolymeric materials and their suitable modification to introduce different organic moieties capable of showing molecular interactions with proteins and nucleic acids.

Atom Transfer Radical Polymerization (ATRP) has been carried out using both PVDF or model ATRP-initiator anchored PVDF systems with various methacrylate monomers at elevated temperatures (60^{o}C or 90^{o}C) using Cu/bpy based catalyst complex in N-methyl Pyrrolidone (NMP). In the subsequent step post polymerisation, modifications have been carried out either in solution or in surface of fabricated films. The kinetics of the copolymerisation of GMA/DEGMEM using modified PVDF initiator and their molecular weight evolution with time has indicated towards controlled nature of grafting. In the post polymerisation modification steps various synthetic strategies including coupling or cycloaddition reactions have been used. Formation of the graft copolymer and, in the subsequent steps, introduction of various functionalities has been confirmed by ^{1}H-NMR and other techniques. FE-SEM analysis has shown development of porosity in the casted membrane. PVDF-g-P(GMA-alt-DEGMEM) copolymeric films have shown appreciable amount of adsorption of Bovine serum albumin (BSA) from its aqueous solution.

Keywords: *ATRP; modified PVDF membrane; affinity chromatography*

Introduction

Polyvinyledenedifluoride (PVDF) is a technologically very much important crystalline polymer because of its excellent piezo and pyro electric properties[1], good biocompatibility[2] and excellent membrane forming capability[3,4]. Apart from this PVDF is a very much robust polymer system, which shows tolerance towards different chemicals and solvents. PVDF contains highly polar C-F bond which is capable of showing ionic interactions with the polar solvents in spite of staying in a highly hydrophobic skeleton. Therefore this polymer system shows excellent gelation with different polar solvents like ketones, esters or amides or lactums. These differential interactions with solvent molecules along with the tendency for crystallization is considered to be the principal reason behind formation of porous films by PVDF via different techniques such as phase inversion[5], solvent casting[6,7] or application of "breath figure" technique[8] etc.

Accordingly, PVDF based membranes have received wide range of applications as high throughput filtration membrane materials. Further development in PVDF based membranes for filtration or separation may be done by anchoring suitable organic moieties by using different synthetic strategies to have more specificity in action. The anchored moieties may be capable of undergoing specific interactions with various molecules present in the analyte for filtration and therefore the synthesized membrane materials may be useful for "affinity chromatography" applications.

There are some interesting reports in this field which demonstrates modifications of surfaces of commercially available membranes or silica particles with highly reactive functional groups like epoxides which may subsequently react with nucleophilic functional groups present in the target molecule of the analyte and hence filtration or separation may be possible. Polyglycidyl methacrylate (PGMA) is a very good option in this strategy for coating or attaching over the surface of the materials so that appreciable population of epoxide functionalities may be found. Now this strategy may work well if the functionalities present in the surface of the materials show good interactions with PGMA, for example hydroxyl groups present on the silica surface may interact well with the oxygen atom of the epoxide group. Hence PGMA may be efficiently deposited over silica surface. An alternative approach for getting PGMA chains on the silica surface, as reported by Klok et.al.[9], is to carry out surface initiated Atom Transfer Radical Polymerization (SI-ATRP) to anchor polyglycidyl methacrylate (PGMA) and subsequently the modified silica particles have been used for selective anchoring of proteins like bovine serum albumin (BSA) etc. through the covalent interactions of amine groups present in the protein molecules with reactive epoxy groups. Husson et.al.[10] have reported deposition of PGMA over commercially available PVDF membrane surface, however, it should be rather difficult due to absence of any suitable functional groups on PVDF surface which may interact with the PGMA molecules. However, the overall strategies narrated above depend on the degree of attachment of reactive functional groups in the surface modification step to generate good results in respect of filtration or separation performance. Now, as the above strategies only deal with the surface

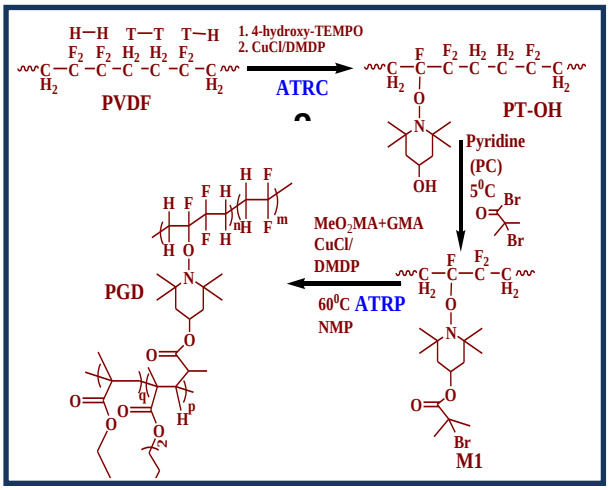
modification therefore an alternative approach with bulk modification of the materials with reactive functional groups followed by membrane fabrication evidently would have provided much better performance

The present work demonstrates controlled growth of random copolymers of polymethcrylates including polyglycidyl methacrylate (PGMA) or polyfurfuryl methacrylate (PFMA) having reactive pendant moieties like epoxide or furan ring respectively, on PVDF backbone. Grafting on PVDF backbone has been done by ATRP in solution phase using CuCl.DMDP(4,4'-dimethylbipyridine) catalyst in N-methylpyrrolidine (NMP) solvent.

Experimental

PVDF (M_n = 71000) were purchased from Aldrich Chemicals and was used after recrystallization from acetophenone. 4-hydroxyTEMPO, 4,4'-dimethylbypyridine were purchased from Aldrich Chemicals and were used without any further purification. GMA (98%), FMA (98%), n-butyl methacrylate (nBMA) (98%), diethyleneglycolmethylether methacrylate (DEGMEM) (98%) was purchased from Aldrich Chemicals and passed through neutral alumina column before use. CuCl was purchased from Loba Chemicals and was purified by washing in 10% HCl solution followed by drying with methanol and ether. All other solvents were purchased from local chemical suppliers and purified by distillation under reduced pressure.

^{1}H-NMR through a Bruker 500 MHz spectrophotometer, XPS, XRD analysis done from IACS, Kolkata and SEM, TEM analysis were done from IACS Kolkata, IIT Kharagpur and CRNN Calcutta University.



Scheme-1

Results and discussion

Grafting of random copolymers of PGMA and PDEGMEM carried out following Scheme-1 through model ATRP initiators anchored on PVDF backbone. The polymerization followed first order kinetics and showed linear development of molecular weight determined from PMR spectroscopy. The polymerization reached 86% monomer conversion after 30 hrs and the sample thus synthesized is named PGD-30.

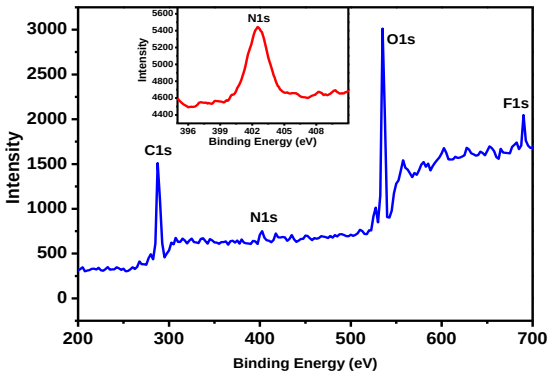


Figure 1: XPS analysis of PT-OH

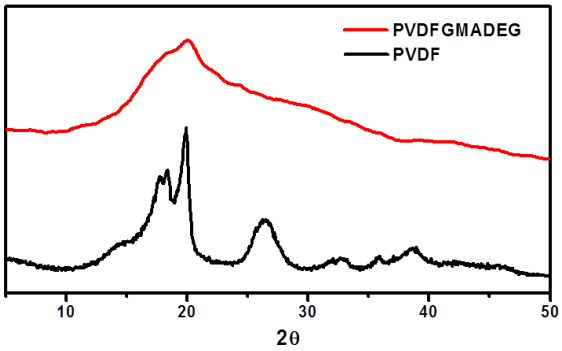


Figure 2: WAXS analysis of PVDF and PGD-30

The successful operation of ATRC technique for attaching TEMPO moiety on the PVDF backbone has been proved from XPS analysis as shown in Figure 1. Figure 2 shows the XRD analysis of PVDF and PGD-30, the development of amorphous hump in case of PGD-30 in sharp contrast with PVDF indicates loss of PVDF crystallization upon grafting of polymethacrylate chains. Similarly Figure 3 is the TEM micrograph of PVDF and PGD-30 which also show much increase in domain size in case of graft copolymer along with much increase in electron density which is indicated by increased brightness of the domains in PGD-30. Therefore TEM analysis also indicates towards successful grafting of polymethacrylate chains on PVDF backbone.

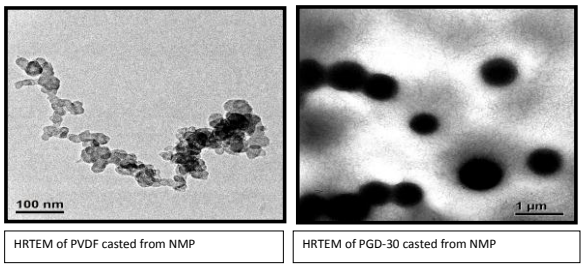


Figure3: HRTEM images of PVDF and PGD-30

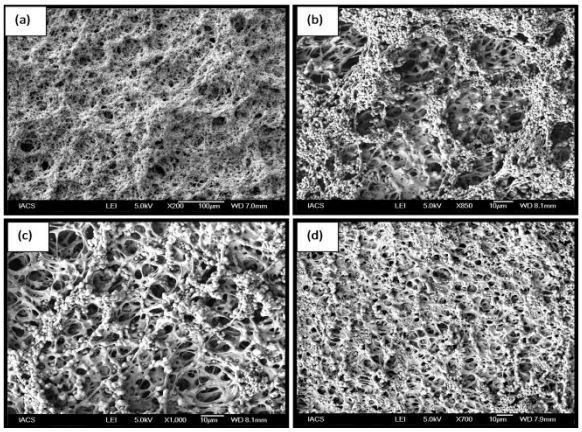


Figure 4: FESEM images of PGD-30

The ^{1}H-NMR spectrum of PGD-30 shows $M_{n(NMR)}$ for PGMA and PDEGMEM to be 174000 and 202000 respectively. Hence a significant amount of PGMA is anchored along with appreciable amount of PDEGMEM which should provide water permeability and anti fouling property to the membrane. This sample was then film casted using phase inversion technique from its 10% NMP solution in cold water. The FE-SEM images of the casted films are shown in Figure 4. The FESEM image of PGD-30 shows a highly porous morphology but the pore sizes are rather large and uncontrolled/polydisperse in nature having pore sizes in the range of 1 micrometer to about 8 micrometers. This indicates that the conditions of phase inversion was not very much appropriate and at the same time relatively hard and brittle nature of the graft copolymer may also be one reason behind poor phase inversion as observed.

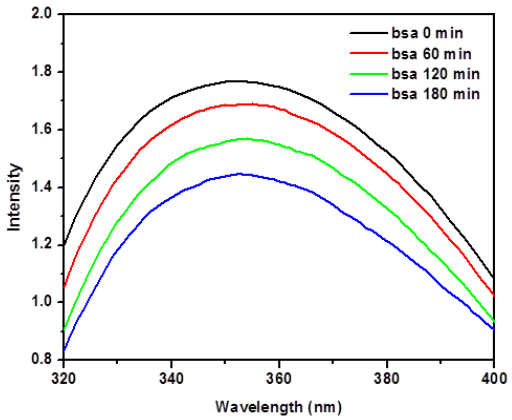


Figure 5: PL Spectra of BSA solution after adsorption by PGD-30 film (with different time)

However this copolymeric material has shown adsorption of proteins like BSA in PBS buffer through the interaction of amine groups of the protein molecules with the epoxy groups of GMA units. Klok and coworkers[9] have reported similar protein adsorption through epoxy groups of GMA anchored on silica substrate. Figure 5 shows the BSA adsorption profile of PGD-30 sample with time as has been observed from the decrease in fluorescence intensity of the BSA molecules. In an alternative approach for anchoring furan moieties on PVDF backbone, random

polymerization of FMA, nBMA and DEGMEM carried out through ATRP using similar reaction conditions with only exception of using PVDF as the macroinitiator instead of using modified PVDF. This is a first time report for grafting of FMA on PVDF backbone by ATRP. The ^{1}H-NMR analysis shows development of signals in the range of (5-7.5)δ corresponding to the furan ring and adjecent methylene protons. The synthesized material has been further subjected to DA reaction for anchoring maleimide units. Application of this finally synthesized material and possible control over the pore morphology of the membrane is matters of further studies which are currently undergoing in our laboratory.

Conclusions

The present work aims for the synthesis of PVDF based graft copolymers which may be used for affinity chromatography applications. Synthesis of random copolymeric polymethacrylate graft chains have been done using model ATRP initiator modified or unmodfied PVDF as macroinitiators using copper/bipyridine based complex. PGMA or PFMA chains have been anchored on PVDF backbone to bring reactive functionalities on the membrane material so that further post polymerization modifications may be done conveniently to introduce desired interacting functionalities. Hydrophilic PDEGMEM block has been introduced to provide water permeability and anti fouling property to the membranes. The synthesized materials have been subjected to phase inversion technique for development of pores. This has resulted microporous materials with rather large and polydisperse pore formation. The PGMA containing graft copolymer shows adsorption of BSA from PBS buffer solutions.

Further studies with alternative graft copolymers having PFMA grafted chains and their post polymerization modifications to develop novel affinity chromatography materials are currently undergoing.

Acknowledgements

We thankfully acknowledge for the grant sanctioned by Department of Science and Technology (DST), Govt. of India, having the Sanction Order No and date: **SB/FT/CS-189/2011 dated 27.06.2014 under Fast Track Project Scheme for Young Scientists.** We also thank IACS, Kolkata, IIT Kharagpur and CRNN, the University of Calcutta for providing instrumental support.

References

1. Lovinger, A. J. *Development in Crystalline Polymers*s *I*; Elsevier, Applied Science: London and New York, 1981.
2. Braga, F. J. C., Rogero, S. O., Couto, A. A. *Mater. Res. 10,* 247, 2007.
3. Hester, J. F., Banerjee, P., Won, Y.-Y., Akthakul, A., Acar, M. H., Mayes, A. M. *Macromolecules 35,* 7652, 2002.
4. Chen, Y., Ying, L., Yu, W., Kang, E. T., Neoh, K. G. *Macromolecules 36,* 9451, 2003.
5. Zhai, G.; Shi, Z. L.; Kang, E. T.; Neoh, K. G. *Macromol. Biosci. 5,* 974, 2005.
6. Samanta S., Chatterjee, D.P., Layek, R.K., Nandi, A.K. *J. Mater. Chem. 22***,** 10542, 2012.

7. Kuila, A., Chatterjee, D.P., Layek, R.K., Nandi, A.K. *Journal of Polym. Sci. Part A: Polymer Chemistry 52*, 995, 2014.
8. Samanta, S., Chatterjee, D.P., Layek, R.K., Nandi, A.K. *Macromol.Chem.Phys.212*, 135, 2011.
9. Barbey, R., Klok, H.-A. *Langmuir 26(23)*, 18219, 2010.
10. Sing, N., Husson, S.M., Zdyrko, B., Luzinov, I. *Journal of Membrane Science 262*, 81, 2005.

MACRO 228

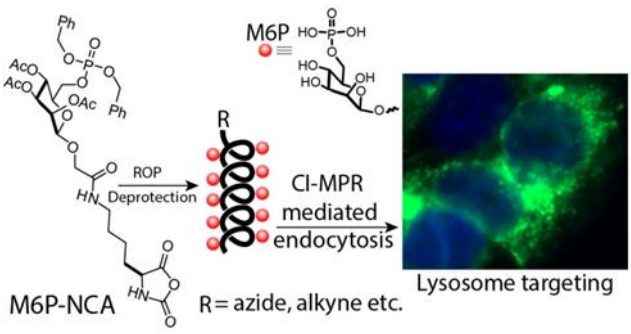
Controlled Synthesis of End-Functionalized Mannose-6-phosphate Glycopolypeptides for Lysosome Targeting

Das, Soumen* Parekh, Nimisha Mondal, Basudeb and Sen Gupta, Sayam *

CReST Chemical Engineering Division, CSIR National Chemical Laboratory, Dr. Homi Bhabha Road, Pune 411008, India

*E-mail: ss.sengupta@ncl.res.in. sh.das@ncl.res.in.

ABSTRACT: The ubiquitous expression of the mannose-6-phosphate receptor on the majority of human cells makes it a valid target in the quest to deliver therapeutics selectively to the lysosome.[1-6] In this work end-functionalized polyvalent mannose-6-phosphate glycopolypeptides (M6P-GPs) with high molecular weights (up to 22 kDa) have been synthesized via NCA polymerization. These synthetic M6P-GPs were found to display minimal toxicity to cells in vitro and show exceptional selectivity for trafficking into lysosomes in various cell lines. Comparison of the cellular uptake behavior of M6P-GP and the corresponding mannose-GP polymer reveals that incorporation of the phosphate moiety at the 6-position of mannose completely alters its trafficking behavior and becomes exclusively lysosome specific.[7,8] We also demonstrate that trafficking of M6P-GPs in mammalian cells is likely associated with the CI-MPR receptor pathway.



References

[6] Kornfeld, S. Annu. Rev. Biochem. 1992, 61, 307−330.
[7] Alberts, B.; Johnson, A.; Lewis, J.; Raff, M.; Roberts, K.; Walter, P. Mol. Biol. Cell, 4th ed.; Garland Science: New York, 2002; Chapter 317
[8] Ghosh, P.; Dahms, M. N.; Kornfeld, S. Nat. Rev. Mol. Cell Biol.2003, 4, 202−212.
[9] De Souza, A. T.; Hankins, G. R.; Washington, M. K.; Orton, T. C.; Jirtle, R. L. Nat. Genet. 1995, 11, 447−449.
[10] O'gorman, B. D.; Weiss, J.; Hettiaratchi, A.; Firth, M. S.; Scott, D. C. Endocrinology 2002, 143, 4287−4294.
[11] Gary-Bobo, M.; Nirde, P.; Jeanjean, A.; Morere, A.; Garcia, M. Curr. Med. Chem. 2007, 14, 2945−2953.
[12] Pati, D.; Das, S.; Patil, N. G.; Parekh, N.; Anjum, D. H.; Dhaware, V.; Ambade, A. V.; Sen Gupta, S. Biomacromolecules 2016,17, 466−475.

[13] Wienke, D.; Davies, G. C.; Johnson, D. a.; Sturge, J.; Lambros, M. B. K.; Savage, K.; Elsheikh, S. E.; Green, a. R.; Ellis, I. O.;Robertson, D.; Reis-Filho, J. S.; Isacke, C. M. Cancer Res. 2007, 67, 10230−10240.

MACRO 231

Strategic Catalyst Designing for Insertion Copolymerization of Polar Olefins with ethylene

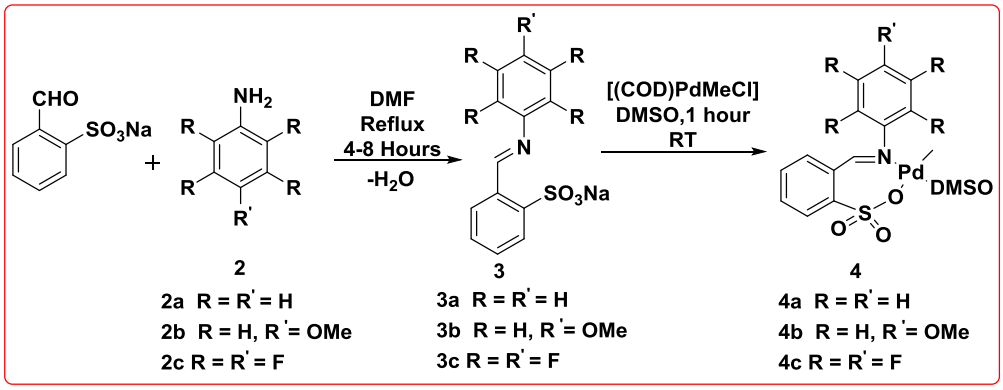
Deshmukh Satej S.[a]; Gaikwad Shahaji R. [a]; Chikkali Samir H.*[a,b]

[a]*Polyolefin Lab, Polymer Science and Engineering Division, National Chemical Laboratory, Pune-411008, India*

[b]*Academy of Scientific and Innovative Research, Anusandhan Bhawan, 2 Rafi Marg, New Delhi 110001, India*

**E-mail: s.chikkali@ncl.res.in.*

The ground breaking discovery by Prof. Ziegler and Prof. Natta led the foundation of olefin polymerization and today we produce about 160 million tons of polyolefins annually. Despite of this progress, the field of insertion co-polymerization of functional olefins is still in its infancy, though it has witnessed sudden resurge after the induction of neutral phosphinesulfonate Pd-complexes by Prof. Drent.[1] There are still many pressing issues associated with this polymerization.[2,3,4] In our endeavor to address those issues we propose a catalytic system as depicted in scheme **1**. The characteristic features of the catalyst are i) the proposed catalyst would be less oxophilic and more tolerant to functional groups in insertion co-polymerization, ii) electron rich *neutral* palladium centre would favor formation of *trans* π-complex over *cis* σ-complex.



Scheme 1: Synthesis of imine sulfonate ligand and subsequent complex

Existence of 3 was unambiguously established using a combination of 1-2D NMR, ESI-MS and analytical methods. The reaction of these ligands with palladium precursor [(COD)PdMeCl] yields the desired metal complexes. Performance of these catalytic systems in ethylene and functional olefin co-polymerization will be presented.

Reference:

(1) Drent, E.; van Dijk, R.; van Ginkel, R.; van Oort, B.; Pugh, R. I. *Chem. Commun.* **2002**, 744-745.
(2) Nakamura, A.; Anselment, T. M. J.; Claverie, J.; Goodall, B.; Jordan, R. F.; Mecking, S.; Rieger, B.; Sen, A.; van
Leeuwen, P. W. N. M.; Nozaki, K. *Acc. Chem. Res.* **2013**, *46*, 1438-1449.
(3) Gaikwad, S.; Deshmukh, S.; Chikkali, S. H. *J. Polym. Sci. A Polym. Chem.* **2014**, *52*, 1-6.
(4) Gaikwad, S. R.; Deshmukh, S. S.; Gonnade, R. G.; Rajamohanan, P. R.; Chikkali, S. H. *ACS Macro Lett.* **2015**, *4*,
933-937.

MACRO 240

Synthesis of amino phosphonate grafted resin and their extraction behaviour towards Actinides

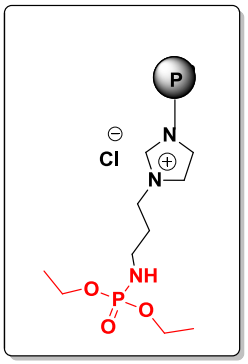
Dhrubajyoti Das[a], Kari Vijayakrishna[a]*, Akella Sivaramakrishna[a], C.V.S. Brahmmananda Rao[b]

[a] *Department of Chemistry, School of Advanced Sciences, VIT University, Vellore 632 014, Tamil Nadu*

[b] *Chemistry Group, Indira Gandhi Centre for Atomic Research, Kalpakkam 603 102, Tamil Nadu*

*Corresponding Author: kari@vit.ac.in

Actinides are toxic heavy metals which, if ingested or swallowed, can stay inside the human body for long period of time leading to acute chemical as well as radio toxic effects [1]. It is a challenging task to quantitatively recover these trace metal ions from these systems due to high acidic matrix environment [2]. Various organic extractants were employed in solvent extraction (SE) technique for the selective extraction of actinides from high acidic wastes [3]. Amongst them, phosphorus based ligands are known to be more selective for actinide ions [4-5]. But the main problems encountered in SE technique are: (a) the third phase formation; (b) disposal of large volumes of extractants and diluents; (c) multi-stage extraction procedures. To solve this, more recently polymer based sorbents are being employed in these extraction studies. Polymers have been frequently used for solid phase extraction as they provide good stability, high sorption capacity for the metal ions and good flexibility in the working conditions.



On that search we focused our interest towards the synthesis a new class of resin grafted amino phosphonate. A series of amino phosphonate were synthesized by Atherton –Todd reaction with a good yield. These amino phosphonate were hooked on to Merrifield's resin and used for the extraction of actinides by solid-liquid extraction. In the presentation we will discuss about the synthesis of amino phosphonate grafted resin, its characterization and their extraction behaviour towards Actinides.

References

1. X. Sun, H. Luo, S. Dai. *Chem .Rev.*, 112**,** (2012) 2100.
2. E.P. Horwitz, M.L. Dietz, D.M. Nelson, J.J. La Rosa, W.L. Fairman, Anal. Chim. Acta 238 (1990) 263.
3. W. Lewis, M. J. Hudson, L. M. Harwood. *Synlett*, 18, (2011), 2609.
4. C.V.S. BrahmmanandaRao, T.G.Srinivasan, P.R. VasudevaRao. *Solvent Ext. Ion. Exch*., 30, (2012), 262.
5. D. Das, E.V. Goud, S. Annam, S. Jayalakshmi, G. Gopakumar, C. V. S. Brahmmananda Rao, N. Sivaraman, A. Sivaramakrishna and K. Vijayakrishna, *RSC Adv.*, 5, (2015), 107421

MACRO 249

Synthesis, Characterization and property investigation of PVDF/rGO Nanocomposites for Energy Harvesting application

Chandan Kumar[1*], Anupama Gaur[2], Pralay Maiti[3] and Sanjay Kumar Rai[4]

[1,4] School Of Biomedical Engineering, Indian Institute Of Technology-BHU, Varanasi, India
[2,3] School Of Materials Science and Technology, Indian Institute Of Technology-BHU, Varanasi, India

*ckumar.rs.bme13@itbhu.ac.in

ABSTRACT

Graphene possess extraordinary electrical, mechanical and thermal properties and also have potential applications in many areas such as biosensors, conducting agent and composites. PVDF/rGO nanocomposites were prepared using in-situ solvothermal reduction of grapheme oxide in the PVDF solution. The nanocomposites were prepared with different concentrations of filler. The extent of interaction is determined by Transmission Electron Microscopy. The structural changes determined by UV-visible spectroscopy and X-ray diffraction studies. Surface morphology is determined by Scanning Probe Microscopy.

Dielectric studies of pure PVDF and nanocomposites were compared over a range of frequencies (20 Hz- 1MHz) and temperature 25-37^{o}C, which shows significant improvement in dielectric constant and decrease in dielectric loss in nanocomposite as compared to pure PVDF. Electrical conductivity of the composites is also measured. Further this material is used in Energy Harvesting application.

Keywords: PVDF, Graphene oxide, Dielectric properties

INTRODUCTION:

The decreasing energy consumption of today's portable electronics has raised the prospect of energy harvesting from the ambient environment for self-power supply. One common and simple method for vibration energy harvesting is to exploit the direct piezoelectric effect. In the last few years it has been a growing demand of low power and portable energy sources due to the advancement and mass consumption of portable electronic devices. Further, the portable energy sources must be linked with environmental issues and regulations. These demands support the research in the areas of portable energy generation methods.

Converting mechanical energy to electrical energy using piezoelectric materials has been the choice for many energy harvesting applications. In between the piezoelectric device and the actual electrical loads, an energy harvesting circuit is inserted as the electrical interface such that the power conditioning, impedance matching [1,2] or more complicated active boundary control [2,3] can be applied. Therefore well designed energy harvesting interfaces are highly desired.

Graphene, a two-dimensional sheet of sp2-bonded carbon atoms with honeycomb crystal lattice structure, has attracted tremendous attention due to its admirable mechanical strength, extraordinary flexibility, large specific surface area, high aspect ratio, as well as upright electrical and thermal conductivities [4]. One way to harness these desirable properties is to integrate graphene nanosheets (GNS) into composite materials and to form a new class of functional materials. Poly(vinylidene fluoride) (PVDF) is an important polymer having piezo and pyroelectric properties. It exhibits five different crystalline polymorphic structures (α, β, γ, δ, θ) of which β polymorph is piezoelectrically active [5]. This polymer is about 50% crystalline and it crystallizes in the stable a polymorph from the melt. PVDF is a biocompatible polymer [20], so its composites with graphene would be very much useful for biomedical applications. In particular, electrically conductive composites [6-8] have attracted considerable attention because graphene enables the insulator to conduct at a significantly lower filler loading due to the large particle aspect ratio. Stankovich and coworkers have reported that electrical percolation of isocyanatetreated graphite oxide (GO) takes place in polystyrene at 0.1 vol% and this composite has a conductivity of w0.1 Sm_1 at 1 vol% [9]. Stankovich's study has benefited high-dielectric-constant (high-k) materials used in microelectronics and other applications [10].

It is crucial to accomplish uniform filler dispersion within the polymer matrix and good interfacial adhesion between fillers and polymer matrix. For graphene-based composites, the dispersion of GNS in a polymer matrix can be an issue because GNS is not compatible with some polymer materials. Several techniques such as physical absorption and chemically linking between functional groups and graphene sheets have been developed to solve the problem [11].

In this paper, we describe the simplistic and effective synthesis of GNS/PVDF composites by reduction of graphene oxide in Dimethylformamide (DMF). The dielectric properties and electrical breakdown strength were studied. Dielectric Studies of the PVDF/rGO composites and pure PVDF were compared over a wide range of Frequencies (20 Hz-1 MHz) and temperature (25-37^{0C}). The result suggests that the PVDF/rGO composites showed a significantly improved dielectric constant

with a decrease in the dielectric loss. Furthermore for Energy harvesting the voltage produced by the material were also studied.

EXPERIMENTAL:

Materials:

PVDF(sigma Aldrich), Graphite (Aldrich, USA), sodium nitrate and potassium permanganate (Merck, Mumbai) are used as received. N, N dimethyl formamide (DMF), Hydrazine hydrate solution (Merck, Mumbai) is used as received.

Preparation of Reduced Graphene:

Graphene oxide (GO) is prepared from graphite powder by oxidizing with $KMnO_4/NaNO_3$ mixture in concentrated H_2SO_4 medium using Hummers method.

Reduction of graphene oxide is done by hydrazine hydrate. For this 32.1 m mol hydrazine hydrate is added to graphene oxide solution and heated at 100^oC for 24 hours. After that it is filtered and vaccum dried at 50^oC for 24 hours. Obtained product id reduced graphene oxide abbreviated as R-GO.

Preparation of Nanocomposite and Samples:

To prepare the reduced GO-PVDF composites, PVDF is dissolved in DMF and RGO is dispersed in DMF separately. Then both the solutions are mixed to make homogeneous solution. The evaporation of the solvent in a Petri dish at 60^oC gives films of the nanocomposites which are kept at 60^oC for three days in vacuum. Prepared nanocomposite is abbreviated as NC.

Sample preparation for characterization: The Compression moulding technique was used to prepare the specimens. Special care has been taken to produce air bubble free samples.

RESULT AND DISCUSSIONS:

Structure:

Reduced graphene oxide nanoparticles have strong influence on structure of Pure PVDF. As we can see in X-ray diffraction pattern there is a peak at 19.2^o which get shifted to 20.4^o because of piezoelectric phase induced in the nanocomposites. We can further elaborate the phase fractions by deconvolution of the peaks. Similarly peak at 17.6 also get reduced in nanocmposite as compared to pure PVDF.

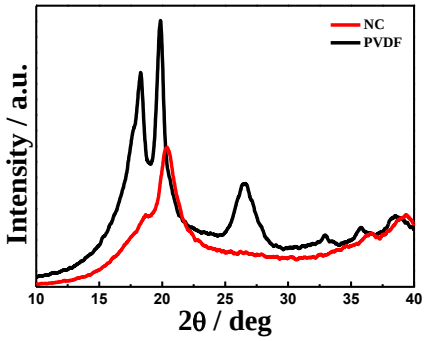


Figure 1: X-ray diffraction Pattern for Pure PVDF and PVDF-RGO nanocomposite.

Voltage response:

Voltage response of pure PVDF and nanocomposite is measured under same load. Same size specimens of pure PVDF and nanocomposites are taken and pressed under same load and we can see the difference in output voltage in *figure 3*. The output voltage is direct measure of piezoelectric properties developed in nanocomposite with respect to pure PVDF.

It can be seen in the graph that the voltage generated from the nanocomposite is around 0.4V and peak to peak voltage is around 0.8-0.9 volt.

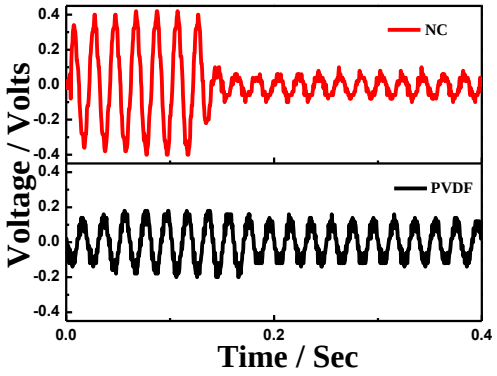


Figure 3: Voltage response under load for pure PVDF and nanocomposite.

CONCLUSIONS:

Nanocomposite of PVDF and RGO shows better piezoelectric properties than pure polymer. X-ray diffraction studies shows structure changes in the nanocomposite and its effect is shown in decrease in tanδ value with frequency. Also the voltage output with same applied load shows that

nanocomposite has better piezoelectric properties than pure PVDF, which is responsible for better voltage output and can be used for device fabrication.

ACKNOWLEDGEMENTS:

Chandan Kumar acknowledges the Institute for his teaching assistantship.

REFERENCES:

1. Roundy, S. (2005). On the effectiveness of vibration-based energy harvesting.*Journal of intelligent material systems and structures*, *16*(10), 809-823
2. Shenck, N. S., & Paradiso, J. A. (2001). Energy scavenging with shoe-mounted piezoelectrics. *IEEE micro*, (3), 30-42
3.Piguet, C. (Ed.). (2004). *Low-power electronics design*. CRC press
4. Kim, Hyunwoo, Yutaka Miura, and Christopher W. Macosko. "Graphene/polyurethane nanocomposites for improved gas barrier and electrical conductivity." *Chemistry of Materials* 22.11 (2010): 3441-3450.
5. Lotz, Bernard, Andrew J. Lovinger, and Rudolf E. Cais. "Crystal structure and morphology of syndiotactic polypropylene single crystals." *Macromolecules*21.8 (1988): 2375-2382.
6. Ansari, Seema, and Emmanuel P. Giannelis. "Functionalized graphene sheet—Poly (vinylidene fluoride) conductive nanocomposites." *Journal of Polymer Science Part B: Polymer Physics* 47.9 (2009): 888-897.
7. Ganguli, Sabyasachi, Ajit K. Roy, and David P. Anderson. "Improved thermal conductivity for chemically functionalized exfoliated graphite/epoxy composites." *Carbon* 46.5 (2008): 806-817.
8. Lee, Yu Rok, et al. "Properties of waterborne polyurethane/functionalized graphene sheet nanocomposites prepared by an in situ method."*Macromolecular Chemistry and Physics* 210.15 (2009): 1247-1254.
9. Stankovich, Sasha, et al. "Graphene-based composite materials." *nature*442.7100 (2006): 282-286.
10. Chu, Baojin, et al. "A dielectric polymer with high electric energy density and fast discharge speed." *Science* 313.5785 (2006): 334-336.
11. Hou, Shifeng, et al. "Formation of highly stable dispersions of silane-functionalized reduced graphene oxide." *Chemical Physics Letters* 501.1 (2010): 68-74.

MACRO 250

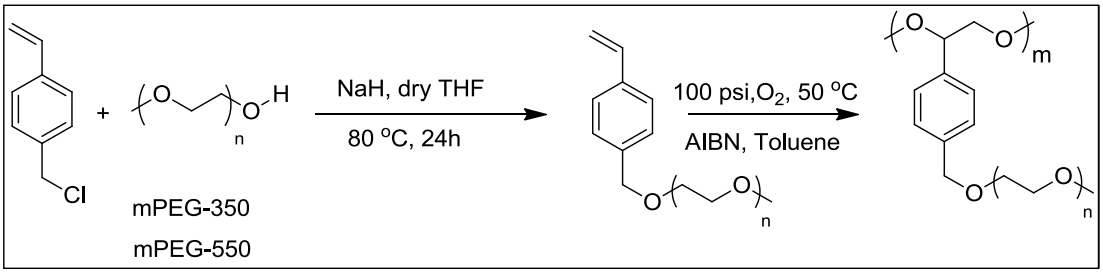
Water Soluble Polyperoxides

Mete, Sourav; De, Priyadarsi*

Polymer Research centre, Department of Chemical Sciences, Indian Institute of Science Education and Research Kolkata, Mohanpur - 741246, Nadia, West Bengal, India.

* *Corresponding author E-mail: p_de@iiserkol.ac.in*

Free radical polymerization of vinyl monomers in the presence of high oxygen pressure yields polyperoxides, which are strictly alternating copolymers of vinyl monomers and molecular oxygen. Polyperoxide polymers are unique due to their highly exothermic decomposition, in contrast to common polymers which generally degrade endothermically. Polyperoxides find application as autocombustible fuel, polymeric macroinitiator, dismantlable adhesive, curatives in coating and moulding compositions, drug delivery carrier, etc. Although polyperoxides are known since 1922's, only few water soluble vinyl polyperoxides have been reported in the literature.[1] Therefore, in this work we have prepared 4-vinyl benzyl polyethylene oxide (VBPEG) and reacted with oxygen under high pressure at 50 ^{o}C in the presence of 2,2' - azobisisobutyronitrile (AIBN) as a radical initiator. We got water soluble polyperoxides of poly(VBPEG peroxide) (PVBPEGP). Electron-impact mass spectroscopy (EI-MS), FT-IR and NMR spectroscopy have been used to verify the alternating copolymer structure with peroxy (–O–O–) bonds in the main chain. The rate of polymerization (R_p) was calculated from the slope of the oxygen consumption against time plot. Highly exothermic thermal degradation of polyperoxides have been investigated by differential scanning calorimetry (DSC).[2] The obtained polyperoxides showed temperature induced phase separation, and the transition temperature decreased according to the decrease of the ethylene oxide groups in the vinyl monomer (Scheme 1). Therefore, cloud point in the polyperoxides can be altered by changing the number of ethylene oxide groups in the monomer.



Scheme 1: Synthesis of 4-vinyl benzyl PEG and their polyperoxides.

References

1. Pal, S; De, P. *Chem Commun*, 48 (2012) 4229.
2. Pal, S; Das, A; Maiti, S; De, P. *Polym Chem*, 3 (2012) 182.

MACRO 259

Synthesis of Polyaniline & Polypyrrole Nanofibers via Continuous flow And Microfluidic Droplet generator method

Bajpai Rishab, Kumar Anil*

[a] *Chemistry Department IIT Bombay, Mumbai, India*
** anilkumar@iitb.ac.in*

Continuous Flow Processes provide an attractive alternative for an environmentally friendly, economically viable and safe operation for large chemical plants. It has been projected as the process of choice for the chemical factories of tomorrow. In this direction, we have been working on development of continuous flow process for the synthesis of nano particles and nano fibers. Some of the salient features of continuous flow process for nano particle syntheses are fast mixing, excellent heat exchange, previse control over the concentration gradient and the control over the particle size.

In chemical oxidative polymerization of aniline there are two factors for the growth of aniline monomer homogenous nucleation and heterogeneous nucleation. [1] Homogenous nucleation of polyaniline formation nanofibers, while Heterogeneous nucleation leads to granular particulates. [1] Kaner and coworkers, in their seminal work, have shown that the polymerization process for the synthesis of polyaniline proceeds via the formation of 100% nanofibers in the initial phase of polymerization. These nanofibers then act as nuclei resulting in secondary nucleation leading to the synthesis of particles. The key factor for the synthesis of Polyaniline and Polypyrrole nanofibers is to suppress the secondary growth. In continuous flow method one can suppress the secondary growth by fast mixing as well by the continuous removal of product from the fresh starting material. [3] Therefore, we expect that continuous flow synthesis of Polyaniline should result in nano fibers formation via Homogenous nucleation. As expected, it resulted in the synthesis of 100% nanofibers **(figure 1**) without any secondary nucleation. It was observed that the fiber deposition happens at the reactor walls leading to fouling of the reactor and decreasing yield.

Particle deposition can be avoided by switching to droplet flow reactor in which an immiscible phase is injected into the channel alongside the reagent phase, causing the reagent phase to divide into a succession of droplets. [3] By this method one can get monodisperse and shape control nanofibers without fouling the reactor with high yield **(figure 2-3).** Our recent results in this direction will be highlighted in this poster.

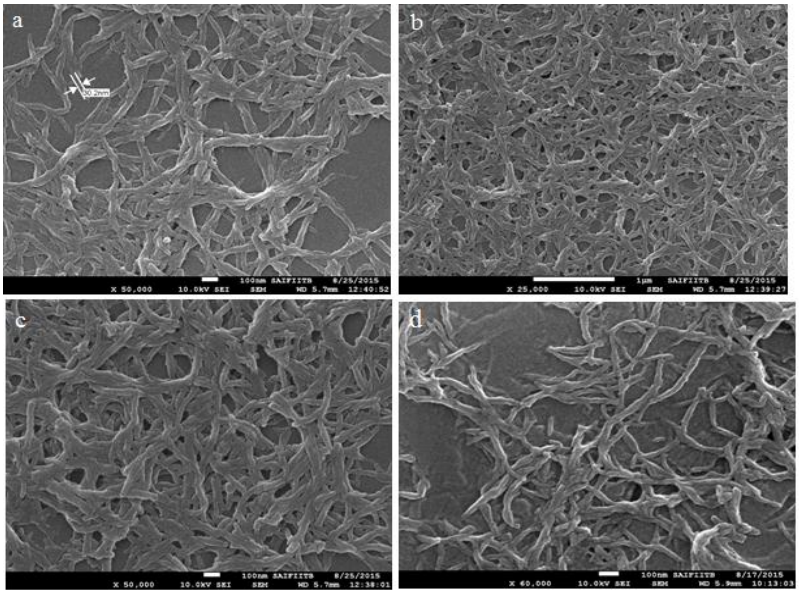


Figure 1. SEM images of HCl-doped polyaniline synthesized by continuous flow method

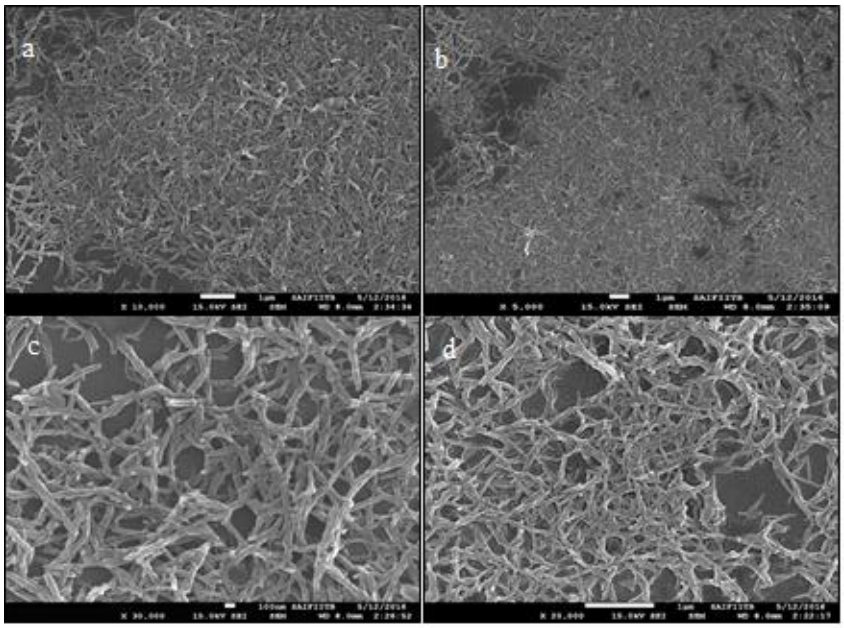
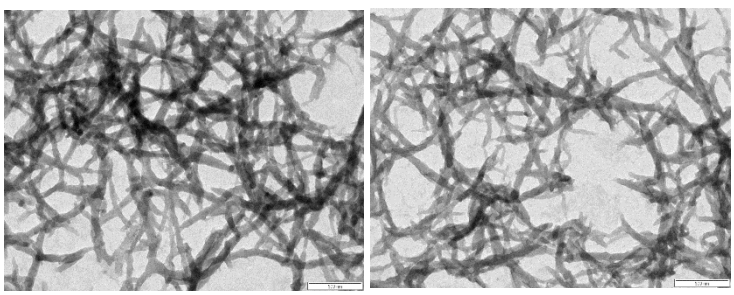


Figure 2. SEM images of HCl-doped polyaniline synthesized by microfluidic droplet method

(a) **(b)**



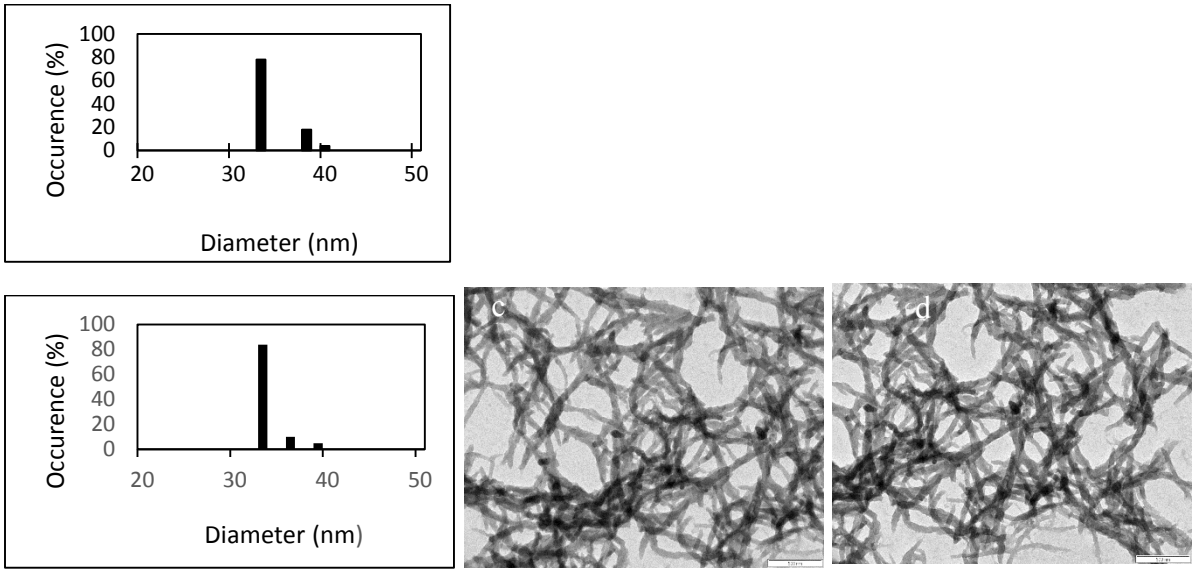


Figure 3. (a) The particle size distribution and (b) TEM images of HCl-doped polyaniline synthesized by microfluidic droplet method.

References

3. Huang J, Kaner B. R. *Angew. Chem. Int. Ed*. 43 (2004) 5817.
4. A.M.Nightingale, S.H.Krishnadasan, D.Berhanu and J.C.de Mello *RSC Adv*., 2011, 11, 1221-1227.
5. Kumar Anil and Bajpai Rishab, Indian Patent Application No 3030/MUM/2015, filed on 10 August 2015.

MACRO 260

Synthesis of 'Living' Poly(Dimethylaminoethyl Methacrylate) Using CuCl.PMDETA Complex in Environmentally Benign Conditions

Basak, U[a].; Majumdar, S.[b]; Ghosh, T.[a]; Ball, R.[c]; Chatterjee, D.P.[a]*

[a]*Department of Chemistry, Presidency University, Kolkata, India*
[b]*Department of Chemistry, Indian Institute of Technology Kharagpur- 721302, India*
[c]*Department of Chemistry, Indian Institute of Technology Bombay, Powai, Mumbai-400076, India*
** e-mail id: dhruba.chem@presiuniv.ac.in*

Abstract

The present contribution describes a novel method for synthesis of controlled polydimethylaminoethyl methacrylate (PDMAEMA) via atom transfer radical polymerization (ATRP) under solvent free condition at 30^0C using CuCl/pentamethyldiethylenetriamine

(PMDETA) complex as catalyst. A quaternaryammonium chloride salt, tricaprylylmethylammonium chloride (AQCl), is used in double molar proportion with respect to CuCl during the reaction to solubilize the deactivator cupric complexes formed after initiator addition. The polymerization kinetics in presence and in absence of AQCl is measured. A linear first order kinetic plot is observed when AQCl is present unlike the case when AQCl is absent. The linear kinetic plot indicates steady radical concentration throughout the polymerization as a result of the proper functioning of the ATRP equilibrium. However, in absence of AQCl due to the precipitation of the cupric complex, ATRP equilibrium could not be established and therefore, formation of uncontrolled polymers resulted. The molecular weight and poly dispersity index (PDI) of the synthesized polymers are characterized by GPC technique. The monomer conversion in presence of AQCl reached even up to 98% , therefore, the synthesized PDMAEMA-Cl polymers are used as macroinitiator for chain extension with another very interesting monomer MeO_2MA in single pot under solvent free conditions. The GPC analysis shows a clean sweep of GPC trace corresponding to the block copolymer PDMAEMA-b-$PMeO_2MA$ from the PDMAEMA-Cl macroinitiator without any significant bimodality or peak residue. This clearly indicates towards the living nature of the PDMAEMA-Cl synthesized by the present technique. Therefore, we believe this is the first time report of solvent free ATRP of DMAEMA under ambient temperature using CuCl.PMDETA catalyst system which proceeds with remarkable control over polymer molecular weight and polydispersity index (PDI) and shows proper living character of the synthesized polymers through successful block copolymerization.

Keywords: *polymer; ATRP; living polymers; block copolymers;*

Introduction

A significant development has occurred in biomedical field in respect of *in-vitro* delivery of drugs or nucleic acid molecules etc. In most of these cases, delivery vehicles used are polymers which are biocompatible or biodegradable. These polymer systems should be water soluble and undergo association or dissociation under various physiological conditions either reversibly or irreversibly. The aggregated forms may be used as polymer scaffolds for loading of drugs or other molecules and dissociation should release the molecules to the target areas.[1] Now increasing degree of sophistication in applications such as targeted drug delivery or sustained release requires more sophisticated polymer systems which may behave differently under the influence of different stimulus in a reversible fashion. These are called 'smart' polymeric materials. Polymer molecules with varying degrees of structural complexities (block, graft, gradient etc.) responding under two most biologically important stimulus, pH and temperature are most attractive in this respect. Introduction of structural complexities in a tailor made approach may introduce many interesting properties for specific applications. However, this would require development of efficient synthetic strategies for exerting precise control over polymer molecular weight and architecture, preferably under environmental friendly conditions in a cost effective way.

Poly(2-dimethylaminoethyl methacrylate)(PDMAEMA) is a very much important, water soluble, thermo and pH responsive polymer system. It has found significant applications in biomedical field such as in gene delivery, bioseparation,, antimicrobial or antibacterial agents etc.[2,3] Protonation or quaternization of -NMe_2 groups of PDMAEMA forms polycationic derivatives which are typically used as carriers for nucleic acids or used as antimicrobial or antibacterial agents. Dual stimuli responsive block copolymers containing PDMAEMA are particularly very much useful for the preparation of stimuli responsive micelles capable of being used as delivery vehicles.

Atom Transfer Radical Polymerization (ATRP) has emerged as a very important tool for controlled radical polymerization because of its requirement of less stringent reaction conditions and tolerance towards different monomers or solvents. ATRP operates via generation of radicals by reaction of redox active metal complexes in the initiation step and subsequently propagation occurs by monomer addition in repetitive cycles of activation and deactivation provided by the metal complex. Although complexes of various metal ions may be used but copper based ATRP has been most successful. Literature reports show that DMAEMA has been polymerized by ATRP, but in most of them either very much expensive tetradentate ligand system has been used for complex formation with copper salts or bipyridine based complexes are used in aqueous medium. One major disadvantage of Cu.bpy complex based ATRP is the issue of copper contamination in the final product even after repeated attempts of purifications and furthermore, polymerization of DMAEMA in water or alcohol medium suffers from the problem of trans-esterification, as reported by Armes et.al.[4]

Pentamethyldiethylenetriamine (PMDETA) has been a very much useful ligand in Cu based ATRP of (meth)acrylates, particularly because it provides appreciably high value of rate of activation (k_a) during ATRP initiation, it is commercially very much available and cheap. However, the Cu.PMDETA complex has not been very much successful for carrying out controlled / living radical polymerization of polar monomers having pendant reactive functionalities. This may be attributed to the tridentate nature of PMDETA ligand which forms relatively less stable complex with cuprous salts and therefore competitive ligation with monomer functional groups leads to catalyst deactivation.[5] However, given the high ATRP activation rate constant with Cu(I)/PMDETA complex if strategies may be developed to restrict monomer complexation to the copper ions, polymerization of such reactive monomers may be done in presence of much reduced amount of copper catalyst also.

Here we report a new method for ambient temperature solvent free ATRP of DMAEMA with CuCl/PMDETA complex as catalyst in presence of catalytic amount of tricaprylylmethylammonium chloride (AQCl), a quaternaryammonium salt. Kinetic analysis of the bulk polymerization of DMAEMA in presence and in absence of AQCl carried out under ambient temperature conditions. Polymerization in presence of AQCl operates nicely in concurrence with the features of a controlled/living polymerization. Furthermore, the synthesized PDMAEMA-Cl has been efficiently used as macroinitiator for polymerization of methoxyethoxyethyl methacrylate

(MeO_2MA) to prepare a thermo and pH responsive diblock copolymer at 30^0C and solvent free conditions in one pot. On the other hand, polymerization in absence of AQCl under the similar conditions although has reached very high monomer conversion but the features of polymerization including reaction kinetics and molecular weight evolution are quiet in non-conformity with the conditions of controlled polymerization.

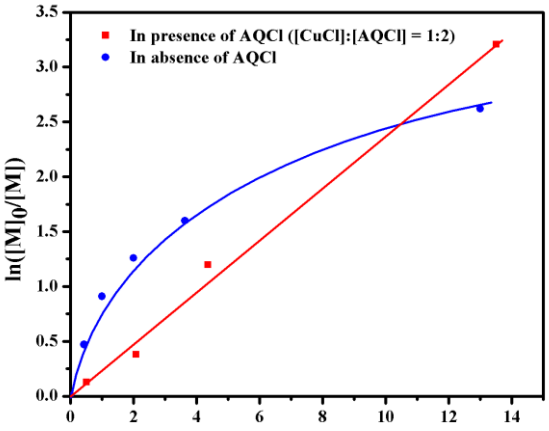
Experimental

Dimethylaminoethyl methacrylate (DMAEMA) (98%), diethyleneglycolmethylether methacrylate (DEGMEM) (98%) are purchased from Aldrich Chemicals and passed through basic alumina column before use. And also PMDETA, EBIB, AQCl are also purchased from Aldrich Chemicals. CuCl was purchased from Loba Chemicals and was purified by washing in 10% HCl solution followed by drying with methanol and ether. All other solvents were purchased from local chemical suppliers and purified by distillation under reduced pressure.

The polymerization is conducted in a glass tube fitted with B-14 standard joint. The monomer is purged thoroughly with nitrogen gas and then in it AQCl, CuCl, PMDETA is added. After formation of the completely soluble system, initiator EBiB is added. The polymer formed after desired time period is precipitated after diluting the reaction medium with THF in pet ether.

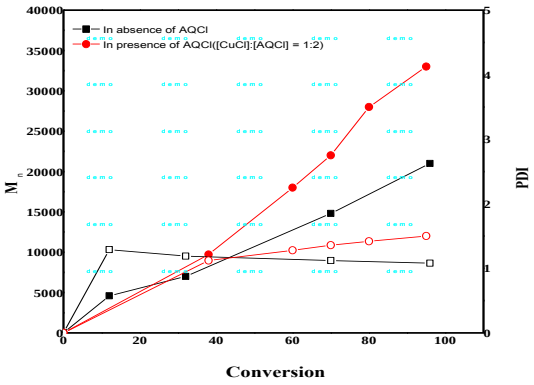
Results and Discussions:

Figure 1 shows the first order kinetic plots of bulk polymerization of DMAEMA conducted in bulk at 30^0C using CuCl/PMDETA catalyst with EBiB as initiator both in presence and in absence of AQCl. Halide exchange technique is used here to ensure faster rate of initiation over propagation and to have relatively stronger C-Cl bond at the chain end to minimize the possible loss of chain end functionality via elimination or substitution reactions by the reactive tertiary amine groups of the polymer. A linear kinetic plot indicating a steady radical concentration all through the polymerization is found when (1:2) molar ration of CuCl and AQCl respectively is used. This is very much expected when ATRP equilibrium of activation and deactivation is reached. However, a non linear kinetic plot is observed in absence of AQCl. This indicates a decreasing concentration of radicals which occurs due to the presence of appreciable amount of termination reactions occurring all through the reaction. However, notably in either of the cases, the monomer conversion reached appreciably high value (>95%). It is observed visually that, during polymerization in absence of AQCl, some green colored precipitation is developed even before initiator addition. This green coloured precipitate must be due to $CuCl_2$/PMDETA complex



(Figure 1): Kinetics of bulk polymerization of DMAEMA

formation from the residual amount of $CuCl_2$ which remains contaminated with CuCl due to aerial oxidation even after purification of CuCl. The formation of green colored insoluble material continues to occur throughout the polymerization. However, with advancement of polymerization, due to sharp increase in medium viscosity it does not show precipitation but a dispersion is rather observed. However, due to such phase separation of deactivator cupric complex, deactivation reactions occur only through heterogeneous reaction in the interface of monomer and insoluble cupric catalyst. Therefore, inefficient deactivation is provided to the propagating radicals leading to the formation of dead polymer chains. However, due to insolubility of the deactivator complex, deactivation reactions are obstructed but not completely absent. This probably explains very high conversion of DMAEMA polymerization even in absence of AQCl. On the other hand, on presence of AQCl (1:2) molar ratio with respect to CuCl, the reaction system shows formation of completely transparent light green coloured solution which deepen somewhat after initiator addition and shows a steady colour with complete transparency till the end of the reaction. Hence unlike the previous condition, here the deactivator complex remains soluble in the reaction medium. This helps in establishing ATRP equilibrium and the reaction proceeds with all through steady radical concentration.



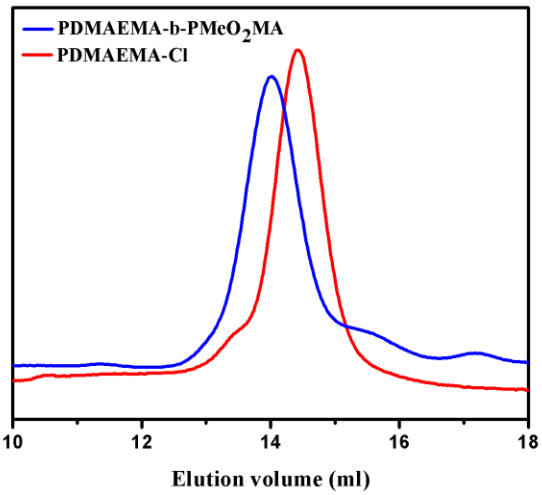
(Figure 2): Variation of $M_{n(gpc)}$ and PDI with conversion

Figure 2 shows that when AQCl is present, increase in PDMAEMA molecular weight occurs almost linearly with increasing conversion by keeping an appreciably good agreement with the theoretically predicted molecular weight. Another very interesting observation is, during polymerization in this condition, the PDI of the polymer samples show a gradual decrease with increasing conversion and reaches a minim um value of 1.07 at the highest conversion (99%)(closed symbols indicate M_n and open symbols PDI). This feature is typical of a controlled polymerization. However, in absence of AQCl, the development of molecular weight with increase in conversion observed but with a rather poor agreement with the theoretically predicted value and the dispersity of the synthesized polymers increased with increasing conversion. Therefore, both of these features indicate towards an uncontrolled polymerization.

The PDMAEMA synthesized in presence of AQCl is subsequently used for block copolymer synthesis with MeO_2MA in one pot. The conversion of DMAEMA in the first step reached about 99%, hence the target block copolymer

PDMAEMA-b-$PMEO_2MA$ should be free of any random copolymer contamination within the block copolymer chain. Figure 3 shows the clean sweep of gpc trace from PDMAEMA macroinitiator to PDMAEMA-b-$PMEO_2MA$ without any bimodality or any

residue in the molecular weight range of the macroinitiator. This proves the living nature of PDMAEMA-Cl polymers synthesized in presence of AQCl without any ambiguity.



(Figure 3): Overlay of gpc traces

Conclusions

Atom transfer radical polymerization of DMAEMA carried out under ambient temperature using CuCl.PMDETA complex in solvent free conditions. Tricaprylylmethylammonium chloride used in catalytic amount is helpful in making the corresponding cupric complex soluble in the reaction medium which is otherwise highly insoluble. The polymerization in presence of AQCl is well controlled showing good agreement with the theoretically predicted molecular weights and lower PDI is observed unlike in case of polymerization when AQCl is absent. Block copolymer with $PMeO_2MA$ is synthesized successfully using PDMAEMA-Cl macroinitiator synthesized during ATRP of DMAEMA in presence of AQCl. This clearly establishes the living nature of the polymers produced.

Acknowledgements

We thank Presidency University for providing financial support and laboratory set up. Chatterjee D.P. also thanks UGC, Govt. of India for providing the financial support through UGC, Start Up Grant No. F.30-92/2015 (BSR) dated March, 2015 (FD Diary No. 11758 Date 26.03.2015).

References

1. Zhang, B.-U. He, W.-D. Li, W.-T. Li L.-Y., Zhang K.R., Zhang H. *Polymer 51*, 3039, 2010.
2. Cordeiro R.A., Rocha N., Mendes J.P., Matyjaszewski K., Guliashvilli T., Serra A.C., Coelho F.J. *Polym. Chem. 4*, 3088, 2013.
3. Huang J., Murata H., Koepsel R.R., Russel A.J., Matyjaszewski K. *Biomacromolecules 5*, 877, 2004.
4. Bories-Aaeau X., Armes S.P. *Macromolecules 35*, 10241, 2002.
5. Nanda A.K., Matyjaszewski K. *Macromolecules 36*, 1487, 2003.

MACRO 272

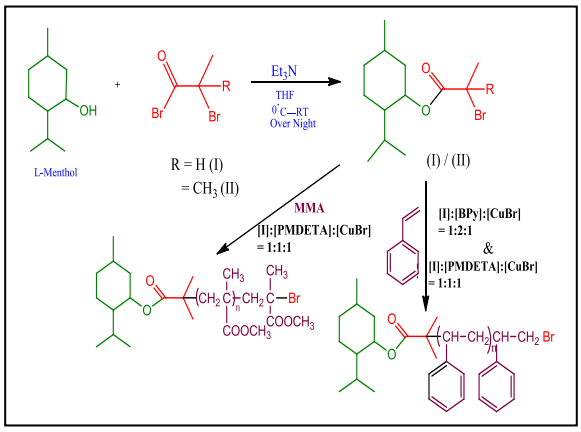
Novel L-Menthol-Based Initiators for Atom Transfer Radical Polymerization (ATRP)

Vishwakarma Sambhav,[a] Kumari Archana,[a] Singh Rajshree,[a]Ramesh K.,[a,b] Misra Nira,[b] Ray Biswajit[a]*

[a]*Department of Chemistry, Institute of Science, Banaras Hindu University, Varanasi-221005, India.*
[b]*School of Biomedical Engineering, Indian Institute of Technology (Banaras Hindu University), Varanasi-221005, India.*

Corresponding author email i.d.: biswajitray2003@yahoo.co.in

L-Menthol-based atom transfer radical polymerization (ATRP) initiators, namely, 2-isopropyl-5-methylcyclohexyl 2-bromo-2-methylpropionate (**I**), and 2-isopropyl-5-methylcyclohexyl 2-bromopropionate (**II**), have been synthesized with 82 and 60% yields, respectively, by the reaction of L-menthol with 2-bromo-2-methylpropinyl bromide / 2-bromo-propinyl bromide in the presence of triethyl amine in THF. Successful formation of the initiators has been confirmed by FTIR, ^{1}H NMR, and ^{13}C NMR spectroscopic techniques. These newly synthesized initiators have been used to initiate the bulk ATRP of styrene and methyl methacrylate (MMA) at 100 and 90°C, respectively, in the presence of Cu(I)Br. The polymerization has been studied by using two ligands, namely, 2,2′-bipyridyl and *N*,*N*,*N*′,*N*′,*N*″-pentamethyldiethylenetriamine (PMDETA). Obtained polymers has been purified and characterized by ^{1}H NMR and gel permeation chromatography (GPC). PMDETA as ligand has showed better yield and control over polymerization procedure. On increasing monomer loading, molecular weight of the resulted polymers has been increased linearly. Polystyrenes having low (1.08-1.27) polydispersity (PD) have been synthesized with high conversion (80-90%) compared to that (~ 70%) of polyMMAs with PD in the range of 1.20-1.27.



The end-group analysis by ^{1}H NMR has indicated the presence of the initiator fragments at the both chain-ends of the polymer. The controlled nature of the polymerization has also been confirmed by kinetic study. The livingness of the formed polymers has been confirmed by successful homo-chain and hetero-chain extension experiments. The resultant polymers and block-copolymers have been characterized by ^{1}H NMR and GPC. Thus, these ATRP initiators have shown a novel synthetic methodology to generate well-defined L-menthol- terminated polystyrene and polyMMA homo-polymers and their block copolymers.

References

6. Mishra A. K, Patel V.K., Vishwakarma N. K., Biswas C.S.,Raula Manoj, Misra Arvind, Mandal T.K.and Biswajit Ray. *Macromolecules* 44 *(*2011) *2465*.
7. Vishwakarma N. K, Mishra A K, Mishra A, Paira T, Patel V K, Biswas C S , Mandal T K , Maiti P., *Appl. Polym. Sci*. (2012) doi:10.1002/app.38279,
8. Patten E. Timothy and Matyjaszewski Krzysztof, *Acc. Chem. Res.* 32(1999) 895.

9. Coessens, V., Pintauer, T., Matyjaszewski K., *Prog. Polym. Sci. 26* (2001) 337.

MACRO 273

Synthesis of amphiphilic block copolymers through RAFT polymerization and their application as surf-RAFT agent for the miniemulsion polymerization of styrene

Kishor Pawar [a,b], S. N. Raju Kutcherlapati [b], Niranjan Yeole [b], Dilip Hundiwale [a] and Tushar Jana*[b]

[a] *School of Chemical Sciences, North Maharashtra University, Jalgaon-425 001*
[b] *School of Chemistry, University of Hyderabad, Hyderabad-500 046*
E-mail:tusharjana@uohyd.ac.in

Amphiphilic block copolymers (Am-BCPs) are special class of materials due to their unique properties and enormous potential applications in various fields. The properties of Am-BCPSs can be tuned by varying the block length and composition of block copolymers. The unique amphiphilic character of the block copolymers (BCPs) enables them to self-assemble to form a range of different morphologies in aqueous solution, including spherical micelles, vesicles, cylinders, rods and worm-like micelles etc. Am-BCPs are also used as surfactant as well as stabilizer for the colloidal systems. Here, we report the synthesis of Am-BCPs based on hydrophilic NIPAAm and hydrophobic 9-anthracene methylmethyacrylate (AnMMA) through RAFT polymerization. In the first step hydrophilic PNIPAAm macro-RAFT was synthesized using (3-(Benzylsulfanylthiocarbonylsulfanyl)-propionic acid (BSPA) as chain transfer agent, this PNIPAAm macro-RAFT was chain extended with hydrophobic AnMMA to get amphiphilic poly(NIPAAm–b–AnMMA) block copolymers. The formation of copolymers of different hydrophobic block length with fixed hydrophilic block is confirmed by GPC analysis. These Am-BCPs were self-assembled in aqueous media to produce spherical micelles consisting of hydrophobic AnMMA as a core and hydrophilic PNIPAAm as a corona. The formed micelles of different sizes were characterized by transmission electron microscopy (TEM) and dynamic light scattering (DLS) analyses. The Am-BCPs were later used as surf-RAFT agent i.e. surfactant as well as RAFT agent for the miniemulsion polymerization of styrene. TEM analysis showed that the synthesized polystyrene emulsion had a core-shell morphology. The particle size and particle size distributions of the polystyrene latex were determined by DLS, FE-SEM and TEM analysis. The spherical micelles of amphiphilic block copolymers may prove to be useful tool as nanoreactor for the synthesis of nanoparticles.

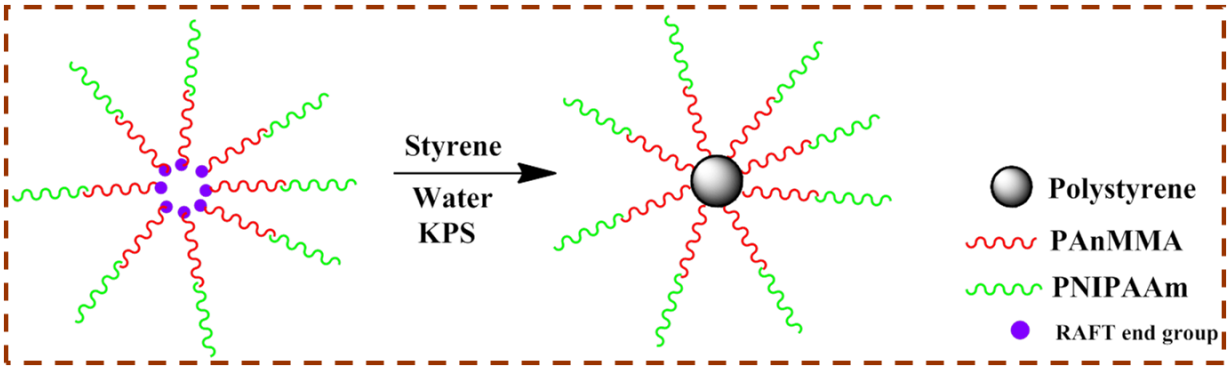


Figure 1. Synthesis of polystyrene core shell nanoparticle using Am-BCP as surf-RAFT agent

References:

[1] B. Koiry.; A. Chakrabarty.; N. Singha. *RSC Adv.*, 5 (2015) 15461.
[2] T. Lodge. *Macromol. Chem. Phys.*, 204 (2003) 265.
[3] H. Datta.; N. K. Singha, *J. Polym. Sci., Part A: Polym. Chem.*, 46 (2008) 3499.
[4] K. Pawar.; S. N. R. Kutcherlapati.; N. Yeole.; D. Hundiwale.; T. Jana (Manuscript under preparation).

MACRO 281

Arm First Approach Towards the Synthesis of Core Cross-Linked Star Polymer with Hydrophobic Corona via Click Chemistry

Samanta, Pousali; Banerjee, Rakesh; Maiti, Saikat; and Dhara, Dibakar*

Department of Chemistry
Indian Institute of Technology Kharagpur
West Bengal 721302 India

** Email: dibakar@chem.iitkgp.ernet.in*

Cross-linked star polymers are very useful because of their applications in tissue engineering, chemical sensing, cosmetics, etc. In this presentation, we present two different types of approaches towards the synthesis of cross-linked star polymers. In one approach, a well-defined block copolymer with azide functionalized middle-block was synthesized by controlled radical polymerization (RAFT) in the initial step. Then, core cross-linked star (CCS) polymers were synthesized by reacting the above block copolymer and alkyne-functionalized cross-linkers (tri- and tetra-functional). We have demonstrated the synthesis of core cross-linked star (CCS) polymers using 'click reaction' between azide functionalities in a polymer chain and alkyne groups from a cross-linker.

In another approach, instead of the conventional copper-based reagents for the development of star-branched polymers, we have established a novel and environmentally benign method, whereby a 1,3-dipolar cycloaddition reaction using a non-toxic reagent, iodosobenzenediacetate [$PhI(OAc)_2$]. Two well-defined block copolymer chains having acrylate-functionalized middle-block and oxime-functionalized middle-block was synthesized by RAFT AGENT. CCS polymer was synthesized by reacting the above two block copolymer chains via the formation of isoxazoline ring using 'click reaction' between acrylate functionalities in one polymer chain and in situ generated nitrile oxide groups from another polymer chain. In aqueous medium these CCS polymers produces polymeric nanoparticles, which could potentially serve as a carrier of hydrophobic drug molecules. Their drug loading capacity was investigated using coumarin dyes through steady state and time resolved fluorescence spectroscopy studies.

References

10. Banerjee, R; Maiti, S; Dhara, D. Green Chemistry, 16 (2014) 1365.
11. Samanta, P; Maiti, S; Dhara, D. Unpublished results

MACRO 284

Synthesis of PEG and NIPA Containing Cationic Block Copolymers with Different Architectures and their Interaction with DNA

Sahoo, Satyagopal; Dey, Debabrata,; Dhara, Dibakar*

Department of Chemistry
Indian Institute of Technology Kharagpur,
West Bengal 721302 India

**Email: dibakar@chem.iitkgp.ernet.in*

Investigation into the spontaneous polyion coupling between DNA and water soluble cationic polymers have recently attracted significant attention, particularly owing to their potential applications in the field of non-viral gene delivery and gene transfection. One of the potential routes by which this DNA-binding modulation or switching may be achieved is via the use of responsive or 'smart' polymers that are capable of conformational or phase changes under different regimes of pH and temperature. On the other hand, with recent developments in the area of controlled radical polymerization particularly reversible addition fragmentation transfer (RAFT), block copolymers with well-defined compositions, different architectures and functionalities can be synthesized from a wide range of available monomers.

We have synthesized two sets of PEGylated cationic copolymers – linear block copolymers (BCPs) and bottle-brush copolymers (BBPs) - by sequential polymerization of (3-methacrylamidopropyl)-trimethylammonium chloride (MAPTAC) and poly(ethylene glycol) based monomers, and a set of thermo-responsive block copolymers having a sharp LCST from 2-(dimethylamino)ethyl methacrylate (DMAEMA) and N-isopropylacrylamide (NIPA) monomers employing RAFT polymerization technique. After characterization of the polymers using GPC and NMR spectroscopy, we have studied the interaction behavior of these copolymers with nucleic acid (DNA). Equilibrium studies and thermo-responsive properties of these polyplexes were done using UV-visible, steady-state fluorescence spectroscopy, circular dichroism (CD), gel electrophoresis and dynamic light scattering (DLS) techniques. Kinetic studies were performed by stopped-flow fluorescence technique and time-resolved fluorescence spectroscopy to understand the complexation process. Results showed that at physiological pH, PEG containing cationic blocks interact with negatively charged DNA more strongly compared to PMAPTAC homopolymer where PEG content is nil. Here, hydrophobic interaction between PEG and DNA acts in a synergetic manner in addition to normal electrostatic binding force. Stopped-flow fluorescence technique was employed to monitor the fast kinetic pathway of the binding process. All the results of BCP-DNA binding studies suggested a two-step reaction mechanism - a rapid electrostatic binding between the cationic blocks and DNA, followed by a conformational change of the polyplexes in the subsequent step that led to DNA condensation. The relative rate constant ($k_1^{'}$) of the first step was much higher compared to that of the second step ($k_2^{'}$). The charge ratios as well as the PEG content with different architectures in the cationic blocks had marked effect on the kinetics of the DNA-BCP polyplex formation. The time-resolved fluorescence measurements revealed that the behavior of the polyplexes formed after the DNA compaction process depends largely on the nature and structure of the cationic polymers under study. In case of low generation PAMAM dendrimers, the DNA dendriplexes formed were seen to have a relatively less relaxed complex state, as compared to the polyplexes formed between

PEGylated cationic BCPs with DNA. In case of cationic BCP37 with the maximum PEG content, the resultant DNA polyplex existed in the most easily relaxed state i.e., DNA was not folded into a fixed conformation but rather existed in several conformations. Thermo-responsive studies showed that a complex is tightly formed between the carrier polymer and DNA above the transition temperature by hydrophobic aggregation of the polymer. Below the transition temperature this complex is dissociated or becomes loosely bound because of the decrease in hydrophobic nature of the polymer. The details of the results including the effect of polymer architecture will be presented.

References

1. Dey, D; Maiti, C; Sahoo, S; Dhara, D. *J Mol. Liq*, 221 (2016) 547.
2. Dey, D.; Kumar, S; Maiti, S; Dhara, D. *J. Phys Chem B*, 117 (2013) 13767 .
3. Dey, D.; Kumar, S; Banerjee, R; Maiti, S; Dhara, D. *J Phys Chem B*, 118 (2014) 7012.
4. Dey, D; Maiti, C; Maiti, S; Dhara, D. *Phys. Chem. Chem. Phys.*, 17 (2015) 2366.
5. Sahoo, S.; Dey, D.; Dhara, D. Unpublished results

MACRO 285

Modified Dendritic Amine Grafted on Mesoporous Silica: A Highly Effective Reusable Catalyst for One-Pot Synthesis of Conjugated Nitroalkenes and Nitroaldols

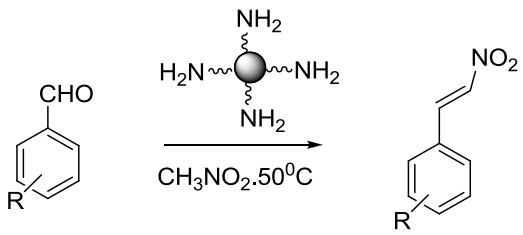
K.A. Jisha, K. Sreekumar* and S. Prathapan*

Department of Applied Chemistry, Cochin University of Science and Technology

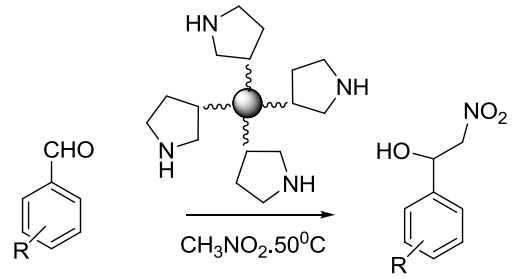
Cochin, India

* ksk@cusat.ac.in

The Henry reaction is one of the fundamental carbon- carbon bond forming reactions in organic synthesis. It is one of the most useful methods for the preparation of β-nitroalkanols, which are considered as useful, intermediates in organic and nitroalkenes which have wide application in pharmaceuticals.[1-3] We synthesized three generations of amine and proline grafted on mesoporous silica (G0-G2) through stepwise growth technique and characterized by BET surface area analysis, Low angle X-ray diffraction (XRD), solid state ^{13}C NMR, TG analysis and IR spectroscopy.[4] We present a new, simple and practical procedure for direct transformation of aryl aldehydes into conjugated nitroalkenes and nitroaldols using nitromethane as nitrating agent in the presence of proline and amine modified dendrimers grafted on mesoporous silica given in the scheme1 and 2 respectively. The reaction between aldehyde and nitromethane was performed under solvent-free condition at 50 °C in the presence of 4.8 mol% of both catalysts to produce corresponding products. The maximum yield was observed with second generation dendrimer (G2). After the reaction is over, the catalyst can be separated and reused up to 4 cycles without appreciable loss in its activity.



Scheme 1 Synthesis of conjugated nitroalkene



Scheme 2 Synthesis of conjugated nitroalkene

References

[1] Makowska-Janusik, M.; Kassiba, A; Errien N.; Mehdi A., *J. Inorg Organomet Polym*, 20 (2010) 761.
[2] Anjoy M.; Santosh T. K.; Sung S. K., *Bull. Korean Chem. Soc., 30* (2009) 1767.
[3] Yang, J.; Dong, J.; Lü, X.; Zhang, Q.; Ding; Wei Shi; Xiaoxin; *Chin. J. Chem.*, 30 (2012) 2827.
[4] Bhagiyalakshmi M.; Do Park S.; Seog Cha W.; Tae Jang. H, *Applied Surface Science* 256 (2010) 6660.

MACRO 290

Synthesis and Photovoltaics Applications of Novel Fluorene based Donor-Acceptor Cross-Conjugated Polymers

Bhavna Sharma and Josemon Jacob*

[1]*Centre for Polymer Science and Engineering, Indian Institute of Technology, Hauz Khas, New Delhi 110016, India*

**Corresponding author. Tel.: +91 99 1106 1890; fax: +91 11 2659 1421.*

E-mail address: jacob@polymers.iitd.ac.in (J. Jacob).

Low band gap cross-conjugated donor-acceptor type materials for polymer solar cells based on fluorene were synthesized by Yamamoto polymerization and direct arylation polycondensation approach. Fluorene based donor monomer was polymerized with benzothiadiazole moiety to obtain the target polymers in good yields and high molecular weight. The resulting polymers were found to have good solubility in the common organic solvents. Cross-conjugated polymers are expected to be more planar due to the in-plane arrangement of the side alkyl chains which favour strong solid state interactions of polymer chains by π-stacking. Optical properties of these polymers were investigated in solution as well as thin film by UV-visible and photoluminescence (PL) spectroscopy. The absorption maxima ranged from 490 to 520 nm in THF solutions. A distinct red-shift is observed in absorption maximum of solid-state UV-visible spectrum compared to solution spectrum suggests a significant face-to- face interchain stacking of the polymer chains in solid state. Thermal properties were studied by thermo-gravimetric analysis and the thermal decomposition onset temperatures were found to be in range of 250-350 °C. Electrochemical studies were done by Cyclic Voltammetry in 0.1M TBAP solution in acetonitrile by which HOMO-LUMO levels and electronic band gaps were calculated. These cross-conjugated polymers are potentially impressive narrow

band gap (~1.7 eV) donors for bulk heterojuntion (BHJ) type organic solar cells with power conversion efficiency (PCE) of 1.4%. This result indicates that cross-conjugated polymers can be classified as potential donors for BHJs as the PCE obtained is the highest class among this type of cross-conjugated polymers.

References

[1] L. Han, X. Bao, T. Hu, Z. Du, W. Chen, D. Zhu, Q. Liu, M. Sun, R. Yang, Macromolecular Rapid Communications ***2014****, 35, 1153.*
[2] X. Gong, C. Li, Z. Lu, G. Li, Q. Mei, T. Fang, Z. Bo, Macromolecular Rapid Communications ***2013****, 34, 1163*

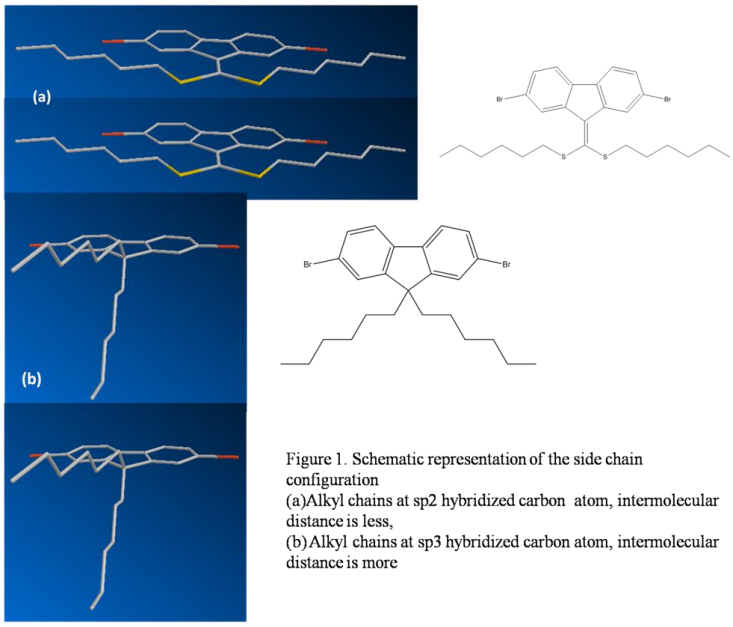


Figure 1. Schematic representation of the side chain configuration
(a)Alkyl chains at sp2 hybridized carbon atom, intermolecular distance is less,
(b)Alkyl chains at sp3 hybridized carbon atom, intermolecular distance is more

MACRO 291

Synthesis and Third-order Nonlinear Optical Properties of Phenothiazine-Triazine Copolymer

S. Narayanan[a]*, S. Mathew,[b] K. Sreekumar,[c] C. Sudha Kartha,[d] R. Joseph,[e] K. S. Devaky[a]

[a] *School of Chemical Sciences, MG University, Kottayam, India*

[b] *International School of Photonics, CUSAT, Cochin-22, India*

[c] *Department of Applied Chemistry, CUSAT, Cochin-22, India*

[d] *Department of Physics, CUSAT, Cochin-22, India*

[e] *Polymer Science and Rubber Technology, CUSAT, Cochin, India*

* *e-mail id: sonachalil@gmail.com*

Abstract

Design and synthesis of conjugated polymers is important to the development of organic photonic devices. With the extensive use of high power laser in various applications, much interest is currently being directed towards the search for new nonlinear optical materials for good optical limiters, to protect human eyes and sensitive optical devices from intense laser damages. Conjugated phenothiazine-N-piperidine substituted triazine copolymer, (P(PH-TZ)) has been designed by employing density functional theory (DFT) in the periodic boundary condition (PBC) formalism at HSE06 and B3LYP level of theory. Copolymer was synthesized via standard Suzuki cross-coupling method. The copolymer exhibited optical band gap of 2.5 and 2.2 eV in THF solution and as thin film, respectively. The optical band gap value is in good agreement with theoretical prediction. Third-order nonlinear optical properties of the copolymer were investigated by simple method, Z-scan technique. The copolymer showed third-order nonlinear optical susceptibility and optical limiting threshold of 1.27×10^{-11} esu and 0.22 GW/cm^2, respectively.

Keywords: *phenothiazine; s-triazine; suzuki polymerization; nonlinear optical property*

Introduction

Organic π-conjugated structures with 1,3,5-triazine as the core unit have received significant attention due to their promising applications in liquid crystalline materials,[1,2] magnetic materials,[3] solar cells[4,5] and light emitting diodes (LEDs).[6] Owing to their high thermal stability, polymers containing 1,3,5-triazine unit are widely used in industry. Recently, some new polymers bearing 1,3,5-triazine units have been reported.[6,7] The π-conjugated organic compounds have emerged as promising candidates due to their fast response time, large third-order susceptibility and processability.[8] The nonlinear optical (NLO) properties of organic molecules can be tuned by adopting suitable synthetic strategies, such as donor–π–acceptor (D–π–A), donor–π–donor (D–π–D), donor–acceptor–donor (D–A–D), and acceptor–donor–acceptor (A–D–A).[9] Here, we are mainly interested in the alternating donor-acceptor copolymer since their optoelectronic properties can be tuned by efficient intramolecular charge transfer. The strong donor-acceptor intramolecular interaction and delocalized π-electron system yields NLO properties in π conjugated organic compounds. This in turn intrigued our research interest in the third-order NLO behaviour of D-π-A type copolymer, P(PH-TZ). In this paper, we discuss the electronic structure, synthesis and optical properties of phenothiazine-triazine copolymer and have demonstrated the applicability of the polymer as active material in nonlinear optical devices.

Experimental

All the chemicals used were of analytical grade and used as received. The solvents used were dried and distilled when necessary according to standard procedures. The nonlinear optical property of the copolymer was measured by Z-scan technique performed with a Q-switched Nd:YAG laser system (Spectra Physics LAB-1760) continuum with pulse width of 7 ns at 10 Hz repetition rate

and 532 nm wavelength. A solution of 1 mm cell of the sample in THF at 1.0 $\times 10^{-3}$ mol/L was put in the light path, and all measurements were carried out at room temperature. The relation between the normalized transmittance T(z) and z position was obtained by moving the samples along the axis of the incident beam (z-direction) with respect to the focal point. The incident and transmitted energies were detected simultaneously by an energy meter (REj7620, Laser Probe Corp.). The input energy applied was 112 μJ. The data were analyzed by using the procedure described by Bahae et al.,[10] and the nonlinear optical coefficients were obtained by fitting the experimental z-scan plot with the theoretical plots.

Results and discussion

Theoretical calculation

All the DFT[11] calculations were carried with Gaussian 09 program. The monomer geometries were optimized by B3LYP/631-G method. Figure 1 shows the frontier molecular orbitals of monomeric unit, PH-TZ. It reveals that the HOMO (highest occupied molecular orbital) level of PH-TZ was located on phenothiazine unit and LUMO (lowest unoccupied molecular orbital) level was located on triazine moieties. This large degree of polarization might be responsible for the small band gap value for P(PH-TZ) compared to homopolymer, poly(phenothiazine) (P(PH)).

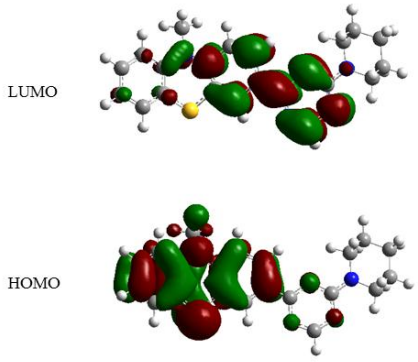


Figure 1: Frontier molecular orbital distribution of monomeric unit of P(PH-TZ) by B3LYP/6-31G method.

The electronic properties of the P(PH) and P(PH-TZ) were studied by PBC calculation at two different energy levels (B3LYP/6-31G and HSE06/6-31G) and the band structure obtained by HSE06/6-31G level have been plotted in Figure 2.

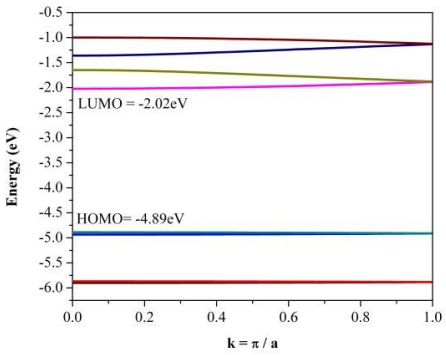


Figure 2: Band structure of P(PH-TZ) by HSE06/6-31G method.

Table 1 lists the calculated theoretical HOMO-LUMO energy levels and band gaps of the homopolymer, (P(PH)) and copolymer, P(PH-TZ). The lower band gap of P(PH-TZ) compared to that of P(PH), indicated a significant effect of intramolecular charge transfer between the phenothiazine and triazine moieties.

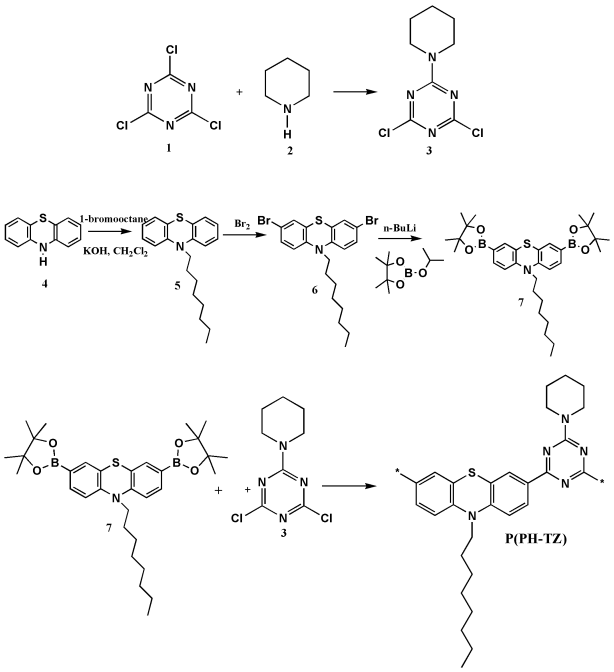
Table 1. Computational data of P(PH) and P(PH-TZ) with DFT/B3LYP/6-31G and DFT/HSE06/6-31G methods.

Polymer	HOMO (eV)	LUMO (eV)	E_g (eV)
P(PH)	-4.76	-1.41	3.35
P(PH-TZ)[a]	-5.02	-1.75	3.27
P(PH-TZ)[b]	-4.89	-2.02	2.87

[a]Obtained by the DFT/B3LYP/6-31G method, [b]Obtained by the DFT/HSE06/6-31G method.

Synthesis and Characterization

The synthetic procedures towards the synthesis of monomers and copolymer are outlined in Scheme 1. Suzuki polycondensation reaction was used to synthesize phenothiazine-triazine polymer, P(PH-TZ). Repeated purification by soxhlet extraction was performed using methanol and hexane to remove oligomers and dried under reduced pressure. The polymer was obtained as yellowish green powder with 60 % of yield.



Scheme 1: Synthesis of copolymer, P(PH-TZ)

The copolymer was readily soluble in common organic solvents, such as THF, chloroform, dichloromethane and chlorobenzene. The molecular weight of polymer was determined by gel permeation chromatography (GPC) in THF referring to polystyrene standards. GPC analysis showed that copolymer had number average molecular weight (Mn) of 3580, weight average molecular weight (Mw) of 4928 and polydispersity index (PDI) of 1.66. The molecular structure of the copolymer was verified by FT-IR, ^{1}H NMR and XPS analysis. Results clearly indicated that copolymerization was successfully achieved.

The photophysical characteristics of copolymer were investigated by both UV-visible absorption (Figure 3) and photoluminescence (PL) spectra in dilute THF solution and as thin film. The optical band gap of P(PH-TZ) was calculated to be 2.5 eV, from the cut-off wavelength of optical absorption in THF solution.

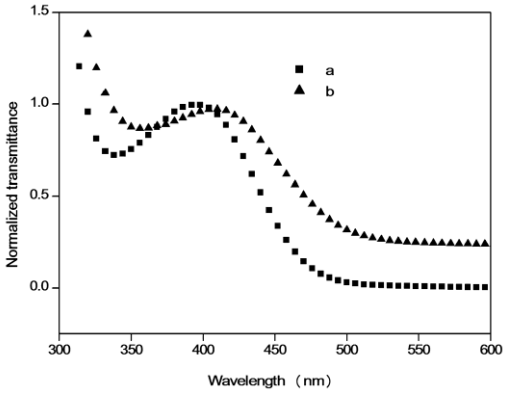


Figure 3: UV-visible spectra of copolymer, P(PH-TZ) in (a) THF solution and (b) as thin film.

Optical band gap derived from the absorption edge of the polymer film was 2.3 eV, differed 0.2 eV, from the solution band gap. As expected, the copolymer has lower band gap than the conjugated homopolymer, poly(phenothiazine) (2.76 eV)[12] due to better charge transfer between the units. The PL emission maximum of P(PH-TZ) in THF solution and film are observed at 529 and 535 nm, respectively.

Nonlinear optical (NLO) properties

The measurement of third-order NLO properties of copolymer, P(PH-TZ) was performed with the z-scan technique at 532 nm by the reported method.[10] The open-aperture (OA) z-scan signal in dilute $CHCl_3$ is shown in Figure 4. The normalized transmittance valley of light at the focus suggests that the copolymer is reverse saturation absorber (RSA) with positive NLO absorption coefficient.

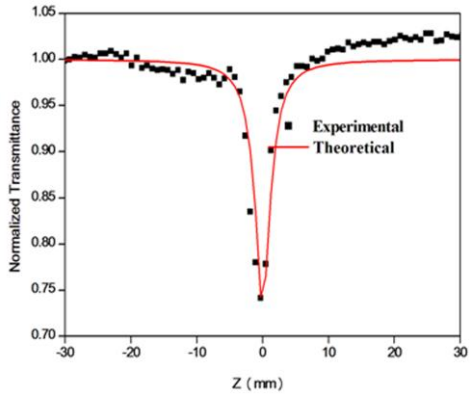


Figure 4: Open aperture z-scan trace of P(PH-TZ).

The nonlinear optical absorption coefficient, β is obtained by fitting the experimental data using equation:[47] $T(z)=\frac{C}{q_0\sqrt{\pi}}\int_{-\infty}^{\infty}\ln(1+q_0\,e^{-t^2})\,dt$ and it is obtained to be 3.75×10^{-10} m/W.

Optical limiting property

An optical power limiter is a device which has very high transmission for weak optical signals, but becomes opaque for intense optical signals.[13] The optical power limiting property is mainly due to nonlinear absorption property of a molecule. The optical power limiting behavior of the polymer obtained from the OA z-scan curve is shown in Figure 5.

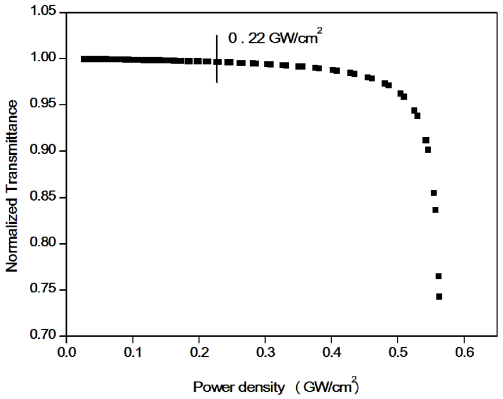


Figure 5: Optical limiting curve of P(PH-TZ).

The optical limiting threshold will determine the ability of the limiter. The lower the limiting threshold value, the better is the optical limiter. Optical limiting threshold of the copolymer, P(PH-TZ) is obtained to be 0.22 GW/cm^2.

Conclusions

In conclusion, we have developed a new soluble conjugated copolymer of phenothiazine and triazine via standard Suzuki coupling reaction. Structural characterization was performed by FT-IR, ^{1}H NMR and XPS. We have performed a theoretical investigation on the copolymer, P(PH-TZ) using density functional theory calculations at two different energy levels. The band gap obtained by DFT/HSE06 method reveals good agreement with the optical band gap. Compared to the homopolymer, copolymer exhibited decreased band gap value (2.5 eV) and red shifted emission. The third-order nonlinear optical parameters were studied using z-scan technique. The z-scan results indicate that the polymer exhibits positive nonlinear absorption and it is calculated to be 3.75×10^{-10} m/W. The copolymer exhibits optical power limiting behaviour at 532 nm wavelength. Hence, the polymer investigated seem to be promising candidate for photonic and optoelectronic applications.

Acknowledgements

The authors gratefully acknowledge financial support from University Grants Commission Kothari Cell (UGC-DSKPDF) and Department of Science and Technology (DST).

References

1. C. -H. Lee, T. Yamamoto, *Tetrahedron Lett*., 2001, 42, 3993.

2. R. Bai, S. Li, Y. Zou, C. Pan, *Liq. Cryst*., 2001, 28, 1873.

3. S. Hayami, K. Inoue, *Chem. Lett*., 1999, 28, 545.

4. Y. Zhou, L. Wang, J. Wang, J. Pei, Y. Cao, *Adv. Mater*., 2008, 20, 3745.

5. O. Alévêque, P. Leriche, N. Cocherel, P. Frère, A. Cravino, J. Roncali, *Sol. Energy Mater. Sol. Cells*, 2008, 92, 1170.

6. P. Zhou, C. Zhong, X. Chen, J. Qin, I. Mariz, E. Maçôas, *Macromolecules*, 2014, 47, 6679.

7. D. Saikia, C. -G. Wu, J. Fang, L. -D. Tsai, H. -M. Kao, *J. Power Sources*, 2014, 269, 651.

8. H. S. Nalwa, S. Miyata, Nonlinear optics of organic molecules and polymers, CRC Press, Boca Raton, Florida, 1997.

9. M. Albota, D. Beljonne, J. L. Brebas, J. E. Ehrlich, J. Y. Fu, A. A. Heikal, S. E. Hess, J. T. Koge, M. D. Levin, R. S. Marder, D. M. Maughon , J. W. Perry, H. Rockel, M. Rumi, G. Subramaniam, W. W. Watt, X. L. Wu, C. Xu, *Science*, 1998, 281, 1653.

10. M. Sheik-bahae, A. A. Said, T.-H. Wei, D. J. Hagan, E. W. Van Stryland, IEEE *J. Quantum Electron*., 1990, 26, 760.

11. R. G. Parr, W. Yang, Density-Functional Theory of Atoms and Molecules, Oxford University Press, New York, 1989.

12. X. Kong, A. P. Kulkarni, S. A. Jenekhe, *Macromolecules*, 2003, 36, 8992.

13. G. S. He, G. C. Xu, P. N. Prasad, B. A. Reinhardt, J. C. Bhatt, A. G. Dillard, *Opt. Lett.*, 1995, 20, 35.

MACRO 292

Synthesis of N-Vinyl Pyrrolidone Based Smart Polymers and their Application as Self- Immolative Polyprodrug and Targeted Delivery Vehicles

Maiti, Saikat; Dhara, Dibakar*

Department of Chemistry

Indian Institute of Technology Kharagpur
West Bengal 721302 India

** Email: dibakar@chem.iitkgp.ernet.in*

Poly(N-vinyl pyrrolidone) (PVP) is an attractive polymer for its pharmaceutical applications such as in drug delivery or tissue engineering. PVP is neutral amphiphilic, nontoxic, and biocompatible with living tissue and soluble in water as well as in many organic solvents. However, due to the unavailability of the functional groups along the polymeric chains, the biotechnological and bioconjugation application of PVP is somehow restricted. To overcome this problem, N-vinyl pyrrolione (NVP) has been substituted at the 3- position with different types of substituent. The random copolymers of NVP and 3-substituted NVP show excellent temperature responsiveness and exhibit lower critical solution temperature (LCST) in water. The LCST of the copolymeric systems can be regulated by changing the feed ratio of NVP and 3-substituted NVP. In this presentation, we report various thermoresponsive copolymers of NVP and 3-substituted NVP monomers containing other stimuli (pH, enzyme, and reduction/oxidation) responsive groups producing smart delivery vehicles with multi stimuli responsive behavior. Additionally, the polymeric systems were made specific to the cancer cells through the incorporation of the targeted agents like folic acid, biotin, or sugar moiety in the polymeric chain. Moreover, anticancer drug molecules were covalently conjugated to some the copolymers through stimuli-labile covalent bonds making the copolymers as potential anti-cancer prodrugs.

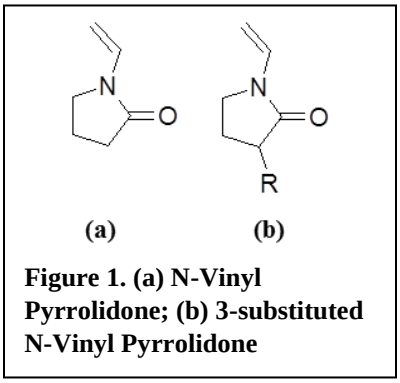


Figure 1. (a) N-Vinyl Pyrrolidone; (b) 3-substituted N-Vinyl Pyrrolidone

References

1. Chen, G-T; Wang, C-H; Zhang, J-G; Wang, Y; Zhang, R; Du, F-S; Yan, N; Kou, Y*; and Li, Z-C*. *Macromolecules*, 43 (2010) 9972.
2. Maiti, S.; Dhara, D. Unpublished results.

MACRO 295

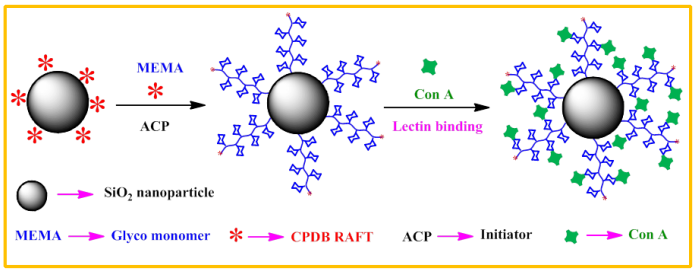
Synthesis of Lectin Binding Glycopolymer Coated Silica Nanoparticles using *Grafting from* RAFT Polymerization

*S N Raju Kutcherlapati, Rambabu Koilapu, Tushar Jana**
School of Chemistry, University of Hyderabad, Hyderabad-500 046
E-mail: tusharjana@uohyd.ac.in

Abstract

Here, we report the synthesis of glycopolymer (GP) grafted silica nanoparticles (SiO_2) called as GNPs by using Reversible Addition Fragmentation chain Transfer (RAFT) polymerization through *grafting from* approach. The glycopolymer chains have been synthesized from RAFT attached SiO_2 nanoparticles using mannosyloxyethyl methacrylate (MEMA) as a monomer and 4,4′-Azobis(4-cyanopentanoic acid) (ACP) as an initiator in DMF as well as water / ethanol mixture for different chain length as well as different chain density of glycopolymers on the surface of SiO_2 nanoparticles. The surface functionalization of glycopolymers on SiNPs is confirmed by fourier transform infrared spectroscopy (FTIR), nuclear magnetic resonance spectroscopy (NMR) and thermo gravimetric analysis (TGA). The mean diameter of the GNPs is measured by transmission electron microscopy (TEM) and hydrodynamic diameter is obtained by dynamic light scattering (DLS). These GNPs shows strong binding with mannose specific lectin Con A, and was studied by using Isothermal Titration Calorimetry (ITC) and proves to be valuable tools for further investigating glycobiological, biomedical, material science and especially in our case mannose functionalized SiNPs (GNPs) can be used as targeting cancerous cells.

Keywords: *Carbohydrates; glycopolymers; RAFT polymerization; protein binding.*



Introduction

Carbohydrates have the highest abundance of all biomolecules in nature. They participate and perform many biological things, for example energy storage and metabolic intermediates. The carbohydrates which are conjugated to proteins or lipids mediate many biological processes like molecular recognition, signal transduction, cell adhesion, inflammation and molecular trafficking. However, the interaction between carbohydrates and proteins is in general recognized to be with very low affinity and this can be compensated by presenting multiple ligands (as glycopolymers) to receptors leads to multivalent interaction,[1] thus increasing the interaction of multi valent ligands with their corresponding receptors by manifold than corresponding monovalent interaction.[2]

The synthesis of glycopolymers with different morphologies is an important topic towards understanding how these glycopolymers behave with their corresponding receptors and more importantly the polymer morphology has a profound influence on the binding between glycopolymer and their corresponding proteins. For this reason and to study carbohydrate–carbohydrate and carbohydrate–protein interactions there is a need to develop a versatile method for the preparation of these glycopolymers especially in the form of glyconanoconjugates. The development of carbohydrate functionalized nanomaterials is the topic of interest towards the understanding of lectin-carbohydrate interactions, which play crucial roles in a variety of biological processes, including fertilization, cell migration, cancer therapy, and host-pathogen interactions.[3]

In particular, silica nanoparticles provide several interesting features like they are biocompatible as well as low toxicity. Therefore, carbohydrate modified SiNPs nanoparticles have recently attracted much attention for understanding lectin-carbohydrate interactions and find applications in a variety of biological processes, including fertilization, cell migration, cancer therapy, and host-pathogen interactions. Carbohydrate modified SiNPs nanoparticles were able to target exactly at the site of tumor cells, owing to cancer cell death leaving the normal tissue unaffected.

A number of methods have been practiced to modify nanoparticle surfaces with polymers. More often, polymers are attached to nanoparticle surfaces by the covalent linkages. Generally, for grafting carbohydrates on nanoparticle surfaces several different conjugation chemistries have here been used, including CuAAC, amide coupling, nucleophilic substitution, and photo coupling.[2] Usually, two methods are used for modification of nanoparticle surfaces with polymers. Where, one is grafting polymer chains to the nanoparticle (*grafting to*), or two, the grafting reaction can be proceed by polymerizing monomers from the nanoparticle surface (*grafting from*). In both cases, a thin polymer layer can be formed on the nanoparticle surface. However, in *grafting to* method is simple to be performed, but the graft density is fairly low since the diffusion of oligomeric/polymer chains to the particle surface is sterically hindered. Therefore, we have chosen the *grafting from* the method to graft GP onto the surface of SiNPs.

Various polymerization techniques, including conventional free radical, cationic, anionic], ring-opening and controlled radical polymerizations (CRPs) have been used for grafting polymers on the surface of a class of inorganic particles among which, CRPs have more advantages because they can control the architecture, molecular weight and molecular weight distribution when compared to the conventional radical polymerization. Amongst the CRPs, nitroxide-mediated polymerization (NMP), atom transfer radical polymerization (ATRP) and reversible addition fragmentation chain transfer polymerization (RAFT) have been used to graft polymers from nanoparticle surface. Comparing to the NMP and ATRP, RAFT polymerization exhibits the advantage on compatibility with a wide range of monomers including functional monomers and free of transition metal ion contamination more over reactions can be conducted in mild conditions and proven to be a versatile approach for grafting organic polymers with controlled molar mass, composition, and functionality on both planar as well as nanoparticles particle surfaces.[4]

In consideration of this background, to the best of our knowledge no report studied the controlled radical polymerization of a glycopolymer from the surface of a SiNP using *grafting from* RAFT polymerization. In this work, we report the structurally well-defined, glycopolymer-SiNP hybrids were prepared by modifying the surface of SINPs with RAFT agent and then GP grafted SiNP was prepared using the *grafting from* RAFT-controlled radical polymerization method.

Experimental

The synthesis CPDB, SiO_2 and SiO_2-CPDB were conducted according to the literature reported procedures.

Polymerization of MEMA using SiO_2-CPDB

We have carried out the reactions in two different solvents (water: ethanol mixture 7:3 ratio and DMF) to check the suitability of solvent so as to get good amount of glycopolymer loading on particle surface.

DMF based reactions:

Into a series of Schlenk tubes containing DMF (1.4 mL), SiO_2-CPDB (0.1 g, 7.607 μmol by RAFT), MEMA (calculated amount, we have varied for different chain lengths), free CPDB (2.13 mg, 7.607 μmol) and ACP (0.426 mg, 1.521 μmol) were added by keeping [SiO_2-CPDB]: [free CPDB]: [ACP] = 1:1:0.2 constant throughout all the reactions. These reaction vials were then sealed and subjected to three freeze-pump-thaw cycles followed by sonication for 10 min and stirred for 16 h in preheated oil bath at 70 ^oC. After completion the reaction, the reaction mixture was quenched using liquid nitrogen, the glycopolymer coated particles were precipitated from large excess of hexane and isolated by using centrifugation. The obtained precipitate was redispersed in methanol (40 mL) and centrifuged at the rate 7000 rpm for 30 min. This step was repeated for thrice and the obtained glycopolymers were dried under vacuum at 70 ^oC for 48 h. We have altered the amount of sugar monomer in the reaction medium by keeping all the other reagents constant so as to obtain different chain length of glycopolymer chain on the particle surface and finally cleavage of the GP from the GP-grafted silica was carried out according to the procedure described elsewhere.[4] The recovered GP was then subjected to GPC analysis.

Results and discussion

In this article, we report the successful grafting of glycopolymers on silica nanoparticles using *grafting from* RAFT polymerization. The activated RAFT agent was attached to silica nanoparticles by reacting with amine modified SiO_2 nanoparticles and the FESEM and TEM images of bare SiO_2, SiO_2-NH_2 and SiO_2-CPDB are presented in supporting information Fig S2.

Fig. 1compares the FT-IR spectrum of the SiO_2-CPDB (Fig. 1) produced in this work with those which in turn from the bare SiO_2 (Fig. 1a). The FT-IR spectrum of SiO_2-CPDB (Fig. 1b) shows a sharp band at 1645 cm^{-1}, which is attributed to the C=O stretching of the amide carbonyl, also a peak at 1551 cm^{-1} is attributed to the C-N stretching and N-H bending from the amide group. Although the characteristic bands of thiocarbonyl (C=S) around 1060 cm^{-1} overlapped with the strong absorption of the bare silica (Fig. 1a), a band at 2948 cm^{-1} is for alkyl C-H stretching, the band at 1450 cm^{-1} is attributed to phenyl ring from CPDB RAFT agent and a band at 2254 cm^{-1} is attributed to cyano group in the CPDB. This indicates that the dithiobenzoate group of CPDB RAFT agent is covalently attached to the surface of the silica particles.

Fig. S3 shows the TGA analysis of bare SiO_2, SiO_2-NH_2 and SiO_2-CPDB. As can be seen from the figure the final weight loss is increasing from bare SiO_2 to SiO_2-NH_2 to SiO_2-CPDB indicates that the attachment organic groups (propyl amine or CPDB) to the surface of the SiO_2 nanoparticles. The relative amount of RAFT (CPDB) agent which is covalently attached on the SiO_2 nanoparticles was calculated by using TGA analysis as explained elseware. Calculation based on TGA shows that the content of dithiobenzoate group on the particles is 21.3 mg/g (76 μmol/g).

MEMA monomer initially was synthesized using established literature protocol as explained in the experimental section (Scheme 1) and $^{1}H/^{13}C$ NMR were presented in supporting information Fig. S1 SiO_2-CPDB particles was used for the RAFT mediated controlled radical polymerization of MEMA in two different solvents initially, water/ethanol mixture (7:3) or DMF (Scheme 3). We have performed the polymerization of MEMA in the presence of SiO_2-CPDB and CPDB as a free chain transfer agent using ACP as an thermal initiator at 70 °C by keeping [SiO_2-CPDB]: [free CPDB]: [ACP] = 1:1:0.2 constant, with a variation of MEMA to get different chain lengths

The relative amount of GP grafted to silica particles in the products can be estimated by TGA method. Fig. 2 shows the TGA curves for the SiO_2-CPDB, GP grafted SiO_2 nanoparticles and polyMEMA prepared using two different solvents and obtained after purification. The decomposition temperature range is 250-600 °C for all the TGA curves shown in Fig. 2. Assuming that the GP is decomposed completely, as can be seen from the TGA graphs with increase in GP chain length the final weight loss is increasing attributing that the more amount of GP loading on the SiO_2 nanoparticle surface. This result can be better understand by keeping it in mind that the same no of initiating groups on the particle surface and with increase in GP chain length will increase the amount of GP attached to the particle surface.

Fig.2. TGA analysis of GP grafted SiO_2 nanoparticles obtained after purification for different chain lengths in water/ethanol (A), DMF (B) as a solvent. The details of individual components are presented in the figure.

Fig. 3 shows the FT-IR spectra of SiO_2-CPDB, GP grafted SiO_2 and polyMEMA. FT-IR spectrum of GP grafted SiO_2 (Fig. 3b) show a peak around 1217 cm^{-1}, which correspond to C-O bond stretching of the mannose moiety, which is also apparent in the polyMEMA (Fig. 3c). The bands observed at 1379 cm^{-1} and 1735 cm^{-1} is assigned to the C-O-C group and C-O ester double bond of the mannose sugar, which is also observed in polyMEMA (Fig. 3c). Further the band observed around 2890−2985 cm^{-1} is attributed to the C-H stretching of the alkyl (polymer backbone) chains. The FT-IR spectrum of GP grafted SiO_2 (Fig. 3b) shows a broad peak around 3150−3600 cm^{-1} attributed to vibrations of the four −OH groups of the mannose moiety. The broad band observed at 1020−1250 cm^{-1} is attributed to Si-O, C-O, Si-CH2 and C-OH. The broadening and the high intensity of this peak are due to the four hydroxyl (-OH) groups of the mannose as well as Si-O bond, which can be clearly seen in both spectra in Fig a, b and c. All these observations confirm that the SiO_2 are grafted with GP.

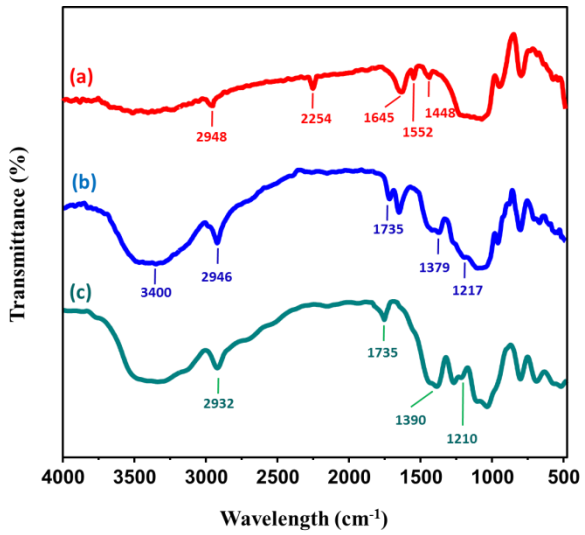


Fig. 3 FT-IR spectra of (a) SiO_2-CPDB, (b) GP grafted SiO_2 and (c) polyMEMA.

Fig. 4 shows the FE-SEM and TEM images of GP grafted SiO_2 nanoparticles. The surface of SiO_2-CPDB (Fig. S2c) is smooth and without roughness, but in case of GP grafted SiO_2 nanoparticles show a rough surface, and also the gray surface layer of the silica particles in TEM images (right panel) is visible clearly, which is attributed to the GP formed on their surface. The increase in particle agglomeration with chain length in GP grafted nanoparticles when compared with their precursor SiO_2-CPDB (Fig. S2c) and the increase in particle size from 48 nm (±2, SiO_2-CPDB) to 57 nm (±4, P6) after grafting the GP chains may reveal that the GP chains are chemically bound to the silica nanoparticles. FE-SEM and TEM analysis of the SiO_2 nanoparticles before and after reaction showed that the shape and size distribution of the particles remained unchanged, indicating that the nanoparticles were stable under the used conditions.

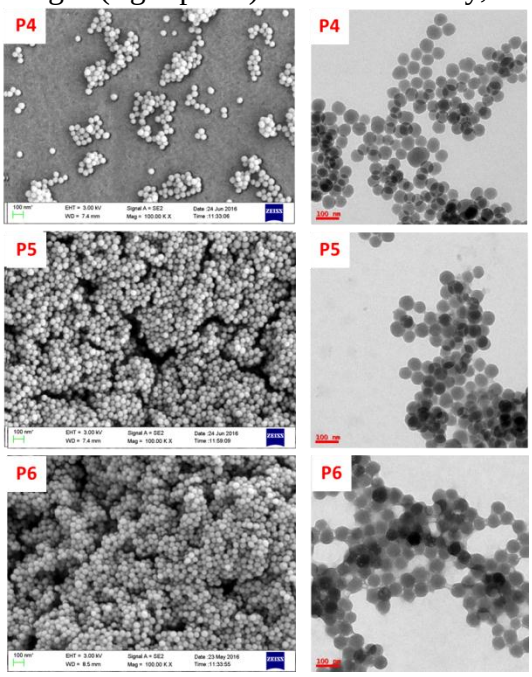


Fig. 4 FE-SEM images (left panel) and TEM images (right panel) of GP grafted SiO_2 nanoparticles and he details of individual components are presented in the figure.

^{13}C-NMR spectra of GP grafted SiO_2 nanoparticles in D_2O solvent is presented in Fig. 5a. In the spectrum, a peak at 170.9 ppm attributes the carbonyl carbon (C=O) of the ester from the polyMEMA. The peak at 105.8 ppm is due to the anomeric carbon of mannose in MEMA. The 7 peaks between 64 ppm to 77 ppm is attributed to the five remaining carbon from the mannose ring and the remaining two peaks is due to the ethylene part of MEMA. Two peaks at 48.6 ppm and 29.2 ppm is due to the polymer backbone indicating the successful grafting of MEMA on the SiO_2 nanoparticle surface.

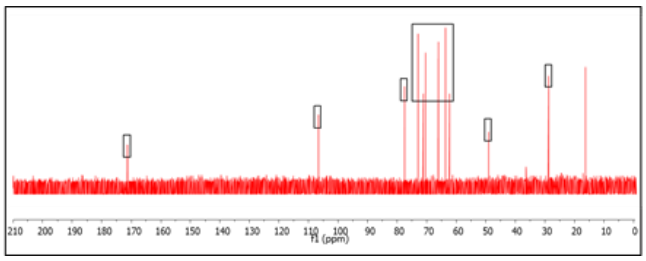
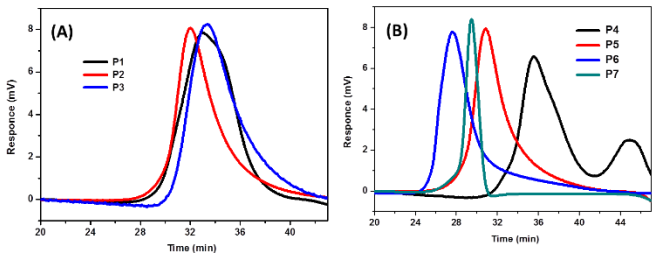


Fig. 5 13 C NMR spectra of GP grafted SiO_2 nanoparticles

The particle size and size distribution of GP grafted SiO_2 nanoparticles were measured in water by using DLS and presented in Fig. 5b and 5c . Fig 5b and 5c, shows the size distribution of GP grafted SiO_2 nanoparticles. Even though the core (SiO_2-CPDB) diameter of all the particles are same (as prepared from the same sample of CPDB-SiO_2), the hydrodynamic diameter of GP grafted SiO_2 nanoparticles are increased by two to three fold indicating that the GP grafted SiO_2 nanoparticles possesses the graft polyMEMA chains which are highly hydrophilic and are in the swollen state and the size from DLS in proportional to the GP chain length on the particle surface. These above results indicate that the grafting of GP on the SiO_2 nanoparticle surface was successfully achieved by RAFT mediated controlled radical polymerization of MEMA using SiO_2-CPDB. Information about the molecular weights and molecular weight distributions of the grafted polyMEMA chains were measured using GPC and



presented in Fig. 6a and 6b. As shown in Fig. 6a and 6b, the GPC curves are all symmetric and unimodal, the narrow GPC curves indicate that the polymerization proceeded in a controlled manner. The narrow PDI values (<1.3) indicated that the polymerization proceeded in accordance with a controlled/living radical polymerization mechanism.

Fig. 6. GPC curves of GP chains cleaved from GP grafted SiO_2 nanoparticles

Conclusions

A mannose containing glycopolymer chain was grown on the surface of SiNP using a *grafting from* RAFT polymerization. The chain length of the GP on the SiO_2 nanoparticle surface has been varied and the resulting SiNP grafted GP core-shell particles displays a narrow size distributions obtained from GPC analysis after cleaving the GP from the SiO_2 nanoparticles confirms the formation of GP grafted SiO_2. The microscopic, spectroscopic, thermal and DLS studies unequivocally confirms the formation of silica (core) -glycopolymer (shell) particles. The mannose containing GP grafted SiO_2 nanoparticles retained their binding affinity and selectivity towards lectin Con A and was studied using ITC. The present methodology delivers a controlled synthesis of well-defined core-shell nanoparticles with protein binding glycopolymer on the surface of the particles which may be useful for delivering new carbohydrate based therapeutics.

Acknowledgements

SNRK thanks the CSIR-SRF for fellowship. and Industrial Research (CSIR), Govt. of India for the research funding

References

3. C. Bartholome, E. Beyou, N. Zydowicz, *Polymer* 46, 8502, 2005.
4. A. Dureault, D. Taton, Y. Gnanou, *Macromolecules* 37, 5513, 2004.
5. Q. Zheng, CY. Pan. *Macromolecules* 38, 6841. 2005.
6. K. W. Jayawadena, S. A. Wijesundera, M. Yan, Chem. Commun. 51, 15964, 2015.

MACRO 303

Synthesis and Characterization of Blue Emitting Materials for Organic Light Emitting Diode Applications

Kaur Banpreet, Jacob Josemon*
Centre for Polymer Science and Engineering, Indian Institute of Technology Delhi Hauz Khas, New Delhi

jacob@polymers.iitd.ac.in

Blue emitting materials have attracted considerable scientific and industrial interest, since electroluminescence using small organic molecules was first demonstrated by Tang and VanSlyke [1]. This

was soon extended to polymers by Prof. Friend and co-workers [2] and led to the development of Organic Light Emitting Diode (OLED) technology. OLED technology since then has garnered significant interest due to its applications in full colour displays and solid state lighting. They possess the advantages of flexibility, low cost and low power consumption. To realize full colour display, highly efficient red-, green- and blue- emitting materials of equal stability and colour purity are required. However, highly pure and stable blue emission is still a challenging task [3]. High performance blue emitters are difficult to generate because of the presence of intrinsic wide band gap, which makes it hard to inject charges into emitters. Some of the prerequisites for blue emitting materials are - appropriate molecular mass for solution processability, good thermal and morphological stabilities. Otherwise, the formation of aggregates, or keto-defects, lead to emissions different than that of desired colour.

The present work is aimed at developing truxene (10,15-dihydro-5H-diindeno[1,2-a;10 ,20 -c]fluorene) based blue emitting materials, utilizing various cross-coupling reactions. This heptacyclic polyarene with C_3 symmetry, has been found to possess high thermal stability, with T_d>300^{o}C, which along with the ease of chemical tailoring makes truxene derivatives highly suitable candidates as blue emitters [4]. To obtain the target molecules, functionalization of the core by side moieties was done by Palladium catalyzed- Suzuki and the Buchwald-Hartwig cross coupling reactions. To improve the solution processability of the material, long and branched alkyl chains were used as substituents. The synthesized derivatives were purified through recrystallization and column chromatography and were characterized by ^{1}H-NMR and ^{13}C-NMR technique. The coupling of the truxene core with bulky aryl groups removes the planarity of the truxene core resulting in a three dimensional structure, thus preventing stacking. The basic optical properties- UV-vis and photoluminescence, of the materials were investigated in tetrahydrofuran solution and in film. From the absorption spectra, λ_{max} was observed at 356 nm (T_1) and 330 nm (T_5), exhibiting a red shift due to increased effective π-conjugation, in comparison with the truxene moiety (307 nm). From the emission spectra, λ_{max} for emission was observed at 425 nm (T_1) and 385 nm (T_5). Also, electrochemical studies were done using cyclic voltammetry for the determination of the band gap of the synthesized molecules. The preliminary optical and electrochemical investigations indicate that the materials emit blue colour in solutions.

References

1. Tang, C. W.; VanSlyke, S. A. *Appl. Phys. Lett* .(1987), 51(12), 913-15
2. Burroughes, J. H.; Bradley, D. D. C.; Brown, A. R.; Marks, R. N.; Mackay, K.; Friend, R. H.; Burn, P. L.; Holmes, A. B. *Nature* (1990),347, 539.
3. Schols, S. Device Architecture and Materials for Organic Light-Emitting Devices; Springer, (2011); pp. 1–171
4. Pei, J.; Wang, J.; Cao, X.; Zhou, X.; Zhang, W. *J. Am. Chem. Soc*. (2003) 9944-9945

MACRO 313

Synthesis and Characterization Of β-CD Induced Block Copolymers via ARGET-ATRP of Vinyl and Acrylate monomers

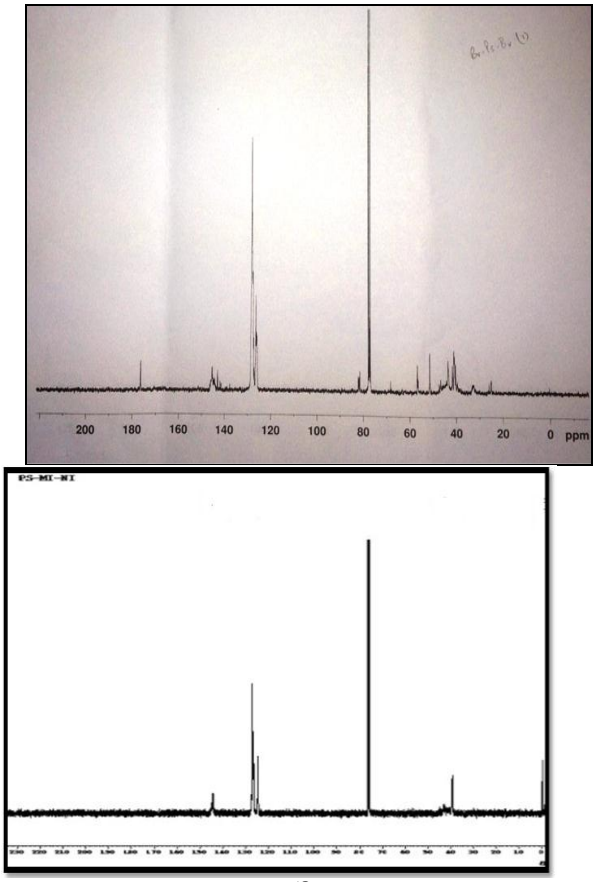
Karkare P., Murthy C. N.*[a]

[a]*Macromolecular Materials Laboratory, Applied Chemistry Department , Faculty of Technology and Engineering, The Maharaja Sayajirao University of Baroda, Vadodara, India.*

The synthesis of block copolymers (BCP) with precise and controllable architecture is of immense technological importance due to their applications in drug delivery,

protein-polymer conjugates, stimuli responsive assemblies and to polymer-inorganic hybrid materials [1,2]. Among the all controlled polymerization techniques, atom transfer radical polymerization has shown to be versatile and easily approachable technique even in aqueous systems [3].

Activators regenerated by electron transfer atom transfer radical polymerization (ARGET-ATRP) is the technique in the prime focus since last few years since it uses simple reducing agents such as ascorbic acid, glucose, phenols, hydrazines, sulphites but unfortunately this numbers is limited to very few due to the limitation of solubility and the regeneration of the reducing activity. Cyclodextrin and their derivatives are interesting molecules for supramolecular host-guest structures and recently we have found then to have active reducing character for the synthesis of core-shell silver@gold and gold@silver nanoparticles [4]. In present work we utilise the reducing character of cyclodextrin for the regeneration of activators for the ATRP. We synthesized two different molecular weight domain di-functional polystyrene macroinitiators using dimethyl 2,6-dibromo heptanedioate (DMDBHD) and 1,3-dibromo propane (1,3-DBP) via ATRP. These macroinitiators were used were used in block copolymerization with acrylates in aqueous and in solvent systems as well. The control over the molecular weight was comparable for the di-functional polystyrene macroinitiators and tri, penta – block copolymers. The effect of molecular weight on the efficiency of block copolymerization was studied. The resultant macroinitiators and block copolymers were characterized by Gel Permeation Chromatography (GPC), C^{13}-NMR for the carbon sequence, Thermogravimetric analysis (TGA), Fourier Transform Infrared Spectroscopy (FT-IR), Differential Scanning Calorimeter (DSC). The morphology study was characterized by Transmission Electron Microscope (TEM). These results will be discussed in this presentation.



C^{13}-NMR (PS macroinitiator with DMDBHD) C^{13}-NMR (PS macroinitiator with 1,3-DBP)

References

5. Massimo L; Guojun L; Sebastien L. *Block Copolymers in Nanoscience*, Weinheim: Germany. Wiley-VCH (2006).
6. Kumar, S.; Lee, J-S.; Murthy C. N.; *Macromole. Res*. 19 (2011) 10.
7. Matyjaszewski K.; Tsarevsky N. V. *J. Am. Chem. Soc*, 18 (2014) 136.
8. Bhoi, V. I., Kumar S.; Murthy C. N., *New J. Chem.*,40 (2016) 1396.

MACRO 314

Synthesis and Aggregation Behavior of Poly(2-oxazoline)-Based Light- and Thermo-responsive Block and Random Copolymers

Jana Somdeb, Saha Anupam, Bose, Avijit and Mandal, Tarun Kumar*

Polymer Science Unit, Indian Association for the Cultivation of Science,

Jadavpur, Kolkata 700 032, India

*E-mail: psutkm@iacs.res.in

Recent direction of polymer research has been dedicated to the design and development of "environmentally sensitive" smart macromolecules that are sensitive to several physical, chemical or biochemical stimuli. Here, we report the synthesis of photoresponsive poly(2-ethyl-2-oxazoline)-*block*-poly(2-nitrobenzyl acrylate) (PEtOx-*b*-PNBA) block copolymers (BCPs) via combination of microwave-assisted cationic ring-opening polymerization (ROP) and ATRP techniques.[1] The amphiphilic nature of this BCP direct them to self-assemble into unit micelles in THF/H_2O, which further undergo secondary aggregation into nanostructured compound micelles. Upon UV light irradiation, the photocleavage of the PNBA block of the BCP leads to the formation of the doubly hydrophilic PEtOx-*b*-poly(acrylic acid) (PEtOx-*b*-PAA) BCP causing the rupture of micelles. The photoinduced release of encapsulated guest molecule from the BCP micellar core is also investigated. Furthermore, PEtOx-*b*-PNBA amphiphiles also self-assemble into reverse micelles in non-aqueous media, which can encapsulate anionic dye, Eosin B, and facilitate its solubilization in organic media. We further describe the synthesis of oligo(2-oxazoline) acrylate (OOxA) by direct termination of living OOx chains by triethylammonium acrylate and finally a series of graft copolymers (CPs) are prepared by copolymerizing OOxA with NBA via RAFT polymerization. It is already reported that, poly(2-oxazoline) have thermo-responsive property. Thus, the presence of P(OOxA) sequence introduces the thermo-sensitivity into the as-synthesized graft copolymers. Upon UV light irradiation, the irreversible photocleavage of *o*-nitrobenzyl ester moieties into carboxylic acid increases the hydrophilicity of the CP molecules and consequently, increases the cloud point by more than 10 °C. In aqueous medium, the as-synthesized CP molecules can also self-assemble into micelles at room temperature. Upon UV light irradiation, photolysis of *o*-nitrobenzyl ester units takes place and therefore, causing the dissociation of micelles into unimers.

Reference

[1] Jana, S., Saha, A., Paira, T. K., & Mandal, T. K. *J. Phys. Chem. B* **2016**, *120*, 813-824

MACRO 319

Poly(vinylidenefluoride)(PVDF) graft Copolymer in Alcohol-Water Environment

Kuila, A.; Maity, N.; Chatterjee, D. P.[a]; Nandi, A. K.*

Polymer Science Unit, Indian Association for the Cultivation of Science, Jadavpur, Kolkata 700032, India, Fax: (+) 91 33 2473 2805
[a]Present address: Department of Chemistry, Presidency University, Kolkata-700073

** Correspondence to: A. K. Nandi (E-mail: psuakn@iacs.res.in)*

Grafting of different monomers (methacrylates, acrylates, and acrylamide) on PVDF backbone is designed using atom transfer radical coupling (ATRC) [1] followed by ATRP. Initially, 4-hydroxy TEMPO moieties are anchored on PVDF backbone by ATRC followed by attachment of ATRP initiating sites at pendant –OH groups. And from the initiators a series of comonomers can be polymerized according to the reactivity of monomers of our need[2]. With model macro initiators on PVDF, grafting of a several co-monomers with high conversion are now possible. In this context, a water soluble polymer poly(diethylene glycol methyl ether methacrylate) ($PMeO_2MA$) is grafted on PVDF backbone(Figure 1). Dynamic light scattering (DLS) data indicate this graft copolymers(PD) possess a lower critical solution temperature (LCST) at ~30 ^{0}C which can be tuned by changing the composition of the graft copolymer. The antifouling properties of the PD-24 film, produced specifically by water treatment at 15 ^{0}C (PD-24-15) and 37 ^{0}C (PD-24-37), are tested with bovine serum albumin (BSA) at below and above the LCST and a lower protein adsorption is noticed at 37 ^{0}C indicating a temperature triggered antifouling property of the PD graft co-polymers. Again the filtration of BSA solution using these two films monitored through fluorescence intensity indicates ~60% protein absorption during filtration through the PD-24-15 film but PD-24-37 does not exhibit any change of fluorescence intensity, indicating *superior antifouling properties*[3]. Further the thermal transitions of that particular graft co-polymer are studied in different solvents like methanol and isopropanol and in mix-solvents consisting of water, methanol and isopropanol. Temperature dependent ^{1}H NMR and DLS size studies are done to observe the thermal transitions. Solvent polarity in mix solvents and the hydrophobic-hydrophilic balance among the side chains and main chains of $PMeO_2MA$ and also PVDF backbones plays a vital role behind this thermo responsiveness in solution state. We have drawn a quasibinary phase diagram which indicates an approximate *inverted hourglass phase diagram*[4] where a swelled state exists between two single phase boundary produced from LCST and UCST type phase transitions for a particular solution.

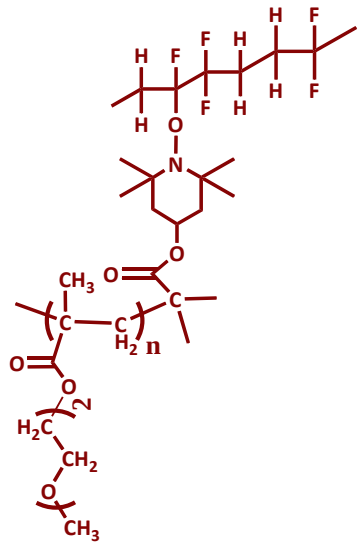


Figure 1. Poly(vinylidene fluoride) graft Poly(diethylene glycol methyl ether methacrylate).

References

1. Matyjaszewski, K.; Woodworth, B. E.; Zhang, X.; Gaynor,S. G.; Metzner, Z. *Macromolecules* 31 (1998**)** 5955.
2. Kuila, A.; Chatterjee, D. P.; Layek, R. K.; Nandi, A. K. *J. Polym. Sci., Part A: Polym. Chem.*, 52 (2014**)** 995.
3. Kuila, A.; Maity, N.; Chatterjee, D. P.; Nandi, A. K. *J. Mater. Chem. A* 3 (2015) 13546.
4. Kuila, A.; Maity, N.; Chatterjee, D. P.; Nandi, A. K. *J. Phys. Chem. B,* 120 (2016) 2557.

MACRO 323

Synthesis of Fluorescent Water-Soluble Amphiphilic Peptide-Polymer Bioconjugate: for Cell Imaging and RNA Binding

Dule, Madhab; Biswas, Yajnaseni and Mandal, Tarun Kumar*

Polymer Science Unit, Indian Association for the Cultivation of Science, Jadavpur, Kolkata 700 032, India

E-mail: psutkm@iacs.res.in

Peptide-polymer conjugate is a new class of soft matters in which synthetic polymers are immobilized to biomolecules to enhance the solubility, stability, activity, or therapeutic utility of the biological entity such as peptide.[1] In recent days, the multifunctional self-assembled polymer micelles based on peptide-polymer conjugates have been used for designing of drug delivery vehicles, gene transfer agents, or bioimaging agents.[2] A fluorescent amphiphilic FITC-tagged dipeptide-poly(vinyl imidazole) [PVim-Cys(FITC)-Trp-OMe] bio-conjugate is synthesized by 'grafting from' technique based on thiol-initiated polymerization followed by attachment of fluorescein isothiocyanate (FITC). PVim-Cys(FITC)-Trp-OMe conjugate characterized by NMR and fluorescence spectroscopy techniques. The presence of peptide ad FITC end groups in the conjugate are identified from the analysis of MALDI-TOF-MS spectra. The amphiphilic polymer-peptide conjugates undergo self-assembly into micelles in aqueous solution as confirmed from TEM, FESEM and DLS. The aqueous solution of the peptide-polymer bioconjugate as well as its miclles emits green light and exhibits a fluorescence emission band at 520 nm. Further, the highly stable and non-toxic fluorescent PVim-Cys(FITC)-Trp-OMe conjugate micelles are used for imaging of CHO cells. Finally, the formation of polyplex between peptide-polymer, PVim-Cys(Boc)-Trp-OMe bioconjugate and nucleic acid (RNA) is studied using fluorescence spectroscopic technique.

Reference

[1] Paira, T. K.; Saha, A.; Banerjee, S.; Das, T.; Das, P.; Jana, N. R.; Mandal, T. K. *Macromol. Biosci. 14(***2014)**, 929-935.

[2] Vandermeulen, G. W. M.; Klok, H.-A. *Macromol. Biosci. 4(***2004)**, 383-398.

MACRO 326

Synthesis of Superporous PolyHIPE Hydrogels as a Scaffold Material for Tissue Engineering Application

Nalawade A. C.[a]* Qureshi. M. S, N.N Chavan, S. P. Ponrathnam

[a] *Polymer science division, NCL, Pune-411008, India.*

[b] *Chemical Engineering and process Development Division, NCL, Pune-411008,India.*

* *e-mail id: archana.thorave@gmail.com*

Abstract

Emerging field of tissue engineering aims to regenerate damaged tissue with the highly porous scaffold material with the requisite properties which acts as template for tissue regeneration.
In this work, a series of novel superporous polyHIPE hydrogels were successfully synthesized by inverse high internal phase emulsion polymerization (i-HIPE) of monomers glycerol monomethacrylate, 2-hydroxy ethyl methacrylate and glycerol dimethacrylate as a flexible cross-linker at the physiological temperature using liquid paraffin oil, a non toxic organic solvent, as dispersed phase. The morphology and the properties of the materials could be altered by changing the monomer ratio. The morphological studies showed that the pore diameter varied between 19-31 μm and the pore throats (interconnecting windows) diameter in the range of 3-8 μm. The initial cytotoxicity study performed according to ISO-10993-5 indicated cytocompatibility (97% cell viability) and the subsequent cell seeding and proliferation study exhibited 55 - 88 % cell viability. The described super porous hydrogels showed sufficiently high swelling ratio, porosity, hydrophilicity and thereby increased degradability, improved biocompatibility and therefore can be considered as promising materials for tissue scaffolding.

Keywords: *polyHIPE; superporous hydrogel, Tissue scaffold, biocompatible*

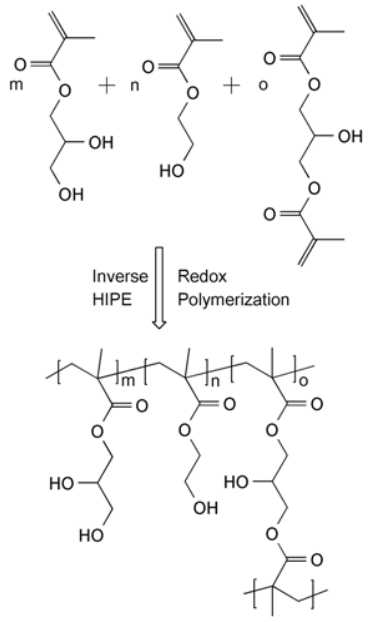
Introduction

Polymer based porous materials, such as scaffolds, have attracted the attention of researchers due to their versatile properties and applications in tissue engineering. [1] The material to be used as a scaffold permits cells adhesion and promotes their growth and allows for the retention of differentiated cell functions besides being biocompatible.[2] A scaffold should have high enough porosity to provide sufficient space for cell adhesion, extracellular matrix regeneration and it must allow spatial cell distribution throughout the scaffold to facilitate homogeneous tissue formation.[3] The porous hydrogels are promising materials as scaffolds for tissue engineering because of their inherent hydrophilic nature; favorable mass transport properties for molecules such as drugs, nutrients, oxygen, and cell wastes; structural similarity to the extracellular matrix of tissues; and they are amenable to relatively mild processing conditions. [4, 5] The polymerized high internal phase emulsions (PolyHIPEs) are more recently explored materials as scaffolds. PolyHIPEs have been synthesized using high internal phase emulsions (HIPEs) as templates. [6] HIPEs are emulsions that have an internal phase volume greater than 74% dispersed in a continuous (external) phase. Polymerization of the continuous phase of HIPEs gives rise to porous polymers (polyHIPEs) with open cells and interconnected pores after removal of the dispersed internal phase. To overcome the intrinsic hydrophobicity of polyHIPEs synthesized via the water-in-oil route, synthesis of hydrophilic polyHIPE was suggested following oil-in-water methodology using hydrophilic monomers in an aqueous (continuous) phase.[7] However, hydrophilic polyHIPEs remain less explored systems for biomedical applications mainly for poor emulsion stability, relatively limited synthesis windows, low porosity and/or poor interconnectivity. In this study, we report the synthesis of superporous polyHIPE hydrogels for tissue engineering applications by copolymerization of glycerol monomethacrylate (GMMA), 2-hydroxy ethyl methacrylate (HEMA) and glycerol dimethacrylate (GDMA) as a crosslinker following inverse (i.e. oil-in-water) HIPE polymerization methodology using a nontoxic oil phase. To date, no study has been reported on the preparation of porous hydrogels based on inverse HIPE polymerization of HEMA, GMMA and GDMA.

Experimental

PolyHIPE hydrogel synthesis

In a typical experiment, liquid paraffin oil (dispersed phase 80 vol. % on total volume) was added drop wise to the continuous (aqueous) phase consisting of Triton X-305(10 wt% on total volume), GMMA and HEMA in various molar concentrations and fixed amounts of cross-linker GDMA (25 mol % of GMMA and HEMA) and initiator APS (2 mol% of monomers and cross-linker) in deionized water while constant stirring at 1000 rpm was maintained. After the complete addition of the oil phase, the HIPE was further stirred for five minutes to improve emulsion uniformity (similar to mayonnaise consistency) and then the reducing agent TEMED (2 moles % of monomers and cross-linker) was added. The HIPEs were covered and kept at 37 °C in a water bath for polymerization for 6 h during which cross-linking of polymer chains locked-in the emulsion geometry of HIPE with the suspended oil droplets as pore template to form polyHIPE monoliths. After the polymerization was over, the polyHIPEs were washed thoroughly with deionized water to remove unconverted monomers, surfactant etc. and Soxhlet extracted for 12 h with acetone to remove the oil phase. Finally, the resulting polyHIPEs were dried overnight to constant weight under vacuum at 65°C to produce white fluffy monoliths.



Scheme 1 Copolymerization of GMMA, HEMA and GDMA

Results and discussion

Cross-linker concentration

To study the effect of cross-linker concentration in the continuous phase for obtaining stable emulsion with desired morphology, the polyHIPE hydrogels were synthesized with 1, 5, 10 and 25 mole percent concentration of GDMA while keeping the rest of the composition, including the monomers concentration fixed (GMMA:HEMA, 100 : 0). It was observed that the polyHIPE

morphology progressively improved from almost nonporous to highly porous as the cross-linker concentration increased. At 1 mol% concentration of GDMA, almost no porosity developed (Figure 1A) and only rudimentary porosity (with very irregular pore shape and without pore interconnectivity) started emerging at 5 mol% concentration (Figure 1B).

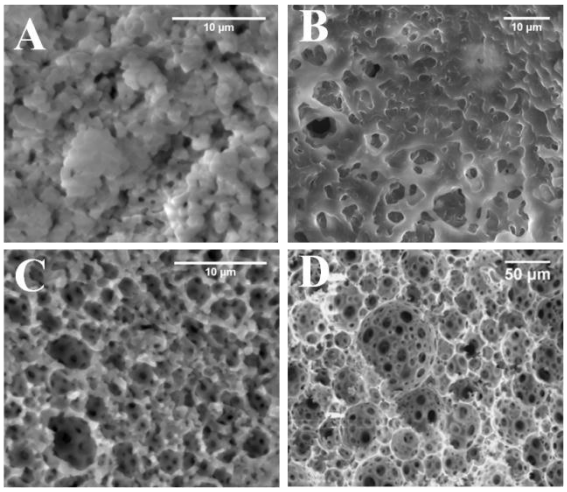


Figure 1 SEM micrograph showing effect of cross-linker concentration on polyHIPE hydrogel morphology; (GMMAHEMA,1000) and GDMA A)1 mol %, B)5 mol %, C)10 mol % and D) 25 mol %.

As the concentration of the cross-linker was increased to 10 mol%, the porosity of the polyHIPE improved further (the pore shape became better) but with thicker pore walls and fewer interconnects (Figure 1C). At 25 mol%, GDMA concentration a polyHIPE hydrogel with desired porous structure and having highly interconnected open-pore architecture resulted (Figure 1D). Therefore, all the polyHIPE hydrogels, reported in this study, were synthesized maintaining the crosslink density at 25 mol%.

Effect of molar ratio of monomers

Initially, we tried to synthesize the superporous hydrogel of HEMA by the inverse HIPE methodology using GDMA as a cross-linker but the emulsion was not stable. The co-monomer GMMA was incorporated in the formulation along with HEMA in different mole ratios and it was noted that the addition of GMMA vastly
improved the emulsion stability.

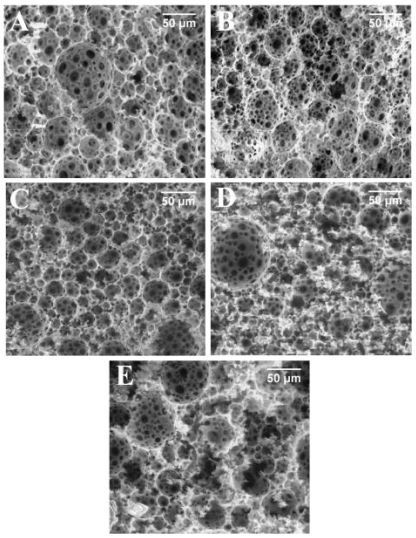


Figure 2 SEM micrographs of polyHIPE hydrogels A) GHG-1, B) GHG-2, C) GHG-3, D) GHG-4, E) GHG-5.

Further, we observed that when the molar ratio of GMA: HEMA was increased beyond 40: 60, the emulsions were not stable. The effect of molar concentration of HEMA and GMMA on the morphology of polyHIPE hydrogels was studied by SEM.

The SEM images (Figure 2) show that all the hydrogels exhibited open porous bimodal morphologies with high porosity ranging from 92.3% to 96.6% that is typical of the polyHIPE porous structures.49 The surface area of the polyHIPE hydrogels varied between 2.89 and 23.1 $m^2 g^{-1}$. With the increased proportion of HEMA of up to 60 mol% in the copolymer, the porosity of the hydrogels increased (consequently, the surface area and the pore volume increased as well), whereas the pore size, pore throat size and pore wall thickness decreased. This led to the formation of relatively stiffer (GHG-1) to softer (GHG-5) hydrogels.

Swelling kinetics in water

A study of the swelling behavior of the polyHIPE hydrogels was carried out in water because the wettability and the swelling are very important properties of a scaffold for tissue engineering. [8] The scaffold's wettability determines the cell seeding and proliferation, whereas the swelling is responsible for the nutrient transport[9] to (and removal of toxic metabolites from) the cells growing on the polymer matrix. It was observed that the swelling of all the five polyHIPE hydrogels occurred very rapidly and reached the equilibrium swollen state in around 10 min. (Figure 3)

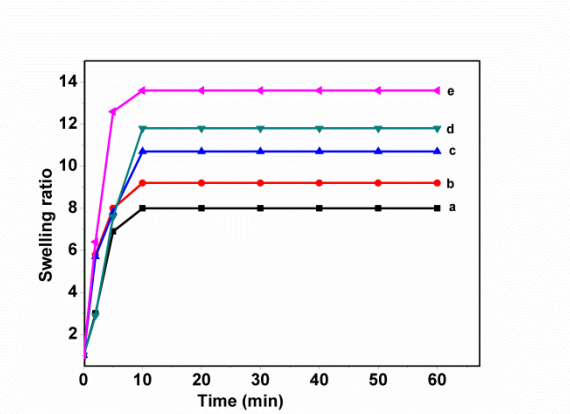


Figure 3 Swelling kinetics of polyHIPE hydrogels a) GHG-1, b) GHG-2, c) GHG-3, d) GHG-4, e) GHG-5.

The highest value of Q (13.6 ± 0.05) was observed for GHG-5 GMMA: HEMA, 40: 60), whereas GHG-1 (100% GMMA) showed the lowest values of Q (8.1 ± 0.05).

Biocompatibility Cell adhesion and proliferation

To investigate the potential of the polyHIPE hydrogels as a scaffold for tissue engineering, assessment of their biocompatibility was carried out using a well characterized NIH3T3 cell line. The cell adhesion and proliferation study was carried out. The assessment revealed that the polyHIPE hydrogel samples exhibited greater than 55% cell viability after 7 days.

The cell viability was assessed for 5 days relative to TCPS as a cytocompatible control. The assessment indicated that the hydrogels exhibited greater than 97% cell viability after 5 days. The images of NIH3T3 cells in the presence of hydrogels and the control after 5 days are shown in figure r. The percentage cell viability on the polyHIPE hydrogels increased monotonously from GHG-1 to GHG-5 and correlated well with their physical and chemical properties as expected (Figure 5).

The increase in the percentage cell viability could be attributed to the increase in porosity (i.e. decrease in pore and pore throat size), pore volume, surface area, area to volume ratio and hydrophilicity.

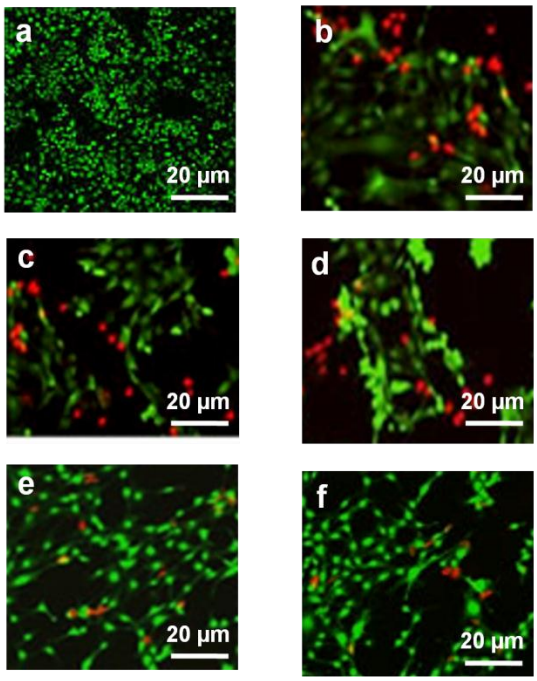


Figure 4 Fluorescence microscopy images of NIH3T3 cells seeded on polyHIPE hydrogels: (a) control, (b) GHG-1, (c) GHG-2, (d) GHG-3, (e) GHG-4 and (f) GHG-5 after 7 days.

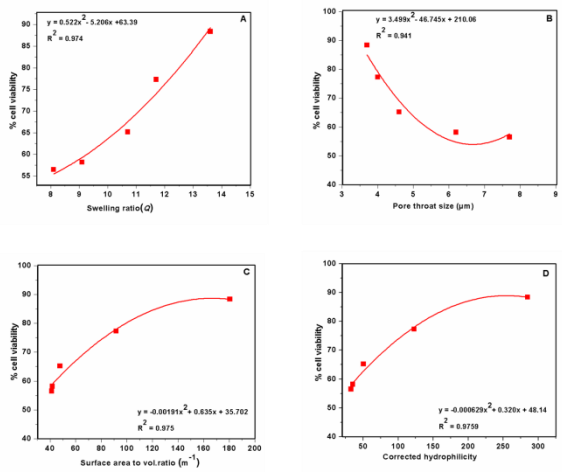


Figure 5 Variation of cell viability with (A) swelling ratio, (B) pore throat size, (C) surface area to volume ratio and (D) corrected hydrophilicity

The increasing hydrophilicity (increased –OH groups and increased surface area) of the polyHIPE hydrogels promoted cell adhesion, migration and proliferation of the seeded cells

Conclusions

In this study, a series of superporous polyHIPE hydrogels were successfully synthesized by inverse high internal phase emulsion polymerization. The described materials showed a sufficiently high

swelling ratio, porosity, hydrophilicity and thereby increased degradability and improved biocompatibility. The open porous morphology, a key design criterion for a tissue scaffold, of the reported polyHIPE hydrogels permitted fast enough convective mass transport of nutrients and oxygen, which resulted in cell growth and proliferation. Assessment of in vitro cell adhesion and proliferation has shown that these materials supported the cell adhesion, penetration and proliferation. Overall, the described polyHIPE hydrogels resembled many human body soft tissues and therefore can be considered as promising materials for tissue scaffolding.

Reference

[1] B. Dhandayuthapani, Y. Yoshida, T. Maekawa, D. Kumar, Int. J. Polym. Sci., 2011, 1, 2011.

[2] S. J. Hollister, Nat. Mater., 4, 2005, 518
[3] R. Ravichandran, S. Sundarrajan, J. Venugopal, S. Mukherjee, S. Ramakrishna, Macromol. Biosci., 12 2012, 286n
[4] S. Varghese, J. Elisseeff, Adv. Polym. Sci., 203, 2006, 95

[5] A. Hoffman, Adv. Drug Delivery Rev., 54, 2002, 3

[6] M. S. Silverstein, Polymer, 55, 2014, 304
[7] P. Vishwanathan, S. Chirasatitsin, K. Ngamkham, A. j. Engler G. Battaglia, J. Am. Chem. Soc., 134, 2012, 134, 20103
[8]S. Zhou, A. Bismark, J. H. G. Steinke, Macromol. Rapid Commun., 33, 2012, 33, 1833
[9] A. L. Gatta, C. Schiraldi, A. Esposito, A. D. Agostino, A. D. Rosa, J. Biomed. Mater. Res., Part A, 90, 2009, 90, 292

MACRO 327

Thermo-, pH-, and Anion-Responsive Phosphonium and Imidazolium Poly(ionic liquid)s

Biswas, Yajnaseni; Maji, Tanmoy; Dule, Madhab; Mandal, Tarun K*

Polymer Science Unit, Indian Association for the Cultivation of Science, Jadavpur, Kolkata 700 032, India
**psutkm@iacs.res.in*

Poly(ionic liquid)s (PILs) have attracted considerable attention to the research community as fascinating polymer materials due to their wide range of applications such as CO_2 sorbents, porous materials, carbon precursors, catalytic materials and specially as a stimuli-responsive materials.[1] Stimuli responsive polymers exhibit a drastic change in their solution property upon small changes in external stimuli such as temperature, pH, light and ionic strength of solution. In this study, a cationic phosphonium PIL, poly(triphenyl-4-vinylbenzylphosphonium chloride) (P[VBTP][Cl]) of varying and

controllable molecular weight is synthesized via reversible addition-fragmentation chain transfer (RAFT) polymerization. The transparent aqueous solution of this cationic phosphonium PIL turns into a turbid solution in presence of halide ions, forming insoluble microgel aggregates. The intra- and/or inter-chain crosslinking through halide ion bridges between PIL chains eventually screen the positively charged phosphonium groups of PIL chains resulting in microgel aggregates. Further, upon heating this turbid solution transforms into clear solution exhibiting a distinct upper critical solution temperature (UCST)-type phase transition due to disruption of ion bridges present in the gel bead.[2] This is contrast with many of the water-soluble PILs that often exhibit a lower critical solution temperature (LCST)-type transition.[3]

Beside this, a series of novel carboxybetaine type immidazolium-based zwitterionic PILs containing varying chain length of alkane spacer group present in between imidazolium cation and carboxylate anion moiety are synthesized by RAFT polymerization technique. Among them, poly(1-(2'-dimethyl propionic acid)-3-(4"-vinyl benzyl)-1H-imidazole-3-ium bromide) (P[VBIMBA][Br]) exhibits a soluble to insoluble transition in presence of BF_4^- and I^- ions. The ion-induced cloudy solution further exhibits a clear insoluble to soluble (UCST-type) phase transition. Furthermore, in the pH range of 5.1−6.9, the aqueous P[VBIMBA][Br] solution appears as a two-phase system due to the formation of insoluble aggregates through the intra- and inter-molecular electrostatic interaction between the pendent imidazolium cation and carboxylate groups of the neighboring zwitterionic PIL molecules. Furthermore, in this pH range, the two-phase P[VBIMBA][Br] solution becomes one-phase upon heating, exhibiting distinct reversible UCST-type phase transition. The cloud point temperatures are measured through turbidimetry and dynamic light scattering (DLS). The cloud point temperature of the aqueous PIL solution can be tuned in terms of concentration, molecular weight, pH and ionic strength of the externally added electrolytes. Moreover, this PIL is applied as a smart stabilizer to promote water borne stimuli-responsive dispersion of multi-walled carbon nanotubes (MWCNTs) towards ions and temperature.[2] This opens up the applicability of this PIL as an important material for sensing of pH, halide ions and other temperature responsive applications.

References

[1]Yuan, Jiayin; Mecerreyes, David; Antonietti, Markus. *Progress in Polymer Science*, 38 (2013)1009.
[2]Biswas, Yajnaseni; Maji, Tanmoy; Dule, Madhab; Mandal, T. K. *Polymer Chemistry*, 7 (2016) 867. [3]Men, Yongjun; Schlaad, Helmut; Yuan, Jiayin. *Acs Macro Letters*, 2 (2013) 456.

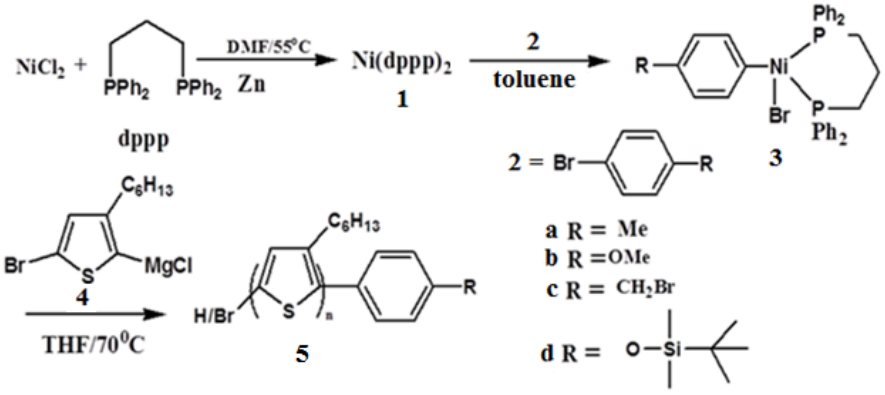
MACRO 340

A Simple Approach For Synthesis Of Externally Initiated Regioregular Poly(3-Hexylthiophene)

Khawas Koomkoom and Kuila Biplab K.*
Centre for Applied Chemistry, Central University of Jharkhand, Brambe, Ranchi, India, Pin-835205,
Email: biplab.kuila@cuj.ac.in

Poly (3-hexyl thiophene) (P3HT) has remain frontrunners in the research on conjugated polymer and work horse for organic electronic devices, such as photovoltaics, organic field effect transistors (OFETs)[1]. A milestone in the development of their synthetic strategy was the discovery of the controlled chain-growth polymerization of poly(3-hexylthiophene) by Yokozawa and McCullough groups[3,4]. However, these synthetic strategies suffer from its limitation as polymerization cannot be initiated from an external moiety as required for synthesis of block copolymer and P3HT based complex architectures. There are few example[8] of externally initiated polymerization of P3HT[5-8] where initiator is generated from direct oxidative addition of Ar-X(Ar = aromatic group and X= Cl/Br) to either $Ni(PPh_3)_4$or $Ni(dppp)_2$ resulting Ar-Ni(dppp)-X or Ar-$Ni(PPh_3)_2$-X . But the major drawback of this polymerization technique is that the starting Ni(0) complexes are highly unstable and difficult to handle. In alternative method[8], the initiator Ar-Ni(dppp)-X is synthesized through the reaction of Et_2Ni(bipy) with Ar-Br and further exchanging the ligand "bipy " by "dppp". This reaction itself involves several tedious steps, synthesis of commercially nonavailable Et_2Ni(bipy) from highly reactive and hazardous organoaluminum compounds like diethylaluminum ethoxide or triethylaluminum.

Here, we have demonstrated a very simple approach to initiate the polymerization from in-situ generated Ni(II) initiator [bromo(aryl)(dppp)Ni(II)] resulting end functionalized regioregular P3HT with controlled molecular weights, narrow distribution. The advantages of this method are the easy synthesis of the Ni(II) initiator from readily available reagents and the in-situ nature of all the steps which will reduce the cost-effectiveness and viable for industrial scale preparation. The synthesis of desired initiating complex and polymerization is depicted in scheme-1. First the nickel complex, $Ni(dppp)_2$ (orange in color) was synthesized by the reduction of anhydrous Nickel (II) chloride with Zinc dust in DMF followed by the addition of ligand 1,3 bis(diphenylphosphino) propane [dppp] under argon atmosphere. Further oxidative addition of aryl bromide to $Ni(dppp)_2$, at room temperature resulted in the formation of bromo (aryl)1,3-bis(diphenylphosphino)propane nickel(II). The polymerization was initiated by adding the monomer 2-bromo-5-chloromagnesio-3-hexylthiophene. The reaction mixture was quenched with a small amount of dilute HCl, extracted with chloroform and further precipitated in methanol. The polymers were further characterized by NMR, MALDI-TOF and GPC to verify the end functionality, molecular weight and PDI.



Scheme-1 Total reaction scheme for synthesis of P3HT

References

[1] Perepichka, I. F.; Perepichka D. F. Handbook of Thiophene Based Materials: Applications in Organic Electronics and Photonics, Volume One: Synthesis and Theory, ed., (2009).
[2] Loewe, R. S.; Khersonsky, S. M.; McCullough, R. D. *Adv. Mater. 11* (1999) 250.
[3] Miyakoshi, R.; Yokoyama, A.; Yokozawa, T. *J. Am. Chem. Soc. 127* (2005) 17542.
[4] Bronstein, H. A.; Luscombe, C. K. J. Am. Chem. Soc. *131* (2009) 12894-12895.
[5] Senkovskyy, V.; Khanduyeva, N.; Komber, H.; Oertel, U.; Stamm, M.;Kuckling, D.; Kiriy, A. *J. Am. Chem. Soc. 129* (2007) 6626.
[6] Chavez, C.A., Choi J, Nesterov EE *Macromolecules 47* (2014) 506–516.
[7] P3HT revisited from molecular scale to solar cell devices, Advance in polymer Science 265, Sabine Ludwigs, Springer-Verlag Berlin Heidelberg (2014).
[8]

MACRO 341

Designing of Multi-Responsive Amino Acid-Based Zwitterionic Polymers

Maji, Tanmoy, Biswas, Yajnaseni and Mandal, Tarun Kumar*

Polymer Science Unit, Indian Association for the Cultivation of Science, Jadavpur, Kolkata 700 032
*psutkm@iacs.res.in

In recent year, polyzwitterions attract substantial interest due to their structure, flexibility and promising applications for their tunable properties and excellent antifouling properties. The polyzwitterion contains both the positively and the negatively charged moiety on the same repeating unit, which is also referred as polybetaines. This class of polymer usually undergo conformational changes in presence of external stimuli like pH, temperature and ionic strength. Biocompatibility and stimuli-responsiveness are the promising features of polybetaines. However, incorporation of amino acid into a polymer makes the polymer more bio-friendly. In this work, L-serine-based zwitterionic polymer, poly(L-serinyl acrylate)s (PSA) of controllable molecular weights and low polydispersities are designed and synthesized via RAFT polymerization technique in water. The aqueous PSA solution appears as a two-phase system in the pH range of 2.4-3.4 where it forms insoluble aggregates through the intra- and inter-molecular electrostatic interaction between the pendent ammonium and carboxylate groups of the neighbouring zwitterionic PSA molecules. Furthermore, another phase transition from the biphasic PSA solution to clear solution is observed upon heating of that pH ranges, exhibiting a distinct reversible upper critical solution temperature (UCST). The cloud point is found to increase with increasing molecular weights of PSAs. It is also observed that the cloud point changes with changing its molecular weights, the solution pH and the externally added electrolyte such as brine solution. Finally, fluorescein isothiocyanate (FITC) tagged PSA with dual-responsiveness is prepared by the post modification of pendent amino groups of PSA for futuristic application in sensors and bioimaging.

Furthermore, we also describe the design of a new type of amino acid-based sufobetaine type zwitterionic, 3-[Boc-L-methionine-(2-methacryloylethyl)]propanesulphonate (METMAS) monomer followed by its RAFT polymerization to polysufobetaine (PMETMAS). The synthesized monomer shows UCST-type phase transition in aqueous medium near pH 5.75 because of the reversible formation of intermolecular linking through ionic interaction between cationic sulfonium and anionic sulfonate groups. Whereas the zwitterionic PMETMAS remain soluble in water in acidic pH but exhibits salt (NaCl, NaBr) induced LCST-type phase transition in alkaline solution. The polyzwitterions show polyelectrolyte-type effect in presence of external

salt. The larger halide anions interact more with sulfonium ion than the smaller one which increase its cloud point temperature in aqueous solution. It is also observed that the cloud point can be tuned by changing the solution pH, anion size and also on concentration of the salt in solution.

References

[1] Kramer, J.; Deming, T. J. Biomacromolecules **2012**, 13, 1719−1723
[2] Arjunan Vasantha, V.; Junhui, C.; Ying, T. B.; Parthiban, A. *Langmuir* **2015,** *31* (40), 11124-11134.
[3] Banerjee, S.; Maji, T.; Paira, T. K.; Mandal, T. K., *Macromol. Rapid Commun.* **2013,** 34, (18), 1480-1486.
[4] Maji, T.; Banerjee, S.; Biswas, Y.; Mandal, T. K.,*Macromolecules* **2015,** 48, (14), 4957-4966

MACRO 343

Synthesis and composition dependent optical, electronic properties of poly (3-hexyl thiophene)-b-poly(N-isopropyl acrylamide)

Pallavi Kumari and Biplab K. Kuila *
Centre for Applied Chemistry,
Central University of Jharkhand, Brambe, Ranchi, India, Pin-835205,
Email: biplab.kuila@cuj.ac.in

Abstract

Here, we have reported the facile synthesis of poly(3-hexyl thiophene)-b-poly(N-isopropyl acrylamide) block copolymers of varying composition of both the block using click reaction between alkyne terminated P3HT and azide terminated PNIPAM. The composition dependent solubility, thermo-responsive property in water, phase behaviour, and electronic properties of these block copolymers were systematically investigated. The block copolymers with higher volume fraction of PNIPAM form thermo-sensitive spherical micelles with P3HT-rich crystalline cores and PNIPAM coronas. AFM study indicates that the blocks copolymers show well defined microphase separated nanostructures and the structure depends on the composition of the blocks. The block copolymers show improved or similar charge carrier mobility compared to the pure P3HT depending on the composition of the block copolymer. These P3HT-b-PNIPAM copolymers might be interesting for fabrication of optoelectronic devices capable of thermal and moisture sensing and for studying the thermo-sensitive colloidal structures of semiconductor amphiphilic systems.

Keywords: *Block copolymers, Conjugated polymer, Thermo-responsive, Self-assembly*

Introduction

Design and synthesis of new conjugated polymeric materials with novel functionality and wide processability has attracted significant research attention because of their enormous potential applications in sensors, energy storages, corrosion inhibitors, optoelectronic devices, etc1-2. Poly (3-hexyl thiophene) (P3HT) is one of the mostly studied conjugated polymer and work horse for organic electronic devices3.4. P3HT has been incorporated into different types of block copolymers in order to manipulate its solubility, optical, electronic properties3,5. Particularly, there is a significant demand of water-soluble conjugated polymeric materials related to their applications achieved from environmentally friendly steps and applications centred on their use in biological environments6. Whereas poly(N-isopropylacrylamide) (PNIPAM) is one of the most famous thermally responsive polymer, which shows a rapid coil-to-globule transition in aqueous solutions above its LCST (320C) and wide range of applications3,7,8 in therapeutic delivery tissue engineering and sensing. There will be a significant progress if we can develop smart hybrid polymeric materials by blending the thermoresponsive properties of PNIPAM and the unique optical and electronic properties of P3HT. Synthesis of block copolymer by combining P3HT and a thermoresponsive polymer is a smart approach to synthesize such thermoresponsive optical and electronic materials.

Here, we have demonstrated the facile synthesis of poly(3-hexyl thiophene)-b-poly(N-isopropyl acrylamide) block copolymers of varying composition of both the block using click reaction between alkyne terminated P3HT and azide terminated PNIPAM. We investigated how the solubility, thermoresponsive property in water, phase behaviour, optical and electronic properties of the block copolymers depend on block ratio. We believe that these novel block copolymers might be interesting for fabrication of optoelectronic devices capable of thermal and moisture sensing as well as for studying the thermosensitive colloidal structures of semiconductor amphiphilic systems.

Experimental

All chemical including Magnesium, 1-bromohexane, 3-bromothiophene, Na_2SO_4, N-Bromosuccinimide, $Na_2S_2O_3$, KOH, etc. were purchased from Sigma Aldrich Pvt. Ltd. and used as received. Other solvents like THF, Ether, Methanol, Chloroform etc. were obtained from Rankem.

Characterization:

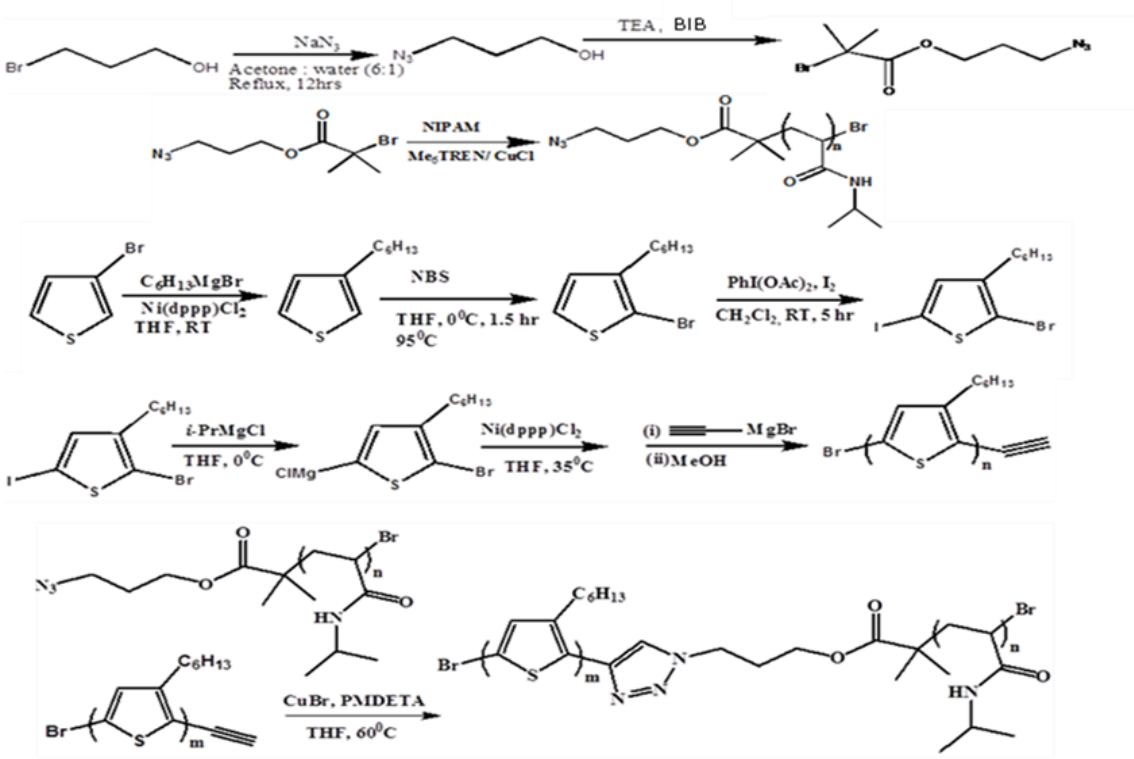
Fourier transform infrared (FTIR) spectra were recorded in Perkin Elmer FTIR spectrometer [Spectrum two]. Nuclear magnetic resonance spectra were record on 300MHz Bruker instrument. The number-average molecular weight (Mn) and polydispersity index (Mw/Mn) of P3HT samples were determined by Shimadzu prominence in THF as solvent. Atomic force microscopy (AFM) imaging was performed using AFM NT-MDT, Solver Pro 47 in the tapping mode. UV-vis absorption spectra were recorded in chloroform and thin film state on a Simadzu UV 3600+, UV-vis spectrophotometer.

Synthesis of block copolymer

The typical synthesis procedure of the P3HT-b-PNIPAM is as follows (Scheme-1). Into a 25 mL Schlenk flask were added 221.06 mg (16.87 μ mol) of alkyne-terminated P3HT[9], 3.873 mg (27 μmol) of CuBr, 500 mg (13.5 μmol) of PNIPAM-N_3[3] and 30 mL of dry THF. The tube was degassed by three freeze-thaw cycles in liquid N_2 and then 5.629 μL (27 μmol) degassed PMDETA was added to the reaction mixture and refluxed at 60 °C for 24 h. After opening the reaction mixture in air, it was further diluted with THF and passed through neutral alumina column to remove Cu catalyst. After that THF was removed by rotary evaporator and the polymer was further dissolved in DMF. The unreacted P3HT was removed by filtering the DMF solution. Finally, the purple colour polymer was obtained by removing DMF in rotary evaporator and drying the sample in a vacuum oven for 48 h at 60 °C (60% yield).

Result & discussion

Scheme-1 depicts the straightforward route for the synthesis of conjugated block copolymers P3HT-b-PNIPAM of varying composition by copper (I) catalysed click reaction. First, the ethynyl modification of P3HT was checked by ^{1}H NMR spectrum, singlet at 3.52 ppm[10] (Figure-1) and the appearance of CH stretching frequency ~ 2100 cm^{-1}, in FTIR. The successful synthesis of the azide modified PNIPAM was also confirmed by ^{1}HNMR (proton peak near 3.4, Fig.-1) and FTIR study (azide stretching frequency at 2094 cm^{-1}).



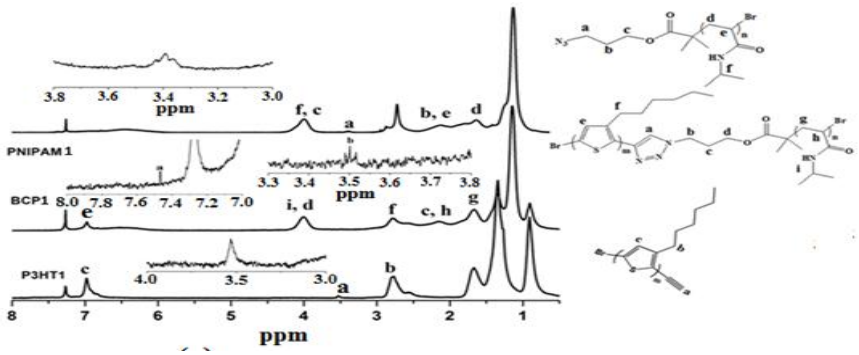
Scheme1.Total reaction scheme for synthesis of P3HT-b-PNIPAM

Table-1

Characteristics of homopolymers and the block copolymers

Sample	P3HT block	PNIPAM block	P3HT-b-PNIPAM

	Name	DP_{P3HT}	M_n	PDI	Name	DP_{PNIPAM}	M_n	PDI	DP ratio (DP_{P3HT}/DP_{PNIPAM})	M_n	PDI
BCP1	P3HT1	9	1,792	1.36	PNIPAM1	23	4,000	1.17	1:2.54	5,780	1.35
BCP2	P3HT2	69	10,517	1.10	PNIPAM2	55	14,287	1.34		24,408	1.03
BCP3	P3HT2	69	10,517	1.10	PNIPAM1	23	4,000	1.17	2.90:1	14,517	1.38



Sample	P3HT block				PNIPAM block				P3HT-b-PNIPAM		
	Name	DP_{P3HT}	M_n	PDI	Name	DP_{PNIPAM}	M_n	PDI	DP ratio (DP_{P3HT}/DP_{PNIPAM})	M_n	PDI
BCP1	P3HT1	9	1,792	1.36	PNIPAM1	23	4,000	1.17	1:2.54	5,780	1.35
BCP2	P3HT2	69	10,517	1.10	PNIPAM2	55	14,287	1.34		24,408	1.03
BCP3	P3HT2	69	10,517	1.10	PNIPAM1	23	4,000	1.17	2.90:1	14,517	1.38

Figure 1 ^{1}H NMR spectra of low molecular weight polymers P3HT 1, BCP 1 and PNIPAM 1 with expanded spectra and chemical structure of the polymers

The synthesis of three block copolymers with one predominantly P3HT chain length, one with predominantly PNIPAM chain length and one with both having almost equal chain length were confirmed by the disappearance of both ethynyl proton at (δ =3.52 ppm) in ^{1}HNMR, azide stretching frequency at 2100 cm^{-1} and appearance of the singlet triazole proton at δ = 7.78 ppm[10].

For click reaction, one of the homopolymers is taken in excess amount in order to promote the reaction in the forward direction. Block copolymers are soluble/dispersible in nonselective solvent like chloroform, THF and in selective solvent like methanol, water and DMF depending on the chain length of P3HT. In thin film, the block copolymers exhibit varieties of nanostructured morphology depending upon solvent chosen for thin film fabrication and block composition. In selective solvent like water and methanol, the block copolymers show micellar morphology whereas in nonselective solvent show microphase separated nanostructured morphology characteristic of block copolymer. The AFM images of block copolymer (BCP2) (Figure-2) having almost equal weight fraction of PNIPAM and P3HT, shows mixed morphology with lamella and cylinders. Whereas, BCP1 having lower molecular weight of both the block with higher weight fraction of PNIPAM shows fibrilar morphology and the BCP3 shows cylindrical morphology. However, in all the cases, the morphology is not very well defined and ordered indicate a non-equilibrium state morphology and equilibrium morphology may be obtained by further optimization of annealing condition, film thickness, and cooling rates. The DLS study clearly shows that BCP1 and BCP2 exhibit a well-defined LCST similar to PNIPAM by an abrupt increase of z average size at the transition point. At lower temperatures, the micelles are stabilized in water through the PNIPAM block by hydrogen bonding.

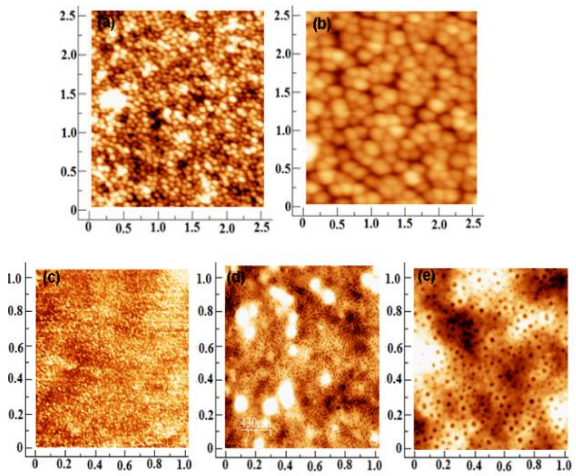


Figure 2 AFM phase images of block copolymers in different solvents (a) BCP1 in water (b) BCP 2 in water (c) BCP 1 in chloroform (d)BCP2 in chloroform (e)BCP 3 in chloroform

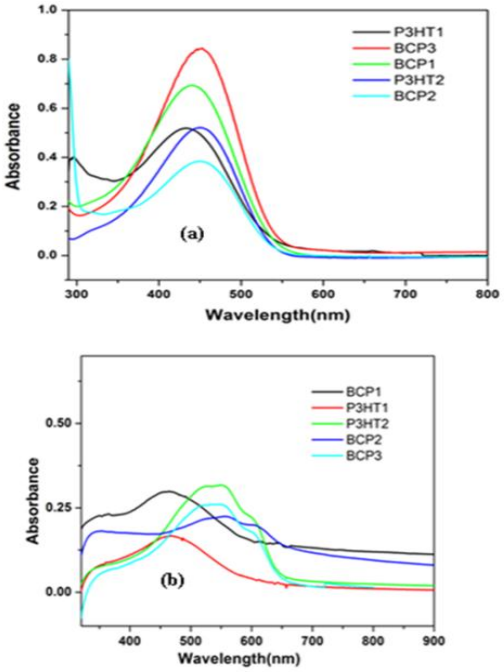


Figure 3 UV−vis spectra of P3HT and block copolymer samples(a) in solution and (b) thin film state.

When the temperature rises above the LCST, the PNIPAM segments undergo abrupt dehydration due to breaking of the hydrogen bonding and results in conformational change of the PNIPAM from an extended hydrated coil to a collapsed hydrophobic globule.

Figure-3 shows the UV−vis spectra of P3HT and different block copolymers in chloroform. It can be seen that λ_{max} value of P3HT shows absorption peak in the region 400-500 nm, due to π−π* transition. In case of BCP1, BCP2 and BCP3, the λ_{max} does not show any significant change compared to the precursor P3HT in solution but In thin film, P3HT1 and P3HT2 show π−π* absorption peak at 467, and 551 nm and BCP1, BCP2 and BCP3 show π−π* absorption peak at 463, 555 and 534 nm. The change in spectral shift compared to pure P3HT is due to the change in the conjugation length caused by different type of assembly in thin film compared to P3HT.We have investigated their optical band gap of block copolymers and pure P3HT from the λ_{onset} of the UV-vis spectra in thin film. The optical band gap values are 2.01eV, 1.89eV, 1.79eV, 1.63eV and 1.88eV for P3HT1, P3HT2, BCP1, BCP2 and BCP3 respectively. The transport properties in the direction perpendicular to the substrate of P3HT and block copolymer samples in diode geometry were investigated. The carrier mobility values are 1.26 X 10^{-6} (cm^2/Vs), 1.4 X 10^{-5} (cm^2/Vs), 2.80 X 10^{-5} (cm^2/Vs), and 4.1 X 10^{-6}(cm^2/Vs) for P3HT1, P3HT2, BCP1, BCP2, and BCP3, respectively. The charge carrier mobility values clearly indicate that both the BCP1 and BCP2 show higher charge carrier mobility than their pristine P3HTs. The improvement of charge carrier mobility in BCP1 and BCP2 compared with pristine P3HT is also supported from the optical band gap study. The current voltage study of the devices clearly indicates that these block copolymers will be useful for electronic device fabrications like FET, photovoltaic devices. The additional

presence of thermoresponsive and water soluble block PNIPAM may be helpful for fabrication of future thermo and moisture sensitive optoelectronic devices.

Conclusion

In conclusion, we have successfully synthesized a series of well-defined P3HT b-PNIPAM block copolymers via a click reaction between varying molecular weight of P3HT-Alkyne and PNIPAM. The composition dependent solubility, thermoresponsive property in water, phase behaviour, and electronic properties of the block copolymers were systematically studied. The block copolymers in aquaouas solution form micelles consist of a crystalline P3HT core which is surrounded by PNIPAM coronas. The block copolymers show improved or similar charge carrier mobility compared with the pure P3HT depending on the composition of the block copolymer. These P3HT-b- PNIPAM block copolymers are interesting for fabrication of optoelectronic devices capable of thermal and moisture sensing as well as for studying the thermosensitive colloidal structures of semiconductor amphiphilic systems.

Acknowledgement: P.K. and B.K.K acknowledge Ramanujan Fellowship (SR/S2/RJN-81/2010, DST), CSIR project (02(0117)/13/EMR-II), DST fast track project (SR/FT/CS-169/2011), Centre for Excellence in Green and Efficient Energy Technology (GEET) (under FAST scheme of MHRD, Government of India, New Delhi) for financial support.

References

1. F. H. Schacher, P. A. Rupar, I. Manners, *Angew. Chem. Int. Ed*. 51, 7898. 2012.

2. H. Sirringhaus, N. Tessler, R. H. Friend, *Science*, 280, 1741, 1998.

3. P. Kumari, K. Khawas, S. Hazra and B. K. Kuila, *J. Polym. Sci. polym. Chem. Part A*, 54, 1785, 2016.

4. A. Marrocchi, D. Lanari, A. Facchettibc, L. Vaccaro, *Energy Environ. Sci.*, 5, 8457, 2012.

5. K.-K. Huang, Y. K. Fang, J. C. Hsu, C.-C. Kuo, W. H. Chang, W. C. Chen, *J. Polym. Sci. Part A: Polym. Chem.* 49, 147, 2011,

6. K. P. R. Nilsson, O. Inganas, *Nat. Mater*., 2, 419, 2003.
7. Y. Ono, T. Shikata, *J. Am. Chem. Soc.* 128, 10030, 2006.
8. H. Wei, S. X. Cheng, X. Z. Zhang, R. X. Zhuo, *Prog. Polym. Sci.*, 34, 893, 2009.
9. A. Yokoyama, R. Miyakoshi, T. Yokozawa, *Macromolecules* 37, 1169, 2004.
10. H. Yang, H. Xia, G. Wang, J. Peng, F. Qiu, *J. Polym Sci. Part A: Polym. Chem.* 50, 5060, 2012.

MACRO 344

Amphiphilic, thermoresponsive conjugated block copolymer of poly(3-hexyl thiophene)

Kuila Biplab K.*

Centre for Applied Chemistry, Central University of Jharkhand, Brambe, Ranchi, India, Pin-835205, Email: biplab.kuila@cuj.ac.in

Abstract
Here, we have demonstrated a new class of amphiphilic, thermoresponsive rod−coil conjugated block copolymer having regioregular poly(3-hexyl thiophene) and poly(N-isopropylacrylamide). The optical and luminescence properties of theses polymers highly depend on the self-assembled nanostructures formed in different solvent and are easily tailored by changing the solvent composition or external stimuli like heat. Unique optical and electronic properties of these block copolymers are believed to make it promising for applications like sensor, fluorescence thermometer, optoelectronic, and bioelectronics devices.

Keywords: *Block copolymer, thermo-sensitive, Conjugated polymer*

Introduction
Development of new conjugated polymeric materials with novel functionality and wide processability has attracted lot of research attention because of their enormous potential applications in sensors, energy storages, corrosion inhibitors, optoelectronic devices, etc[1-2]. Particularly, there is a significant demand of water-soluble conjugated polymeric materials related to their applications achieved from environmentally friendly steps and applications centered on their use in biological environments[3]. Poly (3-hexyl thiophene) (P3HT) is one of the mostly studied conjugated polymer and work horse for organic electronic devices[4,5].

P3HT has been incorporated into different types of block copolymers in order to manipulate its solubility, optical, electronic properties[6-9].
Here, a novel class of amphiphilic, thermosensitive rod−coil conjugated block copolymer (P3HT-b-PNIPAM) composed of regioregular P3HT and a thermoresponsive polymer poly(Nisopropylacrylamide) (PNIPAM) has been synthesized in order to manipulate the properties of P3HT. The optical and luminescence property of P3HT-b-PNIPAM is different from P3HT and deeply depends on the nature of the solvent or composition in a mixed solvent. P3HT-b-PNIPAM shows lower critical solution temperature (LCST), detected from both UV−vis and luminescence studies.

Experimental All chemical including Magnesium, 1-bromohexane, 3-bromothiophene, Na_2SO_4, N-Bromosuccinimide, Na_2S_2O3, KOH, etc. were purchased from Sigma Aldrich Pvt. Ltd. and used as received. Other solvents like THF, Ether, Methanol, Chloroform etc. were obtained from Rankem.

Characterization: Fourier transform infrared (FTIR) spectra were recorded in Perkin Elmer FTIR spectrometer [Spectrum two]. Nuclear magnetic resonance spectra were record on 300MHz Bruker instrument. The number-average molecular weight (Mn) and polydispersity index (Mw/Mn) of P3HT samples were determined by Shimadzu prominence in THF as solvent Atomic force microscopy (AFM) imaging was performed using AFM NT-MDT, Solver Pro 47 in the tapping mode. UV-vis absorption spectra were recorded in chloroform and thin film state on a Simadzu UV 3600+, UV-vis spectrophotometer.

Synthesis of P3HT-b-PNIPAM
The typical synthesis procedure of the P3HT-b-PNIPAM is as follows. Into a 25 mL Schlenk flask were added 221.06 mg (16.87 μ mol) of alkyne-terminated P3HT, 3.873 mg (27 μmol) of CuBr,

500 mg (13.5 μmol) of PNIPAM-N_3 and 30 mL of dry THF. The tube was degassed by three freeze -thaw cycles in liquid N_2 and then 5.629 μL (27 μmol) degassed PMDETA was added to the reaction mixture and refluxed at 60 °C for 24 h. After opening the reaction mixture in air, it was further diluted with THF and passed through neutral alumina column to remove Cu catalyst. After that THF was removed by rotary evaporator and the polymer was further dissolved in DMF. The unreacted P3HT was removed by filtering the DMF solution. Finally, the purple colour polymer was obtained by removing DMF in rotary evaporator and drying the sample in a vacuum oven for 48 h at 60 °C (60% yield). The resulting block copolymer was further characterized by GPC and NMR. ^{1}H ($CDCl_3$) 6.98 (1H, s), 2.80 (t, 2H), 2.8−0.89 (m, aliphatic H of PNIPAM and P3HT), 7.78 (s, 1H, triazole −CH−), 4.0(m, 1H, $(CH_3)_2CHNH$, PNIPAM).

Result & discussion

P3HT-b-PNIPAM was prepared successfully by connecting two homopolymers through Cu-catalyzed click

The presence of the triazole proton at δ = 7.78 ppm as well as the disappearance of both ethynyl proton at (δ =3.52 ppm) in 1H NMR (Figure 1) and the azide stretching frequency ∼2110 cm−1 in FTIR confirm the successful synthesis of P3HT-b-PNIPAM. The Mn and PDI of P3HT-b- PNIPAM are around 44,000 and 1.4 respectively. At room temperature, the synthesized P3HT-b- PNIPAM is soluble/dispersible in several solvents such as chloroform, THF (good solvent for both the block), and water, methanol, DMF (poor solvent for P3HT). In nonselective polar solvent like water, P3HT-b-PNIPAM forms self-assembled into core/shell−type nanostructure with hydrophobic P3HT in the core and hydrophilic PNIPAM in the shell (Fig-2).The Z-average particle size of P3HT-b-PNIPAM in water and methanol are 129 and 167 nm, respectively The higher Z-average particle size of P3HT-b-PNIPAM in methanol compared to water may be explained from the higher solubility of the PNIPAM in methanol resulting more extended chains and formation of larger aggregates. UV−vis spectra of P3HT and P3HT-b-PNIPAM in various solvent are presented in Figure 3a. From the figure it is clear that the λmax value for π−π* transition of P3HT changes from 449 nm to 429 nm upon grafting with PNIPAM. The spectral shift is the result of change in the effective conjugation length as the P3HT chains adopt more coil conformation due to the steric interaction with the PNIPAM chain as well as change in the solvophobic environment near the polythiophene main chain. The block copolymer shows different λmax value depending on solvent where it is dissolved or dispersed. In solvent like methanol and water where P3HT is not hydrated, two absorption peaks at 429 and 510 nm are observed. The peak at 429 is assigned to π-π* transition of P3HT and 510 nm is possibly originated from the aggregation of P3HT- b-PNIPAM. The different λmax for different solvent is result of the different conformation adopted by P3HT-b-PNIPAM causing change in the effective conjugation length as evidenced by AFM study. The block copolymer shows solvent dependent colour emission, orange in THF, purple in water and blue in methanol (Figure 2b). Figure 3c demonstrates the PL spectra of the block copolymer in four different solvents. The PL emission peaks are 577, 574, and 566 nm (with additional intense peaks at 460 and 491 nm) for chloroform, THF and methanol, respectively. In the case of water, the PL intensity substantially decreases and the peak becomes broader and red-shifted. The different colour emission originates from different type of nanostructures attributed to the different conjugation length formed in different solvents. The dramatic decrease of PL intensity in water is due to the increased interchain Froster energy transfer from more close proximity of the P3HT chains in micelles. In thin film state P3HT generates a peak at

648 nm, whereas the peak shifted to 711 nm in case of P3HT-b-PNIPAM (Figure 3d). The red shift in PL spectra is due to the energy transfer to low energy sites in the packed

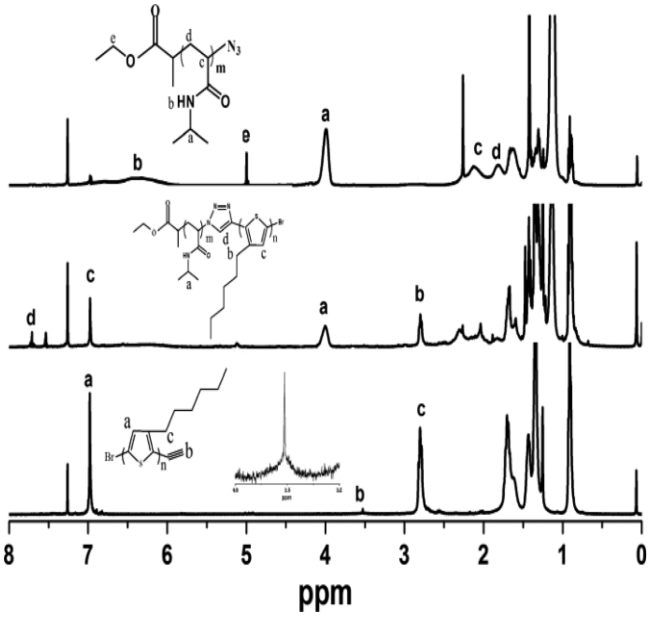


Figure 1. 1H NMR spectra of P3HT-alk, P3HT-b-PNIPAM,
PNIPAM-N_3 in $CDCl_3$.

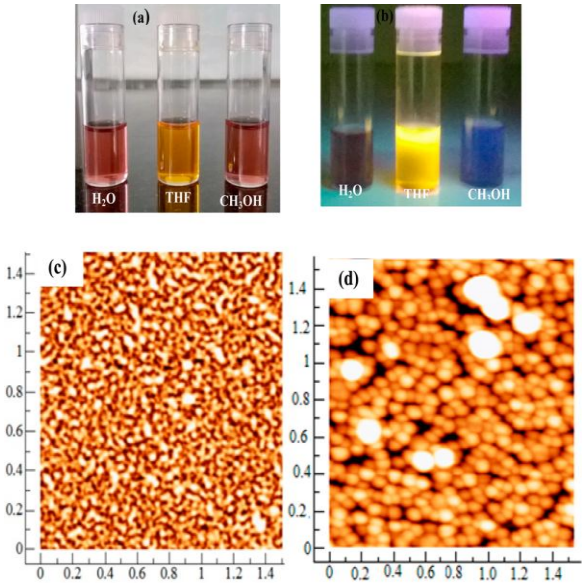
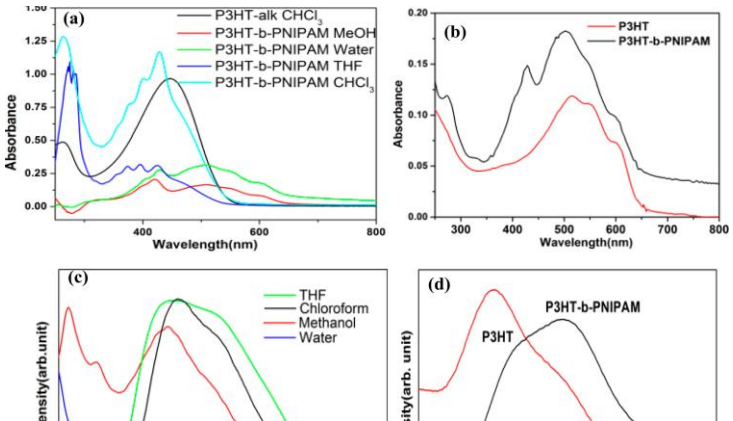


Figure 2. (a) color of the P3HT-b-PNIPAM in various solvent, (b) distinct color emission under UV illumination, (c, d) AFM phase images of P3HT-b-PNIPAM thin films deposited from (c) THF and (d) water.

P3HT chains induced by PNIPAM. Figure 4a displays the temperature dependent PL intensity for P3HT-b-PNIPAM in water upon heating. A sharp reversible change in the PL intensity between 30 to 35 °C has been observed. The sudden increase of the PL intensity is due to reversible conformational change of the PNIPAM from an extended hydrated coil to a collapsed hydrophobic globule (as shown in the inset of Figure 3a) at LCST. In collapse conformation, the PL intensity will be high as the intercalated PNIPAM chain will separate the P3HT chains from each other and prevent PL quenching through interchain mechanism. The reversible change of conformation from an extended hydrated coil to a collapsed hydrophobic globule near LCST is also supported by temperature dependent DLS study. There is a sharp decrease in the average particle size from 126 to 101 nm on heating from 30 to 35 °C. On further heating the average particle size again



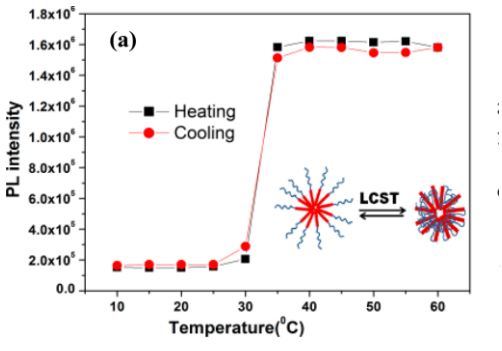


Figure 4. Variation in PL intensity at

increases (at 40 °C, 153 nm) as these collapse chain conformation is unstable and forms larger aggregation. The water solution of the polymer also shows sudden increase of absorption intensity at 510 nm between 30 to 35 °C upon heating. Both the observations clearly demonstrate the potentiality of P3HT-b-PNIPAM for fabrication of delicate temperature sensor.

The nonlinear I−V characteristics curve of the polymer shows semiconducting behaviour and confirms its applications for electronic and optoelectronic devices.

Conclusion:

In summary, an amphiphilic, thermoresponsive rod−coil conjugated block copolymer P3HT-b-PNIPAM has been successfully synthesized by a Cu-catalyzed click reaction which couples ethynyl-terminated regioregular poly(3-hexylthiophene) and azide-terminated PNIPAM. In nonselective solvent, the block copolymer is self-assembled into phase separated nanostructure whereas in polar solvent like water aggregated into core/shell−type nanostructure. The optical and luminescence property of the block copolymer is different from its pure analogue and highly depends on the nature of the solvent or composition in a mixed solvent. Temperature dependent photoluminescence and UV−vis study clearly indicate that between 30 and 35 °C in water P3HT-b-PNIPAM undergoes a reversible phase transition from a collided structure to collapsed globule (Fig.-4). By varying the composition of the P3HT block in the block copolymer one can further tune the solubility, nanostructured morphology and thereby can tune its optical and electronic properties in a controlled manner. We believe that the unique optical and electronic properties will make it promising for many applications like sensor, fluorescence thermometer, optoelectronic, and bioelectronics devices.

Acknowledgement: B.K.K acknowledge Ramanujan Fellowship (SR/S2/RJN-81/2010, DST), CSIR project (02(0117)/13/EMR-II), DST fast track project (SR/FT/CS-169/2011), Centre for Excellence in Green and Efficient Energy Technology (GEET) (under FAST scheme of MHRD, Government of India, New Delhi) for financial support.

References:

1. F. Wang, H. Gu, T. M. Swager, *J. Am. Chem. Soc.*, 130, 5392, 2008.
2. 2 D. T. McQuade, A. E. Pullen, T. M. Swage, *Chem. Rev.*, 100, 2537, 2000.
3. 6. K. P. R. Nilsson, O. Inganas, *Nat. Mater.*, 2, 419, 2003.
4. A. Marrocchi, D. Lanari, A. Facchettibc, L. Vaccaro, *Energy Environ. Sci.*, 5, 8457, 2012.
5. F. Y. Yang, K. J. Chang, M. Y. Hsua, C. C. Liu, *J. Mater. Chem.*, 18, 5927, 2008.
6. P. Kumar, M. K. Bera, S. Malik and B. K. Kuila, *ACS Applied Material and Interfaces* 7,12348–12354, 2015

7. M. Sommer, A. S. Lang, M. Thelakkat, *Angew. Chem., Int. Ed.,* 47, 7901, 2008.
8. Q. Zhang, A. Cirpan, T. P. Russel, T. Emrick, *Macromolecules* 42, 1079, 2009.
9. E. Kaul, V. Senkovskyy, R. Tkachov, V. Bocharova, H. Komber, M. Stamm, A. Kiriy, *Macromolecules* 43, 77, 2010.

MACRO 351

BUF Resins Synthesis: An Experimental Study & Characterization of Resins by Changing Bu/U Mole Ratio

Amin, Shital[a], Dayal Pratyush[b], Padhiyar Nitin*

[a] *Department of Chemical engineering, Indian Institute of Technology Gandhinagar, Gandhinagar 382355, Gujarat, India*

nitin@iitgn.ac.in

Abstract

Butylated Urea Formaldehyde (BUF) resins properties changes depending upon the amount of alcohol used in the synthesis. In this work, characterization experimental investigations of the BUF resins have been performed, which will be useful for the process systems engineering. In present work, we present the characterization techniques for identification of the various functional groups and oligomers formed during resins synthesis using ^{1}H-NMR and LCMS respectively, measurement of butanol content using GC, and the water content in the BUF resins using KF. Characterization results indicate that the resins formed are partially alkylated. The butanol concentration has an influence on the final resin viscosity; lower the B/U ratio higher is the viscosity.

Keywords: *butylated urea formaldehyde resins; NMR; LCMS; reactant mole ratio;*

Introduction

Butylated Urea Formaldehyde (BUF) resins are industrially known as amino cross-linking agents or aminoplasts. [1–3] BUF finds widespread applications in baking and stoving enamel formulations, plywood baking and as air-drying amino alkyd enamels.[4] BUF is prepared by alkylation using an alcohol such as *n*-butanol for enhancing the water resistance property of Urea Formaldehyde (UF).[5] Synthesis of the BUF is a three-step process.[4,6,7] Reaction of urea and formaldehyde takes place in the first step, which is also called methylolation reaction.[4,6,7]In the second step - the methylolated intermediates react with each other to form oligomers with methylene (-CH_2-)[8,9] and di-methylene ether (-CH_2-O–CH_2-)[10,11]linkages. Alcohol reacts with methylol group in the butylation or etherification reaction in the third step. Our approach to study BUF resins characterization is based on UF resins due to common reactions of methylolation and condensation.

Different grades of BUF are produced commercially based on their diverse applications in paint and coating industry.[12] The resin properties are likely to change with different extent of alkylation.[1]

The control of the reaction and, therefore, of the degree of condensation and butylation are important in order to obtain a product with tailor made properties. Reaction parameters that mostly affect the properties of the final product are the molar ratio of reactants, pH, temperature, concentration and time.

The complex UF and BUF resins chemistry has been the subject of numerous structural investigations.[13] ^{1}H-NMR are found to be useful technique for the identification of methylol intermediate, which can be synthesized by controlling reaction parameters.[13] An overview of the NMR studies of the UF system in the literature is given in the work of Minopoulou et al.[13] They have recorded ^{1}H-NMR spectra for model compounds and developed the method for the quantification of functional group in the UF resin. They have reported that UF resins produced at high temperatures and acidic pH values exhibit higher degrees of condensation, presumably because of the development of more cross-linked structures. Kambanis and Vasishth[14] reported procedure for analyzing UF and BUF resins and performed quantitative determination of functional groups in resins using ^{1}H-NMR spectroscopy. Christensen[15] have performed inter laboratory study concerning the analysis of functional groups in amino resins, in particular UF, BUF and melamine resins and established technique for the estimation of functional group concentration. Meyer[16] has reported spectra of UF resins and characterized various functional groups present in the resins system based on the model compound. For identification of oligomeric structure of resins, Liquid Chromatography Mass Spectrometry (LCMS) is found to be useful technique. Recently, Favretto et al.[2] described characterization method for the structure analysis of *n*-butylated melamine formaldehyde and *i*-butylated formaldehyde resins using HPLC coupled with electron spray ionization. Chang[17] reported the characterization of methoxymethyl melamine resins by LCMS technique and identified monomeric and dimeric compounds formed during the resins synthesis.

In this study, particular emphasis is given to improve the understanding of the available characterization techniques and its applicability to understand the BUF structure. Three sets of experiments were performed in a semi batch reactor to form resins by varying Bu/U mole ratio (2.6 to 4) while keeping the other process parameters constant such as temperature, pressure, pH and catalyst concentration. Various functional groups linkages were identified by H^{1}-NMR. The BUF structures of oligomers were predicted using LCMS analysis. The butanol consumed during the reaction was measured using Gas Chromatography (GC) and by performing material balance. Further, BUF resins were characterized by measuring % solids, viscosity and Moisture Content (MC).

Experimental section

A schematic of the semi batch process along with the vapour phase separation and butanol recycle is shown in Figure 1.

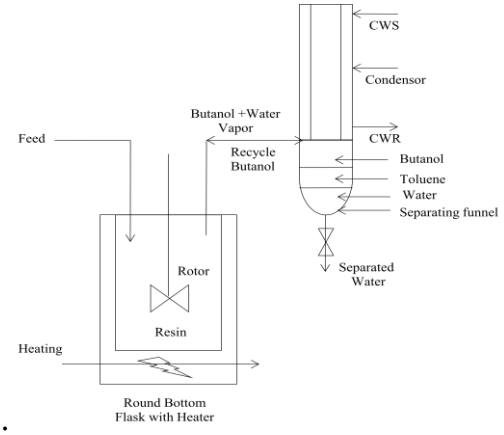


Figure 1: Semi batch production of butylated amino resins

Formalin and butanol are charged at required experimental temperature into the reactor. The pH of the reaction mixture is adjusted to neutral by addition of 1 N NaOH solution and formic acid with 98% purity. A pre-calculated amount of urea is charged to a glass reactor. The experiments were performed with varied Bu/U mole ratio (2.6 to 4) and with constant F/U ratio 2.03 for preparation of resins. For the methylolation reaction, temperature is maintained at the desired value of 70 ± 3 ˚C and the reaction mass is kept idle for 60 min. Again, the heating is started and the temperature is set at 90℃. The condensation process starts now; pH is adjusted to 4.5 by adding acid catalyst such as phosphoric acid and oxalic acid. Small amount of toluene is added to the bottom of the separating funnel to facilitate the effective separation of butanol and water from condenser. Water is removed from the bottom of the separating funnel and the butanol rich layer is recycled into the vessel. Completion of the BUF resins synthesis process is checked by resins *o*-xylene tolerance test.

^{1}H-NMR are recorded for BUF resins by using Bruker 500 MHz with 1000 scan. In present analysis, LCMS measurement is performed on SynaptG2-S model with ESI detector. Formaldehyde is measured using the sulphite method.[11] The GC analysis is used to get the concentration of butanol in water rich and toluene rich phases. GC-1000 Chemito gas chromatography, equipped with a flame ionization detector is used for analysis. **V**olumetric analysis using Karl Fischer (ANALAB Make) was performed for determining the water content (percentage by weight) in resins samples. The percentage solid test is carried out by keeping the sample for 2 hrs at 120 ºC in oven. Viscosity is measured by the Gardner Bubble Viscometer method at 25 ºC.

Result and Discussion

Table 1 shows the analysis of ^{1}H-NMR spectra of resins prepared with Bu/U ratio 2.6. Analysis shows the presence of various functional groups such as urea, mono/di/tri-substituted urea, butylated ether linkages and linkages such as di-methylene ether and methylene linkage corresponding to various NMR peaks (ppm).

Table 1: ^{1}H-NMR analysis of BUF resins prepared with Bu/U ratio: 2.6

Structure	Frequency in ppm	Literature
=NCH$_2$OCH$_2$NH, =NCH$_2$NH	7-7.3	1
NHCH$_2$OCH$_2$NH, -CONH-	6.8-7	1,2,3,4
NH$_2$CO, -CONH-	5.6-6	1,2,3,4
OHCH$_2$N, NCH$_2$OCH$_2$N, NCH$_2$N	4.3-4.8	1,2,3,4
ROCH$_2$(CH$_2$)$_2$CH$_3$	3.3-3.5	1,2,3,4
OCH$_2$CH$_2$CH$_2$CH$_3$	1-1.5	3,4
OCH$_2$(CH$_2$)$_2$CH$_3$	0.7-1	3,4

Figure 2 shows ^{1}H-NMR spectra of resins prepared with Bu/U ratio 2.6.

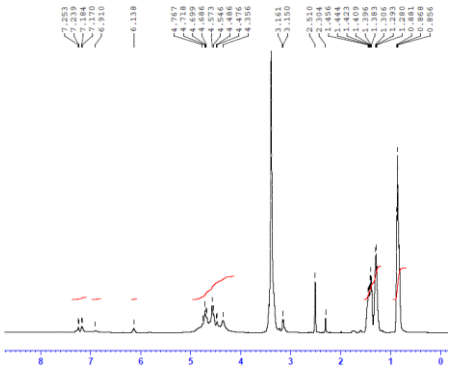


Figure 2: ^{1}H-NMR spectra of BUF resins having Bu/U ratio 2.6

The integration of the spectra is based on the assumption that -CONH- peak contains only one hydrogen. ^{1}H-NMR spectra consist of bands corresponding to -CH$_2$-, -NH$_2$ and -NH- protons and can be used for quantitative characterization of the resins.[13] By calculating the relative peak areas of the above mentioned groups, the percentage abundances of the non-substituted, N-substituted and N,N-di-substituted amide groups can be obtained. Results are listed in Table 2. Resins formed with Bu/U ratio 2.6 shows higher abundance of di-substituted group, which indicates higher degree of condensation compared to resins formed with other Bu/U ratios. It also indicates low abundance of the tri-substituted group compared to resins formed with Bu/U ratio 3.08.

Table 2: Percentage abundances of characteristic groups in BUF resins

Characteristic groups	Bu/U : 4	Bu/U : 3.08	Bu/U : 2.6
% - NH$_2$	3.229	1.491	2.132
% - NH-	0.0694	3.550	4.6055
% - N=	89.83	94.95	93.26

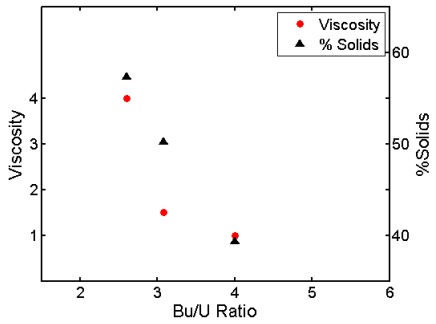


Figure 3 : Viscosity and %solids vs. Bu/U ratio for BUF resins

To draw any further conclusion, we have measured the resin properties such as viscosity and % solids. Figure 3 depicts that viscosity and % solids increase with decrease in Bu/U ratio. Resins formed with Bu/U ratio 2.6 shows higher viscosity compared to other two. It may contain more concentration of $-CH_2OH$ and -NH- groups which can form hydrogen bond with the solvent and lead to higher viscosity. Another reason could be $-CH_2OH$ groups react with each other to form $-CH_2-$ linkage with long chain oligomers giving higher viscosity.

BUF resins are further characterized to verify extent of butylation. It has been assumed that 2 % butanol is lost during the synthesis and solvent phase of the BUF resins contains free formaldehyde, water and unconverted butanol. The GC analysis is utilized to measure butanol in water rich and toluene rich phases which are removed during the semi batch process of BUF resins synthesis. Bu_c (moles of butanol consumed) is calculated by subtracting the amount of butanol present in solvent phase, butanol lost with toluene and water phases from total butanol input. Mass of solvent phase is calculated by considering the % solids of resins mixtures to get mass of solid resins which is subtracted from total mass of resins mixtures. Table 3 shows that butanol consumption is more for the resin prepared with Bu/U ratio 2.6. It also indicates the % FF content increases with decrease in Bu/U ratio. FF content and % solids in Figure 3 indicates resins formed are partially alkylated resins.[18] Polymerization reactions are reversible in nature hence there are possibilities of formaldehyde evolving during the reverse reaction of polymerization or conversion of di-methylene ether linkage into the methylene linkage.

BUF model resins are further characterized to predict the structure using LCMS. The LCMS chromatograms of percentage relative abundance vs. retention time are recorded in Figure 4A for BUF resins.

Table 3: Butanol consumption for resins

Bu/U Ratio	4	3.08	2.6
F/U Ratio	2.03	2.03	2.03
Bu concentration in toluene (T_{out}) rich phase	62.84	55.06	56.06
Bu concentration in water (W_c) rich phase	3.92	4.31	3.34
% Moisture content of resins product	3.94	3.11	3.25
% Solid of final resins product	39.35 %	50.21 %	57.30 %
% FF content of final resins product	1.04 %	1.07 %	1.15 %
% Butanol Conversion	25.03	33.95	41.97

The ESI mass spectra of the BUF resins prepared with Bu/U ratio 2.6 eluting at 7.55 min are reported in Figure 4B. It shows the relative abundances of various masses are present in corresponding peak.

Table 4: BUF resins mass fragments and corresponding predicted structure

RT (min)	Molecule Type	Free valance of N	$-CH_2OH$	$-C_4H_9OH-O-CH_2$	H	Mw	Structure
7.55	dimer_a	6	4	1	1	338	$C_{12}H_{26}O_7N_4$
7.55	dimer_b	6	3	1	2	338	$C_{12}H_{26}O_7N_4$
6.60	trimer_a	8	4	1	3	410	$C_{14}H_{30}O_8N_6$
6.60	trimer_b	8	2	1	5	410	$C_{19}H_{40}O_9N_6$
6.60	trimer_c	8	3	1	4	410	$C_{14}H_{30}O_8N_6$

Table 5: The structure of the backbone polymer chain

dimer_a	N-CO-N-CH_2-N-CO-N
dimer_b	N-CO-N-CH_2-O-CH_2-N-CO-N
trimer_a	N-CO-N-CH_2-N-CO-N-CH_2-N-CO-N
trimer_b	N-CO-N-CH_2-O-CH_2-N-CO-N-CH_2-O-CH_2-N-CO-N
trimer_c	N-CO-N-CH_2-N-CO-N-CH_2-O-CH_2-N-CO-N

Polymer molecules are classified such as dimer, trimer, tetramer etc. Table 5 shows the structure of the backbone polymer chain of dimer and trimer having linkages such as $-CH_2-$ or $-CH_2-O-CH_2$. The backbone polymer chain can be attached to various functional groups such as $-CH_2OH$, $-C_4H_9OH-O-CH_2$ and H depending on the free valences of nitrogen atom and the structure could be predicted by trial and error method. Table 4 shows the mass fragments (340 and 412) obtained for BUF resins with their retention time.

Similarly, the structure of other 12 molecular masses can be predicted. Resins prepared with varying Bu/U ratio show similar masses for the major peaks, mainly 340, 498, 412, 656 and 814. Structure of mass fragment 340 is reported in Figure 4D, which indicates that the resins formed are of partially alkylated type. The elemental composition analysis of the component with Mw 340 is reported in Figure 4C. This indicates that the predicted formula by trial and error matches with the result shown by LCMS.

CONCLUSIONS

The effect of Bu/U ratio on BUF resins was investigated by manufacturing BUF resins in semi batch process with different initial reactant concentration. The result shows more amount of butanol is consumed at lower Bu/U ratio.

Based on the values of FF content and % solids, and structure predicted by LCMS, it is concluded that resin formed are partially alkylated type.

Reactant mole ratio of Bu/U play significant role in the reaction between urea, formaldehyde and butanol and has significant effect on the type of linkages and groups formed during synthesis, which determines the final resin properties.

Reactant mole ratio of Bu/U play significant role in the reaction between urea, formaldehyde and butanol and has significant effect on the type of linkages and groups formed during synthesis,

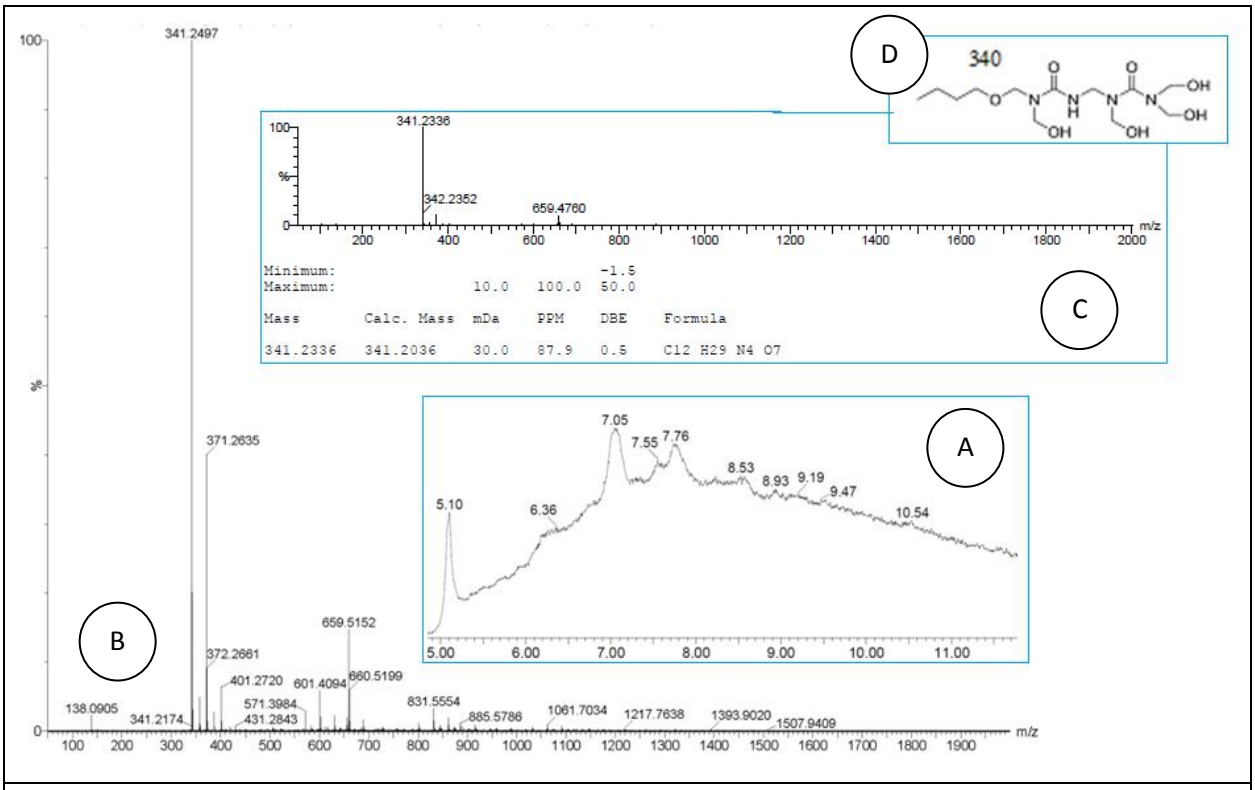


Figure 4: (A) The LCMS spectra of BUF model resins model with Bu/U ratio 2.6, (B) ESI mass spectra of the component with the retention time 7.55 min and(C) Elemental composition report corresponding mass found 341 with the retention time 7.55 (D) Predicted structure of mass fragments in LCMS analysis

which determine the final resin properties.

Resins prepared at lower Bu/U ratio shows higher degree of condensation, resulting in molecules with higher molar masses and yield more N,N-disubstituted amide groups and -CH_2OH groups and that account for the formation of longer chain molecules.

Higher quantity of butanol confers little advantage however, it is added to maintain the viscosity of the resins.

Acknowledgement

Financial support of this work by IIT Gandhinagar is gratefully acknowledged.

References

(1) Oldring, P. K. T.; Limited, S. T.; Tuck, N. *Resins for Surface Coatings: Polyurethanes, polyamides, phenolplasts, aminoplasts, maleic resins*; Wiley, 2001.

(2) Favretto, D.; Traldi, P.; Marcelli, A. *Eur. Mass Spectrom.* **1998**, *4* (5), 371–378.

(3) Hart, W. F. Storage-stable butylated urea-formaldehyde cross-linking agent and process for the manufacture thereof. US3957731 A, May 18, 1976.

(4) Koleske, J. V. *Paint and Coating Testing Manual*; ASTM International, 1995.

(5) Blais, J. F. *Amino resins*; Reinhold Pub. Corp., 1959.

(6) Vaughan, G. D. *Paint and Coating Ind.*; 1998; Vol. 58.

(7) Leach, R. H. *The Printing Ink Manual*; Springer Science & Business Media, 1993.

(8) WICKS JR, Z. W. *Encycl. Polym. Sci. Technol.* **2003**, *1*, 340.

(9) Ibeh, C. C. *Handb. Thermoset Plast. 2 Pp* **1999**, 72–96.

(10) Carvalho, L. M. H.; Costa, M. R. P. F. N.; Costa, C. A. V. *J. Appl. Polym. Sci.* **2006**, *102* (6), 5977–5987.

(11) Kumar, A.; Katiyar, V. *macromolecules* **1990**, *23* (16), 3729–3736.

(12) Freitag, W.; Stoye, D. *Paints, Coatings and Solvents*; John Wiley & Sons, 2008.

(13) Minopoulou, E.; Dessipri, E.; Chryssikos, G. D.; Gionis, V.; Paipetis, A.; Panayiotou, C. *Int. J. Adhes. Adhes.* **2003**, *23* (6), 473–484.

(14) Kambanis, S. M.; Vasishth, R. C. *J. Appl. Polym. Sci.* **1971**, *15* (8), 1911–1919.

(15) Christensen, G. *Prog. Org. Coatings* **1980**, *8* (3), 211–239.

(16) Meyer, B. *Urea-Formaldehyde Resins*; Addison-Wesley, 1979.

(17) Chang, T. T. *Anal. Chem.* **1994**, *66* (19), 3267–3273.

(18) Stoye, D.; Funke, W.; Hoppe, L.; Hasselkus, J.; Curtis, L. G.; Hoehne, K.; Zech, H.-J.; Heiling, P.; Yamabe, M.; Dören, K.; others. *Ullmanns Encycl. Ind. Chem.* **2006**.

MACRO 358

Poly (methylated pyridinium benzimidazolium): A new class of anion exchange membrane

Balakondareddy Sana, Tushar jana*

School of chemistry, University of Hyderabad, Hyderabad, India

Email: tusharjana@uohyd.ac.in

Poly (methylated pyridinium benzimidazolium) iodides (PMPBI) were synthesized successfully by methylation of pyridine bridge polybenzimidazoles (Py-PBIs) using excess methyl iodide and this method allows avoiding the use of toxic chloromethylation method. The Py-PBI polymers were synthesized from tetra amine 2, 6-bis (3', 4'-diaminophenyl)-4-phenyl pyridine (Py-TAB) monomer and various kinds of dicarboxylic acids. Here, both pyridinium and benzimidazolium groups acted as anion exchange sites. The PMPBI membranes were prepared by casting in DMSO solvent. The PMPBOH and PMPBCO_3 anion exchange membranes (AEMs) were obtained by anion exchange of PMPBI with KOH (0.5 M, 0.1 M) and K_2CO_3 (0.5 M) solutions, respectively. The PMPBI and PMPBOH membranes were characterized by the FT-IR and ^{1}H NMR spectroscopy. The AEMs were fully characterized by IEC, water uptake, ionic conductivity and for thermal, mechanical and chemical stability using both 0.5 M KOH and K_2CO_3 aqueous

alkaline solutions. The PMPBOH membranes displayed higher IEC and higher ionic conductivity to that of $PMPBCO_3$ membranes. The PMPBOH membranes demonstrated high ionic conductivity (10.24×10^{-2} S/cm) and mechanical strength which were proved by the cross-section morphology. The pyridinium groups helped in improving the ionic conductivity by preventing the formation of pyridone. Among all the polymers, PMPBI-OBA membrane was more stable and PMPBI-IPA membrane was least stable towards alkaline solutions. In this study, the PMPBI-OBA membrane exhibited excellent AEM properties. These results highlighted the feasible approach for enhancing the ionic conductivity and other membrane properties which have potential applications as AEMs.

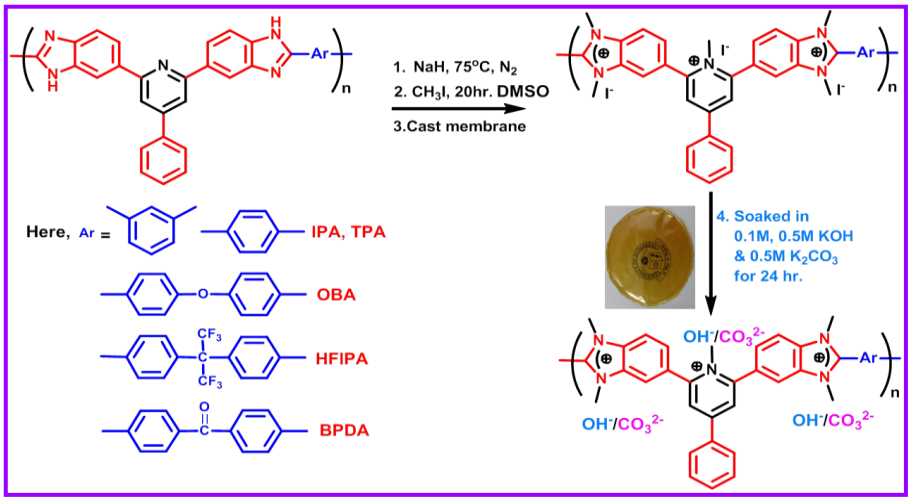


Figure 1. Synthesis of poly (methylated pyridinium benzimidazolium) and anion exchange membranes from it.

References

5. L, Yan; M, A, Hickner; *Macromolecules* 43 (2010) 2349.
6. S, Maity; T, Jana; *Macromolecules*, 46 (2013) 6814.
7. X, Li; Y, Yu; Y, Meng; *ACS Appl. Mater. Interfaces* 5 (2013) 1414.
8. K, M, Meek; Y, A, Elabd; *Macromolecules* 48 (2015) 7071.

MACRO 372

Synthesis and Characterization of Stereo-Di-Block Polylactides with Varying Block Length Compositions

Mili, Medha[a], Masutani, Kazunari[b], Sakurai, Shinichi[c], Kimura, Yoshiharu[b], Katiyar,Vimal[a,*]

[a]Department of Chemical Engineering, Indian Institute of Technology Guwahati, Guwahati-781039, Assam, India
[b]Center for Fibre and Textile Science, Kyoto Institute of Technology, Japan-606-8585
[c]Department of Biobased Materials Science, Kyoto Institute of Technology, Japan-606-8585

** Email: vkatiyar@iitg.ernet.in*

The present work reports the synthesis of stereo-di-block Polylactides (PDLA-b-PLLA) via two-step ring opening polymerization (ROP) of L-and D-lactides [1] having composition ratios 20/80 and 30/70. In addition, silk nanocrystal (SNC) as a filler have also been incorporated and its affect on the properties of the synthesized stereo-di-block PLA have been studied. Herein, PDLA prepolymers with monohydroxyl terminals are first synthesized which then acts as the macroinitiators in the next step ROP of L-lactide to obtain the target stereo-di-block PLA in the presence of stannous octoate as the catalyst. ^{1}H NMR spectra confirms the synthesis of stereo-di-block PLA having short PDLA block and long PLLA block composition. The resultant stereo-di-block PLA having molecular weight~100kDa were then fabricated into hot pressed film which are then annealed at various temperatures. To investigate the crystal phases present in the annealed samples, WAXD measurements have been performed which clearly suggests preferential stereocomplex crystal (sc) formation without any homochiral (hc) crystal formation [2]. Further, SAXS analysis has been carried out to investigate the affect of annealing temperature on the Long period and Lamellae thickness and was found that with the increase of annealing temperature there is increase in the Long period and Lamellae thickness.

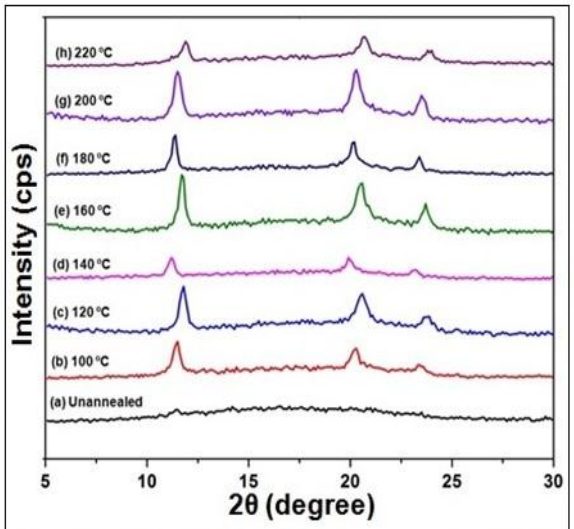


Figure 1:- WAXD profile of di-b-PLA having composition ratio of 20/80

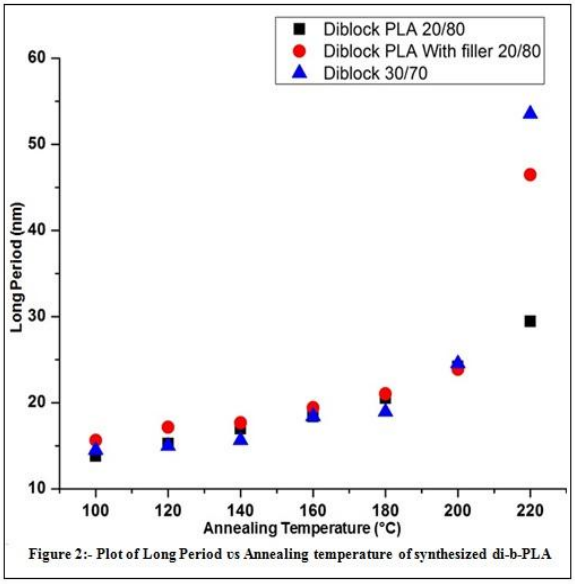


Figure 2:- Plot of Long Period vs Annealing temperature of synthesized di-b-PLA

References

1 Hirata, Masayuki; Kobayashi, Kaori; Kimura, Yoshiharu. *J Polym Sci Part A: Polym Chem* 48 (2010) 794.

2. Masutani, Kazunari; Lee,W.C; Kimura,Yoshiharu. *Macromol Chem Phys 213* (2012) 695.

.

MACRO 392

Synthesis and Characterization of New Semifluorinated Sulfonated Polyimides for Proton Exchange Membrane Application

[a]Singh Asheesh, [a]Banerjee Susanta*

[a]*Materials Science Centre, IIT, Kharagpur 721302, India*

*susanta@matsc.iitkgp.ernet.in

A series of new semifluorinated sulfonated polyimide (PTNQSH-XX) copolymers were prepared by the click polymerization of bis-N,N'-(prop-2-ynyl)-1,4,5,8-naphthalenetetracarboxylic diimide (TN) with a mixture of two diazide monomers: 4,4-bis[3-trifluoromethyl-4(4-azidophenoxy)phenyl]biphenyl (QAZ) and 4,4′-Diazido-2,2′-stilbenedisulfonic acid disodium salt hydrate (DADSDB). The degree of sulfonation (DS) of the polyimides was controlled by variation of ratio of DADSDB to QAZ. The structures of the polyimides were confirmed by FTIR and ^{1}H NMR spectroscopy. The polyimides exhibit high molecular weights and good solubility and film forming capabilities. The copolymer films showed good thermal stabilities, oxidative stabilities and mechanical properties depending upon their chemical compositions. The copolymers showed good dimensional stability and low water uptake values. Transmission electron microscopy (TEM) images of the membranes showed phase separated morphology with ionic cluster sizes from 10 to 75 nm. Ion exchange capacity of the copolymers was calculated ^{1}H NMR spectroscopy and determined by titration. The proton conductivities of PTNQSH-XX (XX-50, 60, 70, 80) membranes were found in the range of 6-32 mS/cm at 30 °C and 14-79 mS/cm at 80 °C.

References

1. Huang, Yao Jheng; Ye, Yun Sheng; Yen, Ying Chieh; Tsai, Li Duan; Hwang, Bing Joe; Chang, Feng Chih. *International Journal of Hydrogen Energy*, 36 (2011) 15333.
2. Singh, Asheesh; Mukherjee, Rajdeep; Banerjee, Susanta; Komber, Hartmut; Voit, Brigitte. *Journal of Membrane Science*, 469 (2014) 225.
3. Singh, Asheesh; Banerjee, Susanta; Komber, Hartmut; Voit, Brigitte. *RSC Advances*, 6 (2016) 13478.

Macro-395

Synthesis and Characterization of Perfluorochain Bearing Crosslinked System via Hydrosilylation Reaction.

Sandeep P.B, Monisha Baby, Ranajit Pal*, and Suraj S.
Polymers Division, Vikram Sarabhai Space Centre, Trivandrum-695022, India
** e-mail id: monishababy87@gmail.com*

Abstract

A hybrid compound bearing perfluorochain 1H,1H,2H,2H Perfluorooctyl triallylsilane (PFOTAS) was synthesized via allyl Grignard reaction of 1H,1H,2H,2H perfluorooctyltrichlorosilane (PFOTCS) and was characterized by using Fourier transform infrared spectroscopy (FTIR), ^{1}H and ^{13}C nuclear magnetic resonance (NMR) spectroscopy. The PFOTAS thus synthesized undergoes hydrosilylation reaction with 1,3,5,7-tetramethylcyclotetrasiloxane (TMCTS) to form a crosslinked system in presence of Platinum catalyst in vinyl polydimethylsiloxane (PDMS). The curing behavior of the system is monitored by using FTIR and Differential Scanning Calorimetry (DSC). From FTIR data, disappearance of C=C bond peak of PFOTAS during the course of reaction indicates the formation of the cross-linked product. Exothermic peak obtained from DSC analysis shows the curing reaction. The kinetic parameters such as activation energy (Ea) and Arrhenius pre-exponential factor (A) were also computed from DSC using Borchardt Daniel method. Contact angle measurement showed the hydrophobic nature of the cross-linked system. Surface energy of the cured product is evaluated by contact angle measurement using harmonic mean method.

Keywords: *perfluoro-crosslinked system; kinetic parameters; hydrophobic;*

Introduction

Perfluorinated compounds (PFCs) belong to a special class of chemicals which are used in a wide range of commercial and industrial products in order to change physico-chemical properties of the product. The use of PFCs in products make them resistant to water, stains, oil, fire *etc.* since PFCs contain predominantly C-F bonds. The overall lower

dipole moment of these compounds also contribute to their oil and water repellency, as well as their low surface tension, low refractive index and low coefficient of friction. These perfluoro compounds can be converted to other multifunctional groups bearing perfluoro chains in the backbone.[1] PFCs containing silicon are featured for the low surface tension properties as well.[2] Therefore crosslinked systems bearing perfluorochains should also possess these superlative properties. In this work, we report the synthesis of perflouro compound monofunctionalised with triallylsilane 1H,1H,2H,2H-Perfluorooctyltriallylsilane (PFOTAS) which was obtained via allyl Grignard reaction of 1H,1H,2H,2H Perflurooctyltrichlorosilane (PFOTCS) and its curing reaction with 1,3,5,7-tetramethylcyclotetrasiloxane (TMCTS) via hydrosilylation[3-5] in presence of Pt catalyst dispersed in vinyl polydimethylsiloxane (PDMS). The curing reaction monitored by differential scanning calorimetry (DSC) and Fourier transform infrared spectroscopy (FTIR) studies. Kinetic parameters like activation energy and rate constant were computed using Borchardt and Daniel method.

Experimental

Materials:

1H,1H,2H,2H Perfluorooctyltrichlorosilane (PFOTCS), allyl magnesium bromide and ammonium chloride (NH_4Cl) were purchased from Sigma-Aldrich Pvt limited. 1,3,5,7-tertramethylcyclotetrasiloxane (TMCTS) and the catalyst Pt(0)-1,3-Divinyl-1,1,3,3-tetramethyldisiloxane complex in vinyl terminated polydimethylsiloxane (PDMS) were purchased from Gelest, INC and the solvent diethyl ether was purchased from FINAR Pvt limited.

Synthesis of 1H,1H,2H,2H Perfluorooctyltriallylsilane.

To a dried 250 ml, three necked RB fitted with a condenser and a guard tube in an inert atmosphere containing allyl magnesium bromide (100 ml, 585.7 mmol), mixture of PFOTCS (2.2154 ml, 2.88g, 6 mmol) and diethyl ether (50 ml, 480.9 mmol) are added via a pressure equalizing funnel. The reaction mixture was stirred at ambient for 24 hours under inert condition. The saturated aqueous ammonium chloride was slowly added to the reaction mixture to decompose the complex. The organic layer was separated and the water layer was further extracted by ether. The combined organic portion was washed with water, brine, dried over anhydrous $NaSO_4$ and a liquid pale yellow product was obtained on solvent evaporation under reduced pressure.

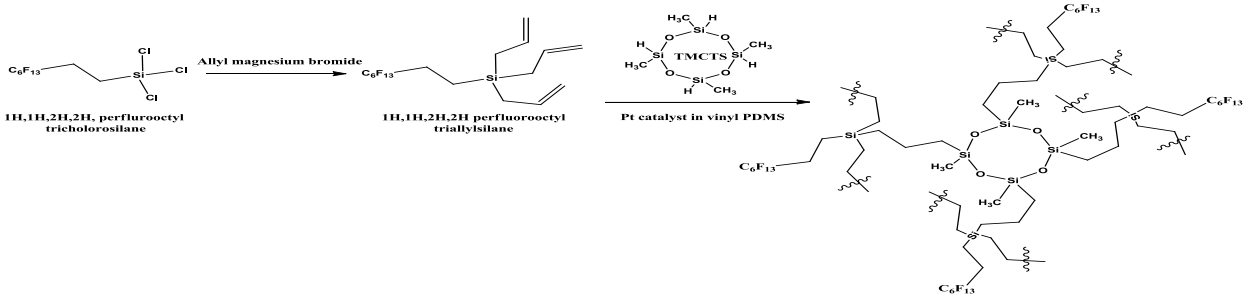
Hydrosilylation reaction between 1H,1H,2H,2H Perfluorooctyltriallylsilane and 1,3,5,7-tetramethylcyclotetrasiloxane.

PFOTAS (0.4 g, double bond equivalent = 0.0024), TMCTS (0.144g, Si-H equivalent = 0.00239) and 30% Pt catalyst in vinyl PDMS (10-15 mg) are mixed in a closed environment, blanketed with nitrogen gas and cured in an inert atmosphere oven at 70 °C for 3 hours. The curing behavior of the mixture at every one hour is monitored by using FTIR analysis.

Characterisation

Nicolet Is50 FTIR spectrometer in wave number range of 4000-400 cm^{-1}, Bruker Avance 400MHz Nuclear Magnetic

Resonance Spectrometer with tetramethylsilane as internal standard and sweep width of 10300 Hz. The contact angle and the surface energy characteristics of the



Scheme 1

cross-linked system is measured using a video based contact angle measuring equipment aided by OCA20 software. DSC studies were performed in TA instruments TA-Q600 under nitrogen atmosphere, using aluminium sample pans. Dynamic DSC was performed at 10°C per minute heating from RT to 200 °C under nitrogen atmosphere.

Results and discussion

The perfluoro chain bearing cross-linked polymer PFOTAS was synthesized by a two-step reaction. The first step is the synthesis of

PFOTAS via allyl Grignard reagent reaction of PFOTCS and the products were characterized using FTIR, ^{1}H and ^{13}C NMR spectra. The second step is the formation of cross linked thermoset by hydrosilylation in presence of Pt-based catalyst. The scheme of the entire reaction is illustrated in scheme 1.

Spectral analysis.

PFOTAS was completely characterized by FTIR, ^{1}H and ^{13}C NMR spectra. The FTIR spectra of the product (Fig.1) confirmed the conversion of PFOTCS to PFOTAS possessing characteristic signatures at 2976 (alkane C-H stretch), 1633 (Si-CH_2-$CH=CH_2$), 1240, 1209, 1145 (C-F stretch). The ^{1}H-NMR spectra (Fig.2) also confirms the formation of PFOTAS. The characteristic peaks are 0.8 ppm corresponding to protons of carbon atom attached to silicon in perfluoro chain **(Si-CH_2-CH_2-C_6F_{13}).** The peak at 1.18 ppm indicates the protons of the substituted allyl group that is attached to the silicon atom **(Si-CH_2-$CH=CH_2$)**. Peak at 1.6 ppm indicates the presence of protons attached to carbon in perfluoro chain **(Si-CH_2-CH_2-C_6F_{13})**. The peaks between 4.8 and 4.9 ppm indicate the terminal protons of the allyl group **(Si-CH_2-$CH=CH_2$)** and that between 5.6 to 5.8 ppm indicates the peak for protons of the internal alkene carbon **(Si-CH_2-$CH=CH_2$)**. ^{13}C-NMR spectra is shown in (Fig.3). Assignments of the chemical shifts were as follows. The peak at 4 ppm indicates the carbon atom of the perfluoroalkyl chain that is attached to silicon atom **(Si-CH_2-CH_2-C_6F_{13})** and that at 22 ppm indicates the carbon atom **(Si-CH_2-CH_2-C_6F_{13})**. The peak at 25 ppm indicates the carbon atom of the allylic group attached to the Si atom **(Si-CH_2-$CH=CH_2$)**. The other 8 peaks for carbon atoms appeared between 115 to 130 ppm.

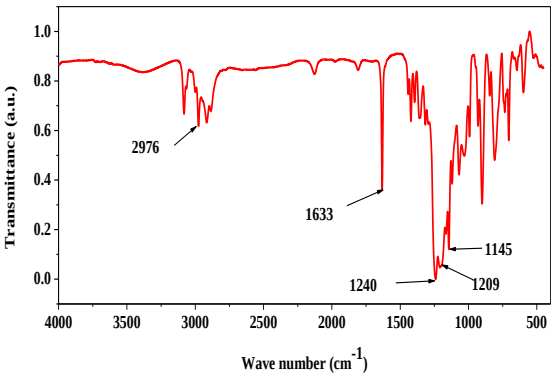


Figure.1: FTIR spectra of PFOTAS

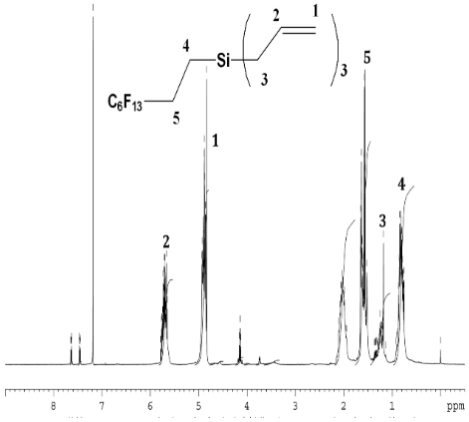


Figure.2: ^{1}H-NMR spectra of PFOTAS

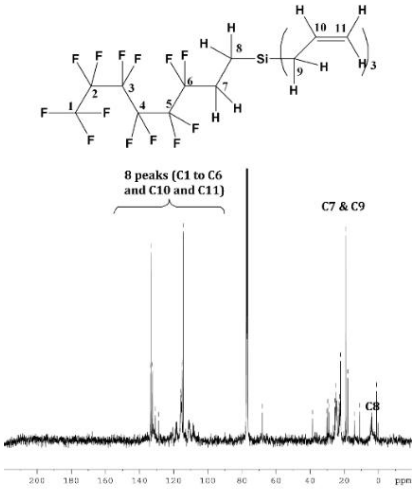


Figure.3: ^{13}C-NMR spectra of PFOTAS

Curing study of PFOTAS via Hydrosilylation reaction with TMCTS.

The curing reaction between PFOTAS and TMTCS (stoichiometric ratio) with platinum catalyst is monitored by using FTIR and DSC.

FTIR spectra

The sample was analyzed for FTIR at the time of mixing (t = 0) and kept at inert atmosphere oven at 70°C. It was analyzed at an interval of 1 hour up to 3 hours for FTIR. From FTIR (Fig.4), it is observed that the intensity of double bond (1633 cm^{-1}) is diminishing with time and after 3 hours of reaction, the peak was completely vanished. This ensures the complete conversion of double bond resulting into a solid cross-linked product.

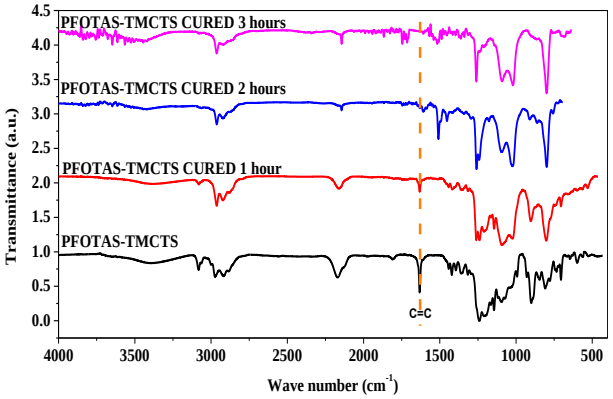


Figure 4: Curing of PFOTAS-TMCTS using FTIR analysis.

DSC analysis

The curing of the mixture is further evaluated by using DSC. The sample is heated from 40 °C to 200 °C under nitrogen atmosphere at a heating rate 10 °C. The curing parameters obtained from the DSC (Fig.5) are tabulated in Table (1).

Table.1: Calorimetric data of PFOTAS-TMCTS

Sample	T Initial	T Peak	TFinal	ΔH(J/g)
PFOTAS-TMCTS	60.12°C	122.06°C	182°C	61.51

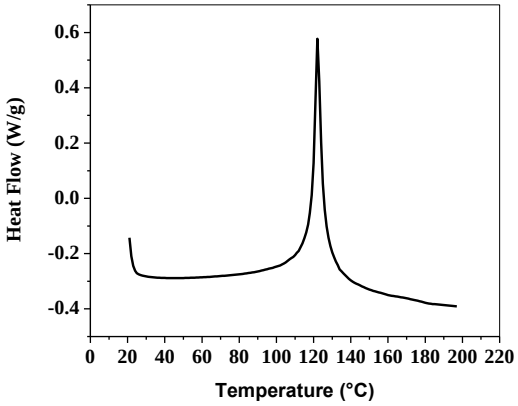


Figure 5: DSC of PFOTAS-TMCTS

Cure kinetics

The kinetic parameters such as activation energy (Ea) and Arrhenius pre-exponential factor (A) were also computed from DSC using Borchard Daniel method**.** For reaction kinetics, any n^{th} order kinetic rate equation is expressed as;

$$\frac{d\alpha}{dt} = k(T)(1-\alpha)^n \qquad (1)$$

Where,

$\alpha = fractional\ conversion,$

$\frac{d\alpha}{dt} = rate\ of\ reaction,$

$k(T) = rate\ constant\ dependent\ on\ temperature$

$k(T)$ is related to Ea and is expressed by Arrhenius equation as given in equation (2)

$$k(T) = Ae^{-\frac{E}{RT}} \qquad (2)$$

Where,

$A = frequency\ factor,$

$E = activation\ energy,$

$R = universal\ gas\ constant,$

$T = temperature\ in\ absolute\ scale.$

Kinetics of PFOTAS-TMCTS

Therefore, $k(T)$ can be calculated for every α (below 10% conversion to be considered to minimize error) from the DSC trace and $lnk(T)$ is to be plotted against inverse of temperature in absolute scale ($\frac{1}{T}$) to obtain a straight line. In this case, 5 to 7 % conversion was considered for computing kinetic parameters. Frequency factor can be calculated from the intercept and activation energy will be obtained from slope of the plot (Fig.6). From linear fit curve, the straight line equation obtained is $\ln k(T) = 1.36 - \frac{1367}{T}$. Ea and A obtained in this experiment are 11.3 kJ.mole^{-1} and 0.4 min^{-1} respectively. The dependency of rate constant with temperature is plotted (Fig.7) and it is obvious that the rate constant is dependent on temperature.

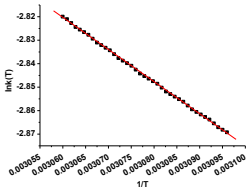


Figure 6: Arrhenius plot of lnk (T) against inverse of temperature

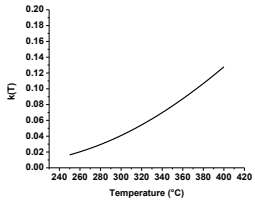


Figure 7: Predicted Temperature dependency of rate constant.

The glass transition temperature (T_g) of the cured system PFOTAS-TMCTS is evaluated using DSC analysis and it is found to be -46 °C.

Contact angle measurement and surface energy calculation.

The sample OPFTAS-TMCTS was smeared in a glass plate and cured in air oven at 70 ˚C for 3 hours. Contact angle measurements are carried out for different liquids over the surface of the cured system. The contact angle of water (polar) over the surface is 107.8° (fig.8a), that for ethylene glycol (semi-polar) is 101.7° (fig.8b) and that for di-iodomethane (non-polar) is 97.1° (fig.8c). From the values of contact angle of these liquids the surface energy of the cured sample can be calculated by using harmonic mean method using the equation (3).

$$\gamma_{SL} = \gamma_S + \gamma_L - \frac{4\gamma_S^d \gamma_L^d}{\gamma_S^d + \gamma_L^d} - \frac{4\gamma_S^p \gamma_L^p}{\gamma_S^p + \gamma_L^p} \quad (3)$$

The surface energy (γ) of the cured OPFTAS-TMCTS is found to be 16.14 mN/m. The dispersion value (γ^d) and polar value (γ^p) can also be calculated from this method and it is found to be 13.31 and 2.83 mN/m respectively.



(Figure 8a, 8b, 8c: contact angle of water, ethylene glycol, di-iodomethane respectively on the surface of cured PFOTAS-TMCTS)

Conclusion

PFOTAS was synthesized by the reaction of PFOTCS with allyl magnesium bromide. PFOTAS is characterized by FTIR, ^{1}H-NMR and ^{13}C-NMR. PFOTAS was further reacted with TMCTS in presence of Pt based catalyst to yield cross-linked polymer PFOTAS-TMCTS. The curing characteristics were evaluated by FTIR and DSC. The disappearance of the peak at 1633 (Si-CH_2-$\underline{CH{=}CH_2}$) for PFOTAS indicates the progress of curing reaction and the reaction was completed within 3 hours (1633 cm^{-1} peak completely vanished). Kinetic parameters were also computed from DSC analysis using Borchardt and Daniel method. Activation energy of 11.3 $kJ.mole^{-1}$ and Arrhenius pre-exponential factor of 0.4 min^{-1} were computed from the experiment for PFOTAS Water contact angle on the cured polymer was found to be 107.8° indicating its hydrophobicity. Surface energy is measured by harmonic mean method and the value is found to be 16.14 mN/m. The dispersion value (γ^D) and polar value (γ^P) were also be calculated from this method as 13.31 and 2.83 mN/m respectively.

Acknowledgment

Authors thank DD (PCM), GD (PSCG), Head, PSCG for their support and Head, ASD for characterization.

References

1. FL Qing, Min Ji, J. Fluorine chem. 113 (2002) pp: 139-141.

2. M.J. Owen, D.E. Willams, J. Adhes. Sci.Technol. 5 (1991) 307.

3. Rieko van Heerbeek, Paul C. J. Kamer,.*Org. Biomol. Chem.*, (2006),4, pp:211-223.

MACRO 415

Styrene based Comb Copolymers by Click Chemistry and Free Radical Polymerization

*[a]Sunitha K, [b]Unnikrishnan G, [a]Reghunadhan Nair C P**

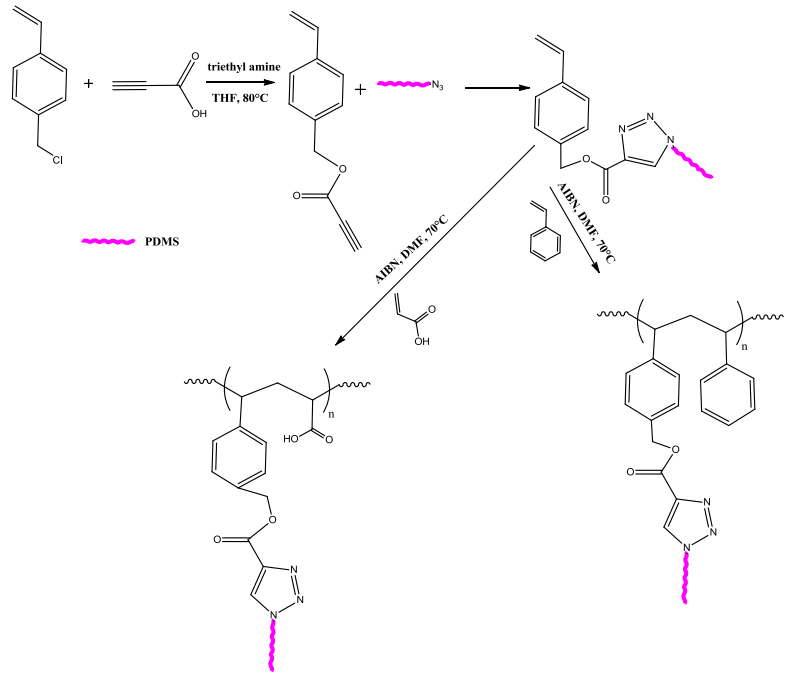
[a]Polymers and Special Chemicals Division

Vikram Sarabhai Space Centre, Thiruvananthapuram-695 022, India

[b]Department of chemistry, National institute of technology, Calicut-673601, India

**cprnair@gmail.com*

Styrene encapped PDMS based macro monomers were synthesized by azide-alkyne click chemistry and characterized. For this monoglycidyl PDMS (molecular weight~5000) was converted to corresponding monofunctional azide. 4-vinyl benzyl chloride was reacted with propiolic acid to derive alkyne containing styrene monomer. This one was reacted with azide functional PDMS by copper catalysed azide-alkyne (CuAAC) reaction to get the macromonomer. The macromonomers were independently copolymerized with monomers such as styrene and acrylic acid. Kinetics of copolymerization revealed a statistical activity of styrene. The derived comb like polymer exhibited very interesting behavior in solutions of different polarity and in bulk because of the difference in polarity of the two segments and these properties were followed as a function of comb of polymer.



Scheme 1. Synthesis of graft copolymers through click reaction

References

4. Eissa, A M; Khosravi, E Macromol. Chem. Phys. (**2015)** DOI: 10.1002/macp.201400604.

5. Demirci, G; Tasdelen, M.A. Eur. Polym. J. 66 (**2015)** 282.

MACRO 417

Phenolic resin based organic-inorganic hybrid polymer networks: Synthesis and properties

[a] Satheesh Chandran M, [b]Gayathri D S, [a]Sunitha K, [a]Dona Mathew*

[a]Polymers and Special Chemicals Division

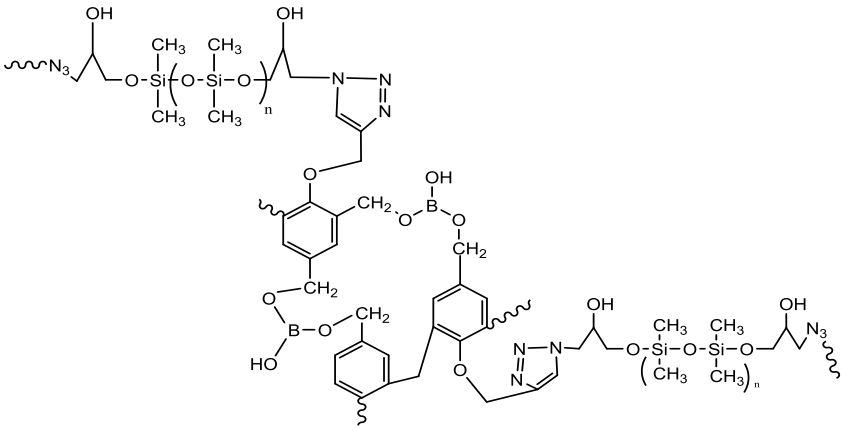
Vikram Sarabhai Space Centre, Thiruvananthapuram-695 022, India

[b]Department of chemistry, SN College Varkala, Kollam-, India

**satheeshchandran.m@gmail.com*

Innovative research is focused on means to address the limitations of phenolic resins such as low mechanical properties, low thermal stability and high brittleness for application as TPS materials

for re-entry missions. Modified phenolic resins containing flexible groups and concept of inorganic-organic hybrid systems gain importance in this context. In this paper, boron containing phenolic-siloxane hybrid polymer bridged through triazole groups were realized by azide- alkyne click chemistry (Scheme 1). The thermal stability and char yield of the copolymers were found to increase with boron content. During the ceramic conversion via pyrolysis at 1450°C, formation of heterogeneous compounds including B4C, SiC and SiB4 mixed phase was confirmed. The obvious effect of boron in improving the thermal stability and promoting the formation of graphite crystallites during pyrolysis was manifested by the transformation from flaky whisker carbon structure to graphitic ordered structure was evidenced by XRD , Raman and SEM.



Scheme 1: Probable cured network of boron containing phenolic-siloxane hybrid polymer

References

1. Eissa, A M; Khosravi, E Macromol. Chem. Phys. (**2015)** DOI: 10.1002/macp.201400604.
2. Shujuan Wang , Xinli Jing , Yong Wang , Jingjing, Poly. Degradation and Stability 99 (**2014**) 1

MACRO 426

Hyperbranched Polymers as Scaffolds for Supported Catalysis

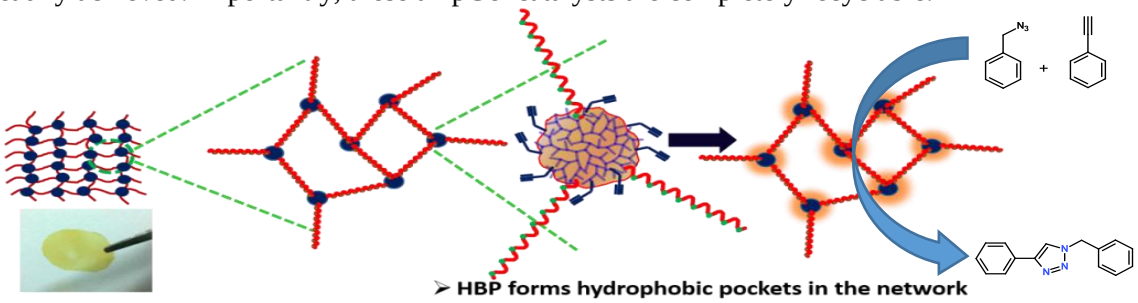
Perala Suresh Kumar and S. Ramakrishnan*

Department of Inorganic and Physical Chemistry
Indian Institute of Science, Bangalore 560012
e-mail: raman@ipc.iisc.ernet.in

HBPs are a class of highly branched macromolecules having low viscosity, low melting, high solubility and large number of modifiable peripheral functional groups. Unlike dendrimers, these are prepared by single step and therefore make them more scalable for a variety of applications. During the past decade, we have developed some of the simple methodologies to access peripherally *clickable HBPs* bearing propargyl/allyl terminal groups; it was shown that these terminal groups can be readily modified by alkyne-azide or thiol-ene click reactions.[1, 2]

In the present study, we have utilized *azide-yne clickable HBPs* to anchor catalysts and examined their efficacy as recyclable systems; two different formats were examined for this purpose. In the first study, the periphery has been clicked with polyethylene glycol monomethyl ether (MPEG-750) azide and the resulting triazole rings were used to complex Cu for the catalysis of azide-yne click reaction in aqueous medium; here the motivation was to use sparingly water soluble substrates that would have a strong tendency to partition near the hydrophobic core region of the HBP and thereby enhance the catalysed reaction; the Cu-triazole complex is expected to be located at the interface of the hydrophilic PEG segments and the hydrophobic core of the HBP. Earlier studies by Christophe et al. have shown similar catalytic activity using Dendrimer anchored Cu (I)-catalyst the azide-alkyne click reaction in the water under mild conditions.[3]

In an alternate approach, the *clickable HB polyesters* bearing numerous peripheral propargyl groups were used to prepare amphiphilic gels (*ampGels*) by crosslinking with PEG-diazides; the PEG length was varied (PEG 600 to 6000) to modify both the crosslink density as well as the hydrophilic content of the gel. As the length of the PEG segment increased the extent of swelling, both in aqueous as well as organic solvents expectedly increased. Furthermore, since majority of the peripheral propargyl groups were not utilized for the crosslinking, the residual propargyl groups were clicked with a simple hydrophobic azide, like benzyl azide, to generate an additional hydrophobic shell around the HBP core; the purpose being to try and locate the triazole rings within the hydrophobic pockets in the amphiphilic gel. Complexation of the triazoles with Cu (II) generated an amphiphilic gel with catalytic sites possibly encapsulated within the hydrophobic pockets. These Cu-containing ampGels were used to very effectively catalyze azide-yne click reactions of a variety of substrates, in the presence of added ascorbate as a reducing agent; it was shown that ppm-levels of the Cu(I) was adequate and turn-over numbers (TON) as high as 100000 was readily achieved. Importantly, these ampGel catalysts are completely recyclable.



References

3. Ramkumar, S. G.; Amala Rose, K. A.; Ramakrishnan, S. *J. Polym. Sci. Chem. Ed.* **2010**, *48*, 3200-3208; Rajkumar, R.; Ramakrishnan, S. *J. Polym. Sci. Chem. Ed.* **2011**, *49*, 1735-1744; Shree Varaprasad, N. S.; Venkatesh, P.; Ramakrishnan, S. *J. Apll. Polym. Sci.* **2014**, *131*, 40248.
4. Ashok, Z. S.; Ramakrishnan. S. *Macromolecules* **2012**, *45*, 2348-2358; ibid *Langmuir* **2013**, *29*, 1245-1257.
5. Christophe D.; Noel Pinaud, and Didier Astruc *J. Am. Chem. Soc.* **2014**, *136*, 12092-12098.

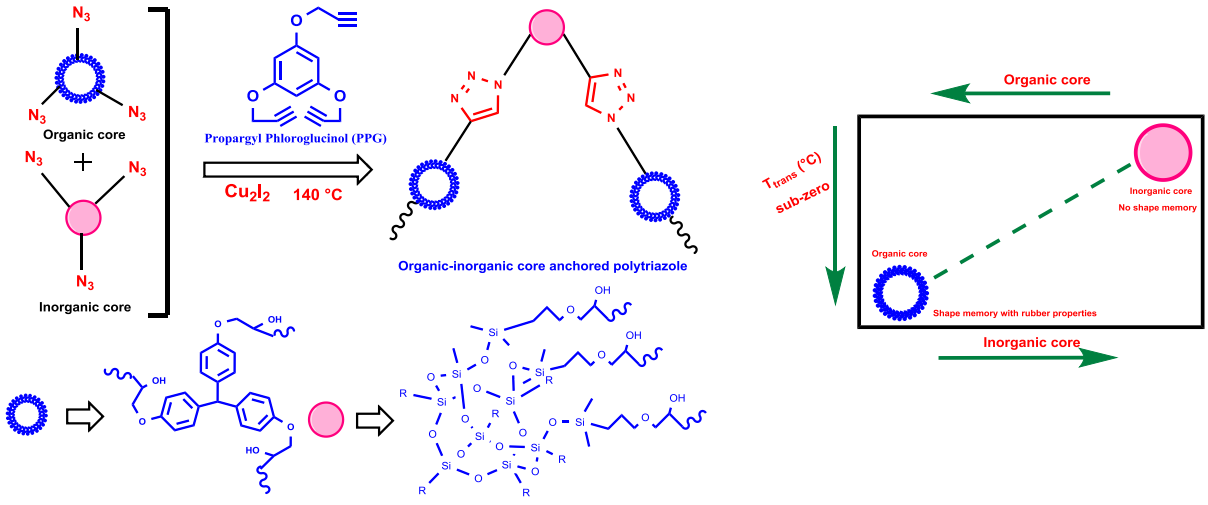
MACRO 427

Organic - inorganic hybrid polytriazoles; Synthesis and shape memory properties

Ragin Ramdas M., Reghunadhan Nair C.P., Santhosh Kumar K.S.*

Polymers and Special Chemicals Division, Vikram Sarabhai Space Centre, Thiruvananthapuram-22
**E-mail: santhoshkshankar@yahoo.com*

Shape memory polymers (SMPs) are intelligent visco-elastic materials, which exhibit recovery of original shape upon exposure to external stimuli like temperature, light, solvents etc. In this work, new SMPs are synthesized *via* copper catalyzed azide-alkyne cycloaddition (CuAAC) reaction. Towards this, polyhedral silsesquioxane azide (inorganic core), trisphenyl azide (organic core) and propargylated phloroglucinol (PPG) are click cross-linked at 140 °C. For purely inorganic core based film, no shape memory property is observed and the film is brittle. However film derived from 100 % organic core exhibits good shape memory properties at sub-zero temperature and is a rubber with tensile properties (at ambient temperature). In the hybrid SMPs, transition temperatures increase to above 0 °C and display good shape memory properties. The shape retention and recovery of these hybrid polymers are > 95 % and they are thermally stable up to 250 °C.



Scheme 1: Click polymerization of inorganic/organic azides with PPG to form hybrid polytriazoles

References

[1] Xu J., Song J., *PNAS*, 2010, 107, 7652–7657.
[2] Chatani S., Wang C., Podgorski M. and Bowman C. N., *Macromolecules*, 2014, 47, 4949–4954
[3] Ragin Ramdas, M., Santhosh Kumar, K.S., Reghunadhan Nair, C.P. *J. Mater. Chem. A*, 2015, 3, 11596.

MACRO 429

Electrically Conductive Oligomeric Conjugated Aromatic Schiff Base- Synthesis and Characterization

Apparao Thota[a] and Chepuri R. K. Rao*
[a]*Polymers and Functional Materials Division, CSIR-Indian Institute of Chemical Technology (CSIR-IICT), Hyderabad-500007, Telangana state, India*

*Email i.d: *ramchepuri@gmail.com*

An oligomeric Schiff base- Ligand has been synthesized by the condensation of benzenedicarbaldehyde (terephthalaldehyde) and conjugated aromatic amine (dianiline) [1]. This novel Schiff base-Ligand model compound (SBL) has been oxidized with ammonium persulphate (APS) in presence of 1 M HCl solution to get conducting Schiff base-Ligand (OSBL). The products (SBL and OSBL) were characterized by ^{1}H NMR, Fourier transform infrared, ESI-MASS, ultraviolet–visible, fluorescence, elemental analyses and field emission scanning electron microscopy (FE-SEM). The UV-vis band at 431nm due to azomethines (CH=N) moiety. In oxidized state one extra band was observed at 624 nm due to π-π* transition (quinoid ring). The emeraldine bases of the polymers are insulators ($\sigma \leq 10^{-10}$ S/cm) [2]. The electrical conductivity of OSBL at room temperature range is $4.51\times10^{-2} - 2.84\times10^{-1}$ S/cm. Thermogravimetric analysis (TGA and DSC) was used to determine the thermal stability of the SBL and OSBL oligomers. The

redox behavior of the SBL and OSBL oligomers was investigated by electrochemical method using cyclic voltammetry. Spectroscopic and conductivity measurements all suggest that there is considerable electron delocalisation through the -CH=N-linkage along the molecular structure.

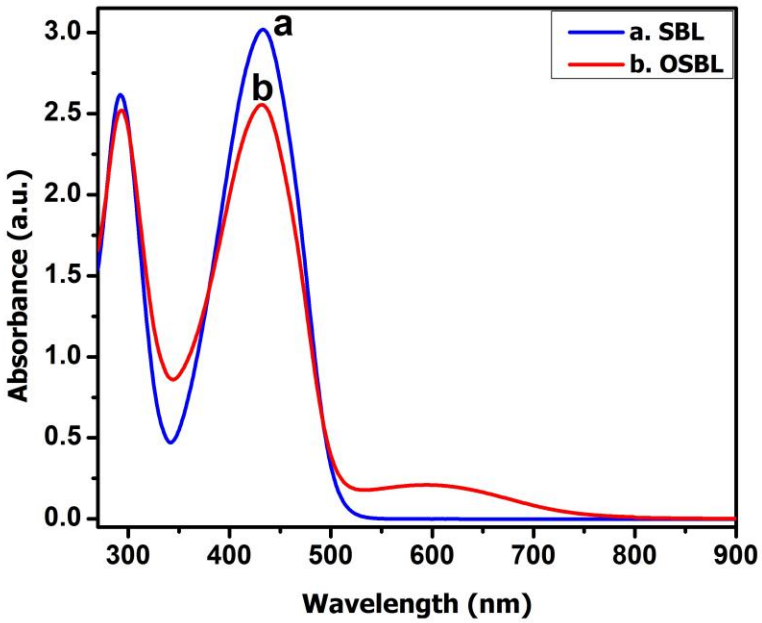


Figure 1: UV-vis spectra in DMF solution of (a) SBL and (b) OSBL

References

1. Liu, Huan; Fu, Zien ; Xu, Kai; Cai, Hualun; Liu, Xin; Chen, Mingcai. *J. Phys. Chem. B,* 115, (2011) 7568–7577.
2. Wei, Y; Focke, W. W; Wnek, E. G; Ray, A; MacDiarmid, A.G. *J. Phys. Chem*. 93, (1989) 495-499.

MACRO 430

Cross-stitching Folded Polymeric Systems

Sujoy Bej and S Ramakrishnan*
Department of Inorganic and Physical Chemistry
Indian Institute of Science, Bangalore 560012
e-mail: raman@ipc.iisc.ernet.in

Block copolymers form a remarkably wide range of interesting microphase separated morphologies that strongly depends on the relative volume fractions of the two blocks. Whereas diblock and triblock copolymers have been extensively studied far fewer studies have focussed on multi-block copolymers. Recently, we demonstrated that immiscibility between the

backbone and pendant graft segments in periodically graft copolymers can coerce the polymer to undergo self-segregation by folding in a zigzag manner leading to microphase separation at the nanoscale; crystallization of either backbone and/or pendant units often provides substantial stabilization to these sub-10 nm nanometer morphologies that are formed.[1-3] Similar folding has also been postulated for multi-block copolymers when specific strong interactions are present in one of the blocks while the other block is soft and flexible.[4]

We have synthesized a series of amphiphilic multiblock copolymers carrying hydrophobic C-20 alkylene segments bearing diacetylene segments (DA) and hydrophilic PEG segments in an alternating fashion. The polymers were synthesized by transesterification of docosa-10, 12-diyne-1, 22-diester with PEGs of varying length (tetraethyleneglycol, PEG-300 and PEG-600). Earlier studies from our lab has shown that the amphiphilic multiblock copolymers containing alternating C-18 alkylene segment and PEG segments undergo self-segregation, possibly by folding; this permits the alkylene segments to crystallize by excluding out the PEG segments. It is well known that diacetylene undergoes topochemical polymerization in the crystalline solid provided they are arranged in the required geometry.[5] As shown in the figure, the folding of the chain in the DA-TEG polymer could bring the DA units in close proximity to permit cross-polymerization. We will discuss various aspects of this photochemical cross-polymerization and the possibility of preparing self-crosslinked single chain nanoparticles using this approach.

In another approach we attempt the cross-dimerization of pendant anthracene units located at periodic intervals along a polyethylene-like polyesters bearing long crystallizable alkylene segments along the backbone. The bulky anthracene segments we postulated would exclude the paraffinic alkylene lattice formed by the backbone segments and in doing so would collocate the anthracene units above and below the folded chain. We expect that once collocated the anthracene units could be dimerized at random locations along the folded chain to transform the folded chains into 2-D polymers. The design, synthesis and photo-reaction studies in both these novel systems will form the essence of the presentation.

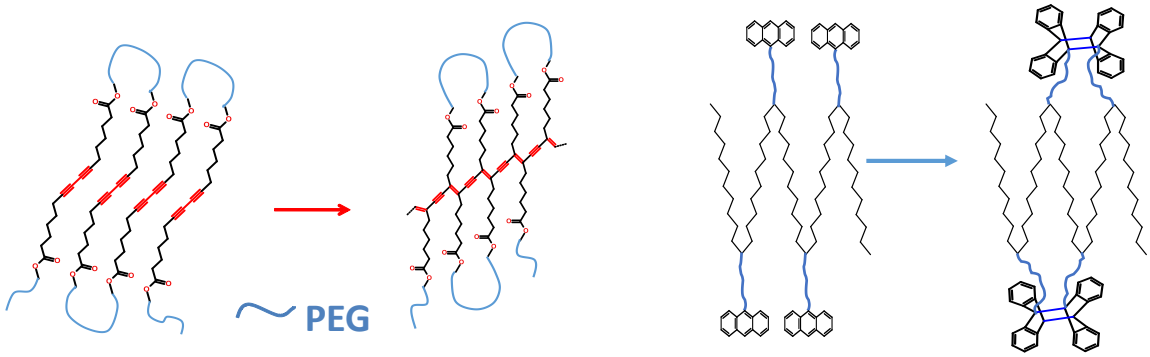


Figure: Topochemical polymerization of diacetylene (left) and Photochemical dimerization of anthracene (right).

References

1. Roy, R. K.; Gowd, E. B.; Ramakrishnan, S. *Macromolecules* **2012**, 45, 306.
2. Mandal, J; Krishnaprasad, S; Shankar Rao, D. S; Ramakrishnan, S. *J. Am. Chem. Soc*. **2014**, 136, 2538.
3. Chanda, S; Ramakrishnan, S. *Macromolecules* **2016**, 49, 3254.
4. Ikeda, T. *Angew. Chem. Int. Ed.* **2013**, *52*, 4845.
5. Wegner**,** G. *Die Makromolekulare Chemie* **197**1, 145, *85.*

MACRO 443

Synthesis of Amphiphilic Block Copolymers Using New method of Catalysing Thiol-Ene Reaction

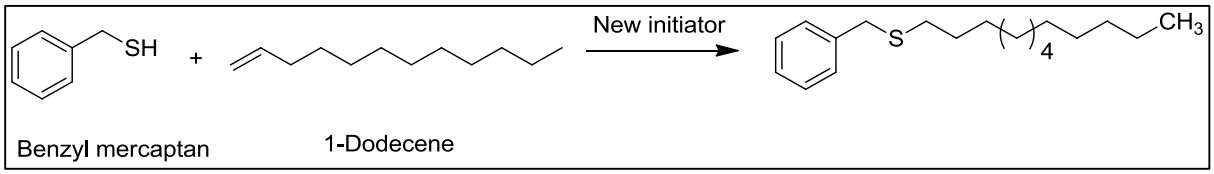
Hafeez Sumbul* and Nebhani Leena[1*]

[1]*Centre for Polymer Science and Engineering, Indian Institute of Technology, HauzKhas, New Delhi 110016, India*

**Corresponding author. Tel.: +91 11 2659 6691; fax: +91 11 2659 1421.*

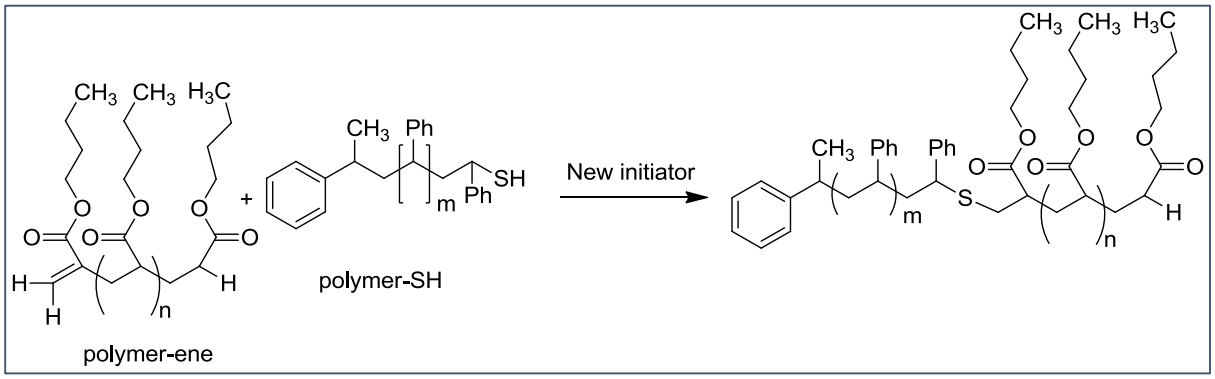
**E-mail address: sumbulhafeez03@gmail.com, leena.nebhani@polymers.iitd.ac*

Thiol-ene click chemistry is widely used for synthesis of hydrogels [1], dendrimer [2], convergent star synthesis [3], microfluidic-devices [4], for polymer post functionalization [5] and surface functional ization [6]. Thiol-ene reaction can be catalyzed using several methods, for example, thiol-ene reaction can be catalyzed using a photo initiator [7] or a thermal initiator [8]. It can also be catalyzed using a base (such as triethylamine and diphenylphosphine) [9]. In this work, we have reported a new method for initiating thiol-ene reaction.



Scheme 1. Model reaction between benzyl mercaptan and 1-dodecene.

Several model reactions between low molecular weight thiol and ene were carried out to establish this new method of catalysing thiol-ene reaction as shown in **Scheme 1**. Further, this new method of catalysing thiol-ene reaction was utilized for construction of amphiphilic block copolymers. For the synthesis of amphiphilic block copolymers, first styrene was polymerized using RAFT polymerization. The synthesized polystyrene was characterized using several techniques, for example, size exclusion chromatography ($\bar{M}_{n:}$ 3181, $\bar{M}_{w}$: 3841, PDI 1.1), ^{1}H NMR, ^{13}C NMR, FTIR-spectroscopy, Mass spectroscopy. To provide polystyrene with thiol functionality, polystyrene with RAFT end group was aminolyzed using excess of base in the presence of triphenylphosphine (acting as a reducing agent). The thiol functionalized polystyrene was characterize by various techniques, for example, size exclusion chromatography ($\bar{M}_{n:}$ 2916, $\bar{M}_{w}$: 3484, PDI 1.1), ^{1}H NMR, ^{13}C NMR, FTIR-spectroscopy, Mass spectroscopy. To follow the conversion of trithiocarbonate functionality to thiol functionality UV-Visible spectroscopy was utilized. UV-Visible spectrum of polystyrene shows a peak at 299 nm corresponding to π-$\pi*$ transition of C=S bond. While the polystyrene sample containing thiol group shows no peak at 299 nm. Ene functionalized polymers were utilized for conjugation with thiol functionalized polystyrene. Ene functionalized polymer used in this study is macromonomer based on different acrylates, for example, n-butyl acrylate, t-butyl acrylate, methyl acrylate, ethyl acrylate, methyl methacrylate. The synthesized macromonomer containing double bond at the end was characterized using different techniques, for example, size exclusion chromatography ($\bar{M}_{n:}$ 1550, $\bar{M}_{w}$: 1770, PDI 1.1), ^{1}H NMR,(showing the presence of vinyl double bond at end) ^{13}C NMR, FTIR-spectroscopy, Mass spectroscopy. The conjugation of thiol functionalized polystyrene and ene functionalized polyacrylates was performed using new method of initiating thiol-ene reaction as shown in **Scheme 2.**



Scheme 2. Synthesis of amphiphilic block copolymer using thiol-ene chemistry.

The prepared block copolymer was also characterized using different techniques, for example, size exclusion chromatography, ^{1}H NMR, ^{13}C NMR, FTIR-spectroscopy, mass spectroscopy.

References

[1] Lutolf, M. P., Tirelli, N., Cerritelli. S., Cavalli L., Hubbell, J. A., *Bioconjug. Chem.*, 12 (2001) 1051.
[2] Killops, K. L.; Campos, L. M.; Hawker, C. J. *J. Am. Chem. Soc., 130* (2008) 5062.
[3] Chan, J. W.; Yu, B.; Hoyle, C. E.; Lowe, A. B. *Chem. Commun.* (2008) 4959.
[4] Khire, V. S., Yi, Y., Clark N. A., Bowman, C. N., *Adv. Mater. 20*, (2008) 3308.
[5] Pogantsch, A., Rentenberger, S., Langer G., Keplinger J., Kern, W., Zojer E., *Adv. Funct. Mater. 15* (2005) 403.
[6] Goldmann, Anja S., Walther, A., Nebhani, L., Joso, R., Ernst, D., Loos, K., Barner-Kowollik, C., Barner, L., Muller, A.H. E., *Macromolecules, 42* **(**2009) 3707.
[7] Brummelhuis N. ten, Diehl C., and Schlaad H., *Macromolecules, 41* **(**2008) 24.
[8] Uygun, M., Tasdelen M. A., Yagci Y., *Macromol. Chem. Phys., 211* (2010) 103.
[9] B. D. Mather, K. Viswanathan, K. M. Miller and T. E. Long, *Prog. Polym. Sci., 31* (2006) 487.

MACRO 444

Defect-Free Regioregular Poly(3-hexylthiophene) *via* Nickel Zero Catalyzed Kumada Catalyst-Transfer Polymerization

Tarange Dattatray, Gopinathan Sreelekha, Kumar Anshu, Kumar Anil*

Department of Chemistry, Indian Institute of Technology Bombay, Powai, Mumbai, 400076, India
**Email-* anilkumar@iitb.ac.in

In recent times, electronic devices has become a valuable and interesting part of our life style because of low cost material as well as cheaper fabrication techniques. Regioregular Poly(3-hexylthiophene), (rr-P3HT) is a widely studied conjugated polymer in organic electronics. Most common method for the synthesis of rr-P3HT is Kumada Catalyst –Transfer Polymerization (KCTP) with Ni(dppp)Cl_2 as catalyst. The *in-situ*

catalyst cycle starts with trasmetalation and reductive elimination to form a tail-to-tail (T-T) coupled dimer, then sequence of oxidative addition, transmetalation and reductive elimination continues resulting in the formation of rr-P3HT. The regioregularity obtained via this route is only 95-99%. Kiriy and co-workers reported the *ex-situ* as an alternative route for 100% rr-P3HT, (defect-free rr-P3HT), for the first time, but synthetic route for the preparation of nickel initiator is longer as well as tedious. We develop a one-pot synthesis *via* a soluble nickel zero catalyzed *ex-situ* KCTP. The defect free nature and end groups were confirmed by NMR and MALDI-TOF. This is the first example of a Ni(0) catalyzed Kumada catalyst-transfer polymerization. Ni(0) catalyst was synthesized in quantitative yield using a conventional, off the shelf, Ni(II) catalyst. The catalyst was found to be highly stable in solution at ambient conditions and hence can be prepared in advance and stored. Polymerization follows a pseudo-living mechanism wherein the final molecular weight can be controlled by monomer to initiator ratio. The process was found to be amenable for continuous flow process resulting in the synthesis of defect-free rr-P3HT with very low polydispersity (1.1). The current process has excellent batch-to-batch reproducibility even at large scale making it economically viable for bulk production for large area applications.

References

6. McCullough, R. D.; Lowe, R. D. *Chem. Commun.* 1 (1992) 70.
7. Kiriy, A.; Senkovskyy, V.; Sommer, M. *Macromol. Rapid Commun*. 32 (2011) 1503.

MACRO 455

GT-g-P (DADMAC): Synthesis, Characterization and Evaluation of Its Cationic Properties as Flocculant for Model Aqueous Suspensions

Pal, Pinki, Pandey, J. P., Sen, Gautam*

Department of Chemistry, Birla Institute of Technology, Mesra, Ranchi – 835215, Jharkhand, India.

Corresponding author: gsen9@hotmail.com (Sen, Gautam)

ABSTRACT

A functionalized positively charged polymeric flocculant was fabricated by microwave-assisted [1, 2] polymerization of diallyldimethylammonium chloride (DADMAC) on gum tragacanth (GT-g-P(DADMAC). The graft copolymerization was initiated by potassium persulphate (KPS) in synergism with microwave radiation.

Free radical chain polymerization occurs with monomer units having double bonds e.g. vinyl, allyl etc. In this reaction, a polymer molecule of high molecular weight can be produced from an active centre in a very short time. The grafted chains of poly(DADMAC) get attached at these centers through initiation, propagation and termination reaction (usual free radical mechanism), and leading to the formation of graft copolymer [3, 4]. The synthesis details of synthesized GT-g-P(DADMAC) have been given in Table 1.

Table 1. Synthesis Details of various grades of GT-g-P(DADMAC)

Polymer grade	Wt. of Gum (g)	Wt. of KPS (g)	Wt. of Monomer (g)	Percentage Grafting	Flocculation Efficacy (Reduction in Turbidity, %)
GT-g-P(DADMAC) 1	1	0.5	5	144.8	65.31
GT-g-P(DADMAC) 2	1	1	5	213.1	85.21
GT-g-P(DADMAC) 3	1	2	5	405.7	87.46
GT-g-P(DADMAC) 4	1	3	5	521.2	85.60
GT-g-P(DADMAC) 5	1	2	2.5	205.5	8.25
GT-g-P(DADMAC) 6	**1**	**2**	**7.5**	**470.1**	**90.69**
GT-g-P(DADMAC) 7	1	2	10	8.058	86.36
Gum Tragacanth	--	--	--	--	13.71

The copolymer produced was characterized through FTIR spectroscopy, Elemental analysis, SEM, TGA and DTA. The effect of reaction conditions onto the flocculation efficacy was studied.

The grafted chains of poly(DADMAC) have cyclic unit and a charged quaternary ammonium group in each monomer unit which contribute the graft copolymer with enhance water solubility and high cationic functionality. The material thus developed has been studied for its efficacy as a flocculant in model aqueous suspensions of kaolin, coal fine etc through standard jar test procedure.

The approach established in this investigation constitutes the coagulation, through interdependent electrostatic attraction and flocculation by bridging mechanism [5. 6].

Flocculation is a **surface phenomenon** which involves the accumulation of individual dispersed particles and eventual splitting of the **solid- liquid interface**. By this process, the sedimentation or filterability of small and fine particulates improves due to the formation of larger flocs.

The aqueous suspension with colloidal particles is stable due to the repulsion induced by the charges on the particles. The lengthy, dangling cationic chains of poly(DADMAC) get adhered onto the stiff and solid backbone of polysaccharide and develop comb like structure. This modified structure creates bridges between suspended colloidal particles due to increase in their approachability [7] and each particle may connect two or more such type of links. In this technique, the particles draw closer to each other and concentrate in the form of floc thus causes destabilization of the suspension.

Polysaccharide graft copolymer as clarifying agent in water treatment is green and competitive substitute as manifestated by biodegradability, physiological inertness and immense flocculation competencies.

The optimal dosage of GT-g-P(DADMAC) as flocculant in kaolin suspension has been found at 1.25 ppm and maximum flocculation efficacy (percentage reduction in turbidity) has been found at 90.69

% (Figure 1). The results exhibit the excellence of the synthesized graft copolymer. It is worthwhile to note that this technology may be further useful for clarification of other aqueous suspensions, fruit and vegetable juices, alcoholic and nonalcoholic beverages etc.

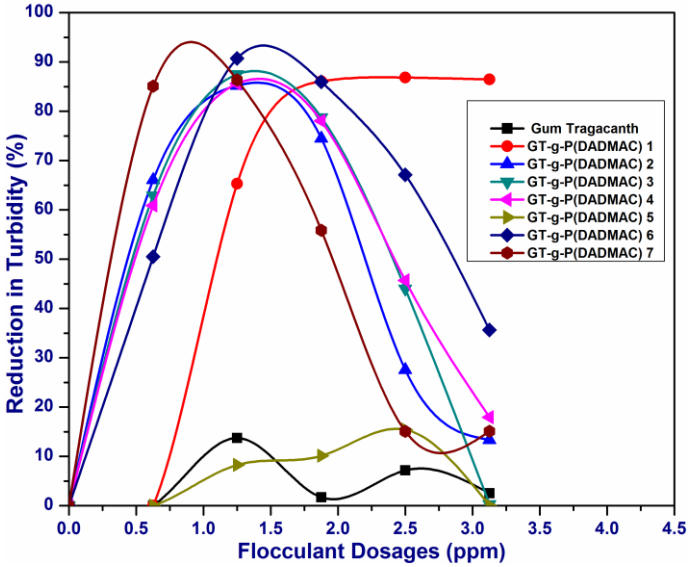


Figure1. Flocculation efficacy of various grades of GT-g-P(DADMAC) in kaolin suspension

References

[1] Mishra, S.; Mukul, A.; Sen, G.; Jha, U. *International Journal of Biological Macromolecule*, 48 (2011) 106.
[2] Sinha, S.; Mishra, S.; Sen, G. *International Journal of Biological Macromolecules*, 60 (2013) 141.
[3] Odian, G. *Principles of polymerization*. New York: John Wiley & Sons (2002).
[4] Gowariker, V. R.; Viswanathan, N. V.; Sreedhar, J. *Polymer science*. New Delhi: New age International (p) Ltd. (1986).
[5] Brostow, W.; Pal, S.; Singh, R.P. *Materials Letters.* 61 (2007) 4381.
[6] Ruehwein, R.A.; Ward, D.W. *Journal of soil sciences.* 73 (1952) 485.
[7] Singh, R.P.; Karmakar, G.P.; Rath, S.K.; Karmakar, N.C.; Pandey, S.R.; Tripathy, T. *Polymer Engineering & Science.* 40 (2000) 46.

MACRO 466

Synthesis and Chemical Modification of Polyesters Containing Allyloxy functional Groups by "Click Chemistry" Approach.

Dr. Verma Savita (Mail.ID – savitanit@gmail.com)

Dr. Prakash P. Wadgaonkar,
Scientist, Polymer Science and Engineering Division,

National Chemical Laboratory (**NCL**), Dr. Homi Bhabha Road, **Pune** 411008, India,
Email: pp.wadgaonkar@ncl.res.in
Tel: +91-20-25902306; Fax: +91-20-25902615

Abstract

High performance polymers such as aromatic polyesters and polyamides have received considerable attention due to their notable high impact on industry. These polymers find applications in various industries such as aero-space, automobile, electronics, packaging, coatings, etc, due to their excellent mechanical and thermal properties, good chemical resistance and insulating properties. However, for more specific applications these polymers are limited in scope because of the lack of functionalities on the polymer backbone for further modifications and tailoring.[1-4] The research concerning functionalization of step-growth polymers in general and polyesters and polyamides in particular has been moving towards the use of recently discovered click chemistry approach, as introduced by Sharpless and co-workers in 2001.[3, 5-13]

The click philosophy, has been heavily exploited in polymer and material sciences by means of the copper-catalyzed azide-alkyne cycloaddition (CuAAC) and has led to a convenient approach to synthesize functionalized polymers.[14, 15] Due to the toxicity of copper and the risk inherent in working with azides, a growing interest has risen in thiol-ene chemistry, which works under mild conditions and is copper- and zide- free and and ready availability of an enormous range of thiols.[16-21] One of the greatest utilities of thiol– ene click chemistry is rapid modification of existing polymers to tailor physical, mechanical, optical, solubility, and other key properties over a wide range, in high yield. In recent years, significant effort has been expanded towards polymer functionalization using thiol–ene free-radical reactions.[20, 22-25]

Polymers containing pendent allyl(oxy) groups are of interest as they provide a versatile option to ready functionalization *via* radical addition of thiols, epoxidation, halogenations and hydroboration, among others.[14-19] So here we focused on synthesis of polysters containing functional groups and their post modifications by "**Click chemistry**" approach.

Experimental methods- We synthesized allyloxy functionalized polyester by polycondensation of a diacid chloride containing pendent allyloxy group (synthesized by me in lab) and commercially available bisphenol A. Copolyester was also synthesized by polycondensation of a mixture of diacid chloride containing pendent allyloxy group and isophthaloyl chloride with bisphenol A. Polyesters were characterized by inherent viscosity measurements, GPC, solubility tests, FT-IR, ^{1}H and ^{13}C-NMR spectroscopy. Futher copolyester containing 25 mol % Allyloxy functional groups was post-functionalized using four different thiols *viz;* 1-butanethiol, 2-mercaptoethanol, 3-mercaptopropanoic acid and 11-marcaptoundecyl phosphoric acid *via* **thiol-ene click** reaction.

Result- The functionalized polyesters were characterized by FT-IR and ^{1}H-NMR spectroscopy. In result we found that Copolyester containing 25 mol% allyloxy functionality was successfully functionalized by four different thiols.

Conclusion- Depending on the various demand of applications we can easily functionalize aromatic polyesters by **thiol-ene click** reaction.

References

[1] Leen, B.; David, F.; Du Prez, F. E. *Polymer 50*, **2009**, 3877.
[2] Tailoring. *J. Polym. Sci., Part A: Polym. Chem. 46,* **2008,** 6552.

[3] Williams, C. K. *Chem. Soc. Rev. 36,* **2007,** 1573.
[4] Lecomte, P.; Riva, R.; Jerome, C.; Jerome, R. *Macromol. Rapid. Commun. 12,* **2008**, 982.

[5] Hng, M.; Jing, Y. L. *Macromolecules 44,* **2011**, 5659.
[6] Budhathoki, J.; Noval, U. B. *Macromolecules 44,***2011,** 5947.
[7] Mohammad, N. J.; Vora, A. *Macromol. Chem. Phy. 212,* **2011,** 539.
[8] Conner, D. M.; Robert, M. K.; Collard, D. M. *J. Polym. Sci., Part A: Polym. Chem. 38,* **2000,** 1291.
[9] Taufik, N.; Karsten, B.; Jorg, K. *Biomacromolcules 11,* **2011,** 3660.
[10] Martin, W. M.; Claudia, H.; Bart, V. *Macromol. Chem. Phy. 209,* **2008,** 1887.
[11] Bunyamin, K.; Yuksel, Y.; Bahadir, N. *Des. Monomers Polym. 12,* **2009,** 511.
[12] Kolb, H. C.; Finn, M. G.; Sharpless, K. B. *Angew. Chem. Int. Ed. 40,* **2001,** 2004
[13] Leen, B.; David, F.; Du Prez, F. E. *New Smart Materials via Metal Mediated Macromolecular Engineering* **2009**.
[14] Hoyle, C. E.; Lowe, A. B.; Bowman, C. N. *Chem. Soc. Rev. 39,* **2010,**1355.
[15] Iha, R. K.; Wooley, K. L.; Nystrom, A. M.; Burke, D. J.; Kade, M. J.; Hawker, C. *J. Chem. Rev. 109,* **2009,** 5620.
[16] Hoyle, C. E.; Bowman, C. N. *Angew. Chem. Int. Ed. 49,* **2010,** 1540.
[17] Ende, A. E.; Harrell, J.; Sathiyakumar, V.; Meschievitz, M.; Katz, J.; Adcock, K.; Harth, E. *Macromolecules 43,* **2010,** 5665.
[18] Stanford, M. J.; Dove, A. P. *Macromolecules 42,* **2009,** 141.
[19] Ende, A. E.; Kravitz, E. J.; Harth, E. *JACS 130,* **2008,** 8706.
[20] Lowe, A. B.; Harvison, M. A. *Aust. J. Chem. 63,* **2010,** 1251.
[21] Ates, Z.; Thornton, P. D.; Heise, A. *Polym. Chem. 2,* **2011,** 309.
[22] Yang, T.; Long, H.; Malkoch, M.; Gamstedt, E. K.; Berglund, L.; Hult, A. *J. Polym. Sci., Part A: Polym Chem. 49,* **2011,** 4044.
[23] Sun, J.; Schlaad, H. *Macromlolecules 43,* **2010,** 4445.
[24] Imbesi, P. M.; Raymond, J. E.; Tuckera, B. S.; Wooley, K. L. *J. Mater. Chem. 22,* **2012,** 19462.
[25] Xi, W.; Wang, C.; Kloxin, C. J.; Bowman, C. N. *ACS Macro Lett.* **2012,** 1, 811.

MACRO 475

Synthesis and characterization of PMMA/PEDOT and graphene based hybrid materials for conductive transparent thin films

P. A. Saeed, Dr. A. Sujith*

Department of Chemistry, Materials Research Laboratory,
NIT Calicut, India
*Saeedp10@gmail.com

PMMA(poly-methylmethacrylate) coated PEDOT(poly-ethylene dioxythiophene) hybrid materials have been synthesized and their conductive thin films were fabricated using these materials as filler. In addition, have been studied the influences of graphene based dopants on PMMA coated PEDOT materials and

fabricated their composite films. Also, have been extensively characterized the conductive composites and their films using scanning electron microscopy (SEM), differential scanning calorimetry (DSC), thermogravimetric analysis (TGA), fourier transform infrared (FTIR) and UV-Vis spectroscopies, and electrical conductivity measurements. FTIR results and conductivity measurements exhibited successful incorporation of PEDOT on PMMA with graphene based dopants and improvement of conductivity comparable with current materials. These results will exploit the future application of conductive transparent thin films based on PEDOT/PMMA system.

References

8. H. Shirakawa; E.J. Louis; A.G. MacDiarmid; C.K. Chiang and A.J. Heeger. J Chem Soc Chem Comm, (1977) 579.
9. J. Prasad Rao; Kurt E. Geckeler. Progr. Polym. Sci., 36 (2011) 887.
10. By Jyongsik Jang and Joon Hak Oh. Adv. Funct. Mater., 3 (2005) 15.
11. V H Pham; T T Dang; S H Hur; E J Kim and J Chung. Appl. Mater. Interfaces., 4 (2012) 2630.
12. H G Chandhuri and S Paria. Chem. Rev, 112 (2012) 4 2373.

MACRO 483

Surface initiated ATRP from GO: Precision Synthesis and Control of Nanocomposite properties

Kattimuttathu I. Suresh* ,Rajender N

Polymers & Functional Materials Division,
CSIR-Indian Institute of Chemical Technology,
Hyderabad – 500 007, India.
E-mail: kisuresh@iict.res.in

ABSTRACT

Surface-initiated polymerization (SIP) from nanoparticle surfaces offers several advantages in the preparation of polymer nanocomposites. The technique can be applied to a wide range of monomers under varying reaction conditions, offering the possibility to prepare nanocomposites with different functionalities present on the surface. One major advantage of SI-ATRP performed from solid surface is good control over the polymer molecular weight, polydispersity index, composition and end group functionality. In this presentation the effect of functionalized graphene initiators on the synthesis and materials properties of graphene-polyacrylate nanocomposites will be discussed. The effect of ligand, monomer type, ligand:CuBr ratio and supported initiator concentration on the synthesis and properties of the hybrid nanocomposites were studied using bulk ATRP. The nanocomposite films were characterized for thermal stability, glass transition, rheological, stress-strain behavior and surface properties. The nanocomposites prepared via SI-ATRP showed improved damping and film formation characteristics as compared to the peroxide polymerized sample prepared from acrylated GO. The nanocomposites also showed improved thermal stability, rheological and mechanical properties that varied with the graphene initiator content. The surface and film formation properties of the nanocomposite were also found to be influenced by the nanofiller content.

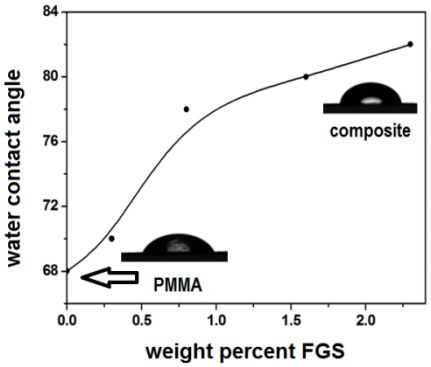


Figure 1. Image showing the effect of functionalized graphene sheets on the surface properties of Graphene - PMMA nanocomposite.

References:

1. Rajender, N. and Suresh, K. I. *Macromol. Mater. Eng*., **2016**, 301: 81–92.
2. Lee, S. H.; Dreyer, D. R.; An, J.; Velamakanni, A.; Piner, R. D.; Park, S.; Zhu, Y.; Kim, S. O.; Bielawski, C. W.; Ruoff, R. S. *Macromol. Rapid Commun*. **2010**,*31*, 281-288.
3. Kim, J. B.; Huang, W.; Miller, M. D.; Baker, G. L.; Bruening, M.L. *J.Polym. Sci., Part A: Polym. Chem.* **2003**, *41*,386.

MACRO 488

Fluorene Based Cardo Semifluorinated Poly(Ether Imide)S: Synthesis, Characterization and Gas Transport Properties

Chatterjee, Rimpa and Banerjee, Susanta*

Materials Science Centre, Indian Institute of Technology, Kharagpur, India 721302

Email: susanta@matsc.iitkgp.ernet.in

Membrane based gas separation has already established itself as a highly efficient technique over conventional separation techniques like cryogenic distillation and adsorption processes. Aromatic polyimides are an important class of high performance polymer with excellent thermal stability, chemical resistance, film forming ability, mechanical strength and thus can be used as promising membrane materials for different gas separation applications. Considering the general tradeoff between gas permeation and selectivity, a series of new organo-soluble aromatic polyimides (PI) was synthesized using the diamine monomer 9,9-bis-[3-phenyl-4-{2′-trifluoromethyl-4′-(4″-nitrophenyl) phenoxy}phenyl]fluorene with three different commercially available aromatic anhydrides namely 4,4'-(4,4'-isopropylidenediphenoxy) bis(phthalic anhydride) (BPADA), 2,2-bis(3,4-dicarboxyphenyl) hexafluoropropane (6FDA) and 4,4'-oxydiphthalic anhydride (ODPA). All synthesized PIs exhibited excellent thermal stability (up to 510 ºC in synthetic air for 10% weight loss), high glass transition temperature (243-280 ºC) and excellent mechanical properties (tensile strength up to 76 MPa, modulus up to 1.92 GPa and elongation at break up to 9%) depending on their repeat unit structure. Gas transport properties of these membranes were investigated for the four different gases (e.g., CH_4, N_2, O_2 and CO_2) at

35 ºC at an applied pressure of 3.5 bar. These PIs showed high gas permeability [$P(CO_2)$ up to 70.3 and $P(O_2)$ up to 16.7] and permselectivity [$\alpha(CO_2/CH_4)$ up to 73.57 and $\alpha(O_2/N_2)$ up to 13.39) in comparison to many other reported PIs.

References

[1] Bandyopadhyay, P.; Bera, D.; Ghosh, S.; Banerjee, S.; *RSC Adv.*, 4 (2014) 28078.
[2] Koley, T.; Bandyopadhyay, P.; Mohanty, A. K.; Banerjee, S.; *Eur. Polym. J.*, 49 (2013) 4212.
[3] Ghosh, A.; Sen, S.K.; Banerjee, S.; Voit, B.; *RSC Adv.*, 2 (2012) 5900.
[4] Sen, S.K.; Banerjee, S.; *RSC Adv.*, 2 (2012) 6274.

MACRO 489

Synthesis and optoelectronic properties of hybrid *rr*-Poly-3-hexylthiophene (P3HT) GO nanocomposites.

M. Jakeer Hussain

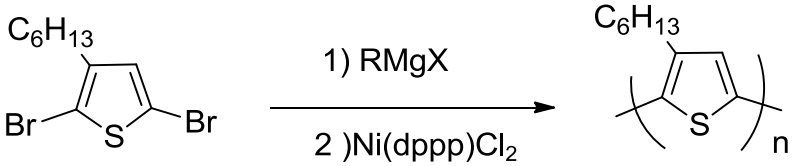
Polymers & Functional Materials Division, CSIR-Indian Institute of Chemical Technology.
Uppal Road, Hyderabad - 500007.

Dr.K.I.Suresh* ***E-mail:* *kisuresh@iict.res.in*

ABSTRACT

Hybrid nanocomposites of conjugated polymers with graphene are widely studied materials for solar cells and other optoelectronic devices [1]. Solar cells based on polymer-nano particle blend systems in particular, bulk hetero junction (BHJ) solar cells, have shown much improved results [2].

In the present work, we studied the synthesis of rr-P3HT and its hybrid nanocomposites, which are used as active layers in solution-processed solar cells. The hybrid system consist of blends of regioregular P3HT with different carbon nanomaterials like graphene oxide, graphene quantum dots and carbon nano spheres incorporated into rr-Poly (3-hexylthiophene) (P3HT) [3] [4]. The nanoparticle can alter the structure ordering of the conjugated polymer and thereby its optical properties. The microstructure of the composites solution and films were analysed by various techniques including x-ray diffraction, ultraviolet–visible absorption, Raman spectroscopy, Fourier-transform infrared spectroscopy and cyclic voltammetry, and spectroscopic ellipsometry. The results show that the presence of these nano particles improves the crystallinity and increase the conjugation length of P3HT in the films. Furthermore, increase in absorption wave length, and photoluminescence quenching is observed in the P3HT/ graphene oxide, and graphene quantum dot films, suggesting the possibility of photo induced electron transfer between P3HT and these nano particles as a result of the π–π interaction among the constituents. The blend systems may be suitable for application in bulk hetero junction solar cells and organic photo-detectors.



2,5 di bromo-3-HT P3HT

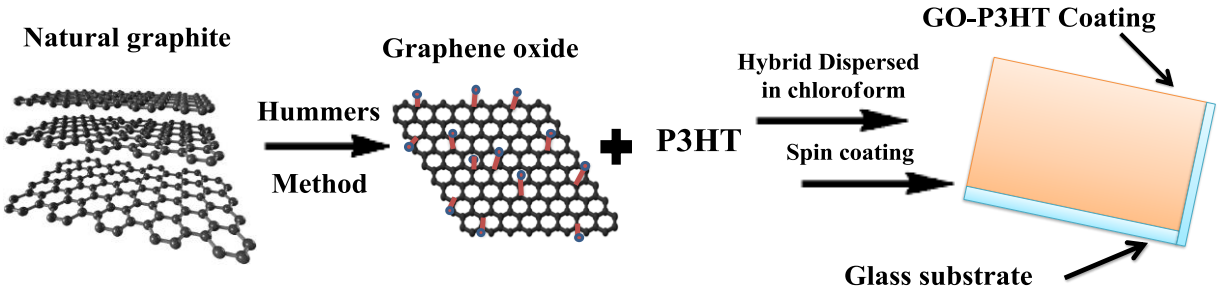


Figure 1: Schematic representation of synthesis of GO, rrP3HT hybrid and spin coating of the nano composite.

References:

[1] S, A, McDonald. G, Konstantatos. S, Zhang. P, W, Cyr. E, J, D, Klem. L. Levina. E. H. Sargent. *Nat.Mater* ,4 (2005) 138

[2] H, C. Leventis. S, P, King. A. Sudlow. M, S, Hill. K. C. Molloy. S. A. Haque. *Nano Lett*, 10 (2010) 1253-1258.

[3] McCullough RD, Lowe RS, Kherson sky SM. *Adv Mater*, 11 (1999) 250.

[4] Shuai Wang et al. *J,Phys.Chem. Lett*, 3 (2012) 2332−2336

MACRO 495

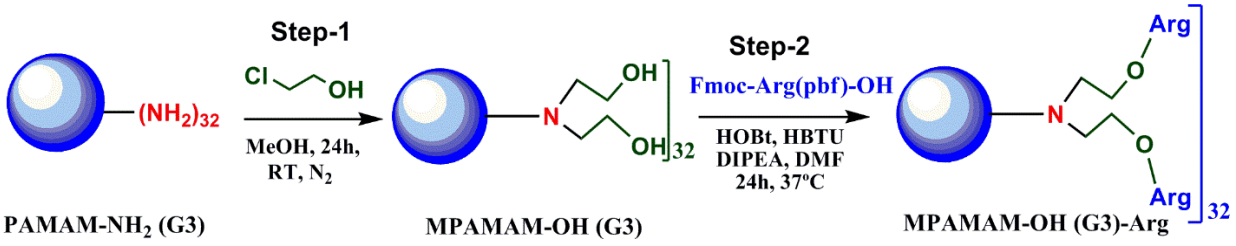
Synthesis of Surface Modified Poly (amidoamine) Dendrimer Functionalized Arginine for Solubility Enhancement of fat soluble Vitamin

E. Murugan*, V.Yogaraj and C. R. Akshata

Department of Physical Chemistry, School of Chemical Sciences, University of Madras, Guindy Campus, Guindy, Chennai-600 025, Tamil Nadu, India.
Email: dr.e.murugan@gmail.com

Vitamins are essential micronutrients which are importantly associated with major biological processes. Particularly, uptake of vitamins through routine diet is very crucial for maintaining good human health. However, biologist and medicos are facing several challenges due to partial or poor solubilization of fat soluble vitamins in aqueous phase due to its higher hydrophobicity which accounts for their diminished therapeutical efficiency. In order to exclude this problem, there is a need for benign solubiliser to accelerate the solubility of fat soluble vitamins in aqueous phase. Hence, in this work, it was aimed to enhance the aqueous solubility of fat soluble vitamins by employing modified Poly (amidoamine) (MPAMAM) dendrimer of third generation with surface functionalized amino acid for solubility enhancer.

Dendrimers are a new class of monodisperse macromolecules with regular and highly branched three dimensional architecture and surface functionality [1]. In this study, poly (amidoamine) (PAMAM) dendrimer having third generation was surface modified [2] and subsequently functionalized with Arginine (amino acid) [3] and thus obtained modified Poly (amidoamine) dendrimer with surface functionalized arginine (MPAMAM-OH (G3)-Arg). This product was in turn characterized with FT-IR and UV-vis spectroscopic techniques. The newly synthesized material viz., MPAMAM-OH (G3)-Arg was subsequently employed as a solubiliser and investigated the solubility of fat soluble vitamins in aqueous phase. The observed experimental results have strongly evidenced that MPAMAM-OH (G3)-Arg has proved to be an excellent solubiliser for fat soluble vitamins. It is also worth to mention here that the solubility of fat soluble vitamins noticed in the presence of MPAMAM-OH (G3)-Arg may be attributed due to the presence of internal cavities in dendrimers which leads to hydrophobic interaction of vitamins and further the basic nature of arginine favours the solubility enhancement. Hence, MPAMAM-OH (G3)-Arg is proved to be a promising candidate or solubility enhancer for fat soluble vitamins and thus have enormous scope in pharmaceutical applications.



Acknowledgement

One of the authors wishes to acknowledge DST-SERB, Govt. of India for financial assistance.

References

[1] H. Tokuhisa, M. Zhao, L. A. Baker, V. T. Phan, D. L. Dermody, M. E. Garcia, R. F. Peez, R. M. Crooks, and T. M. Mayer. *J. Am.Chem. Soc*, 120 (1998) 4492.
[2] E. Murugan, D.P.Geetha Rani. *Expert. Opin. Drug Deliv*, 10 (10) (2013) 1319.
[3] Hye Yeong Nam, Hwa Jeong Hahn, Kihoon Nam, Woo-Hyung Choi, Yunseong Jeong, Dong-Eun Kim, Jong-Sang Park. *Int. J. Pharm*, 363 (2008) 199.

MACRO 501

Click Chemistry Route to Covalently Link PVA and Cellulose

Kousar Jahan[a], Verma, Vivek[a, b, *]

[a]*Department of Materials Science and Engineering, Indian Institute of Technology Kanpur, Kanpur 208016, India*
[b]*Centre for Environmental Science & Engineering, Indian Institute of Technology Kanpur, Kanpur 208016, India*

[*]*corresponding author: Email: vverma@iitk.ac.in*

Click chemistry route to covalently link cellulose and polyvinyl alcohol (PVA) is demonstrated in present study. Polyvinyl acetate azide (PVAA) was synthesized via

chloroacetylation of Poly(vinyl alcohol) and subsequent azidation of as prepared poly vinyl chloroacetate (PVCA). Propiolic ester of cellulose was synthesized via esterification of cellulose by propiolyl chloride. Azide and alkyne derivatives of PVA and cellulose respectively were then coupled using Cu (I) catalyzed Huisgen azide-alkyne 1,3-dipolar cyclo-addition click reaction (CuAAC), resulting in triazole linkage between cellulose and PVA.

Functionalization of cellulose and PVA (using alkyne and azide derivatives, respectively) and click chemistry product were confirmed using FTIR. Thermal stability and crystallinity, performed using TGA and XRD, were also studied and compared to that of non-functionalized PVA and cellulose.

.

References

1. Huisgen, R; Szeimies,G; and Mobius,L. *Chem.Berichte*, 100 (1967) 2494–2507.
2. Binder, W. H. and Sachsenhofer, R. *Macromolecular Rapid Communication*, 28 (2007) 15-54.

MACRO-529

Cyclophane as a conformationally twisted monomer in high performance polymers

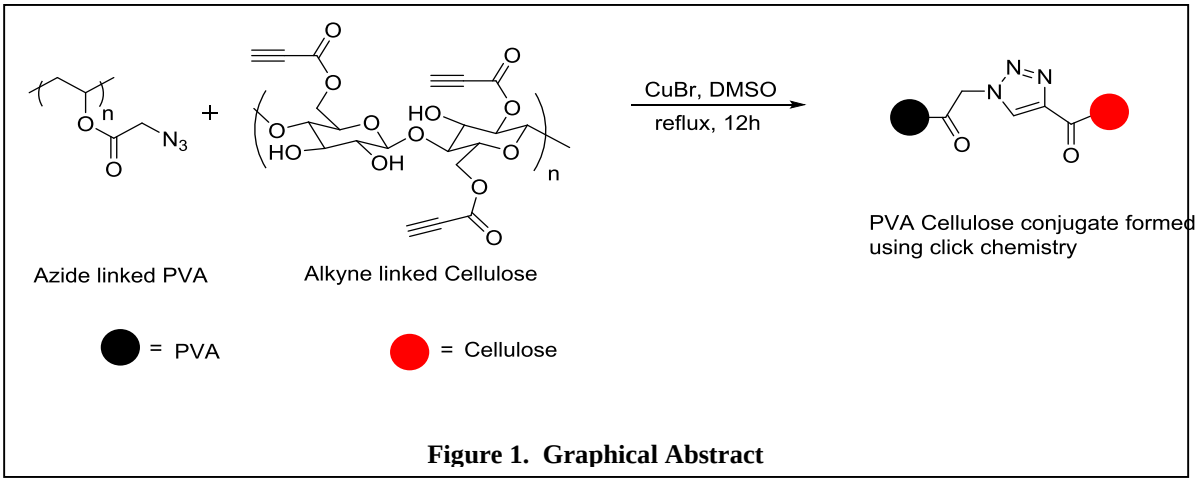


Figure 1. Graphical Abstract

Shyambo Chatterjee [a] , Vikas Kumar [a] , S. Sivaram *[b],

[a]Polymer Science and Engineering Division,
CSIR- National Chemical Laboratory, Pune 411008, India and
[b] Indian Institute of Science Education and Research, Pune 411008, India
email id: s.sivaram@iiser.ac.in

Abstract

Intrinsic microporosity in polymers is defined as "a continuous network of interconnected intermolecular voids, which forms as a direct consequence of the shape and rigidity of the component macromolecules". Our approach to creating intrinsic microporosity is by the use of a novel conformationally twisted cyclophane monomer for the synthesis of polybenzimidazoles which may have potential applications as membranes for selective proton or lithium ion transport.

Keywords: *Intrinsic microporosity, Free volumes, Paracyclophane, Polybenzimidazoles*

Introduction

Porous polymers are polymeric materials containing one or more types of pores. Opportunity to create high value applications provide an incentive for developing reliable methods for preparation of porous polymers, with designed pore architectures, customized framework and pore surface functionalities.[1] Several important structural characteristics of porous polymers are important for defined applications. These include, pore geometry, pore size, pore surface functionality and polymeric framework structure including composition, topology, and functionality. Recently, Intrinsically microporous polymers (IMP) have attracted attention as a class of new materials for creating microstructured and microporous polymers.[2] Intrinsic microporosity in polymers is defined as "a continuous network of interconnected intermolecular voids, which forms as a direct consequence of the shape and rigidity of the component macromolecules".

Poly(benzimidazole)s (PBIs) are a class of high-performance polymers which have been receiving increasing interest during the last years due to their high potential as constituents of membrane materials. In earlier work, porous PBIs were mainly prepared through the template method by use of soft templates.[3]

Our approach to maximizing intrinsic microporosity has been to design polymers with highly contorted molecular structures to provide "awkward" macromolecular shapes that cannot pack efficiently. Such intrinsically microporous PBI's may find useful applications as membranes for selective transport of proton (in fuel cells) and transport of lithium ions (as separator films for lithium ion batteries).

[2.2] *para*-Cyclophane is a key compound of the cyclophane family partly because of the ease of its synthesis.[4] The most important features of this class of compounds are the electronic interaction of the closely stacked π systems and the high amount of molecular strain which manifests itself in the distortion of the benzene rings into a boat shape. As cyclophane is a twisted bulky structure, its incorporation into rigid polymer networks is expected to result in packing defects and large free volume leading to the appearance of accessible microporosity.

Experimental

^{1}H and ^{13}C NMR spectra were recorded on a JEOL JNM-EX400 spectrometer. FTIR spectra were obtained on a Perkin-Elmer 1600 spectrometer. Analytical thin-layer chromatography (TLC) was performed with silica gel 60 Merck F254 plates.

Materials

[2.2] *para*-Cyclophane was obtained from Aldrich, 3,3'-diaminobenzedene (Sigma), isophthalic acid (Sigma), polyphosphric acid (Sigma), N,N-dimethylacetamide (Sigma) were used as received. The chemical structure of aromatic dicarboxylic acid 4, 16-dicarboxyl[2.2] *para*-cyclophane used in this work is well established.

Results and discussion

The derivatization of cyclophane was accomplished via electrophilic bromination as originally described by Reich and Cram.[5] Reaction was carried out using 2 equiv of bromine and was kept overnight in refluxing condition and monitored by thin layer chromatography. Pure pseudo-*para*-dibrobromo [2.2] cyclophane was separated by recrystallization process and the structure was established by single crystal XRD (**Figure 1**). The synthetic procedure of 4, 16-dicarboxyl[2.2] *para*- cyclophane is found to depend on the concentration of n-BuLi.

The synthetic procedure used for polybenzimidazoles is outlined in **Scheme 1**. Polymerization of p-dicarboxy [2.2] *para*-cyclophane in different mole percent with isophthalic acid and 3,3'-diaminobenzidine in polyphosphoric acid at 180°C gave poly (benzimidazo1e) PBI-I (5 % cyclophane di carboxylic acid) and PBI-II (10 % cyclophane dicarboxylic acid). Polyphosphoric acid solvent is selected for polymerization because a full conversion could be obtained well below

the strain release temperature of the [2.2] *para* cyclophane. The reference copolymer m-PBI was synthesized in the same manner at 200 °C. **Figure 2** shows the ^{1}H NMR spectrum of 10 mole % cyclophane dicarboxylic acid containing PBI where 3 imidazole protons exhibited a singlet at 13.27 δ, ppm, 16 aromatic protons of isophthalic acid and 3,3'-diaminobenzidene exhibited a multiplet between 9.16-7.65 δ, ppm, 6 aromatic protons of cyclophane dicarboxylic acid exhibited a triplet between 6.89-6.61 δ, ppm.

The copolymers were fully amorphous in nature and showed single glass transition temperatures (Tg). The results of thermogravimetric analysis (TGA) given in **Figure 3** indicate that poly(benzimidazole)s as a class possess outstanding thermal stability. The onset degradation temperature (Td) of the PBI II is about 590 °C and the weight loss is about 63 % at 900 °C. A small weight loss in the temperature range 270 °C is also observed. This can be ascribed to the homolysis of cyclophane ring (**Scheme 2**) leading to crosslinking. Inherent viscosity measurements of the copolymers were performed in DMAc at 30 °C with a concentration of 0.2 g/dL. The value obtained for PBI I and PBI II are 0.54 and 0.6 dL/g, respectively.

TEM micrographs reveal the preservation of the pore system in the co-PBI network **(Figure 4).** TEM micrograph of porous PBI indicates porous bicontinous sponge-like network. For all the samples, the distribution of the pores is not uniform.

Membrane Preparation

1 wt % polymer solution was dissolved at 80 ^{o}C in 10 mL of DMAc. The solution was stirred overnight and then filtered before being cast onto a clean glass plate. The solvent was evaporated at 180 ^{o}C overnight under nitrogen flux and then heated gradually to 200 ^{o}C and maintained at this temperature for 1 h. After cooling to room temperature, the membrane was unstuck from the glass plates by immersion in water. To remove the residual solvent, the membrane was dried under high vacuum for 5 h at 120 °C and then immersed in water and methanol.

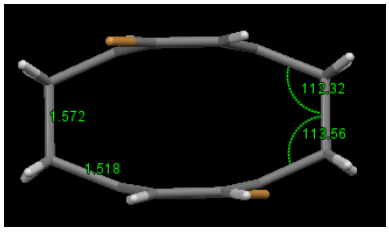
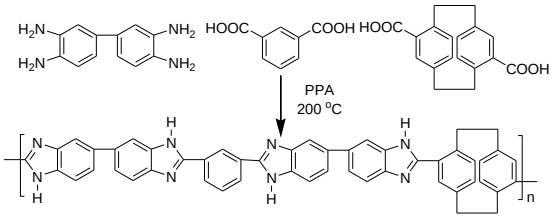


Figure 1. Crystal structure of pseudo para-dibrobromo [2.2] cyclophane with bond angle and bond length.



Scheme 1. Synthesis of polybenzimidazole based on 3,3'-diaminobenzidine, 4,16-dicarboxyl[2.2]paracyclophane and isophthalic acid.

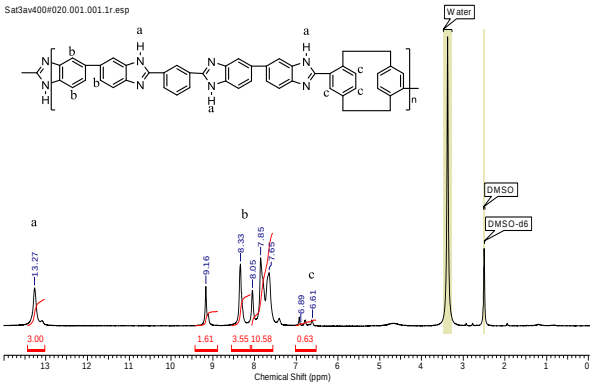


Figure 2. ^{1}H-NMR (DMSO-D$_6$) spectrum of co-polybenzimidazole based on 3, 3'-diaminobenzidine, cyclophane dicarboxylic acid (10 mole %) snd isophthalic acid.

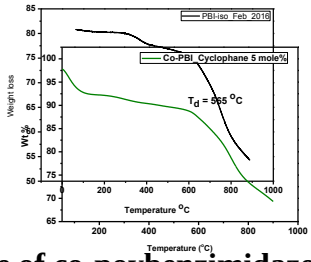
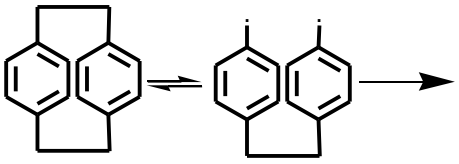


Figure 3: TGA curve of co-poybenzimidazole PBI-II and PBI-I .



Scheme 2. The paracyclophane units of the poly(benzimidazole) may undergo homolysis and combine in an intermolecular fashion to give the desired ethylene ladder crosslinks.

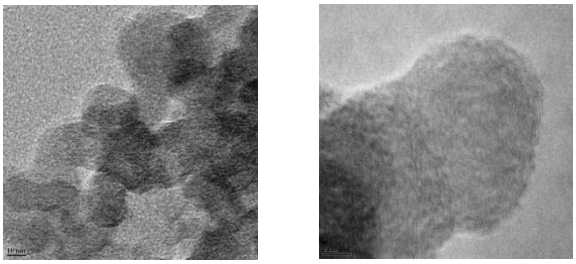


Figure 4. TEM micrographs of mesoporous PBI networks.

Table 1. Thermal characteristics of m-PBI, PBI-I and PBI-II.

Polymer	T_d (°C) (onset)	Tg (°C)
m-PBI	600	438
PBI-I	565	427
PBI-II	590	411

Conclusions

Copoly-benzimidazoles were successfully synthesized using upto 10 mol % 4, 16-dicarboxyl[2.2] *para*-cyclophane as a conformationally twisted comonomer. This polymer, consist of sites of contortion within a rigid amorphous polymer backbone. These copolymers could be cast in the form of a free standing film. The polymer has been characterized for its molecular and thermal properties.

Acknowledgements

SC gratefully acknowledges financial support from CSIR, New Delhi in the form of a Research Associateship. VK gratefully acknowledges grant of a Senior research fellowship from UGC, New Delhi

References

[1] Jenekhe, S. A. Chen, X. L. *Science* 372, 283, 1999.

[2] McKeown, N. B. Budd, P. M. *Chem. Soc. Rev.* 35, 683, 2006.

[3] Asensio, J. A. Sanchez, E. M. Gomez-Romero, P. *Chem. Soc. Rev*. 39, 3239, 2010.

[4] Hopf, H. *Angew. Chem. Int. Ed.* 47, 9808, 2008.

[5] Reich, H. J. Cram, D. J. *J. Am. Chem. Soc.* 91, 3534, 1969.

MACRO-530

Synthesis of aliphatic polyesters from a bio derived AB monomer

Y.R. Nevare[a],D. J. Nemade[a] and S. Sivaram*[b]

[a]*Polymer Science and Engineering Division, CSIR-National Chemical Laboratory, Dr. Homi Bhabha Road, Pune 411008, India*

[b]*Indian Institute of Science Education and Research, Dr Homi Bhabha Road, Pune 411008, India*

** e-mail id: s.sivaram@iiser.ac.in*

Abstract

Methyl 12-hydroxy stearate (Me 12-HS) is an AB monomer prepared by esterification of 12-hydroxy stearic acid (12-HSA), a bio-renewable material and readily available from castor seed oil. Commercial 12-HSA has mono carboxylic acids as impurities which are not desirable since they act as chain terminators. In this study an attempt was made to prepareMe 12-HS in high purity which was subjected to transesterifcation as well as transesterifcation-polycondensation using titanium isopropoxide and distannoxane catalysts. The degree of polymerization increased by 3-4 units every 3 h. The rate of polymerization, as evidenced by the change of DP with time, indicates that the rate is faster with a titanium based catalyst. MALDI-TOF analysisindicates formation of cyclics along with linear chains. The fact that intramolecular reactions can compete with chain growth reaction in the melt phase adds to the complexity of polymerizing this monomer.

Keywords: *polyester; 12-HSA; Me 12-HS, Trans-esterification; Polycondensation*

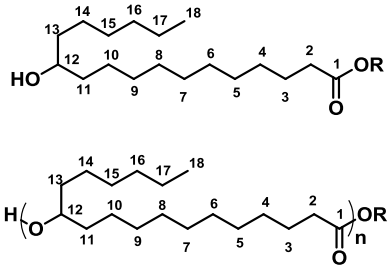
Introduction

Methyl 12-hydroxy stearate (Me 12-HS) is an AB monomer prepared by esterification of 12-hydroxy stearic acid (12-HSA), a bio-renewable material whichis readily available from castor seed oil. India is the world's largest producer of castor seeds[1]. Short chain aliphatic polyesters

containing AA + BB type monomers namely,poly(ethylene succinate), poly(butylene adipate)etc have been synthesizedby transesterification of the corresponding diesters with diols. This reaction is facilitated by the easy removal of low boiling byproduct formed during the reaction. However, in case of longer chain aliphatic diol and diestermonomers, it is difficult to remove the byproduct diol on account of its poor volatility and high boiling point,. For example, 1,14-tetradecane diol has a boiling point of >200°C at 9 Torr[2]. Short chain AB type monomers, namely, poly(lactic acid) and poly(glycolic acid) are generally synthesized by ring opening polymerization (ROP) of the corresponding cyclic lactides. Naturally occurring long chain AB type monomers, such as, fatty acids from plant seed oils are attractive substrates as they contain long chain linear or branched segments. The most common fatty acids in plant oils have C16 and C18 aliphatic chains. Aliphatic segments of this chain length in polyesters provide significant enahancement of crystallinity and improved melting points[2].

Only few references are available in the literature on the polymerization of aliphatic long chain AB monomers with a methylene number more than 14[2]. Liu et. alsynthesized a long chain aliphatic polyester from 14-hydroxytetradecanoic acid using titanium tetraisopropoxide as a catalyst with the molecular weight of 53,000 to 140,000 g/mol[3]. The resulting polymer showed improved mechanical properties. Poly(18-hydroxyoctadecanoic acid) has also been prepared by the melt polycondensation using titanium alkoxide as catalyst[4].

Me 12-HS is an AB monomer which could be used for the synthesis of long chain aliphatic polyesters (Fig.1).



Where, R= -CH_3

Fig. 1: Chemical structure of Me 12-HS and its polyesters.

The resulting long chain aliphatic polyesters are likely to be amorphous thermoplastics with a low T_g in view of the presence of a branch at the 12-carbon atom. 12-HSA has been polymerized by polycondensation in melt at 160^{o}C under vacuum in presence of PTSA as catalyst.The polymer with a M_n of 3500-4000 was obtained in 5 h as a colorless and transparent, viscous liquid. The[5] presence of n-hexyl pendant (side chain) affects any parallel arrangement of the backbone polymer chains, which is essentially required for crystallization. This is clear evidence of the fact that softness and amorphous nature of poly(12-HSA) is due to the n-hexyl side chain. Surprisingly,

there is only one report of the polymerization of 12-HSA and no report of polymerization of any of its esters. Therefore, an objective of the present work is to obtain chemically pure monomer quality Me 12-HS suitable for polymerization. Me12-HS can be polymerized by transesterification-polycondensation reaction. The chemical structure and properties of the oligomers and polymers thus obtained has been examined.

Experimental

Materials

12-HSA (75 % GC), was procured from TCI, Tokyo, Japan. Dibutyltin dichloride and stannous oxide (99.99%),chloroform-d (99.8%), Concentrated HCl (35 to 38 %), sulfuric acid (98 %), and titanium isopropoxide (97%) were procured from Aldrich Chemicals, USA and used without further purification.

Measurements

For NMR measurements, the samples were dissolved in chloroform-d in a 5 mm diameter NMR tube at room temperature. Proton-decoupled ^{13}C NMR spectra (nuclear Overhauser effect) were recorded on a Bruker DRX 500-MHz NMR spectrometer working at 125-MHz. $CDCl_3$ served as a solvent and tetramethylsilane served as an internal standard for all NMR measurements. Melting points were recorded on a Barnstead Mel-Temp 1001D electrothermal melting point apparatus. All melting points are uncorrected and are recorded on the Celsius scale.MALDI-ToF MS analysis was performed on a KratosKompact MALDI IV spectrometer. All experiments were carried out at an accelerating potential of 20 kV. In general, mass spectra from 200 shots were accumulated to produce a final spectrum. The samples were dissolved in tetrahydrofuran (1 mg/mL) and mixed with the matrix (15 mg/mL of THF) before drying on the sample plate. 2,4,6-trihydroxyacetophenone (THAP) was used as the matrix. The sample plate was inserted into the apparatus under high vacuum (~ 10^{-5} Pa).

Synthesis of 1,1-dichloro-1,1,3,3-tetrabutyl-distannoxane (9)

1,3-dichloro-1,1,3,3-tetrabutyl-distannoxane (9) catalysts was prepared as per reported procedure[6].

Synthesis of methyl 12-HS

Me 12-HS was prepared by the esterification of 12-HSA using sulfuric acid as catalyst as per reported in the literature[7].

Transesterification-polycondensation of Me12-HS

In a three neck flask equipped with a nitrogen inlet and a condenser connected to vacuum pump through cold trap was charged with 5 g of **2**, and 0.5 wt % of $Ti(O^iPr)_4$ catalyst under nitrogen purging. The reactor was immersed into the oil bath and the temperature was slowly increased to 180^oC within half an hour with a constant flow of nitrogen. Samples were withdrawn at 3, 6, 9 and

12 h. Thereafter, the pressure was slowly decreased to 0.5 mm Hg at 180^{o}C. Again samples were withdrawn at 15, 18, 21 and 24 h. The number average degree of polymerization of the samples was calculated using NMR.

Results and discussion

Synthesis

Characterization of 1,3-dichloro-1,1,3,3-tetrabutyl-distannoxane catalysts

The chemical structure of 1,3-dichloro-1,1,3,3-tetrabutyl-distannoxane is shown in Fig. 2.

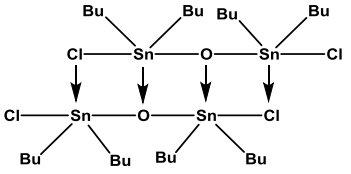
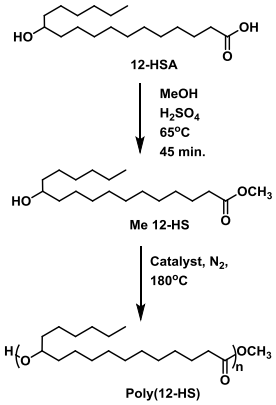


Fig. 2: Chemical structure of distannoxane catalysts.

Melting point of distannoxane was found to be 105-110^{o}C (lit. 110-112^{o}C).



Scheme 1: Synthesis and transesterification of Me12-HS.

Me 12-HS were prepared by the esterification of 12-HSA in methanol using sulfuric acid as catalyst (Scheme 1). The product was distilled under vacuum. The distillate solidified upon cooling. Chemical structure of Me 12-HS (distilled sample) was confirmed by using NMR spectroscopy (Fig. 3 and 4). The peak assignments are in good agreement with the chemical structure of Me 12-HS.

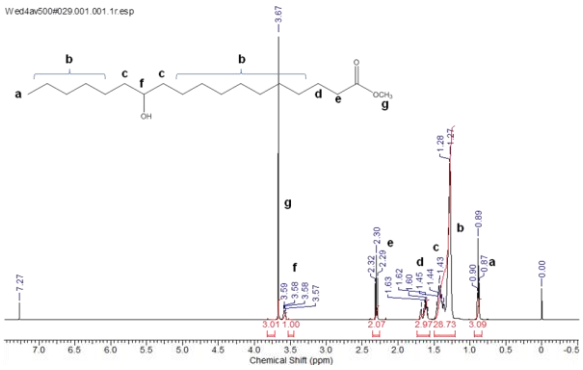


Fig. 3: ^{1}H NMR (500MHz) spectrum of vacuum distilled Me12-HS in $CDCl_3$.

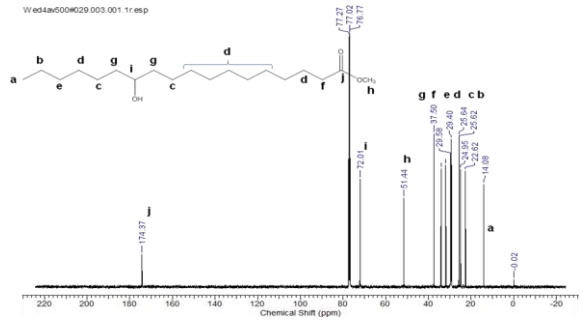


Fig. 4: ^{13}C NMR spectrum of vacuum distilled Me 12-HS in $CDCl_3$.

The number average degree of polymerization increased by 2-3 units after each 3 h. The number average degree of polymerization after at the conclusion of the reaction was found to be 18. Transesterifcation-polycondensation of Me 12-HS was performed in presence of a distannoxane catalyst and analyzed as described in experimental section. NMR spectrum of 3, 6, 9, 12, 15, 18, 21 and 24 h was recorded. Fig. 6 shows NMR scpetrum of sample taken after 24 h. The peak assignments (chemical shift in ppm) have been shown in fig. 5. The peak signal at 3.66 ppm which is corresponds to the $–OCH_3$ end group has been used for the determination of number average degree of polymerization as well as number average molecular weight.

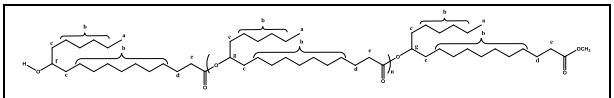


Fig. 5: Chemical structure of poly(Me 12-HS).

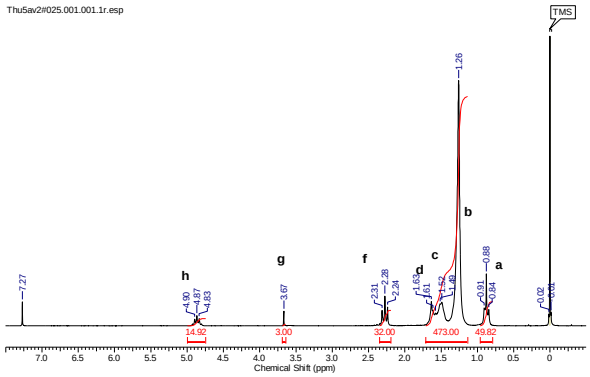


Fig. 6: ^{1}H-NMR (200 MHz) spectrum of sample 8 (after 24 h) in $CDCl_3$.

The number average degree of polymerization increased by 1-2 units after intervals of 3 h.

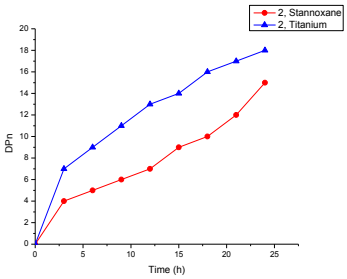


Fig. 7: Variation of DPn with time .

Thus, Me 12-HS could be polymerized using distannoxane as catalyst. The number average degree of polymerization after 24 h was found to be 15.The relative reactivity of the titanium and stannoxane catalyst for transesterifcation-polycondensation of Me 12-HS is shown in Fig. 7. The titanium based catalyst was found to be more effective than tin based catalyst. However, the reaction rates are slow with both the catalysts.

MALDI-TOF-MS

The MALDI-TOF spectrum shown in fig. 8 presents the complete MALDI spectrum of poly(me 12-HS). The zoomed region shown in inset for the identification of series of peaks. The most intense peaks in the region 353 to 1765 Da corresponding to the potassiated adduct molecular ions of empirical formula H-(O-CH($(CH_2)_5CH_3$)$(CH2)_{10}CO)_n$-OCH_3 and molecular weight (282n + 32 + 39), where, n ranges from 1 to 18. There is another series of intense peak from 321 to 1362 Da which can be assigned to cyclic oligomers having molecular weight (282n + 39), where, n ranges from 1 to 5. This indicates that the linear polymer formation is accompanied by formation of macrocyclics during the TE-PC. Two more series of peak are observed which corresponds to sodiated adduct molecular ions having molecular weight (282n + 32 + 23) and (282n + 23) respectively.

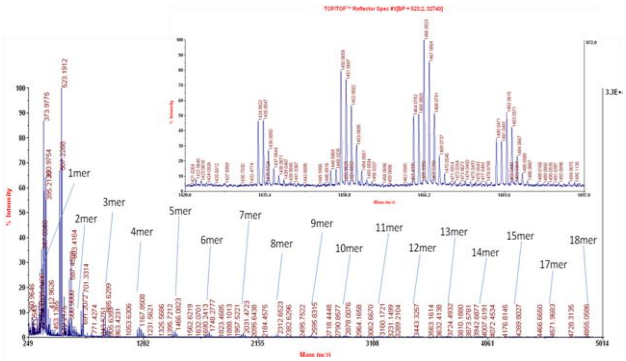


Fig. 8: MALDI spectrum of poly(me 12-HS).

Conclusions

Me 12-HS was prepared from 12-HSA which is a material that can be readily obtained from renewable resources and is a potentially useful AB monomer.The product was obtained in high purity by vacuum distillation. The purity of the monomer was ascertained by a multiplicity of analytical methods. Me 12-HS was subjected transesterifcation as well as transesterifcation-polycondensation using titanium isopropoxide and distannoxanecatalysts. The degree of polymerization increased by 3-4 units every 3 h. After 24 h the number average degree of polymerization was found to be 4000-4500 g/mol in both the cases. The rate of polymerization, as evidenced by the change of DP with time, indicates that the rate is faster with a titanium based catalyst. MALDI-ToF analysis shows the formation of cyclics along with linear chains. Cyclics begin to form even at early stages of transesterification. The concurrent formation of cyclics could restrict the efficient polymerization of this monomer.

Acknowledgements

YRN acknowledges DST for INSPIRE fellowship.

References

1. Mutlu, H.; Meier, M.A.R. Eur. J. Lipid Sci. and Technol. **2010**, 112, 10.
2. Stempfle, F.; Ortmann, P.; Mecking, S. Chem. Rev. **2016**,116,4597.
3. Liu,C.; Liu,F.; Cai,J.; Xie,W.; Long, Y.E.; Turner,S.R.; Lyons, A.; Gross,R.A. Biomacromolecules**2011**,12,3291.
4. Jose,J.;Pourfallah,G.;Merkley,D.;Li,S.;Bouzidi.L.;Leao, A. L.; Narine, S. S. Polym. Chem. **2014**, 5, 3203.
5. Bawn, C. E. H.; Huglin, M. B. Polymer **1962**, 3, 257.
6. Okawara, R.; Wada, M. J. Organomet. Chem. **1963**, 1, 81.
7. Madison, T. M. S. A.; Bijan, H.; Jose, J. R.; Helen, M.; Jianmimg, L. **2012**, US20120122936 A1.

MACRO 535

Syntheses and characterization of block copolymers of methacrylates bearing POSS as well as fluoro alkyl group

Siva Ponnupandian, Nikhil K. Singha

Rubber Technology Centre, Indian Institute of Technology Kharagpur, Kharagpur - 721302, West Bengal, India. E-mail: psiva1990@gmail.com Tel: + 91-8768757323

Abstract: Fluorinated polymers, especially fluoroacrylates find enormous applications in hydrophobic surface coating. This investigation reports preparation of block copolymers (BCPs) of fluorinated and non-fluorinated monomers via Reversible Addition Fragmentation chain Transfer (RAFT) polymerization technique. In this case, BCPs of methacrylol isobutyl polyhedral oligomeric silsesquioxane (POSS) and 2,2,2-trifluoroethyl methacrylate (TFEMA) were prepared using 2-(dodecylthiocarbonothioylthio)-2-methylpropanoic acid (DDMAT) as RAFT agent. POSS was polymerized using DDMAT and have been used as macro-RAFT agent to polymerize TFEMA. The homo and block copolymers were characterized using FTIR, ^{1}H NMR and GPC analyses. The thermal properties of the BCPs were studied using DSC and TGA analyses. The morphology of the BCPs was studied using SEM, TEM and AFM analysis. The BCPs exhibits core-shell type morphology. The prepared BCPs were coated over glass substrates and their hydrophobicity and the surface energy were measured using contact angle analysis. The coating showed improved hydrophobicity on increasing the block length of the fluorinated polymer.

Keywords: Fluoroacrylate, block copolymer, RAFT polymerization, hydrophobicity.

References:

1. Q. Hong, M. Xiaoyan, L. Zhiguang, C. Fang, and Z. Qilu, Materials & Design, 2016, **96,** 1-9.
2. A. Chakrabarty, P. Siva, K. Naskar and N.K. Singha, RSC Advances, 2016, **6**, 34987-34995.
3. K. Zhang, L. Xiaohui, Z. Yunhui, Z. Kongying, L. Yancai, T. Chao, and Y. Xiaoyan, Progress in Organic Coatings, 2016, **93**, 87-96.
4. H. Hussain, B.H. Tan, C.S. Gudipati, Y. Xaio, Y. Liu, T.P. Davis, and C.B. He, Journal of Polymer Science Part A: Polymer Chemistry, 2008, **46**(22), 7287-7298.
5. B.P. Koiry, P. Siva, S. Choudhury, and N.K. Singha. Journal of Fluorine Chemistry, 2016. doi: 10.1016/j.jfluchem.2016.06.021.

MACRO 536

Synthesis and Characterisation of Polyamides containing thiazolidine unit

V.P. Ubale[a]; A. A. Ghanwat[b]; P.H. Basutkar[a]; J. N. Mahindrikar[b], N. N. Maldar[b] and R.A. Patil[a]*

[a] D.B.F. Dayanand College of Arts and Science, Solapur, Maharashtra, India.

[b] *School of Chemical Sciences, Solapur University, Solapur, Maharashtra, India.*
**e-mail id: vpubale@yahoo.co.in*

Abstract

Aromatic polyamides are well accepted as high performance and high temperature resistant materials. They exhibit favorable balance of physical and chemical properties and show excellent thermal, mechanical and electrical properties. They are widely used in microelectronic and aerospace engineering. .

The present investigation deals with the synthesis of a new diamine containing thiazolidine unit N, N'-Bis-[3-(2-amino-thiazol-4-yl)-phenyl]isophthalamide (ATPIPA) was synthesised by reaction of isophthaloyl chloride with m/p-aminoacetophenone followed by reaction with iodine, thiourea and characterized by different spectroscopic methods. IR spectrum of ATPIPA exhibited the absorption bands at 3345 (N-H asymmetric stretching), 3440 (N-H symmetric stretching), 1625 (N-H bend.) and 1150 cm^{-1}(C-S stretch.). N, N'-Bis-[3-(2-amino-thiazol-4-yl)-phenyl]-isophthalamide (ATPIPA) was used to synthesise aromatic polyamides by polycondensation with aromatic acids such as isophthalic acid (IPA), terephthalic acid (TPA), dicarboxy diphenyl sulphone (DCDPS) etc.

These polyamides exhibited solubility in polar aprotic solvents like NMP and DMAc, DMF. Thermal analysis showed that polymers possess good thermal stability exhibited glass transition temperature (Tg) in the range 207-225ºC.The T_{10} value means 10% weight loss determined from thermo gravimetric analysis in nitrogen atmosphere was in the range 270-340 ºC demonstrating good thermal stability. Synthesised polyamides showed the inherent viscosity in the range 0.3 -0.6 dLg^{-1}

Keywords: Polyamide, thermally stable polymers, high performance materials.

Introduction:-

Aromatic polyamides are one of the most important class of high performance polymers, because they possess excellent mechanical properties, thermal stability, chemical resistance and low flammability [1- 2.] However, they encounter processing difficulties due to limited solubility in organic solvents and high glass transition or melting temperatures. It is a result of chain stiffness and intermolecular hydrogen bonding between amide groups [3-4]. However, these wholly aromatic polyamides usually shows poor solubility in common organic solvents and their extremely high melting temperatures, which lie above their decomposition temperatures, give rise to processing difficulties and so limit their applications [5-6]. In order to overcome these drawbacks, considerable efforts have been made to modify their chemical structure to improve processability and solubility, so that to facility their use in a specific field .There are various approaches for improvement of the solubility and processability of polyamides without sacrificing their high thermal stability and mechanical properties, these methods include incorporation of kinked units or flexible spacer units into the diamine fragment [9–12]. The introduction of bulky pendant (cardo) groups into the backbone

of polymers is another approach to improve solubility and thereby process ability such as, the incorporation of the flexible linkages (e.g. –O–,–SO_2–, etc.) [14], lowers the segmental rotational barrier and increase the conformational freedom, cardo groups (such cyclododecylidene, pyrene, and naphthalene, etc.) [13-14] or molecular asymmetry (*ortho*, *meta* versus linkages) [15-16] into the backbone or addition of bulky side group (such as *tert*-butyl, norbornane units) [17–21].

Tg increases by the introduction of rigid rod like structure along the polymer backbone. On the other hand kinked structures such as m-phenylene linkages make the polymer more soluble in organic solvents. However the Tg temperature decrease. Korshak [23] and Imai et.al. synthesised polyamides having high solubility and glass transition temperature by introducing bulky and stiff structure into the polymer backbone. Introducing heteroaromatic rings, such as the thiazole unit, into the main chain of a synthetic polymer is expected to impart certain properties such as chemical stability, thermal and thermo-oxidative stability to the polymer. Heteroaromatic ring of thiazole was expected to provide molecular irregularity and decrease interchain interaction and the ability for polymer chains to pack while providing a barrier to segmental mobility, thus resulting in an enhanced solubility and increased Tg of the polymers.

Experimental

Material:-

Dimethyl formamide (DMF), thionyl chloride, methanol, m-aminoacetophenone, isopthalic acid, terepthalic acid,4,4'-diphenoxy diphenyl ether, m-cresol, ethanol (S. d.fine), triphenyl phosphite (TPP) were used after purification. N, N, Dimethyl acetamide (DMAc) was refluxed over barium oxide over 4 h distilled under vaccum and stored over Linde type 4A molecular sieves. Pyridine, lithium chioride, N-methyl-2-pyrrolidone (NMP) were purified prior to use.

2.2 Characterization

IR spectra were recorded at a resolution of 4 cm^{-1} with co-addition of 32 scans using a Thermo-scientific Nicolet iS10 smart IR. ^{1}HNMR spectra were recorded with a Bruker 400 MHz and 100 MHz for ^{13}CNMR measurements using $CDCl_3$ or DMSO solvent. Thermogravimetric analysis (TGA) was performed with Perkin-Elmer TGA-7 system at a heating rate of 10ºC/min in a nitrogen atmosphere from 60 to 1000ºC..

DSC was conducted on a Metler Toledo DSC at a heating rate of 10ºC/min over a temperature range of 50-350ºC under a nitrogen flowing atmosphere.

XRD patterns of polymer were obtained with a Rigaku Micromax-007 X-ray diffractometer operating at 40 kV and 30 Ma Measurements.

Inherent viscosity (η_{inh}) of the polyamides was determined using an Ubbelhode suspended level viscometer with a solution of polymer in DMAc at a concentration of 0.5% (W/V) at 30±0.1ºC. It was calculated using the equation

$$\eta_{inh} = 2.303/C \log t/t_0$$

Where t and t_0 are flow times of polymer solution and solvent, respectively and C concentration of polymer solution.

Synthesis of monomers:-

A) Synthesis of N,N'- bis (3- acetyl phenyl) isophthalimide (I)

In 100 mL three neck round bottom flask equipped with magnetic stirrer, a nitrogen gas inlet, thermowell and $CaCl_2$ guard tube were charged with m-aminoacetophenone 0.274 g (0.002mol) and dry DMAc (6 mL) .The mixture was stirred under nitrogen atmosphere till the complete dissolution takes place and it was cooled to -15ºC. In a cooled reaction mixture add lot wise isophthalyol chloride 0.166 g (0.001 mol) and few crystals of LiCl. The mixture was stirred at 0ºC for 1.5 h and then for 1.5 h at 25ºC

The solution was stirred at room temperature for 24 h. The viscous solution was poured in methanol with stirring to get white solid. Then filtered and washed with methanol to obtain white colored product.

Yield: - 0.38 g (95%)

Melting point: - 210ºC

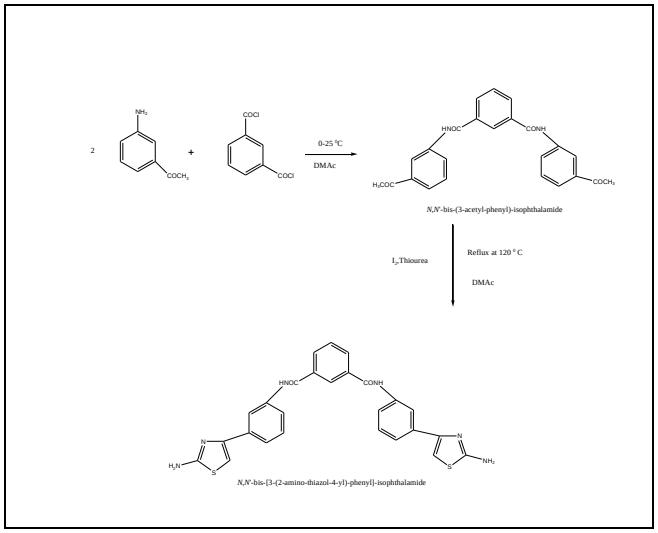
IR (cm^{-1}) : 1667 cm^{-1} (–C=O stretching of (CONH)) , 2908 cm^{-1} (aliphatic CH stretching) and 1602 cm^{-1} (NH bending) ^{1}HNMR: 10.36 ppm (s,2H) amide proton .The singlet peak at 2.86 ppm (s,6H) was due to aliphatic methyl proton. 7.45-8.35 ppm (multiplate) aromatic protons were observed in range^{13}C NMR spectra showed the 16 peaks for 16 different carbon atoms. (26.96 ppm) as assigned to methyl carbon, (165 ppm) assigned to carbonyl carbon of amide group and at (197 ppm) due to carbonyl carbon of acetyl group.

B) Synthesis of N**, N'-Bis-[3-(2-amino-thiazol-4-yl)-phenyl]isophthalamide (II)(ATPIPA)**

In a 100 mL three neck round bottom flask added compound (I) 0.4 g(0.001mol) and iodine 0.252 g (0.002mol) and thiourea 1.2 g (0.004 mol) and stirred the mixture in DMAc at 120ºCfor 24 h. Then poured the solution with stirring in water, the yellow solid was obtained. The precipitate was washed successively with water and then by ethanol. Recrystallised the product in acetone.

Yield:-0.460 (90%). (IR) 1672 cm^{-1} (–C=O stretching of (CONH)) 3365 cm^{-1} (NH stretching of primary amine) . ^{1}HNMR(200 MHz ,DMSO; ppm) 10.38 ppm(s 2H) ,6.97 ppm (s,2H) was assigned to proton of NH_2 group.The aromatic protons were exhibited peaks in range(7.33-8.60 ppm. (multiplate) ^{13}C NMR(50 MHz,DMSO;PPM) showed the 15 peaks for 15 different carbon atoms. The peak at 165 ppm was assigned to carbonyl carbon of amide group.

Mass: The molecular ion peak at 512 m/e^+ was assigned as a base peak. This confirmed the Thiazole diamine structure



Scheme 1:-Synthesis of compound (I)

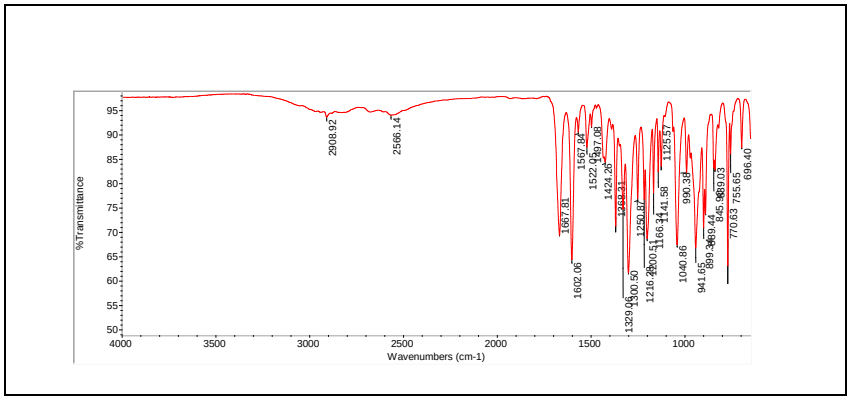
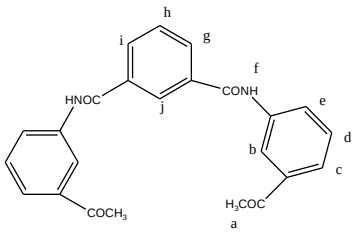
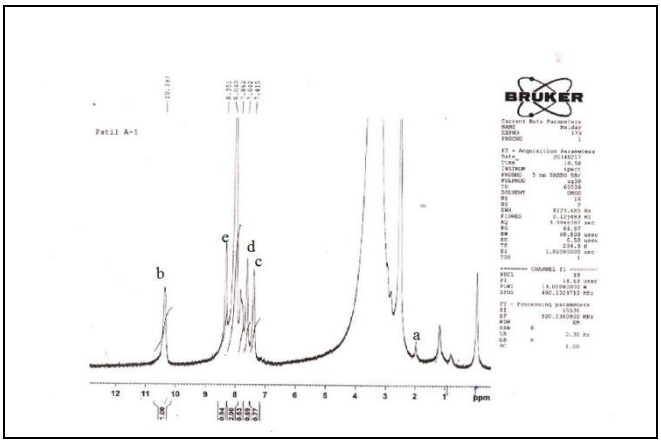


Figure :-1 IR spectra of compound (I)

^{1}HNMR, ^{13} CNMR spectra confirms the structure of compound (I).





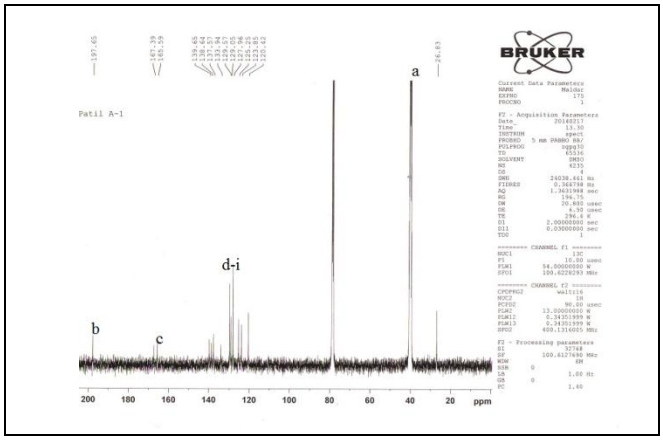


Figure 2:-^{1}HNMR spectra of compound (I)

Figure 3:-^{13}CNMR of compound (I)

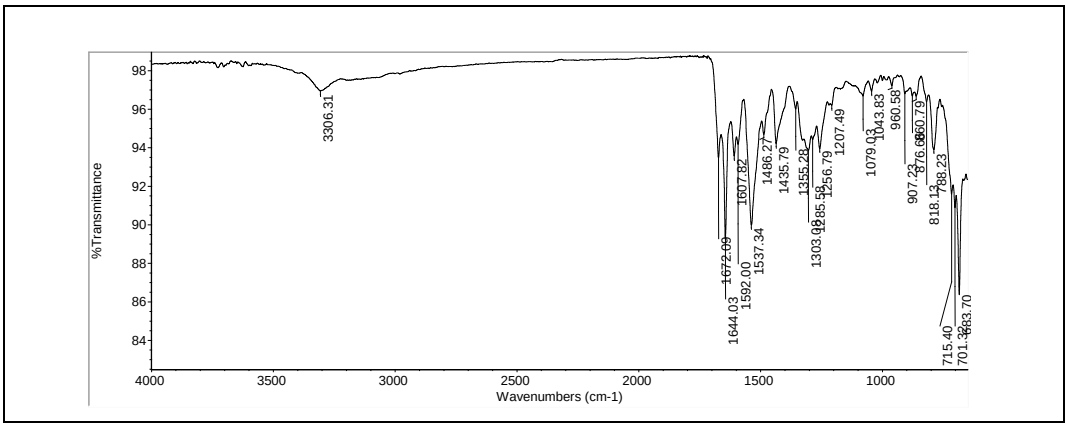
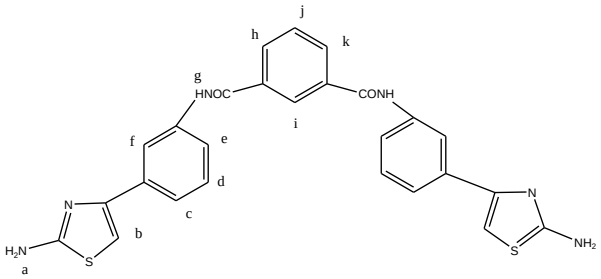
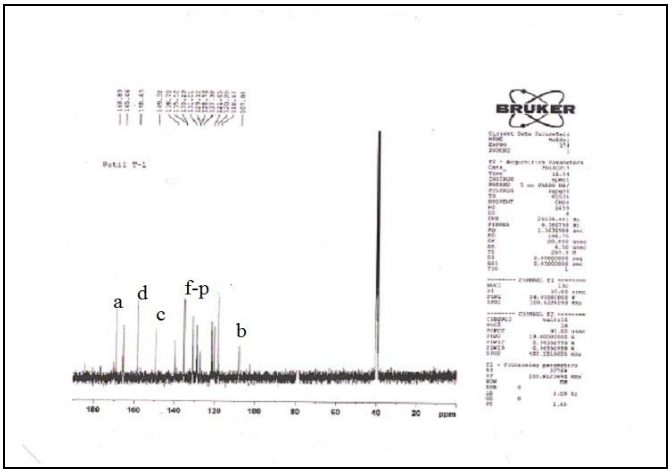


Figure 4:- IR spectra of compound (II)

^{1}HNMR , ^{13} CNMR spectra confirms the structure of compound (II).





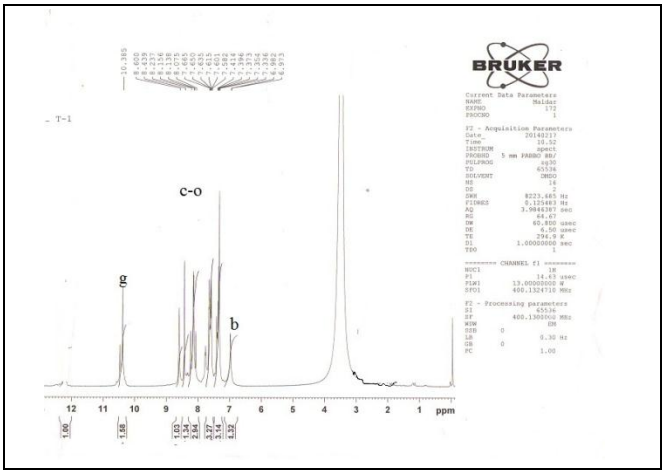


Fig:-5 ^{1}HNMR of compound (II)

Figure 6:-^{13}CNMR compound (II)

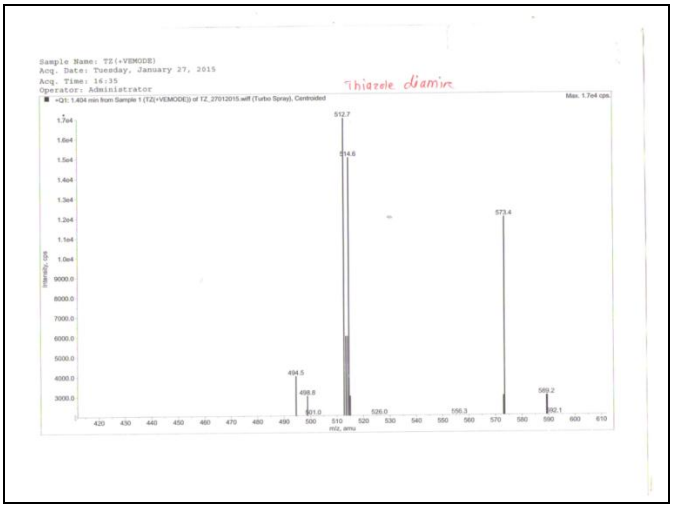


Figure-7:-mass spectra of compound (II)

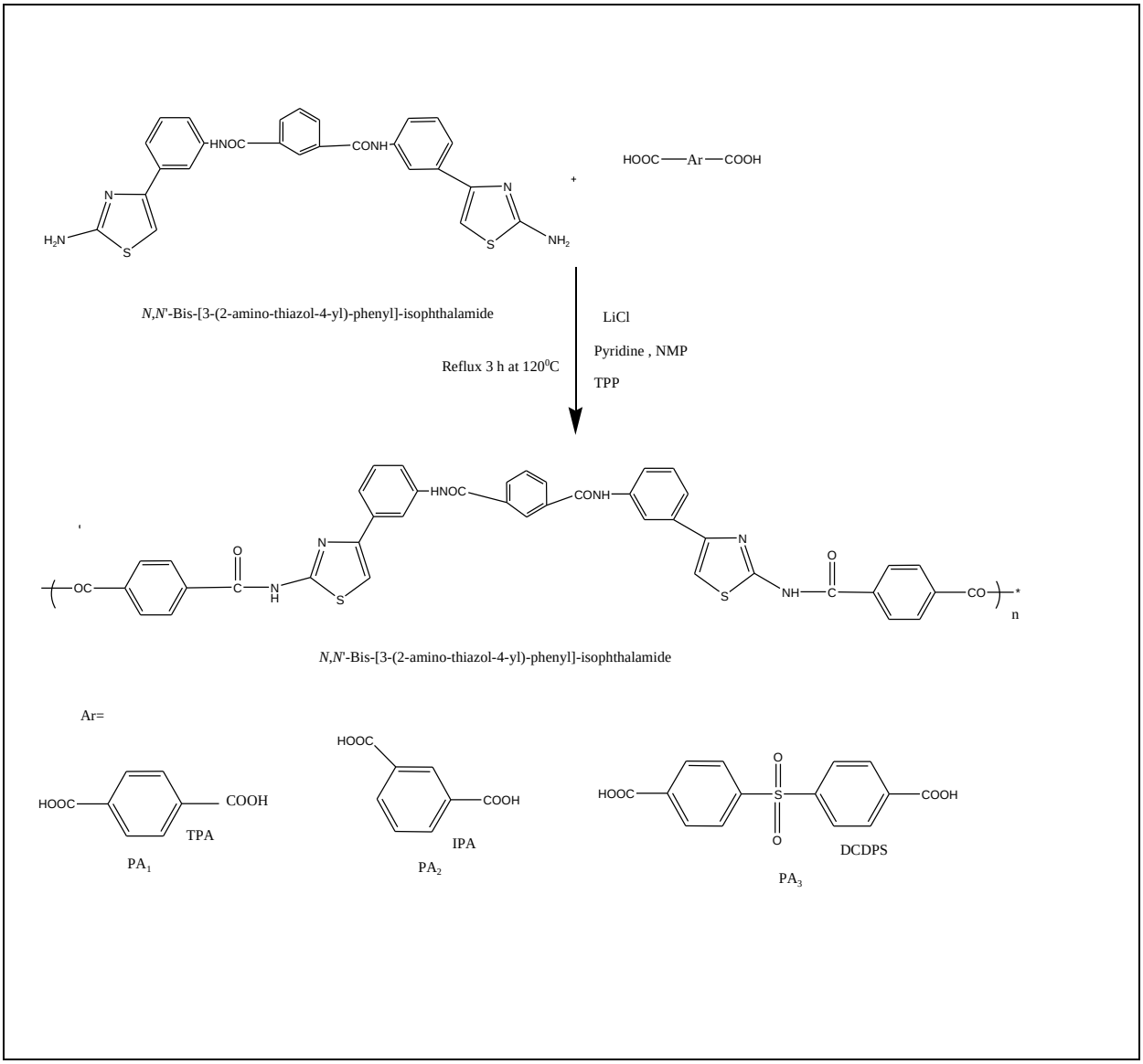
Results and discussion:-

Polymer synthesis

In a 100 mL three neck round bottom flask equipped with reflux condenser, magnetic stirrer and calcium chloride guard tube and nitrogen gas inlet were placed 0.512g (0.001mol) and 0.166g(0.001mol) isopthalic acid,0.200g lithium chloride (8wt% based on solvent N-methyl pyrrolidone(NMP) and pyridine mixture) and 0.744 g (0.63 mL,2.4 mmol) triphenyl phosphite (TTP),0.5 mL pyridine,2 mL NMP. The mixture was stirred well and temperature was slowly raised to 100ºC and heated at 100ºC for 3 h. under nitrogen. After cooling the resulting viscous mixture was poured into rapidly stirred methanol. The precipitated polymer was filtered, washed with methanol and air dried. Polymer was purified by dissolving in N,N-dimethyl acteamide (DMAc) and reprecipitating by methanol. The precipitate was filtered, washed with methanol and dried under vacuum at 80ºC for 8 h. The yield was 85% and the reduced viscosity of polymer in DMAc at 30ºwas 0.45dL/g. All other polyamides i.e PA-2 to PA-9 were prepared by similar procedure

Scheme 3:-Synthesis of polyamide from compound (I) and aromatic diacidsSPECTRAL

Analysis of Polyamide



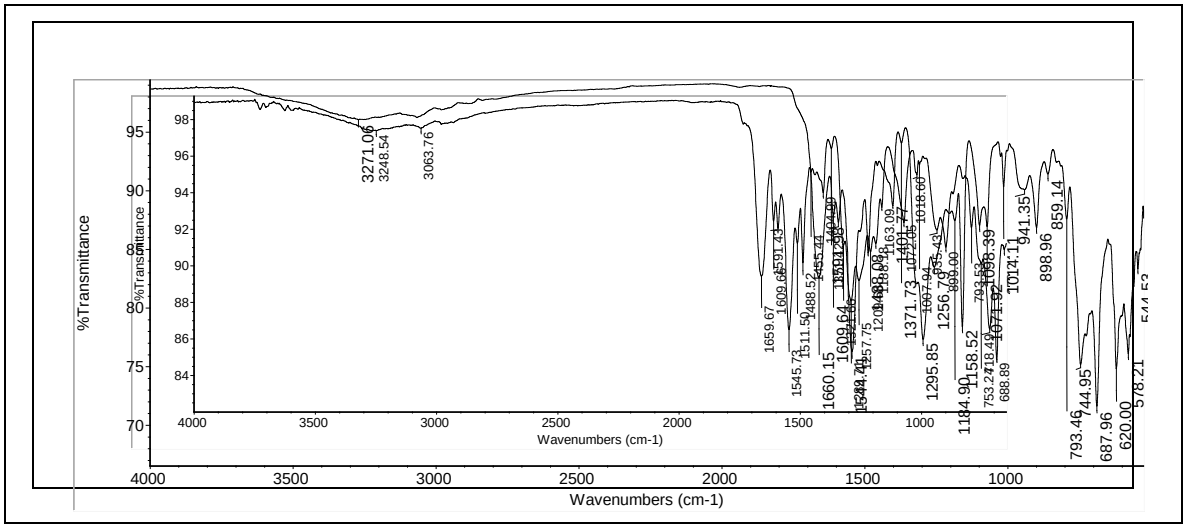
Polyamide synthesized by using isophthalic acid and thiazole diamine was confirmed by spectral analysis.

IR SPECTRA OF PA-2 (compound II and IPA)

The absorption peak at 1659 cm^{-1} and 3063cm^{-1}due to –C=O stretching of (CONH) group

Figure 8:- IR spectra of compound (II) and IPA

Figure 9:- IR Spectra of compound (II) and DCDPS(PA-3)



[1]HNMR:-

The peak at 10.27 ppm was assigned to amide proton. The disappearance of peak at 6.97 ppm indicates the polyamide formation

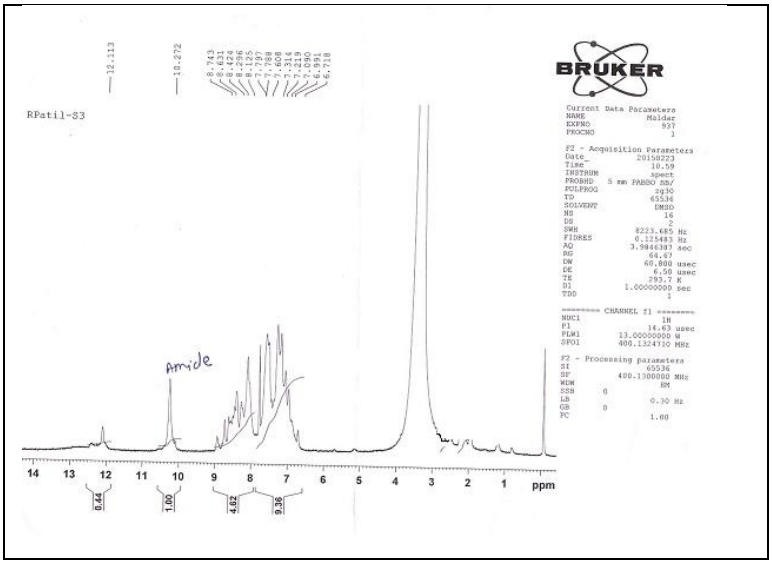


Figure 10:-[1]HNMR of polyamide from Thiazole diamine and IPA

[13]CNMR OF Thiazole diamine and IPA

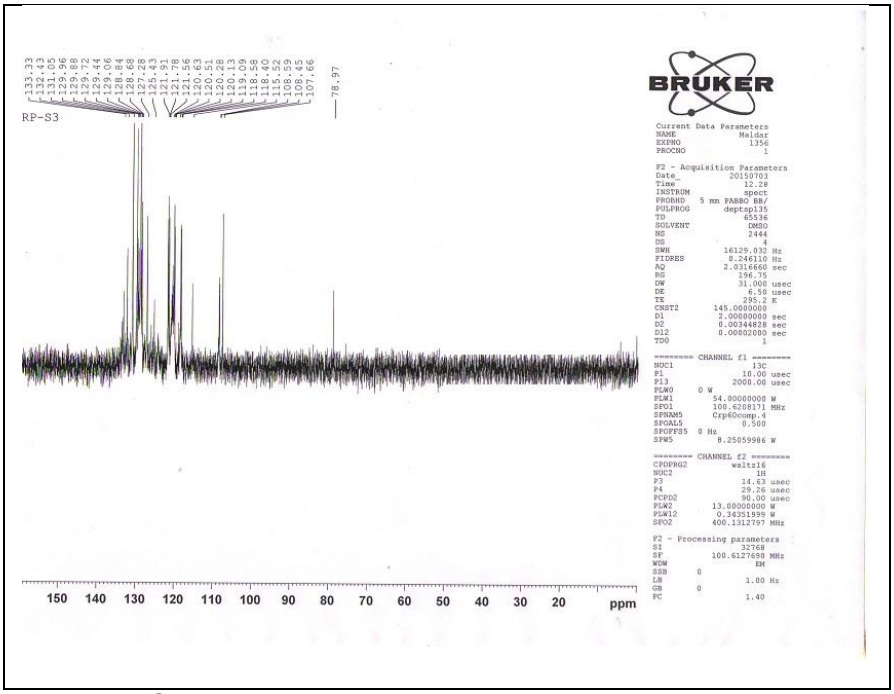


Fig.11:- ^{13}CNMR of compound (II) and IPA

TGA and DSC analysis of thiazole diamine and aromatic diacids

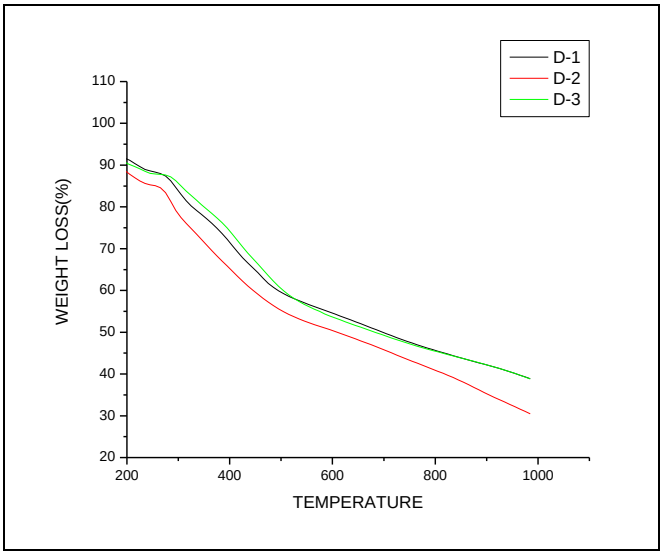


Fig.12 TGA of polyamide

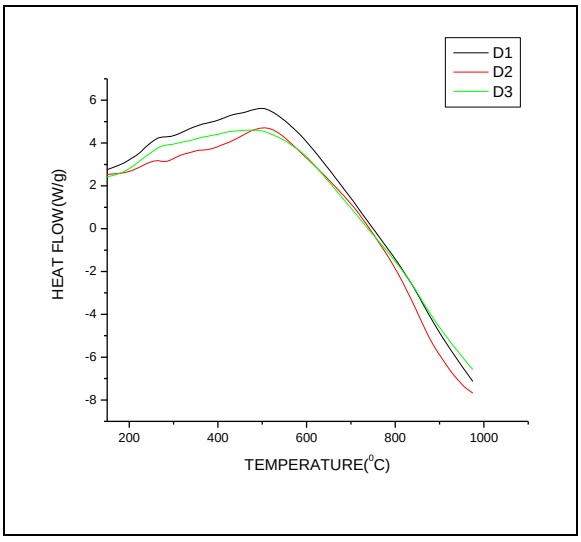


Fig.13 DSC of polyamide

Table-1-synthesis and properties of polyamides from thiazole diamine and aromatic diacid

[a] *n*inh was measured with 0.5%(w/v) solution of polyamide at 30±0.1^{0}c in DMAc.

Polymer	Diamine	Diacid	Yield (%)	n_{inh} (dL/g)[a]	T_i (^{0}C)[b]	T_{10} (^{0}c)[c]	T_{30} (^{o}C)[d]	Residue at 900 ^{0}C (%)[e]	T_g (^{o}c)[f]
PA-1	TZD	IPA	80	*O.33*	140	340	620	38.76	210
PA-2	TZD	TPA	85	*0.43*	121	270	560	30.37	225
PA-3	TZD	DCDPS	80	*0.56*	135	350	610	38.77	207

[b] Initial decomposition temperature.

[c] Temperature at which 10% weight loss is observed.

[d] Temperature at which 30% weight loss is observed

[e] % of char yield

[f]Glass transition temperature measured on DSC at a heating rate of 10ºC /min under N_2

From thermogravimetric analysis the 10% weight loss in the range of 270-350ºC in nitrogen and 30% weight loss in the range of 550-620ºC.Char yield at 900ºC is about 40% shows good thermal stability. From DSC the exothermic peak the glass transition temperature is about 210ºC.

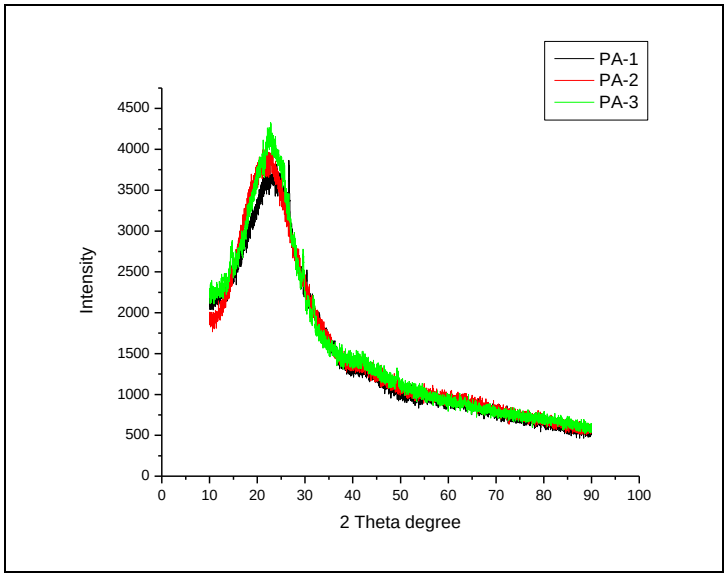


Fig 14 XRD of Polyamide

From XRD analysis the polyamides were semicrystalline in nature

Table-2 :-Solubility of Thiazole polyamide

Polymer	SOLVENT										
	DMAc	DMSO	DMF	NMP	PYRIDINE	cresol	Nitrobenzene	DCM	CHCl3	ethanol	Acetone
PA-1	++	++	++	++	++	+-	+-	--	--	--	--
PA-2	++	++	++	++	++	+-	+-	--	--	--	--
PA-3	++	++	++	++	++	+-	+-	--	--	--	--
PA-4	++	++	++	++	++	+-	+-	--	--	--	--
PA-5	+-	+-	+-	++	+-	+-	+-	--	--	--	--
PA-6	++	++	++	++	++	+-	+-	--	--	--	--
PA-7	++	++	++	++	++	+-	+-	--	--	--	--
PA-8	+-	+-	+-	++	++	+-	+-	--	--	--	--
PA-9	+-	+-	+-	++	++	+-	+-	--	--	--	--

[a] ++ soluble at room temperature +- soluble on heating; -- insoluble

PA-1 = TZD +IPA PA-2=TZD+TPA

PA-3= TZD+ DCDPS PA-4=ODA+IPA

PA-5=ODA+TPA PA-6=ODA +DCDPS

PA-7=TZD +ODA(75:25) PA-8=TZD +ODA(50:50) PA-9=TZD+ODA(25:75)

Table-3:- Synthesis of polyamides using aromatic diamines and dicarboxylic aciid

Sr. No.	Polymer code	Diacid	Diamine	Yield (%)	η_{inh} Viscosity dL/g
1	PA-1	IPA	TZ	80	*O.33*
2	PA-2	TPA	TZ	85	*0.43*
3	PA-3	DCDPS	TZ	80	*0.56*
4	PA-4	IPA	ODA	75	0.31
5	PA-5	TPA	ODA	85	0.28
6	PA-6	DCDPS	ODA	80	0.34
7	PA-7	IPA	(TZ+ODA)	75	0.36
8	PA-8	IPA	(TZ+ODA)	70	0.41
9	PA-9	IPA	(TZ+ODA)	80	0.28

Conclusions

Solubility of polyamides synthesized by using various aromatic dicarboxylic acids and Thiazole diamine were soluble in polar aprotic solvent such as DMAc, DMF, DMSO, Pyridine, NMP. While the PA-5 shows less solubility which was synthesized from ODA and TPA. The yield of synthesized polymers were quantitative 70-85% showed the built of moderate molecular weight polymer. The inherent viscosity range between 0.2-0.6 dL/g.

XRD data showed that all polymers were semicrystaline in nature.

Acknowledgements:
We sincerely thank the authorities of D.B.F Dayanand College of Arts and Science, Solapur for providing us all the necessary facilities and extend our gratitude to Prof (Dr) N.N.Maldar, Vice Chancellor, Solapur University, Solapur for extending valuable cooperation and guidance to complete the aforesaid research work.

References:-

1) R.Kant.K.Singhal,S.K.Shukla,K.chandrashekhar,A.K.Saxena,A.Ranjan,P.Raj,*J.Phosphorous, sulphur,silicon.*183,2029,2008.
2) Cassidy P. E, Thermally stable polymers. Marce Dekker, New York ,1980.
3) Yang H. H,Aromatic high-strength fibers. Wiley, New York ,1989.
4) Negi Y. S.,-ASuzuki Y-I., Kawamura I., Kakimoto MA., Imai Y, *Journal of Polymer Science Part A: Polymer Chemistry,* 34,1663 ,1996.
5) Ubale, V. P., Sagar, A. D., Maldar, N. N., & Birajdar, M. V. *Journal of applied polymer science*, ***79***,566. (3),2001.
6) *Li et al. – eXPRESS Polymer Letters,* Vol.3, No.11, 703, 2009.
7) Wu S-C., Shu C-F, *Journal of Polymer Science Part A: Polymer Chemistry,* 41, 1160–1166, 2003.
8) Mehdipour-Ataei S., Heidari H,*J Macromolecular Symposia*, 193, 159–168,2003.
9) Cheng L., Jian X. G., Mao S. Z, *Journal of Polymer SciencePart A: Polymer Chemistry*, 40, 3489–3496, 2002.
10) Yang C. P., Su Y. Y, *J Polymer,* 44, 6311–6322, 2003.
11) Sciannamea V., Catala J-M., Jérome R., Detrembleur C, *Journal of Polymer Science Part A: Polymer Chemistry*, 45,1219–1235, 2007.
12) Kim H-S., Kim Y-H., Ahn S-H., Kwon S-K, *J Macromolecules*, 36, 2327–2332 ,2003.
13) Espeso J. F., de la Campa J. G., Lozano A. E., de Abajo J, *Journal of PolymerScience Part A: Polymer Chemistry,* 38, 1014–1023, 2000.
14) .Espeso J. F., Ferrero E., de la Campa J. G., Lozano A.E., de Abajo J, *Journal of Polymer Science Part A: Polymer Chemistry*, 39,475–485, 2001.
15) Yang C-P., Chen R-S., Yu C-W, *Journal of Applied Polymer Science*, 82, 2750–2759, 2001.
16) Takashi K., Atsushi S., Shoji T. Japanese Patent 2000-297067,Japan ,2000.
17) Myung B. Y., Kim J. J., Yoon T. H, *Journal of Polymer Science Part A: Polymer Chemistry*, 40, 4217–4227, 2002.

18) Myung B. Y., Kim J. S., Kim J. J., Yoon T. H, *Journal of Polymer Science Part A: Polymer Chemistry,* 41, 3361, 2003.
19) Li et al., *eXPRESS Polymer Letters,* Vol.3, No.11 703, 2009.
20) Banerjee S., Madhra M. K., Salunke A. K., Jaiswal D. K, *Polymer*, 44, 613, 2003.
21) Wang C-Y., Li P-H., Li G., Jiang J-M Colloid and Polymer Science, 287, 495,2009.
22) Liaw D-J., Chen W-H., Hu C-K., Lee K-R., Lai J-Y, *Polymer*, 48, 6571, 2007.
23) Hsiao S-H., Yang C-P., Tsai C-Y., Liou G-S, *European Polymer Journal*, 40, 1081, 2004.
24) Sheng S-R., Pei X-L., Huang Z-Z., Liu X-L., Song CS, *European Polymer Journal*, 45, 230, 2009.
25) Qiu Z., Wang J., Zhang Q., Zhang S., Ding M., GaoL, *Polymer*, 47, 8444, 2006.
26) Liu B. J., Hu W., Chen C. H., Jiang Z. H., Zhang W.J., Wu Z. G., Matsumoto T, *Polymer*, 45, 3241, 2004.
27) Yang C-P., Chen Y-P., Woo E. M, *Polymer*, 45, 5279, 2004.
28) Barikani M., *Polym. J.* 11, 215, 2002.
29) Rozhanskii I., Okuyama K., and Goto K., *Polymer*, 41, 7057, 2000.
30) Der-Jang L., Been-Yang L., and Chia-Wei Y, *Polymer*, 42, 5175-5179, 2001.

MACRO-537

Synthesis and Gas sensing studies of polyazomethines polymers

Y. S. Patil[a], *V.B. Patil*[b], *P.H. Salunkhe*[a], *V .P. Ubale*[c], *N. N. Maldar*[a] *and A. A. Ghanwat*[a*]

[a.] *School of Chemical Sciences, Solapur University, Solapur, Maharashtra, India.*

[b.] *School of Physical Sciences, Solapur University, Solapur, Maharashtra, India.*

[c.] *DBF Dayanand College of Arts and Science, Solapur, Maharashtra, India.*

E-mail:*anil_ghanwat@yahoo.com*

Abstract

The new series of polyazomethines were synthesized by the polycondensation of a new diamine monomer 2, 5-Bis (4-(2-aminothiazole) phenyl)-3, 4-diphenyl thiophene, with equimolar proportion of aromatic dialdehydes. Inherent viscosities of these polymers were in the range 0.14 to 0.27 dL/g. These polymers were soluble in formic acid and sulphuric acid. Thin films of semiconducting polyazomethines were prepared on glass substrates using spin coating technique. Physical properties of polyazomethines films were characterized and analyzed by XRD, SEM and TEM techniques, FTIR, UV–Vis and electrical resistivity measurement techniques. SEM and TEM analysis showed presence of nanostructured particles having size in the range of 5 to 10 nm. Room temperature gas sensing performance of the polyazomethines films have been studied for various oxidizing (NO_2) as well as reducing (H_2S) gases. It was observed that, the polyazomethines films were highly selective towards NO_2 gas at room temperature with high sensitivity and good

selectivity. These results have been gained on polyazomethines thin films which contain five member active nucleuses of thaizole rings.

Keywords: *Polyazomethines thin film, FTIR, SEM, NO_2 sensor*

Introduction

The improvement of well organized devices for detection of toxic gases present in the environment is an important demanding in the field of gas sensor development. Therefore, the current research in the field of gas sensor devices has been focused on the development of sensors for the detection of flammable, hazardous and toxic gases, which have the characteristics of immense sensitivity, superior selectivity, active response and low cost. Nitrogen dioxide (NO_2) is one of the highly toxic and maximal harmful gases exude from combustion of the exhaust of home heaters, furnaces, plants and automobile engines [1]. It is a chemical suffocate, which involve in human's nervous system and could cause people to lose sensibility at a very low concentration. The threshold limit value of NO_2 gas is 25 ppm. Therefore, it is necessary to have sensors which can detect NO_2 gas at a small concentration (10-100) is very crucial to protect human lives [2, 3]. The recent improvements in the field of conducting polymers promise future progress in certain areas of latest technology such as gas sensors, biosensors, microelectronics, chemical and biochemical engineering, as well as adequate and inexpensive solar cells, due to their significant electrical and mechanical properties such as adjustability and easy processability, low cost, low operating temperature and so on [4–8]. In recent decades, conducting polymers such as polyaniline, polypyrrole, polyazomethines, polyacetylene, and polythiophene have been widely used as potent materials for the detection of hazardous, toxic and flammable gases, due to their ease of synthesis and low cost [9]. The very important advantage of these conducting polymer sensors is their room temperature operation and high sensitivity [10]. Among different conducting polymers, polyazomethines has a contour because it is easily synthesized by condensation of two bifunctional monomers and solution polycondensation; it has comparatively good chemical stability against atmospheric conditions, having moderate electrical conductivity [4, 11]. Many approaches for fabricating films of polyazomethines have been proposed. Some of them include vapor deposition polymerization [12], deposition of Langmuir–Blodgett film [13], UV-photo polymerization [14], electrochemical deposition [15] and chemical deposition by dip coating [16]. Polyazomethines has been reported interesting nitrogen dioxide (NO_2) and (H_2S) gas sensing properties operating at room temperature [17]. It is notable that the toxic limit of nitrogen dioxide is 25 ppm in air and therefore it is necessary that the sensors should be constructing in such a way that they sense the gas concentrations well below this limit. Therefore, we made an attempt to develop a usable NO_2 sensor based on polyazomethines thin film, which detect lower concentrations of NO_2 gas. Polyazomethines have been successively prepared using solution polycondensation polymerization technique. Films of polyazomethines were fabricated by spin coating technique on a glass substrate and characterized by using FTIR, SEM, UV–Vis and TEM techniques respectively, as well as their gas sensing performance was studied for various reducing

(NH_3, H_2S) and oxidizing (NO_2,Cl_2) gases at room temperature. The other gas sensing properties, such as selectivity, stability, response and recovery times and reproducibility were also investigated and explored. We report our findings in this paper and developed a usable NO_2 sensor based on polyazomethines thin film.

Measurements

The chemical structure of Monomer, Polymers and Thin films was analyzed by IR spectra were recorded on a Thermo Nicolet iS-10 Mid Fourier transform infrared (FTIR) spectrometer in the 500–4000 cm^{-1} frequency range.^{1}H NMR (400MHz) spectra were obtained with a Bruker spectrometer. Chemical shifts (d values) are given as parts per million with tetramethylsilane (TMS) as an internal standard. Ultraviolet–visible (UV–Vis) spectra were recorded on a Beckman DU-640 spectrometer. XRD was recorded on X-ray Diffraction System Ultima IV with ULTIMA IV Goniometer. The surface microstructure of the thin film was investigated using scanning electron microscopy (SEM Model: JEOL 6360).Viscosity measurements were made with 0.5% (W/V) solution of polymers at 30^0C using Ubbelohde suspended level viscometer. The solubility of polymers was determined at 3% (w/v) concentration in various solvents at room temperature or by warming, if needed. Gas sensing measurements were performed by using custom fabricated room temperature gas sensing measurement unit. In order to measure the gas response, the resistance of the films was measured in air ambient and in gas atmosphere. For resistance measurement, two silver electrodes separated by 1 cm were deposited on film using silver paint and dried at room temperature. The sensor films were mounted in an air tight stainless steel chamber having volume of 250 cm^3. The change in resistance of the sensor films was measured using a Keithley 6514 System Electrometer, which was controlled by a computer. Required concentration of a various reducing (H_2S, NH_3, CH_3OH, and C_2H_5OH) and oxidizing (NO_2, Cl_2) gases in the chamber was attained by introducing a measured quantity of desired gas using a syringe. All the gas sensitivity measurements were carried out at room temperature. Once a steady state was achieved, recovery of sensors was recorded by exposing the sensors to air, which is achieved by opening the lid of the chamber.

The sensitivity (S) of the sensors was calculated from the response curves using the relation:

$$S\ (\%) = |Ra - Rg|Ra * 100$$

Where, ‘Ra’= resistance of the sensor in clear air and ‘Rg’= resistance of the sensor in testing gas.

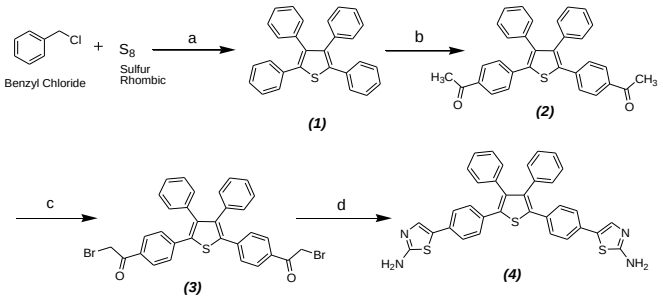
Experimental

2.1 Materials

All materials and solvents were purchased either from Sigma Aldrich or s d fine, through a local agency. Sulphur powder, thiourea, iodine (I_2), aluminium chloride ($AlCl_3$) acetyl chloride, Br_2 Solution, isophthalaldehyde (IPA), terephthalaldehyde (TPA). Solvents Such as THF, DCM, methanol, ethanol, glacial acetic acid were used as received. N,N'-dimethyl foramide (DMF) and N,N'-dimethyl acetamide (DMAc) were purified by distillation over P_2O_5 under reduced pressure and stored over $4A^0$ molecular sieves. terahydrofuran (THF) and Dichlomethane (DCM) were dried by sodium and calcium hydride respectively before use. LiCl was dried at 180^0C in vacuum oven for 14hrs.

2.2 Synthesis of the Monomer and Polymers

The synthesis route for the monomer and polymers are illustrated in Scheme1 and scheme2. Detail on the preparation and characterization of monomers and polymers are given below.



Scheme1. ***2, 5-Bis (4-(2-Aminothiazole) phenyl)-3, 4-diphenyl Thiophene (4)***

Reagents and conditions:

a)reflux, 240^0C, 3 days: b) CH_3COCl, $AlCl_3$, DCM 10-15^0C: c) Br2, AcOH, 80^0C, 2 h: d) I_2, Thiourea,THF, reflux, 24h.

2.2.1 Synthesis of Monomer

2, 5-Bis (4-(2-Aminothiazole) phenyl)-3, 4-diphenyl Thiophene **(4)** was synthesized in four steps.

2.2.1.a) 2, 3, 4, 5-Tetraphenylthiophene (TPTP) (1)

Compound **(1)** was prepared according to a literature procedure [18]. TPTP (1) was recrystallized from a dichloromethane–methanol system to produce white needles (yield: 51%; mp: 184–186°C).

2.2.1.b) 2, 5-Bis (4-acetyl phenyl)-3, 4-diphenyl Thiophene (TPTPDAc) (2)

TPTP (1) (3.5 g, 9.01 mmol), anhydrous DCM (50mL), and $AlCl_3$ (2.5 g, 18.75 mmol) were added to a three-neck flask under nitrogen atmosphere. The whole mixtures were then cooled to 0 ^{0}C by ice-water bath. Acetyl chloride (1.47 g, 18.75 mmol) was then added drop wise to the stirred reaction mixture at 0^{0}C. The reaction was allowed to warm to room temperature and continued for overnight. The resulting mixture was poured into ice water (300 mL), and the organic layer was collected, evaporated to give crude product (2). Recrystallized from toluene to get pure (2) as pale yellow needles (yield: 70%, mp: 250–252°C).

2.2.1.c) 2, 5-Bis (4-(alpha-Bromo) acetyl phenyl)-3, 4-diphenyl Thiophene (3)

Suspend 4.72gm (10 mmol) of (2) in 200mL glacial acetic acid in a 500mL three neck flask, warm gently on a oil bath until a clear solution result. Then cool as far as possible without formation of crystal. To this solution add 3.199gm (1mL 20 mmol) of bromine; do not allow the temperature to rise above 80^{0}C during this addition. The brominated product separates from the solution when about three-quarters of the bromine has been added. After 2hrs, cool the flask in a bath of ice and salt, filter the product, and wash with a little cold glacial acetic acid followed by small volumes of water until all the acid has been removed. The yield of crude material, m.p. 224-226^{0}C is 6gm (83 %). Recrystallize from hot rectified spirit and add a little decolourising carbon to remove the colour: pure, colourless **(3)** 79%,m.p. 224-226^{0}C

2.2.1.d) 2, 5-Bis (4-(2-Aminothiazole) phenyl)-3, 4-diphenyl Thiophene (4)

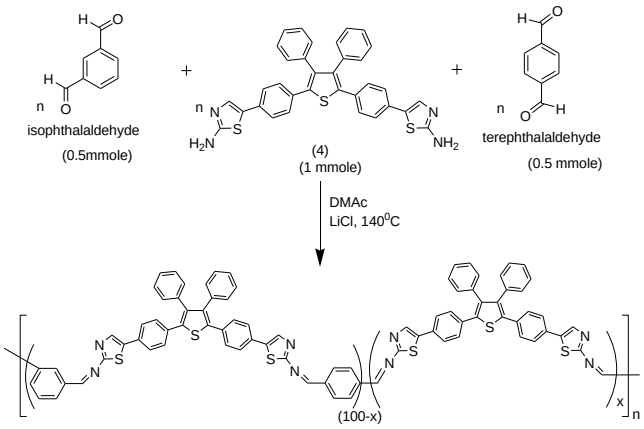
A mixture of **(3)** (5.6g, 8.88mmol)and thiourea (2.24g, 29.47mmol) in 70mL THF in single neck 100mL round bottom flask was refluxed, completion of the reaction was confirmed by TLC. After completion of reaction cool the flask, this clear solution reaction mass was poured onto cold sodium acetate solution and precipitated product was collected by filtration and recrystallized from ethyl acetate as yellowish crystals. M.p.236-238^{0}C and yield 75%.

2.2.2 Polymerization

By using the novel monomer 2, 5-Bis (4-(2-Aminothiazole) phenyl)-3, 4-diphenyl Thiophene **(4)** a series of five polyazomethines was prepared.

Synthesis of Co-polyazomethines (CP-PAM-01 to CP-PAM-05)

In a 100-mL three-neck round-bottom flask equipped with magnetic stirrer, reflux condenser, calcium chloride guard tube, and nitrogen gas inlet were placed 0.584 g (1 mmol)2, 5-Bis (4-(2-Aminothiazole) phenyl)-3, 4-diphenyl Thiophene**(4)** and dry N,N'-dimethyl acetamide (3mL) containing ***Scheme2.Synthesis of Polyazomethines (CP-PAM-01 to CP-PAM-05) from (4)***



0.150 g lithium chloride [5 wt % based on solvent N,N'-dimethyl acetamide (DMAc)]. The mixture was stirred well at room temperature to get clear solution, then [0.067 g (0.5mmol) Isophthalaldehyde (IPA) and 0.067 g (0.5mmol) terephthalaldehyde (TPA)] was added. The reaction mixture was stirred overnight at room temperature under nitrogen atmosphere. Finally the mixture was refluxed for 4hrs. at 140^{0}C. Then solution was cooled to room temperature and sufficient quantity of water was added so as to precipitate the polymer. The polymer was collected by filtration, washed with water, ethanol and dried under vacuum at 80^{0}C for 8hrs. The yield of polymer was 0.682gm (100%) and reduced viscosity of polymer was 0.14dL/g. All other polyazomethines, that is, CP-PAM-01 to CP-PAM-05, were prepared by similar procedure.

Table I Synthesis of Polyazomethines[a]

Polymer Code	Diamine	Dialdehyde		Yield (%)	Viscosity[b] $\eta_{sp/c}$ (dL/g)
	mol %				
	TD (4)	TPA (X)	IPA (100 -X)		
CP-PAM-01	100	100	00	99	0.27
CP-PAM-02	100	75	25	100	0.21
CP-PAM-03	100	50	50	100	0.14
CP-PAM-04	100	25	75	97	0.17
CP-PAM-05	100	00	100	93	0.27

[a]Polymerization was carried out with 1mmol each of diamine(4) and dialdehyde.

[b]Measured at a concentration of 0.5g/dL in Formic acid at 30°C.

3. RESULTS AND DISCUSSION

3.1 Analysis of Monomers

In the present investigation the synthesis of highly phenylated thiophene containing thaizoline diamine was performed. The monomer was characterized by IR, NMR and MASS. Thus, the novel 2, 5-Bis (4-(2-aminothiazole) phenyl)-3, 4-diphenyl Thiophene (4) was synthesized from benzyl chloride in four steps (Scheme 1). 2, 5-Bis (4-acetyl phenyl)-3, 4-diphenylthiophene (2) was synthesized as per procedure described in the literature [18].

a) FTIR analysis

The infrared spectrum of **(4)** showed absorption bands at 3400–3150 cm^{-1}(-NH_2 stretch) and the absence of a carbonyl (C=O) peak in dicating the presence of primary amine group.

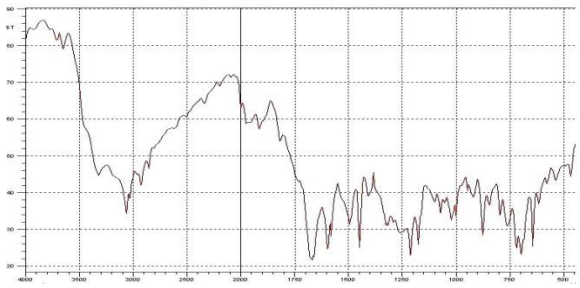


Fig. 3.1 (a) IR Spectrum of 2, 5-Bis (4-(2-Aminothiazole) phenyl)-3, 4-diphenyl Thiophene (4)

b) ^{1}H-NMR analysis

The proton NMR spectrum of **(4)** showed the NMR signal at 4.0 δ, corresponding to an amine (4H) group of the2-amino thaizole. It appeared as a singlet. The NMR signals in the range of 6.4–7.6δ (16H) are attributed to the aromatic protons of the tetraphenyl moiety.

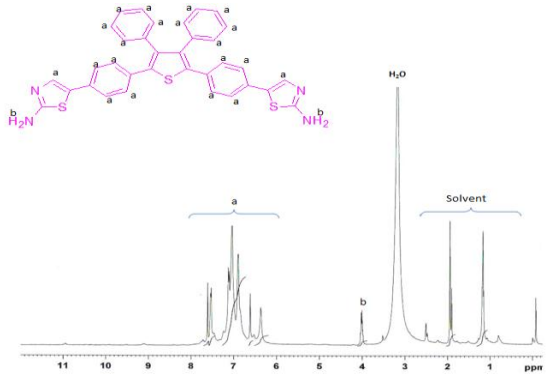


Fig. 3.1(b)* ^{1}H-NMR*Spectrum of 2, 5-Bis (4-(2-Aminothiazole) phenyl)-3, 4-diphenyl Thiophene (4)

c) *MASS Spectrum*

The mass spectrum of (4) was consistent with the proposed structure as the peak at m/e 584 corresponding to the molecular ion peak of 2, 5-Bis (4-(2-aminothiazole) phenyl)-3, 4-diphenyl thiophene **(4)** is clearly seen. The other fragmentation peaks at m/e 555,537 and 385 indicate the loss of 2-amino thiazole units.

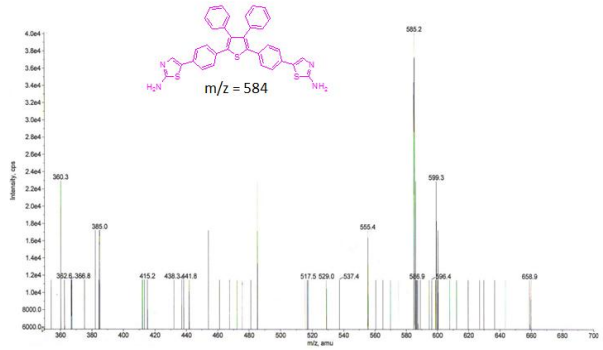


Fig. 3.1(c) MASS Spectrum of 2, 5-Bis (4-(2-Aminothiazole) phenyl)-3, 4-diphenyl Thiophene (4)

3.2 Analysis of Polymers

a) FTIR analysis

The polymers were also characterized by IR spectroscopy. The IR spectrum of CP-PAM-03 showed characteristic azomethine absorptions at 1598cm^{-1}(C=N-).The disappearance of bands at 1700 and3400-3150 cm^{-1} indicated that all the aldehyde and amine groups had reacted to yield high molecular weight polyazomethines.

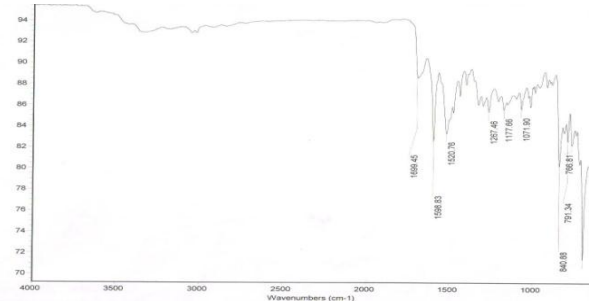


Figure 3.2 (a) IR Spectrum of CP-PAM-O3 polyazomethine from (4)

b) XRD Analysis

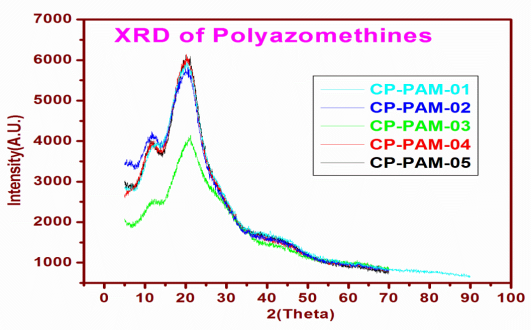


Figure 3.2 (b) X-ray diffraction of polyazomethines (CP-PAM-01 to CP-PAM-05)

X-ray diffraction (XRD) techniques have been used to check the crystallinity of the five CP-PAMs [Fig. 3.2(b)]. In good agreement with the reported literature, linear PAM is amorphous with broad diffractive peaks in the 2θ range of 5°–90°. [19] X-ray diffraction analysis of polyazomethines was conducted at room temperature to obtain information on both the mesophase structure and crystallinity of polyazomethines. The measurements exhibited several peaks in the range of 2θ= 15 – 25° as observed in Figure 3.2(b) and this indicated semi crystalline character possessed by polyazomethines.

c) Solubility and Viscosity

1. The reduced viscosities were in the range of 0.14–0.27 dL/g.

	CP-PAM-01	CP-PAM-02	CP-PAM-03	CP-PAM-04	CP-PAM-05
DMAc	+-	+-	+-	+-	+-
DMF	+-	+-	+-	+-	+-
NMP	+-	+-	+-	+-	+-
DMSO	+-	+-	+-	+-	+-
m-cresol	+-	+-	+-	+-	+-
Pyridine	+-	+-	+-	+-	+-
H_2SO_4	++	++	++	++	++
Formicacid	++	++	++	++	++
$CHCl_3$	--	--	--	--	--
DCM	--	--	--	--	--
THF	--	--	--	--	--

++ Soluble + soluble on heating +- partly soluble --Insoluble

3.2 (c) Table2. Solubility of (CP-PAM-01 to CP-PAM-05)

2. The solubility characteristics were determined in different common organic solvents. A 3% solution of polymer in solvent was taken as a criterion for solubility. The polyazomethines showed better solubility (Table2) in solvents such as formic acid and conc. H_2SO_4 but were partly soluble in DMAc, DMSO, NMP, DMF, pyridine, m-cresol, and insoluble in chlorinated solvents such as chloroform, DCM, and so forth. [20,21]

d) Electrical conductivity study

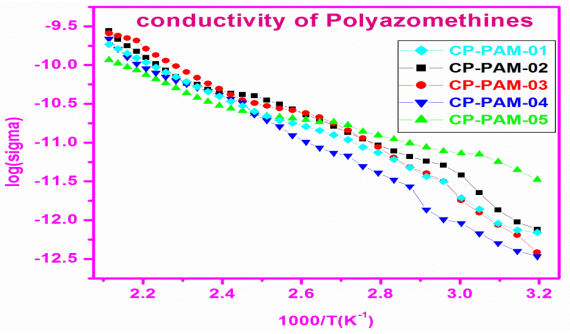


Figure 3.2 (d) Electrical Conductivity of polyazomethines (CP-PAM-01 to CP-PAM-05)

The temperature dependence of conductivity of polyazomethine films are shown in Fig. 3.2(d). The dc conductivity of polyazomethine has an activated character, including two regions with different slopes for the 1000/T dependence of log σ. The room temperature dc electrical conductivity of polyazomethine films was found to be 9.5 x 10^{-7} S/cm to 9.9 x 10^{-7} S/cm. The conductivity increases with increases of temperature which is the characteristic behavior of semiconductors. The temperature dependence of the conductivity σ (T) of disordered semiconducting materials is generally described by the Mott variable range hopping (VRH) model

$\sigma(T)=\sigma_o \exp[(T_0/T)^{\gamma}]$……..(1)

Where σ_o is the high temperature limit of conductivity and To is Mott's characteristic temperature associated with the degree of localization of the electronic wave function. The exponent γ= 1/ (1 + d) determines the dimensionality of the conducting medium. The possible values of γ are 1/4,1/3 and 1/2 for three, two and one-dimensional systems respectively. The plot of log σ against 1000/T indicates that three-dimensional (3D) charge transport occurs in all the samples. Polyazomethine films follow the three-dimensional VRH electrical conduction process. Fig.3.2 (d). shows the plot of conductivity vs. the equimolar portion of [isophthalaldehyde (IPA) and terephthalaldehyde (TPA)] in the polyazomethine films. The plot shows that the conductivity of polyazomethine films

increases remarkably after insertion of 1, 3 linkage means isophthalaldehyde (IPA) in the polyazomethine matrix. Polyazomethine films are of P-type semiconducting materials having large number of free charge carrier available for the purpose of conduction. [22]

e) UV–vis analysis

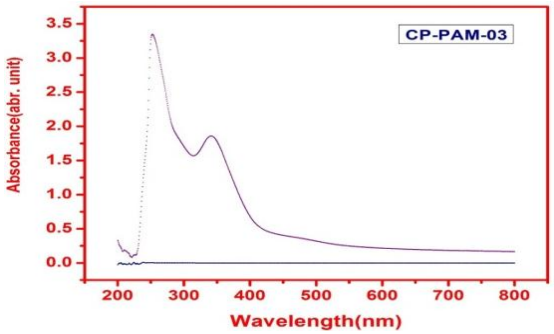


Figure 3.2 (e) UV-Vis spectrum of polyazomethines (CP-PAM-03)

Figure 3.2(e) shows the optical absorption spectra Polyazomethine nano films on quartz substrates. The high-energy absorption bands between 255 nm and 342 nm arise from to the π–π* transition of the conjugated backbone. Generally the optical band gap in semiconductor is determined by assuming the nature of transition (m) and plotting $(\alpha\ hv)^{1/m}$vshv where m represents the nature of transition. The exponent 1/m may have different values, such as ½, 2, 3/2, 3 for allowed direct, allowed indirect, forbidden direct and forbidden indirect transitions respectively. The optical absorption coefficient ‘‘α’’ near the absorption edge for direct interband transition is given by a

$$\alpha = B\ (hv - E_g)^{1/2}/hv \text{----------(2)}$$

Where B is the absorption constant for direct transition and Eg is the band gap. For allowed direct transition one can extrapolate the linear portion of to α = 0 value to obtain the corresponding band gap [17]. The presence of –C=N (azo linkage) in the polyazomethines matrix was confirmed using UV–vis spectra. The UV-Vis spectra Fig. 3.2(e). shows blue shifting of the corresponding peaks from 342 nm for –C=N (azo linkage) π–π* 255 nm for –C=C-(olefine linkage) n–π* which suggest that the polymerization showing highly conjugated in the chain of Polyazomethines. This change is attributable to the interaction in the Polyazomethines films, which increases the degree of orbital overlap between the p electrons of the heteroaromatic rings with the lone pair of the nitrogen atom in the polyazomethines.

f) Scanning electron microscopy (SEM) analysis

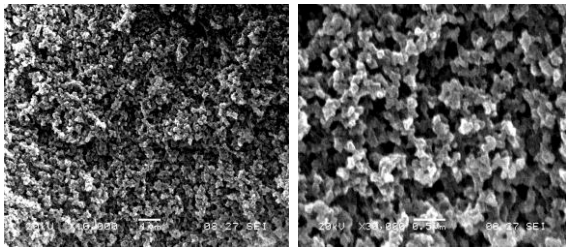


Figure 3.2 (f) SEM of polyazomethine(CP-PAM-03)

Figure 3.2 (f) Shows the scanning electron micrograph of CP-PAM-03 film. The micrograph shows the spherical granular morphology with high porosity. Such a porous granular morphology could give a fine pathway for electron transfer in the gas sensing process and is expected to be advantageous for gas sensing application due to availability of diffusion channel inside the polymeric network. On the other hand, porous and loose structure surface morphology provides higher surface area to volume ratio and which enormously contributes to the gas diffusion process, results in the improvement of the gas sensing properties. This is due to the fact that the gas diffusion occurs more easily in porous structure and hence increases the reaction between gas molecules and the film.

g) Compositional analysis

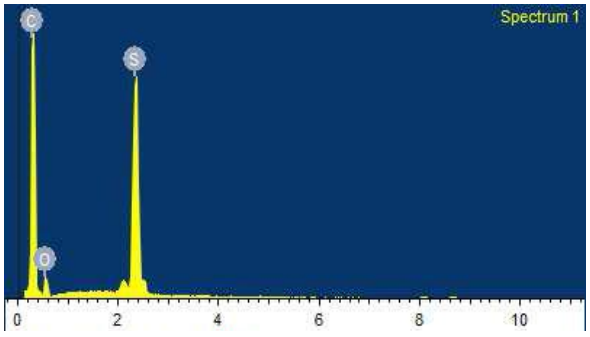


Figure 3.2 (g) EDAX of polyazomethine(CP-PAM-03)

Fig. 3.2 (g) shows EDAX spectra of polyazomethine thin film. The EDAX analysis revealed the presence of sulfur, carbon and oxygen and other elements from the glass substrates. That there were only sulfur, carbon and oxygen elements in the organic samples [(Fig. 3.2 (g)], it indicated that high purified copolyazomethines have been prepared by using solution polycondensatoin technique.

h) Transmission electron microscopy (TEM) analysis

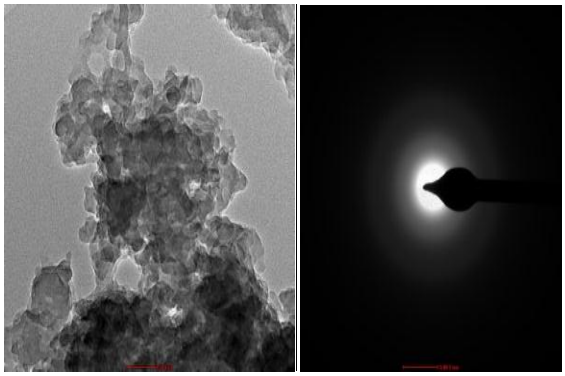


Figure 3.2 (h) TEM of polyazomethine (CP-PAM-03)

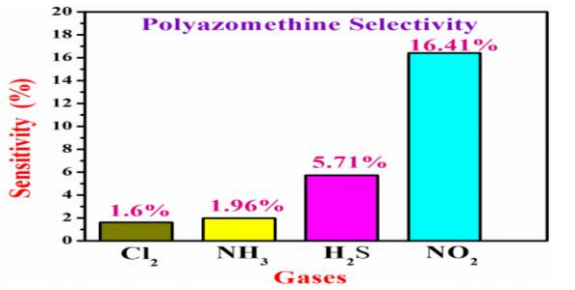
Figure 3.2 (h) shows transmission electron microscopy (TEM) image of polyazomethines(CP-PAM-03).The TEM image shows that polyazomethines matrix were uniformly elongated and formed loose aggregates. The micrographs indicate that average particle size of the polyazomethines (CP-PAM-03) was in the 45-50 nm range. It can be concluded from TEM images that nucleation of polyazomethines matrix.

Gas sensing properties

a) Selectivity of Polyazomethines sensor

An important parameter of gas sensors is selectivity. The ability of a sensor to respond to a certain gas in presence of other gases is known as selectivity and the selectivity coefficient (Q) of 'target gas' to another gas is estimated using the relation, Q= (SA/SB). Where, SA is the response of film to the target gas 'A' and SB is the response of film to the other gas B. Theoretically, the sensors should have high response to some gases but on the other hand there is little or no response to other gases in the same surroundings. Therefore, in order to study the selective behavior of the Polyazomethines sensor, gas sensing measurements were carried out for various reducing (NH_3, H_2S, CH_3OH, C_2H_5OH) and oxidizing (NO_2, Cl_2) gases, each with a fixed concentration of 100 ppm. All the gas sensing measurements were carried out at room temperature and the corresponding results are shown in [Fig. 3.3a)]. The histogram shows, the polyazomethines sensor exhibit higher response to NO_2 gas (16.41 %), whereas it shows a considerably lower response towards NH_3, H_2S, and Cl_2. The larger value of selectivity coefficient for a specific gas denotes the sensor has a better competency to differentiate the target gas (NO_2 herein) from the mixture gases. Therefore, we could find that polyazomethines sensor had a good sensing performance to NO_2 gas. This may be due to the different gases have different energies for reaction to occur on

the surface of sensor film. The plausible mechanism of selectivity for NO_2 gas may be traced to the characteristics of vapor adsorbed over the surface of Polyazomethines.A high response for NO_2 indicates that the polyazomethines films are selective for this gas. The higher response towards NO_2 than NH_3, H_2S, and Cl_2 can be explained on the basis of different interactions between sensing film and adsorbed gas. Polyazomethines film is a p-type material and when it interacts with reducing gas like NH_3 and H_2S, there is reduction in charge carrier density. Since the majority carriers (holes) density gets decreased due to electron donating nature of these gas. This results in decreasing the conductivity of material and film resistance increases. In case of oxidizing gas like NO_2 and Cl_2 there is an increase in charge carrier concentration, since NO_2 and Cl_2 gas is electron accepting in nature. Hence it increases the conductivity of the material. The interaction of NH_3, H_2S, and Cl_2 with polyazomethines film is very less as compared to NO_2, hence it shows very less and sluggish response Therefore, further dependence of NO_2 response for polyazomethines sensor is studied for various concentration of NO_2 gas operating at room temperature.



Selectivity Response of Gases at different ppm Level

Sr. No.	Operating Temperature (°C)	Name of Oxidizing/ Reducing Gases	Volume of Gas (ppm)	Response (%)
1.	25°C	NO_2	100ppm	16.41%
			50ppm	15.44%
			25ppm	9.06%
			05ppm	4.8%
			01ppm	0.7%
2.	25°C	H_2S	100ppm	5.71%
3.	25°C	NH_3	100ppm	1.92%
4.	25°C	Cl_2	100ppm	1.6%

Fig.3.3.a) Selectivity Polyazomethines sensor for 100 ppm of various gases operating at room temperature

b) Sensitivity of polyazomethines sensor to NO_2 gas

The dependence of the gas response of the polyazomethines sensor to the NO_2 gas concentration operating at room temperature is shown in [Fig. 3.3b)]. The sensitivity of polyazomethines sensor

to NO_2 gas concentration (1, 5, 25, 50 and 100 ppm) operating at room temperature was found to 1.6%, 1.96%, 9.06%, 15.44%, and 16.41% respectively. It was found that, polyazomethines sensor had the highest response of 16.41% towards 100 ppm of NO_2 gas. This behaviour was related to the adsorption of NO_2 gas molecules on the surface of the polyazomethines film. As the concentration of NO_2 gas increased then increases active sites for adsorption, causing the increase in response. On the other hand, the enhanced gas sensing performance of the polyazomethines sensor is due to porous microstructure of the material which offers more chemical reactions to occur at the interface and ultimately results into increased gas response. It was conclude that, the polyazomethines sensor able to detect at 100 ppm of NO_2 gas with the good response (16.41%) and the linearity of the gas response in the low NO_2 gas concentration range (10–100 ppm) suggests that, the polyazomethines sensor can be reliably used to monitor the concentration of NO_2 gas over this range.

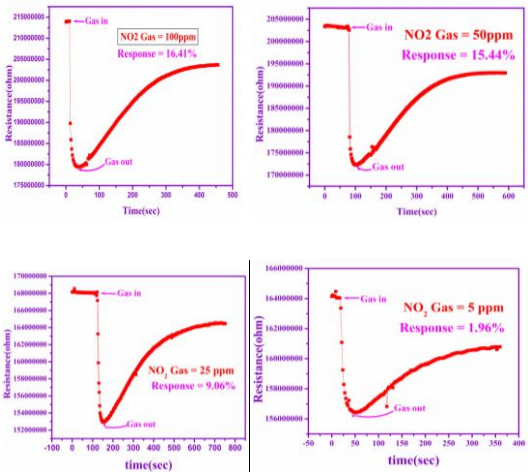
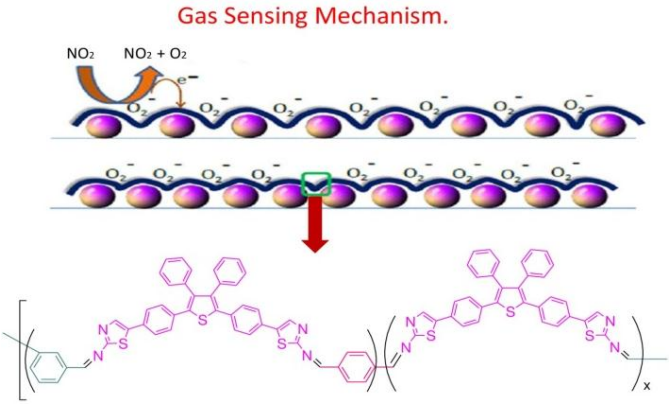


Fig.3.3.b.) Electrical response of Polyazomethines sensor towards various concentration of NO_2 gas

c) Sensing mechanism of polyazomethine sensor

The change in the resistance of the sensing element (polyazomethines film) as a function of time was recorded at room temperature and displayed in [Fig. 3.3c)]. It was found that, to exposure the oxidizing NO_2 gas molecules with polyazomethines film produced the sudden decrease in the value of resistance. The original resistance value achieved when the NO_2 gas had been turned off and fresh air is introduced into the test chamber. The observed change in the resistance of sensor with NO_2 gas molecules is due to the adsorption of gas on the surface of polyazomethines film as well as the response for a particular gas or vapour is mainly related to adsorption kinetics of gas

on active sensing layer. polyazomethines is a p-type material in which majority charge carriers are holes. On the other hand, NO_2 is an oxidizing gas (electron accepter) and when it interacts with the p-type polyazomethines then it capture electrons from the polymer matrix resulting in the decrease of the resistance. Since the majority carriers (holes) density gets increased due to electron accepting nature of NO_2 gas. This results in increasing the conductivity of material and film resistance decreases.



Conclusions

The new series of polyazomethines were synthesised by the polycondensation of a new diamine monomer 2, 5-Bis (4-(2-aminothiazole) phenyl)-3, 4-diphenyl thiophene, with equimolar proportion of aromatic dialdehydes. Inherent viscosities of these polymers were in the range 0.14 to 0.27 dL/g. These polymers showed soluble in formic acid and sulphuric acid. The room temperature dc electrical conductivity of polyazomethine films was found to be 9.5 x 10^{-7} S/cm to 9.9 x 10^{-7} S/cm. The plot of polyazomethines conductivity contents the equimolar portion of [isophthalaldehyde (IPA) and terephthalaldehyde (TPA)] in the polyazomethine films. The plot shows that the conductivity of polyazomethine films increases remarkably after insertion of 1, 3 linkage means isophthalaldehyde (IPA) in the polyazomethine matrix. Polyazomethine films are of P-type semiconducting materials having large number of free charge carrier available for the purpose of conduction. The presence of –C=N (azo linkage) in the polyazomethines matrix was confirmed using UV–Vis spectra. The NO_2 gas sensor based on polyazomethine thin films was successfully fabricated by spin coating technique on a glass substrate. The structure and morphology of the polyazomethine thin films is confirmed by using FTIR, SEM, TEM and XRD techniques. These films were found to be highly sensitive and selective to the NO_2 gas operating at room temperature. Taking into account all the results of gas sensing experiments it is concluded

that, the polyazomethine sensor have good sensing properties such as selectivity towards NO_2 gas than other interfering gases, higher gas response 16.41%. These results indicate that, the polyazomethine is found to be very attractive NO_2 gas sensing material and has potential application in the field of gas sensors. These results have been gained on polyazomethines thin films with containing five member active nucleus thaizole rings.

Acknowledgements

Y.S. P. grateful to University Grants Commission (UGC) New Delhi, India for financial assistance in the form of Junior Research Fellowship (JRF).

References

1. Y. Shimizu, M. Egashira, *MRS Bull*. 18–24, 1999.
2. G. Martinelli, M.C. Carotta, M. Ferroni, Y. Sadaoka, E. Traversa, *Sens. and Actua*, B 55 99, 1999.
3. V.E. Bochenkov, G.B. Sergeev, Adv. Colloid Interface Sci. 116, 245–254, 2005.
4. H. Yan, L. Zhang, J. Shen, Z. Chen, G. Shi, B. Zhang, Nanotechnolg*y* 17 3446–3450, 2006.
5. K. Potje-Kamloth, Critical Rev. Anal. Chem.32, 2,121–140, 2002.
6. B. Adhikari, S. Majumdar, Prog. Polym. Sci. 29, 699–766, 2004.
7. M. Woodson, J. Liu, *J. Am. Chem. Soc.* 128,3760–3763, 2006.
8. J.H. Wu, Q.H. Li, L.Q. Fan, Z. Lan, P.J. Li, J.M. Lin, S.C. Hao, J. Power Sources 181, 172–176, 2008.
9. Q.H. Li,J.H.Wu, Q.W. Tang, Z. Lan, P.J. Li,J.M. Lin, L.Q. Fan, Electrochem.Commun. 10, 1299–1302, 2008.
10. D.S. Sutar, N. Padma, D.K. Aswal, S.K. Deshpande, S.K. Gupta, J.V. Yakhmi, Sens. Actua. B 128, 286–292, 2007.
11. H.K. Jun, Y.S. Hoh, B.S. Lee, S.T. Lee, J.O. Lim, D.D. Lee, J.S. Huh, Sens. Actuators. B 96,576–581, 2003.
12. E. Stussi, S. Cella, G. Serra, G.S. Venier, Mater. Sci. Eng. C 4 27, 1996.
13. M. Penza, E. Milella, M.B. Alba, A. Quirini, L. Vasanelli, Sens. Actuators B 40,205–209, 1997.
14. P.G. Su, L.N. Huang, Sens. Actua. B 123, 501, 2007.
15. Q. Fang, D.G. Chetwynd, J.A. Covington, C.S. Toh, J.W. Gardner, Sens. Actuat. B 84, 66–71, 2002.
16. J.H. Cho, J.B. Yu, J.S. Kim, S.O. Sohn, D.D. Lee, J.S. Huh, Sens. Actuat. B 108 389, 2005. 17. M. penza, E. Milella, V.I. Anisimkin, Sens. Actua. B 47, 218–224, 1998.
17. M.A. Chougule, Shashwati Sen, V.B. Patil, Sensors & Transducers Journal 139, 122–132, 2012.
18. Imai, Y.; Maldar, N. N.; Kakimoto, M. J Polym Sci Polym Chem 1985, 23, 1797.
19. J. Roncali, P. Leriche and A. Cravino, Adv. Mater., ,19, 2045, 2007.
20. Hsiao S. H., Liou G. S., Polymer Journal, 34, 917–924 2002.
21. Patra S.; Lenka S., Nayak P. L.: Journal of Applied Polymer Science, 32, 5071–5083 1986.

22. M.A. Chougule, S.G. Pawar, P.R. Godse, R.N. Mulik, S. Sen, V.B. Patil, Soft Nanoscience Letters 1, 6–10, 2011.

MACRO-545

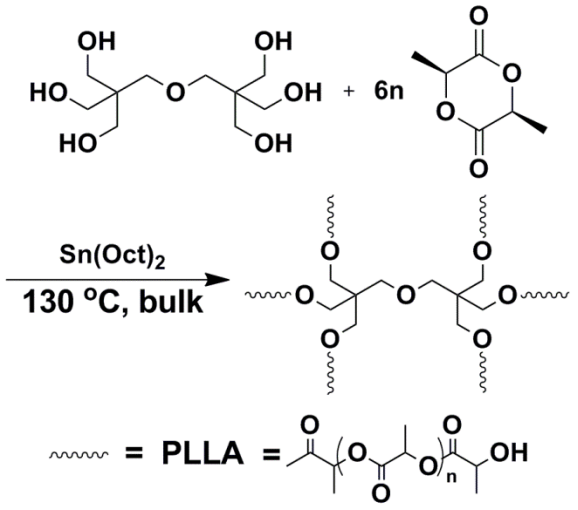
Synthesis and chemical characterization of high molar mass star-shape poly(L-lactides) (PLLA's).

Adam Michalski*[a], Grzegorz Łapienis[a]

[a] *Department of Polymer Chemistry, Centre of Molecular and Macromolecular Studies, Polish Academy of Sciences, Sienkiewicza 112, 90-363 Lodz, Poland*
Phone: +48-42-684-71-13,
**E-mail: michadam@cbmm.lodz.pl; michalski.a.k@gmail.com*

Abstract

In this communication the synthesis of high molar mass star-shaped PLLA's with 4 and 6 arms is presented. Di(trimethylolpropane) (4-OH groups) and dipentaerythritol (6-OH groups) were used as initiators and $Sn(Oct)_2$ was applied as a catalyst in the ring-opening polymerization (ROP) of L-lactide (L-LA) Scheme 1. The prepared star-shaped PLLA's and their linear analogs having similar molar masses were characterized by SEC, ^1H NMR, FT-IR, DSC, and TGA analysis. The analytical data of both types of polymers were compared.



Scheme 1 Scheme of six arms star PLLA synthesis.

Keywords: *poly(L-lactide); ring-opening polymerization, NMR; thermal stability*

Introduction

PLLA is a renewable, biodegradable, and compostable thermoplastic polymer with mechanical properties similar to polystyrene. It is one of the most promising candidates capable to replace petrochemical polymers, but it has inherent brittleness and low toughness which restrict the range of applications. Recently, it is observed an increased interest of star-shaped PLLA materials as they exhibit highly desirable rheological, mechanical and biomedical properties that are inaccessible in the case of linear polymers. These branched polyesters have higher concentration of functional end groups that additionally influenced their properties. (1)

Experimental

Tin(II) octoate (2-ethylhexanoate; $Sn(Oct)_2$) (Aldrich, 92,5%-100%) was purified by two consecutive high-vacuum distillations at 140°C/3×10^{-3} mbar. The purified $Sn(Oct)_2$, kept in vacuum glass ampoules, was finally directly distributed under vacuum into thin-walled vials or ampules equipped with break-seals and then sealed off and stored at −12°C. *n*-Butanol (Sigma-Aldrich, 99%) was purified by distillation with butyl phthalate and Na metal, stored on the vacuum line, finally was directly distributed into thin-walled ampules equipped with break-seals and then sealed off and stored at −12°C. Di(trimethylolpropane) (Aldrich, 97%) and dipentaerythritol (ACROS Organics, 90%) were dried few hours under high vacuum (10^{-3}mbar, 85°C) before use. L-lactide (Purac, 99%) was consecutively crystallized from dry 2-propanol and purified just before use by sublimation in vacuum (10^{-3} mbar, 85°C). Tetrahydrofuran (THF, POCH, 99%) was kept for several days over KOH pellets, filtered off, and refluxed over Na metal. Eventually, it was distilled, degassed, and stored in a closed glass ampule over a liquid Na/K alloy, and it developed a blue color. Methanol (pure, Chempur) was used as received.

The number–average molar masses M_n of polymers were determined by size exclusion chromatography (SEC) using an Agilent Pump 1100 Series (preceded by an Agilent G1379A Degaser), equipped with a set of two PLGel 5μ MIXED–C columns. Wyatt Optilab Rex differential refractometer and a DawnEOS (Wyatt Technology Corporation) laser photometer were used as detectors. Dichloromethane was used as eluent at a flow rate of 0.8 mL min^{-1} at room temperature.

^1H NMR spectra were recorded in $CDCl_3$ using a Bruker Avance III 500 spectrometer operating at 500 MHz. Traces of the nondeuterated chloroform were used as an internal standard.

DSC analysis was performed under nitrogen at a heating and cooling rate equal to 10°C min^{-1} on a DSC 2920 Modulated TA Instrument. Both temperatures and heat flow were calibrated with indium.

Star-shaped poly(L-lactides), having 4 and 6 arms, were synthesized by the coordination polymerization using tin octoate as a catalyst and di(trimethylolpropane) or dipentaerythritol as an initiators, according to the method previously described. (2)

Results and discussion

The molar masses of the obtained star-shaped PLLA's (determined by ^{1}H NMR and SEC) were close to those calculated from the $[M]_0/[I]_0$ ratio, and their dispersity was in the range of typically observed for the ROP of lactides. To confirm the structure of obtained star-shaped polymers, the radii of gyration for linear and star macromolecules were compared, according the following equation:

$$g = \frac{< R_g >_{br}^2}{< R_g >_{lin}^2}$$

where: g - branching index, R_g - radius of gyration for branch or linear polymers.
E.g. for our star-shaped polymers with 6 arms g = 0.56 was determined, that agrees with the literature data (g = 0.50 ÷ 0.60) for stars with statistical distribution length of arms and dispersity near 1.50. (3) The observed linear constant function for relation between g factor and M_n, denotes that obtained PLLA's have star-shaped structures in the whole interval of molar masses.
In our project we will compare the mechanical, thermal and rheological properties of star-shaped PLLA's with their linear analogs with similar molar masses. Therefore, the analyzed samples of polymers should have a high thermal stability and do not contain any labile impurities (e.g. residue of monomer). The presence of unreacted L-LA could be degrade to lactic acid at processing temperature, that causes further degradation of PLLA's.

Thus, the resulting raw polymers were purified by precipitation into cold methanol from methylene chloride solution, filtration and finally drying. The content of the residual amount of L-LA in the polymer was determined on the bases on the analysis of ^{1}H NMR spectra. (4) The methine proton of main chain of PLLA has chemical shift δ = 5.16 ppm different from methine proton of LA (δ = 5.04 ppm). Therefore, the amount of lactide present in polymer was possible to estimate by comparison of the respective intensities of signals. In raw polymerization product the content of unreacted L-LA was below 0.50%. After purification the content of L-LA decreased below of the sensitivity of using NMR equipment. During purification (precipitation) the catalyst (tin octanoate) was also removed. It is well-known that the presence of many hydroxyl end-groups, as it is in the case of star-polymers, can accelerate the thermal degradation of PLLA.
Therefore, to all commercial PLLA were added respective stabilizers in a small amount not exceed 0.50%.
Our raw polymers and/or after purification without stabilization degrade at high temperature ~200°C with lowering their molar masses. After adding thermal stabilizer (0.2% irganox 1010) and catalyst deactivator (0.2% irganox 1024) polymers with high thermal stability were obtained (cf. Figure 1).
No considerable lowering of molar masses were observed even after keeping polymer 1 h at 200°C, that is much longer time than applied in normal manufacturing.

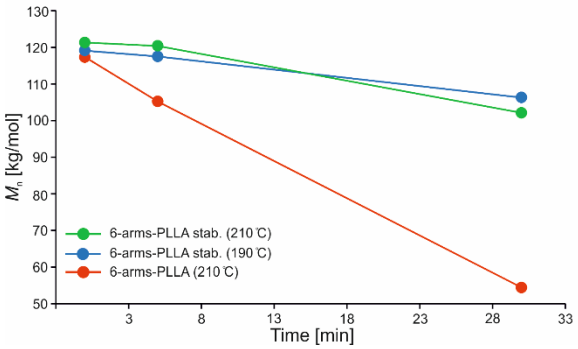


Figure 1 Thermal stability of 6-armed star-shaped PLLA before and after stabilization

DSC analysis disclosed that 6-arms star-shaped PLLA's have slightly lower melting temperatures (T_m) than their linear analogs with this same molar masses (cf. Figure 2).

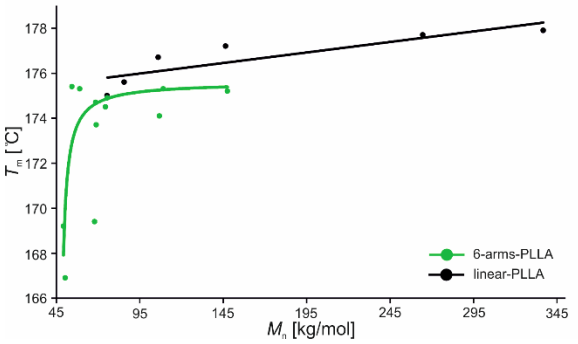


Figure 2 Melting temperatures (T_m) of 6-armed star-shaped PLLA's and their linear analogs.

Conclusions

1. The synthesis and characterization of 4- and 6-arms PLLA's with high molar masses from 8.0 × 10^4 up to 2.5 × 10^5 was described.

2. Star-shaped polymers with high thermal stability were obtained and their thermal properties were compared with linear analogs.

Acknowledgements

This research project has been supported by the National Science Centre, Poland, grant No UMO-2013/09/B/ST5/03619

References

1. **Auras, Rafael, et al.** *Poly(lactic acid) sythesis, structires, propeties, processin, and application.* s.l. : Wiley, 2010.
2. **Michalski, Adam, et al.** *Polymer.* 2016, Vol. 90, 242-248.
3. **Biela, Tadeusz, et al.** *Macromolecules Symposium.* 2006, Vol. 240, 47-55.

4. **Ksapabutr, Boua-In and Chaiyut.** *Rapid Communication.* 2010, Vol. 4, 1404-1407.

MACRO-546

Triblock poly(trimethylene carbonate) and polylactide copolyesters: synthesis, properties and stereocomplex formation

M. Socka*,[a] A. Duda,[a]

[a] *Department of Polymer Chemistry, Centre of Molecular and Macromolecular Studies, Polish Academy of Sciences, Sienkiewicza 112, 90-363 Lodz, Poland*
** e-mail id: msocka@cbmm.lodz.pl*

Abstract

The controlled synthesis and characterization of the series of the ABA and BAB copolymers comprising segments of the repeating units derived from lactides (L,L-LA or D,D-LA) and trimethylene carbonate (TMC) is reported. The copolymers were obtained by coupling of the dihydroxyl polyesters using diisocyanates as chain extenders [hexamethylene diisocyanate (HDI), dicyclohexylmethane and isophorone diisocyanate (IPDI)] in the presence of dibutyltin laurate (DBTL) as the catalyst. The homopolymers, namely PTMC and PLA diols, as well as corresponding monohydroxyl-terminated polyesters, were obtained via coordination polymerization catalysed with stannous 2-ethylhexanoate.
In order to improve the thermal properties of thus obtained materials, triblock copolymers of the opposite configuration of PLA blocks, have been used for preparation of the corresponding stereocomplexes.

Microstructure, morphology, and thermal properties of the prepared copolymers and their stereocomplexes have been investigated by ^{1}H NMR, SEC, SEM and DSC respectively.

Keywords: biodegradable copolyesters, block polymers, coupling with diisocyanates, stereocomplex, morphology and thermal properties.

Introduction

Block copolymers and terpolymers that comprise aliphatic polycarbonate segments became promising bioresorbable materials because through changing the block lengths and the composition one can easily modify mechanical properties, hydrophilic-hydrophobic balance, biodegradation rate and thermal sensitivity of the final materials. PTMC emerged as an interesting component for introducing modifications to rigid PLA. Materials that merge strength and

flexibility can be obtained by blending of PTMC and PLA homopolymers or by a copolymerization of the cyclic monomers. The synthetic route, most widely used for the preparation of biodegradable and biocompatible copolyesters, is based on the ring-opening polymerization (ROP) of corresponding monomers [1]. The ROP provides sufficient copolymerization control and results in polymers of the required molar masses (M_n), low dispersity (*Đ)*, microstructure, desired end-groups. However, this method requires appropriate conditions for the elimination of even traces of impurities [2]. More convenient method of aliphatic esters block copolymer synthesis is based on the coupling of the corresponding polyester (α,ω) diols. Thus, this synthetic route was applied for preparation of the polymers with defined molecular masses at the conditions of excluded transesterification.

The approach for improving the properties of PLA copolymers is stereocomplexes formation between enantiomeric chains of poly(L-lactide) (PLLA) and poly(D-lactide) (PDLA) [3,4]. It is well known that stereocomplexes formed from homopolylactides melt at temperatures up to 60 deg higher comparing to that of the homochiral components, as well as show better mechanical properties and degradation stability [5-7].

The present contribution reports on the synthesis of the triblock copolyesters obtained via coupling of corresponding polyester (α,ω) diols using hexamethylene diisocyanate (HDI) and isophorone diisocyanate (IPDI) as the chain extenders. In this study, the enantiomeric ABA and BAB triblock copolymers consisting of PLLA or PDLA as the A block, were synthesized. Finally, the resulting triblock copolyesters with the opposite configuration of PLA blocks, were used for a preparation of the corresponding stereocomplexes. The microstructure, molar masses, morphology, and thermal properties of the obtained copolymers were investigated by ^{1}H NMR, SEC, SEM, and DSC measurements respectively.

Experimental

Materials

L,L- and D,D -LA (Boehringer Ingelheim, Germany) were crystallized from dry 2-propanol and then purified by sublimation in vacuum (10^{-3} mbar, 90 ^{o}C). Trimethylene carbonate (TMC) (Boehringer Ingelheim, Germany, > 99%) was crystallized from dried THF: ethyl ether mixture (3:1) and sublimated (10^{-3} mbar, 45 ^{o}C). The purified monomers were distributed into the glass ampules equipped with break-seals.

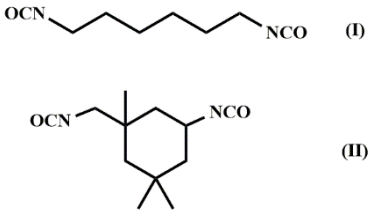
1,5-pentandiol (Aldrich), 2-propanol (POCh, Gliwice, Poland) were dried with Na metal and distributed by vaccum distillation into the thin walled vials. Hexamethylene diisocyanate (HDI) and isophorone diisocyanate (IPDI) (98%, Aldrich) were distillated under reduced pressure and storage in low temperature (< 4 ^{o}C). Tin (II) octoate ($Sn(Oct)_2$) (95%, Aldrich), and tetrahydrofuran (THF) (99%, POCh, Gliwice, Poland)) were purified as described in ref 8. Dibutyltin dilaurate (DBTL) was used without purification (95%, Aldrich).

Synthesis of the LA and TMC homopolymers

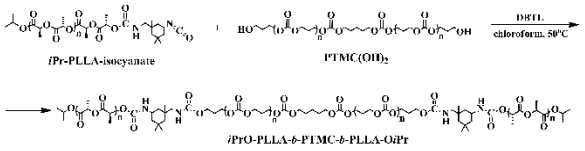
The homopolymerizations of L,L-LA, D,D-LA and TMC were performed according to the coordination mechanism, with stannous 2-ethylhexanoate ($Sn(Oct)_2$) as the catalyst and 2-propanol or 1,5-pentandiol as the initiators. Polymerization were carried out for 24 h at 80 °C, using the standard high-vacuum technique. The resulting polymers were precipitated into methanol and dried under reduced pressure at room temperature.

Synthesis of LA and TMC copolymers

The coupling of corresponding PTMCs and PLAs with HDI (I) and IPDI (II) was carried out under nitrogen atmosphere, in the presence of dibutyltin dilaurate (DBTL), using chloroform as a solvent.



As a representative example, triblock ABA copolymer was synthesized by the following procedure: First a mixture containing monohydroxyl-terminated polyester and diisocyanate in chloroform ([OH]/[-NCO] equal to 1:4) was stirred for 48h at 50°C. The obtained isocyanate-terminated polyester was precipitated into an excess of *n*-hexane, filtered and dried under vacuum. At the next step, the isolated isocyanate-ended polyester was used in DHBL-catalysed reaction with the dihydroxyl polycarbonate (Scheme 1).



Scheme 1. Synthesis of the triblock ABA copolymer.

The use of HDI allowed obtaining the high molar mass copolymers, however, the formation of insoluble fraction of products was observed. For this reason, only the products obtained with IPDI as a coupling agent were widely characterized and use further in stereocomplex formation.

Stereocomplex formation

The precipitated and dried PTMC-*b*-PDLA-*b*-PTMC and PTMC-*b*-PLLA-*b*-PTMC as well as PLLA-*b*-PTMC-*b*-PLLA and PDLA-*b*-PTMC-*b*-PDLA copolymers were then used for the preparation of the stereocomplexes. The samples of the D,D-LA and L,L-LA copolymers were dissolved separately in 1,4-dioxane.

The solutions were mixed together and stirred using a magnetic stirrer for 24 h. The stereocomplex was precipitated into methanol and dried under vacuum.

Characterization

Monomer conversion and (co)polymer composition were determined by NMR spectroscopy. ^{1}H NMR spectra were recorded on Bruker DRX 500 (Germany) with $CDCl_3$ (99.8% D). The actual number-average molar mass (M_n) and molar mass distributions (M_w/M_n) of PLA were determined using an Agilent 1100 HPLC pump and set of two PLGel 5μ mixed-C columns. An Optilab rex Wyatt interferometric refractometer and DOWN EOS Wyatt laser photometer were applied as detectors.

The (co)polymers structure were confirmed by Fourier-Transformed infrared (FTIR) spectroscopy. Infrared spectra were obtained using Avatar TM 330 FTIR Spectrometer (Nicolet) in the HATR mode.

The thermal properties of materials were measured by a differential scanning calorimetry (DSC Q200, TA Instruments and DSC 2920, TA Instruments). The thermal parameters of the each sample were measured under nitrogen flow at a heating rate of 10 °C min^{-1}. The thermal stability of the materials was investigated with a thermogravimetry (TGA) (Hi-Res TGA 2950 Thermogravimetric Analyzer, TA Instruments) under the nitrogen flow by heating with the rate of 10 °C min^{-1}.

The morphology of the materials was observed with scanning electron microscopy (SEM). Samples were coated with a fine gold layer by ion sputtering (JEOL JFC-1200) and then examined with the JEOL JSM-5500 LV scanning electron microscope.

Results and discussion

The present paper reports the convenient method for the synthesis of the ABA and BAB aliphatic esters triblock copolymers, consisting of PLLA or PDLA as the A block and the PTMC as the B block. It has been shown that the coupling of corresponding polyester diols is a good alternative for the common used ring opening sequential copolymerization.

The formation of (co)polymers was proved by SEC and ^{1}H NMR methods. In the SEC traces the monomodal molar masses distribution with relatively low dispersity ($M_w/M_n < 2$) for all (co)polymers were observed.

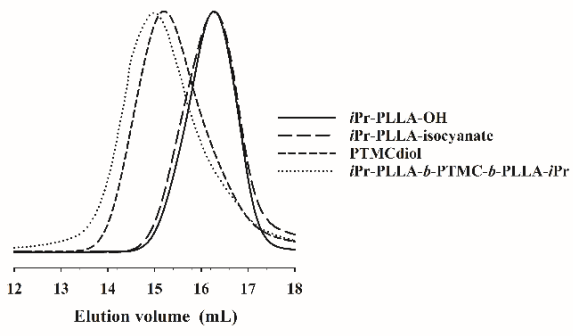


Figure 1. GPC traces of the *i*Pr-PLLA-*b*-PTMC-*b*-PLLA-*i*Pr copolymer (M_n ~ 10.0 kg mol^{-1}) and its homopolymers.

Figure 1 shows SEC chromatograms of homopolymers, prepolymer and the coupling product. The expected shift to the lower elution volume (higher molar masses range) after coupling step, clearly indicate copolymer formation.

In ^{1}H NMR spectrum of the final product (Figure 2), the signals at δ = 3.82 ppm (t, 4H, CH_2O) and 4.35 ppm (quintet, 2H, CH_2), coming from protons in the PTMC and the PLA end-groups respectively, disappear. It shows the polymer chains extension.

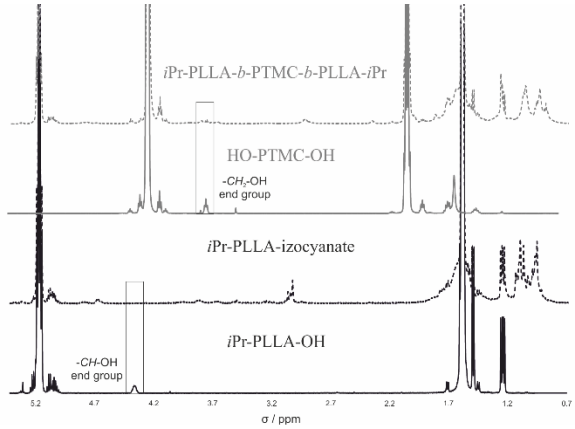


Figure 2. ^{1}H NMR analysis confirming formation of the *i*Pr-PLLA-*b*-PTMC-*b*-PLLA-*i*Pr.

Table 1. Comparison of the predicted (M_n(theor.)) and measured (M_n(SEC) and M_n(NMR)) molar masses of the ABA copolymers.

LA/TMC copolymers synthesis:				
Copolymer	M_n (theor.)[a] (kg mol^{-1})	M_n (GPC, MALLS)[b] (kg mol^{-1})	M_n (NMR)[c] (kg mol^{-1})	$Đ$[d]
*i*Pr-PLLA-*b*-PTMC-*b*-PLLA-*i*Pr	10.0	15.1/10.3	9.7	1.5
*i*Pr-PLLA-*b*-PTMC-*b*-PLLA-*i*Pr	40. 0	50.5/36.9	38.9	1.8
*i*Pr-PDLA-*b*-PTMC-*b*-PDLA-*i*Pr	10.0	12.3/9.2	11.7	1.6
*i*Pr-PDLA-*b*-PTMC-*b*-PDLA-*i*Pr	40.0	51.2/37.4	37.4	1.7

[a] The number-average molar based on the starting concentrations of the comonomers.
[b] The number-average molar masses determined by SEC with a laser light scattering detector on the basis of the assumption that dn/dc = 0.035 (PLA) and 0.048 mL g^{-1} (PTMC) respectively.
[c] The number-average molar masses determined from the ratio of the relative intensities of the main-chain and end-group signals in the ^{1}H NMR spectra.
[d] $Đ = M_w/M_n$ measured by SEC with RI detector.

The molar masses determined by SEC (MALLS) were in satisfactory agreement with values determined from NMR and were close to the theoretical (predicted) values based on the starting concentrations of the comonomers and initiators (Table 1).

The resulting triblock copolyesters with the opposite configuration of PLA block, were used for a preparation of the corresponding stereocomplexes. The thermal properties of the copolymers and stereocomplexes were analyzed by DSC. The melting peaks at temperature characteristic for stereocomplex [6] were observed in the first DSC heating runs at 210.6 °C (Figure 3). A higher melting temperature (T_m) of the stereocomplex in comparison to T_m of L- or D-PLA isomers is very well known and widely described in the literature [6,7].

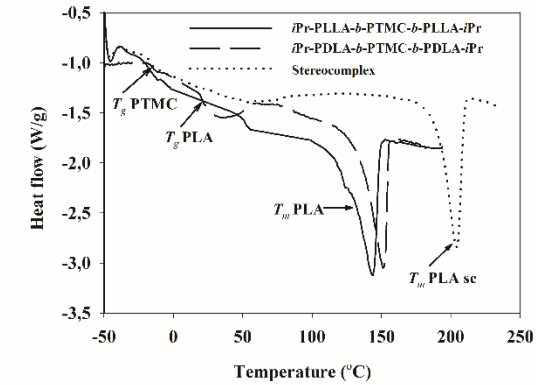


Figure 3. DSC thermograms (rate of heating and cooling: 10 °C·min^{-1}) LA/TMC copolymer (M_n ~10 000 g mol^{-1}) and stereocomplex during first heating.

SEM was chosen as a tool for direct observation of the morphological differences between copolymers of different composition. An aggregation of copolymers chains into microparticles were observed for the copolymers and stereocomplex samples. SEM pictures show the particles from copolymer suspension, obtained by dropping non-solvent methanol to the homo- or copolymers solutions in tetrahydrofuran (THF) (0.5 %w/v).The particles of TMC/LA triblock copolymers, depending on the distribution of carbonate units along polymer chains, showed two types of the morphology (Figure 4), the fusiform particles of PLA-*b*-PTMC-*b*-PLA copolymer and the fusiform particles of PTMC-*b*-PDLA-*b*-PTMC with the fraction of relatively regular, close to spherical shape particles. The typical thickness of the fusiform particles was about 0.5 μm, whereas diameters of spheres of the latter copolymer were from about 0.2 to 1 μm. The SEM image of stereocomplex samples presents spherical shaped particles with diameters from 0.1 to 2 μm.

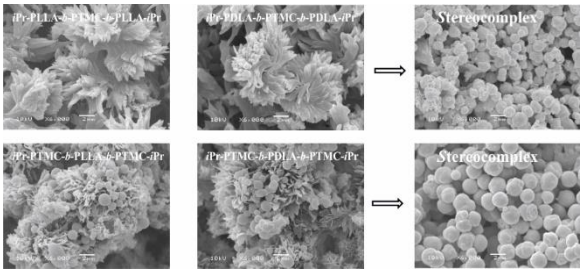


Figure 4. SEM micrographs illustrating the morphology of *i*Pr-PLA-*b*-PTMC-*b*-PLA-*i*Pr and *i*Pr-PTMC-*b*-PLA-*b*-PTMC-*i*Pr copolymers and its stereocomplex (copolymers with M_n ~ 10 000 g mol^{-1}).

Conclusions

In summary, we have demonstrated that the end-to-end coupling of corresponding polyester (α,ω) diols is a convenient method for synthesis of aliphatic esters block copolymer allowing preparation of the LA/TMC triblock copolymers (both ABA and BAB structure). ^{1}H NMR, GPC, DSC analyses confirmed the tailor-made and well-defined microstructures of these copolymers.

The thermal properties of the obtained copolymers were significantly different than their stereocomplex formed from the enantiomeric copolymer components. Additionally, it can be concluded that the composition as well as microstructure of copolymers chains, has a strong influence on the observed morphology of the synthesized materials.

Acknowledgements

This work was realized in a frame of the project LACMAN PBS2/A1/12/2013 financed by a National Centre for Research and Development (NCBiR).

References

1. A. Duda, Polymer Science: A Comprehensive Reference, K. Matyjaszewski and M. Moeller Eds., Elsevier Vol. 4, 213–246, 2012.
2. M. Socka, A. Duda, A. Adamus, R. A. Wach, P. Ulanski, *Polymer* 87, 50, 2016.
3. K. Kobayashi, S. Kanmuri, Y. Kimura, K. Masutani, *Polym. Int.* 64, 641, 2015.
4. M. K. Kang, Y. Jung, S. H. Kim, *Macromol. Res.*, 21, 1036, 2013.
5. H. Tsuji, *Macromol. Biosci.* 5, 569, 2005.
6. M. Brzezinski, T. Biela, Encyclopedia of Polymeric Nanomaterials: Stereocomplexed Polylactides, S. **Kobayashi** and K. **Müllen** Eds., Springer, 2274-2281, 2015.
7. A. Kowalski, A. Duda, S. Penczek, *Macromol. Rapid Commun*. 19, 567, 1998.

MACRO 551

High Performance Liquid Crystalline Polymers from 2,5-furandicarboxylic acid; Synthesis, Characterization and Properties

Wilsens, C.H.R.M.[a,b,*]; Deshmukh, Y.S. [a,b]; Auhl, D. [a,b,]; Yao, Y.[c]; Rastogi, S[a,b].

[a]*Department of biobased materials, Maastricht University, P.O. Box 616, 6200MD Maastricht, The Netherlands.*

[b]*Aachen-Maastricht Institute for BioBased Materials (AMIBM), Urmonderbaan 22, 6167 RD, Geleen, The Netherlands*

[c]*Shanghai Key Laboratory of Magnetic Resonance, East China Normal University, North Zhongshan Road 3663, 200062 Shanghai, P.R. China*

** corresponding author: karel.wilsens@maastrichtuniversity.nl*

Thermotropic polyesters are an important class of materials for high performance applications. Their low melt viscosities, low thermal expansion coefficients, high use temperatures, and ease in processing allow for the production of high strength and high modulus fibers, films, or compression-molded articles. In this work we explore the synthesis, melt extrusion, fiber spinning, and performance of thermotropic liquid-crystalline polyesters from renewable resources. Special focus is on the application of the bio-based co-monomers 2,5-furandicarboxylic acid and vanillic acid and on their effect of the material properties.

Using a high-temperature acidolysis melt-polycondensation reaction at temperatures up to 360 °C, fully aromatic bio-based thermotropic polyesters with melting temperature around 300 °C have successfully synthesized. [1] Unfortunately, processing at these high temperatures causes degradation of the monomers during the polymerization, resulting in discoloured and low molecular weight material (M_n of 8,000 g/mol). Instead, synthesis at mild temperatures (< 260 °C) and the inclusion of aliphatic dicarboxylic acids to suppress the melting temperature yields materials with molecular weight (M_n) above 20,000 g/mol [2]. Using various characterization tools, we demonstrate that a judicious selection of the aromatic and aliphatic monomers gives excellent control over the glass transition temperatures, melting temperatures, overall crystallinity, and the degree of segmental block formation inside the polymeric chains.

As anticipated, the thermotropic characteristics of the polymer melt eases the melt-processing, yielding highly oriented fibers after melt-drawing. Preliminary fibre spinning experiments yield single-filament fibres with a high orientation parameter ($<P_{2n}(\cos\varphi)>$ up to 0.9), a tensile modulus of 10 GPa, and a tensile strength in the range of 150 – 200 MPa. [3] Although these values are promising, they are not comparable to performance of commercial liquid crystalline fibers. This is likely resulting from the large percentage of aliphatic content, which is generally 30 mole%.

Despite the moderate performance of the pure thermotropic fibres, we demonstrate that the developed materials are efficient fillers in polyester blends: Detailed Tunnelling Electron Microscopy, differential scanning calirometry, small angle X-ray diffraction, and tensile testing studies indicate that these bio-based thermotropic liquid crystalline polyesters both reinforcing and provide surface for nucleation for the polyester matrix. [4] The resulting enhancement in interfacial interaction between the matrix and filler allows for the development of fibres from renewable polyester blends with enhanced tensile modulus and tensile strength, without mitigating on the strain at break (> 600 %).

References

[1] Wilsens, C.H.R.M.; Noordover, B.A.J.; Rastogi, S.; *Polymer*, 55, **2014**, 2432

[2] Wilsens, C.H.R.M.; Verhoeven, J.M.G.A.; Noordover, B.A.J.; Hansen, M.R.; Auhl, D.; Rastogi, S.;
Macromolecules, 47, **2014**, 3306.

[3] Wilsens, C.H.R.M.; Deshmukh, Y.S.; Liu, W.; Noordover, B.A.J.; Yao, Y.; Meijer, H.E.H.; Rastogi, S.; *Polymer*, 60, **2015**, 198.

[4] Wilsens, C.H.R.M.; Pepels, M.P.F.; Spoelstra, A.B.; Portale, G.; Auhl, D.; Deshmukh, Y.S.; Harings, J.A.W.; *Macromolecules*, 49, **2016**, 2228.

MACRO-553

Synthesis and Characterization of Polystyrene Using Modified Graphene oxide based Polymeric Nano-Surfactant via Emulsion Polymerization

Rajender Nutenki,[a] *Dr.K.I.Suresh,*[a, b]*

[a, b] *Polymers & Functional Materials Division,*

[b] *Academy of Scientific and Innovative Research (AcSIR),*

CSIR-Indian Institute of Chemical Technology, Hyderabad – 500 007, India.
** e-mail: kisuresh@iict.res.in*

Abstract

In the present work we report the synthesis and characterization of a Graphene modified polymeric surfactant via surface initiated atom transfer radical polymerization (SI-ATRP) and its evaluation. Mono disperse polystyrene (PS) Nanoparticles are synthesized using modified graphene polymeric surfactant through emulsion polymerization technique. The prepared surfactant was characterized for structure and surface tension properties. The effect of Graphene surfactant on the synthesis, and polymer properties have been studied by using various techniques like IR, DLS, DSC, SEM, TGA. The influence of Graphene surfactant on the synthesis, film formation and film properties has been studied.

Keywords: *Modified graphene polymer surfactant; Mono disperse PS; thermal properties*

Introduction

During the last two decade Graphene Polymer Nano composites have attracted extreme interest in industrial and academic field.[1, 2] This is attributed to its exceptionally high surface area as well as incredible electrical, optical, thermal, and mechanical properties. But pristine unmodified graphene is insoluble and infusible, which makes it difficult the preparation and processing of polymer-graphene Nano (PGN) composites. Oxidized graphene containing various functional groups like, −OH, −COOH, epoxy prepared via acid oxidation of graphite resembles single layer graphene sheet in several aspects. It has good water solubility and amenable to chemical reactions to modify the interphase between graphene oxide Nano filler and polymer matrix via chemical attachment.

Generally, synthesis of stable PGN via emulsion polymerization technique was not successful due to instability of the composite emulsions. In this work, to facilitate the preparation of stable PS-GO Nano composite emulsion, a novel polymeric graphene oxide based Nano surfactant was synthesized. To prepare the Graphene modified polymer surfactant, poly (Pentadecyl phenyl methacrylate) (PDPMA) was grafted on graphene oxide (GO) sheet via surface initiated atom transfer radical polymerization. The polymer grafted graphene was later sulfonated with chloro-sulfonic acid and subsequently treated with aqueous Na_2CO_3. Polymer grafted graphene oxide Nano surfactant could be useful in various other fields, such as (mini)emulsion polymerizations,

coatings, biotechnology, nanotechnology, medicine, pharmacology, cosmetics, agriculture, water purification, electronic, optoelectronic, and enhanced oil recovery. [4]

The synthesized narrow disperse stable Polystyrene Nano composites has been characterized by techniques like FTIR, DLS, SEM and TGA. The Graphene surfactant was found to compose the film formation and film properties of PS emulsion.

Experimental

Materials

Styrene (99%, Sigma-Aldrich) purified by washing with aqueous 5% NaOH, (SD.Fine Chem.,Mumbai) followed by distillation at 40°C under reduced pressure. Distilled and Deionized (DDI) water was obtained from a Millipore Milli-Q water purification system. . Potassium persulphate (KPS) was obtained from Sigma-Aldrich. The grafted graphene –poly PDPMA sample was reacted with Chloro-sulfonic acid (Avra synthesis, Hyderabad) and subsequently treated with aqueous Na_2CO_3 (SD. Fine Chem.,Mumbai) Solvents Chloroform and dichloromethane analytical grade (SD. Fine Chem.,Mumbai) was used.

Instrumentation techniques

The IR spectrum was recorded on a Perkin Elmer machine. The particle size of the GPDPMA dispersions and the zeta potential was measured with a Malvern Nanosizer from Malvern Instruments, UK. Thermal transition temperatures (Tg) of the samples were recorded on a TA-Q100 differential scanning calorimeter at a heating and cooling rate of 10°C/min under nitrogen atmosphere. TGA measurements were carried out on a Q500 thermogravimetric analyzer (TA instruments). Scanning electron microscopy (SEM) and energy dispersive X-ray spectroscopy analysis was carried out to study the surface morphology, elemental composition of sulfonated-GPDPMA and the PS nanoparticles. The EDS-SEM analysis was performed on JEOL 7610FS-3000N machine under high vacuum.

Preparation of water soluble graphene supported polymeric surfactant (S-GPDPMA)

In a typical reaction (Scheme.1) 0.7 gm of PDPMA grafted graphene synthesized via SI ATRP was dispersed in 10ml of DCM and purged with nitrogen gas for 10 min. 200µl (2eq of PDPMA) choro-sulfonic acid dissolved in 2ml of DCM was add through dropping funnel to the polymer solution at 0°C. After the addition of sulfonating agent the reaction was continued at R.T. for 4 hrs. The sulfonated copolymer was ionisable with 5% $NaCO_3$ solution to adjust the pH to 8. Then aqueous solution was freeze dried and analyzed for composition.

.

Emulsion polymerization of Styrene using Graphene –based surfactant.

The nanocomposites emulsion was prepared using the aqueous solutions of S-GPDPMA as a seed in the emulsion polymerization. In a typical experiment, 50 g of S-GPDPMA–water dispersion was taken in a three-neck round bottom flask. Five milliliter of styrene monomer was added through a syringe and stirred at 250 rpm for 1 h using a mechanical stirrer under N_2 atmosphere. The pH of the solution was shown at 9.0–10.0 range according to the weight of surfactant.

The reaction mixture was heated to 75 ± 2°C, and 50mg of $K_2S_2O_8$ was added to initiate the polymerization. The reaction was run for 24 h to achieve the maximum conversion in all cases.

The same reaction was carried out at different surfactant concentration under identical reaction conditions.

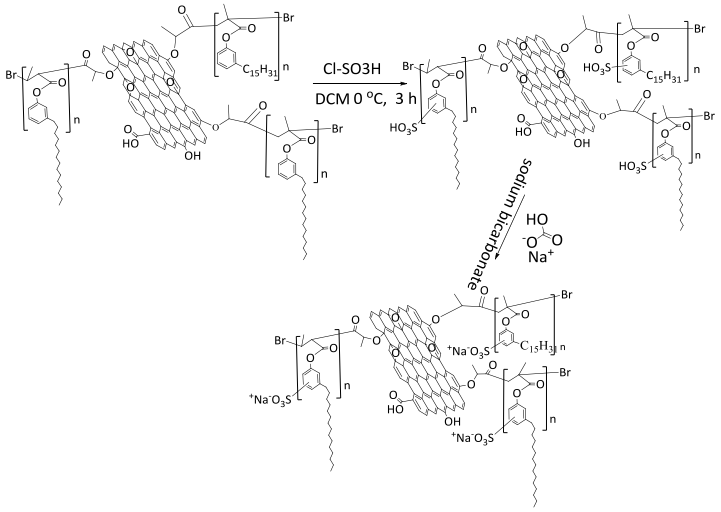
Results and discussion

In this work, the evaluation of a new graphene modified polymeric surfactant abbreviated as S-GPDPMA, in the emulsion polymerization of styrene was under taken with the aim of studying its effect on synthesis and polymer properties**.**

Synthesis & characterization of water soluble graphene based polymeric surfactant

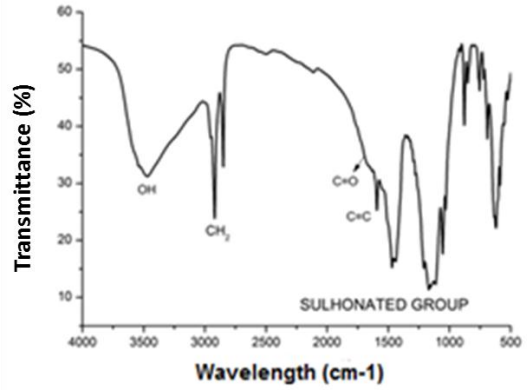
The synthesis of the surfactant starting from the polymer (PDPMA) grafted graphene is presented in scheme 1. The surface initiated polymerization PDP methacrylate using GO based ATRP initiator is reported in another paper.

Sheme.1. Schematic representation of water soluble graphene supported polymeric surfactant (S-GPDPMA)



The prepared aqueous dispersion of S-GPDPMA was freeze dried by lyophilisation to obtain a solid powder. The powder surfactant was characterized for sulphur content, surface morphology, particle size and zeta potential using techniques like FT-IR, EDS-SEM, & DLS.

Fig 1. FT-IR spectrum of Surfactant



The IR spectrum shown in fig.1 has characteristic absorption bands of sulfate groups at 1380 and 1060 cm^{-1} indicating the formation of the Phenyl-Sulphur linkage. Remaining functional groups corresponds to GPDPMA through SI-ATRP.

EDS Analysis

The EDS of S-GPDPMA further confirms the functionalization of sulfate groups on phenyl ring and corresponding elemental composition significantly increased comare to initiated functionalized graphene (GO-Br).

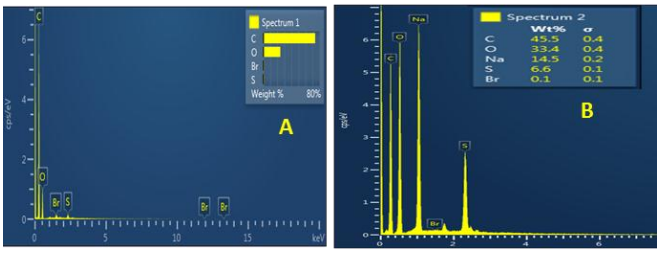


Figure 2. EDS of A. GO-Br, B. S-GPDPMA

Dynamic Light Scattering study (DLS)

The particle size distribution and zeta potential of particle of S-GPDPMA in aqueous medium was studied. The aqueous dispersion of different concentration fed in the batch emulsion such as 25mg/ml to 100mg/ml particle and Z-average size in the range 280 to 300nm, (fig.3) showing unimodal and narrow disperse. The corresponding seeded water disperse zeta potential showing in the range -30 to -35mv, though it shows anionic in nature.

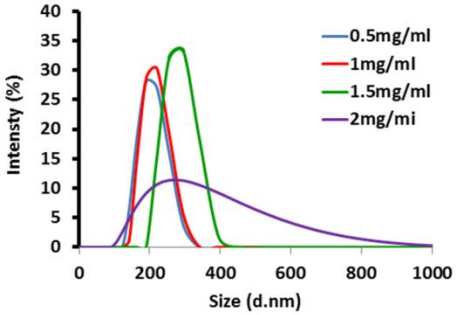
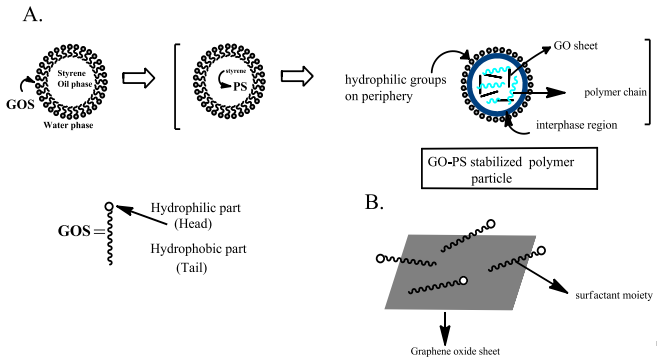


Figure 3. Particle size variation of polymeric surfactant with concentration in water.

The surfactant was later evaluated in the emulsion polymerization of styrene at various concentrations. The schematic of the procedure used is given in scheme 2.

Sheme.2. Schematic representation of emulsion polymerization of styrene with graphene modified surfactant..



The emulsion polymerization of styrene was under taken with the aim of studying its effect on synthesis and polymer properties**.**

Synthesis and characterization composite dispersions.

The performance of the polymeric surfactant in batch emulsion polymerization (Scheme 2) was explored using styrene as monomer and characterizing the surfactant effect on particle size, size distribution, and morphology of the resulting particles. Stable dispersions were obtained in all cases; Table 2 gives composition, and characteristics of the synthesized dispersions.

Table.2 Composition and characteristics of GO-PS emulsion using with modified S-GPDPMA surfactant.

Sample code	Surfactant weight (%)to monomer [b]	Conversion (%)	Particle diameter (nm)[d]
GOPS-1	0.5	70	162
GOPS-2	1	72	164
GOPS-3	1.5	71	190
GOPS-4	2	68	219

a= 1wt% of $K_2S_2O_8$ initiator, 4.65gm of styrene were used as the, in all cases. b= seed dispersions have a size 280 to 300nm in range. c= determined by gravimetric method. d= determined from Malvern Nanosizer

Figure 4 along with the data presented in Table 2 shows that the particle diameter 160 to 200nm range, in all cases monomial and narrow disperse.

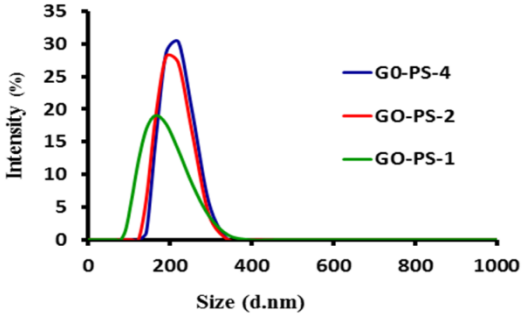


Figure 4. Particle size distribution of PS emulsion with varying S-GPDPMA loading.

Surface Properties

From the SEM images the morphology of the particles shows spherical with size 120±20nmm. The wettability of water of Pickering emulsion coated on glass slide has been studied through contact angle measurements. While increasing the surfactant ratio the contact angle also increasing 84 (GO-PS-1) to 124° (GO-PS-4) angle significantly, it suggesting that hydrophobicity increasing. This is expected due to the graphene grafted polymer chain having the C-15 long alkyl side chain in every monomer unit.

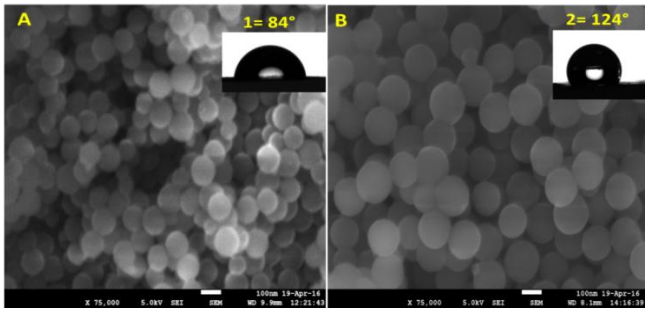


Figure 5. Scanning electron micrographs of A. GO-PS-1, B.GO-PS-4 and in side showing corresponding contact angle images.

Thermal properties.

Thermal properties like glass transition temperatures of the graphene modified surfactant samples were studied using DSC, and the results are summarized in Fig. 6.

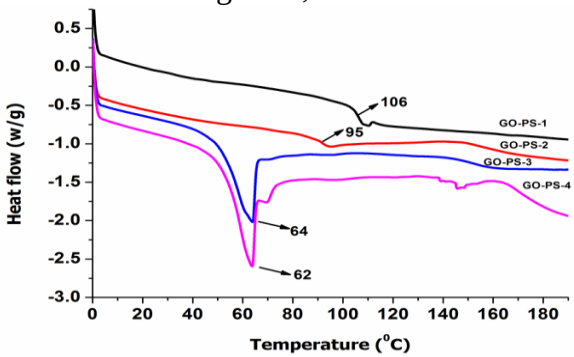


Figure 6. DSC thermos graphs of polystyrene nano composite emulsion.

Figure 6 shows that, initially, the glass transition temperature at 106°C is nearly same as that of pure PS (GO-PS-1) which decreases to 95°C for GO-PS-2 prepared with 1wt% graphene surfactant. While increasing surfactant concentration 1.5wt% (GO-PS-3) to 2wt% (GO-PS-4) becoming

Sharp melting curves around 64 and 62°C was observed. These results suggest that clear interaction between polystyrene chain and the surfactant. This is due to the S-GPDPMA exhibiting the ordered, flexible and low Tg, attributed by the crystalized side chains on phenyl ring moiety.

To evaluate the influence of the polymeric surfactant on the thermal stability of polystyrene, the decomposition behavior was studied by thermogravimetric analysis (TGA). The weight loss thermogram no appreciable difference is observed in all case. The thermal decomposition pattern of samples GO-PS3 showed in Fig. 7. The figure shows, up to 400°C no decomposition was observed, the peak decomposition temperature obtained from the derivative plot (not shown) was

430 °C. Thus, the TGA studies indicate that the surfactant does not influence the decomposition characteristics of the polymer.

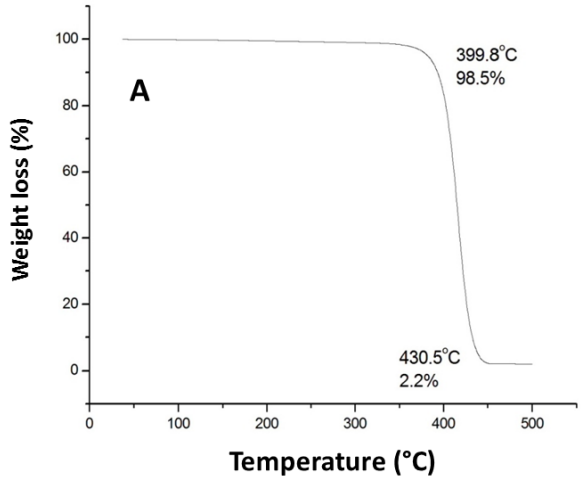


Figure 7. Weight loss curves of polystyrene prepared with 75mg surfactant in the feed.

Conclusions

The polymeric Graphene modified surfactant, sulfonated poly 3-pentadecyl phenyl methacrylate, was synthesized and evalauated in the emulsion polymerization of styrene. The stable nano sized poly styrene particles of narrow size distribution was obtained as confirmed by Dynamic light scattering and SEM. While increasing the surfactant ratio highest loading (GO-PS4) a melting peak at 62°C due to crystallization was observed. This is attributed to the crystallization of the side chain of polymeric surfactants. The results show that the incorporation of a novel graphene based surfactant enhances the film formation and film properties. The water contact angle of the films increased from 84° to 124° with 2wt% load of surfactant. The composite dispersions yield flexible films which are being characterized in detail for the dynamic mechanical, thermal and tensile properties to assess the suitability in coatings and adhesisves.

Acknowledgements

N.Rajender thanks to UGC for senior research fellowship and to Director IICT for granting permission to carry out this work.

References

1. H. W. Kim, A. A. Abdala, C. W. Macosko, *Macromolecules* 2010, 43, 6515.

2. J. R. Potts, D. R. Dreyer C. W. Bielawski, R. S. Ruoff, *Polymer* 2011, *52*, 5-25.

3. J. Kim , L. J. Kote , F. Kim , W. Yuan , K. R. Shull , J. Huang , *J. Am.Chem. Soc.* 2010, 132, 8180–8186.

4. A. Durand, E. Marie, *Adv. Colloid Interface Sci*. 2009, 150, 90−105.

MACRO-558

Synthesis and Characterization of Novel Poly(vinyl alcohol-*co*-styrenesulfonic acid) for Membrane Applications

R.R. Choudhury, J.M. Gohil*, A.K. Palai, S. Mohanty

Laboratory for Advanced Research in Polymeric Materials (LARPM), Central Institute of Plastics Engineering and Technology (CIPET), Bhubaneswar, Odisha-751024, India

Presenting author e-mail id: rikarani.choudhury@gmail.com (R.R. Choudhury)

** Corresponding author e-mail id: jay21480@yahoo.co.in* (J.M. Gohil)

Abstract

Tailored polymer synthesis is most important aspect for the development of next generation of membrane materials. The synthesis of polymers, especially those with designed structure, and subsequent membrane formation is very promising for water desalination and fuel cell applications. This study first time elaborates the synthesis protocol for the preparation of novel poly(styrenesulfonic acid-co-vinyl alcohol). Copolymer has designed to bear both ion conducting and crosslinkable segments from varying molar ratios of vinyl acetate (VAc) and SSA by free radical polymerization. Mild alkaline hydrolysis of polyvinyl acetate and copolymers were carried out to get hydrolyzed polyvinyl alcohol and poly(styrenesulfonic acid-co-vinyl alcohol) respectively. The solubility of resultant copolymers of different molar composition were studied using different ratios of water:methanol. Formations of copolymer were confirmed by fourier transform infrared spectroscopy (FTIR) peaks for sufonate and hydroxyl groups. Thermal stability of poly(styrenesulfonic acid-co-vinyl alcohol) was higher than that of unhydrolysed poly(styrenesulfonic acid-co-vinyl acetate). Differential scanning calorimetry thermogram showed single T_g peak for copolymers formed.

Keywords: poly(styrenesulfonic acid-co-vinyl alcohol); synthesis; fourier transform infrared spectroscopy; membrane

MACRO-559

Functional Intrinsic Microporous Polymers for Energy Applications: Synthesis and Characterization

A. K. Palai, J. M. Gohil*, S. Mohanty

Laboratory for Advanced Research in Polymeric Materials, Central Institute of Plastics Engineering & Technology, Bhubaneswar, Odisha, India 751 024.
Presenting author e-mail id:apalai@gmail.co

m
**e-mail id:* jay21480@yahoo.co.in

Abstract

Polymers of intrinsic microporosity (PIMs) are a new class of polymers with molecular sieve behaviour due to their rigid, contorted macromolecular backbones. They show great potential in solvent-resistant nanofiltration, organophilic pervaporation and gas and vapour separations. However, little is known about its use as material for energy applications, e.g., as polymer electrolyte membrane for fuel cells.

In this regard, a series of functionalized intrinsic microporous polymers (PIM) were synthesized. The PIM-1 starting material used for the hydrolysis experiments was gel-free and had high molecular weight (M_n = 44000, PDI = 1.5), which was obtained under an optimized polycondensation process. Sulphonated PIM-3 (named as PIM-SO_3H) was synthesized by post-synthesis modification method using trimethysilyl chlorosulfonate as reagent at room temperature. The protocol enjoys mild reaction conditions, easy work-up procedure and moderate conversion yield. Elemental analysis and FT-IR spectra indisputably confirmed that pure PIMs were obtained with no traces of nitrile groups. The PIM-SO_3H/COOH conveys high solubility in polar aprotic solvents such as DMSO, DMF, and NMP. The present study improves the understanding of the relationship of structure/ properties and also extends the PIM spectrum beyond those reported previously. In addition, the incorporation of sulphonic/carboxylic acid sites has the potential for further use as a proton exchange membrane for fuel cell applications.

Keywords: Polycondensation, Intrinsic microporosity, Sulphonation reaction, Fuel cell



FOCUS AREA

POLYMERS FOR ENERGY AND SENSING APPLICATIONS

MACRO 111

Fabrication of A Polyaniline Transduced Imidazole Based Conductometric Sensor for Rapid Detection of Cyanide

Paul Anirban [ab], Perween Mosarrat [ab], Saha Sukdeb [ab], Srivastava Divesh N.[ab], Das Amitava*[abc]*

[a] *Analytical Division and Centralized Instrument Facility, CSIR-Central Salt and Marine Chemicals Research Institute, Gijubhai Badheka Marg, Bhavnagar 364002, India.*

[b] *Academy of Scientific and Innovative Research-CSMCRI, Gijubhai Badheka Marg, Bhavnagar 364002, India.*

[c] *Organic Chemistry Division, CSIR-National Chemical Laboratory, Dr. Homi Bhabha Road, Pune 411008, India.*

E-mail: dnsrivastava@csmcri.org (D. N. Srivastava), a.das@ncl.res.in (A. Das)

Materials having lethal toxicity are of prime concern in the scientific community as they play a perilous role as pollutants in environmental and biological world.[1] Cyanide ion is one of such species having fatal impacts on the living cells and found to be extremely hazardous for nature and environment. It can rigorously restrain the cellular respiration in humans and mammals by suppressing the transport of oxygen as it has a higher affinity towards cytochrome-c oxidase.[2] Accumulation of high concentration of cyanide in the body can cause cardiac arrest, coma and even death within a few minutes[3]. The United States environmental protection agency (USEPA) circulated a guideline for maximum contamination of cyanide ion in drinking water is 7.69×10^{-6} mol/Lit,whereas as per World health organization (WHO), the maximum contamination of cyanide in drinking water is 2.7×10^{-6}. Despite of these harmful effects, use of cyanide cannot be avoided in the areas like electroplating, metallurgy and mining industry. As per an estimate every year 1.4 million tons of toxic cyanide is produced by various industries worldwide which is a great environmental concern.[4]Consequently several methods have been reported for cyanide sensing like

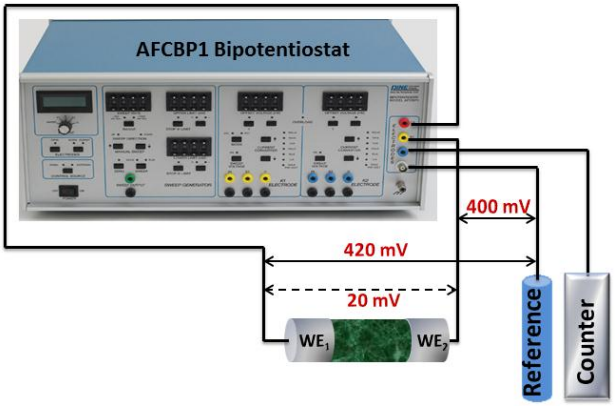


Fig. 1: Schematic diagram of the experimental protocol

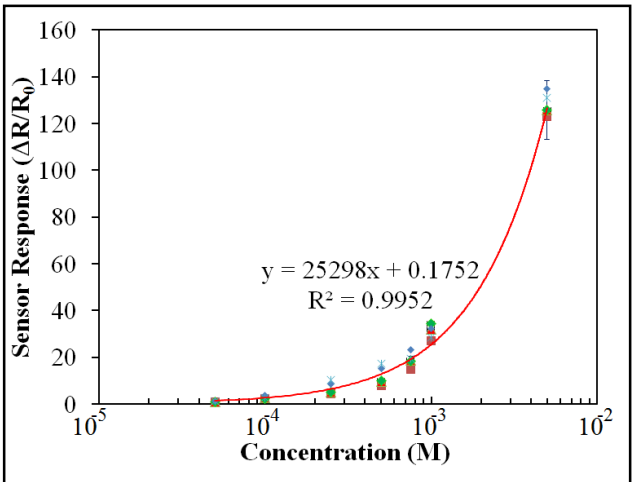


Fig.2: Calibration plot of conductometric sensor response

titration,spectrophotometry,fluorometry,luminescence,phosphorescence,electrophoresis,voltammetryetc.[5]The excellent electro activity of polyaniline coupled with the excellent electroactivity of this receptor, due to the presence of the quinone moiety, has been exploited to develop a conductometric sensor. The primary doping of conducting polyaniline is generally utilized for fabrication of conductometric sensors, albeit there are few reports of exploiting secondary doping also.[6]The primary doping comprises protonation/ deprotonation of the polymer leading to few orders of magnitude change in the conductance (Fig 1). Specific and efficient hydrogen bonding interaction between cyanide and the $H_{N\text{-}H}$ [Imidazole] in aqueous medium had been utilized for selective recognition of the cyanide in physiological condition and pH. Possibility of utilizing such an interaction for developing any practical device for specific detection of cyanide in aqueous environment has not been explored earlier. Here, we report a simple dip and read conductometric sensor for cyanide ion using a tailored electrode in aqueous media. The purpose built reagent, 2-phenyl-1H-anthra-[2,3-d]-immidazole-5,10 dione was immobilized in polyaniline matrix to fabricate this conductometric device. The homogeneous immobilization of the receptor in polyaniline was confirmed by FT-IR mapping. Proposed transduction mechanism is charge neutralization on polyaniline moiety, which ultimately inhibitsthe protonation resulting decrease in conductance. The sensor responses were differentiated from the artifacts by means of various control experiments. The responses have been investigated under various conditions, like different pH and electrochemical state of the polymer. The current sensor has been found to be better closer to the neural pH and at 400 mV vs. Ag/AgCl potential.The minimum detection limit of this conductometric sensor was found 1×10^{-8} mol/Lit which is 200 times less than the maximum amount of cyanide contamination in water approved by WHO. The linear range was found from5×10^{-5}mol/Lit to 5×10^{-3} mol/Lit concentration of cyanide under various conditions (Fig. 2). The reproducibility and repeatability of the sensor was investigated and the interference studies were performed.

References

[1] S. K. Mehta, K. Salaria, A. Umar, *Electrochim. Acta*, 2012, **81**, 308-312.
[2] M. R. Ajaykumar, P. Mukhopadhyay, S. Yadav, S. Ghosh, *Org. Lett.*, 2010, **12**, 2646-2649.
[3] Y. M. Hijji, B. Barare, Y. Zhang, *Sens. Actuators, B*, 2012, **169**,106-112.
[4] A. Taheri, M. Noroozifar, M. K.-Motlagh, *J. Electroanal. Chem.*, 2009, **628**, 48-54.
[5] J. Ma, P. K. Dasgupta, *Anal. Chim. Acta*, 2010, **673**, 117-125.
[6] C. Muthukumar, S. D. Kesarkar, D. N. Srivastava, *J. Electroanal. Chem.*, 2007, **602**,172-180.

MACRO 114

Strain Rate Sensitivity Of Epoxy Composites Toughened With 2D Molybdenum Disulphide

Parthsarthy, S. Chaudhary, S. Roy, P. K*.

Centre for Fire, Explosive and Environment Safety, DRDO, Timarpur, Delhi 110054, India.

**pk_roy2000@yahoo.com, pkroy@cfees.drdo.in*

Transition metal dichalcogenides belong to the category of two-dimensional (2D) plate type materials, which offer distinctive opportunities in terms of tailoring the mechanical, thermal, electronic and optical properties of polymer nanocomposites. In the present work, molybdenum disulfide (MoS_2) was exfoliated into nanoplatelets using ultrasonication and subsequently dispersed in a cycloaliphatic epoxy resin at low loading fractions (< 1% w/w) to form toughened compositions. The tensile and fracture properties of the nano composites were determined which revealed that MoS_2 nanoplatelets are highly effective at enhancing the mechanical properties of epoxy at low nanofiller loading fractions (below 0.3 % w/w). The tensile strength and fracture energy (G_{IC}) increased by 41 % and 50 % respectively upon introduction of 0.3 % nano filler. This was also accompanied with an increase in the tensile modulus (~ 40%) with no decrease in glass transition temperature. Our results clearly highlight the potential of 2D nanoplatelets as reinforcing fillers in polymeric composites. Post-mortem morphological studies of the fracture surfaces was performed to arrive at the principal toughening mechanisms behind the experimental findings. High strain rate studies were performed using Split Hopkinson pressure bar, and the results were compared with those obtained under quasi-static conditions, to establish the strain rate sensitivity of the composites.

References

[1] Eksik,O.; Gao,J.; Shojaee,A.; Thomas,A.; Chow,P.; Bartolucci,F.; Lucca,D.A.; Koratkar,N.; *ACS NANO*, (2014) doi: 10.1021/nn5014098
[2] Matusinovic, Z.; Shukla,R.; Manias,E.; Hogshead,C.G.; Wilkie,C.A.; *Polymer Degradation and stability*. 97 (2012) 2481
[3] Chaudhary,S.; surekha,P.; Kumar,D.; Roy,P.K.; *Polymer Composites*, (2014) doi: 10.1002/p.c.22927.

MACRO 140

Preparation and Characterization of Terpolymer Based Cation Exchange Membrane for Water Desalination by Electrodialysis

[a]Bhadja Vaibhavee, [b]Jewrajka Suresh K and [a]Chatterjee Uma*

[a]Electromembrane Processes Division,[b]Reverse Osmosis membrane Division, CSIR-Central Salt & Marine Chemicals Research Institute,G. B. Marg, Bhavnagar, Gujarat, India

*Mail-id: * umac@csmcri.org*

Cation exchange membranes (CEMs) are widely used in fuel cells [1, 2] water desalination via electrodialysis (ED) [3, 4], and reverse electrodialysis [5]. The advantages of ED over reverse osmosis is the lower energy consumption during desalination of brackish water, minimal requirement of feed water pre-treatment, easier and lower cost of system maintenance, higher membrane life owing to relatively low bacterial/pathogenic fouling and higher recovery of water. The CEM contains negative charge on its surface and allows the passage of cation under electric potential. The CEM should possess high selectivity, high ionic conductivity and appropriate mechanical and chemical stability for the applications in desalination and fuel cells. The suitability of any desalination process via ED mainly depends on the value of power consumption and current efficiency. The power consumption and current efficiency values are largely influenced by the water uptake, ion exchange capacity, conductivity and transport number of membrane.

Our objective is the preparation of mechanically strong copolymer based cation exchange membrane with suitable electrochemical and mechanical properties for water desalination by ED process. Herein, a process for the preparation of terpolymer-based CEM by avoiding post sulfonation reaction is reported. Films were fabricated from terpolymers of polyacrylonitrile (PAN), polystyrene sodium sulfonate ($PStSO_3Na$) and polyn-butyl acrylate (PnBA) for use as CEM for water desalination via ED. Terpolymer composition was adjusted by optimizing the AN to $StSO_3Na$ and nBA ratio (w/w) in the copolymerization feed. The terpolymer synthesized by copolymerization of 75% (w/w) AN, 15% (w/w) $StSO_3Na$ and 10% (w/w) nBA in a feed mixture yielded copolymer containing 31.7 wt% $PStSO_3Na$. The casting of copolymer gave CEM which exhibited 8.7 MPa tensile stress and 34% strain under water wet state and is suitable for use in ED unit.

Table-1 shows the comparative physical and electrochemical properties of the prepared CEM and two other commercial CEMs (IONSEP and FujiFilm type -II).

Table 1. Physical and Electrochemical Properties of different CEMs

Membranes	Ion Exchange Capacity (IEC) ($meq.g^{-1}$)	Membrane Conductivity (K^m) ($mS.cm^{-1}$)	Water uptake (%)	t^+
CEM	1.72	1.56	13	0.87
Ionsep	3.2	2.45	40	0.85
FujiFilm type-II	2.17	2.07	30	0.88

The prepared CEM exhibited 0.87 transport number which is close to the value obtained with commercial membranes. The water uptake, IEC and K^m values were 13%, 1.72 $meq.g^{-1}$ and 1.56 $mS.cm^{-1}$ respectively. These values are lower than the values obtained for commercial membranes. The CEM is stable at pH window 2 to 12. Five pieces of prepared CEM along with commercial AEM was employed for dilute sea water desalination (total dissolved solid**,** TDS=2000 mg/L) by ED process in a small ED unit of effective area 65 cm^2 at 10 volt applied potential. The power consumption and current efficiency by the membrane during desalination were 1.06 $KWhKg^{-1}$ and 86% respectively**.** The TDS value of finally obtained water was reached to 500 mg/L.

References

[1] Asano, N; Aoki, M; Suzuki, S; Miyatake, K; Uchida, H; Watanabe, M. *J. Am. Chem. Soc.,* 128 (2006) 1762.

[2] Gil, S C; Kim, J C; Ahn, D; Jang, J-S; Kim, H; Jung, J C; Lim, S; Jung, D-H; Lee, W. *J. Membr. Sci*., 417-418 (2012) 2.

[3] Adhikary, S K; Narayanan, P K; Thampy, S K; Dave, N J; Chauhan, D K; Indusekhar, V K. *Desalination*, 84 (1991) 189.

[4] Shah, B G; Shahi, V K; Thampy, S K; Rangarajan, R; Ghosh, P K. *Desalination,* 172 (2005) 257.

[5] Hong, J G; Chen, Y. *J. Membr. Sci*., 473 (2015) 210.

MACRO 141

Modulation of Protein Adsorption and Cell Proliferation on Polyethylene Immobilized Graphene Oxide Reinforced HDPE Bionanocomposites

Upadhyay, Rahul [a]; *Naskar, Sharmistha* [c]; *Bhaskar, Nitu* [a]; *Bose, Suryasarathi* [b*]; *Basu, Bikramjit* [a, c*]

[a]*Laboratory for Biomaterials, Materials Research Center, Indian Institute of Science, Bangalore, India*

[b]*Department of Materials Engineering, Indian Institute of Science, Bangalore, India*

[c]*Center for Biosystems Science and Engineering, Indian Institute of Science, Bangalore, India*

E-mail addresses: rahulupadhyay8303@gmail.com *(Rahul Upadhyay)*

Abstract

The uniform dispersion of nanoparticles in a polymer matrix, together with an enhancement of interfacial adhesion is indispensable towards achieving better mechanical properties in the nanocomposites. In the context to biomedical applications, the type and amount of nanoparticles can potentially influence the biocompatibility. In order to address these issues, High Density Polyethylene (HDPE) based composites reinforced with graphene oxide (GO) were prepared by melt mixing followed by compression moulding. In an attempt to tailor the dispersion and to improve the interfacial adhesion, polyethylene (PE) was immobilized onto GO sheets by nucleophilic addition-elimination reaction.

A good combination of yield strength (ca. 20 MPa), elastic modulus (ca. 600 MPa) and an outstanding elongation at failure (ca. 70 %) were recorded with 3 wt % polyethylene grafted graphene oxide (PE-g-GO) reinforced HDPE composites. In order to assess the cytocompatibility, osteoblast cell line (MC3T3) and human mesenchymal stem cells (hMSCs) were grown on HDPE/GO and HDPE/PE-g-GO composites, *in vitro*. The extensive proliferation of cells with oriented growth pattern also supported the fact that tailored GO addition can support cellular functionality, *in vitro*.

Keywords: *cytocompatibility; graphene oxide; HDPE; nanocomposites; grafting; toxicity; osteoblast; hMSC*

Introduction

Natural bone is a composite of collagen, a polymer matrix and hydroxyapatite, an inorganic reinforcement.[1-2] The load bearing capabilities of the bone gain needs to be critically considered in developing an artificial bone implant.[3-4]

In this work, the hybrid composites of HDPE with graphene oxide (GO) and polyethylene grafted graphene oxide (PE-g-GO) have been developed in the present study. In biomedical field, GO has been used for applications such as tissue engineering, drug delivery, gene delivery and bioimaging. It is envisaged that the dispersion of nanoparticles in a polymer matrix decides the mechanical and cytocompatibility properties of the developed implant. Therefore, polyethylene is grafted onto GO for enhancing the interfacial adhesion with the matrix and henceforth, the dispersion.

In the present study, PE chain is immobilized onto GO surface to improve the structural

properties and enhance the biocompatibility. The stress transfer from the matrix to the filler is expected to improve which eventually will result in enhancing the structural properties to a considerable extent. Efforts were therefore made to improve the mechanical properties of HDPE based composites in which surface modified GO nanoparticles were melt mixed with HDPE. The mechanical and cytocompatibility properties were assessed and compared with the composites filled with unmodified GO sheets. Protein adsorption studies have been performed as it is precursor to cell growth on any substrate. Cell viability and cell adhesion analysis were evaluated for HDPE/GO and HDPE/PE-g-GO composites. Mouse osteoblast cell line (MC3T3) and human mesenchymal stem cells (hMSCs) were selected for all the *in vitro* experiments. It was observed that osteoblast and hMSC growth/adhesion systematically increases with increasing GO content and substantial cell growth was observed for PE-g-GO based composites as compared to unmodified GO based composites. Taken together this study opens up new avenues in designing unique polymeric substrates with enhanced cell growth.

Experimental

Materials and methods

High density polyethylene (HDPE) of density 0.95 g/cc was obtained from Swasan Chemicals (India). Graphite flakes, maleated polyethylene (PE-g-MAH), 4,4-methylene dianiline (MDA), Bovine Serum Albumin (BSA) and WST-1 Assay (Roche) were procured from Sigma Aldrich (USA). The solvents tetrahydrofuran (THF), xylene, toluene, ethanol, and methanol were obtained from Merck (India).

Synthesis of polyethylene grafted graphene oxide (PE-g-GO)

PE-g-MAH and GO-NH_2 (amine functionalized graphene oxide) were blended in HAAKE mini lab melt extruder at a speed of 60 rpm at 100°C in a weight ratio 3:1 to ensure a complete conversion of amine groups of GO-NH_2 to imide groups. From FTIR spectra, it is confirmed that there is no free amine group in PE-g-GO suggesting that all amine groups of GO-NH_2 are converted to imide groups.

This part consists of materials and instrumentation techniques used in the work.

Preparation of nanocomposites

All the nanocomposites (HDPE/GO and HDPE/PE-g-GO) were prepared by using HAAKE minilab melt extruder at rotation speed of 60 rpm maintained at 220°C for the duration of 20 min. The extruded composites were then subsequently compression moulded at 150 °C for 2 min at pressure of 10 Psi.

Mechanical Characterization

Uniaxial tensile testing was carried out using INSTRON 5967 in an effort to measure the yield strength, elastic modulus and % elongation until failure. All the samples were prepared according to ASTM standard, D-638 Type-V for tensile testing. In particular, the dumbbell shape specimens were tested under a cross head speed of 5 mm/min and the loading was continued till specimens were fractured.

Structural and morphological analysis of GO and PE-g-GO

The attenuated total internal reflection fourier transform infrared spectra (ATR-FTIR, Perkin- Elmer) of GO and PE-g-GO were recorded from 4500 to 500 cm^{-1}. Raman spectroscopy (Horiba LabRAM HR) of GO and PE-g-GO were carried out with a 532 nm monochromatic laser. The percentage grafting of polyethylene was evaluated using Netzsch STA 409 PC Thermogravimetry Analyzer (TGA). The SEM micrographs of tensile fractured composites were acquired using FEI, QUANTA (USA) at 10 kV (see figure S2, supporting information).

Cell Culture

Two cell lines, mouse osteoblast precursor cells (MC3T3) and human mesenchymal stem cell (hMSC) were selected to observe their responses towards all the substrate (HDPE, HDPE/GO and HDPE/PE-g-GO composites).

Results and discussion

Characterization of polyethylene grafted GO (PE-g-GO)

The synthesized PE-g-GO was further characterized with the spectroscopic techniques. FTIR spectra of GO and PE-g-GO are shown in Figure 1. The characteristic peaks of PE-g-GO around 2920 cm^{-1} and 2850 cm^{-1} were assigned to stretching frequency of $–CH_2$, while peaks at 1376 cm^{-1} and1640 cm^{-1} were assigned to stretching frequency of C-N (imide) and stretching frequency of imide C=O (Figure 1), respectively.

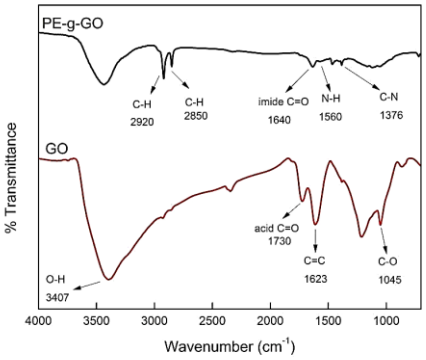


Figure 1: FTIR spectra recorded from as synthesized GO and PE-g-GO

Raman spectroscopy provides signatures of molecular vibrations of Raman-active compounds. In Raman spectrum of GO, the G band was observed at 1585 cm^{-1} which is attributed to the first order scattering of the E_{2g} mode of the sp^2 domain of graphite (C–C scattering).[51] In contrast, the D band at 1351 cm^{-1} corresponds to the defects or breakdown of translational symmetry arising at the edges.[52] The relative intensity ratio of the disorder induced D band to G band (I_D/I_G) of GO was 0.97. In Raman spectrum of PE-g-GO, the position of D and G band were approximately same as in GO but the relative intensity ratio of the disorder induced D band to G band (I_D/I_G) was relatively lower at 0.89. The above observations suggest that the defect and disorder in PE-g-GO are minimum than that of GO.

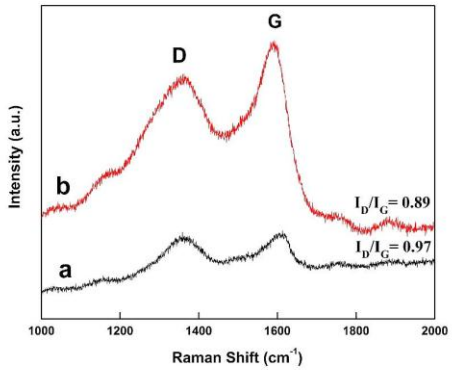


Figure 2: Raman spectra acquired from as synthesized (a) GO and (b) PE-g-GO

Thermogravimetric analysis (TGA) is a technique in which the mass of a compound or a material is dynamically monitored as a function of temperature or time. Figure 3 shows the TGA profile for GO and PE-g-GO. From the measured weight loss, it can be suggested that the percentage of grafted polyethylene in PE-g-GO was approximately 65 %, which is independent of GO content.

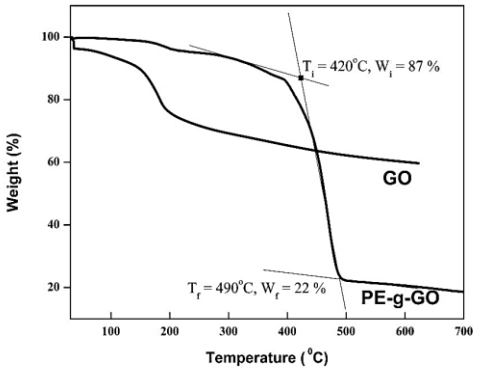


Figure 3: TGA profile recording weight loss for GO and PE-g-GO.

Mechanical Properties of HDPE/GO and HDPE/PE-g-GO bionanocomposites

The uniaxial tensile deformation properties of all the composites were evaluated using ASTM standards at a constant cross head speed of 5 mm/min. The representative engineering stress-strain response of the composites is shown in Figures 4 and 5. Irrespective of the filler type and amount, the initial elastic response was recorded in the entire composite. The non-linear deformation behavior started prior to reaching the yield strength and continued.

The magnitude of the yield strength, elastic modulus and failure strain varied significantly, depending on the presence of GO content (see Table 2 and Figures 4 and 5). The yield strength and the elastic modulus of pure HDPE were found to be 16.4 MPa and 490 MPa respectively, at a cross head speed of 5 mm/min. A significant improvement could be observed in the yield strength (17.4 MPa) and elastic modulus (586 MPa) with the addition of 1 wt % GO (Table 2). The yield strength and elastic modulus were however decreased with the addition of 2 wt % GO and 3 wt % GO, possibly because of the agglomeration or restacking of GO nanoparticles due to hydrogen bonding or electrostatic interaction.

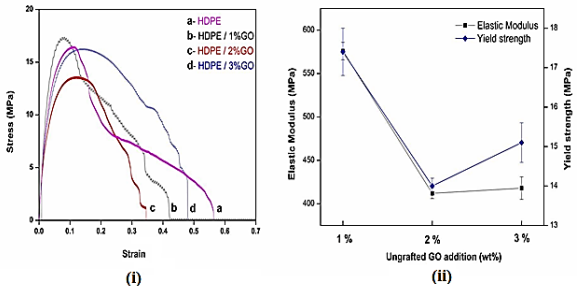


Figure 4: (i) Engineering stress-strain plot for HDPE, HDPE/GO 1 %, HDPE/GO 2 % and HDPE/GO 3 % **(ii)** Plot showing the variation of elastic modulus and yield strength of HDPE composites with different amount of fillers

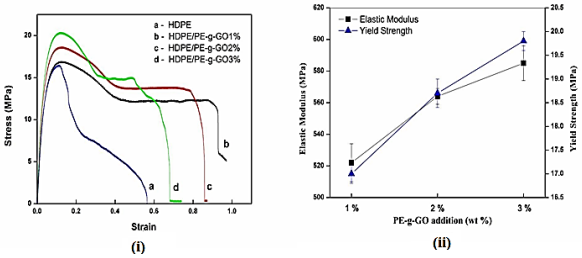


Figure 5: (i) Engineering stress- strain plot for HDPE, HDPE/PE-g-GO 1 %, HDPE/PE-g-GO 2 % and HDPE/PE-g-GO 3 % **(ii)** Plot showing the variation of Elastic Modulus and yield Strength of HDPE composites with different amount of fillers.

Protein adsorption analysis

Protein adsorption study was performed on different substrates (HDPE, HDPE/GO and HDPE/PE-g-GO composites) as per the methodology described in subsection 2.1.4. There is a marked decrease in the absorbance of the bulk solution for HDPE with 3wt% PE-g-GO (figure 8). The depletion of protein infers increased adsorption of protein on the substrate surface. With respect to protein adsorption, the difference between HDPE reinforced with 3 % GO and 3 % PE-g-GO is ca. 13.8 % at 1000 µg/ml bulk concentration. HDPE without any reinforcement shows 29.1 % lower adsorption compared to HDPE reinforced polyethylene grafted 3 wt % GO at the same initial bulk concentration.

MC3T3 osteoblast cell viability analysis using WST-1 assay

Cell proliferation is significantly enhanced for the specified duration of the *in vitro* culture (2 days, 4 days and 6 days) as reflected from the increased OD values (figure 11). The enhanced cell viability can be explained in relation to the substrate composition. The substrate containing 3 % modified graphene oxide in HDPE matrix has been found to have an impressive 150 % enhancement in cell viability at the first observation (i.e. after 2 days of culture), which at the end of 6th day resulted in ca. 300 % increase, with respect to the control (figure 12). As far as the growth rate was concerned, HDPE/PE-g-GO 3 % has supported the highest cell growth. Moreover, surprisingly pure HDPE has also supported osteoblast growth.

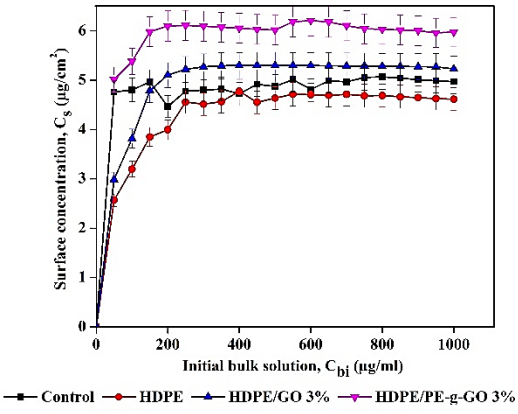


Figure 6: Adsorption of BSA form the bulk solution onto the substrate surfaces.

Conclusions

Taken together, the present study demonstrated the modulation of protein adsorption and cell proliferation on 3 % PE-g-GO reinforced HDPE compared to 3 % GO reinforced HDPE composite together with better comparison of elastic modulus and yield strength. Therefore, it is believed that this developed material could bring a promising candidate for moderate load bearing orthopedic applications.

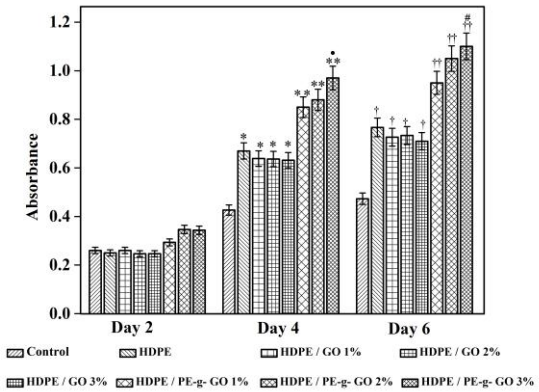


Figure 11: The bar graph for WST-1 assay for MC3T3 shows increased optical density for after modification of the graphene oxide.

Acknowledgements

The authors are grateful for financial support from Department of Biotechnology (Govt. of India) and 'Centres of Excellence and Innovation in Biotechnology' scheme through the Center of excellence project - Translational Center on Biomaterials for Orthopedic and Dental Applications.

References

1. Lombardi, A. V.; Mallory, T. H.; Vaughn, B. K.; Drouillard, P., J. Bone Jt. Surg., Am.Vol. 1989, 71 (9), 1337-1342.
2. Ramay, H. R.; Zhang, M., Biomaterials 2004, 25 (21), 5171-5180.
3. Ng, T. P.; Koloor, S. S. R.; Djuansjah, J. R. P.; Kadir, M. R. A. Adv. Mater. Res. 2014; pp 324-329.
4. Moro, T.; Takatori, Y.; Ishihara, K.; Konno, T.; Takigawa, Y.; Matsushita, T.; Chung, U.-i.; Nakamura, K.; Kawaguchi, H., Nat. Mater. 2004, 3 (11), 829-836.
5. Vasileiou, A. A.; Kontopoulou, M.; Docoslis, A., ACS Appl. Mater. Interfaces 2014, 6 (3), 1916-1925.
6. Gao, L.; Li, Q.; Li, R.; Yan, L.; Zhou, Y.; Chen, K.; Shi, H., Nanoscale 2015, 7 (25), 10903-10907.

MACRO 144

Preparation and Characterization of Crosslinked Anion Exchange Membrane for Water Desalination by Electrodialysis

[a]Chatterjee Uma*, [a]Bhadja Vaibhavee and [b]Jewrajka Suresh K*

[a]*Electromembrane processes Division, CSMCRI, Bhavnagar, Gujarat, India*

[b]*Reverse Osmosis Membrane Division, CSMCRI, Bhavnagar, Gujarat, India*

correspondance to Uma Chatterjee (umac@csmcri.org)

Electrodialysis (ED) technique is based on the transportation of ions through selective membranes under the influence of electrical field. ED process for removal of ionic species in an aqueous medium has been proven to be a efficient technique [1]. The advantages of ED over other separation techniques include low energy cost during desalination, minimum requirement of pre-treatment of feed water and higher membrane life. Thus main applications of ED process are purification of salty water, separation and concentration of high value chemicals. As regards to ED, Anion Exchange Membrane (AEM) is one of the important components used for any separation process. AEMs are also widely employed in different fields of industry, such as in power sources (fuel cells) [2]. Efficient AEMs are mostly prepared through chloromethylation of aromatic ring attached to polymer chains of polysulfone, interpolymer of polyethylene polystyrene followed by quaternization with trimethyl amine [3,4]. However, most of this AEM preparation uses highly carcinogenic and hazardous chloromethyl methyl ether (CME). An alternate method of preparation of AEM is the graft copolymerization of vinyl monomers, such as 4-vinylpyridine and vinylbenzylchloride onto various polymer films using various grafting techniques [5,6]. Homogeneous AEMs were also prepared from poly(2,6-dimethyl- 1,4-phenylene oxide), poly (aryl ether ketone) by benzylic bromination followed by amination reaction [7-9].

Our main objective is the preparation of homogeneous, fully cross-linked conetwork-based AEMs for water desalination by ED. We have prepared two types of ampiphilic conetworks for this purpose [10,11]. The first conetwork has been prepared from amphiphilic copolymer of polyacrylonitrile-co-poly(2-dimethylaminoethyl)methacrylate (PAN-co-PDMA) containing 28 wt% of PDMA in the copolymer. The second conetwork has been prepared from the terpolymer of polyacrylonitrile-co-polyn-butylacrylate-co-poly(2-dimethylaminoethyl)methacrylate (PAN-co-PnBA-co-PDMA) containing 17-18wt% PnBA and 28-30wt% PDMA part. Both the PAN-co-PDMA copolymer and PAN-co-PnBA-co-PDMA terpolymer easily undergoes quaternization and forms cross-linked network by treatment with alkyl iodide and hydrazine hydrate respectively. Table 1 shows the comparative physical properties such as equillibrium water uptake and electrochemical properties such as ion-exchange capacity, membrane conductivity and trasport number of the prepared AEMs and also for three different types of commercial AEMs.

Table 1. Physical and electrochemical properties of AEMs

AEM	Water uptake (%)	Ion exchange capcity ($meqg^{-1}$)	Transport number	Membrane conductivity ($mScm^{-1}$)
PAN-co-PDMA	19	1.30	0.92	2.22
PAN-co-PnBA-co-PDMA	13	1.45	0.93	4.57
ACS (commercial)	25	1.2-1.4	0.95	2.50
ARA (commercial)	12.4	0.92	0.90	1.50
IONSEP (commercial)	40	1.8-2.2	0.91	3.23

The water uptake of PAN-co-PnBA-co-PDMA based AEM is close to the ARA membrane and is lower than that of other membranes listed in Table 1. The water uptake of this AEM is also lower than bicomponent PAN-co-PDMA based AEM. This may be due to presence of phase separated hydrophobic PnBA. Both type of prepared AEMs exhibited high ion exchange capacity, high trasport number and high ionic conductivity like the commercial membranes. This is attributed to the synergistic effect of both higher PDMA content (higher anion exchange site, QPDMA) and low degree of water uptake (low diffusion of water) in both types of AEMs.

The water desalination experiments were carried out separately using 5 pieces of both types of AEMs and polyethylene-polystyrene interpolymer based CEM in small ED unit (effective area 65 cm^2) under recirculation mode of operation at 10 volt applied potential. The feed NaCl solution of concentration 2000 mg/L was circulated in both the diluate and concentrate compartments at a flow rate 5.4 L/hr. Figure 1 shows the decrease of NaCl concentration with time during ED experiment using both types of AEMs.

The power consumption and current efficiency during desalination process have been calculated. The terpolymer based AEM exhibited 0.95 $KWhKg^{-1}$ power consumption and 96% current efficiency whereas the bicomonent copolymer exhibited 1.15 $KWhKg^{-1}$ power consumption and 80% current efficincy.
Therefore, the remarkable effect on the desalination performance of AEM was observed when the AEM contains 18 wt% of PnBA and minimum of 32 wt% of PDMA [10, 11].

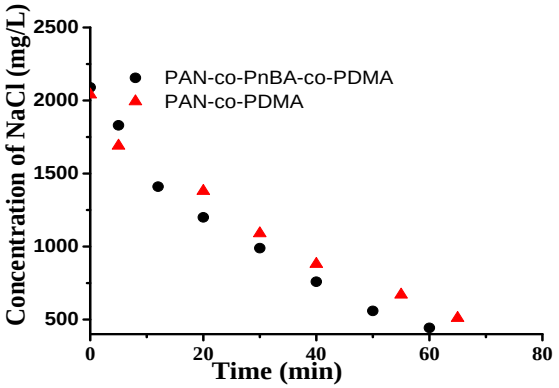


Figure 1. Concentration of NaCl vs desalination time during ED with both types of AEMs

References

[1] Tanaka, Y. *Desalination*, 249 (2009) 809.

[2] Hickner, M A; Ghassemi, H; Kim, Y S; Einsla, B R; McGrath, J E. *Chem. Rev*., 104 (2004) 4587.

[3] Wang, G; Weng, Y; Chu, D; Chen, R; Xie, D. *J. Membr. Sci.*, 332 (2009) 63.

[4] Shah, B G; Shahi, V K; Thampy, S K; Rangarajan, R; Ghosh, P K. *Desalination*, 172 (2005) 257.

[5] Kostov, G; Turmanova, S. *J. Appl. Polym. Sci.*, 64 (1997) 1469.

[6] Merle, G; Chairuna, A; Van de Ven, E; Nijmeijer, K. *J. Appl. Polym. Sci*., 129 (2013) 1143.

[7] Xu, T W; Zha, F F. *J. Membr. Sci*., 199 (2002) 203.

[8] Shen, K; Pang, J; Feng, S; Wang, Y; Jiang, Z. *J. Membr. Sci.*, 440 (2013) 20.

[9] Xu, T W; Yang, W H. *J. Membr. Sci.*, 190 (2001) 159.

[10] Chatterjee, U; Jewrajka, S K. *J.Mater.Chem. A*, 2 (2014) 8396.

MACRO 146

Thermally and pH Responsive Poly(dimethyl aminoethyl)methacrylate-*b*-Poly(N-isopropyl acrylamide)/Polycaprolactone Amphiphilic Conetwork Gels

[a,b]Jewrajka Suresh Kumar*, [a,b]Chandel Arvind K Singh and [a]Bhingaradiya Nutan

[a]Reverse Osmosis Membrane Division, AcSIR-Central Salt and Marine Chemicals Research Institute, CSIR-Central Salt and Marine Chemicals Research Institute, G. B. Marg, Bhavnagar, Gujarat 364002, India

[b]AcSIR-Central Salt and Marine Chemicals Research Institute, CSIR-Central Salt and Marine Chemicals Research Institute G. B. Marg, Bhavnagar, Gujarat 364002, India

Email: skjewrajka@csmcri.org

Amphiphilic conetwork (APCN) gel is a cross-linked polymer network which swells both in water and organic solvent. APCN gels attracted wide attention due to their varieties of applications. For example, APCN gels are used in tissue culture [1, 2], controlled delivery of hydrophobic and hydrophilic drugs [3, 4], electrodialysis membranes [5], and immunoisolation membranes [6]. APCN are mostly synthesized by macromonomer method via polymerization of macromonomer containing at least two polymerizable groups in presence of molecular weight monomer.

Our main objective is the synthesis of biodegradable/biocompatible as well as pH and temperature responsive APCN gels for biomedical application using multifunctional polymers and copolymers. We selected naturally available FDI approved polycaprolactone (PCL) or its copolymer with polyethylene glycol e.g. PCL-*b*-PEG-*b*-PCL and pH and temperature responsive di-block copolymer such as poly(dimethyl aminoethyl)methacrylate-*b*-poly(N-isopropyl acrylamide) (PDMA-*b*-PNIPAM) for construction of APCN gels. Tertiary amine functional Agr and activated halide terminated PCL was combined to obtain APCN gels [4, 5]. The property of the obtained APCN gels were controlled by the use of halide terminated tri-block copolymer of PCL and polyethylene glycol i.e. PCL-*b*-PEG-*b*-PCL [4]. Herein, we report pH and temperature responsive APCN gels of PDMA-*b*-PNIPAM and PCL or PCL-*b*-PEG-*b*-PCL. Sequential nucleophilic substitution reaction of tertiary amine groups of PDMA-*b*-PNIPAM and activated halide groups PCL or PCL-*b*-PEG-*b*-PCL gave multicomponent gels which swell both in water and in toluene. The gels containing different amount of PCL were prepared (Table 1). These gels were prepared by reacting DMF solution of PDMA-*b*-PNIPAM and halide terminated PCL or PCL-*b*-PEG-*b*-PCL. Rapid gelation occurs at 50 ^{o}C. Removal of solvent by evaporation followed by extraction with water gave highly transparent gels.

Table 1 shows the composition, swelling and sol fraction of the different APCN gels obtained by the sequential nucleophilic substitution reaction. Low degree of sol fraction in DMF indicates efficient gelation reaction between PDMA-*b*-PNIPAM and halide terminated PCL or PCL-*b*-PEG-*b*-PCL. This APCN gels swelled in water as well as in toluene while maintained the transparency of the films. This indicates co-continuous nanophase morphology of the gels. A negatively charge Rose Bengal dye distributed into the gel matrix homogeneously. This also indicated nanophase co-continuous structure and positive charge character of the gels.

All the APCN gels (Table 1) exhibited pH and temperature responsive water swelling. The swelling of gels were higher at lower pH and temperature. This effect is due to pH and temperature responsive property of PDMA-*b*-PNIPAM copolymer which was synthesized by reversible addition and fragmentation chain transfer polymerization (RAFT). The unreacted DMA moieties of the copolymer in the gels undergo enhanced protonation at lower pH and enhanced the water swelling. On the other hand, PNIPAM chains showed enhanced water swelling at lower temperature due to enhanced formation of hydrogen bond with water. The lower critical solution temperature of PNIPAM is reported to be ca. 32 ^{o}C.

The swelling of the gels can be controlled by changing the PCL amount in the gel. For example, Gel-1showed lower amount of water swelling than that of Gel-2 and Gel-3. Mechanically milled particles of the gels were soft and were injectable through hypodermic syringe of needle size 20-G. The gels particles also exhibited similar swelling properties as that of films.

Table 1. Synthesis conditions, sol fraction and water swelling of APCNs gels.

APCN	PCL or PCL-*b*-PEG-*b*-PCL/PDMA-*b*-PNIPAM-2 (w/w, %)	Sol fraction in DMF (%)	Equilibrium Swelling[z]	
	Reaction mixture		pH 7.4	pH 5
[x]Gel-1	1/1	3.2	197/169/120	220/190/140
[y]Gel-2	1/1	3.5	210/185/142	240/201/156
[x]Gel-3	1/0.5	5.7	240/201/174	267/226/190

x-PCL; y- PCL-*b*--PEG-*b*-PCL, z- swelling was measured at 17 ºC, 27 ºC and 37 ºC.

References

[1] Rimmer, S; German, M J; Maughan, J; Sun, Y; Fullwood, N; Ebdon, J; MacNeil, S. *Biomaterials*, 26) 2005(2219.
[2] Behravesh, E; Jo, S; Zygourakis, K; Mikos, A G. *Biomacromolecules*, 3) 2002 (374.
[3] Bera, A; Chandel, A K S; Kumar, C U; Jewrajka, S K. *J. Mater. Chem. B*, 3)2015(8548.
[4] Chandel, A K S; Kumar, C U; Jewrajka, S K. ACS *Appl. Mater. Interfaces*, 8) 2016(3182.
[5] Chatterjee, U; Bhadja, V; Jewrajka, S K. *J. Mater. Chem. A*, 2) 2014(16124.
[6] Guzman, G; Nugay, T; Nugay, I; Nugay, N; Kennedy, J .P Cakmak, M. *Macromolecules*, 48)2015(6251.

MACRO 147

Tailoring pyrazoline–aromatic donor based luminescent polymers for organic-electronics.

T.Vandana, A.Karuppusamy, P. Kannan*,[a]

[a] *Department of Chemistry, Anna University, Chennai, 600025, India*

* *e-mail id:* pakannan@annauniv.edu

Abstract

Four pyrazoline–aromatic donors forming polymers were synthesized successfully by Suzuki coupling method and described. The Pyrazoline (PP) was synthesized from Claisen-Schmidt condensation followed by cyclisation to give luminescent monomer. Pyrazoline are well-known for their blue fluorescence. Here we are able to tailor their conjugation length and band gap by polymerizing them with electron rich donor group like phenylene (PPB), anthracene (PPA) and thiophene (PPT) and benzathiadiazole (PPBta) an electron deficient compound by Suzuki cross-coupling polycondensation .The polymers band gap had be tailored such that it emits a part of visible spectrum from blue to orange. Structural conformation and stability pattern were determined. Polymers are soluble in common organic solvents and display absorption of 360 nm to 460 nm. The polymeric solutions exhibit emission from blue to orange in the range of 440 nm to 570nm. Absorbance and emission spectra experience a bathochromic shift with increasing aromatic ring to heteroaromatic ring systems. Cyclicvoltammetry studies reveals quasi-reversible oxidation potentials for the polymers synthesized falls in the range of 1.0 to 1.4 V and reduction potential of -0.05 to -0.3 V through which HOMO–LUMO energy levels were determined. Electrochemical band gap had been calculated as they fall in between 1.3 to 1.6eV. Both Photophysical and electrochemical behavior made the polymers apt for Organic-Electronics.

Keywords: *PLED; Organicelectrinics; chalcones; Pyrazolines*

Introduction

The semiconducting polymers have been developed signaling the birth of a futuristic technology of polymerelectronics and molecular-electronics. Polymer light emitting devices (PLEDs) have drawn much attention because of their large p-conjugated backbones, delocalizedelectronic structures, low cost, ease of modification of properties by appropriate substitution, and of solvent processability[1-3]. Among various PLEDs, the blue emitting material is still scarce and desired much more for the development of current PLEDs[4]. Compared to organic small molecule light-emitting materials, the most obvious advantage of the polymer light-emitting materials lies in allowing adjustment of their properties by the facile design and modification[5-7].

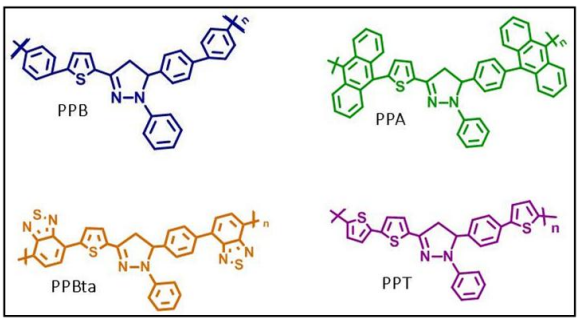


Fig. 1 The molecular structures of polymers.

Pyrazoline is a typical hole-transfer material, and these dyes containing various aromatic units have excellent photo-conductivity and relatively intense luminescence. Conjugated polymers with pyrazoline units on aromatic backbone display strong brightness and high stability have been widely applied as reasonable host materials in OLED and PLED[8-11]

Our contribution is aimed in describing the synthesis and characteristic property of newly synthesized polymers one very attractive aspect of the polymers are they can be accessed from relatively simple methodology as shown in Scheme 1.The raw materials chosen are phenylene, anthracene, thiophene and benzathiadiazole as the chromophores on pyrazoline polymer backbone. The aim of preparing electron-rich materials that possess inheritant hole transporting ability of pyrazoline would be for application in OLEDs, organic photovoltaics (OPV), and organic thin-film transistors (OTFTs). To achieve solution processability, phenyl groups are capped on pyrazoline the conjugated moieties. As illustrated in Scheme 1, all the polymers were synthesized by Claisen smidt condensation to cyclisation followed by Suzuki cross-coupling reaction, respectively All of the compounds are readily soluble in common organic solvents such as $CHCl_3$, CH_2Cl_2, THF, and toluene, and recrystallized by ethanol. ^1H and ^{13}C NMR spectra and IR were employed to confirm the structure and purity of all compounds. Molecular weight distribution, optical and electrochemical properties were investigated using GPC, UV, fluorescence spectroscopy and cyclic voltammetry.

Experimental

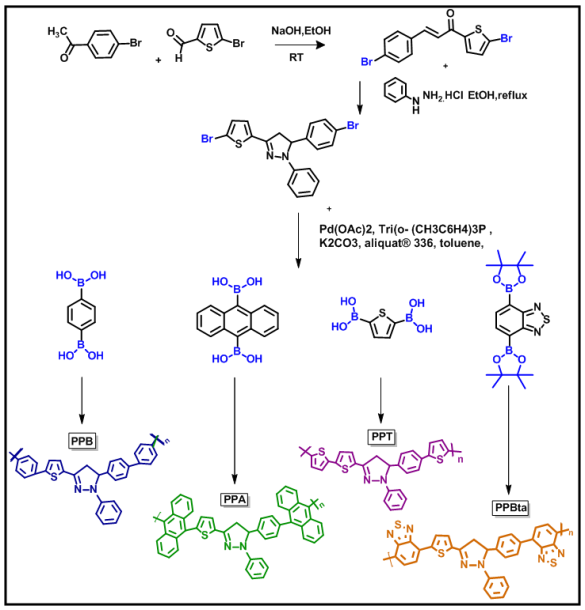
Materials and methods

All the chemicals 4-bromoacetophenone, 5-bromo-2-thiophenecarboxaldehyde, sodium hydroxide, ethanol, Phenylhydrazine hydrochloride, Palladium (II) acetate, Tri(o-tolyl)phosphine, potassium carbonate, aliquat®336, toluene, 1,4-Benzenediboronic acid bis(pinacol) ester, 2,5-Thiophenediylbisboronic acid, 9,10-Anthracenediboronic acid bis(pinacol) ester, 2,1,3-Benzothiadiazole-4,7-bis(boronic acid pinacol ester, were purchased from Sigma Aldrich

The synthesized polymers are structural analysised by FT-IR, ^1H NMR and GPC. The photophysical properties are studied by Absorption, Emission Spectrophotometer and life time analysis. The electrochemical behaviors of polymers are determined by cyclic voltammetry.

Chalcones were synthesized by reacting equimolar quantity of 5-bromo-2-thiophenecarboxaldehyde and 4-bromoacetophenone in ethanol at RT. These are then cyclised using phenylhydrazine hydrochloride under reflux in ethanol. The pyrazoline formed are

polymerized by Suzuki cross coupling reactions



Scheme 1 The synthesis route of polymers.

Results and discussion

Photophysical Properties

Fig.1 display an UV-Vis absorption and photoluminescence (PL) spectra for all the four polymers are (PPB, PPA, PPT, PPBt) in dichloromethane (CH_2Cl_2) (10^{-5} mol L^{-1}). The absorption spectra for all the compounds exhibit their bands at 307-450 nm. Polymers (PPB, PPA, PPT) exhibit absorption maxima (λ_{max}) at 366, 374, 388 nm which is reasoned due to π-π* transfers from donors linked to pyrazoline polymer backbone. PPBt alone exhibits three absorption bands in from 304-450 nm and (λ_{max}) at 444 nm. A gradual red shift on introducing a polyheterocycle as relative strength of donating ability benzathiadiazole which is well known for its electron delocalisation nature, that tunes the properties of pyrazolines polymers on their absorption spectra.

Emission images and spectra were recorded for all the polymers in solution state as shown in Fig.2. and Fig.3. The luminescence spectra was recorded for the first three polymers (PPB, PPA, PPT) with an excitation wave length 376 nm while the fourth polymer (PPBt) was carried out with 445 nm respectively. The three polymers with donors of benzene, anthracene, and thiophene exhibit a similar kind of emission 446 nm, 458 nm, 465nm and intense red shift seen in the polymer (PPBt) at 570 nm.

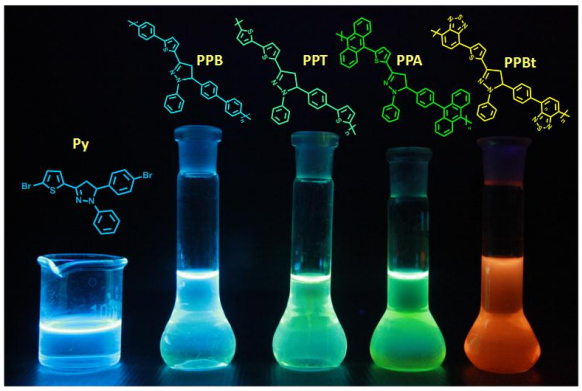


Fig.2 The emission images of polymers

The first three polymers wherein aromatics and heterocyclic segments on pyrazoline polymer backbone exhibit emission from 440-470 nm due to mainly charge transfer transitions. Whereas fused heterocyclic of benzathiadiazole on pyrazoline polymer framework are duly determined by non planarity in these heterocyclic chromophores is deemed to effectively reduce the intermolecular π-π stacking and prevent chromophore aggregation, thus diminishing the fluorescence quenching. In addition to that emission band is more or less like a mirror image to the absorption band with a minimum strokes shift of 83, 77 nm in (PPA, PPT)polymers, while in (PPB, PPBta) it is

110, 126 nm. The large strokes shift is seen in those conjugated polymers that undergo additional energy migration. PPB polymer depict an surprisingly an large stoke shift as due to para substituted phenylene to pyrazoline results for more intramolecular charge transfer due to less twisted molecular configurations. Polyheterocycle (PPBt) polymers are prone to large stokes shift as it undergoes an easy energy transfer process and conformational relaxation.

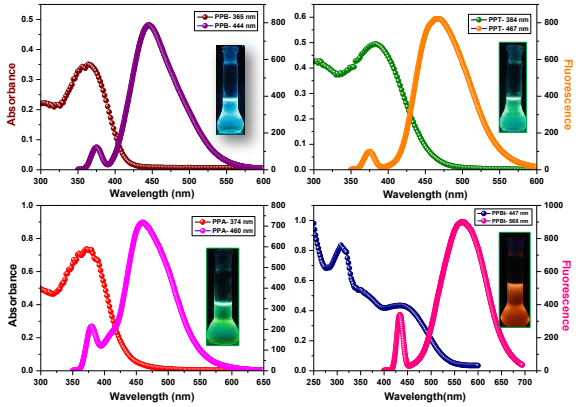


Fig. 2 The absorption and emission spectra of polymers.

Fluorescence lifetime

Quantitative fluorescence lifetime measurements enable investigators to distinguish between fluorophore that have similar spectral characteristics but different lifetimes, and can also yield clues to the local environment. Hence the fluorescence lifetime values of four polymers were measured by TCSPC analysis using $CHCl_3$ as solvent and depicted in Fig.3. It is observed that the decay time varies depending on donors in the molecular structure of polymers. The calculated decay time of polymers are PPB for 2.97, PPT for 3.2, PPA for 3.8 and PPBt for 1.64 ns respectively. PPT is accompanied with exponential decay of high fluorescence quantum yield (Φ) that reveals domination of radioactive relaxation pathway.

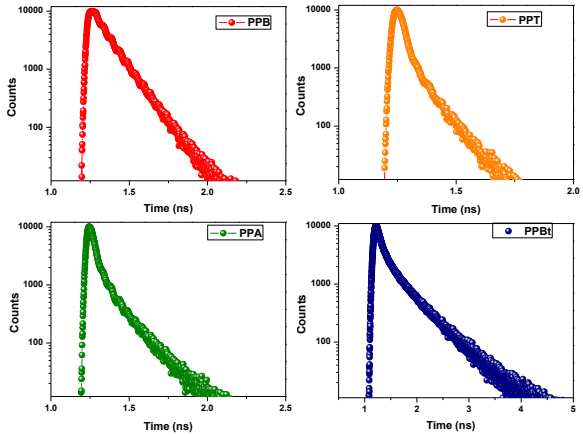


Fig. 3 The lifetime decay curves of polymers

Electrochemical studies

Electrochemical methods such as cyclic voltammetry provide a means of calculating the HOMO and the LUMO energies of conjugated systems and there by band gaps. These values are playing a major role in choosing cathode and anode materials in an OLED or photovoltaic device, selecting an appropriate host polymer in a PLED. Cyclic voltammetry (CV) in CH_2Cl_2 solution yielded determines the oxidation and reduction potential for the respective polymers and values to estimate their HOMO and LUMO energy levels. From their respective onset oxidation potentials (E_{onset}^{ox}) and onset reduction potentials (E_{onset}^{red}) of the polymers, their LUMO and HOMO energy levels from which their electrochemical band gap were calculated based on the Bredas equations. The results suggest that PPT has an HOMO level could be reached lowest value of -6.13 eV and that of PPB has the highest value of -5.97 eV and PPA, PPBt appear to be in between values of

-6.03, -6.09 respectively. Corresponding LUMO energy level of polymers PPB, PPA, PPT, PPBt are -4.5, -4.71, -4.52 and 4.75 eV respectively. Polymers PPA and PPBt posses negatively higher values indicating that electron injection process is easier in them when compared to rest of the other two polymers. The electrochemical band gaps for the polymers (PPB, PPA, PPT, and PPBta) are 2.9, 2.7, 2.61, and 2.2 respectively.

Conclusions

Here we come with the synthesis of various pyrazoline hooked polymers where its photophysical and electrochemical properties are studied and determined. The polymer is synthesized in good yields and portrays a wide solubility in most of the organic solvents. A well dependency on the electronic properties is significantly influenced by the substituents. The UV-visible absorption and emission pattern of these showcase colors of blue, green and orange based on the substituents that much in need for a fluorescence-based application. Looking on to further their electrochemical properties reveal their Homo energy can well tuned ranging from -5.9 to 6.09 eV opens flexibility during fabrication module.

Acknowledgements

T.V and A.K gratefully acknowledge the UGC-BSR and DST-SERB for their respective fellowship. The instrumentation facility provided under DST-FIST and UGC-DRS to Department of Chemistry, Anna University is sincerely acknowledged.

References

7. Suzuki, Mitsunori, "Highly efficient polymer light-emitting devices using ambipolar phosphorescent polymers." Applied Physics Letters 86.10 (2005): 103507.
8. Brédas, Jean-Luc, "Conjugated polymers and oligomers: Designing novel materials using a quantum-chemical approach." Advanced Materials 7.3 (1995): 263-274.
9. Yip HL, Jen AK, Recent advances in solution-processed interfacial materials for efficient and stable polymer solar cells. Energy & Environmental Science. 2012;5(3):5994-6011.
10. Li Y, Wu Y, Zeng W, Li Y, Xu L, Qiu X, Chen R, Huang W. Improving Efficiency of Blue Organic Light-Emitting Diode with Sulfobutylated Lignin Doped PEDOT as Anode Buffer Layer. ACS Sustainable Chemistry & Engineering. 2016 Mar 23;4(4):2004-11.
11. Ajantha, Joseph, "Photophysical and charge transport properties of pyrazolines." RSC Advances 6.1 (2016): 786-795.
12. Kim, Myoung Ki, "A bipolar host containing 1, 2, 3-triazole for realizing highly efficient phosphorescent organic light-emitting diodes." New Journal of Chemistry 34.7 (2010): 1317-1322.
13. Vandana, T., V. Ramkumar, and P. Kannan. "Synthesis and fluorescent properties of poly (arylpyrazoline)'s for organic-electronics." Optical Materials 58 (2016): 514-523.
14. Osken, Ipek "Fluorene–dithienothiophene-S, S-dioxide copolymers. Fine-tuning for OLED

applications." Macromolecules 46.23 (2013): 9202-9210.
15. Parker, Timothy C, "Heteroannulated acceptors based on benzothiadiazole." Materials Horizons 2.1 (2015): 22-36.
16. Parker TC, Patel DG, Moudgil K, Barlow S, Risko C, Brédas JL, Reynolds JR, Marder SR. Heteroannulated acceptors based on benzothiadiazole. Materials Horizons. 2015;2(1):22-36.
17. Dias FB, Pollock S, Hedley G, Pålsson LO, Monkman A, Perepichka II, Perepichka IF, Tavasli M, Bryce MR. Intramolecular charge transfer assisted by conformational changes in the excited state of fluorene-dibenzothiophene-S, S-dioxide co-oligomers. The Journal of Physical Chemistry B. 2006 Oct 5;110(39):19329-39**.**

MACRO 155

Planar Heterojunction Perovskite Solar Cell with Poly(3-thiophene acetic acid) as Hole Transporting Layer under Ambient Condition

Arnab Shit and Arun K. Nandi*

Polymer Science Unit, Indian Association for the Cultivation of Science, Jadavpur, Kolkata -700 032, India
**E-mail: psuakn@iacs.res.in*

The properties of a methyl ammonium lead iodide ($MAPbI_3$) perovskite solar cell with poly(3-thiophence acetic acid) (P3TAA) as hole transporting material (HTM) and a dense layer of ZnO nanoparticles film as electron transporting material (ETM) is described using the conventional ZnO(n)/Perovskite (i)/P3TAA(p) (n-i-p) architecture. The interface between different layers of the perovskite solar cell may have large effects on the power conversion efficiency (PCE) and in an attempt here an acid derivative of polythiophene e.g. P3TAA has been chosen where the –COOH groups have a possibility to interact with perovskites through their NH3 group, which may provide a good mixing at the interface facilitating easy transfer of holes.

The X-ray diffraction (XRD) patterns of $MAPbI_3$ represent the diffraction planes of its tetragonal phase suggesting the complete conversion of PbI_2 to $MAPbI_3$ under the device preparation procedure. The FT-IR spectra of $MAPbI_3$/P3TAA mixture indicates shift of N-H stretching peak and abolition of N-H bending peak indicating an interaction between the components. The UV-Vis spectra of the mixture exhibit a large red shift of π-π* transition peak of the conjugate chain arising from the interaction causing increase of conjugation length. The surface SEM image shows the formation of packed crystallites of $MAPbI_3$. The cross sectional SEM image of the device shows the sequence of the individual layers of ZnO, $MAPbI_3$, P3TAA and Ag, respectively with the thickness of the individual layers are measured to be 222, 228, 70 and 105 nm, respectively. The current density (J) – voltage (V) curves on illumination with a light intensity of 100 mW/cm^2 indicate a hysteresis in the reverse bias than that of forward bias and the average PCE is measured to be 7.38±0.59% at ambient atmospheric condition. The IPCE values of this cell reach about 63% across a broad range of wavelength (300–800 nm). The HOMO and LUMO of P3TAA is measured from cyclic voltammetry and optical band gap and the relative energy level of the components explain the operation of photocurrent in the cell. The longevity of the cell is found to be satisfactory for storing under ambient condition without encapsulation.

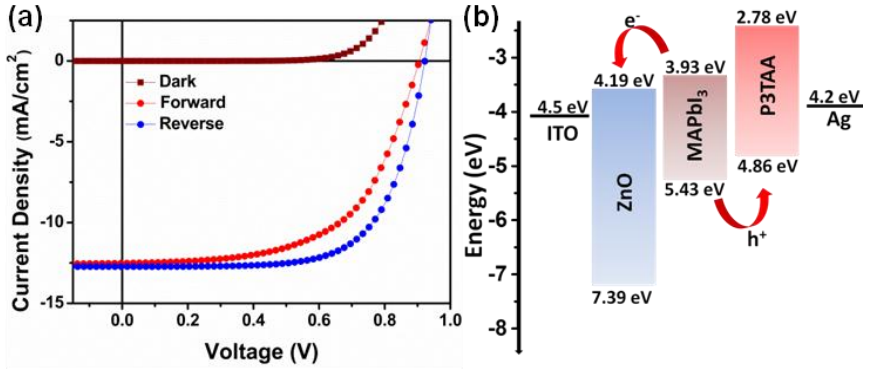


Figure 1. (a) J-V characteristics plot for the ITO/ZnO/$MAPbI_3$/P3TAA/Ag device under dark and AM 1.5G 100 mW/cm^2 illumination measured with forward and reverse scan directions, (b) Schematic representation of the band energy diagrams.

A device using P3HT as the HTM instead of P3TAA have also been fabricated under similar conditions for comparison purposes and the PCE is found to be 5.85±0.51%, which is lower than that of the P3TAA system. The longevity of the P3TAA based cell is found to be better than that of the P3HT based cell for storing under ambient conditions in air. The UV-Vis and impedance spectral results clearly explain the influence of interface on the PCE of the hybrid solar cells.

References

[6] Shit, A; Nandi, A, K; *Phys.Chem.Chem.Phys.*, 18 (2016) 10182.

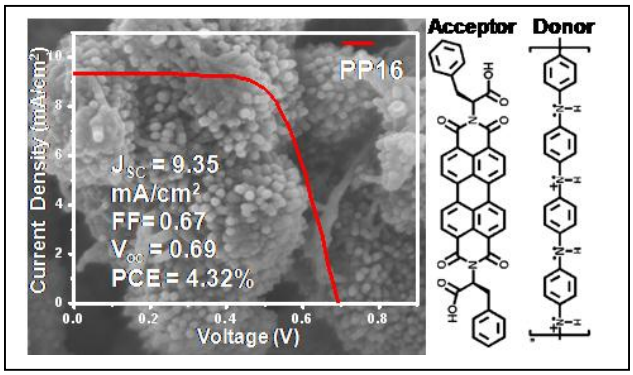
MACRO 156

A Potential polyaniline and Perylene Diimide Based Acceptor Material for Highly Efficient Dye sensitized solar cell with 4.32% Efficiency.

Pousali chal, Arnab Shit, and Arun K. Nandi*

The Polymer Science unit, Indian Association for the Cultivation of Science, Jadavpur, Kolkata-700032, India.
E-mail: psuakn@iacs.res.in

Abstract: In last two decades, organic photovoltaic devices, primarily bulk heterojunction solar cells, have progressed much in device performances but the requirement of crystalline nanoscale phase separated domain has limited the modular characteristic of the approach and very specific donor : acceptor blends are preferred. Here, we show an alternative organic photovoltaic platform with dye sensitized architecture pertaining excellent modular characteristic. Aniline in situ polymerized in presence of different amounts of N,N-di((S)-1-carboxylphenylalanine)-3,4:9,10 perylenetetracarboxyldiimide(PPA, 10, 12, 16, 20 mg) in citric acid medium, results the composites designated as PP10, PP12, PP16 and PP20, respectively. Dye-sensitized organic solar cells fabricated with PP16 and N719 dye exhibit highest power conversion efficiency (PCE) of 4.32 %. SEM study reveals dense rod like nanoshpere morphology; FTIR, UV-Vis, and photoluminescence spectra suggest the presence of π-stacking interaction between PPA and PANI. IPCE results exhibit a maximum of 62% conversion of incident photon absorbing in the range 360–650 nm. The impedance spectra of the devices displayed three semicircles for all the different composites systems, representing a complex equivalent circuit diagram consists of three resistance and capacitance circuits. Lifetime of photo-injected electron measured from the impedance spectra confirm that PP16 device has highest lifetime (7.7mS) accounting the highest PCE. Comparison with the PCE of a reference device clearly indicates the influence of dopant acid of PANI and influence of interfacial interaction through π-stacking process towards photovoltaic performance. The work presented here will open up a new paradigm for further development of novel organic photovoltaic solar cells.



References

[7] Chal, P.; Shit, A.; Nandi, A. K., *J. Mater. Chem. C*, 4 (2016), 272.

MACRO 158

Development of Electrochemical Sensor for the Detection of Creatinine with Silane Functionalized Graphene Oxide Based Molecularly Imprinted Polymer film

Anirudhan T S*, Deepa J R, Nisha Stanly, Shainy F, Anoop. S. Nair, Manasa Mohan.A

[a]*Department of Chemistry, School of Physical and Mathematical Sciences, University of Kerala, Kariavattom, Trivandrum-695 581, Kerala*

* *tsani@rediffmail.com*

Creatinine is a break down product of creatine which is an important part of muscle and is normally removed from the blood by kidney. But when kidney functions slows down, Creatinine (Cn) level rises [1]. Chronic kidney disease (CKD) is often observed in diabetes and hypertension persons. Glomerular filtration rates (GFR) reveals how much kidney dysfunctions and may be estimated from the level of Cn. If GFR falls below 15 indicates that need to start treatment towards kidney dysfunction. Hence detection of Cn is very important. Cn, 2- amino-1-methyl -2- imidazoline 4-one is the final product of creatine metabolism in mammals. It is essential that the clinical measurements of Cn level in human blood and urine is done periodically because it partly reflects the renal muscular and thyroid function [2]. In hem- dialysis therapy it is also useful for biomedical diagnosis of acute myocardial infarction. In contrast to urea, the concentration of Cn in these body fluids is not influenced by protein intake. So its level is more reliable indicator of renal dysfunction. Kidney transplant recipient who have abnormally high Cn levels in their blood often have allograft dysfunction secondary to rejection. The patients having kidney dysfunction, should periodically check to determine the Cn level, since it is an important marker for renal dysfunction of kidney [3]. Jaffe's reaction or enzymatic colorimetric method is the most common method for analysis of Cn, which is affected by numerous metabolites and drug found in biological samples. To overcome these limitations, cylic voltammetric technique can be used for Cn determination. It is an attractive method due to fast response, high sensitivity, feasibility and suitability for real time detection. Among all the sensors, electrochemical Cn sensors are used due to its simplicity of design and construction. Molecularly imprinted polymer (MIP) technique is one of the most convenient methods for recognition of Cn due to its selectivity and sensitivity [4].

In the present work, a biomolecule sensor, silynated GO co polymerized with Methyl Methacrylate and 2-HydroxyMethacrylate [TMSPMA-GO-co-HEMA/MMA] was synthesized as shown in **Fig. 1.** Silane functionalized GO was prepared, to create a double bond on the GO surface. Here 3-(tri methoxy silyl propyl) methacrylate (TMSPMA) as silynation agent, whose long chain could impart more spacing between polymer chain and GO above which creatinine imprinted polymer was synthesized by means of polymerization. silynated GO polymerized with a pre-polymerization mixture. Thus the polymer chains grafted onto the surface of the silynated GO, form a strong covalent bonding between silynated GO and polymer matrix. Pre-polymerization mixture was prepared by using 2-Hydroxyethyl methacrylate (HEMA), Cn (template) and Methyl methacrylate (MMA). Two monomers can effectively interact with two functional moieties in the Cn. In the first part of grafting, the silyl functionalized GO undergoes reaction with pre-polymerization mixture in presence of ethylene glycol dimethacrylate (EGDMA) as cross linker and 2,2'-azobisisobutyronitrile(AIBN) as initiator. The physical and chemical properties of resulted material was characterized by FTIR, NMR, RAMAN, XRD, SEM and AFM techniques.

The IR data successfully explains the formation of bond between GO and TMSPMA. MIP without Cn gave peak at 1718 and 1631 cm^{-1} clarifies the functionalities of MMA and HEMA onto the MIP Matrix. The peak at 1150cm^{-1} is due to the retaining of Si-O-C bond in MIP. A broad peak at 3379 – 2974 cm^{-1} indicates the –OH functionalities of MIP. By comparing XRD pattern of Cn-MIP and MIP the peak at 6.60^0 of Si-GO broadened than that of MIP without Cn on the TMSPMA-GO-co-HEMA/MMA polymer. In NIP, XRD peaks are entirely different from MIP, indicating the non-specificity of NIP for the Cn binding in the polymer surface. In the SEM image of MIP-TMSPMA-GO-co-HEM/MMA some visible irregular and large number of pores is present on the surface of MIP. The effective pH for the response of the sensor material was found to be 6.0. Voltammetric profiles typically arising from the direct oxidation of Cn at concentrations ranging between 0 mM and 200 mM in pH 9.4 PBS with 150 mM NaOCl electrolyte. The feasibility of prepared sensor material in real life situation was successfully verified to determine Cn in blood and urine samples collected from kidney patients.

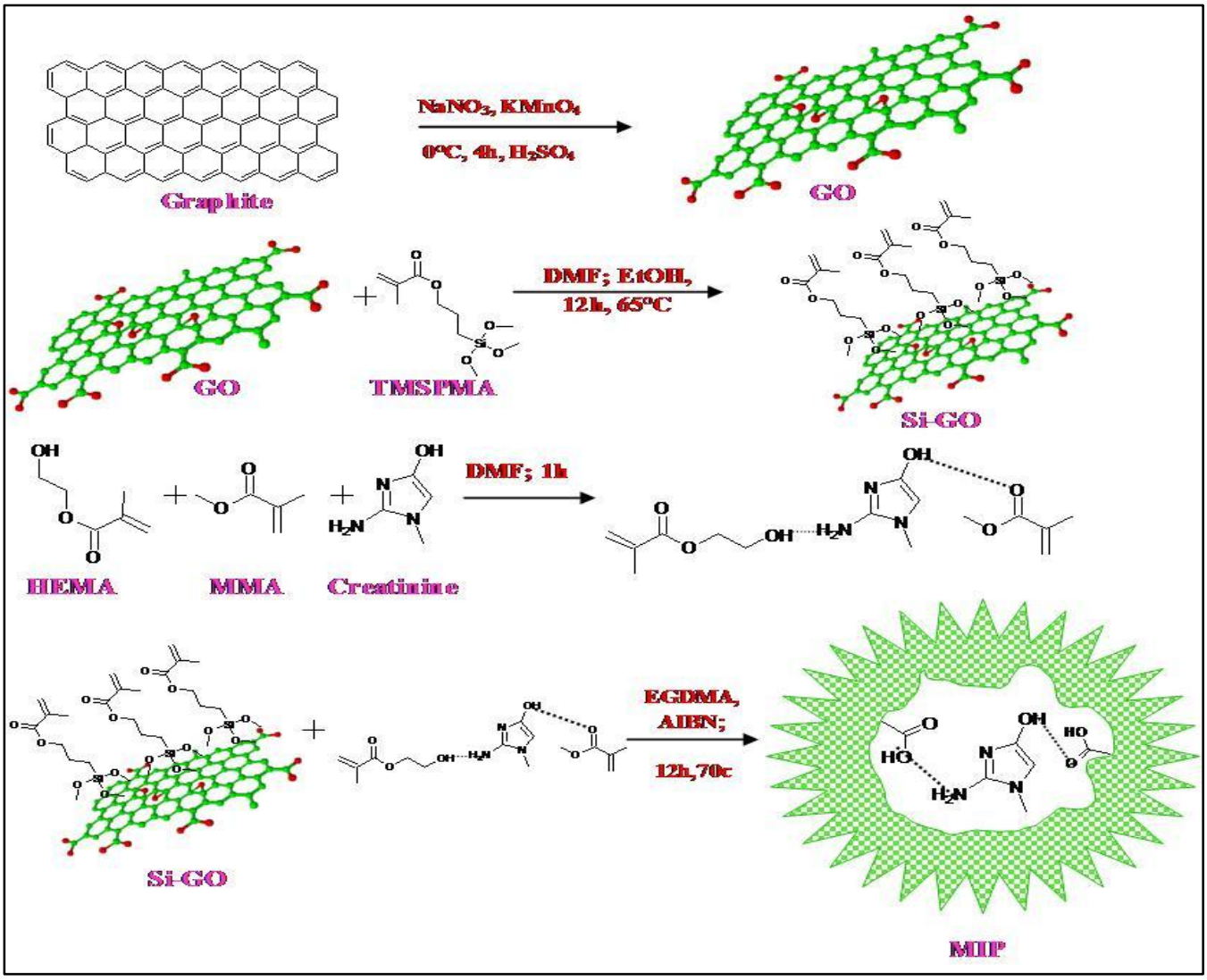


Figure 1. Synthesis of TMSPMA-GO-co-HEMA/MMA

References

[1]. Garbati,P. Salis, A; Adriano,E;Galatini, A; Damonte, G.; Balestrino, M.;E. Millo, ,*Amino Acids*.45 (2013) 821.

[2]. Chena, J.C.; Kumara, A.S.; Chunga, H.H.; Chien, S.H; Kuo,M.C. , Zena, J.-M.; *Sensors and Actuators*, B. 115 (2006) 473–48.

[3]. Wei, F.; Cheng, S; Korin, Y; Reed, E. F.; Gjertson, D.; Ho, C.M.; Gritsch, H. A.; Veale, J. ; *Analytical chemistry*, 84(2012) 7933

[4]. Pundir, C.S.; Yadav, S; Kumar**,** A., *Trends in Analytical Chemistry*. 50 (2013) 42.

MACRO 164

Fabrication of Graphene Quantum Dot-Doped Polyaniline Nanostructure and Its Opto-electronic and Photovoltaic Properties

Maity, Nabasmita; Kuila, Atanu and Nandi, Arun. K.*

Polymer Science Unit, Indian Association for the Cultivation of Science, Jadavpur, Kolkata-700 032, INDIA

**For correspondence: Arun. K. Nandi, Email: psuakn@iacs.res.in*

Aniline is in-situ polymerized in aqueous dispersions of graphene quantum dots (GQDs), produced by Sono-Fenton method, fabricating different polyaniline (PANI)-GQDs hybrids (PAGD) without using any external dopant. As evidenced from both FTIR and UV-vis spectroscopy, the carboxylic acid groups of GQDs dope PANI well. The bulkier and poly-dentate nature of GQDs counter anions attached to the doped PANI chains cause gradual uncoiling of the chains and thus increasing the conjugation length causing the red shift in π to polaron band transition of PAGD hybrids for increasing amount of GQDs. The fluorescence intensity of GQDs drastically quenches in the PAGD hybrids suggesting effective charge transfer between the GQDs and PANI chains. The X-ray diffraction pattern suggests the presence of lamellar structure with lamellar thickness of 13.57 Å. The morphology of the PAGD hybrids studied from field emission scanning electron microscopy display a change from nanoflakes to nanorods with increasing GQDs concentration attributing to the change from the flat-on to cylindrical lamella formation. The result from thermogravimetric analysis indicates that PAGD hybrids exhibit better thermal stability in comparison to HCl-doped PANI. In PAGD composites the dc-conductivity increases by three orders from that of GQDs due to formation of polarons in the PANI chains. The Current-Voltage (I-V) characteristics of PAGD hybrids signify semiconducting behaviour and almost a reversible photoresponse occurs on irradiation with light. Dye-sensitized solar cell (DSSC) fabricated with PAGD hybrids and N719 dye indicate highest power conversion efficiency (PCE) of 3.12%. Semicircular Cole-Cole plots obtained from impedance study of the hybrids indicate the presence of resistance (R)-capacitance (C) circuit where capacitance is in parallel to the bulk resistance which increases with increase in GQDs concentration. The Debye plot and the dielectric permittivity values also support the variation of photovoltaic property of the PAGD hybrids. The impedance spectra of the DSSCs indicate the presence of three semicircles exhibiting a complex equivalent circuit comprising of three R-C circuits and analysis of the data yield the life time values of photo-injected electrons supporting the PCE variation of PAGD hybrids.

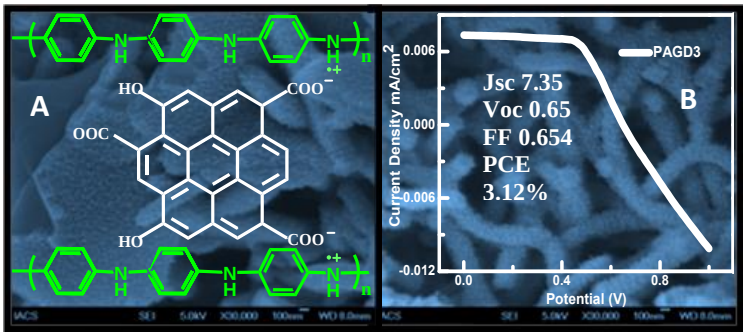


Figure 1. (A) Scheme of PANI-GQDs (PAGD) nanocomposites preparation and (B) J-V curve of PAGD sample with highest power conversion efficiency with a background having FESEM image of PAGD nanoflakes (A) and nano rods (B) .

References

[8] Maity, N; Kuila, A; Das, S; Mandal, D; Shit, A; Nandi, A. K.*J. Mater. Chem. A*, 3 (2015) 20736.

MACRO 169

Safe and Non-toxic Carbohydrate Polymer Based Pollutant Sensor Gold Nanoparticles having Fluorescence Quenching Ability

Pattanayak, Sutanuka[a], Maity, Dipanwita[b], Chattopadhyay, Dipankar[b], Chakraborty, Mukut[a]*

[a]*Department of Chemistry, West Bengal State University, Barasat, 700126, India*
[b]*Department of Polymer Sc. & Tech., University of Calcutta, 92, A.P.C. Road, Kolkata 700009, India*

* *mukutchem@yahoo.co.in*

This work deals with a natural polymer or more precisely the carbohydrate polymer named β-glucan (beta glucan) extracted from an edible mushroom [1]. β-Glucans are polysaccharides of D-glucose monomers linked by β-glycosidic bonds and have been used to synthesize gold nanoparticles (Au NPs). As glucan is water soluble the Au NPs sol was prepared in water, the green solvent. The synthesized Au NPs have been characterized using UV-Vis spectroscopy, TEM, EDX, XRD and FT-IR spectroscopic studies.

The synthesized Au NPs act as a very good fluorescence quencher obeying Stern-Volmer equations in presence of fluorophore. The β-D-Glucan capped Au NPs are safe and non-toxic having possible medicinal usage [2]. Stern-Volmer plots of fluorophore-Au NPs system in solvents of different viscosities were also carried out and the Stern Volmer constant (Ksv) values were calculated. The results indicate that the probable quenching process was dynamic rather than static in nature.

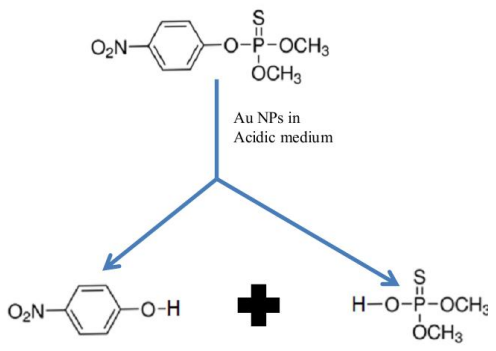


Figure 1. Cleavage of phospho-ester linkage of Methyl parathion by Au NPs in acidic medium

The obtained Au NPs also show chemosensing property against Methyl Parathion (MP). MP a common pesticide, renowned for its highly neurotoxic agricultural chemical property is extensively used world-wide to manage a wide range of insect pests [3] and its residue remains in the soil causing severe pollution. We have studied the sensor properties of glucan stabilized Au NPs sol by examining the UV-Vis spectral change due to the addition of methyl parathion and its subsequent degradation at the ppm level. Our carbohydrate polymer capped Au NPs therefore are able to dissociate the phospho-ester linkage as per Figure 1. This fact has been established using UV-Vis and FT-IR spectrophotometric studies.

References

[9] Sen, Ipsita K.; Maity, Kousik; Islam, Syed S. *Carbohydrate Polymers*, 91 (2013) 518.
[10] Mason, Roger. *What is Beta Glucan?* Printed in the U.S.A.: Safe Goods, 561 Shunpike Road, Sheffield, MA 01257 (2011).
[11] Pakala, Suresh B.; Gorla, Purushotham; Pinjari, Aleem Basha; Krovidi, Ravi Kumar; Baru, Rajasekhar; Yanamandra, Mahesh; Merrick, Mike; Siddavattam, Dayananda. *Applied Microbiology and Biotechnology*. 73 (2006) 1452.

MACRO 182

All-polymer Solar Cell Performance Of N-type Napthalenediimide/ Perylenediimide - Bithiophene Copolymer

Sharma Sandeep[ab], Kolhe Nagesh B.[a], Asha S. K.,*[ab]

[a] *Polymer Science and Engineering Division, CSIR-NCL, Pune, India-411008.*
E-mail: sk.asha@ncl.res.
[b] *Academy of Scientific and Innovative Research, New Delhi, India*

Naphthalenediimide-bithiophene P(NDI2OD-T2) is a well known donor-acceptor polymer. P(NDI2OD-T2) is used in all-PSCs and OFET applications because of its desirable photo-physical and semiconducting properties. It exhibited high electron mobility > 0.85 $cm^2V^{-1}s^{-1}$ in OFET, high PCE efficiency ~5% in all-PSCs. The optical, bulk, electrochemical and semiconducting properties of P(NDI2OD-T2) polymer was tuned via random incorporation of perylenediimide (PDI) as co-acceptor. Three random copolymers containing 2, 2'-bithiophene as donor unit and varying compositions of napthalenediimide (NDI) and perylenediimide (*x*PDI, *x* = 15, 20, 30 mole% of PDI) as two mixed acceptors were synthesized by Stille coupling copolymerization.

All the random copolymers exhibited broad absorption (in the region of 300-800 nm) and high bulk crystallinity, as evidenced from their UV-Visible absorption spectra and X-diffraction patterns respectively. The newly synthesized random copolymers were further investigated as electron acceptors in BHJ all-PSCs in combination with PTB7-Th (PCE10) as donor polymer and their performance was compared with P(NDI2OD-T2) as reference polymer

Table1. Photovoltaic properties of PCE10: NDI-Th-PDI*x* blend all-polymer solar cells.

Active layer	Voc(V)	Jsc (mA/cm2)	FF (%)	PCE (%)
PCE10: P(NDI2OD-T2)	0.797	9.05	41.3	2.97
PCE10: NDI-Th-PDI15	0.792	10.71	49.7	4.22
PCE10: NDI-Th-PDI30	0.795	11.43	55.4	5.03
PCE10: NDI-Th-PDI50	0.797	10.16	41.2	3.33

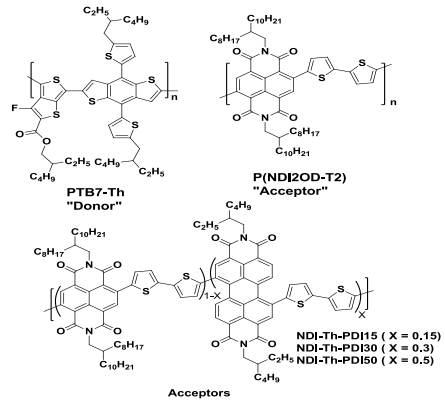


Figure 1. Structures of Donor and acceptor Polymers

The reference acceptor polymer P(NDI2OD-T2) exhibited Power conversion efficiency (PCE) of 2.97% in BHJ all-PSCs. Excitingly, the random copolymers(NDI-Th-PDI*x*) showed maximum PCE of 5.03% (NDI-Th-PDI30; Table 1). This PCE value obtained for NDI-Th-PDI30 device is so far the best reported for all-PSCs using PCE10 as donor. This work demonstrate the importance of molecular design via random copolymer strategy to control the bulk crystalinity, compatibility, blend morphology and solar cell performance of n-type copolymers.

References

[12] Hwang, Y.-J.; Earmme, T.; Courtright, B. A. E.; Eberle, F. N.; Jenekhe, S. A. *J. Am. Chem. Soc.*, 137 (2015) 4424–4434.
[13] Kolhe, N. B.; Ashar, A. Z.; Narayan, K. S.; Asha, S. K. *Macromolecules,47 (* 2014) 2296–2305.
[14] Kolhe, N. B.; Shinde, S.; Saibal, B.; Asha, S. K. *Org. Photonics Photovolt, 3 (*2015) 71-100.

MACRO 183

Glutamic Acid Appended Water-Soluble Conjugated Polymer for Fluorescence Sensing and Imaging of Fe^{2+} Ions in Live Cells

Nikam, Shrikant B. [a,b] T. Sethilkumar,[a] Parekh Nimisha [c] and S. K. Asha,*[a,b]

[a] *Polymer Science and Engineering Division, CSIR-NCL, Pune, India-411008.*
E-mail: sk.asha@ncl.res.
[b] *Academy of Scientific and Innovative Research, New Delhi, India*
[c] *Chemical Engineering and Process Development Division, CSIR-NCL, Pune, India-411008*

The ferrous state of iron (Fe^{2+}) is predominantly favoured inside the cell by inherent factors such as reductive environment, higher water solubility and the presence of ferric reductase enzyme. Iron flexibly shuttles between Fe^{2+}/Fe^{3+} oxidation states. It is very important that the levels of iron and the balance in the oxidation states are maintained as overloading of iron causes variety of disorders such as cell damage, abnormal production of reactive oxygen species, hepatitis, organ dysfunction, Alzheimer's and Parkinson's diseases. Intracellular detection and imaging of labile iron(II) pools is very important in tracking physiological processes, cell metabolism and in addition it facilitates an access for understanding the mechanisms of biological reactions that demand new and rapid sensing probes.

In this report, we present a water soluble polymer based probe for the fluorescence sensing and live cell imaging of labile Fe^{2+} ions with high selectivity for the first time. The polymer probe was based on conjugated polyfluorene which was appended with amino acid (L-glutamic acid). Simple glutamic acid did not show selectivity towards any of the divalent ions. However, glutamic acid appended polyfluorene exhibited selective chelation to Fe^{2+} ions resulting in immediate sensing activity for Fe^{2+} ions in water and living cells with fluorescence turn-off response. The biocompatibility of the polymer was confirmed from an MTT assay which demonstrated > 90% cell viability even at 300 mg ml^{-1} loading of polymers. The limit of detection of the PF-Ph-GA polymer probe was 46 (±2) nM which indicated high sensitivity for Fe^{2+} over other ions reported in the literature. The polymer also exhibited improved sensing activity in the range of intracellular pH (5–9) which is advantageous in differentiating endogenous changes. The probe was successfully applied for the fluorescence imaging of intracellular and supplemented labile iron(II) pools in living HeLa cells.

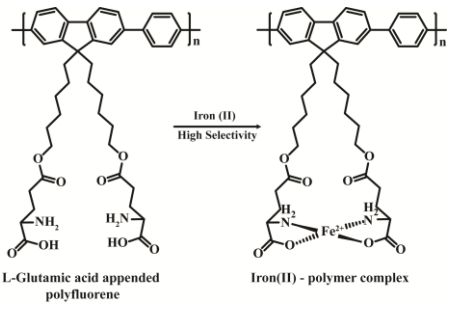


Figure1: Schemetic representation for the sensing of iron(II)

References

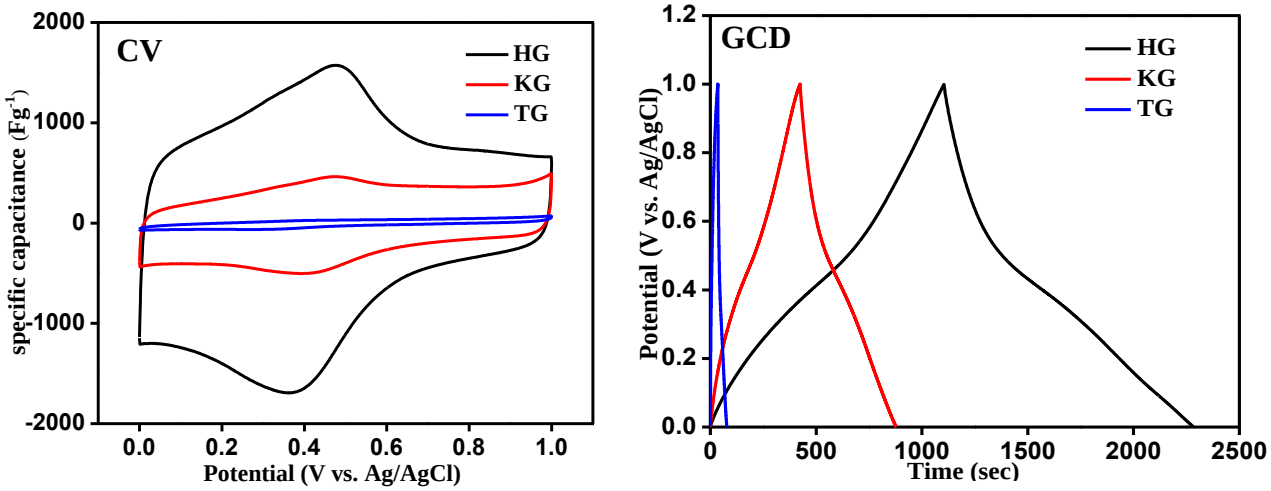
[15]Senthilkumar, T; Parekh, N; Nikam, S. B; Asha, S. K. *J. Mater. Chem. B*, 4 (2016) 299.
[16]Ho, J. A; Change, H.-C; Su, W.-T. *Anal. Chem. Sci.*, 84 (2012) 3246.
[17]Sui, B; Tang, S; Liu, T; Kim, B; Belfield, K. D. *ACS Appl. Mater. Interfaces*, 6 (2014) 18408.

MACRO 184

Highly Efficient Supercapacitor Performance of Iodine Doped Reduced Graphene oxide Produced via Mild Reaction Condition

Mandal, Debasish[a]; Routh, Parimal[b] and Nandi, Arun K[a].*
[a]*Polymer Science Unit, Indian Association for the Cultivation of Science, Jadavpur, Kolkata-700 032, INDIA*
[b]*Department of Chemistry, Charuchandra College, 22 Lake Road, Kolkata 700 029, India*
**For correspondence: A. K. Nandi, Email: psuakn@iacs.res.in*

Various techniques including control reduction of graphene oxide, functionalization, conducting polymer grafting, doping of redox active elements, metal oxide and etc. are being applied to improve the supercapacitor performances of graphene based materials. Herein, synthesized iodine doped reduced graphene oxide (HG) by a simple one step efficient reduction method using HI reducing agent, exhibits excellent specific capacitance of 1180 F g^{-1} at 1 A g^{-1} and about 30 times larger than that of thermally reduced graphene oxide (TG) and 2.5 times compare to potassium iodide reduced graphene oxide (KG). The intrinsic charge storage mechanism is based on the electrochemical double layer capacitance and pseudo capacitance due to the presence of different redox active oxygenated functional groups and doped iodine. Other important and useful properties of these electrode materials for suprcapacitor operations include long cyclic stability (~ 93 % after 10,000 cycles), excellent rate capability (73.7 % retention at current density of 50 A g^{-1}). Also the symmetric supercapacitor based on this electrode material exhibit excellent energy density of 32.53 W h kg^{-1} at a power density of 125 W kg^{-1} and the maximum power density of 12.5 kW kg^{-1} with energy density of 18.12 W h kg^{-1}. This chemical modification is also very useful to improve the electrical conductivity of 0.6 S cm^{-1} compare to that of thermal reduction (2.2×10^{-6} S cm^{-1}). Physical properties are characterized by transmission electron microscopy, Fourier transform infrared spectroscopy, thermogravimetric analysis, Raman spectroscopy, X-ray diffraction, X-ray photoelectron spectroscopy, electrical conductivity, cyclic voltammetry and impedance measurements.



References

[18]Xu, B; Yue, S; Sui, Z; Zhang, X; Hou, S; Cao, G; et al. Energy Environ. Sci., 4 (2011) 2826.
[19]Lin, Z; Liu, Y; Yao, Y; Hildreth, O. J; Li, Z; Moon, K; et al. J. Phys. Chem. C, 115 (2011) 7120.

MACRO 188

A New class of Polymeric Network as an Efficient Water Toxicant Remover

Rajan Kumar,[a] Raja Shunmugam*

[a] *Polymers Research Centre, Department of Chemical Sciences,*
Indian Institute Of Science Education and Research Kolkata (IISER K), Mohanpur,
India - 741246
** e-mail id:* sraja@iiserkol.ac.in

Abstract: Photo-irradiated thiol-yne click chemistry[8,14] based biodegradable as well as water insoluble Porous Organic Frame (POF) is preferred to test the adsorption[1, 2] as well as release using the principle of Host-Guest complexation. Here, the study is linked to incubation of Low Molecular Weight (LMW) colorant dye as guest into host (POF)[12,13]. The study is extended to removal of heavy metal with POF network which is functionalized with thiol (-SH) groups. In general, The POF is hard in nature but swelled[9-11] in organic solvents such as chloroform and DMSO.

Keywords: *polymer organic frame (POF); NMR; host-guest; adsorption; trapper*

Introduction

Unlike non-degradable adsorbents like Zeolite and Metal Organic Framework (MOF), biodegradable micro POF can prove itself as an influential tool with super adsorbent property invoked in them. Controlled rigidity and insolubility in aqueous phase are the desired conditions that needed to be taken care for their development. Here, we introduce facile route towards synthesis of thiol-yne Click chemistry for the synthesis of micro POF with bifunctional alkyne and pentaerythritol tetrakis (3-mercaptopropionate).We have successfully prepared covalently crosslinked micro POF network with controlled swell ability. They can be grown into pores of different diameters on demand with switch in hydrocarbon chain. This is very interesting as the controlled architectural design of pores in them can show selectivity for specific toxicant. Water bodies close to industrialization region are contaminated with toxicants such as dyes and non degradable heavy metal ions - mercury, plumbum, cadmium, etc. These Low Molecular Weight (LMW) toxicants cause serious concern towards body metabolism when inhaled. Symptoms such as skin diseases, bone deformation, cancer, etc are the prime consequence that arises due to intake of these toxicants. Their removal from water bodies is the prime objective. We have demonstrated our newly designed micro POF for the adsorption of fluorescein dye, which is frequently used in water bodies. We have also trapped toxic ions from aqueous phase with –SH functionalized micro POF. The material has responded well and it is elaborated in discussion section.

Experimental

Physical and Analytical Method

^{1}H- NMR spectra were acquired with a Jeol -400 spectrometer operating at 400 MHz. Chemical shifts were reported relative to residual non-deuterated solvent. Chemical shift and coupling constant (*J*) are reported in parts per million (ppm) and Hertz respectively. The abbreviations for splitting patterns are s, singlet; and m, multiplet. Photo chamber equipped with set of UV black light bulbs (NARVA, LT 8W T5) of wavelength 365 nm. UV spectra were recorded on UV spectrometer (UV-1800, Shimadzu) maintained at IISER Kolkata. The snapshots to study the adsorption of Dye were also taken. SEM as well as Cryo SEM images were obtained from Scanning Electron Microscope. The SEM microscope was acquired from Carl Zeiss Pvt. Ltd. All analyses were done at 25 °C.

Procedures

Synthesis of Diacid chloride:

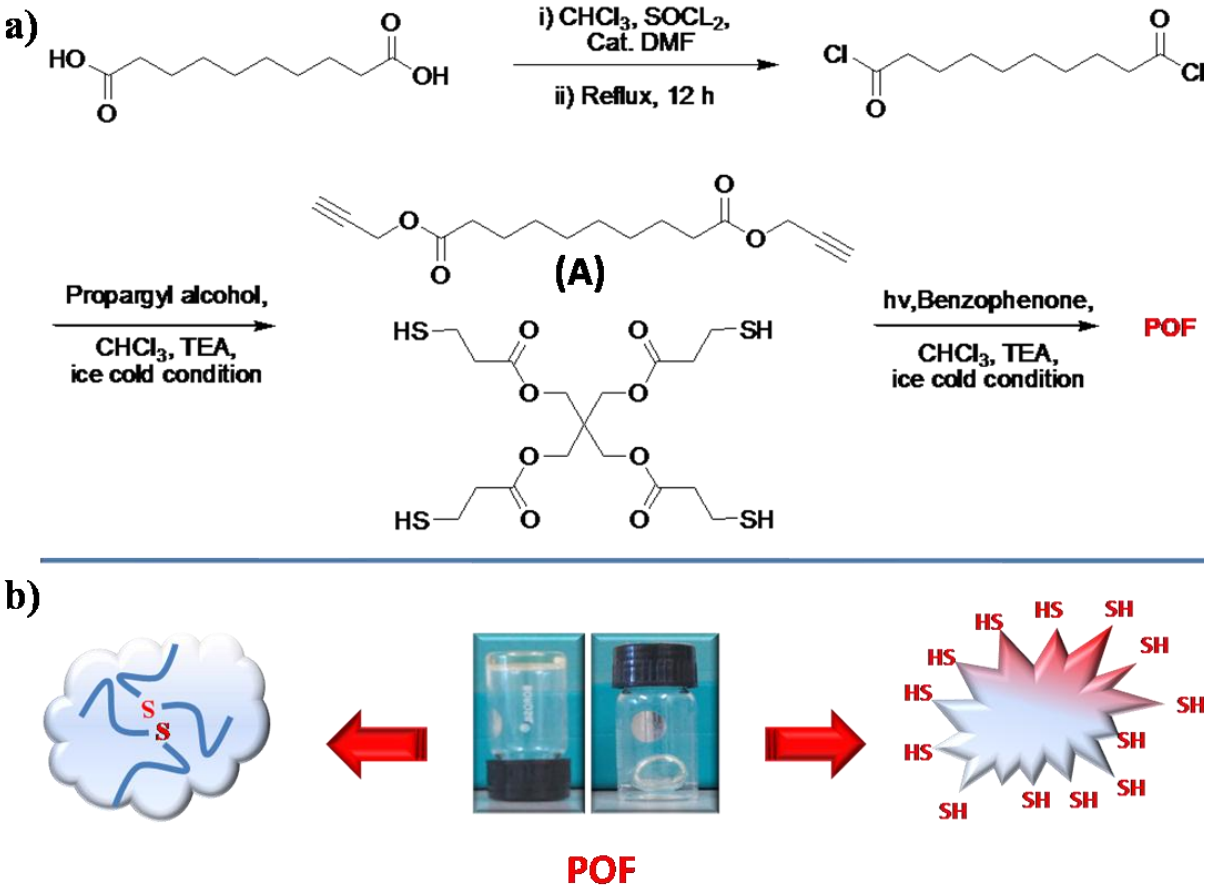
Diacid (1 eq.) was added into 100 mL round bottom flask equipped with magnetic stirrer. Dry DCM was added. Thionyl Chloride (2 eq.) along with catalytic amount of DMF were added under ice cold condition. The reaction mixture was stirred at room temperature for 2 h followed by reflux. After refluxing for 12 h, the solvent and excess thionyl chloride were removed using high vacuum. Finally, the viscous acid chloride was collected as product.

Synthesis of Dialkyne, A:

Acid chloride dissolved in dry DCM was treated with triethylamine (2.1 eq) and propargyl alcohol (2.1 eq) under ice cold condition and constant stirring. The reaction mixture was stirred for overnight at room temperature. The compound extracted with DCM-water was dried over anhydrous sodium suphate. The compound was purified by column chromatography using silica. The silica used was of 100-120 mesh. The system used was 5% MeOH in DCM.

Synthesis of Micro POF:

Compound A (1eq.), pentaerythritol tetrakis (3-mercaptopropionate) (1eq.), and benzophenone (0.001 eq.) were taken in a vial. Nitrogen was purged to the mixture followed by addition of dry DCM (0.5 mL). The solution was exposed to UV irradiation for 0.5 h. A transparent solid material was obtained.



Scheme 1: (a) Synthesis of POF via Thiol-Ene click reaction, (b) Cartoon for the growth of neutral and –SH functionalized POF.

Results and discussion

Condensed Dialkyne, A: The synthetic pathway towards investigation of dialkynes is showed in **Scheme 1(a)**. The pure product was analyzed via ^{1}H NMR spectroscopy as shown in Figure 1(a). The POF so grown via thiol-ene click reaction was characterized by TGA Curve which showed two break points – The first break point at temperature range 300 °C – 400 °C represent ester (-OCO-) bond while the second breakpoint in the range 450 °C - 500 °C represent C-S bond (Figure 1b). The presence of pores within the micro POF was confirmed by SEM and Cryo-SEM data captured over range from μm to nm showed in Figure 1(c; d). The swelling property was calculated POF in DMSO using equation –

$$\text{Wt. Gain \%} = \frac{\text{Wet Weight - Original Weight}}{\text{Original Weight}} \times 100$$

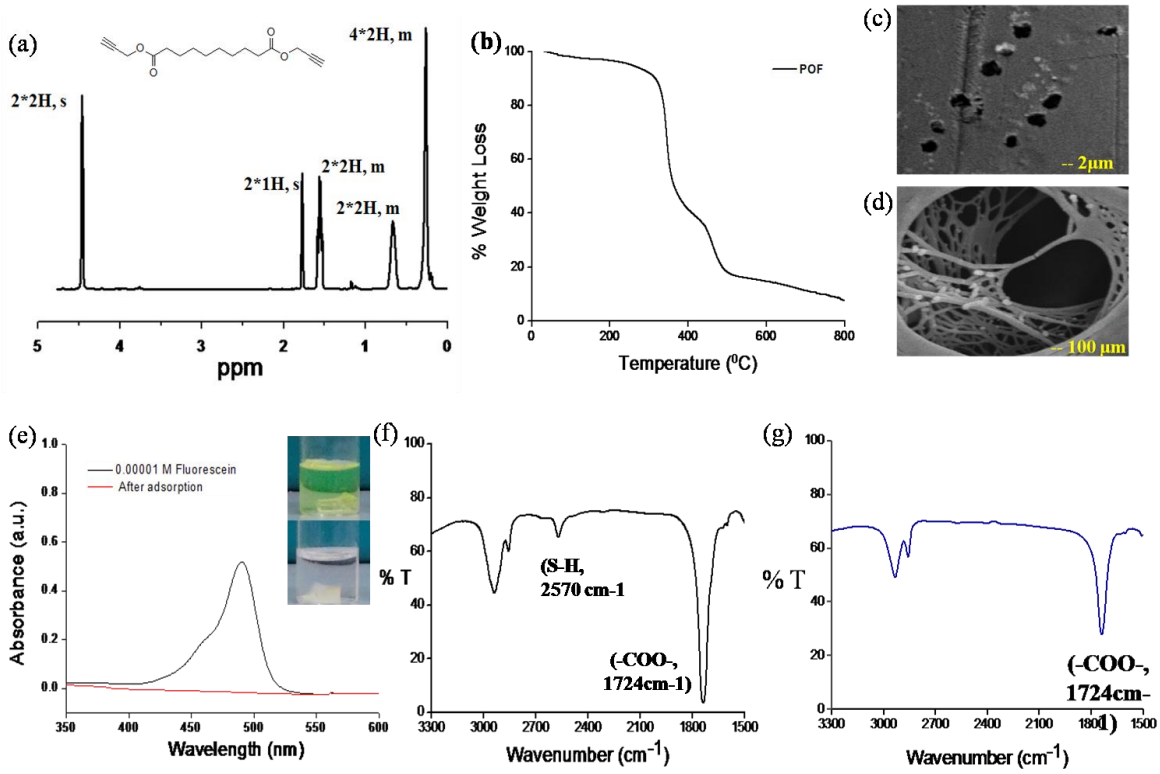


Figure 1. (i) (a) ^{1}H NMR for dialkyne ($CDCl_3$ – 400 MHz), (b) TGA curve for functionalized POF, (c) SEM images, (d) Cryo-SEM images for POF, (e) UV absorption of fluorescein by compact non-functional POF, (f) FTIR for –SH functionalized POF, (g) FTIR for –SH functionalized POF after exposure to metal ion.

The material swelled upto 182.1 wt% at its maximum when allowed to stand for 24 h in DMSO. When compound A was treated with 2 equivalent of Pentaerythritol tetrakis(3-mercaptopropionate)_thiol functionalization occurred. To confirm the product, FTIR was performed as shown in Figure 1(f). The FTIR stretching frequency at 2570 cm^{-1} clearly confirms the presence of S-H stretch.

Adsorption and Trapping of Toxicants:

We introduced the POF network to adsorption and trapping[3-7] of non-biodegradable inorganic low molecular weight toxicants such as plumbum (Pb), arsenic (As), zinc (Zn) and other heavy metals having affinity for sulfur(S). Based on Host – Guest principle, the phenolphthalein derived dye fluorescein, which was tested for 70 mg of POF in 1 mL showed 100% adsorption. This was clearly confirmed from the UV spectra as shown in Figure 1e. Trapping was done using Hard Soft Acids Bases (HSAB) principle by Ralph Pearson. The trapping of heavy metal was analyzed

too. The disappearance of weak sharp stretching for –**SH** at 2570cm^{-1} in Figure 1(g) confirmed the positive response towards trapping of heavy metal ion; lead(Pb).

Conclusions

We have developed micro POF via click chemistry. The porous POF network is not only effective but also can be prepared with cost efficient method. It showed efficient adsorption. POF network can dominate the industrial sector with its application as trapper towards the waste generated. From the preliminary observation and experiments, the material has showed very positive response. The effort in our group is in progress to confirm its efficiency towards organic and inorganic toxicants.

Acknowledgements

RK thank DBT for research fellowship. RS thank DBT and DST for funding. We thank IISER-Kolkata for the infrastructure facility.

References

18. Shi, B.; Li, G.; Wang, D.; Feng, C.; Tang, H. *J. Hazard Mater*. **143**, 567, 2007.
19. Liu, H.; Chen, L.; Ding, J. *RSC Advances*. **6**, 48884, 2006.
20. Bhattacharya, S.; Sarkar, S.; Shunmugam, R. *J. Mater. Chem. A,* **1**, 8398, 2013.
21. Shunmugam, R.; Gabriel, G. J.; Smith, C. E.; Aamer, K. A.; Tew, G. N. Chem. Eur. J. **14**, 3904, 2008.
22. Bhattacharya, S.; Sarkar, S.; Shunmugam, R. J. Mater. Chem. A. **1**, 8398, 2013.
23. Sarkar, S.; Shunmugam, R. *ACS Appl. Mater. Interfaces*. **5**, 7379, 2013.
24. Bhattacharya, S.; Shunmugam, R. RSC Adv. **5**, 74973, 2015.
25. Ganivada, M. N.; Kumar, P.; Shunmugam, R. RSC Adv. **5**, 50001, 2015.
26. Mondal, T.; Ghosh, S. *Journal of Polymer Science Part A: Polymer Chemistry*. **52**, 2502, 2014.
27. Basak, D.; Kumar, R.; Ghosh, S. *Macromol. Rapid. Commun*. **35**, 1340, **2014.**
28. Roy, S.G.; Haldar, U.; De, P. *ACS Appl. Mater. Interfaces.***6**, 4233, 2014.
29. Zhang, C.; Peng-Cheng Zhu P. C.; Tan, L.; Liu, J. M.; Tan, B.; Yang, X. L.; Xu, H. B. Macromolecules. **23**, 8509, 2015.
30. Kandanelli, R.; Sarkar, A; Maitra, U.; *Dalton Trans.* **42**, 15381, 2013.
31. Vizer, S. A.; Sycheva, E. S.; Quantar, A. A. A. A.; Kurmankulov, N. B.; Yerzhanov, K. B.; Dembitsky, V. M. *Chem. Rev.* **115**, 1475-1502, 2015.

MACRO 191

A New Class Of Norbornene Based Dyes For In-field Rapid As(III) Sensing

Tapendu Samanta[a], Vikas Verma[b], Raja Shunmugam[*]

[a,b,*]*Polymer Research Centre, Department of Chemical Sciences,*
Indian Institute of Science Education and Research, Kolkata.
Mohanpur-741246
[*]*E-mail:* ***sraja@iiserkol.ac.in***

Abstract

We have synthesized norbornene derived dyes (Nor-FT).Monomer was synthesized and thoroughly characterized and confirmed the pure products. The main objective of this work is to sense heavy metals and their salts due to their environmental issues. Also the preparation of polymeric materials of these norbornene derived dyes would provide in-field application.

Keywords: *Fluorescein**;** Nor-FT; NMR; ESI-MS; Fluorescence.*

Introduction

The arsenic toxicity in water is actually from arsenite, As(III) and arsenate, As(V) forms of arsenic, which can be deposited from mainly agricultural and industrial areas.[1] Basically the inorganic arsenic form is more harmful and toxic than organic form.[2] Arsenic exposure can cause a wide range of physiological effects like neurologic, cardiovascular, carcinogenic effects, diabetes, ischemic heart disease etc..[3] According to a report of 2007, it is found that over 137 million peoples from approximately 70 countries are effectively affected by arsenic poisoning which mainly causes from drinking water.[4]Maximum concentration of arsenic (III) in-water should not be greater than 10 ppb according to WHO and EPA.[5a,b]There are so many spectroscopic methods like HG-AAS, neutron activation analysis, X-ray fluorescence etc. which are conventionally and frequently used to determine arsenic. But these method are so much cost effective and not that much useful for environmental samples for arsenic.[6-12]

So many As (III) sensors using gold nanoparticles, are reported.[13-15] But the practical application of these sensors is not that easy, as well as cost effective and complicated. Now in recent time, fluorescence technique[12] having so much importance to determine toxic heavy metals like Zn(III), Hg(II), Pb(II), Cd(II), Cu(II) effectively. Though there is nothing proper solution for As (III) in organic or inorganic form. Recently a Cumarin based As(III) sensor has been reported which only works in organic solvent.[16] Cysteine fused tetraphenylethene has been reported as fluorimetric sensing platform for As(III).[17] A water soluble inorganic co-crystal has been reported as a luminescent sensor for As (III) in water medium.[18] Both colorimetric and fluorometric sensor for As(III) in aqueous medium is less reported till now. Recently from our lab one rhodamine derived sensor (Nor-Rh) has been reported[19], which indirectly sense As(III) in aqueous medium by both colorimetrically and fluorometrically till ppb level. The reported compound sense As(III) when it converts to As(V) and liberates iodine, which changes the color and fluorescence of the solution. Direct sensor for As (III) in aqueous medium is till now not available according to our best of knowledge.

Here we have tried to synthesize fluorescein based compounds and their

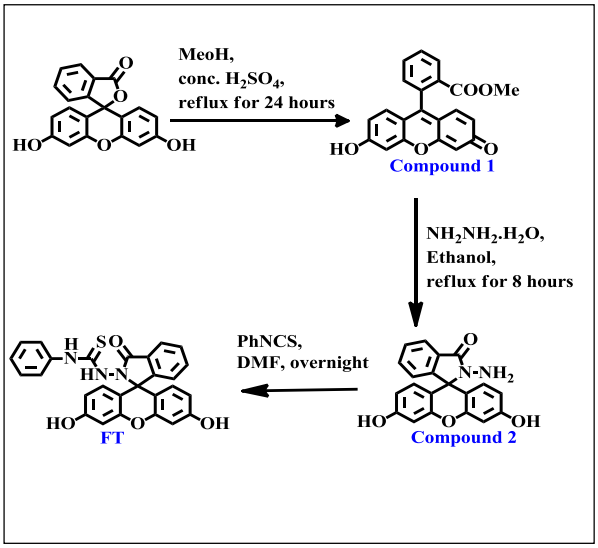
nobornene derivatives for the purpose of heavy metal sensing. In future we also have the intention of making polymeric materials of these above mentioned monomers.

Experimental

Preparation of fluorescein derivative is given in scheme 1.

Synthesis of compound 1

Compound **1** was synthesised by modifying already established procedure.[20] To a 30 mL methanolic solution of fluorescein (3.0 g, 9.3 mmol) in a round-bottom flask, 4 mL of concentrated H_2SO_4 was added dropwise fashion under vigorous stirring condition. After the addition of H_2SO_4.The solution was monitored continuously by thin layer chromatography technique. After observing single spot in TLC, the reaction mixture was added to a beaker containing crushed ice, and followed by the addition of excess water. A red solid was precipitated as product. It was washed several times with water till the filtrate became colorless, then it was washed with hexane for two times. 2.9 g of compound **1** was obtained having yield 92%. ^{1}H-NMR(DMSO-d_6, 500 MHz): δ(ppm) 10.15(s,1H), 8.23 (d, J = 7.86 Hz, 1H), 7.88(d, 2H), 7.5(d,J=7.54 Hz,1H), 6.95(d,J=9.21 Hz,2H), 6.67(d,J=1.8 Hz, 2H), 6.7(dd,J=2 Hz,2H), 3.57(s, 3H)^{13}C-NMR(DMSO-d_6, 500 MHz): δ(ppm)172.8, 165.1, 156.7, 155.0, 133.7, 133.1, 130.7, 130.6, 130.5, 130.2, 129.3, 121.2, 115, 103, 52.3(O-CH_3)ESI-MS: m/z 347.2 $[M + H]^+$.



Synthesis of compound 2

Compound 2 was synthesized by following already established literature.[21] Compound 1(1 g, 0.0028 mol) was dissolved in 30 mL of ethanol in a 250 mL round-bottom flask and stirred vigorously, followed by the dropwise addition of excess hydrazine monohydrate (2 mL, 0.028 mol). Then the reaction mixture was refluxed for 8 hours. Then the reaction mixture was cooled to room temperature and solvent was removed under reduced pressure. The resulting oily solution was added to a beaker containing 200 mL of water. A yellow coloured precipitate was generated which was filtered and washed with water followed by cold ethanol. A yellow powdered product (compound **2)** was obtained with the yield of 88%. ^{1}H-NMR(DMSO-d_6, 500 MHz): δ(ppm)9.7(s,2H), 7.78(dd,J=5.51 and 2.78 Hz,1H), 7.49(dd,J=3.5 and 3.5 Hz,2H), 6.99(dd,J=5.8 and 2.8 Hz,1H), 6.59(d,J=2.31 Hz,2H), 6.45-6.39(m, 4H), 4.36(s, 2H)^{13}C-NMR(DMSO-d_6, 500 MHz): δ(ppm)165.43, 158.16, 152.38, 151.49, 132.56, 129.32, 128.37, 127.9, 123.39, 122.32, 111.97, 109.94, 102.3, 64.59 ESI-MS: m/z 347.1 $[M+H]^+$.

Synthesis of FT

FT was prepared using already known procedure[22] with slight modification. Compound 2(1 g, 0.0028 mol) was dissolved in dry DMF and phenyl isothiocyanate(0.4 g, 0.0029 mol) was added to the solution. Reaction was purged with N_2 and left for 24 hours in stirring condition. Reaction mixture was poured into saturated brine solution and resulting brown precipitate was filtered. Residue was washed with ethanol. Light brown coloured solid product was obtained (1.15 g, 83%). Recrystallization was done from acetonitrile.^{1}HNMR (DMSO-d_6, 500 MHz): δ(ppm)10.0(s, 1H), 9.4(s,1H), 8.9(S,1H), 7.92(d,J=7.21Hz,1H),7.68(m, 2H),7.23-7.07(m, 8H), 6.6(s,2H), 6.46(s,2H)

^{13}CNMR(DMSO-d_6,500MHz):δ(ppm)181.3, 166.1, 158.8, 152.9, 150.2, 138.8, 133.8, 129.5, 128.9, 127.8, 125.8, 125.7, 125.2, 124.2, 123.1, 112.3, 108.8, 102.2, 65.7ESI-MS:m/z 482.12$[M+H]^+$.

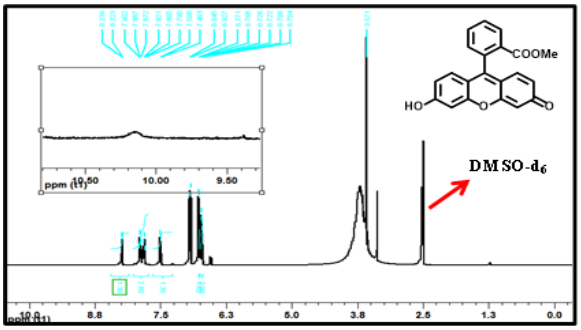


***Figure 1**: ^{1}HNMR spectrum of compound 1*

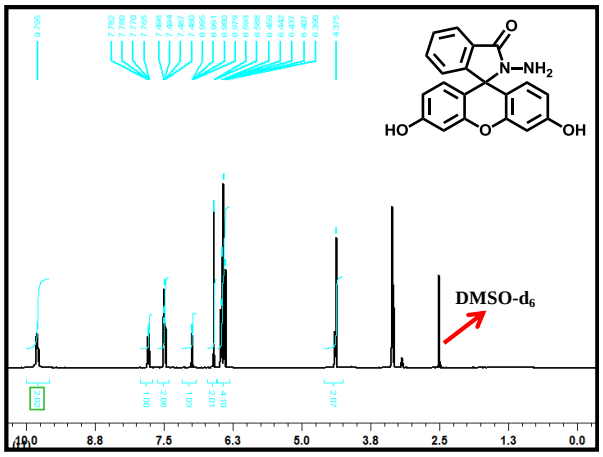


***Figure 2**: ^{1}HNMR spectrum of compound 2*

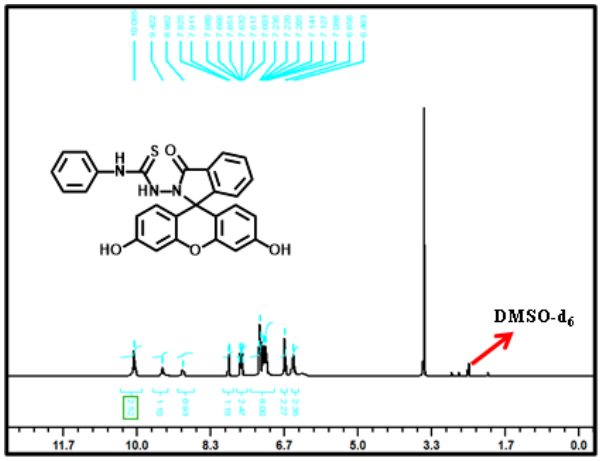


***Figure 3**: ^{1}HNMR spectrum of compound FT*

Complete characterization of Nor-FT has confirmed the formation of the pure product.

Results and discussion

After the successful synthesis and characterization of the compounds, we conducted UV-Vis and fluorescence study of final molecule **FT**.

In UV-Vis, **FT** showed no significant peak but in fluorescence a weak band appeared at 532 nm (Figure 4).

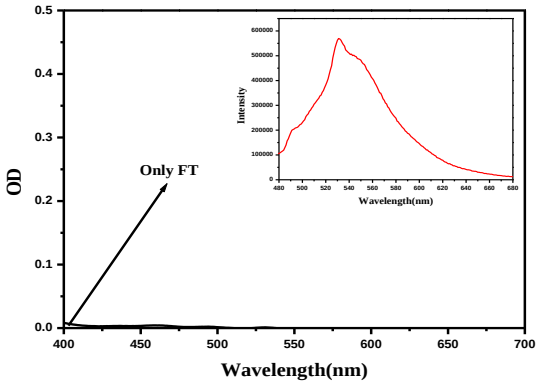


Figure 4: UV-Vis spectra of **FT**, in inset fluorescence spectra of FT in DMF.

Fluorescence of **FT** was in 'OFF' mode which was expected due to the spirolactam ring closed form. Using this spirolactam ring we wanted to use it for the sensing of heavy metals. Our main concern was to detect any of As(III) salt ion, Cd^{2+}, Pb^{2+} metal ion by using FT and it's norbornene derivatives. As Hg^{2+} was detected by Using **FT** so we ignore Hg^{2+} as analyte. Sensing behavior of **FT** is in under investigation.

Conclusions

We have successfully synthesized the compound and characterized them. UV-Vis and fluorescence study have been done for the prepared compound. Norbornene derived monomers are under investigation. Once the norbornene derivatives prepared we want to make their polymeric materials and keenly have the intention to use them n real life application.

Acknowledgements

Authors are thankful to IISER-K for funding and infrastructure.

References

32. J. C. Saha, A. K. Dikshit, M. Bandyopadhyay and K. C. Saha, Crit. Rev. Environ. Sci. Technol., 1999, 29, 281.
33. Wikpedia, arsenic poisoning.
34. Tseng CH, Chong CK, Tseng CP, et al. (January 2003). "Long-term arsenic exposure and ischemic heart disease in arseniasis-hyperendemic villages in Taiwan". Toxicol. Lett 137(1–2): 15–21.
35. "Arsenic Poisoning". IHC World. Retrieved 2 May 2014
36. (a) R. K. Kalluri, T. Arbneshi, S. A. Khan, A. Neely, P. Candice, B. Varisli, M. Washington, S. McAfee, B. Robinson, S. Banerjee, A. K. Singh, D. Senapati and P. C. Ray, Angew. Chem., Int. Ed., 2009, 48, 1; (b) V. C. Ezeh and T. C. Harrop, Inorg. Chem., 2012, 51, 1213.
37. G. Samanta, A. Chaterjee, D. Das, P. P. Chowdhary, C.R. Chanda and D. Chakraborti, Environ. Technol., 1995, 16, 223.
38. D. Das, A. Chatterjee, G. Samanta and D. Chakraborti, Chem. Environ. Res., 1992, 1, 279.
39. M. Shull and J. D. Winefordner, Anal. Chem., 1984, 56, 2617.
40. Y. Madrid, D. Chakraborti and C. Camara, Microchim. Acta, 1995, 120, 63.
41. D. Melamed, Anal. Chim. Acta, 2005, 532, 1.
42. (a) T. P. Jahn and G. P. Bienert, in Advances in Experimental Medicine and Biology, Landes Bioscience, Austin, TX, 2010; (b) W. R. Cullen and K. J. Reimer, Chem. Rev., 1989, 89, 713.
43. H. N. Kim, W. X. Ren, J. S. Kim and J. Yoon, Chem. Soc. Rev., 2012, 41, 3210.
44. X. Dai , O. Nekrassova , M.E. Hyde and R.G. Compton, Anal. Chem.,2004, 76(19), 5924-5929.
45. Y. Wu, L. Liu, S. Zhan, F. Wanga and P. Zhou, Analyst, 2012, 137, 4171–4178.
46. Y. Wu,S. Zhan, F. Wang, L. He, W. Zhia and P. Zhou, Chem. Commun., 2012, 48, 4459–4461.
47. V. C. Ezeh and T. C. Harrop, Inorg. Chem., 2012, 51, 1213.
48. M. Baglan and S. Atilgan, Chem. Commun., 2013,49,5325-5327.

49. B. Dey, R. Saha and P. Mukherjee, Chem.Commun.,2013,49,7064-7066.
50. S. Bhattacharya, S. Sarkar and R. Shunmugam, J. Mater. Chem. A, 2013, 1, 8398–8405.
51. L. Jianga, L. Wang, M. Guoa, G. Yina, R.Wang, Sensors and Actuators B 156 (2011) 825–831.
52. X. Yang, Y. Li, Q. Bai, Analytica Chimica Acta 584 (2007) 95–100

MACRO 195

Fluorene Based Triazine Framework as Chemosensor for Selective Sensing of Nitroaromatic Explosives.

*Saumya Krishnan, T. S. Aruna., C. V. Suneesh**

Department of chemistry, University of Kerala, Kariavattom campus, Thiruvananthapuram, Kerala, 695581

suneeshcv@gmail.com

Abstract

Detection of nitroaromatic explosives has attracted considerable interest in the field of material science, as they cause serious harm to the humanity. In this work, we synthesized the fluorene based Triazine framework, **PTF** through Friedel Crafts reaction. The results indicate that the **PTF** is having high thermal stability and shows significant fluorescence quenching effects in presence of nitro aromatics especially with picric acid (PA). Quenching constant obtained for PA was higher than that of other nitroaromatic compounds. Simple synthetic procedure, high chemical and thermal stability and high selectivity and sensitivity make **PTF** as a better chemosensor for the detection of picric acid.

Keywords: *porous polymer-fluorescence quenching-stern volmer plot- life time measurement-sphere of action model*

Introduction

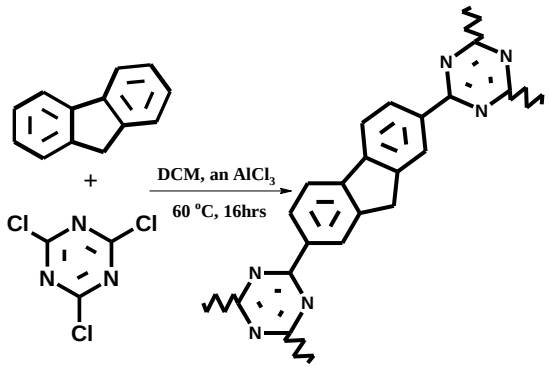
Nitro aromatic compounds (NACs) such as picric acid (PA), 2, 4, 6-trinitrotoluene (TNT) etc., are highly explosive in nature. There are many health concerns relating to nitroaromatics in addition to their explosive nature. Identification of NACs in soil, groundwater, and land mine areas have high demand, therefore suitable sensors[1] with high sensitivity and discriminating ability for the trace detection of NACs are highly sought out for. Sophisticated methods and techniques are now used for the detection of explosives. These methods are difficult to handle in on-field use. Microporous organic polymers (MOPs) are new class of materials which are finding extensive applications in gas adsorption, chemical separation, sensing, light emitting, catalysis and high energy material applications.[2] Triazine based networks are interesting class of highly stable Microporous polymers that have enjoyed popular attention in aforementioned applications.[3]

The aim of the present work is design and synthesis of microporous polymer like luminescent triazine based network for the facile detection of nitro aromatic explosives. In this work we have synthesized a triazine based Microporous polymeric network, (**PTF**) in high yield using Fluorene and Cyanuric chloride, by simple Friedel Craft reaction.[4,5] **PTF** exhibit luminescent properties and the fluorescent intensity decreases with various nitroaromatic analytes especially picric acid (PA).

Experimental

All the chemicals were purchased from spectrochem and used as received.

Synthesis of (PTF): Synthesis was carried out by slight modification of reported procedure [6] (Scheme 1).



Scheme 1 synthesis of **PTF**

To a 250 mL round bottom flask was added sequentially fluorene (1g, 6.01 mmol), cyanuric chloride (2.218g, 12.03 mmol), DCM (70 mL) and anhydrous $AlCl_3$ (3.2g, 24.04mmol). The flask was fitted with a condenser and heated for 16 hours under reflux. The resulting mixture was cooled to RT. The solid dark brown coloured precipitate was filtered off, washed several times with DCM, Methanol and Water to completely remove the unreacted starting precursors and catalysts and done the soxhlet extraction for 24 hours in methanol, dried in a vacuum for 6 hours to obtain the solvent free material in 86% yield.

Result and Discussion

PTF was synthesized by Friedel Craft reaction of fluorine with cyanuric chloride. In FTIR spectrum of **PTF**, the band centered at 850 cm^{-1} associated with C−Cl in cyanuric chloride vanishes and new bands at 1337 (C-N), and 1520 (C=N) cm^{-1} appears, indicating the presence of triazine moiety (figure 1a). The FTIR spectrum obtained is in good agreement with previous reports of the similar networks.[6]

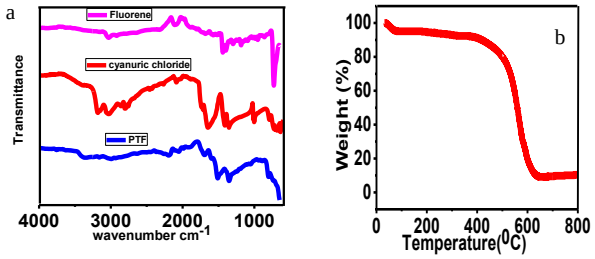


Figure 1 (a) FT-IR spectra of the **PTF** and precursors. (b)TGA thermogram of the **PTF** under nitrogen atmosphere.

The thermal stability of **PTF** was studied by TGA and the polymer remains stable up to 400 °C (figure 1b). ^{13}C CP-MAS Solid State NMR signals of **PTF** are obtained in expected range, which suggests the formation of triazine based frame works (Figure 2a). **PTF** shows a peak at 37 ppm, which can be assigned to the methylene bridge carbon in the fluorene unit. The other

major peaks at 115-150 ppm correspond to the aromatic carbons in the fluorene unit. A peak for the triazine ring carbons is observed at 172 ppm. The amorphous nature of the product was assessed by PXRD (figure 2b).

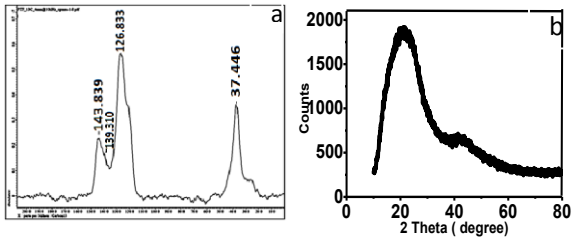


Figure 2 (a) ^{13}C solid-state MAS NMR spectrum of **PTF**. (b) Powder XRD pattern of **PTF**.

The ability of **PTF** to detect nitro aromatic explosives by fluorescence quenching was investigated by adding different analyte to **PTF**. Figure (4) shows the absorption and emission spectra of **PTF** in chloroform.

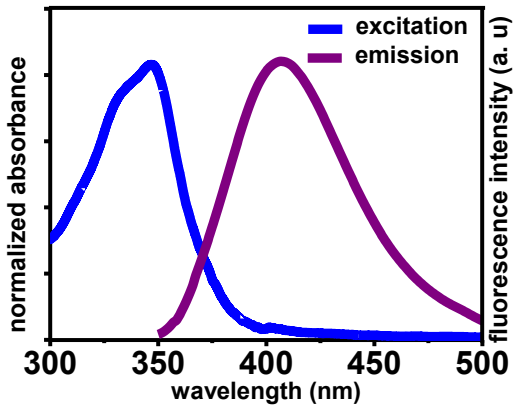


Figure 4. The absorption and fluorescence spectra of **PTF** in chloroform (red line) and (blue lines) respectively (λ_{ex} = 330 nm)

The long wavelength absorption of **PTF** occurs with a λ_{max} at 347 nm. The compound shows emission maximum peak at (λ_{max}) 409 nm upon excitation at 330 nm. With a stokes' shift of 4369 cm^{-1}. The fluorescence quantum yield of **PTF** was found out to be 0.5, which is one of the highest values reported for any MOP.

The fluorescence quenching studies of **PTF** was carried out using nitro and non nitro aromatic compounds. The non nitro aromatics did not show any appreciable quenching effect on the fluorescence. But the nitro aromatic compounds quenched the fluorescence to different extend. Twelve analyte molecules viz., Picric Acid (PA), 4-Nitro Phenol(NP), meta-dinitrobenzene(MDNB), trinitrotoluene (TNT), para-dinitrobenzene (PDNB), nitrobenzene (NB), dinitrotoulene(DNT), Aniline (A), Bromobenzene (BB), Benzene (B), Toluene (T), Xylene (X) were selected as quenchers. Different amount of analyte were added in to the dispersed solution of **PTF** in chloroform**.** Fluorescence intensity was found to decreases with the increase in concentration of nitro aromatics. Picric acid shows most efficient quenching of **PTF** emission. The reason for the fluorescence quenching can be attributed to the photoinduced electron transfer between the excited **PTF** (electron donor) and the electron acceptor analytes. The fluorescence quenching behaviors of **PTF** with various analytes are shown in figure 5a.

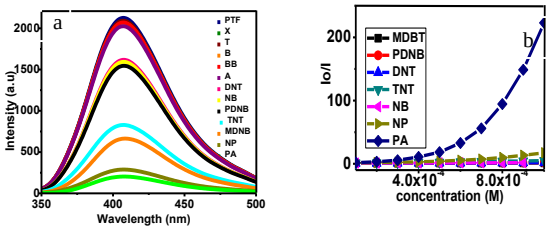


Figure 5(a) Concentration dependent fluorescence quenching of **PTF** upon the addition of same concentrations (0.4 mM) of different analytes (λ_{ex} = 330 nm). (b) Stern–Volmer plots of fluorescence quenching of **PTF** with different analytes

There is tremendous decrease in intensity with increase of analyte concentration. The percentage quenching can be calculating using the equation:

$$\% \text{ QE} = \frac{I_0 - I}{Io} \times 100 \ldots\ldots\ldots (1)$$

The polymer **PTF** shows high sensitivity for PA. The quenching efficiency is 93.3 % for PA. Quenching in fluorescence intensity of **PTF** is also observed on addition of various other quenchers like NP, MDNB, TNT, PDNB, NB, DNT, A, BB, B, T, X and percentage quenching (quenching efficiency) obtained is 86.4, 68.79, 61.04, 30.1, 25.07, 23.9, 4.77, 2.64, 2.98, 1.61, 1.93 respectively.

Stern-Volmer plot is constructed for all the quenchers using Stern-Volmer equation.

$$\frac{I_0}{I} = 1 + K_{SV}[Q] \ldots\ldots\ldots (2)$$

I_0 is the initial fluorescence intensity without the quencher, I is the fluorescence intensity after adding quencher of concentration [Q] and K_{SV} is Stern-Volmer quenching coefficient.

We obtained a non linear upward bending Stern-Volmer plot (figure 5b) which corresponds to a super-amplified quenching effect. From this plot it is clear that fluorescence quenching capability of picric acid is very high compared to other nitroaromatics. Hence **PTF** is very sensitive and selective for the detection of picric acid. The non linear nature of Stern-Volmer plot may be explained by assuming a coexistence of static and dynamic quenching. Dynamic quenching is happening due to the collisional interaction between an excited state fluorophore with a ground state quencher, whereas static quenching involves the formation of ground state complex of fluorophore and the quencher.

Figure 7a and 7b shows the fluorescence quenching of **PTF** with addition of increasing concentration of picric acid (PA) and p-nitrophenol (NP). Results indicate the super-amplified quenching, through a clear upward bending Stern-Volmer plot for PA and NP. Therefore a simultaneous existence of static and dynamic quenching may be presumed. Luminescence life-time of **PTF** is unaltered during the addition of increasing concentration of PA and NP, hence ruling out any dynamic contribution to the quenching (insets of figure 7c and 7d).

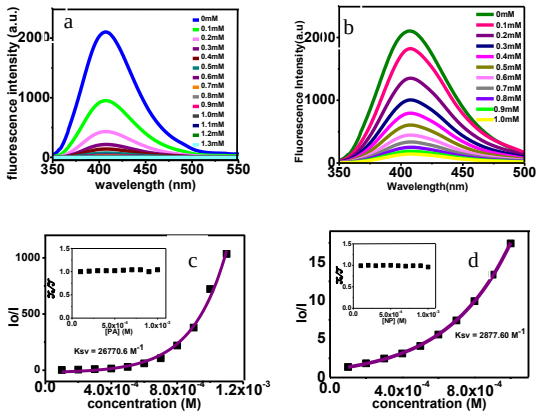


Figure 7 Emission spectra of **PTF** with addition of increasing concentration of

(a) PA, (b) NP.Non-linear Stern-Volmer plots of Io/I against concentration for (c) PA and (d) NP. Insets refer to the plots of relative fluorescence lifetimes against the concentrations of the corresponding analytes.

The upward bending Stern-Volmer plots can be explained by invoking Perrin's sphere of action model. This model describes an 'active sphere' as the volume around a fluorophore such that a quencher present within this volume will deactivate fluorescence with unit efficiency. Quenchers outside of this zone do not influence the excited state.[7] In this case fluorescence intensity decreases exponentially with quencher concentration and the quenching sphere of action model is explained by equation (3)[8]

$$Io/I = e^{V[Q]} \text{---------- (3)}$$

Where, V is the static quenching constant. If R is the radius of the quenching sphere, then

$$V = 4\pi R^3 N_A/3000 \text{ ---------- (4)}$$

By fitting quenching data shown in Fig 7(c& d) yielded equ (5) & (6) for NP and PA respectively.

$$Io/I = 1.00\, e^{2854[Q]} + 0.016 \text{ ---------- (5)}$$

$$Io/I = 5.58\, e^{4793[Q]} - 23.61 \text{---------- (6)}$$

$$Io/I = A\, e^{k[Q]} + B \text{----------(7)}$$

where equation (7) is general form of equations (5) and (6). Static quenching constant K is given by the product of k and A. Static quenching constants obtained from this methods are 2.9×10^3 M^{-1} and 2.7×10^4 M^{-1} for NP and PA respectively, and corresponding radii of quenching spheres are 10.4, 22.03 nm respectively. The high value of radius of the quenching sphere may be due to the large extent of exciton migration in conjugated MOPs. Limit of detection (LOD) of PA was calculated to be $1.87 \times 10^{-4}\, M$ (187 μM), showing the high sensitivity of **PTF** towards PA.

The fluorescence quenching studies reveals that the **PTF** is efficient in detecting the nitro aromatic explosives and it shows very high selectivity and sensitivity towards the detection of picric acid.

Conclusion

In this work we have synthesized fluorescent triazine based micro porous organic polymer **PTF**, by reaction of cyanuric chloride with fluorene via Friedel Crafts reaction. The synthesized polymer was used for the detection of various nitro aromatic compounds by fluorescence quenching method. The super-amplified quenching by nitroaromatics is explained by invoking Perrin's sphere of action model. Stern-Volmer plots showed that **PTF** exhibits high sensitivity and selectivity towards the detection of picric acid.

Acknowledgements

The authors thank University Grants Commission for UGC-BSR research start up grant to CVS. The authors also thank Dr.

Mahesh Hariharan, IISER Trivandrum for helping with TCSPC measurements.

References

MACRO 200

Fluorene based Polymers and Copolymers as Sensors

Malik Sudip

Polymer Science Unit, Indian Association for the Cultivation of Science, 2A & 2B Raja S. C. Mullick Road, Jadavpur, Kolkata – 700032, India.
E-mail: psusm2@iacs.res.in

Polyfluorene(PF), a relatively new conjugated polymer, consists of rigid planar biphenyl units, bridged by a carbon atom at 9-position, providing higher degree of conjugation. Additional substituents at 9-position have given opportunity to modify the polymer processability and interchain interactions in solid films, without significant change of electronic structure of individual polymer chain. Star shape copolymer having different core have designed, synthesized and correlations of physical properties with these copolymer structures [1-5] will be discussed. By changing the chemical structure at 9-position of monomer, fluorescent PF have been developed and their sensing properties and molecular mechanism will be explored. Several PF copolymers have been designed to detect metal ions.

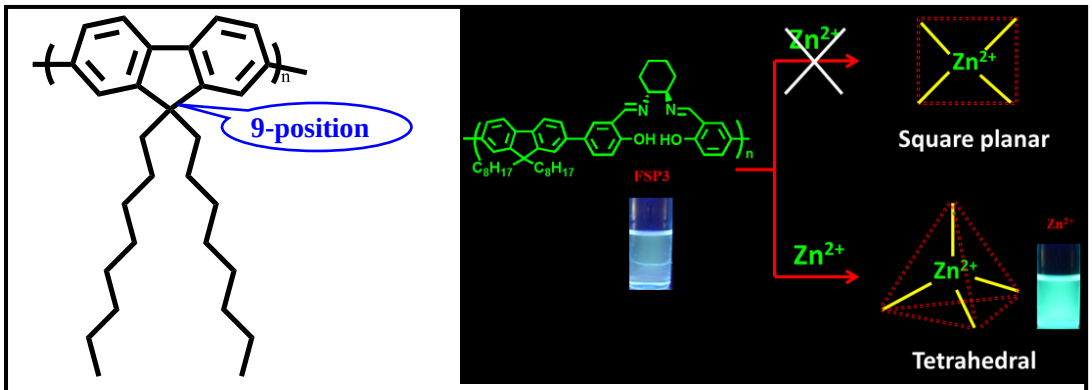


Figure 1. Chemical structure of polyfluorene, and the representation of Zn^{+2} detection by fluorene copolymers.

References

[20] Scherf U.; List, E. J. W. *Adv. Mater.*, 14 (2002), 477.
[21] Bera, M. K.; Chakraborty, C.; Singh, P. K.; Sahu, C.; Sen, K.; Maji, S. K.; Das, A. K.; Malik, S. *J. Mater. Chem. B* , 2 (2014) 4733.
[22] Bera, M. K.; Chakraborty, C.; Malik, S. *New J. Chem.*, 39 (2015) 9207.
[23] Chakraborty, C.; Bera, M. K.; Rana, U.; Malik, S. *Chem. Commun.*, 51 (2015) 13123.
[24] Bera, M. K.; Chakraborty, C.; Malik, S. *unpublished results*.

MACRO 202

Fluorescent Polystyrene Nanobeads for Biosensing and Imaging

Sarabjot Kaur [ab], Asha S. K.,*[ab]

[a] *Polymer Science and Engineering Division, CSIR-NCL, Pune, India-411008.*
E-mail: sk.asha@ncl.res.
[b] *Academy of Scientific and Innovative Research, New Delhi, India*

Fluorescent cross-linked polymer nanobeads are highly valuable for various applications in areas as diverse as sensors, bioimaging, optoelectronics and biolabelling. For instance, fluorescent polystyrene beads have been used in cell marker studies due to their proven biocompatibility. Polystyrene beads are also available commercially but they are developed either by dye encapsulation which often leads to dye leakage or by post modification where controlling particle size is an issue.

We have developed PS nanobeads incorporating fluorescent crosslinkers based on Perylene bisimide (PBI) and oligo-phenylenevinylene (OPV). The crosslinkers were incorporated covalently in varying amounts into polystyrene beads via miniemulsion polymerization to give a series of monodisperse fluorescent nanobeads of size ranging from 100-150 nm, which are ideal for cell marker studies. The size and morphology were confirmed using scanning electron microscopy and dynamic light scattering. The method is a simple one pot strategy to prepare water based fluorescent nanobeads which gave both solid state fluorescence as well as water based fluorescence directly from latex. Incorporation of as low as 10^{-7} mol% fluorophore into polystyrene nanobeads (as determined by absorption spectroscopy) was sufficient to result in solid state as well as water based fluorescence. The synthetic methodology could be extended to develop modified PS, where the surface of the fluorescent PS beads would be functionalized with moieties like glucuronic acid that could sense bioanalytes like bilirubin.

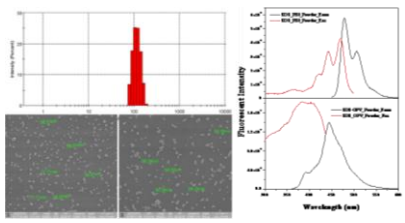


Figure1: Characterisation of fluorescent polystyrene nanobeads

References

[25]Sonawane, S. L.; Asha S. K. *ACS Appl Interfaces.*, 5 (2013) 12205.

[26]Lanfester, K. et al. *Macromol. Chem. Phys*., 206, (2005) 2440.

[27]Tuncel, D.; Demir, H. V. *Nanoscale*, 2 (2010) 484.

MACRO 205

Synthesis and characterization of partially fluorinated, quaternized anion exchange membrane for alkaline water electrolyser applications

A. Kalaiyarasi, S. Hosimin, S. Vengatesan*, G. Sozhan

CSIR- Central Electrochemical Research Institute, karaikudi – 630006, Tamilnadu, India

** e-mail id:* venki781@gmail.com

Abstract

In this study, anion exchange membrane is prepared by poly(PFBE and VBC) in this ratio is 3:1 and 5:1 (partially fluorinated co-polymer was synthesized from hydrocarbon and perfluourinated monomers through free radical polymerization). The membrane was characterized by TGA, FT-IR and NMR. Thermal analysis results showed that the composite membranes have good thermal properties they shows two stage degradation,the first 320 ^{o}C and the second at 435 ^{o}C.

Keywords:*anionexchangemembrane ;perfluourinated monomer;*

Introduction

Hydrogen is an attractive fuel for future energy demands, since it is a clean and renewable energy source. Water electrolysis produces ultra-pure hydrogen from more abundant water as a resource. There are three main types of water electrolysis processes, namely, alkaline water electrolysis, polymer electrolyte membrane water electrolysis and high temperature steam electrolysis. Of these, alkaline water electrolysis is more preferred since it affords the benefits of fast kinetics as well as the flexibility in using non-noble metal catalysts. Hydrogen is considered as a compact, zero-emmission fuel with greater flexibility and overall efficiency[1]. Advanced water electrolysis is the most efficient and economical way to obtain high purity hydrogen (>99.999 %), since it does not produce any green house gases as by-products [2]. A number of water electrolysis processes such as alkaline water electrolysis, proton exchange membrane (PEM) electrolysis and steam electrolysis have been developed for the production of hydrogen [3],[4],[5],[6]and[7]. Commercial Nafion® membranes that are widely used in these systems have good thermal, chemical and mechanical stability along-with high proton conductivity. However, the highly acidic environment of these membranes necessitates noble metal catalysts to be used in such systems. To overcome these issues, alkaline anion exchange membranes (AAEM) is considered as a suitable candidate that requires non-noble metal catalysts.

Experimental

Materials

PFBE from SigmaeAldrich , and vinylbenzylchloride (VBC) from Acros Organics (purity > 99%) were purchased and used as the monomers ;2 ,20

azobisisobutyronitrile(AIBN) purchased from SigmaeAldrich was used as initiator. Trimethylamine(TMA), 30% solutionwas purchased from Agros organics and used as amination agent, and solvents such as N-methyl pyrrolidone (NMP), dimethyl formamide (DMF), methanol and chloroform were analytical grade and used as-received. De-ionised water was used throughout the study.

Synthesis of poly (PFBE-co-VBC) co-polymer and amination:

Poly (PFBE-co-VBC) co-polymer was synthesised via free radical polymerization[11]and[12], the procedure is as follows: vinylbenzyl chloride and PFBE was dissolved in THF and taken in a 250 mL round bottom flask. Nitrogen gas was purged through the solution for 30 min, and AIBN was added into the solution under N2 atmosphere. The polymerisation reaction was carried out at 60·C for 24 h. Then, the solution was cooled and precipitated in methanol. The precipitate was dried under vacuum to yield poly (PFBE-co-VBC). The synthesized poly (PFBE-co-VBC) co-polymer was dissolved in DMF and TMA solution was added. The mixture was stirred for 12 h at ambient temperature to obtain the quaternized polymer as a viscous gel.

Membrane preparation:

The quaternized co-polymer was dissolved in NMP solvent for 30 min to obtain homogeneous solution. Then, the viscous solution was casted on a glass plate using doctor blade and dried at 110·Cfor over neight. The prepared membrane was peeled-off from the glass plate and soaked in de-ionised water.

Characterisations

FT-IR spectra of synthesized poly (PFBE-co-VBC) co-polymers and quaternized membranes were recorded in KBr pellets using Bruker27 Tensor FT-IR spectrophotometer with a resolution range of 0.125 cm^{-1}. 1H NMR analysis of the polymerisation products was performed on a Bruker Avance 400 MHz instrument using chloroform-d (CDCl3) as solvent and tetramethylsilane (TMS) as an internal reference. Thermal degradation and stability of the prepared membranes were investigated using a simultaneous TGA/DTA analyser (Model: SDT Q600, TA Instruments) under nitrogen atmosphere at a heating rate of 5 _C/min from 25 to 800 _C.

Results and discussion

In this work, partially fluorinated co-polymer was synthesized from hydrocarbon and perfluourinated monomers through free radical polymerization. Zonyl®PFBE and vinylbenzyl chloride (VBC) are used as monomers. The co-polymers with PFBE to VBC ratios of 3:1, 5:1 were synthesized and the obtained polymer was quaternized by trimethylamine.

Results:

(i) FT-IR studies

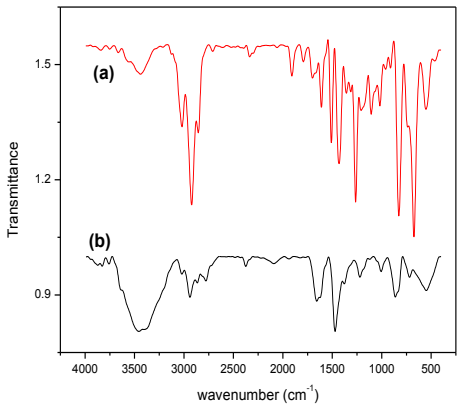


Fig.1 IR spectrum of (a) (PFBE-co-VBC) copolymer and (b) Quaternized copolymer

FT-IR spectra of synthesized poly (PFBE-VBC) co-polymer and quaternized polymer were recorded in KBr pellets using Bruker 27 Tensor FT-IR spectrometer. From the copolymer spectrum, peaks appear in the region of 700-850 cm^{-1} is due to C-Cl stretching and 1260 cm^{-1} is assigned to CH_2Cl wagging. The peak at 1609 cm^{-1} is assigned to aromatic C=C stretching. However, the peaks in the region of 700 – 850 cm^{-1} as well the peak at 1260 cm^{-1} disappeared in quaternized polymer spectrum which confirms the quaternization.

(ii) NMR Studies

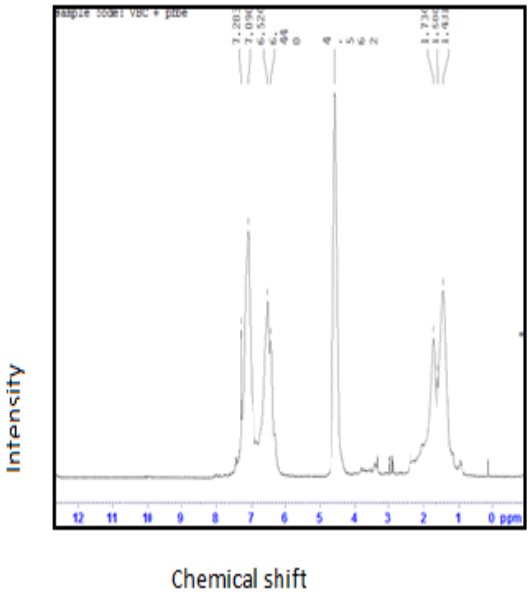


Fig.2 ^{1}H-NMR spectrum of PFBE-co-VBC polymer

The co-polymer synthesized was dissolved in Chloroform-d1 (NMR grade solvent) and subjected to ^{1}H-NMR studies. In the spectrum, The VBC group present in the co-polymer was confirmed by $–CH_2Cl$ peak present in the chemical shift 4.6 ppm. The peak around 6-8 ppm represents the aromatic protons and the solvent peak appears at 7. 3ppm. The peaks in the range of 1-2.5 ppm represent the aliphatic protons present in the side chain of VBC as well as the aliphatic protons of PFBE.

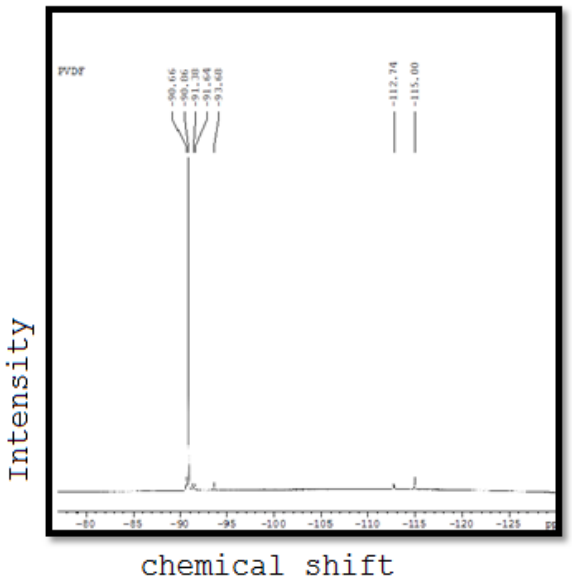


Fig.3 ^{19}F-NMR spectrum of (PFBE-co-VBC) copolymer

The ^{19}F spectrum of copolymer shows 3 distinct peaks at the chemical shift values of -90ppm, -112ppm and -115 ppm corresponding to CF, CF_2, CF_3 groups, respectively. This confirms the presence of PFBE in the co-polymer.

(iii) TGA analysis

From the TGA curves, the co-polymer shows two stage degradation: first degradation at 320 ^{o}C and the second at 435 ^{o}C showing the decomposion of monomers of the co-polymer. However, the quaternized polymer represents three degradation steps, (i) 85 ^{o}C , (ii) 250 ^{o}C and (iii) 400 ^{o}C which confirms the thermoplastic behavior of quaternized polymer

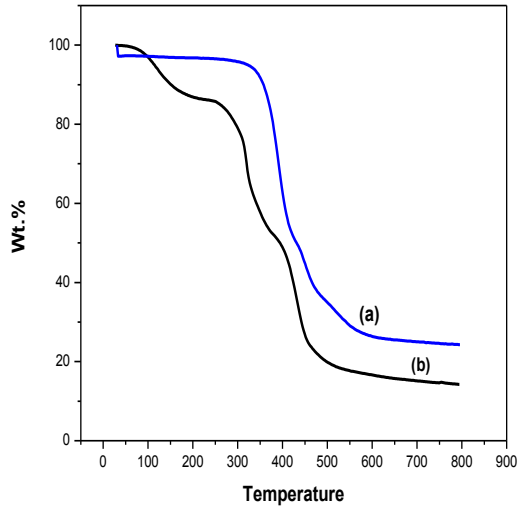


Fig.4 TGA curves for (a) PFBE-co-VBC copolymer and (b) quaternized copolymer

Conclusions

Poly (PFBE-co-VBC) based anion exchange membranes have been prepared via partially fluorinated co-polymer from hydrocarbon and perfluourinated monomers through free radical polymerization. Zonyl®PFBE and vinylbenzyl chloride (VBC) are used as monomers. PFBE toVBC ratio of co-polymer plays a vital role in achieving the membrane with good mechanical and chemical properties. The membrane with optimum PFBE to VBC ratios (3:1 and 5:1) exhibits good mechanical properties.

Acknowledgements

The authors acknowledge DST-SERB for providing the financial support through the grand-in-aid project (project code: GAP-05/14).

References

53. S. Vengatesan, S. Santhi, S. Jeevanantham, G. Sozhan Journal of Power Sources 284 (2015) 361e368

54. A. Ursua, L.M. Gandia, P. Sanchis, Hydrogen production from water electrolysis:current status and future trends, Proc. IEEE 100 (2012) 410e426

55. J. Fischer, H. Hofmann, G. Luft, H. Wendt, Fundamental investigations and Electrochemical engineering aspects concerning an advanced concept for Alkaline water electrolysis, AIChE J. 26 (1980) 294e802.

56. J.C. Ganley, High temperature and pressure alkaline electrolysis, Int. J. Hydrog.Energy 34 (2009) 3604e4361.

57. S.A. Grigoriev, V.I. Porembsky, V.N. Fateev, Pure hydrogen production by PEM electrolysis for hydrogen energy, Int. J. Hydrog. Energy 31 (2006) 171e175.

58. F. Barbir, PEM electrolysis for production of hydrogen from renewable energy sources, Sol. Energy 78 (2005) 661e669.

59. F.J. Salzano, G. Skaperdas, A. Mezzina, Water vapor electrolysis at high temperature:systems considerations and benefits, Int. J. Hydrog. Energy 10 (1985) 801e809.

60. G. Merle, M. Wessling, K. Nijmeijer, Anion exchange membranes for alkaline fuel cells: a review, J. Membr. Sci. 377 (2011) 1e35.

61. G. Couture, A. Alaaeddine, F. Boschet, B. Ameduri, Polymeric materials as anion-exchange membranes for alkaline fuel cells, J. Prog. Polym. Sci. 36(2011) 1521e1557.

62. Y.C. Cao, X. Wu, K. Scott, A quaternary ammonium grafted poly vinyl benzylchloride membrane for alkaline anion exchange membrane water electrolysers with no-noble-metal catalysts, Int. J. Hydrog. Energy 37 (2012) 9524e9528.

63. T. Ameringer, F. Ercole, K.M. Tsang, B.R. Coad, X. Hou, A. Rodda, D.R. Nisbet,H. Thissen, R.A. Evans, L. Meagher, J.S. Forsythe, Surface grafting of electrospunfibers using ATRP and RAFT for the control of bio-interfacial interactions,Biointerphases 8 (2013) 16.

64. Y.S. Lee, Y.S. Byoun, Poly (styrene-co-4-vinylbenzyl chloride) conjugated with 3 (dimethylamino) phenol: synthesis and antibacterial activity, Bull. Korean Chem. Soc. 23 (2002) 1833e1835.

MACRO 212

Surfactant Triggered Fluorescence Turn "on/off" Behavior of a Polythiophene – graft - Polyampholyte

Ghosh, Radhakanta[a]; Das, Sandip[a]; Chatterjee, Dhruba. P[b]. and Nandi, Arun. K[a].*

[a]Polymer Science Unit, Indian Association for the Cultivation of Science, Jadavpur, Kolkata-700 032, INDIA

[b]Dept. of Chemistry, Presidency University, Kolkata-700 073

**For correspondence: A. K. Nandi, Email: psuakn@iacs.res.in*

Polythiophene graft polyampholyte (PTP) is synthesized by atom transfer radical polymerization using N,N-dimethylaminoethyl methacrylate (DMAEMA) and tert-butyl methacrylate (TBMA) monomers from the polythiophene backbone, followed by hydrolysis. The side-chains present both

amine and carboxylic acid groups, which impart pH responsivity into the polymer. These polyampholyte shows aqueous solubility via formation of small sized miceller aggregates with hydrophobic polythiophene core and radiating polyionic side chains at the outer periphery (cationic or anionic depending on the pH of the medium). In acidic media, the amine groups are protonated and the PTP coassembles forming compound micelles with the anionic surfactant, sodium dodecyl benzene sulfonate (SDBS), resulting in a blue-shift in the absorption maximum and increase in the fluorescence intensity which diminishes the quenching of PTP exitons with water. The aggregates can be disassembled through the addition of a cationic surfactant cetyltrimethylammonium bromide (CTAB), regenerating the optical properties of the free PTP. Conversely, in basic media, the carboxylic acid group is deprotonated and the PTP co-assembles with CTAB, delivering a change in the optical properties, which can be subsequently reversed through the addition of SDBS. Thus the polymer shows repeatedly reversible fluorescence on and off with the sequential addition of differently charged ionic surfactants response in both acidic and basic medium. This result shows that PTP has potential for surfactant induced reversible fluorescence turn on and off using ionic surfactant (SDBS and CTAB) through ionic aggregates formation and de-assembly of that aggregates.

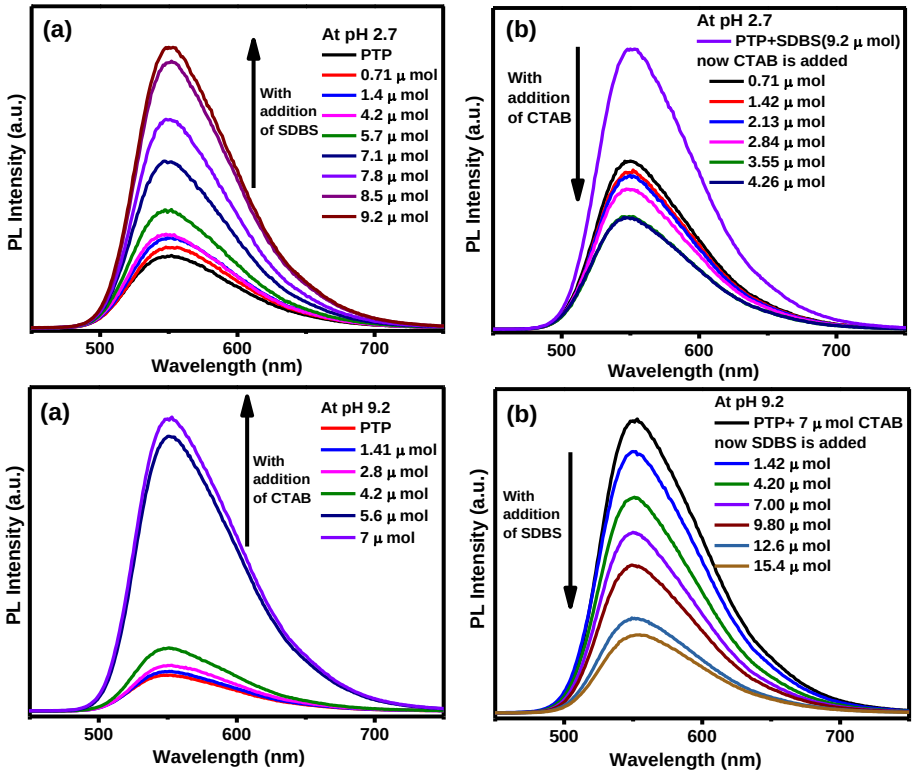


Figure 1. PL intensity vs wavelength plot of PTP in aqueous solution at pH 2.7 with increasing amounts of (a) SDBS and (b) CTAB and at pH 9.2 with increasing amounts of (a) CTAB and (b) SDBS.

References

[28]Li, Y; Bai, H; Li, C; Shi, G; *ACS Applied Materials & Interfaces*, 3 (2011) 1306.

[29]Evans, R. C; Knaapila, M; Willis-Fox, N; Kraft, M; Terry, A; Burrows, H. D; Scherf, U; *Langmuir*, 28 (2012) 12348.

MACRO 230

Carbamoylmethylphosphine Oxide (CMPO) Derived Cross-Linked Polymers for Uptake of Uranium (VI) From Nitric Acid Media

Suresh Annam,[a] Kari Vijayakrishna, [a]* Akella Sivaramakrishna,[a] C.V.S. Brahmmananda Rao,[b] and N. Sivaraman[b]

[a] *Department of Chemistry, School of Advanced Sciences, VIT University, Vellore-632014, Tamil Nadu, India.*

[b] *Chemistry Group, Indira Gandhi Centre for Atomic Research (IGCAR), Kalpakkam-603102, Tamil Nadu, India.*

* *e-mail id:* kari@vit.ac.in

Abstract

A new class of three different porous crosslinked polymers functionalized with carbamoylmethyl phosphineoxide (CMPO) was developed via the post-derivatization of a vinyl-anchored precursor, which were used as adsorbents for removal of uranium (VI) from aqueous solution. These materials were characterized by FT-IR, NMR, SEM, CP-MAS, nitrogen adsorption/desorption experiments. The effect on uranium (VI) as well as Th(IV) and Am(III) sorption behaviors of the functionalized polymers as was studied. The influence of porogens on the porous structures of polymers and their effect on uranium (VI) sorption was also discussed. As a result, CMPO grafted crosslinked polymers possessed not only a good sorption ability and a desirable selectivity for U(VI) over a range of competing metal ions.

Keywords: *phosphine oxides, uranium, porous polymers, distribution ratio.*

Introduction

Uranium is important element not only in energy but also in environmental problems. Recovery of uranium from waste generated from mining, hydrometallurgy of uranium and spent nuclear fuel is very important not only from the view of its limited resources of availability but, also for the reduction of its quantum for disposal as radioactive waste.[1] The development of efficient and economically viable methods for separation of uranium from waste water is desirable. For this purpose, numerous suitable separation techniques have been applied, including solvent extraction, precipitation, ion exchange, reverse osmosis, hyperfiltration, electrodialysis and sorption.[2-3] Solid phase extraction (SPE) is an appealing technique to realize the enrichment of uranium in extreme dilute media. In the past decade, a variety of sorbents such as montmorillonite clays, silica gels, macroporous adsorbents (XAD-4, XAD-7) have been used as solid support for

the sorption of uranium and other actinide elements from the dilute aqueous media.[4] Recently, meso-porous materials have attracted much attention in chemistry because of high surface areas, large ordered pores, diverse morphology and surface properties, as well as acid and radiation-resistance. Therefore, recent efforts have been devoted to prepare the porous functional materials with organic ligands which contain O, N, S and/or P donor atoms, and have affinity to bind with the actinide elements.[5]

Organo-phosphorous based solvents or extractants or ligands have been used to separate U(VI) and other fission products from aqueous solution. Tributyl phosphate (TBP) is the unanimous choice of extractant, which is used in PUREX process.[6] Several phosphorus-based extractants such as dialkyl alkylphosphonates,[7] 2-ethylhexylphosphonic acid[8] and octyl (phenyl)-N,N-diisobutylcarbamoylmethylphosphine oxide (CMPO) have been extensively studied for the separation and pre-concentration of actinide elements from aqueous solutions. Among various chelating molecule, carbamoylmethyl phosphineoxide (CMPO), a bifunctional organo- phosphorous ligand, for use in the TRUEX process (TRansUranic Extraction) for separation of many kind of the actinide and fission products ions.[9] Furthermore, CMPO shows fairly excellent chemical-stability in acidic medium. In 2003 suresh et.al studied the extraction behavior of actinides with CMPO adsorbed on the various macro-porous polymeric resins (XAD-4, XAD-7).[10]Similarly, in 2007, Subramanian et al. bound CMPO ligands to insoluble polymer resins, a process that has been established with several ligand systems.[11]

Herein, we present the study on a new class of mesoporous cross-liked polymers bearing CMPO ligands with different substituents. For the synthesis of cross-linked polymers, three kinds of vinyl-anchored CMPO derivatives with different alkyl chains at the amide end were prepared in advance, followed by the polymerization with ethylene glycol dimethacrylate (EGDMA) as a cross-linking agent, which serves a backbone to the polymer. In this study, a facile way was presented the bonding of CMPO ligands to the meso-porous crosslinked polymers, developed via the post-derivatization of a vinyl-anchored precursor. The synthesis scheme is illustrated in Figure 1. The CMPO functionalized mesoporous polymers were labeled as MPP 5a-c. The polymers were characterized by ^{1}H NMR, ^{31}P-CP-MAS NMR, and IR spectroscopies. The synthesized porous cross-linked polymers were evaluated for the extraction of uranium from nitric acid media ranging from 0.01-6M by batch sorption methods. The influence of porogens on the porous structures of polymers and their effect on the extraction of uranium (VI) was reported. The kinetics of equilibrium and the distribution ratios for other actinide elements Thorium(IV) and Amerecium(III) were also reported.

2 Experimental

2.1 Chemical Materials: 4-vinyl benzyl chloride, ethylene glycol dimethacrylate (EGDMA), Azobisisobutyronitrile (AIBN)

were purchased from Sigma-Aldrich India. All the reagents and solvents used for the synthesis of precursor molecules were of reagent grade. Solvents were dried prior to the use. The actinides, ^{241}Am and ^{233}U tracers were used from laboratory stock solutions and their radiochemical purity was established prior to use.

2.2 Synthesis of CMPO functionalized meso-porous cross-linked polymers

The CMPO derivatives functionalized with vinyl benzene was synthesized as per the procedure described below (Fig. 1).

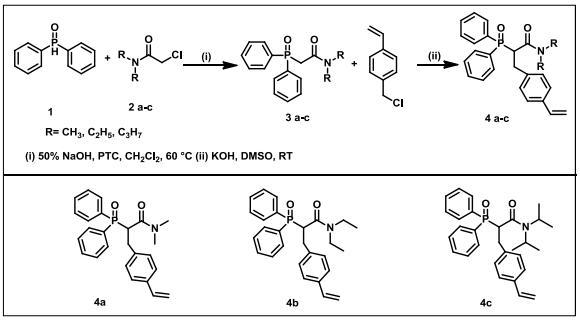


Figure 1: synthesis of vinyl-functionalized CMPOmonomer

2.2.1 **Synthesis of CMPO functionalized meso-porous cross-linked polymers.**

CMPO functionalized mesoporous polymers were synthesized by precipitation polymerization (figure 2). In a typical polymerization, required quantities of CMPO monomer, cross linker EGDMA and radical initiator AIBN were dissolved in the porogenic solvent in a schlenk tube. The solution was degassed in an ultrasonic bath, sparged with oxygen-free nitrogen for 10 min and the tube was sealed with a screw cap. The temperature of the oil bath was increased from room temperature to 60°C .over a period of 2 h, and then held at 60°C for a further 24 h. At the end of this period, the polymer particles were separated from the reaction medium simply by filtration on a 0.2 µm nylon membrane filter, washed sequentially with corresponding porogen in order to remove unreacted starting materials, and then dried in vacuum overnight at 60°C.

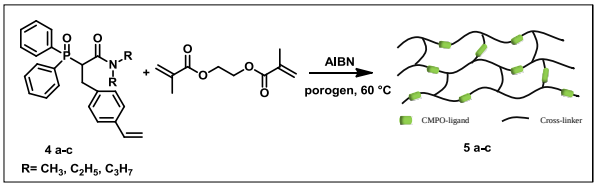


Figure 2: Schematic illustration of the synthesis process of CMPO-grafted crosslinked polymers.

2.3 Characterization Methods.

The ^{1}H, ^{13}C, and ^{31}P{1H}-NMR spectra of precursor molecules were recorded using BRUKER DMX-400 and all ^{1}H chemical shifts were reported relative to the residual proton resonance in deuterated solvents. The synthesized mesoporous silica was characterized by scanning electron microscopy (SEM), N_2 sorption/desorption isotherm experiments, solid-state magic angle spinning (MAS)-NMR spectra, thermo gravimetric analysis (TGA) and Fourier transform infrared spectroscopy (FTIR).

2.4 Batch Sorption Experiments

The sorption of U(VI), Th(IV) and Am(III) from aqueous solutions onto MPP5a-c at room temperature was studied by batch sorption methods as a function of nitric acid concentration ranging from 0.01-6M. In a typical experiment, to 0.1g of MPP5a-c was added equal volume of aqueous phase (containing requisite quantity of 233U/ 241Am tracer) and equilibrated in a rotary thermostated water bath for 4 h at 298K. After attainment of equilibrium, suitable aliquots from the both the phases (e.g.100µL)

were taken for radiometric assay of the actinides. For, Th(IV) estimation, 200 ppm of stock solution in corresponding nitric acid was equilibrated for 4 h. After the mixture was centrifuged, the concentrations of thorium ions in the solutions were determined by spectrophotometry using Arsenazo-III[12] as a chromogenic agent. The amount of the metal ions adsorbed on the polymers was calculated by using the following equation.

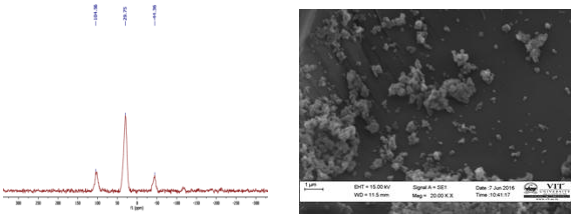
$$D_M = \left[\frac{[M]_{org}}{[M]_{aq}}\right] \frac{W}{V} \qquad (1)$$

Where D represents the amount of the metal adsorbed on the polymer, $M_{org.}$ and $M_{aq.}$ represents the amount of metal in organic (polymer) and aqueous phases respectively. W is the amount of polymer (g) and V is the volume of metal solution (L).

3 Results and discussion

3.1. Characterization of the adsorbents

The characterization results of the crosslinked polymers MPP5 a-c are shown in figure 3. ^{31}P CP-MAS NMR showed that the presence of carbomylmethyl phosphineoxide covalently bonded to the polymer matrix, whose resonance signal were observed at 30 ppm along with side bands at 24 and 36. The SEM image indicates that the polymer sample is composed of uniformly dispersed beads.



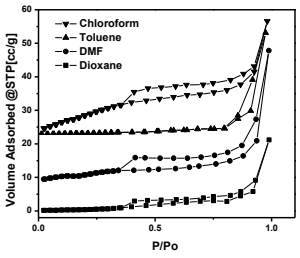
(a) (b)

Figure 3: Characterization MPP (a) 31P CP/MAS NMR (b) SEM image

3.2 Screening of porogen in polymer

Polymers with different pore sizes and porosities have been obtained using porogenic solvents viz. chloroform, toluene, dimethyl formamide and 1,4-dioxane. The effect of porogen on porous properties, N_2 Nitrogen gas adsorption–desorption isotherm tests were done to investigate the changes in the pore structure of resulted polymers and their subsequent effect on the extraction behavior was studied for U(VI) were shown in figure 4.

Porogen	Specific Surface area(g^2m^{-1})	Average pore diameter(nm)
chloroform	3.9	2.91
Toluene	0.514	7.31
DMF	1.98	10.78
Di-oxane	25.52	18.01



(a) (b)

Figure 4: (a)The N_2 sorption isotherms (b) physical parameters of the cross-linked polymers prepared in various porogens.

Figure 4 shows the effect of porogen on pore size and distribution of U(VI). Polymers obtained in Di-oxane are having higher pore volume and resulted the high distribution values for U(VI) from nitric acid media. The distribution data shows that how porogen having great influence on pore structure and sorption percentage of U(VI).

3.3 Extraction Kinetics

The U(VI) sorption by MPP-c for different contact time from 30 min to 7 h was performed to evaluate the sorption rate. The results are shown in figure 5.

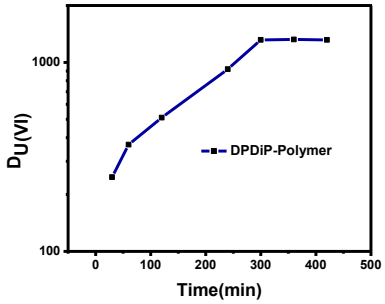
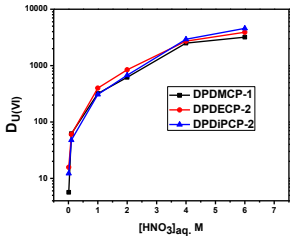


Figure 5: Kinetics of extraction of U(VI) from by CMPO polymer at 303 K.

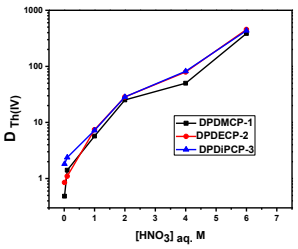
It is clear that the sorption process of U(VI) is slow and increased steadily up to 4 h. After 4 h, the sorption seems to be an equilibrium with the U(VI).

3.4 Actinide Extraction Properties of Functionalized Porous Polymers

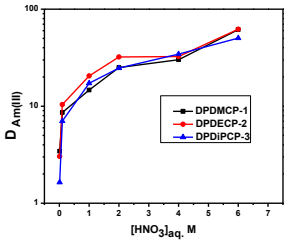
Extraction studies for actinide metals U(VI), Th(IV) and Am(III) were carried using three polymers functionalized with derivative CMPO chelating ligands. 50 mg polymer for U(VI) and 100mg for Th(IV) and Am(III) was used for the studies. Extraction studies were carried out as a function of nitric acid concentration from 0.01 to 6M at 303K.



(a)



(b)



(c)

Figure 6: Variation of (a) $\mathbf{D}_{U(VI)}$, (b) $D_{Th(IV)}$ and (c) $D_{Am(III)}$ with equilibrium aqueous phase nitric acid for the three CMPO-polymer at 303 K.

Fig. 6 a-c shows the distribution ratios of U(VI), Th(IV) and Am(III) for the three polymers. As increase in acid concentration distribution values are increased. Highest distribution values are obtained for the U(VI) as compared to that of Th(IV) and Am(III). All the polymers are showing the same distribution. i.e. change of substitution at the amide end is not showing much effect on the extraction of actinides.

Conclusions

In summary, a new category of mesoporous polymeric adsorbents functionalized with carbamoyl methyl phosphineoxide (CMPO) ligands was introduced. These porous polymer materials were characterized for surface area and pore-size distribution. Due to the favorable coordination properties of CMPO ligands with the actinide elements, these porous polymers showed good binding ability towards uranium (VI) in strong HNO_3 solutions than other actinides elements Thorium (IV) and Americium (III). For this reason, these adsorbent materials might find potential application in separation of

uranium(VI) from dilute nitric acid media.

Acknowledgements

Kari thanks IGCAR-Kalpakkam, [IGCAR/FChD/SCSS/Project-1/2014] for the financial support and Authors also thank DST-VIT-FIST for NMR, VIT-SIF for GC-MS and other instrumentation facilities.

References

65. H. J. Park and L. L. Tavlarides, Ind. Eng. Chem. Res. 49, 12567, 2010.
66. S. Lawrosky, Chem. Eng. Prog. 51, 461, 1955.
67. V.I. Grebenschikova, R.V. Bryzgalova, Radiokhimia 2 (1960) 265–273.
68. K.Vidya, SE. Dapurkar, P. Selvam, SK. Badamali, NM. Gupta, Micropor Mesopor Mat, 50, 173, 2001.
69. GE. Fryxell, YH. Lin, S. Fiskum, JC. Birnbaum, Environ Sci Technol, 39, 1324, 2005.
70. W.W. Schulz, L.L. Burger, J.D. Navratil, K.P. Bender (Eds.), Science and Technology of Tributyl Phosphate, CRC Press Inc., Boca Raton, 1984, p. 55.
71. C.K. Vyas, C. Brahmmananda Rao, S. Jayalakshmi, P.M. Joshirao, V.K. Manchanda, Radiochim. Acta, 103, 277, 2015.
72. C. Brahmmananda Rao, S. Jayalakshmi, N. Sivaraman, P. Vasudeva Rao Radiochim. Acta, 103, 235, 2015.
73. E. P. Horwitz, A. C. Muscatello, D. G. Kalina, L. Kaplan, Sep. Sci.Technol. 16, 417, 1981.
74. A. Suresh, C. V.S. Brahmmananda Rao, R. Deivanayaki , T. G. Srinivasan,P.R. Vasudeva Rao, Solvent Extr. Ion Exch. 3, 449, 2003.
75. Ch. Siva Kesava Raju, M.S. Subramanian, J. Hazard. Mater.145, 315, 2007.
76. P.R.V. Rao, S.K. Patil, J. Radioanal. Chem. 42, 399, 1978.

MACRO 235

Luminescence Study of Pyrene-tagged Poly-(*N*-Vinyl-2-pyrrolidone)

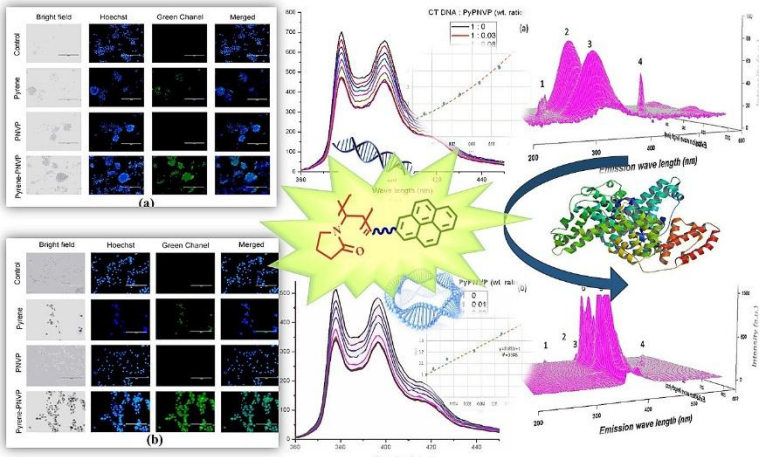
Mitra Kheyanath,[a] Singh Shikha,[a] Hira Sumit K.,[b] Patel Vijay K.,[a] Singh Deovrat,[a] Manna Partha Pratim,[b] Ray Biswajit[a*]

[a] *Department of Chemistry, Institute of Science, Banaras Hindu University, Varanasi – 221005, India*

[b] *Immunobiology Laboratory, Department of Zoology, Banaras Hindu University, Varanasi – 221005, India*

** Corresponding author email i.d.: biswajitray2003@yahoo.co.in*

Poly-(*N*-Vinyl-2-pyrrolidone) (PNVP) has been widely used in both chemical and biomedical fields for various applications like drug delivery, stabilization, phase transfer catalyst and selective chelating agent due to its low toxicity, high water solubility and bio-compatibility.[1-4] On the other hand, pyrene is a fluorescent, hydrophobic polycyclic aromatic hydrocarbon. Pyrene and its derivatives have been exploited widely in the field of chemical, environmental and biomedical sciences as fluorescent sensor and probe.[5-6] For controlled synthesis of PNVP with tunable chain-end reversible addition fragmentation chain transfer (RAFT) polymerization has been evolved as one of the most successful method.[1-4] In earlier study we have synthesized azide terminated PNVP by RAFT polymerization using [(*S*)-2-(4-azidobutyl propionate)-(*O*-ethyl xanthate)] as mediator and there off synthesized pyrene-tagged PNVP (PyPNVP) *via* click chemistry of 1-prop-2-ynyloxymethyl-pyrene.[4]



Here, we have explored the fluorescence based application of this amphiphilic PyPNVP having higher water solubility, biocompatibility and complexation ability compared to hydrophobic pyrene. The PyPNVP has successfully acted as turn off chemosensor for metal ions Cu^{+2}, Hg^{+2}, and Pb^{+2}. It has also successfully acted as fluorescent probe for critical micellar concentration (CMC) determination of amphiphilic block copolymer. It has also successfully showed interaction with both plasmid and calf thymus (CT) DNAs as evidenced by its fluorescence quenching. Different magnitude and type of quenching has been observed for both the cases which may be useful in distinguishing different kinds of DNAs. In order to further understand the potential of PyPNVP in various biotechnological processes, binding property of it with bovine serum albumin (BSA) has also been studied. The efficient quenching of intrinsic fluorescence of BSA by PyPNVP through binding and occurrence of the fluorescence resonance energy transfer (FRET) type of interaction have been studied using steady state, synchronous and 3D fluorescence spectroscopies. Such protein and DNA binding properties can make PyPNVP suitable for the therapeutic delivery purpose and other biotechnological uses like biosensors assay, biomaterial separations etc. Fluorescence microscopic cell imaging study reveals the significant uptake of PyPNVP in HEPG2 (human hepatocellular carcinoma) and U87 (human glioblastoma) cells compared to free Py. Thus, PyPNVP can also be used as efficient cell tracker.

References

[30] Hira, S. K.; Ramesh, K.; Gupta, U.; Mitra, K.; Misra, N.; Ray, B.; Manna, P. P. *ACS Appl. Mater. Interfaces*, 7 (2015) 20021.

[31] Mishra, A. K.; Patel, V. K.; Vishwakarma, N. K.; Biswas, C. S.; Raula, M.; Mishra, A.; Mandal, T. K.; Ray, B. *Macromolecules*, 44 (2011), 2465.

[32] Patel, V.K., Viswakarma, N. K., Mishra, A. K., Biswas, C. S., Maiti, P.; Ray B. *J. Appl. Polym. Sci.*, 127 (2013) 4305.

[33] Patel, V. K.; Viswakarma, N. K.; Singh, S.; Mitra, K.; Ramesh, K.; Misra, N.; Ray, B.; *Int. J. Polym. Mater. Polym. Biomater.*, 65 (2016), 269.

[34] Zhang, J.; Chen, W.; Tang, B.;, Zhang, W.; Chen, L.; Duan, Y.; Zhu, Y.; Zhu, Y.; Zhang, Y.; *RSC Adv.*, 6 (2016) 23622.

MACRO 242

Design and synthesis of new organic electronic materials based on hetero doped organic polymers

X-Yu Cao[a] and A. Pradhan[b] *
[a] *Xiamen University, Xiamen-361005, China*
[b] *Department Material Science, DST-Inspire Faculty, IACS, Kolkata-700032, India*
* *e-mail id:* msap5@iacs.res.in

Abstract: New centrosymmetric star-shaped thiolated hole-transporting materials (HTMs) including a truxene core have been successfully synthesized and investigated for high performance perovskite solar cells. These findings open the opportunities for efficient HTMs based on the functionalized truxene utilizing the strong interactions of their functional groups with perovskite. Maximum power conversion efficiency (PCE) of 11.87 % has been achieved by employing thiolated truxene derivatives.

Since the first reported in 2009 by Miyasaka,[1a] perovskite-based solar cells (PSCs) have great interest because of their unique optical and electrical properties and rapidly become the hottest topic in photovoltaics. The organic-inorganic hybrid perovskite solar cells (PSCs) have drawn great attentions as a real competitor to silicon solar cell,[1] due to their high power conversion efficiencies, easy fabrication, and low cost. Moreover, the organic-metal halide perovskites are direct band gap materials which exhibit strong light harvesting characteristics within the visible solar spectrum.[2a] In PSCs, lead halide perovskite $CH_3NH_3PbI_3$ widely used as perovskite semiconductors, act as photo absorbers to generate free carriers that can be collected in the electrodes through both p- and n-type buffer layers.[2] PCEs in a relatively short period for such cells have been substantially increased, mainly improvements of the fabrication protocols for the perovskite layer.[3] However, a large amount of the converted photon energy is wasted by the surface recombination resulting from the imperfect crystal passivation and undesirable interfacial behaviour. Therefore, further efficiency enhancement mainly relies on minimizing the interface losses by interface modification between the active layers [4] Recently, a breakthrough in PCE has been achieved by replacing traditional dyes with organic−inorganic hybrid perovskite.[4] The HTMs at the other side of perovskite layer also play an important role in the most efficient PSCs. Recently, an impressive PCEs was achieved over 18% with 5,10,15-trihexyl-3,8,13-tris(4-methoxyphenyl)-10,15-dihydro-5H diindolo[3,2-a:3′,2′-c]carbazole (triazatruxene derivative)[5] as an HTM. In these PSCs, triazatruxene (TAT) derivatives has been utilized to be an excellent HTM, even though other small-molecule HTMs such as 3,4- ethylenedioxythiophene-,[6] pyrene-,[7] linear π-conjugated-,[8] butadiene-,[9] and spiro-OMeTAD derivatives-[10] based HTMs gave high conversion efficiencies of 11 to 20%. Some polymer HTMs [11] with excellent electrical properties also resulted in high photovoltaic performances. The development of alternative HTMs is left an attractive goal because they are cheaper and easier to purify than that of the spiro-OMeTAD. An ideal HTM generally requires compatible energy level, sufficient charge extraction and transferability.

In our previous work we observed that introducing thiols unit into the hexabenzocoronene (TSHBC)[12] skeleton worked as a HTM for PSCs. Although it has poor hole mobilities which limit the fill-factor and thus overall efficiency of perovskite solar cells but larger intermolecular π-orbital overlap, improved stability, and ease of functionalization also. To the best of our knowledge, our group first employed thiolated nanographenes (TSHBC) in PSCs as HTMs to date.

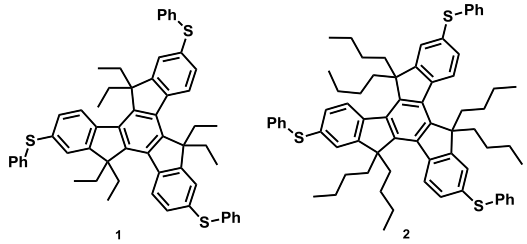


Figure 1. Structures of synthesized star-shaped HTMs.

Star-shaped truxene and triazatruxene derivatives are potential new HTMs for PSCs, since they have been known as hole selective layers for organic solar cells.[13] Truxene have been used for nonlinear optical (NLO) [14], organic photovoltaics (OPVs) [15], and organic light-emitting diodes (OLEDs) [16]. Truxene core being structured from three indene units combined by one benzene ring can be considered as a two-dimensional π-system, which provides a large aromatic surface to overlap with each other for efficient intermolecular charge hopping. In addition, it offers large chemical versatility to tune electronic and morphological properties. Considering these advantages and high hole mobility values,[17, 18] herein, we use thiolated star shaped rigid plannar 10,15-30 dihydro-5*H*-diindeno[1,2-*a*;10,20-*c*]fluorine (truxene) (the structures shown in **Figure 1**) as the HTMs in the pristine form in PSCs. The peripheral thiol groups form Pb−S coordination bonds at the interface of perovskite and HTM. The tight binding of thiolated truxene

helps to rapidly extract charge from perovskite, resulting in a low energy loss at the interface. The performance is readily improved by doping with plannar thiolated truxene to enhance the hole transporting property within HTM.

The synthesis started from alkylations of the known 10,15-dihydro-5H-diindeno[1,2-a:1',2'-c]fluorine (truxene)[19] **3** (**Figure 2**) with 1-bromoethane and 1-bromobutane respectively in the presence of KOH to give compounds **4a** and **4b** in a quantitative yield. Six alkyl groups were introduced onto the truxene core to increase the solubility and also to increase their hydrophobicity. Compounds **4a** and **4b** was brominated with bromine in chloroform with a catalytic amount of $FeCl_3$ at 0 °C, giving compounds **5a** and **5b** respectively in a high yield. Compounds **5a** and **5b** was then treated with thiol and a catalytic amount of $[Pd(OAc)_2]$ to give **1** and **2** respectively (See SI), despite the three nucleophilic substitution reactions.

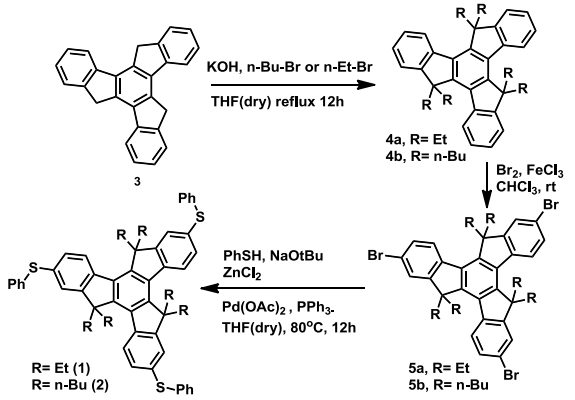


Figure 2. Synthesis of thiolated truxene.

The normalized UV−vis absorption spectra of **1** and **2** in DCM solution are shown in **Figure 3a**. Absorption bands appear in the spectral region between 250 and 350 nm, which are assigned to the π−π* transitions of the conjugated system. The experimental HOMO energy levels of the thiolated truxene derivatives were estimated from cyclic voltammogram with ferrocene as external reference (**Figure 3b**). The LUMO/HOMO values were determined as -5.95/-2.80 eV and -5.92 eV/-2.82 eV *vs* vacuum for **1** and **2**, respectively (Table 1). The HOMO levels are slightly higher than that of $CH_3NH_3PbI_3$ perovskite (-5.40 eV). The alkyl chains almost didn't influence their energy levels. To further understand their electronic structures, the molecular orbitals (MO) of thiolated truxene were calculated through the density functional theory (DFT) method at the B3LYP/6-311G(d,p) level in gas phase. Alkyl chains were replaced by methyl. As shown in **Figure 4**, the introduction of thiophenyl influence both HOMO and LUMO of truxene derivatives due to the delocalization of HOMO and LUMO to thiophenyl. And the planar and large π-conjugated backbone contribute to their ordered packing in solid state, thus enhance their carrier transport abilities.

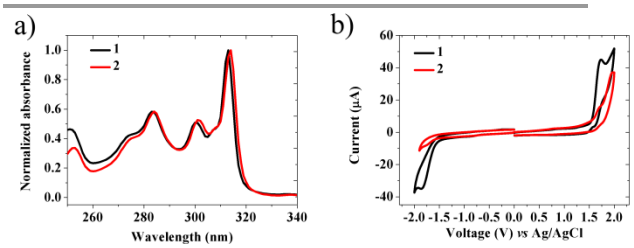


Figure 3. a) Normalized absorption spectra of **1** and **2** in CH_2Cl_2 (1×10^{-5} M). b) Cyclic voltammetry of **1** and **2** in CH_2Cl_2 with 0.1 M *n*-Bu_4NPF_6 as the supporting electrolyte.

Table 1. Summary of optical and electrochemical data.

	HOMO (eV)	LUMO (eV)	Eg (eV)
1	-5.95	-2.80	3.91
2	-5.92	-2.82	3.90

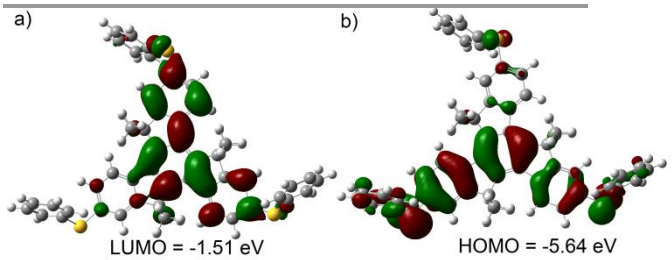


Figure 4. a), b) LUMO and HOMO of thiolated truxene optimized at the B3LYP/6-311G(d,p) level. Alkyl chains were replaced by methyl to facilitate the calculation.

Compound **1** and **2** were used as HTMs. The PSCs had a typical p-i-n configuration of FTO/TiO_2/$CH_3NH_3PbI_3$/Thiolated truxene/Au. In a typical fabrication procedure, the compact TiO_2 layer and mesoporous TiO_2 layer were deposited on a FTO (fluorine doped tin oxide) conducting glass substrate, to achieve electron extraction and transport. We employed here thiolated truxene derivatives (20 nm thickness) on top of perovskite layer as HTMs. The entire fabrication procedure was in the open air at a common relative humidity of 45%. The fabricated perovskite devices were characterized by SEM (**Figure 5**) and XRD (**Figure S4**).

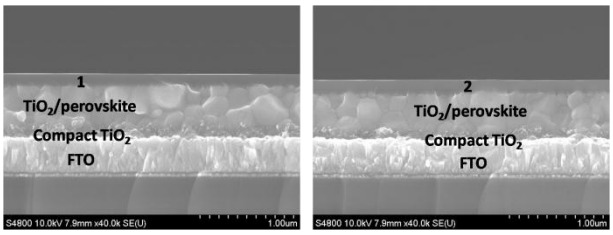


Figure 5. (1 & 2) Cross-sectional SEM image of the device of FTO/TiO2/perovskite/Truxene derivatives film.

To evaluate whether thiolated truxene derivatives could serve as effective materials to extract photogenerated holes from the perovskite layer, the *J*−*V* characteristics of FTO/TiO_2/$CH_3NH_3PbI_3$/Thiolated truxene/Au devices were measured under the illumination of AM 1.5, 100 mW cm^{-2}. As shown in **Figure 6a**, when ~80 nm thick thiolated truxene was deposited on the top of the perovskite layer as HTM, the best efficiency of compounds **1** and **2** was achieved 11.45 % and 11.87 % respectively. The open-circuit voltage (V_{oc}), short-cut current (J_{sc}), and fill-factor (FF) were measured to be 0.97 V, 19.32 mA·cm^{-2}, and 61.12 % respectively for ethyl substituted thiolated truxene **1** but in the case of butyl substituted thiolated truxene **2** these values are little different 0.98 V, 19.43 mA·cm^{-2}, and 62.34 % (**Table 2**). The measurements over 30 devices gave an average efficiency of 10.8 ± 2.0% (**Figure 6c**). The incident photon-to-current conversion efficiency spectra (IPCE) of the device spanned from the UV region to 800 nm (**Figure 6b**), matching well with UV−vis absorption spectra of perovskite. Introducing different alkyl chain length (ethyl to butyl) in thioated truxene derivates increased hydrophobicity of the HTM, which is readily provided as an effective molecular sealing approach to improve the stability of PSCs. Hydrophobic long chain alkylated thiolated truxene derivatives on perovskite surface immediately inhibited to enter water molecules into perovskite film and significantly enhance the stability of PSCs.

The excellent performance of PSCs, involving the use of thiolated truxene as HTM, suggested a unique hole-extracting interface between perovskite and thiolated truxene. The higher efficiency also suggested the formation of Pb−S coordination-bond between thiolated truxene derivatives and perovskite.[12] This work confirm the concept that the formation of Pb−S coordination bonds between TSHBC derivatives and perovskite contribute the efficient electron extraction at the interface.

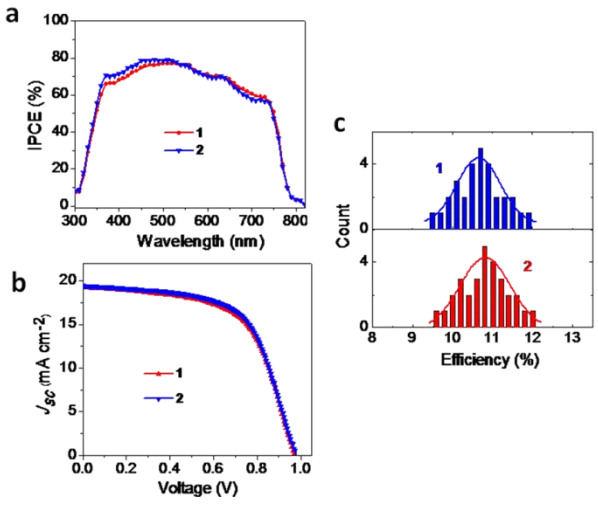


Figure 6. (a) Best I−V characteristics. (b) The IPCE spectra of the devices. (c) Comparison of the performance distributions of 30 individual devices of the cells.

Table 2. Photovoltaic parameters of the champion cells.

HTM	J_{sc}/mA·cm^{-2}	V_{oc}/V	*FF*/%	*η*/%	*Rs*/Ω·cm^{-2}
1	19.32	0.97	61.12	11.45	11.31
2	19.43	0.98	62.34	11.87	11.28

Conclusions

In summary, we report a rapid and efficient synthesis of two thiolated truxene-based two-dimensional HTMs, comprising electron-rich thiol engineered substituent's. HTMs are obtained from simple and inexpensive starting materials merely in four scalable synthetic steps, offering potentially much lower production costs. Thiolated truxene derivatives exhibit surface interaction with perovskite material resulting in efficient hole injection from the valence band of perovskite into the HOMO of HTM. Power conversion efficiency of 12.0 % was realized when **1** and **2** were used as HTM.

Our study demonstrates a potential of two-dimensional materials like thiolated truxene derivatives as an alternative for the existing cost ineffective and synthetically challenging spiro- OMeTAD and PTAA HTMs in PSCs. We expect that further modification of the thiolated truxene core by molecular engineering of functional groups not only improves interfacial properties and efficiency but also protects from humidity and UV induced degradation of PSCs.

Notes and references

1 (a) A. Kojima, K. Teshima, Y. Shirai and T. Miyasaka, *J. Am. Chem. Soc.* 2009, **131**, 6050. (b) J. H. Im, C. R. Lee, J. W. Lee, S. W. Park and N. G. Park, *Nanoscale* 2011, **3**, 4088. (c) H. S. Kim, C. R. Lee, J. H. Im, K. B. Lee, T. Moehl, A. Marchioro, S. J. Moon, R. Humphry-Baker, J. H. Yum, J. E. Moser, M. Gratzel and N. G. Park, *Sci. Rep*. 2012, **2**, 1. (d) M. M. Lee, J. Teuscher, T. Miyasaka, T. N. Murakami and H. J. Snaith, *Science* 2012, **338**, 643. (e) H. Zhou, Q. Chen, G. Li, S. Luo, T. B. Song, H. S. Duan, Z. Hong, J. You, Y. Liu and Y. Yang, *Science* 2014, **345**, 542. (f) N. J. Jeon, J. H. Noh, W. S. Yang, Y. C. Kim, S. Ryu, J. Seo and S. I. Seok, *Nature* 2015, **517**, 476. (g) N. J. Jeon, J. H. Noh, Y. C. Kim, W. S. Yang, S. Ryu and S. I. Seok, *Nat. Mater*. 2014, **6**, 897. (h) W. S. Yang, J. H. Noh, N. J. Jeon, Y. C. Kim, S. Ryu, J. Seo and S. I. Seok, *Science* 2015, **348**, 1234. (i) A. Mei, X. Li, L. Liu, Z. Ku, T. Liu, Y. Rong, M. Xu, M. Hu, J. Chen, Y. Yang, M. Grätzel and H. Han, *Science* 2014, **345**, 295. (j) W. Nie, H. Tsai, R. Asadpour, J.-C. Blancon, A. J. Neukirch, G. Gupta, J. J. Crochet, M. Chhowalla, S. Tretiak, M. A. Alam, H.-L. Wang and A. D. Mohite, *Science* 2015, **347**, 522.

2 (a) K. Lim, M-S. Kang, Y. Myung, J-H. Seo, P. Banerjee, T. J. Marks and J. Ko, *J. Mater. Chem. A*, 2016, **4**, 1186. (b) Y. Yamada, T. Nakamura, M. Endo, A. Wakamiya and Y.

Kanemitsu, *J. Am. Chem. Soc.* 2014, **136**, 11610. (c) J. S. Manser and P. J. Kamat, *Nat. Photonics* 2014, **8**, 737. (d) C. La-o-vorakiat, T. Salim, J. Kadro, M.-T. Khuc, R. Haselsberger, L. Cheng, H. Xia, G. G. Gurzadyan, H. Su, Y. M. Lam, R. A. Marcus, M.-E. Michel-Beyerle and E. E. M. Chia, *Nat. Commun*. 2015, **6**, 7903.

3 (a) M. Xiao, F. Huang, W. Huang, Y. Dkhissi, Y. Zhu, J. Etheridge, A. Gray-Weale, U. Bach, Y.-B. Cheng and L. Spiccia, *Angew. Chem., Int. Ed*. 2014, **53**, 9898. (b) N. Ahn, D.-Y. Son, I.-H. Jang, S. M. Kang, M. Choi and N.-G. Park, *J. Am. Chem. Soc*. 2015, **137**, 8696.
4 (a) J. Min, Z.-G. Zhang, Y. Hou, C. O. Ramirez Quiroz, T. Przybilla, C. Bronnbauer, F. Guo, K. Forberich, H. Azimi, T. Ameri, E. Spiecker, Y. Li and C. Brabec, *J. Chem. Mater*. 2015, **27**, 227. (b) L. Liu, A. Mei, T. Liu, P. Jiang, Y. Sheng, L. Zhang and H. Han, *J. Am. Chem. Soc*. 2015, **137**, 1790.(c) L. Zuo, Z. Gu, T. Ye, W. Fu, G. Wu, H. Li and H. Chen, *J. Am. Chem. Soc*. 2015, **137**, 2674.
5 K. Rakstys, A. Abate, M. I. Dar, P. Gao, V. Jankauskas, G. Jacopin, E. Kamarauskas, S. Kazim, S. Ahmad, M. Grätzel, and M. K. Nazeeruddin, *J. Am. Chem. Soc*. 2015, **137**, 16172.
6 H. Li, K. Fu, A. Hagfeldt, M. Gratzel, S. G. Mhaisalkar and A. C. Grimsdale *Angew. Chem., Int. Ed*. 2014, **53**, 4085.
7 N. J. Jeon, J. Lee, J. H. Noh, M. K. Nazeeruddin, M. Gratzel and S. I. Seok, *J. Am. Chem. Soc*. 2013, **135**, 19087.
8 J. Wang, S. Wang, X. Li, L. Zhu, Q. Meng, Y. Xiao and D. Li, *Chem. Commun.* 2014, **50**, 5829.
9 S. Lv, L. Han, J. Xiao, L. Zhu, J. Shi, H. Wei, Y. Xu, J. Dong, X. Xu, D. Li, S. Wang, Y. Luo, Q. Meng and X. Li, *Chem. Commun*. 2014, **50**, 6931.
10 N. J. Jeon, H. G. Lee, Y. C. Kim, J. Seo, J. H. Noh, J. Lee and and S. Seok, *J. Am. Chem. Soc* 2014, **136**, 7837.
11 Y. Xiao, G. Han, Y. Chang, H. Zhou, M. Li and Y. Li, *J. Power Sources*, 2014, **267**, 1.
12 J. Cao, Y. M. Liu, X. Jing, J. Yin, J. Li, B. Xu, Y. Z. Tan and N. Zheng, *J. Am. Chem. Soc* 2015, **137**, 10914.
13 S. W. Shelton, T. L. Chen, D. E. Barclay and B. Ma, *ACS Appl. Mater. Interfaces* 2012, **4**, 2534.
14 J. Shao, Z. Guan, Y. Yan, C. Jiao, Q. H. Xu, and C. Chi, *J. Org. Chem.* 2011,**76**, 780.
15 T. Bura, N. Leclerc, S. Fall, P. Leveque, T. Heiser and R. Ziessel, *Org. Lett.* 2011, **13**, 6030.
16 W. Y. Lai, Q. Y. He, R. Zhu, Q. Q. Chen and W. Huang, *Adv Funct Mater* 2008, **18**, 265.
17 A. B. Hernandez, U. K. Pandey, E. Cavero, R. Termine, E. M. G. Frutos, J. L. Serrano, A. Golemme and B. G. Lor, *Chem. Mater*. 2013, **25**, 117.
18 F. J. Ramos, K. Rakstys, S. Kazim, M. Gratzel, M. K. Nazeeruddin and S. Ahmad, *RSC Adv*. 2015, **5**, 53426.
19 H. Tsuji, Y. Ota, S. Furukawa, C. Mitsui, Y. Sato and E. Nakamura, *Asian J. Org. Chem.* 2012, **1**, 34.

MACRO 246

Flexible Micro-Supercapacitors using Silk and Cotton Substrates

Chayanika Das[a] and Kothandam Krishnamoorthy.*[a]

[a] *Polymers Science and Engineering Division, CSIR- National Chemical Laboratory, Pune-411008, India*

* *e-mail id:* kkrishnamoorthy1976@gmail.com

Abstract

Flexible micro supercapacitors in the form of yarn are among the sources of energy for wearable devices. Recently, many forms of carbon and conducting polymers and their composites are being exploited for making such yarn supercapacitors. Making yarns out of such materials involves biscrolling or spinning methods. To avoid such involved processes, we thought of making yarn supercapacitors by using silk fibers (SFs) which can be drawn from a silk cocoon. Since SFs are insulators, they require surface modification by conducting materials (viz. gold) to impart conductivity. A new method of gold deposition was introduced where polyphenols in green tea was used as protective and reductive layer which reduces Ag^+ to Ag. Electropolymerized Poly(3,4-ethylenedioxythiophene) (PEDOT) was used as an active material for the supercapacitor. The device was fabricated by twisting a PEDOT@ GSF and a GSF. The device showed an impressive performance with high energy and power densities.

Keywords: *Flexible microsupercapacitors; silk fibers; cotton fiber; green tea*

Introduction Micro-supercapacitors (MSCs) are required to power miniaturized electronic devices.[1] Towards this objective, polymers and its composites were deposited on microelectrodes to fabricate MSCs.[2] Flexible MSCs are desired for the fabrication of wearable electronics.[3] Furthermore, a method devoid of micro patterning facilitates easier and cost effective fabrication of MSCs. In fact, MSCs with the shape of threads are desirable for easy integration with flexible clothes.[4] Towards this objective, biscrolled yarns comprising carbon nanotubes and conjugated polymers were prepared.[5,6] Niobium yarns coated with poly(3,4-ethylenedioxythiophene) showed a volumetric capacitance of 158 F/cm^3.[7] Polyaniline is a well known pseudocapacitive material, which upon coating on top of CNT yarn showed areal capacitance of 38 mF/cm^2.[8] Often, carbon fibers are used as current collector and base substrate to fabricate yarn supercapacitors.[9] In these experiments, carbon nanotubes are converted to its yarns using variety of simple and involved approaches.

Silk fibers (SFs) that form cocoons are few tens of microns in diameter and few centimeter in length.[10] These fibers are mechanically very strong. Thus, SFs could be an useful substrate for the fabrication of MSCs. However, the SFs are insulators. Deposition of metals to impart conductivity by conventional approaches affect the mechanical stability of SFs. We have used polyphenols from green tea as protective as well as reductive coating to prepare gold film on top of SFs. One of the very stable and commercially exploited conjugated polymers, PEDOT, was used as pseudocapacitive material. The MSCs showed highest specific capacitance of 500 F/g, areal capacitance of 62 mF/cm^2 and volumetric capacitance of 120 F/cm^3. Coiled devices were also prepared to demonstrate

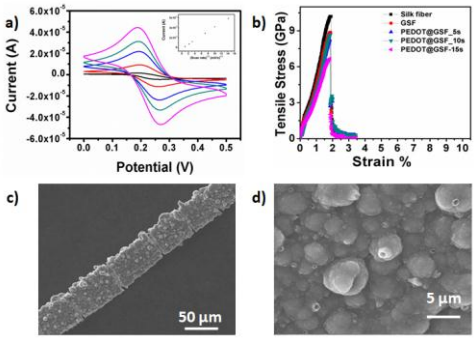


Figure 1 a) CV of 1 mM ferrocenemethanol recorded using GSF as working electrode. The inset shows the linear plot of square root of scan rate vs peak current. b) Stress-strain curve for GSF and PEDOT@GSFs c) SEM image showing the morphology of PEDOT@GSF_15s. d) Enlarged SEM image showing the morphology of PEDOT in PEDOT@GSF_10s

the suitability of MSCs as flexible devices. The performance of the coiled devices was same as that of uncoiled devices.

To demonstrate that the diameter is not restricted to microns and the substrate doesn't have to be single fiber like SFs, we used cotton threads as base to coat gold. Cotton threads comprise bundle of smaller threads and they are insulators. The polyphenol based gold coating was used to prepare gold coated cotton threads (GCTs). These threads were used for the deposition of PEDOT. While using GCTs as substrate and PEDOT as active material, a specific capacitance of 250 F/g was observed. The best energy and power densities were found to be 5.5 Wh/kg and 1118 W/kg. The performances of coiled devices are comparable to that of uncoiled devices, which indicates that the charge storage properties are unaffected upon bending the devices.

2. RESULTS AND DISCUSSION

The SFs of defined length was dipped in green tea extract to obtain a colourless coating of polyphenol. The polyphenol is capable of reducing silver ions to silver.[11,12] Thus, silver nanoparticles could be easily synthesized by immersing the polyphenol coated SFs in ammoniacal silver nitrate solution. This process results in the formation of silver nanopartcile decorated SFs. Silver nanoparticles can reduce gold ions due to the commensurate electrochemical potential. Thus, further immersion of silver nanoparticle coated SFs in gold plating solution results in gold coated SFs (GSFs). The gold coating was confirmed by EDAX analysis as well as SEM imaging. The GSFs were used as working electrode to record cyclicvoltammograms (CVs) and study the electroactivity of the surface. CVs were recorded in 1 mM ferrocenemethanol using 0.1 M $LiClO_4$ as supporting electrolyte. The well defined redox peaks of ferrocenemethanol indicate that the GSFs are conducting. The CVs were recorded at various scan rates and the plot of square root of scan rate vs current was found to be linear (Figure 1a). This indicates the redox species don't adhere on the surface of the GSFs. These experiments encourage us to use GSFs as substrate to fabricate MSCs. PEDOT was coated on top of GSFs by applying a constant potential of 1.3 V vs Ag/AgCl in EDOT monomer solution.[13,14] PEDOT coated GSFs were prepared at three polymerization times, (*i*) 5 s, (*ii*) 10 s and (*iii*) 15 s. This variation permits us to identify the optimum PEDOT thickness to achieve best MSCs performance. PEDOT coated GSFs prepared at various polymerization will be mentioned as PEDOT@GSFs-5 (5 s), PEDOT@GSFs-10 (10 s) and PEDOT@GSFs-15 (15 s). Together, they will be mentioned as PEDOT@GSFs. Before fabrication of MSCs, the mechanical stability of the SFs, GSFs and PEDOT@GSFs were studied using tensile measurements (Figure 1b). The Youngs modulus of SFs was found to be 5.2 GPa. This decreased marginally upon coating gold (5.0 GPa) and further decreased to 4.7 GPa for PEDOT@GSFs-5. The lowest Young's

modulus of 3.5 GPa was measured for PEDOT@GSFs-15. Thus, the gold coating and thinner PEDOT coatings don't affect the mechanical strength of SFs. However, thicker PEDOT coating does affect the mechanical strength. The SEM images of the GSFs and PEDOT@GSFs (Figure 1c) were recorded to study the morphology of surfaces. The PEDOT coating impart roughness to the surface of GSFs. Similar morphology is observed for the PEDOT@GSFs (Figure 1d). The redox characteristics of PEDOT@GSFs were studied using CV. The potential was swept between 0 and 0.8 V vs Ag/AgCl, while using the PEDOT@GSFs as working electrode. The CVs didn't show Faradaic peaks. From the box type CVs, areal capacitance could be calculated. The capacitance was found to increase linearly as a function of polymerization time. Next, the PEDOT@GSFs were used as electrode in a MSCs. In the first set of experiments, PEDOT@GSFs were used as working electrode with GSFs as counter electrode. The electrolyte was 1 M $LiClO_4$. The charge discharge experiments were carried out between 0 and 0.8 V at various current densities. PEDOT@GSFs-5 showed symmetrical charge discharge profiles. On the other hand, PEDOT@GSFs-15 showed unsymmetrical charge discharge profile, which indicates increased IR drop. This is due to the poor conductivity of the thick PEDOT film. Furthermore, the 15 s polymerization results in the formation of uneven and discontinuous film (Figure 1c), which also contributes to the increased resistance. In Figure 2a, the charge discharge profiles of PEDOT@GSFs at 1 A/g is shown. The highest specific capacitance was measured for PEDOT@GSFs-10 (500 F/g) at a current density of 1 A/g. The impedance spectra of PEDOT@GSFs were recorded using the experimental conditions that are used for capacitance measurements. A linear line in the nyquist plot indicates ion transport (Figure 2b). The resistance was calculated from high frequency intercept and it was not significantly different among the PEDOT@GSFs. Among the three PEDOT@GSFs, PEDOT@GSFs-10 is the best performing electrode. Therefore, we carried out all the forthcoming experiments using this electrode. Furthermore, gel electrolyte comprising poly(vinyl alcohol) and 1M $LiClO_4$ was used in all the forthcoming experiments. The MSCs were fabricated by immersing PEDOT@GSFs-10 and GSFs in gel electrolyte, which were then scrolled to form the device. CV of the device were recorded at various scan rates. At a scan rate of 5 mV/s, the areal and volumetric

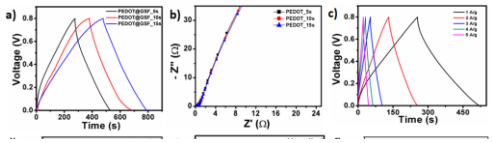


Table 1. Length, areal, volumetric and gravimetric capacitances of uncoiled and coiled PEDOT@GSFs-10 devices.

Current density (mA/cm)	Uncoiled device				Coiled device			
	C_s (F/g)	C_l (mF/cm)	C_{vol} (F/cm^3)	C_{areal} (mF/cm^2)	C_s (F/g)	C_l (mF/cm)	C_{vol} (F/cm^3)	C_{areal} (mF/cm^2)
0.0012	500	0.6	120	62	500	0.6	120	62
0.002	333	0.3	80	41	333	0.3	80	41
0.004	214	0.3	51	26	230	0.3	55	28
0.005	182	0.2	43	22	200	0.25	48	24
0.006	161	0.2	38	20	166	0.2	40	21

capacitances are 51 mF/cm^2 and 128 F/cm^3, respectively. The volumetric capacitance is calculated by taking the whole electrode comprising gold coated silk fiber as well as PEDOT into account. These values decreased upon increase in scan rate. The charge discharge experiments were carried out using the MSCs between 0 and 0.8 V (Figure 2c). The specific capacitance was calculated based on the length of the PEDOT@GSFs-10, which was found to be 0.6 mF/cm while discharging at 0.001 mA/cm (1 A/g). Upon increase in discharge current densities, the specific capacitances have been found to decrease. We also calculated areal and volumetric capacitances which are tabulated in table 1. In order to test the devices' flexibility, coiled MSCs were prepared. For this purpose, 10 cm MSCs were coiled around a plastic cylinder. Then, the performance of the device was measured. The CV were found to be devoid of any Faradaic peaks. From the box type CVs, the areal and volumetric capacitance was calculated. At a scan rate of 5 mV/s, areal and volumetric capacitance was found to be 51 mF/cm^2 and 127 F/cm^3, respectively. Thus, the coiling doesn't affect the performance of MSCs. The charge discharge experiments were carried out between 0 and 0.8 V. The charge discharge curves were not perfectly symmetric with IR drop during the discharge cycle. The volumetric and areal capacitance of the device was found to be 120 F/cm^3 and 62 mF/cm^2, respectively, while discharging at 0.001 mA/cm (1 A/g) (Table 1). We attribute this impressive performance to the conductivity imparted to the SFs by gold. Please note that the gold coating is possible on SFs using polyphenols extracted from green tea. The stability of the uncoiled and coiled devices were studied over 10000 cycles. It is gratifying to note that the capacitance decrease was only 15% for both coiled and uncoiled devices. The Ragone plot that compiles the energy and power density of a energy device is shown in Figure 2e. Highest energy density of 44 Wh/kg and power density of 2667 W/kg was calculated for the silk fiber based uncoiled devices. The energy and power density didn't vary significantly upon coiling (Figure 2e). The other factor that is likely to affect the performance of MSCs is length of the device. The performances of the devices were measured by varying the length of the device between 2 cm and 10 cm. The capacitance as a function of length was found to decrease by 34% in capacitance for a 80% increase in length, which is small (Figure 2f).

Cotton threads were coated with gold by following the procedure used for SFs (SEM image shown in Figure 3a). PEDOT was coated by applying a constant potential of 1.3 V vs Ag/AgCl for 10 s. This electrode will be mentioned as PEDOT@GCTs-10. For device

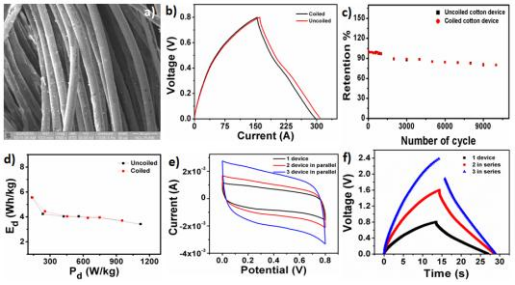


Figure 3: a) SEM image of GCTs. b) Charge discharge profiles of PEDOT@GCTs-10 recorded in gel electrolyte at 1 A/g. c) Stability study showing the variation if specific capacitance of PEDOT@GCTs-10 based coiled and uncoiled devices as a function of number of chare discharge cycles. d) Ragone plot showing the change in energy and power density of PEDOT@GCTs-10 for uncoiled and coiled devices. e) The CV of three PEDOT@GCTs-10 based devices connected in parallel. f) The charge discharge profile of three PEDOT@GCTs-10 based devices connected in series.

fabrication, the GCTs were used as counter electrode. From the box type CV, the capacitance as a function of length was calculated to be 0.82 mF/cm while sweeping the potential at 5 mV/s. This value decreased

to 0.63 mF/cm upon increasing the scan rate to 100 mV/s. The charge discharge experiment was performed between 0 and 0.8 V at various current densities. The discharge curves were linear with IR drop. The specific capacitance was found to be 250 F/g while discharging at 1 A/g (Figure 3b). This decreased to 166 F/g upon increase in discharge current density to 10 A/g. The devices were coiled around a plastic cylinder. The coiled device showed a specific capacitance of 250 F/g while discharging at 1 A/g. This decreased to 153 F/g upon increase in discharge current density to 10 A/g. The decrease is likely due to the bundle of threads, which has several twisting points. At these places, the ions transport is hindered at higher current densities. This issue is not present in SFs, hence the device performance doesn't vary as a function of coiling. The specific capacitance decreased by 20% after 10000 cycles (Figure 3c). The variation in energy and power density for coiled and uncoiled devices are shown in Ragone plot (Figure 3d). Highest energy and power densities of 5.5 Wh/kg and 1118 W/kg, respectively were observed for uncoiled PEDOT@GCTs-10. The PEDOT@GCTs-10 based devices were connected in series and parallel. While the devices are connected in parallel, the current is expected to increase due to addition of current as a function of number of devices. Indeed, we do observe linear increase in current while connecting two and three devices. A single device showed a current of 0.7 mA in CV which increased to 2 mA on connecting three such devices in parallel. On the other hand, the potential will increase upon connecting the devices in series. This was demonstrated by recording charge discharge curves. The voltage was found to increase as function of number of devices. While a single device could be charged to 0.8 V, three devices when connected in series could be charged to 2.4 V.

Acknowledgements

KK acknowledges the funding from CSIR through TAPSUN (NWP 54) project. CD thanks UGC India for the fellowship.

References

1. Huang, P.; Lethien, C.; Pinaud, S.; Brousse, K.; Laloo, R.; Turq, V.; Respaud, M. ; Demortière, A.; Daffos, B.; Taberna, P. L.; Chaudret, B.; Gogotsi, Y.; Simon, P. *Science*, 351, 691, 2016.
2. Aradilla, D.; Gaboriau, D.; Bidan, G.; Gentile, P.; Boniface, M.; Dubal, D.; G´omez-Romero, P.; Wimberg, J.; Schubert, T. J. S.; Sadki, S. *J. Mater. Chem. A* 3, 13978, 2015.
3. El-Kady, M. F.; Kaner, R. B. *Nat. Commun.* 4, 1, 2012.
4. Chen, T.; Hao, R.; Peng, H.; Dai, L. *Angew. Chem. Int. Ed*. 54, 618, 2015.
5. Kim, S. H.; Sim,H. J.; Shin, M. K.; Choi, A. Y.; Kim, Y. T.; Lima, M. D.; Baughman, R. H.; Kim, S. J. ***RSC Adv.* 3**, 24028, 2013.
6. Lee, J. A.; Shin, M. K.; Kim, S. H.; Cho, H. U.; Spinks, G. M.; Wallace, G. G.; Lima, M. D.; Lepró, X.; Kozlov, M. E.; Baughman, R. H.; Kim, S. J. *Nat. Commun*. 4, 1, 2013.
7. Mirvakili, S. M.; Mirvakili, M. N.; Englezos, P.; Madden, J. D. W.; Hunter, I. W. *ACS Appl. Mater. Interfaces* 7, 13882, 2015.
8. Wang, K.; Meng, Q.; Zhang, Y.; Wei, Z.; Miao, M. *Adv. Mater.* 25, 1494, 2013.
9. AU - Ren, J.; Li, L.; Chen, C.; Chen, X.; Cai, Z.; Qiu, L.; Wang, Y.; Zhu, X.; Peng, H. *Adv. Mater.* 25, 1155, 2013.
10. Kim, D-H.; Viventi, J.; Amsden, J. J.; Xiao, J.; Vigeland, L.; Kim, Y-S.; Blanco,J. A.; Panilaitis, B.; Frechette, E. S.; Contreras, D.; Kaplan, D. L.; Omenetto, F. G.;

Huang, Y.; Hwang, K-C.; Zakin, M. R.; Litt, B.; Rogers, J. A. *Nat. Mater*. 9, 511, 2010.

11. Das, C.; Krishnamoorthy, K. ***Chem. Commun.* 50,** 5905, 2014.
12. Das, C.; Jain, B.; Krishnamoorthy, K. ***Chem. Commun.* 51,** 11662, 2015.
13. Huang, S.; Zhang, Y.; Shi, J.; Huang, W. *ACS Sustainable Chem. Eng.* 4, 676, 2016.
14. Zhou, C.; Liu, Z.; Yan, Y.; Du, X.; Yiu-Wing Mai, Y-W.; Ringer, S. *Nanoscale Res. Lett*. 6, 364, 2011.

MACRO 248

BODIPY based Polymers for Organic Field Effect Transistors

Singh, Saumya[a]; Singh, Anup Kumar[a]; and Krishnamoorthy, Kothandam[a]*

[a]*Polymer Science and Engineering Division, CSIR-National Chemical Laboratory, Pune, India*

**k.krishnamoorthy@ncl.res.in*

BODIPY (4, 4-difluoro-4-bora-3a, 4a-diaza-*s*-indacene) fluorophores exhibit excellent thermal/photochemical stability and intense absorption/emission profiles [1]. BODIPY based small molecules and polymers have been widely explored in different areas for a variety of applications such as sensors, biological labelling, photodynamic therapy, etc. By bringing structural variations on dipyrromethene core, redox properties of these dyes can be easily tuned, which is an important parameter for organic semiconducting material design. Also, the core is rigid and helps in intermolecular stacking in the solid state. Despite these, BODIPY based organic semiconductors are rare. There are few reports of BODIPY based systems for OFETs, but charge carrier mobility values have been moderate so far [2-4]. In this work, we have attempted the design and synthesis of conjugated polymers incorporating BODIPY dyes, and their application in organic field effect transistors. Three p(BODIPY-alt-DPP) polymers (P1 – P3) are synthesized with a variation on the BODIPY core, and their physical, thermal, and electronic properties are studied. These polymers are thermally stable up to 362 °C with 5% weight loss, hence suitable for device fabrication at a higher temperature. Field effect transistors devices fabricated from these polymers show ambipolar charge transport. P3 exhibits highest mobility values with a hole mobility of 3.1 x 10^{-2} cm^2/Vs and electron mobility of 1.5 x 10^{-2} cm^2/Vs.

References:

[1] Loudet, A and Burgess, K. *Chemical reviews*, 107 (2007) 4891.
[2] Popere, C.; Della Pelle, A.M.; and Thayumanavan, S. *Macromolecules*, 44 (2011) 4767.
[3] Singh, S.; Venugopalan, V.; Krishnamoorthy, K. *Phys. Chem. Chem. Phys.* 16 (2014) 13376.
[4] Debnath, S.; Singh, S.; Bedi, A.; Krishnamoorthy, K.; Zade, S. S. *J. Phys. Chem.* 119 (2015) 15859.

MACRO 251

Highly Acid/Oxidative Resistant Cation-Exchange for Membrane Electrolysis

Arindam Kumar Das[a], and Vinod K. Shahi*

[a] *Electro-Membrane Processes Division and Academy of Scientific and Innovative Research,*

CSIR-Central Salt and Marine Chemicals Research Institute,

Council of Scientific & Industrial Research,

Gijubhai Badheka Marg, Bhavnagar 364002, Gujarat, India

E-mail: arindamkumar91@gmail.com, vkshahi@csmcri.org

For developing acid/oxidative resistant aliphatic polymer based cation-exchange membrane (CEM), macromolecular modification of poly (vinylidene fluoride-co-hexafluoropropylene) (PVDF-co-HFP) was carried out by controlled chemical grafting of 2-acrylamido-2-methyl-1-propanesulfonic acid (AMPS). To introduce the unsaturation suitable for chemical grafting, dehydrofluorination of commercially available PVDF-co-HFP was achieved under alkaline medium. Sulphated copolymer (SCP) was prepared by the free radical copolymerization of dehydofluorinated PVDF-co-HFP (DHPVDF-co-HFP) and AMPS in presence of free radical initiator. Prepared SCP based CEMs were analysed for their morphological characteristics, ion exchange capacity (IEC), water uptake, conductivity and stabilities (mechanical, chemical and thermal) in compare with state-of-art Nafion117 membrane. High bound water content avoids the membrane dehydration, and most optimal (SCP-1.33) membrane exhibited about ~2.5 fold high bound water content in compare with Nafion117 membrane.

Bunsen reaction of iodine-sulphur (I-S) was successfully performed by direct contact-mode membrane electrolysis in a two-compartment electrolytic cell using different SCP membranes. High current efficiency (83-99%) confirmed absence of any side reaction and 328.05 kJ mol-1-H2 energy was required for to produce 1mol of H2 by electrolytic cell with SCP-1.33 membrane. In spite of low conductivity for reported SCP membrane in compare with Nafion117 membrane, SCP-1.33 membrane was assessed as suitable candidate for electrolysis due low-cost nature and excellent stabilities in highly acidic environment may be due to partial fluorinated segments in the membrane structure.

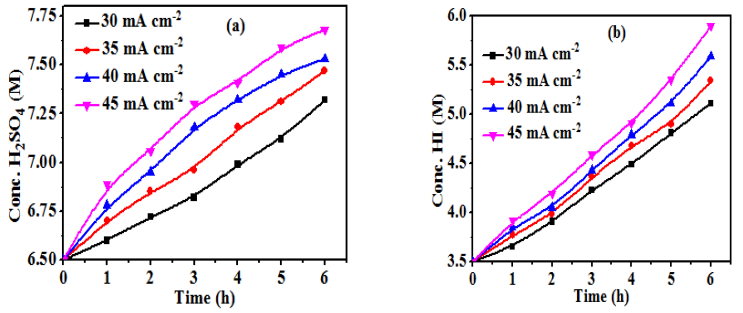


Figure 1. Effect of current density on concentration of acids: (a) H_2SO_4 and (b) HI; using SCP-1.33 membrane during electrolysis. Experimental conditions: I_2/HI ratio = 1; effective membrane area; 60 cm^{-2}, temperature; 35°C

In the electrochemical Bunsen reaction, SO2 is oxidized to H2SO4 at the anode while I2 is reduced to HI at the cathode. I_2/HI molar ratio in the catholyte and H2SO4 concentration in the anolyte were examined. New polymer SCP was synthesized for this process which exhibits good stability as well as conductivity compare to nafion 117. Electrolyte membranes were applied in an electro-membrane process (electro-electrodialysis, EED) to increase the HI molality of HIx solution (HI + I_2 +H_2O mixture) to be over quasi-azeotropic.

Membrane structure with fluorinated segments responsible for good stability and conductivity and low co-ion/mass permeation. The Bunsen reaction was successfully performed in a two compartment electrolytic cell separated by SCP membrane in the batch mode of operation. About 83−99% current efficiency at the cathode and close to 85−100% at the anode indicated the absence of another side reaction (either at the electrode or in bulk). For the production of H_2, energy required for electrolysis decreased significantly (about threefold) with an increase in membrane conductivity or IEC. About 328.05 kJ mol-H_2 $^{-1}$ energy is required for producing 1 mol of H_2 by an electrolytic cell utilizing SCP-1.33 membrane, confirming its suitability for electrolytic water splitting by the I−S cycle (Bunsen reaction).

References

[1] Tanaka, N; Yamaki, T; Asano, M; Maekawa Y; Onuki. K. *J. Membr. Sci,* 346 (2010) 136.
[2] Gokul, K. U; Immanuel, V; Sant, S; Shukla, A. *J. Membr. Sci* 13 (2011) 380.

[3] Gokul, K. U; Immanuel, V; Sant, S; Shukla. *J. Hydrogen Energy* 37 (2012) 3595.

MACRO 268

HDPE - Sillimanite Mineral Based Composites For Electronic Applications

[a] I.J. Induja, [a] M. R. Varma, [b*] M.T Sebastian

[1]*Materials Science & Technology Division*
National Institute for Interdisciplinary Science & Technology
Trivandrum, 695019 India.

[2*] Microelectronics Research Unit
Faculty of Information Technology & Electrical Engineering ,
University of Oulu, 90014, Finland.

E-mail Id: mailadils@yahoo.com

The ever growing increase in electronic and telecommunication industry demands new materials having better properties for various applications. The performance of high speed microelectronic devices is determined by the dielectric properties of the packaging materials [1]. For microelectronic packaging applications the materials should satisfy low dielectric constant (ε_r), low dielectric loss (tanδ), high thermal conductivity (TC), low coefficient of thermal expansion (CTE), low moisture absorption, mechanical stiffness etc. Among the materials polymers plays a significant role in electronic packaging owing to their low dielectric constant, cost effectiveness, lighter weight, great variety of mechanical properties, easy processing etc [1]. The low thermal conductivity, high (CTE) values of polymers delimits their wider usability [2]. The ceramics materials have high processing temperature; brittle nature prevents them from circuit applications. So by integrating polymers and ceramics, it is possible to tailor the dielectric, thermal and mechanical properties of the newly developed polymer-ceramic composites for practical applications. The judicious selection of individual components in a polymer-ceramic composite is very crucial since it determines the dielectric, thermal, mechanical properties of the composite [1]. In literature, several reports can be seen based on HDPE-ceramic composites. High Density Polyethylene (HDPE) is one of the important thermo plastic [8] .The polymer HDPE is having better microwave dielectric properties, easy processibility, low cost etc. The ceramic filler used for the present study is a cost-effective mineral sillimanite (Al_2SiO_5), which is abundant in nature. It is having an orthorhombic structure. In the present study HDPE-sillimanite composites were prepared by sigma mixing. The structural, moisture absorption, dielectric studies and thermal expansion studies were carried out and discussed.

References

[1] M. T. Sebastian, H. Jantunen, Polymer–Ceramic Composites of 0–3 Connectivity for Circuits in Electronics: A Review, Int. J. Appl. Ceram. Technol., 7 (2010) 415–434.

[2] A.J. Bur, Polymer review Dielectric properties of polymers at microwave frequencies: a review, Polymer, 26 (1985) 963-977.

MACRO 274

Porous Benzimidazole linked Aryl-imide polymers in The Application of Gas Storage Capacity

Roy, Arkapal[a]; Halder, Arijit[b]; Mondal, Sanjoy[a]; Ghoshal, Debajyoti[b]; Malik, Sudip*[a]

[a]*Polymer Science Unit, Indian Association for the Cultivation of Science, Jadavpur, Kolkata-700032, India*

[b]*Department of Chemistry, Jadavpur University, Jadavpur, Kolkata-700032, India*

email i.d: psusm2@iacs.res.in

Considering the major problems in this era we have given special preference to global warming, i.e the capturing of green house gases like carbon dioxide, methane etc. There are few reports which have told us the carbon dioxide capturing through the porous organic polymers and the major interaction point for physisorption is benzimidazole part.[1-4] Keeping all these things in mind, we have designed and synthesized benzimidazole linked aryldiimide polymers which are subsequently characterized by solid state ^{13}C-CPMAS NMR & FT-IR spectra. Morphological studies of these polymers have been studied with FESEM, suggesting the presence of spherical aggregates. Porosity of the polymers has checked through adsorption and desorption isotherms of N_2 gas at 77K, which provides BET surface area around 120 m^2/gm, however carbon dioxide adsorption isotherms have showed good results with one of the polymer (CO_2 uptake upto 14.56 wt%).

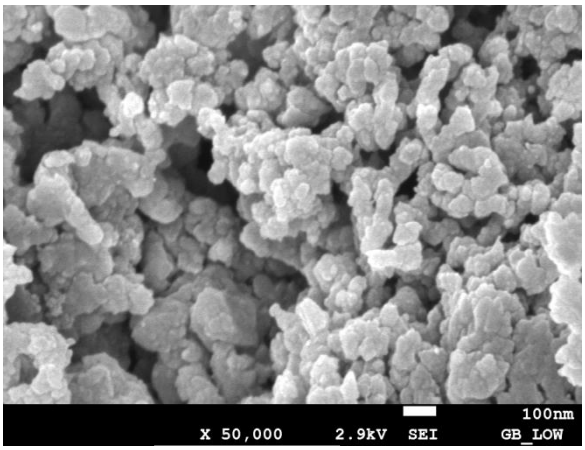


Figure 1a

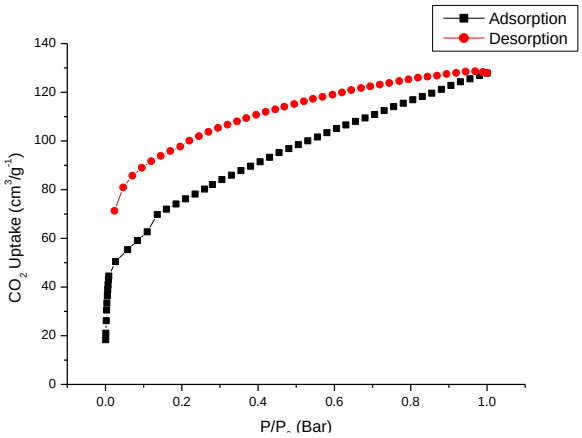


Figure 1b

Figure 1a: FE-SEM Image of Naphthalene containing Benzimidazole polymer; 1b: CO_2 Adsorption Isotherm of Naphthalene containing Benzimidazole polymer;

References

[35] Dawson, R.; Stockel, E.; Holst, J. R.; Adams, D. J.; Cooper, A. I. *Energy Environ. Sci* , 4 (2011) 4239.
[36] Furukawa, H.; Yaghi, O. M. *J. Am. Chem. Soc.*, 131(2009) 8875.
[37] Suh, M. P.; Park, H. J.; Prasad, T. K.; Lim, D.-W. *Chem. Rev.*, 112(2012) 782.
[38] Murray, L. J.; Dinca, M.; Long, J. R. *Chem. Soc. Rev.*, 38 (2009) 1294.

MACRO 301

Nano-porous Coordination Framework for Electro-sensing of Atropine Sulphate

Vinita; Tiwari, M.; Kumar, A.; Prakash, R.

School of Materials Science and Technology, Indian Institute of Technology (Banaras Hindu University), Varanasi-221005, India,
Email:vinita.rs.mst15@itbhu.ac.in, rprakash.mst@iitbhu.ac.in

Abstract

The advancement in chemistry of the coordination polymers having designable architectures fabricated from functionalized building blocks is an emerging area from last two decades. The further challenges are construction of coordination network assembly having electro-active nano-pores. We report a nano-porous coordination polymeric framework (NPCNPs; DMTD-Ag) derived from 2-5-Dimercapto-1,3,4-thiadiazole and silver nitrate. The NPCNPs consist of one dimensional infinite array of individual components of DMTD and Ag (I), in which Ag (I) get coordinated by endocyclic thiol groups of individual DMTD synthons [1]. The nano-porous architecture of DMTD-Ag is investigated by FE-SEM and the amorphous nature along with the oxidation state of silver is studied through XRD, TEM and XPS respectively [2]. Furthermore, the efficient electron transfer kinetics is probed by using Fe (II)/Fe (III) redox couple in phosphate buffer pH 10 via cyclic voltammetry. Thereafter this excellent electroactivity is employed in the electro-detection of an anticholinergic drug, Atropine sulphate. The anodic peak current revealed a linear dependence with atropine sulphate concentration with sensitivity and limit of detection as 0.02 μA/μM and 46.00 nM, respectively. The effective assay of drug is caused by the excellent channeling of electron through porous veins. Further the concept is extended and established in the pharmaceutical formulation of atropine sulphate with a sensitivity of 0.02 μA/μM, and limit of detection as 72.50 nM.

References

[39]Tiwari, M.; Gupta, S.; Prakash, R.; *RSC Adv*. 4 (2014) 25675.
[40]Bourg, M. C.; Badia, A.; Lennox, R. B.; *J. Phys. Chem. B.*104 (2000) 6562.

MACRO 304

Polypyrrole Coated Fabrics for EMI Shielding Application

Gahlout Pragati and Choudhary Veena *

Centre for Polymer Science and Engineering

Indian Institute of Technology Delhi, New Delhi-1100106, India

*veenach@hotmail.com

Rapid growth of electronic devices and telecommunication industry has become a major cause of severe electromagnetic pollution, which not only affects the normal functioning of the other electronic devices (e.g. buzzing sound in speakers when placed near mobile phones) but it has reached to the level where it is believed that exposure to certain radiation may have adverse health effects on humans and possibly affecting human behavior. To decrease the harmful effect of these radiations on humans and electronic equipment, a protective shield is required [1-6]. In the present study we are trying to prepare and compare flexible shields using cotton and polyester fabric and conducting polymer (polypyrrole) which is able to attenuate electromagnetic radiation in an effective way. The shield attenuate the incident radiation predominantly by absorption mechanism.

Preparation of conducting polymer fabric was carried out by in-situ polymerization of pyrrole in the presence of surfactant and oxidant. By this method, a thin layer of conductive polypyrrole (PPy) was formed on cotton or polyester fabrics by a surfactant template. Coating of polymer on fabrics was analyzed by scanning electron microscope (SEM). Structural characterization was done by FT-IR and XRD. Thermal stability of fabric was analyzed through thermogravimetric analysis (TGA). Electrical conductivity was measured using four point probe low resistance meter. Electromagnetic interference response of conducting polypyrrole-coated fabrics in the microwave range (X-band range) has been studied by vector network analyzer (VNA). In the frequency range from 8.2-12.4 GHz, conducting polypyrrole-coated conducting fabrics (thickness 0.2-0.4 mm) shows a total shielding effectiveness in the range 4-8.9 dB.

Keywords: PPy, conducting fabric, EMI shielding.

References:

[1] Haknsson Eva, Amiet Andrew, Kaynak Akif, *Synthetic metals*, 156 (2006) 917–925.
[2] Hun Kim Seong, HoJang Soon, Weon Byun Sung, Young Lee Jun, Soo Joo Jin, Hoon Jeong Sung, Park Myung-Ja, *Applied polymer science*, 87(2002)1969-1974.
[3] Dhawan S.K, Singh N, Venkatachalam S. *Synthetic Metals*, 129 (2002) 261-267.
[4] Yue B, Wang G, Ding X, Wallace G. *Electrochimica Acta*, 68 (2012) 18-24.
[5] Kincal D, Kumar A, Child AD, Reynolds JR; *Synthetic Metals*, (1998)53-56.
[6] Lekpittaya Porntip, Yanumet Nantaya, Grady Brian P, A. Edger, O'Rear. *Journal of Applied Polymer Science*, 92(2004)2629-2636.

MACRO 308

Nitrogen-Enriched Porous Carbon Derived From Polymer of Sucrose and Urea with High CO_2 Capture Performance

Deepthi L. Sivadas*,[a,b] Sujith Vijayan,[b] Rajeev, R,[a] Prabhakaran K.[b], and Ninan K. N.[b]

[a]*Analytical and Spectroscopy Division, Vikram Sarabhai Space Centre, Thiruvananthapuram-695 022, India*
[b] *Department of Chemistry, Indian Institute of Space Science and Technology, Thiruvananthapuram- 695 547, India.*

** e-mail id* deepthisivadas@gmail.com

Abstract

Nitrogen enriched carbon with well-developed microporosity and superior CO_2 adsorption capacity were prepared by KOH activation of a nitrogen-containing polymer obtained by heating sucrose and urea. The maximum surface area, total pore volume and nitrogen content of the activated carbon achieved are 2366 m^2/g, 1.157 m^3/g and 10.5 wt.%, respectively. Maximum CO_2 adsorption capacity of 4.3 mmol/g (19 weight %) was achieved at 25 ^oC and 1 bar pressure. The CO_2 adsorption capacity of all prepared carbon materials was well correlated with the nitrogen content and microporosity. The CO_2 adsorption on the activated carbon materials showed excellent selectivity over nitrogen, with one of the highest selectivity factor of 38, hence an ideal candidate for CO_2 removal from flue gases.

Keywords: *Sucrose; urea; carbon; CO_2 capture*

Introduction

CO_2 is the primary anthropogenic greenhouse gas contributing 77% of the total human contribution to greenhouse gas.[1] During the past few decades, much effort has been devoted for the development of new solid CO_2 capture materials, viz., Metal Organic Framework, amine on solid support, porous carbons etc.[2] Numerous carbon materials, including activated carbon, polymer derived carbon, biomass-derived carbon and nitrogen-doped carbon has been thoroughly investigated for CO_2 adsorption.

Many studies have proven that the CO_2 capture capacity of activated carbon (AC) sorbents can be significantly increased by introducing nitrogen (N) functional groups into their structures.[3-6] N-containing functionalities increase the surface polarity and basicity of AC materials, which is beneficial for the adsorption of CO_2. Microporosity is another factor that affects CO_2 uptake in N-doped carbon. [7]

Synthesis of advanced materials from naturally renewable bio-resources is of utmost importance for sustainable development. Sucrose is an economical,

commercially available, and naturally renewable carbon source, and urea is a bio-molecule rich in nitrogen. However, the combination of sucrose and urea is not yet exploited for the synthesis of N-doped AC materials. This study is designed to develop an economical and simple method for the synthesis of high N-doped (6–10 wt% nitrogen) porous carbon from sucrose and urea. The N-containing polymeric materials obtained by heating sucrose and urea are activated by KOH at varying concentrations to produce the N-doped AC. The N-doped and N-free porous carbon materials thus produced were evaluated for CO_2 adsorption capacity. The effect of N-doping and microporosity of the AC materials on the CO_2 adsorption has been studied in detail.

Experimental

Sucrose (AR grade) and urea (AR grade) from Merck India Pvt. Ltd were used as such.

Preparation of N-containing carbon:

Sucrose and urea were thoroughly mixed and melted at 150°C in an air oven. The temperature of the oven was then increased to 250°C, melt becomes a brittle foamy solid polymer. The resultant polymeric products are denoted as **SU-x-250**, where x represents the wt% of urea in sucrose-urea mixture. The polymeric products obtained were mixed with various amounts of KOH and heated in a platinum crucible at 650°C for 2 h in an ultra-high pure nitrogen atmosphere in a tubular furnace. The resulting samples were washed with distilled water until KOH was completely removed. The samples were dried at 150°C in a vacuum oven for 24 h. Thus, the synthesized carbon materials were designated as **SU-x-y-650**, where y denotes the weight ratio of KOH to SU-x-250.

Structure identification:

The carbon, hydrogen and nitrogen content of the prepared carbon materials were determined using Perkin Elmer PE 2400 model CHNS elemental analyser. The FTIR spectra were recorded in a Perkin Elmer Spectrum GX-A FTIR spectrometer. The morphology of the samples was analyzed using a field emission scanning electron microscope (FE-SEM JEOL Microscope JSM 6060).

Textural property evaluation:

The porous textural properties of materials were analyzed using volumetric N_2 adsorption–desorption at −196 °C using a surface area analyzer (Micromeritics Tristar II, USA).

Results and discussion

The sucrose-urea mixtures form homogeneous melts on heating at temperatures nearly 150^{o}C. These melts give brittle foamy solids on heating at 250^{o}C for 3 hours. The urea in the melt undergoes trimerization into cyanuric acid when heated at 200^{o}C (**Figure 1**). The setting of the melt is due to polymerization of glucose and fructose anhydrides formed from sucrose (**Figure 2**) and cross-linking of the resulting polymer by the cyanuric acid molecules through –OH to –OH condensation (**Figure 3**). The foaming is due to the ammonia generated during the trimerization of urea and water vapor produced as a result of –OH condensation.

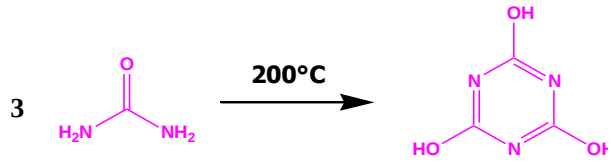


Figure 1 Formation of cyanuric acid by the trimerization of urea

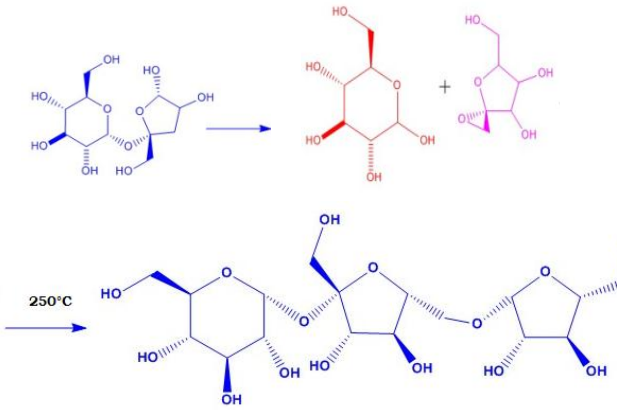


Figure 2 Trimerization of sucrose decomposition products

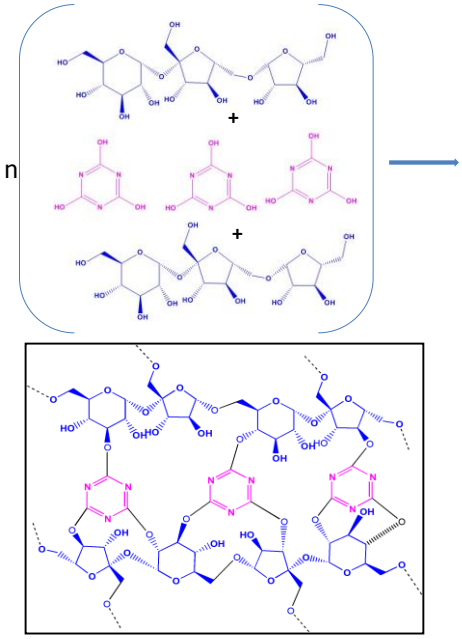


Figure 3 Proposed reactions and the structure of the polymeric product formed by heating sucrose and urea

The IR spectrum (**Figure 4**) of SU-0-250 (polymeric product without urea) shows peaks at 776 cm^{-1} (sp^2 C–H bend), 1110 cm^{-1} (–C–O stretch), 1615 cm^{-1} (alkyl C=C stretch), 1700 cm^{-1} (C=O), and 3440 cm^{-1} (–OH stretch). The C=C and C=O groups are formed by the α-elimination of water and thermal oxidation of $–CH_2OH$ in the polymeric structure produced by intermolecular condensation of glucose and fructose anhydride, respectively. SU-25-250 shows an additional peak at 1226 cm^{-1}, which can be attributed to aliphatic C–N– stretching vibration. The signal at 1600 and 3426 cm^{-1} can be identified as originating from N–H in-plane deformation vibration and N–H symmetric stretching vibration and/or –OH stretching vibration, respectively. SU-50-250 has two more additional bands at 1690 cm^{-1} (C=N stretch) and 2186 cm^{-1} (C≡N). The peaks observed at frequencies in the ranges of 1535–1560 cm^{-1}, and 784–800 cm^{-1} in SU-75-250 are characteristic of the triazine ring (Seifer, 2002). One IR signal observed in SU-75-250 at 2830–2900 cm^{-1} was attributed to the imido group of cyanuric acid.

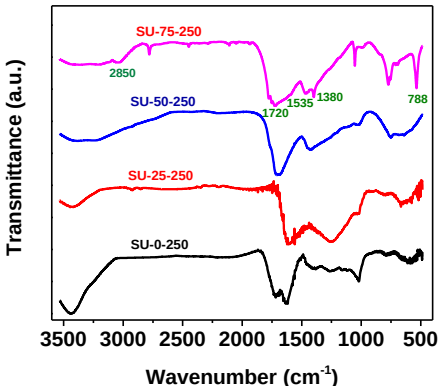


Figure 4 FTIR spectra of SU-x-250

The elemental analysis of the polymeric products shows an increase in the N content when the weight percentage of urea in the sucrose–urea mixture increases. The N contents of SU-25-250, SU-50-250, and SU-75-250 are 14.4, 21.2, and 28.8 wt%, respectively.

The KOH activation of the polymeric product is expected to develop microporosity, retaining nitrogen in the carbon structure, which will result in increased CO_2 adsorption capacity.

The carbon materials obtained after KOH activation (SU-x-y-650) show well-developed hierarchical pore structure as evidenced from the SEM analysis. The interconnected macropores are clearly visible in the high-magnification SEM image of the AC material. In contrast, the foamy polymeric products (**SU-x-250**) obtained have a cellular morphology and the cell walls are dense and smooth (**Figure 5)**.

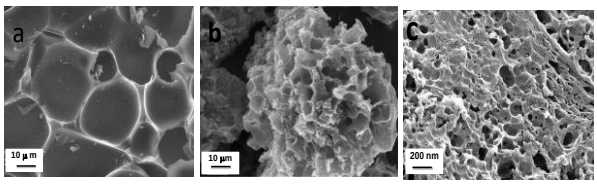


Figure 5 FESEM images of (a) SU-50-1-250 and (b) SU-50-1-650 at low magnification and (c) SU-50-1-650 at high magnification

Although the hierarchical pore structure is developed, KOH activation results in a decrease in N content. The N content of the prepared ACs varies from 6.0 to 10.5 wt% **(Table 1)**. At a particular KOH concentration, the N content of the ACs increases with an increase in urea concentration.

Textural property evaluation

The porous textures of carbon are characterized by N_2 sorption at −196 °C and CO_2 sorption at 0 °C. An increase in KOH concentration is found to increase the BET surface area and total pore volume of the carbon.

Table 1 Textural properties, %N and CO_2 adsorption capacities of the prepared carbon materials

Samples	S_{BET} ($m^2\ g^{-1}$)	V_p ($cm^3\ g^{-1}$)	V_m ($cm^3\ g^{-1}$)	N (wt%)	*CO_2 adsorption capacity*	
					25 °C	*0 °C*
SU-0-1-650	624	0.34	0.22	0	2.3	4.1
SU-0-2-650	693	0.35	0.22	0	2.2	4.4
SU-0-3-650	716	0.58	0.06	0	2.0	4.1
SU-25-1-650	1745	0.90	0.53	7.7	4.3	7.0
SU-25-2-650	1995	1.1	0.48	7.5	4.1	7.0
SU-25-3-650	2260	1.1	0.42	7.4	3.9	6.9
SU-50-1-650	1413	0.73	0.44	8	4.0	6.3
SU-50-2-650	1994	0.97	0.41	6.3	3.8	6.6
SU-50-3-650	2366	1.1	0.35	6.1	3.7	6.9
SU-75-1 -650	634	0.39	0.37	10.5	3.8	5.9
SU-75-2- 650	936	0.41	0.24	8.9	3.0	4.7
SU-75-3-650	1276	0.64	0.21	6.7	2.4	3.4

Carbon prepared from sucrose in the absence of urea exhibits relatively low surface area ranging from 623 to 716 m^2/g and total pore volume in the range of 0.33–0.58 cm^3/g. On the contrary, KOH activation of the polymer obtained by heating sucrose and urea produces N-doped carbon with high specific surface area ranging from 634 to 2366 m^2/g.

CO_2 adsorption evaluation

The CO_2 adsorption isotherms of the N-doped ACs are shown in **Table 1**. SU-25-1-650 shows the highest CO_2 adsorption capacities of 4.3 mmol/g at 25 °C.

The effect of factors such as N content and micropore volume on the CO_2 adsorption capacity of this N-doped carbon is also studied. **Figure 6** shows the correlation between CO_2 adsorption capacity and the corresponding micropore volume. **SU-0-3-650** with the lowest micropore volume shows the lowest and **SU-25-1-650** with the highest micropore volume shows the highest CO_2 adsorption capacity.

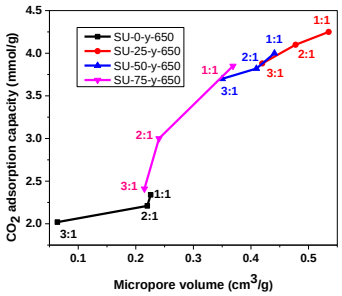


Figure 6 Correlation between micropore volume and CO_2 adsorption capacity.

Correlation between N content and CO_2 adsorption capacity of the prepared carbon is shown in **Figure 7**. Within a set of N-doped AC prepared at a particular urea concentration using various amounts of KOH, the CO_2 adsorption capacity increases with an increase in N content.

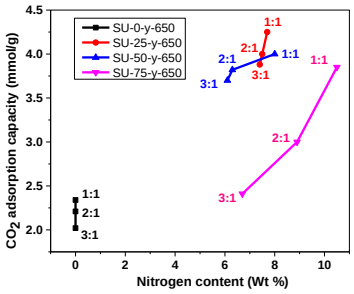


Figure 7 Correlation between N content and CO_2 adsorption capacity.

When all the prepared carbon with different pore volume/N content are compared for CO_2 adsorption, SU-75-1-650 with the highest N content shows only moderate CO_2 adsorption capacity. This result suggests that in addition to the nitrogen, porous textures of the carbon also plays an important role in determining CO_2 uptake for these N-doped AC materials.

Conclusions

Nitrogen-doped AC adsorbents having a hierarchical pore structure with high microporosity and N content were successfully synthesized with high yield by the KOH activation of the polymeric structures obtained by heating sucrose (carbon source) and urea (nitrogen source). The synergistic effect of microporosity and N-doping on CO_2 adsorption capacity of the AC is established through the investigation of the textural characteristics, N content, and CO_2 adsorption capacity of a series of N-free and N-doped AC prepared at various urea and KOH concentrations. Highest CO_2 adsorption capacity of 4.3 mmol/g was achieved by SU-25-1-650. The synergy of

textual properties and N-doping on CO_2 adsorption capacity is also evident from a comparative study of CO_2 adsorption capacity, textural properties and nitrogen content of all the four carbon materials prepared in different modes, which give the highest CO_2 adsorption capacity in each class.

References

77. Yamasaki, A., *J. Chem. Eng. Jpn*. 36, 361, 2003.
78. Su, F. and Lu, C., *Energy Environ. Sci*.,5, 9021, 2012.
79. Sevilla, M. and Fuertes, A. B., *Adv. Funct. Mater*. 21, 2781, 2011.
80. Liu, L., Deng, Q.-F., Hou, X.-X., Yuan, Z.-Y. *J. Mater. Chem.*, 22 , 15540, 2012.
81. Ma, X., Cao, M., Hu, C. *J. Mater. Chem. A* 1, 913, 2013
82. Bai, R., Yang, M., Hu, G., Xu, L., Hu, X., Wang, S., Dai, W., Fan, M., Li, Z., *Carbon*, 81, 465, 2015.
83. Zhang, Z., Zhou, J., Xing, W., Xue, Q., Yan, Z., Zhuo, S., Qiao, S. Z. *Phys. Chem. Chem. Phys.* 15, 2013, 2523.

MACRO 309

Microwave Assisted Synthesis of Poly (indole-5-carboxylic acid) for Sensing Application

Tiwari, P; Prakash R.

School of Materials Science and Technology, Indian Institute of Technology (Banaras Hindu University), Varanasi-221005, India,

*Email: tiwari.preeti602@gmail.com, rprakash.mst@iitbhu.ac.in

Abstract

We report here, a rapid, facile, one-pot synthesis of poly (indole -5- carboxylic acid) using microwave radiation. Bathochromic shift observed in UV-Vis spectra revealed extension in conjugation length as compared to its monomer. Structural information was further confirmed via ^{1}H-NMR and FT- IR. Globular texture morphology was examined via Scanning Electron Microscopy (SEM). Thermal stability was investigated by thermogravimetric analysis (TGA) to get an insight about its thermal degradation behaviour. Its redox behaviour was analysed using cyclic voltammetry (CV) technique. As-prepared poly (indole -5-carboxylic acid) was found to be electro active. Taken together, this polymer can be a promising material for sensing applications. Graphite paste electrode was modified using this polymer for sensing application in aqueous medium.

References

1. Tiwari, M.; Kumar A.; Umre H.S.; Prakash, R**.** *J. Appl. Polym. Sci*. 132 (2015).
2. Joshi, L.; Prakash, R. *Mater Lett.* 65 (2011).

MACRO 311

Thin Film Composite Membranes Containing Functionalized Carbon Nanotubes for Low Pressure Desalination Process

Km Nikita[a], Aswal V. K .[b], Murthy C. N.[a*]

[a] *Applied chemistry Department, Faculty of Technology and Engineering, The M. S. University of Baroda, Vadodara, India*
[b] *Solid State Physics Division, Bhabha Atomic Research Centre, Mumbai, India*

***E-mail**:chivukula_mn@yahoo.com*

Membrane technology has been commonly used all over the world for the purification of water. Separation and purification techniques have become industrially feasible because of the high separation efficiency of these membranes, depending on the membrane technology. The composite membranes are much efficient because of their barrier tendency towards different salts and heavy metals and carbon nanotubes show potential low pressure desalination. In the present study we have prepared thin film composite membrane of functionalized multiwalled carbon nanotubes (CNT) with poly sulfone, polyether sulfone and poly phenylene oxide as the membrane matrix. The purified CNTs were functionalized with different chemical functionality to enhance the interaction of carbon nanotubes and matrix. The thermal stability of composite membranes analyzed by Thermo gravimetric analysis (TGA) showed enhance thermal properties and better stability to degradation than the pristine membranes. The surface morphology of the composite membranes were studied by small angle neutron scattering (SANS) to evaluate the pore structure of the membranes that were cast by the phase inversion technique. Analysis showed the uniform distribution of pores and the pore diameter as well (Figure 1). It is also observed that smaller pore dimensions were detected when the composite membranes where soaked in the D_2O compared to when it is soaked in the DI water (Figure 2). Thus the detection limit could be improved. The further analysis have been carried out to calculate the salt rejection of the composite membranes and these will be discussed in this presentation.

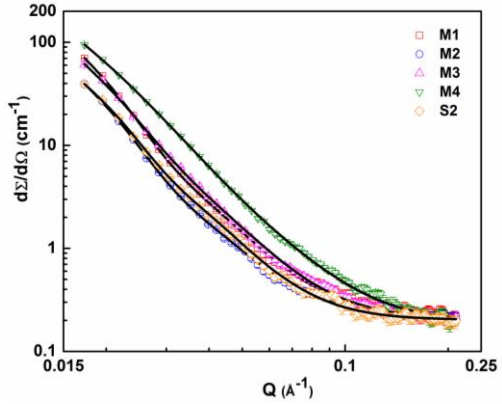


Figure 1.SANS profile of membranes soaked in DI water

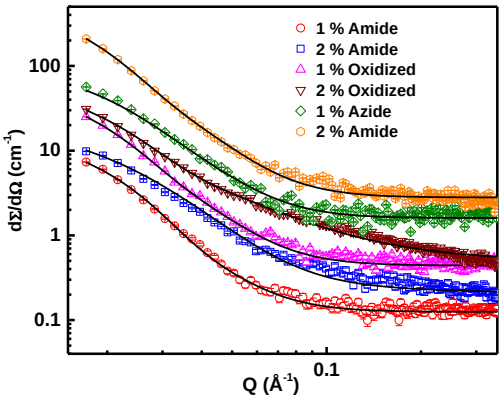


Figure 2.SANS profile of membranes soaked in D_2O

References

[41] Mangukiya S.; Prajapati S.; Kumar S.; Aswal V. K.; Murthy C. N., Polysulfone-based composite membranes with functionalized carbon nanotubes show controlled porosity and enhanced electrical conductivity, *J. Appl. Polym. Sci.*, (2016).

[42] Liu J. , Shi G., Guo P., Yang J., Fang H., Blockage of Water Flow in Carbon Nanotubes by Ions Due to Interactions between Cations and Aromatic Rings; *American Physical Society;* 115 (2015) 164502.

[43] Shah P.; Murthy C. N., Studies on the porosity control of MWCNT/ Polysulfone composite membrane and its effect on metal removal; *J. Membr. Sci.*; 437 (2013) 90-98.

MACRO 324

Redox polymers for electro-kinetic flow-in-a cell

Selvam Mathi and Rajaram K. Nagarale*

Electro Membrane Processes Division, CSIR-Central Salt and Marine Chemicals Research Institute, Bhavnagar,364002 Gujarat, India
** e-mail id:* rknagarale@csmcri.org ; rknagarale@gamil.com

Abstract

Redox polymers like polyaniline are associated with electron transport accompanied by proton transport. Here we are utilizing this property to make a flow-in-a cell device. The polymer was synthesize by an interfacial polymerisation technique with three dopant, PSS, PA and alum. The synthesized polymer was characterized by recording FTIR, SEM, and cyclic voltammogram. A device was assembled by sandwiching a silica membrane between two flow through polyaniline coated electrodes made up of mixing, powdered PANI, TimCal graphitic carbon and Nafion solution. The developed assembly successfully demonstrated with generation of electroosmotic flux of 33 μL/min/cm^2/V with the application of 1V across the cell. The flow increased linearly with the applied voltage and persisted till the 80% consumption of coulombic capacity. It is the best known non-gassing, non-contaminating and low voltage electroosmotic pump in literature operates at 1V applied voltage exclusively by electro-oxidation/reduction of PANI on respective electrodes.

Keywords: *Polyaniline, Electro-osmotic pump, Alum, Phytic acid, Polystyrene Sulfonic acid, Redox polymer, Silica membrane*

Introduction

In recent years, development of microfluidic devices where controlled flow at micro-liter level is an urgent requirement.[1] Our research group is involved in development of electro-osmotic pumps (EOP), an integral part of micro fluidic devices, which can coulometrically control the flow rate of liquid flow at micro liter level.[2-5] We have successfully demonstrated the EOP using redox-polymer electrodes like poly(hydroquinone/benzoquinone)[4] and polyaniline wrapped aminated graphene electrodes.[5] The flow of the EOP was resulted from the electro-oxidation of redox polymer at anode, which generates the protons. At cathode electro reduction consumes the protons. In the process the electrons pass through the silica membrane, where concerted shifting of protons drags the sheet of water molecules and hence results into flow. The maximum electro-osmotic flux obtained 40 μL/min/cm^2 reported for polyaniline wrapped aminated graphene electrodes is enough to make at least one microfluidic device such as insulin pump.

Herein, we are demonstrating effect of different acid dopant on electro-osmotic flow of the polyaniline electrodes. The flow through electrodes were made by dip coating carbon paper into paste consisting of polyaniline, conducting carbon filler and Nafion® solution as binder. The sandwich assembly was used to make the pumps. The performance was demonstrated at constant potential.

Experimental

Materials.

Aniline was procured from Loba chemicals, India. Graphitic carbon C45 was purchased from Timcal. Ammonium per sulphate, isopropanol was purchased from SD fine chemicals India. 50% phytic acid solution (PA) , polystyrene sulphonic acid (PSS) and Nafion solution (20% in water) were purchased from Aldrich chemicals. Carbon paper was procured Spectrochem. All the chemicals were used as received. The distilled water was used in all the experiments.

Synthesis.

The polyaniline with different acid dopant was synthesized by interfacial polymerization technique.[6] In brief, 3.2 mmol of aniline dissolved in 10 mL of chloroform was taken in 20 mL glass vial. Separately, 0.8 mmol of ammonium peroxydisulfate in 10 mL of 1 M dopant acid solution was taken. The both solution were mixed slowly and kept without disturbing overnight. The precipitate of polyaniline formed was filtered, washed with water and dried. The dry powder was used for making electrode paste.

Pump assembly:

The sandwich assembly was used to make the electro-osmotic pump. The silica membrane was sandwiched between two polyaniline coated flows through electrodes. The silica membrane was prepared by palletizing 1 micron size phytic acid treated silica particles followed by calcination at 700^0C for 4 h.[2] The electrodes were made by dip coating nitric acid treated carbon paper in a paste composed of 300 mg of polyaniline, 100 mg of conducting carbon, 200 μL of 20% Nafion® solution and 8 mL of isopropanol. Electrodes were washed, dried and punched to 8 mm diameter disks and used to assemble EOP.

Characterization

FTIR spectra were recorded with a Perkin Elmer (Germany) GXFTIR system at 400–4000 cm^{-1} wavelength. The surface morphology was visualized using a JSM-7100F, Japan field emission scanning electron microscope. The flow rate of the assembled EOP was measured by a home-built system. The voltage across the cell was applied using a CHI 760E Electrochemical Analyzer (CH Instruments).

Results and discussion

We successfully synthesized the polyaniline with different dopant by Interfacial polymerization technique. The polymer formation was monitored by FTIR. Figure 1 shows the FTIR spectra recorded in KBr. The presence of vibrational band at 1481 cm^{-1} corresponds to the C=C deformation vibration of the quinoid and benzene ring of PANI, while the peak at 1293 cm^{-1} is assigned to C−N stretching in the benzoid ring. The range of peaks from 1250-1020 cm^{-1} arise from C−N stretching in aromatic amines. The peaks at 815 and 1637 cm^{-1} confirms the presence of sulfonic acid in polystyrene sulfonic acid doped PANI, while, peats at 1275–1250 cm^{-1} confirms the phosphonic acid in phytic acid doped PANI.[7]

The alum doped PANI showed the peak at 1125 cm^{-1}.[8]

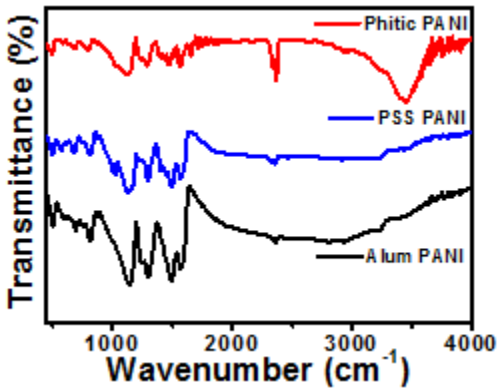


Figure 1. FTIR spectra of polyaniline doped with Alum, Polystyrene sulfonic acid and phytic acid.

Figure 2 shows the SEM images of the PSS, PA and alum doped PANI. Unlike reports on the formation of fibrous structures [6,9], none of the present dopant gave the fiber structure. Instead, aggregates of different size and shapes were observed. This is due to polymeric or multi acidic nature of the dopant.

Electrochemical characterization was performed by recording the cyclic voltammogram in 1 M H_2SO_4 as electrolyte with drop coated paste (consisting of 300 mg of polyaniline, 100 mg of conducting carbon, 200 µL of 20% Nafion solution and 8 mL of isopropanol) on printed carbon electrode as working, platinum wire as counter and Ag/AgCl as reference electrode. The recorded voltammogram at different scan rates were presented in Figure 3. From the figure it is clear that at slow scan rate i.e. 5mV/s, the PANI with all three dopant showed the typical two wave redox behavior, similar to the reported in literature.[10]

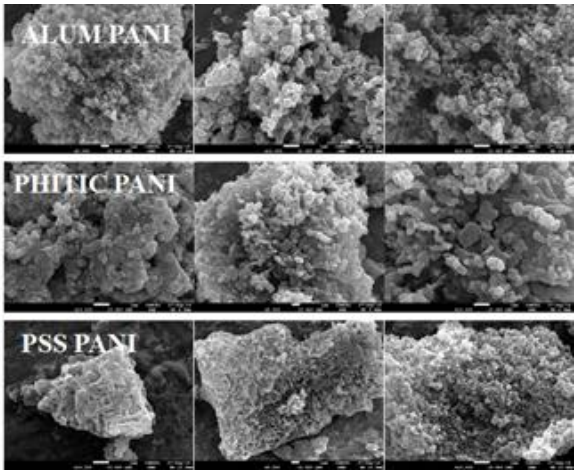


Figure 2. SEM images of the polyaniline doped with Alum, PSS and PA at similar magnifications. Scale bar corresponds to one micro.

The first oxidation/reduction peak appears at 187 and 29.00 mV while second oxidation/reduction appeared at 606 and 328 mV. As the scan rate increased theses peaks gets overlapped and became single peak due to ohmic resistance of the electrode. When we plot the graph of peak current versus scan rate, straight line was observed indicating surface confined phenomena. Of the three dopant, phytic acid (PA), polystyrene sulfonic acid (PSS) and alum; low ohmic resistance was observed for PA followed by alum and PSS indicating multi functionality of the dopant molecule plays important role in redox behavior of PANI. PSS is polymeric and has the molecular weight of 75000 mol/g, whereas alum and PA has 4 and 6 sulfonic acid functionality with molecular weights of 474.38 and 660.04. This was also supported by calculated resistance of the electrodes from impedance measurements.

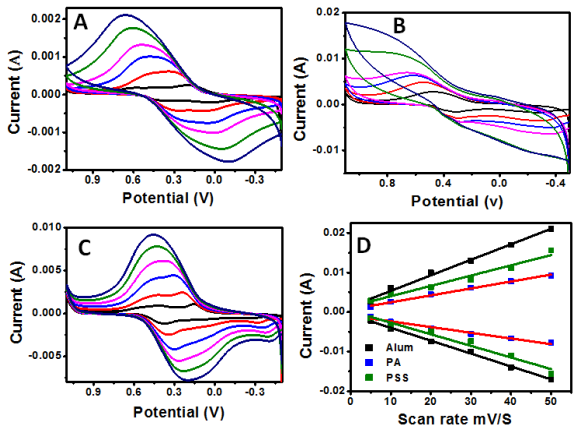


Figure 3. Cyclic voltammogram with normalized current for A) Alum, B) PSS and C) Phytic acid doped PANI. D) Shows the normalized current versus scan rate

Figure 3 (D) shows the Nyquist plot for the PSS, PA and alum doped PANI. The Typical Nyquist plots consist of three parts: (i) a semicircle in the high-to-medium frequency region, with the starting cross-point at the Z' axis indicating the combined series resistance of the electrolyte, electrode, current collectors, electrode/current collector contact resistance, and the diameter of the semicircle representing the charge transport resistance (ii) A straight line with a slope of 45^0 in the low-frequency range, which corresponds to the semi-infinite Warburg impedance, resulting from the frequency dependence of ion diffusion/transport in the electrolyte. (iii) A vertical line at very low frequencies caused by the accumulation of ions at the bottom of the pores of the electrode. The nearly vertical line indicates good capacitive behaviour without diffusion limitations. Herein, we observed the two arcs in Nyquist plots, a small in high frequency region and big arc in low frequency region. A small arc in high frequency region indicates the low resistance. The calculated resistance values were 2.37, 2.87 and 8.14 ohms for PSS, PA and alum respectively. The PSS has the lowest resistance of 2.37 Ω followed by PA, 2.87 Ω and alum, 8.14 Ω. Second arc indicates the efficacy of proton diffusion. A slope of ~ 45^0 in PSS doped PANI indicates the efficient proton diffusion by pathway of proton hopping. The PA and alum has the lower slope suggesting poor diffusion of protons in compare to PSS dopant.

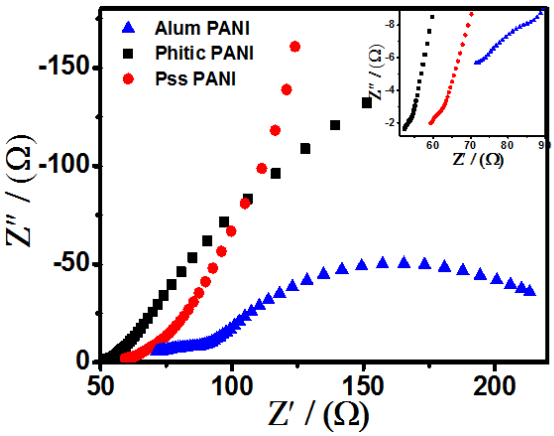


Figure 4. Nyquist plots of PAA, PA and alum doped PANI in 1 M H_2SO_4 solution with three electrode system.

The electro-osmotic pumps was assembled by sandwiching silica membrane between PANI paste coated flows through electrodes. The schematics of pump assembly is shown in figure 5 along with representative electrode reactions. The performance of the pump was tested by applying constant potential. Figure 6 shows the plot of flow rate versus applied constant potential. From the graph it was clear that the flow rate was linearly dependent on applied potential. The minimum potential at which the flow observed was 1V.

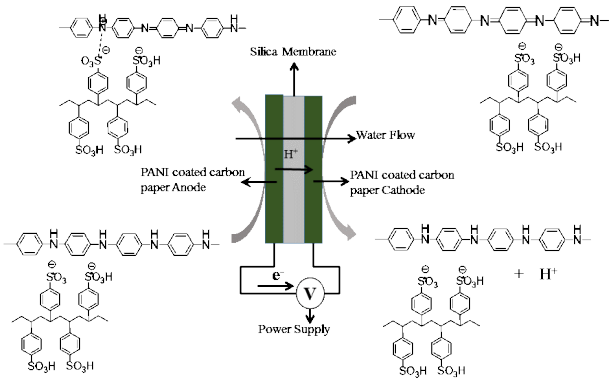


Figure 5. Schematics of electro-osmotic pump showing PSS doped PANI as anode and cathode with clean generation and consumption of protons.

This potential is well below the thermodynamic potential of water oxidation indicating operation of the pump was purely from the electro oxidation/reduction of polyaniline present on respective electrodes. The generated proton pass through the silica membrane. In the process it drags the surrounded sheet of water molecules which results into flow. The maximum electro-osmotic flux obtained was 30µl/min for PSS doped PANI followed by PA and alum. It follows the trend of resistance values suggesting effective potential available for PSS doped PANI is higher than the PA and alum doped PANI. Lower the resistance of the electrode higher the potential available to flow the water and hence higher the flow.

The obtained electro-osmotic flux of about 33µl/min is similar to our earlier report for polybenzoquinone based EOP and higher than the reported PEDOT based EOP.[11] But smaller than the Ag/Ag_2O[1] and silver ferricyanide based electrodes.[3] This variation in flow may be due to the relative proton generating and consuming kinetics of the electrodes.

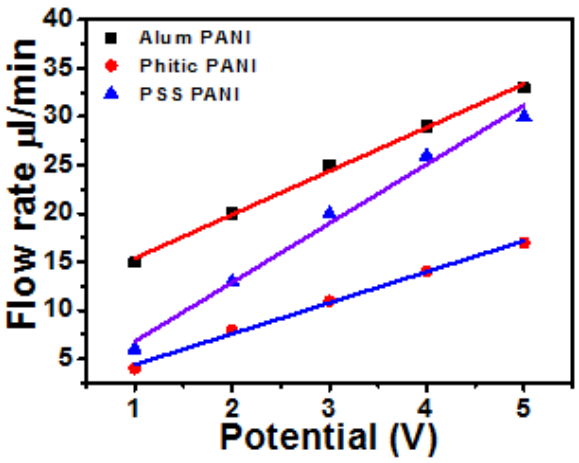


Figure 6. Plot of flow rate versus applied constant potential for PSS, PA and alum doped PANI.

Conclusions

We have successfully fabricated and demonstrated non-gassing electro-osmotic pump with PSS, PA and alum doped PANI. The PANI was synthesized by interfacial polymerization of aniline with ammonium persulphate catalyst. The FTIR spectra confirm its formation. The electrodes were made by dip coating paste composed of PANI, conducting carbon and Nafion® solution. Cyclic voltammogram and impedance measurements confirms dopant dependent electrochemical behavior. The pump assembly showed the linear dependence of electroosmotic flux with applied potential. The maximum flux of about 33 µl/min/V obtained for PSS doped PANI without generation of either oxygen or hydrogen neither on anode nor cathode. The operation of the ump was purely electro oxidation/reduction of PANI on respective electrodes.

Acknowledgements

This work was supported by the Department of Science and Technology, Government of India, by awarding Ramanujan Fellowship

(SR/S2/RJN-18/2011) and the financial assistance, (grant no. SR/S3/CE/034/2013). Authors thank Dr Amitava Das, Director, CSIR-CSMCRI for his encouragement and support.

References

1. C. He, J.J. Lu, Z. Jia, W. Wang, X. Wang, P. K. Dasgupta, S. Liu, *Anal. Chem*. 83, 2430, 2011.
2. W. Shin, J. M. Lee, R. K. Nagarale, S. J. Shin, A. Heller, *J.Am.Chem.Soc*. 133, 2374, 2011.
3. S. Mathi, R.K. Nagarale, *J. Electrochem. Soc*. 163, H657, 2016.
4. V. K. Sachan, A. K. Singh, K. Jahan, S. G. Kumbar, R.K. Nagarale, P. K. Bhattacharya, *J. Electrochem. Soc*. 161, H3029, 2014.
5. R. Kumar, K. Jahan, R. K. Nagarale, A. Sharma, *ACS Appl. Mater. Interfaces* 7, 593, 2015.
6. J. Huang, R.B. Kaner, *J. Am. Chem. Soc*. 3, 126, 2004.
7. Y. Li, S. Cai, G. Xu, S. Shen, M. Zhang, T. Zhang, X. Sun, *RSC Adv*. 5, 25708, 2015.
8. M. V. Barashkov, A. I. Komyak, S. N. Shashkovb, *Journal of Applied Spectroscopy*, 71, 3, 2004.
9. P. Dallas, V. Georgakilas, *Adv. Colloid Interface Sci*. 224, 46, 2015.
10. N. Gospodinova, L. Terlemezyan, *Prog. Polym. Sci*. 23, 1443, 1998R.
11. P. G. Erlandsson, N. D. Robinson, *Electrophoresis*, 32, 784, 2011.

MACRO 355

Gas Separation Membranes Made From Tröger's Base-based Polyamide

Bisoi, Soumendu
Materials Science Centre, Indian Institute of Technology, Kharagpur- 721302, India
*Susanta Banerjee** (E-mail: susanta@matsc.iitkgp.ernet.in)

Gas transport properties have been tested to see the effects of Tröger Base (TB) moiety on polyamide (PA) membranes. In view of that, here we report a series of four novels TB derived PAs, synthesised from previously reported diamine monomer and four commercially available diacids via conventional polycondensation method.[1] Dense membranes were prepared by solution casting and solvent evaporation techniques. The synthesized PAs showed high glass transition temperature (283-290 °C), 10% weight loss up to temperature 431 °C in air, and tensile strength up to 91 MPa. The PA membranes showed good gas permeability (P_{CO2} up to 109 and P_{O2} up to 21 barrer) and high permselectivity (P_{CO2}/P_{CH4} up to 53.7 and P_{O2}/P_{N2} up to 7.52) in comparison to many other published literature.[2]

References

[44]S, Bisoi; P, Bandyopadhyay; D, Bera; S, Banerjee. *Eur. Polym. J.*, 66 (2015) 419–428.
[45]D, Bera; V, Padmanabhan; S, Banerjee; Macromolecules, 48 (2015) 4541–4554.

MACRO 366

Fe-N integrated metal organic gel- melamine formaldehyde derived porous carbon structures- a novel catalyst system for alkaline fuel cells

N.S. Sumitha[a], G.S. Sailaja[a*], K. Shijina[b], U. S. Hareesh [b]*,
G.M. Anilkumar[c], Balagopal N. Nair [c], I. V. Rajith[d], K. Sreekumar [d]

[a]*Department of Polymer Science and Rubber Technology, Cochin University of Science and Technology, Cochin, India*
[b]*Materials Science and Technology Division, CSIR-NIIST, Thiruvananthapuram, India*
[c]*R&D Centre, Noritake Co. Ltd, Aichi, Japan*
[d]*National Chemical Laboratory CSIR, Pune, India*
** e-mail id:* sailajags@cusat.ac.in; hareesh@niist.res.in

Abstract

Porous carbon based electrocatalysts with activity comparable to that of Pt/C is of utmost importance for fuel cell applications. Here we present synthesis of a novel class of Fe and N doped porous graphitic carbon precursor derived from polymerization of melamine formaldehyde and metal-organic gel system. Pyrolysis of the IPN at 900°C under N_2 atmosphere resulted in graphitic network structures with sufficient Fe and N doping as substantiated by TEM micrographs. The derived carbon network has a high surface area value of 430m^2/g as evidenced by BET surface area analysis. Ultrastructural evaluation exemplified a structure integrated with two morphologies; one having a flower-like structure and second having nano-rod shaped graphitized carbon. The existence of Fe was evident from the TEM-EDX analysis. This new class of catalysts exhibited onset potential of 0.86 V for Oxygen Reduction Reaction (ORR) offering feasibility to derive extended versions of Fe-N doped porous carbon structures with better ORR activity from IPN based structures via systemic modulations of synthetic protocols.

Keywords: *Metal-organic gel; porous carbon; Oxygen reduction reaction; Fuel Cell*

Introduction

Oxygen Reduction Reaction (ORR) plays a key role in the energy conversion mechanism in fuel cells.[1] Platinum and Pt-based alloys have been known as the state of the art catalyst for ORR.[2] However, the high cost and scarcity of Pt limits its large-scale application.[3, 4] Porous carbon materials have attracted extensive interest due to their large surface area and conductivity.[5] However, usually these materials exhibit low ORR activity.[6] Recently it has shown that the incorporation of hetero atoms like nitrogen[7, 8] and metals like iron can improve the electrocatalytic activity[9, 10] of carbon by destroying the electroneutrality of carbon resulting in the formation of catalyticaly active sites. Zeolitic Imidazolate Framework (ZIF) and Metal Organic Frame work (MOF)

are the major sources of heteroatom-doped carbon.[11, 12] However, the syntheses of these materials are cumbersome and include the use of toxic solvents.[13] Metal Organic gel, an extended network of MOF are new class of materials with easier syntheses protocols and are widely used in gas storage applications.

In this study we report the synthesis of Fe-N *in situ* doped carbon from Metal Organic Gel and melamine formaldehyde network.

Experimental

(i) Materials

Trimesic acid (Sigma Aldrich), Anhydrous ferric chloride (Sigma Aldrich), Ethanol(Jiangsu Huaxi International Trade Co-Ltd, China), Naphthalene (TCI Chemicals, India Pvt. Ltd), Melamine (Sigma Aldrich), Formaldehyde (Sigma Aldrich) were used.

(ii) Synthesis of Fe-N in situ doped porous carbon

The Fe MOG samples were synthesized by formulating a network generated by reacting a metal organic gel derived from $FeCl_3$ and H_3BTC and melamine formaldehyde, cross-linked at 120 °C. The green precursors were pyrolysed at 900°C under N_2 atmosphere. The carbonized samples were washed with 1M KOH and characterized (Fe-MOG 1). In a subsequent reaction, porosity was modulated by a porogen (denoted as Fe-MOG 2)

(v) Characterization

The microstructural analysis of samples were done using a Scanning Electron Microscope (SEM) (Hitachi 2240 Japan SEM microscope). The Transmission Electron Microscopic Analysis (HR-TEM) were carried out using a FEI Tecnai 30 G2 S-TWIN microscope. The specific surfacearea of samples were measured using BET surfacearea measurement technique with Mictromeritics Gemini 2375 Surface area analyzer. The electrochemical measurements were carried out in a Biologic Electrochemical Workstation (VMP-3) using a three-electrode setup.

Results and discussion

The SEM image of Fe-MOG 1 (figure 1 a) has distributed pores along its surface while Fe-MOG 2 (figure 1b) has a flower-bunch like microstructure, where the individual flower is characterized by elongated needle-like petals generating elongated void spaces with higher porosity. Due to this intrinsic feature, we anticipate a higher surface area for this sample.

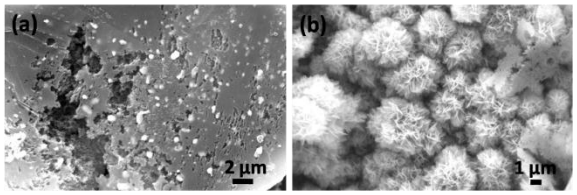


Figure 1 SEM images of carbonized (a) Fe-MOG 1 and (b) Fe-MOG 2

The HRTEM images of Fe-MOG 1 and Fe-MOG 2 are given in figure 2. Fe-MOG 1 is composed of multi-layered branched carbon nanotubes (Figure 2a-c). The size of branches ranges from 10 nm to 40 nm. The HR-TEM images of Fe-MOG 2 (Figure 2d-f) have

characteristic aggregated cube-like morphology. The modulated morphology of the derived carbon is accounted due to the incorporation of naphthalene into the gel-polymer network.

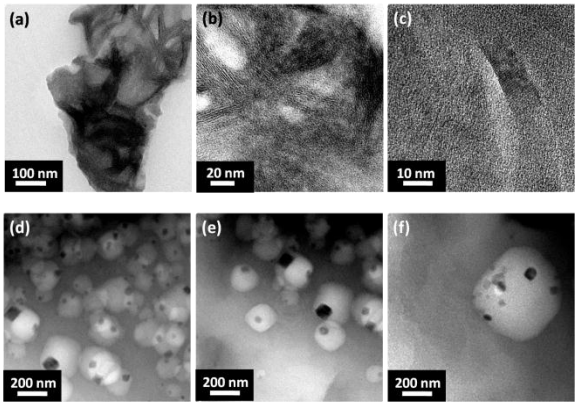


Figure 2 HRTEM images of carbonized (a-c) Fe-MOG 1 and (d-f) Fe-MOG 2.

The EDX patterns of the samples given as figure 3 confirm the presence of Fe in both the samples.

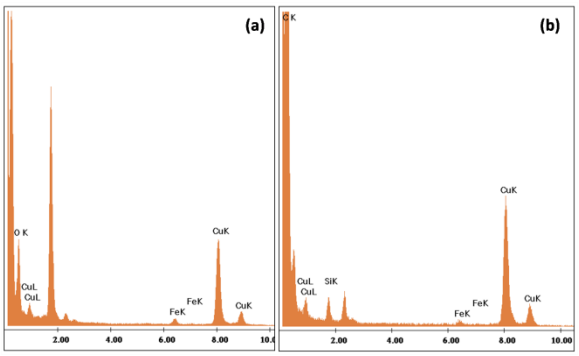


Figure 3 EDX patterns of carbonized (a) Fe-MOG 1 and (b) Fe-MOG 2

Typical nitrogen adsorption-desorption isotherm of the Fe-MOG 2 demonstrated to have type 1 isotherm with microporous structure and BET surface area 430 m^2/g.

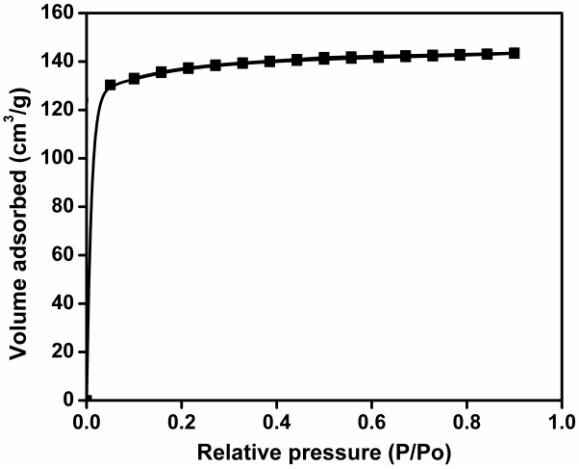


Figure 4 N_2 adsorption isotherm of carbonized Fe-MOG 2

The electrochemical measurements were conducted using a biologic electrochemical work station using a three electrode set up with glassy carbon as the working electrode, mercury mercurous oxide as the reference electrode and graphitic carbon as the counter electrode. The electrodes were dipped in 0.1 M KOH solution. A catalyst slurry was prepared by mixing 5 mg catalyst with 1mL water: IPA (3:1) mixture and 40 µL nafion solution using ultrasonication. 10µL of the slurry was dropped on GC electrode and dried and used as working electrode.

The electrocatalytic studies were carried out using linear sweep voltammetry (LSV) using Rotating Disc Electrode (RDE) analysis with a scan rate of 5 mVs^{-1} and rotation speed 1600 rpm in oxygen saturated 0.1 M KOH solution. The two samples exhibited an onset potential of 0.86 V. ORR results indicate that the material has potential to be employed as catalyst for fuel cell applications. Further work to tailor the composition and morphology of the materials are in progress

now. Recently, we have successfully modified the process resulting in materials with higher surface area values of 868m^2/g. It is therefore anticipated that the modified system will show significantly better ORR activity. Full evaluations of the new materials including electrochemical characterization are being measured now and will be reported in subsequent papers.

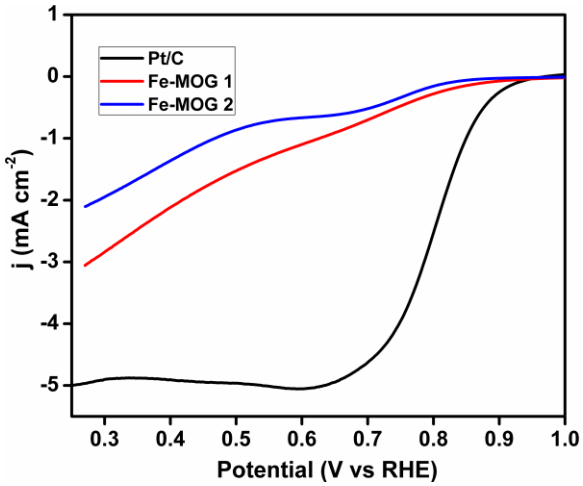


Figure 5 Linear sweep voltammograms of Fe-MOG 1, Fe-MOG 2 and Pt/C

Conclusions

We have developed two novel Fe-N doped porous carbon systems from Fe-MOG-melamine formaldehyde IPN's. Modulation of microstructure, porosity and surface area was accomplished by incorporation of naphthalene in the system in one case. Typical ORR results exhibited an onset potential of 0.86 V.

Acknowledgements

Authors acknowledge Council of Scientific and Industrial Research (CSIR), Government of India and Noritake Company, Ltd., Japan for the joint collaborative project (CLP 218739)

References

1.C. Zhu, H. Li, S. Fu, D. Du, Y. Lin, *Chem. Soc. Rev.*, 45, 517-531 (2016).

2. Y. Nie, L. Li and Z. Wei, *Chem. Soc. Rev.*, 44, 2168-2201 (2015).

3. J. Liang, X. Du, C. Gibson, X. W. Du, S. Qiao, *Adv. Mater*. 25, 6226–6231 (2013)

4. Y. Liang, Y. Li, H. Wang, J. Zhou, J. Wang, T. Regier, H. Dai, *Nat Mater.*, 10, 780-786 (2011).

5. R. Silva, D. Voiry, M. Chhowalla, T. Asefa, *J. Am. Chem. Soc*., 135, 7823–7826 (2013).

6. H. Wang, R. Cote, G. Faubert, D. Guay, J. P. Dodelet, *J. Phys. Chem. B*, 103, 2042–2049 (1999).

7. K. P. Gong, F. Du, Z. H. Xia, M. Durstock, L. M. Dai, *Science*, 323, 760–764 (2009).

8. P. Chen, T. Y. Xiao, Y. H. Qian, S. S. Li, S. H. Yu, *Adv. Mater*., 23, 3192–3196 (2013).

9. R. Zhou, S. Z. Qiao, *Chem. Commun.*, 51, 7516-7519 (2015).

10. J. Zhang, L. Dai, *ACS Catal.*, 5, 7244-7253 (2015).

11. S. J. Yang, T. Kim, J. H. Im, Y. S. Kim, K. Lee, H. Jung, C. R. Park, *Chem. Mater.*, 24,464-470 (2012).

12. P. Zhang, F. Sun, Z. Xiang, Z. Shen, J. Yun, D. Cao, *Energy Environ. Sci.*, 7,442-450 (2014).
13. W. Xia, B. Qiu, D. Xia, R. Zou, *Sci. Rep.*, 3, 1935 (2013).
14. L. Cui, J. Wu, H. Ju, *ACS Appl. Mater. Interfaces*, 6, 16210-16216 (2014).
15. L. Zhang, B. Marzec, R. Clerac, Y. Chen, H. Zhang, W. Schmitt, *Chem. Commun.*, 49, 66-68 (2013).

MACRO 369

Polyamine phosphate ester blends with oxypolybezimidazole to improve the properties of proton exchange membrane

K Rambabu, Balakondareddy Sana, Tushar Jana*

School of chemistry, University of Hyderabad, Hyderabad, India

Email: tusharjana@uohyd.ac.in

Current work focussed on increasing the thermal, mechanical and chemical stability of poly (4,4'-diophynyl ether-5,5'bibenzimidazole) (OPBI) membrane and increasing the proton conductivity of membranes for the application in high temperature proton exchange membrane fuel cell (HTPEMFC). Polyamine phosphate ester (PAPE) have been successfully synthesized by prudovik reaction by using polyschiff's base. The blend formation of PAPE and OPBI was observed from NMR and FT-IR. The hydrogen bond interaction between –P=O in PAPE and –NH in OPBI was observed. Membranes were analysed by TGA, DMA, Impedance for thermal stability, glass transition temperature and conductivity analysis respectively. 75% of OPBI blend showed good mechanical, thermal and conductivity properties.

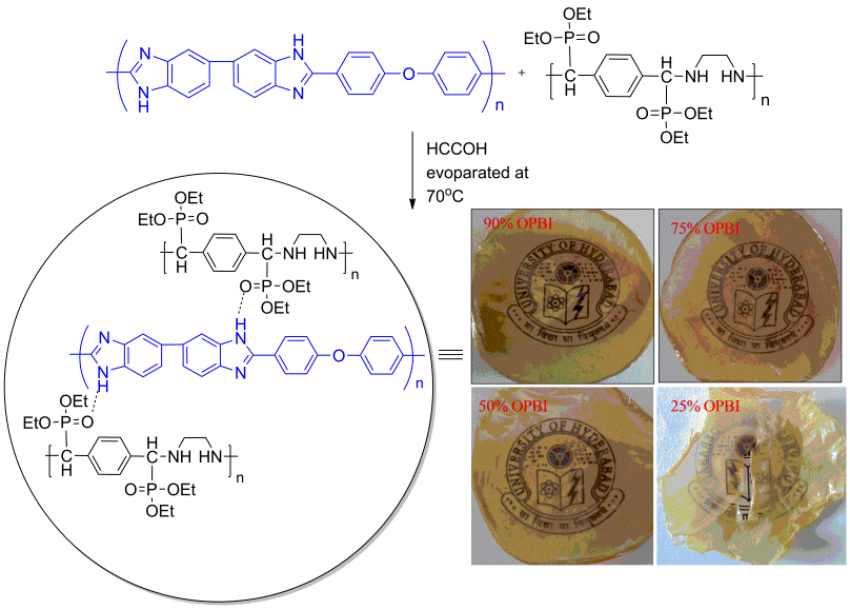


Figure 1: Preparation of OPBI/PAPE blended membranes

References

[1] Ghosh Sandip; Sannigrahi Arindam; Maity Sudhangshu; Jana Tushar; *Journal of physical chemistry B* 114 (2010) 3122.

[2] Yan Liu; Yan Zhang; Zhenhu Cao; Mao Peng; Zhengping Fang; *Polym. Adv. Technol.* 24 (2013) 197.

MACRO 376

Fabrication of Poly(vinyl chloride)-Chitosan-Cellulose Nanocrystals based Solid Electrolyte Membrane for Direct methanol Fuel Cells: A Sustainable Approach

Gaur, Surendra Singh; Dhar, Prodyut; Sonowal, Amrita; Sharma, Akanksha; Kumar, Amit; and Katiyar, Vimal*

Department of Chemical Engineering, Indian Institute of Technology Guwahati, Guwahati, Assam, India – 781039

** Corresponding Author: vkatiyar@iitg.ernet.in*

Abstract: The study reports the use of cellulose nanocrystals (CNCs) as bionanofiller for fabrication of solid electrolyte membranes for direct methanol fuel cells (DMFCs). CNCs were synthesized by hydrolysis process by using three types of acids H_2SO_4, HNO_3 and HCl. The acids used in hydrolysis had effect on the shape, size and morphology of CNCs, which affected the properties of electrolyte membranes also. Poly (vinyl alcohol) (PVA) and chitosan were used as the polymer matrix, but they are unstable at higher temperatures [1]. Crosslinking of PVA and chitosan provided the stability to the membranes. CNCs are incorporated in the polymer matrix to improve the ion conductivity. The methanol permeability of prepared membranes was ~10^{-8} cm^2 s^{-1}, which is significantly lower than the base PVA membrane. Further, these membranes had good thermo-mechanical properties, low swelling characteristics and higher ion conductivity. It is found that HNO_3 hydrolysed CNCs based membrane showed better performance in water uptake, ion conductivity and swelling, whereas HCl hydrolysed CNCs based membrane have demonstrated better methanol barrier properties. As the methanol permeability of HNO_3 CNCs based membrane was almost equal to HCl CNCs based membrane and it was superior in other properties, so it can be concluded that HNO_3 hydrolysed CNCs based membrane can be a suitable and sustainable option for solid electrolyte used in DMFCs.

Acknowledgements: The authors are thankful to the Department of Chemicals and Petrochemicals (GoI) funded Centre of Excellence for Sustainable Polymers, IIT Guwahati and Central Instruments Facility, IIT Guwahati for utilizing their research facilities.

References

[1] Gaur, Surendra Singh; Dhar, Prodyut; Kumar, Amit; & Katiyar, Vimal. *Journal of Renewable and Sustainable Energy*, 6(5) (2014) 053135.

MACRO 387

Tunable Photoluminescence of Carbazole Based Quinoline Conjugated Polymer by Doping Cds Quantum dot and Poly(vinyl alcohol)

S. Karpagam* and Anjali Upadhyay
Department of Chemistry,
School of Advanced Sciences,
VIT University, Vellore -14. Tamil Nadu, India
**Email: skarpagam80@yahoo.com*

Carbazole and quinoline combined donor-acceptor conjugated polymer was synthesized by Wittig route [1,2,3]. The resulting polymer structure was well established by FTIR, NMR, Gel permeation chromatography (GPC) and elemental analysis.

This polymer was electrospun with Cds quantum dots and polyvinylalcohol to prepare composite nanofiber (PVA/Polymer/Cds) using electrospinning technique. The synthesized nanofiber were characterized by UV-Visible, photoluminescence (PL) spectrophotometer, XRD, TEM and SEM. Figure 1 represents the SEM, TEM and PL spectra of the polymer nanofiber. From the figure, there are two emission peaks were appeared at 340 nm and 398 nm for naofibers. The PL spectrum of polymer was observed and blue shifted after doping of CdS and PVA. It was found that the changes in PL spectra of polymers originated from the chemical interactions between polymer and Cds.

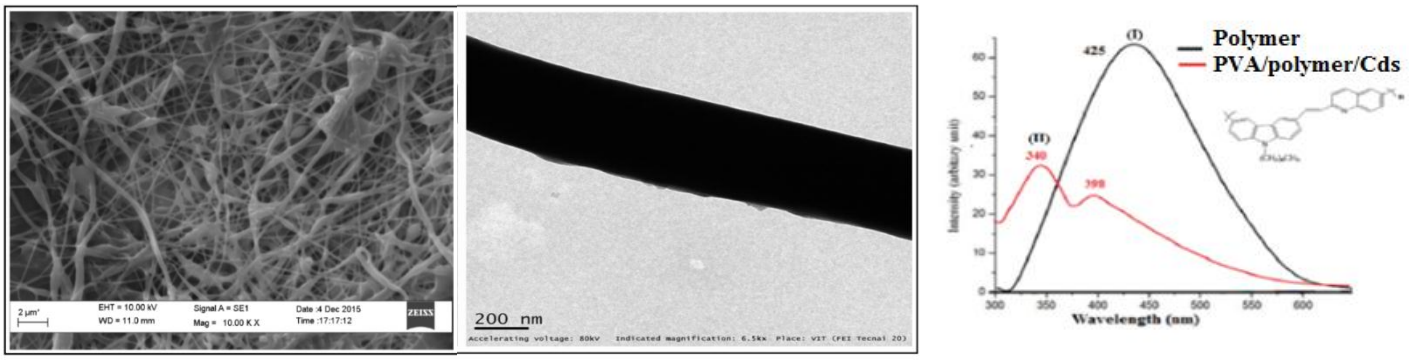


Figure 1: SEM ,TEM images and PL spectra of PVA/Poymer/CdS composite nanofibers

As can be seen from the figure 1, the average diameter of these fibers was found to be 290 nm. The long electrospun nanofibers exhibited like random orientation like a spider with uniform thickness and were distributed in a fibrous mat. TEM micrographs illustrated that the resulting nanofibers were smooth and exhibited uniform diameter in the range of 250–260 nm along their entire length.

References

[1] Anjali Upadhyay and S.Karpagam, Synthesis and opto-electrical properties of carbazole functionalized quinoline based conjugated oligomer for luminescent devices, *J. Photopolym sci tec*,6 (2015) 755.

[2] Anjali Upadhyay and S.Karpagam, Studies of luminescence performance on carbazole donor and quinoline acceptor based conjugated polymer, *J fluores*,26 (2016) 439-449.

[3] Anjali Upadhyay and S.Karpagam, Synthesis, photophysical and electrochemical properties of carbazole-containing 2,6-quinoline-based conjugated polymer, *Polym. Bull*, (2016) (DOI 10.1007/s00289-016-1619-1).

[4] Cho, H., S.Y. Min and T.W. Lee, Electrospun organic nanofiber electronics and photonics, *Macromol. Mater. Eng. 298* (2013) 475–486.

MACRO 389

Förster's Resonance Energy Transfer (FRET) as a Technique to Monitor the Aggregation Phenomenon of Amphiphilic Polymer

Rajdev, Priya*, Basak, Dipankar and Ghosh, Suhrit*

Polymer Science Unit, Indian Association for the Cultivation of Science, 2A & 2B Raja Sc. Mullick Road, Jadavpur, Kolkata – 700032, India

* psupr2@iacs.res.in; psusg2@iacs.res.in

For the last few decades amphiphilic polymers have gained immense importance due to the structurally diverse nano-assemblies (micelles, polymerosomes, fractals etc.) with container properties, formed by these polymers, which find applications in biological and biomedical fields. One of the most important parameters, which is to be considered for biomedical application, is the dynamics/stability of these aggregates. FRET is a highly sensitive technique and recently, we have studied [1] the kinetic stability of aggregates from a family of amphiphilic random copolymers by non-covalent encapsulation of FRET dyes. Hence, more recently, we have synthesized a pair of block copolymers, also from a single parent polymer, where the D and A chromophores were covalently attached to the hydrophobic block in a random fashion, via the post polymerization modification of the –OH groups present in the hydrophobic block [2]. Detail investigation on individual and co-mixed aggregates of D- and A- functionalized block copolymers showed remarkably slow dynamics (high stability), high thermal stability and low critical aggregation concentration for the micellar aggregates. To rationalize the remarkably high stability of these polymer aggregates, the structure of the polymers were analyzed which hinted at the presence of unreacted pendant –OH groups. FT-IR experiments highlighted the presence of H-bonding among these OH groups which supramolecularly cross-linked the micellar core. Thus, this non-covalent core-cross linking was responsible for such astonishingly slow mixing dynamics or remarkably high stability further corroborated by similar experiments with control polymers lacking such -OH groups (acetylation or protonation of OH groups). In this presentation we will discuss the unique kinetic stability of the micelles and the role of supramolecular core cross-linking and focus on the utilization of FRET in context of studying dynamics of amphiphilic polymer aggregates.

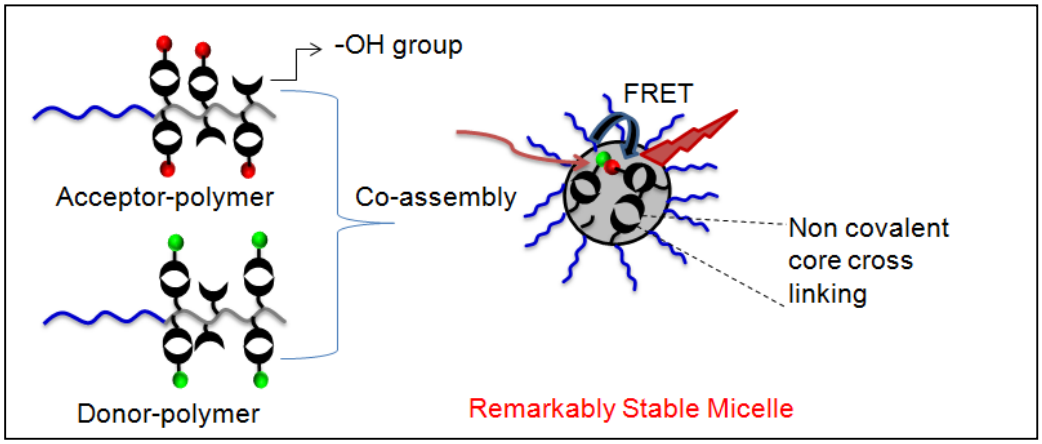


Figure 1: FRET between D- and A-polymer as a tool to measure the dynamics of mixing in amphiphilic polymers.

References

[46]Dan, K; Rajdev, P; Deb, J; Jana, S. S.; Ghosh, S. *J. Pol. Sc. Part A: Pol. Chem.*51 (2013), 4932.

[47]Rajdev, P; Basak, D; Ghosh, S. *Macromolecules* 48 (2015) 3360.

MACRO 391

Ambient dried carbon aerogel as an anode material for lithium ion cells

Ancy Smitha Alex[a], Ananda Lekshmi. M.S[a], Sekkar. V[a]*, Bibin John[b], Gouri. C[c], SA Ilangovan[d]

[a]*Analytical Division,* [b] *Energy Systems Division,* [c] *Propellants and Special Chemicals Group,* [d] *Chemical Systems Group*

PCM Entity, Vikram Sarabhai Space Centre, Thiruvananthapuram-695022, India

**email id*: vsekkar@gmail.com, v_sekkar@vssc.gov.in

Abstract

Carbon aerogel synthesised through a cost effective and easy method was evaluated as an anode material for lithium ion cells. Carbon aerogel was prepared by carbonizing resorcinol-formaldehyde (RF) aerogel which in turn was prepared through sol gel polymerization of resorcinol with formaldehyde using sodium carbonate as catalyst adopting ambient pressure drying route. The structure and the morphology of the prepared carbon aerogel are investigated using XRD, SEM and TEM and surface area determined using N_2-BET method. The evaluation of carbon aerogel as an anode material revealed promising specific capacity synergized with outstanding cyclability. The first cycle specific capacity was 288 mAh/g with an efficiency of 63% at C/10 rate. The material retained a capacity of 96.9% of the initial capacity with about 100 % efficiency after 100 cycles, showing the excellent cyclability of the material.

Keywords: Carbon aerogel; lithium ion battery; anode

Introduction

Lithium ion (Li-ion) cells have gained considerable attention in recent years as power source for various applications owing to their high voltage, high energy density, low self discharge and good cycle life. A typical Li-ion cell consists of three basic components: cathode, anode, and electrolyte. The performance of the Li-ion cell has strong dependence on the nature of the electrodes and electrolyte employed [1]. Carbon/graphite is the most commonly employed anode material in Li-ion cells because of low cost, low Li^+ ion intercalation potential and satisfactory cycle life [2]. Materials like Si, Sn, transition metal oxides, etc. have attracted attention in recent times due to their high specific capacity. However, these materials suffer from volumetric expansion during cycling which limits their cyclability. Non-graphitic, porous, carbon-based materials are gaining importance as anode by virtue of their high surface area, large pore volume, thermal and chemical stability [1]. Among the various non-graphitic carbonaceous materials, carbon aerogels (CAs) have recently gained considerable attention. CAs are novel class of nanostructured carbon materials with a continuous solid framework and an open pore

structure associated with a wide variety of applications [3]. CAs exhibit attractive properties including low density, well-defined and controlled pore structure, large surface area, mechanical strength and high electrical conductivity, which make them promising candidates for energy applications [2].

Several methods for the synthesis of CAs have been developed [4-7]. Conventionally, aerogels are obtained through super critical drying of the wet gels in which the drying process is associated with negligible shrinkage [8]. However, supercritical process involves very high pressure which makes the drying process highly unsafe and uneconomical. On the other hand, sub critical drying process has been developed which is quite safe to handle and scalable [8].

In the present study, we have chosen to adopt ambient pressure drying route. CA was synthesised from resorcinol-formaldehyde through ambient pressure drying route followed by heat treatment at 1050°C under Ar atmosphere. The material was characterised by XRD, Raman spectra, SEM, TEM, BET nitrogen sorption and finally evaluated as anode material in Li-ion cell.

Experimental

Carbon black (M/s. Timrex, Switzerland), polyvinylidene fluoride (Sigma Aldrich) and 1-methyl-2-pyrrolidinone (Sigma Aldrich) were used for electrode processing. 1M $LiPF_6$ in ethylene carbonate: diethyl carbonate: ethyl methyl carbonate (1:1:1, w/w/w) (Charslton Technologies, Singapore) was used as electrolyte and Celgard 2320 was used as separator. Resorcinol was procured from M/s. Merck Speciality chemicals Inc., Bangalore, India. Formalin (37% aqueous solution of formaldehyde, stabilized with methanol) was procured from M/s. Poly formalein Pvt. Ltd., Cochin, India. Sodium carbonate was procured from M/s.NICE India Ltd., Cochin, India.

CA was synthesised by carbonizing Resorcinol Formaldehyde (RF) aerogel at 1050 °C under Ar atmosphere. RF aerogel was synthesized by polymerizing resorcinol and formaldehyde (1:2 mole ratio) catalysed by sodium carbonate (R/C = 3000) at room temperature for 24 h followed by heat treatment at 50 °C for 24 h and 90 °C for 72 h. R/C denotes the ratio of equivalents of resorcinol to the catalyst. The total solid content in the pre-gel solution was kept at 30 %. Afterwards the RF gels were immersed in 2 % acetic acid at room temperature for 24 h. Then the aqua gels were exchanged with fresh acetone for three times once in 24 hours. Final drying was done under ambient conditions in acetone atmosphere for 48 h followed by vacuum drying for 2 h.

XRD measurements were carried out by a Bruker D8-Discover X-ray diffractometer operating with a Cu anode (40 kV, 40 mA). Microstructural characterization was undertaken by using FEI Quanta 200 Scanning electron microscope (SEM) and FEI Technai-$20G^2$ (200 kV) high resolution transmission electron microscope (TEM). Raman spectrum is recorded using WiTec alpha 300R confocal raman microscope, employed with a laser 532 nm, and 600 lines/min grating and the integration time is 1 s. The BET surface area and BJH pore size analysis was carried out by nitrogen adsorption/desorption technique using

surface area analyser (Micrometrics, USA, ASAP 2020 models)

CA and carbon black were dried at 100 °C for 24 h and polyvinylidene fluoride at 70 °C for 5 h, under vacuum. Electrode slurry was prepared using CA, carbon black and polyvinylidene fluoride (ratio 80:10:10, by weight) using NMP as solvent. The slurry was then coated onto a copper foil of 10 µm thickness and dried at 100 °C for 10 h under vacuum. CR 2032 coin cells were then assembled using this electrode along with lithium metal as reference electrode, using 1M $LiPF_6$ in EC:DEC:EMC (1:1:1, w/w/w) as electrolyte and Celgard 2320 as separator. The cell was assembled in a glove box filled with dry argon gas (H_2O < 1 ppm, O_2 < 1 ppm).

Results and discussion

Morphology and physical properties of CA

The XRD pattern of the synthesised carbon aerogel is shown in Figure 1. It shows graphitic-like structure with broad reflection peaks at ca. 24° and 44° which can be assigned to the lattice planes of graphite [1,2]. The broad reflection peaks compared to those of graphite indicate that the as-prepared CA is amorphous in nature with a low degree of graphitization [1]. In such amorphous carbon, Li is considered to be trapped inside the cavities located at the amorphous areas as well as in the graphene layers of the carbon [1].

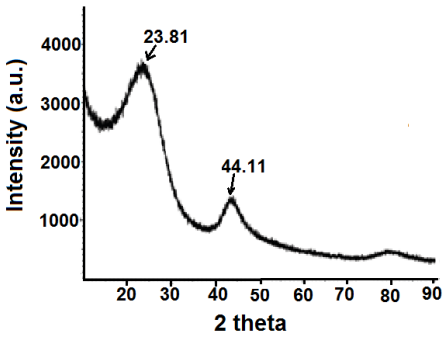


Figure 1. XRD pattern of CA

The Raman spectra of CA is shown in Figure 2. It has strong D (1324 cm^{-1}) and G (1579 cm^{-1}) bands which are similar to the known Raman peaks for CAs [9]. The I_D/I_G ratio is 1.03 suggesting amorphous nature of CA considered for the present study.

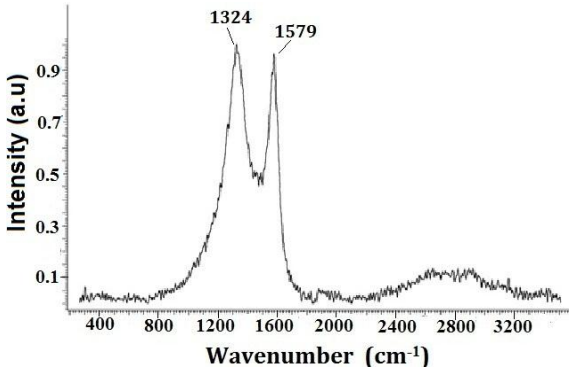


Figure 2. Raman Spectra of CA

The characteristic SEM micrograph of the synthesized CA for present investigation is shown in Figure 3. SEM images indicate that carbon nano-particles are aggregated to form nearly spherical particles. It is clearly seen from the figure that the CAs possess pearl like spherical particles aligned along a string. Average size of these particles is observed to be 6-7 µm. The pearl like particles are connected through well defined necks. The neck connects the particles making them to exist together rather than getting separated. The existence of necks suggests high mechanical strength of these CAs. Thus, the

process of drying under ambient pressure conditions does not lead to any discernable shrinkage.

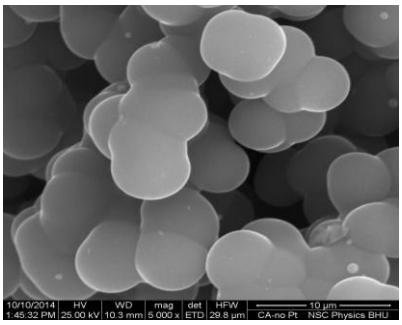


Figure 3. SEM image of CA

The TEM image of as prepared CA is shown in Figure 4 at various magnifications. It can be clearly seen that the entire region is populated with micropores (less than 5 nm) revealing the microporous morphology. Close examination of TEM images reveal that the pore diameter ranges from 0.3 to 1.4 nm which fall under the category of submicropores.

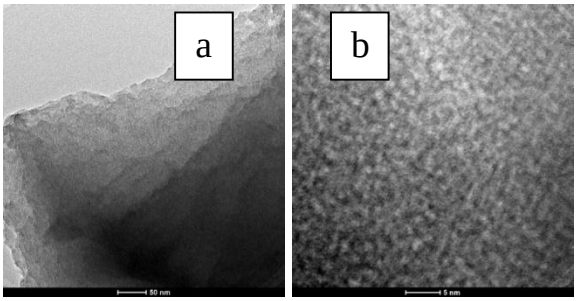


Figure 4. TEM image of CA at different magnifications with scale bar of (a) 50 nm and (b) 5 nm

The nitrogen adsorption/desorption isotherm recorded at 77 K is shown in Figure 5. By applying the BET-BJH model calculations on the adsorption/desorption data the following parameters were calculated: BET surface area: 534.3 m^2/g; Langmuir Surface area: 776.0 m^2/g; Micropore Area: 466.9 m^2/g; Total pore volume: 0.2845 cm^3/g; Total micropore volume: 0.2465 cm^3/g; Average pore diameter: 2.51 nm. The nitrogen adorption/desorption isotherm corresponds to type I isotherm on Brunauer, Deming, Deming, Teller (BDDT) classification. Such isotherms arise when the adsorptions are limited to a few molecular layers. This situation may be possible with the micro-porous materials whose pore size does not exceed a few adsorbate molecular diameters.

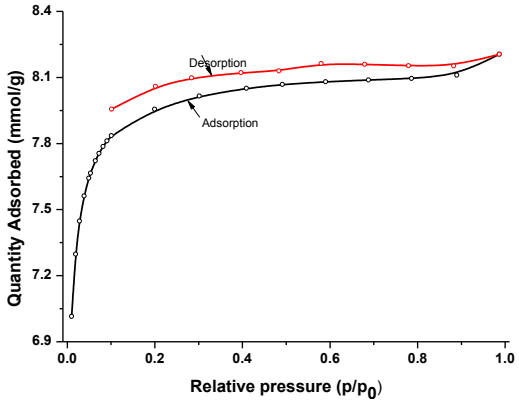


Figure 5. Nitrogen adsorption/desorption isotherm at 77K for CA

Electrochemical studies

The electrochemical evaluation of the CA electrodes was carried out by assembling cells using CA as one electrode versus metallic Li as counter electrode. The assembled cell was subjected to charge-discharge cycling in the voltage range 0.005 to 3.0 V. The cell was subjected to 100 charge-discharge cycles at C/10 rate. The charge-discharge curves at 1^{st}, 2^{nd}, 50^{th} and 100^{th} cycles are shown in Figure 6. The first cycle discharge capacity was 456 mAh/g and charge capacity was 288 mAh/g corresponding to a charge efficiency of 63%. This value is higher than that reported for CAs synthesized from nanobacterial

cellulose [2]. The irreversible capacity in first cycle may be attributed to the formation of solid electrolyte interface (SEI) at electrode surface. This large irreversible capacity occurring in the first discharge/charge cycle is a common phenomenon for carbon materials [1]. The first cycle efficiency of 63.15 % is improved to 93 % in second cycle and further to ~100 % in subsequent cycles. This is due to the stabilization of SEI during cycling. The charge-discharge pattern shown in Figure 6 is consistent with that obtained for CA derived from bacterial nanocellulose [2]. The cycling performance of the cell at C/10 rate is shown in Figure 7. The capacity showed a slight decrease initially and then increased with cycling which may be attributed to the activation of the disordered structure. Similar observation of increase in capacity has been reported by Wang et al [2].

The specific capacity at the end of 100 cycles was 279 mAh/g which shows that 96.9 % of the initial capacity was retained during cycling (Figure 6). The efficiency was maintained at the end of 100th cycle also. Thus, CA based electrodes exhibited excellent capacity retention when evaluated as anode material in Li-ion cells. After the cycling at C/10, the performance of the cell was evaluated at higher rates viz. C/5, C/2 and 1C. The stabilised specific capacity at C/5, C/2 and 1C is 259, 184 and 109 mAh/g respectively. The efficiency got stabilised at 100 % after a few cycles at each rate.

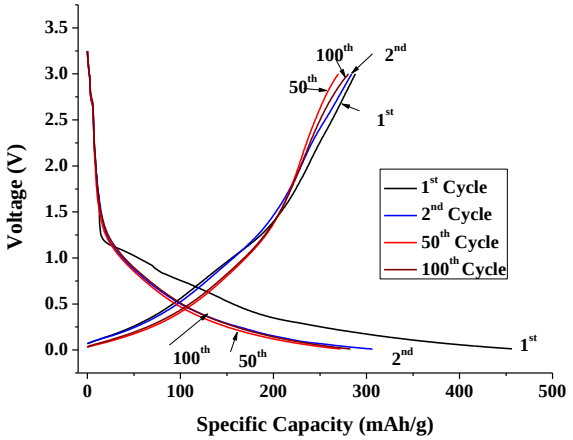


Figure 6. Charge-discharge cycle of carbon aerogel electrode at 1st , 2nd , 50th and 100th cycle

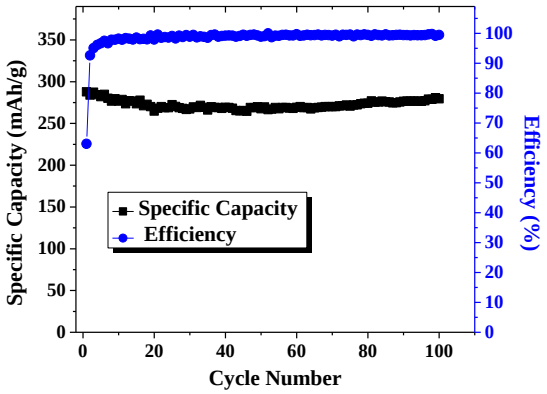


Figure 7. Cycling performance of CA electrode at C/10 rate

Conclusions

The carbon aerogel with microporous structure derived from resorcinol-formaldehyde by an ambient drying route has been successfully evaluated as an anode material in lithium ion cells. The material exhibited a specific capacity of 288 mAh/g at C/10 rate and retained 97 % of the initial capacity after 100 cycles. The material also exhibited promising performance at higher rates. The efficiency got stabilised at 100 % after a few cycles during the evaluation at

different rates, showing the excellent reversibility of the aerogel.

Acknowledgements

The authors thank Director, VSSC for granting permission to publish this paper.

References

1.X. Yang, H.Huang, G.Zhang, X. Li, D. Wu, R.Fu, *Mat. Chem. Phy.* 149-150, 657, 2015.

2.L.Wang, C.Schutz, G. Salazar-Alvarez, M.-M.Titirici, *RSC Adv*., 4, 17549, 2014.

3. H. Kabbour, Jr. Baumann, T. Satcher, A. Saulnier, C.C. Ahn, *Chem. Mater*., 18, 6085, 2006.

4. R. A. Ganeev, P. A. Naik, J. A. Chakera, H. Singhal, N. C. Pramanik, P. A. Abraham, N. Rani Panicker, M. Kumar, P. D. Gupta*J Opt Soc Am B*, 28,360, 2011.

5. R.W.Pekala, *J.Mater.Sci.*, 24, 3221, 1989.

6. R.W. Pekala, S.T. Mayer, J.L. Kaschmitter, F.M. Kong, *Sol Gel Process Appl*,369, 1994.

7. D. Wu, R. Fu, S.Zhang, M.S. Dresselhaus, G.Dresselhaus *Carbon*, 42, 2033, 2004.

8. S.A. Muhtaseb, J.A. Ritter, *Adv. Mater.*, 15, 101, 2003.

9. K.Balakumar, N.Kalaiselvi. *RSC Adv*., 5,340, 2015.

MACRO 393

Electromagnetic Interference Shielding of Nickel Electroplated Fabrics.

K.S.Dijith[ab], C.V.Sruthy[a], K.P.Surendran[ab]*

[a]*Materials Science and Technology Division,*
CSIR-National Institute for Interdisciplinary Science and Technology,
Trivandrum, Kerala, India
[b]*Academy of Scientific and Innovative Research (AcSIR), India*
kpsurendran@niist.res.in

Electromagnetic interference (EMI) is the disturbance that adversely affects an electrical circuit due to either electromagnetic induction or electromagnetic radiation emitted from an external source. The factors like miniaturization and abundance of electronic equipments in industrial and domestic environments, have given rise to a great number of sources and receptors, which increases the potential for interference. Hence the need for protection of sophisticated instruments and components in military, nuclear weapons, aerospace, data cables etc from this interference is a major industrial challenge [1]. The effects of electromagnetic interference can be reduced or diminished by suitably designed EMI shielding materials. In principle, EMI shielding materials either reflect and/or absorb the electromagnetic radiation, which thereby acts as a shield against the penetration of the radiation through the shield. In defense sector, the EMI shielding materials are in huge demand since they can avoid radars and thereby protect these high security installations from the enemy's reach [2].

Metals are the foremost candidates for EMI shielding due to their high electrical conductivity and reflectivity. Metal coated or metal reinforced polymers are useful candidates for shielding applications. Shielding by conductive painting, insertion of conducting meshes, injection molding with highly conductive particles/fibers, electro-less coatings and electro plating technique have been widely proposed for converting a non conductive substrate into an EMI shielding one[3][4]. Here in this work, we have adopted electro plating as a strategy to make a non conductive fabric substrate to a conducting one. Since the electromagnetic wave consists of electric and magnetic fields, it is better to select a material which can interact both electrically and magnetically with the incoming electromagnetic waves. The

metal chosen for electro deposition is nickel, which is conducting as well as ferromagnetic. Nickel chloride and boric acid are taken in the bath solution to get a proper nickel deposition. Different fabrics such as linen, polyester, nylon and silk, are used as the substrate to deposit the metals.

The phase purity of the deposit was analyzed by XRD. The morphological characteristics and thickness of coating were analyzed using scanning electron microscope (SEM) and optical microscope. The microwave dielectric properties of the different bare fabrics selected were analyzed using split post dielectric resonator (SPDR). The magnetic properties of the deposited metals were analyzed using vibrating sample magnetometer (VSM). The shielding studies were done in a vector network analyzer (VNA) using transmission wave guide method in the frequency range of 8.2-12.4 GHz (X band). Out of the four different fabrics sheet analyzed, the nickel deposited linen fabric shows better value with 99% shielding effectiveness in the X band range and the rest of the fabric with nickel coating showed 90% or more efficiency. The contributions from both reflection and absorption are believed to be the reason behind the enhanced EMI shielding in metallized fabrics.

References

[1]ParveenSaini, VeenaChoudhary, N. Vijayan, and R. K. Kotnala. *J. Phys.Chem.C*116(2012) 13403−13412.

[2]Chung DDL.*J Mater Eng Perform*, 9(3) (2000) 350-354.

[3]Ho-Chul Lee, Jin-Young Kim, Chang-Ho Noh, Ki Yong Song, Sung-Heon Cho.*Appl. Surf. Sci.* 252 (2006) 2665–2672.

[4]John T. Hoback and John J. Reilly.*J. Elastomers Plast.*20 (1988) 54-69.

MACRO 408

Renewable Resource Based Ionic Liquid Crystals for Safe and Sustainable Energy Storage

Renjith Sasi, and Sudha J. Devaki*
Chemical Sciences and Technology Division, CSIR-National Institute for Interdisciplinary Science and Technology (CSIR-NIIST), Thiruvananthapuram, 695019, India
** sudhajd2001@yahoo.co.in*

Ionic liquid crystals are unique molecules having combined properties of liquid crystals (LCs), and ionic liquids (ILs). They find applications in areas such as energy storage devices, sensors, regioselective synthesis, anisotropic conductors, separation membranes, power sources and so forth [1-2]. ILCs form mesophases through various non-covalent interactions and may exhibit properties like macroscopic orientation, ionic conductivity and the transportation of charges in liquid crystalline phases. Unlike conventional liquid crystals, ILCs will self-assemble by means of specific non-covalent interactions results in the formation of nano channels within the mesophases for effective charge transport. As the mesophase formation is highly responsive to the external stimuli, it could be possible to align the charge carriers and to modulate the charge transport pathways by applying stimuli such as temperature, electric or magnetic field, metallic ions, mechanical rubbing, solvents and light.

Even though ILCs are having excellent functional properties, their expensive nature makes them less available for commercial applications. Low cost and environmentally benign alternates are the ultimate necessity of the current century ailing from fierce environmental back lashes like global warming, green-house effect, etc. due to the senseless exploitation of fossil fuels. In the present work, we describe the preparation, properties and applications of novel ionic liquid crystals derived from 3-pentadecylphenol, a bio-based low cost material obtained from cashew nut shell liquid (CNSL). Amphotropic liquid crystalline phase formation were characterised using a combination of techniques such as DSC, PLM, XRD, SEM, and rheology which revealed the formation of one-,two- and three dimensionally ordered mesophases in different length scales. Based on these results, a plausible mechanism for the formation of specific modes of packing in various mesophases was proposed [3]. Further the observation of anisotropic ionic conductivity, electrochemical stability and lower charge transport resistance suggests its application as a safe and sustainable electrolyte for energy storage systems. Anisotropic mesophase with excellent capacitive behaviour explored as a high performing electrolyte for symmetric supercapacitors which yielded a very good specific capacitance of 131.43 F/g at 0.37 A/g with an excellent capacitance retention (80%) over 2000 cycles [4].

.

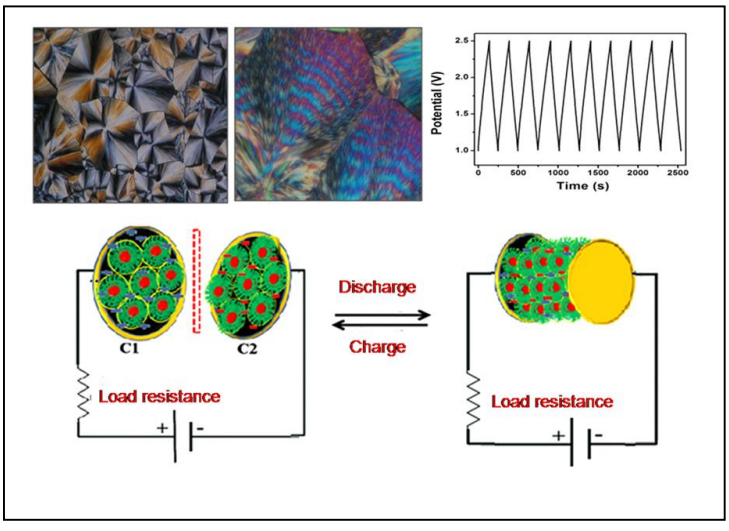


Figure 1. PLM images of the Columnar and Smectic mesophases, charge-discharge cycles and schematic diagram of symmetric supercapacitor on operation

References

[48]Brennecke, J. F.; Maginn, A. J. *AIChE J.*, 47 (2001), 2384.
[49]Lee, C. K.; Huang, H. W.; Lin, I. J. B. *Chem. Commun*., 2000, 1911.
[50]Sasi, Renjith; Rao, T. P.; Sudha, J. D. *ACS Apply. Mater. Interfaces*, 6 (2014), 4126.
[51]Sasi, Renjith; Sarojam, Sujatha; Sudha, J. D. *ACS Sustainable Chem. Eng.*, 4 (2016), 3535.

MACRO 413

Liquid Crystalline Template Driven Conductive PEDOT Transducer for Nicotine Sensor

Neethu K. S. and Sudha J. Devaki
Chemical Sciences and Technology Division, CSIR-National Institute for Interdisciplinary Science and Technology, Thiruvananthapuram 695 019, India
* sudhajd2001@yahoo.co.in

Nanostructured conducting polymer exhibit unique opto-electronic properties and they find applications in the field of sensors, electro chromic devices, organic light emitting diodes, solar cells, drug delivery systems, actuators and so forth.[1,2] Among the various conducting polymers, PEDOT has been identified as a reliable functional material for a wide range of applications because of its tunable conductivity, high charge carrier mobility, optical transparency, flexibility, ease of preparation and bioconjugation. Liquid crystalline (LC) template driven synthetic process is receiving importance since LC phase of specific texture with well-organized channels can be exploited to tune the size and shape of the formed conducting polymers.[3] Nicotine is a neuro active pyridine derivative alkaloid present in tobacco leaves. Despite of its toxic effects, nicotine has many therapeutic applications in variety of disorders like Parkinson's disease, anxiety, obesity, depression, Tourette's syndrome, and attention deficit disorder.[4,5] Thus, the detection of nicotine is important in several areas such as chemistry, toxicology, pharmacology, clinical and environmental fields.

Glassy carbon electrode was modified with well-ordered PEDOT using bio-based liquid crystalline template polymerization approach. Enhancement in the performance of transducer was monitored by performing Fourier transform electrochemical impedance spectroscopy. Electrochemical oxidation of nicotine was investigated by cyclic voltammetry and was observed that for modified electrode, the oxidation of nicotine occurs at lower potential (0.83V) with high current (54.63 µA) compared to bare electrode. Under optimized conditions, the linear range (R^2 =0.9971) and detection limit for nicotine determined were observed to be (5µM to 10mM and 2.5nM).This developed ecofriendly sensor is very simple, low cost with high sensitivity and selectivity which may find application in clinical as well as pharmaceutical fields.

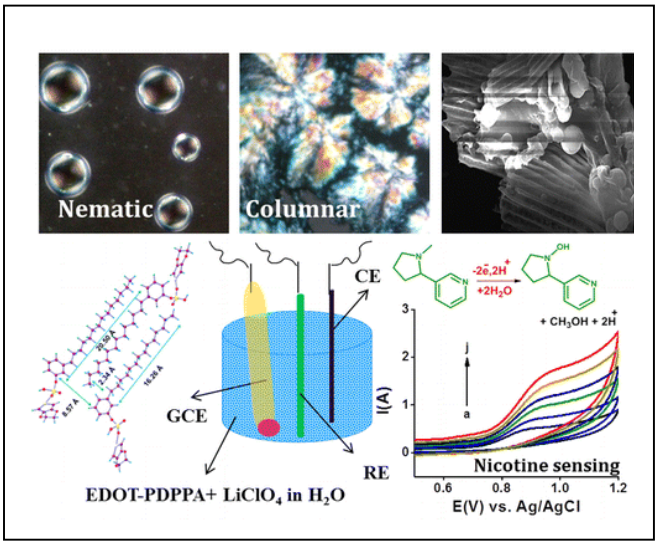


Figure 1. Scheme showing the PEDOT modified Glassy carbon electrode used as a transducer for Nicotine detection.

References

[52]Ramakrishnan, R.; Devaki, S. J.; Aashish, A.; Thomas, S.; Varma, M. R.; KPP, N. *J. Phys. Chem. C*, 120 (2016), 4199.

[53]Belaidi, F. S.; Civélas, A.; Castagnola, V.; Tsopela, A.; Mazenq, L.; Gros, P.; Launay, J.; Temple-Boyer, P. *Sensors Actuators B Chem.*, 214 (2015), 1.

[54]Devaki, S. J.; Sadanandhan, N. K.; Sasi, R.; Adler, H.-J. P.; Pich, A. *J. Mater. Chem. C,2(* 2014**)**, 6991.

[55]Yildiz, D. *Toxicon*, 43(2004), 619.

[56]Alberg, A. J. *Drugs of Today* 44(2008), 895.

MACRO 439

Polyaniline salt catalyzed synthesis of hyper branched polyester and its use as dopant in polyaniline salt for coating, fluorescence and supercapacitor electrode

Sangam Naidu Karri,[a] Uma Shankar Male,[a] Palaniappan Srinivasan*, [a, b]

[a] Polymers & Functional Materials Division, CSIR-Indian Institute of Chemical Technology, Tarnaka, Hyderabad-500007, INDIA. [b] CSIR–Network Institutes for Solar Energy(NWP0056), New Delhi, INDIA.
*** palani74@rediffmail.com**

Synthesis of novel polyaniline salts is an important work for their use in industrial applications. The objective of this work is to use alcohol in the polymerization of aniline instead of hazardous protic acids, [1] which are mostly being used. For this purpose, hyper branched polyesters (HBPEs) containing many alcohol groups were selected. In the HBPEs, alcohol groups could be increased via preparation of first(G1), second(G2) and third(G3) generation of HBPE [2]. HBPEs were synthesized from the reaction of bis-MPA as ABx monomer and TEA as a nitrogen containing core. This reaction was promoted using polyaniline salt containing high strength protic acid, trifluoromethanesulfonic acid, as catalyst for the first time [3]. Interestingly, used these HBPEs in the aqueous polymerization of

aniline to polyaniline salt containing HBPEs. Properties of these novel polyaniline salts in terms of yield, density, conductivity, solubility, crystalline nature, morphology and application as electrode in supercapacitor were determined. These polyaniline salts containing dual dopants of H_2SO_4 and HBPE are stabile up to 210 ^oC and showed highly ordered semicrystalline nature with nano rods morphology (35 to 60 nm). Yield, density and conductivity of the PANI-HBPEs salts are independent of the generation of HBPEs. Polyaniline salt containing third generation hyper branched polyester sample showed higher specific capacitance (450 F g^{-1}). These polyaniline salts are insoluble in most of the common organic solvents. Polyaniline salts containing HBPEs in organic solvent were synthesized via emulsion polymerization pathway (E-PANI-HBPEs). These polyaniline salts contains three dopants, HBPE, DHS and H_2SO_4, were isolated in chloroform solvent, which showed particle size around 85 nm, with fluorescence property, and hydrophilicity. Polyaniline-HBPEs prepared via emulsion polymerization showed higher conductivity than that of the samples prepared via aqueous polymerization pathways.

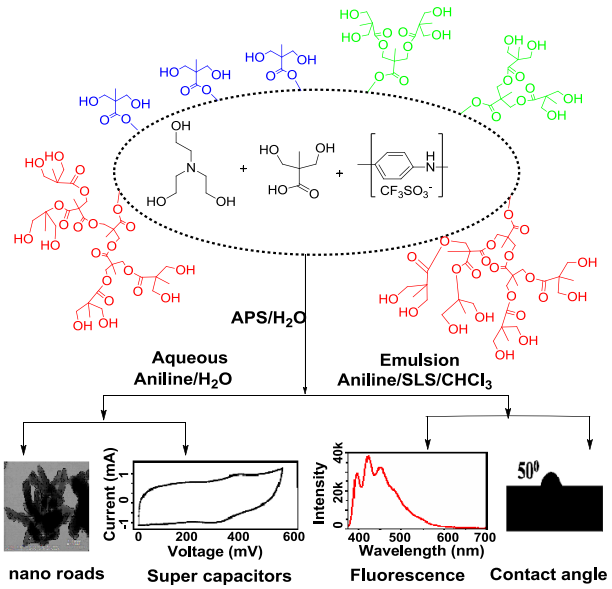


Figure 1. Schematic Representation of HBPEs Doped Polyaniline Salt Synthesis

References

[1] R, Gottam; P, Srinivasan. *New Journal of Chemistry*, 39 (2015) 8545.
[2] A, Goswami; A K, Singh. *Reactive and Functional Polymers*, 61 (2004) 255.
[3] P, Srinivasan; R, Boddula. *Advanced Synthesis & Catalysis*, 352 (2010) 250.

MACRO 442

Polybenzimidazole – Polydimethylsiloxane composite films: morphology and mechanical properties

Satheesh Kumar B*[1], G Unnikrishnan[2], Santhosh Kumar K.S*[1]

[1]*Polymers and Special Chemicals Division, Vikram Sarabhai Space Centre, Thiruvananthapuram-22*
[2]*National Institute of Technology, Calicut*
**skbisro@gmail.com, santhoshkshankar@yahoo.com*

Polybenzimidazoles (PBI) are known for their high thermal stability and are stable up to 500°C. In the present work, pyridine based PBI powders were synthesized (M_w 24000 g/mol) and blended with polydimethylsiloxane (PDMS) to form PBI-PDMS films. The pristine PDMS film marked a $T_{10\%}$ (temperature at which 10% weight loss) value of 365°C whereas $T_{10\%}$ got increased to 470°C by the introduction of 10 wt% PBI powder into PDMS

(10 PBI). The tensile modulus also enhanced from 0.26 to 0.31 MPa. However, elongation decreased to one fourth of pristine PDMS film. This is due to the rigid structure of PBI which was integrated into the PDMS matrix (evidence from FESEM images). On further increase of PBI content (20% and 30%), elongation decreased further as expected. Morphological examination of the blends revealed micro-phase separation of PBI (evidence from SEM and AFM images).

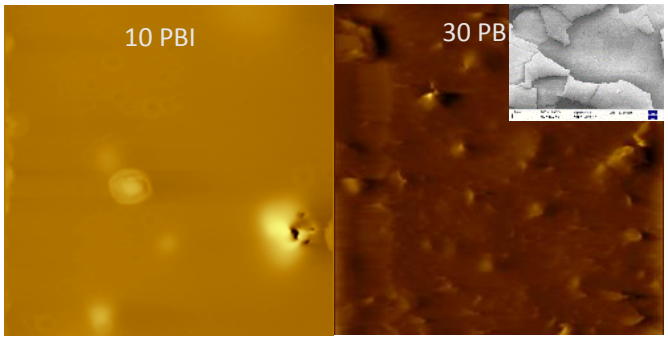


Fig: 1 AFM images of 10 and 30 wt% of PBI containing PDMS films (inset: micro phase separation in SEM image of 30 PBI)

References

[1] Jin-Woo Lee1, Sher Bahadar Khan2,*, Kalsoom Akhtar3, Kwang-In Kim1, Tae-WonYoo1, Kwang- Won Seo1, Haksoo Han1,* Abdullah M. Asiri2, *Int. J. Electrochem. Sci.*, *2012*, *7*, 6276 – 6288

[2] Kathryn A .Berchtold a,n, Rajinder P.Singh a, Jennifer S. Young b, Kevin W .Dudeck, *J. Membr. Sci*., 2012, 415-416, 265-270

[3] P. Staiti*, M. Minutoli, *J. Power Sources*, 2001, 94, 9-13

MACRO 447

Air stable n-type diketopyrrolopyrrole based oligomers for high performance field-effect transistors

Tushita Mukhopadhyay, S. Patil

Indian Institute of Science, Bangalore

e-mail: twinkling.tush@gmail.com

Abstract:

The design and synthesis of *n*-type organic semiconductors pose challenges such as they are prone to oxidation under to ambient conditions. Herein, we report design and synthesis of diketopyrrolopyrrole (**DPP**) based oligomers for ambipolar organic thin film transistors (**OFETs**) with excellent air and bias stability at ambient conditions. Structural and electronic properties have been probed by UV-visible spectroscopy, atomic force microscopy (**AFM**), and thin film X-ray diffraction (**XRD**) and grazing incidence small angle X-ray scattering (**GISAXS**) measurements. Changes in morphology and thin-film microstructural order induced by different processing conditions were investigated by AFM and GISAXS measurements. These measurements also highlight the significance of chalcogen atom from sulphur to selenium on the photophysical, optical, electronic and solid-state properties of DPP-DPP oligomers. Consistent electron mobilities of ~0.2 $cm^2V^{-1}s^{-1}$ and high on/off ratios $>10^4$ were obtained by solvent and thermal annealing, with the retention of field-effect behaviour up to ~ 4 week. This work paves the way towards the development of *n*-type DPP-DPP based oligomers exhibiting retention of field effect behaviour with superior stability at ambient conditions.

MACRO 451

Indolo[3,2-b]carbazole-based Poly(arylene ethynylene)s: Modulation of Their Optoelectronic Properties by Changing Monomers

M. Vintu and G. Unnikrishnan

Dept. of Chemistry, National Institute of Technology, NIT campus, Calicut- 673601

Email: vintu09@gmail.com, unnig@nitc.ac.in

Abstract

Charge transport in many organic devices depends strongly on the molecular order and morphology of their organic semiconductors. In the design of new organic semiconductors, the selection of an appropriate core plays a key role in their molecular packing and charge transport characteristics. In the present work, a novel family of indolo[3,2-b]carbazole (ICZ)-based polymers was designed and synthesized using Sonogashira cross-coupling reaction between dibromoindolo[3,2-b]carbazoles and 2,7-diethynylfluorene or 9,10-diethynylanthracene. The new polymers have an arylene ethynylene structure with ICZ moiety interconnected in the main chain by 2, 8 positions. The polymers were obtained as partially soluble materials, in chlorinated, aromatic and aprotic polar solvents. The structures of the polymers were confirmed by methods such as Fourier transform infrared, proton nuclear magnetic resonance, ultraviolet–visible and photoluminescence spectroscopies and thermogravimetry. Electrochemical properties were investigated by cyclic voltammetry, using a platinum disc working electrode. The optical and electronic properties have also been investigated.

Keywords: *Indolo[3,2-b]carbazoles, Sonogashira cross-coupling, poly(arylene ethynylene)s, tuning optical properties, cyclic voltammetry*

Introduction

Polycyclic π-conjugated systems based on fused aromatic and heteroaromatic rings have gained considerable attention, by now, due to their wide applications in the development of photo- and electroactive organic materials for advanced electronic and optoelectronic devices[1-3]. 1,2 5,11-dihydroindolo[3,2-b]carbazoles (indolo[3,2-b]carbazoles, (ICZ) represent an important class of ladder-type N-heteroacenes, which have a large planar and rigid backbone. A great variety of ICZ derivatives have been stated previously as efficient hole-transporting, electroluminescent or sensitizing materials for organic light-emission diodes (OLEDs), organic field effect transistors (OFETs) and organic photovoltaics (OPVs), due to their excellent electrical and optical properties, and high resistance to photo, thermal and electrochemical degradation [4-5]. In this work, two polymers were prepared by Sonogashira cross-coupling reaction,using the ICZ monomer either with 9,10-diethynylanthracene or with 2,7-

diethynylfluorene. It has been found that the connection position of ICZs in the backbone allows the easy tuning of optical and electronic properties.

Experimental

Materials

9,10-Diethynyanthracene, copper(I) iodide (CuI), bis(triphenylphosphine) palladium (II) dichloride ($PdCl_2(PPh_3)_2$), 2,7-Diethynylfluorene, 5-bromoindole, benzaldehyde, 2-ethylhexyl bromide, tetraethyl ammonium bromide ($(C_2H_5)_4NBr$) and triphenylphosphine (PPh_3) were purchased from Sigma Aldrich and used without further purification. N,N-Dimethyformamide (DMF), tetrahydrofuran (THF), acetonitrile, dimethyl sulphoxide (DMSO), toluene and triethylamine (TEA), all from Sigma Aldrich, were dried by usual methods and distilled before use.

Instrumentation techniques

Proton (^1H; 400MHz) nuclear magnetic resonance (NMR) spectra were measured on a Bruker Avance DRX 400 MHz NMR spectrometer , using DMSO as solvent and tetramethylsilane as an internal standard. Fourier transform infrared (FTIR) spectra were recorded using Jasco FTIR spectrophotometer. Ultraviolet–visible (UV-Vis) absorption and fluorescence spectra of polymers were recorded with a Jasco spectrophotometer and a Perkin Elmer apparatus respectively, using dilute monomer and polymer solutions and very thin films of polymers deposited on quartz plates by a drop-cast technique. Thermogravimetric analyses (TGAs) were done using TGA/DTA STA 449 F1 Jupiter (Netzsch, Germany) under nitrogen atmosphere at a heating rate of 10 ^0C min. Electrochemical studies were carried out with a potentiostat–galvanostat (Bioanalytical System (BASi) 100B/W; West.

Results and discussion

Synthesis of monomers

5-bromoindole was used in condensation with equimolar quantities of benzaldehyde in presence of HCl as catalyst to obtain the corresponding dibromine-substituted indolo [3,2-b]carbazole (M1). The second monomer, diethynylanthracene (M2) was synthesized from 9,10-dibromoanthracene with trimethyl silylacetylene. The same method was employed for the third monomer 2, 7-diethynylfluorene (M3). The synthesized monomers were characterized by FTIR and NMR. The melting points of monomers have been found to be as high as 250 ^0C.

Polymer synthesis

Two novel polymers viz; anthracene containing (ICZP1),and fluorene containing (ICZP2), with ICZ cores were synthesized by Sonogashira crosscoupling reaction is shown in Scheme 1. The new polymers have been found to be partly soluble in THF and aromatic and chlorinated organic solvents such as $CHCl_3$ and methylene chloride. Although the long and branched alkyl chains at N-5 and N-11 positions can effectively enhance the solubility of the product, in the present case, the alkyl substituent is not long enough to assure the solubility of the rigid polymers at higher molecular weights. The structures of polymers were characterized by ^1H and FTIR spectra. A tentative assignment of NMR peaks of ICZP1 and ICZP2 are presented in Figures 1 and 2 respectively. From ^1H NMR spectra it is seen that all the peaks are broader. For both the polymers, the aromatic protons are observed between 8.20

and 6.00 ppm, the signal of the methylene adjacent to nitrogen atom appeared around 3.82 ppm. The characteristic resonance peaks of 2-ethylhexyl chains appear in the range 0.55–2.30 ppm.

Thermal properties

The thermal stability of ICZ-cored polymers were examined by thermogravimetric analysis (TGA) at a scanning rate of 10 ^{0}C min^{-1} under nitrogen atmosphere. The results are shown in Fig 3. Both of them exhibit high thermal resistance, which is important for many optoelectronic applications. Their decomposition temperatures (Td) exceed 400 ^{0}C.

Photophysical properties

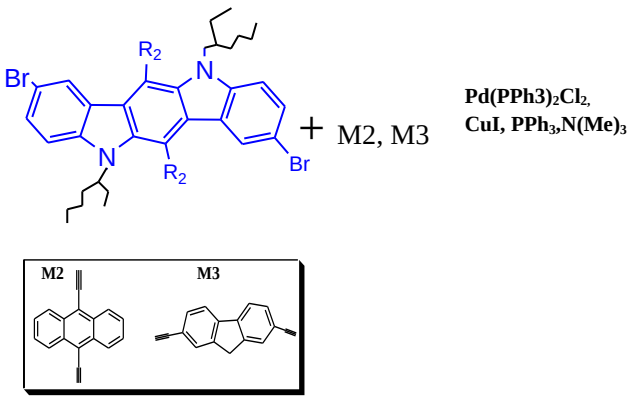
The UV-visible absorption and photoluminescence spectra of ICZ-cored compounds were recorded at ambient temperature in CH_3Cl solution. The UV-visible absorption spectra of all the polymers recorded in solution as well as thin films deposited on quartz substrate are shown in Fig 4. The absorption and emission data are summarized in Table 1. In dilute chloroform solution (10^{-5} mol L−1) both the polymers exhibit absorption maxima ranging from 240 to 470 nm; red-shifted as compared to ICZ. The absorptions located at shorter wavelengths (244–295 nm) can be assigned to $\pi-\pi^*$ transitions from the aromatic rings while the bands at longer wavelengths (325–430 nm) can be assigned to $\pi-\pi^*$ electronic transitions of the entire conjugated backbone. The absorption spectra of the polymers are bathochromically shifted in the order ICZP2>ICZP1 and are decided by the effective conjugation length.

In solid film, the absorption maxima are little red shifted and appear broader compared to their solution counterpart with absorption tails until 500 nm (Fig.5). This slight bathocromic shift in absorption may be attributed to the weak intermolecular interactions of the polymer backbone in the solid state.

The fluorescence spectra of polymers were also recorded in solution as well as in solid film and are presented in Fig 6. Both polymers in solution exhibit broad emission spectra with asymmetrical shape and maxima between 460 and 500 nm.

Electrochemical Analysis

Unlike most p-channel semiconductor compounds, indolo[3,2-b]carbazole based compounds have a relatively wide band gaps and low-lying HOMO levels. This could suggest an easier hole injection into films from ITO electrodes in optoelectronic device applications. The cyclic voltammograms of ICZP1 and ICZP2 are given in Fig.7 & 8 respectively.



Scheme 1: Synthesis of poly(arylene ethynylene)s by Sonogashira couplin

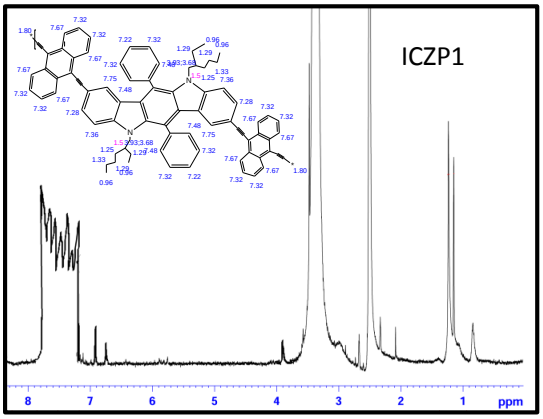


Fig 1: ^{1}H NMR of ICZP1

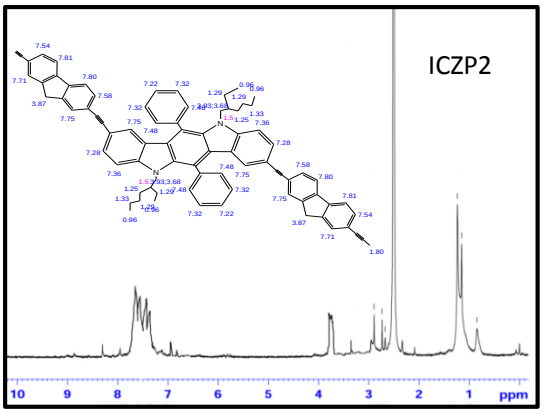


Fig 2: ^{1}H NMR of ICZP2

The ـy levels were estimated by CV in combination with the optical absorption gap (Eg) values and are shown in Table 2. The HOMO energy levels of the polymers were estimated from E_{OX}^{onset}. The LUMO energy levels of the ICZP1 and ICZP2 were estimated as -3.40 eV,-3.76 respectively. The lower HOMO energy level of ICZP2 than that of ICZP1 results from a better electron delocalization in the former.

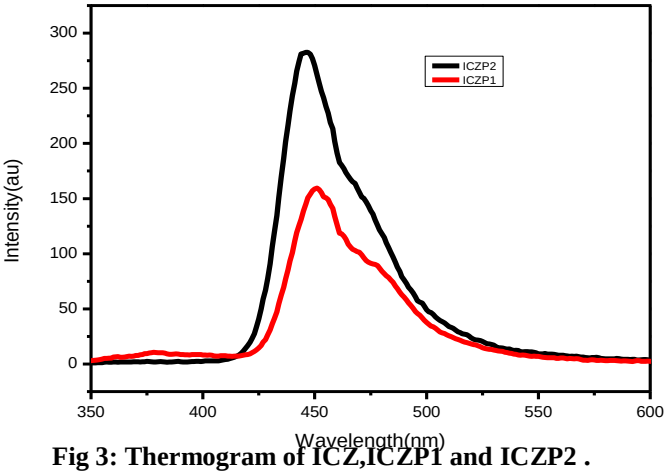
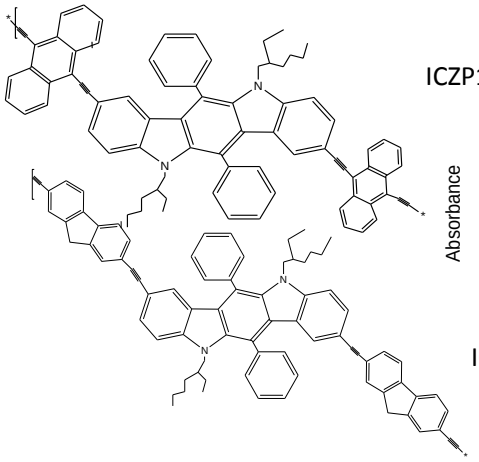


Fig 3: Thermogram of ICZ,ICZP1 and ICZP2 .



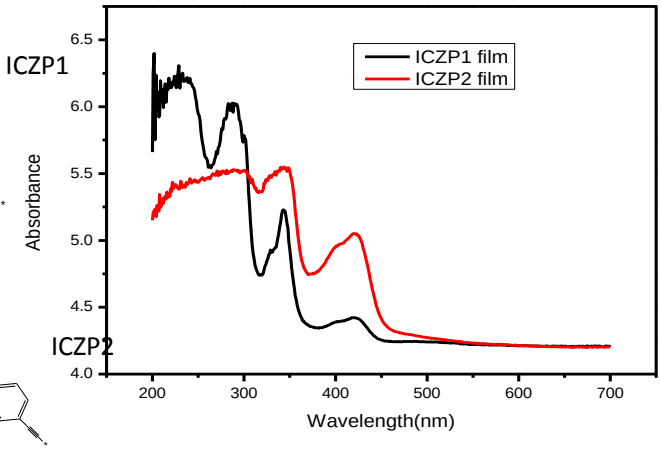


Fig 5: UV-VIS spectra of ICZP1and ICZP2 films

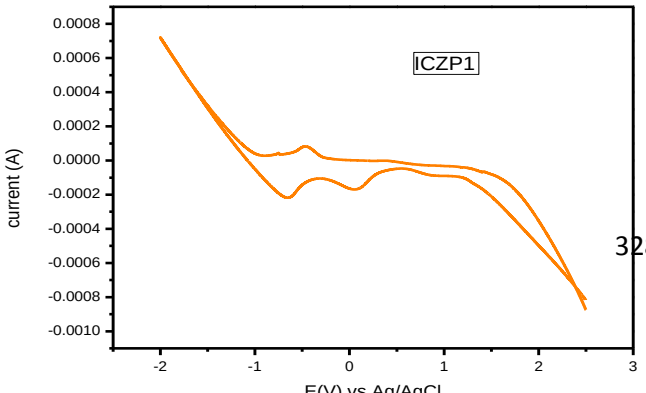


Fig 7: CV analysis of ICZP1

	Solution		Films
	λ^{abs}_{max} (nm)	λ^{pl}_{max} (nm)	λ^{abs}_{max} (nm)
ICZ	207,276,339,413	433	210,280,340,420
ICZP1	242,293,340,423,541	441	232,290,342,423
ICZP2	246,281,344,421,537	443	297,345,423,

Fig 6: Fluorescence spectra of ICZP1 and ICZP2

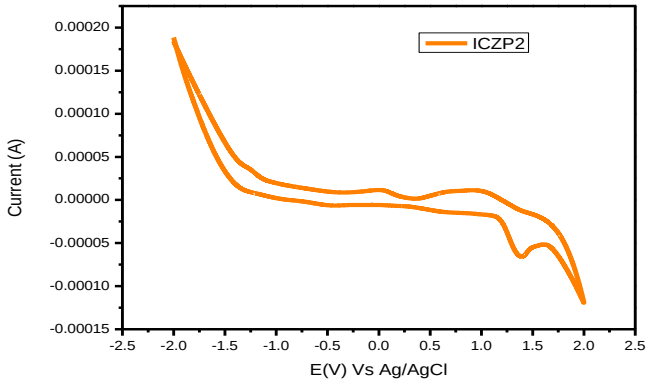


Fig 8: CV analysis of ICZP2

Table 1. Photophysical properties of polymers

Conclusion

Two novel ICZ-based polymers were synthesized using Sonogashira cross-coupling reaction between bisbromine ICZ and 9,10-diethynylanthracene, or 2,7-diethynylfluorene. The characterization has been done by spectroscopic methods, themogravimetry and electrochemical analysis .The photophysical properties were investigated by UV-VIS spectroscopy and fluorescence emission spectroscopy. The band gap, HOMO and LUMO valuesof the new polymer have been found to be perfectly matching with the requirements for semiconducting devices.

Acknowledgement

This work was supported by strategic grants from MHRD of India.

Table 2. Electrochemical properties of the polymers.

Polymer	Eg (eV)	Eox V	HOMO (eV)	LUMO (eV)
ICZP1	**2.22**	**1.22**	**-5.62**	**-3.40**
ICZP2	**2.76**	**1.15**	**-5.55**	**-3.76**

References

1. O.I. Negru, A.M. Solonaru, M. Grigoras, *Polym Int* (2016), DOI 10.1002/pi.5200
2. P.L.T. Boudreault, S .Beaupre and M .Leclerc, *Polym Chem* **1**: 127–136 (2010).
3. S. Wakim, B.R. Aich, Y. Tao and M. Leclerc, *Polym Rev* **48**: 432–462 (2008).
4. H.P. Zhao, F.Z Wang, C.X Yuan, X.T. Tao, J.L Sun, D.C. Zou., *Org Electron* **10**: 925–931 (2009).

5. L. H. Chan, L.C. Lin, C. H. Yao, Y.R. Liu, Z. J. Jiang and T.Y. Cho, *Thin Solid Films* **544**: 386–391 (2013).
6. H. Shi, J .Dai, X .Wu, W .Shi, J .Yuan, L. Fanf, *Org Electron* **14**: 868–874 (2013).
7. G .Zhao, H .Dong, H. Zhao, L. Jiang, X. Zhang, J. Tan, *J Mater Chem* **22**: 4409–4417 (2012).

MACRO 467

Synthesis and Characterization of Carboxylic Acid Funtionalised Sulfonated Polytriazoles for Proton Exchange Membrane

Saha, Sayantani and Banerjee Susanta* (Last/Surname, First name or initials)

Materials Science Centre, Indian Institute of Technology, Kharagpur 721302 India

Email: susanta@matsc.iitkgp.ernet.in

A series of new semifluorinated sulfonated polytriazoles containing carboxylic acid functionality with different degree of sulfonation was synthesized employing the click reaction between a newly synthesized diazide monomer; 4,4-bis[3-trifluoromethyl-4(4-azidophenoxy)phenyl]benzene (TAZ), a commercially available monomer 4,4'-diazido-2,2'-stilbenedisulfonic acid disodium salt (DADSDB) and a bis-alkyne monomer 3,5-bis(prop-2-ynyloxy)benzoic acid (DPBA). The degree of sulfonation was varied by controlling the molar ratio of the sulfonated azide monomer. The structures of the sulfonated polytriazoles were analyzed by FTIR and NMR spectroscopic techniques. All the polymers exhibited good solubility and film forming ability along with good thermal and chemical stabilities and high mechanical properties. Excellent phase separated morphology was observed under transmission electron microscopy (TEM) indicating the formation of hydrophilic and hydrophobic domains throughout the membrane. The ionic cluster size ranged from 10–65 nm. The membranes exhibited moderately high water uptake and swelling due to the presence of hydrophilic –COOH groups. The proton conductivity values of the sulfonated membranes were found in the range of 38–152 mS/cm at 80 °C in completely hydrated condition.

References

[1] Huang, Y.J.; Ye, Y.S.; Yen, Y.C.; Tsai, L.D.; Hwang, B.J.; Chang, F.C. *Int. J. Hydrogen Energy*, 36 (2011) 15333.
[2] Singh, A.; Mukherjee, R.; Banerjee, S.; Komber, H.; Voit, B.; *J. Membr. Sci.*, 469 (2014) 225.
[3] Singh, A.; Banerjee, S.; Komber, H.; Voit, B.; *RSC Adv.*, 6 (2016) 13478.

MACRO 469

Novel Gel Polymer Electrolyte films: Preparation and characterization

Nisha Balachandran*, Parvathy C, Sadhana R, Rajeev R

Analytical and Spectroscopy Division, PCM Entity,

Vikram Sarabhai Space Centre, Thiruvananthapuram-695022

* *e-mail id: nishapzm@gmail.com*

Abstract

Application of gel polymer electrolytes in lithium-ion polymer batteries can address many shortcomings associated with liquid electrolyte lithium-ion batteries. A novel gel polymer membrane comprising poly(vinylidene difluoride) (PVdF) polymer and ionic liquids, viz., tetrabutyl ammonium bromide and methyl triphenyl phosphonium bromide were prepared by phase inversion and solvent drying method. The films were characterised using various techniques viz., Fourier Transform Infrared (FTIR) spectroscopy, Impedance Analysis, Contact Angle measurement and Field Emission Scanning Electron Microscopy (FE-SEM). The porosity of the films was also evaluated using Gas pycnometry. The properties such as ionic conductivity, porosity, and wettability of films prepared by two different methods and compositions were compared with that of pristine PVDF films. The correlation between the porosity and ionic conductivity of the films was also investigated.

Keywords: *PVDF, ionic liquid, ionic conductivity*

1. Introduction

Gel polymer electrolyte (GPE) based films are used for diverse applications, including secondary batteries, electrochromic displays, sensors, and various ionic devices [1]. PVDF is a prominent polymer known to be a promising matrix for an electrolyte material. It has a high dielectric constant of $\varepsilon = 8.4$ which can assist in greater dissociation of salt. It also comprises of both amorphous and crystalline phases. The amorphous phase of this polymer assists for ionic conduction whereas the crystalline phase acts as a mechanical support. PVDF films are expected to have a high anodic stability due to the presence of strong electron-withdrawing functional group (-C-F-) [2]. Traditional polymer electrolytes can easily be prepared from solutions consisting of a polar organic solvent and electrolyte salts in a polymer matrix. However, there are several critical problems, such as volatility and flammability, when organic solvents are used in a severe temperature range. Hence the use of ionic liquids as a substitute for conventional organic solvents has recently been of great interest in research on electrochemical devices. Ionic liquids exhibit interesting physiochemical properties with low vapour pressure, high ionic conductivity and electrochemical stability [3]. Ionic liquids immobilised or incorporated

within PVDF matrix was chosen for the present study.

Generally, two methods of preparing polymer electrolytes have been employed: one is dissolution of the polymer host and ionic liquid in a non-volatile solvent which is evaporated to form films; the second method, called phase inversion or activation process, involves soaking the polymer film in a non-solvent. The ionic conductivity of this porous membrane mainly depends on the conductivity of the electrolyte entrapped in the pores of the membrane. Therefore, the membrane's porosity, conductivity of the electrolyte, thickness of the membrane, and the extent to which the electrolyte wets the pores of the membrane are the properties to be considered for the membrane preparation.

Ionic liquids used for the present study includes tetrabutyl ammonium bromide and methyl triphenyl phosphonium bromide. Preparation of PVDF-gel electrolytes films was done by two different methods - phase inversion and solution casting method. The film casting solution was prepared by dissolving known weight of ionic liquid and PVDF in N,N-Dimethyl acetamide (DMAC) solvent. The prepared films were characterised using various techniques viz., Fourier Transform Infrared (FTIR) spectroscopy, Impedance Analyser, Gas pycnometry, Contact Angle measurement and Field- Emission Scanning Electron Microscopy (FE-SEM). The properties of the Gel polymer electrolyte films prepared via, phase inversion and solution casting were compared with that of pristine PVDF films. The crystalline phases of the films were obtained from FTIR analysis. The porosity of the films was evaluated using Gas pycnometry and wettability properties were studied using contact angle measurement. The membranes were gelled and subjected to impedance analysis and ionic conductivity was evaluated.

2. Experimental

2.1 Materials

PVDF and ionic liquids viz., tetrabutyl ammonium bromide and methyl triphenyl phosphonium bromide from Alfa Aesar, and HPLC grade N,N'-Dimethyl acetamide (DMAc) from Spectrochem were used for the preparation of film casting solution. Millipore water with 18 Mohm conductivity was used in coagulation bath as non- solvent in phase inversion method.

2.2 Preparation of nanocomposite

PVDF films were prepared by phase inversion (PI) and solvent drying (SD) methods. PVDF powder was dried overnight at 100 °C prior to processing. PVDF–ionic liquid doped films were prepared using 0.5 wt % of ionic liquid in DMAc (50 mL) and sonicated for 10 minutes. Casting solutions were prepared by dissolving PVDF (10 wt %) in the ionic liquid dispersion. The solutions were kept at room temperature for 24 hours. Composition of the casting solution is given in Table 1. PVDF film without addition of ionic liquid was also prepared by both methods for comparison.

Table 1. Composition of the casting solutions

Film Name	Composition of the casting solutions				Method
	PVDF Wt. (g)	Ionic liquid		DMAc (mL)	
		Name	Wt. (g)		
P-PI	5	--	--	50	PI
P-PI-IL-1	5	Tetrabutyl-ammonium bromide	0.025	50	PI
P-PI-IL-2	5	Triphenyl-phosphonium bromide	0.025	50	PI
P-SD	5	--	--	50	SD
P-SD-IL-1	5	Tetrabutyl-ammonium bromide	0.025	50	SD
P-SD-IL-2	5	Triphenyl-phosphonium bromide	0.025	50	SD

The solutions were casted on a glass plate using doctor blade (set at 35 rotations). In phase inversion method the casted films were immersed in the distilled water and dried, whereas in solvent drying method the casted films were dried in air oven set at 80°C for 1 hour.

2.3 Instrumentation techniques

2.3.1 FTIR spectroscopy

PVDF films were characterized using Nicolet iS50 FTIR spectrometer equipped with diamond ATR accessory. The spectra were recorded in the wavelength range 4000-550 cm^{-1} with number of scans 16 and resolution 4 cm^{-1}.

2.3.2 Contact angle measurement

Hydrophilic or hydrophobic characteristic nature of samples were estimated by measuring contact angle (θ) value. The wetting liquid was Milli-pore-grade distilled water [liquid surface tension (γl) = 72.8 mJ·m−2] [4]. 5 µl of water was added uniformly over the surface of the membrane. Contact angle was measured after 1 minute of water addition to provide the configuration between the measurements. When a drop of liquid is brought into contact with a flat solid surface, the final shape taken by the drop is expressed by "θ". The increased value of θ denoted higher wettability characteristics of a material.

2.3.3 Gas Pycnometry

Gas pycnometry analysis was carried out using Accu Pyc II 1340 pycnometer. A sample cup having volume of 10 cm^3 was used for the analysis. Helium gas was used for purging. The gas pycnometer measures skeletal density of the sample. Bulk density can be obtained from the sample dimensions. Porosity can be measured by the equation,

$\rho = (1- \rho_b/\rho_s) * 100.$

ρ_b - Bulk density (Mass/Volume)

ρ_s – Skeletal density

2.3.4 FE-SEM analysis

Scanning electron microscopy of the samples were carried out using Carl Zeiss with an acceleration voltage of 10 kV with a magnification of 17 K X.

2.3.5 Impedance Analyser

The ionic conductivities were measured by the impedance method of the Au/ polymer film / Au at room temperature, using Biologic electrochemical work station over the frequency range of 100 mHz to 1 MHz. An ionic conductivity cell was assembled by sandwiching the polymer film between two gold plated nickel electrodes (ϕ-1.5 cm). The electrolyte resistance *R* was measured using AFRA technique. The data were analysed by Z-plot software. The ionic conductivity of the membrane σ was then calculated by the equation $\sigma = l/RA$, where *l* is the thickness of the film, *R* is the resistance of electrolyte and *A* is the area of the film.

3. Results and Discussion

3.1 FTIR spectroscopy

Fig. 1 shows overlaid FTIR spectra of PVDF films prepared by drying and phase inversion method. Stretching vibrations at 840 and 1275 cm^{-1} were attributed to β conformation. 1233 cm^{-1} and a broad peak at 835 cm^{-1} with a small shoulder peak at 812 cm^{-1} was observed for γ phase. The spectrum 1 and 2 in Fig. 1 shows γ and β phases of PVDF whereas β phase is more prominent in spectra 3 and 4.

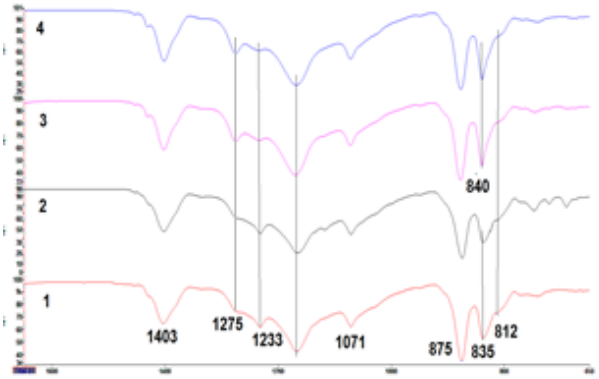


Fig. 1 Overlaid FTIR spectrum (1) P-SD-IL-1, (2) P-SD-IL-2 (3) P-PI-IL-1 (4) P- PI-IL-2

3.2 Contact angle measurement

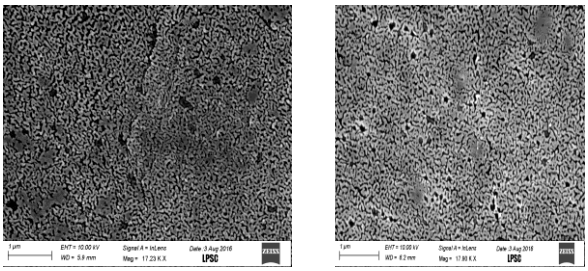
A droplet of water on a PVDF (highly hydrophobic) surface will give a contact angle which is larger than 90°. If the film surface is porous the contact angle will have a value between 0° and 90°. The contact angle was found to be less than 60° for the films prepared by phase inversion method due to high porosity and have a possibility of penetrating the water into the pores of the material. As the films prepared by solvent drying also have porous surface, its contact angle is around 80°.

3.3 Gas Pycnometry

From gas pycnometry, the porosity obtained for the films, P-PI-IL-1 and P-PI-IL-2 prepared by phase inversion method was about 68% and 66% respectively while that of while P-SD-IL-1 and P-SD-IL-2 was around 39 and 33% respectively. So the above analysis shows that porosity is more for phase inversion films.

3.4 FE-SEM analysis

From FE-SEM analysis, films prepared by both the methods have small pores below 1 micrometer but uniform distribution of pores is observed in films prepared by phase inversion method. Figure. 4 shows the FE-SEM images of (a) P-SD and (b) P-PI



(a) (b)

Fig. 2 FE-SEM images of (a) P-SD and (b) P-PI

3.5 Impedance Analyser

Figure 3 and 4 shows the impedance data of PVDF films and Figure 5 shows ionic conductivity comparison of PVDF with different compositions and preparation methods. Since the ionic conductivity largely depends on the pore structure that entraps liquid electrolytes the formation of pores in films is very important for obtaining proper channel of ionic conduction [5]. Resistance of pristine PVDF film by both the methods showed a higher value (>300 ohm). Incorporation of ionic liquid into the PVDF films improves the ionic conductivity of the films. The ionic conductivity is higher for the films prepared by phase inversion method than solvent drying due to the higher porosity in the films, which was confirmed by gas pycnometry.

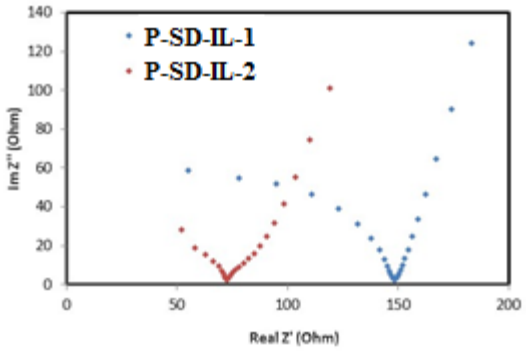


Fig. 3 Nyquist plots of (a) P-SD-IL-1 (b) P- SD IL-2 at 100 mHz to 1 MHz frequency

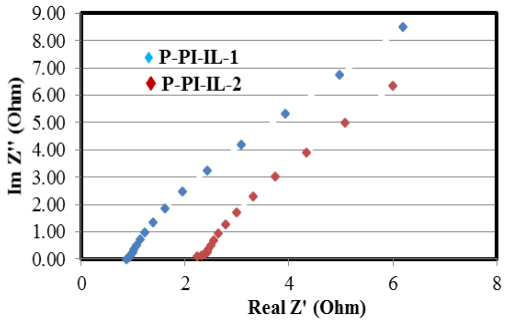


Fig. 4 Nyquist plots of (a) P- PI-IL-1 (b) P- PI-IL-2 at 100 mHz to 1 MHz frequency

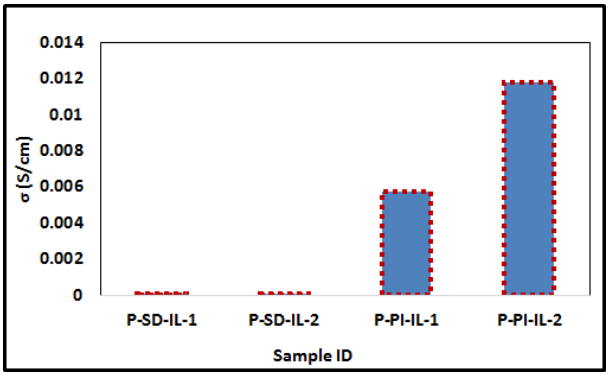


Figure 5. Ionic conductivities with different compositions and different preparation methods

4. Conclusions

Addition of ionic liquids to PVDF matrix improved the ionic conductivity of the films. The films prepared by phase inversion method were found to be highly porous as compared to the films prepared by solvent drying. Due to the high porosity films prepared by phase inversion method, it showed higher ionic conductivity values. The films prepared with different ionic liquids by solvent drying method showed similar ionic conductivity values. Whereas, for the films prepared by phase inversion method there was difference in ionic conductivity with a higher value for P- PI-IL-2.

5. Acknowledgements

I Acknowledge Deputy Director, PCM Entity and Director, VSSC.

6. References

[57] Martin Tosoni, Michael Schulz, Thomas Hanemann, *Int. J. Electrochem. Sci.,* 9 3602 – 3617, 2014

[58] Renard, I., Li, H.,Marsan, B. *Electrochim. Acta, 48,* 831-844, 2003

[59] Ohno, H., Yoshizawa, M.,Ogihara, W.,*Electrochim. Acta, 48,* 2079-2083, 2003

[60] Lugscheider E., Bobzin K., *Surface & Coating Technology*, 165, 51-57, 2003.

[61] S. Rajendran, O. Mahendran and R. Kannan, *Materials Chemistry & Physics*, Vol. 74, 52-57, 2002.

MACRO 472

Multifunctional Porous Organic Polymers

Bandyopadhyay Sujoy, Anil G, Amith , Deshmuk Arundhati, and Patra Abhijit*
Department of Chemistry, IISER, Bhopal, India
* *abhijit@iiserb.ac.in*

Starting from the grand old activated charcoal to zeolites, porous materials have been utilized for environmental and technological benefits for mankind. Of late, porous organic polymers (POPs) have emerged as a new class of functional materials with applications ranging from gas adsorption, gas and liquid separtion, catalysis, light harvesting to chemo/ bio-sensing.[1] However, fabrication of a single porous material capable of exhibiting a range of different applications still remain a challenge. In this regard, we have developed POPs based on a new core of tetraphenyl-5,5-dioctylcyclopentadiene (TPDC).[2] Apart from gas adsorptions, these solution processable POPs were employed for nitroaromatics sensing by amplified fluorescence quenching. In order to understand the quenching process, we have investigated a broad set of analytes ranging from nitrophenols, nitrotoluenes, nitroanilines, quinones to nitrobenzenes. Interestingly, nitroanilines are found to be the most efficient quenchers in contrast to the extensively studied picric acid.[3] Further, the variation of comonomer led to the formation of solution-processable POPs with tunable fluorescence and high surface area.

We also fabricated POPs having 4,4-difluoro-4-bora-3a,4a-diaza-s-indacenes (BODIPY) core with tunable surface areas and porosities. Detailed gas adsorption studies of the polymers revealed a high uptake of CO_2 and H_2. POPs developed in the present study were found to be promising materials for generating singlet oxygen. The BODIPY based POPs turned out to be excellent catalysts for visible-light-driven photooxidation of thioanisole with 96% conversion. These polymers are currently being probed for supercapacitive energy storage.

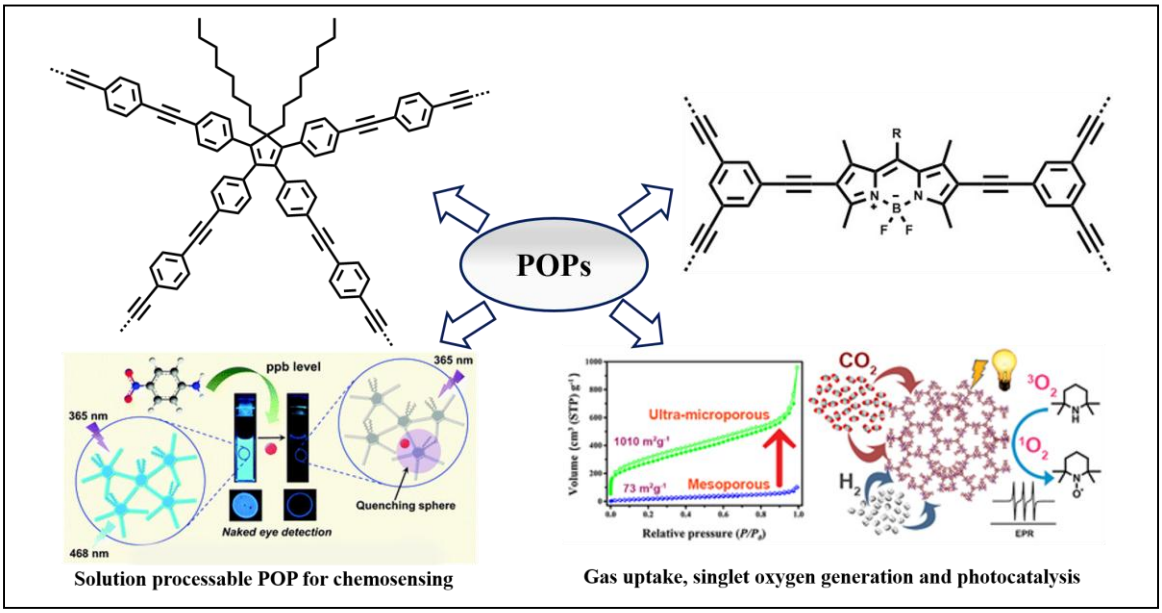


Figure 1 Schematic illustration of diverse application of porous organic polymers.

References

[62] Slater, A. G.; Cooper, A. I. *Science* **2015,** 348 (6238).
[63] Bandyopadhyay, S.; Pallavi, P.; Anil, A. G.; Patra, A. *Polym. Chem.* **2015,** *6* (20), 3775.

[64] Deshmuk, A.; Bandyopadhyay, S.; James, A.; Anil, Patra, A. ***J. Mater. Chem. C*, 2016, *4*** (20), 4427.

MACRO 481

Novel process for coating of polyaniline salt on stainless steel electrode: Flexible electrode for High performance supercapacitor

Gopi Chintada[a], Ramesh Gottam[a], Palaniappan Srinivasan*[, a, b]

[a] *Polymers & Functional Materials Division, CSIR-Indian Institute of Chemical Technology, Hyderabad-500007, INDIA.*

[b] *CSIR–Network Institutes for Solar Energy(NWP0056), New Delhi, INDIA.*

* *Corresponding author's email:* ***palani74@rediffmail.com***

Increasing energy demand and the development of alternative sources to meet such demand, energy storage technologies are increasingly becoming a crucial component of many renewable energy systems. Super capacitor is an important energy storage system. Three types of materials, such as carbon [1], metal oxide [2] and conducting polymers [3] are being used as electrode materials in supercapacitor. Preparation of electrode via coating the active material on conductive substrate is an important aspect for supercapacitor device. In this work, a novel process was developed for the preparation of composite of polyaniline salt containing p-toluenesulfonic acid dopant with activated carbon (PANI-PTSA-CARBON). The composite sample was well characterized by physical, spectral, electrical and thermal methods. Thus prepared sample was coated on stainless steel sheet along with activated carbon and without any binder. This coated sheet (10 x10 cm) is used as electrode in symmetric supercapacitor cell configuration (Figure). Performance of supercapacitor cell was carried by cyclic voltammetry, charge-discharge and impedance spectral measurements. PANI-PTSA-CARBON flexible electrode showed specific capacitance of 528 F g^{-1} and energy density of 73 W h kg^{-1} at a power density of 250 W kg^{-1}. The specific capacitance of PANI-PTSA-CARBON was higher than that of PANI-PTSA salt (180 F g^{-1}). Cell of PANI-PTSA-CARBON electrodes (2 × 2 cm^2 area) was subjected for 10,000 charge-discharge cycles at heavy current density 4 A g^{-1} and it showed 70 % retention of its initial capacitance of 380 F g^{-1}. Novelty of this work is scalable and easy synthesis and v flexible electrode for supercapacitor and in this work PANI-PTSA salt is used as binder for carbon.

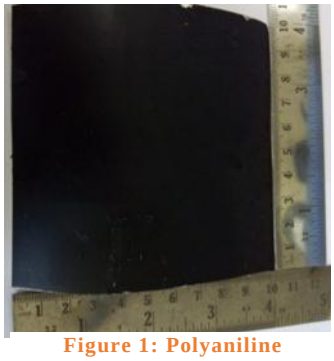


Figure 1: Polyaniline composite coated stainless steel electrode



Figure 2: Laminated super capacitor cell

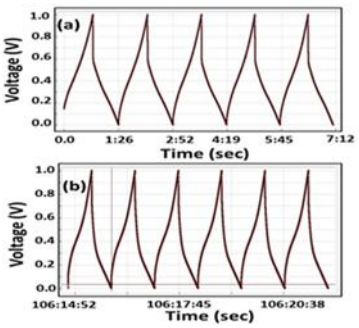


Figure 3: 1st and last five charge-discharge cycles of 10,000 cycles

References

[65]A, Ghosh; Y H, Lee. *Chemsuschem*, 5 (2012) 480.

[66]W, Deng; X, Ji; Q, Chen; C E, Banks. *RSC Advances*, 1 (2011) 1171.

[67]T, Liu; L, Finn; M, Yu; H, Wang; T, Zhai; X, Lu; Y, Tong; Y, Li. *Nano Letters,* 14 (2014) 2522.

MACRO 482

Fabrication and electrical performance of PEDOT:PSS/graphene nanocomposites

R.Aiswarya[a,b], R.Mitra[a] and K.P.Surendran[a,b*]

[a] *Electronic Ceramics group, Materials Science and Technology Division, CSIR-NIIST,Pappanamcode, Thiruvananthapuram, Kerala – 695019, India*
[b] *Academy of Scientific and Innovative Research(AcSIR),India*

* *Email: kpsurendran@niist.res.in*

Polyanilines, polypyrrole and poly thiophenes are different types of conducting polymers employed in electronic applications. Poly(3,4-ethylenedioxythiophene)-poly(styrenesulfonate), abbreviated as PEDOT:PSS, is a promising conducting polymer for bioelectronics applications due to its non toxicity and stability at ambient temperature.[1] It is a p type semiconductor and can be integrated into thin film transistors (TFTs) to form sensors.[2] Its solubility in aqueous solution can be attributed to the presence of negatively charged PSS.[3] Inkjet printing and spin coating are widely employed in literature to develop thin films using PEDOT:PSS. The conductivity of the film can be improved with ethylene glycol, methanol and DMSO treatment. The transparency of the film makes it a suitable candidate for fabrication of transparent electrodes in touch screen incorporated devices. It is a suitable replacement for ITO electrodes in solar cells. Addition of various conducting fillers like carbon nanotubes, graphene and silver can drastically improve the electrical performance of the film.

Graphene is a single layer of hexagonally arranged sp^2 bonded carbon atoms and is a semimetal with zero band gap which exhibits excellent thermal and electrical properties.[4] The thermal properties are described by the presence of flexural(Z) phonons and electrical properties such as hall effect can be described by the massless Dirac fermions. Graphene is widely used as conducting element in RFID tag antennas, supercapacitor, and Hall effect sensors.

In this work, graphene oxide was synthesised by modified Hummers' method and the subsequent reduction of graphene oxide to reduced graphene oxide (RGO) was performed using hydrazine hydrate. This was followed by synthesis of PEDOT:PSS and PEDOT:PSS/graphene composites through solution techniques. The wide angle x-ray scattering (WAXS), scanning electron microscopy (SEM) and transmission electron microscopy (TEM) were performed for the structural as well as morphological analysis of the nanocomposites. The thermogravimetric studies (TGA), Raman spectra and UV-Visible data have also been obtained for the composites. The electrical characteristics of PEDOT:PSS as well as PEDOT:PSS/graphene composites were studied using Keithley 2400 series source meter. From the I-V measurements, the improvement of conductivity of PEDOT:PSS with addition of graphene could be observed. TFT incorporating PEDOT:PSS/Graphene composites have been tested and their transistor characteristics have yielded promising results. Hence, PEDOT:PSS/graphene nanocomposites could be qualified as promising candidates for sensor fabrication.

References

[68]L.Wan, B.Wang, S.Wang, X.Wang, Z.Guo, B.Dong, L.Zhao, J.Li, Q.Zhang, T.Zuo. *J.Mater.Sci.,* 50 (2015) 2148.
[69]E. Bihar, Y.Deng, T.Miyake, M.Saadaoui, G.G.Malliaras, M.Rolandi. *Sci. Rep.*, 6 (2016) 27582.
[70]Y. H. Kim, C. Sachse, M. L. Machala, C. May, L. Müller-Meskamp, K. Leo. *Adv. Funct. Mater.*, 21 (2011) 1076.
[71]G.Wang, B.Wang, J.Park, Y.Wang, B.Sun, J.Yao. Carbon, 47 (2009) 3242.

MACRO 484

Poly(aniline-co-pyrrole) - Nanocomposite for Room Temperature Sensing of Carbonmonoxide

Khadeeja Sherin P. R.[a], Bhuvaneswari S.*[b], Eapen Thomas[b], Sadhana R.[b], Rajeev R.[b], Benny K. George[b]

[a] *University of Calicut, Malappuram*
[b]*Analytical, Spectroscopy and Ceramics Group, PCM entity, Vikram Sarabhai Space Centre*
** sbvssc@gmail.com*

Unswerving detection of gases is of prime concern in environmental pollution, industrial emission monitoring, public security, agriculture, space missions and a variety of industries. As there is increasing demand for effective sensing of $CO_{(g)}$ in various fields, the present study aims at developing a sensing material with good sensitivity at room temperature (RT) and reusability after exposure. The tremendous potential of conducting polymers (CPs) as sensors can be tailored by copolymerisation with another CP [1] or by using a suitable dopant such as carbon nano tube (CNT) [2]. Nanomaterials possess potential for unsurpassed sensitivity towards changes in its chemical environment thus making them promising candidates for gas sensing applications [2].

Preparation of CNT based conducting poly(aniline-co-pyrrole) (PAC) composites and its posterior use for sensing of $CO_{(g)}$ are attempted through this work. PAC composites were synthesized by microemulsion polymerization (MP) via soft template (ST) method using sodium hexametaphosphate (SHMP) and 1-hexadecyl-3-methylimidazolium chloride (HMIC) in aqueous and alcoholic medium with different loadings of multi-walled CNT (MWCNT). The synthesized composites were characterized using various techniques viz. FTIR and Raman spectroscopy, XRD, surface area analysis and AFM. The resistance of all composites was evaluated.

PAC composite synthesized in aqueous medium possessed a high resistance initially, but the response towards gas was not linear and the response time taken when compared to the composite synthesized in ethanol medium was high. The polymer synthesized by chemical oxidative polymerization has spherical particles in micrometer range. PAC synthesised by MP using SHMP resulted in irregular platelet morphology whereas when HMIC is employed uniform spherical nanospheres (Figure 1) were obtained. PAC-composite synthesized using SHMP tends to pick up moisture and also the response was not linear compared to that of composite synthesized using HMIC as ST.

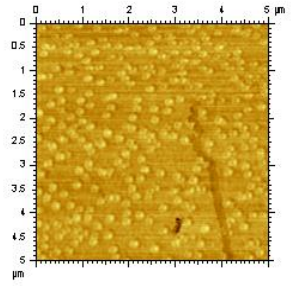


Figure 1. Topography image of PAC-nanocomposite synthesized by MP using HMIC as ST

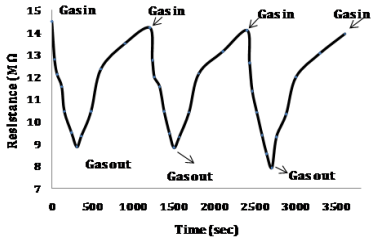


Figure 2. Repetitive response of PAC-nanocomposite to 10 ppm of CO

The resistance measurements of the composites revealed that PAC polymerized with 0.2 wt% of CNT in presence and absence of HMIC had higher resistance. Hence, for further experiments on sensing $CO_{(g)}$, these systems were chosen. PAC-nanocomposite was exposed to varying concentration of $CO_{(g)}$ and the changes in the resistance were monitored. PAC-nanocomposite synthesized via ST method using HMIC showed a good sensitivity even towards 0.5 ppm of $CO_{(g)}$ with response time less than 30 sec. The repetitive response of PAC nanocomposite synthesised by MP was stable (Figure 2), whereas the response of nanocomposite prepared by chemical oxidative polymerization was varying after subsequent exposure. Hence, PAC-nanocomposite with 0.2wt% of CNT synthesized by MP employing HMIC as ST in ethanol medium with controlled morphology is preferred as a potential candidate for $CO_{(g)}$ sensing with good response time and repetitive recovery at room temperature.

References

[1] Hua Bai, Gaoquan Shi, Gas Sensors Based on Conducting Polymers, *Sensors***,** 7 (2007) 267.

[2] Zhang, T., Mubeen, S., Myung, N. V., & Deshusses, M. A. Recent progress in carbon nanotube-based gas sensors. *Nanotechnology*, 19 (2008) 332001.

MACRO 492

Thermoreversible gelation of cycloaliphatic poly (urethane *acyl*semicarbazides) in DMSO and selective adsorption and separation of dyes from waste water by using xerogels

Sravan Baddi, Aruna Palanisamy*

Polymers and Functional Materials Division, CSIR-Indian Institute of Chemical Technology, Tarnaka, Hyderabad, India, 500007

** e-mail id:* aruna@iict.res.in

Abstract

A series of linear segmented poly (urethane *acyl*semicarbazides) were synthesised from polypropylene glycol (M_n~1000 and 2000), HMDI and cyclohexane-1, 4-dicarboxylic acid dihydrazide. The polymers with specific NCO/OH ratios exhibited thermoreversible gelation at a concentration of 25 mg/mL in DMSO. IR studies revealed the H-bonded nature of the chains in the gel state. SEM analysis of the xerogel revealed that slight changes in hard segment content leads to drastic changes in the morphology. Extent of H-bonding and hard segment length were quantified by WAXS. The xerogels of the self-assembled polymers exhibit a remarkable ability to remove dye molecules selectively, rapidly and efficiently. The gels retain their original structure and performance even after they are recycled 20 times. This was quantified by carrying out UV-vis studies.

Keywords: *Gelation, H-bond, polyurethane, hard segment*

1. Introduction

Among the numerous techniques available for the removal of these dyes, the adsorption technique is most effective, eco-friendly, economical and easily regenerated way for environmental clean-up.[1] Despite various adsorbents used to remove dyes from aqueous solutions from that physically cross-linked polymer based hydrogels, [2] dendritic polymers, [3] biopolymers (Chitosan and cellulose) [4, 5] and organic-inorganic hybrid gel materials[6] have been commonly used to remove toxic dyes from waste-water. Recently the selective removal of dyes from polluted water is more attractive and extremely important.[7, 8]

Self-assembled supramolecules have a three dimensional network like structure in which the gelator molecules hold the solvent in their interstices. The increased porosity and availability of both hydrophilic and hydrophobic groups in their backbone are desirable qualities for a material to possess adsorption of dyes. With this understanding, the present work has been carried out to design polyurethanes which can self assemble under stimuli, leading to gelation. To the best of our knowledge there is no report on self-assembling polyurethane based xerogels that have been used for waste-water treatment. The xerogels demonstrated in this work were found to remove dye molecules selectively and efficiently.

2. Experimental

2.1. Synthesis of polyurethanes

A mixture of poly propylene glycol (PPG), hexa methylene diisocyanate (HDI) and DBTDL were reacated till the NCO content reached the theroretical value. The prepolymer was diluted with dimethyl acetamide (DMAc) and then chain extended with 1, 4-Cyclohexanedicarboxylicacid dihydrazide (CHDH dissolved in DMAc) at room temperature till the NCO peak 2270 cm^{-1} disappeared completely. The polymer was recovered by precipitating in water.

2.2.Gelation Test & Preparation of PU xerogels

The gels were prepared in test tubes by taking appropriate amounts of polymer in 1 mL of DMSO, which was sealed and then left until

the compound dissolved. To that solution we have added MeOH in different ratios. The solution was then heated and allowed to cool to room temperature when gelation took place.

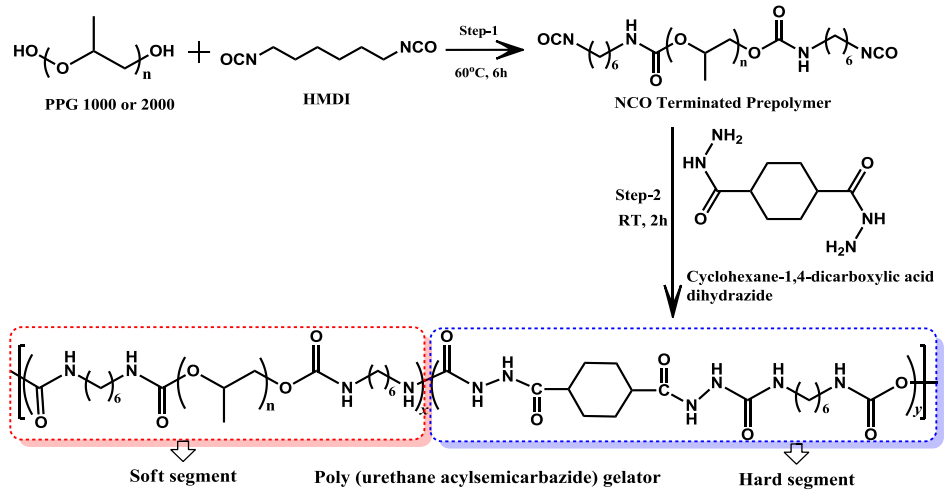


Figure 1. Synthetic route of poly (urethane *acyl*semicarbazide) gelator

3. Results and discussion

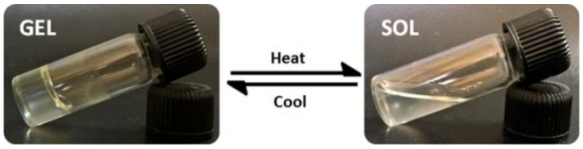


Figure 2. The digital photograph of thermoreversible gel–sol transitions of P_{2000}-1:3 gel.

Table 1. Codes, composition and minimum gelation concentration (MGC) of polyurethane gelators

Sample Code	PPG M.Wt	PPG: HMDI: TDH mole ratio	HSC (wt%)[a]	DMSO MGC (mg/mL)	T_{gel}(°C)	G_T (min)	Glass transition temperature (T_g) of gelators	
							Soft segment	Hard segment
P_{1000}-1:2.5	1000	1:2.5:1.5	41	25 (G)	131.3	35	-53.03	37.96
P_{1000}-1:3	1000	1:3:2	47	20 (G)	137.6	30	-46.82	47.62
P_{2000}-1:3	2000	1:3:2	30	25 (G)	107.4	45	-63.12	34.04
P_{2000}-1:3.5	2000	1:3.5:2.5	34	20 (G)	115.1	35	-63.22	39.96

[a] hard segment content= [mass of CHDH + HMDI]/[mass of PPG + HMDI + CHDH], T_{gel}=Gel melting point, G_T=Gelation time.

Four compositions listed in table 1 exhibited gelation in DMSO upon warming the gelators of specific concentration and then cooling the resulting solutions. Among them, P_{2000}-1:3 and P_{2000}-1:3.5 are effective gelators for mixture of solvents (DMSO/MeOH) in different ratios (1:1, 1:2, 1:3 and 1:4 by volume). All the gels obtained were transparent, thermoreversible (Figure 2) mechanically stable without any visible

structural disintegration under mechanical agitation and stable at ambient temperature for more than 6 months.

3.1.Thermal properties of gels

From table 1 it was observed that when the NCO/OH ratio increased the melting temperature increased from 131 to 137 ^{o}C and 107 to 115 ^{o}C for PPG1000 and PPG2000 based gels. When the gelator concentration increased from 25 to 100 mg/mL the peaks shifted to higher temperatures. The high gel–sol phase-transition temperatures confirm that the thermal stability of the PU gels is higher and introduction of extra hydrogen bonding moieties leads to stronger gelator–gelator interactions (intermolecular attraction of hard to hard segments). This is because of the higher hard segment content (semicarbazide moieties), where the urethane groups form dense domains.

3.2. FT-IR

The FTIR spectra of P_{2000}-1:3 gelator in gel and solution state were recorded in DMSO. (Figure 3).The stretching vibrations of N-H, appeared at 3455 cm^{-1}(υ_{N-H} stretch) and 1660 cm^{-1}($\upsilon_{C=O}$ of amide), respectively for the solution. Upon gelation, the bands shifted to 3398 cm^{-1}(υ_{N-H} stretch) and 1652 cm^{-1}($\upsilon_{C=O}$ of amide) respectively. The decrease in N-H, C=O stretching frequencies in gel state are the characteristic transmissions of the extensive intermolecular hydrogen-bonded amide group. This is an evidence for the participation of the N-H group in the formation of hydrogen bonds, which should be one of the driving forces for the formation of the gel. We observed a noticeable decrease of CH_2 stretching peak intensity in gel state. These lower intensities of υ_{asym} and υ_{sym} of CH_2 stretching frequencies indicates the decrease in fluidity of the hydrophobic chains.

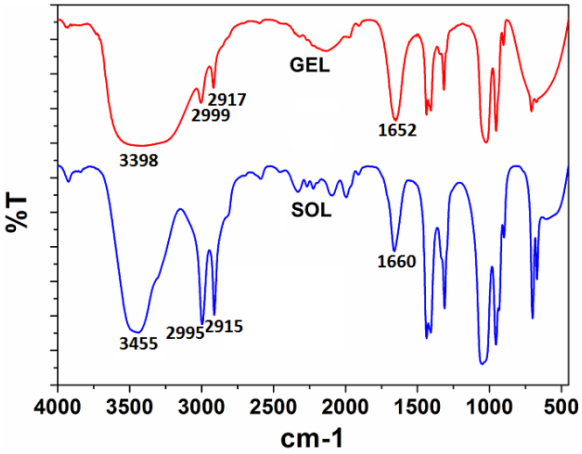


Figure 3. FT-IR spectrum of P_{2000}-1:3 in solution and gel state

3.3. Morphology

We observed an entangled fibrillar network type of morphology for PPG1000 based systems while PPG2000 based systems exhibited both microsphere and fibre like morphology depending on the NCO/OH ratio. When the polyol molecular weight is fixed, a lower NCO/OH ratio leads to good phase separation. As the polyol molecular weight increases, for a fixed ratio of NCO/OH (1:3), there is an enhancement in phase separation (Figure 4). Hence a phase separation induced gelation mechanism can be proposed for this system.

3.4. X-ray Diffraction Analysis

The wide-angle X-ray diffraction patterns reveal a series of prominent peaks in the region 2θ = 7-22^{o}.

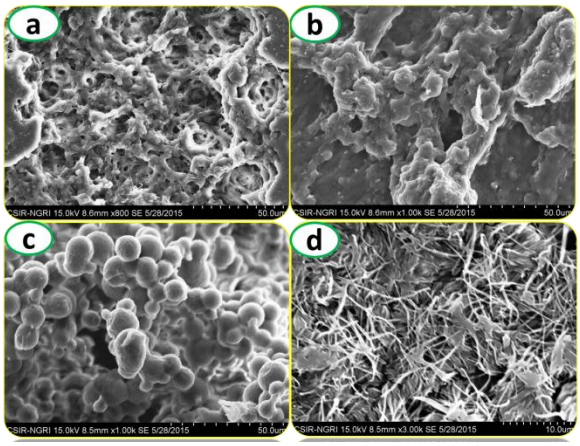


Figure 4. SEM images of xerogels of (a) P_{1000}-1:2.5 (b) P_{1000}-1:3 (c) P_{2000}-1:3 and (d) P_{2000}-1:3.5 respectively.

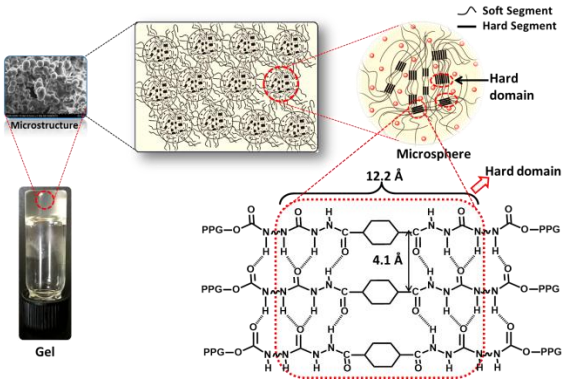


Figure 5. Plausible mechanism of formation of microspheres and fiber through Hydrogen bonding

The peak around 12 Å might be assigned to the diffraction related to the CHDH and HMDI hard domain unit (Figure 6) indicating some degree of crystallinity. The crystallinity increases and hence intensity of peak increases with increasing HSC and higher melting temperature suggest better ordering of crystallites due to significant hydrogen bonding. The diffractograms exhibit broad peaks on 2-theta-scale around 21˚ angle. The reflection with a lattice spacing of 4.1 Å corresponds to the plane that is formed by hydrogen bonding of amide groups in hard segments as depicted in Figure 5.

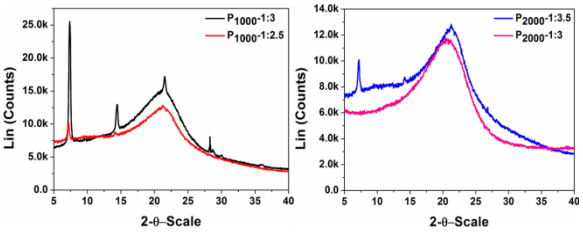


Figure 6. X-ray difractograms of PU (*acyl*semicarbazide) xerogels.

3.5.Dye adsorption and specificity in aqueous solution

PUG xerogel (20 mg) was added to an aqueous solution (5 mL) of crystal violet (c= 1×10^{-5} mol·L^{-1}). The xerogels efficiently adsorbed the CV molecules from water after 24 h (adsorption equilibrium) as monitored using UV-visible spectroscopy. (Figure 11a). The time-dependent adsorption curves of CV on xerogel are depicted in Figure 7.

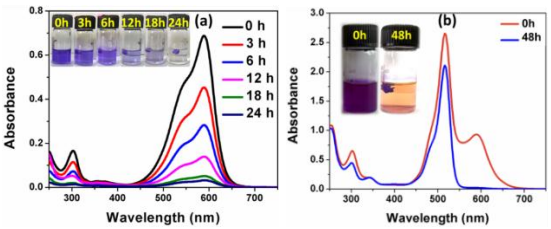


Figure 7. (a) Time-dependent UV–vis spectra of CV solution after addition of the xerogel, **(b)** UV- Visible spectra of mixture of aqueous dye solutions of CV&EY, the inserted photos are dye solutions acquired for the clear liquids (left to right).

The adsorbed amount of dyes by the PUs was measured using the following equation.

$$Q_{eq} = \frac{(C_0 - C_{eq})V}{m}$$

Where Q_{eq} (mg g^{-1}) is the amount of adsorbed dyes by the PUG xerogel, C_0 (mg L^{-1}) is the initial concentration of dyes, C_{eq} (mg L^{-1}) is the equilibrium concentration of dyes in

water. V (L) is the volume of the dye solution and m (g) is the mass of the PUG xerogel used in this adsorption experiment. Using the above equation, it was found that one gram of xerogel can adsorb 201.6 mg of CV.

To confirm selectivity we have chosen four water soluble dyes- crystal violet (cationic CV), amaranth, eosin yellow and methyl orange (anionic AM, EY and MO). The xerogels were added separately to the aqueous solutions containing two dyes with different charges (CV & AM, CV & EY, CV & MO).The adsorption behaviour of xerogels was monitored by UV-visible spectroscopy. The intensity of the absorption band of CV (λ max= 589 nm) decreases with time in the presence of xerogel. However, the intensity of the absorption bands of AM, EY and MO (λ max= 529, 516 and 464 nm respectively) remains unchanged (Figure 7b). The results revealed that the xerogels can rapidly and selectively adsorb CV dye molecules into their networks and the adsorption rate is very high in the first 18 h. The adsorption of the anionic dyes was negligible. These results indicate that these xerogels can efficiently purify and separate cationic dyes from water. After adsorption, the xerogels were collected from water by decantation of faded water. The 20 mg of CV@xerogel (CV adsorbed xerogel) was placed in 5 mL methanol or acetone solution and the UV visible spectra were recorded at different time intervals. It was found that the intensity of the absorption maximum increases and the colour of the solution changed within 20 min (Figure 8d). As expected, the colour of xerogel changes to white (Figure 8c) and it was again used for the dye adsorption. During recycling, it maintained the rapid and selective adsorption having the almost same adsorption capacity up to 20 cycles without losing its physical structure.

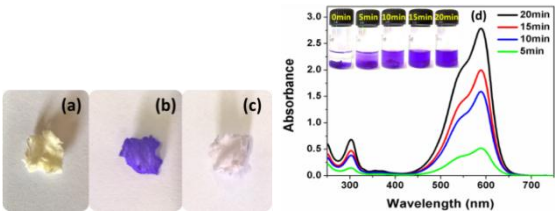


Figure 8. Digital photograph of PUG xerogel (a) before adsorption; (b) after adsorption of CV; (c) after desorption in MeOH (d) UV-Vis spectra of xerogel during desorption in 5ml of MeOH. The inset images are before after dye desorption (left to right).

4. Conclusions

In summary, a series of linear segmented poly (urethane *acyl*semicarbazides) with cycloaliphatic groups in the hard segment exhibiting gelation in DMSO and DMSO: Methanol mixtures were successfully synthesized. Effect of hard segment content and polyol molecular weight on gel properties was systematically studied to propose a suitable phase separation induced gelation mechanism. The xerogels had the ability to remove dyes selectively from water with 98% efficiency and excellent recyclability; these materials are promising candidates for water purification.

Acknowledgements

Sravan Baddi is indebted to Council of Scientific and Industrial Research (CSIR), India, for Senior Research Fellowship (SRF).

References

1. M. T. Yagub, T. K.Sen, S.Afroze, , & H. M Ang, (2014). *Advances in colloid and interface science*, *209*, 172-184, 2014.

2. X. Guan, K. Fan, T. Gao, A. Ma, B. Zhang,J.Song. *Chemical.Communications*, *52*(5), 962-965, 2016.
3. M. Arkas, D. Tsiourvas, C. Paleos, M. *Chemistry of materials*,*17*(13), 3439-3444, 2005.
4. Y. C. Wong,., Szeto, Y. S., Cheung, W. H., & McKay, G. *Langmuir*, *19*(19), 7888-7894, 2003.
5. G. Annadurai, R. S. Juang, D. Lee, *Journal of hazardous materials*, *92*(3), 263-274, 2002.
6. V. Bekiari, P. Lianos, *Chemistry of materials*, *18*(17), 4142-4146, 2006.
7. C. K. Karan, M. Bhattacharjee, *ACS applied materials & interfaces*, *8*(8), 5526-5535, 2016.
8. N. Cheng, Q. Hu, Y. Guo, Y. Wang, L. Yu, .*ACS applied materials & interfaces*, *7*(19), 10258-10265, 2015.

MACRO 500

Molecular interactions in lithium ion batteries: Identification of lithium species in non-aqueous propylene carbonate electrolyte by NMR

Vikas Kumar[a], C.V. Avadhani[a], P.R. Rajamohanan[b], S. Ganapathy[b] and S. Sivaram[c*]
[a]Polymer Science and Engineering Division and [b]Central NMR Facility, National Chemical Laboratory, Pune 411008, India
[c]Indian Institute of Science Education and Research, Pune 411008, India
email id: s.sivaram@iiser.ac.in

Abstract

The electrolytic dissociation of lithium hexafluorophosphate ($LiPF_6$) in non aqueous cyclic propylene carbonate has been investigated in the 0.2 – 3.5 M concentration range by ^7Li solution state NMR spectroscopy. ^7Li NMR spectra provide evidence for the presence of different cationic species in the electrolyte. Using a spectral deconvolution procedure we have determined their relative composition at any given salt concentration. In the solvent rich regime (0.2 - 1.4 M) the free dissociated Li^+ ions and the solvent separated ion-pairs (SSIP) are the dominant species, whereas in the salt rich regime the contact ion-pairs (CIP) become the dominant species. Additionally, our results show that the Li exchange among these sites occurs on a sufficiently slow NMR chemical shift time scale at room temperature ($k < 15$).

Key Words: Li-ion battery, electrolyte, non-aqueous carbonate solvent, ^7Li NMR spectroscopy, lithium speciation

Introduction

Lithium ion batteries (LIBs) power our digital life and are extensively used in electronic devices. LIBs consist of electrodes, electrolyte and a separator. The

most widely used electrolyte for LIBs is $LiPF_6$ in a non-aqueous carbonate solvent mixture, consisting of a cyclic carbonates, e.g, ethylene carbonate (EC), with one or more linear carbonates, e.g, dimethyl carbonate (DMC). The key to the battery performance is the Li-ion conduction in the liquid electrolyte medium which, in turn, is determined by the nature of Li ion species that exist in solution and the factors that govern the dynamics of the ion pairs. Considerable research has been reported in the last few years to better understand the nature of the Li-ion species formed in terms of solvation and coordination using a variety of experimental and theoretical studies.

In so far as studies of Li-ion complexation in non-aqueous carbonate solvent is concerned, recent studies have dealt with the application of various techniques such as Raman,[1-2] vibrational, infrared[2-3] and molecular rotation[1,3] spectroscopy. NMR spectroscopy, using ^{13}C and ^{17}O of the solvent molecule, has also been employed to glean valuable atomic level insights from the observed chemical shifts and analyzing them in term of the Li-ion coordination with the organic solvent molecules to determine the coordination number.[3-5] Theoretical studies based on molecular dynamics simulations and density functional theory as well as quantum chemical calculations have been reported which not only complement the experimental findings but have enabled the determination of thermodynamic parameters.[6]

By and large, the studies on neat and mixed electrolytes reported thus far are mostly solvent focused and invariably studied in the solvent rich regime. While they do provide valuable insights on the nature of primary and secondary solvation and also enable the determination of the solvent coordination number, no information about the non-solvated cation environments, such as the contact ion pairs (CIP) are provided from such studies.

The direct observation of Li-cation using ^{7}Li NMR spectroscopy as a molecular characterization tool offers new opportunities to probe the cationic environments in the electrolyte at the atomic level. The lithium cation can be expected to exist in either of the three major species, namely, (i) the solvated and fully dissociated Li^+; (ii) the solvent separated ion pair (SSIP) and (iii) the contact ion pair (CIP), which are the major species formed during the electrolyte dissociation.[2,4] ^{7}Li NMR thus enables the inspection of all these cation environments and hence affords their characterization. Besides, the evolution and build up of the different Li-species can be

monitored and ascertained when ^{7}Li NMR studies are conducted as a function of salt concentration. ^{7}Li NMR offers a high detection sensitivity due to its large natural abundance (92.6 %) and, despite being quadrupolar (I=3/2), a high spectral resolution is expected due to its small quadrupole moment. ^{7}Li NMR, therefore, provides a direct access to the local Li environments present under high resolution conditions and renders a study of lithium speciation in electrolytes readily feasible.

The present work deals with the direct application of ^{7}Li NMR spectroscopy to study the dissociation of $LiPF_6$ in non-aqueous cyclic propylene carbonate (PC) over the salt concentration range of 0.2 - 3.5 M with the main objective of providing first hand information on lithium ion speciation and their relative population at each concentration.

Experimental

Lithium hexafluorophosphate was purchased from Sigma Aldrich and used without further purification. Commercially available battery grade carbonate solvents, propylene carbonate (PC) was obtained from Sigma Aldrich and used after distillation. Electrolyte solutions of different concentrations (0.2 - 3.5 M with 0.2M incremental step) in PC solvent were prepared in an argon filled glove box (both H_2O and O_2 < 0.1 ppm) and transferred into 5 mm NMR tube and stored under a moisture free environment.

NMR experiments were carried out in the solution state at ambient room temperature (22-24 ^{o}C) on a Bruker Avance III 400 MHz NMR spectrometer at the Larmor frequency of ^{7}Li (155.506 MHz). ^{7}Li NMR spectra were acquired in the single pulse mode with a 30^{o} flip angle pulse (4 μsec) and a 1 sec relaxation delay. Typically 40 free induction decays were acquired and Fourier-transformed with 1 Hz exponential line broadening. The ^{7}Li chemical shifts were referenced externally to 1M LiCl solution. All the spectral deconvolutions were carried out using DMFIT software.[7] A mixed Gaussian/Lorentzian line shape (G/L =0.5) was used and the experimental spectra were iteratively fitted to arrive at the lithium species present and estimate their relative population.

Results and Discussion

Figure 1 (A) shows the ^{7}Li-NMR spectra of $LiPF_6$ at different concentrations in the range 0.2 – 3.5 M in non-aqueous organic propylene carbonate solvent. The NMR spectra mainly show a dominant signal with clearly noticeable shift of the resonance with increasing concentration. A careful

inspection of the ^{7}Li-NMR spectra shows that the line shape is not a single Lorentzian as expected for an exchange narrowed line which is typical for a dynamically averaged cationic environment in dynamic equilibrium. This is clearly not the case as seen by the marked asymmetry in the line

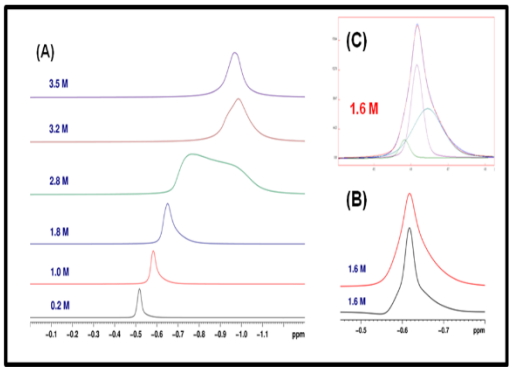


Figure 1. (A) ^{7}Li-NMR spectra of $LiPF_6$ in propylene carbonate at different salt concentrations. (B) Resolution enhanced ^{7}Li-NMR spectrum of 1.6 M. (C) Spectral deconvolution of (B) using a mixed Gaussian/Lorentzian (0.5) line shape function.

shape which can be noticed in **Figure 1**, especially in the spectra recorded at higher concentrations. This can be attributed to the spectral overlap among distinctly different lithium sites which have small difference in their chemical shifts. The observed signal line shape and the intensity profile are entirely governed by the lithium species present and their actual composition in a given concentration. This can be more readily seen from the resolution enhanced spectrum, such as the one shown in **Figure 1 (B)** for 1.6 M solution, which clearly shows that there are three overlapping signals which constitute the observed ^{7}Li spectral line shape. Independent ^{7}Li spin-lattice (T_1), spin-spin (T_2) relaxation time measurements of 1.6 M solution reveal a triple exponential relaxation behaviour for the total integrated signal intensity and additionally confirm our above spectral interpretation.

The observed ^{7}Li NMR spectra at each concentration was de-convoluted to reveal the various lithium species present. De-convolution of the of 1.6 M solution is shown in **Figure 1 (C)** and the presence of three distinct lithium sites is at once identified. The concentration dependence of the ^{7}Li NMR response shows that at low concentrations down to 1.4 M the NMR spectrum comprises only two components, whereas, at higher concentrations an additional component is required to fit the observed ^{7}Li line shape. These observations and the de-convolution procedure that we have used have therefore enabled us to monitor not only the Li species formed, but also get quantitative estimates of their relative population at any given concentration. The lithium cation speciation from ^{7}Li NMR has also enabled the determination of ^{7}Li chemical shifts at each concentration for the different species

present. It may be remarked that the chemical shifts ascribed to each species are determined more accurately in the present study when compared to previous studies which assume that the ^{7}Li NMR spectrum consists of a single unresolved resonance.[8] This has, in turn, allowed monitoring the NMR behaviour for the dissociated Li-ion, SSIP and CIP species in a way that had not been possible before.

The lithium cation speciation of $LiPF_6$ in propylene carbonate is shown in **Figure 2**. The three lithium species detected from ^{7}Li NMR are labeled as Li (1), Li (2) and Li (3), respectively. Plots in **Figure 2** show the variation of the relative population for the above three Li species as a function of the salt concentration. Li (1) and Li (2) begin to emerge at the lowest concentration of 0.2 M with a large number of lithium cations getting preferentially populated at Li (1) sites. This enables us to associate the two species Li (1) and Li (2), detected in the 0.2 - 1.4 M range, to the dissociated and charged Li^{+} ions in the propylene carbonate solvent and the solvent separated ion pairs (SSIP), respectvely.[6] Initial confinement of lithium

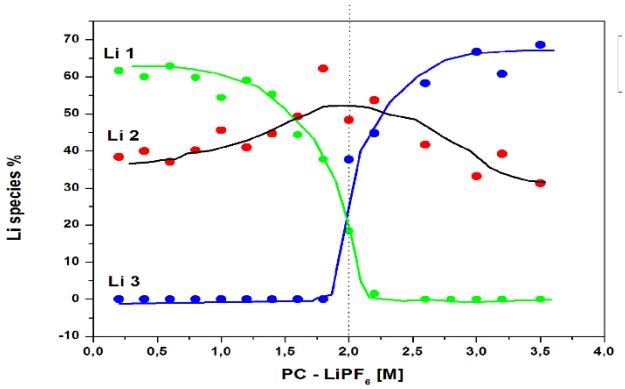


Figure 2. Lithium speciation determined from ^{7}Li-NMR and the variation in lithium site population for the electrolyte solution of $LiPF_6$ and propylene carbonate.

into the Li (1) and Li (2) environments and the large deficiency at Li (2) sites tends to allow the Li (2) population to grow as more and more lithium is consumed from the electrolyte at increasing concentrations. Since the total lithium is distributed only among Li (1) and Li (2) sites, increase in the population of Li (2) sites would tantamount to a progressive decrease of the Li (1) site population as the concentration of the salt solution is increased. This is indeed noticed in **Figure 2** in the concentration range 0.2 - 1.6 M until an equitable distribution of lithium into Li (1) and Li (2) sites is seen to occur at 1.6 M. Remarkably, Li (3) emerges only beyond 1.6 M and becomes the dominant species at 2.6 M and above. Since for the cyclic carbonate contact ion pairs are favoured only at high salt concentrations, Li (3) can be readily assigned to the lithium cation belonging to CIPs. Our ^{7}Li NMR results show that in the solvent rich regime the lithium speciation occurs in a way that the fully dissociated and solvated charged (Li^{+})

and solvent separated ion pairs (Li^+ - solvent - PF_6^-), i.e., Li (1) and Li (2), respectively, are the dominant species. On the other hand, in the high salt rich regime, cations in the contact ion pairs ($Li^+...PF_6^-$) are the dominant species, although the fully solvated lithium ions are by no means insignificant in number.

Conclusions

^{7}Li-NMR spectroscopy has been utilized to study the lithium cation speciation in the electrolyte solution of $LiPF_6$ in non-aqueous organic propylene carbonate. Lithium belonging to the solvated and fully dissociated (Li^+), solvent separated and ion paired (SSIP) and contact ion pairs (CIP) have been identified from ^{7}Li NMR spectra and their populations at different salt concentration have been quantitatively determined. The dominance of the former two species in the solvent rich regime and that of the latter two species at high salt concentrations have been borne out from these studies.

Acknowledgement

We gratefully acknowledge funding from Council of Scientific and Industrial Research, New Delhi under the NWP 56 TAPSUN programme. VK gratefully acknowledges grant of a Senior research fellowship from UGC, New Delhi

References

1. Qiao, H.; Luan, H.; Fang, X.; Zhou, Z.; Yao, W.; Wang, X.; Li, J.; Chen, C.; Tian, Y. *J. Mol. Stru.* **2008**, *878*, 185.

2. Burba, C. M.; Frech, R. *J. Phys. Chem. B* **2005**, *109*, 15161.

3. Seo, D. M.; Reininger, S.; Kutcher, M.; Redmond, K.; Euler, W. B.; Lucht, B. L. *J. Phys. Chem. C* **2015**, *119*, 14038.

4. Yang, L.; Xiao, A.; Lucht, B. L. *J. Mol. Liq.* **2010**, *154*, 131.

5. Bogle, X.; Vazquez, R.; Greenbaum, S.; Cresce, A. v. W.; Xu, K. *J. Phys. Chem. Lett.* **2013**, *4*, 1664.

6. Aroca, R.; Nazri, M.; Nazri, G. A.; Camargo, A. J.; Trsic, M. *J. Sol. Chem.* **2000**, *29*, 1047.

7. Massiot, D.; Fayon, F.; Capron, M.; King, I.; Le Calvé, S.; Alonso, B.; Durand, J.-O.; Bujoli, B.; Gan, Z.; Hoatson, G. *Mag. Reson. Chem.* **2002**, *40*, 70.

8. Kondo, K.; Sano, M.; Hiwara, A.; Omi, T.; Fujita, M.; Kuwae, A.; Iida, M.; Mogi, K.; Yokoyama, H. *J. Phys. Chem. B* **2000**, *104*, 5040.

MACRO 504

Interesting Results Shown By Perovskite-Polymer Hybrid Solar Cell with Enlarged Absorption Spectra and Greater External Quantum Efficiency

Bavane Swapnil Ravindrakumar

Department of Chemical Engineering, University Institute of Chemical Technology, North Maharashtra University, Jalgaon
swapnilbavane@gmail.com

The urgent need for high-performance, large-scale, and low-cost thin film photovoltaic is driving extensive research on new light absorber materials. Among them, perovskite cells with significantly higher power conversion efficiency, usually $CH_3NH_3PbX_3$ based and polymer solar cells with aesthetic properties like flexibility and cost effective manufacturing, are a way more popular than and among many others. The work comprises of new characteristics shown by newly constructed hybrid of perovskite cell and traditional third generation polymer solar cell (Bulk hetero-junction), which leads to reduction in regular limitations observed in each of the pure forms of the respective component cells. Due to the high absorption coefficient (about 10^5 cm^{-1}) of perovskite (say CH3NH3PbI3) compared to that of a polymer (10^4 cm^{-1}), it is replaced as an absorber. Moreover, bipolar charge transport characteristics, low exciton binding energy, and long exciton diffusion lengths led to considerably as high PCE as about 12%.

References

(1) Chun-Chao Chen, Sang-Hoon Bae, Wei-Hsuan Chang, Ziruo Hong, Gang Li, Qi Chen, Huanping Zhou and Yang Yang, *Mater. Horiz.*, 2015,**2**, 203-211

(2) Agnese Abrusci, Samuel D. Stranks, Pablo Docampo, Hin-Lap Yip, Alex K.-Y. Jen, and Henry J. Snaith, *Nano Lett.*, **2013**, *13* (7), pp 3124–3128

(3) Long Ye, Benhu Fan, Shaoqing Zhang, Sunsun Li, Bei Yang, Yunpeng Qin, Hao Zhang and Jianhui Hou, *Sci. China Mater*. (2015) 58: 953.

MACRO 515

POLYMERIZATIONS WITH ELEMENTAL SULFUR: A ROUTE TO IMPROVED NEXT GENERATION BATTERIES

Jeffrey Pyun,[†,‡] Kookheon Char, [‡] Richard S. Glass[†]

[†]*Department of Chemistry & Biochemistry, University of Arizona, Tucson, AZ 85721;* [‡]*School of Chemical & Biologial Enegineering, Seoul National University, Seoul, Korea*

E-mail: jpyun@email.arizona.edu

The development of chemistry and processing methods for the utilization of elemental sulfur into polymeric materials provides a unique opportunity for addressing the substantial waste surfeit of sulfur generated via petroleum refining.[1-3] We recently demonstrated the use of liquid sulfur as the reaction medium for the synthesis of chemically stable and processable copolymer materials using a methodology, termed, *inverse vulcanization*.[1] In the *inverse vulcanization* process, the thermal ROP of S_8 is initiated by heating liquid sulfur to T = 185 ºC, however, the addition of 1,3-diisopropenylbenzene (DIB) to this free radical reaction enabled the synthesis of a chemically stable, branched copolymer of poly(sulfur-*random*-1,3-diisopropenylbenzene) (poly(S-*r*-DIB) (Figure 1). These sulfur copolymers were further shown to be electrochemically active when formulated into cathodes of lithium sulfur (Li-S) batteries exhibiting enhanced cycle lifetimes and charge capacity retention relative to elemental sulfur batteries.[1,2] We discuss new advances in the synthesis and processing of sulfur based electroactive materials for Li-S batteries sulfur copolymers, along with the unique electrochemical and optical properties of these materials.[3]

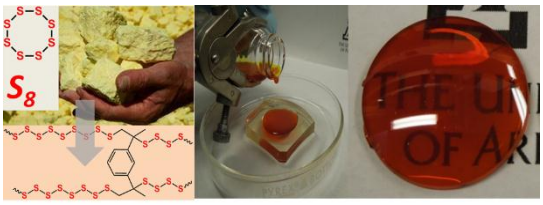


Figure 1: Representative scheme for the preparation of high sulfur content copolymers as electroactive cathode materials for Li-S batteries

Acknowledgements

We acknowledge the NSF (CHE-1305773), the University of Arizona Renewable Energy Network, Kuraray, the WCU Program through the NRF of Korea funded by the Ministry of Education, Science and

Technology (R31-10013) for support of this work. KC acknowledges the support from NRF for the National Creative Research Initiative Center for Intelligent Hybrids (2010-0018290).

References

1. Chung, W. J.; Griebel, J.J.; Kim, E.-T.; Yoon, H. –S.; Simmonds, A.G.; Ji, H.-J.; Dirlam, P.T.; Glass, R.S.; Wie, J.J.; Nguyen, N.A.; Guralnick, B.W.; Park, J.; Somogyi, A.; Theato, P.; Mackay, M.E.; Sung, Y.-E.; Char, K.-C.; Pyun, J. *Nature Chem.* **2013**, 5, 518-524.
2. Kim, E.-T.; Park, J.-J.; Kim, C.; Simmonds, A.G.; Sung, Y.; Pyun, J.; Char, K. *ACS Macro Lett.* **2016**, *5(4)*, 471-475
3. "Polymerizations with Elemental Sulfur: A Novel Route to High Sulfur Content Polymers for Sustainability, Energy and Defense," Griebel, J.J.; Glass, R.S.; Char, K.; Pyun, J. *Prog. Polym. Sci.* **2016**, *58*, 90-125.

MACRO 543

Copolymers of waste raw materials: sulphur and naturally occurring phenol derivatives for Lithium Sulphur battery

Swapnil Shukla,[a] Arnab Ghosh,[b] Sagar Mitra,[b] Bimlesh Lochab*, [a]

[a] *Department of Chemistry, School of Natural Sciences, Shiv Nadar University, Gautam Budh Nagar, Uttar Pradesh 203207, India*

[b] *Electrochemical Energy Storage Laboratory, Department of Energy Science and Engineering, Indian Institute of Technology, Bombay, Powai, Mumbai 400076, India*

** e-mail id: bimlesh.lochab@snu.edu.in*

Abstract

Secondary storage energy devices such as Lithium Sulphur (Li-S) batteries are receiving widespread attention due to their inherent high theoretical energy density (2600 Whk/g) and capacity (1672 mAh/g) of elemental sulphur (S) along with its abundant availibility. However, certain drawbacks *viz.* sulphur dissolution in the electrolyte, crack formation and reduced performance have impeded their performance and demand scientific solution towards their the further development. The chemical confinement of sulphur is one the most recent measure to counter such drawbacks using inverse vulcanisation strategy. In this study, sustainable benzoxazines have been explored as novel comonomers to yield random sulphur copolymers with a very high loading of S (~ 90%). These copolymers were derived from a bulk polymerisation methodology utilising sustainable origin materials namely sulphur (industrial waste) and cardanol (agro waste). The copolymers were successfully characterised by Raman, UV-visible, FTIR, and NMR spectroscopy. The copolymer structure was further studied by thermal and gel permeation chromatography confirming the copolymerisation reaction. They have shown the promising potential as cathodic materials for future Li-S battery, which will be discussed in the presentation.

Keywords: *Benzoxazine, Cardanol, Lithium Sulphur Batteries, sustainability*

Introduction

Sulphur is an intriguing element in terms of its diverse properties and a wide array of consequent applications ranging from energy storage devices to infrared transmitting materials. Amongst, various sources of sulphur, elemental sulphur generated as a waste by-product of petroleum industry can be considered as the most abundant one. Certain issues such as low solubility in organic solvents has hindered the utilization of elemental sulphur to its full potential till now. Recently, Pyun *et al*. have come up with an elegant chemistry of inverse vulcanisation[1] which has made it possible to incorporate up to 99 wt.% of sulphur in the polymeric architecture. A diverse range of monomers such as1,3-diethynylbenzene,[2] 1,4-diphenylbutadiyne,[3] carbyne

polysulphide polymers[4] and polythiophenes[5] have since been explored to extend the work to various possible applications. While, these findings certainly address the advancements in this field, dependence on petroleum sources makes this arrangement unsustainable in the wake of rapidly depleting petro sources. Hence, the avenues for including sulphur in polymeric framework via greener routes using sustainable building blocks demand immediate attention and exploration.

In this work we intend to explore a new class of materials as potential comonomers in the inverse vulcanisation process with an emphasis on sustainability. It can be inferred from the existing literature that a monomer in order to be incorporated in polysulphane framework must possess certain set of properties. These include reactivity towards free radical reactions, high temperature stability and non-volatility. Cardanol, an agro based phenol derived from cashew nut industry waste is one such promising candidate fulfilling the aforementioned criteria.[6] More so, the presence of long alkyl chain at meta-position renders low viscosity to it thereby easing the synthetic requirements of melt polymerisation resulting in a facile, scalable synthetic methodology. The only drawback is the presence of phenolic group which inhibits the polymeric chain growth by forming stabilised phenoxy radicals. This drawback can be countered by conversion of this phenolic group into oxazine ring, paving way for the exploration of benzoxazine. Benzoxaines are a new class of monomers which have gained prominence in the recent decade owing to a plethora of functionalities and unique properties and can be considered as potential comonomers for polysulphur compounds. Cardanol based benzoxazines, in particular not only satisfy the criteria adjudged suitable for inverse vulcanisation but also bring the factor of sustainability into the picture.[7] Here, it must be emphasized that being derived from a renewable waste is not the only highlight of the cardanol based benzoxazine. Its unique architecture is suited for the high temperature melt polymerisation apart from offering a multitude of reaction sites to react with polysulphane diradical. Taking into account all these factors, we have synthesized sustainable copolymers with high loading of sulphur (~95%) in the copolymer.

The wide chasm between the energy demand and supply calls for more efficient energy storage devices. Li-S batteries due to its high theoretical capacity (1672 mAh/g) and high theoretical energy density (2600 Wh/kg) are one of the emerging candidates to bridge this gap.[1] Polymers with chemically incorporated sulphur in high loading are ideal for the preparation of LiS cathodes. Thus, Li-S batteries could be considered as a major application of this work.[8] The only drawback in this case is the insulating nature of the commoner. This was countered by addition of carbon based nanofillers, MWCNT and reduced graphene oxide (rGO). Simultaneously, a comparison was also sought between the efficacies of these fillers where MWCNT is commercially available expensive option while rGO is derived via green route at cheaper costs. Latter was found to be a more efficient option with improved cathodic performances at lower loadings compared to its costlier counterpart.

Experimental

Materials

Cardanol was procured from Satya Cashew Chemicals Pvt. Ltd. (India), paraformaldehyde, sulphuric acid, sodium nitrate, potassium permanganate, hydrogen peroxide, hydrazine hydrate, aniline and liquor ammonia from Fisher scientific, gallic acid and MWCNT from Sigma Aldrich, chloroform from Finar, anhydrous sodium sulphate from Chemlabs, graphite flakes and sulphur (S8, 325 mesh, reagent grade) from Alfa Aesar. All the reagents were used as received.

Characterisation

Fourier Transform Infrared (FT-IR) spectra were recorded on a *Nicolet iS5* spectrometer equipped with iD5-ATR accessory, in the range of 4000 to 400 cm−1. Raman spectra were obtained using a JobinYvon HR800 Raman Microscope at 514.5 nm. Bruker AC 500 MHz FT-NMR spectrometer was used to record the 1H-NMR of the samples in $CDCl_3$ using tetramethylsilane as the internal standard. Calorimetric studies were performed on a Differential Scanning Calorimeter (DSC, TA instruments Q 20). For dynamic DSC scans, samples (10±2 mg) were sealed in aluminium pans, and heated from 50 to 160 °C at 10 °C min^{-1} under nitrogen atmosphere. The morphology and microstructure of bulk rGO and S90-2.5% rGO composite were characterized through field emission scanning electron microscopy (FESEM, Carl Zeiss Ultra 55) and high resolution transmission electron microscopy (HRTEM, JEOL-2100F).

Synthesis

Cardanol benzoxazine was synthesised by a previously reported procedure[9] involving solventless heating of a mixture of cardanol (0.33 mol), aniline (0.33 mol) and paraformaldehyde (0.66 mol) followed by extraction into organic layer which was dried to yield C-a in quantitative yields. Sulphur based copolymer was synthesised by adding desired weight percent of monomer to molten sulphur at 185 ^oC followed by stirring for ~10 minutes. Graphene oxide was synthesised *via* Hummer's method[10] followed by reduction using gallic acid in aqueous media.[11]
Polymer was further blended with MWCNT and rGO *via* ultrasonication.[12,13]

Results and discussion

Cardanol benzoxazine monomer (C-a) was synthesized using solventless method as reported (Figure 1).[9] Elemental sulphur was heated to 185 ^oC followed by subsequent copolymerisation with C-a. Amiable miscibility of C-a monomer made it possible to synthesize a series of sulphur copolymers varying the sulphur content from 95% to 20%. As mentioned earlier the capability of C-a to polymerize sulphur in large excess (~95%) may be explained by the numerous available reactive sites in the moiety including double bonds, benzylic carbon and oxazine ring.

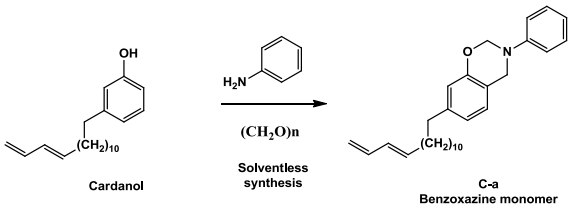


Figure 1: Synthesis of cardanol benzoxazine monomer, C-a.

Benzoxazine ring is susceptible to ring opening polymerisation (ROP) in presence of

thiols by COLBERT (Catalytic Opening of Lateral Benzoxazine rings by Thiols) ionic mechanism.[14] Polysulphane diradicals generated from large excess of sulphur can also be expected to result in the ROP at the reaction temperature leading to a further crosslinked system. This again supports the possibility of sulphur being chemically included in the polybenzoxazine network and eliminating the possibility of electrolyte assisted leaching which is one of the major limiting factor for device cyclability. This factor also expands the scope of applications to include lithium sulphur batteries where soluble polysulphide formation is a prominent drawback.

Structural Characterization

Confirmation of efficient polymerisation between elemental sulphur and C-a was sought utilizing UV-Vis, FTIR, Raman spectroscopy and ^{1}H-NMR analysis (Fig 2). UV Vis spectra (Fig 2a) exhibits a red shift for polymers with higher C-a content with polymer having 20% C-a content exhibiting a peak at 340 nm.

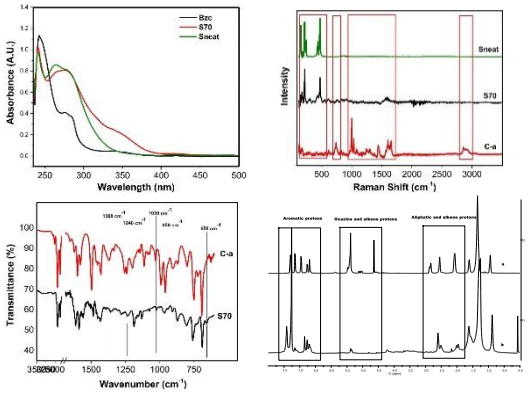


Figure 2. a) UV-Vis spectra of C-a, S70 and S; b) Raman spectra of C-a, S70 and S; c) FTIR spectra of C-a and S70 ; d) 1H-NMR of C-a and S70.

In Raman spectroscopy characteristic peaks (Fig 2b) were observed in the copolymers due to bending and stretching vibrations at 150, 220 and 472 cm^{-1} respectively accounting for the presence of S-S bonds. The characteristic benzoxazine peak at 750-770 cm^{-1} confirmed the reaction between diradical and benzoxazine. Significant observations from FTIR spectroscopy (Fig 2c) include broadening of bands at ~1240, 1350, ~1030 and 950 cm^{-1} corresponding to oxazine ring along with appearance of a band at ~658 cm^{-1} associated with the formation of C-S bond. ^{1}H-NMR spectra (Fig 2d) of all the copolymers showed absence, intensity variations and accompanied by broadening of signals at aliphatic-alkene, oxazine-alkene and aromatic region at 2-3, 4.5-5.5 and 6.5-7.5 ppm respectively suggesting reaction of polysulphane radicals at these positions in C-a and formation of copolymers. ^{1}H-NMR of C-a remain the same under the reaction conditions employed suggesting absence of homopolymerisation.

Graphene by the virtue of high specific area and excellent electronic conductivity of graphene can create a percolation network through polymer and thus remarkably improve the conductivity of sulphur copolymer.[15] Conductive filler, rGO was synthesized from graphene oxide (GO) where latter itself was derived from graphite via Hummer's method. Synthesis of rGO was carried out by Gallic acid mediated reduction of GO, making it a greener process.

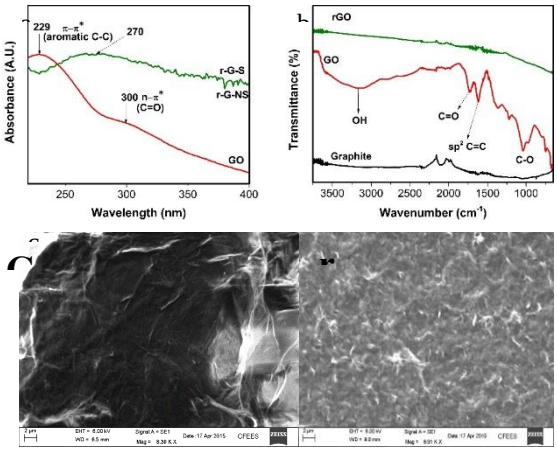


Figure 3. a) UV-Vis spectra of GO and rGO; b) FTIR spectra of GO and rGO ; c) SEM images of GO and rGO

FTIR analysis showed absence of hydroxyl, carboxyl, carbonyl, aromatic C=C, epoxy, ester stretching vibrations confirming efficient GO reduction (Figure 3a). UV-Vis analysis was also concurrent with the same showing the shift in absorbance from 230 nm (GO) to 270 nm (rGO) confirming restoration of conjugation (Figure 3b). SEM images, showed the presence of wrinkles, ripples and scrolls in the rGO sheets pointing towards synthesis of few-layered graphene sheets (Figure 3c).

Thermal Characterization

Dynamic DSC analysis (Figure 4a) of elemental sulphur exhibited two melting transitions at 109 °C and 119 °C.

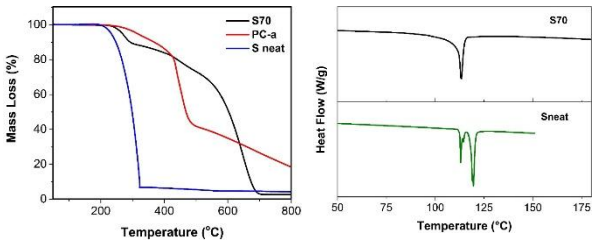


Figure 4. a) TGA of S, S70 and PC-a; b) DSC scan of S and S70

The copolymers also showed melting transitions confirming the existence of crystalline domains. Increase in C-a content on the other hand lead to the broadening of endotherms while increase in sulphur content was accompanied by a similar melting behaviour which can be attributed the formation of more crystalline domains. Thermal analysis (Figure 4b) also showed variation in decomposition steps with varying monomer and sulphur content.

Electrochemical performance

Cathode material was synthesized after doping the polysulphur and C-a copolymer with the rGO (2.5 wt%).

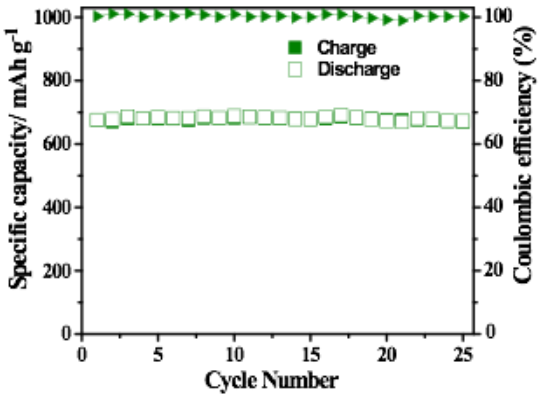


Figure 5. Cycling experiment of electrode-A at C/8 current rate

The cycling experiment was carried out in CR2032 coin cell using lithium foil as counter electrode and 0.25(M) LiTFSI + 0.1 (M) LiNO3 in 1:1 (v/v) 1,2-dimethoxyethane + 1,3-dioxolane as electrolyte. This rGO doped sulphur copolymer exhibited specific capacity of ~700 mAh/g with good capacity retention and excellent Coulombic efficiency

at C/8 rate exhibiting promising properties and scope for further exploration (Figure 5).

Conclusions

A facile, scalable and sustainable approach for the preparation of polymers based on waste materials, elemental sulphur and cardanol is demonstrated. This is a new synthetic methodology which showed maximum incorporation of elemental sulphur into a polymer demonstrating the reverse of traditional vulcanisation process. Naturally occurring phenolic compound, cardanol, was chemically modified to form benzoxazine monomer (C-a) which undergoes crosslinking reaction with polysulphane diradicals at three places oxazine ring, double bonds of the alkylene chain and the benzylic position as demonstrated by the FTIR, Raman and ^{1}H-NMR studies. The cross-linking reaction occurs via free radical addition reaction of polysulphane radicals on to the cardanol monomer, C-a, leading to formation of sulphur cross-linked polymers with different set of properties. Ring opening cross-linking reaction of C-a with elemental sulphur was further confirmed using DSC studies. Both GPC and thermogravimetry analysis suggested incorporation of sulphur into the polymer and a different polymer architecture can be achieved by altering the feed ratio of the both the monomers. Copolymers showed the possibility of both solution and melt processing leading to more opportunities of their incorporation in devices. These polymers could prove their usefulness in advanced material applications such as energy storage devices and high refractive index materials, which is currently being explored in our research group.

Acknowledgements

A.G. and S.M. are thankful to the project DST/RCUK/SGES/2012/13 (instrumental and financial supports), NCPRE funded by Ministry of New and Renewable Energy, Government of India and IRCC (instrumental support) and IIT Bombay (infrastructure). S.S. and B.L. would like to acknowledge the Shiv Nadar University and DST/BL/2014/15 (financial support).

References

1. Chung, W. J., Griebel, J. J., Kim, E. T., Yoon, H., Simmonds, A. G., Ji, H. J., Dirlam, P. T., Glass, R. S., Wie, J. J., Nguyen, N. A., Guralnick, B. W., Park, J., Somogyi, A., Theato, P., Mackay, M. E., Sung, Y.- E., Char, K. and Pyun, J., *Nat. Chem.* 5, 518-524 2013.

2. Sun, Z.; Xiao, M.; Wang, S.; Han, D.; Song, S.; Chen, G. and Meng Y., *J. Mater. Chem. A*, 2, 9280, 2014.

3. Dirlam, P. T.; Simmonds, A. G.; Kleine, T. S.; Nguyen, N. A.; Anderson, L. E.; Klever, A. O.; Florian, A.; Costanzo, P. J.; Theato, P.; Mackay, M. E.; Glass, R. S.; Char, K and Pyun, J., *RSC Adv.*, 5, 24718, 2015.

4. Duan, B.; Wang, W.; Wang, A.; Yu, Z.; Zhaob H.; Yang, Y., *J. Mater. Chem. A*, 2, 308, 2014.

5. Dirlam, P. T.; Simmonds, A. G.; Shallcross, R. C.; Arrington, K. J.; Chung, W.– J.; Griebel J. J.; Hill, L. J.; Glass, R. S.; Char, K. and Pyun, J., *ACS Macro Lett.*, 4, 111, 2015.

6. Lochab, B., Shukla, S. and Varma, I. K., *RSC Adv.*, 4, 21712, 2014.

7. Shukla, S., Mahata, A., Pathak, B. and Lochab, B., *RSC Adv.*, 5, 78071, 2015.

8. Ji, X. and Nazar, L. F., *J. Mater. Chem.*, 20, 9821, 2010.

9. Lochab, B., Varma, I. K. and Bijwe, J., *J. Therm. Anal. Calorim.*, 102, 769, 2010.
10. Hummers, W. S. and Offeman, R. E., *J. Am. Chem. Soc.*, 80**,** 1339, 1958.
11. Li, J., Xiao, G., Chen, C., Li, R. and Yan, D., *J. Mater. Chem. A*, 1**,** 1481, 2013.
12. Shukla, S., Ghosh, A., Shaligram, A., Kumar, U. K., , Prasun Kumar Roy, Sagar Mitra and Bimlesh Lochab, *ChemistrySelect*, 1, 594, 2016.
13. Ghosh, A., Shukla, S., Khosla, G. S. K., Lochab, B. and Mitra, S., *Sci. Rep.*, 6, 25207, 2016.
14. Z. Beyazkilic, M. U. Kahveci, B. Aydogan, B. Kiskan and Y. Yagci, *J. Polym. Sci. Part A: Polym. Chem.*, 50, 4029, 2012.
15. Soldano, C., Mahmood, A. and Dujardin, E., *Carbon*, 48, 2127, 2010.

MACRO 560

Synthesis and characterisation of zinc sulphide quantum dots encapsulated zeolitic imidazolate frame works-8

A. Asif * and M.S. Sreevidya

Department of Chemistry, University College, Thiruvananthapuram- 695034
**Email: asifibnuazeez@gmail.com*

Abstract
Zinc sulphide (ZnS) quantum dots (QDs) have been encapsulated in zeolitic imidazolate frame works-8 (ZIF-8) via a simple chemical co-precipitation method. The corresponding ZnS@ZIF-8 has shown good optical properties and high thermal stability. The structure and morphology of the system has been confirmed by PXRD, FTIR and SEM analysis. Well defined PXRD patterns and characteristic functional groups in FTIR spectra indicated the crystalline topology and imidazolate frame work. SEM pictures revealed the homogenous encapsulation of QDs particles with relative size ca. 100-200nm and having a hexagonal shape.

Key words*: Quantum dots, Zeolitic imidazolate frameworks, SEM, XRD, thermal stability*

Introduction

Metal–organic frameworks (MOFs) are among the most exciting, high-profile developments in nanotechnology in the last ten years. Composed of metals (or metal clusters, chains, or layers) connected by organic linkers, they show some of the highest porosities known, with pore sizes between 0.4 and 6 nm, which is ideal for capture, storage, and/or delivery applications[1]. Their promising properties coupled with the ease by which their structures can be modified make MOFs one of the most exciting, diverse, and rapidly growing areas of modern chemistry research[2].

Zeolitic Imidazolate Frameworks (ZIFs) are one important subclass of metal–organic frameworks (MOFs), where transition metals (Zn/Co) are connected tetrahedrally via the imidazolate (Im) type of linkers. Recently, a couple of approaches have been made for the incorporation of functional species (nanoparticles, oligomers, drug molecules, etc.) into MOFs/ZIFs to construct hybrid materials especially for catalytic, magnetic and optical applications.

However, many of these lack long term stability [3]. A series of zeolitic imidazolate frameworks (ZIFs) have been developed. Among them, ZIF-8 attracted much attention because of its large pores of 11.6 A° that are accessible through small apertures of 3.4 A°[4-7].

QDs offer some advantages compared with conventional chromophores, including wide absorption bands, narrow and symmetrical emission bands, low photo bleaching, long lifetimes and high quantum yields. The characteristic UV–vis exciton peak of QDs is strongly related to the size of the particle, with smaller QDs displaying shorter wavelengths and consequently fluorescence emission is tuneable. This phenomenon is often affected by the number of surface defects (referred to as trapped surface states), essentially imperfections in the crystalline structure that can lead directly to QD fluorescence quenching. Constant efforts to reduce the number of trapped states and increase the fluorescence quantum yield of the QDs are thus under investigation.

Controllable integration of MOFs and functional materials is leading to the creation of new multifunctional composites/hybrids, which exhibit new properties that are superior to those of the individual components through the collective behaviour of the functional units. This is a rapidly developing interdisciplinary research area. The applications of QD@MOF composites, which also provide an interesting platform to explore synergistic and/or symbiotic effects arising from the combination of the quantum confinement of semiconductor nanoparticles and the vast diversity of MOF compositions available, which can additionally confer higher stability to the nanoparticle.

The present work aims on the preparation and characterization of QD@MOF composites using ZnS as QDs and ZIF 8 as metal organic framework. The QDs encapsulated Zeolitic imidazolate frameworks (ZIFs) provide various applications might be expected that a composite material containing embedded photoactive particles such as QDs will be used mainly in light-dependent applications such as fluorescence sensing, photocatalysis, imaging drug release and other areas where light-induced mechanisms can be exploited.

Experimental

Zinc sulphate and Zinc nitrate (Spectrum reagents and chemicals Pvt. Ltd), Na_2S and EDTA, (Nice chemicals Pvt. Ltd), 2-methyl imidazole (Himedia Laboratories Pvt. Ltd) and Methanol (Sysco Research Laboratories Pvt. Ltd) were used as received.

Synthesis of ZnSQDs@ZIF-8

The solution consists of Zn $(NO_3)_2.6H_2O$ was slowly added to the solution of ZnS QDs and stirred for 1h. After, the solution consists of 2-methyl imidazole was dropped to the solution of Zn $(NO_3)_2.6H_2O$ and ZnS QDs under stirring. The mixture slowly turned to milky and was kept stirring for 4 h, ZnS@ZIF-8 nanocrystals were separated by centrifugation and washing with methanol for three times, to remove the unreacted reagents completely. The solids dried overnight in air oven at room temperature.

Characterization

The crystalline nature and the particle size of the synthesized samples were characterized using powder X–ray diffractometer (D8 Advanced Bruker) with Ni–filtered Cu Kα (λ = 0.154060 nm) radiation. The IR spectra of the nanoparticles were recorded on SCHIMADZU DR 43 S spectrophoto-meter using KBr pellets in the range 4000-400 cm^{-1}. The morphology of the synthesized samples was recorded on a scanning electron microscope (Nova Nano SEM 450), with an acceleration voltage of 15 kV. The Electronic spectra of the nano particles were recorded on Perkin Elmer Lambda 25 UV-Vis spectrophotometer. Photo luminescence spectra of the nano particles were recorded on Perkin Elmer Fluorescence Spectrometer. Thermo gravimetric measurements were made on Perkin Elmer Thermo gravimetric instrument, with heating rate of 20 ^{0}C/ min in an atmosphere of nitrogen in the temperature range of 0-900 ^{0}C.

RESULTS AND DISCUSSIONS

Powder X-ray diffraction (PXRD)

The crystalline nature of the prepared nano size ZnS powder is evident from the X-ray diffraction pattern (Fig 1). The most significant feature within the observed pattern, at 2θ=28.6264, is assigned to the (111) reflection of the cubic zinc blende structure of ZnS. Two other prominent features are observed at 2θ = 47.7355 and 56.5339, which belong to (220) and (311) reflections. From the X-ray patterns , the mean calculated crystallite size of the ZnS nanoparticles shows that the synthesized nanoparticles are in the quantum confinement regime as 1-3 nm. Thus, these nanoparticles may also be called the quantum dots. It is known that decreasing particle size results in a broadening of the diffraction peaks. Pure ZnS have an average particle size of 2.8 nm is calculated using XRD data and Debye-scherrer formula.

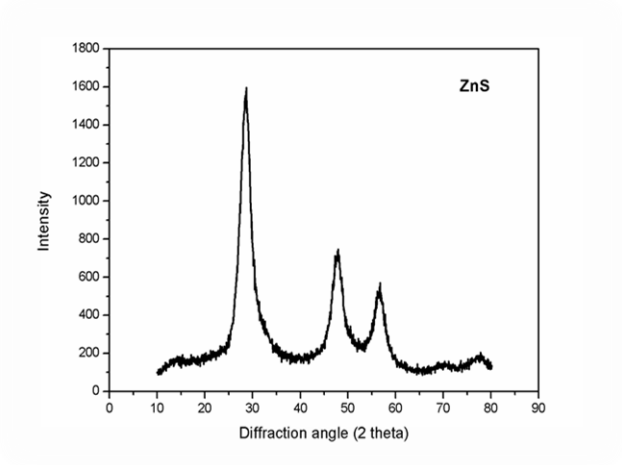


Fig 1 XRD patterns of pure ZnS nanoparticles.

The encapsulation of ZnS in ZIF-8 was further demonstrated by powder X-ray diffraction (PXRD) analysis (Fig 2). ZnS@ZIF-8 particles exhibit a similar XRD pattern compared to ZIF-8 indicating that the sodalite structure of ZIF-8 crystals remained unaffected after loading the ZnS nano particles. The XRD pattern of ZnS QDs is displayed in Figure 9. It can be identified as the cubic zinc blende structure with a comparison to the standard card (JCPDS, no. 05-0566).

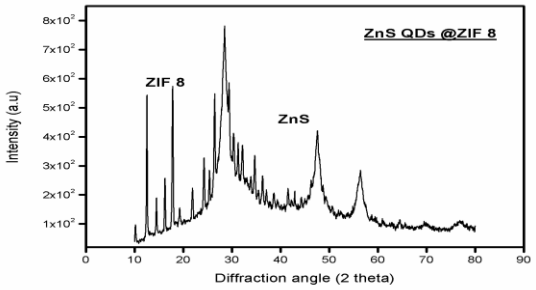


Fig 2. XRD patterns of ZnSQDs@ZIF-8 nanoparticles.

The diffraction patterns of the ZnSQDs@ZIF-8 nano composites are in perfect agreement with that of pure ZIF-8, indicating the existence of the well-defined framework units in the synthesized materials, confirming that ZnS incorporation does not disturb or destroy the formation of the ZIF-8 crystal structure. The average particle size of ZnS in ZnS QDs @ZIF- 8 is 1.73nm.

FTIR spectra

The FTIR spectrum ZnS@ZIF-8 nanoparticles are shown in Fig. 3. The characteristic major peaks of ZnS can be observed at about 1083, 925, and 644 cm^{-1} and the broad absorption peaks in the range of 3100 cm^{-1} –3600 cm^{-1} correspond to O–H stretching modes arising from the absorption of water. The peaks at 1537, 1681, 1693 cm^{-1} are due to C–H stretching mode of EDTA, which is used as the capping agent in the preparation of ZnS. The peak at 586 cm^{-1} assigned to the C=N bending mode in 2-

methylimidazole, which is the dominating ligand in the ZIF structure. The 1365 and 1090 cm^{-1} peaks correspond to the axial and transverse stretching modes of the C–N–C of the imide 5-membered ring respectively. The bands at 644 and 719 cm^{-1} in the spectral region are associated with out of plane bending of the imidazole ring. The peaks at 1537cm^{-1} attributed to the bending N–H vibration of the imidazole ring. From these spectral lines, it is assumed that ZnS QDs might have been encapsulated in ZIF-8 framework.

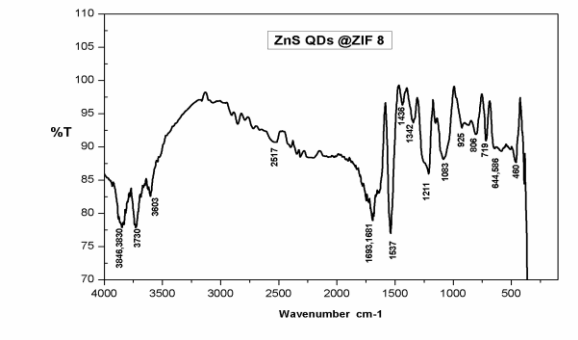


Fig 3. FTIR spectra of the ZnSQDs@ZIF-8 nanoparticles

Scanning Electron Microscopy

The SEM image of ZnSQDs@ZIF-8 nanoparticles is shown in Fig 4. The SEM micro structural analysis shows that the synthesized ZnSQDs@ZIF-8 contains mainly the grains of ZnS particles (crystallite) with regular Hexagonal shape. One can see that nearly hexagonal nanoparticles have an almost homogenous size distribution with a mean size of 75 nm. Incorporation of EDTA as capping agent causes the stabilization of the small ZnS particles and the inhibition of this agglomeration.

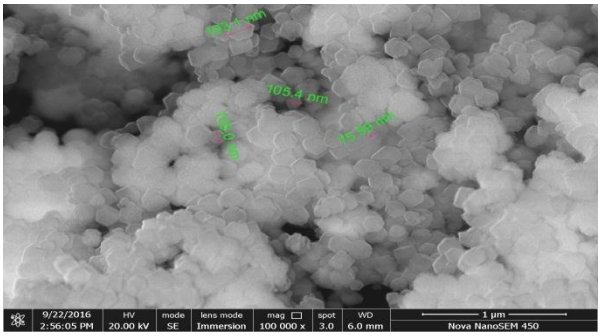


Fig 4. SEM images of ZnSQDs@ZIF-8 nanoparticles.

UV- Visible spectra

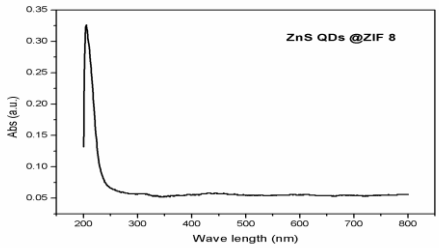


Fig 5. UV-Vis absorption spectra of ZnSQDs@ZIF-8 nanoparticles

Fig 5 represents the UV-Visible spectra of ZnSQDs @ZIF-8. It has a strong absorption band centered at 221 nm. Compared to free ZnS QDs nanoparticle, which shows absorption peak around 320 to 345nm, the encapsulation causes a blue shift in absorption indicating that ZnS is encapsulated into the framework of ZIF-8.

Photoluminescence (PL) Spectra

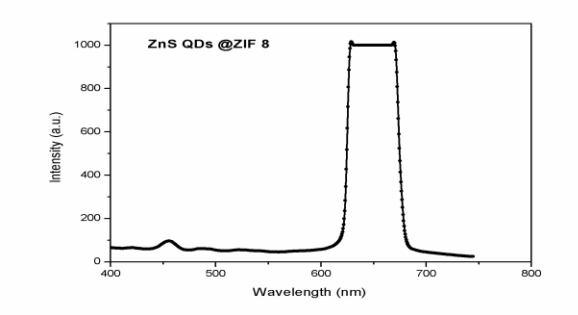


Fig 6. PL spectra of the ZnSQDs@ZIF-8 nanoparticles

The room temperature photo-luminescence spectrum of ZnS QDs@ZIF-8 for excitation wavelength of 221nm is shown in Fig 6, which shows strong emission peak at longer wavelength of about 650 nm and a less intense emission peak at 460 nm. The emission at 650 nm may be caused by the transition from the conduction band to the zinc vacancies in the lattice. It is reported that appearance of emission peak at 460 nm is attributed to the presence of sulphur vacancies.

Thermo gravimetric Analysis (TGA)

The thermo gravimetric analysis (TGA) of ZnSQDs@ZIF-8 was performed under nitrogen flow is shown Fig 15. As shown in Fig 7, a long plateau with less than 10% weight loss is observed in the temperature range of 50−400 °C indicating the high thermal stability of ZnS@ZIF-8. Thermo gravimetric analysis (TGA) indicates that ZnS@ZIF-8 particles have a slightly lower stability than ZIF-8 crystals. For ZIF-8, the sharp weight loss was observed at ca. 500°C, corresponding to the decomposition of the 2-methyl imidazole (Hmim) linker. A gradual weight loss of 17.79 % up to 636 °C is observed. The relatively lower decomposition temperature of ZnSQDs@ZIF-8 (473°C) compared to pure ZIF-8 might be attributed to the gradual decomposition of the EDTA molecule, used as capping agent in ZnS nanoparticles, between 473 °C and 636 °C.

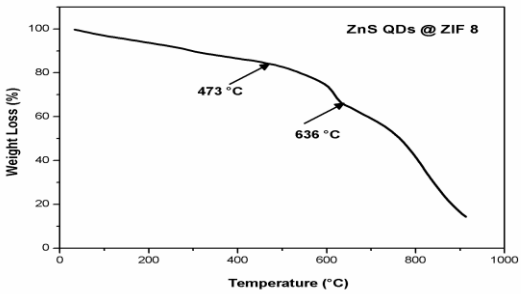


Fig 7. TGA curve of ZnSQDs@ZIF-8 nanoparticles

Conclusions

In the present study, ZnS QDs was successfully encapsulated in to the zeolitic imidazolate frame works such as ZIF-8 and the ZnS QD@ZIF-8 are characterized by FTIR, UV, PL, XRD, TG, and SEM. Overall the study suggest that QD@ZIF-8 has wide

applications and used as photo catalyst, super capacitors, sensing etc.

References

1. Alistair C, McKinley, Russell E. Morris, Patricia Horcajada, Grard Frey, Ruxandra Gref, Patrick Couvreur, and Christian Serre, *Angew. Chem. Int. Ed.* 2010, 49, 6260 - 6266.
2. Inhar Imaz, Marta Rubio-Martı´nez, Jihyun An, Isabel Sole´-Font, Nathaniel L. Rosi and Daniel Maspoch, *Chem. Commun.*, 2011, 47, 7287-7302 .
3. Bishnu P. Biswal, Dhanraj B. Shinde, Vijayamohanan K. Pillai and Rahul Banerjee, *Nanoscale*, 2013, 5, 10556-10561.
4. Yi Han, Jian-Rong Li, Yabo Xie and Guangsheng Guo, *Chem. Soc. Rev.*, 2014, 43, 59520-5981.
5. Iewei Liu, Lianfen Chen, Hao Cui, Jianyong Zhang, Li Zhang and Cheng-Yong Su, *Chem. Soc. Rev.*, 2014, 43, 6011- 6061.
6. Shilun Qiu, Ming Xue and Guangshan Zhu, *Chem. Soc. Rev*., 2014, 43, 6116-6140.
7. Chih-Wei Tsai, Ernie H.G. Langner, *j.micromeso.*2015.08.041 1387- 1811.

1. S. J. Toal, W. C. Trogler, *J. Mater. Chem.* 16, 2871 – 2883, 2006.
2. Z. Xiang, D. Cao, *J. Mater. Chem. A*, 1, 2691, 2013.
3. S. Ren , M. J. Bojdys , R. Dawson, A. Laybourn , Y. Z. Khimyak , D. J. Adams, A. I. Cooper, *Adv.mater*. 24, 2357-2361, 2012.
4. H. Lim, M. C. Cha, J. Y. Chang *Macromol. Chem. Phys.* 213, 1385−1390, 2012,
5. P. Puthiaraj, S-S. Kim, W-S Ahn *Chem. Eng.*, 283, 184-192, 2016.
6. S. Dey, A. Bhunia, M. D. Esquivel C. Janiak, *J. Mater. Chem. A*, 4, 6259–6263, 2016.
7. J. R Lakowicz Principles of Fluorescence Spectroscopy, Plenum Press. New York and London,1986
8. J. Liu, Y. Zhong, P. Lu, Y. Hong, J. W. Y. Lam, M. Faisal, Y. Yu, K. S. Wong, B. Z. Tang, *Polym. Chem.*, 2010, 1, 426-429.



FOCUS AREA

GREEN, SUSTAINABLE AND BIOPOLYMERS

MACRO 113

Metal organic frameworks as accelerators for ring opening polymerisation of bio-based benzoxazines

Sharma Pratibha [a,b], Srivastava Manju [a,c], Lochab Bimlesh [d], Kumar Devendra [b], Ramanan Arunachalam [c], Roy Prasun Kumar [a*]

[a]*Centre for Fire, Explosive and Environment Safety, DRDO, Timarpur, Delhi 110054, India.*
[b]*Department of Applied Chemistry and Polymer Technology, Delhi Technological University, Delhi 110042, India.*
[c]*Department of Chemistry, Indian Institute of Technology Delhi, New Delhi-16, India*
[d]*Department of Chemistry, School of Natural Sciences, Shiv Nadar University, UP 201314, India.*
** E-mail addresses:pk_roy2000@yahoo.com*

Abstract

Benzoxazine resins offer attractive properties but suffers from a major drawback associated with its high curing temperature. MOF5, exhibits Lewis acidic Zn_4O nodes, therefore we considered it of interest to explore its potential as a curing accelerator for a representative biobased benzoxazine resin. MOF5 was solvothermally synthesized and characterized. Introduction of MOF5 led to a shift in the curing profile of benzoxazine resin to lower temperature, the extent of which was proportional to the amount of MOF5 in the formulation. In addition, other MOFs like copper terephthalate and HKUST 1 were also evaluated for their ability to accelerate the curing process. The activation energy for curing, as calculated using Kissinger Akahira Sunose method, was found to concomitantly decrease upon addition of MOF5 (5% w/w).

Keywords: *MOF5, 1,3-benzoxazine, accelerator, ring-opening polymerization*

Introduction

Metal organic frameworks (MOFs) are a rapidly developing class of microporous materials, which are finding increasing applications in varied fields including gas adsorption[1], separation, chemical sensing and catalysis[2-4]. Inherent characteristic properties of MOFs, particularly in terms of their ultra-high surface areas, possibility of pore structure modification and a high degree of chemical and thermal stability bestow them excellent candidature for the aforementioned applications. One such application, of particular interest to our group, concerns catalytic curing of bio-based benzoxazine resins[5-7].

Benzoxazines are capable of undergoing ring-opening polymerization reaction [8-10] to form cross-linked networks with exceptional thermal stability[9,11,12]. However, majority of benzoxazine resins polymerize at elevated temperatures[13,14] which is definitely a matter of concern for practical applications. Sudo et.al[14] studied the efficiency of acetylacetonato complexes of 4th period transition metals as catalysts for ring opening polymerisation of benzoxazine. The examination revealed that acetylacetonato complexes of manganese, iron, cobalt and zinc exhibited the highest activity, which inspired us to explore the potential of zinc based MOFs in the context of curing of benzoxazine monomer [14]. The possibility of tailoring the chemical environment around the metal centre with exceptionally high surface area of MOFs leave enormous scope for these MOFs in the context of catalysis.

MOF5 is a three dimensional zinc carboxylate framework ($[Zn_4O(BDC)_3]$, BDC = 1,4-benzenedicarboxylate), reported by Yaghi et.al[15]. The crystal structure of MOF 5 is comprised of oxocentered Zn_4O nodes, connected through linear BDC units forming an extended 3D cubic network with interconnected pores of 0.9 nm. Zinc oxide clusters (Zn_4O) of atomic precision, which are available throughout the framework confer it excellent candidature for applications where acidic catalysis is desirable which has led researchers to explore its potential in representative applications e.g. Friedel craft reaction[16-18]. Although application of MOF's as heterogeneous catalysts has been well reported[19-22], studies concerning their ability to accelerate the polymer curing reactions are virtually absent.

Herein, we report the exploration of the potential of MOFs towards accelerating the ring opening polymerization of cardanol based monofunctional benzoxazine resin. Differential Scanning Calorimetric (DSC) analysis was performed to quantify the extent of acceleration in the ring opening polymerization behavior.

Experimental

Materials

Cardanol was obtained from Satya Cashew Chemicals Pvt. Ltd. (India). Zinc acetate dihydrate ('AR', E.Merck), Copper nitrate trihydrate ('AR', E.Merck), Copper acetate trihydrate ('AR', E.Merck), 1,4-benzene dicarboxylic acid (BDC) ('AR', Aldrich), Benzene-*1,3,5*-tricarboxylic acid (BTC) (Aldrich) and N,N-dimethyl formamide (DMF) (HPLC grade, Aldrich), 2-methyl imidazole (MeIm) ('AR', Aldrich) was used without further purification. Paraformaldehyde, aniline, sodium sulphate, zinc dust, zinc oxide and chloroform from CDH were used as received. Double distilled water was used throughout the course of this work.

Characterization method

Calorimetric studies were performed on a Differential Scanning Calorimeter (TA instruments Q 20).

Results and discussion

Benzoxazine monomers undergo thermally accelerated cationic ring opening polymerisation leading to the formation of a thermally stable crosslinked polymer. The ring opening polymerisation has been reported to be auto catalytic as the phenolic -OH generated in situ act as an additional initiator. Accelerators employed, alleviates the kinetics of the oxazine ring opening stage through several proposed mechanisms [8,28-32]. To investigate the curing behavior of the benzoxazine resins in the presence of accelerators, non-isothermal calorimetric studies were performed and the representative curing profiles of formulations containing MOF5 are presented in Figure 1.

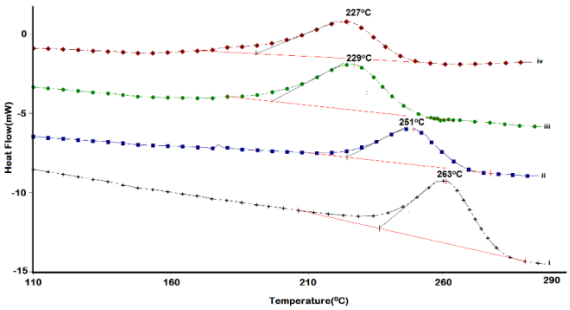


Figure 1: DSC curves for i) C-a, ii) M1C-a, iii) M5C-a and iv) M10C-a

It can be seen that the curing of the synthesized cardanol based benzoxazine exhibits a peak at 263°C (Figure 1(i)). There was a pronounced shift in the curing profile towards lower temperature upon addition of MOF 5, the extent of which was found to be proportional to MOF5 loading. The ability of MOF5 to accelerate the curing process can be credited to the presence of acidic Zn_4O nodes of the MOF5 crystal lattice. To gain insight on the role of the chemical environment around the central zinc species, curing studies were also performed in the presence of Zn, ZnO, BDC and another zinc based metal organic framework ZIF8, with high surface area (900 m^2/g) but differing predominantly with respect to the chemical environment around the central zinc atom. ZIF8 reportedly features a sodalite topology (Si-O-Si bonds in zeolites being replaced by Zn-Im-Zn bonds) with cavities of diameter 1.16 nm, connected via 6- and 4-ring apertures[33,34].

Another set of experiment was performed using two MOFs, HKUST-1 and Cu(BDC).DMF. The selection for the study stemming from the similarity in the nature of ligand i.e. BDC for copper terephthalate and BTC for HKUST-1. Copper terephthalate exhibits a sheet type structure in which the Cu^{II} atoms are coordinated to the terephthalic acid linkers specific planes which are bonded through weak stacking interactions. HKUST-1 is made up of interconnected $[Cu_2(O_2CR)_4]$ units (where R is an aromatic ring), creating a three dimensional network with a pore size of 1nm. The building block of HKUST-1 comprises of Cu^{2+} dimer coordinated with four oxygen atoms of benzene tricarboxylate forming a paddle wheel type structure.

The DSC traces associated with the curing of benzoxazine in the presence of different MOFs is presented in Figure 2. It can be seen that among all the MOFs studied, MOF5 led to the maximum decrease in the curing temperature,

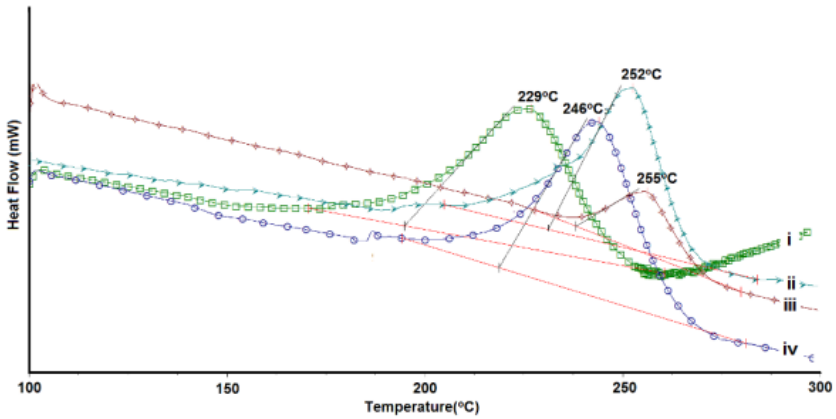


Figure 2: DSC traces i) M5C-a, ii) H5C-a, iii) CT5C-a and iv) Z5C-a

The results of the DSC analyses in terms of characteristic curing temperatures are summarized in Table 1.

Acids, such as BDC have been reported to accelerate oxazine ring opening by the preferable protonation of oxygen atom generating a reactive species which undergoes condensation with the phenolate or other benzoxazine molecule resulting in phenolic structure (Figure 3(ii)).

Table 1: Effect on introduction of accelerators on characteristic curing temperatures (β=10°C/min)

Sample designation	T_o (°C)	T_{10} (°C)	T_{50} (°C)	T_{peak} (°C)	% Decrease in terms of T_{peak}	% Decrease in terms of T_o
C-a	240	235	250	263	-	-
BDC10C-a	231	224	240	253	2.6	3.7
ZnO10C-a	214	206	223	237	4.9	10.8
Zn10C-a	220	212	231	244	6	8.3
Z5C-a	218	197	218	246	6.5	9.1
CT5C-a	237	228	253	255	2.7	1.2
H5C-a	230	219	239	252	4.2	4.2
M1C-a	228	214	234	251	4.8	5
M5C-a	184	185	210	229	12.8	23.3
M10C-a	178	168	206	227	13.6	25.8
M15C-a	231	223	237	248	5.7	3.7

Metal centered accelerators such as metal oxides and MOFs accelerate benzoxazine polymerisation through the formation of aryl ether structures (Figure 3(iii)). The curing of benzoxazine in the presence of MOF5 as accelerator is proposed to proceed through coordination of zinc present in the Zn_4O cluster with the benzoxazine oxygen atom resulting in the formation of reactive iminium species. The electrophile generated condenses with other benzoxazine molecule resulting in unstable aryl ether structure which rearranges to more stable phenolic structures at elevated temperature (Figure 3(iv)).

As is evident from Table 1, among all the additives studied, MOF5 leads to the most pronounced decrease in the curing temperature of C-a. However, increasing the amount of MOF5 beyond 5%, does not lead to any considerable decrease in the curing temperature further.

In view of the same, M5C-a was chosen for establishing the kinetic parameters associated with the polymerisation reaction.

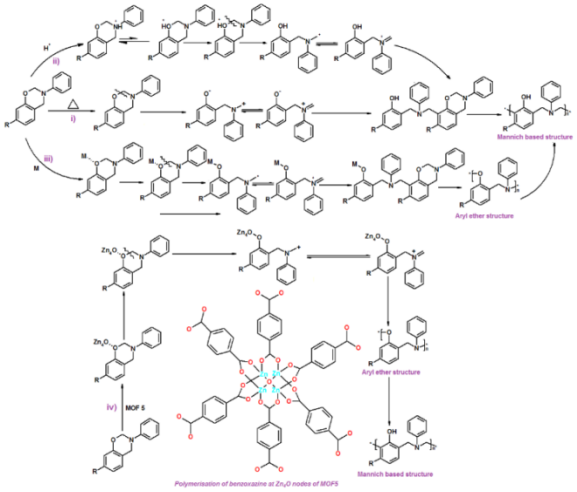


Figure 3: Probable mechanisms i) thermally accelerated polymerisation of benzoxazine resin ii) polymerization by protonation iii) polymerization in the presence of metal based accelerators iv) polymerization in the presence of Lewis acidic Zn_4O nodes present in MOF5

It is interesting to note that ZIF8, although containing the same metal centre (Zn) and exhibiting high surface area did not lead to any substantial curing acceleration of the benzoxazine in terms of decrease in the curing temperature. ZIF8, comprises of individual Zn nodes as against Zn_4O nodes available throughout the MOF5. In addition, the presence of Cu(BDC) and HKUST-1, does not lead to any substantial decrease in the curing temperature. Our studies lead us to believe that, it is primarily the availability of the acidic Zn_4O nodes in MOF5, which is responsible for the acceleration of the benzoxazine curing.

The DSC traces of a representative formulation (M5C-a) at various heating rates viz. 5, 7 and 10 °C/min are presented in Figure 4. Increasing the heating rate (β) leads to systematic shift in the trace towards higher temperatures, which can be attributed to the reduced time available with the reactive molecules. The characteristic parameters associated with the curing of the resin i.e. ΔH_{cure}, T_{onset} and T_{peak} are summarized in Table 2.

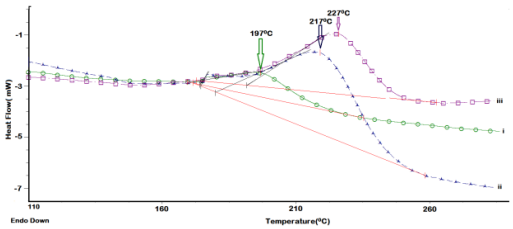


Figure 4: Effect of heating rate (β) on the curing profile of M5C-a a) 5, b) 7 and c) 10 °C/min.

The extent of conversion, α at any particular temperature (T_α) was calculated as the ratio of the areas under the exothermic DSC peak and expressed as:

$$\alpha = \frac{\Delta H_{T_\alpha}}{\Delta H_{cure}} \quad \ldots\ldots\ldots\ldots\ldots\ldots 1$$

where ΔH_{T_α} is the heat of reaction of partially cured samples (till temperature T_α) and ΔH_{cure} is the total heat of curing. The increase in the degree of conversion with temperature for C-a and M5C-a at a particular heating rate (5°C/min) is presented in Figure 5. It can be seen that the complete curing of neat monomer is achieved at 280°C while in the presence of MOF5, the same is attained at 230°C, which is indicative of the ability of MOF5 as an accelerator for curing of benzoxazines.

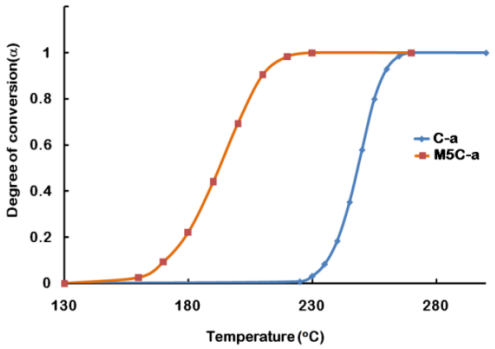


Figure 5: Effect of temperature on the degree of conversion of cardanol based benzoxazine in the presence and absence of MOF 5 (β = 5 °C/min).

In view of its simplicity, Kissinger–Akahira–Sunose equation[35] was applied for determination of activation energies (E_α) from the plot of $ln\left(\frac{\beta_i}{T_{\alpha,i}^2}\right)$ against $1/T_\alpha$.

$$ln\left(\frac{\beta_i}{T_{\alpha,i}^2}\right) = \text{Constant} - \frac{E_\alpha}{RT_{\alpha,i}} \quad \ldots\ldots\ldots\ldots\ldots\ldots 2$$

Where, β is the heating rate, T_α is the temperature associated with a particular conversion (α) at the corresponding heating rate, E_α is the activation energy at that α and R is the gas constant.

Table 2: Characteristic curing parameters of neat benzoxazine and M5C-a

Sample	β (°C/min)	T_{onset} (°C)	T_{peak} (°C)	Activation energy α= 10% (kJ/mol)
	5	224	246	
C-a	7	236	255	98
	10	241	263	
	5	173	196	
M5C-a	7	178	217	58
	10	184	229	

The presence of MOF 5 led to a substantial decrease in the activation energy from 98 kJ/mol (for neat resin) to 58 kJ/mol (M5C-a).

Conclusion

The accelerating ability of MOF 5 on the ring opening polymerisation of a representative biobased cardanol- benzoxazine(C-a) was systematically studied. The presence of MOF 5 was found to decrease the curing temperature of neat benzoxazine from 263 °C to 229°C (12.6 % decrease). Our studies indicate that Zn_4O nodes of atomic precision, which are available throughout the framework, are responsible for the decrease in the curing temperature. KAS method was used to

determine the activation energy of polymerization, which was found to decrease from 98 kJ/mol (neat resin) to 58 kJ/mol for formulation containing MOF 5 (5%w/w).

References

1. Mallick, A.; Saha, S.; Pachfule, P.; Roy, S.; Banerjee, R., J. Mater. Chem. 20, 9073 2010.
2. Zhang, Z.; Zhao, Y.; Gong, Q.; Li, Z.; Li, J., Chem. Commun. 49, 653 2013.
3. Qiu, S.; Xue, M.; Zhu, G., Chemical Society Reviews 43, 6116 2014.
4. Li, J.-R.; Kuppler, R. J.; Zhou, H.-C., Chem. Soc. Rev. 38, 1477 2009.
5. Sharma, P.; Lochab, B.; Kumar, D.; Roy, P. K., J. Appl. Polym. Sci. 1322015.
6. Sharma, P.; Shukla, S.; Lochab, B.; Kumar, D.; Kumar Roy, P., Mater. Lett. 133, 266 2014.
7. Arslan, M.; Kiskan, B.; Yagci, Y., Macromolecules 48, 1329 2015.
8. Riess, G.; Schwob, J. M.; Guth, G.; Roche, M.; Laude, B. In Adv. Polym. Syn.; Culbertson, B. M.; McGrath, J. E., Eds.; Springer US: Boston, MA, 1985.
9. Ning, X.; Ishida, H., J. Polym. Sci., Part A: Polym. Chem. 32, 1121 1994.
10. Yagci, Y.; Kiskan, B.; Ghosh, N. N., J. Polym. Sci., Part A: Polym. Chem. 47, 5565 2009.
11. Ishida, H.; Allen, D. J., J. Polym. Sci., Part B: Polym. Phys. 34, 1019 1996.
12. Ishida, H.; Sanders, D. P., J. Polym. Sci., Part B: Polym. Phys. 38, 3289 2000.
13. Ishida, H.; Rodriguez, Y., J. Appl. Polym. Sci. 58, 1751 1995.
14. Sudo, A.; Hirayama, S.; Endo, T., J. Polym. Sci., Part A: Polym. Chem. 48, 479 2010.
15. Li, H.; Eddaoudi, M.; O'Keeffe, M.; Yaghi, O. M., Nature 402, 276 1999.
16. Phan, N. T. S.; Le, K. K. A.; Phan, T. D., Applied Catalysis A: General 382, 246 2010.
17. Lee, J.; Farha, O. K.; Roberts, J.; Scheidt, K. A.; Nguyen, S. T.; Hupp, J. T., Chemical Society Reviews 38, 1450 2009.
18. Akimbekov, Z.; Wu, D.; Brozek, C. K.; Dinca, M.; Navrotsky, A., PCCP 18, 1158 2016.
19. Lee, J.; Farha, O. K.; Roberts, J.; Scheidt, K. A.; Nguyen, S. T.; Hupp, J. T., Chem. Soc. Rev. 38, 1450 2009.
20. Gao, S.; Zhao, N.; Shu, M.; Che, S., Appl. Catal., A 388, 196 2010.
21. Czaja, A. U.; Trukhan, N.; Müller, U., Chem. Soc. Rev. 38, 1284 2009.
22. Sabo, M.; Henschel, A.; Fröde, H.; Klemm, E.; Kaskel, S., J. Mater. Chem. 17, 3827 2007.
23. Lochab, B.; Varma, I. K.; Bijwe, J., J. Therm. Anal. Calorim. 102, 769 2010.
24. Manju; Kumar Roy, P.; Ramanan, A.; Rajagopal, C., Materials Letters 106, 390 2013.
25. Manju; Roy, P. K.; Ramanan, A.; Rajagopal, C., RSC Adv. 4, 17429 2014.
26. Majano, G.; Pérez-Ramírez, J., Helv. Chim. Acta 95, 2278 2012.
27. Manju; Roy, P. K.; Ramanan, A., RSC Adv. 4, 52338 2014.
28. Dunkers, J.; Ishida, H., J. Polym. Sci., Part A: Polym. Chem. 37, 1913 1999.
29. Sudo, A.; Kudoh, R.; Nakayama, H.; Arima, K.; Endo, T., Macromolecules 41, 9030 2008.
30. Chutayothin, P.; Ishida, H., Macromolecules 43, 4562 2010.
31. Liu, C.; Shen, D.; Sebastián, R. M.; Marquet, J.; Schönfeld, R., Macromolecules 44, 4616 2011.
32. Wang, Y.-X.; Ishida, H., Macromolecules 33, 2839 2000.
33. Pan, Y.; Liu, Y.; Zeng, G.; Zhao, L.; Lai, Z., Chem. Commun. 47, 2071 2011.
34. Srivastava, M.; Roy, P. K.; Ramanan, A., RSC Adv. 6, 13426 2016.
35. Budrugeac, P.; Segal, E., Journal of Thermal Analysis and Calorimetry 88, 703 2007.

MACRO 112

Mesoporous and Hollow Polymers Nanostructure for Drug Delivery

Paik Pradip*

[a]*School of Engineering Sciences and Technology, University of Hyderabad , Hyderabad 500 046*

** Corresponding author's email i.d.: pradip.paik@gmail.com, ppse@uohyd.ernet.in, paik@uohyd.ac.in*

In this work, a series of amino acid based block-co-polymers have been synthesized through ring-opening polymerization and characterized through H^1 NMR, MULDI-TOF, and CD spectroscopy. These polymers further have been utilised for creating nanostructure mesoporous polymers of PCL and inorganic polymers. The pore size of the mesostructured are found to be 4-5 nm and with hollow core of 120-150 nm in diameter with an overall diameter of the capsules of 200-250 nm. The final nanocapsules are found to be biocompatible c.a. 95% which has been measure through MTT assay. Further the mesoporous of the nanocapsules of polymers are characterized and found to be chiral in nature. That is the pores are chiral pores. These chiral mesoporous polymer capsules are suitable for chiral resolution and stereo selective chiral recognition useful for chiral memory applications [1,2]. The second part of this work is on the hollow and porous structure of polymer Nano capsules. These special nanocapsules were used to design the nanoformulation with the siRNA, DNA and various anticancer drugs e.g, DOX, imatinib etc. The kinetics of release studied revealed that these nanoformulation exhibits sustained delivery of medicines at various pH and temperatures. Based on these results the Nano formulations were used to challenge the carcinoma cells such as leukaemia (K562), kidney and liver cancer (HepG2) cells. The cell based studies exhibited a potential improvement of IC_{50} against the cancer cells with low doses of nanoformulations with respect to the free drugs and exits a very high mortality of cancer cells (up to ~96.6%). Our nanoformulations arrest the cell divisions due to "*cellular senescence"* and kill the cancer cells specifically through apoptosis. Our findings could be enriched the effectiveness of idiosyncratic, hollow nanoporous polymer capsules to use them in various other nanomedicinal and biomedical applications such as for killing cancer cells, immune therapy and gene delivery [3-5].

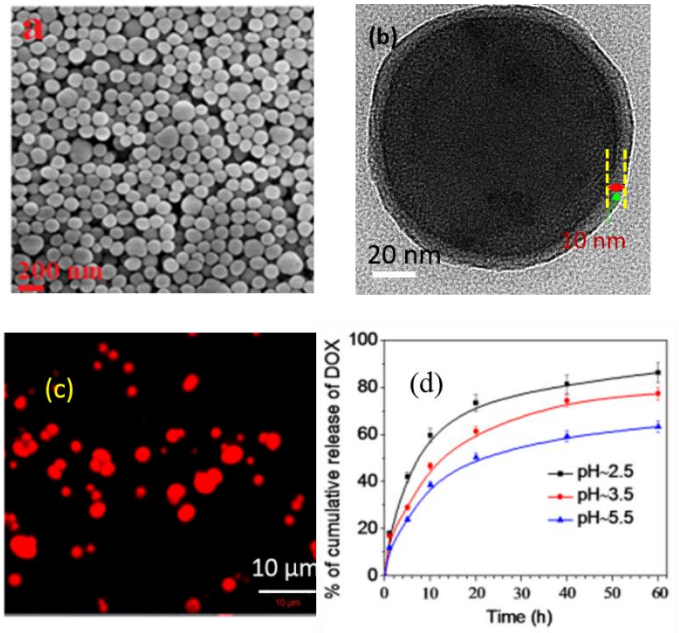


Figure 1 (a) Representative SEM image (b) HRTEM image for polymer nanocapsules. (c) confocal microscopy image for nanoformulation of anticancer drugs and (c) release kinetics for nanoformulation used for anti-cancer treatment.

References

1. Paik, Pradip Paik; Gedanken Aharon; Mastai, Yitzhak Mastai. *Journal of Materials Chemistry*, 20 (2010) 4085.
2. Paik, Pradip Paik; Gedanken Aharon; Mastai, Yitzhak Mastai, *ACS Applied Materials & Interfaces*, 1(8) (2009), 1834.
3. Paik, Pradip Paik; Zhang,Yong *Nanoscale, 3 (*2011)2215.

4. Vijay Bhooshon Kumar, Aharon Gedanken, Pradip Paik. Facile Synthesis of Self-Assembled Spherical and Mesoporous Dandelion Capsules of ZnO: Efficient Carrier for DNA and Anti-cancer Drugs, *J. Mater. Chem. B*, 2014, 2, 3956.
5. Kumar, Vijay Bhooshon; Medhi, Himadri; Zhang, Yong; Paik, Pradip Paik. *Nanomedicine: Nanotechnology, Biology, and Medicine 12(3 201,)579.*

MACRO 126

Galactitol Based Polyesters for Biomedical Applications

Janeni Natarjan[1], Sahitya Movva[2], Kaushik Chatterjee[3], Giridhar Madras[2*]

[1]*Centre for Nano Science and Engineering, Indian Institute of Science, Bangalore 560012, India*
[2] *Department of Chemical Engineering, Indian Institute of Science, Bangalore 560012, India*
[3]*Department of Materials Engineering, Indian Institute of Science, Bangalore 560012, India*

** Corresponding author. E-mail address: giridhar@chemeng.iisc.ernet.in (G. Madras)*

There is always a need for investigating perfect biomaterials though we have made significant advances in drug delivery and tissue engineering applications. Subsequently, the objective of this study is to synthesize a novel polyester poly (galactitol adipate) and form a crosslinked network by adding various monomers like tartaric acid, citric acid etc to improve the mechanical properties and decrease the degradation rate of the polyesters. Galactitol and adipic acid are bio-degradable and biocompatible. They are endogenous to human metabolism. While hydrolysis of lactose gives glucose and galactose, galactose on further reduction produces galactitol. Adipic acid is easily removed from the body by β-oxidation pathway. Both of them are non-toxic in nature and have a low cost. Hence, they make a good choice to synthesize a novel polyester. FT-IR confirmed the presence of ester bond in all the polyesters. ^{1}H NMR confirmed the chemical structure of the polymer synthesized. Thermal characterization was performed by DSC disclosing that the polymers have amorphous nature and the cross-linking increases the glass transition temperature. Contact angle measurements revealed that the cross-linker gives hydrophobic nature to the polyester. *In vitro* hydrolytic degradation studies and dye release studies showed that addition of cross-linker to the polymer imparted hydrophobic nature and hence decreased the rate of degradation of the polyester. *In vitro* cell studies confirmed the cytocompatibility nature of the polyesters. Tailored degradation, release and cytocompatibility properties make them promising materials for use in drug delivery and tissue engineering.

Keywords: Polymer cross-linking, Poly (galactitol adipate), Cytocompatible, Drug delivery, Tissue Engineering

References

[1] Natarajan, Janeni; Chatterjee, Kaushik; Madras, Giridhar. *Int. J. of Bio. Macro.*, (2016).

[2] Cao, N; Chen, X; Schreyer, D. *ISRN Chem. Eng. 2012* (2012).

[3] Chen, B; Liu, M; Zhang, L; Huang, J; Yao, J; Zhang, Z; *J. Mater. Chem.*, 21 (2011)7736–7741.

MACRO 137

Electrospun Matrices from Advanced Emulsion Electrospinning Approach

Archana Samanta,[a] Bhanu Nandan,[a] Rajiv Srivastava*[a]

[a] *Department of Textile Technology, Indian Institute of Technology-Delhi, Hauz Khas, New Delhi 110016 India*

** e-mail id: rajivsriva@gmail.com*

Abstract

An approach for production of electrospun matrices from a hydrophobic polymer with minimized solvent content is reported. Electrospun matrices from advanced emulsion i.e, High Internal Phase Emulsions (HIPE) with aqueous dispersed phase volume fraction over 0.74 and Pickering emulsions with minimized organic solvent, without emulsifier systems were adopted to electrospun poly(ε-caprolactone) meshes as a path forward towards green electrospinning technology. Pickering emulsions use solid particles instead of emulsifiers to stabilize emulsions. Hence inclusion of a Pickering agent helped in enhancing mechanical properties of the composite electrospun matrices.

Keywords: *HIPE, Pickering*

Introduction

Electrospinning is a simple technique to generate fibers with versatile properties. High surface area to volume ratio, innate porosity, controlled fiber fineness aids to the aptness of the electrospun meshes in the field of filtration, membrane separation, scaffolds for tissue engineering[1],[2] and others. Parameters like voltage, flow rate of polymer solution, needle to collector distance paly a paramount role in controlling fiber morphology.

With the advent of eco-friendly and intensification of sustainable technologies, the need of the day encourages on the minimized usage of toxic solvents in the electrospinning system too. Usage of water is not an issue of concern for producing electrospun composite matrices from hydrophilic polymer like polyvinyl alcohol, poly ethylene oxide, poly ethylene glycol and others. But for

hydrophobic polymers like poly styrene, poly caprolactone, poly acrylonitrile, usage of organic solvents is a mandatory compulsion[3].

Emulsion, Clay, composite, crystallinity Emulsion electrospinning is a novel concept which can be adopted to minimize the usage of organic solvents. There are handful of literature on emulsion electrospinning. A novel concept of High internal phase Emulsion (HIPE) electrospinning was adopted in this study with aqueous phase volume fraction over 0.74 Pickering emulsion can be considered an advantage over conventional emulsion systems which does not require a surfactant to stabilize the emulsion. Instead of surfactants solid particles are used to stabilize the oil water interfaces[4]. Unlike surfactants, such solid particles are not soluble in aqueous media and notably the addition of these particles can enhance functionality of the system which can later be channelized to the electrospun fibers system.

Instead of conventional process of composite fiber formation using polymer-solvent electrospinning, an innovative and sustainable approach of High Internal Phase Emulsion (HIPE) with volume fraction of aqueous dispersed phase over 0.74 and Pickering emulsion electrospinning is adopted without the usage of any water soluble template polymer or surfactant with minimized usage of organic solvents.

Experimental

Materials

Poly(ε-caprolactone) (PCL) with average molecular weight (sigma Aldrich Mn=80,000 g/mol), Poly(vinyl alcohol) (PVA) (average molecular weight Mw=125,000 g/mol, CDH India), Brij-58 (non-ionic emulsifier, having linear formula $HO(CH_2CH_2O)_{20}C_{16}H_{33}$ and reported number average molecular weight Mn = 1124 g/mol) (Sigma Aldrich India), DI water (Millipore India), toluene (Merck India) were used as received without any purification. Shelsite 30B, modified montmorillonite clay of purity 99% and average particle size 80 nm (as reported by supplier) and unmodified montmorillonite clay were purchased from Nanoshel LLC, Wilmington, DE, USA, and Human breast cancer cell line (MCF7, a kind gift from Indianapolis University, source ATCC) were maintained in RPMI 1640 (GIBCO) medium supplemented with 10 % FBS (Fetal Bovine Serum) and 1 % penstrep.

Results and discussion

HIPE electrospinning and factors governing morphology of fibers

Preparation of HIPE

Organic phase was made of PCL and Brij-58 solution in toluene. Aqueous phase was made by dissolving PVA in DI water. Aqueous phase was added drop wise to the oil phase in pre-determined volume fractions (oil: aqueous phase at 0.26: 0.74, 0.85: 0.15 or 0.90: 0.10) under a high speed homogenizer (IKA Ultra Turrax T25) operating at 15000rpm

Stable water-in-oil High Internal Phase Emulsions (HIPE) of PCL and PVA were obtained using Brij-58 as the emulsifier. Optical microscopic images Figure 1 showed an increase in dispersed

phase droplet size with increase in volume fraction of dispersed phase (Φ_d) (from 0.74 to 0.9). All HIPEs were then subjected to electrospinning. The morphology of the fibres was observed under SEM, figure 1.

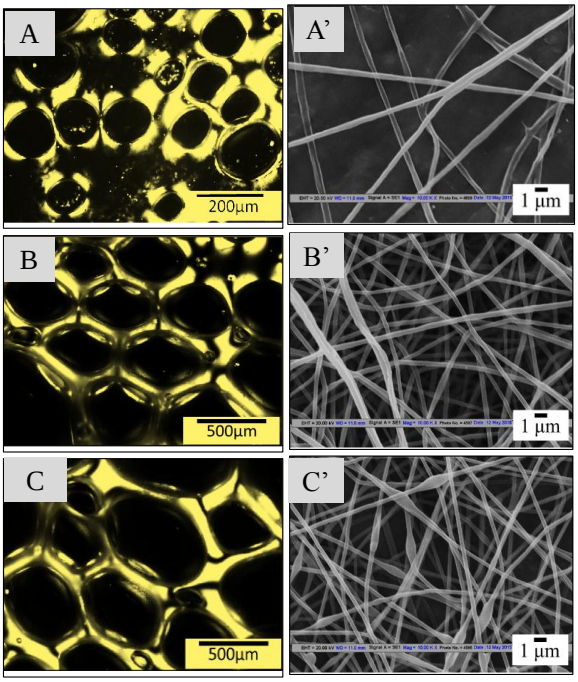


Figure 1. Optical microscope images of HIPE with ϕ_d 0.74(A), 0.85(B) and 0.9(C). A', B' and C' represent the corresponding SEM images of electrospun fibers from these HIPEs.

Thermal Analysis

Fibers obtained were of uniform diameter without any beads. The diameter of the fibers reduced with increase in continuous phase containing polymer and emulsifier. This was due to reduction in total solid content of the emulsion from 1.26 to 1.09g/ml with increase in continuous phase from 0.74 to 0.9 with emulsifier in oil phase

Neat PCL and neat Brij-58 show a melting peak at 55°C and 40°C respectively. And show a crystallization peak at 30 and 31°C respectively, as shown in figure 2. Interestingly in case of HIPE films a homogenous crystallization peak was observed at around -3°C signifying the confinement effect of polymer and emulsifier. The crystallization peak at 30°C was reduced with increase in dispersed phase volume fraction signifying the reduction in thickness of continuous PCL phase which is in correlation with the optical images. In case of electrospun fibers both homogenous as well as heterogeneous crystallization peaks at -4 and 30°C respectively were profound. This clearly

indicates a co-continuous arrangement of PCL-PVA domains instead of a core shell morphology which is generally produced in emulsion electrospun fibers. This observation was in agreement with TEM images of electrospun samples. As the content of PCL/B58 is reduced distinct separated domains of PCL is formed which leads to more pronounced surface nucleation mechanism of crystallization occurring at much higher degrees of supercooling. And this effect is profound both in case of fibers as well as films.

Figure 2. (a)Crystallization peaks of HIPE films. (b) Crystallization peaks of HIPE films.
This study enabled in production of electrospun fibers from HIPEs with at least 75% reduction in organic solvent. Factors affecting emulsion stability and governing fiber morphology are studied in detail. Change in crystallization behavior with variation in polymer concentration was studied and was related to fiber and film morphologies[5].

Pickering Emulsion (PE) electrospinning and factors governing morphology of fibers

Usage of electrospun fibers produced from HIPE technique enabled in reduction of organic content. But exposure of fibers containing emulsifier as well as water soluble template polymer may hamper the mechanical properties of fibers in an aqueous environment. To overcome this issue Pickering emulsion electrospinning was developed as a novel approach.

In this study instead of emulsifier modified montmorillonite clay with hydrophilic and hydrophobic groups to stabilize the emulsion was adopted. Emulsions were formed by dispersing clay in toluene. PCL was added to toluene phase and later neat DI water was added dropwise under stirring to toluene phase to form the Pickering emulsions. WAXD indicated the interaction of clay in the resulted matrix.

Figure 3 shows the ternary phase diagram of stable emulsion region formed by varying PCL and clay concentration with an intention of maximum replacement of organic phase with water. PCL concentration was varied from 10, 15, 20 to 25wt%. clay concentration was varied from 0.5 to 1wt. %. Further increase in clay content beyond 1wt% resulted in settling down of clay even after 30 minutes of sonication. An increase in PCL concentration with constant clay% resulted in increase in water uptake. Increase in polymer concentration resulted in increase of oil phase viscosity which then was able to separate dispersed water droplets. More the polymer concentration less the tendency of water droplets to coalesce had hence more is the water uptake. An increase in clay concentration resulted in enhanced water uptake against respective PCL concentrations. This was because of accumulation more number of nano particles at oil water interface and reducing the tendency of droplet coalesce which may reduce emulsion stability.

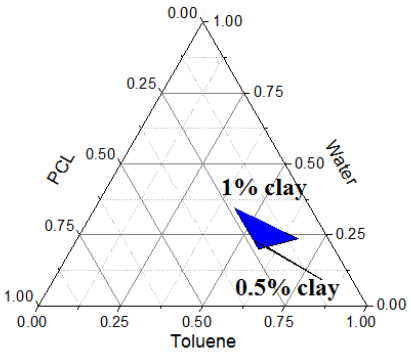


Figure 3. Ternary phase diagram of PCL, clay and water systems.

Electrospinning of stable emulsions with 1wt% clay (as it can uptake more water compared to 0.5% clay) and oil/water 0.74/0.3 was conducted. Diameter of fibers increased with increase in PCL content from 10 to 25% due to increase in overall solid content. Electrospun matrices with 20 and 25% PCL showed pores due to phase separation of oil water phases. Clay particles are found to be aligned along the fiber axis shown in figure 4.

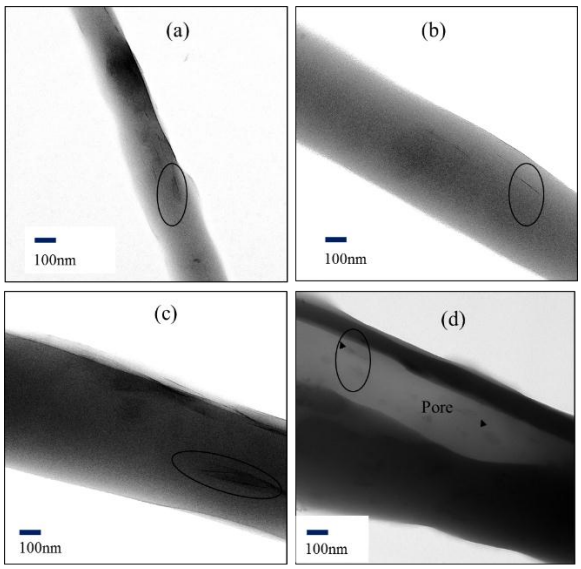


Figure 4 TEM imaging of PCL-clay Composite fibers. (a) PCL10 (b) PCL 15 (c) PCL20 (d) PCL 25 weight percent

Crystallinity of the electrospun samples enhanced with increase in polymer concentration as compared to neat PCL samples. This is due to nucleating effect of clay and increase in number of polymer chains with increase in polymer concentration. Mechanical property was also enhanced with increase in PCL concentration. This is due to formation of thicker fibers with increase in polymer concentration. Hence more axial force is required to break a thicker fiber than a thinner one**.** Also the enhancement in crystallinity as added to the mechanical strength[6].

As PCL scaffolds are mostly used in tissue engineering applications, cell viability assay of the electrospun composite matrices were analyzed shown in figure 5. Composite matrices showed similar cell proliferation efficiency as that of neat PCL samples.

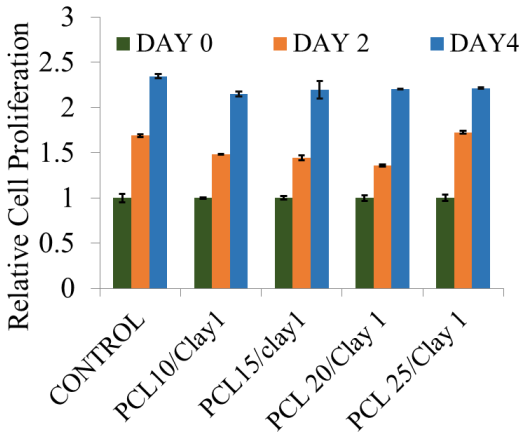


Figure 5 Cell viability Analysis of PCL-Clay composites

Conclusions

In this study a novel approach of emulsion electrospinning was adopted for electrospinning hydrophobic polymer with minimized organic solvent content. Organic solvent content was reduced to over 0.74 volume fraction. Pickering Emulsion electrospinning has further reduced the risk of leaching out of emulsifier and/or template polymer along with added advantage of minimized organic solvent usage. Inclusion of clay as a Pickering agent enhanced the crystallinity and mechanical properties of electrospun matrices. Composite matrices produced via advanced emulsion electrospinning are found to be suitable as fibrous scaffolds for cell attachment and growth.

Acknowledgements

Authors gratefully acknowledge the financial support provided by Indian Institute of Technology Delhi and Department of Science and Technology, India (grant no. SERB/F/3988/2014-15) to perform this research.

References

[1] S. Agarwal, J. H. Wendorff, and A. Greiner, “Use of electrospinning technique for biomedical applications,” *Polymer*. 49, 5603, 2008.

[2] F. H. Anka and K. J. Balkus, “Novel Nanofiltration Hollow Fiber Membrane Produced via Electrospinning,” *Ind. Eng. Chem. Res.* 52, 3473, 2013.

[3] R. M. Mohamed and K. Yusoh, “A Review on the Recent Research of Polycaprolactone (PCL),” *Adv. Mater. Res.* 1134, 249, 2015.

[4] Y. Chevalier and M.-A. Bolzinger, "Emulsions stabilized with solid nanoparticles: Pickering emulsions," *Colloids Surf. Physicochem. Eng. Asp.* 439, 23, 2013.

[5] A. Samanta, B. Nandan, and R. K. Srivastava, "Morphology of electrospun fibers derived from High Internal Phase Emulsions," *J. Colloid Interface Sci.* 471, 29, 2016.

[6] A. Samanta, S. Takkar, R. Kulshreshtha, B. Nandan, and R. K. Srivastava, "Electrospun composite matrices of poly(ε-caprolactone)-montmorillonite made using tenside free Pickering emulsions," *Mater. Sci. Eng. C.* 69, 685, 2016.

MACRO 145

Amphiphilic Co-network Gels of Agarose Graft Copolymer and Polycaprolactone-*b*-Polyethylene glycol-*b*-Polycaprolactone for Biomedical Application

[ab]Chandel, Arvind Kumar Singh, [a]Bhingaradiya, Nutan, [ab]Jewrajka Suresh Kumar *

[a]Reverse Osmosis Membrane Division, CSIR-Central Salt and Marine Chemicals Research Institute, Bhavnagar, Gujarat 364002, India
[b]AcSIR-Central Salt and Marine Chemicals Research Institute, CSIR-Central Salt and Marine Chemicals Research Institute G. B. Marg, Bhavnagar, Gujarat 364002, India

Email: skjewrajka@csmcri.org

Amphiphilic conetwork (APCN) gel is a smart material which swells both in water and in organic solvent [1-3]. The important advantage of APCN gel over hydrogel is the solubilisation of both hydrophobic and hydrophilic drugs by the former material. The mechanical property of APCN gel is generally better than that of hydrogel [4, 5]. Thus APCN gel may be better candidate for specific tissue engineering application. Recently, APCN gels have attracted wide attention due to their application in tissue culture [6, 7], drug delivery [4, 8, 9] and antifouling coating [10]. APCN gels of biodegradable and biocompatible polymers are highly desirable for biomedical application. Agarose (Agr), polycaprolactone (PCL) and polyethylene glycol (PEG) are well known biocompatible polymers. The copolymer of Agr is also biocompatible and biodegradable. The triblock copolymer of PEG and PCL i.e. PCL-*b*-PEG-*b*-PCL is also biocompatible/biodegradable [11]. Hence, APCN gels of Agr copolymer and PCL-*b*-PEG-*b*-PCL is highly useful for biomedical applications.

Herein we report synthesis of multicomponent APCN gels of Agr-based amphiphilic graft copolymer and PCL-*b*-PEG-*b*-PCL. Amphiphilic graft copolymer of Agr and polymethyl methacrylate-*b*-poly(dimethyl aminoethyl)methacrylate (Agr-g-PMMA-*b*-PDMA) was synthesized by atom transfer radical polymerization (ATRP) using Agr-based macroinitiator (Agr-I) [12]. First, ATRP of MMA was conducted using Agr-I to obtain Agr-g-PMMA-X (where X= halide). Further ATRP of DMA using Agr-*g*-PMMA-X as macro-initiator gave Agr-g-PMMA-*b*-PDMA with controlled molecular weight. The precursors of APCN gels were characterized by NMR, FTIR and GPC. Multifunctional APCN gels were prepared by reacting Agr-*g*-PMMA-*b*-PDMA with activated halide terminated PCL-*b*-PEG-*b*-PCL [4]. The rapid sequential nucleophilic substitution reaction between tertiary amine unit of Agr-PMMA-*b*-PDMA and halide end group of PCL-*b*-PEG-*b*-PCL was realized. This reaction avoids any side product due to quaternization of DMA moieties by the nucleophilic substitution reaction. Table 1 summarizes the composition, sol fraction, and equilibrium water swelling of the gels.

The gels are pH responsive as evident from the enhanced swelling of the gel at pH 5 compared to that at pH 7.4 (Table 1). This is due to presence of unreacted DMA moieties in the gels. The unreacted DMA moieties undergo enhanced protonation at low pH and enhanced the swelling of the gel.

Table 1. Composition, sol fraction and equilibrium water swelling of the APCN gels.

APCN	APCN composition				Extractive value, %	Eq. Swelling (%)	
	Agr	PDMA	PMMA	Cl-PCL-PEG-PCL-Cl			
APCN-1	56	25	13	6	7.2	148	199
APCN-2	38	17	10	35	8.5	114	164
APCN-3	20	30	29	20	7.1	83	104

These APCN gels exhibited good biocompatibility as well as hemocompatibility as confirmed by MTT assay and in vitro haemolysis assay respectively. All the APCN gels undergo degradation in presence of lipase as well as at pH 5. The lipase catalysed degradation of the APCN is due to degradation of PCL backbone whereas Agr backbone undergoes degradation at acidic pH. One application of these gels is the controlled release of drugs. For example APCN-1 showed controlled release of anticancer 5-fluorouracil (Figure 1). The release of drug was faster at pH 5 than that at pH 7.4. This is due to enhanced swelling of the gel at lower pH. The Drug containing APCN gels remained transparent due to enhanced solubilisation of the drug into the matrix of APCN gel.

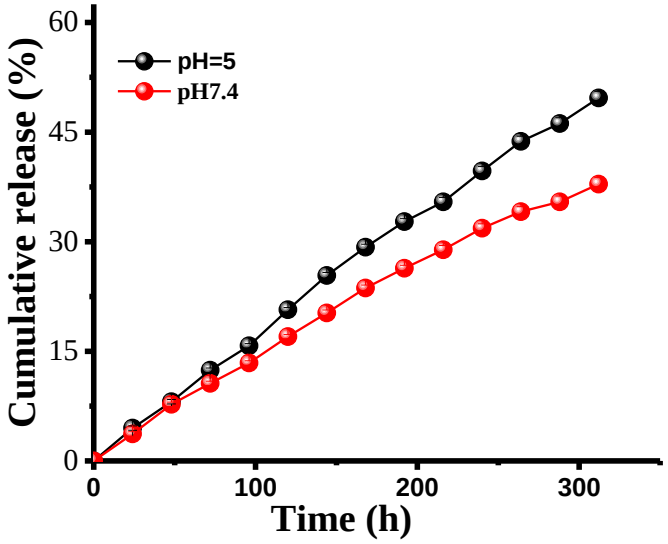


Figure 1. Cumulative release of water soluble 5-fluorouracil from APCN-1 at pH 5 and 7.4 and at temperature 37 ºC.

These APCN gels can also entrap and release hydrophobic drug. For example, the APCN-1 showed controlled release of prednisolone acetate. The mechanically milled particles of the gels were injectable through hypodermic syringe of needle size 20-G.

Reference

[1] Erdodi, G; Kennedy, J. P. *J. Polym. Sci., Part A: Polym. Chem*., 43 (2005) 4965.

[2] Triftaridou, A. I.; Hadjiyannakou, S. C; Vamvakaki, M; Patrickios, C. S. *Macromolecules,* 35 (2002) 2506.

[3] Loizou, E.; Triftaridou, A. I; Georgiou, T.; Vamvakaki, K. M; Patrickios, C S. *Biomacromolecules*, 4 (2003) 1150.

[4] Bera, A.; Chandel, A. K. S; Kumar, C U; Jewrajka, S K. *J., Mater. Chem. B*, 3 (2015) 8548.

[5] Chandel, A. K. S.; Kumar, C. U; Jewrajka, S. K. *ACS Appl. Mater. Interfaces,* 8 (2016) 3182.

[6] Behravesh, E; Zygourakis, S; Jo, K; Mikos, A. G. *Biomacromolecules*, 3 (2002) 374.
[7] Rimmer, S.; German, M. J.; Maughan, J.; Sun, Y.; Fullwood, N; Ebdon, J.; MacNeil, S. *Biomaterials*, 26 (2005) 2219.
[8] Iva´n, B; Kennedy, J P; Mackey, P. W. *ACS Symposium Series*, Washington, DC, 469 (1991) 203.

[9] Lin, C; Gitsov, I. *Macromolecules, 43* (2010) 10017.

[10] Tiller, J. C; Sprich, C.; Hartmann, L. *Journal of Controlled Release*, 103 (2003) 355.

[11] Zhang, Y.; Zhuo, R-X. *Biomaterials,* 26 (2005) 6736.

[12] Muppalla, R; Jewrajka, S. K; Prasad, K. *J. Biomed. Mater. Res*., 101A (2013) 163.

MACRO 157

Water Soluble Poly(ethylene glycol) Methyl Ether Acrylate Containing Polysulfide Polymers *via* Interfacial Polycondensation

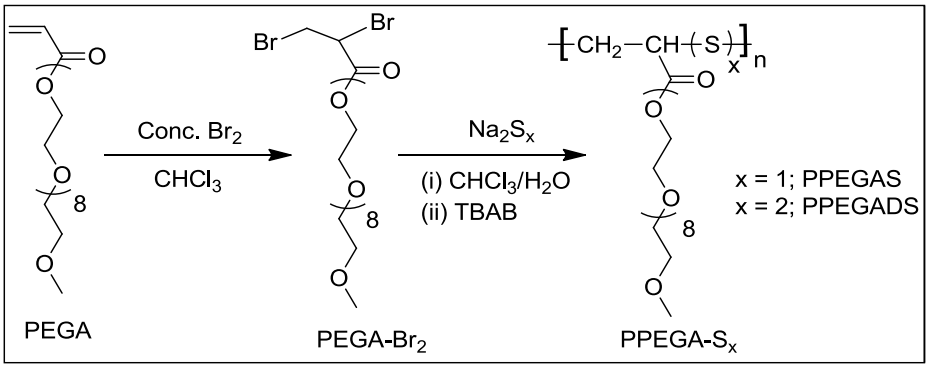
Kapil Dev Sayala,[a] Ujjal Haldar and Priyadarsi De[a,]*

[a] *Polymer Research Centre, Department of Chemical Sciences, Indian Institute of Science Education and Research Kolkata, Mohanpur - 741246, Nadia, West Bengal, India.*

* *p_de@iiserkol.ac.in*

Polysulfide polymers are unique amidst main chain weak-link polymers owing to their high thermal stability in comparison with other main chain weak-link polymers such as polyperoxides and polyselenides. They demonstrate exceptional characteristics concerning weatherability, solvent and oil resistance. Polysulfide polymers are gaining escalating attention attributable to their substantial applications as sealants, adhesives, vulcanizing agents for diverse naturally occurring rubbers, stabilizer for vinyl polymers, macroiniferter to make branched polymers, etc. In this work, we have designed water soluble poly(ethylene glycol) methyl ether acrylate containing polysulfide polymers *via* conventional interfacial polycondensation polymerization technique (Scheme 1). Formation of polysulfide polymers are confirmed by means of gel permeation chromatography (GPC), FT-IR, ^{1}H

and ^{13}C NMR spectroscopy. Thermal behavior of these polysulfide polymers are investigated by thermogravimetric analysis (TGA) and differential scanning calorimetry (DSC). Major degradation products have been identified by electron ionization-mass spectrometry (EI-MS). Incorporating -S- or -S-S- weak-links in the main chain did not influence the thermal stability of polysulfide polymers compared to the poly(poly(ethylene glycol) methyl ether acrylate) (PPEGA). These polysulfide polymers are soluble in most of the common organic solvents, as well as in water. Although the PPEGA is a thermoresponsive polymer, main chain sulphur containing PEGA based polymers did not show any temperature dependent phase transition in aqueous medium. The presence of disulphide linker in the main chain of water soluble poly(poly(ethylene glycol) methyl ether acrylate disulfide) (PPEGADS) is expected to manifest potential biological applications. This interesting class of polymer can also be employed as chain transfer agents to control molecular weight of conventional free radical polymerization of vinyl monomers in aqueous medium.



Scheme 1. Synthesis of PEGA containing polysulfide polymers *via* interfacial polycondesation method.

References

[1] Haldar, U; Ramakrishnan, L; Sivaprakasham, K; De, P. *Polymer*, 55 (2014) 5656.
[2] Kishore, K; Ganesh, K. *Macromolecules*, 26 (1993) 7109.
[3] Kishore, K; Mukundan, T. *Nature*, 130 (1986) 324.

MACRO 159

Adsorption and Photocatalytic Degradation Studies of Enrofloxacin using Polyacrylic Acid- grafted-Carboxylic Graphene/Titanium Nanotube Composite

Anirudhan T S*, Shainy F, Deepa J R, Anoop S Nair, Manasa Mohan A

Department of Chemistry, School of Physical and Mathematical Sciences, University of Kerala, Kariavattom, Trivandrum -695 581, India

* *tsani@rediffmail.com*

Nowadays antibiotic is widely used as a feed additive to promote animal growth. Enrofloxacin (ENR) is a fluoroquinolone bacterial antibiotic [1]. The application of ENR has increased equally in human and veterinary medicine for disease treatment. ENR is used in veterinary medicine in cattle, pigs, poultry, dog and cat. Antibiotics are introduced to various environments as parent compounds or byproducts by excretion, disposal of expired drugs or unused drugs and accidental spills [2]. A large number of antibiotics have been found in waste water effluents and natural waters at different concentrations. ENR shows a wide spectrum of activity at very less concentrations in comparison to traditional antibiotics such as pencillins, cephalosporias, macrolides, tetracyclines and sulphonamides [3]. Therefore the removal and degradation of these antibiotics is very important.

Adsorption followed by advanced oxidation process (AOP) play an important role for the removal of toxic pollutants [4]. Among the various AOP techniques, photo degradation has proved to be the most efficient method which involves the production of highly reactive hydroxyl free radicals (OH·**)**. Various semiconducting materials such as ZnO, CdS, ZnS, Fe_2O_3 and TiO_2 were recently used to remove organic pollutants because of their photo catalytic activity [5]. TiO_2 nanoparticles are the most suitable materials for the degradation of antibiotics due to their nontoxicity, low cost, high reactivity, physical and chemical stability. But the use of TiO_2 as such will have some limitations such as low adsorption capacity and recombination of charge carriers [6]. When TiO_2 is converted to titanium dioxide nanotubes (TNT), its inner and outer surface area increases. To overcome the limitations of TNT, carbon materials are used to improve adsorption efficiency and electrical properties. The carbon materials act as electron sink and avoid the recombination of electron-hole pairs. Graphite is the most widely used photo catalytic filler because of good electrical conductivity, large surface area and appreciable stiffness [7]. Graphite is hydrophobic in nature. So they are aggregated together in hydrophilic media and it has poor dispersion in composite. When graphite is oxidised to graphene oxide (GO) its dispersion capacity increases because of the presence of polar groups such as hydroxyl, ether, epoxide and carboxylate groups. When GO is converted to carboxylic graphene (CGR), all the hydroxyl groups are converted to carboxyl groups and hence adsorption efficiency increases. Polyacrylic acid (PAA) is a pH and electrical sensitivity material. When PAA is treated with CGR, the epoxide is broken and PAA is grafted onto CGR.

In the present work, a novel material - polyacrylic acid-grafted-carboxylic graphene/titanium nanotube composite (PAA-g-CGR/TNT) was prepared via ultra-sonic treatment under normal conditions as shown in **Fig. 1.** In the first step graphite powder was converted into GO and then to CGR. Then the solution was irradiated through ultra-sonication and then mixed with TNT. The photo catalytic activity of PAA-g-CGR/TNT composite was investigated in the decomposition of the antibiotic ENR under visible light. Photo catalytic activity occurs when TNT absorbs a photon with an energy equal/greater than the materials band gap energy that results in the formation of electron-hole pairs which can migrate to the PAA-g-CGR/TNT composite surface and react with adsorbed ENR to generate reactive species such as H_2O_2, superoxide anion radical ($O_2^{-}\cdot$) and hydroxyl radical (OH·). These species are strong oxidising and highly reactive agents that can degrade the pollutant to harmless compounds. The adsorbent cum photocatalyst, was characterized by FTIR, XRD, SEM, DRS and UV-visible absorbance spectra analyses.

The photo catalytic activity of PAA-g-CGR/TNT composite was evaluated on the basis of the degradation of pollutants by using natural sunlight. The band gap of the prepared photo catalyst was found to be 2.6 eV which is in the visible region. The removal of the antibiotic enrofloxacin (ENR) was achieved by two step mechanism based on adsorption and photo degradation. Maximum adsorption was observed at pH 5.0. The kinetic models pseudo-first-order and pseudo-second-order kinetic model were used to study the adsorption mechanism of ENR onto PAA-g-CGR/TNT composite. The best fitting was observed by pseudo-second-order kinetic model. Maximum adsorption was observed at 30 ^{o}C. The maximum adsorption capacity was found to be 13.40 mg/g. The kinetics of photo degradation of ENR onto PAA-g-CGR/TNT composite follow first-order kinetics and optimum pH was found to be 5.0. The regeneration and reuse of the adsorbent was also examined upto five cycles and it was observed that PAA-g-CGR/TNT composite was very efficient adsorbent as well as photo catalyst.

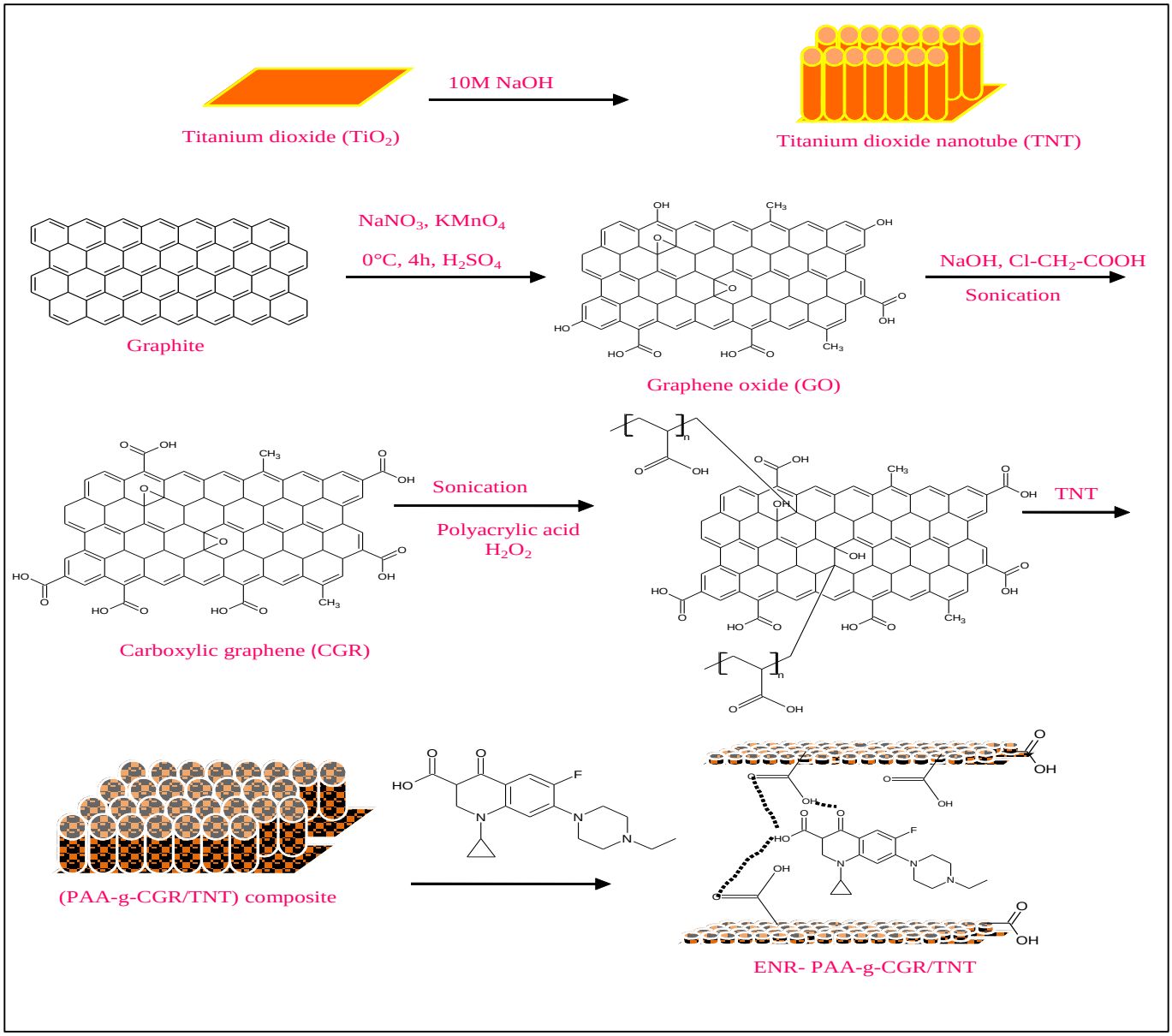


Figure 1. Synthesis of (PAA-g-CGR/TNT)

References

[1]. Chamani, M; Panahi, H.A; Tayebi, P; Aminafshar, M; Sadeghi, A.A, *European J. Experimental Bio.*, 3 (2013),
35-42.
[2]. Jorgensen, S.E; Halling-Sorensen, B; *Chemosphere* 40 (2000) 691-699.
[3]. Rivier, J.E; Papich, M.G; Veterinary Pharmacology and Therapeutics, 9th Edition, Wiley-Blackwell, USA,
(2009).
[4]. Klauson, D; Babkina, J; Stepanova, K; Krichevskaya, M; Peris, S; *Catal. Today*, 152 (2010) 39-45.

[5]. Lin, C.C; Chiang, Y.J; *J. Ind. Eng. Chem*. 18 (2012) 1233-1236.
[6]. Ullah, K; Zhu, L; Meng, Z.D; Ye, S; Sun, Q; Oh, W.C; Chem.Eng.J. 231 (2013) 76-83.
[7]. Stankovich, S; Dikin, D.A; Dommett, G.H.B; Kohlhaas, K.M; Zimney, E.J; Stach, E.A; Piner, R.D; Nguyen, S.T; Ruoff, R.S; Nature 442 (2006) 282-286.

MACRO 160

Fabrication of solvent responsive transdermal device for the efficient treatment of skin cancer

Anirudhan T S[a], Anoop S Nair[a], Sabari J Bino[a], Deepa J R[a], Shainy F[a], Manasa Mohan A[a]

[a] *Department of Chemistry, School of Physical and Mathematical Sciences, University of Kerala, Kariavattom,Trivandrum-695581, Kerala, India*

** e-mail id: tsani@rediffmail.com*

Abstract

Ozone depletion due to various human activities has allowed large influx of harmful solar radiation to enter into the earth's atmosphere thereby causing serious adverse effects on human health. The most prominent among them is skin cancer. Even though, efficient drugs have been discovered for its treatment, lack of proper administration routes that can bring about their complete efficacy is highly challenging. Herein, we report the fabrication of a novel solvent sensitive transdermal device that can elute out the drug from its matrix as a function of the eluting solvents. The prepared polymer consists of alginate coated aminated nanodextran (ALG@AND) that could efficiently entrap and exhibit sustained release of 5-flurouracil (5-FU) after wetting with ethanol (EtOH). All reaction procedures were monitored by ATR-FTIR, XRD and SEM techniques. The potential applicability of the material was further elucidated using swelling studies, mechanical strength evaluation, water vapour permeability and average visible transmittance studies. The ability to sustain 5-FU release was ascertained by *in vitro* permeation profiles on rat skin using modified Franz diffusion cell. Physiological acceptance of the prepared material was further confirmed using MTT assay on human keratinocyte cell line, HaCaT.

Keywords: *transdermal drug delivery; 5-flourouracil; solvent selectivity; chitosan*

Introduction

Industrial revolution and world war have revolutionized the modern world. Even though there was an industrial boom in this period, contamination of earth was a serious issue that arose. This led to influx of large toxic chemicals and harmful radiation into the earth's atmosphere leading to a variety of diseases. The most fatal among them is said to be cancer. Of the various cancers, skin cancer is very common and as per the world health organization (WHO), around 13,20,000 cases are reported each year. Even though a lot of anti-cancer drugs like curcumin, 5-FU, doxorubicin, etc. have been discovered, convenient route for their administration so as to reduce the adverse effects of chemotherapy is under serious discussion around the world.

To address this issue, the most promising solution seems to be alternate routes of drug administration like transdermal drug delivery where neither the drug carriers nor the drug enters directly into the bloodstream. When hybrids of nanoparticle and transdermal delivery are used, it can offer greater skin permeation, better encapsulation and sustained release of drug.[1, 2]

It was in this aspect, that we fabricated a matrix diffusion controlled transdermal film comprising of alginate coated aminated nanodextran (ALG@AND). 5-FU was loaded onto the hydrophilic core of dextran (DEX) and owing to similar log p values, 5-FU could be leached out from the polymeric matrix using specific solvents. Based on the previous observations that drugs could elute rapidly through moist skin, a list of eluting solvents were tried and best results were obtained with EtOH.[3] Histological studies revealed the non-toxicity when organic solvents are used. MTT assay on skin cell lines suggested the potential usefulness of the material to treat skin cancer.

Experimental

1. Equipments and Methods of Characterization

Experimental steps were monitored using Cary 630 ATR spectrophotometer (model-Spectrum 400, USA). Absorbance measurements of drug loading and release were performed on a JASCO V-530 UV-Visible spectrophotometer at λ_{max} of 266 nm, characteristic of 5-FU. DLS and zeta potential studies were performed on Horiba SZ-100 instrument equipped with a 532 nm Diode Pumped Solid State (DPSS) laser. X-ray diffraction (XRD) patterns of the samples were performed using Siemens D5005 X-Ray Diffractometer, employing nickel filtered Cu-K_α radiation at 25 ^{0}C. The surface morphology of all the samples was recorded using a Carl Zeiss EVO-18 scanning electron microscope operated in vacuum. Cell viability of the prepared polymer in skin cell lines-HaCaT was measured using MTT assay.

2. Preparation of alginate coated aminated nanodextran (ALG@AND)

Aminated dextran nanoparticle was synthesized by a slightly modified procedure.[4] 5-FU was loaded onto the hydrophilic core of aminated nano dextran. Briefly, 20 mL 5-FU solution at a concentration of 2.0 mg/mL was added to 0.2 g of aminated nanodextran at a pH of 4.0, to make 5-FU neutral and to protonate the amino groups for facilitating polymer- drug interaction. The

resultant solution was then stirred for about 4 hours. After loading, surface amino groups of aminated nano dextran was coupled to carboxylic groups of alginic acid (ALG) by DCC. 44.1 mg of ALG was initially dissolved in methanol together with DCC at a molar ratio of 1:1. This solution was added dropwise into a 1.5 M aminated nano dextran solution with constant stirring at room temperature for 24 hours. After completion of the reaction, pH was adjusted to 8.0 and was washed with deionised water. The drug loading (%), encapsulation efficiency (%), drug loading (%) and theoretical loading (%) were calculated using the following equations (equations 4-7):

$$\text{Drug loading (\%)} = \frac{\text{amount of loaded drug}}{\text{amount of polymer}} \times 100 \quad (1)$$

$$\text{Encapsulation efficiency (\%)} = \frac{\text{total amount of drug} - \text{free drug}}{\text{total amount of drug}} \times 100 \quad (2)$$

$$\text{Theoretical loading (\%)} = \frac{\text{amount of drug added}}{\text{amount of copolymer}} \times 100 \quad (3)$$

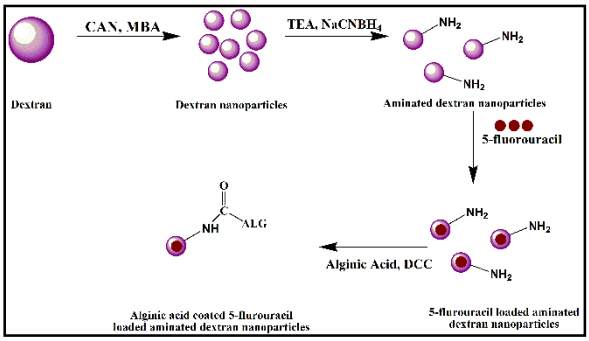
Schematic preparation of CUR loaded nanoparticle is as shown in **Scheme 1.**

3. Determination of swelling degree %

Swelling measurements were performed by immersing the DDS taken in tea bag in 1.2 and 7.4 pH. The weight of swollen copolymer were measured at different time after removing the surface water with filter paper. Degree of swelling was calculated using equation (4) as:

$$\text{Degree of swelling \%} = \frac{(Ws - Wi)}{Wd} \times 100 \quad (4)$$

where, 'W_s' is the weight of the swollen copolymer at a given time during swelling, 'W_i' is the initial weight, 'W_d' is the weight of the dry copolymer.



Scheme 1. Preparation of 5-FU loaded ALG@AND

4. *In vitro* permeation profile

Sustained release from the drug-loaded matrix patches was evaluated on wistar rats using modified Franz diffusion cell having a permeation area of 0.95 m^2 and with a receptor volume of 4 mL. Each drug loaded patches was placed in the intact epidermal membrane of the donor compartment and

wetted with various organic solvents. The receptor fluid was constantly mixed and aliquots from the stirred receptor compartment were withdrawn at definite time intervals and the amount of drug in the receptor fluid was determined by UV-Vis. Spectroscopic method.

5. Cosmetic attractiveness

Thickness of the drug loaded film was measured with a hand held micro meter with ten replicates at different points. Average visible transmittance of the films was measured over the range 400-700 nm using UV-Vis. Spectrophotometer. Water vapour permeability of the fabricated film was carried out in accordance with the method stated by British Pharmacopoeia (BP) with slight modifications.[5]

6. Determination of cell viability

The cells were initially seeded using a 200 µl cell suspension in a 96-well plate at a cell density of 25,000 cells per well. It was then allowed to adhere to the culture plate for about 24 hours. Test solutions of definite concentrations were added to this along with a control having no test solution. The plates were incubated at 37°C for 48 hours. After incubation, plates were removed and MTT reagent was added to a final concentration of 10.0 % of total volume. The absorbance at 570 nm was noted using the spectrophotometer to determine the % cell viability.

Results and discussion

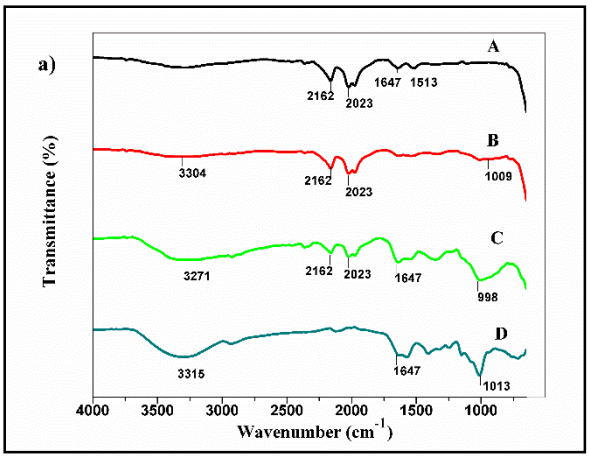


Figure 1 FTIR spectrum of A) nano DEX, B) aminated nano DEX, C) 5-FU loaded aminated nano DEX and C) CS coated 5-FU loaded aminated nano DEX

Nano dextran was initially aminated using hexamethylenediamine, where the primary hydroxyl groups of DEX were bonded to hexamethylenediamine facilitated by $NaCNBH_3$, forming an amine terminated alkyl chain. 5-FU was then loaded onto the hydrophilic core of nano DEX. In addition, 5-FU was also held together by the non-covalent interactions from the amine and hydroxyl groups present in DEX. Drug loading %, encapsulation efficiency and theoretical loading were obtained

as 15.0 %, 77.3 % and 15.7 % respectively. The –COOH groups of ALG were then reacted with the 1^0 amine of aminated DEX via carbodiimide chemistry which gave grafting efficiency of 82 %. All the synthetic procedures for the preparation of 5-FU loaded aminated nano DEX was monitored using FTIR and the spectrum obtained is as shown in **Figure 1.** FTIR spectrum of nano DEX obtained peaks that were identical to those reported already in the literature.[6] In aminated nano DEX, the intensity of $–NH_2$ peaks increased as expected. In 5-FU loaded sample, peaks of 5-FU at 3327 and 1639 cm^{-1} due to –NH and >CO stretching respectively of the uracil moiety pointed out the successful encapsulation of 5-FU. It was then coated with ALG in the ratio 1:2. Evidence for the formation of newly formed amide bond was observed by identifying characteristic peak at 1639 cm^{-1} in the ALG coated 5-FU loaded aminated nano DEX sample.

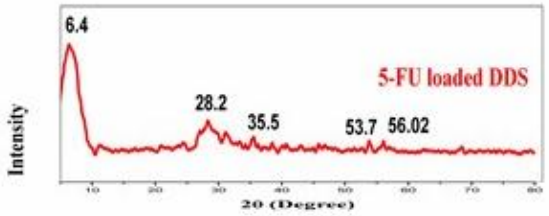


Figure 2 XRD patterns of 5-FU loaded DDS.

The XRD patterns observed for the 5-FU DDS are as shown in **Figure 2.** In ALG@5-FU loaded aminated DEX (5-FU DDS), characteristic peaks of 5-FU were found at 2θ = 6.4, 28.2, 35.5 and 56.0°. The broad peak obtained at 6.4 and 28.2° revealed successful loading of 5-FU onto the polymer. On modification, crystallinity was found to be disappearing. Peaks at 2θ=35.5° is of DEX and at $2\theta=53.7^0$ is of aminated DEX. Decrease in the intensity of peaks at 6.4 and 28.2° indicated the intercalation of drug inside DEX core. The amorphous nature of the polymer evident from the broad nature of peaks proved to be beneficial for inducing uniform surface charges.

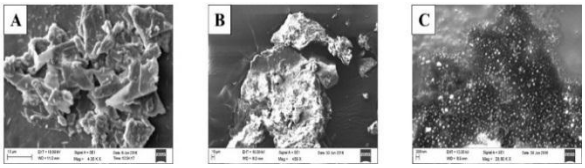


Figure 3 SEM Images of A) Aminated DEX, B) 5-FU Loaded Aminated DEX and C) ALG Coated 5-FU Loaded Aminated DEX

Figure 3 shows the SEM images of the prepared samples. In aminated DEX, the surface appeared to be porous with cavities unlike granular appearance of pristine DEX. On incorporating 5-FU, particles were found to aggregate. On coating with ALG, the particles were much more dispersed with a size of 340.5 nm. In addition, it showed smooth and spherical surface morphology, evident of efficient coating by ALG. The variation of tensile strength (T_S) and elongation of break (Eb) was also measured to assess the shelf life. The values of T_S and E_b were observed to be 0.5225

MPa and 204 %, respectively. Film thickness is an important parameter in TDDS which is proportional to the drug efflux from the film. The fabricated film was found to have a thickness of 0.4 ±1 mm. Smooth transparent films that are easy to be handled are generally preferred. The average visible transmittance of the prepared film was calculated to be 86.0 %. Swelling studies at 1.2 and 7.4 pH initially showed a burst swelling and equilibrium was attained after 24 hours. Even in the initial hours, SD % was below 300 % only, indicative of its lesser swelling capability. At pH 7.4, the copolymer showed an identical trend, and after 24 hours, it showed almost a constant SD of 80.0 %. Permeability of water vapour was evaluated to be 0.39 gcm^2/24hr. Thus it could be said that the TDDS prepared could firmly bind to the skin surface without causing any damage. Sustained release of 5-FU from the polymer after wetting with EtOH was observed as shown in **Figure 4 A.** The maintenance of surface topology even after EtOH treatment was confirmed from optical images as shown in **Figure 4 B.**

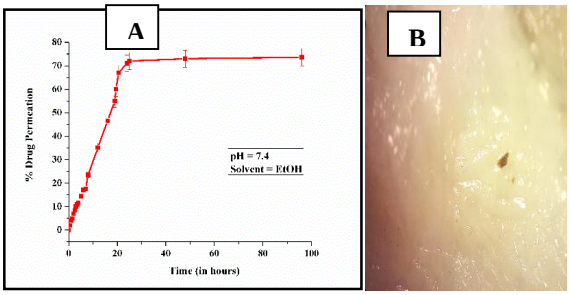


Figure 4 A). *In vitro* skin permeation of 5-FU from 5-FU loaded DDS, B). Optical photo of rat skin after EtOH treatment

Cell viability studies of 5-FU loaded DDS showed viability greater than 80.0 % at sample concentrations ranging from 1.5 to 25.0 µg/mL (**Figure 5**).

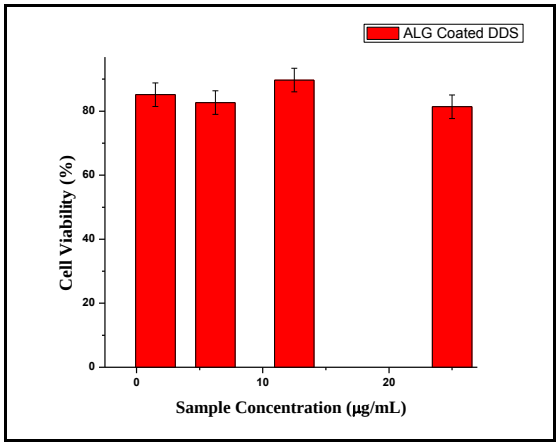


Figure 5 Cell viability studies of 5-FU loaded DDS

Typically, viability above 80.0 % is considered to be highly beneficial to transdermal systems and high value observed may be the contribution of biopolymers. Optimal viability % was observed for 12.5 µg/mL of the sample where it exhibited 89.3 % viability. To conclude, the fabricated system has excellent biocompatibility with skin, making it an ideal candidate for regular and prolonged use.

Conclusions

The present investigation deals with the fabrication of a novel solvent selective TDDS which could efficiently encapsulate 5-FU and could release it as a function of eluting solvents. Appreciable mechanical strength and physical properties that are essential for any TDDS were achieved. Drug was loaded onto ALG@AND and was coated with CS. All the reaction steps were thoroughly characterized. *In vitro* permeation studies on rat skin showed the solvent selectivity of the drug carrier. Further, biological studies performed on skin and melanoma cancer cell lines projected out the potential usefulness of the prepared TDDS. It can also gateway a new economical and patient compliant 5-FU therapy.

Acknowledgements

The authors are thankful to Professor and Head, Department of Chemistry, University of Kerala, Trivandrum, India for providing the laboratory facilities. One of the authors (Anoop S. Nair) is grateful to Kerala State Council for Science Technology and Environment (KSCSTE), for providing assistance in the form of a research fellowship for this work (Grant No. 001/FSHP-MAIN/2014/KSCSTE).

References

1. L. Juan, H. Yuran, K. Anil, T. Aaron, J. Shubin, M. Anbu, X. J. Liang, *Biotechnol. Adv.* 32, 693, 2014.
2. M. R. Saboktakina, A. Shahab, A. Fizuli, *Int. J. Biol. Macromol.*, 69, 442-446, 2014.
3. S. Nikhil, A. Geta, A. C. Rana, Z. A. Bhat, K. Dinesh, *IJDDR* 3, 70, 2011.
4. M. Tang, H. Dou, K. Sun, *Polymer* 47, 728, 2006.
5. Water-vapour permeability, in: British Pharmacopoeia, Appendix XXJ, 1993.
6. C. Zhang, S. Yang, Y. Zhu, R. Zhang, X. Liu, *Carbohydrate Polymers* 32, 637, 2015.

MACRO 163

Preparation and Characterization of Novel Dual Drug Loaded Hydrogel for Combination Therapy

T. S. Anirudhan[*a], Manasa Mohan A[a] , Shainy F[a], Deepa J R[a], Anoop S Nair[a],

[a]*Department of Chemistry, School of Physical and Mathematical Sciences, University of Kerala, Kariavattom, Trivandrum-695 581, Kerala, India.*

e- mail id: manasamohan42@gmail.com

Abstract

In the present work a novel dual drug loaded gelatin hydrogel was prepared and characterized. Drug resistant bacteria are now a challenge to the medical field, only combination therapy can solve this problem. Thus combination of two drugs, Gentamicin (GS) and Ampicillin (Amp), having synergistic activity to treat bacterial infection has been used. The carrier was well characterized using FTIR, XRD and SEM. Swelling and drug release studies were carried out to find the pH dependent behavior of the hydrogel. The release studies revealed the extended activity of the hydrogel, to release the drugs in a controlled manner and remain inactive during the absence of severe infection. Antimicrobial studies revealed the increased efficiency of the drug combination in killing bacteria.

Keywords: *gelatin; antibiotics; gentamicin; combination therapy*

1 Introduction

Bacterial diseases are the most prevalent and serious infections in humans. Most common routes of administration of several drugs include the preferred non-invasive peroral (through the mouth) and topical on skin. Such therapy not only takes a long time but it is also toxic for the living organisms because the antibiotic also kills other, non-pathogenic bacteria in the human body. The alternative to a medicine administered orally is an antibiotic released from biomaterials which were needed to be used as an implant. This can serve to protect the body during the regeneration process, because, in this case, the drug is located in the place of damage, and it does not influence the whole system. Most of the bacterias became drug resistant. Hence due to the molecular complexity of diseases and strengthening resistance of bacteria, "Combination therapy" is becoming increasingly important for a better long term prognosis and to decrease side effects. Any two antibacterial drug combinations for an active disfunction of bacteria are possible. But it is better to take two drugs having synergism. Among various classes of antibacterial drugs the synergism is finding to be better in between the aminoglycosides and beta lactum antibiotics. Here

we choose GS, as aminoglycoside and Amp, as beta lactum antibiotics. GS has nephrotoxicity; this may be due to the release of reactive oxygen species by it [1,2] .

2 Experimental

2.1 Reagents

Gelatin (Gelatin purified Type B), Methacrylic acid, potassium per sulphate (KPS) were purchased from MERK Specialities pvt Ltd. Methacrylic anhydride (MAA), N-hydroxy succinimide, GS were purchased from Sigma- Aldrich USA. Ethylene Glycol Dimethacrylate (EGDMA), 1-(3-Dimethylaminopropyl)-3-ethylcarbo diimide Hydrochloride (EDC), Amino guanidine, Ampicillin were purchased from Tokyo Chemical Industry Co.Ltd. HCl, NaOH, $NaHCO_3$, etc were purchased from S.D Fine Chemicals, India and were used as received. Distilled water with specific conductivity less than 1μ Ohm/cm was used throughout. Other solvents and chemicals were of analytical grades and used without further purification

2.2 Swelling studies

Swelling studies were performed by immersing dried 0.1g each of GMA, GMA/MAA and GMA/MAA-GS taken in pre weighed dialysis bags in the phosphate buffer of pH 7.4 and KCl buffer of pH 5.0. The weights of swollen composites were measured at different time after removing the surface water with filter paper and Degree of swelling was calculated

2.3 In vitro drug release

Invitro release studies were carried out in two different pH conditions (pH 7.4 and 5.0) Dialysis sacs were equilibrated with the dissolution medium for a few hours prior to experiments. 0.1 g each of GMA/MAA-GS and DDLHG is taken in two solution bottles of different pH containing 50 mL each, placed in Julabo shaking water bath (sw23) shaked at 31^{o}c for 168 h. The shaking frequency was kept at 100rpm, 4 mL of sample was withdrawn at regular time intervals and the same volume was replaced with a fresh dissolution medium. Samples were analysed for GS, 2- Amino guanidine and Amp content by UV Spectrophotometer at λ_{max}=215, 212 and 254 nm respectively. The studies were performed in triplicate for each sample and the average values were used in data analysis.

2.4 Antibacterial activity

The samples GMA/MAA, GS, Amp, GMA/MMA-GS and DDLHG were tested for the antibacterial activity against a gram negative and gram positive bacterial pathogens such as E-Coli and Staphylococcus aureus respectively following Agar well diffusion method. Petriplates containing 20ml Muller Hinton Agar Medium were seeded with bacterial culture of *E.coli* and *S. aureus* (growth of culture adjusted according to McFards Standard, 0.5%). Wells of approximately 10 mm was bored using a well cutter and samples were added. The plates were then incubated at

37°C for 24 h. The antibacterial activity was assayed by measuring the diameter of the inhibition zone formed around the well .Streptomycin was used as a positive control.

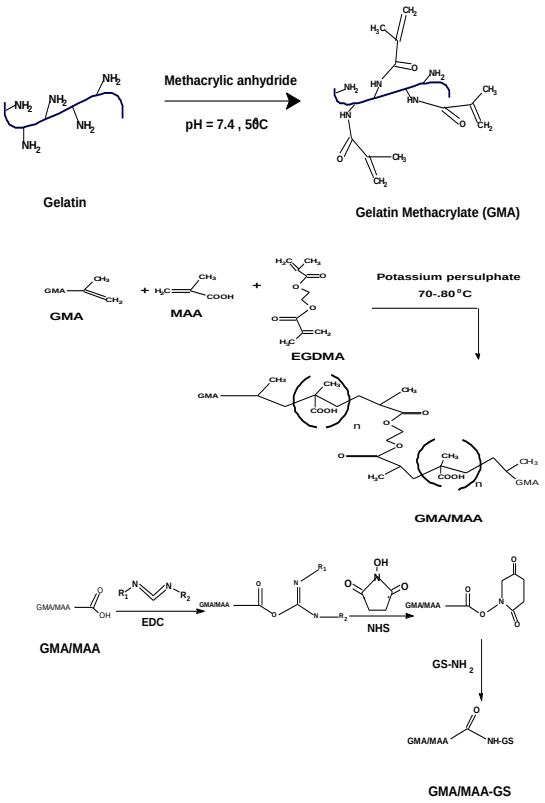
3. Results and discussion

3.1 Characterisation of hydrogel

All the steps in synthesis were closely monitored using FTIR as shown in Figure 1. Gelatin undergoes methacrylation with methacrylic anhydride forming gelatin methacrylate (GMA). The absence of the peak around 3500 cm^{-1} indicates the absence of free $–NH_2$ group and presence of a peak around 3200-3300 cm^{-1} is due to N-H stretching of amide substantiates the formation of GMA. Presence of intense peaks around 3000-3500 cm^{-1}, 1600-1750 cm^{-1} in GMA/MAA indicates the introduction of carboxyl groups by methacrylic acid to GMA. For GS, major absorbance peaks were at 619 and 1100-1400 cm^{-1}. The spectrum of GMA/MAA-GS has both the characteristic peaks of GMA/MAA and GS, i.e. the peaks around 3000-35000 cm^{-1}, but the peaks at 1600-1750 cm^{-1} are absent that shows that the carboxylic groups are used for conjugation with GS. Peak at 1100-1400 cm^{-1} is also present which shows that GS is well conjugated to the polymer. The spectra of DDLHG and of GMA/MAA-GS are almost identical indicating that the cargos are buried deep inside hydrogel matrix and only GS is on the surface.

XRD patterns of GMA, GMA/MAA, GMA/MAA-GS and DDLHG were recorded to determine the possible differences in the crystallinity of the structures (Figure 2). The interaction of GMA with methacrylic acid results in the appearance of peaks in the XRD pattern at 2θ values 30.9, 53.0^0. The XRD pattern GS conjugated GMA/MAA has peaks at 2θ= 16.3, 31.2, 53.4^0, the presence of new peaks may be due to the conjugation of GS through amide linkage. The drug carrier retains almost all the peaks of its constituents with slight modifications and was found that after each modification the crystallinity of the samples decreases. The XRD pattern of DDLHG was found to be amorphous in nature giving a clear evidence for the effective encapsulation of drugs deep inside the matrix.

SEM analysis was carried out to investigate the morphology as well as crystalline nature of the polymer materials. Figure 3 illustrates the SEM images of Gelatin, GMA, GMA/MAA, GMA/MAA-GS and DDLHG. From the figure it can be seen that the surface morphological features of each sample differed entirely. GMA has a rough surface with lot of channels. GMA/MAA has non uniform wrinkled surface morphology and is found to be amorphous. It may be due to the increase of carboxylic groups, which makes it highly hygroscopic. The SEM images of GMA/MAA-GS and DDLHG are almost similar



Scheme 1. Synthesis of GMA/MAA-GS

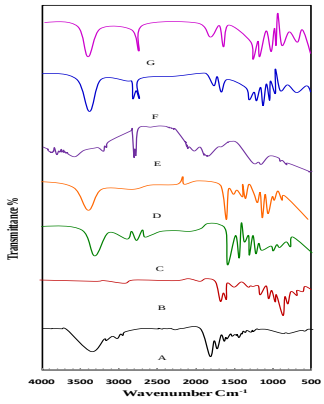


Figure 1 FTIR spectra of Gelatin (A), Methacrylic anhydride (B), GMA (C), GMA/MAA (D), G.S (E), GMA/MAA-GS (F) and DDLHG (F).

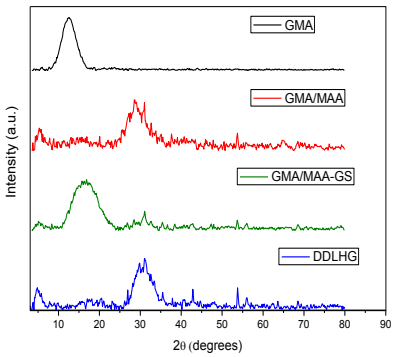


Figure 2 XRD patterns of GMA, GMA/MAA, GMA/MAA-GS and DDLHG

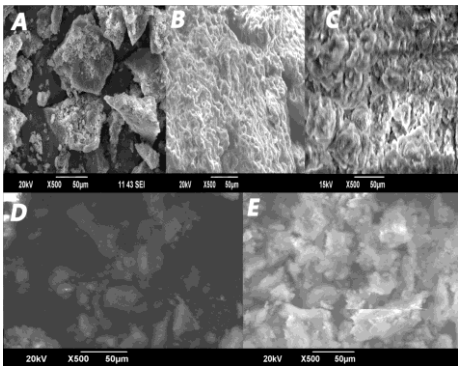


Figure 3 SEM images of Gelatin (A), GMA (B), GMA/MAA (C), GMA/MAA-GS (D) and DDLHG (E)

3.2 Swelling studies

The pH dependent swelling of gelatin, GMA/MAA and GMA/MAA-GS is shown in Figure 4. At acidic pH, GMA/MAA and GMA/MAA-GS has almost same swelling, this is due to the release of GS at this pH. At low pH conditions, -COOH groups remain unionised. This leads to the elimination of the main anion-anion repulsion and hydrogen bonding interaction is high. Due to the above reasons, the network tends to shrink and consequently the swelling is decreased. GMA/MAA has higher swelling, GMA/MAA-GS has low swelling at basic pH is due to the absence of free carboxyl groups. At this pH carboxyl groups are ionized, consequently the electrostatic attraction between the ions increases and the hydrogen bonding interaction weakens.

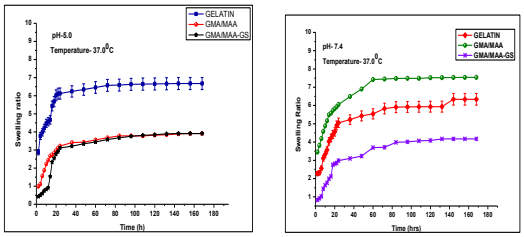


Figure 4 Effect of pH on swelling for Gelatin, GMA/MAA and GMA/MAA-GS

3.3 Drug release studies

The percent release of all the three components as a function of time was determine at pH 5.0 and 7.4 at 37.0 ^{0}C to investigate the effect of pH on drug release and the data is shown in Figure 5 a and b. From figures it is evident that release of GS is high at low pH condition and viceversa. This is due to the breakage of amide bond at this pH conditions. The release of other two is less than 50% at this pH, this may be due to the low swelling of the hydrogel network. The possibility of triggering the drug release in response to certain external stimuli is used to improve the efficacy of antibiotics. During *staphylococcus* infection the pH shift from physiological to acidic [3]. The amide bond is stable at physiological pH and broken in acidic conditions[4] is used here to conjugate GS to GMA/MAA.Release profile of GS shows a biphasic pattern consisting of an initial burst release during the first 24 hrs, this may be due to the release of the unconjugated drug molecules that may be adsorbed on the surface of carrier, followed by a slow and steady release for the next 6 days. At higher pH condition the release of GS is less than 20% and that of other two is high and the other two is released at this pH as a result of swelling of hydrogel matrix

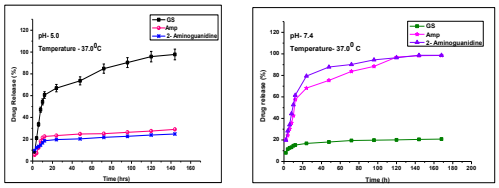


Figure 5 a and b Drug release at pH5.0 and 7. 4 for GS, Amp and 2-Amino guanidine.

3.*4 Antimicrobial studies*

The antimicrobial activities of GMA/MAA (A), Amp(B), GS(C), GMA/MAA-GS(D) and DDLHG(E) were studied against *E Coli* and *S. aureus* and the obtained results are shown in Figure 6. The zonal area is small for GMA/MAA for both bacteria, which indicates that it is highly biocompatible. For *E Coli* the zone is same for GMA/MAA-GS and DDLHG. This can be explained on the basis of the high activity of GS against *E Coli* and also on the basis of the structure of the drug conjugate in which GS is exposed to the environment and free to exhibit its properties. *S. aureus* is a gram positive bacteria, for which GS alone has minimum activity. Compared to pure drug, DDLHG show somewhat lesser antibacterial effect; as the release rate of

drug is slow and controlled from it [5].But combining with Amp it has high activity, due to the synergism in their activity.

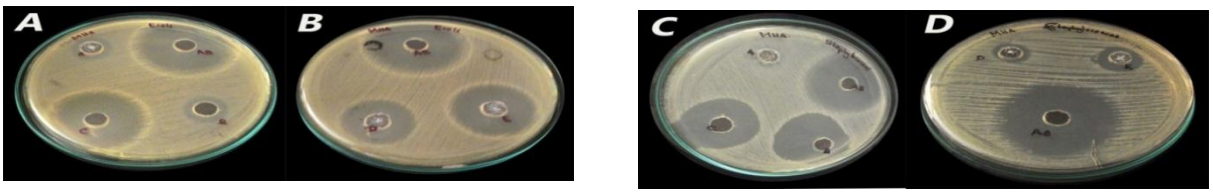


Figure 6 Antimicrobial activities of GMA/MAA (A), Amp(B), GS(C), GMA/MAA-GS(D) and DDLHG(E)

4. Conclusions

In the present work, design and fabrication of a novel DDLHG which can efficiently encapsulate three payloads and release them in a prolonged and controlled manner in response to the pH shift was successful. FTIR confirms the chemical modifications in each step of carrier synthesis. Swelling and drug release studies confirms the external pH as the triggering force for drug release. The presence of 2-Amino guanidine nullifies the big side effect of GS. The antimicrobial studies firmly confirms the increased anti bacterial effect of the drug combination. In short the present work confirmed the physiological acceptance, increased bioavailability of drug, prolonged anti bacterial activity as well as good bio compatible and biodegradable properties and our novel carrier is an excellent medium for the combination therapy against bacteria.

Acknowledgements

The authors are thankful to Professor and Head, Department of Chemistry, University of Kerala, Trivandrum, India for providing the laboratory facilities. One of the authors, A. Manasa Mohan is grateful to Department of Science and technology, Govt of India (DST) for providing assistance in the form of INSPIRE fellowship with grand number IF140061 for this work

References

1. P. Balakumar, A. Rohilla, A. Thangathirupathi, *Pharmacol Res.* 62, 179-86, 2010.

2. Muhammad R Khan, Iram Badar, AishaSiddiquah, *BMC Complementary and Alternative Medicine.* 11, 113, 2011.

3. S. K. Bajpai, J. Sonkusley, *J. Appl. Polym. Sci.* 84, 1133-1145, 2002, 133–1145.

4. T. S. Anirudhan, A. Manasa mohan, *RSC Adv.* 4, 12109-12118, 2014.

5. T. S. Anirudhan , P. L. Divya, J. Nima, *Chem. Eng. J.* 284, 1259–1269, 2016.

MACRO 166

Prodrug immobilized nanoparticles of Human Serum Albumin and PLGA for Treatment of Colorectal Cancer

Patel Pratikshkumar R,[a] Rathna Gundloori*,[a]

[a]*Polymer Science and Engineering, CSIR National Chemical Laboratory, Pune 411008,India.*

** e-mail id: rv.gundloori@ncl.res.in*

Abstract

Prodrug nanoparticles targeted for cancer treatment is considered to be more preferable over the conventional method to treat cancer because of reduced toxicity with effective treatment to cancer cells. Therefore, we proposed to develop nanoparticles that are drug immobilized and targeted to colon cancer using biocompatible polymers. We have designed and successfully made nanoparticle of human serum albumin (HSA) and Polylactic glycolic acid (PLGA) in oil phase by double emulsion method. To target and protect the Nanoparticle from acidic pH in stomach we modified the PLGA with Glucosamine by N,N'-Dicyclohexylcarbodiimide (DCC) Coupling. Conjugation is confirmed by ^{1}H, and C13. The dimension of nanoparticle were in range of 300 nm to 400nm with E-SEM and TEM.

Keywords: *PLGA-glucosamine; interaction studies; Double emulsion method; colorectal cancer.*

Introduction

More than 1·2 million patients are diagnosed with colorectal cancer every year, and more than 600 000 die from the disease. Incidence is higher in men than women and strongly increases with age; median age at diagnosis is about 70 years in developed countries. The cornerstones of therapy are surgery, neoadjuvant radiotherapy (for patients with rectal cancer), and adjuvant chemotherapy (for patients with stage III/IV and high-risk stage II colon cancer).[1]

After the surgery or with combination with radiation therapy, chemotherapy is given to patients to completely remove the cancer cells form body. So, it is necessary to develop the system which can kill cancer cells more effectively against cancer cells and doesn't harm to normal cells.

In present paper, we have made PLGA and HSA immobilized with glucosamine as targeted moiety and characterized delivery system by double emulsion method W/O/W. In this whole system we have used biodegradable and biocompatible polymers and protein-PLGA has been conjugated with Glucosamine. Here, Glucosamine is used as targeting moiety and to protect from acidic stomach. Human serum albumin is used to encapsulate the drug and to release the drug for longer time and help to undergo extracellular drug delivery. Polyvinyl alcohol (PVA) is used as emulsifier.

Experimental Materials:-Polyvinyl alcohol (PVA) was purchased from SDFCl. Glucosamine was purchased from Himedia. PLGA RG752S obtained as gift sample from evonik, Mumbai. Human Serum Albumin was purchased from Millipore.

Conjugation PLGA and glucosamine:-PLGA glucosamine conjugation is done by DCC Coupling.[2] 200mg of PLGA is dissolved in 3ml of DMSO (dimethyl sulphoxide) kept on stirrer. Then in PLGA solution 2 mole (11.56mg) of NHS (N-Hydroxysuccinimide) was added and kept for 1 hour at room temperature. Then glucosamine 6 mole (53.75mg) and DCC 3 mole (30.94 mg) was dissolved in DMSO. Glucosamine solution is added drop wise in PLGA solution total volume kept was 5ml and the reaction is allowed to heat at 60^{o} for 24 hour. The reaction is filtered and unconjugated Glucosamine is removed and dialyzed for 3 days in dialysis bag (2000 Da). Finally, purified conjugated PLGA-Glucosamine was lyophilized until it become dry. The percentage yield was found to be 96.8 %. The schematic diagram was show in (Figure 1).

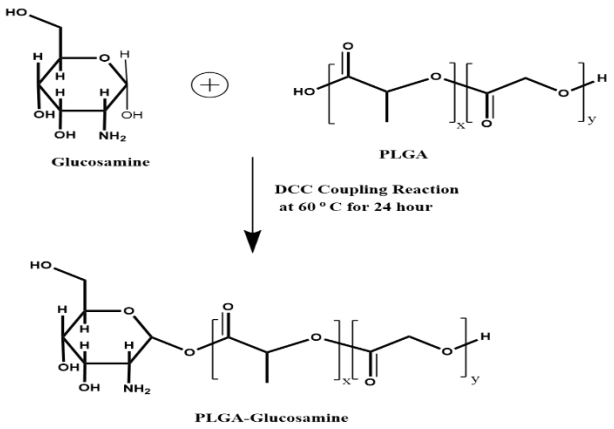


Figure 1:-Synthesis of PLGA-Glucosamine

Preparation of Nanoparticles:-

Nanoparticles were prepared by double emulsion solvent evaporation Method[3].For oil phase, PLGA-glucosamine (10mg) was dissolved in acetone (0.5ml) and DCM (2.5ml) using magnetic stirrer. In inner water phase, HSA (10mg) is dissolved in phosphate buffer pH 7.4. The oil phase is kept under sonication and water phase was added dropwise, then emulsified for 60s using the sonicator which resulted in w/o emulsion. This emulsion was dispersed in the outer water phase containing 2 wt% PVA (10ml) and using the same, sonicated for 1–3 min to obtain w/o/w double emulsion. The DCM was evaporated to solidify PLGA-Glucosamine NPs under continuous stirring (500 rpm) for 2 h using a magnetic stirrer. After the evaporation of DCM, dispersed solid PLGA NPs were dried by lyophilization and stored for further experimental analysis. All Sonication processes were always carried out in an ice bath. Utilization of an ultrasonic probe

leads to an increase in bulk temperature. If the temperature is not controlled using ice bath, some undesired effects may occur. The most obvious is the degradation of compounds of interest.

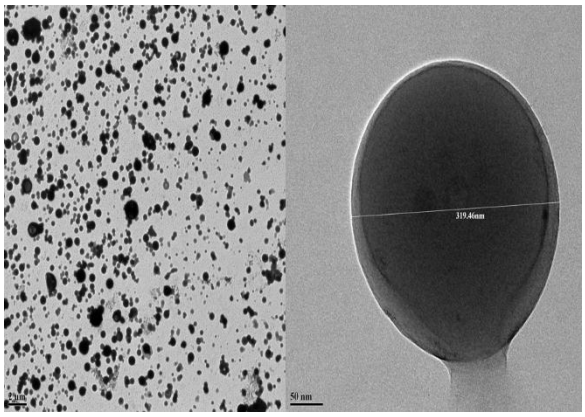


Figure 2:- TEM Images of PLGA-glucosamine

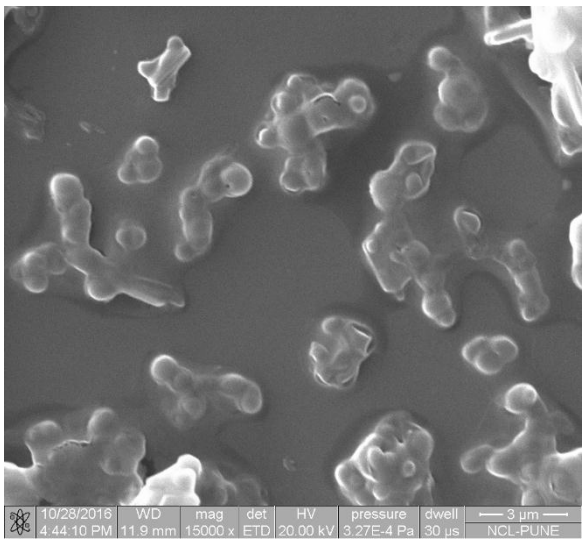


Figure 3:- E-SEM Images of PLGA-glucosamine

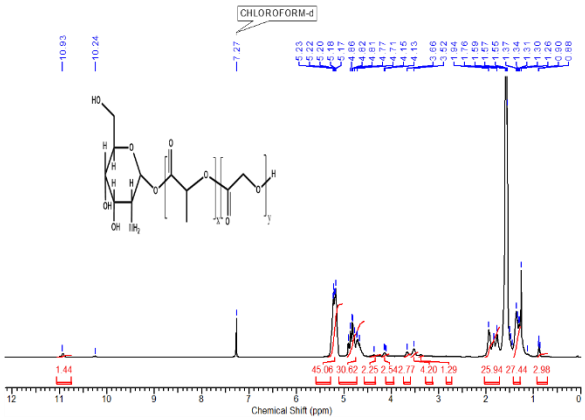


Figure 4:- ^{1}H NMR proton shifts of the conjugated PLGA–GlcN.



Figure 5:-Carbon13 of PLGA-Glucosamine

Conclusions

We have successfully synthesized and characterized by NMR the PLGA-glucosamine prepared by DCC Coupling. By double emulsion method, we have prepared prodrug PLGA-Glucosamine incorporated HSA nanoparticle in range of 300-400 nm. By this nanoparticle system we can incorporate Drugs for possible use against cancer cells.

Acknowledgements

PR Patel and RG would like to thank Council of Scientific and Industrial Research CSIR, CSIR-CSC0134, CSC0302, for funding the project. NCL and AcSIR for providing infrastructure and academic support.

References

1.Brenner, H.; Kloor, M.; Pox, C. P., *The Lancet* **2014,** (383), 1490 - 1502.
2. Mohana Marimuthu, Devasier Bennet and Sanghyo Kim Polymer Journal ***2013,*** 45, 202–209.
3.Panyam, J.; Dali, M. M.; Sahoo, S. K.; Ma, W.; Chakravarthi, S. S.; Amidon, G. L.; Levy, R. J.; Labhasetwar, V., *Journal of Controlled Release* **2003,** *92* (1), 173-187.

MACRO 167

Biodegradable copolymer for stimuli responsive sustained release of doxorubicin

Sayantani Bhattacharya,[a] Raja Shunmugam*[a]

[a] *Polymer Research Centre, Department of Chemical Sciences,*
Indian Institute of Science Education Research (IISER) Kolkata
e-mail id: sraja@iiserkol.ac.in

Abstract

In this work, we have synthesized a polymeric nanocarrier for the controlled release of anti cancer drug Doxorubicin. Motivated by the hydrolytically labile prospects of acylhydrazine bonds along with fascinating self-assembly properties of amphiphilic block copolymers; this work delineates on the design and synthesis of the **POLY-PE-PC-DOX** consisting of acylhydrazine tethered DOX and PE chains in the caprolactone backbone. Targeting optimal properties for controlled drug delivery, we pursued rational structural design of **POLY-PE-PC-DOX**. The incorporation of PE block makes the system advantageous as it shows no toxicity and can significantly promote water-solubility and increase plasma clearance half-life of nanostructures. Secondly, acid-sensitive acylhydrazine-based linkage is chosen to conjugate doxorubicin to trigger the sustained drug release. The inclusion of enzymatically cleavable disulphide linkage in the backbone is adding to the advantage of stimuli-responsiveness of our design.

Keywords: *polymer; caprolactone; biodegradable; doxorubicin*

Experimental

Materials: Sodium azide, copper (II) sulfate, Lithium diisopropylamide (LDA), propargyl bromide, tin (II)-trifluoromethanesulfonate [$Sn(OTf)_2$], ε-caprolactone, cyclohexanone, monomethoxy poly(ethylene glycol),carbo-di-imidazole,2-hydroxyethyl disulfide,1,8-diazobicyclo[5,4,0]undec-7-ene (DBU), THF, toluene, deuterated chloroform ($CDCl_3$), dimethyl sulfoxide-d_6 (DMSO-d_6).

Instrumentations:

NMR**:** ^{1}H NMR and ^{13}C NMR were done on Bruker 500 MHz and 125 MHz respectively. FT-IR: Spectra were obtained from Perkin-Elmer Spectrometer. Fluorometry: Emission recorded from Horiba Jobin Yvon, Fluromax-3, Xe-150 W. GPC: Waters Gel Permeation Chromatography in THF. DLS: Particle size was measured using Malvern Zetasizer nano with 4.0 mW He-Ne laser at λ=633 nm. TEM: Low resolution TEM was performed on JEOL 200 CX microscope.

Introduction

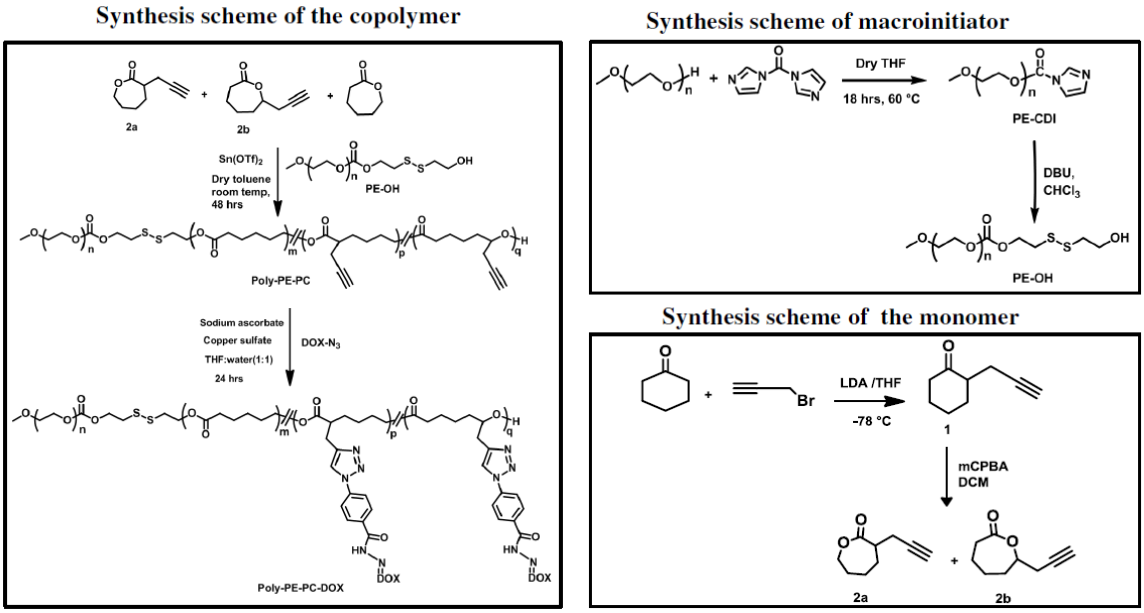
Polymeric nanoparticles serve as efficient drug carriers because of enhanced permeability and retention (EPR) effect.[1-3] In the field of drug delivery, biodegradable polymers receive great deal of attention as they break down into small fragments and can be readily excreted from the body. Some of the widely used biodegradable polymers are poly (lactic acid) (PLA), poly ε-caprolactone (PCL), and their copolymers.[4] Doxorubicin is a well known anti cancer drug but it lacks site specificity and is toxic to normal cells.[5-7] Now, there are two ways to deliver the toxic drugs specifically to the tumour cells, namely, covalent and non-covalent approach. Covalent approach is superior to the non-covalent ones, as it eliminates burst mechanism.[6] The release of drugs attached via covalent approach is based on stimuli responsive linkers. The most widely used linkers are imines, oximes, acetals acylhydrazine.[8-12] Among these, acylhydrazine linker is promising because of the highly pH- responsive nature in the field of drug delivery. There are a handful of

reports which describes the reductive nature of disulphide bonds present in the polymeric prodrug.[13-16] The disulphide bond is stable under physiological conditions but in the intracellular region, it gets reduced to the corresponding alcohol as the glutathione concentration is very high (GSH, 10mM).[17-20]

Herein, we have designed and synthesised a polymeric nanocarrier **POLY-PE-PC-DOX** which is both pH as well as reduction responsive. The amphiphilicity present in the design brings about self-assembly. Scanning Electron Microscopy (SEM) and Transmission Electron Microscopy (TEM) analysis suggests the vesicular nature of the nanoaggregates. The pH-sensitivity of the acylhydrazine linker is tested by dialysis against acidic environment. The biodegradability of the backbone is confirmed by the reductive behaviour in presence of dithiothreitol (DTT). Cell viability studies suggest biocompatibility while epifluorescence microscopy and flow cytometry analysis shows increased internalisation of the drug into the cells.

Results and discussion

The present work describes an efficient method to covalently attach the anti cancer drug DOX and poly (ethylene glycol) to the biodegradable caprolactone with S-S linker (Scheme 1). The reaction scheme can be divided into three parts. In the first step, the macroinitiator **PE-OH** was synthesised. Then the caprolactone functionalised monomer was synthesised by alkylation and followed by Baeyer-Villiger oxidation. The isomeric mixture of lactones 3-((prop-2-ynyl) oxepan-2-one) 2a and 7-((prop-2-ynyl) oxepan-2-one) 2b was obtained. The mixture of compounds was thoroughly characterised by ^{1}H NMR and ^{13}C NMR spectroscopy. For the copolymerisation, compound mixture 2a and 2b was copolymerised with ε-caprolactone under nitrogen atmosphere via Ring Opening Polymerisation (ROP) for 48 hrs. **PE-OH** was used as macroinitiator and $Sn(OTf)_2$ as catalyst. The ratio was maintained at [2a and 2b]:[ε-CL]:[$Sn(OTf)_2$]: [PE-OH] =10:90:5:1). The resulting copolymer was characterised by ^{1}H NMR, FT-IR spectroscopy and GPC techniques. The GPC trace of the copolymer **PE-PC** was unimodal with the mol wt 7700g/mol and PDI = 1.25. After copolymerisation, azide functionalised doxorubicin with acylhydrazine linker (DOX-N_3) was synthesised following an already reported procedure.[21] Then DOX-N_3 was conjugated with the polymer employing alkyne-azide click chemistry. The reaction was carried out using sodium ascorbate and copper (II) sulphate in THF and water mixture (1:1). The product formation was confirmed by ^{1}H NMR spectroscopy (Figure 1) where all the characteristic peaks of PE, DOX appeared in addition to a new triazole peak at δ 7.37 ppm. In the FT-IR spectroscopy, azide stretching frequency at 2095 cm^{-1} disappeared which further confirms successful click reaction. Next, the CAC of **POLY-PE-PC-DOX** was measured in water using pyrene as fluorescent probe. The CAC value was 180 μg/mL. The size of the aggregate was determined from DLS measurements. The radius was about 104 nm with PDI = 0.26. Both SEM and TEM analysis revealed vesicular morphology. The diameter of the aggregate was about 200 nm which was comparable with the DLS data. (Figure 2)



Scheme 1: Synthesis of macroinitiator, monomer and the copolymer.

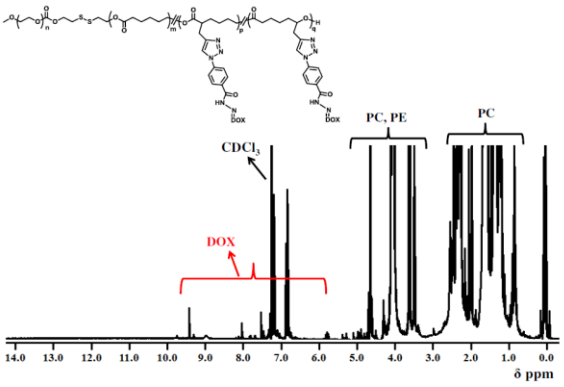
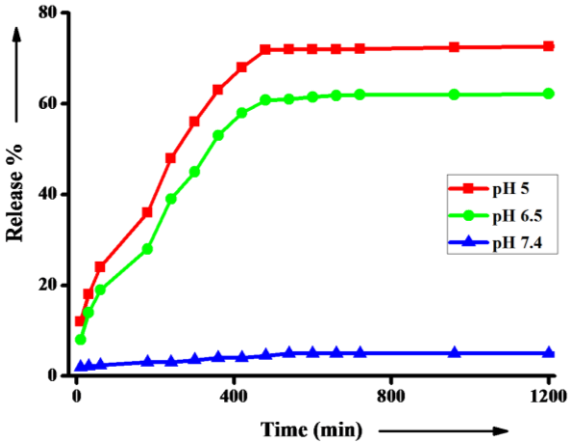


Figure 1: ^{1}H NMR of **POLY-PE-PC-DOX** in $CDCl_3$.



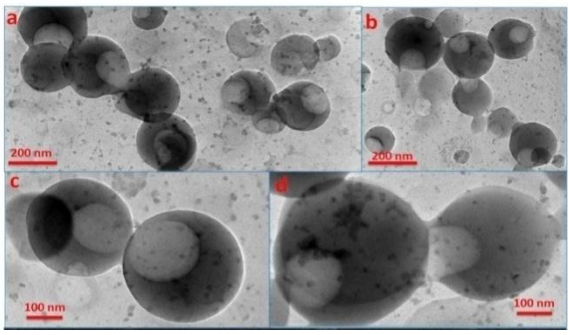


Figure 2: (a-d) TEM images of **POLY-PE-PC-DOX.**

To investigate the stimuli responsiveness of the nanocarrier, dialysis study was performed at different pHs e.g. 7.4, 6.5 and 5. For this purpose, 1 mg of **POLY-PE-PC-DOX** was dissolved in 1 mL phosphate buffer solution then it was loaded in a dialysis tube and dialyzed against 80 mL water at pH 5 by gentle stirring. For the fluorescence spectrum, the excitation wavelength was set at 510 nm and emission intensities were monitored at

560 and 588 nm. The aliquot was added back to the solution each time to maintain the constant volume. This process was carried out at every 1 hr and continued up to 48 hrs. The increase in fluorescence intensity was not significant after 10 hrs. Similar procedure was involved to monitor the drug release at pH 6.5 and 7.4. The drug release was more at acidic pH compared to the physiological pH (Figure 3). This result clearly indicated the pH responsiveness of acylhydrazine linker.

Figure 3: DOX release profile at different pH.

In the polymeric backbone, disulphide bond was preset, making the copolymer reductively degradable by the treatment of GSH and DTT. To demonstrate the reduction responsiveness, the copolymer **POLY-PE-PC-DOX** was treated with 10 mM GSH (intracellular GSH concentration in tumour cells). The particle sizes were monitored by DLS at different time intervals. We observed immediate increase of the average diameter to 1000 nm within 10 mins. This prompt increase in diameter in presence of GSH was caused by the disassembly of the vesicular architecture. We believed that the increment in size was due to rupture of polymer chain by disulphide bond followed by recombination of the chains. Interestingly the aggregate size did not vary when it was not treated with GSH, indicating stability of the nanocarrier under physiological medium. The degradation behaviour of the copolymer in presence of DTT was also confirmed by GPC analysis. The copolymer peak shifted to higher retention time with three fragments. The disaggregation of the copolymer was further supported by SEM analysis, which revealed the rupture of self-assembled morphology.

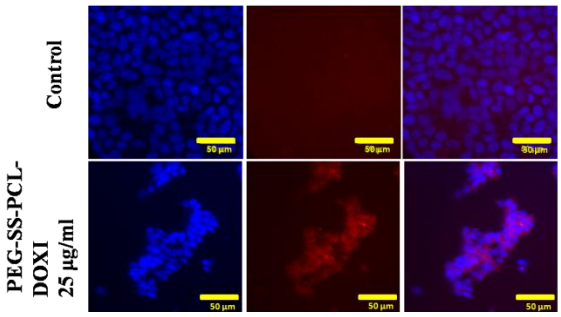


Figure 4: Epifluorescence microscopy images of the MCF-7 cell line with **POLY-PE-PC-DOX.**

Cellular uptake studies were carried out using epifluorescence microscope (Figure 4). MCF-7 cells were treated with free DOX and **POLY-PE-PC-DOX** having concentrations 25, 50 and 100 µg/mL at 37 ºC for 24 hrs. Microscopic observations showed that both free DOX and the nanocarrier entered the cells with increased concentrations. Cell viability of free DOX was more than that of **POLY-PE-PC-DOX,** but the nanocarrier showed a gradual change which indicated sustained and controlled release of the drug. Flow cytometry results revealed that the mean fluorescence intensities and the fold change for free DOX and **POLY-PE-PC-DOX** were comparable. Biological studies have shown that free DOX was more effective for killing cancer cells but it did not have site-specificity. It was noteworthy that the nanocarrier disaggregated through disulphide bonds only in the cancer cells due to the presence of GSH and released the drug employing pH responsive acylhydrazine linker in sustained manner.

Conclusions

This article reports the synthesis of the nanocarrier **POLY-PE-PC-DOX**, in which, the anti cancer drug DOX was covalently attached to the biodegradable caprolactone backbone via pH-sensitive acylhydrazine linker, thereby releasing the drug in stimuli responsive controlled way. Owing to the inherent Amphiphilicity, the nanocarrier self-assembled to form a vesicular aggregate which was suggested by SEM and TEM analysis. Cell viability studies demonstrated effective internalisation of the nanocarrier into the tumour cells.

Acknowledgements

S.B. thanks IISER Kolkata for fellowship. R.S. thanks the DST for Ramanujan fellowship, DBT for funding. R.S. and J.D.S. thank IISER Kolkata for infrastructure.

References

1. R. Duncan, *Nat. Rev. Cancer*. 6, 688, 2006.
2. M. J. Stukel, C. R. Li, D. H. Maynard R. M. Caplan, *Biomacromolecules,* 11, 160, 2010,
3. D. Li, H. Sun, J. Ding, Z. Tang, Y. Zhang, W. Xu, X. Zhuang, X. Chen, *Acta Biomater*. 9, 8875, 2013.
4. M. Mizutani, C. S. Arnold, T. Matsuda, *Biomacromolecules*, 3, 668, 2002.
5. L. Zhou, R. Cheng, H. Tao, S. Ma. W. Guo, F. Meng, H. Liu, Z. Liu, Z. Zhong, *Biomacromolecules*, 12, 1460, 2011.
6. R. E. Gillies, J. M. J. Frechet, *Bioconjugate Chem*. 16, 361, 2005.
7. R. E. Gillies, J. M. J. Frechet, *Chem. Commun.* 14, 1640, 2003.
8. J-M. Lehn, A. Eliseev, *Science*, 291, 2331, 2001**.**
9. J-M. Lehn, *Chem. Soc. Rev.* 36, 151, 2007.
10. Y. Jin, L. Song, Y. Su, L. Zhu, Y. Pang, F. Qiu, G. Tong, D. Yan, B. Zhu, X. Zhu *Biomacromolecules*, 12, 3460, 2011.
11. R. E. Gillies, J. M. J. Frechet, *Pure Appl. Chem*. 76, 1295, 2004**.**
12. B. J. Matson, I. S. Stupp, *Chem. Commun*. 47, 7962, 2011.
13. J. Li, M. Huo, J. Wang, J. Zhou, M. J. Mohammad, Y. Zhang, Q. Zhu, Y. A. Waddad, Q. Zhang, *Biomaterials*, 33, 2310, 2012.
14. J. Liu, Y. Pang, W. Huang, Z. Zhu, X. Zhu, Y. Zhou, D. Yan, *Biomacromolecules*, 12, 2407, 2011.
15. H. Sun, F. Meng, R. Cheng, C. Deng, Z. Zhong, *Expert Opin. Drug Delivery*, 10, 1109, 2013.
16. N. Chan, Y. An, K. J. Oh, *Polym. Chem.* 5, 1637, 2014.
17. Y. Yan, Y. Wang, K. J Heath, C. E. Nice, F. Caruso, *Adv. Mater.* 23, 3916, 2011**.**
18. P. D. Jones, L. J. Carlson, Jr. V. C. Mody, J. Cai, J. M. Lynn, Jr. P. Sternberg, *Free Radical Biol. Med.*, 28, 625, 2000.
19. H. Sun, B. Guo, X. Li, R. Cheng, F. Meng, H Liu, Z. Zhong, *Biomacromolecules*, 11, 848, 2010**.**
20. G. Saito, A. J. Swanson, K-D. Lee, *Adv. Drug Delivery Rev.* 55, 199, 2003.
21. M. N. Ganivada, V. N. Rao, H. Dinda, P. Kumar, J. Das Sarma, R. Shunmugam, *Macromolecules,* 47**,** 2703, 2014**.**

MACRO 172

Polymer-Chlorambucil Drug Conjugates: A Dynamic Platform of Anticancer Drug Delivery

Saha, Biswajit; Haldar, Ujjal; De, Priyadarsi*

Polymer Research Centre, Department of Chemical Sciences, Indian Institute of Science Education and Research Kolkata, Mohanpur - 741246, Nadia, West Bengal, India.

** Corresponding author E-mail: p_de@iiserkol.ac.in*

In recent years, alkylating agents have been attracting too much attention towards cancer therapy. Among many types of alkylating agents, the nitrogen mustard chlorambucil (CBL) is one of the classic examples of bifunctional alkylating agent as anticancer drug, which has already been approved for cancer treatment. The nitrogen mustard moiety in CBL is the most attractive part, because it interferes in the replication of deoxyribonucleic acid (DNA) through the alkylation of nucleobases by forming aziridinium ion as an intermediate and it is important to mention that carboxylic side in CBL is pharmacokinetic but not dynamic. Therefore, binding of a non-toxic molecule to this carboxylic side of CBL will only affect its absorption and half-life, not the effectiveness.

At present, the polymeric prodrugs have attracted considerable attention to achieve low toxicity and potential drug delivery towards cancer cells. Polymer-drug conjugates (PDCs) in which drug molecules are covalently bound to polymeric systems *via* biodegradable linkers are promising co-delivery carriers. In this work, we have developed a simple strategy to make PDCs of an antitumor alkylating agent, chlorambucil, using a biocompatible disulphide linker. Chlorambucil based chain transfer agent was used to prepare various homopolymers and block copolymers in a controlled fashion via reversible addition-fragmentation chain transfer (RAFT) polymerization. Chlorambucil conjugated block copolymer, poly(polyethylene glycol monomethyl ether methacrylate)-*b*-poly(methyl methacrylate) (PPEGMA-*b*-PMMA) formed well-defined spherical nanoparticles (NPs) in aqueous medium, as confirmed by ^{1}H NMR, DLS and FE-SEM study. The block copolymer enabled the release of CBL in the presence of D, L-dithiothreitol (DTT) as reducing agent and also can load hydrophobic dye/drug molecules. In response to reductive reactions, CBL released from the micelles does not affect the aggregated nature of PPEGMA-*b*-PMMA, which was confirmed by DLS and FE-SEM study. These significant results suggest that a well-defined thiol-responsive spherical NP can act as a drug-delivery systems (DDS) towards cancer therapy through alkylating the nucleobases of DNA.

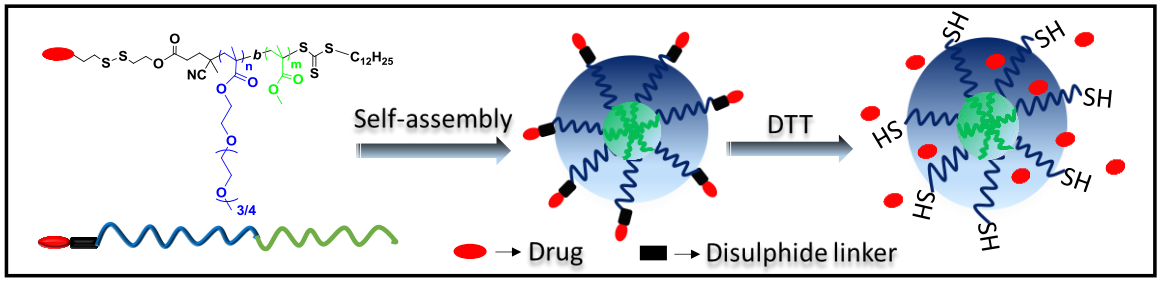


Figure 1. Schematic representation of self-assembly of PPEGMA-*b*-PMMA block copolymer and their thiol-responsive degradation with DTT.

References
[4] Esencay, M; Hamad, B. *Nat. Rev. Drug Discov*., 14 (2015) 381.
[5] Aleksanian, S; Khors, B; Schmidt, R; Oh, J. K. *Polym. Chem*., 3 (2012) 2138.
[6] Omoomi, F. D; Siadat, S. D; Nourmohammadi, Z; Tabasi, M. A; Pourhoseini, S; Agha, R. *J. Cancer Sci. Ther.,* 5 (2013) 075.
[7] Pal, S; Roy, S. G; De, P. *Polym. Chem*., 5 (2014) 1275.
[8] Saha, B; Haldar, U; De, P. *Macromol Rapid Commun*, DOI: 10.1002/marc.201600146.

MACRO 173

PEGylated Polymeric Nanogel For Theranostic Applications

Vineeth M Vijayan, Muthu Jayabalan*.

Polymer Science Division, BMTWing,

Sree Chitra Tirunal Institute for Medical Sciences and Technology,

Thiruvananthapuram –695012, Kerala, India,

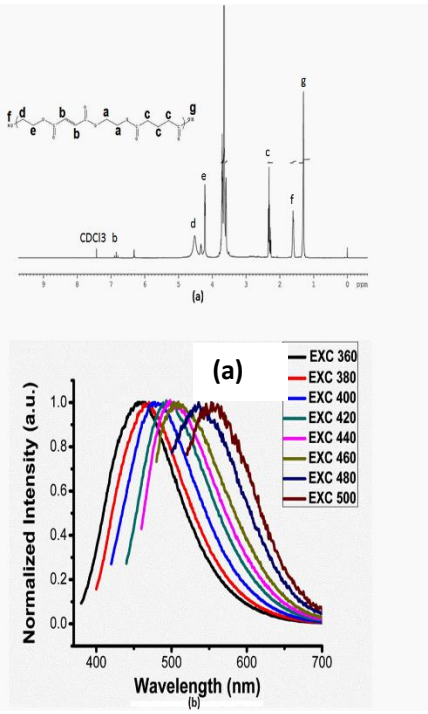
**Fax:0091-471-234814; Tel: 0091-471-2520212; E-Mail. mjayabalan52@gmail.com*

Introduction: Theranostics is an emerging area in nanomedicine which offers tremendous advantages such as monitoring and quantification of drug release and non invasive assessment of drug accumulation at the target site. Polymer-based theranostic agents are of particular interest as they possess useful properties such as stability, biocompatibility and availability of functional groups for specific cancer cell targeting [1]. The current strategy of constructing a polymer-based theranostic agent relies on the incorporation of fluorophores and magnetic resonance imaging contrast agents, which have inherent drawbacks such as toxicity, high cost, low sensitivity and non-biodegradability. Nanogels are nanosized hydrogel particles which are formed by the physical or chemical crosslinking of polymeric networks [2]. Nanogels offer several advantages as a drug carrier such as high drug loading capacity, high stability and responsiveness to environmental factors such as ionic strength, pH and temperature. Hence, photoluminescent polymeric nanogels having innate fluorescent property and biocompatibility could serve as an ideal theranostic platform. The present paper deals with PEGylated Polymeric Nanogel For theranostic Applications

Methods: Synthesis of fluorescent PEGylated comacromer: The PEGylated comacromer was synthesized by non-catalysed melt polycondensation of PEG with maleic acid and glutamic acid. The structure and photoluminescence properties of the PEGylated comacromer formed were

analysed using proton NMR and fluorescence spectroscopy respectively.The comacromer was further crosslinked with diethyleneglycoldimethacrylate to form nanogel. The cancer cell imaging capability of this nanogel was evaluated by cellular uptake studies using cervical cancer cell line Hela.

Results and Discussion: Proton NMR spectrum of the comacromer (Figure 1 a) shows peaks at 6.8 ppm (CH=CH of maleic acid), 3.6 ppm (-CH_2 groups of PEG), 1.3 ppm (-OH from glutamic acid) which proves the formation of comacromer. The studies on fluorescence characteristics of the comacromer in aqueous condition reveal emissions red-shifted from 420 nm to 680 nm for excitations from 360 nm to 500 nm with reduced intensity with increase in excitation ascertaining the excitation wavelength dependent fluorescence characteristics (Fig1b).The nanogel has smooth spherical morphology with particle size around 40 nm (Fig 2a). The nanogel also exhibited good dispersion stability, which may be attributed to the PEG chains present on the surface of the comacromer. The cellular uptake studies on Hela cells with nanogel and imaging with excitation at 488 nm reveal green fluorescence which reveals cancer cell imaging capability (Fig 2b). The inherent EDF characteristics associated with C-PLM NG enable cellular imaging when excited at 488 nm. Imaging of the cells was accomplished by the bright green fluorescence produced by the nanogel.



.

Fig.1. Proton NMR spectra of comacromer (a), Fluorescent spectra of comacromer (b)

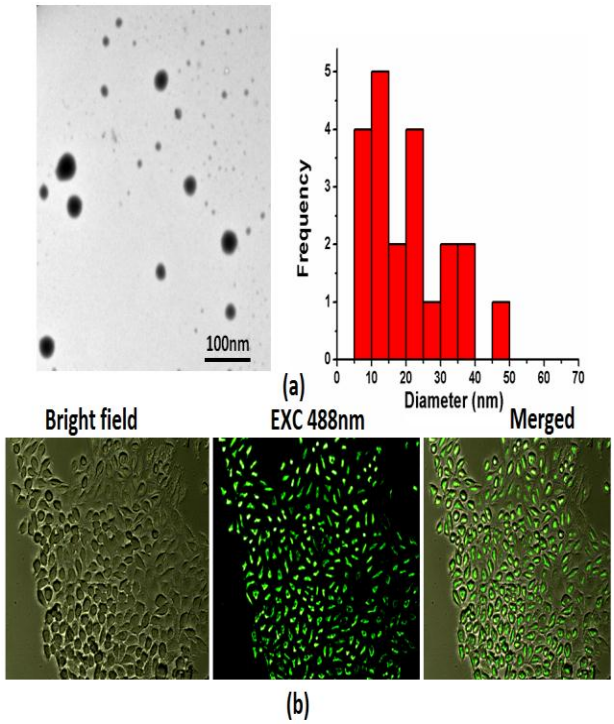


Fig.2. Morphology and size distribution of nanogel (a), cancer cell imaging capability of nanogel (b)

Conclusion: The synthesized nanogel displayed good diagnostic capability on cancer cells. As nanogels are ideal drug carriers, the present self fluorescent nanogel has promising potential as biocompatible theranostic agent. In the current area of nanomedicine, such self-fluorescent PEG-based polymeric nanogel systems with innate theranostic capabilities are not well-established or explored, despite the potential impact that they could have in the field.

References

[1] Xie, J.; Lee, S.;Chen, X.Adv. Drug Deliv. Rev, *62* (**2010)** *1064.*

[2] Kumar, N.; Asok, N.; Nair, S.; kumar, G.Int J Nanomedicine,*7* (**2012)** 5769.

MACRO 175

Injectable, Elastic and Conducting Hydrogel for Tissue Engineering Applications

Komeri Remya and Muthu Jayabalan *

Sree Chitra Tirunal Institute for Medical Sciences and Technology, Polymer Science Division, BMT Wing, Thiruvananthapuram – 695 012, Kerala State, India.

**Fax:0091-471-234814; Tel: 0091-471-2520212;E-Mail.* mjayabalan52@gmail.com.

Introduction*:* The tissue engineered constructs for electro responsive nervous, cardiac and bone tissues require electrically conducting matrices for better tissue formation. Electrical conductivity is reinforced in tissue- engineered constructs using carbon nanotubes or gold nanowires which have drawbacks such as inhomogeneous distribution, non biodegradability and unknown long term effects [1]. Polymers like poly pyrrole, poly aniline and poly thiophene are identified with metal-like conducting property. However cytotoxicity, non biodegradability and water insolubility limits the use of these conducting polymers for tissue engineering applications. Due to ease of synthesis, processibility, and antibacterial effect, poly aniline is recently recommended for conducting films for cardiac and nerve growth [1]. However, injectable hydrogels containing poly aniline for cell therapy is rarely reported. Here we report an injectable, elastic and conducting hydrogel prepared from poly aniline conjugated fumarate-co-PEG-co-sebacate comacromer for tissue engineering applications.

Experimental section

Synthesis of sulfonated poly aniline: Sulfonated poly aniline was synthesized by oxidative polymerization of anilinium hydrochloride as per the published report [2]. 0.5 g of poly aniline emaraldine salt was mixed with 10 ml cold conc.sulfuric acid at 4 ^{0}C for 1 h. The sulfonated poly aniline was precipitated in ice : water (75 : 25) mix and centrifuged at 3000 rpm. The pellet of sulfonated poly aniline was dried at 40 ^{0}C. Sulfonated polyaniline is coded as PANIS.

Synthesis of carboxy terminated poly fumarate-co-PEG-co-sebacate comacromer: 1.5 M maleic anhydride, 1.5 M sebacic acid, 3 M poly ethylene glycol 300 were refluxed in round bottom flask for 1 h at 160 ^{0}C in nitrogen atmosphere. 0.5 g morpholine and 0.25 g sodium acetate were used as catalyst. Vacuum condensation was done at 180 ^{0}C for 5 min. The polymer was precipitated in cold diethyl ether. The solvent was evaporated using rotary evaporator at 40 ^{0}C and stored at 4 ^{0}C.

Synthesis of conducting comacromer: 0.5 g fumarate-co-PEG-co-sebacate comacromer was neutralized with sodium bicarbonate in a round bottom flask at room temperature. Carboxyl groups of polymer was activated with equal volumes of 0.4 M 1-Ethyl-3-(3-dimethylaminopropyl) carbodiimide **(**EDC) and 0.1 M N-hydroxysuccinimide (NHS) for 10 min. 300 mg sulfonated poly aniline was slowly added into the reaction mix and stirred continuously for 24 h. The reaction mix was dialyzed, lyophilized and stored at 4 ^{0}C. The conducting comacromer is coded as PANIS-P. Structural analysis was done with FT-IR, ^{1}H-NMR and UV-Visible spectroscopy.

Preparation of hydrogel*:* The conducting PANIS-P comacromer was diluted at 20:80 ratio with distilled water and mixed with 20 mg PEGdiacrylate (PEGDA) to prepare PANIS-P/PEGDA hydrogel.

Characterisation of hydrogel*:* Swelling and crosslink density of PANIS-P/PEGDA hydrogel was determined in distilled water at 37 ^{0}C. *In vitro* ageing profile of PANIS-P/PEGDA hydrogels was studied at 37 ^{0}C for 28 days in PBS. Compressive mechanical property and stress-strain behaviour of PANIS-P/PEGDA hydrogel was determined using universal mechanical analyser. ESEM analysis of PANIS-P/PEGDA hydrogel was carried out to analyse surface and internal morphology. DPPH radical scavenging activity of PANIS-P/PEGDA hydrogel was investigated to determine antioxidant property. Cytocompatibility of PANIS-P/PEGDA hydrogel was analysed with L929 cells and H9c2 cardiomyoblast cells by MTT assay and direct contact assay. Electrical resistance of cylindrical PANIS-P/PEGDA hydrogel was determined using multimeter. The conductivity of hydrogel was calculated using the following formula

Conductivity= Length/ (Resistance x Area of cross section)

Results and discussion: The presence of trans fumarate double bonds in PANIS-P comacromer facilitate *in situ* crosslinking with vinyl crosslinker, PEGDA. FT-IR spectral responses at 1653 cm $^{-1}$ and ^{1}H-NMR chemical shift of protons at 6.2-6.7 ppm substantiate the presence of trans fumarate double bonds in PANIS-P comacromer. The formation of amide bonds between fumarate-co-PEG-co-sebacate comacromer and poly aniline is confirmed with the spectral responses at 1570 cm^{-1} and 1345 cm^{-1} in FT-IR spectrum of PANIS-P (Fig.1A). The UV-Visible spectral absorbance of PANIS-P comacromer at 685 nm indicates the presence of conducting electrons (Fig. 1B) [3]. PANIS-P/PEGDA hydrogel hold 84.08% water on equilibrium swelling and retains the compressive Young's modulus of 442 kPa (Table 1). Compressive Young's modulus of the present hydrogel lies in the range of stiffness of native tissue counterparts which is suitable for skin and cardiac applications [4]. Moreover the hydrogel return to the original size even after 60% compression which also reveals elastic property. PANIS-P/PEGDA hydrogel looses 47% and 90% of initial weights after 8 and 28 days of *in vitro* ageing at 37 ^{0}C under continuous shaking conditions. The present hydrogel is porous with wide interconnected internal pores suitable for cell encapsulation (Fig.1C). The porous nature is beneficial for better oxygen, nutrient transport and vascularization. The present hydrogel exhibit conductivity of 3 x 10^{-4} S/cm (Table 1). The electrical conductivity of native murine myocardium is 0.16 x 10^{-2} S/cm [5]. The PANIS-P/PEGDA hydrogel scavenge 63% DPPH radical which is significant when compared with 50 µM ascorbic acid (Fig.1D). MTT assay and direct contact assay of hydrogel reveal cytocompatibility with L929 fibroblast and H9c2 cardiomyoblast cells. L929 cells exhibit more than 80% viability with the hydrogel extract. L929 cells and H9c2 cardiomyoblast cells retain its original morphology even after 12 h of contact with hydrogel (Fig. 1E&1F). The green fluorescing live cells observed in live dead assay of L929 cells after 12 h of direct contact with PANIS-P hydrogel confirm cytocompatibility of hydrogel (Fig. 1G).

Table 1. Physico-chemical properties of hydrogel.

Properties	PANIS-P/PEGDA
1.Injectable formulation	
Comacromer concentration (%)	20%
Crosslinker (mg)	20
0.4 M APS (µl)	20
6 M TEMED (µl)	3
2. Setting characteristics	
Setting time (min)	6
Setting temperature (^{O}C)	35
3.Swelling properties	
Weight swelling ratio	6.3
Equilibrium water content (%)	84.08
Cross linking density (mol/cm^3)	0.030
Molecular weights between Crosslinks (g/cm$^{3)}$)	32
4.Mechanical properties	
Maximum load(N) at break	2.86
Youngs modulus (kPa)	442
Compressive stress(kPa)	44
5. Conducting property	
Resistance (Ω)	1986
Conductivity (S/cm)	3 x 10^{-4}

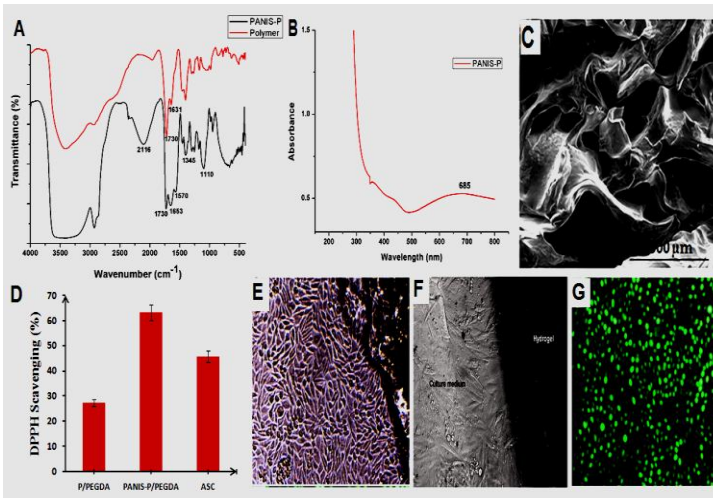


Fig 1: FT-IR spectrum of PANIS-P comacromer (A), UV-Visible absorption spectrum of PANIS-P (B), ESEM image of hydrogel cross section (C), DPPH scavenging assay of hydrogel (D), direct contact assay of PANIS-P hydrogel with L929 cells (E) and H9c2 cardiomyoblast cells (F), live dead assay of L929 cells after direct contact test (G).

Conclusion: The present PANIS-P/PEGDA hydrogel is injectable, cytocompatible and porous which is suitable for tissue engineering applications such as cell encapsulation and cell delivery. The candidate hydrogel has conducting and elastic property favourable for cardiac tissue engineering. Moreover, the free radical scavenging property of hydrogel is beneficial to reduce the hypoxic microenvironment at the infarcted or inflamed tissue zone, which can fasten the repair process. Briefly, the PANIS-P/PEGDA hydrogel is a potential injectable system for minimally invasive tissue engineering applications.

References

[9] Qazi TH, Rai R, Boccaccini AR. Tissue engineering of electrically responsive tissues using polyaniline based polymers: a review, Biomaterials. 35 (2014) 9068–9086.

[10] Azhar FF, Olad A, Salehi R. Fabrication and characterization of chitosan–gelatin/nanohydroxyapatite–polyaniline composite with potential application in tissue engineering scaffolds, Des. Monomers Polym. 17 (2014) 654–667.

[11] Cui H, Liu Y, Cheng Y, Zhang Z, Zhang P, Chen X, Wei Y. *In vitro* study of electroactive tetraaniline-containing thermosensitive hydrogels for cardiac tissue engineering, Biomacromolecules. 15 (2014) 1115–1123.

[12] Miller K, Biomechanics of soft tissues, Med. Sci. Monit. Int. Med. J. Exp. Clin. Res. 6 (2000) 158–167.

[13] Raghavan K, Porterfield JE, Kottam ATG, Feldman MD, Escobedo D, Valvano JW *et al*. Electrical conductivity and permittivity of murine myocardium. IEEE Trans. Biomed. Eng. 56 (2009) 2044–2053.

MACRO 178

Synthesis, characterization and *in-vitro* studies of folic acid decorated graphene oxide/chitosan nanocomposites for cancer drug delivery

Ananya Deb, Vimala.R*

School of Biosciences and Technology, VIT University, Vellore, Tamilnadu, India-632014

***vimala.r@vit.ac.in**

Graphene oxide nanomaterials are widely used to achieve effective cancer treatment. In this study, a novel graphene oxide mediated drug delivery system was synthesized by combining anticancer drug camptothecin (CPT) to the large surface area of graphene oxide by π-π stacking. Initially graphene oxide was synthesized by hummer's method and to obtain a more precise drug delivery, the system was decorated with folic acid conjugated chitosan. The resultant conjugate was characterized by FTIR, XRD, UV, Ramam spsctroscopy, SEM, TEM and AFM. The cationic and hydrophobic nature of chitosan was found to impart stability to the nano drug delivery system. The graphene-oxide-folic acid-chitosan-camptothecin (GO-FA-CHI-CPT) drug delivery system showed a pH dependent drug release as observed by UV analysis. The anticancer activity of the synthesized drug delivery system was studied by MTT assay using MCF-7 breast cancer cell lines. The conjugate showed enhanced anticancer activity thus could be used as a potential candidate for drug delivery.

Key Words: Graphene oxide, drug delivery, chitosan, natural polymer, camptothecin

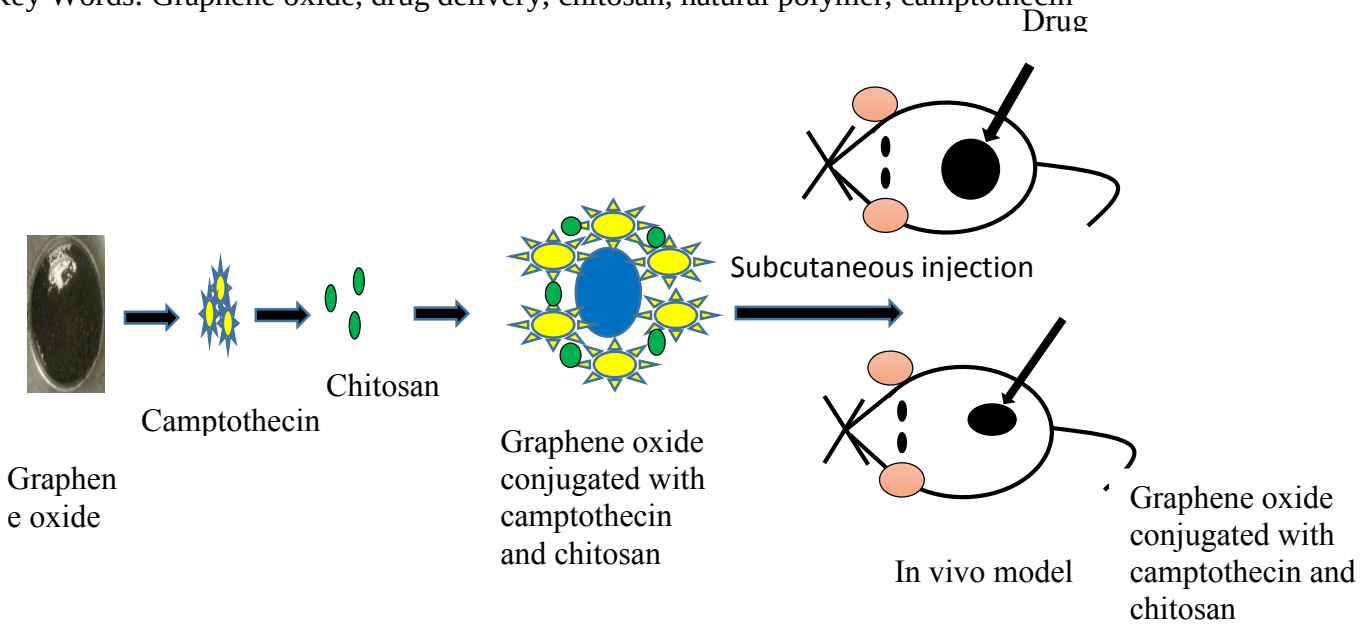


Figure: In vivo tumor bearing rat model treated with Graphene oxide conjugated camptothecin and chitosan

MACRO 179

Synthesis and Characterization of Sodium Alginate / Gelatin / Hydroxyapatite Green Nanocomposites

Mohanan, A*

Department of Chemistry, Nehru Arts & Science College, Kanhangad, Kerala, India

Email id : drmohanan75@gmail.com

Nanocomposite is a composition having a dispersed material that has one or more dimensions, such as length width and thickness, in the nanometer size range. Nano-sized materials possess uniqueness in their properties and designes as compared to their bulk counterparts. The nano sized materials have emerged as suitable alternatives to overcome drawbacks of composite and microcomposite materials. Biopolymer/Hydroxyapatite nanocomposites are a novel class of materials which have recently attracted interest as biomaterials and as drug delivery items. The objectives of the present study were the synthesis and characterization of green nanocomposites consists of sodium alginate, gelatin & hydroxyapatite. The nanocomposites of various composition were made by changing the ratio of the components. The prepared nanocomposites beads were characterized by means of XRD, Zeta sizer and SEM for better understanding regarding their composition and surface morphology. Poly dispersity index of particles and mean particle sizes were measured by zeta sizer. XRD reports confirm the nanocrystalline composition and crystalline size. SEM Provided the nanocomposite shapes and their surface morphology.

References

[1] Daemi, H; Barikani, M. Scientia Iranica F 19 (2012) 2023.

[2] Krishna Sailaja, A; Amareshwar, P; Chakravarthi,P. International Journal of Pharmacy & Pharmaceutical Sciences 3(2011) 45

MACRO 187

MICROWAVE ASSISTED POLYMERIZATION OF WATER SOLUBLE MONOMERS

Poorvi M. Purohit, Gajanan M. Pawar and Deepa A. Dhoble*
Polymer Science and Engineering Division,
National Chemical Laboratory,
Pune 411008, India.
da.dhoble@ncl.res.in

Abstract:

The present work highlights free radical solution polymerization of acrylamide (AM) and 2-acrylamido-2-methyl-1-propanesulfonic acid (AMPS) monomers using a microwave oven (MW) as well as by conventional method (CM) as a function of AM and AMPS feed ratio. Preliminary results of polymerizations carried out in a microwave oven show improved molecular weights and comparable thermal properties with a several fold decrease in reaction times compared to polymers obtained under conventional polymerization conditions.

Key Words: Microwave synthesis, Water soluble polymers, AM - AMPS copolymers

Introduction:

The advent of microwaves in chemical syntheses has opened up several new opportunities to a synthetic chemist. It provides a comfortable, safe, and clean way of working. Instantaneous, selective and rapid heating results in uniform heating of the reaction mixture with accelerated polymerization rates, which result in shorter polymerization times and better yields as compared to conventional methods.

Free radical polymerization of vinyl monomers is widely practiced in polymer chemistry. McCormick et al [1] and others have extensively studied AM - AMPS copolymers synthesized by traditional techniques. Thermal properties and microstructure of these polymers are well documented in literature. In most of these reports, solution polymerization technique using free radical initiators has been employed. Though solution polymerization is simple and easy to carry out, it has certain limitations. One among these is the restriction on molecular weight built up due to the increase in viscosity during the course of polymerization. An alternative route to prepare high molecular weight polymer is by inverse emulsion polymerization technique [2]. Compared to solution polymerization, emulsion polymerization technique demands critical experimental conditions and entails cumbersome experimental set up. To overcome the difficulties of solution and emulsion polymerization technique, preparation of high molecular weight polymers have been attempted using microwave assisted polymerization technique.

Experimental:

i) Homo- and Copolymer Synthesis:

Homo- and copolymers of AM - AMPS monomers were prepared using MW and CM [3] following standard free radical polymerization technique [3]. AM was recrystalized from acetone and dried in vacuum oven at 40°C. Analytical grade AMPS (Lubrizol 2404) and AR grade $K_2S_2O_8$ were used without further purification. Polymerization was carried out with 10% monomer and 0.5% initiator concentration. Sodium salt of AMPS was prepared prior to polymerization by adding slight molar excess NaOH required for neutralization of the acid. Copolymers were prepared with varying comonomer compositions (AM: AMPS: 10:90, 50:50 and 30:70). The temperature was maintained at 70 ± 3°C during the course of reaction. These conditions were employed for polymerization reactions by MW as well as CM. MW polymerizations were carried out in a domestic microwave oven equipped with four stirrers and four condensers with a minimum power setting of 140W. Polymerization temperature was maintained at 70 ^{0}C, by keeping a 1L water heat sink along with the reaction flask inside the microwave oven.

The polymers obtained were purified by repeated precipitations using anti-solvent acetone and freeze-dried using Heto Power Dry LL3000 freeze dryer. Residual monomer traces were removed by washing the freeze dried samples with acetone and drying at 60^{0}C for 48 h in a vacuum oven.

Table 1: **AM-AMPS copolymer molecular weights and composition**

Polymer (Feed ratio)/ Method	[η], dl/g	Mv	Mw	PDI	%Comp. by ^{1}H - NMR	% Improvement
AM: AMPS (50:50) / MW	1.67	874000	391300	4.3	58	29 (1.5 times)
AM: AMPS (50:50) / CM	1.25	617600	314100	5.4	56	
AM: AMPS (30:70) / MW	1.31	655000	349000	6.4	38	64 (3 times)

AM: AMPS (30:70) / CM	0.56	233100	225200	5.0	31	
AM: AMPS (10:90) / MW	0.74	330800	224200	5.8	16	23 (1.3 times)
AM: AMPS (10:90) / CM	0.60	256700	179400	5.3	19	
Homo PAMPS / MW	0.37	142200	153600	5.1	------	23 (1.3 times)
Homo PAMPS / CM	0.30	110100	109200	4.6	------	

ii) Polymer Characterization:

Measurements of intrinsic viscosity for the polymers synthesized by MW and CM were carried out on 1% polymer solution in 0.5M NaCl using an Ubbelohde type viscometer mounted in Schott Gerate automatic viscometer at 30 ± 0.01^0C. Viscosity average molecular weights were calculated using the measured [η] and reported MHK constants for poly AMPS at 30^0C [4].

FTIR spectra were recorded on Perkin Elmer Spectrum GX FTIR spectrophotometer using polymer-KBr discs.

^{1}H-NMR spectra were recorded on Bruker Avance DRX 200 spectrometer at 298 K, using approximately 4-5 % (w/v) copolymer in D_2O.

Homo- and copolymer molecular weight and molecular weight distribution (MWD) were determined on Waters Alliance system using TSKgel columns (G3000PW, G3000PW, and G3000PW) and polyacrylamide standards (PSS) with 0.2M $NaNO_3$ as a mobile phase at a flow rate of 1 mL/min.

Result and Discussion:

Most of the reports on microwave synthesis exist for organic reactions [5]. There are scanty reports on the use of microwaves for polymer forming reactions [6]. Solution polymerizations of AM-AMPS monomers were performed in a suitably modified domestic microwave oven with $K_2S_2O_8$ as an initiator and deionized water was used as a solvent at 70^0C for 10 min. Similar conditions (with 4h polymerization time) were used to carry out the polymerization by conventional method. Polymers obtained were characterized by Viscosity, FTIR spectroscopy, ^{1}H-NMR, TGA, DSC and GPC.

Copolymer composition:

Spectroscopic techniques were employed for the structural elucidation of homo- and copolymers. FTIR spectroscopy was used to confirm the presence of the functional groups in the polymer and to highlight the similarities between the copolymers synthesized by MW and by CM. ^{1}H-NMR was useful in establishment of the structure of the copolymer as well as for the determination of the copolymer composition.

Evidence of AM-AMPS polymerization can be seen by the FTIR spectra. Figure. 1 shows the typical FTIR spectra for AM, AMAPS monomers along with the copolymers synthesized under MW and CM. The absorption frequencies are in good agreement with the reported frequencies [3,7]. The C=O stretching of AM appears at 1674cm^{-1} while the two stretching vibrations of NH_2 group appear at 3354 cm^{-1} and 3191 cm^{-1}. The NH_2 deformation band appears at 1614 cm^{-1} and the absorption band of primary amide group is seen at 1429 cm^{-1}. In the FTIR spectrum of AMPS, in addition to the C=O and NH_2 bands in AM, asymmetric and symmetric stretching for sulfonic acid group are seen at 1245 cm^{-1} and 1079 cm^{-1}, respectively.

FTIR spectra for the typical copolymers synthesized by two different techniques are almost identical and show shifts in the frequencies as compared to the corresponding monomers. The spectra show two characteristic absorption bands of NH_2 at 3471 cm^{-1} and 3338 cm^{-1}, the deformation band of NH_2 at 1549 cm^{-1}, the stretching bands for C=O at 1668cm^{-1}, asymmetric and symmetric bands of SO_2 at 1216 cm^{-1} and 1045 cm^{-1}, respectively. The polymerization can be confirmed by the disappearance of the characteristic frequency of C=C at 982 cm^{-1} in the copolymer spectra, which is seen in the spectra for the individual monomers. The chemical shifts for the ^{1}H-NMR were in agreement with the reported values [3]. A typical ^{1}H-NMR spectrum for AM-AMPS copolymer is given in Figure 2. The peak assignments were as follows: The chemical shifts at 1.42-1.67 δ, ppm, 2.04 δ, ppm, 3.33 δ, ppm corresponds to -CH_2 - (AM+AMPS), -CH_3 (AMPS) overlapping, -CH- (AM+AMPS) and -CH_2-SO_3 (AMPS), respectively. The calculated copolymer composition by ^{1}H-NMR was in good agreement with the

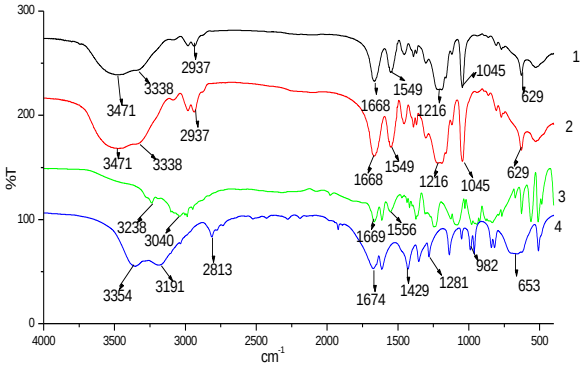


Figure 1 : IR Spectra of (1) copolymer AM-AMPS oven, (2) Copolymer AM-AMPS by conventional method, (3) AMPS monomer and (4) AM monomer

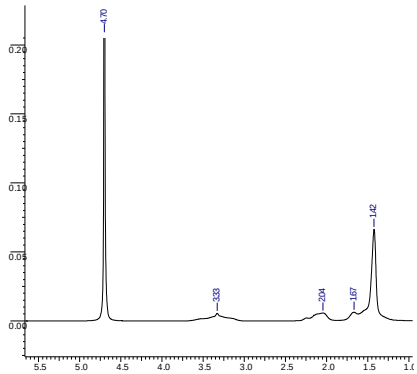


Figure 2 : ^{1}H-NMR spectrum (D_2O) of AM-AMPS in microwave

theoretical composition (Table 1). Also, it was observed that the copolymer composition was independent of the method of synthesis employed. In all the cases, the AM content in the copolymer was slightly higher than in the feed. This may be attributed to the higher reactivity ratio of AM as compared to AMPS [3]. It was observed that AM incorporation in case of MW synthesized polymer was higher than in polymers synthesized by CM, except for 10:90 composition, where percentage composition of AM was higher than that of corresponding MW synthesized copolymer. The increase in the AM % in case of MW synthesis can be attributed to increase in the rate of polymerization [8] due to the dielectric heating mode of MW [6].

Molecular weight:

The major difference in MW and CM lies in the process of heating. In case of heating in a water bath, heat propagates from outside the reaction vessel to inside the reactants. Thus, the reaction mixture gets heated gradually. Since $K_2S_2O_8$ is a thermal initiator, it decomposes as the temperature raises to its decomposition temperature and the polymerization starts. On the contrary, the dielectric heating mode of microwaves directly heat up the reactive centers and the solvent due to dipole moment. Thus, due to faster energy transfer, spontaneous decomposition of the initiator takes place, giving rise to significant increase in the decomposition rate of the initiator [9], in turn increasing the rate of polymerization and shortening the time for polymerization. In our study almost quantitative conversion was obtained within 10 minutes while it took about 4 hours in case of conventional method. Also, the MW polymerizations show improved yields (98% vs 92%) as compared to CM. Significant molecular weight built up (25 to 60%) was observed in case of MW polymerization. This was reflected in increasing intrinsic viscosity also (Table 1). This may be due to the fact that the rate of polymerization was high enough for the growing radical to attain sufficient chain length before it colliding with the other growing radical, thus terminating the polymer growth.

Conclusion:

Free radical solution polymerization of AM with AMPS in MW gave copolymers with 25 to 60 % increase in molecular weight as compared to CM under similar conditions and with better yields and good reproducibility.

References:

[1] C. L. McCormick and G. S. Chen, J. Polym. Sci. Polym. Chem. Ed., 20, (1982) 817

[2] X. Zushun, C.Yuanchun, Z. Gueijun, C.Shiyuan, and F. Linxian, Journal of Polymer Science: Part A, 37, (1999) 2719

[3] J. Travas-sejdic, A. Easteal, Journal of Applied Polymer Science, 75, (2000) 619

[4] L. W. Fisher, A. R. Sochor and J. S. Tan, Macromolecules, 10, (1977) 949

[5] C. O. Kappe, Angewandte Chemie - International Edition, 43, (2004) 6250

[6] C. Koopmans, M. Iannelli, P. Kerep, M. Klink, S. Schmitz, S. Sinnwell and H. Ritter, Tetrahedron, 62, (2006) 4709

[7] F. Rosa,J. Bordado, M. Casquilho, Journal of Applied Polymer Science, 87,(2003)192

[8] J. Jacob, L. H. L. Chia, F. Y. C. Boey, Journal of Applied Polymer Science, 63, (1997) 787

[9] S. Sarkar, M. S. Adhikari, M. Banewee, and R. S. Konar, Journal of Applied Polymer Science, 35, (1988) 1441

MACRO 190

Designing Double Network Hydrogels for Biomedical Applications

Sanoop B. Nair, Arun Torris A. T., Manohar V. Badiger*

Polymer Science and Engineering Division,

CSIR – National Chemical Laboratory, Pune-411008, India

** e-mail id: mv.badiger@ncl.res.in*

Abstract

Polymeric hydrogels continue to find wide range of applications in drug delivery, tissue engineering, bio-implants, scaffolds, due to their special physico-chemical properties such as softness, biocompatibility, water permeability, stimuli responsiveness, self healing etc. One of the major drawbacks of hydrogels is the lack of mechanical strength. Many efforts are being made to overcome this drawback and "Double Network Gels" (DN) are one among them. The toughness in DN hydrogels originates from the combination of two polymeric networks wherein, the first network is hard and tightly crosslinked and the second network is soft and loosely cross linked. In this work, we synthesized a DN hydrogel consisting of tightly crosslinked carboxymethylcellulose (CMC) as the first network and loosely crosslinked poly(hydroxyethylacrylate) (PHEA) as a second network. The second network also contain small amount of stearyl methacrylate (SM), which has a hydrophobic chain that helps in energy dissipation mechanism.

Keywords: *double network hydrogels; carboxymethyl cellulose; poly(hydroxyethyl acrylate); mechanical strength; hysteresis energy*

Introduction

It is well established that biocompatible and hydrophilic hydrogels mimic the natural extra-cellular matrix (ECM), which is a dynamic three-dimensional structure surrounding cells in organs and tissues. This unique property is due to their ability to retain large amounts of water and soft consistency. Moreover, their network design closely resembles to that of living tissues.

Traditional gels used for biomedical applications are vulnerable to stress-induced formation of cracks and voids, which affects the integrity of gel network, resulting in the loss of functionality and service life. Tough gel networks with inherent energy dissipation mechanism are ideal for such environments, which mimic the self-regeneration mechanism of natural tissues. These two major properties can be merged through the design of double-network (DN) gels[1], where one network contributes towards the toughness of the gel whereas the second one imparts ductility. The first network is tightly cross-linked and the second network is loosely cross-linked[2] (**Figure 1**). New Hybrid gels with such multi-functional properties are proposed for the development of innovative medical devices, which can overcome the practical limitations imposed by metals and ceramics.

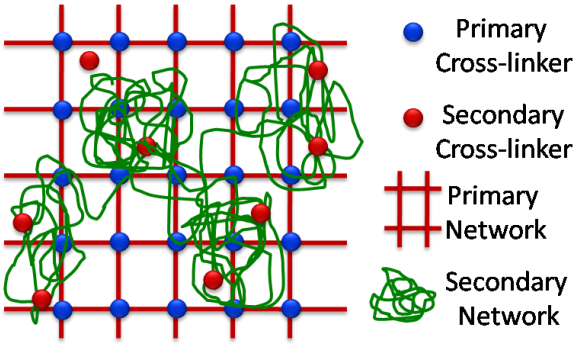


Figure 1: *Schematic representation of DN hydrogel*.

Our aim was to design and synthesize robust hydrogels adopting double network design using carboxymethyl cellulose (CMC) and hydroxyethyl acrylate (HEA) as 1st and 2nd networks respectively. Deploying advanced dynamic mechanical experimental methodologies in simulated environments can bring forward a critical evaluation of the mechanical deliverables of these hybrid gels.

Experimental

Materials and methods:

Carboxymethyl cellulose (Merck, India), hydroxyethyl acrylate (Sigma Aldrich, India), Divinly sulphone (Sigma Aldrich), Stearyl methacrylate (Sigma Aldrich), 2-Hydroxy 2-methylpropiophenone (HMPP) (Sigma Aldrich, India), Sodium dodecyl sulphate (SDS) (Thomas Baker, India), Sodium hydroxide (Merck, India) were procured.

Preparation of CMC gels:

A stock solution of CMC was prepared by adding 1.05 gm of sodium salt of CMC in 30 ml of distilled water, to obtain 3.5 Wt% concentrations and dissolution was carried out using roller mixer. In roller mixer CMC solution was loaded using 50ml closed cylindrical glass vial and subjected to rotation at 25 RPM in horizontal axis overnight to obtain homogenous solution of CMC. To 2ml of CMC stock solution, 4 to 5 drops of 1 M NaOH solution was added to increase the pH upto 12, followed by the addition of 20, 25 and 30% wt of DVS. Solution was vortexed for 5 minutes and poured on to cylindrical Teflon moulds (15 mm dia. x 15 mm height) and kept at

15^0C overnight for 24 hours to obtain CMC hydrogels. Hydrogel was washed thrice with distilled water to remove residual DVS and stored under refrigeration.

Swelling studies of CMC gels

For swelling studies, CMC gels were prepared with uniform size and shape as detailed above. These as-prepared gels were washed with water; swollen to equilibrium in distilled water and dried in oven at 50^0 C. There dried xerogels were allowed to swell upto equilibrium in distilled water at pH 7. During the process the weight gain was noted at specific time intervals.

Preparation of PHEA and PHEA-co-SM gels:

An aqueous solution of HEA (30 % wt.) was prepared and photopolymerized in the presence of HMPP and UV radiation for 27 minutes. As-prepared gels were washed with distilled water and swollen to equilibrium. SDS is added (0.04 % wt/vol.) to the aqueous solution of HEA and mixed for 2 hours. Stearyl methacrylate (SM) was added drop-wise to this solution (2, 4 and 6 mol %) and stirred for 6 hours. The homogenous solution was later mixed with HMPP and poured onto cylindrical teflon moulds (15 mm dia. x 15 mm height) and subjected to UV radiation for 21 minutes. As-prepared gles of PHEA-co-SM was washed with distilled water and allowed to attain equilibrium swelling in distilled water.

Preparation of double network (DN) gels from CMC and PHEA:

As-prepared CMC gels with 30 Wt.% DVS was washed with distilled water to removed NaOH, dried in vacuum and immersed in an aqueous solution of HEA (30 Wt.%) and SM (2, 4 & 6% wt.) containing SDS, until it attained equilibrium swelling and later photo-polymerized in the presence of HMPP to obtain as-prepared DN gel. As prepared DN gel was swollen to equilibrium in distilled water, during which water was replenished at specific time intervals.

Mechanical studies:

Mechanical strength of CMC, PHEA, PHEA-co-SM and DN gels (as-prepared and equilibrium swollen) were measured using Instron 5943 material testing system equipped with 1 kN load-cell capacity and compression platens of 5cm diameter. Un-confined uni-axial compression measurements were performed on gels of 15 mm diameter and 15 mm height with 3 mm/min cross-head speed up to its failure. Stress applied during the compression was measured and plotted as a function of strain.

Hysteresis energy of gels:

Cyclic uni-axial compression experiments were performed on gels in which they were compressed for upto 50 % strain at 10 mm/min speed and relaxed to its initial state in a water bath maintained at 37^0C. This cycle is repeated for upto 50 cycles and the resultant stress and strain were plotted. Hysteresis energy was calculated from the histogram of compressive stress versus compressive strain following the **equation (1)** given below:

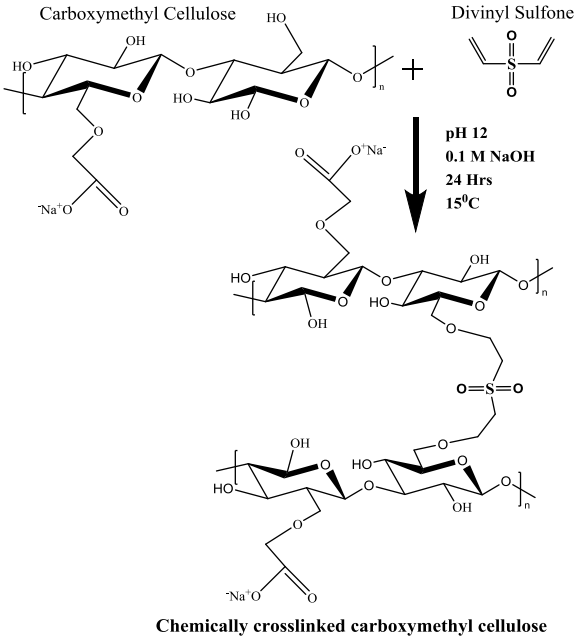
$$U_{50\%} = \frac{\int_0^{0.5_{loading}} F\mathrm{d}s - \int_0^{0.5_{unloading}} F\,\mathrm{d}s}{\pi R^2} \quad \textbf{(1)}$$

Where, $U_{50\%}$ represents the dissipated energy for 50% compressive strain, *F* is the loading, *s* is the displacement to the corresponding strain and *R* is the radius of the gel.

Results and discussion

Preparation of CMC gels:

Preparation of CMC gels follows a base-catalysed Michael-type addition reaction as illustrated in **scheme 1**.



Scheme 1: *Preparation of carboxymethyl cellulose (CMC) gels cross-linked with DVS.*

Aqueous solutions of polysaccharides are generally highly viscous due to polyelectrolyte effect and hence pose a practical difficulty in handling these viscous solutions during the gelation after adding cross-linker. Bases such as NaOH is added to reduce the viscosity which enhances efficient mixing of cross-linker, but higher concentration of base reduces the time required for gelation, which in turn pose difficulty during the preparation of gels. Therefore, optimum conditions were obtained.

Swelling studies of CMC gels:

It's been observed that with respect to the cross-linker concentration, swelling profile (**figure 2**) shows a gradual decrease in swelling from 20 to 30 Wt. % of DVS.

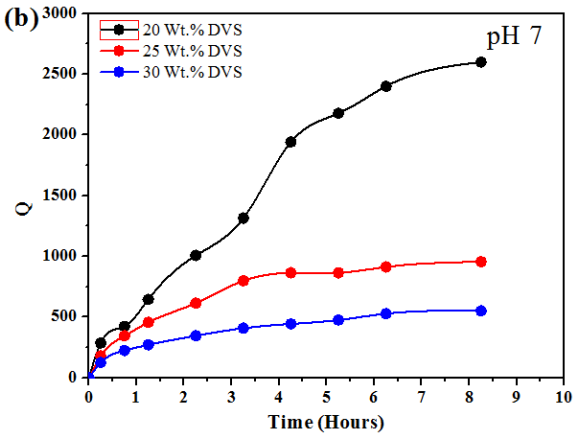
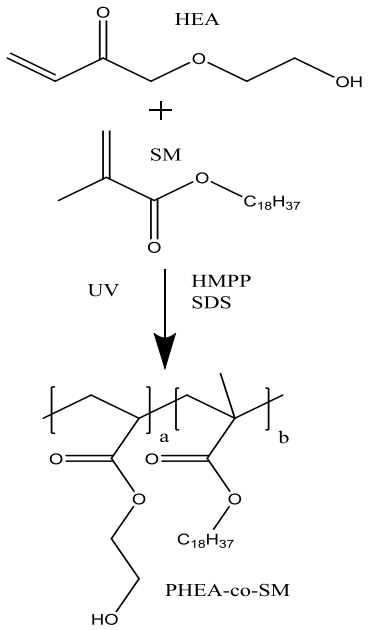


Figure 2: *Swelling profile of CMC gels with different concentration of DVS in pH 7 and ambient temperature.*

Preparation of PHEA and PHEA-co-SM gels:

Poly (hydroxyl ethyl acrylate) (PHEA) is selected as the secondary gel network and prepared by photo-polymerization induced by UV irradiation in the presence of photo-initiator and cross-linker. To tailor the mechanical properties of the secondary network comprising of PHEA, stearyl methacrylate (SM) is used as a co-monomer during the UV assisted photo-polymerization of HEA (**scheme 2)**.



Scheme 2: *Schematic representation of the UV-assisted micellar co-polymerization of PHEA-co-SM.*

Due to the immiscibility of SM in aqueous solutions, we adopted micellar co-polymerization technique[3], wherein SM is added at 2, 4 and 6 % wt. of HEA, to an aqueous solution of HEA containing surfactant.

Mechanical behavior of CMC gels:

True stress versus true strain plot of as-prepared CMC gels with varying cross-linker concentration is shown in **figure 3**. With increase in the concentration of cross-linker, stress at break is increased. It is evident that the increase in cross-link density has apparently increased the stress required for failure of these gels.

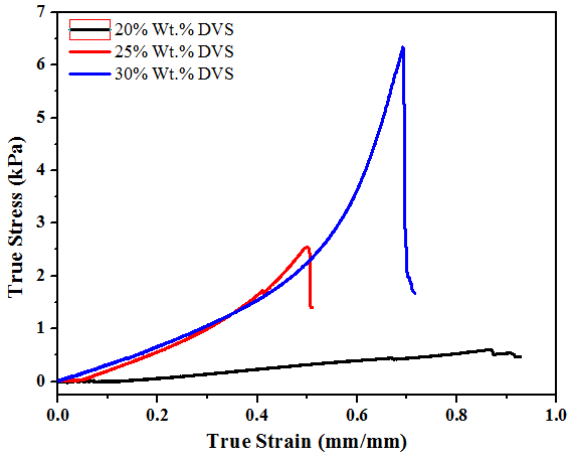


Figure 3: *True Stress vs. true strain plot of as-prepared CMC hydrogels with varying cross-linker concentration.*

Mechanical behavior of DN gels:

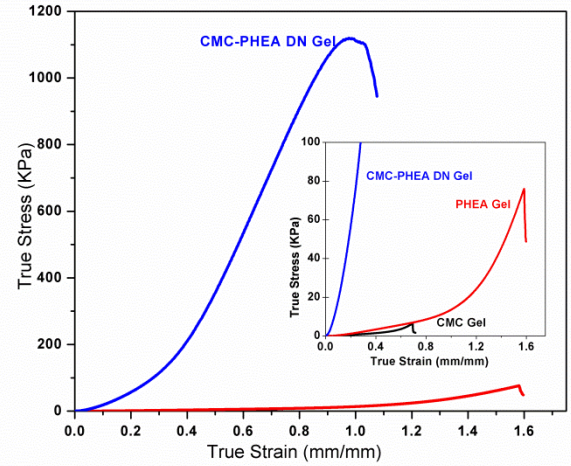


Figure 4: *True Stress vs. true strain plot of DN hydrogel, primary and secondary gel networks.*

Enhancement in the mechanical strength of DN gels with respective to their primary and secondary counterparts are shown in **figure 4**. DN gel shows a compressive strength of 1100 kPa, whereas

second network shows that of 75 kPa and primary network shows that of <10 kPa (shown in inset graph).

Hysteresis energy of DN gels:

Hysteresis energy is a direct indication of the energy dissipation mechanism of gels, which is a ratio of energy absorbed during its mechanical compression and released during the reversal of compressive force. Lower the loss of energy during the reversal of compressive force, higher the efficacy in the dissipation of energy by the gels. With increasing the weight fraction of SM, the hydrophobic fraction increases in the gel, which increases number of pendent chains and increase the mobility of polymer chains within the confined environment for DN gels. (For example, 6% SM in **figure 5)**.

Conclusions

Bio-polymer derived DN gels (CMC-PHEA-co-SM DN gels) are a new class of DN gels which can be employed for various biomedical applications with respect to their other purely synthetic counterparts.

The synergistic combination of the brittle as well as hard primary network (CMC) and ductile secondary network (PHEA-co-SM) play a key role in the dynamic energy

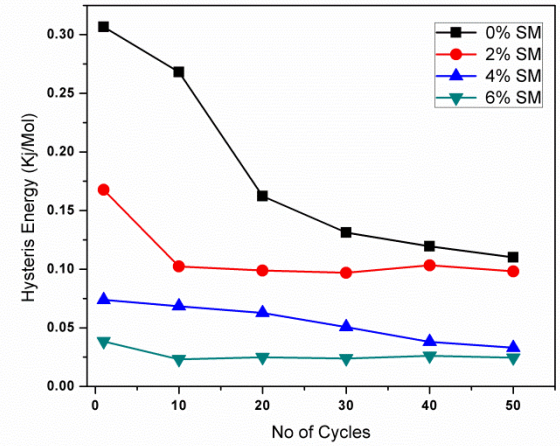


Figure 5: Hysteresis energy of CMC-PHEA-SM DN gels with 2, 4 and 6 wt. % SM from 1st to 50th cycles.

dissipation mechanism of the resultant DN gel systems. Energy dissipation mechanism could be tailored to suit the end applications and may be applied or extended to other similar DN gel concepts.

Acknowledgements

Authors are grateful to the research grant received from DST-SERB, New Delhi (SB/S3/CE/023/2015).

References

1. Jian Ping Gong, Yoshinori Katsuyama, Takayuki Kurokawa, Yoshihito Osada**,** *Adv. Mater.* 14, 1155, 2003.
2. Jian Ping Gong, *Soft Matter* 6, 2583, 2010.
3. Umit Gulyuz, Oguz Okay, *Soft Matter* 9, 10287, 2013.

MACRO 192

Polycarbonate-based biodegradable copolymers for stimuli responsive targeted drug delivery

P. Kumar, M. N. Ganivada, P. Kanjilal, R. Shunmugam*

Polymer Research Centre, Department of Chemical Sciences,

Indian Institute of Science Education and Research Kolkata,

Mohanpur-741246

*E-mail: sraja@iiserkol.ac.in

Abstract

A novel tumour targeted polymer nanocarrier is developed using polylactide and polycarbonate as polymeric backbone. Using ring opening polymerization (ROP) and click chemistry. Biotin and doxorubicin are attached covalently to the polymeric backbone with end group as well as side chain functionalization. Standard analytical techniques are used to characterize the monomer and copolymer followed by self-assembly study using DLS and FE-SEM. Acid labile oxime linker is used to attach doxorubicin with **BPLC-Doxm** copolymer. Higher intracellular doxorubicin accumulation observed at cancer cell by biotin and doxorubicin conjugated nanocarrier **BPLC-Doxm** copolymer. It's unique design, biocompatible and biodegradable nature will open path for cancer therapy.

Keywords: *polymer; NMR; thermo-reversible; thermal stability*

Introduction

Small molecule is always difficult for drug delivery due to its hydrophobicity and lack of specificity.[1] In literature many biodegradable polymers are reported for drug delivery of anticancer drugs.[2] In literature, anticancer drugs or receptors are attached covalently or non-covalently with the polymeric backbone. But, covalently attached anticancer drug as well as receptor (like biotin[3], etc..) is not much explored. In literature, copolymer made by either side chain or end group

functionalization.[4-6] Functionalization by side chain as well as end group is not explored so far.

Here, we have reported aliphatic polyester and polycarbonate as polymeric backbone due to its low toxicity, biodegradability and biocompatibility[7-10] with side chain as well as end group functionalization in the copolymer using ROP and click chemistry. DOXI and PEG-biotin is attached to polymeric backbone, where PEG-biotin is attached by end group and DOXI is grafted as pendent motif. So, we believe this polymeric nanocarrier will behave as smart targeted delivery vehicle for the cancer therapy.

Experimental

Instrumentations

GPC, Fluorometry**,** NMR, FT-IR, UV-Vis, DLS, SEM, CLSM were used for the characterization of the compounds.

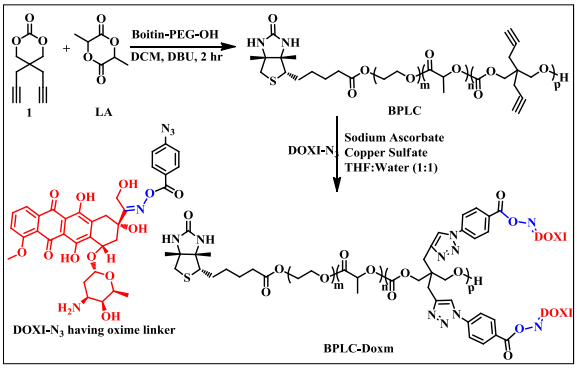
Materials

Malonic ester was purchased from Alfa Aesar. $LiAlH_4$, NaH, propargyl bromide, sodium azide, copper (II) sulfate, anhydrous tetrahydrofuran, PEG (M_n = 1,450 g/mol), doxorubicin hydrochloride, 4-aminobenzoic acid were purchased from Sigma-Aldrich. DCC, DMAP, HOBT, EDC-HCl, TFA were purchased from spectrochem. Toluene, CH_3OH, DMF, ethyl acetate, hexane, $CHCl_3$, acetone, HCl, CD_3OD, $CDCl_3$, DMSO-d_6, acetonitrile, DCM were purchased from Sigma-Aldrich and used as received without further purification. All other solvents were of highest purity and purchased from Sigma-Aldrich.

Results and discussions

Toward this goal, monomer (compound 1) was synthesized in three steps according to literature. PEG-biotin was prepared by the coupling reaction between HO-PEG-OH (Mn = 1,450 g/mol) and biotin in presence of DCC/ DMAP and DMF as solvent. Above all the compounds were characterize by standard analytical techniques (**Figure 1**).

Copolymerization of lactide and monomer (compound **1**) were explored using DBU as catalyst and PEG-biotin as initiator under inert condition (**Scheme 1**). DBU is basic in nature, gives better control over PDI (<1.1) and low catalytic activity.[11] Three different types of copolymers were prepared namely **BPLC-1** (**Figure 1**), **BPLC-2** and **BPLC-3** with different monomer and lactide feed ratio and at constant M/I = 50 and mol 1% catalyst w.r.t initiator. For further studies **BPLC-2** ([1]:[LA]:[DBU]:[PEG-biotin] :: 15:35:0.5:0.5) was used. Formation of compound was confirmed by ^{1}H NMR and GPC technique. GPC trace of **BPLC-2** copolymer was observed unimodal with Mn = 6,400 g /mol and controlled PDI = 1.1.



Scheme 1: Synthesis of **BPLC-Doxm** copolymers.

Next, DOXI motif attachment was explored with **BPLC-2** copolymer. Towards this motivation, DOXI-N_3 having oxime linker

was synthesized in five steps.[12-13] By diazotization reaction, 4-aminobenzoic acid was converted to 4-azidobenzoic acid. Then, boc-protection of amine group of H_2N-OH.HCl was explored followed by attachment of 4-azidobenzoic acid using EDC.HCl and HoBT and DMF as solvent. Resulting compound was deprotected with TFA with DCM as solvent to give o-(4-azidobenzoyl)hydroxylamine. Then DOXI-N_3 having oxime linker was prepared by attachment of DOXI and o-(4-azidobenzoyl)hydroxylamine in methanol with catalytic amount of TFA. Formation of above all compound was confirmed through standard analytical techniques. In ^{1}H NMR, the signals at δ 7.94 - 7.95 (m, 2H), 7.79 - 7.80 (m, 2H), 7.77 - 7.78 (m, 1H), and 7.36 - 7.39 (m, 1H) ppm were responsible for doxorubicin aromatic group protons which indicated the formation of product. Also, in FTIR spectroscopy, the stretching frequency at 2100 cm^{-1} (due to azide), which indicated the formation of DOXI-N_3 having oxime linker.

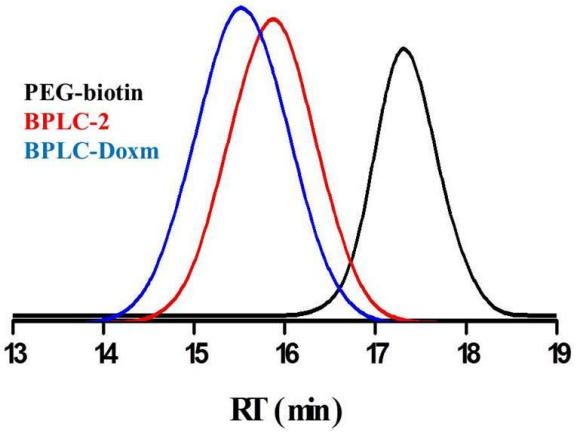


Figure 1: GPC data of PEG-biotin, BPLC-2 and BPLC-Doxm.

After successful synthesis of acetylene functionalized **BPLC-2** and DOXI-N_3 having oxime linker, azide-alkyne click chemistry was explored in presence of sodium ascorbate and $CuSO_4.5H_2O$ with H_2O:THF (1:1) solvent mixture to get our targeted **BPLC-Doxm** copolymer. The obtained **BPLC-Doxm** copolymer was purified dialysis with 3500 dalton cutoff in phosphate buffer solution (PBS) for 24 hrs at room temperature. Then water was evaporated with high vacuum and further it was characterize by ^{1}H NMR, FT-IR and GPC (**Figure 1**). In ^{1}H NMR of **BPLC-Doxm** copolymer showed all characteristic peaks of DOXI, PEG and biotin with a new signal at δ ppm 7.34 for triazole moiety. In FT-IR spectroscopy, absence of peak at 2100 cm^{-1} confirms the successful click reaction. GPC trace shows the Mn = 9,300 g/mol with controlled PDI = 1.2.

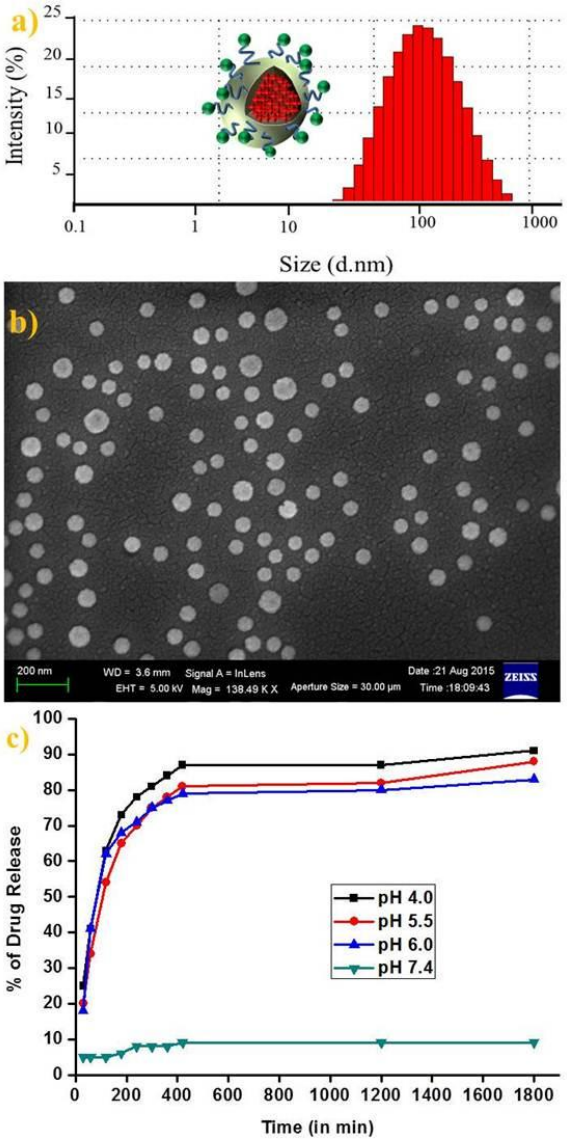


Figure 2: a) DLS data of **BPLC-Doxm** copolymer in water b) SEM images of **BPLC-Doxm** copolymer in water, and c) DOXI release profile from **BPLC-Doxm** copolymer micelles at 37 °C in comparison with pH 4.0, 5.5, 6.0 and 7.4.

After successful synthesis of **BPLC-Doxm** copolymer self-assembly studies was carried out inwater and methanol solvent mixture. 1 mg of **BPLC-Doxm** copolymer was dissolved in methanol. From the above solution an aliquot of 2.5 ml water taken out and in a vial and 18% of water was added under constant stirring. According to DLS, size of polymeric nanoaggregates was observed about 90 nm with PDI = 0.30 (**Figure 2a**). Morphology study of **BPLC-Doxm** copolymer was done by SEM, which gives spherical shape with 70 nm of particle size i.e. in good agreements with DLS (**Figure 2b**).

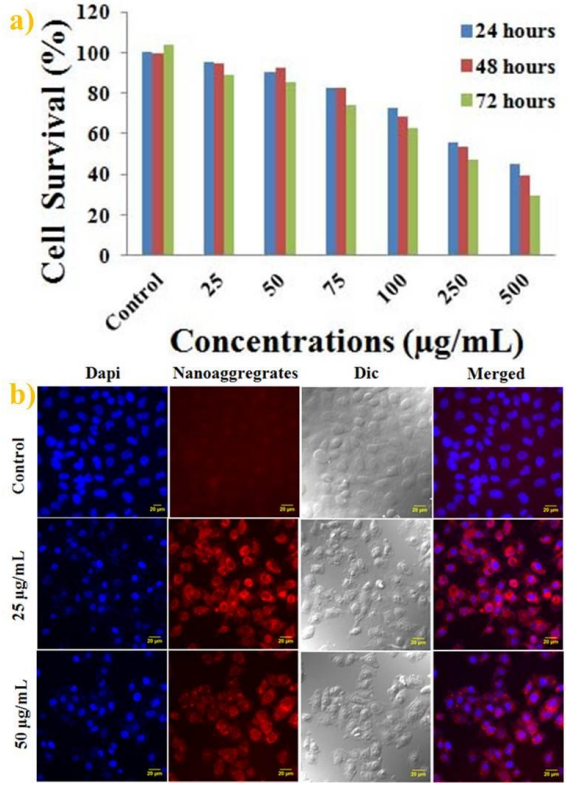


Figure 3: a) Cytotoxicity profile of **BPLC-Doxm** copolymer in Hela cells and b) **CLSM** images of control molecule, the nucleus are staind with **DAPI** and uptake of **BPLC-Doxm** copolymer in HeLa cells with different concentration.

Drug release study was carried out at different pH 4.0, 5.5, 6.0, and 7.4 in PBS of **BPLC-Doxm** copolymer (**Figure 2c**). 1 mg of **BPLC-Doxm** copolymer was dissolved in 1 ml of distilled water and loaded in dialysis tube with 3500 dalton cutoff. Dialysis was done against 100 ml of PBS at different pH

4.0, 5.5, 6.0 and 7.4. An aliquot was taken out from the solution after every 1 hr for 48 hrs to study absorbance and fluorescence of DOXI release. Absorbance was observed at 480 nm and fluorescene was performed by exciting the solution at 510 nm. Sample was poured back to the solution to maintain the volume. Interestingly, drug release was observed below 5% for pH 7.4, which shows the stability of **BPLC-Doxm** copolymer at physiological condition. Maximum release was observed at higher pH 4.0, 5.5 and 6.0, which shows the importance of acid labile oxime linker in **BPLC-Doxm** copolymer.

HeLa wt cells were used for cell viability study for different concentration from 25 µg/mL to 500 µg/mL (**Figure 3a**). From, the cell viability assay it was clear that when the concentration of the **BPLC-Doxm** nanoaggregrates was high, and then cells cytotoxicity increased gradually. In 250 µg/mL and 500 µg/mL of concentration, cells were died almost 50% to 60% of the total number of cell population.

Cellular uptake study was done in biotin positive HeLa wt cells. Cells were treated with **BPLC-Doxm** nanoaggregrates with different drug concerntration (25 and 50 µg/mL) at 37 °C for 24 hrs (**Figure 3b**). From the cellular uptake studies it was evident that the nanoaggregrates were internalized more with increasing concentration and it mainly concentrated around the nucleus of the cells. The observed increase in internalization also suggested the importance of site specific internalization due to biotin motifs present in the nanocarrier.

Conclusions

In conclusion, **BPLC-Doxm** copolymer was successfully synthesize by ROP and click chemistry. DOXI and biotin was covalently attached with side chain and end group, respectively in **BPLC-Doxm** copolymer. DLS and SEM studies shows the miceller formation of **BPLC-Doxm** copolymer in aqueous environment. Maximum release of DOXI at different pH shows the importance acid labile oxime linker in **BPLC-Doxm** copolymer. Cell viability studies in *in vitro* shows the micelles is effective in inhibiting the tumour cell growth at low concentration. So, according to above observation, we believes that the newly designed biodegradable copolymer will open a new path for effective cancer treatment.

Acknowledgements

We thank Prof. Jayasri Das Sarma for providing biology lab facility and Himadri Dinda for biological study.

GMN thanks UGC for the research fellowship, PK thanks INSPIRE for the research fellowship, PINTU thanks INSPIRE for scholarship. RS thanks Department of Science and Technology, New Delhi for Ramanujan fellowship and DST. RS and JDS thank IISER-Kolkata for providing the infrastructure and start-up funding.

References

1. D. Peerl, J. M. Karp, S. Hong, O. C. Farokhzad, R. Margalit, R. Langer, *Nature Nanotechnology* 2, 751, 2007.
2. M. N. Ganivada, V. N Rao, H. Dinda, P. Kumar, J. D. Sarma, R. Shunmugam, *Macromolecules* 47, 2703, 2014.

3. S. Mukherjee, J. D. Sarma, R. Shunmugam, *ACS Omega* DOI:10.1021/acsomega.6b00167.
4. M. Mizutani, S. C. Arnold, T. Matsuda, *Biomacromolecules* 3, 668, 2002.
5. F. Nederberg, T. Bowden, J. Hilborn, *Macromolecules* 37, 954, 2004.
6. A. Cordova, T. Iversen, K. Hult, *Polymer* 40, 6709, 1999.
7. A. C. Albertsson, I. K. Varma, *Biomacromolecules* 4, 1466, 2003.
8. D. Greenwald, S. Shumway, P. Albear, L. Gottlieb, *J. Surg. Res.* 56, 372, 1994.
9. B. Parrish, R. B. Breitenkamp, T. Emrick, *J. Am. Chem. Soc.* 127, 7404, 2005.
10. S. Bhattacharya, M. N. Ganivada, H. Dinda, J. D. Sarma, R. Shunmugam, *ACS Omega* 1, 108, 2016.
11. F. Nederberg, B. G. G. Lohmeijer, F. Leibfarth, R. C. Pratt, J. Choi, A. P. Dove, R. M. Waymouth, J. L. Hedrick, *Biomacromolecules* 8, 153, 2007.
12. L. Li, J. Han, B. Nguyen, K. J. Burgess, *Org. Chem.* 73, 1963, 2008.
13. M. N. Ganivada, P. Kumar, P. Kanjilal, H. Dinda, J. D. Sarma, R. Shunmugam, *Polym. Chem.* 7, 4237, 2016.

MACRO 198

Norbornene Based Copolymer for Site-specific Theranostic Application

S. Mukherjee, D. Patra, R. Shunmugam*

[a] *Polymers Research Centre, Department of Chemical Sciences, IISER- Kolkata, Mohanpur, Nadia-741246, India*

** e-mail id:* sraja@iiserkol.ac.in

Abstract

Theranostic is a concept, deals with therapy and diagnosis which actually helps to increase the survival rate against the terminal illness. Cancer is one of those which cause a huge death in each year, so early detection of cancer helps to start the proper treatment which increases the survival rates. Polymeric systems are having widespread application in biomedical field due to their high biodistribution and retention effect. Among several polymerization techniques Ring opening metathesis polymerization (ROMP) is a versatile technique to make highly functional polymers for biomedical application due to its functional group tolerance. So different norbornene based copolymers have been synthesized for the purpose of diagnosis and therapy simultaneously. The presence of imaging agent also helps to monitor the therapeutic pathway. Inclusion of site-specific group to the polymeric backbone.

Keywords: co*polymer; theranostic; ROMP*

Introduction

Small molecule chemotherapeutic agents suffer from poor bio-distribution and pharmacokinetics which causes for severe side-effects, so it is always necessary to protect this drug from other healthy cells and tissues inside body.[1] There are several different models available to guide this drug more precisely into the tumour cells, for example, polymer, nanoparticle, liposome.[3] However, polymer based delivery vehicle emerged as a superior over all other existing systems due to its pharmacokinetics and biodistribution profiles via the enhanced permeability as well as retention (EPR) effect.[1] These systems also helps to maintain the therapeutic concentration over long periods of time.

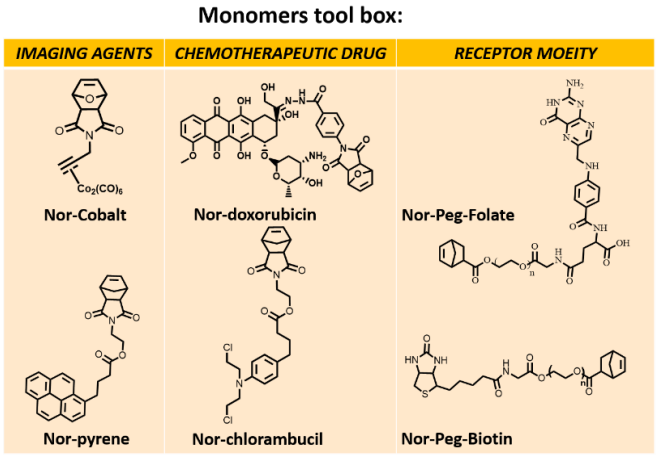
Cancer detection at the primary level is the key factor for successful cancer therapy, which improves the survival rates. To detect the primary level, multimodal bioimaging has been emerging as a promising diagnosis technique which is also having broad clinical application. The site-specific delivery of such imaging agents has become an important area of research.[1-3]

There are few diagnostic techniques available in which magnetic resonance imaging (MRI) is a technique, advantageous for greatest resolution and isotropic depth of imaging. Theranostic is a concept which integrates therapy and diagnosis in a single system. Theranostic nano-medicine is emerging system which have the ability to carry drug and imaging agent simultaneously. This

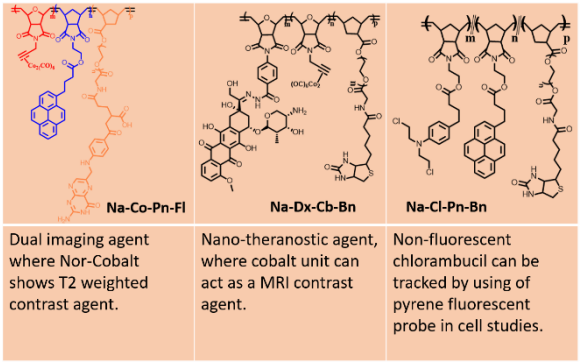
theranostic medicine capable of diagnosis and monitoring the therapeutic response is playing a significant role in the era of personalized medicine.[1]reduces the cytotoxicity towards the normal cells.

In this work, we have synthesized different polymeric nano-system for theranostic application. All the monomers are characterized by standard analytical techniques. The MRI and cellular uptake studies have been done to explore the theranostic capability of the nano-carrier.[4-6]

Experimental



Scheme 1: A toolbox comprising the different monomers



Scheme 2: A tool box comprising the copolymers used for theranostic application

Results and discussion

General polymerization procedure:

A known amount of three monomers were weighed separately and taken in a 15-mL glass vial. Then desired amounts of Grubbs' third generation catalyst were weighed in a separate vial and dissolved in minimum amount of dry CH_2Cl_2. Polymerization was done in an inert atmosphere inside the glove box. The final copolymer **Na-Co-Pn-Fl, Na-Dx-Cb-Bn, Na-Cl-Pn-Bn** were characterized by standard analytical technique.

1. **Dual imaging agent (Na-Co-Pn-Fl):**

MRI study:

To prove the **Na-Co–Pn-Fl** nano aggregates as potential MRI agent, relaxivity measurements were performed.[5] All relaxation studies were performed on a standard bore Bruker 500 MHz Avence III spectrometer at room temperature. We have made NMR samples of seven different concentrations (in millimolar) of synthesized final copolymer, dissolved in a mixture of H_2O and D_2O, taken in 1:5 ratios. We applied conventional inversion recovery and CPMG pulse sequences on water proton in order to study respectively T_1 and T_2 relaxation of water peak, affected due to the presence of polymer in aqueous medium. All experimental data were fitted by using Matlab programs.

Both T_1 and T_2 values were found to be decreasing with increasing concentration. But the relative changes of T_2 values with respect to concentrations were much more prominent than the relative change of T_1 values.
The $1/T_2$ (R_2) and $1/T_1$ (R_1) values were plotted in same graph with respect to concentrations. The behaviour of experimental data was found to be linear and was fit with straight line functions given by the following equations.

$1/T_1 = 1/(T_1)_0 + r_1.C$
$1/T_2 = 1/(T_2)_0 + r_2.C$
Where, $1/(T_1)_0$ and $1/(T_2)_0$ were the longitudinal and transverse relaxation rate of the sample without any polymer solute (only 1:5 H_2O and D_2O mixture) and r_1 and r_2 were the relaxivity constants of T_1 and T_2 process

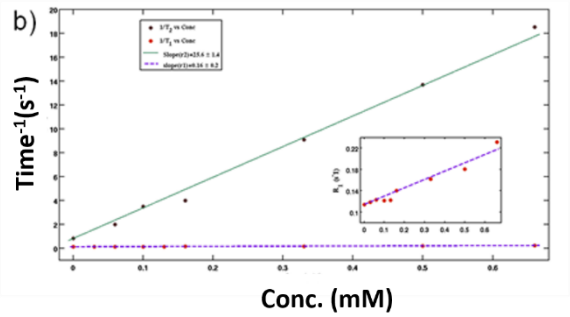


Figure 1. Transverse relaxation rates ($1/T_2$) and longitudinal relaxation rates ($1/T_1$) versus concentration of final triblock copolymer **(Na-Co-Pn-Fl).**
respectively, measured from the slope of two straight lines. In this case, r_2 was 25.6 $mmol^{-1}s^{-1}$, much higher than the r_1, which was 0.16 $mmol^{-1}s^{-1}$ (**Figure 1**).

2. **Theranostic agent (Na-Dx-Cb-Bn)**

MRI study:

In a NMR tube the 0.3 mL blank solution (H_2O and D_2O mixture in 1:5 v/v ratios) was added at the bottom. Then a separator was created using some NMR inactive materials (cotton and wax) and then approximately 0.3 mL of nano-carrier in D_2O–H_2O mixture in 1:5 v/v ratio sample

solution was added on the top.[4] Here, the gradient of strength 4.3 Gauss/cm was used for the sample slice selection. It was observed that with respect to blank solution, the nano-carrier solution peak relaxed faster as time τ changed from 1ms to 45 ms .

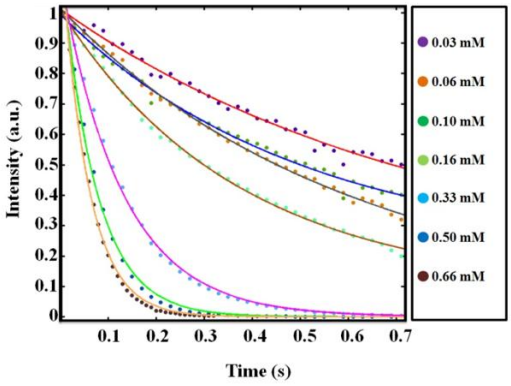


Figure 2. The curves shown above are the transverse relaxation (T_2) curves of water peaks, present in H_2O and D_2O (1:5) solution of synthesized compound in different concentrations.

Flat region between the two peaks were due to the presence of NMR inactive separator. The difference of relaxation behavior of two solutions could be easily visualized by this image, which confirmed the MRI contrast capability of our nano-carrier system (**Figure 2**).

3. **Theranostic agent (Na-Cl-Pn-Bn):**
   To track the therapeutic pathway of fluorescent inactive drug chlorambucil, we have designed a polymeric prodrug functionalized with pyrene, which shows promising activity in cell in vitro studies.[6]

Biological studies:

To reveal the importance of nanoaggreates, two cell lines were taken. HeLa wt cells (human cervical cancer cell line) were maintained in MEM (Minimum Essential Medium) medium containing with 10% fetal bovine serum (FBS), penicillium (100 U/mL) and Streptomycin (100 µg/mL) were incubated at 37 °C in 5% CO_2 environment according to ATCC recommendations.

Cellular uptake studies:

The epifluorescence microscope was used to track pyrene emission in **Na-Cl-Pn-Bn and Na-Co-Pn-Fl** and doxorubicin emission for **Na-Dx-Cb-Bn**. As observed in **Figure 3**, nano-carriers incubated with HeLa wt cells showed promising fluorescent intensity. This obvious fluorescent intensity was due to the receptor mediated internalization **(Figure 3).**

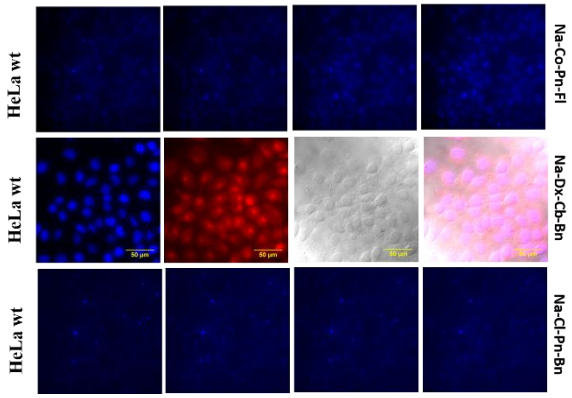


Figure 3. Cellular uptake studies of three different nano-carrier in HeLa wt. cell lines.

Conclusions

In conclusion, we have synthesized different norbornene based copolymer for theranostic application. The **Na-Co-Pn-Fl** shows promising activity towards dual imaging whereas the copolymer carries imaging agent along drug i.e. theranostic nano-carrier shows promising activity towards invitro studies.

Acknowledgements

S.M. thanks CSIR for the research fellowship, R.S. thanks Department of Science and Technology, New Delhi, for Ramanujan Fellowship and DBT for funding. R.S. thank IISER-Kolkata for providing the infrastructure and start-up funding.

References

1. Y. Li, T-Y. Lin, Y. Luo, Q. Liu, W. Xiao, W. Guo, D. Lac, H. Zhang, C. Feng, S. Wachsmann-Hogiu, J. H. Walton, S. R. Cherry, D. J. Rowland, D. Kukis, C. Pan, K. S. Lam, *Nat. Commun* .,2014, 5, 4712.
2. V.N. Rao, H. Dinda, M. N. Ganivada, J. Das Sarma, R. Shunmugam, *Chem. Commun.*, 2014, 50, 13540.
3. S. Bhattacharya, M. N. Ganivada, H. Dinda, J. Das Sarma, R. Shunmugam, *ACS Omega* 2016, 1, 108−117
4. S. Mukherjee, D. Patra, H. Dinda, I. Chakraborty, L. Shashank, R. Bhattacharyya, J. Das Sarma and R. Shunmugam, *Macromolecules*, 2016, 49, 2411−2418
5. S. Mukherjee, H. Dinda, L. Shasank, I. Chakraborty, R. Bhattacharya, J. Das Sarma, R. Shunmugam; *Macromolecules*, 2015, 48 (19), pp 6791–6800.
6. S. Mukherjee, J. Das Sarma, R. Shunmugam; *ACS Omega* 2016, DOI: 10.1021/acsomega.6b00167**.**

MACRO 199

A New Class of Fe(III) Containing Norbornene Copolymer: Very Efficient Theranostic Agent for Cancer Therapy

Patra, D[a] and Shunmugam, R[*]

[a]*Polymer Research Centre, Department of Chemical Sciences,*

Indian Institute of Science Education and Research Kolkata,

Mohanpur-741246

[*]*E-mail: sraja@iiserkol.ac.in*

Theranostic deals with diagnostic and therapy simultaneously. For chemotherapeutic agent it is always necessary to monitor its therapeutic pathway. Among the several polymerization techniques, we utilized ring opening metathesis polymerization (ROMP) due to its functional group tolerance and capability of making polymers with narrow PDI. Here we synthesized norbornene based polymeric prodrug (NOB-PFL-DXR-Fe(III)) by using the ROMP polymerization technique. The chemotherapeutic drug, doxorubicin was functionalized through pH sensitive hydrazone linker. Fe(III)-Terpyridine complex was generated for MRI contrast agent applications. For the site specificity and solubility, PEG functionalized folate moiety was used to guide the nano-theranostic agent to reach the cancer cell site specifically. All the monomers and polymers were characterized through NMR, IR, mass spectroscopy and GPC techniques. As the copolymer was amphiphilic in nature, thus the self assembly behavior was explored by using DLS, SEM, and TEM techniques. The biological results showed the potentiality of our system as an efficient nano-theranostic agent for cancer therapy.

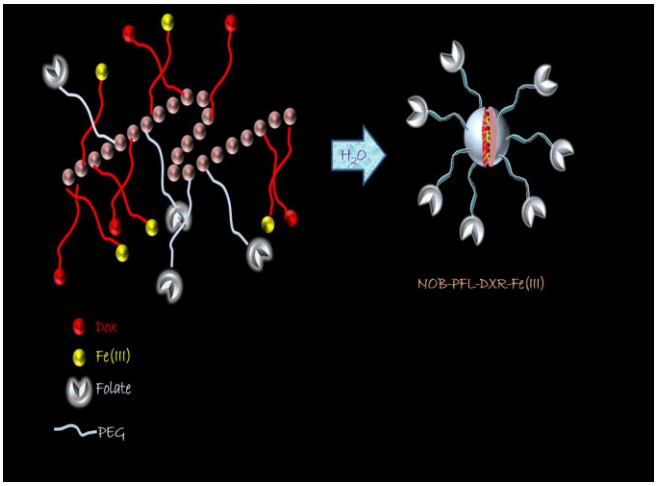


FIGURE 1. CARTOON REPRESENTATION OF NANO-

References
[14]Mukherjee, S; Patra, D; Dinda, H; Chakraborty, I; Shashank, L; Bhattacharyya, R; Das Sarma, J; Shunmugam, R*. Macromolecules 49 (2016) 2411.
[15]Nakayama, Y; Baba, Y; Yasuda, H*; Kawakita, K; and Ueyama, N. Macromolecules 36 (2003) 7953.
[16]Rao N, V; Ganivada, M, N; Sarkar, S; Dinda, H; Chatterjee, K; Dalui, T; Das Sarma, J; and Shunmugam, R*. | Bioconjugate Chem. 25 (2014) 276.

MACRO 204

Synthesis and Characterization of N-Vinyl-2-Pyrrolidone based Graft copolymers for Delivery of levofloxacin

Kumar Ashok, Deepak, Sharma Swati, Afgan Sere and Kumar Rajesh*

Organic Polymer Laboratory, Department of Chemistry, Centre of Advanced Studies in Chemistry, Banaras Hindu University, Varanasi-221005, UP, India, rkr_bhu@yahoo.com

A series of graft copolymers (XG-g-PNVP-1 to XG-g-PNVP-5) based on xanthan gum (XG) and poly(N-vinyl-2-pyrrolidone) (PNVP) has been synthesized by free radical polymerization using peroxymonosulphate/thiourea redox pair in an inert atmosphere. The optimum conditions for maximum grafting have been determined by varying the concentrations of N-vinyl-2-pyrrolidone as well as time duration and temperature. The grafting parameters have been increased up to the certain concentration of N-vinyl-2-pyrrolidone while thereafter grafting parameters have been decreased. The synthesized graft copolymers have been characterized by ^{1}H NMR and FTIR spectroscopies, scanning electron microscopy (SEM), thermogravimetic analysis (TGA) and atomic force microscopy (AFM). Among all the grades of graft copolymers, the one which is having highest percentage of grafting (XG-g-PNVP-3) has been used for drug loading and *in-vitro* releasing studies of levofloxacin. Drug loaded polymer (XG-g-PNVP-D) hybrid has been used in *in-vitro* studies of drug release in phosphate buffer solution (PBS) at 37±0.1 °C and pH 7.4. The corresponding drug loading and releasing studies have been analysed by UV-visible spectrophotometer.

MACRO 206

Modulation of Protein Adsorption and Cell Proliferation on Polyethylene Immobilized Graphene Oxide Reinforced HDPE Bionanocomposites

Upadhyay, Rahul [a]; Naskar, Sharmistha [c]; Bhaskar, Nitu [a]; Bose, Suryasarathi [b]; Bikramjit Basu [a, c*]*

[a]Laboratory for Biomaterials, Materials Research Center, Indian Institute of Science, Bangalore-560012, India

[b]Department of Materials Engineering, Indian Institute of Science, Bangalore-560012, India

[c]Center for Biosystems Science and Engineering, Indian Institute of Science, Bangalore-560012, India

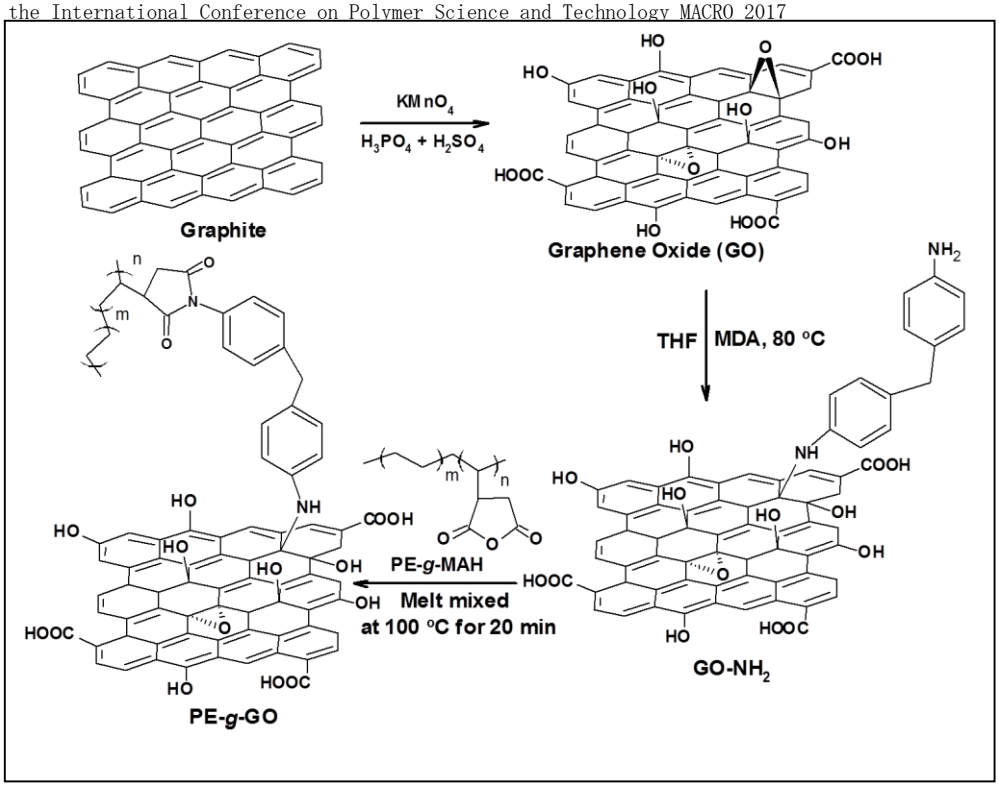
E-mail addresses: bikram@mrc.iisc.ernet.in (B. Basu), sbose@materials.iisc.ernet.in (S. Bose)

Abstract

The uniform dispersion of nanoparticles in a polymer matrix, together with an enhancement of interfacial adhesion is indispensable towards achieving better mechanical properties in the nanocomposites. In the context to biomedical applications, the type and amount of nanoparticles can potentially influence the biocompatibility. In order to address these issues, High Density Polyethylene (HDPE) based composites reinforced with graphene oxide (GO) were prepared by melt mixing followed by compression moulding. In an attempt to tailor the dispersion and to improve the interfacial adhesion, polyethylene (PE) was immobilized onto GO sheets by nucleophilic addition-elimination reaction.

A good combination of yield strength (ca. 20 MPa), elastic modulus (ca. 600 MPa) and an outstanding elongation at failure (ca. 70 %) were recorded with 3 wt % polyethylene grafted graphene oxide (PE-g-GO) reinforced HDPE composites. Considering the relevance of protein adsorption as a biophysical precursor to cell adhesion, the protein adsorption isotherms of bovine serum albumin (BSA) were determined to realize three times higher equilibrium constant (K_{eq}) for PE-g-GO reinforced HDPE composites as compared to GO reinforced composites. In order to assess the cytocompatibility, osteoblast cell line (MC3T3) and human mesenchymal stem cells (hMSCs) were grown on HDPE/GO and HDPE/PE-g-GO composites, *in vitro*. The statistically significant increase in metabolically active cell over different time periods in culture for upto 6 days in MC3T3 and 7 days for hMSCs was observed, irrespective of the substrate composition. Such observation indicated that HDPE with GO or PE-g-GO addition (upto 3 wt %) can be used as cell growth substrate. The extensive proliferation of cells with oriented growth pattern also supported the fact that tailored GO addition can support cellular functionality, *in vitro*. Taken together, the experimental results suggest that the PE-g-GO in HDPE can effectively be utilized to enhance both mechanical and cytocompatibility properties and can further be explored for potential biomedical applications.

KEYWORDS: *cytocompatibility; graphene oxide; HDPE; nanocomposites; grafting; toxicity; osteoblast; Hmsc*



Scheme 1. Synthetic approach followed in grafting of polyethylene on graphene oxide (GO). PE-g-MAH**:** polyethylene grafted maleic anhydride**;** MDA**:** 4,4-methylene dianiline; PE-g-GO**:** polyethylene grafted graphene oxide

Table 1: Summary of the tensile properties obtained for HDPE and its composites, designed using melt mixing followed by compression moulding.

Matrix	Filler (wt %)	Yield Strength (MPa)	Elastic Modulus (MPa)	Elongation at failure (%)
HDPE	Neat	16.4±0.8	490±16	56±10
HDPE	GO 1%	17.4±0.6	586±10	41±3
HDPE	GO 2%	14.0±0.2	412±6	36±5
HDPE	GO 3%	15.3±0.5	418±13	48±4
HDPE	PE-g-GO 1%	17.0±0.7	522±18	70±9
HDPE	PE-g-GO 2%	18.7±0.3	564±3	92±6
HDPE	PE-g-GO 3%	20.0±0.4	595±14	71±15

Reference

[1] Ratner, B. D.; Hoffman, A. S.; Schoen, F. J.; Lemons, J. E.; Dyro, J.; Martinsen, O. G.; Kyle, R.; Preim, B.; Bartz, D.; Grimnes, S., *Biomedical Engineering E-Mega Reference*, 1st ed.; Academic Press: Amsterdam, Netherlands and Boston MA, (2009).
[2] Dikin, D. A.; Stankovich, S.; Zimney, E. J.; Piner, R. D.; Dommett, G. H.; Evmenenko, G.; Nguyen, S. T.; Ruoff, R. S., *Nature* (2007) 448.
[3] Vasileiou, A. A.; Kontopoulou, M.; Docoslis, A., *ACS Appl. Mater. Interfaces* (2014) 6.
[4] Lee, W. C.; Lim, C. H. Y. X.; Shi, H.; Tang, L. A. L.; Wang, Y.; Lim, C. T.; Loh, K. P., *ACS nano* (2011) 5.
[5] Burg, K. J. L.; Porter, S.; Kellam, J. F., *Biomaterials* (2000) 21.
[6] Moro, T.; Takatori, Y.; Ishihara, K.; Konno, T.; Takigawa, Y.; Matsushita, T.; Chung, U.-i.; Nakamura, K.; Kawaguchi, H., *Nat. Mater.*(2004) 3.
[7] Dreyer, D. R.; Park, S.; Bielawski, C. W.; Ruoff, R. S., *Chem. Soc. Rev.* (2010) *39* .
[8] Lombardi, A. V.; Mallory, T. H.; Vaughn, B. K.; Drouillard, P., *J. Bone Jt. Surg., Am.Vol.* (1989) *71*.

MACRO 223

Novel *Borassus* fiber-reinforced polylactic acid composites: processing and mechanical properties

Y. N. Marathe [a] and M. V. Badiger*[a]

[a] *Polymers Science and Engineering Division, CSIR-National Chemical Laboratory, Dr. Homi Bhabha Road, Pune-411008, India*

**e-mail id: mv.badiger@ncl.res.in*

Abstract

This paper reports on the development of bioplastic which consist of Poly (lactic acid) (PLA) and borassus fruit fibers. It also summarizes the structural characterization of fibers by FT-IR, SEM and WAXS. *Borassus* fibers were alkali treated with 5% concentration Sodium hydroxide solution, dried and powdered. Treated and untreated powder was melt mixed with PLA at different concentrations of 5%, 10% and 15wt%. Dispersability of the fiber was studies by Scanning Electron Microscopy (SEM). Composites were prepared and evaluated for their processing and mechanical properties. These composites (PLA/*Borassus* fiber powder) show better performance in comparison with neat PLA.

Keywords: *Natural Fibers; Biopolymer; Biocomposite*

1. Introduction

Over the years, plastics have molded the modern world and transferred the quality of life. Right from clothing to shelter, from transportation to communication and from entertainment to healthcare, plastics have played a key role. However, the fact that plastics are made from

hydrocarbons derived from petroleum, which is non-renewable, has raised environmental issues. Further, the non-biodegradability of plastics can cause damage to our eco-system if and only if the plastics are not disposed and recycled properly. In this context, bio-plastics for making durable products are gaining importance. Particularly, fiber reinforced bio-plastics are becoming more and more attractive. Many researchers have examined and studied natural fibers such as kenaf [1], flax, jute and abaca [2] as reinforcing materials for plastic composites.

Borassus (Palmyra Palm) (Figure 1) belongs to a palm tree family, native of tropical regions of Africa, Asia and New Guinea. It is one of the most important trees and the fruit of which can be used as food product.[3] These fruits contain cellulosic clumps which are reinforced by coarse and fine fibers. These fibers show better tensile properties [4], mechanical and thermal properties.[5] However, they have not been fully explored for polymer composite applications.



Figure 1: A) *Borassus* tree, B) Fruits, C) Dried fruits and D) Raw fibers

In the present work, we report on the synthesis and characterization of *Borassus* fiber reinforced Polylactic acid (PLA) composites. The *Borassus* fibers were initially treated with alkali to remove hemicellulose, lignin and other impurities from the fiber which helped in better fiber-polymer matrix interface with better wetting properties. The processing and material properties were studied and compared between the neat PLA matrix, PLA/treated fibers and PLA/untreated fibers. Preliminary results showed that the mechanical properties of the borassus fiber incorporated composites improved significantly.

2. Experimental

2.1 Materials

Borassus fruit fibers were obtained as a gift sample from Osmania University (Hyderabad, India). PLA (3051D) was obtained from NaturWorks, USA. Sodium hydroxide pellets and concentrated Hydrochloric acid were procured from Thomas Baker co. India.

2.2 Estimation of fiber content

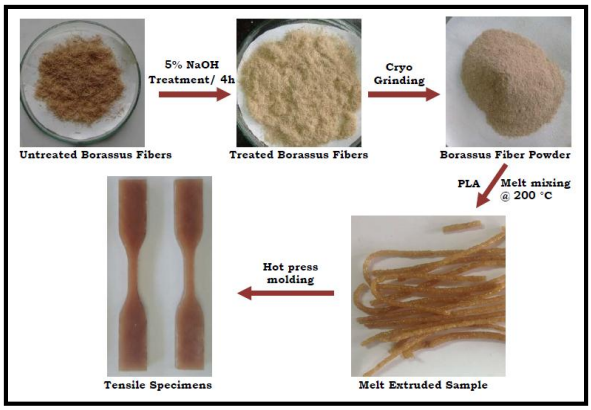
Compositions of *Borassus* fruit fiber were estimated, as reported elsewhere.[6] Content of Cellulose, Hemicellulose and lignin was measured.

2.3 Surface treatment

Fibers were treated with 5% NaOH solution for 5 hr at room temperature. Before water wash, solution was neutralized with 35% of HCl. The fibers were taken out and washed thoroughly with water and dried in oven at 70°C for 24hr. Liquid ratio maintained here for alkali treatment of fiber was 1:30. The dried treated and untreated fibers were cryo grinded to make a powder using CryoMill, Retsch, USA.

2.4 Composite fabrication

The dried, treated and untreated Borassus fiber powder was melt mixed with PLA powder in twin screw extruder (DSM Micro5) at 195 ± 5°C. The screw speed, feeding time and time of holding mixture in barrel was 100 rpm, 1 min and 3 min respectively. Extrudate was pelletized manually using wire stripper. Pellets were dried in oven at 70°C for 24hr and test specimens for tensile were obtained with Polymer Press (PFM 15, Technosearch Instruments) as per the standard ASTM-638V. A 10kN load cell was used and a constant cross head speed of 5 mm min^{-1} was maintained. At least five dog bone shaped specimens were prepared for each type of composite and average value was considered. Various stages involved in the process of composite fabrication are shown in Scheme 1.



Scheme 1: Schematic representation of preparation of tensile specimens

2.5 Instrumentation

Before performing micro-compounding at high temperature, PLA and *Borassus* powder were analyzed for their stability at high temperature using Simultaneous Thermogravimetric Analyzer (STA 6000, PerkinElmer, USA). FT-IR spectra of treated and untreated fibers were recorded on ATR-FTIR (attenuated total reflection) PerkinElmer spectrometer (Spectrum GX). The WAXS measurements in transmission mode were carried out using a Rigaku Micromax-007HF

diffractometer operating at 40 kV and 30 mA. Mechanical properties were determined using Universal Testing Machine (INSTRON 33R4204) at room temperature.

3. Results and Discussion

3.1 Structural characterization of *Borassus* fruit fibers

Composition of treated and untreated *Borassus* fibers was assayed by chemical method. It was found that the 5% NaOH treated fiber reduced the hemicellulose and lignin content as mentioned in Table 1.

Table 1: Composition of *Borassus* Fibers

	UTF (%)	TF (%)
Cellulose	70.2	85.91
Hemicellulose	13.51	2.89
Lignin	10.1	8.52

Alkali treatment caused cellulosic fiber to swell and removed hemicellulose and other impurities from fiber surface. It leads to better wettability, strength and fiber matrix adhesiveness. Figure 2A shows that cellulosic fibers remained unaffected in structure due to alkali treatment and the fiber surface was smoother than the untreated fiber (Figure 2B) due to removal of impurities.

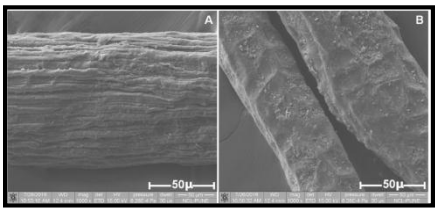


Figure 2: SEM micrographs of A) Treated and B) Untreated *Borassus* fibers

To confirm the changes in the composition of alkali treatment of *Borassus* fiber, FT-IR was performed. Figure-3A shows disappearance of characteristic peak at 1737 cm^{-1} of C=O stretching vibration from acetyl group of hemicellulose.[7]

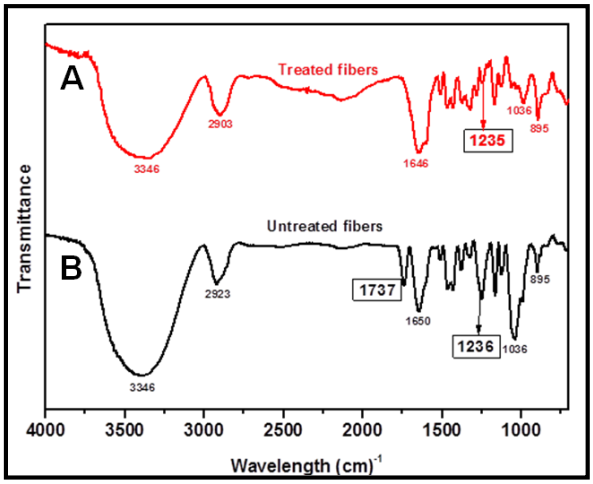


Figure 3: FT-IR spectra of treated and untreated *borassus* fibers

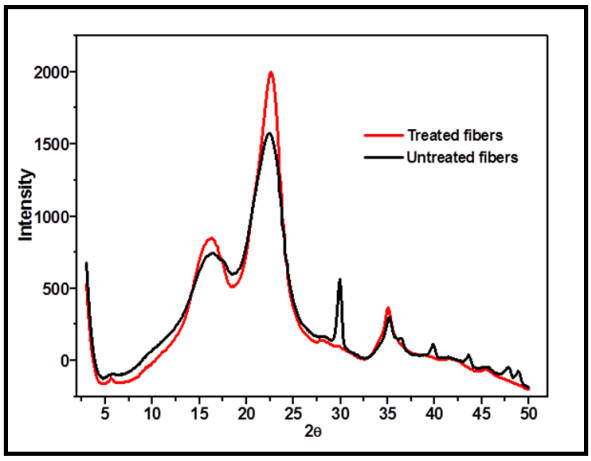


Figure 4: WAXS pattern of treated and untreated *Borassus* fibers

WAXS pattern of treated fibers confirmed that hemicellulose and lignin were washed out of fiber (Figure 4). Peak attributed to hemicellulose at 2θ=30° was not observed and the crystallinity of treated fiber increased due to removal of hemicellulose and lignin which contribute to amorphous part.[8]

Borassus fibers characterized by the SEM, FT-IR and WAXS indicated the removal of hemicellulose and other impurities from the surface on alkali treatment. Prior to processing for composite, thermal stability of treated and untreated fibers as well as that of polymer matrix was estimated. It was observed that the thermal stability of treated fibers was found to be slightly higher than that of untreated fibers. But both were quite stable at processing temperature of 200°C (Figure 5). These fibers were then cryo-grinded and processed with PLA to obtained tensile specimens as show in Scheme 1.

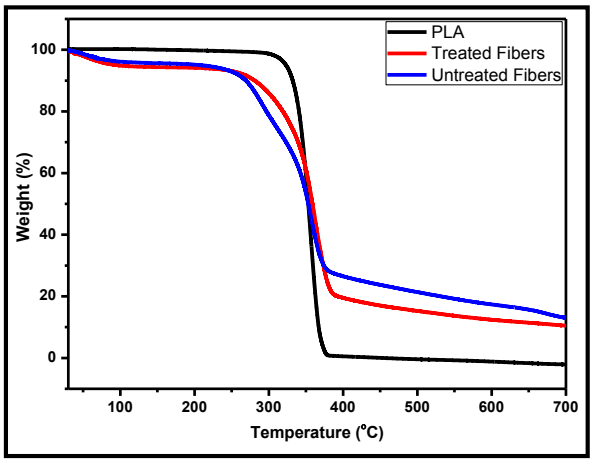


Figure 5: Thermogravemetric analysis for PLA and *Borassus* fibers

3.2 Fabrication of Borassus fiber powder/ PLA composites

We have fabricated a new Borassus fiber powder/ PLA biocomposites using a different concentration of fiber powder. It was reported that the alkali treated fibers showed better characteristic properties as compare to raw fibers. In this paper, we have made powder of borassus fiber for better dispersion in polymer matrix. Composites were prepared using 5, 10 and 15-wt% of borassus fiber powder using melt extruder. Test specimens were prepared using these compositions.

Extrudate was cryo-fractured and observed under SEM for dispersability of powder in the polymer matrix. SEM micrograph in Figure 6 show better dispersion as the concentration of powder increases from 5wt% to 15wt%.

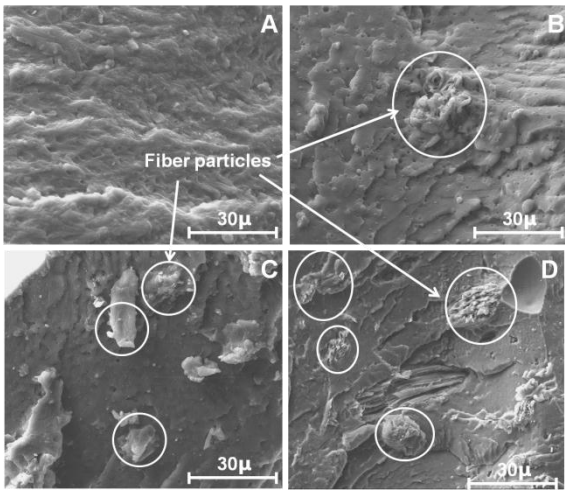


Figure 6: SEM micrograph of **A)** Neat PLA, **B)** 5%, **C)** 10% and **D)** 15% - treated powder / PLA

Figure 7A shows cryo-fractured samples of 5%-untreated/PLA extrudate which indicates poor interfacial interaction between fiber powder causing poor mechanical properties. In contrast, 5%-treated/PLA extrudate showed strong interaction between fiber and matrix (Figure 7B).

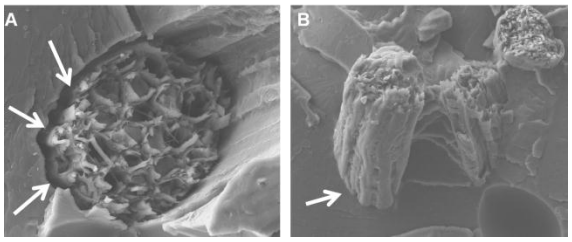


Figure 7: SEM micrograph of **A)** 5% untreated and **B)** 5% treated fiber powder /PLA

Specimens for tensile testing were prepared as per the standard ASTM-638V (63.30 × 3.15 × 3.05 mm) as shown in Scheme 1. Table 2 shows mechanical properties of PLA and its corresponding treated and untreated fiber powder / PLA composite. The results show that the treated as well untreated powder/PLA composites are having more strength as compare to neat PLA. Whereas, TFP composite is slightly better than UTFP composites. Strength increased with increasing fiber powder concentration from 5% to 15%, beyond which fibers or powder can agglomerate.[9]

Tensile strengths were increased for 15%TFP/PLA and 15% UTFP/PLA by 30% and 27% respectively.

Table 2: Mechanical properties of composites

	Tensile Strength (MPa)	Young's Modulus (GPa)	Elongation (%)
PLA	32.18	2.06	3.07
5%TFP/PLA	39.66	2.30	4.12
10%TFP/PLA	34.88	2.08	3.78
15%TFP/PLA	41.70	1.76	5.02
5%UTFP/PLA	32.10	1.80	3.57
10%UTFP/PLA	32.32	2.08	3.22
15%UTFP/PLA	40.71	1.83	5.20

(TFP= Treated fiber powder, UTFP= Untreated fiber powder)

Conclusions

The aim of this study was to synthesize and characterize *Borassus* fiber / PLA green composite in terms of their processing conditions and mechanical properties. The fibers were treated with 5% NaOH solution to remove impurities and make smooth surface. It was observed that dispersability increased for fiber powder in polymer matrix. Strength of PLA composite increased upon fiber reinforcement. % elongation was higher for TFP in contrast to UTFP. Removal of hemicellulose from fiber leads to closer packing of cellulose chains.

Acknowledgements

YNM thanks DST-INSPIRE programme, Delhi for a DST-INSPIRE fellowship.

References

4. Serizawa S, Inoue K, Iji M. *Journal of Applied Polymer Science*, 100 (2006) 1.
5. Petinakis KL, Yu L, Simon G, Dean K. *Fiber Reinforced Polymer-Technology Applied for Concrete Research*. Martin Alberto Masuelli. Rijeka, Croecia: InTech. (2013) 41-59.
6. Shibata M, Ozawa K, Teramoto N, Yosomiya R, Takeishi H. *Mocromolecular Materials & Engineering*, 288 (2003) 11.
7. Sudhakara P, Reddy KO, Prasad CV, Jagadessh D, Kim HS, Kim BS, Bae SI, Song JI. *Composites Research*, 26 (2013) 48-53.

8. Reddy KO, Rao GB, Rajulu AV. *Journal of Applied Polymer Science*, 114 (2009), 603–611.
9. Boopathi L, Sampath PS, Mylsamy K. *Composites: Part B*, 43 (2012), 3044-52.
10. Silva FA, Chawla N. *Composites Science and Technology*, 68 (2008) 3438-43
11. Kumar A, Negi YS, Chaudhary V, Bhardwaj N. *Journals of Material Physics and Chemistry*, 2 (2014), 1-8.
12. Sudhakara P, Reddy KO, Wang Y, Prasad V, Devi APK, Balakishnan G, Kim HS, Kim BS. *Carbohydrate Polymers*, 98 (2013) 1002-10.

MACRO 233

Enhanced Drug Release by Selective Cleavage of Crosslinks in a Double Crosslinked Hydrogel

Neha Tiwari,[a] Manohar V. Badiger*,[a]

[a] *Polymer Science & Engineering Division, National Chemical laboratory, Pune-411008, India*

** e-mail id: mv.badiger@ncl.res.in*

Abstract

In the present paper, we report on the synthesis and characterization of redox sensitive double cross linked poly(acrylic acid) hydrogels using two different cross linking agents namely, Jeffamine and Cystamine. Jeffamine provides mechanical stability to the hydrogels while cystamine incorporates redox sensitivity. The elastic modulus, E' of the double cross linked hydrogels were determined from the stress-strain plots. The disulfide bonds (S-S) in the Cystamine were cleaved selectively in the presence of dithiothreitol which increased the degree of swelling of the hydrogels and consequently could enhance the release of drug. The implication of selective breaking of crosslinks on the swelling-controlled release of an anti-cancer drug, doxorubicin was demonstrated.

Keywords: *hydrogels; redox; drug*

Introduction

The controlled release of active ingredients such as drugs, proteins and other micronutrients at the required site on demand is a biggest challenge in medical and pharmaceutical areas. In this context, smart responsive polymeric hydrogels have become promising materials for drug delivery[1,2] and tissue engineering applications[3-5] due to their controlled swelling-deswelling kinetics and tunable properties. Hydrogels contain hydrophilic polymeric chains that are crosslinked either physically[6] or chemically[7] thus imparting a 3-dimensional network structure to the hydrogel. Major efforts are being continuously made in designing and synthesizing smart hydrogels that are sensitive to external stimuli such as temperature[8,

[9], pH[1, 9-13], magnetic[14] and electric field[15] etc. Recently, redox stimuli is becoming important in hydrogels.[4,16-18] In redox stimuli, the volume transition is effected by breaking and reformation of crosslinks triggered by reduction and oxidation.

In the present work, we have synthesized double crosslinked Poly(acrylic acid) hydrogels using two different crosslinking agents namely Jeffamine (jeff) and Cystamine (cys). The jeffamine provides a good mechanical strength while the cystamine with disulphide bonds incorporates the redox sensitivity to the hydrogels. The hydrogels were easily prepared in aqueous medium at room temperature and the gelation could be completed within a few minutes. Poly(acrylic acid) (PAA) based hydrogels have been extensively studied for controlled drug delivery applications.[1, 9, 12] Large number of pharmaceutical formulations of creams, ointments etc. contain PAA with FDA approval and acts as a rheological control agent. We demonstrated the selective cleavage of one crosslinking by DTT and its implications on the controlled release of an anticancer drug, Doxorubicin (Dox).

Experimental

2.1. Materials

Poly(acrylic acid) (MW=2,50,000) (PAA), Cystamine di-hydrochloride, 1-Ethyl-3-(3-dimethylaminopropyl) carbodiimide hydrochloride (EDC.HCl), dithiothreitol (DTT) were obtained from Sigma Aldrich, USA. Jeffamine (MW=2,000) was obtained from Texaco Chemical Company, USA. Doxorubicin HCl was obtained from Prolab Marketing Pvt. Ltd., New Delhi. Silver nitrate (AgNO3) was procured from S.D. Fine chemicals Ltd (India) and sodium borohydride (NaBH4) was purchased from Merck(India). All the chemicals were of analytical grade and used as received.

2.2. Method

300mg of Poly(acrylic acid) was dissolved in distilled water followed by addition of varied compositions of cystamine dihydrochloride and jeffamine. The pH of the solution was adjusted to 7.5-8.0 by adding 1M NaOH solution followed by the addition of EDC.HCl to it. The total volume of the reaction was kept constant at 10ml for all the experiments. The solution was poured immediately into cylindrical teflon molds of different sizes. The gels were removed from molds after 2 hours and used for further studies. The gels were then kept in distilled water for 4 days with periodic replenishment with fresh water for the removal of any unreacted reagents and polymer.

2.3. Instrumentation Techniques

The stress-strain measurements in the unidirection were carried out using Instron 5943 mechanical tester at room temperature. The in-situ gelation of PAA with two cross- linking agents in aqueous medium was studied using Anton Paar MCR-301 controlled stress rheometer with cup and bob geometry (CC17). Transmission Electron Microscopy (TEM) was performed on JEOL (JEM 2000) operating at 200kV. FT-IR spectra of the hydrogels were recorded on Perkin Elmer.

Results and discussion

3.1 Synthesis of double cross linked PAA hydrogels

The reaction pathway for the crosslinking between PAA and the two crosslinking agents is shown in **Scheme 1**.

Scheme 1: Reaction scheme for synthesis of PAA-cys-jeff double crosslinked hydrogels

3.2 Swelling behavior of double crosslinked hydrogels

The swelling behavior of PAA hydrogels was studied using gravimetric method in four different solvents (**Fig.2**) using the following equation:

$$Q_e = \frac{W_s - W_d}{W_d} x100 \qquad (1)$$

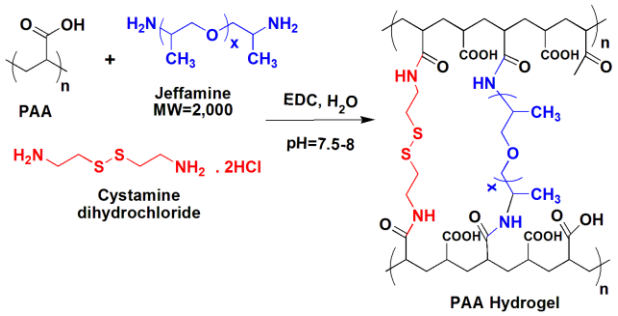
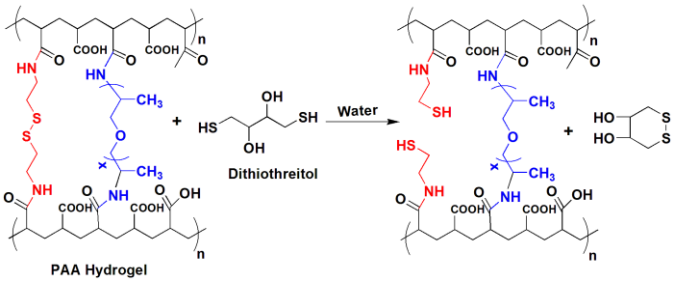


Fig.2. Equilibrium swelling ratios of double crosslinked PAA hydrogels in water, NaCl (0.1M), PBS (pH 7.4, 0.01M)

Where W_s and W_d are the weights of the swollen and dried samples respectively. Expectedly, it is clear from **Fig.2**. that as the crosslinking density increases in a hydrogel the swelling decreases. Also, jeffamine undergoes more efficient crosslinking in the hydrogel formation as is evident from the compared to cystamine.



3.5 Selective breaking of one crosslinking in a double crosslinked hydrogel and its influence on swelling

The schematics of selective breaking of S-S bonds in cystamine without affecting the jeffamine crosslinks is shown in **Scheme 2**. The selective breaking of S-S bonds in cystamine resulting into decrease in the degree of crosslinking was manifested in the increase in equilibrium swelling ratios of hydrogels. We show in **Fig.3**, the equilibrium swelling ratios of PAA hydrogels in water, NaCl and PBS (pH 7.4, 0.01M) solution after the cleavage of cystamine crosslinking. It can be seen that

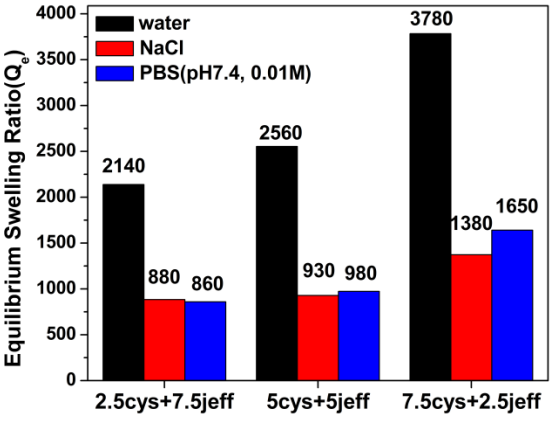
Scheme 2: Selective cleavage of cystamine in the presence of DTT in double cross linked PAA hydrogels
Fig.3. Equilibrium swelling ratios of double crosslinked PAA hydrogels in water, NaCl (0.1M), PBS (pH 7.4, 0.01M) in presence of DTT

there is a significant increase in the swelling ratio due to decrease in the degree of crosslinking as a result of the breaking of S-S bonds in cystamine.

3.7 Mechanical Properties

The stress values at break/rupture of the as-prepared and equilibrium swollen mono and double crosslinked PAA hydrogels were measured from the stress v/s strain curves **Table 1**. The results reveal that, in both the mono crosslinked hydrogels independently
by cystamine and jeffamine, the ultimate stress values (i.e. the stress values at break) increase with the increase in degree of crosslinking indicating the enhancement in the mechanical strength of the hydrogels. Interestingly, jeffamine crosslinked hydrogels showed higher ultimate stress values (6-8times) as compared to Cystamine crosslinked hydrogels. This clearly indicates that jeffamine undergoes more efficient crosslinking in the hydrogel formation. It is also observed that the equilibrium swollen hydrogels showed lower ultimate stress and lower mechanical strength as compared to the as-prepared hydrogels. This could be attributed to the fact that, equilibrium swollen hydrogels contain large amount of fluid which makes them soft resulting in to lower mechanical strengths.

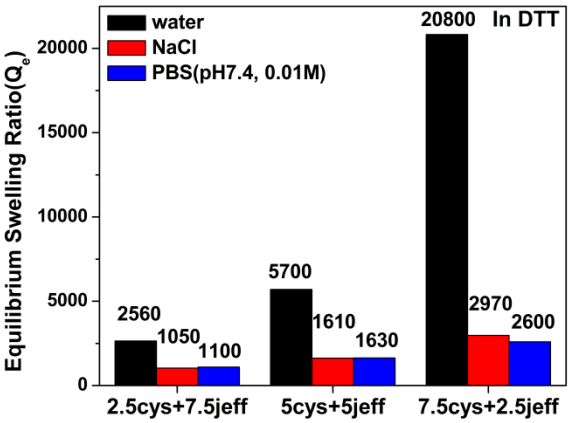
Table 1: Stress at break point for mono and double cross linked PAA hydrogels with different degree of crosslinking



Sample	Stress at break point (kPa)	
	As Prepared	Equilibrium Swollen in PBS
5cys	10	6.0
7.5cys	11	8.0
10cys	17.1	12.5
5jeff	51.4	33.5
7.5jeff	72.6	65.4
10jeff	130.5	125
7.5cys+2.5jeff	47.2	35.3
5cys+5jeff	82.7	69.2
2.5cys+7.5jeff	103.2	91.2

3.8 Drug loading and release from double crosslinked PAA hydrogels

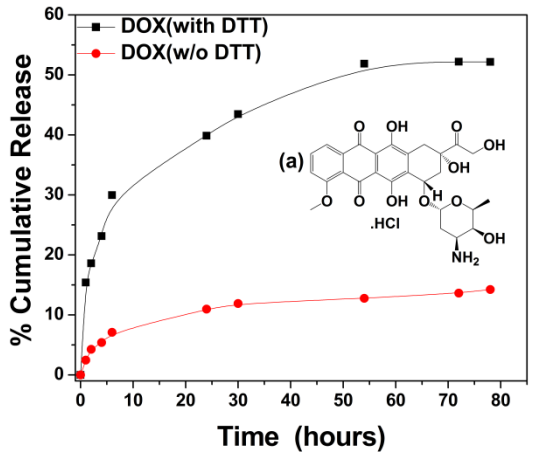
In order to see the implication of selective breaking of one crosslinking in the drug delivery applications, we incorporated an anticancer drug, doxorubicin hydrochloride into double crosslinked PAA hydrogel (PAA-5cys+5jeff) and studied the release of dox in PBS (pH 7.4,



0.01M) upon selective breaking of disulphide (S-S) bonds in cystamine using DTT. The loading of dox in to the hydrogel was performed by immersing the dry PAA-5cys+5jeff xerogel into PBS containing dox hydrochloride. The swelling of the hydrogel induced the diffusion of dox into the hydrogel. We show in **Fig.3**, the cumulative release of dox from PAA-5cys+5jeff as a function of time with and without the treatment of DTT. It is seen from the figure that, the hydrogel without the treatment of DTT showed ~15.0% dox release in 40-80hrs whereas, the DTT treated hydrogel cleaved the di- sulphide linkage and reduced the degree of crosslinking and inturn increased the swelling of hydrogel. The increase in swelling of the hydrogel influenced the faster and higher amount (~ 60 %) of dox release from the hydrogel over a period of 40-80hrs.

Fig.3. Cumulative release of DOX with time from PAA-5cys+5jeff in the presence and absence of DTT and (a) Structure of Doxorubicin HCl

The release of dox from the xerogel involves the simultaneous absorption of water/buffer and desorption of dox via a swelling controlled diffusion mechanism.



Conclusions

We have successfully synthesized double crosslinked PAA hydrogels simultaneously using two crosslinking agents namely, cystamine and jeffamine. The two diamines were coupled to PAA using EDC coupling agent. All the hydrogels were characterized in terms of structure, morphology, swelling and mechanical strength. The hydrogels obtained showed good mechanical strength in terms of compressive strength and exhibited strong dependence on the degree of crosslinking and extent of swelling. Jeffamine showed more efficient crosslinking compared to cystamine. The selective breaking of disulfide linkage in the cystamine was effected using DTT which resulted in decrease in the degree of crosslinking and increase in the swelling of the hydrogels. This phenomenon of in-situ breaking of one crosslinking and increasing the swelling ratio could be used in the swelling-controlled drug delivery systems. The implication of selective breaking of crosslinks on the swelling-controlled release of an anti-cancer drug, doxorubicin was demonstrated. These double cross linked hydrogels show great promise in drug delivery and tissue engineering applications.

References

1. S. M. H. Bukhari, S. Khan, M. Rehanullah and N. M. Ranjha, *International Journal of Polymer Science*, 2015, Article ID 187961, 15.

2. A. Chang, *Iranian Polymer Journal*, 2015, 24, 161-169.

3. Z. A. Hamid, A. Blencowe, B. Ozcelik, J. A. Palmer, G. W. Stevens, K. M. Abberton, W. A. Morrison, A. J. Penington and G. G. Qiao, *Biomaterials*, 2010, 31, 6454-6467.

4. S.-Y. Choh, D. Cross and C. Wang, *Biomacromolecules*, 2011, 12, 1126-1136.

5. J. Choi, H. J. Kung, C. E. Macias and O. K. Muratoglu, *Journal of biomedical materials research*. Part B, Applied biomaterials, 2012, 100, 524-532.

6. S. S. Halacheva, T. J. Freemont and B. R. Saunders, *Journal of Materials Chemistry B*, 2013, 1, 4065.

7. X. Zhang, S. Malhotra, M. Molina and R. Haag, *Chem. Soc. Rev*., 2015, 44, 1948-1973.

8. Z. M. Rzaev, S. Dincer and E. Pişkin, *Progress in Polymer Science*, 2007, 32, 534-595.

9. D. Das, P. Ghosh, S. Dhara, A. B. Panda and S. Pal, *ACS applied materials & interfaces,* 2015, 7, 4791-4803.

10. X. Gao, C. He, C. Xiao, X. Zhuang and X. Chen, *Polymer*, 2013, 54, 1786-1793.

11. Q.-B. Wei, F. Fu, Y.-Q. Zhang and L. Tang, Journal of Polymer Research, 2015, 22, 1-8.

12. H. Hosseinzadeh, Journal of chemical sciences, 2010, 122, 651-659.

13. I. Manavi-Tehrani, M. Rabiee, M. Parviz, M. R. Tahriri and Z. Fahimi, 2010, 296, 457-465.

14. J. Dobson, Drug development research, 2006, 67, 55-60.

15. T. Shiga, Y. Hirose, A. Okada and T. Kurauchi, Journal of applied polymer science, 1992, 44, 249-253.

16. J. Zhang, F. Yang, H. Shen and D. Wu, ACS Macro Letters, 2012, 1, 1295-1299.

17. X. Z. Shu, Y. Liu, Y. Luo, M. C. Roberts and G. D. Prestwich, Biomacromolecules, 2002, 3, 1304-1311.

18. A. N. Zelikin, Q. Li and F. Caruso, Chemistry of materials, 2008, 20, 2655-2661.

MACRO 236

Study of swelling characteristics and mechanical properties of 2-Acrylamido-2-Methylpropane Sulphonic Acid (AMPS) based hydrogels

Chaurasia Siddhant[a], Singh Neelima[b], Shaikh Vasi[c], Tiwari Neha[d], Badiger Manohar*

[a]*Student, Polymer Engineering, Maharashtra Institute of Technology, Pune, India.* [b]*Student, Polymer Engineering, Maharashtra Institute of Technology, Pune, India.* [c]*Professor, Polymer Engineering, Maharashtra Institute of Technology, Pune, India.*

[d]*Senior Research fellow, Polymer Science and Engineering, CSIR-National Chemical Laboratory, Pune, India.*

** Chief Scientist, Polymer Science and Engineering, CSIR-National Chemical Laboratory, Pune, India.*

** e-mail id: neelimasinghbhati@gmail.com*

Abstract

Hydrogels from 2-Acrylamido-2-Methyl Propane Sulphonic acid were prepared using N,N'-Methylenebisacrylamide (MBA) as a cross linking agent by free radical polymerisation. Two different kinds of hydrogels have been studied by varying the mole% of crosslinking agent (keeping accelerator constant) and varying the mole% of accelerator (keeping crosslinker constant). The effect of reaction variables, crosslinker and accelerator on swelling of hydrogels has been studied in detail in different solvents like water, 0.9 & 3.5% NaCl, basic medium, acidic medium and different ratios of water and ethanol mixtures. FTIR Spectroscopy was also performed to determine the functional groups for AMPS. Compression studies were performed on all the hydrogels and their mechanical properties were studied by changing the reaction variables. The results indicate that both change in the cross linker and accelerator concentration has significant effect on the swelling and mechanical properties.

Keywords: *Hydrogels, AMPS, FTIR Spectroscopy, Compression, Swelling.*

Introduction

Hydrophilic gels, usually referred as hydrogels are networks of polymer chains that are sometimes found as colloidal gels in which water is the dispersion medium. Researchers, over the years, have defined hydrogels in many different ways[1]. The most common of these is that, a hydrogel is a water-swollen and cross-linked polymeric network produced by the simple reaction of one or more monomers. The ability of hydrogels to absorb water arises from hydrophilic functional groups attached to the polymeric backbone, while their resistance to dissolution arises from cross-links between network chains.[2]

Recently, 2-Acrylamido-2-MethylPropane Sulphonic acid (AMPS-H^+) has gained attention which is a strongly acidic ionic monomer and is easily dissolved in water. The polymer properties enhanced by AMPS-H^+ are its hydrophilicity, thermal stability, stability over a broad pH range,

resistance to hydrolysis and ionic character.[3]Organogels are materials which can solidify organic solvents; they may be composed of low molecular weight or polymeric materials. Alcohol specific super-swelling organogel (i.e. superalcogels) can be used for various applications such as fuel gels or pharmaceutical formulations.[4]

Experimental

Materials

2-Acrylamido-2-Methylpropanesulfonic acid (AMPS), N,N'-Methylene-bisacrylamide (MBA), Ammonium persulphate (APS) and Tetramethylethylenediamine (TEMED) were purchased from Sigma Aldrich. All the chemicals were of analytical grade and used as received.

Synthesis

AMPS was dissolved in distilled water in a closed vial and stirred until the solution became homogeneous. Neutralization of AMPS was done. After that MBA and APS were added and further the solution was stirred for complete homogenization. Total volume of the solution was kept constant to 20ml by adding distilled water. N_2 was bubbled through the solution (to maintain inert conditions) followed by the addition of TEMED before sealing the vial. After complete gelation gels were placed in distilled water to remove all the unreacted molecules completely. The gels were finally filtered using sieve, rinsed with acetone and dried in oven at 50° C for 2-3 days or till the gels dried completely. The powdered gels were weighed and sealed in vials for further studies. Same procedure was used to obtain the gels in bead form. After the N_2 bubbling and addition of TEMED to the beaker, the mixture was immediately poured into Teflon mould. After the completion of reaction the beads were demoulded and kept in distilled water for washing. The stoichiometry of the gels are mentioned in Table 1.

Table 1 Stoichiometry for the synthesis of PAMPS Hydrogels

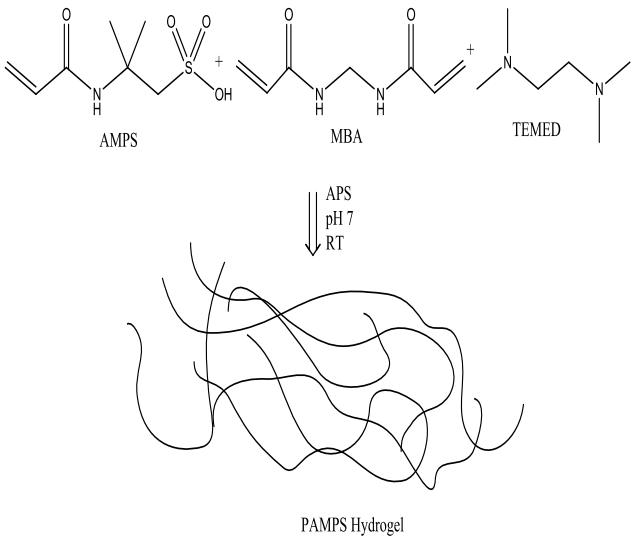
Composition	AMPS (x 10^{-3} mols)	MBA (x 10^{-3} mols)	APS (x 10^{-3} mols)	*TEMED (x 10^{-3} mols)*
6%C + 0.5% A	9.65	0.579	0.409	*0.051*
6% C + 1% A	9.65	0.579	0.409	*0.102*
6% C + 2% A	9.65	0.579	0.409	*0.205*
6% C + 3% A	9.65	0.579	0.409	*0.307*
6% C + 4% A	9.65	0.579	0.409	*0.409*
8% C + 4% A	9.65	0.772	0.416	*0.416*
10% C + 4% A	9.65	0.965	0.423	*0.423*
15% C + 4% A	9.65	1.448	0.444	*0.444*

FTIR Spectroscopy

Samples of each hydrogel were dried in an oven at 40°C until constant weight. Pellets were prepared by taking 3 mg of sample with 97 mg KBr powdered in a mortar. IR spectra were recorded over the range 400–4000 cm-1, in ALPHA FTIR spectrophotometer and the results were analyzed to confirm the presence of AMPS.

Swelling behavior of hydrogels

The swelling behavior of the hydrogels was studied. The "as synthesized" hydrogels were immersed in distilled water for several days to remove the unreacted molecules. The hydrogels were then dried in oven till the hydrogels get dried completely. These xerogels were then immersed in different solvents namely distilled water, ethanol solution with varying concentration(V/V), NaCl(3.5%) in distilled water, NaCl(0.9%) in distilled water, HCl solution (pH 2.2) and NaOH solution(pH 11.5). The swollen gels in different solvents were removed from solution at specified time intervals and excess water was removed using filter paper and weighed in the analytical balance. Weights of the samples were recorded till they become constant/reaches equilibrium swelling. The swelling ratio was determined using the formula:



$$Q = \frac{W_s - W_d}{W_d} \times 100$$

Where Ws and W_d are the weights of the swollen and dry samples respectively and Q being the swelling ratio.[5]

Mechanical studies

Unidirectional stress–strain measurements were performed with an Instron 5943 mechanical tester at room temperature. The compression studies were performed on as synthesized (15mm in diameter 15mm in height) mounted on parallel plates with constant speed of 2mm/min and 1kN pre-tension load. Three samples of each cross-linked hydrogels, "as synthesized" were tested for reproducibility and the results were averaged.[6] As shown in Figure 1.

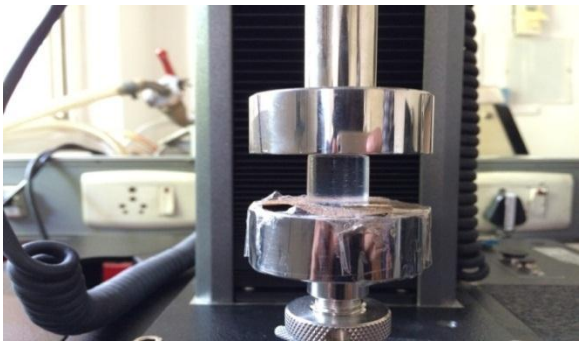


Figure 1 Compression studies of as synthesized gel.

Results and discussion

Synthesis of cross linked PAMPS hydrogel

The hydrogels were prepared successfully. The time taken for the gelation was found to be inversely proportional to the amount of cross linking reagent used which was expected. The mechanical strength of the beads was proportional to the amount of crosslinking reagent. The reaction scheme is given in Scheme 1.

Scheme 1 Reaction scheme of PAMPS hydrogel.

Characterization

The absorption of the peak between 1040 -1050 cm^{-1} is the characteristic peak of AMPS due to S=O asymmetric stretch. The spectra is shown in Figure 2 and Figure 3.

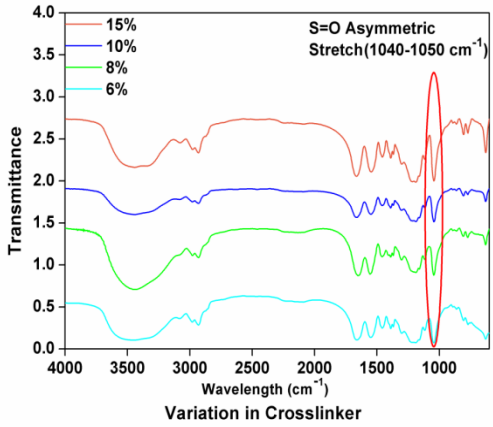


Figure 2 FTIR spectra of hydrogels with different crosslinker keeping the accelerator constant 4%.

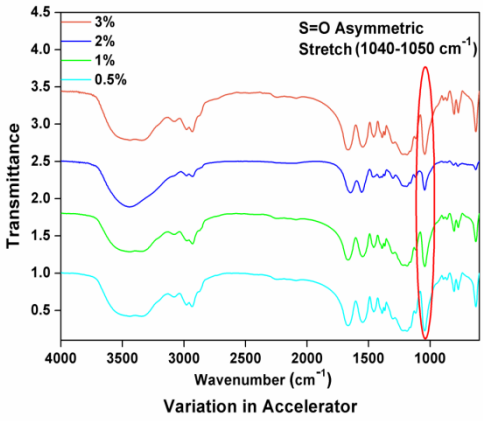


Figure 3 FTIR spectra of hydrogels with different accelerator keeping the crosslinker constant 6%.

Swelling Studies

The hydrogels shows maximum swelling in distilled water which is devoid of any ions. At neutral pH all the sulphonic groups are in their anion form and hence the sulphonic groups on swelling shows electrostatic repulsion and hence maximum swelling.

As the amount of accelerator increases the swelling increases this is due to the fact that on increasing mole% of accelerator the time of gelation decreases because of this fast gelation all the monomers don't take part in reaction and hence the crosslinking do not take place effectively. This explains the anomalous swelling behavior in case of changing accelerator concentration. Figure 4 depict the swelling studies in distilled water.

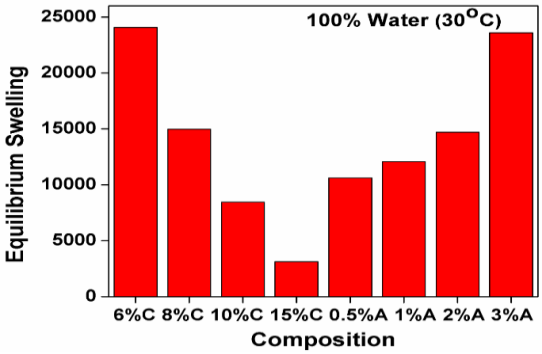


Figure 4 Equilibrium swelling of PAMPS hydrogels with different crosslink and accelerator in water.

As the percentage of ethanol increases from 10% to 70% there is a decrease in the swelling. The swelling is inversely proportional to that of crosslinker showing a decrease from 6% crosslinker to 15% crosslinker. As the accelerator increases the swelling increases this is due to the fact that all the crosslinks are not formed as the time of reaction is less. Figure 5 shows swelling in ethanol and water.

At acidic pH (pH 2.18), all the sulphonic groups are protonated and the repulsion between sulphonic groups are eliminated and thus hydrogels shows negligible swelling compared to other solvents. Also, due to the neutralization of the sulphonic groups the hydrogels get precipitated and shows minimum swelling behavior. At basic pH (pH 11.52) screening effect due to the cation eliminates the repulsion between sulphonic groups.

In NaCl(0.9% and 3.5%)the sulphonic groups are in their anion state but unlike distilled water, the swelling in hydrogels are not observed to be too high. This phenomenon can be explained by the screening effect caused by the cations present in the salt solutions. The cations effectively screen the anionic sulphonic groups and hence due to the reduction in the electrostatic repulsion between the sulphonic groups, the hydrogels shows less swelling compared to as in the distilled water. There is not much reduction in swelling observed from 0.9% concentration to 3.5% this is due to the number of cations present in 0.9% is enough to effectively screen the anionic sulphonic

groups. Hence further increase in concentration will not affect the swelling. and Figure 6 depict the swelling studies in solvents.

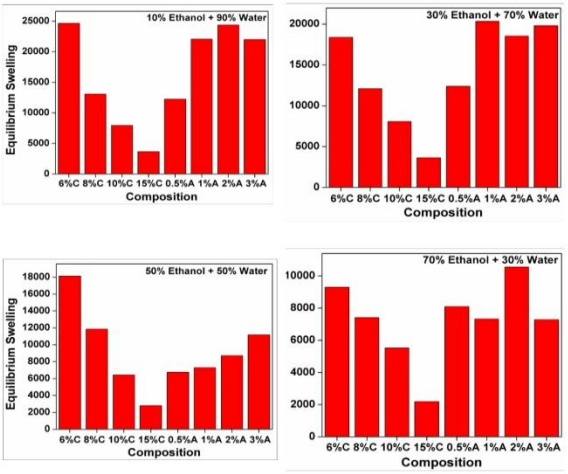


Figure 5 Swelling in various Ethanol -Water Mixtures.

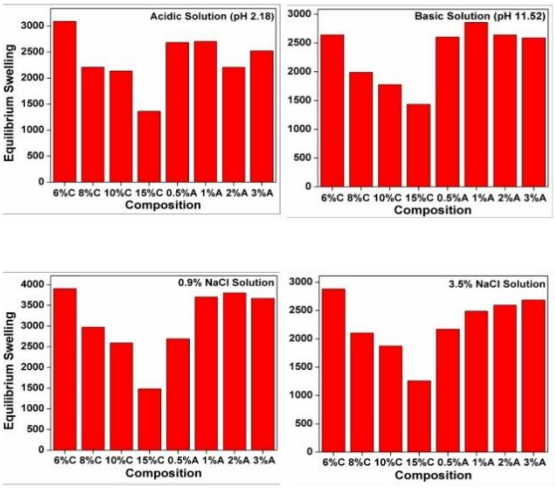


Figure 6 Swelling in Acidic, Basic and Salt Solution

Compression Studies

The compressive modulus of the hydrogels increases linearly on increasing the cross linking density as expected and decreases with increasing the accelerator. Where as the compressive strength of the hydrogels decreases linearly on increasing the cross linking density and increases with increasing the accelerator as depicted from Figure 7 Figure 8

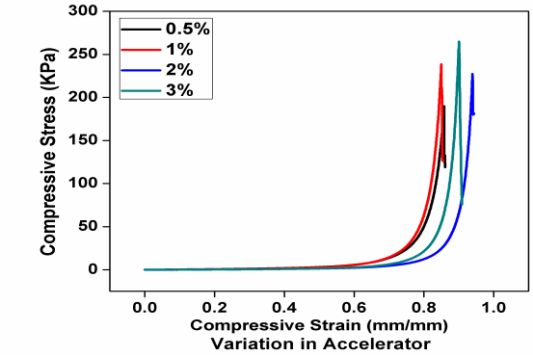


Figure 7 Compression studies of hydrogels with different mole% of accelerator, with constant mole% crosslinker as 6%.

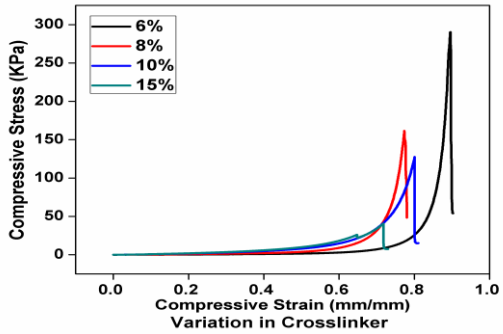


Figure 8 Compression studies of hydrogels with different mole% of crosslinker, with constant mole% of accelerator as 4%.

Conclusion

We have successfully synthesized AMPS based hydrogels with varying cross linker and accelerator using MBA and TEMED respectively. We have studied the effect of different solvents on the swelling behaviour of the cross linked hydrogels and it was observed that cross linking density, pH change and ionic strength plays a major role in the swelling profile. The hydrogels obtained have reasonably good mechanical strength as obtained from the compression studies. Compressive strength and modulus also depends on the degree of cross linking and the ionic strength of the solvent. From the compression studies we concluded that increasing MBA increased Compression Modulus and increasing TEMED increased Compressive Strength. Hydrogels with super-absorbency of alcohols such as ethanol and methanol are used as fuel gels, fire starters, etc. due to their ability for alcohol super absorbency, these gels can be used as fuel gel for warming, cooking or boiling water. They can also be used for hygienic applications such as sanitizers and controlled release of fragrance and drugs. These gels can also be used for slow water release in agriculture and farming and playing fields.

References

1. Ahmed Enas M, Aggor Fatma S, Awad Ahmed M, El-Aref Ahmed T. An innovative method for preparation of nanometal hydroxide superabsorbent hydrogel, CarbohydrPolym 2013; 91:693–8.
2. Enas M. Ahmed Hydrogel: Preparation, characterization, and applications Journal of Advanced Research (2013).
3. Kanarat Nalampang, Nantarat Suebsanit, Chinanat Witthayaprapakorn, and Robert Molloy Design and Preparation of AMPS-Based Hydrogels for Biomedical Use as Wound Dressings Chiang Mai J. Sci. 2007; 34(2) : 183-189.
4. KouroshKabiri, AzadehAzizi, GholamBagheriMarandi, HosseinBouhendi, and Ahmad Jamshidi. Super-alcogels Based on 2-Acrylamido-2-methylpropane Sulphonic Acid and Poly(ethylene glycol) MacromerIranian Polymer Journal 20 (3), 2011, 175-183.
5. Rosalia Rodriguez, Carmen Alvarez-Lorenzo, Angel Concheiro, Journal of Controlled Release 86 (2003) 253–265.
6. Anumon V Divakaran, Arun Torris AT, Ashish K Lele and Manohar V Badiger, Porous poly(ethylene glycol)–polyurethane hydrogels as potential biomaterials, Wiley Online Library.

MACRO 238

Modification and Hydrogel preparation of Chitosan for Controlled Drug Delivery and Tissue Engineering

Arun Kumar Mahanta and Pralay Maiti*
School of Materials Science and Technology, IIT (BHU), Varanasi- 221 005, India.
***e-mail id:** chem.arun11@gmail.com

Abstract

The present investigation focuses on the grafting of chitosan (CHT) with diisocyanate terminated polyurethane. Solid state ^{13}C NMR spectroscopy confirms the grafting reaction and the degree of substitution (DS) was calculated from the deconvoluted area of the corresponding NMR peak. Solubility studies, swelling behavior and contact angle measurements support the hydrophobic chemical modification on CHT molecules and higher DS leads to the crosslinking of CHT molecules having polyurethane bridges resulting insolubility and regulated swelling in the graft copolymer. Molecular relaxations phenomena due to the constraint associated with the grafting have been revealed using spin lattice relaxation tine (T_1) and shifting of peak position in tan δ curve toward lower temperature in dynamic mechanical measurement at constant frequency indicating flexible nature of graft copolymers as compared to pure CHT. The sustained drug delivery has been achieved using graft copolymers.

Keywords: Chitosan; grafting; drug delivery

Introduction: In last few decades, significant progress has been made on fundamental and biomedical research on chitosan technology. Chitosan is one of the most important biopolymers, composed of β-(1,4) linked 2–deoxy-2-amino-D-glucopyranose and partially of β-(1,4) linked2–deoxy-2-acetamido-D-glucopyranose[1,2] and is obtained by alkaline deacetylation of chitin[3,4] which is the major component of the exoskeletal in crustaceans.[5] Owing to its special characteristics like nontoxic, biodegradable and biocompatible, various biomaterials of chitosan and its derivatives have been developed for its use in pharmaceuticals applications.[6-9] Chitosan can also be used in a wide range of applications such as membrane,[10] drug delivery system,[11-14] gene delivery,[15,16] cell culture,[17-19] tissue engineering,[20] biosensors,[21] and scaffold generation.[22] Although, chitosan is an interesting biomacromolecule, it is insoluble in most common organic solvents and water, which greatly affects its applications in a various fields. A few chitosan derivatives have been chemically modified and characterized for their possible use in controlled release and targeted delivery of pharmaceuticals.[23,24] Some of these chitosan derivatives are self assembled and have the capability to form nanoparticles for controlled release and targeted delivery of bioactive components. Among them, N-alkyl-O-sulfate,[25,26] crosslinked chitosan[24,25] and O-carboxymethylate,[24] as well as derivatives containing hydrophobic branches on chitosan backbone[25] are of great interest. N–alkyl-O-sulfate showed nanomicelles formation and due to its self assembly and poor solubility, slow release of paclitaxel, a hydrophobic anticancer compound, is reported in the literature.[27] Chemical modification may also improve the mucoadhesive and penetration enhancing properties of chitosan.[28] Use of chitosan derivatives for controlled release and targeted delivery of bioactive component in pharmaceutics may promote the value added use of crab and shrimp shells and enhance the growth of seafood industry.

Now a day, the synthesis of novel blood compatible polymer based biomaterials has been drawing a great attention. Currently, much interest is being paid to use natural material for designing new biomaterial. Very large swelling characteristics along with its first release of drug make pure chitosan not suitable for many applications, especially in biomedical uses. Further, very low elongation at break or brittle nature of pure chitosan limits its use as biomaterials. Polyurethane modified chitosan has become a new frontier.[29,30] Many interesting properties are expected, such as excellent mechanical property, good thermal stability, increasing anticoagulant, low hydrophilicity, and so on.

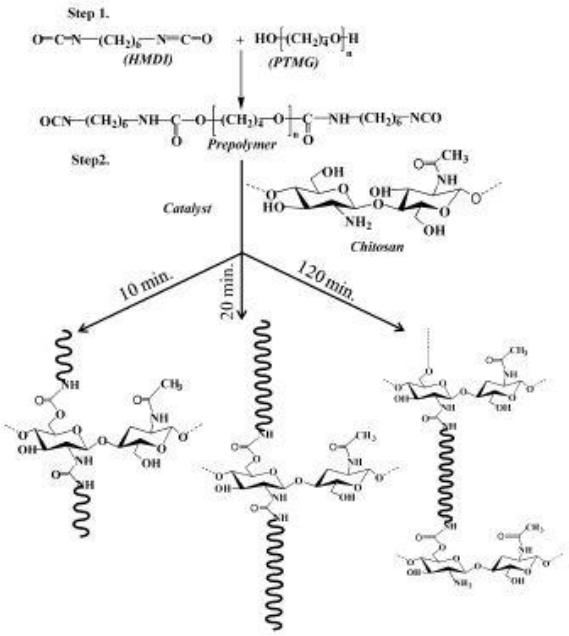
In this work, isocyanate terminated polyurethane (prepolymer) was grafted on to chitosan molecules and various degree of substitutions with varying chain length were obtained to control the hydrophilic nature. Network structure has also been developed through crosslinking of chitosan molecules with polyurethane bridges. Grafting was confirmed by using ^{13}C solid state NMR and other spectroscopic techniques. Solubility and swelling profile of the copolymers also endorse the grafting followed by crosslinking
Introduction text goes here.[1] The introduction should be relevant with the focus of work.[2, 3]

Experimental : Chitosan (CHT), from shrimp shells with ≥75% degree of deacetylation was used for this work, was obtained from Sigma Aldrich, USA. Poly(tetramethelene glycol) (PTMG) (Terathane, Sigma Aldrich), number average molecular weight (M_n) 2900 g / mol was used as received. 1, 6 – hexamethylene diisocyanate (HMDI), glacial acetic acid (100%) and solvent dimethyl formamide (DMF) were purchased from Merck, Germany. The catalyst dibutyltin

dilaurate (DBTDL) was purchased from Himedia. The antibacterial drug, tetracycline hydrochloride was procured from Sigma Aldrich, USA.

Preparation of *CHT -g- PU:* Polyurethane grafted chitosan copolymers were synthesized in two steps as (1) preparation of polyurethane prepolymers, and, (2) copolymerization through grafting. The prepolymers were obtained through condensation reaction between HMDI and PTMG in the –NCO/–OH ratio of 1.05:1, using few drops of 0.1 wt% DBTDL solution in toluene as catalyst. The reactions were performed at 80 ºC for 2h to form an isocyanate terminated prepolymer in a closed reaction vessel. Chitosan (1 g) was dispersed into glacial acetic acid / DMF mixture (30 ml) in the ratio of 50/50 and left overnight to obtain good swollen chitosan and consequently the grafting reaction was carried out. The isocyanate terminated polyurethane prepolymer solutions were cooled down to room temperature then fully swollen chitosan was added to the mixture. The reactions were continued at 80 ºC under constant stirring for predetermined times (***Table 1***) to obtain various degrees of grafting/substitution. After the completion of the reaction, the reaction mixture was transferred to distilled water. Grafted copolymers were separated by filtration and successively washed with DMF, methanol, acetone to remove the pure polyurethane from grafted specimen. The final products were dried under vacuum oven at 60 ºC. The reaction details were given in **Scheme 1**.

Scheme 1: Scheme of the reaction showing time dependent chain length of grafted species and subsequently crosslinking between CHT molecules at higher degree of substitution.



Characterization:

Solid state NMR spectroscopy: Solid-state ^{13}C NMR measurements of the samples were carried out on a Bruker 400 MHz spectrometer at the resonance frequency of 100.628 MHz using 4 mm double resonance cross polarization magic angle spinning probe. Around 100 mg of sample was tightly packed into a 4 mm diameter cylindrical zirconium oxide rotor with a Kel-F end cap. ^{13}C CP/MAS NMR spectrum was acquired with a cross-polarisation contact time of 2 ms and a recycle delay of 5s at a MAS speed of 10 kHz. A 1s recycle delay was used for HP/MAS experiments in

order to observe the fast relaxing components. CPT_1 experiment used here was a modified CP inversion recovery experiment where a single pulse delay was used between carbon pulses instead of a collection of delays. In order to observe selectively the most rigid fractions of the polymer, the single pulse delay should be about five times to that of the lowest relaxing component. A 5s single pulse delay determined from spin-lattice data of $CPXT_1$ experiment was used for CPT_1 experiment. All experiments were carried out at ambient probe temperature (25 ^oC) with high power proton decoupling during acquisition. All ^{13}C NMR spectra were assigned using adamantane as an external reference.

FTIR: Infrared spectra of the solid polymer film were recorded on a Thermo Nicolet 5700 instrument with the resolution of 4 cm^{-1} taking 100 scans at room temperature.

UV- Visible spectroscopy: The UV-Visible measurements were performed by using Shimadzu (UV-1700), pharma speck, UV-Visible spectrophotometer operating in 200-1100 nm spectral range. The transparent thin films were prepared through solvent casting method.

Swelling Studies: The swelling capacity of the copolymers including CHT was determined through gravimetric technique. A known weight of the dry polymer was immersed in beaker containing 50 ml of a solution of 0.1 M AcOH and DMF mixture in the ratio of 70:30. The polymer films were taken out from the solution at different times and the excess water was removed by soaking with tissue papers. The swollen polymers were weighed and then placed in the solution again. The dynamic weight change of the polymers with respect to time was calculated using the formula below: **[31]**

$$\% \text{ weight change} = \frac{W_f - W_i}{Wi} \times 100\%$$

where, w_f is the weight of the polymer in the swollen state and w_i is the initial weight of the polymer in dried condition.

Contact angle: Determination of the contact angle of the graft copolymers is essential to examine their hydrophilicity. The contact angles of the copolymers were measured using the Kruss F-100 tensiometer at ambient condition. Three specimens of each sample in the form of thin strips were used to measure contact angle in water. The accuracy of the measurement was $\pm 1^o$.

Differential scanning calorimetry (DSC): The heat of fusion of the pure CHT and its graft copolymers was determined by using DSC, Mettler 832 at a scan rate of 10^o min^{-1}. The peak temperature and enthalpy of fusion were measured from the endotherms with the help of a computer attached to the instrument. The DSC was calibrated with indium before use.

The degradation temperature of the specimens was estimated using Mettler thermogravimetric analyzer at a heating rate of 20^o min^{-1} under nitrogen atmosphere.

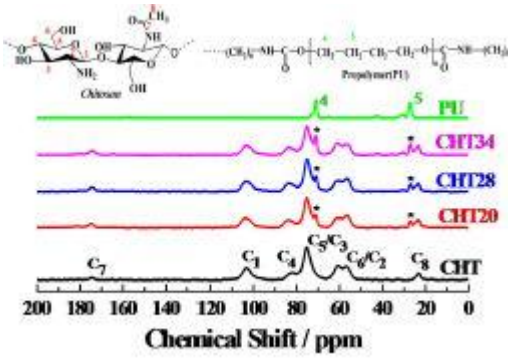
Drug assay and release study: In *vitro* release studies were carried out in PBS buffer at pH~7.4. Anti bacterial drug, tetracycline hydrochloride, standard stock solution (1 mg/ml) was prepared first. The standard curve was drawn after taking absorbance using UV – visible spectrophotometer (Shimadzu 1700) taking the absorption at 358 nm in the concentration range of 1 to 10 mg/ml. CHT and its graft copolymers containing the drug were put into 100 ml of release medium in an incubator shaker (50 rpm) at 37^{o}C. Aliquot from drug containing solutions were taken at constant time intervals from the release medium and were replaced with same amount fresh buffer. The concentration of anti bacterial drug in the samples was measured by determining the absorbance at 358 nm.**[32]** Drug loaded (3 wt.%) polymer film was prepared by dissolving the purified polymers and drug in a mixed solvent of 0.1M AcOH and DMF in the ratio of 70:30. The mixture was stirred

for overnight to ensure the complete dissolution of polymer and drug. The Homogeneous solution of polymer and drug was poured into a Petri dish and then heated at 60 ^{o}C to evaporate solvent. After the complete evaporation of solvent the drug embedded polymer films were used for drug release studies.

Results and discussion:

Grafting on chitosan:

Polyurethane chain extension on chitosan backbone has been done through the reaction of isocyanate terminated polyurethane prepolymer and hydroxyl/amine linkages present in chitosan. ^{13}C solid state NMR spectroscopic technique has been used to characterize the grafting and to measure the degree of substitution. **Figure 1** shows the ^{13}C NMR of prepolymer PU, pristine CHT and their graft copolymers



sample identification	degree of substitution	time of reaction	
		step 1 (h)	step 2 (min)
CHT20	20	2	10
CHT28	28	2	20
CHT34	34	2	120

Figure 1: ^{13}C solid state NMR Spectra of chitosan, PU and their graft copolymers as indicated.

and the assignment of each peak has been made on the basis of literature reports.[36-38] The grafting of polyurethane onto chitosan occurred through the formation of urethane (-OCONH-) linkage either the reaction between –NH_2 groups at C_2 and/or –OH groups at C_6 position of the chitosan with the –NCO terminal groups of polyurethane prepolymers resulting no change in characteristic ^{13}C NMR peak of chitosan rather two new peaks are observed at 26.9 and 71 ppm, respectively, in the copolymers. Moreover, the intensities of those peaks gradually enhanced with increasing the time of reaction between prepolymer (PU) and pristine CHT indicate greater incorporation of PU chain in CHT backbone at longer reaction time. The degree of substitution (DS) has been calculated from the peak area of the deconvoluted peaks and, henceforth, termed the copolymers as CHT20, CHT28 and CHT34, where the numbers after CHT represent the percentage substitution (**Table 1**). Degree of substitution per chitosan monomeric unit was estimated from NMR data using the following equation:

Table 1: Reaction conditions and nomenclatures of the graft copolymers.

$$DS\ \% = \frac{\text{Area of } I_{26.9ppm}}{\text{Area of } I_{26.9ppm} + \text{Area of } I_{23.35ppm}} \times 100 \quad \ldots\ldots\ldots\ldots (1)$$

This is to be noted that DS increases with reaction time as newer sites are grafted and longer PU chains are attached with CHT molecules resulting crosslinking between CHT molecules through

PU chain as described in **Scheme 1**. However, varying length of grafted PU chain has been prepared by changing the reaction time / degree of substitution which lead to the ultimate crosslinking of CHT molecules through PU chains, thereby, modifying the chemical nature of CHT from hydrophilic to hydrophobic in nature. As there are three different sites from where chain extension of PU may start, it is important to find out the exact locations of chain reaction. Spin–lattice relaxation time (T_1) has been measured using inversion recovery experiments to understand the dynamics of various carbon atoms of CHT.[39] Relaxation time of C_2 and C_6 nuclei are considerably affected with degree of substitution (**Table 2**). T_1 increases systematically with DS both for C_2 and C_6 nuclei indicating slower dynamics arising from longer PU chains attached or actual reaction sites of chain propagation Relaxation behavior as a function of time has been shown in exhibiting a relaxation peak at higher time. However, it is clear from spin – lattice relaxation time (T_1) that rigidity occurs in C_2 and C_6 nuclei with increase in reaction time as compared to other site and suggests the chain extension at those sites leading to ultimate crosslinking

Table 2. ^{13}C Spin–Lattice Relaxation Time (T_1, s) for Chitosan and Its Graft Copolymers for Indicated Carbon Positions

CHT	CHT10	CHT20	CHT34
10.1 (C_2), 0.84 (C_6)	11.8 (C_2), 0.92 (C_6)	13.4 (C_2), 1.1 (C_6)	13.6 (C_2), 1.4 (C_6)

Table 2: ^{13}C Spin lattice relaxation time (T_1) for chitosan and its graft copolymers for indicated carbon positions.

Polyurethane grafting on CHT has been analyzed through spectroscopic techniques. FTIR spectra of chitosan and its graft copolymers CHT20, CHT28 and CHT34 are shown in **Figure 2.** The well known characteristics peaks of chitosan are at 1650 and 1580 cm^{-1} for distinct amide I and amide II band, respectively.[40] The broad peaks in the region of 3200 – 3500 cm^{-1} were assigned for N-H and O-H stretching vibration of inter- and intra-molecular hydrogen bonds appears from the $–NH_2$ and –OH groups of the chitosan molecule.[40,41] Observed band of pure CHT at 3370 cm^{-1} becomes narrower as well as shifted to lower region at 3313 cm^{-1} in graft copolymers with increasing the degree of substitution suggest that the inter- and intra-molecular hydrogen bonding become weak as the $–NH_2$ and –OH groups of CHT have been transformed into corresponding urea and urethane linkages. The shifting of the band is attributed to the interaction between grafted PU and CHT molecules mainly due to dipolar interaction including hydrogen bonding.

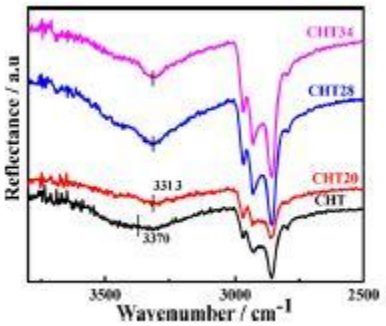


Figure 2: FTIR Spectra of CHT and its indicated copolymers. The vertical lines indicate the peak positions.

The UV–Vis spectra of polyurethane, pure chitosan and its graft copolymers are shown in **Figure 3**. Pristine CHT shows no absorption peak in the range of 200 – 400 nm[42] while PU shows

one band at 230 and 318 nm due to the $\pi - \pi^*$ and $n - \pi^*$ transition, respectively.[43] Notably, the UV–Vis absorption peaks of grafted copolymer are shifted to longer wavelengths at 278 and 307 nm. The red shifts are attributed to the interaction between PU and CHT chains. These results are consistent with the literature reported value of grafted chitosan.[42,44]

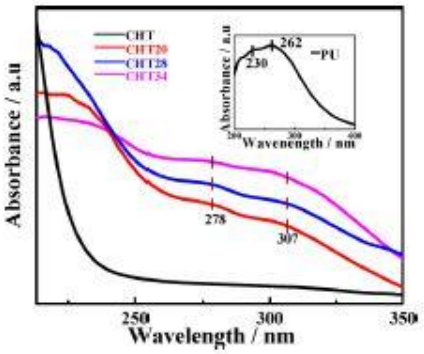


Figure 3: UV- Visible spectra of CHT and its indicated copolymers. The vertical lines indicate the peak positions. Inset figure represent the UV-Vis pattern of pure PU showing absorption peaks.

Effect of grafting:

Grafting plays an important role for modifying the properties and makes the polymer suitable for different applications. CHT is soluble in dilute mineral acid while PU is soluble in DMF. The solubility of the copolymers has been carried out in 0.1 M acetic acid and in acetic acid / DMF mixture in the ratio of 70/30. The grafted copolymer CHT20 is soluble in both acetic acid and acetic acid/DMF mixture, whereas CHT28 is partially soluble in 0.1 M acetic acid but soluble in acetic acid/DMF mixture. On contrary, CHT34 is insoluble in both the solvents. It is evident from the solubility studies that slightly longer grafting of PU chain makes CHT partially soluble in acetic acid solution while crosslinking of CHT at longer reaction time (CHT34) convert into insoluble system.

Swelling studies provide important indication of the extent of crosslinking in a polymer network.[45] **Figure 4** exhibits the swelling behavior of graft copolymers indicating poor swelling for higher DS copolymers. The swelling decreases considerably with increase in crosslink densities. Swelling behavior of pure CHT has been presented in the inset of Fig. 4 showing very high swelling (6000%) of pure CHT and it can be tuned nicely up to 200% by controlling the DS or crosslink density through grafting. Grafting of CHT with polyurethane transforms the polymer toward hydrophobic in nature as evident from the higher contact angle of copolymers as

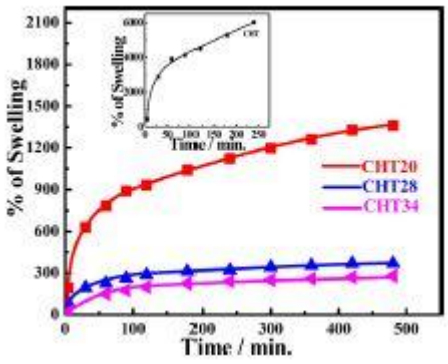


Figure 4: Swelling profile of chitosan (inset figure) and its indicated graft copolymers in acetic acid and DMF mixture

compared to pure CHT.Further, the contact angle enhances with DS indicating wrapping up of hydrophobic PU on CHT molecules. However, the degree of swelling systematically decreases to 1360, 370 and 280% for CHT20, CHT28 and CHT34, respectively, while increase of contact angle is noticed as 66.6, 70.7 and 72.2^{o} for the same order of specimens. However, the solubility, swelling ability and contact angle of grafted and crosslinked chitosan have particular importance as a drug carrier.

Effect of grafting on thermal and mechanical responses:

Thermal degradation profiles for pristine and chemically modified chitosan are quite different. The mass losses curves, evaluated under nitrogen atmosphere, are shown in F**igure 5a.** Pure polymers exhibit single step degradation while graft copolymers show two steps degradations corresponding to the copolymer components. The initial mass loss, occurred at 45 ^{o}C which continued up to 150 ^{o}C with gradual weight loss of 5%, is associated with the loss of adsorbed water molecules due to hydrophilic nature of polymer. The second stage of degradation started at 281^{o}C with 50% weight loss corresponding to the decomposition of chitosan.[47,48] The third stage of weight loss in graft copolymers corresponds to the PU degradation at ~400 ^{o}C. The thermogravimetric analysis was used to determine the thermal stability of chitosan where it is expected to decrease its weight with increasing crosslinking due to disappearance of hydrogen bonding associated with N-acetyl and free amino groups in graft copolymers.[46] Pure prepolymer (PU) shows single stage degradation which starts at higher temperature (395 ^{o}C) as compared to chitosan and nearly complete degradation occurs at 450 ^{o}C. On the other hand, around 60% degradation occurs for CHT due to formation carbon shoot which get enhanced considerably in graft copolymer.

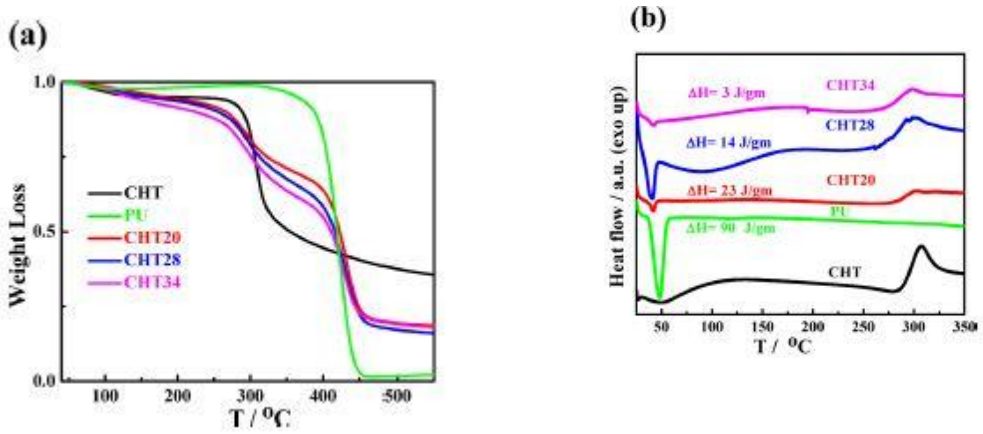


Figure 5: (a) *TGA* and (b) *DSC* thermograms of CHT and its graft copolymers. The heat of fusion gradually decreases with increasing DS as mentioned.

DSC curves of chitosan and its graft copolymers under nitrogen atmosphere are shown in **Figure 5b**. A broad endothermic peak around 50 °C is observed in the DSC curve of chitosan which is attributed to the loss of absorbed water and another strong exothermic peak centered near 307 °C due to the decomposition of chitosan which is in good agreement with the TGA analysis.[49,50] Prepolymer (PU) shows a sharp endotherm at 48.1 °C indicating its melting point while the graft copolymers show endothermic peak at ~ 40 °C. The lowering of melting temperature is presumably due to the dilution effect and greater interaction between PU and CHT chains. The interactions are further reflected in reduced heat of fusion (ΔH) of copolymers as compared to pure PU. ΔH gradually decrease with increasing DS due to reduction in crystalline part after crosslinking.[48] However, chitosan does not show any characteristics glass transition temperature (T_g) in its DSC curve. It is well known that chitosan is a semicrystalline polymer and shows strong intra- and inter-molecular hydrogen bonding along with a rigid amorphous phase of its heterocyclic units. The variation in heat capacity corresponding to the change in specific volume near T_g is too small to be detected by using DSC. A more sensitive method by applying sine wave frequency (DMA measurement) has been used to detect the T_g.

Controlled release of drug:

The aim of a controlled drug delivery system is to supply a biologically active molecule depend on the need of the physiological environment over a required time period maintaining the drug level in the body within the therapeutic window. *In vitro* drug release kinetics were performed in phosphate buffer solution (pH~ 7.4) at 37 °C using tetracycline hydrochloride loaded biocompatible and hemocompatible pristine CHT and polyurethane grafted chitosan films. **Figure 8** shows the cumulative percentage release of tetracycline hydrochloride as a function of immersion time. The sustained release of drug from PU grafted CHT copolymers is obvious vis-à-vis pure CHT. Pure CHT exhibits burst release of drug and release rate remain high at longer period and the total drug release attains 60% in 72 hrs. On the other hand, gradually sustained release has been noticed in graft copolymers with higher degree of substitution (only 15% release for CHT34 in 72 hrs). Moreover, the burst release completely disappears in graft copolymers and the cumulative releases are 60, 30, 20 and 15% for pure CHT, CHT20, CHT28 and CHT34, respectively, during first 72 hrs. If we look into the mechanism of drug release from a polymer

matrix, liquid penetration into the matrix, dissolution of the drug and diffusion of drug out of the matrix are the three distinct steps.[61] The rate determining

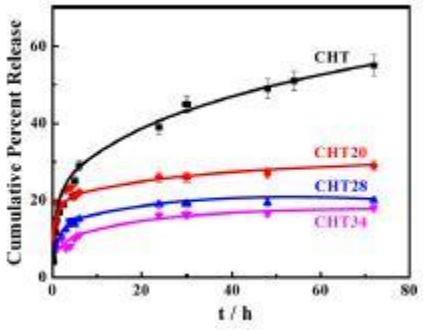


Figure 8: Cumulative drug release profile for CHT and its indicated graft copolymers.

step for drug release may be any one of these processes. It is observed that the release of drug molecules is significantly delayed from the graft copolymers than the pristine CHT. Polyurethane grafted chitosan systems show greater extent of network structure through crosslinking with increase in degree of substitution on to chitosan backbone. Increased crosslinking produces denser network and exhibits restricted swelling due to larger retraction forces caused by the higher number of covalent bridges within in the system and simultaneously prevents the diffusion out of the drug molecules from the network to the release medium. Zero order, first order and Higuchi models are also verified but the correlation coefficient (r^2) values corresponding to those models are not satisfactory while Korsmeyer-Peppas model is a perfect fit. Hence, slower diffusion is considered to be the rate determining step which is strongly influenced by the sluggish swelling ability of grafted copolymer as compared to pure CHT. Based on the release rate, a model has been proposed in **Scheme 2** to reveal the controlled release of drug from pure and graft copolymer. Extra covalent bonds arising from the extensive grafting form the network structure and diffusion of drug becomes slower from the graft copolymer cage. In summary, the drug release rate can be tuned by changing the network structure via suitable grafting of CHT.

Conclusions

Chemical modification of chitosan has been performed through grafting with isocyante terminated polyurethane and the degree of substitution has been varied until crosslinking between CHT molecules having polyurethane bridge. Degree of substitution has been calculated from the deconvoluted peak areas obtained from solid state NMR studies. Spin lattice relaxation time (T_1) increases with DS due to the relaxation constraints arising from the grafted part on CHT molecules. The extent of solubility and swelling characteristics decreases considerably with increasing DS in graft copolymers as compared to pristine CHT. Simultaneously, hydrophobic character, measured through contact angle, increases due to polyurethane grafting. Significant improvement of toughness has been observed after grafting vis-à-vis pure CHT while crosslinked copolymer exhibit brittle nature under uniaxial elongation.

Acknowledgements

The authors acknowledge the receipt of funding for his fellowship from *CSIR*, New Delhi, India. The authors also acknowledge the kind support of Prof. N. Misra, School of Biomedical Engineering, IIT (BHU), Varanasi, India for UV-Vis and contact angle measurements.

References

1. Onishi, H.; Machida, Y. Biodegradation and distribution of water-soluble Chitosan in mice. *Biomaterials* **1999**, *20*, 175-182.
2. Ravi Kumar, M.N.V.; Muzzarelli, R.A.A; Muzzareli, C.; Sasfiwa, H.; Domb, A.J. Chitosan Chemistry and Pharmaceutical Perspectives. *Chem. Rev*. **2004**, *104*, 6017-6084.
3. Muzzarelli, R. A. A.; Muzzarelli, C. Chitosan Chemistry: Relevance to the Biomedical Science. *Adv. Polym. Sci*. **2005**, *186*, 151-209.
4. Rinaudo, M. Chitin and Chitosan: Properties and applications. *Prog. Polym. Sci*. **2006**, *31*, 603-632.
5. Ifuku, S.; Morooka, S.; Morimoto, M.; Saimoto, H. Acetylation of chitin Nanofibers and their Transparent Nanocomposite Films. *Biomacromolecules* **2010,** *11*, 1326–1330
6. Gong, Xiuqing.; Peng, S.; Wen, W.; Sheng, P.; Li, W. Design and Fabrication of Magnetically Functionalized core/shell Microspheres for Smart Drug Delivery. *Adv. Funct. Mater*. **2009**, *19*, 292-297.
7. Hsieha, W.C.; Changb, C.P.; Gaoc, Y.L. Controlled release properties of Chitosan encapsulated volatile Citronella Oil microcapsules by thermal treatments. *Colloids Surf., B* **2006**, *53*, 209-214.
8. Yamamoto, H.; Amaike, M.; Biodegradation of cross-linked chitosan gels by microorganisms. *Macromolecules* **1997**, *30*, 3936-3937.
9. Risbud, M.V.; Bhonde, R.R.; Polyacrylamide-chitosan hydrogels: in vitro biocompatibility and sustained antibiotic release studies. *Drug Deliv* **2000,** *7*, 69-75.
10. Smitha, B.; Sridhar, S.; Khan, A.A. Chitosan-poly (vinyl pyrrilidine) blends as membranes for direct methanol fuel cell applications. J. Power Sources **2006**, *159*, 846-854.
11. Lubben, I.M.V.; Verhoef, J.C, Aelst, A.C.V, Borchard, G.; Junginger, H.E. Chitosan micropartiloces for oral vaccination: preparation, characterization and preliminary in vivo uptake studies in murine Peyer's patches. *Biomaterials* **2001**, *22*, 687-694.
12. Berthold, A.; Cremer, K.; Kreuter, J. Preparation and characterization of chitoan microsphere as drug carrier for prednisolone sodium phosphate as model for anti inflammatory drugs. *J. Control. Release* **1996**, *39*, 17-25.
13. Agnihotri, S.A.; Mallikarjuna, N.N.; Aminabhavi, T.M. Recent advances on chitosan-based micro- and nanoparticles in drug delivery. *J. Control. Release* **2004**, *100*, 5-28.
14. Trindade, M.C.D.; Lind, M.; Nakashima, Y.; Sun, D.; Goodman, S.B.; Schurman, D.J.; Smith, R.L. Interleukin-10 inhibits polymethylmethacrylate particle induced interleukin-6 and tumor necrosis factore-release by human monocyte/macrophages in vitro. *Biomaterials* **2001**, *22*, 2067-2073.
15. Jiang, X.; Dai, H.; Leong, K.W.; Goh, S.H.; Mao, H.Q. Yang, Y.Y.; Chitosan-g-PEG/DNA complexes deliver gene to the rat liver via intrabiliary and intraportal infusions. *J Gene Med* **2006**, *8*, 477-487.
16. Chen, M.H.; Hsu, Y.H.; Lin, C.P.; Chen, Y.J.; Young, T.H. Interactions of acinar cells on biomaterials with various surface properties. *J. Biomed. Mater. Res. A* **2005**, *74*, 254-62.
17. Mao, J.S.; Liu, H.F.; Yin, Y.J.; Yao, K.D. The properties of chitosan-gelatin membranes and scaffold modified with hyaluronic acid by different methods. *Biomaterials* **2003**, *24*, 1621-1629.
18. Lin, S.J.; Jee, S.H.; Hsaio, W.C.; Lee, S.J.; Young, T.H. Formation of melanocyte spheroids on the chitosan-coated surface. *Biomaterials* **2005**, *26*, 1413-22.

19. Wang, Y.C.; Lin, M.C.; Wang, D.M.; Hsieh, H.J. Fabrication of a novel porous PGA chitosan hybrid matrix for tissue engineering. *Biomaterials* **2003**, *24*, 1047-57.
20. Gingras, M.; Paradis, I.; Berthod, F. Nerve regeneration in a collagen-chitosan tissue-engineered skin transplanted on nude mice. *Biomaterials* **2003**, *24*, 1653-61.
21. Du, Y.; Luo, X.L.; Xu, J.J.; Chen, H.Y. A simple method to fabricate a chitosan-gold nanoparticles film and its application in glucose biosensor. *Bioelechtrochemistry* **2007**, *70*, 342-347.
22. Oliveiraa, J.M.; Rodriguesa, M.T.; Silva, S.S.; Malafayaa, P.B.; Gomesa, M.E.; Viegasac.; Diasc, I.R.; Azevedod, J.T.; Manoa, J.F.; Reisa, R.L. Novel hydroxyapatite/chitosan bilayered scaffold for osteochondral tissue-engineering applications: Scaffold design and its performance when seeded with goat bone marrow stromal cells. *Biomaterials* **2006**, *27*, 6123-6137.
23. Kumar, M. N. V. R. Nano and microparticles as controlled drug delivery devices. *J. Pharm. Pharmaceut. Sci.* **2000**, *3*, 234-258.
24. Bodnar, M.; Hartmann, J. F.; Borbely, J. Preparation and characterization of chitosan-based nanoparticles. *Biomacromolecules* **2005**, *6*, 2521-2527.
25. Zhang, C.; Ping, Q.; Zhang, H.; Shen, J. Preparation of *N*-alkyl-*O*-sulfate chitosan derivatives and micellar solution of taxol. *Carbohydr. Polym.* **2003**, *54*, 137-141.
26. Zhang, C.; Ping, Q.; Zhang, H. Self-assembly and characterization of paclitaxel-loaded *N*-octyl-*O*-sulfate chitosan micellar system. *Colloid Surf., B.* **2004**, *39*, 69-75.
27. Prabaharan, M.; Mano, J. F. Chitosan-based particles as controlled drug delivery systems. *Drug Deli*v **2005**, *12*, 41-57.
28. Brar, S.; Yadav, A. Investigation of microstructure of glycidyl methacrylate/α-methyl Styrene copolymers by 1D- and 2D- NMR Spectroscopy. *Eur. Polym. J.* **2003**, *39*, 15-19
29. Xu, D.; Meng, Z.; Han, M.; Xi, K.; Jia, X.; Yu, X.; Chen, Q. Novel Blood-Compatible Waterborne Polyurethane using Chitosan as an Extender. *J. Appl. Polym. Sci.* **2008**, *109*, 240-246.
30. Lin, W.C.; Tseng, C.H.; Yang, M.C. In vitro Hemocompatibility Evaluation of a Thermoplastic Polyurethane Membrane with Surface-Immobilized water-soluble Chitosan and Heparin. *Macromol.Biosci.* **2005**, *5*, 1013-1021.
31. Pasparakis, G.; Bouropoulos, N. Swelling studies and in vitro release of verapamil from calcium alginate and calcium alginate-chitosan beads. *Int. J. Pharm.* **2006**, *323*, 34-42.
32. Mary, L.A.; Senthilram, T.; Suganya, S.; Nagarajan, L.; Venugopal, J.; Ramakrishna, S.; Giri Dev, V.R. Centrifugal spun ultrafine fibrous web as a potential drug delivery vehicle. *eXPRESS Polymer Letters* **2013,** *7***,** *238–248.*
33. Singh, S. K.; Singh, M. K.; Nayak, M. K.; Kumari, S.; Gracio, J.A.; Dash, D. Size Distribution Analysis and Physical/Fluorescence Characterization of Graphene Oxide Sheets by Flow Cytometry. *Carbon* **2011**, *49*, 684−692.
34. Mishra, A.; Singh, S.K.; Dash, D.; Aswal, V.K.; Maiti, B.; Misra, M.; Maiti, P. Self – assembled aliphatic chain extended polyurethane nanobiohybrids: Emarging hemocompatible biomaterials for sustained drug delivery. *Acta Biomater* **2014**, *10*, 2133-2146.
35. Singh, N.K.; Singh, S.K.; Dash, D.; Gonugunta, P.; Misra, M.; Maiti, P. CNT Induced B-Phase in Polylactide: Uniqe Crystallization, Biodegradation, and Biocompatibility. *J.Phys. Chem.C* **2013**, *117*, 10163-10174
36. Ishida, M.; Yoshinaga. Solid –State 13C NMR Analyses of the Microphase-Separated Structure of Polyurethane Elastomer. *Macromolecules* **1996**, *29*, 8824-8829.

37. Saito, H.; Tabeta, R. High-Resolution Solid-state ^{13}C NMR Study of Chitosan and Its Salts with Acids: Conformational Characterization of Polymorphs and Helical Structures as Viewed from the Conformation-Dependent ^{13}C chemical Shift. *Macromolecules* **1987**, *20*, 2424-2430.
38. Kavianinia, I.; Plieger, P.G.; Kandile, N.G.; Harding, D.R.K. Fixed-bed column studies on a modified chitosan hydrogel for detoxification of aqueous solution from copper (II). *Cabohydr. Polym* **2012**, *90*, 875-886.
39. Breitmaier, E.; Spohn, K.H.; Berger, S. ^{13}C Spin-Lattice relaxation Times and the Mobility of Organic Molecules in Solution. *Angew.Chem.internat.Edit*. **1975**, *14*, 144-158.
40. Chen. C.; Tao, S.; Qiu, X.; Ren, X.; Hu, S. Long-alkane-chain modified *N*-phthaloyl chitosan membranes with controlled permeability. *Cabohydr. polym*. **2013**, *91*, 269-276.
41. Kolhe, P.; Kannan, R.M. Improvement in Ductility of Chitosan through Blending and Copolymerization with PEG: FTIR Investigation of Molecular Interaction. *Biomacromolecules* **2003**, *4*, 173-180
42. Liu, J.; Wen, X.; Lu, J.; Kan, J.; Jin, C. Free radical mediated grafting of chitosan with caffeic and ferulic acids: Structures and antioxidant activity. *Int. J. Biol. Macromol.* 2014, *65*, 97-106.
43. Chen, Y.; Zhou, S.; Yang, H.; Wu, L. Structure Properties of Polyurethane/Nanosilica Composite. *J. Appl. Polym. Sci*. **2005**, *95*, 1032-1039.
44. Bozic, M.; Gorgieva, S.; Kokol, V. Laccase-mediated functionalization of chitosan by caffeic and gallic acids for modulating antioxidant and antimicrobial properties. *Carbohydr. Polym* **2012**, *87*, 2388-2398.
45. Flory, P. J. *Principles of Polymer Chemistry*; Cornell University Press: Ithaca, NY, **1953**.
46. Welsh, E.R.; Schaur, C.L.; Qadri, S.B.; Price, R.R. Chitosan Cross-linked with a Water-Soluble, Blocked Diisocyanate. 1. Solid State. *Biomacromolecules* **2002**, *3*, 1370-1374.
47. Kyzas, G.Z.; Siafaka, P.I.; Lambropoulou, D.A.; Lazaridis, N.K.; Bikiaris, D.N. Poly (itaconic acid)-Grafted Chitosan Adsorbents with Different Cross-Linking for Pb (II) and Cd (II) Uptake. *Langmuir* **2014**, *30*, 120-131.
48. Ganguly, K.; Aminabhavi, T.M.; Kulkarni, R. Colon Targeting of 5-Fluorouracil Using Polyethylene Glycol Cross-linked Chitosan Microspheres Enteric Coated With Cellulose Acetate Phthalate. *Ind. Eng. Chem.Res*. **2011**, 50, 11797-11807.
49. Wan, Y.; Wu, H.; Yu, A.; Wen, D. Biodegradable Polylactide /Chitosan Blend Membranes. *Biomacromolecules* **2006**, *7*, 1362-1372.

MACRO 239

Nanostructure Regulated In Vitro – In Vivo Controlled Delivery of Hydrophobic Anticancer Drug

Sudipta Senapati,[a] Dipak Rana[b], Reshmi Shukla[c], Y.B. Tripathi[c] and Pralay Maiti*[a]

[a] *School of Materials Science and Technology, Indian Institute of Technology (Banaras Hindu University) Varanasi 221005, India*

[b]*Industrial Membrane Research Institute, Department of Chemical and Biological Engineering, University of Ottawa, 161 Louis Pasteur St., Ottawa, ON, Canada KIN 6N5*

[c] *Department of Medicinal Chemistry, Institute of Medical Science, Banaras Hindu University, Varanasi 221005, India*

** e-mail id: pmaiti.mst@itbhu.ac.in*

Abstract

In the current work, we have proposed a new PCL coated LDH-RH nanohybrid to improve the therapeutic efficacy of the hydrophobic anticancer drugs in terms improved bioavailability, in vitro–in vivo prolonged and sustained drug release profile, enhanced cellular uptake properties, better cancer cell killing efficacy while reducing in vivo adverse side effects etc. We found that PCL coated LDH-RH nanohybrid has the ability to suppress the initial burst release of RH and prolonged the release period of 5 days in vitro and more than 3 days in vivo. It has also much better in vitro anti–tumor efficiency and enhanced cellular uptake properties compared to bare RH or polymer embedded RH (PCL–RH). This nanohybrid reduced the adverse side effects of the anticancer drug and improved patient compliances by releasing the drug in more well controlled manner.

Keywords: *layered double hydroxide, poly(ε-caprolactone), controlled drug delivery, in vivo drug delivery*

Introduction

In recent years inorganic nanomaterials have attracted considerable attention as a drug delivery vehicles due to their biocompatibility, bioactivity, large surface area, no or minimum toxic side effects, low susceptibility to immune response, and resistance of high temperature and light.[1] Amongst them, layered double hydroxide nanoparticles are one of the best nanocarrier due to their excellent anion exchange capacity, excellent biocompatibility, no-toxicity, high drug loading efficacy, full protection for the loaded drugs, low cost, ease to prepare, biodegradability, biocompatibility, pH dependent stability, excellent endosome escape and moreover drug release rate can be controlled and tuned according to needs.[2] LDHs are a family of anionic clay materials, commonly defined by the general formula $[M^{II}_{1-x} M^{III} x\ (OH)_2]^{x+}\ (A_n^-)\ x/n.yH_2O$, where M^{II} is a divalent metal ion, such as Mg^{2+}, Zn^{2+}, etc., M^{III} is a trivalent metal ion, such as Al^{3+}, Fe^{3+}, Co^{3+}, etc. and A_n^- is an anion, such as Cl^-, NO_3^-, CO_3^{2-}, etc. However, these LDH-drug nanohybrids have very fast release profile, almost 100% drug release occurs within a few hours.[3] Although the fast release systems are much needed for some cases (such as anti-inflammatory applications etc.), but they may not be the best vehicles where drug exposure require for some days. A number of

biodegradable polymers are attractive materials from the standpoint of biocompatibility, degradability, bioactivity and controlled drug delivery vehicle. Amongst them, FDA approved polymer, poly(Ɛ-caprolactone) (PCL) is one of the biomaterials known for its biodegradability, biocompatibility, chemical stability, thermal stability, good mechanical properties, tissue-compatible nature and permeability used for wide applications, such as in certain implantable devices, has been considered as a potential substrate in drug delivery systems, resorbable sutures and bone graft substitutes.[11-14] Herein, hydrophobic anti-cancer drug raloxifene hydrochloride (RH) was intercalated into a series of zinc iron layered double hydroxide (ZnFe-LDH) using anion exchange technique. LDH nanoparticle intercalated with RH was then encapsulated into PCL matrix through solution route to control drug release. Among the LDH systems, nitrate bound LDH exhibits stronger interaction with drug and consequently sustained the release of the drug delivery against the loosely interacted phosphate bound LDH-drug, which shows fast release. Again the release rate was made more sustained by dispersing the nitrate bound LDH drug complex into PCL matrix (PN–R). The *in vitro* antitumor efficacy pure drug, drug intercalated LDHs and PN–R were investigated against the HeLa cells in a concentration and time dependent manner and it was observed that drug intercalated LDHs and PN–R have better antitumor efficacy than the pure drug (RH). In the *in vivo*, PN–R suppressed the initial burst release of RH in the blood and prolonged the circulation time up to 80 h.

Experimental

Synthesis of layered double hydroxide (LDHs): The ZN-Fe-LDHs were synthesized by using coprecipitation method according to our previous study.(ref) Mixture solution of 0.5 M Zn(NO3)2•6H2O and 0.25 M Fe(NO3)3•9H2O with [Zn2+]/[Fe3+] molar ratio of 2:1 in 100 ml deionized water was prepared first. 100 ml of 1.5 M NaNO3, Na2CO3, and Na3PO4 were prepared separately and were kept in five-neck flat bottom flask. Five necks of the flask were fitted with two burettes, one condenser, one gas inlet-outlet and one pH meter probe. The solutions were degassed by purging purified nitrogen. Previously prepared mixture solution of Zn(NO3)2•6H2O and Fe(NO3)3•9H2O was added drop wise into NaNO3, Na2CO3, and Na3PO4 separately and the solutions were stirred vigorously during mixing. NaOH solution (1.0 M), fitted in one burette, was added drop wise to the three different above mentioned solutions until the pH reached the value of 10. The whole solution was stirred continuously at 60 ºC for 14 h. The appearance of white gelatinous precipitate indicated the formation of Zn-Fe-LDHs having three different intercalated anions (NO3-LDH, CO3-LDH, PO4-LDH and are abbreviated as ZN, ZC and ZP, respectively). The precipitates were recovered by centrifugation (5000 rpm, RT) and were washed thoroughly with deionized water followed by drying in air oven at 50 ºC for 36 h.
Preparation of drug loaded polymer nanocomposite:

In order to prepare drug embedded polymer nanocomposite, ZN–R first sonicated in dichloromethane (DCM) to achieve a good dispersion. PCL was dissolved in DCM separately. Now ZN–R dispersion in DCM was added to the PCL solution (25% ZN–R w/w with respect to PCL) and then the whole solution was stirred for 3 h to ensure proper mixing. This mixture solution was allowed 24 h in a fume hood for solvent evaporation and then vacuum dried at room temperature for an additional 24 h. We termed this PCL and ZN–R nanocomposite as PN–R.

In vitro Drug release study: The drug release studies were performed at 37 oC after suspending drug intercalated LDH in 100 ml phosphate buffer saline of pH 7.4. At predetermined time intervals, 1 ml of aliquots were withdrawn and replaced by 1 ml fresh PBS to maintain the sink condition. The concentration of the released drug was determined through UV absorption at λmax = 295 nm. Further, to understand the release kinetics of the drug from the matrix, several kinetic models were used (details given in the Supplementary document) and fitted with the in vitro drug release data.

Cell viability: Cell viability of pure LDHs, pure polymer, pure drug, drug intercalated LDHs (D–LDH) and polymer D–LDHs nanocomposites (PN–R) were performed through the MTT assay against HeLa cell. In brief, 1×10^5 cm-2 HeLa cells were seeded onto the 96-well culture plates in DMEM. After 24 h of culture, the medium in the wells was replaced with the fresh DMEM containing the samples in the concentrations range 10 to 100 μg/ml and were incubated for 24, 48, and 72 h time intervals. After incubation, 100 μl of MTT dye solution (5 mg/ml in PBS, pH 7.4) was added to each well by replacing the media containing samples and was again incubated for another 4 h. At the end of the assay, purple colour formazan was produced, which was then dissolved in DMSO and the absorbance of each well was read on a microplate reader (DYNATECH MR7000 instruments) at 570 nm. The absorbance of the spectrophotometer was calibrated to zero using culture medium without cells.

The relative cell viability (%) related to control (representing HeLa cells incubated in medium alone) was calculated using the formula:

Results and discussion

Elemental and morphological analysis of layered double hydroxide nanoparticles:

Energy Dispersive X-ray Spectrometry (EDS) technique was used to analyze the chemical composition of the synthesized LDHs nanoparticles. The EDS spectrum of pristine ZN exhibits characteristic emissions for zinc, iron and nitrogen while that of the ZP exhibits the presence of zinc and iron and phosphorus. The atomic composition of the samples obtained from the EDS measurement is presented in Table S1. It shows that Zn:Fe has molar ratio of 1.98:1.00 in ZN which is in agreement with the proportion of metal salt precursors used in the synthesis (2:1). The ratio is also close to that of precursor solution (1.92:1.00) in ZP. The morphology and size of the LDHs particles were examined through TEM. Homogeneous distribution of well-defined monodispersed plate-like particles have been observed in pristine ZN with lateral dimension of 81±4 nm while plate-like morphology with some agglomeration have been observed in pristine ZP

of lateral dimension of 83±4 nm. The selected area electron diffraction (SAED) pattern of ZN and ZP particles shown in Figure 1c clearly shows the presence of concentric diffraction rings of characteristic for the TEM-SAED pattern of Zn-based LDHs and all are crystalline in nature. AFM images of the suspension of the samples after 'drop and dry' procedure on a Si substrate exhibiting similar particle size (86 nm for Zn and 87 nm for ZP) as that of measured from TEM. SEM image of ZN exhibits hexagonal flakes like morphology of dimension of 93±8 nm lying on top of one another while that of ZP exhibits granular morphology of size 91±7 (Figure 1e).

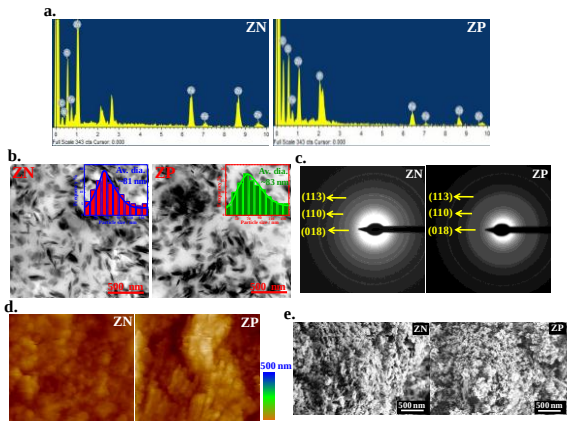


Figure 1: (a) Energy dispersive X-ray spectrum showing strong signals of Zn and Fe, confirm the formation of ZN and ZP LDH nanoparticles; (b) TEM images revealed that average size of ZN and ZP LDH nanoparticles are 81 and 83 nm respectively; (c) SAED patterns of ZN and ZP LDHs. (d) AFM topographical images of the samples and (d) SEM images of ZN and ZP LDH nanoparticles.

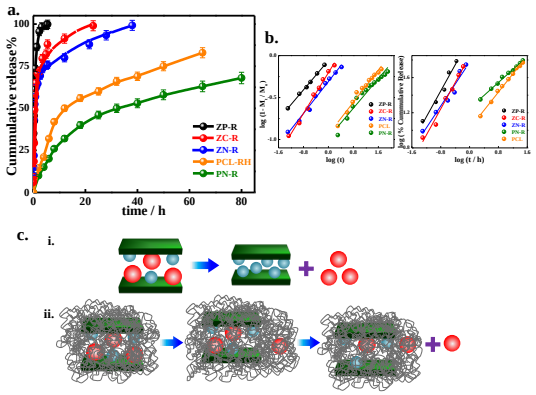


Figure 2: Drug release kinetics and its schematic representation.

Conclusions

Three different Mg–Al based layered double hydroxides (LDHs) have been synthesized with varying interlayer exchangeable anions (NO_3-, CO_3 2− andPO_4 3−) and raloxifene drug was intercalated within the LDH layers through ion exchange reactions. Stronger interactions lead to sluggish delivery in LN-R against relatively weak interaction in LP-R, responsible for fast release. In vitro anticancer studies demonstrate that drug intercalated LDHs efficiently inhibit the growth

of HeLa cells as compared to pure drug. Interestingly, side effects as measured from body weight measurements and histological assessment indicate that drug intercalated LDHs, especially slow releasing system, are safer materials as compared to pure drug.

Acknowledgements
The author (SS) acknowledges the receipt of funding for his fellowship from the University Grants Commission (UGC), India.

References

13. Y. Yang, D. Pan, K. Luo, L. Li, and Z. Gu, *Biomaterials*, 34, 8430–8443, 2013.
14. J. Nicolas, S. Mura, D. Brambilla, N. Mackiewicz, J. Nicolas, and D. M. Haddleton, *Chem. Soc. Rev.* 42, 1147–1235, 2013.
15. J. Lu, M. Liong, J. I. Zink, and F. Tamanoi, *small*, 3, 1341– 1346, 2007.

MACRO 241

Mechanically Tunable Curcumin Incorporated Polyurethane Hydrogels as Potential Biomaterials

V.D. Anumon,[a] B.A. Lal,[b] S.S. Sachin,[c] A.T. Arun Torris,[d] M.V. Badiger*,[e]

[a,b,d,e] *Polymer Science and Engineering Division,* [c] *Physical and Material Chemistry Division, CSIR−National Chemical Laboratory, Dr. Homi Bhabha Road, Pune 411008, India*

** e-mail id: mv.badiger@ncl.res.in*

Abstract
We report here on the one-pot synthesis and characterization of curcumin incorporated polyethyleneglycol−polyurethane(PU-CUR) hydrogels using PEG-4000, 4,4′- methylene bis,(cyclohexyl-isocyanate), curcumin in the presence of a cross-linker, 1,2,6 hexanetriol (HT). Besides the physical entrapment, curcumin also provides a partial crosslinking in the 3-D structure of the hydrogel. The degree of swelling in hydrogels could be controlled by varying the amount of HT and curcumin. The structural characterization of hydrogels was performed using FTIR. SEM and μ-CT imaging of hydrogels showed the presence of interconnected pores. The mechanical strength of the hydrogels was measured using a UTM. *In-vitro* biological experiments showed the biocompatibility of gels, selective toxicity toward cancer cell lines, and antibacterial property. These gels show promising applications as scaffolds and implants in tissue engineering.

Keywords: *Hydrogels; Curcumin; Poly urethane; Polyethylene glycol.*

1. Introduction

Hydrogels are 3D polymer network structures that are hydrophilic in nature and are capable of absorbing copious amount of water without losing their structural integrity.[1-3] Over the past two decades; hydrogels have received increasing attention from researchers because of their special physicochemical properties such as softness, biocompatibility, water permeability, etc. They find applications as scaffolds/implants in tissue engineering,[4-5] vehicles for drug delivery,[6-7] synthetic extracellular matrix,[8] etc. In this context, there is a large scope for designing and developing new hydrogels with the combination of good mechanical strength, elongation, and good self-recovery properties. Polyethylene glycol−polyureth- ane (PEG−PU) based hydrogels represent a class of materials that possess favorable characteristic of PUs along with the ability to mimic soft tissues.[9] In this study, we have incorporated curcumin in the preparation of PU hydrogels. Interestingly, the obtained hydrogels showed enhanced mechanical properties in terms of modulus, percentage elongation, and recovery. The hydrogels were prepared using PEG-4000 as a soft segment and 4,4′-methylene bis(cyclohexyl isocyanate) (H_{12}MDI) as a hard segment in the presence of a cross-linker, namely 1,2,6-hexanetriol (HT). It is well established that curcumin exhibits both antimicrobial and anticancerous properties. Curcumin with −OH groups also took part in partial cross-linking reaction providing a dual cross-linking nature in the hydrogel structure. The structural characterization of hydrogel was performed by Fourier transform infrared spectroscopy (FT-IR). The cryogenic treatment with lyophilization was used to generate porosity in the hydrogel matrix. The cyto-compatibility studies were per- formed in the hydrogels.

2. Experimental

2.1 Materials and Methods

PEG (MW ≈ 4000 g/mol), dibutyltin dilaurate (DBTDL), and tetrahydrofuran (THF) were obtained from Merck India; H_{12}MDI was purchased from Sigma-Aldrich, USA; and HT was obtained from Fluka India. Curcumin was a gift sample from Arjuna Natural Extracts, India. Dulbecco's modified Eagle medium (DMEM) and fetal bovine serum (FBS) were purchased from Invitrogen USA.

2.2 Synthesis of Curcumin Incorporated Polyurethane (PU-CUR) Hydrogels.

PEG [MW ≈ 4000 g/mol] was vacuum-dried at 60 °C for 6 h in a rota vapor to remove

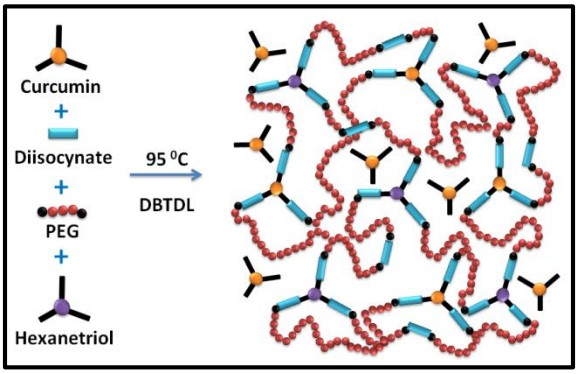


Figure 1. Reaction scheme for the synthesis of PU-CUR xerogel.

any residual moisture and stored in a sealed flask in an oven at 70 °C until use. To the 10 g of molten PEG, 0.06 g of curcumin and 0.335 g of HT were added and kept in a rota vapor for 2 h to form homogeneous solution.

To this solution, 1.5 mL of H_{12}MDI and 13.6 μL of DBTDL were added using a syringe under nitrogen atmosphere. The whole mixture was kept in a rota vapour for 20−30 min at 70 °C until the mixture becomes more homogeneous and then poured in to Petri dishes/molds were kept in oven at 95 °C for 4 h for gelation. The reaction between PEG, H_{12}MDI, HT, and curcumin is shown in **Figure 1.**

2.3 Structural Characterization

The structural characterization of PU-CUR hydrogels was performed by FT-IR, The FT-IR spectra of xerogels were recorded using PerkinElmer spectrum one (USA).

2.4 Swelling Studies

The swelling behaviour of the PU-CUR hydrogels was studied using a gravimetric method.

2.5 Mechanical Properties

Tensile tests were carried out with Instron Universal Testing Machine (UTM-33R) with a load cell of 10kN, at room temperature with an elongation rate of 10 mm/min. Compressive tests were carried out on the same machine with a load cell of 10 kN, at 25 °C with a compression speed of 10 mm/min.

2.6 Morphological Analysis

SEM was employed to investigate the morphology of the hydrogels and porous xerogels using quanta 200 3D dual beam ESEM (FEI, Finland). Three-dimensional non-destructive imaging of PU-CUR xerogels was performed using a high-resolution X-ray micro-computed tomo- graphy (μ-CT), model μ-CT 40 (Scanco Medical AG, Switzerland).

2.7 MTT Assay

MTT solution was prepared freshly by dissolving MTT in serum-free DMEM at a concentration of 5.0 mg/mL. L929 fibroblast and MCF-7 cells were seeded into 48-well plates at a density of 2.5 × 10^4 cells/well. Cells were incubated at 37 °C, 5% CO_2, 95% relative humidity.

3. Results and discussion

3.1 Synthesis of Curcumin Incorporated PEG−PU Hydrogels (PU-CUR). The urethane linkages are formed through the addition reaction between isocyanate groups of H_{12}MDI and the hydroxyl groups of PEG. Curcumin was incorporated during the synthesis of PU-CUR xerogels. The idea of using curcumin in the hydrogel was mainly

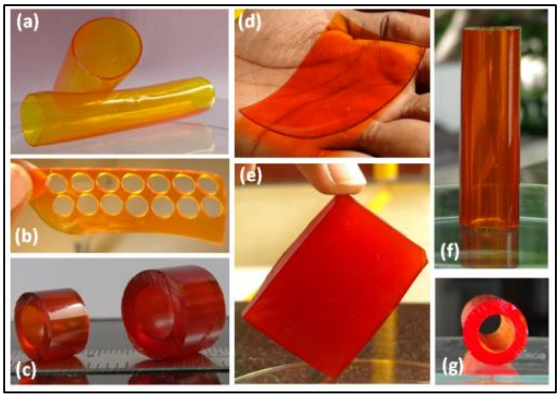


Figure 2. PU-CUR-1.0 gels. (a) Flexible and thin tubes, (b) resistivity to cutting the sample. (c) Dry and water swollen hollow tube, (d) thick film with transparency, (e) block of hydrogel (opaque), (f,g) transparent thick tube and its cross-sectional view.

due to its excellent antimicrobial, antifungal, anti-inflammatory properties, which could make the hydrogels antimicrobial, a desired feature in the tissue engineering applications. Curcumin, commonly known as diferuloyl methane, is a hydrophobic polyphenol derived from the rhizome (turmeric) of the herb curcuma longa. Further, curcumin is soluble in PEG and can be easily incorporated into PU-CUR xerogels without the requirement of any solvent. The network structure in the gel is induced by both HT and curcumin cross-linking in the reaction. The curcumin incorporated PU-CUR xerogels obtained were opaque and orange in colour **(Figure-2).**

3.2 FT-IR Spectroscopy

The structural elucidation of PU-CUR gel was performed by FT-IR spectroscopy. In the case of PU-CUR gel, the characteristic absorption bands of (−NCO) groups from H_{12}MDI (at 2270 cm^{-1}) and (−OH) groups of PEG-4000 (at 3400 cm^{-1}) disappeared indicating the reaction between (−NCO) and (−OH) to form urethane (−NH−COO−) linkages. At the same, a new peak appeared in PU-CUR spectrum at 1716 cm^{-1}, endorsed to the stretching of ester carbonyl groups (>C=O) within the urethane linkages.

These observations in the FT-IR spectrum clearly confirmed the structure of PU-CUR gels.

3.3 Swelling Studies

In PU-CUR hydrogels, the contribution to the swelling comes from the hydrophilic part, PEG, and is controlled by the content of HT and hydrophobic curcumin. We studied the equilibrium swelling capacities of PU-CUR hydrogels with three different contents of curcumin (at constant HT) measured at room temperature. It can be seen that the equilibrium swelling ratio decreases from 800% to 200% with curcumin content increasing from 0.5 to 1.5 wt %.

3.4 Mechanical Properties

We show in **Figure 3 (a)**, the tensile stress-strain curve for hydrogel sample without and with different contents of curcumin. Hydrogels with no curcumin (PU-CUR-0.0)

showed tensile strength of 0.22 MPa with a percent elongation of 72%, whereas hydrogels with curcumin contents of PU-CUR-0.5, PU-CUR-1.0, and PU-CUR-1.5

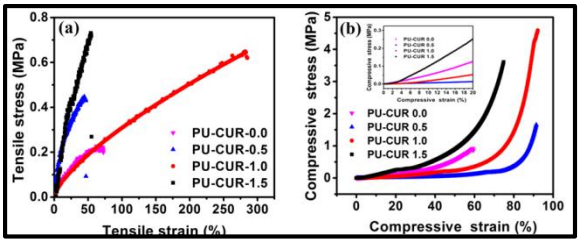


Figure 3. (a) Tensile data for the different amount of curcumin incorporated PU-CUR hydrogels. (b) Uniaxial compression experiment of PU-CUR hydrogels in the swollen state with increasing the amount of curcumin concentration.

showed tensile strengths of 0.48, 0.64, and 0.73 MPa with percentage elongation of 46%, 284%, and 76%, respectively. We have shown in **Figure 3(b)**, the compressive stress−strain curves for equilibrium swollen PU-CUR hydrogels containing curcumin (a) 0.5%, (b) 1.0%, and (c) 1.5% and compared the results with hydrogels containing no curcumin (0.0%). The hydrogels with no curcumin (PU-CUR-0.0) break at 0.9 MPa with % compression of 58%, whereas, hydrogels with PU-CUR-0.5 and PU- CUR1.0 curcumin showed compressive strength of 1.6 and 4.6 MPa, respectively, and could be compressed up to 92% without breaking **(Figure 4a).** The hydrogels with PU-CUR-1.5 of curcumin, however, showed a rupture at compression of 75% with a compressive strength of 3.6 MPa **(Figure 4c).** This could be due to extra cross-linking in the structure, which may cause brittleness. These observations clearly indicate that the curcumin incorporation into PU-CUR hydrogels enhanced the mechanical strength
of the hydrogels with high compressibility

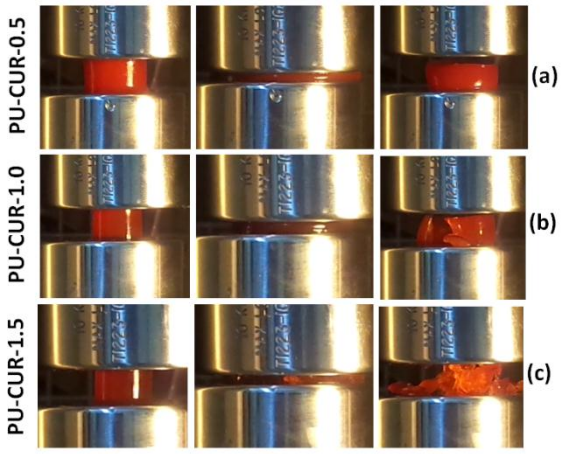


Figure 4. Photographs of compression study demon strating sustainability of (a) PU-CUR-0.5 at higher compression (90% strain), (b) PU-CUR-1.0(90% strain), and (c) PU-CUR-1.5(75% strain), respecti -vely.

(~90%). The increase in both compression and tensile strength of curcumin incorporated hydrogels could be attributed to the fact that curcumin in the hydrogel network is present as both covalently linked to the network and partially physically entrapped in the network structure. The

covalently linked curcumin, along with the HT, can provide a dual cross-linking nature to the hydrogel network. Therefore, both the degree of heterogeneity and energy dissi pation play important role in determining the mechanical strengths of the hydrogels.

3.5 Scanning Electron Microscopy (SEM)

We show in **Figure 5,** the SEM micrographs lyophilized samples of PU-CUR gels with different contents of HT and compare with the untreated samples of PU-CUR gels. It can be revealed from the figure that the

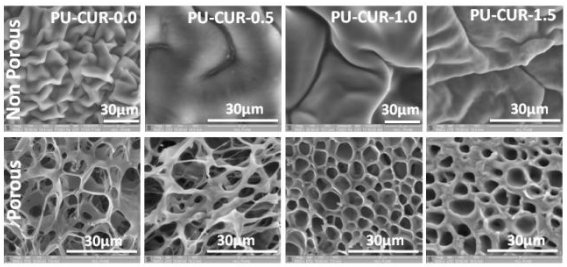


Figure 5. SEM micrographs of the porous PU-CUR xerogels with different curcumin content.

treated sample exhibits porous structure with the pore sizes in the range of 2−15 µm. We found that the pore sizes obtained in our samples are suitable for hosting the endothelial cell transplantation process dur- ing the initial stages of tissue regeneration. **Figure 6 (a),** shows the three-dimensional image of porous PUCUR-1.0 xerogel obtained from µ-CT, which shows homogeneous distribution of pores through- out its volume with an overall porosity of 77%. Pores in the xerogel were imaged by in version of the 3D image and their size distribution based on a colour scale as shown in **Figure 6 (b).**

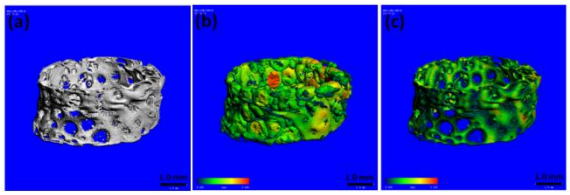


Figure 6. (a) 3D image of the porous PU-CUR-1.0 xerogel obtained from the reconstruction of 2D X-ray projections using µ-CT, (b) pore-size distribution of the xerogel, and (c) wall-thickness distribution of the xerogel. All images are with 1 mm scale bar.

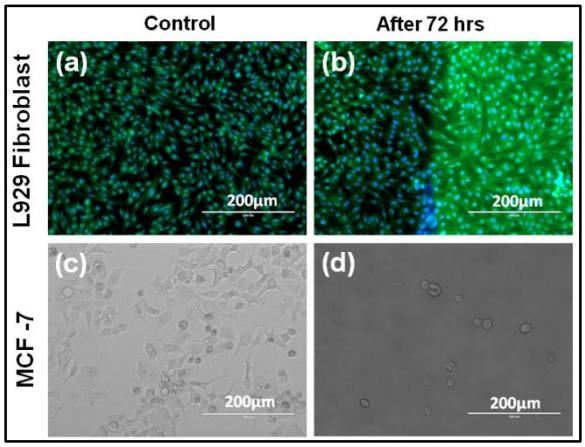


Figure 7. Optical phase contrast images of PU-CUR-1.0 hydrogels in MTT assay with MCF-7 and L-929 fibroblast cells for 72 h at 37 °C. (a) Control for L-929 fibroblast cell lines, (b) L-929 fibroblast cell after 72 h treating with the hydrogels. (c) Control for MCF-7 cell lines, (d) MCF-7 cell lines after 72 h treated with the hydrogels.

3.6 MTT Assay

L-929 fibroblast cells showed cell viability for PU-CUR-0.0 and PUCUR-1.0 97.1 and 94.6%, respectively. But the MCF-7 did not show cell viability for PU-CUR-1.0. Results clearly indicate that PU-CUR-1.0 hydrogels are selectively nontoxic, to L-929 fibroblast cells in **[Figure 7(a&b)],** and toxic to MCF-7 cell line as shown in **Figure 7(c&d).**

4. Conclusions

In the present work, we have synthesized curcumin incorporated PU-CUR hydrogels using PEG-4000 as soft segment and H_{12}MDI as the hard segment by solvent-free one-pot method. Different amounts of curcumin were incorporated with constant amount of HT in the gel. The chemical structure of the gels was characterized by FT-IR spectroscopy. The curcumin was found to be present in the hydrogel in two forms: (i) covalently linked to the hydrogel structure and (ii) physically entrapped in the gel matrix. The mechanical strengths of the curcumin incorporated PU-CUR gels increased due to the presence of curcumin. The heterogeneity and dissipation of energy contribute to the enhancement of mechanical strengths of hydrogels. The morphological characterization by SEM revealed the porous structure with 2−15µm pore size. The cytotoxicity studies of PU-CUR hydrogels showed the continuous growth of cells, which indicated the nontoxic nature of the hydrogels. These hydrogels show promising applications in vascular graft and tissue engineering applications.

References

1. K.Y Lee, D.J Mooney, *Chemical Reviews* 2001, 101, (7), 1869-1879.
2. Y. Qiu, K. Park, *Advanced Drug Delivery Reviews* 2001, 53, (3), 321-339.
3. A.S Hoffman, *Advanced Drug Delivery Reviews* 2002, 54, (1), 3-12.
4. J. Zhu, *Biomaterials* 2010, 31, (17), 4639-4656.
5. S. Van Vlierberghe, P. Dubruel, E. Schacht, *Biomacromolecules* 2011, 12, (5), 1387-1408.
6. T.R Hoare, D.S. Kohane, *Polymer* 2008, 49, (8), 1993-2007.
7. H. Zhang, A. Patel, A.K. Gaharwar, S.M. Mihaila, G. Iviglia, S. Mukundan, H. Bae, H. Yang, A. Khademhosseini, *Biomacromole cules* 2013, 14, (5), 1299-1310.

8. M.W Tibbitt, K.S Anseth, *Biotechnology and Bioengineering,* 2009, 103, (4), 655-663.
9. A.V Divakaran, A.T Torris, A.K Lele, M.V Badiger, *Polymer International* 2015, 64, (3), 397-404.

MACRO 244

Nano-curcumin Encapsulates for Targeted Cancer Therapy

Amarnath Singam and GVN Rathna*,

Polymer Science and Engineering Division, CSIR-National Chemical Laboratory, Pune-411008, India
**rv.gundloori@ncl.res.in*

Abstract

Cancer cells proliferate very fast than the healthy cells therefore, it is essential to inhibit proliferation before eradication of cancer. A natural active component, curcumin possess anti-cancer properties and has potential to inhibit cell proliferation in tumors of cancer without affecting the normal cells. Investigations revealed that curcumin is poorly soluble in water and less bio-available and if taken orally, it gets converted into inactive curcumin analogues due to low gastric pH. The negatively charged nano-curcumin particles were coated layer by layer with bio-compatible polymers to enhance surface potential and stabilization. The developed encapsulates were characterized by particle size analyzer, zeta potential measurement. Nanoparticles formation and size was confirmed using SEM and TEM. Drug loading efficiency, cytotoxicity studies ascertained their utility for biomedical application.

Keywords: *colon cancer; nano-curcumin; bio-polymers; pH sensitive; cytotoxicity*

Introduction

Cancer is a deadly disease and is second leading cause of deaths in world after cardiovascular diseases. Cancer is characterized by formation of tumors and it's metastasis in different organs of the body. The formation of tumor is due to mutations in genes, which confer ability to cells to divide uncontrollably. This lump of cells is called tumor, in cancerous state these cells invade other organs of the body and replicate there. Current treatments aim at removal of tumor and its cancerous form through surgery, radiation and chemotherapy. All these methods are harsh on patient's quality of life, resulting in various side effects. In our work we proposed using natural herb *curcuma longa* content to inhibit cancer cell proliferation. Curcumin a diphenolic compound from rhizome of turmeric is known to have anticancer properties. It is

insoluble in water and has very less bioavailability to be used as drug directly. However, nano-curcumin crystal has greater dissolution rate because of larger surface area compared to bulk curcumin. (1) Extensive literature survey characterized curcumin as an excellent molecule among many naturally occurring compounds for cancer therapeutics. Reports have stated that free curcumin induces cell cycle arrest and/or apoptosis in human cancer cell lines derived from a variety of solid tumors including colorectal, lung, breast, pancreatic and prostate carcinoma, among others(2). Experimental studies have demonstrated that curcumin efficiently sensitizes tumors to first line chemotherapeutics and radiation. Our aim is to deliver this curcumin to colon for treatment of colon cancer. Nano-curcumin is coated with polymers like chitosan (CS) and sodium alginate (NaG) which are biocompatible and biodegradable. Further, due to enhanced permeation effect (EPR) in cancer tissue, nano-curcumin encapsulates enter the tumor via passive targeting.

Experimental

Materials: Curcumin crystalline (SD Fine), Chitosan (medium mol. Wt. Sigma Aldrich), Sodium alginate (Rasayan Chemicals), Scanning Electron Microscope Quanta 200 3D FEI, USA, UV Spectrophotometer Shimadzu.

Method:

Preparation of nano-curcumin

To obtain nano-curcumin, 0.2% (wt/v) crystalline powder was dispersed in deionized water water and sonicated using Sonics Vibra cell probe sonicator at 40% amplitude for 30 min at 5 sec off, 5 sec on.

Solubilization of chitosan (CS) and Sodium alginate (NaG)

0.2% (wt/v) chitosan was solubilized in 1% acetic acid solvent by stirring it for 6-8 hr. Its pH was adjusted to 5.5 using 1M NaOH. 0.2% (wt/v) sodium alginate was dissolved in deionized water.

Preparation of nano-encapsulates:

In chitosan solution curcumin nano-curcumin suspension was added dropwise while stirring at high speed on magnetic stirrer. The charge on the particles was confirmed by zeta potential

measurements using Brookhaven zeta potential instrument. To this solution 0.2% w/v sodium alginate was added dropwise with high speed stirring.

Determination of encapsulation efficiency:

Curcumin loaded encapsulates were dissolved in solvent mixture of acetonitrile, DI water and glacial acetic acid in the ratio of 6:3:1 respectively. This was centrifuged at 16,000rpm for 35min. Supernatant was collected and its absorbance was recorded at 423nm against standard curcumin graph to determine untrapped curcumin concentration.

% Entrapment Efficiency = (weight of cur used - weight of untrapped cur X100) / weight of cur used

Cytotoxicity study:

In vitro cytotoxicity of encapsulates on cancer cells was evaluated by MTT (3-(4,5-dimethylthiazol-2-yl)-2,5-diphenyl tetrazolium bromide) assay using MCF-7 breast cancer cell line. Cells were maintained in MEM (Minimum Essential Media) media supplemented with 10% fetal bovine serum (FBS) in humidified CO_2 atmosphere. Briefly, 10,000 cells per well were seeded in a sterile 96 well plate and UV sterilized sample was added in increasing concentration from 0 to 500 µg/ml. After 48 hr media from wells was piped out, MTT dye solution was added and incubated in dark for 4 hr. Finally, DMSO (Dimethyl Sulphoxide) was added to solubilize formazan crystals and reading was taken at 540nm in plate reader.

Results and discussion

Chitosan is cationic polymer and it has maximum positive charge at pH 5-5.5 From zeta potential measurements (Fig:1) it can be stated that curcumin nanoparticles were coated layer by layer with chitosan polymer first followed by sodium alginate. The coating of NaG will protect the drug from acidic gut environment and safely deliver it in colon at slight alkaline pH where it will degrade. At low acidic pH of cancer microenvironment chitosan wears off and curcumin is released. Size of nano-curcumin with chitosan coating was confirmed by SEM image (Fig.2) and TEM image (Fig.3) In TEM image (Fig. 4) two layers of polymer coatings on curcumin were visual. The percent entrapment efficiency was calculated to be 66% from equation since, supernatant had 34% curcumin concentration. 400µg/ml concentration of nano-encapsulates was IC_{50} value for cancer cell line (Fig.5).

Figures

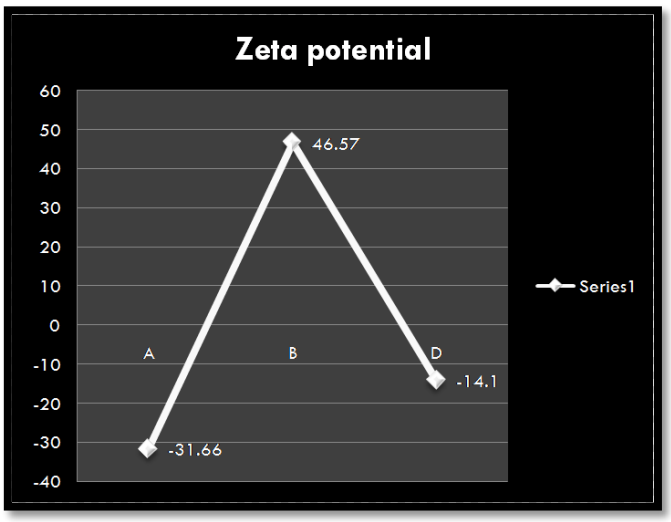


Figure 1: A:Cur, B:Cur-CS, C:Cur-CS-NaG

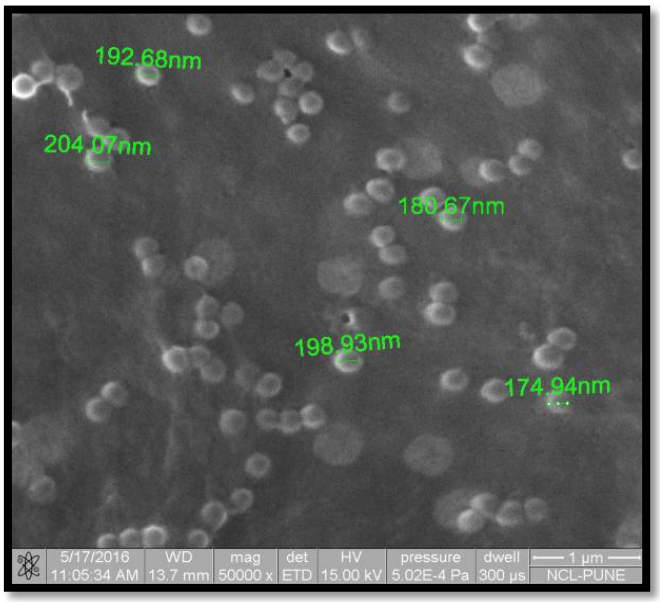


Figure 2: SEM image of Cur-CS-NaG

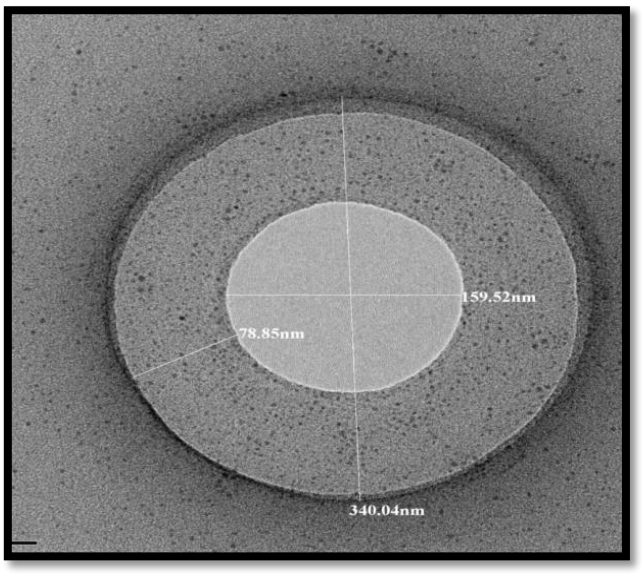


Figure 3: TEM image of Cur-CS

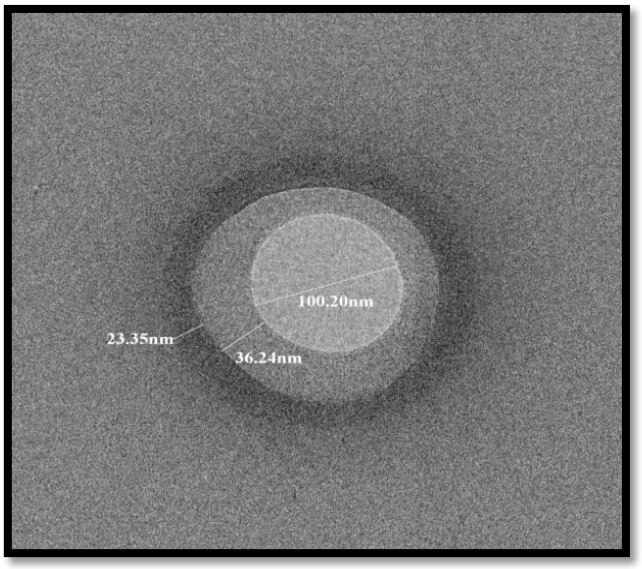


Figure 4: TEM image of Cur-CS-NaG

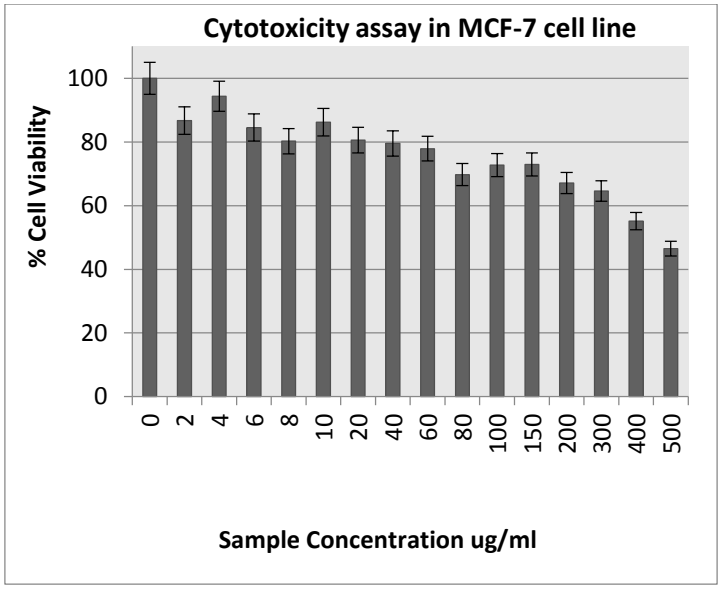
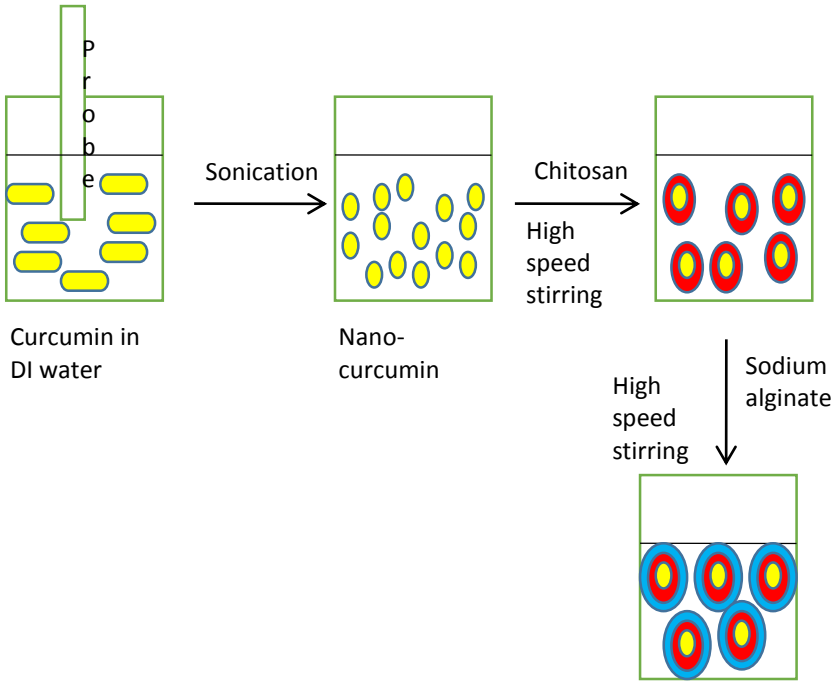


Figure 5: Graph of conc. *vs* % cell viability



Scheme: Method of nano-curcumin encapsulates preparation

Conclusions

Nano-curcumin encapsulates were prepared in the range of 200-300nm. The drug curcumin was entrapped in good amount and showed cytotoxicity to cancer cell line. Bio-polymers CS and NaG are biocompatible, non-toxic and easily eliminated from the body. Releasing curcumin near colon enhances its retention near cancer for longer duration, assisting passive

targeting. Curcumin is safe at permissible amounts and doesn't have any side effects as other chemotherapy drugs.

Acknowledgements

AS would like to thank Department of Biotechnology DBT, CSIR-CSC0134, CSC0302, for funding the project. NCL and AcSIR for providing infrastructure and academic support.

References

16. Yallapu et al, *Drug Discovery Today,* 17; 71-80, 2012.
17. S. Manju, K. Sreenivasan, *Journal of Colloid and Interface Science,* 368; 144-151, 2012.
18. Das et al, *Nanomedicine,* 6; 153-160, 2010
19. Lvov et al, *Langmuir,* 27(3); 1212-1217, 2011.

MACRO 253

Effect of Different Cross – Linkers on Structure and Stability of Polyacrylamide Hydrogels

Khandai Santripti, K. Mithra, and Jena S. Sidhartha*

Department of Physics & Astronomy, National Institute of Technology Rourkela, Rourkela 769008, Odisha, India

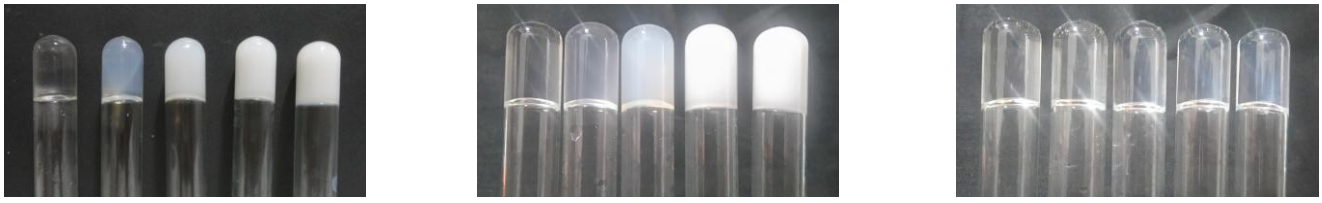
** sid@nitrkl.ac.in*

Hydrogels are three dimensional polymer networks swollen in water medium, having profound use in tissue engineering, biomedical applications, drug delivery, and in various other industries including paint, pharmaceutics, and flavor for their structural flexibility and biocompatibility [1, 2]. The structural properties of hydrogels can be tuned by varying external stimuli like solution pH, ionic strength, polymer and cross – linker concentration, chemistry and chain lengths of monomers, temperature, solvent quality and also with aging of gels itself. Of all gels, polyacrylamide (PAAm) hydrogels are well studied systems for their widespread applications in electrophoresis and sieving technology, in petroleum and oil industries for entrapping water [3, 4]. All of these applications have a considerable dependence on the structure and stability of gel matrix. The structure of polyacrylamide gels can be tailored by varying monomer and cross – linker concentration.

In the current study, we have presented how different cross – linkers and their respective concentration affects the structure and stability of PAAm hydrogels. Polyacrylamide hydrogels were prepared by free – radical polymerization using acrylamide (AAm) as monomer and N, N' methylene bisacrylamide (Bis), N, N′-Bisacryloyl-1,2-dihydroxy-1,2-ethylenediamine (DHEBA), and N, N'-diallyl-tartardiamide (DATD) as cross – linkers. Potassium persulfate (KPS) and N, N, N', N' tetramethylethylenediamine (TEMED) were used as initiator and activator respectively for formation of hydrogels. All the samples were prepared with monomer, AAm, concentration fixed at 7 $wt\%$ while cross – linker concentration used was $1, 3, 5, 7$ and 10 $wt\%$ with respect to the monomer concentration.

To study the structure and stability of prepared hydrogels, we have carried out rheological measurements using $MCR\ 102$ rheometer from Anton Paar having parallel plate configuration with $25mm$ plate diameter. Oscillatory measurements were carried out on all the samples at a fixed temperature of $20\ ^{\circ}C$ and with a constant force of $1N$. The frequency sweep measurements were carried out in a frequency range from $100 - 0.1\ rad/s$ with 0.5% strain which is well within linear viscoelastic region as determined from the strain sweep measurements. The results shown in the present work are average of multiple runs.

Polyacrylamide hydrogels with BIS and DHEBA as cross – linkers, appeared increasingly turbid with rise in cross – linker concentration. On the other hand in case of DATD as cross – linker, the samples remained clear even
for highest cross – linker concentration used in the present study. This observation is depicted in figure 1 below.



(a) **(b)** **(c)**

Figure 1: Visual appearance of PAAm hydrogels with increasing cross – linkers; (a) BIS, (b) DHEBA, (c) DATD. The images shown are for 1, 3, 5, 7, and 10 wt% of cross – linker concentration.

It is well established from earlier studies that the appearance of turbidity is an indication of heterogeneity of gel matrix. With increase in BIS and DHEBA concentration it might be possible that the polyacrylamide gels are getting increasingly heterogeneous with rise in cross-linker density. However this is not the case for gels with DATD as cross – linker. It could be possible in the case of DATD cross-linker it is forming a relatively more homogeneous gels as compared to BIS and DHEBA cross-linkers. Thus in order to determine the macrostructure and stability, we have carried out rheological measurements on the prepared gels. The frequency sweep measurements are signature of individual gel systems that yields the elastic and viscous component of gels. Both these parameters of storage and loss can be extracted from the measured complex moduli, G^*, using the equation; $G^* = G' + iG''$. The more elastic a gel

is, more will be its storage modulus, G', while the viscous component of the system is represented by the loss modulus, G''. The results of frequency sweep for gels with different cross – linker is shown in figure 2.

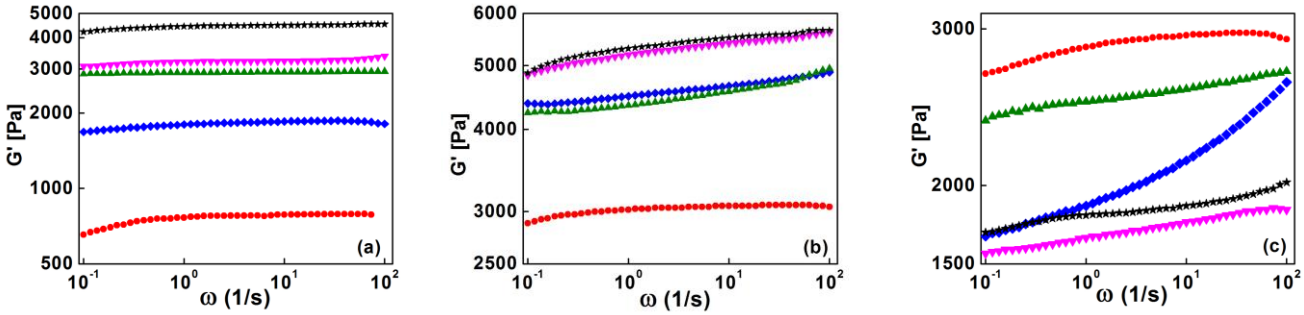


Figure 2: Storage modulus determined from frequency sweep measurements for polyacrylamide hydrogels in presence of (a) DATD (b) DHEBA (c) BIS cross – linker at different concentrations 1% (●), 3% (◆), 5% (▲), 7% (▼) and 10% (★)

In case of gels with DATD cross – linker we find the storage modulus exhibits a monotonous increase with rise in cross – linker concentration from 1 – 10 $wt\%$. This trend has been observed for similar and other kinds of hydrogel systems [4]. The argument for this kind of observation is that, with rise in cross – linker concentration the cross – linking density within gel network increases, thus enhancing gel strength and elasticity. However the gels with DHEBA present a slightly different behavior with rise in cross – linker concentrations. The storage modulus value increases significantly with rise in cross-linker concentration from 1 to 3 $wt\%$, similar to previous observation. But the value of storage moduli for 5 $wt\%$ remained close to that of 3 $wt\%$. On further increasing cross – linker concentration to 7 and 10 $wt\%$, though the elasticity of gel network increases compared to lower cross-linker concentrations, the value for both 7 and 10 $wt\%$ remains same. In the case of BIS, the variation of storage modulus with cross – linker concentration is much more dramatic. The highest modulus value observed in this case is for gels with lowest cross – linker concentration, i.e. 1 $wt\%$. On increasing the cross – linker concentration from 1 $wt\%$ -3 $wt\%$ the storage modulus decreased but increased for 5 $wt\%$. On further increasing the cross – linker concentration to 7 $wt\%$ the storage value decreased relative to 3 and 5 $wt\%$. The moduli value increased slightly on raising cross – linker concentration to 10 $wt\%$ but nevertheless remained well below that of 1 $wt\%$ of cross – linker concentration. The decrease in storage modulus value with increasing cross – linker concentration in case of BIS and DHEBA might be due to phase separation of gel matrix which leads to weakening of gel structure. The phase separation in prepared gels is well substantiated by the observation of turbidity for BIS and DHEBA as cross – linkers. However the increase in storage moduli on further increasing the cross – linking density indicates that there exists a competition between the phase separation and cross – linking density within gel matrix. While the phase separation of gel matrix weakens gel elasticity, at the same time increase in cross-link density increases the storage modulus.

Another noteworthy observation is that hydrogels in presence of BIS and DHEBA cross – linkers at a concentration of 1 $wt\%$, exhibits a comparable value of storage modulus. As opposed to this gels with DATD as cross – linker exhibits ~ four – fold low value of storage modulus for the same concentration. This is in agreement with the polymerization kinetics study by Gelfi and Righetti [3], where they found that the polymerization kinetics is slow in the case of DATD compared to BIS and DHEBA as cross-linker.

In summary the structural stability of polyacrylamide hydrogels exhibits a considerable dependence on the type of cross – linking agent. The gels in presence of BIS exhibited the highest storage at lowest cross – linker concentration beyond which the gel network seems to be phase separated thus decreasing storage moduli value. This is unlike the presence of other cross – linkers which show a significantly higher storage with increasing cross – linking density.

References

[17]Tan H.; Marra K.G. *Materials*, 3 (2010) 1746.
[18]Chirani N.; Yahia L.; Gritsch L.; Motta F. L.; Chirani S.; Fare S. *Journal of Biomedical Sciences*, 4 (2015) 1.
[19]Gelfi C.; Righetti P. G. *Electrophoresis*, 2 (1981) 213.
[20]Al – Muntasheri G. A.; Hussein I. A.; Nasr-El-Din H. A.; Amin M.A. Journal of Petroleum Science and Engineering, 55 (2007) 56.

MACRO 255

SYNTHESIS, CHARACTERIZATION AND APPLICATION OF DEXTRIN GRAFTED POLYURETHANE CO POLYMERS.

Shukla, A[1].and Maiti,P[1].
1. School of Materials Science and Technology, IIT BHU,
Varanasi-221005, Uttar Pradesh.

Email aparna.rs.mst14@itbhu.ac.in, pmaiti.mst@itbhu.ac.in

Abstract

Dextrins are linear *a*-(1, 4)-linked D glucose polymers obtained by enzymatic hydrolysis of corn starch. In this work grafting of (Dex) with di-isocynate terminated polyurethane.The grafting was performed by addition of dextrin to PTMG and HMDI based prepolymer with different weight ratios of dextrin in order to optimise the best one. These copolymers were characterised by GPC (Molecular weight determination), ^{1}HNMR, FTIR, UV-VIS.. Thermal stabilities of graft copolymers were studied by thermogravimetric analysis (TGA). Sustained drug release in graft copolymer in attained by controlling its molecular weight i.e grafting of prepolymer there by creating a tortuous path for drug diffusion.

Keywords*: polymer; dextrin; polyurethane; drug release.*

1. INTRODUCTION

Polymers from natural resources like cellulose, starch, dextrin and guar gum are extensively used in low cost technologies for metal ion removal from water bodies and in bio technological applications like separation and enrichment of nucleic acids, enzymes and bio-organic molecules.Graft copolymerisation is one of the most fascinating approach for incorporation of desired functional groups onto a polymer backbone.When a growing polymerchains are attached to the polymeric backbone by means of chemical bonds then a graft copolymer is formed.[1] The grafting of synthetic polymers on the biodegradable/natural polymer has been conceived to develop polymers with improved as well as enhanced characteristics, properties and applications for sustained drug release systems.[2] Dextrins are linear *a*-(1,4)-linked D glucose polymers obtained by enzymatic hydrolysis of corn starch. They also contain (<5%) 1,6 links thus show branching as well. Dextrin are most commonly used in the manufacturing of adhesives for envelopes gum tapes postage stamps and water labelling due to its low viscosity and solution stability at higher temperature.[3] Diversification of dextrin by grafting/crosslinking is a significant approach that derives the benefit of combining a natural polysaccharide and a synthetic polymer for different bio medical applications including protein delivery, MRI agent superabsorbent materials, crosslinking agent, drug delivery.[4]Starch-based materials are currently being used to prepare biodegradable hydrogels because of the biocompatibility and degradability with applications in areas like pharmacy biology and medicine.[5] These natural polymer based hydrogels are more interesting and mostly used

because of the higher content of functional groups present like hydroxyl, amino, carboxylic acid, sulfate which are utilized for chemical crosslinking with other cross linkers or grafting with other synthetic polymers as well as for bioconjugation with cell targeting agent. [6] Dextrin is one of the most captivating polysaccharide which is hydrophilic easily degradable into glucose by enzymes amylases present in human fluids. Modification of dextrin has been done previously by introducing various synthetic polymers like poly methyl acrylate, polyvinyl acrylate, polyacrylamide and so on dextrin backbone.[7] In this work we have done grafting of polyurethane on dextrin backbone by varying the weight ratios of dextrin. These graft copolymers were characterised via NMR, FTIR and UV-vis spectroscopic methods. These copolymers were further

2. Experimental

2.1 Materials required

Poly(tetramethylene glycol) (PTMG) (Sigma–Aldrich; number average molecular weight, Mn = 2900g mol^{-1}), 1,6-hexamethylene diisocyanate (HDI) (Merck, Germany), dextrin (Dex),Sigma Aldrich,Thecatalyst dibutyltindilaurate (DBTDL) and solvent dimethyl formamide (DMF) were purchased from Himedia and Merck, respectively.

Dexamethasone drug was purchased from Sigma Aldrich.

2.2Synthesis of polyurethane grafted dextrin -Copolymers.

Synthesis was carried out in two steps prepolymer formation and its subsequent grafting on dextrin back bone. Prepolymer synthesis was done using PTMG and HMDI at 70 ^{0}C for 3 hrs to yield isocynate terminated prepolymer in three neck round bottom flask equipped with mechanical stirrer and nitrogen purging inlet in silicon oil bath. Second step involves the chain extension using different concentrations of Dextrin added to prepolymer in the presence of DMF solvent and DBTDL catalyst (0.1 ml of 1 wt % toluene solution) to complete the polymerization reaction with rapid stirring at 70 ^{0}C for 24 h. Polymers was precipitated by pouring the solution in deionised water.It was then dried in vaccum oven @ 70^{o}C for 2 days. studied for sustained drug delivery system.

2.3 Characterisation

NMR

One-dimensional ^{1}H NMR spectra were recorded on a Bruker AVANCE 400 MHz Spectrometer (Germany) using DMSO-d6 (99.98%) as a solvent.

FTIR.

Infrared spectra of the solid polymer film were recorded on a thermo Nicolet 5700 instrument with the resolution of 4 cm^{-1}taking 100 scans at room temperature. Fourier transform infrared (FTIR) spectrum was measured in reflectance mode at room temperature from 650 to 4000 cm^{-1}.

UV- Visible Spectroscopy.

The UV−visible measurements were performed by using Shimadzu (UV-1700), pharma speck, UV−visible spectrophotometer operating from 200-800 nm spectral range. The transparent thin films were prepared through hot pressing.

Thermogarvimetric analysis (TGA)

The degradation temperature of the specimens was estimated using Mettler Thermos gravimetric analyzer (TGA, Mettler-Toledo) at a heating rate of 20° min^{-1}under nitrogen atmosphere in the temperature range from 40 to 600 °C.

Drug assay and release

Standard stock solution of drug was made 1mg/ml and its standard curve was drawn by taking absorbance using UV-vis at wavelength 242 nm with varying concentrations. Drug loaded copolymers were made via solution route by dissolving the polymer and drug in DMF. Solvent was evaporated and films were obtained which were used for drug release study in PBS buffer at pH 7.4.

2.4 Result and Discussion

Grafting of polyurethane on dextrin was done by reacting isocynate terminated prepolymer (PU) with hydroxyl groups on. dextrin .[1] H NMR spectroscopy gives the direct evidence for grafting.

Scheme showing chemical reaction between dextrin and Prepolymer

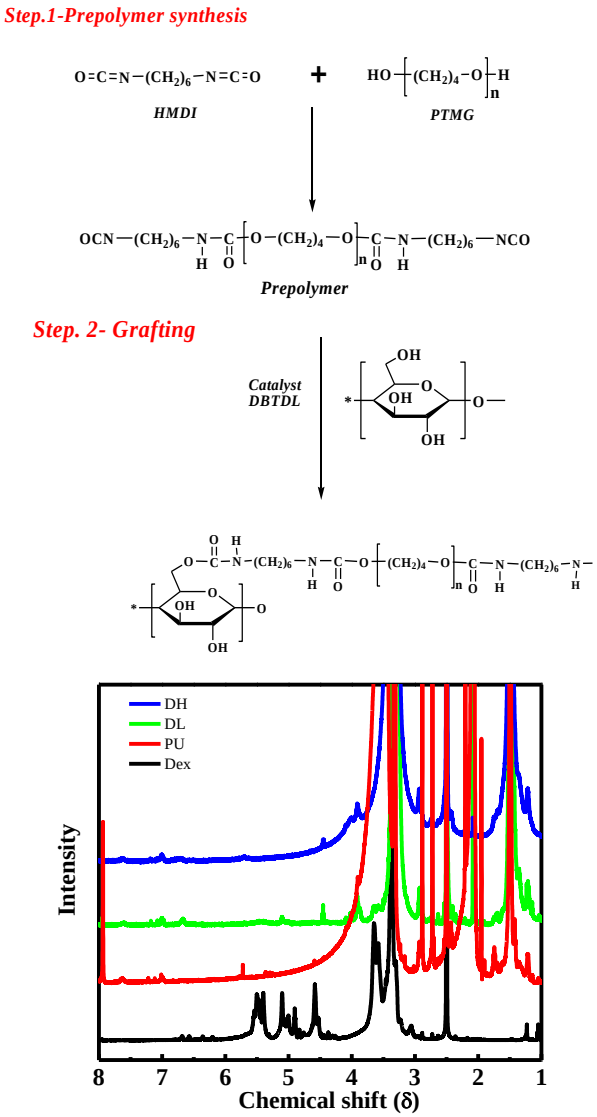


Fig 1.a ^{1}H NMR of Dextrin and its copolymers

NMR spectra of grafted polymers are given in Figure 1a. From the NMR spectra of pure dextrin OH-3 and OH-2 were found to appear between 5.2 and 5.6 ppm clearly separated from the signal of free, more shielded OH-6 groups between 4.2-4.4 ppm. The signal of the urethane proton (NHCOO) was observed at 7.10–7.91 ppm. Appearance of new peaks were at 3.9 ppm and 1.5 ppm assignable to protons of the CH_2N of HMDI and CH_2O of polyol and supports the grafting of PU on dextrin backbone.[8] FTIR spectrum of dex and its PU grafted co-polymers namely dex, DH and DL were shown is shown in Fig. 1(b).Dextrin exhibits a broad band with maximum intensity of about 3400 cm^{-1} due to stretching vibration of hydroxyl group. The bands with intensity at 1642 cm^{-1} are attributed to C-OH bending vibrations.[9]In graft copolymers peaks in region 3500-3200

are due to OH and NH stretching vibrations. FT-IR spectra of all graft copolymers showed a new peak at 1720 $cm^{-1}$for urethane C=O band and 1540 cm^{-1} for the urethane–NH bending and thus confirming the grafting of PU on Dex, a slight shifting in C=O peak is observed in copolymers.[10]

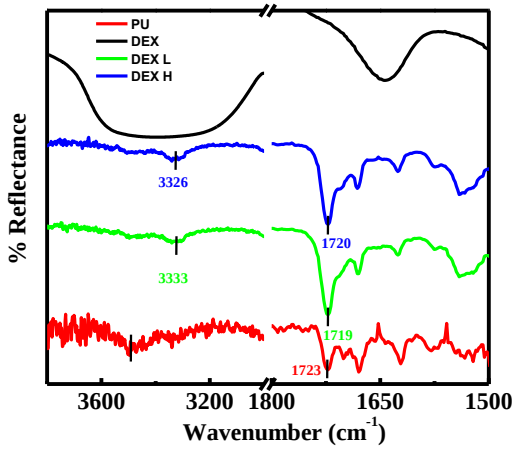


Fig1.b. FTIR spectra of Dextrin and its copolymers

The UV−Vis spectra of PU, pure dextrin and its graft copolymers are shown in Figure 1.c.

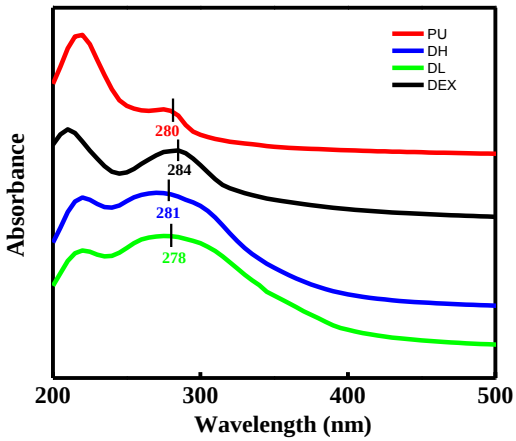


Fig1.c. UV-Vis spectra of Dex and its copolymers.

PU shows two bands at 230 and 280 due to Π-Π* and n-Π*Notably in graft copolymers there is slight shifting in absorption peak due to interaction of prepolymer with dextrin. Pure dextrin exhibits two bands at 211 and 284 nm.[11]

Thermal analysis

TGA

For pure dex weight loss occurs in two step first step involves removal of water and next is complete degradation of dex at 304 ^{O}C. The degradation temperature corresponding to weight loss of 5 % occurs at 376.4 ^{O}C, 341.5 ^{O}C and 353.4 ^{O}C for PU, DH and DL indicating much higher thermal stability of graft copolymers as compared to dextrin.

Drug release study

In vitro drug release kinetics were performed in phosphate buffer solution (pH ~7.4) at 37°C using dexamethasone loaded biocompatible and pristine dextrin and polyurethane grafted dextrin films. .Drug release of pure dextrin, PU and graft copolymers were studied. It is observed that burst release occurs in dextrin and PU but sustained release obtained in graft copolymer. Delayed diffusion of drug in graft copolymer is due to wrapping of PU around dextrin backbone. Grafting results in formation of more covalent bonds, drug release rate can be tuned by controlling the graft density of PU. Pure dextrin shows almost 100% release in less than 1 hour, while in graft copolymer around 40% release occurred within 8 hours and after that a sustained release was observed.

Conclusion

Chemically modifying dextrin by grafting it with isocyanate terminated PU and obtaining highest molecular weight graft copolymer and characterising it by NMR FTIR, UV-Vis, and TGA measurements. Graft copolymers exhibit sustained release of drug and, thereby, overcoming the burst release observed in pure dextrin. The desired biomaterial will be further used for cell culture and animal studies.

Acknowledgement

The author (Aparna shukla) gratefully acknowledges the financial support from CSIR-UGC of funding for fellowship.

References

1. Rajeev Kr. Sharma, Lalita, Ghanshyam S. Chauhan, and Rakesh Verma; International Journal of Polymeric Materials, 59:263–285, 2010.

2. Dipankar Das and Sagar Pal. RSC Adv., 2015, 5, 25014.

3. Bailey, J. E., and Ollis, D. F. (1986). Biochemical Engineering Fundamentals, 2nded., McGraw-Hill Company, New York, p. 38

4. D. Das and S. Pal, *RSC Adv*., 2015, **5**, 25014-25050.

5. Carvalho et al. / European Polymer Journal 43 (2007) 3050–3059.

6. J. K. Oh, D. I. Lee and J. M. Park, Prog. Polym. Sci., 2009, 34, 1261–1282.

7. J. M. Carvalho, M. A. Coimbra and F. M. Gama, Eur. Polym. J., 2009, 75, 322–327 (b) S. Pal, T. Nasim, A. Patra, S. Ghosh and A. B. Panda, Int. J. Biol. Macromol., 2010, 47,623–631.

8. Sitashree Banerjee, Abhinay Mishra, Madan M. Singh, Biswajit Maiti, Biswajit Ray and Pralay Maiti. RSC Adv., 2011, 1, 199–210 | 199

9. Das, D.; Das, R.; Mondal, J.; Ghosh, A.; Pal, S.. J. Appl. Polym. Sci. 2014, 131, 40039. Structure RSC Adv., 2011, 1, 199–210 199.

10. A. Finne and A. C. Albertsson, J. Polym. Sci., Part A: Polym. Chem., 2003,41, 1296–1305

11. G. Bhaskar Raju, Allan Holmgren and Willis Forsling1, Journal of Colloid and Interface Science **200,** 1–6 (1998).

MACRO 256

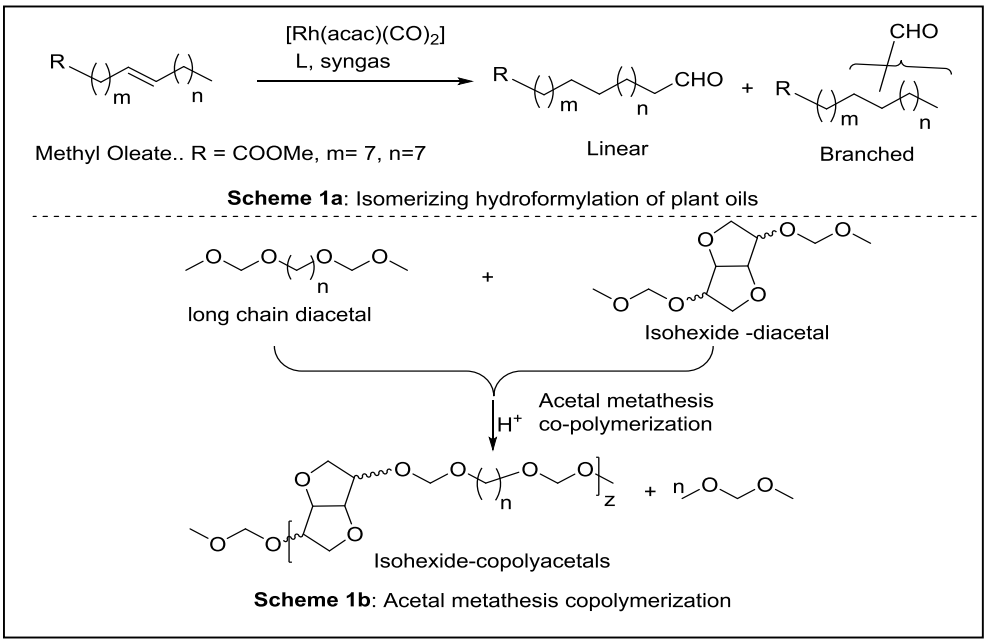
Highly Regioselective Isomerizing-Hydroformylation of Plant Oils to Monomers and Sustainable Polymers

Pandey Swechchha [a]; Rajput Bhausaheb S.[a]; Chikkali Samir H.* [a,,b]

[a]Polyolefin Lab, Polymer Science and Engineering Division, National Chemical Laboratory, Pune-411008, India

*[b]Academy of Scientific and Innovative Research, Anusandhan Bhawan, 2 Rafi Marg, New Delhi 110001, India***E-mail: s.chikkali@ncl.res.in.*

Today's chemical world rely mainly on fossils fuel resources. [1-3] However due to depleting fossils fuel resources and consequently ever increasing prices of crude oil in global market a sustainable alternative is highly desirable. The resurge in the renewable chemical industry has led to the successful launch of several renewable products such as sugarcane-based polyethylene, polylactic acid, and polyhydroxyalkanoates, to name a few. [4] Among the various renewable resources, plant oils stand out, as they provide direct entry to chemical modification. Their easy access and high H/C ratios (almost equivalent to crude oil) make them substrates of choice.[5] Chemically, plant oils are long-chain fatty acids with varying degrees of internal double bonds. The internal double bonds provide an excellent



Scheme 1a: Isomerizing hydroformylation of plant oils

Scheme 1b: Acetal metathesis copolymerization

opportunity to further functionalize plant oils to useful chemicals and materials. A paradigm shift could be achieved if the internal double bond could be isomerized to the terminal position and selectively functionalized. Herein, we present our attempts in the isomerizing hydroformylation of plant oils by using a bisphosphorus Rh complexes and further functionalization of the resultant linear aldehydes to hydroxy–acid bifunctional molecules.[6] These bifunctional molecules were further co-polymerized with isohexides diacetal to prepare renewable and degradable polymers.[7]

References

(1) Biermann, U.; Bornscheuer, U.; Meier, M. A. R.; Metzger, J. O.; Schäfer, H. J. *Angew. Chem. Int. Ed.*
2011, *50*, 3854-3871.
(2) Dapsens, P. Y.; Mondelli, C.; Perez-Ramirez, J. *ACS Catalysis* **2012**, *2*, 1487-1499.
(3) Dodds, D. R.; Gross, R. A. *Science* **2007**, *318*, 1250-1251.
(4) Tullo, A. H. *Chem. Eng. News* **2011**; *89*, 9.
(5) Vennestrom, P. N. R.; Osmundsen, C. M.; Christensen, C. H.; Taarning, E. *Angew. Chem. Int. Ed.* **2011**,
50, 10502-10509.
(6) Pandey, S.; Chikkali, S. H. *ChemCatChem* **2015**, 7, 3468-3471.
(7) Rajput, B. S.; Chander, U.; Arole, K.; Stempfle, F.; Menon, S.; Mecking, S.; Chikkali, S. H. *Macromol.*
Chem. Phys. **2016**, *217*, 1396-1410.

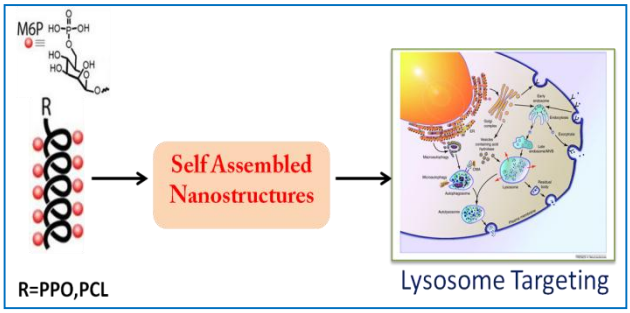
MACRO 258

Self Assembled Nanostructures from Amphiphilic Mannose 6-phosphate Glycopolypeptides for Lysosome Targeting

Pandey, Bhawana[a]; Mondal, Basudeb[a] and Sen Gupta, Sayam[a]*

Chemical Engineering Division, CSIR National Chemical Laboratory, Dr. Homi Bhabha Road, Pune - 411008, India

**ss.sengupta@ncl.res.in*



Glycopolypeptides based nano-carriers represent a very interesting class of drug delivery vehicles as they mimics natural glycoproteins which are involved in regulation of cellular processes through polyvalent interaction with carbohydrate binding receptor proteins that are observed on cell surfaces.[1,2]For selectively targeting and better delivery efficacy, the attractive strategy is to specifically deliver the therapeutic molecule into its intracellular therapeutic active site (targeted organelle).For example, mammalian cells containing mannose 6-phosphate receptors play a critical role in the sorting of lysosomal enzymes from secretory proteins and their delivery into lysosomes.[3,4] These receptors, which include the ~300 kDa insulin-like growth factor-II (IGF-II)/cation-independent mannose 6-phosphate (M6P) receptor (CI-MPR), bind lysosomal enzymes containing phosphomannosyl residues in the trans-golgi network (TGN) and transport them to an acidified compartment where the low pH leads to the dissociation of the ligand-receptor complex.[5] So the incorporation of multiple copies of M6P moieties in glycopolypeptides completely alters their trafficking behavior and becomes exclusively lysosome specific.[6]Therefore, we envisaged that it would be interesting to synthesize nanostructures from the self assembly of amphiphilic M6P-glycopolypeptides which can be used to encapsulate therapeutics for targeting and delivering them exclusively to lysosomes. Herein, we will discuss about synthesis, self assembly and characterization studies of amphiphilic M6P-glycopolypeptides bearing PPO/PCL as hydrophobic block and high molecular weight M6P-glycopolypeptide as a hydrophilic block. By varying the hydrophilic-hydrophobic balance of the amphiphilic M6P glycopolypeptides, we were able to self-assemble them into nanostructures with different morphologies. The multiple pendant M6P moieties on the surface of these nanostructures not only help us understand the complexity and individuality of CI-MPR trafficking for lysosomal targeting but also for efficacious delivery applications towards lysosomes.

References:

1. Mammen, M.; Choi, S.; Whitesides, G. M. *Angew. Chem. Int. Ed.* **1998**, *37*, 2754–2794.
2. Pati, D.; Kalva, N.; Das, S.; Kumaraswamy, G.; Sen Gupta, S.; Ambade, A. V. *J. Am. Chem. Soc.* **2012**, *134*, 7796−7802.
3. Kornfeld, S.; *Annu. Rev. Biochem*., **1992**, *61*, 307-330.

4. *Hoflack, B.; Kornfeld, S. J. Biol. Chem.* ***260*** *(22): 12008–14*
5. Ghosh, P.; Dahms, M N.; Kornfeld, S.; *Nat. Rev. Mol. Cell Biol.*, **2003**, *4*, 202-212.
6. Hoogendoorn, S.; Puijvelde, van M. H. G.; Kuiper, J.; Marel, van der A. G.; Overkleeft, S. H. *Angew. Chem.*, **2014**, *53*, 10975-10978

MACRO 266

Copolymerization Studies of Allyl Glycidyl Ether with Different Hydrophobic Methacrylates: Lipase Immobilization Study

Rajdeo Kishor,[a, b] Tayal Rajiv,[a] Mule Smita,[a] Ponrathnam Surendra,[a] Pardeshi Satish,*[, b] and Chavan Nayaku**[, a]

[a] *Polymer Science and Engineering Division, CSIR-National Chemical Laboratory, Dr. Homi Bhabha Road, Pashan, Pune-411 008, India.*
[b] *Department of Chemistry, Savitribai Phule Pune University (Formerly University of Pune), Ganeshkhind, Pune-411 007, India.*

** *nn.chavan@ncl.res.in*

Binary statistical copolymerisation of allyl glycidyl ether (AGE), a bi-functional monomer, with different hydrophobic methacrylate such as methyl methacrylate (MMA), butyl methacrylate (BMA) and 2-ethylhexyl methacrylate (EHMA) were studied. The copolymerisation studies, particularly, binary monomer reactivity ratios were estimated for the copolymers, over a very wide range of copolymer compositions by free radical solution copolymerisation in methyl isobutyl ketone using 2,2'-azobisisobutyronitrile (AIBN) at 70 ºC. The reactions were quenched at moderate conversions and unreacted co-monomers at stoppage and weight fraction conversions were evaluated by gas chromatography (GC-FID). The instantaneous copolymer composition, utilized to estimate the monomer reactivity ratios by employing four different terminal models, including Fineman-Ross (FR),[1] Kelen-Tudos (KT),[2] extended Kelen-Tudos (Ext. KT)[3] and Mao-Huglin (MH).[4] The copolymer micro-structural parameters, dyad sequence distribution and dyad sequence lengths were computed using Igarashi[5] and Pyun[6] methods respectively. The allyl glycidyl ether-*co*-2-ethylhexyl methacrylate pair fulfills the azeotropic condition and forms the azeotropic copolymer at 0.504 and 0.496 mole fraction of the two comonomers respectively. The average reactivity of allyl glycidyl ether with methyl methacrylate was 0.458 and 1.532 respectively, and showed the tendency towards the formation of random copolymer networks. While allyl glycidyl ether with butyl methacrylate found to be higher reactivity ratio values and were 1.186 and 3.998 respectively. This binary copolymer showed tendency towards the formation of block copolymer networks with more rigid butyl methacrylate comonomer units. The structural and functional characterisation of copolymers were carried out using proton (^{1}H) and carbon (^{13}C) nuclear magnetic resonance (NMR) spectroscopy, Fourier transform infra-red (FTIR) sepectroscopy. Glass transition temperature (T_g) of copolymers were determined by differential scanning calorimetry (DSC).

The beaded, high surface area porous azeotropic polymeric networks based on allyl glycidyl ether with 2-ethylhexyl methacrylate were synthesised employing suspension polymerisation methodology. The pore size-pore size distributions with porosity were studied with the variation of cross link-density (CLD) of the cross-linker. The porosity and the pore size distribution were determined using Brunauer–Emmett–Teller (B.E.T.) via, nitrogen adsorption and isotherm. Enzyme immobilization of commercially important Lipase, *Candida Antarctica* Lipase-B (CAL-B) was carried out on synthesised porous, beaded polymer matrix. The lipase enzyme activity was measured at 30°C with tributyrin (1.3 % V/V) as a substrate using the 0.01 M Tris-HCl assay buffer. The enzyme activity was monitored using pH-metric titration, where the butyric acid produced from the tributyrin was continuously titrated with the standardised 0.2 M NaOH at pH 7.5 for 10 minutes. The enzyme activity in units was expressed in terms of micro moles of NaOH consumed per minute. All the enzyme activities were calculated from the mean of three different readings with standard deviation within limit of ± 5%.

The beaded porous polymers with CLD ranging from 25, 50, 75, 100, 150 and 200 were screened for the Lipase immobilization. The polymer with CLD 100 showed maximum enzyme activity, which retained 95% of the initial activity. The maximum enzyme activity was observed at pH 7 while more acidic and basic pH decreases the enzyme activity. The thermal variation study demonstrated that the temperature 30 °C is optimum and enzyme activity was decreased with the rise in the temperature. Both the pH and thermal study revealed that the immobilised enzymes were having superior enzyme activity as compared to that of free enzyme.

The polymers with and without immobilised enzymes were characterized for their functional, elemental and surface properties by using FTIR, EDX and SEM analytical techniques. All these instrumental techniques have shown the characteristics differentiations with enzyme and without enzyme matrix.

Keywords

Copolymerization; allyl glycidyl ether; binary monomer reactivity ratio; azeotropic copolymer; porous polymers: Enzyme immobilization.

References

[21]Fineman M.; Ross S.D. *J. Polym. Sci*., 5 (1950) 259.
[22]Kelen T.; Tudos F. *J. Macromol. Sci. Part A: Chem.: Pure and Appl. Chem.*, 9 (1975) 1.
[23]Tudos, F; Kelen T.; Földes-berezsnich, T.; Turcsányi, B. *J. Macromol. Sci. Part A: Chem.: Pure and Appl Chem.*, 10 (1976) 1513.
[24]Mao, R.; Huglin, M. B. *Polymer*, 34 (1993) 1709.
[25]Igarashi, S. *J. Polym. Sci. Part B: Polym. Lett.*, 1 (1963) 359.
[26]Pyun, C. W. *J. Polym. Sci. Part A2: Polym. Phys.*, 8 (1970) 1111.

MACRO 270

Novel Silk Fibroin based Coatings for PDMS Breast Implants

Shete Abhijit[a], Nisal Anuya[a]*, Lele Ashish[a], Patil Amrita[b], Prabhune Asmita[b], Dixit Santosh[c], Koppiker Chaitanyanand[c]

[a]*Polymer Science and Engineering Division, CSIR-National Chemical Laboratory, Pune, India*
[b]*Biochemical Sciences Division, CSIR-National Chemical Laboratory, Pune, India*
[c]*Prashanti Cancer Care Mission, Pune, India*

** e-mail id: aa.nisal@ncl.res.in*

Abstract

One of the leading causes of breast implant failure is the formation of a fibrotic capsule surrounding the implant. It has been hypothesized that the primary reasons for this capsular contracture are (a) foreign body response to the implant and (b) bacterial biofilm formation. The objective of this work was to investigate whether coating the PDMS implant surface with an antibacterial polymer such as silk fibroin (SF) may mitigate the bacterial biofilm formation. It was found that SF coating lowered the contact angle of PDMS from103±5º to~ 77±11º. Also, the SF coated PDMS discs showed improved resistance to biofilm formation. The coating was found to be stable for one week in de-ionized water, with negligible fibroin release. It was also evaluated as a drug delivery vehicle, with cephalexin as a model drug.

Keywords: *Silk, PDMS, breast implant, coating, contact angle, bacterial biofilm, drug release.*

Introduction

Cancer is a leading cause of fatalities worldwide, with over 8 million deaths per year[1].Breast cancer is the most common cancer amongst Indian women with Age-standardised Ratio (ASR) of 30-33 (i.e. newly diagnosed cases detected per annum per 1 lakh population). Nearly 1 in 20 urban women (Age 35-45) carry a life-time risk of developing this disease by it[2,3].The general breast cancer management guidelines include surgery (total mastectomy) chemotherapy, radiation therapy and hormonal therapy[4]. Mastectomy procedures may vary according to nature of the disease. Immediate Breast Reconstruction Surgery (IBRS) is fast becoming popular globally as well as in India. In IBRS, the diseased breast tissue is surgically excised and an implant is inserted in the hollow breast pocket in the same setting

Poly (dimethyl siloxane) (PDMS), is the material of choice for breast implants owing to its flexibility (UTS ~ 10 MPa, Elongation at break > 100%)[5], ease of processing and bio-compatibility[6]. Most popular commercial PDMS breast implants are Siltex™ Becker Implants (Johnson and Johnson, USA) and Natrelle 150™ (Allegan Inc., USA).

The main cause of breast implant failure has been attributed to capsular contracture [6]. Though widely used, ~20% of the implants fail due to a fibrotic capsule formation around the implant. Prior art has focused on two hypotheses as primary causes for this capsular contracture:

(1) Exogenous hypothesis: Sub-clinical infection by the formation of bacterial bio-film

Bacteria, such as *Staphylococcus epidermidis*, attach irreversibly to the implant surface, minutes after the implantation [7]. They start colonizing and produce an exopolymer around the colonies which attracts other organisms from the surrounding tissue, leading to the formation of a bacterial bio-film around the implant.

(2) Endogenous hypothesis: Foreign body response (Acute and Delayed)

PDMS is a hydrophobic polymer and the polymer surface has a contact angle for water ~105°. This property leads to the adsorption of various proteins onto the implant surface[8]. This event triggers recruitment of neutrophils, who in-turn signal the macrophages to attack the foreign body as a defense mechanism. As a result, fibroblasts surround the implant surface leading to formation of a fibrotic capsule around the implant [8].

Several approaches have been undertaken by researchers worldwide to address the problem of breast implant induced fibrosis and capsular contracture. These include sub-muscular placement of the implant, texturing the implant, limited pre-operative and operative handling and anti-biotic irrigation of the implant site.

In 2008, Bridges AW and Garcia AJ[11], published an in-depth review on Poly (ethylene glycol) based surface treatments on PDMS. Owing to the hydrophilic nature of PEG, lesser protein adsorption over the surface of the implants is expected, thereby, mitigating the cascade of foreign body response. Surfaces of implants were modified by using treatments such as grafting to form a brush, self-assembling monolayer or coating with a thin film of PEG hydrogel. However, there were limitations to the bio-fouling activity. In 2013, Puskas JE et al[10] developed a non-silicone breast implant using poly (styrene-b-isobutylene-b-styrene) block co-polymer. This novel breast implant is presently undergoing clinical development cycle. In 2013, Scheibel et al[6] coated PDMS breast implants with recombinant spider-silk protein. After *in vitro* and *in vivo* studies, they concluded that the biocompatibility of PDMS had noticeably increased with better cell proliferation and lesser inflammatory responses, rendered by spider-silk coatings.

Here, we propose to coat the surface of PDMS implant with natural silk fibroin protein. Silk fibroin (SF) of silkworm (*Bombyx Mori*) has been an attractive bio-material since 5000 B.C [13]. Though known as a valuable textile component, due to its aesthetic properties; in the recent decades, it has made its mark in the bio-medical sector. The material has good clinical history – SF sutures have been commercialized for decades. More recently a SF scaffold has also received FDA approval. SF is a protein with properties such as high mechanical strength (UTS~ 740 MP, Elongation at break ~ 20%), hydrophilic nature (contact angle: 58-78 degrees), bio-degradability and anti-bacterial activity. It can be regenerated from its nascent form to form films, gels, beads, nano-fibres etc. [14].

Here, we investigate the feasibility of coating regenerated SF onto PDMS surfaces. Furthermore, we aim to evaluate the ability of SF coated PDMS discs to influence bacterial biofilm formation.

Experimental

Casting of PDMS: Sylgard 184 (Dow Corning) two part resin-hardner system was mixed as per the manufacturer's protocoland was casted in a polystyrene petridish to achieve a thickness of 2 mm. The system was cured under vacuum at 40° C for 24h. Cured PDMS discs were peeled off from the petridish and cut into 15mm discs using a punch.

Preparation of PDMS surface: The 15mm discs were cleaned with IPA (Merck) and dried under vacuum at 60°C for 4 hrs. Further these discs were subjected to 1 min of oxygen plasma (RF power: 50 W) to activate the surface. Post plasma treatment, the discs were stored under DI water.

Preparation of regenerated silk fibroin (RSF): Cocoons (35g) of *Bombyx Mori* were degummed in a 0.5% w/v boiling aq. solution of sodium bicarbonate (Merck) twice for 30 minutes each and rinsed thoroughly with DI water thereafter. SF, thus obtained, was vacuum dried at 60° C for 48 hrs. 10g of SF was dissolved in 100 ml, 9.3 M, aq. LiBr (Sigma) solution at 60° C for 4 hrs. This solution of SF was dialyzed for 52 hagainst DI water to ensure complete removal of LiBr salt and centrifuged (10,000 rpm, 30 min) to obtain regenerated silk fibroin solution of 4% w/v.

Dip Coating: RSF was diluted with DI water to prepare dipping solutions with varying concentrations (0.01 % w/v to 4% w/v). Plasma activated PDMS discs were dipped in the solutions for 2 min and dried in air at 25° C for 24h before further characterization.

Scanning Electron Microscopy (SEM): SF coated and uncoated PDMS discs were analyzed using SEM, for surface characteristics and thickness.

Bradford Assay: Discs coated with various concentrations of dipping solution were subjected to Bradford reagent (Sigma) and dried under ambient conditions. The stain was dissolved into acetic acid (Merck) and subjected to UV spectroscopy. The samples were quantified against standard protein curve of BSA.

Stability of coating: RSF (4%w/v) coated PDMS discs were placed under DI water (2ml per disc) for a period of 7 days. Samples of water were analyzed for SF release by using UV-Vis spectrophotometer (peak at 280 nm).

Contact angle studies: 100 µl of DI water was placed onto untreated, plasma activated and SF coated PDMS discs. A picture was taken using a camera and was analyzed in ImageJ image processing software.

Drug Release Study: To add to the anti-bacterial properties of the RSF coating, cephalexin hydrate (Sigma) was blended with the dipping solution. Release of cephalexin in DI water after 24 h was monitored using UV-Vis spectrophotometer (peakat 264 nm).

Inhibition of bacterial biofilm formation: SF coated and uncoated PDMS discs were incubated in a culture of *P.aeruginosa* for 24h. The resulting biofilms were stained using crystal violet stain and observed under optical microscope.

Results and Discussion

Coating thickness: SEM images (Figure 1) taken perpendicular to the plane of the coating dipped in 4% w/v solution of RSF show around 1 µm thick coat. The surface appears to be rough and wavy, as compared to uncoated PDMS.

Subjecting the coated discs to Bradford assay aided quantification of the amount of SF present on the coated surface. This in turn was used to establish a relation between the concentrations of the dipping solution to the thickness of the coating (Figure 2).Thetrend showed a logarithmic relation indicating steady state adsorption of SF onto the PDMS surface.

Stability of the coating: Throughout the seven days of the study, the amount of SF released into the surrounding DI water was negligible (Figure 3). This may be a result of β-sheet formation during drying of the samples after dipping. SF is known to crystallize at the air-water interface[12].

Contact angle studies: The contact angles for uncoated, plasma activated and SF coated PDMS samples were found to be 103±5º, 69±6º and 78±11º respectively. The lowering of contact angle after oxygen plasma is a result of oxygen moieties chemically modifying the methyl group on PDMS to make them hydrophilic. SF later gets physically adhered to these sites and creates a robust coat. SF is an amphiphillic molecule. This increase in hydrophillicity may cause a decrease of protein adsorption on to PDMS surface; in turn reducing the foreign body response associated with it.

Drug release: It was observed that a standard drug like cephalexin was able to diffuse through the SF coat into the surrounding media; which in this case was DI water. The relation between the drug loading and release was linear (Figure 4) at the end of 24 h, as expected.

Inhibition of bacterial biofilm: The number of *P.aeruginosa* colonies significantly reduced on the SF coated PDMS disc (Figure 5).

Figures:

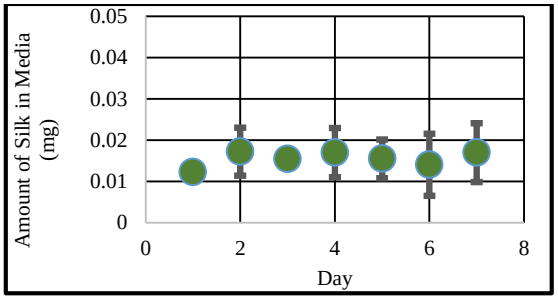


Figure3: Coating stability in DI water

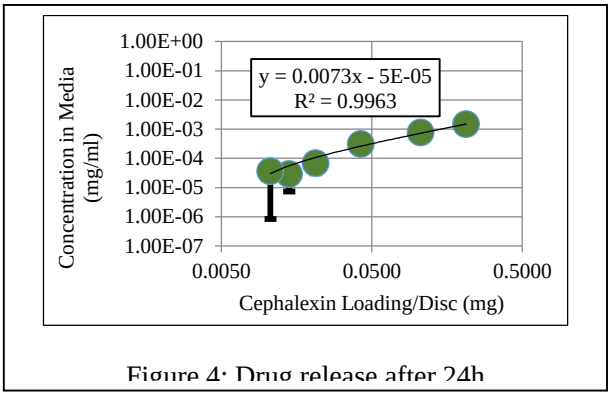


Figure 4: Drug release after 24h

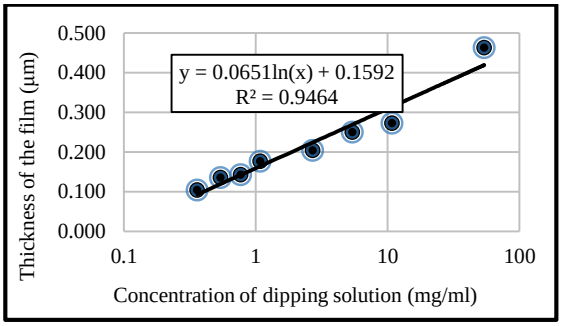


Figure 2: Relationship between concentrations of dipping solution to thickness of SF coat established through Bradford assay

Conclusions

It was successfully demonstrated that SF does form a continuous coat over PDMS substrate. SF coated PDMS discs show a lower hydrophobicity and decreased bacterial activity as compared to untreated PDMS. The study also demonstrated that the SF coating could act as a drug delivery vehicle; with a controlled release of drug molecules. Further studies are underway to assess the performance of SF-coated PDMS surfaces in breast implant-induced fibrosis and capsular contracture.

Acknowledgements

We thank CSIR 12th Five Year Plan Project CSC0134 "Molecules to Materials to Devices"for funding.

References

1. World Health Organization, Fact Sheet No. 297
2. Cooper GM, "Elements of Human Cancer", Jones & Bartlett Learning, 1992, 16
3. Okonkwo QL et al. "Breast Cancer Screening Policies in Developing Countries: A Cost-effectiveness Analysis for India", J Natl Cancer Inst (2008) 100 (18): 1290-1300.
4. Carlson RW, "Breast cancer Clinical Practice Guidelines in Oncology", J NatlComprCancNetw. 2003 Apr;1(2):148-88
5. Mata Alvaro et al., "Characterization of Polydimethylsiloxane (PDMS) Propertiesfor Biomedical Micro/Nanosystems",BiomedicalMicrodevices, 2005, 7:4, 281–293
6. Schiebel T et al.,"Spider Silk Coatings as a Bioshield to Reduce Periprosthetic Fibrous Capsule Formation", Adv. Funct. Mater. 2014, 24, 2658–2666
7. Akers KS et al. AdvExp Med Biol,830 (2015)1
8. Grainger, DW. Nat Biotechnol, 31 (2013) 507
9. Puskas JE et al., "Newbiomaterialasapromisingalternativetosiliconebreastimplants",J Mechbehbiomedmat21(2013)47–56
10. Bridges AW and Garcia AJ, "Anti-Inflammatory Polymeric Coatingsfor Implantable Biomaterials and Devices", J Diabetes SciTechnolVol 2, Issue 6, November 2008, 984-995.
11. West JL, Hubbell JA. "Comparison of covalently and physically cross-linked polyethylene glycol-based hydrogels for the prevention of postoperative adhesions in a rat model" Biomaterials. 1995;16(15):1153–6.
12. VepariCharu, Kaplan DL, "Silk as a Biomaterial", Prog. Polym. Sci. 32 (2007) 991–1007.
13. Rockwood DN et al., "Materials fabrication from *Bombyxmori* silk fibroin", Nature Protocols (2011), 6,1612–1631

MACRO 271

Modified Silk Fibroin based 3D Scaffolds for Bone Tissue Engineering

Parekh Nimisha,[a] , Nisal Anuya [a] *, Sen Gupta Sayam[b], B.L.V. Prasad[c]

[a]*Polymer Science and Engineering Division, CSIR - National Chemical Laboratory, Dr. HomiBhabha Road, Pune-411008, India,*

[b]*Chemical Engineering and Process Development Division, CSIR - National Chemical Laboratory, Dr. HomiBhabha Road, Pune-411008, India.*

[c]*Physical and Materials Chemistry Division, CSIR - National Chemical Laboratory, Dr. HomiBhabha Road, Pune-411008, India.*

** e-mail id: aa.nisal@ncl.res.in*

Abstract

Natural silk fibroin (SF) produced by silkworm *Bombyx mori*, has emerged as a promising biomaterial due to its biocompatibility, biodegradability and excellent thermo-mechanical properties. SF has already been shown to have high potential in bone tissue engineering. In our group, we have recently developed silk fibroin micro-particle scaffolds, which possess excellent mechanical properties appropriate porosities and required pore size and pore architecture. Here, we report a protocol to further enhance the performance of these scaffolds in bone tissue engineering. The SF microparticle scaffolds were coated with a thin layer of collagen type I and *in-vitro* cell culture studies were performed on these scaffolds primarily using osteoblast (MG63) cell line. We observed improved cell adhesion, enhanced cell proliferation and cell viability in collagen coated 3D SF scaffold as compare to uncoated SF scaffold.

Keywords: *3D silk scaffolds; cell adhesion; cell growth; cell viability; bone tissue engineering*

Introduction

In India, where aging is clubbed with obesity and poor physical activity, the bone disorders are expected to double by 2020[1]. Bone is a highly vascularized tissue with a unique capacity to heal and regenerate without leaving a scar. However, this is not always the case and bone grafting is imperative to accelerate bone healing. Bone tissue engineering (BTE) using synthetic materials has been long explored as a potential alternative to the conventional auto/allografts. However, autografts are still the golden standard in the industry today. The primary challenge for development of synthetic bone grafts is the development of a biocompatible 3D scaffold that can provide the adequate morphoroligical, structural and chemical cues for cell adhesion. The scaffold surface must improve the functioning of cells to promote natural bone formation. The scaffold should resorb at appropriate rates according to growth of neonatal tissue. In the recent past, natural silk fibroin (SF) produced by silkworm *Bombyx mori*, has emerged as a promising biomaterial

especially for tissue engineering and biomedical implant applications due to its biocompatibility, biodegradability and excellent thermo-mechanical SF can be produced in large commercial quantities, allows easy chemical modification to obtain required functionality and be processed into 3D materials like hydrogels, sponges, fibers, microspheres, and electrospunfiber mats[3]. The unique mechanical properties and tunable biodegradation rate of these 3D scaffolds allows attachment, proliferation and differentiation of osteoblast cells for BTE[3, 4].The limitation of the scaffolds reported earlier is that they are mostly soft in nature and do not have high load bearing capacity which is essential for BTE[5-12]. Recently high strength silk fibroin scaffold have been fabricated in our group which possess excellent mechanical properties (Dry compression modulus >50MPa) that is essential for load bearing, 40-60% bulk porosity and 100-500 µm pore size coupled with meso and micro porosity[13-15].

Here we report a method to further improve the efficacy of these 3D SF scaffolds by surface functionalizing them with coating of a biocompatible polymer like collagen. SF scaffolds have shown better cell attachment, metabolic activity, cell proliferation, ECM deposition and chondrogenesis as compared to Collagen scaffolds[16, 17]. However, the performances of collagen scaffolds have been limited by their poor mechanical properties and faster rates of bioerosion as compared to silk fibroin[4]. The use of collagen to coat SF microparticle scaffolds helps overcome the limitations posed by either biomaterial. We fabricated the 3D SF microparticle scaffold reported by our group and developed a protocol to coat it with collagen type I and monitored the enhanced efficacy of these modified scaffold for cell adhesion, cell viability, proliferation as compare to non fabricated 3D SF scaffold.properties[2, 3].

Experimental

Materials

Silk microparticles prepared as per protocol reported in our Indian patent application 0045/DEL/2015. Cell line MG 63 purchased from National Centre for Cell Science (NCCS), Pune, India, Collagen type I (Sigma Aldrich), MEM, FBS, Trypsin EDTA, MTT from Invitrogen.

Instruments

Scanning electron microscope (Quanta 200 3D from FEI), Multi scan EX plate reader (Thermo-scientific), Carl Zeiss Axio Observer Z1.

Scaffold preparation

Silk microparticles were made as per the protocol developed in our laboratory. In brief, 3 wt% SF-HFIP solution was infused at a constant rate of 1ml/min using a syringe pump. The drops of SF-HFIP solution were collected in a methanol coagulant bath. The particles so formed were air dried and stored at room temperature for further experimentation. Accurately weighed particles were

placed in a cylindrical mold and 100 µl of aqueous SF solution was added to stick the particles together and form a 3D scaffold. The process has been schematically shown in Figure 1.

Collagen coating and characterisation

1 mg/mL sterile collagen solution was diluted 1:10 times with sterile distilled deionized water. Each scaffold was incubated in 100 µL of 0.01w/v% collagen in a 96 well cell culture plate for 12h at room temperature. The excess solution was then pippeted out and the scaffold was dried at 4ºC for 12h.

Cell viability study by trypan blue assay

MG63 human osteosarcoma cell line was maintained in complete media containing MEM with 10% FBS. Before seeding the cells, scaffolds were incubated in complete media at 37ºC for 12h. 5 x 10^4 cells per scaffold in 100µL of complete media were seeded on both uncoated and collagen coated scaffolds. Cells were trypsinized and counted on the day 1^{st}, 3^{rd}, 5^{th}, and 7^{th} in Neubauer chamber by using the standard trypan blue method. Each count was the mean of triplicate measurement and the viable cell density (VCD) was determined using the formula

VCD = (number of viable cells x dilution factor x 10000) / (Total number of squares counted)

Cell adhesion and proliferation study

Cell proliferation study was determined by MTT (3-(4, 5-Dimethylthiazol-2-yl)-2, 5-diphenyltetrazolium bromide). Before seeding the cells, scaffolds were incubated in complete media at 37ºC for 12h. Cells were seeded in a non-adherent flat bottomed 96-well plate at a density of 5 x 10^4cells per scaffold in 100µL of complete media.The plate was incubated at 37°C with 5% CO_2 for 24 hours. After incubation on the day 1^{st}, 3^{rd}, 5^{th}, and 7^{th}media was replaced with filter sterilized MTT (0.45 mg/mL) prepared in MEM containing 10% FBS and further incubated for 4hrs at 37 °C with 5% CO_2. MTT reagent was replaced by DMSO 100 µL/well. Addition of DMSO dissolves the formazan crystals formed by reaction of cells with MTT and developed color was measured at 550 nm using a Microtitre plate reader (Veroscan, Thermo Scientific).Each absorbance was taken to be the mean of triplicate measurements for both with and without collagen coated scaffolds. To verify the difference in cell adhesion on both the scaffolds after 24 hrs of seeding, DAPI staining was performed. In brief, seeded cells were fixed with 4% paraformaldehyde for 15 minutes followed by 3 times washing with PBS and then stained with DAPI 300nM for 5 minutes. Images were acquired by using epi-fluoresence microscope from Carl Zeiss.

Results and discussion

Collagen coating and characterisation

SEM image of coated scaffold in Figure:2 a shows the presence of layer of collagen on 3D SF scaffold as compare to without coated scaffold (Figure:2).

Cell viability study by trypan blue assay

Figure 3 represents the viable cell density (VCD) on the day 1st, 3rd, 5th, and 7th. As can be seen, there is an increment in VCD with collagen coated scaffold as compare to without coating. From the data there was better cell viability was observed with collagen coated scaffold.

Cell adhesion and proliferation study

Cell adhesion and proliferation were measured by MTT. The collagen coated scaffold consistently showed improved cell adhesion and proliferation as compared to the uncoated scaffold.

DAPI stained images demonstrated improved cell adherence on collagen-coated scaffold (Figure: 5).

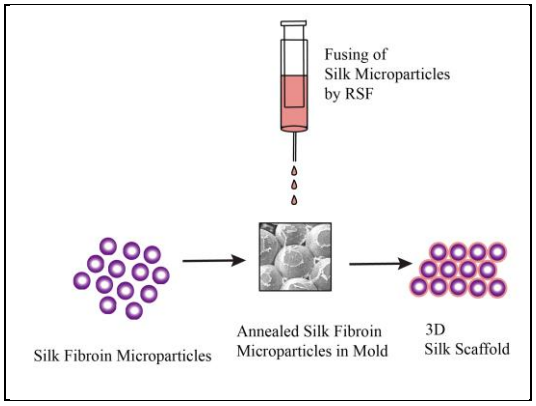


Figure 1. Scaffold making and collagen coating

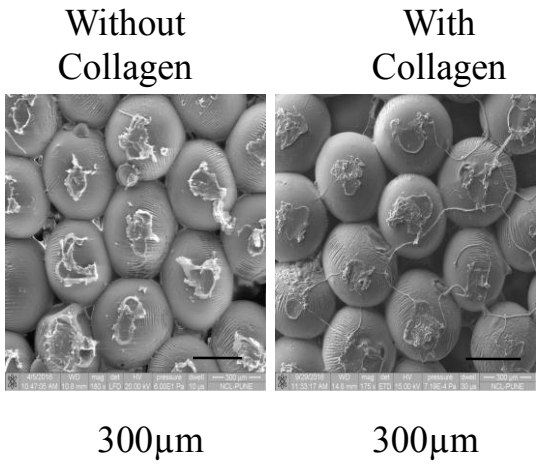


Figure 2.Scanning electron microscopic images of 3D silk scaffold

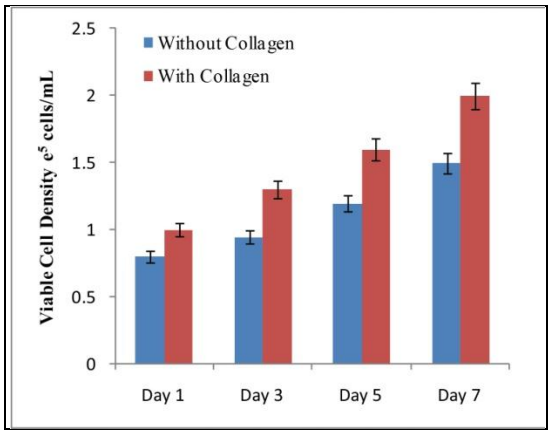


Figure3. Cell viability of MG63 cells by trypan blue assay

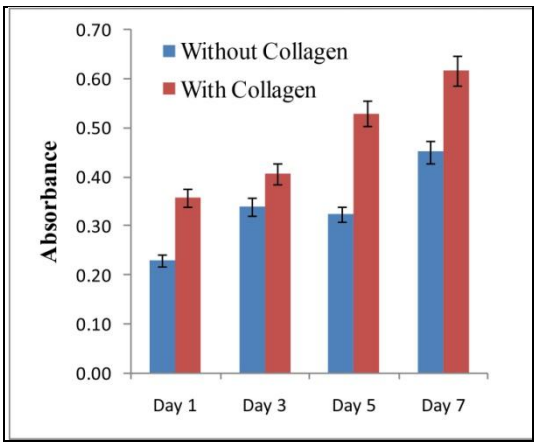


Figure 4. Cell proliferations of MG63 cells by MTT assay

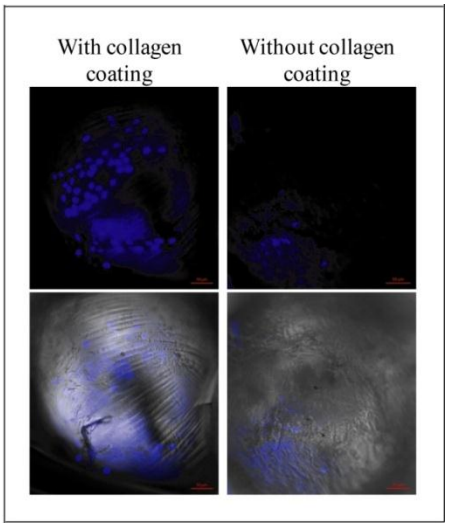


Figure 5.Cell adhesion of MG63 cells by DAPI staining. Images were captured by using objective: 10X; scale bar: 50μm.

Conclusion:

A collagen coating on 3D tensile silk scaffold was done and tested for the cell viability, cell adhesion and proliferation. Result clearly gave confirmation about the better viability with enough cell growth and adhesion on scaffold after coating with collagen. This outcome allow the use of tensile, biocompatibility properties of silk along with adhesion moiety of collagen for further planning of the use of stem cells for bone tissue engineering.

Acknowledgements

The authors would like to thank Ms. Raeesa for providing help in SF particle making and project CSC 0134 for financial support. The authors declare no competing financial interest.

References

1. Amini, A. R.; Laurencin, C. T.; Nukavarapu, S. P.; *Crit Rev Biomed Eng.*,40(5), 363-408, **2012**.
2. Vepari, C.; Kaplan, D. L.; *ProgPolym Sci*., 32(8-9), 991–1007, **2007**.
3. Melke, J.; Midha, S.; Ghosh, S; Ito, K.; Hofmann, S; *Acta Biomater*.,31, 1-16, **2016**.
4. Sundelacruz, S; Kaplan, D. L.; *Semin Cell Dev Biol.*,20(6), 646 – 665, **2009**.
5. Gronau, G.; Krishnaji, S. T.; Kinahan, M. E.; Giesa, T.; Wong, J. Y.; Kaplan, D. L.; Buehler, M. J.; *Biomaterials*, 33, 824-8255, **2012**.
6. Kasoju, N; Bora, U.; *Advanced Healthcare Materials*, 1, 393-412, **2012**.
7. Kundu, B.; Rajkhowa, R.; Kundu, S. C.; Wang, X.; *Advanced Drug Delivery Reviews*, 65, 457-470, **2012**.
8. Chung H.J.; Park T.G.; *Advanced Drug Delivery Reviews*, *59*, 249-262, **2007**.
9. Karageorgiou, V.; Tomkins, M.; Fajardo, R.; Meinel, L.; Snyder, B.; Wade, K.; Chen, J.; Novakovic, G. V.; Kaplan, D. L.; *Biomed. Mater. Res.*, 78A, 324-334, **2006**.
10. Zhang, W.; Zhu, C.; Ye, D.; Xu, L.; Zhang, X.; Wu, Q.; Zhang, X.; Kaplan, D. L.; Jian, X.; *PloS One*, 9 (7), e102371, **2014**.
11. Koh, L. D.; Cheng, Y.; Teng, C. P.; Khin, Y. W.; Loh, X. J.; Tee, S.; Y.; Low, M.; Ye, E.; Yu, H. D.; Zang, Y. W.; Han, M. Y.; *Progress in polymer Science*, 46, 86-110, **2015**.
12. Mandal, B. B.; Grinberg, A.; Gil, E. S.; Panilaitis, B.; Kaplan, D. L.*; PNAS*, 109 (20), 7699-7704, **2012**.
13. Omenetto, F. G.; Kaplan, D. L.; *Science*, 329 (5991), 528-531, **2010**.
14. Das, S.; Pati, D.; Tiwari, N.; Nisal, A.;Gupta, S. S.; *Biomacromolecules*, 13 (11), 3695-702, **2012**.
15. Nisal, A.; Trivedy, K.; Mohammad, M.; Panneri, S.; Gupta, S. S.; Lele, A.; Manchala, R.; Nirmal Kumar, S.; Gadgil, M.; Khandelwal, H.; More, S.; Seeta Laxman, R.; *ACS Sustainability and Engineering*, 2 (2), 312-317, **2014**.
16. Hofmann, S.; Knecht, S.; Langer, R.; Kaplan, D. L.; Vunjak-Novakovic, G.; Merkle HP, et al.; *Tissue Engineering*, 12, 2729-38, **2006**.
17. Meinel, L.; Hofmann, S.; Karageorgiou, V.; Zichner, L.; Langer, R.; Kaplan, D. L., et al.; *Biotechnology and Bioengineering*, 88, 379-391, **2004**.

MACRO 275

Synthesis of Photo Responsive Polymers and their Applications in Photoresponsive Surfaces and Drug Delivery

Biswas, Gargi; Ikbal, Mohammed; Banerjee, Rakesh; Singh, N. D. Pradeep.* and Dhara, Dibakar.*

Department of Chemistry, Indian Institute of Technology Kharagpur, West Bengal 721302 India

**Email: dibakar@chem.iitkgp.ernet.in; ndpradeep@chem.iitkgp.ernet.in*

Over the last few decades photo responsive polymers have created a great interest in drug delivery application. Photo-labile functionality is the fundamental key in photo responsive drug delivery systems (DDS). A number of photo-labile functional groups are reported in the literature. Among them o-nitrobenzyl derivatives are widely used as photo trigger for efficient drug and gene delivery. Likewise, photo acid generators (PAGs) have gained a great interest due to their immense applications in microlithographic industry. Photo irradiation on polymer film containing PAGs generate acid groups which modify the surface [1], [2]. We have synthesized different types of photo responsive homopolymers and their copolymers with methyl methacrylate, styrene, ethyl acrylate, NIPAM, PEG acrylate etc. using well-known free radical polymerization techniques. The synthesized polymers were characterized by IR, 1HNMR and GPC. To investigate the polymers as PAG, polymers were spin coated onto silicon wafers using a headway research spinner. The FT-IR spectra indicated photodecomposition of polymer films on irradiation. The hydrophobicity of the surface was tested by measuring water contact angle [3], [4]. We have also synthesized a new photo labile o-nitrobenzyl derivative [5]. To investigate the polymers as photo responsive drug delivery system, we have synthesized water soluble photo responsive block copolymers using newly synthesized photo labile monomer. An anticancer drug, chlorambucil, was covalently attached to the synthesized polymers. The release at different time interval from the polymer on UV irradiation was monitored by HPLC and UV-vis spectroscopy. The details of the polymers, their synthetic procedures and characterizations will be presented.

References

[27]Ikbal, M; Jana, A; Pradeep Singh, N.D; Banerjee, R; Dhara, D. *Tetrahedron*, 67 (2011) 3733.

[28] Ikbal, M; Banerjee, R; Atta, S; Dhara, D; Anoop, A; Pradeep Singh, N. D. *J. Org. Chem*, 77 (2012) 10557.

[29] Ikbal, M; Banerjee, R; Atta, S; Jana, A; Dhara, D; Anoop, A; Pradeep Singh, N. D. *Chemistry - A European Journal*, 18 (2012) 11968.

[30]Ikbal, M; Banerjee, R; Barman, S; Atta, S; Dhara, D; Pradeep Singh, N. D. *J. Mater. Chem. C*, 2 (2014) 4622.

[31]Biswas, G; Dhara, D. unpublished results.

MACRO 276

Thermal and pH Responsive Polymer-Grafted Magnetic Nanoparticles for Targeted Delivery of Anti-Cancer Drug

Bera, Sharmita; Sahoo, Banalata; Dutta, Sujan; Dhara, Dibakar*

Department of Chemistry
Indian Institute of Technology Kharagpur,
West Bengal 721302 India

** Email: dibakar@chem.iitkgp.ernet.in*

Targeted and efficient delivery of therapeutics to tumor cells is one of the key issues in cancer therapy. In this presentation, we report various nanoparticle-polymer conjugates having capability of temperature and pH dual responsive drug delivery. Core–shell nanoparticles comprising shell coated with smart polymers on magnetic nanoparticles as an anti-cancer drug carrier along with cancer cell-specific targeting agent were developed. Magnetite nanoparticles, prepared by simple co-precipitation method, were surface modified by introducing amine groups using 3-aminopropyltriethoxysilane.[1,2] Various thermal and pH responsive polymers were synthesized by RAFT polymerization. The polymers were then attached to the amine-functionalized nanoparticles.[1] The nanoparticles were characterized by XRD, TEM, SAED, FESEM, EDX, TGA, zeta potential, VSM measurements, and FTIR, UV-Vis spectral analysis. Doxorubicin (DOX) was loaded into the nanoparticles and its release behaviour was subsequently studied as a function of temperature and pH. Result showed a sustained release of DOX preferentially at the desired lysosomal pH and temperature conditions.[2] The biological activity of the DOX-loaded MNPs was studied by MTT assay, fluorescence microscopy, and apoptosis. Intracellular-uptake studies revealed preferential uptake of these nanoparticles into cancer cells compared to normal cells. The in-vitro apoptosis study revealed that the DOX-loaded nanoparticles caused significant death to the cancer cells. These nanoparticles were capable of target specific release of the loaded drug in response to pH and temperature, and hence may serve as a potential drug carrier for in-vivo applications.

References

[32] Sahoo, B; Devi, K S P; Banerjee, R; Maiti, T; Pramanik, P; Dhara, D. ACS Applied Materials and Interfaces 5 (2013) 3884.
[33] Dutta, S.; Parida, S; Maiti, C; Banerjee, R; Mandal, M; Dhara, D. Journal of Colloid and Interface Science 467 (2016) 70.
[34] Bera, S; Dhara, D. unpublished results.

MACRO 277

Temperature, pH and Redox Responsive Carbohydrate based Hydrogels for Protein Delivery

Dutta, Sujan; Deb Barman, Tanay; Dhara, Dibakar*

Department of Chemistry
Indian Institute of Technology Kharagpur,
West Bengal 721302 India

**Email: dibakar@chem.iitkgp.ernet.in*

Carbohydrate based hydrogels are important due to their non-toxicity, biocompatibility and natural origin. In this presentation, we present new set of pH, temperature and redox responsive hydrogels, which were prepared from carboxymethylcellulose (CMC) and poly(N-isopropylacrylamide). Copolymeric hydrogels were synthesized by copolymerizing N-isopropylacrylamide (NIPA) and methacrylated carboxymethylcellulose whereas semi-interpenetrating network (SIPN) hydrogels were prepared by polymerizing NIPA in presence of CMC. Two types of cross-linkers were used – with and without a redox sensitive bond. The structures of the hydrogels were characterized by FTIR and SEM studies. The copolymeric hydrogels were found to be more porous than corresponding SIPNs which resulted in higher swelling for the CP hydrogels. While the swelling of SIPN hydrogels showed discontinuous temperature dependency, CP hydrogels showed gradual decrease in water retention values with increase in temperature.. Lysozyme was loaded in the hydrogels and its in vitro release was studied in various pH, temperature and in presence of a reducing agent, glutathione (GSH). The release rate was found to be maximum at lower temperature, lower pH and in presence of GSH.

References

[35]Dutta, S.; Samanta, P.; Dhara, D. *J. Biol. Mac.* 2016, 87, 92-100
[36]Deb Barman, T.; Dhara, D. Unpublished results

MACRO 278

Synthesis of Glycerol Based Dendrimers for Dual Targeted Drug Delivery Applications

Killi Naresh, Gundloori Rathana VN*

Polymer Science and Engineering Division, CSIR-National Chemical Laboratory,
Dr. Homi bhabha Road, Pune, India-411008

Email ID: rv.gundloori@ncl.res.in

Dendrimers are hyper branched macromolecules with high density functional groups. These are well defined symmetric, nano-sized, homogeneous and monodisperse molecules [1]. The architecture of dendrimers is unique having core, branches and terminal functional groups. The desired physicochemical or biological properties can be attained by changing the terminal functional groups of the dendrimers. Therefore, dendrimers are recommended for different applications like catalysis, sensors, super molecular chemistry and biomedical applications [2]. Dendrimers like polyesters, polyglycerol and polyimine are commercially available and FDA

approved. These are being used in biomedical applications for example, PAMAM and Polyglycerol based dendrimers FDA approved and are being used as drug carriers in drug delivery [3]. Though commercial dendrimers such as Stratus@ CS, Acute Care TM (Dade Behring) are used for cardiac diagnostic testing, Super Fect ™ (Qiagen) is used as gene transfection agent applicable to a broad range of cell lines and PAMAM dendrimers are available for various applications. To expand the scope of the dendrimers and to enhance the properties, there is always a need for designing new dendrimers.

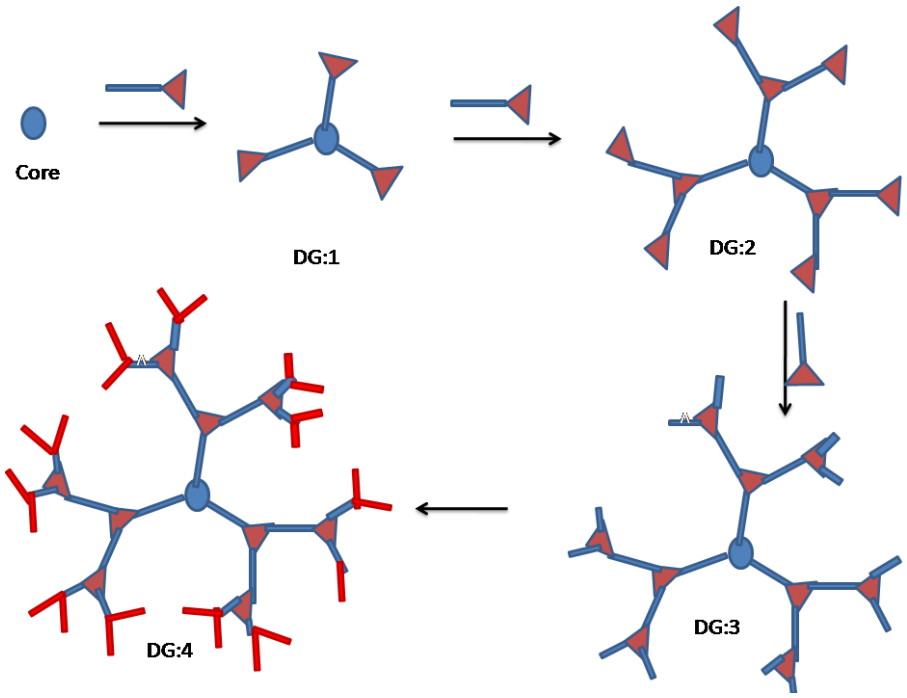


Figure 1: Schematic diagram for synthesis of stimuli responsive dendrimer

Designing and understanding the structural and functional properties of stimuli response dendrimers will definitely provide scope for these in various applications, such as drug delivery, biosensors etc. It is in this context, we propose to design stimuli responsive dendrimers using biocompatible polymers with suitable functional groups. Accordingly we designed and synthesized stimuli responsive dendrimers using polyethylene glycol (PEG) and poly (L-lactide) (PLA) to obtained dendrimer generation 4. Which were confirmed by UV-Visible, FT-IT, NMR and MALDI-ToF. The molecular weight of the dendrimers was determined by GPC. The molecular weight the denderimer is ~ 9000 D. aand the chromatogram peak shifted with increasing the generation of the dendrimer. Cell viability studies were performed and it is found that the dendrimers were viable to normal cells. Stimuli responsive studies were performed using pH 4 and 8 and temperature ranging from 25 to 65 °C. The dendrimer exhibits good stimuli responsive properties. Hence this material can be used for targeted drug delivery and sensor applications.

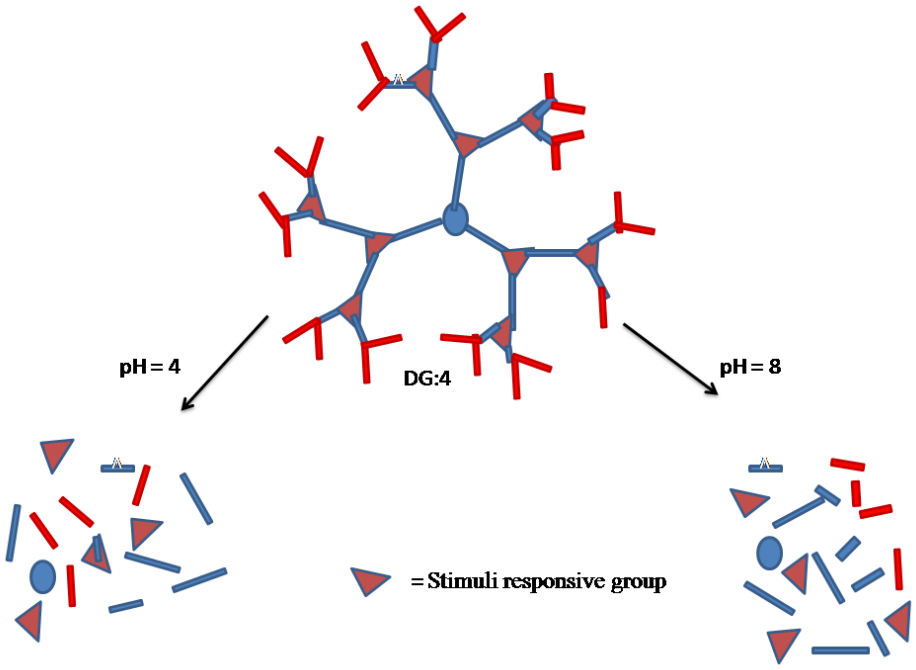


Figure 1: Schematic diagram for pH responsive dendrimer

References

[37] Abbasi, Elham; Aval, Sedigheh Fekri; Abolfazl, Akbarzadeh; Morteza, Milani; Hamid, Tayefi Nasrabadi; Sang, Woo Joo; Younes, Hanifehpour; Kazem, Nejati-Koshki; Roghiyeh Pashaei-Asl. *Nanoscale Research Letters*, 9 **(**2014) 247.

[38] Yulei, Chang; Li, Yapeng; Xinlei, Meng; Nian, Liu; Dexin, Sun; Huan, Liua; Jingyuan, Wanga. *Polym. Chem.*, 4 (2013) 789.

[39] Mura, Simona; Julien, Nicolas; Couvreur, Patrick. *Nature Materials.* 12 (2013) 991.

MACRO 282

L-Amino acid Based Enzyme and pH Dual Responsive Nano-carrier for Multi-drug Delivery to Cancer Cells

Saxena, Sonashree and Jayakannan, Manickam *

Department of Chemistry, Indian Institute of Science Education and Research-Pune, Dr. Homi Bhabha Road, Pune 411008, Maharashtra, India

** Corresponding Author: jayakannan@iiserpune.ac.in*

L-Amino acids are natural building blocks in proteins and new synthetic polymers based on these important bio-resources can mimic functionalities and self-assemblies as observed in the living systems. We

have developed new melt poly-condensation strategies to make a new class of linear and hyper-branched poly (ester-urethane)s and polyesters.[1-5] Here, thermo-selective polymerization was adopted to make new classes of lysosomal enzyme cleavable pH-responsive amphiphilic polyesters based on L-aspartic acid resources. These polyesters were designed having pH responsive BOC urethane units in the side chains of each repeating monomer comprising the polymer. The polymers were also optimized for amphiphilicity by carefully varying the hydrophobic 1, 12-dodecanediol and hydrophilic tri-ethylene glycols in the poly-condensation process. These amphiphilic polyesters self-assembled as nanoparticles and exhibited loading of a wide range of florescent anti-cancer drugs. The BOC units were found to cleave under acidic pH= 6.0-4.0, to generate cationic species which led to the disassembly of the cargo loaded nano-scaffold thereby delivering them into the acidic regions of the cells.[6] At extracellular conditions, i.e. pH=7.4, these nano-scaffold were stable enough to hold the drugs, however were found to degrade in the presence of lysosomal esterase enzyme to deliver the cargo. These studies were performed using *in-vitro* drug release experiments using UV-absorption as a probe. A range of anti-cancer drugs such as doxorubicin (DOX), topotecan (TOP), and curcumin (CUR) were successfully loaded into these nano-scaffolds and were found to kill the cancer cells such as HeLa and MCF-7 cells, despite been highly non-toxic in their nascent state.

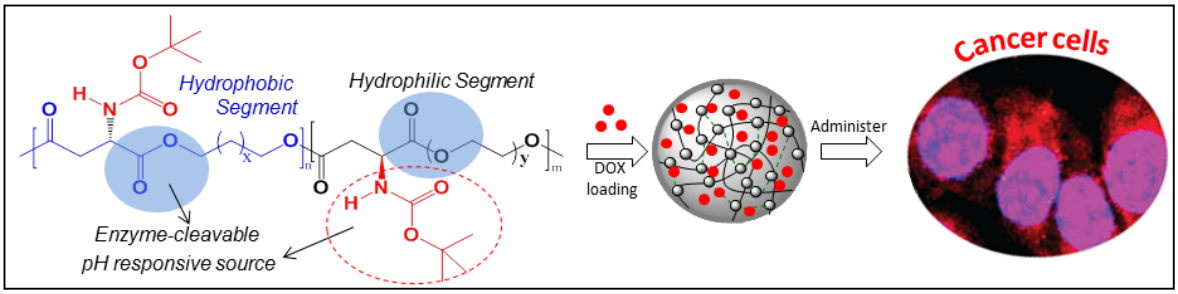


Figure 1. pH Responsive and enzyme biodegradable polymer nano-assemblies from L-amino acid is developed for drug delivery at the intracellular compartments to cancer cells.

References

[1] Santhanaraj, A.; Jayakannan, M. *Biomacromolecules*, 13 (2012) 2446.
[2] Santhanaraj, A.; Jayakannan, M. *Biomacromolecules*, 16 (2015) 1009.
[3] Santhanaraj, A.; Jayakannan, M. *J. Polym. Sci., Polym Chem.*, 2016**, (**10.1002/pola.28172).
[4] Santhanaraj, A.; Jayakannan, M. *J. Polym. Sci., Polym Chem.*, 54 (2016) 1065.
[5] Aluri. R.; Jayakannan, M. *Polym. Chem.***,** 6 (2015) 4641.
[6] Saxena. S.; Jayakannan, M. *J. Polym. Sci., Polym Chem.* 2016, POLA 20160301R1 (in press).

MACRO 283

π-Conjugated Fluorophore-*block*-Biodegradable Polymer Nano-carrier for Cellular Imaging and Drug Delivery

*Kulkarni, Bhagyashree and Jayakannan, Manickam **

Department of Chemistry Indian Institute of Science Education and Research, Dr. Homi Bhabha Road, Pune 411008.INDIA

**Correspondence:* jayakannan@iiserpune.ac.in

Multipurpose polymer nano-scaffolds for cellular imaging and delivery of anticancer drug are required for the cancer therapy. This investigation reports a new polymer drug delivery concept based on biodegradable polycaprolactone (PCL) and highly luminescent π-conjugated fluorophore as dual functional nano-carrier for cellular imaging and delivery vehicles for anticancer drug to cancer cells. A new substituted caprolactone monomer was designed and it was subjected to ring opening polymerization using a blue bishydroxyl oligo-phenylenevinylene (OPV) fluorophore as an initiator[1,2] . A series of A-B-A tri-block copolymer building blocks with a fixed OPV π-core and variable chain biodegradable PCL arm length were tailor-made. These tri-blocks self-assembled in organic solvents to produce well defined helical nanofibers whereas in water they produced spherical nanoparticles with blue luminescence. The hydrophobic pocket of the polymer nanoparticle was found to be an efficient host for loading water insoluble anticancer drug such as doxorubicin (DOX). The photophysical studies revealed that there was no cross-talking between the OPV and DOX chromophores and their optical purity was retained in the nanoparticle assembly for cellular imaging. *In vitro* studies revealed that the biodegradable PCL arm was susceptible to enzymatic cleavage at the intracellular lysosomal esterase under physiological conditions to release the loaded drugs.The nascent nanoparticles were found to be non-toxic to cancer cells whereas the DOX loaded nanoparticles accomplished more than 80 % killing in HeLa cells. Confocal microscopic analysis confirmed the cell penetrating ability of the blue luminescent polymer nanoparticles and their accumulation preferably in the cytoplasm. The DOX loaded red luminescent polymer nanoparticles were also taken up by the cells and the drug was found to be accumulated at the peri-nuclear environment. The present investigation is one of the first examples to demonstrate the dual functional biodegradable luminescence nano-carrier concept and the studies established the proof-of-concept in cellular imaging and drug delivery in cancer cells.

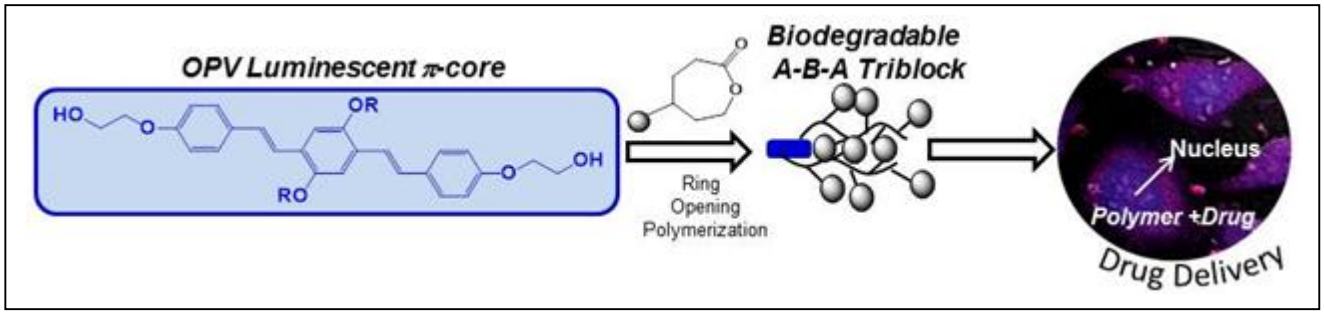


Figure 1. Biodegradable polymer tri-block copolymer approach for drug delivery and imaging in cancer cells.

References

[1] Kulkarni, B; Surnar, B; Jayakannan, M. *Biomacromolecules,* 17 (2016) 1004.
[2] Surnar, B.; Jayakannan, M. *Biomacromolecules,* 14 (2013) 4377.

MACRO 286

Polysaccharide-Cisplatin Vesicular Nano-scaffold for Combination Therapy in Cancer

Deshpande, Nilesh U. and Jayakannan, Manickam *

Department of Chemistry, Indian Institute of Science Education & Research (IISER-Pune)
Dr.Homi Bhabah Road, Pune 411008, Maharashtra, INDIA

** Corresponding Author : jayakannan@iiserpune.ac.in*

Conventional single drug therapy has inherent limitation in cancer treatment and hence combination therapy is often used to prevent the drug induced resistance in the cancer cells. Combination therapy based on the polymer drug conjugates[1] is emerging as one the best anticancer therapy. A single polymer scaffold having more than one drug can act better against the cancer to induce synergistic cell killing.[2-4] Herein we report the polysaccharide based polymer scaffold which is made by modifying the hydrophilic dextran backbone with hydrophobic unit pentadecylphenol along with several carboxylic units as 4-(tert-butoxy)-4-oxobutanoic acid and the formed structure were characterized by NMR techniques.[5] The formed carboxylic dextran scaffold self assembled in aqueous media to form vesicular assemblies, confirmed by AFM analysis, TEM analysis. The formed carboxylic dextran structures upon reaction with cisplatin aqua complex forms the cisplatin stitched dextran vesicles which further used for loading and delivery of hydrophilic doxorubicin (DOX.HCL) and hydrophobic camptothecin (CPT) anticancer drugs. The morphology of this triple loaded dextran vesicles were confirmed by AFM, TEM analysis. These triple loaded dextran vesicles are stable under the physiological condition but immediately rupture upon the exposure to the lysosomal enzymes like esterase at the intracellular compartment. Cytotoxicity studies for the dextran vesicles and its drug loaded form were performed on breast cancer (MCF-7) cells, which shows that dextran vesicles were not cytotoxic upto the concentration of 80 µg/mL where as the cisplatin vesicles could able to bring the 90% cytotoxicity at 10µg concentration of cisplatin. Similarly the cytotoxicity for the double and triple loaded dextran vesicles were checked which shows that 100 % cytotoxicity can be achieved at much lower concentration than the alone cisplatin stitched vesicles.

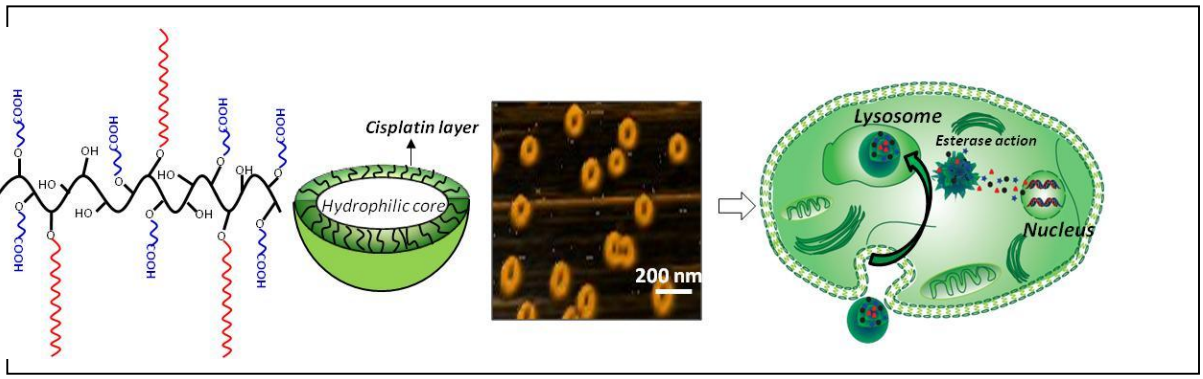


Figure 1. Enzyme-responsive Polysaccharide vesicles for combination therapy in cancer cells

References

[1] Surnar, B.; Sharma, K.; Jayakannan, M. *Nanoscale*, 7 (2015) 17964.

[2] Pramod, P.S.; Takamura, K.; Chaphekar, S.; Balasubramanian, N.; Jayakannan, M.; *Biomacromolecules***,** *13* (2012) 3627.

[3] Pramod, P.S.;Shah,R.; Jayakannan, M**.** *Nanoscale*, 6 (2014) 11841.

[4] Pramod, P.S.; Shah, R.; Jayakannan, M**.** *Nanoscale*, 7 (2014) 6636.

[5] Nilesh, U. D.; Jayakannan, M. *Manuscript submitted*.

MACRO 287

Dynamic Self Assembly of Polyarginine based Polypeptides for Biomedical Applications

Korra,Praveen[a].;Pandey, Bhawana[a] and Sen Gupta,Sayam[a]*

[a]Chemical Engineering Division, CSIR-National Chemical Laboratory, Dr. Homi Bhabha Road, Pune 411008, India

*E-mail: ss.sengupta@ncl.res.in.

Stimuli responsive polymers are growing rapidly, in recent years because of its vast application in biotechnology and drug delivery systems. Usually stimuli responsive nature in amphiphilic polymers incorporated covalently using tedious organic synthesis.[1] In case of "superamphiphile", stimuli responsive nature incorporated in amphiphilic polymers via non covalent interactions, thus excluding tedious organic synthesis. Hence the concept of "superamphiphiles" emerged as an alternative and powerful tool for forming self-assembled stimuli responsive structures. Various non-covalent interactions, such as hydrogen bonding, host-guest interactions, charge transfer interactions, $\pi - \pi$ interactions and electrostatic interactions used as driving force for the formation of superamphiphiles.[2] Various small molecules and polymers used as building blocks in self-assembly of superamphiphiles. There are several reports on the synthesis of stimuli responsive superampiphiles.[3] Herein, we prepared stimuli responsive (pH) superamphiphile from self assembly of cationic block polymer (PEG_{2k} -Ph-Ar_{30}) with anionic form of modified dexamethasone (anticancer drug). The cationic block copolymer is synthesized from polymerisation of NCA of guanidinium modified *L*-Lysine with amine terminated polyethylene glycol $(PEG)_{2k.}$ Synthesis of polymers are well characterised by ^{1}H NMR and GPC techniques. The self assembled structures are characterised by DLS, TEM and AFM. For future application we are trying to use this system in stimuli responsive drug delivery.

References:

1. C. Wang, Y. S. Guo, Y. P. Wang, H. P. Xu, X. Zhang, *Angew. Chem*.2009, 121, 9124.
2. A. Harada,K. Kataoka, *Science* 1999, 283, 65.
3. A. Harada, K. Kataoka, Macromolecules 1995, 28, 5294;

MACRO 288

Random and Block Copolymer Polycaprolactone Nano-assemblies for Drug Delivery

Malhotra, Mehak and Jayakannan, Manickam*

Department of Chemistry, Indian Institute of Science Education and Research-Pune,

Dr. Homi Bhabha Road, Pune 411008, Maharashtra, India

** Corresponding Author: jayakannan@iiserpune.ac.in*

Polycaprolactone (PCL) has been an indispensable part of the biomaterials arena due to its high mechanical strength, low melting point, excellent rheological and viscoelastic properties and superior blend compatibility. Here, we report a new class of complete biodegradable amphiphilic random and block copolymer design based on carboxylic functional polycaprolactone- co-polycaprolactone, wherein we tuned their enzyme-controlled delivering capabilities at the intracellular compartments for doxorubicin (DOX) drug in breast (MCF 7) and cervical (HeLa) cancer cells [1]. The amphiphilic nature was attained by systematically controlling the composition of the hydrophilic carboxylic PCL units in the hydrophobic PCL backbone via ring opening polymerization methodology [2]. For this purpose, a new carboxylic substituted monomer was synthesized and copolymerized with caprolactone to result in the desired random and block copolymers. The amphiphilic polymers self-assembled into < 200 nm nanoparticles in water and exhibited excellent capability for doxorubicin loading in their hydrophobic pocket. *In vitro* drug release kinetics revealed the polymer nano-scaffolds' exclusive susceptibility to rupture in the presence of lysosomal esterase enzyme to deliver DOX. Their 'slow' and 'burst' release kinetics was indirectly controlled by the composition of the random copolymers. For instance, the random copolymer with equimolar amounts of hydrophobic PCL and hydrophilic carboxylic PCL in the backbone was found to undergo "controlled enzymatic-biodegradation" at the intracellular compartment environment. The complete biodegradation of the polymer scaffolds by the enzymatic process was confirmed by *in vitro* dynamic light scattering studies and analysis of the degraded products by mass spectroscopy. *In vitro* cytotoxicity studies in MCF 7 and HeLa cell lines revealed that the newly designed polymer scaffolds are non-toxic to cells and their DOX loaded nanoparticles exhibited more than > 90 % cell death. Confocal microscope analysis confirmed the internalization of the polymer-loaded drugs and indicated that the drugs are predominately delivered at the nucleus of the cells for complete cell killing.

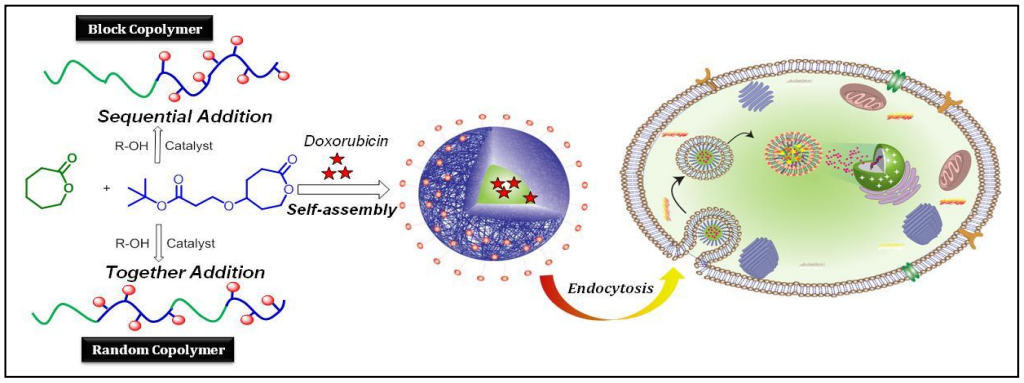


Figure 1. Programming the enzymatic biodegradation of functional polycaprolactone at the intracellular compartments and delivery of DOX to the nucleus of the cancer cells.

References

[40]Malhotra, M.; Surnar, B.; Jayakannan, M. *Manuscript submitted.*
[41]Surnar, B.; Jayakannan, M. *Biomacromolecules*, 14 (2013) 4377.

MACRO 300

Synthesis and design of Curcumin Based Gels

Metta Lokanadham and Gundloori Rathna VN.*

Polymer Science and Engineering Division, CSIR-National Chemical Laboratory,

Dr. Homi bhabha Road, Pune, Maharastra-411008, India.

* *e-mail id*: rv.gundloori@ncl.res.in

Abstract

Gels of acrylic acid are being used as super absorbent for diaper applications. The cross linkers used in these studies are either bis-acrylamide or ethylene glycol dimethacrylate. These chemical cross linkers are toxic, to replace these, we propose to synthesize a new cross linker using curcumin, which is obtained from natural resource, *curcumin longa* (a turmeric herbaceous plant). Accordingly, we synthesized curcumin diacrylates using acryloyl chloride and prepared the gels of acrylic acid using curcumin diacrylate in various concentrations by free radical polymerization method. The synthesized cross linker was characterized by UV, FT-IR, and NMR spectroscopes. The gels were characterized by FT-IR, and DSC.

Keywords: *Curcumin, gels, biomedical applications, acrylate, cross linking.*

Introduction

Curcumin (CUM) which constitutes 90% of turmeric (diferuloylmethane) is extensively used as a spice, food preservative and colouring material in South East Asia [1-2]. In addition, it is being used as a house-hold remedy for various diseases, like biliary disorders, anorexia, cough, diabetic wounds, hepatic disorders, rheumatism and sinusitis. For the past few decades, extensive research has been done on curcumin to establish the biological and pharmacological actions, which posses a wide spectrum of biological properties such as antioxidant, anti-inflammatory, antibacterial, antifungal anti-parasitic anticancer anticoagulant, anti-protozoal, antiviral, anti-fibrotic, anti-venom, antiulcer, hypo-tensive and hypo-cholesteremic properties[1-12]. However poor water solubility of CUM has limited its application. Hence, research is under progress to enhance its water solubility [3]. Generally, phenolic groups of CUM are being modified to enhance the solubility. Studies on CUR and or modified CUR entrapped in polymer matrix used for wound dressing materials showed an initial burst with sustained release[13]. Encapsulation of CUR in various polymeric materials for drug delivery applications have been reported[14-18]. Various biocompatible polymers are being designed and fabricated in the form of gels, films and nanofibers with and without drugs to encounter wound healing by regeneration of tissue[19].

Gels are three dimensional material and used in different application like biomedical, sensors etc. Curcumin based gels will be biodegradable because the starting material obtained by plant. High performance gels with enhanced properties are more in demand for biomedical application. Hence our

objectives of the work are to synthesize curcumin diacrylate as a cross linker and preparation of gels using acrylic acid and curcumin diacrylate.

Experimental

Materials

Curcumin, (Sd fine-CHEM limited Mumbai-30, India), acrylic acid, benzoyl chloride, hydroquinone, 2,2-azobisisobutyronitrile (AIBN), dimethylformamide (DMF), and dichloromethane (DCM) were purchased from Merk Chemicals, Mumbai, India. Acryloyl chloride was synthesized from acrylic acid and benzoyl chloride according to the reported literature.

Measurements

Thin-layer chromatography (TLC) was performed on Silica gel 60 F254 (Merck kGaA 64271 Darmstadt, Germany) with detection by UV light. ^{1}H and ^{13}C NMR spectra were recorded on Bruker AV 200, in solvents, deuterated chloroform ($CDCl_3$) and dimethylsulfoxide (DMSO-d_6). Chemical shifts (δ) were given in ppm. Infrared spectra (KBr disks) were recorded with a Perkins Elmer spectrometer I, FTIR diffused reflectance (DRIFT) mode, USA. The wave numbers (ν) of recorded IR-signals were quoted in cm^{-1}. The mass spectrum was recorded by *Thermo Fisher Q Exactive Focus Mass Spectrometer.* The thermal properties of CUM based gels were determined by differential scanning Calorimetry (DSC). The data for the respective 5 mg sample was recorded on an instrument DSC-TA-Q10, in the temperature ranging from -90°C to 250 °C. A controlled heating and cooling rate was maintained at 5 °C min^{-1}. Experiments were performed under nitrogen atmosphere with a flow rate of 50 mL min^{-1}. Glass transition temperature (T_g) and melting temperature of polymer (T_m) were determined from the heating and cooling scans. UV-vis spectra were recorded using a UV 1601PC UV spectrophotometer, Shimadzu. Melting temperature of compound was determined using Melt-Temp, barnstead/Thermolyne 2555 kerperbaulenvard Dubuque/Iowa 52001, U.S.A.

Methods

Synthesis of acryloyl chloride from acrylic acid:

25 mL (0.3625 gmol) of acrylic acid and 75 mL (0.645 gmol) of benzyl chloride was taken in to the 250 mL of round bottom flask. 1 mL of dried DMF as catalyst and pinch of hydroquinone was added to the reaction mixture for quenching of polymerization then the above complete reaction mixture was kept in oil bath for reflux at 75°C for 6h. After reflux the reaction mixture was distilled at 120°C the distilled acryloyl chloride was received to 50 mL of RB flask and stored less than 4°C. After distillation the remaining reaction mixture was quenched by saturated NaOH solution.

Synthesis of curcumin diacrylate:

5g (0.0135 gmol) of curcumin was dissolved in 50 mL of dried DCM in 100 mL of round bottom flask. 7.755 mL (5.626 gmol) of triethylamine was added to the reaction mixture and stirred for 10min at 0°C. Under same conditions 4.5 mL (5.05 gmol) of acryloyl chloride was added to the reaction mixture drop wise manner. After addition, the reaction mixture was allowed to stir under nitrogen atmosphere for 48 h at room temperature. After compilation of the reaction we conformed by TLC in 35% of ethyl acetate in pet. ether. The crude product was dissolved in ethyl acetate and washed with saturated aqueous solution of sodium bicarbonate. The organic layer was collected and dried using anhydrous sodium sulphate. The obtained product was concentrated by rota evaporation and dried under high

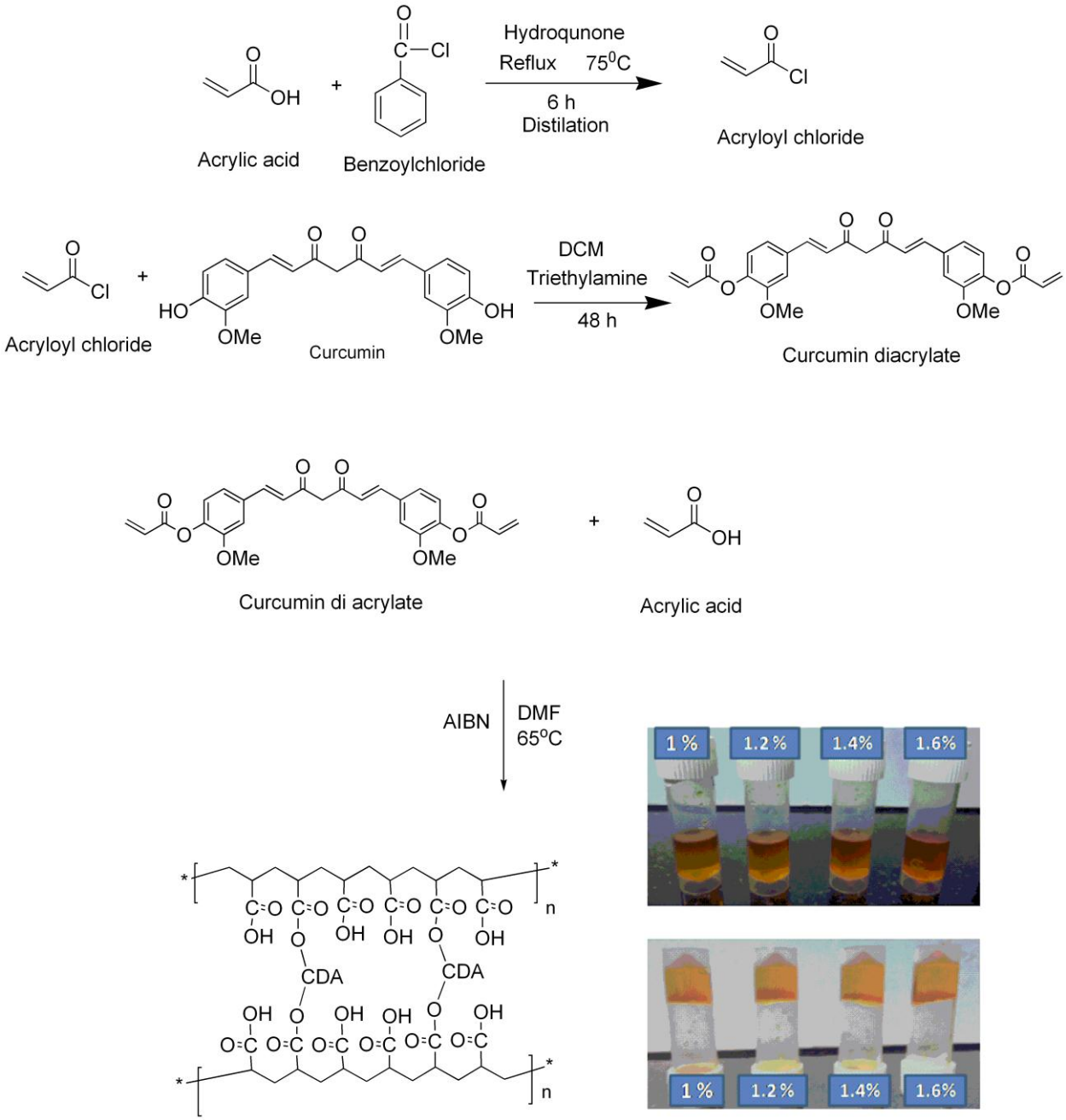
vacuum. The product was purified by column chromatograph, ethyl acetate and pet ether was used as mobile phases. (eluent 15% of ethyl acetate in pet ether) to obtain the pure curcumin diacrylate as a primary product and curcumin monoacrylate as a secondary product.

Synthesis of curcumin based gels:

25 mg (1%) of curcumin diacrylate and 176 µl (185 mg, 7.45%) of acrylic acid were dissolved in 2.5 mL of DMF then purged the reaction mixture with nitrogen gas for 15 min. After purging 4 mg of AIBN was added to the reaction mixture and again purged with nitrogen gas for 15 min. After purging the reaction mixture was kept at 65°C in water bath for crosslinking. Different compositions were prepared as nt concentrations as given in Table 1.

Table 1: Preparation of gels with different concentrations

Sr. No	**Acrylic acid**		**CUDA**		**AIBN**	**DMF**	**Time**	**Formation of gels**
	(µl)	**(%)**	**(mg)**	**(%)**	**(mg)**	**(mL)**	**(h)**	**Yes/No**
1	176	7.4	25	1	4	2.5	24	Yes
2	176	7.4	30	1.2	4	2.5	24	Yes
3	176	7.4	35	1.4	4	2.5	24	Yes
4	165	6.6	40	1.6	4	2.5	24	Yes



Scheme 1: synthesis of curcumin based gel

Results and discussion

Curcumin diacrylate (CUMDA) was synthesized by reacting curcumin with acryloyl chloride and the schematic diagram shown in scheme 1. The pure compound was separated by column chromatography to attain the respective product. As a result, the obtained yield of (CUMDA) was 76 %. The structure of the (CUMDA) was confirmed by UV-vis, FTIR, ^{1}H, ^{13}C NMR and mass spectrometer. The wave length (λ_{max}) of curcumin was 423 nm but the wavelength of (CUMDA) shifted to lower value (413 nm) due to the formation of ester bond between curcumin and acrylic/methacrylic group.

The characteristic absorption bands for (CUMDA) due to the presence of -C=C,-COO, appeared at around 2936 cm^{-1} (H-C=C in alkenes), 2895 cm^{-1} (CH_3-C=C), 1747 cm^{-1} (O=C-O). 1633 cm^{-1} (α, β-unsaturated carbonyl group), 1526, and 1456 cm^{-1} (H-C=C in aromatic). A peak at 1747 cm^{-1} indicated the formation of ester bond due to the reaction between phenolic group of curcumin and acryloyl chloride.

Proton NMR spectra of (CUMDA) showed the characteristic signals, which appeared at 7.76 δ (d, β-hydrogen in α, β- unsaturated C=O group), 7.11-6.41 δ (aromatic hydrogens), 6.16 δ (=CH) (*cis* to carbonyl in acrylic group), 5.9 δ (=CH) (*trans* to carbonyl in acrylic group), 5.75 δ (s, methylene group), 3.87 δ (s, methoxy groups) and 1.78 (t, 1H in acrylic group). ^{13}C NMR spectra of (CUMDA) showed the characteristic signals at 184-181 δ (α, β- unsaturated C=O group), 164 δ (C=O in ester), 151, 148, 139, 134, 127, 123, 121, 111, 101, 56 (CH_2), 56.01 (OCH_3), which conformed the synthesis of (CUMDA).

Curcumin based gels were prepared with different concentration of (CUMDA) by free radical polymerization using AIBN as an initiator. Scheme 1 shows the preparation of gels (1%, 1.2%, 1.4% and 1.6%). The obtained gels were characterized by FTIR, XRD. The FT-IR spectra for gels showed the characteristic absorption bands which appeared at around 3540 cm^{-1} (-OH), 2960 cm^{-1}, (H-C=C in alkanes), 2856 cm^{-1}, (H-C-C in alkanes)1757 cm^{-1} (O=C-O) and 1635 cm^{-1} (α, β-unsaturated carbonyl group), 1526 cm^{-1} and 1462 cm^{-1} (H-C=C in aromatic).

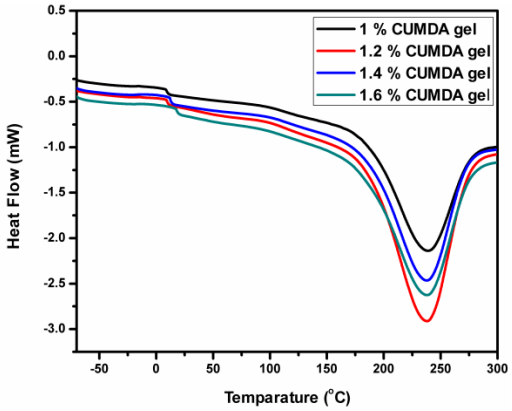


Figure 1: DSC data of gels

The melting temperature (T_m) was studied by DSC. According to literature the CUR melting temperature was 183 °C, however our experimental value ranged from 179-184°C, indicating that

the curcumin used was a mixture of CUR isomers. Gels (1%, 1.2%, 1.4% and 1.6%) showed melting transition temperatures (T_m) ranging from 235-238 °C. Increase in melting temperature.

Conclusions

We successfully synthesis the curcumin diacrylate as a cross linker and it was confirmed by spectroscopic methods. Curcumin based gels were prepared with different concentration of curcumin diacrylate. The swelling studies, DSC, XRD, mechanical properties, and cytoxicity have to be studied

Acknowledgements

Authors are grateful to CSIR, New Delhi for the financial support (projects CSC0302 and CSC0134).

References

1. M. L. Gujral, N. K. Chowdhury and P. N. Saxena, J. Indian Med., Assoc. 22, 273-276, 1953.
2. V. P. Menon and A. R. Sudheer, *Adv. Exp. Med. Biol.,* 595, 105-125, 2005.
3. E. Schraufstatter and H. Bernt, *Nature.*, 164, 456-457, 1949.
4. C. V. B. Martins, D. L. da Silva, A. T. M. Neres, T. F. F. Magalhaes, G. A. Watanabe, L. V. Modolo, A. A. Sabino, A. De Fatima and M. A. de Resende, *J. Antimicrob. Chemoth,*. 63, 337-339, 2009.
5. Md. Shahiduzzaman, and D. Arwid, *Nature Helps*: *Parasitology Research Monograph.,,* 1, 141-152, 2011.
6. B. B. Aggarwal, A. Kumar and A. C. Bharti, *Anticancer Re.*, 23, 363-398, 2003.
7. D. C. Kim, S. K. Ku and J. S. Bae, *BMB Rep.,* 45, 221-226, 2012.
8. H. B. Rasmussen, S. B. Christensen, L. P. Kvist and A. Karazmi, *Planta. Med.*, 66, 396-398, 2000.
9. R. K. Singh, D. Rai, D. Yadav, A. Bhargava, J. Balzarini and E. De Clercq, *Eur. J. Med. Chem*., 45, 1078-1086, 2010.
10. M. Tuorkey and K. Karolin, *Biomed. Environ. Sci*., 22, 488-495, 2009.
11. T. S. Rao, N. Basu, S. D. Seth and H. H. Siddiqui, Indian J. PhysiolPharmacol., 28, 211-215, 1984.
12. M. Kim and Y. Kim, Nutr. Res. Pract., 4, 191-195, 2010.
13. J. G. Merrell, S. W. McLaughlin, L. Tie, C. T. Laurencin, A. F. Chen and L. S. Nair, *Clin. Exp. Pharmacol. Physiol*., 36, 1149-1156, 2009.
14. R. K. Das, N. Kasoju and U. Bora, *Nanomedicine.*, 6, 153-160, 2010.
15. J. Shaikh, D. D. Ankola, V. Beniwal, D. Singh and M. N. V. R. Kumar, *Eur. J. Pharm. Sci*., 37, 223-230, 2009.

16. S. Bisht, G. Feldmann, S. Soni, R. Ravi, C. Karikar and A. Maitra, *J. Nanobiotechn.*, 5, 3, 2007.
17. M. M. Y. K. Vimala, K. Varaprasad, N. Narayana Reddy, S. Ravindra, N. Sudhakar Naidu and K. Mohana Raju *J. Biomate. Nanobiotech*., 2, 55-64, 2011.
18. M. H. L. Phuong Thu Ha1, Thi My Nhung Hoang3, Thi Thu Huong Le4, Tuan Quang Duong5, Thi Hong Ha Tran2, Dai Lam Tran1 and Xuan Phuc Nguyen, *Advances in Natural Sciences: Nanoscience and Nanotechnology*., 3, 035002-035007, 2012.
19. R. Sridhar, K. Madhaiyan, S. Sundarrajan, A. Gora, J. R. Venugopal and S. Ramakrishna, *J. Mat. Chem. B.*, 2, 1626-1633, 2014.
20. Enas M.Ahmed *Journals advanced research* 6, 105-121, 2015.
21. Aysegul Altunbas, SeungJ.Lee, SigridA. Rajasekaran, Joelp.Schneider, DarrinJ.Pochan., *Biomaterials.*, 32, 5906-5914, 2011.
22. Y.ke, Gs.Liu, J.H.wang, w.xue,C.Du, G.Wu., *express polymer Letters*., 8, 841-849, 2014.
23. K.Varaprasad, Y.Murali Mohan, K.Vimala, K.Mohan Raju, *Journal of applied polymers Science*., 121, 784-796, 2011.
24. Yumin Zhang, Cuihong yang, WeiweiWang, Jijian liu, Qiang liu, Fan Huang, chu, Honglingao, Chenli, Deling kong, Qianliu, and Jianfeng liu, *Scientific reports*, 6-21225-2016.

MACRO 312

Rheological behavior of the biocomposites based on

Poly(lactic acid)/jute fibers

Mohammad Tahir Zafar*, Saurindra Nath Maiti, Anup Kumar Ghosh

Centre for Polymer Science and Engineering, Indian Institute of Technology Delhi,

New Delhi 110 016, India

*Corresponding author:

Mob no: +91-9540770072, E-mail: tahir.zafar6@gmail.com

1. Abstract:

In the present research work, biocomposites of poly(lactic acid) (PLA)/jute fibers were prepared by melt compounding the short jute fibers with PLA in a twin screw extruder at different weight percentage (wt%) of jute fiber. Prior to the compounding, in order to improve the matrix fiber interface adhesion, jute fiber were surface treated using NaOH and (NaOH+Silane), separately. The shear and dynamic rheological behavior of the biocomposites prepared with untreated and surface treated jute fibers were studied using capillary and parallel plate rheometer respectively and the effects of jute fiber wt% and surface treatment on the various rheological properties of the biocomposites were studied.

2. Introduction: Due to the growing environmental concern of the non degradable polymeric materials researchers are focusing on the materials such as poly(lactic acid) (PLA), poly(caprolactone) (PCL), poly (butylene adipate terephthalate) (PBAT)which are degradable in nature [1] . PLA is a biobased material which can be produced from the corn. It has some draw backs such as low thermal stability, narrow processing window, and low impact strength. Reinforcement of the PLA using natural fibers such as jute, sisal, hemp, coir can overcome drawbacks associated with PLA [2] . Jute is a natural fiber which has very high percentage of cellulose and is abundant in India. Reinforcing PLA with jute fiber can be a way to overcome the problem associated with PLA.

3. Experimental:

Materials: PLA 3001D was purchased from the nature works® LLC, USA and the jute fibers were procured from the Chandra Prakash & Co. India. 3-Aminopropyltriethoxysilane (APTS) was purchased from M/s Sigma Aldrich.

Surface treatment and fabrication of the composites: In order to improve the matrix-fiber phase adhesion, surface treatment of the jute fibers were carried out as per the procedure describe elsewhere [3] . Compounding of the PLA with untreated and surface treated jute fibers at jute fiber content of 5, 10, 20 and 30wt% were carried out in a twin screw extruder at 200 °C. The extruded strands were pelletized and dried in the oven.

Characterization techniques:

High shear rheology of the PLA and the biocomposites was studied using Rosand RH7 twin bore capillary rheometer (Bohlin Instruments). The twin bore comprise a capillary die in one bore and the other is a reference die (orifice die). The experiment was conducted in the shear rate range of 100-3500 s^{-1} at the temperature of 190 °C, 200 °C, and 210 °C.

The dynamic viscoelastic behavior of the polymers was studied in a parallel plate rheometer by performing frequency sweep in SAOS (small amplitude oscillatory shear) mode. The plate in the rheometer used was

of 50 mm diameter. Linear viscoelastic region (LVR) was initially determined by an amplitude sweep test at constant frequency 10 rad/s by varying strain in the range of 0.001-10 %. Amplitude of 0.01 % was fixed for dynamic frequency sweep test. The viscoelastic parameters of the polymers such as storage modulus (G'), loss modulus (G"), and complex viscosity (η*) were measured using this instrument.

4. Results and discussion: Shear stresses increases with increases in the shear rate as well as with the jute fiber content and decreases with increases in the temperature. Further, shear viscosity also increases with increase in the jute fiber content and decreases with increases in the temperature. Surface treated jute fiber reinforced composites shows higher values of the shear stress and shear viscosity than the untreated jute fiber reinforced composites.

Amplitude sweep was carried out to find out the LVR region and the region near, 0.01% strain was found to be more linear in case of PLA and biocomposites, hence all the frequency sweep test were carried out at 0.01% strain. Addition of jute fibers increases the storage and loss modulus of the composites and the surface treated jute fiber reinforced composites has higher values of the storage and loss modulus than the untreated jute fiber reinforced composites.

4 References

[1] Mathew A. P., Oksman K. and Sain M., Journal of Applied Polymer Science, 97, 2014-2025 (2005).

[2] Biagiotti J., Puglia D. and Kenny J. M., Journal of Natural Fibers, 1, 37-68 (2004).

[3] Zafar M. T., Maiti S. N. and Ghosh A. K., Fibers and Polymers, 17, 266-274 (2016).

MACRO 329

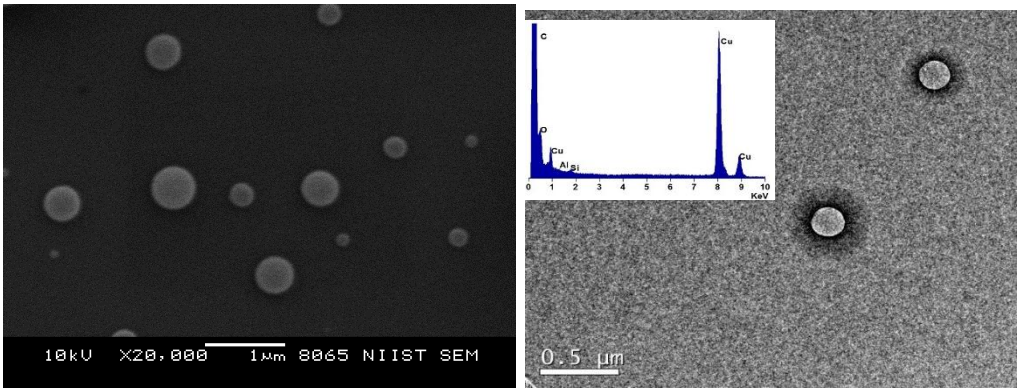
Templated Synthesis of pH Triggered Hydrolytically Cleavable Polylactic Acid Hollow Spheres Using Self-Assembled Layered Silicate Polystyrene Hybrid

Asha Susan Chacko, Vadakkethonippurathu Sivankuttynair Prasad*

National Institute for Interdisciplinary Science and Technology, Trivandrum, INDIA

vsprasad@niist.res.in

One dimensional uniform hollow spheres in nano/micro dimensions of biopolymers such as polylactic acid (PLA) homopolymer find applications in biomedicine in cancer chemotherapy as a biocompatible and biodegradable alternative to polyethylene glycol (PEG). In the present work, stable hollow PLA vesicles were fabricated by a facile synthetic strategy of using self-assembled inorganic-organic hybrid template. Fluorescein tagged protein conjugate of paclitaxel was loaded in this hydrolytically cleavable vesicle and pH dependent release behaviour was studied in vitro as a strategy to targeted delivery. Polystyrene- Montmorillonite (MMT)-Laponite PCN systems were synthesised by in situ block copolymerization using controlled radical polymerization and characterised for the self-assembly in various solvents by SEM, TEM and AFM analysis. The self-assembled soft vesicle template obtained in 0.1-2 µm diameters was used for molding the PLA hollow vesicles by varying the concentration of the polymer and optimized the conditions for fine tuning the size and shell thickness. Significant effect of dimension of layered silicate on the size of self-assembled vesicular template was observed in the case of laponite having lower lateral dimensions compared to MMT. Both of these layered silicate based templates showed considerable stability and showed retention of vesicular morphology with an optimum PLA content of 20 %. The results indicated pH dependent release of cargo from the loaded vesicle was monitored with time using fluorescent microscopy and UV-Vis spectroscopy which showed controlled release with time which may be attributed to the controlled hydrolysis of PLA under acidic conditions. The present result showed a novel strategy for cancer chemotherapy to reduce the toxic effects.



References

[42]Prasad, V. S.; Asha, S. C.; Nair, B. P.; Bijini, T. T.; Pavithran, C. Langmuir, 31(2015) 8260.
[43]Subramaniam, A. B.; Wan, J.; Gopinath, A.; Stone, H. A. Soft Matter, 7(2011) 2600.
[44]Ahmed, F.; Discher, D. E. J. Control. Release. 96(2004) 37.
[45] Liu, G-Y; Chen, C-J; Ji, J. Soft Matter, 8(2012) 8811.

MACRO 332

Biodegradable Nanoparticles for better Encapsulation of Hydrophilic Anticancer Drug Gemcitabine

Sachin S. Surwase, Susheela B. Idage, Bhaskar B. Idage*
Polymer Science & Engineering Division, CSIR-National Chemical Laboratory
Dr. Homi Bhabha Road, Pune - 411 008, INDIA
**e-mail id: bb.idage@ncl.res.in*

Abstract

The most widely used and preferred class of biodegradable polymers are the polyesters and co-polyesters. In the present work, the efforts have been made to prepare mPEG-PLLA, a biodegradable amphiphilic copolymer with a view to improve the entrapment and tuned release of hydrophilic drug Gemcitabine. The mPEG-PLLA copolymers with the varying ratios of L-lactide and mPEG were synthesized by ROP and the copolyesters were characterized by different techniques. Gemcitabine loaded nanoparticles were prepared using mPEG-PLLA copolymers by double emulsion solvent evaporation technique. The nanoparticles were assessed for their *in-vitro* release and also studied for their *in-vitro* cytotoxicity study with the help of cell line culture.

Keywords: *Biodegradable polymers, Gemcitabine, ring opening polymerization, double emulsion, tuned release*

Introduction

Gemcitabine is the first choice drug in several solid tumours. It is having low systemic toxicity as compared to the existing anticancer drugs. In order to get the better effect this drug should retain in the blood circulation for longer time without inactivation by any enzyme. Unfortunately, gemcitabine shows rapid inactivation because of enzyme called deoxycytidine deaminase. This metabolic inactivation is responsible for the short half-life of the very important anticancer drug.[1] It is crucial to protect the drug from this enzyme and to increase the half-life. Gemcitabine is a hydrophilic drug and it is always challenging to encapsulate the hydrophilic drug in order to increase the encapsulation efficiency (EE). Further hydrophilic drug delivery is difficult because of their fragility and poor cellular penetration.[2-3]

PLLA is the important member of the polyester family which is approved by FDA for the biomedical application. It is biodegradable, biocompatible and well studied polymer for the drug delivery application.[4-6] However, PLLA applications are limited due to their hydrophobicity, brittle nature, excessively long degradation time and limited loading of polar drugs. Nanoparticles based on PLLA accumulate blood proteins on their surface as they circulate through the body which attracts attention from immune cells. This nonspecific absorption of proteins results in removal of nanoparticles from circulation before reaching the tumour microenvironment.[7-8]

Architectural modification of degradable polymers by altering the chain length, crystallinity, and morphology has shown to bear significant effects on their degradation and drug-release profiles.[9] Copolymerization is an effective technique for changing and designing such properties of polymers. By using copolymers not only mechanical properties but also degradation and diffusion profiles will be varied.[10-12] Problems associated with delivery of hydrophilic compounds can be solved by careful design of the polymer architecture. This provides the tool to adjust the degradation rate and to vary the release from rapid to controlled release.[13] Drug-release also depends on chemical composition and molecular weight of polymer, which can be adjusted by copolymer hydrophilic-hydrophobic segments.[14] Modification of PLLA biopolymer with mPEG through

copolymerization can results into improved hydrophilicity, degradation rate, and reduced crystallinity.[15-16] The PLLA block of the copolymers provides hydrophobicity and excellent mechanical properties, while the hydrophilic PEG block helps in flexibility, stealth property and results in a significant increase in blood circulation time due to hindered particle uptake into the reticuloendothelial system.[17-18]

Experimental

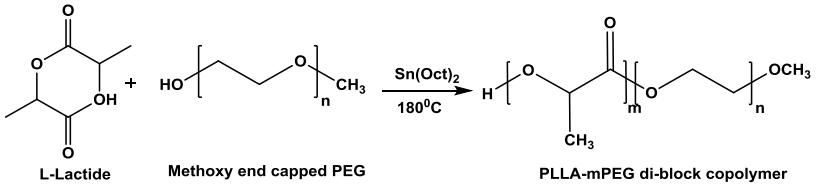
2.1. Materials

Monomethoxy ether polyethylene glycol (mPEG Mw 2000, 5000), Stannous octoate, 3-(4, 5-dimethyl) ethiazole (MTT) and fatal bovine serum (FBS) were purchased from Sigma-Aldrich chemicals, USA. L-lactide was obtained from Purac Biotech, Netherlands. Poly (vinyl Alcohol) (DOH: 85%), Span 80 and EDTA was purchased from Loba Chemie, Mumbai, India. Gemcitabine Hydrochloride was a gift from Sun Pharma, India. Water used in all the experiments was purified using a Milli-Q (Direct- Q3) system. HepG2 cells were purchased from the ATCC (Rockville, MD, USA).

2.2 Methods

2.2.1 Polymer synthesis

To a 50 mL glass ampoule were added the weighed quantities of purified l-lactide, varied amount of PEG and 0.05 wt% of tin octoate catalyst under dry nitrogen atmosphere. The reaction mixture was dried under reduced pressure at 60^{o}C for 3 h. The glass ampoule was sealed under reduced pressure and the ring opening polymerization was carried out at 180^{o}C for 1 h. After polymerization, the glass ampoule was cooled at room temperature, the seal was broken and the copolymer was removed by dissolving in chloroform and precipitating in petroleum ether. The copolymer obtained was separated by filtration, dried at 60^{o}C under reduced pressure and characterized by solution viscosity, gel permeation chromatography and thermal analysis.[19]



2.2.2 Preparation of Gemcitabine loaded mPEG-PLLA nanoparticles

The Gemcitabine loaded mPEG-PLLA nanoparticles (GeNP) were prepared by double-emulsion solvent evaporation method. Briefly, primary emulsion (w/o) was made by adding an aqueous solution (2 mg gemcitabine in 0.2 mL pure water) was added drop wise into an organic solution of the polymer (40 mg mPEG-PLLA in 2 mL chloroform) and was mixed using probe sonicator (Sonics Vibra-cell, USA). The primary emulsion was added drop wise into an aqueous solution that consisted of 40 mL polyvinyl alcohol (PVA) 0.5% (w/v) solution and secondary emulsion (w/o/w) was prepared. The organic phase was evaporated using

rotary evaporator. The suspension of nanoparticles was obtained which was then subjected to centrifugation at 16,000 rpm for 30 minutes. The supernatant containing PVA was decanted and the settled pellet was separated. At last, the resultant nanoparticles slurry was adjusted to 4 mL by addition of distilled water and sonicated and freeze dried further analysis.

2.2.3 Particle size analysis and zeta potential determination

Particle size distribution of mPEG-PLLA nanoparticles and Gemcitabine loaded nanoparticles was determined at 25ºC by particle size analyzer (Brookheaven Instruments, 90 Plus, USA) at a fixed angle of 90º.

2.2.4 Determination of entrapment efficiency

Initially, 1 mL of nanoparticle slurry was added into pre-weighed eppendorf tube and centrifuged at 10,000 rpm for 15 minutes. Then, the supernatant was fully removed and the pellet was dissolved in 0.1mL acetone proceeded by evaporation to dryness. It was sonicated with PBS (pH 7.4) for 15 minutes**.** The solution was filtered and diluted with PBS**.** The amount of Gemcitabine in the solution was determined by measuring the absorbance at 268 nm. Entrapment efficiency (EE) of drug-loaded nanoparticles was calculated.

2.2.5 Environment scanning electron microscopy

The morphology of mPEG-PLLA nanoparticles and GeNP were examined using environment scanning electron microscopy. A drop of nanoparticle suspension was carefully mounted on the silicon wafer fixed on ESEM stub. The mounted stubs were sputtered with gold using a coating unit and imaged.

2.2.6 *In-vitro* drug release study

In-vitro release profile of Gemcitabine from nanoparticle formulations was evaluated by the orbital incubator shaker apparatus. The dialysis membrane, cellulose acetate membrane (molecular mass cut off 14000 Da) was used as a semi-permeable membrane to mimic the natural bodily environment.

2.2.7 *In-vitro* cytotoxicity study

The cytotoxicity of the compounds in the cell lines was determined by the MTT [3-(4, 5 dimethylthiazol-2-yl)-2-5 diphenyl tetrazolium bromide] assay. Cells were seeded at 3 x 10^3 cells per well in 96-well plates. After 24 hours, the cells were treated with different concentrations (10 - 100 µg/ml) of plain drug

concentrations and drug loaded nanoparticles for 24 h and 48 h time periods.

Results and discussion

It is well studied that release of drug from polymer matrix remained slow because of polymer crystalinity and high molecular weight.[20] In order to achieve the controlled degradation of polymer it was integral to combat these limitations. It is well studied that if amount of chain initiator in feed is higher and monomer concentration is kept constant, copolymer is synthesized with decreased molecular weight. Same principle was observed and followed to control the degradation and release in a tuned manner.[15]

Table 1. Properties of PLLA-mPEG copolymer and nanoparticles prepared by double emulsion method

Sr. No.	Polymer Code	Mn (g/mol)	Mw (g/mol)	PDI	IV[c] (dL/g)	Yield (%)	NP Size (nm)	PDI	Zeta Potential	EE (%)
1.	PLLAm-PEG1	33800[a]	51400	1.5	0.62	96	196	0.229	-15	27
2.	PLLA-mPEG2	30100[a]	44800	1.48	0.59	96	160	0.124	-20	26
3.	PLLA-mPEG3	21000[b]	31500	1.5	0.32	95	207	0.137	-19	40

Gemcitabine is a hydrophilic drug and 'highly soluble' in aqueous media. Since nanoprecipitation uses the principle of two miscible solvents, the probability of escape of drug to the aqueous media is high.[21] To overcome this limitation and to increase the drug entrapment, double emulsion solvent evaporation technique was utilized. This method is relatively simple, convenient in controlling process parameters and has higher entrapment efficiency than previously adopted methods. In case of double emulsion method, entrapment efficiency was found to be 40%. Increase in mPEG concentration increased the amount of drug entrapped.[22] It was found that amount of drug loaded was high in case of higher amount of mPEG. This could be due to availability of hydrophilic environment to the drug due to hydrophilic nature of mPEG, which can entrap hydrophilic drug. PDI was also found to be reduced in high mPEG containing polymer and there was no profound effect on zeta potential of the nanoparticles as seen in table 1.

The GeNPs showed increase in release of gemcitabine with increasing the concentration of mPEG. This altered release kinetics of the encapsulated drug may be due to alteration of crystalline nature of PLLA to semi-crystalline copolymer mPEG-PLLA. The release of encapsulated therapeutic agent from biodegradable polymeric matrix occurs mainly through diffusion and degradation. It is well studied that initially diffusion is responsible for release which is followed by both diffusion and degradation.[23] The copolymer containing 5% mPEG released the less amount of drug. This could be due to more crystalline nature of copolymer and higher molecular weight which degrades slowly as compared to 10% and 20% of mPEG. Interestingly, copolymer with 20 % of mPEG degrades readily and release more amount of drug due to its semicrystalline nature attributed to mPEG. With varying the mPEG amount the crystalinity and hydrophobicity of the polymer can be customized, which is responsible for the encapsulation of hydrophilic drug and release of the drug from polymeric nanoparticles. Hence, the release of the drug can be accelerated to the need.

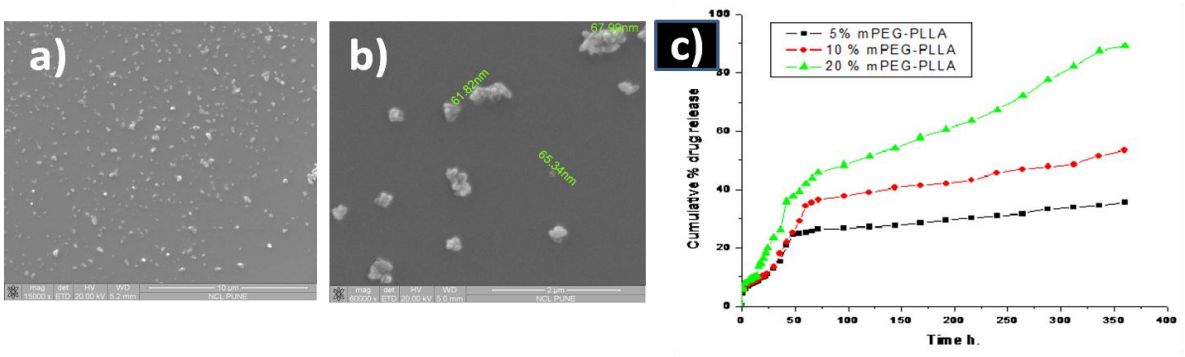


Figure 1. SEM images (a. and b.) of NPs prepared from the copolymers and (c) their release profile

It is observed from Figure 2 that at lower concentration GeNP's inhibits more cells as compared to free Gemcitabine. If the IC50 value of free drug and drug encapsulated inside the NP were compared, it is clear that NP shows better effect than free drug. The IC50 concentration of GeNP is very less as compared to free drug. This effect could be due to controlled release of drug inside polymer which is not available for action. With increase in the concentration of drug inside NP; it constantly inhibited the cell population growth, which is desirable for anticancer effect. Optimum concentration was found to be 50µg/ml, where it showed maximum effect with inhibition of more than 90 % cell population.

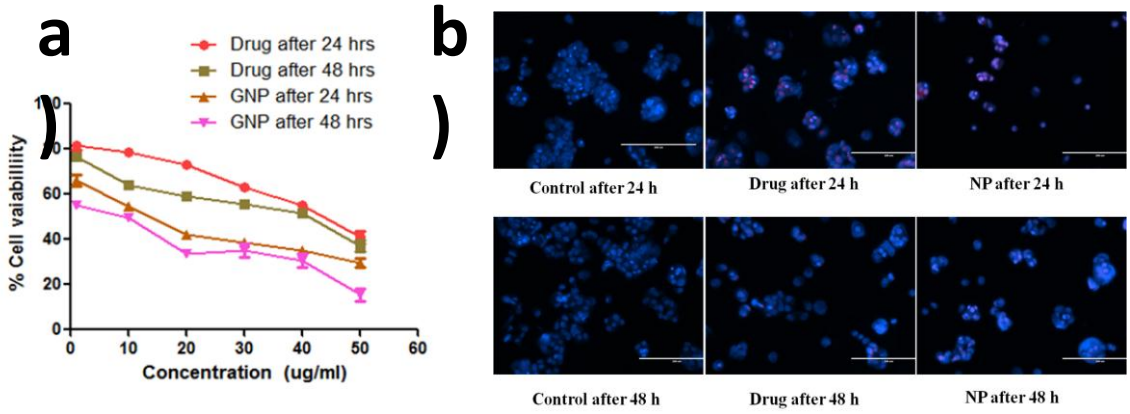


Figure 2. MTT assay and fluorescence microscopy images of the HepG2 cells after treatment with bare drug and NPs containing drug.

Conclusions

This study demonstrates the successful synthesis of mPEG-PLLA copolymers with tailored surface properties of nanoparticles and increased encapsulation of gemcitabine hydrochloride inside the amphiphilic copolymer with modified architecture. Hence, this present study will be useful for successful encapsulation of hydrophilic drug and will also act as attractive tool for tailoring the surface properties of polymeric nanoparticles for controlled and tuned release.

Acknowledgements

The authors gratefully acknowledge the CSIR-NCL for providing the facilities.

References

1. Zhang, Y.; Kim, W. Y.; Huang, L. *Biomaterials* 2013, *34*, 3447.
2. Vrignaud, S.; Benoit, J.-P.; Saulnier, P. *Biomaterials* 2011, *32*, 8593.
3. Cohen-Sela, E.; Chorny, M.; Koroukhov, N.; Danenberg, H. D.; Golomb, G. *Journal of Controlled Release* 2009, *133*, 90.
4. Chen, C.; Lv, G.; Pan, C.; Song, M.; Wu, C.; Guo, D.; Wang, X.; Chen, B.; Gu, Z. *Biomedical materials* 2007, *2*, L1.
5. Xiao, R. Z.; Zeng, Z. W.; Zhou, G. L.; Wang, J. J.; Li, F. Z.; Wang, A. M. *International journal of nanomedicine* 2010, *5*, 1057.
6. Sasatsu, M.; Onishi, H.; Machida, Y. *International journal of pharmaceutics* 2006, *317*, 167.
7. Kyu, S.; Dukjoon, C. *Journal of applied polymer science* 2002, *83*, 435.
8. Panyam, J.; Labhasetwar, V. *Advanced drug delivery reviews* 2003, *55*, 329.
9. Finne-Wistrand, A.; Albertsson, A.-C. *Annu. Rev. Mater. Res.* 2006, *36*, 369.
10. Bergsma, J.; Rozema, F.; Bos, R.; Boering, G.; De Bruijn, W.; Pennings, A. *Biomaterials* 1995, *16*, 267.
11. Barbato, F.; La Rotonda, M. I.; Maglio, G.; Palumbo, R.; Quaglia, F. *Biomaterials* 2001, *22*, 1371.
12. Lucke, A.; Fustella, E.; Teßmar, J.; Gazzaniga, A.; Göpferich, A. *Journal of Controlled Release* 2002, *80*, 157.
13. Otsuka, H.; Nagasaki, Y.; Kataoka, K. *Advanced drug delivery reviews* 2012, *64*, 246.
14. Conti, B.; Bucolo, C.; Giannavola, C.; Puglisi, G.; Giunchedi, P.; Conte, U. *European journal of pharmaceutical sciences* 1997, *5*, 287.
15. Porjazoska, A.; Yilmaz, O. K.; Baysal, K.; Cvetkovska, M.; Şirvanci, S.; Ercan, F.; Baysal, B. M. *Journal of Biomaterials Science, Polymer Edition* 2006, *17*, 323.
16. Hu, D. S.-G.; Liu, H.-J. *Polymer Bulletin* 1993, *30*, 669.
17. Kamaly, N.; Xiao, Z.; Valencia, P. M.; Radovic-Moreno, A. F.; Farokhzad, O. C. *Chemical Society Reviews* 2012, *41*, 2971.
18. Dong, Y.; Feng, S.-S. *Biomaterials* 2004, *25*, 2843.
19. Deokar, M. D.; Idage, S. B.; Idage, B. B.; Sivaram, S. *J. of Appl. Polym. Sci.* 2015.
20. Zhou, D.; Shao, J.; Li, G.; Sun, J.; Bian, X.; Chen, X. *Polymer* 2015, *62*, 70.
21. Barichello, J. M.; Morishita, M.; Takayama, K.; Nagai, T. *Drug development and industrial pharmacy* 1999, *25*, 471.
22. Essa, S.; Rabanel, J. M.; Hildgen, P. *International journal of pharmaceutics* 2011, *411*, 178.
23. Shan, X.; Liu, C.; Li, F.; Ouyang, C, ; Gao Q.; Zheng, K. *Designed Monomers and Polymers* 2015, 18, 678

MACRO 336

Synthesis and Characterization of Surface functionalized and Quaternised Dendrimers for Bio Medical Applications

E. Murugan* and V. Yogaraj

Department of Physical Chemistry, School of Chemical Sciences,

University of Madras, Maraimalai Campus, Guindy, Chennai – 600 025, Tamil Nadu.

Email:dr.e.murugan@gmail.com

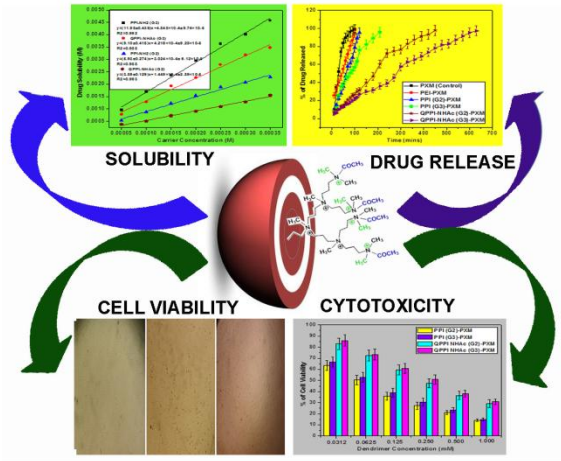
Dendrimers are new branch of macromolecules which can be used as precursors for designing and development of new drug carriers. The dendrimers have specific control over their dendritic structure in terms of size, branching density, surface functionality and thus it is possible to make them ideal for many biomedical applications particularly as a potential drug carriers.It is noteworthy to highlight here that introduction of Dendrimer based drug carriers has solved prevalent challenge faced in the existing drug carriers. Currently, the biomedical and pharmaceutical industries are seriously looking for drug carriers which have extreme biocompatible, non-toxic, effective and inexpensive and thus paved a way for synthesis of new dendrimer based drug carriers for sustained delivery of poorly soluble drugs. In general the biocompatible dendrimer based drug carriers has some specialized properties namely (i) neutral functional group on the surface of the dendrimers (ii) extraordinary potential to maximum retain of drug loading which enables to bind more number of drug molecules invariably at physiological pH (non pH dependent) and (iii) excellent enhancement of bioavailability of the poorly soluble drugs.

Keeping these news in mind, we developed various efficient dendrimer carriers by neutralizing the surface amine groups (-NH_2) of commercially available Poly(propylene imine) (PPI) (G2) and Poly(propylene imine) (PPI) (G3) dendrimers via surface hydroxylation & surface alkylation reactions followed by internal quaternization of the respective hydroxylated & alkylated PPI (G2) and PPI (G3) products. The structure of the resulting dendrimer based drug carriers were established through individual characterizations by FT-IR, ^{1}H &^{13}C NMR and MALDI-TOF spectral techniques. Further, drug delivery investigations of newly developed dendrimer based drug carriers were performed by carrying out their (i) phase solubility (ii) *in vitro* release (iii) cytotoxicity and (iv) anti-bacterial activity studies. That is, by selecting the poorly soluble drugs as representative drugs, the degree of solubility of these drugs under the influence of the dendrimer based drug carriers were examined individually by adopting the phase solubility technique and evaluated the increment of solubility of respective drug with different dendrimer based drug carriers.

The newly developed dendrimer based drug carriers have an excellent drug loading abilities and drug solubilizing potentialfor poorly soluble drugs in aqueous medium and also can sustain the delivery for longer time. The results observed in this study suggested that dendrimer based drug delivery system provides an attractive platform to load and release the poorly soluble drug molecules which improves the

pharmacodynamic and pharmacokinetic behavior of these drugs. Therefore, it is suggested that the dendrimer based drug carriers are proved to be promising and inevitable candidates in the design of polymeric drug delivery systems with high performances and biocompatibility.

Similarly, new efficient quaternized Poly(amidoamine) dendrimer stabilized gold nanoparticle (QDS-AuNPs) was also prepared by adopting the simplified experimental route and demonstrated the same for cancer cell targeting and imaging applications.Initially, amine-terminated Poly(amidoamine) (PAMAM) dendrimerhaving generation 2 was synthesised through Michael addition reactions and the resulting product having surface amine group was neutralised by acetylation followed by quaternization and thus produced quaternizedPoly(amidoamine) dendrimer (QPAMAM). This quaternized product was used as a template for stabilization of gold nanoparticles without adding any external reducing agent and the reactions were completed at room temperature and thus produced quaternized dendrimer stabilised gold nanoparticles which in turn labelled as QDS-AuNPs. ThisQDS-AuNPs were characterized by UV-Vis, FTIR, ^{1}H NMR, MALDI-TOF and TEM analyses. The functionalized nanoparticle is water-soluble and stable for 3 months. Thesynthesis of QDS-AuNPs has provided a straightforward approach for fabrication of various metal nanodevices and thus utilized for range of biomedical applications.



Acknowledgement

I would like to thank UGC-UPE Phase II Theme B Project II for providing financial support.

References

1. H. Tokuhisa, M. Zhao, L. A. Baker, V. T. Phan, D. L. Dermody,M. E. Garcia, R. F. Peez, R. M. Crooks, and T. M. Mayer, *J. Am.Chem. Soc*. 120, 4492 (1998).
2. E. Murugan, D.P.Geetha Rani, Expert. Opin.Drug Deliv. 10 (10), (2013), 1319.

MACRO 339

Green polymer nanocomposites of self assembled polysaccharide hydrogels

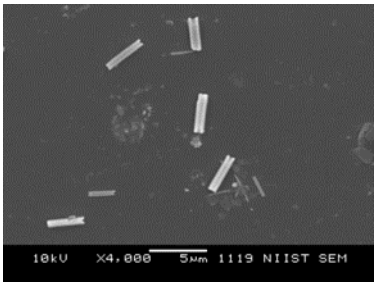
Prasad V S, Asha Susan Chacko, Anju, P., Brahmakumar, M., Sumesh Soman,

Sruthy K. Velayudhan and Tinu Rose, M. P.

CSIR- National Institute for Interdisciplinary Science and Technology, Thiruvananthapuram 695019, India.

vsprasad@niist.res.in

Hydrogels from polysaccharides are of great significance for the applications in nanocomposites especially concerned with the ecological problems associated with non degradable plastics. Long aliphatic chain modified nanocellulose from straight chain polysaccharides and the similar branched chain Xyloglucan showed self assembly in solvents in to giant vesicles and nanotubes respectively. The composites with PLA matrix showed tunable flexibility controlled by cross-linking resulting in inter penetrating network systems as well. The results showed prospects for applications such as transparent packaging films as well as in scaffolds for drug delivery.



References
[46]Kochumalayil, J. Berglund , L. A. Green Chemistry, 16(2014) 1904.

MACRO 364

Tapioca Starch Grafted Polyacrylamide Application in Water Treatment

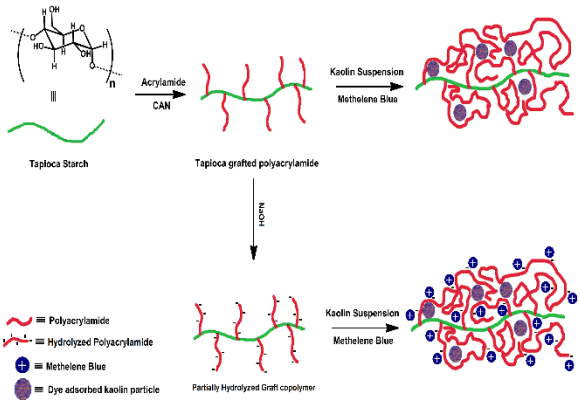
Kranthikumar Tungala[a], Pubali Adhikary[a], **Krishna Kumar[b]**, Abhishek Maurya[a], S. Krishnamoorthi[a]*

[a]*Department of Chemistry, Centre of Advanced Studies, Banaras Hindu University, Varanasi - 221005, India*

[b]*Department of Applied Science, Madan Mohan Malaviya University of Technology, Gorakhpur-273010, India*

Abstract This article deals with the synthesis of five different grades of polymeric flocculants (TAP-g-PAM 1 to TAP-g-PAM 5) by grafting polyacrylamide (PAM) onto the back bone of

tapioca starch. Their molecular weights were estimated from their intrinsic viscosity measurements. Corresponding hydrolyzed products (Hyd TAP-g-PAM 1 to Hyd TAP-g-PAM 5) of TAP-g-PAM 1 to TAP-g-PAM 5 were prepared by partial alkaline hydrolysis. NMR, FTIR, Scanning Electron Microscopy (SEM) and Thermo Gravimetric Analysis (TGA) were supporting the synthesis of grafted and hydrolyzed polymers. The flocculation performances of all grades were evaluated in kaolin suspension by settling and jar test methods. Depending on their flocculation performance, TAP-g-PAM 5 and Hyd TAP-g-PAM 3 were chosen as best grades and employed in removal of methylene blue (MB) dye. Between TAP-g-PAM 5 and Hyd TAP-g-PAM 3, the former one was found as the best performing grade when settling and jar tests were employed, whereas the later one performed best as a dye removing agent. Synthesis and application of tapioca grafted PAM is shown in **scheme 1**.



Scheme 1. Schematic representation of synthesis, and application in dye removal of TAP-g-PAM and Hyd TAP-g-PAM.

Reference

1. Kumar, K., Adhikary, P., Karmakar, N. C., Gupta, S., Singh, R. P., & Krishnamoorthi, S. (2015). *Carbohydrate Polymers* 127, 275-281.
2. Adhikary, P., Krishnamoorthi, S., & Singh, R. P. (2011). *Journal of Applied Polymer Science*, 120, 2621-2626.
3. Yadav, R., & Garg, G. (2013). A Review on Indian Sago Starch and its Pharmacuetical Applications. *International Journal of Pharmaceutical and Life Sciences*, 3, 99-106.

MACRO 370

Thermal Degradation and Mechanistic Study of Guar Gum, Xanthan Gum and Gum Arabic using Hyphenated TGA-FTIR Analysis: A Comparative Study

Monika[a] and Dr. Vimal Katiyar[a*]

[a]*Department of Chemical Engineering, Indian Institute of Technology Guwahati, Guwahati, 781039, Assam, India.*

Email Id: vkatiyar@iitg.ernet.in

Abstract

The present study deals with the thermal degradation behavior and possible byproducts of natural Guar gum (GG), Xanthan gum (XG) and Gum arabic (GA) using hyphenated TGA-FTIR investigations. Thermal stability of these commercial gums is studied at a heating rate of 10 K/min using thermogravimetric (TGA) analyzer. TGA result indicates that the onset degradation (T_{onset}) temperature of GG is higher than other gum which shows the good thermal stability in comparison of other gum. Multiple DTG peaks revealed that the system has a complex reaction mechanism for each gum. The changes in the volatile products distribution and their formation have been characterized by hyphenated TGA- Fourier transform infrared (FTIR) spectroscopy. Detailed investigation of the products confirms that the each gum has different distribution patterns of the gaseous species, depending on the structural properties. Some common volatile compounds such as water, CO_2, CO and different type of aldehydes, acids etc are evolved out due to breaking of glucosidal and carbon-carbon bond, which follows random chain scission. FTIR analysis shows that the both primary and secondary reactions occur in each case. Further, the triplet constants have been quantified for non-isothermal degradation kinetics. It is noteworthy to mention that thermal behavior of these gums is found different due to their varying chemical composition.

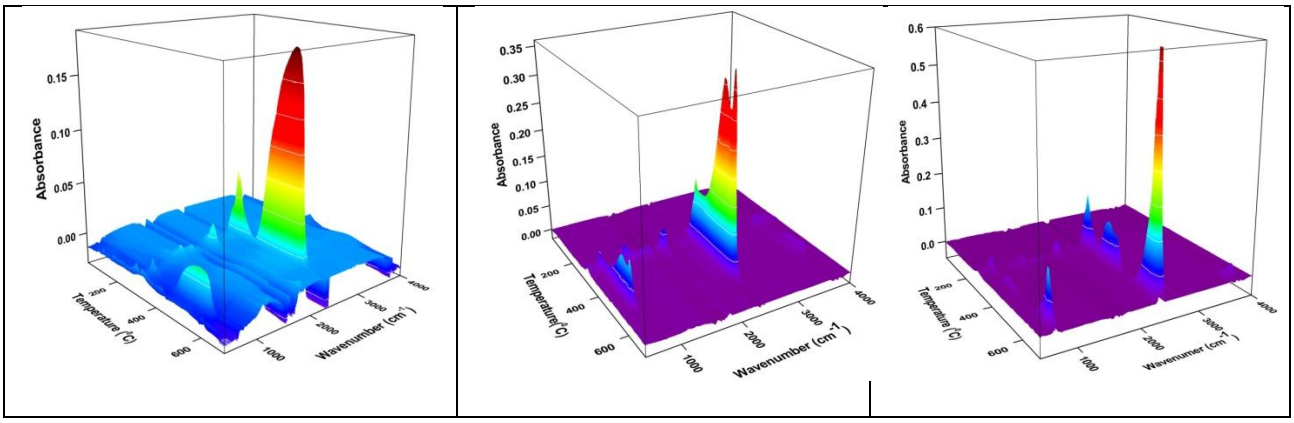


Figure 1. 3D FTIR spectra obtained from thermal decomposition of (a) Gum arabic (b) Guar gum (c) Xanthan gum under nitrogen at 10 K/min.

Keywords: Guar Gum, Xanthan Gum, Gum Arabic, TG-FTIR and thermal analysis.

References

[1] Gonc, C.; Mothe, A.;Freitas, J.S.D.; J Therm Anal Calorim, 116 (2014) 1509.

MACRO 373

Effect of Hydrolytic Degradation on the Wettability Behaviour of Bio-filler Reinforced Poly (lactic acid) Extruded Bionanocomposites.

Kalita, Kumar, Naba.[a]; Patwa, Rahul[a]; Dhar, Prodyut[a]; and Katiyar, Vimal.[a]*

[a]Department of Chemical Engineering, IIT Guwahati, India*
[a]Email: vkatiyar@iitg.ernet.in*

Biopolymers from renewable resources have considerable characteristics for packaging applications [1]. Since Biopolymers tends to degrade both hydrolytically as well as in composting conditions so its superiority as environmental friendly material can be justified[1,2]. Poly(lactic acid) (PLA) is one of the most potentially rich and extensively studied type of synthetic bioplastic which has been on the priority of the scientific community for commercialization in packaging sectors [3,4]. Two important steps of biodegradation associated with polymers are hydrolysis of the polymers and its subsequent assimilation by microbes. So in order to understand the biodegradation behavior of any biopolymers the hydrolytic degradation of the polymers need to be investigated. In this study we have used seven different samples having different combination based upon PLA and having a couple of common fillers as CNC (Cellulose nanocrystals) and DCP (Dicumyl Peroxide) were extruded and nanocomposites were prepared for analysis. Hydrolysis was done at pH 7 and pH 2 for 120 hours at 55°C. We have characterized the samples for understanding wettability behavior.

The polymer nanocomposite surfaces was characterized to understand its wettability behavior prior to degradation and after degradation using a (Kruss, Germany) DSA 25 Contact angle measuring instrument using sessile drop method. 1p in the sample names represents 1% of the fillers used.

Table 1: Contact angle of samples with two different solvent analyzed before and after hydrolytic degradation

	Before hydrolytic degradation		After hydrolytic degradation for 120 hours			
Samples	Water (Solvent I)	Glycerol (Solvent II)	Water (Solvent I)		Glycerol (Solvent II)	
			pH 2	pH 7	pH 2	pH 7
PLA/DCP/CNC/Cellulose 1p	78.58 (±1.85)	71.80 (±1.46)	66.04 (±1.22)	63.62 (±1.09)	85.71 (±2.39)	58.70 (±0.41)
PLA/DCP/CNC/Coconut oil 1p	79.12 (±1.12)	70.74 (±1.48)	60.06 (±0.95)	57.35 (±0.39)	82.32 (±3.05)	70.05 (±1.41)
PLA/DCP/CNC/Carbonfiber 1p	79.72 (±1.46)	72.02 (±0.72)	70.14 (±1.18)	60.98 (±2.37)	64.10 (±1.25)	43.18 (±0.31)
PLA/DCP/CNC/ Alumina 1p	74.42 (±0.99)	72.35 (±0.54)	71.28 (±1.18)	67.63 (±4.14)	85.36 (±1.60)	43.18 (±0.31)
PLA/DCP/CNC/Nanosilica 1p	80.88 (±3.26)	57.17 (±1.28)	67.33 (±1.23)	66.52 (±1.10)	67.48 (±1.19)	75.59 (±1.24)
PLA/DCP/CNC/Starch 1p	67.46 (±1.19)	68.84 (±0.43)	70.84 (±0.85)	55.32 (±11.24)	62.72 (±0.71)	68.70 (±1.45)
Neat PLA	78.43 (±1.81)	73.30 (±2.90)	65.15 (±2.16)	76.34 (±3.39)	69.04 (±1.01)	82.00 (±1.56)

Fig 1 (a)-(g), represents images of water contact angles of the samples as presented in Table 1 at different pH medium.

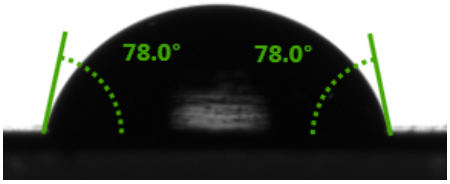


Fig 1 (a)
PLA/DCP/CNC/Carbon 1p before degradation

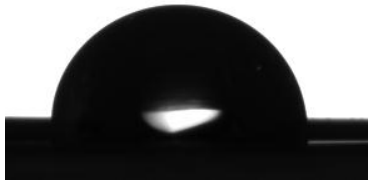


Fig 1 (b)
Neat PLA film before degrdation

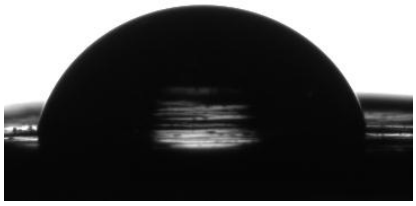


Fig 1 (c)
PLA/DCP/CNC/Carbonfiber 1p subjected at pH 2 for 120 hours of hydrolytic degradation.

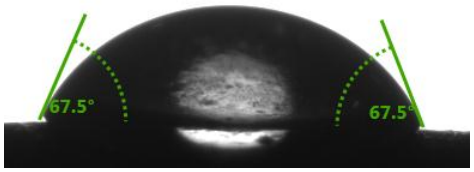


Fig 1 (d)
Neat PLA extruded film subjected at pH 2 for 120 hours of hydrolytic degradation.

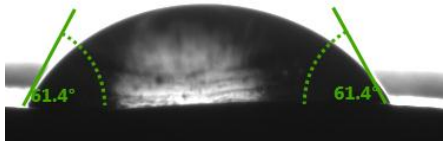


Fig 1 (e)
PLA/DCP/CNC/Carbonfiber1p subjected at pH 7 for 120 hours of hydrolytic degradation.

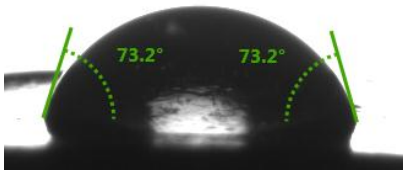


Fig 1 (f)
Neat PLA extruded film subjected at pH 7 for 120 hours of hydrolytic degradation.

Table 2: Surface free energy of the samples with water and glycerol as solvent analyzed for γ, γd and γ^p as total, disperse and polar surface energy respectively, before and after hydrolytic degradation.

Samples	After degradation for 120 hours at pH 2 and at 55 °C			After hydrolytic degradation for 120 hours		
	Water (Solvent I) and Glycerol (Solvent II)			Water (Solvent I) and Glycerol (Solvent II)		
	γ (mN/m)	γ^d (mN/m)	γ^p (mN/m)	γ (mN/m)	γ^d (mN/m)	γ^p (mN/m)
PLA/DCP/CNC/Cellulose 1p	46.90 ±1.89	36.59 ±1.14	10.32 ±0.75	29.29 ±2.97	8.82 ±1.14	20.46 ±1.83
PLA/DCP/CNC/Coconut oil 1p	47.83 ±1.94	32.53 ±1.16	15.30 ±0.78	28.03 ±4.71	16.39 ±2.75	11.64 ±1.96
PLA/DCP/CNC/Carbonfiber 1p	51.93 ±1.50	46.26 ±0.98	5.67 ±0.52	27.16 ±4.23	15.21 ±2.16	11.95 ±2.06
PLA/DCP/CNC/ Alumina 1p	46.62 ±2.70	39.82 ±1.96	6.80 ±0.74	29.29 ±2.97	8.82 ±1.14	20.46 ±1.83
PLA/DCP/CNC/Nanosilica 1p	52.08 ±1.76	44.89 ±1.14	7.19 ±0.62	48.49 ±9.85	46.38 ±7.94	2.11 ±1.90
PLA/DCP/CNC/Starch 1p	33.84 ±3.02	17.66 ±1.57	16.18 ±1.45	35.51 ±3.44	6.44 ±1.02	29.07 ±2.42
Neat PLA	38.66 ±6.42	4.61 ±1.64	34.05 ±4.78	29.67 ±8.49	26.07 ±6.54	3.60 ±1.95

The reasons for the increasing wettability on the surface of the nanocomposite films is due to hydrolytic decomposition of the nanocomposites with time, the surface became more heterogeneous which made it more hydrophilic as can be seen from Table 1 and Fig 1(a-f). The increase in the hydrophilic characteristics of the nanocomposites might be due to the appearance of carboxylic and hydroxyl groups and might be due to the hydrolysis of ester bonds in the polymer chains of the nanocomposites. Increase in Surface Energy with decreasing contact angle can be seen in Table 2. Surface energy results in Table

2 show that the contribution of the polar part is considerably reduced when comparing samples after degradation with samples before degradation due to the insertion of nonpolar groups on the surface of the nanocrystals, increasing their dispersive character in many of the samples after degradation for 120 hrs. Further results will be discussed later.

References

[47] Valapa, Ravibabu; Pugazhenthi G; Katiyar, Vimal. *International Journal of Biological Macromolecules*, 89 (2016) 70–80.
[48] Cadar, Oana; Maria, Paul; Cecilia, Roman; Mirela, Miclean; Cornelia, Majdik. *Polymer Degradation and Stability*, 97 (2012) 354-357.
[49] Magniez, K; Voda, A.S; Kafi, A.A; Fichini, A; Guo, Q; Fox, B.L. *Appl. Mater. Interfaces*, 5 (2013) 276–283.
[50] Valapa, Ravibabu; Sameer, Hussain; Parmeswar, Krishnan Iyer; Pugazhenthi, G; Katiyar, Vimal. *Polymer Bulletin*, 73 (2015) 21-38.

MACRO 375

Melt Extruded Poly Lactic Acid/Chitosan-*grafted*-Oligo L-Lactic Acid Bionanocomposite Films for High Gas Barrier Applications

Pal, Akhilesh Kumar and
Katiyar, Vimal*

Department of Chemical Engineering, Indian Institute of Technology Guwahati, Guwahati, Assam-781039, India

*E-mail: vkatiyar@iitg.ernet.in

The curreent research work is focussed on the fabrication of poly (lactic acid)/chitosan-*grafted*-oligo L-lactic acid (PLA/CH-*g*-OLLA) bionanocomposite films at pilot plant scale using melt extrusion technique with the utilization of two demanded biodegradable polymers i.e. poly (lactic acid) (PLA) and chitosan (CH) in food packaging applications.[1] Both the polymers are biocompatible, non-toxic, biocompostable in nature and most importantly, having film forming ability. It is noteworthy to mention that PLA is hydrophobic in nature whereas, chitosan is hydrophilic in nature. Being a hydrophilic in nature, chitosan is incompatible with most of the hydrophobic polymers. Therefore, current research is performed to increase the functionality of chitosan and converted it into dispersible nanoparticles as a result of grafting of OLLA on its surface. The prepared functionalized chitosan was optimized for its uniform dispersion in PLA via melt extrusion process. Melt extruded films were prepared using twin screw extruder with L/D ratio of 48 and slit die of 20 cm. Extruded films are properly characterized by various techniques such as FTIR, XRD, NMR, DSC, TGA, mechanical and barrier properties for dispersion of chitosan into the PLA matrix.

FTIR analysis confirmed the structural modification with the help of the presence of new peak at 1539 cm^{-1} along with the other regular peaks in bionanocomposite films. The absorption bands at 754 cm^{-1} and 1383 cm^{-1} were attributed to the -CH- bending in the molecular structure of PLA. The absorption band at 870 cm^{-1} was observed in all the film samples except chitosan which denotes -C-C- stretching and also attributed to the amorphous phase of PLA. A sharp and intense peak at 1751 cm^{-1} was observed for all bionanocomposite film samples which showed -C=O (carbonyl stretching) valance vibration. Furthermore, the strong vibrations of amide I band (-C=O stretching) and amide II band (-N-H bending) were confirmed at 1638 cm^{-1} and 1543 cm^{-1} in bionanocomposite films. Very small peak at 1539 cm^{-1} was noticed only in the case of bionanocomposite films which was attributed to the presence of amide ester linkage (–OCONH–) as shown in figure 1.

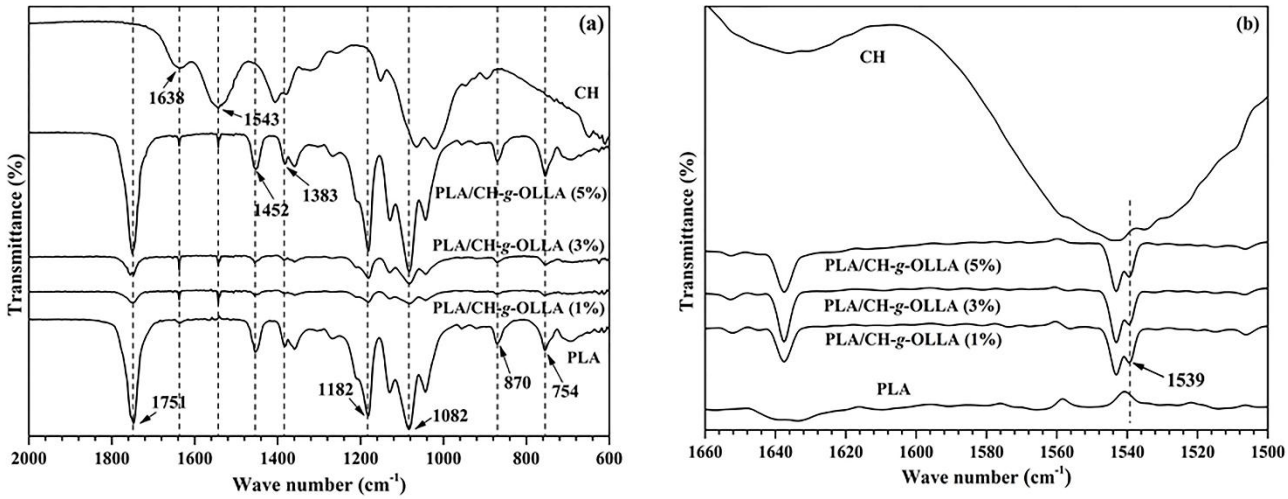


Figure 1. FTIR analysis of PLA, CH and PLA/CH-*g*-OLLA bionanocomposite films (a) in the range of 600-2000 cm^{-1} and (b) in the range of 1500-1660 cm^{-1}.

XRD analysis confirmed the semicrystalline nature of bionanocomposite films, which was reduced continuously with the increase in filler loadings. The intensity of the crystalline peaks was reduced with the increase in filler loadings. DSC analysis confirmed that the glass transition temperature (T_g) of PLA films was reduced significantly up to ~20ºC with an increase in filler loading due to plasticizing effect of low molecular weight of CH-*g*-OLLA. It is noteworthy to mention that T_g value of any polymer can be tuned by changing the molecular weight of polymers. Other parameters such as the degree of deacetylation of chitosan, water amount, crystallinity and OH or amine groups in the macro-molecule chain also responsible for variation in T_g. The heat capacity at constant pressure (C_p) was also reduced along with the increment in filler loading. A small reduction was detected in cold crystallization temperature (T_{cc}) of PLA films with increment in filler loading due to the presence of deformed shape and size of some crystals in PLA matrix. The melting behavior of PLA film showed a unimodal endothermic peak which exhibits α crystalline form of PLA. The slight reduction in melting temperature (T_m) was observed in PLA films by an increase in filler loading due to the heterogeneous distribution of crystals as well as non-uniform crystal thickness. Bimodal endothermic melting peaks, during DSC analysis also corroborate with the presence of two phases (α and β) of PLA which is also confirmed by XRD analysis of PLA/CH-*g*-OLLA bionanocomposite films. Even the thermal stability of PLA/CH-*g*-OLLA films was reduced with an increase in filler percentage though it was found higher than the processing temperature of PLA. Ultimate tensile strength (UTS) of PLA/CH-*g*-OLLA bionanocomposite films was found comparable to that of PLA whereas, Young's modulus was reduced with an increase in filler loading. On the other hand, elongation at break (%E) was improved significantly by incorporating filler in PLA matrix. FESEM and TEM analyses showed that amphiphilic CH-*g*-OLLA nanoparticles were three dimensional, spherical in shape and uniformly dispersed in the form of polymeric micelles in PLA matrix as shown in figure 2. Such morphology supports highly tortuous path for oxygen to move across the film.

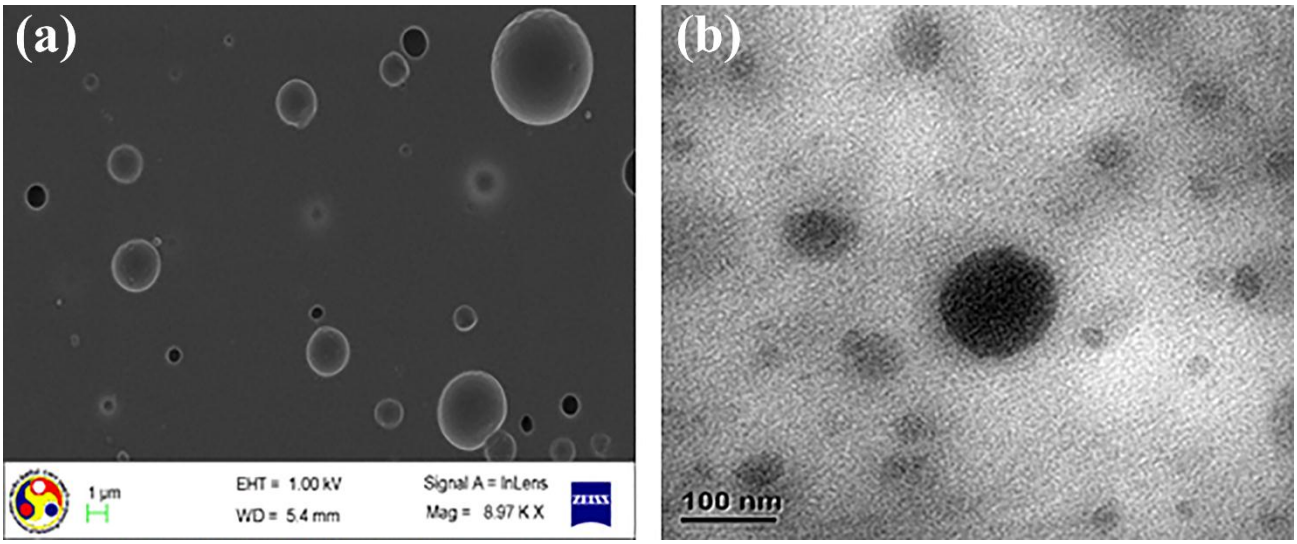


Figure 2. (a) FESEM and (b) TEM analysis of PLA/CH-*g*-OLLA bionanocomposite film.

The permeability coefficient, oxygen permeability and other parameters such as diffusivity, solubility of PLA and PLA/CH-*g*-OLLA bionanocomposite films were also studied to determine the effect of CH-*g*-OLLA on the gas barrier properties. PLA/CH-*g*-OLLA bionanocomposite films showed a significant reduction in oxygen permeability by adding CH-*g*-OLLA up to 5 wt% into PLA matrix. The solubility coefficient reduced continuously with increasing filler loading which clearly indicates the increase in resistance to permeation of oxygen molecules across the core and shell network formed in bionanocomposite films. The formation of unique core and shell network in the polymer matrix may be culpable for the decrement in oxygen permeability across PLA/CH-*g*-OLLA bionanocomposite films. The reduction in solubility coefficient is more responsible for the decrease in gas barrier property because the occupancy of the number of active sites is increased due to nano-filler present in the polymer matrix. Hence, less availability of the number of active sites was found in PLA matrix for physical interaction with oxygen molecules. The lack of active sites in bionanocomposite films was due to the formation of amide ester linkage between PLA and chitosan which can also increase the resistance to the diffusion of oxygen molecules. In this way, the oxygen permeability of bionanocomposite films was reduced by multi-fold as compared to the pristine PLA.[2,3] PLA/CH-*g*-OLLA films can be one of the best substitutes to increase food shelf life in food packaging applications. To conclude, we have developed a melt extrusion process for large scale production of bio-based and biodegradable films containing chitosan as a bio-filler for the targeted application in food storage.

References

[51] Pal, Akhilesh Kumar; Katiyar, Vimal. *Asian Chitin Journal*, 11, (2015) 37.
[52] Pal, Akhilesh Kumar; Katiyar, Vimal. *Biomacromolecules*, 10.1021/acs.biomac.6b00619 (2015).
[53] Katiyar, Vimal; Pal, Akhilesh Kumar; Tripathi, Neelima. *Indian Patent Application*, 981/KOL/2015.

Acknowledgement

We sincerely acknowledge the Centre of Excellence for Sustainable polymers (CoE-SusPol) at IIT Guwahati and Ministry of Food Processing Industries (GoI) for research grant for 'GreenPack' project for providing the research facilities. We also thank to the Central Instruments Facility (CIF), IIT Guwahati for providing characterization facilities.

MACRO 379

An investigation of the viscoelastic and thermal behavior of silk nanoparticles/polylactic acid nanocomposites

P. Rahul, T. Melaku, K. Manash Jyoti, K. Amit and K. Vimal

Department of Chemical Engineering, Indian Institute of Technology, Guwahati-781039, India

** e-mail id: vkatiyar@iitg.ernet.in*

Abstract

In this investigation, we have demonstrated composites of polylactic acid (PLA) and laboratory synthesized silk nanoparticles and investigated their interactions in relation with viscoelastic properties. PLA-silk nanoparticles based nanocomposites were processed in a mini-extruder at 200 °C and 100 rpm. Silk nanoparticles were added at filler loadings of 1, 2 and 5 wt% to the neat PLA and the dynamic oscillatory behavior within the linear viscoelastic region was studied at 180°C and 190 °C respectively. The complex viscosity of the PLA-silk nanocomposites was observed to be inversely proportional to the increase in temperature and silk loading.

Keywords: *polymer; PLA; viscoelastic;*

Introduction

A greater focus on sustainability and sustainable polymers has resulted in extensive research on biodegradable and bio-derived polymers since the last few decades.[1,2] PLA is one of the most widely available and increasingly commercially produced biodegradable polymers. Silk nanocrystals (SNC) are novel nano-fillers derived from silk. With a greater focus on the use of bio-derived polymers and fillers, a study was carried on PLA/SNC nanocomposites. As an extensive body of research is available on the nanocomposites of inorganic non-biodegradable nano-fillers, property comparison between SNC and these nano-fillers are obvious.[2-5] Hence this study on PLA/SNC nanocomposites has been carried out using traditional rheological tools to analyze the flow properties of the compositions. With a correspondence available between the rheological and the molecular weight data, the GPC results of the PLA/SNC nanocomposites have also been presented.

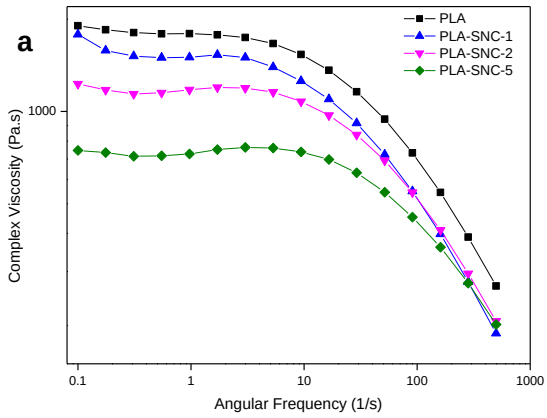
Experimental

Silk particles were prepared using acid hydrolysis from degummed Muga (*antheraea assama*) silk. PLA-silk nanocomposites were processed in a mini-extruder at 200 °C and 100 rpm with a 1 minute residence time. Silk nanoparticles were added at filler loadings of 1, 2 and 5 wt% respectively to the neat PLA. The samples for carrying out the rheological analysis were prepared by drying in hot air oven for 12 hours at 90 °C.

Rheological analysis:
The dynamic oscillatory behavior within the linear viscoelastic region was studied using an Anton Paar rheometer MCR 102 (plate/plate=50 mm diameter). The dynamic frequency sweep was carried out at 180 °C and 190 °C from 0.1 to 500 Hz at 1% strain.

Gel Permeation Chromatography:
Molecular weights and Polydispersity Index (PDI) of nanocomposites after melt compounding were estimated by Size Exclusion Chromatography (SEC) using GPC (LC-20AD, Shimadzu, Japan). A PL gel 5µm column (Polymer Laboratory) and a refractive index detector (Shimadzu RID-10A) were employed. The polymer was dissolved and eluted in chloroform at a flow rate of 1.0 mL/min. The number and weight average molecular weights were calculated using polystyrene standards.

Results and discussion
Complex Viscosity:
The complex viscosity or simply the viscosity (in this case the melt viscosity) is directly proportional to the molecular weight of the polymer. A comparative study of the complex viscosities of PLA/SNC nanocomposites in figure 1 shows that the viscosity of PLA decreases with increase in the temperature. This is expected as more thermal energy is provided to the polymer chains and the polymer starts flowing freely.



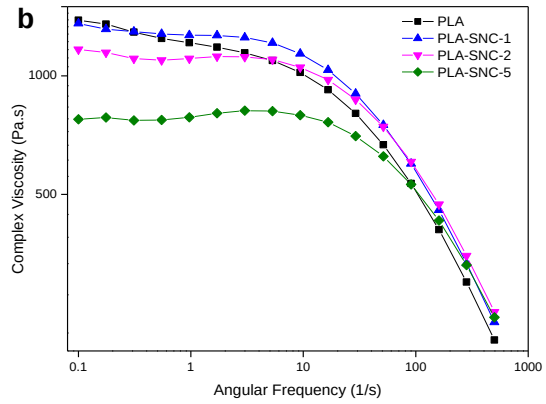


Figure 1: Complex viscosity studies of PLA/SNC nanocomposites at (a) 180 °C and (b) 190 °C.

Table 1 shows the values of complex viscosity at the highest (500 Hz) and the lowest frequencies (0.1 Hz) for the experiment carried out at 180 °C and 190 °C Higher frequencies of the dynamic frequency sweep test correspond to greater shearing of the polymer (between the plates) and hence are expected to result in better flow properties. As can be observed from table 1, the complex viscosities of all the samples (PLA and SNC nanocomposites) are significantly lower at the higher frequency (i.e., 500 Hz).

Table 1: Complex viscosity values at the highest and lowest frequencies for 180 and 190°C.

Freq.	Sample	Complex viscosity (Pa.s) at	
		180° C	190° C
0.1 Hz	PLA	1913	1386
	PLA-SNC-1	1792 (6%↓)	1359 (2%↓)
	PLA-SNC-2	1233 (36%↓)	1168 (16%↓)
	PLA-SNC-5	747 (61%↓)	776 (44%↓)
500 Hz	PLA	269	213
	PLA-SNC-1	189 (30%↓)	237 (11%↑)
	PLA-SNC-2	208 (23%↓)	251 (18%↑)
	PLA-SNC-5	201 (25%↓)	243 (14%↑)

However, the viscosity of the nanocomposites shows a unique behavior with regards to the change in SNC loading. The complex viscosity decreases on increase in the SNC nanofiller loading (1, 2 and 5 wt% respectively) for 0.1 Hz at 180 and 190 °C. There can be two possible explanations for this behavior: (1) a general decrease in viscosity due to the ease of flow promoted by the nanofiller due to polymer chain slippage and hence a general lubricating effect, and (2) chain scission of the PLA and the resulting decrease in polymer molecular weight due to degradation by the residual acidic groups present in the SNC. At lower frequencies, the polymer nanocomposite rheology is dominated by the influence of the SNC nanofiller and hence increase in their concentration led to

marked decrease in the viscosity values. However, at the higher frequency, the complex viscosity at both 180 and 190 °C drastically decrease as the rheological behavior is dominated by the polymer chains which have now more energy to freely flow.

Storage modulus and relaxation times:
The dynamic frequency sweep test provides information about the change in the storage and loss modulus with angular frequency. The storage modulus values have been reported in Figure 2.

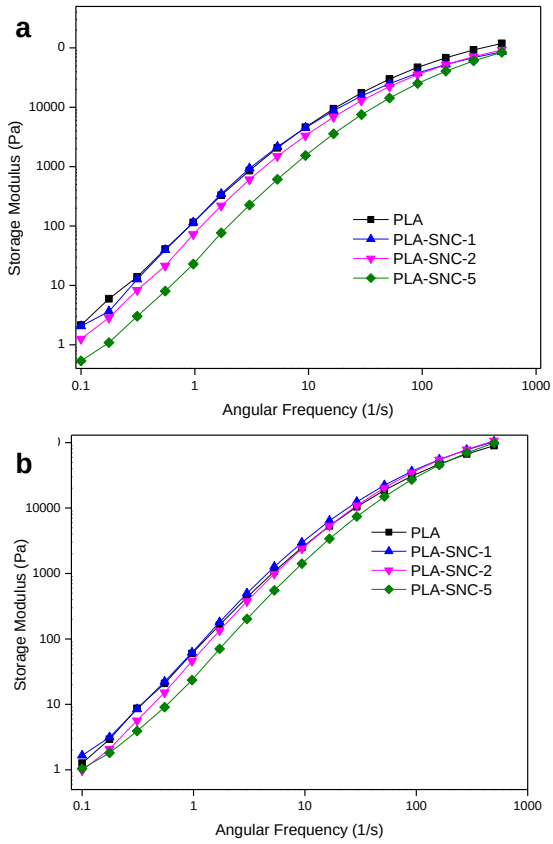


Figure 2: Storage modulus vs. angular frequency at (a) 180°C and (b) 190°C.

The storage and the loss moduli when plotted with respect to the angular frequency cross at a particular frequency value called the crossover frequency. The values of the storage and loss moduli are equal at this point and are called the crossover modulus. The characteristic relaxation times computed from the crossover frequency and the crossover moduli have been reported in Table 2.

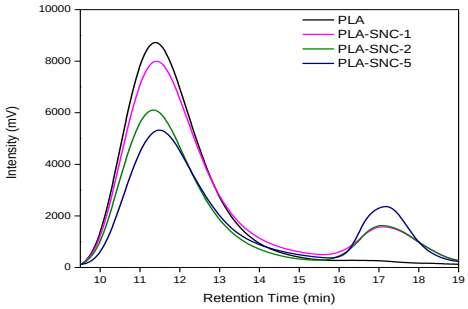
The relaxation or the characteristic relaxation time of the polymer and/or its nanocomposite is dependent on the complexity of the polymer structure. Higher molecular weight polymers are expected to possess greater relaxation times. In the present study, the disentanglement of the

polymer chains is greater at the higher temperature (190 °C) compared to the lower temperature (180 °C) for the same frequency ranges, leading to greater polymer chain mobility and ability to relax.

Table 2: Crossover data from storage and loss modulus vs. angular frequency plots (Figure 2) for PLA/SNC nanocomposites.

Temp. (°C)	Sample	Characteristic relaxation time (s)
180	PLA	0.011
	PLA-SNC-1	0.016
	PLA-SNC-2	0.012
	PLA-SNC-5	0.006
190	PLA	0.007
	PLA-SNC-1	0.009
	PLA-SNC-2	0.007
	PLA-SNC-5	0.005

Hence the the values of characteristic relaxation times at 190 °C are lower. Further, the lower relaxation times of the PLA/SNC nanocomposites compared to the neat PLA can be attributed to the homogenous dispersion of the SNC nanofiller in the PLA matrix which in turn provides a lubricating effect for the polymer chains to slip past each other. This can also be verified from the viscosity behavior of the PLA and the nanocomposites where there was a drop in the viscosity plots on addition of the SNC nanofiller. Further, the lowering of the relaxation times may also have resulted from polymer chain scission due to the degrading effect of the acid traces present in SNC. Decrease in the PLA chain lengths due to degradation leads to smaller polymer chains which in turn easily relax thus lowering the characteristic relaxation times. The lowering of the polymer molecular weight as seen in Figure 3 indicates the polymer degradation occurring on addition of SNC nanofiller to the matrix.



Sample	Mn (kDa)	Mw (kDa)	PDI
PLA	67.2	155.25	2.31

PLA-SNC-1	65.2	151.7	2.32
PLA-SNC-2	60.1	155.9	2.25
PLA-SNC-5	57.3	138.7	2.42

Figure 3: GPC results of PLA/SNC nanocomposites.

Han Plots:

The dispersion of the nanofiller in a polymer influences the rheological properties to a great extent. The dispersion homogeneity of the SNC in PLA can be studied using the Han Plots (plot of storage vs. the loss modulus).

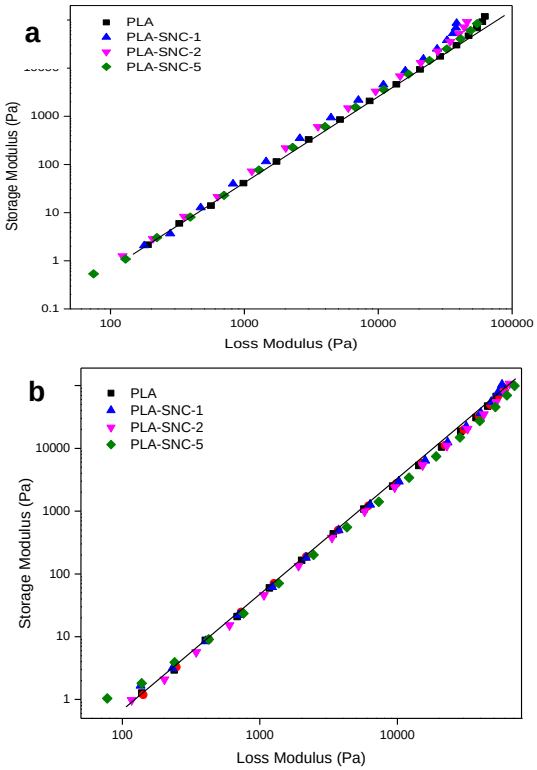


Figure 4: Han plots for PLA/SNC nanocomposites at (a) 180 °C and (b)190 °C.

Figure 4 shows the Han plots for PLA/SNC nanocomposites. If the Han plot for the nanocomposites lie on a straight line and closer to the Han Plot for the neat PLA, a homogenous dispersion of the nanofiller in the polymer matrix can be interpreted. This is found to be true for the PLA/SNC compositions analyzed in this study inferring good homogeneity in dispersion of the SNC in the PLA matrix. The dispersion can be found to be more uniform at 190 °C as evident

from the plot in Figure 4(b), which is expected as the filler can be dispersed at higher temperature and thus lower polymer viscosity with greater ease.

Conclusions

The temperature and SNC nanofiller loading have been found to have a strong effect on the PLA rheology. Increase in temperature resulted in lower viscosity values due to more energy for the polymer to flow, thus resulting in lower relaxation times. Further, higher temperature also led to better dispersion of the nanofiller in the polymer matrix. Addition of SNC nanofiller resulted in characteristic lowering of viscosity at both temperatures due to the nanofiller acting like a flow modifier and lubricating agent probably due to its unique morphology. Polymer chain scission due to the degrading effect of residual acid groups present on SNC nanofiller also lead to lowering of the polymer molecular weight as evident from GPC studies.

Acknowledgements

Authors would like to acknowledge the Centre of Excellence for Sustainable Polymers (CoE-SusPol) for provision of research facilities.

References

1. Dhar, P., Bhardwaj, U., Kumar, A., Katiyar, V. Polym. Compos.. 2015.
2. Aghjeh, M.R.;Asadi, V.;Mehdijabbar, P.;Khonakdar, H.A.; and Jafari, S.H. Composites Part B: Engineering. 86: p. 273, 2016.
3. Ghorbani, F.M.;Kaffashi, B.;Shokrollahi, P.;Akhlaghi, S.; and Hedenqvist, M.S. Mat. Sci. Eng.: C. 59: p. 980, 2016.
4. Nekhamanurak, B.;Patanathabutr, P.; and Hongsriphan, N. Energy Procedia. 56: p. 118, 2014.
5. Solomon, M.J.;Almusallam, A.S.;Seefeldt, K.F.;Somwangthanaroj, A.; and Varadan, P. Macromolecules,. 34(6): p. 1864, 2001.

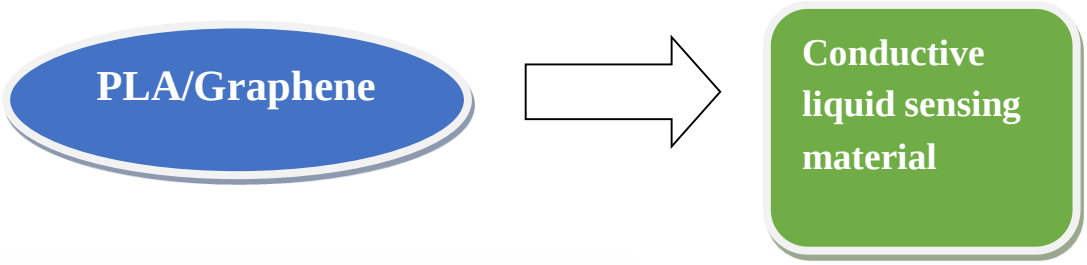
MACRO 381

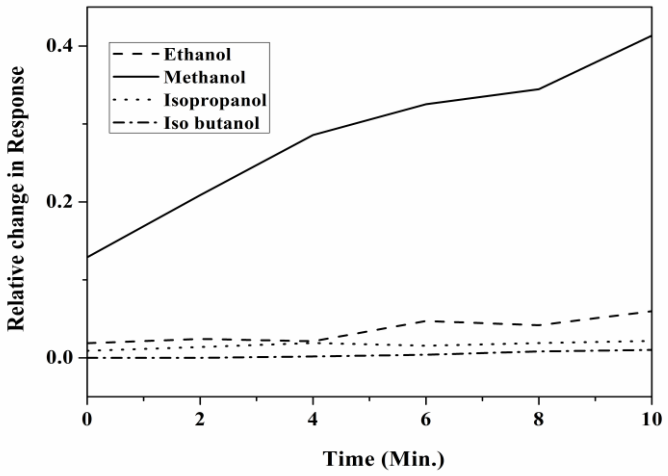
Poly lactic acid (PLA) based conductive biomaterial for the detection of Alcohols

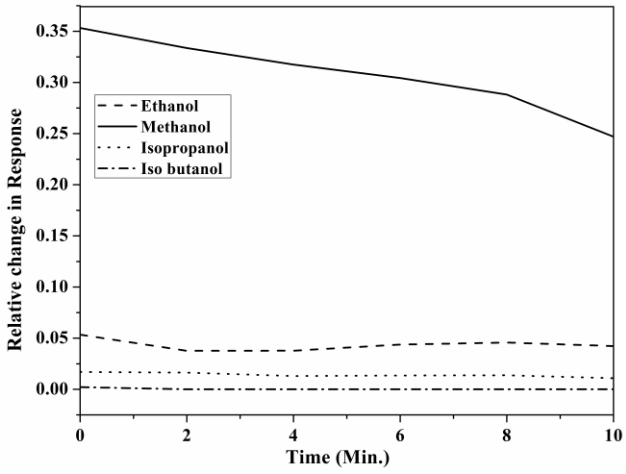
Gourhari Chakraborty*, Vimal Katiyar*, and G. Pugazhenthi*

*Department of Chemical Engineering, IIT Guwahati (Guwahati, Assam, India, PIN-7810389)
*vkatiyar@iitg.ernet.in, *pugal@iitg.ernet.in,

Biodegradable polymers are becoming prime replacement for conventional polymers in almost all the field. Now a days use of bio based materials are extended in the field of biomedical and conductive biomaterials apart from packaging. PLA being a novel thermoplastic biodegradable polymer become exiting material for bio based applications. Introduction of different conductive reinforcement into the PLA matrix leads to conductive bionanocomposites. Nanoparticles like metal based compounds or carbon based fillers like carbon black, carbon fiber, carbon nanotube, and graphene are generally used reinforcement of polymer for conductive applications. PLA based conductive bionanocomposites are now a days can be applicable for sensing liquids, vapours, biological substances, catalyst, energy storage device etc. In this present study we have fabricated PLA, Graphene based conductive nanocomposites and used to detect alcohols like Methanol, Ethanol, Isopropanol, Tertiary butanol using lab made sensing platform. Impedance values are recorded for this work. Impedance of the composites decreased to ~10^3 Ω compared to PLA ~10^{10} Ω. Alcohol sensitivity of the composites fond to be dependent on the molecular weight of the alcohols and it decreases with increase in molecular weight of the alcohols. Sensitivity order found to be MeOH>EtOH>ISOPROPANOL>TERTIARY BUTANOL.







Dipping **Drying**

Figure- Relative change in response (Impedance) at different time for dipping and drying of PLA/Graphene composite in different alcohols.

MACRO 384

Bioactive and non-cytotoxic magnesium incorporated inorganic-organic hybrid resin for biomedical applications.

C Vibha, PP Lizymol*
Biomedical Technology Wing, Sree Chitra Tirunal Institute for Medical Sciences and Technology,Poojappura, Thiruvananthapuram 695012
**Email ID: lizymol@rediffmail.com*

Currently inorganic-organic hybrid materials turn out to be the spot of interest due to the favourable blend of properties of polymers and ceramics. The versatility of its application is due to the covalent bonding of inorganic and organic components within these resins through sol-gel process. In the present study we tried to synthesize inorganic-organic hybrid resin which containing magnesium with polymerisable tetramethacrylate groups through modified sol-gel method. The significant role of magnesium in the stabilization of chemical, physical and electrokinetic states of the surface enamel calcium gives us an insight in the development of biocomposites based on polymerizable multifunctional magnesium containing inorganic-organic hybrid resins. Moreover the combination of magnesium with calcium phosphate nanoparticles in HAP was found to enhance bone forming potential [1-3]. 3-trimethoxy silyl propyl methcarylate propane was used as the silane precursor for the study and the synthesis was done as per the patented procedure [4]. The feasibility of incorporation of magnesium was investigated by evaluating the physico-mechanical properties of photocured composites. Different concentrations of inorganic contents were incorporated into the resin according to the weight percentage of the silane precursor (0-0.5%). Better properties were obtained for photocured composites prepared from resin containing 0.5% of magnesium content [MR1]. This proved that magnesium in the inorganic-organic hybrid resin has significant role in imparting good properties. Better performance obtained for 0.5% of magnesium containing resin based photocured composites is may be due to the availability of multifunctional groups. The synergetic effect of the inorganic content within the resin of this particular composition supplements better properties for the composites. The absence of reaction site hinders the performance of other formulations. This optimized formulation was selected for further studies including *in vitro* cytotoxicity, cell viability, *in vitro* cell adhesion and bioactivity. The test material MR1 was found to be non-cytotoxic [Figure 1] to fibroblast cells as per the cytotoxic test conducted (ISO 10993-5) These novel magnesium containing bio-composites possess lower polymerization shrinkage, good mechanical properties, non-cytotoxic, good cell viability, good cell adhesion and bioactivity. The application of this novel bioactive resin is not limited in the areas of dentistry or orthopaedic but can extent to bioactive coating applications also.

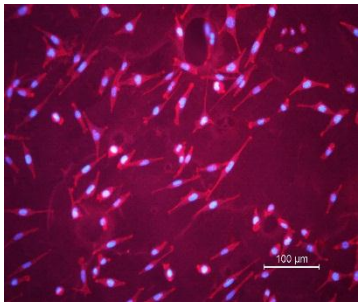


Figure 1. *I*n vitro cytotoxicity study of MR1 using L929 mouse fibroblast cells .

References

[1] Bose, S; Tarafder, S. *Acta Biomater* 8 (2012) 1401–21.

[2] Hickey Daniel, J; Ercan, Batur; Sun, Linlin; Webster, Thomas J. *Acta Biomater* 14 (2015) 175– 184.

[3] Koulourides, H; Cueto, Heriberto T; Pigman, W. *Nature* 189 (1961) 226-227.

[4] Lizymol Philipose Pampadykandathil, Vibha Chandrababu. A process for the synthesis of inorganic-organic hybrid resins comprising of alkoxides or mixture of alkoxides of calcium, magnesium, zinc, strontium, barium and manganese with polymerizable (di/tetra) methacrylate groups, Patent Application Number 4027/CHE/2014.

[5] International Organization for Standardization:ISO 10993-5:2009. Biological evaluation of medical devices Part 5: Tests for in vitro cytotoxicity 3rd ed: 2009.

MACRO 404

Green one step morphosynthesis of silver nanoparticles and their antibacterial and anticancerous activity

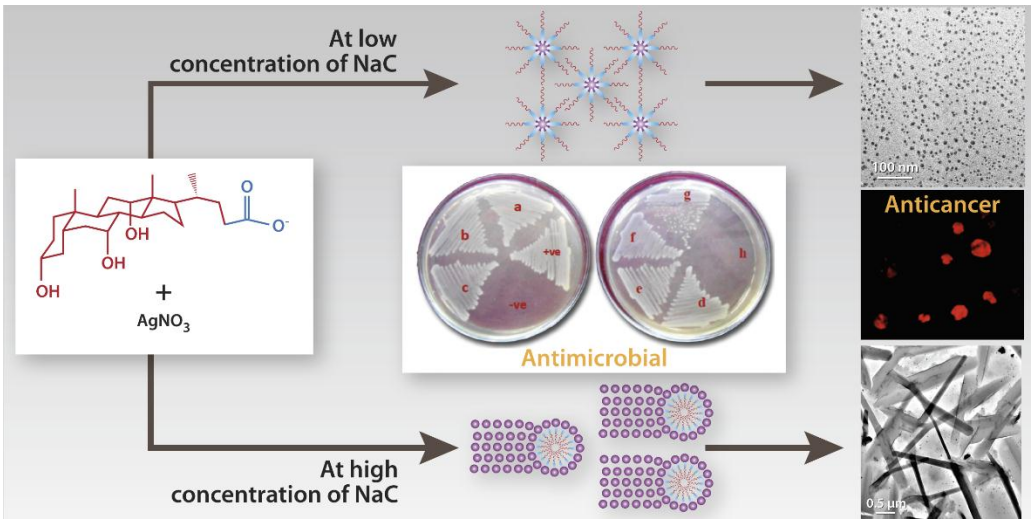
Maity, Dipanwita[a]; Pattanayak, Sutanuka[b]; Chakraborty, Mukut[b]; and Chattopadhyay, Dipankar[a] *

[a]*Department of Polymer Sc. & Tech., University of Calcutta, 92, A.P.C Roy Road, Kol-9*

[b]*Department of Chemistry, West Bengal State University, Barasat, Kol-126*

***dipankar.chattopadhyay@gmail.com**

Keeping the biological perspectives in mind, effort has been made to synthesize Ag NPs using one type of macromolecule “bile salt”. The bile salts play an important role in the digestion of fat and lipids and are naturally occurring steroidal detergents in mammals. Bile salts carry out a vital bioactive responsibility among the various physiologically important molecules. The use of bile acids and their conjugates in nanoscience is a novel idea, which opens up fascinating prospects and gives rise to various versatile properties. A facile, environmentally benign shape-controlled synthesis of anisotropic, crystalline silver nanostructures has been developed using sodium cholate, a biosurfactant as the reducing, stabilizing, and shape-directing agent and has been reported herein. Great latitude in the control of particle size and shape, including formation of hitherto unreported star and wires, could be accomplished through simple variation of the experimental conditions. The silver precursor concentration and the ratio of sodium cholate to silver precursor were found to be the critical factors in morphosynthesis. The formation of nanoparticles (NPs) was monitored using UV-vis spectroscopy. The synthesized NPs were characterized by transmission electron microscopy technique for morphological studies. The interaction between NPs with bile salts was investigated using Fourier transform infrared spectroscopy. The possible mechanistic role of sodium cholate on the reduction and stabilization of silver nanoparticles (Ag NPs) has also been discussed. The obtained Ag NPs exhibit antibacterial and anticancerous activity. The present study also explores the cytotoxic role of Ag NPs on KG-1A (human acute myeloid leukemia) and K562 (human chronic myeloid leukemia) cell lines.

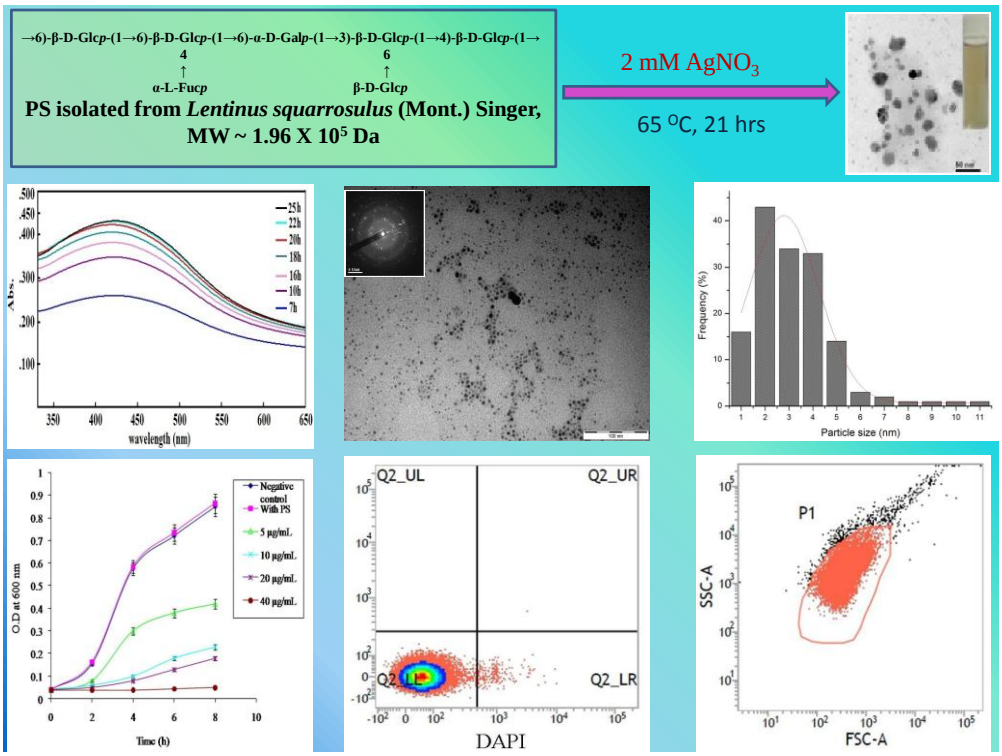


MACRO 405

Antibacterial and DNA degradation potential of silver nanoparticles-polysaccharide composite synthesized via green route

Manna, Dilip Kumar* and Maity, Kankan Kumar
Department of Chemistry & Chemical Technology, Vidyasagar University, Midnapore, West Bengal, 721102.
**dilipmanna99@gmail.com*

In recent years mushroom derived polysaccharides (PS) have drawn the attention of chemist and immunobiologists for their immunomodulation and antitumor properties. It has been observed that the molecular structure, molecular weight, branching pattern, structural modification, conformation, and solubility significantly affect their biological activities. The aims of this study was utilization of properties of both silver nanoparticles (AgNPs) and PS. AgNPs-PS conjugate were synthesized using a hetero polysaccharide (PS) (consisting of glucose, fucose and galactose) isolated from *Lentinus squarrosulus* (Mont.) Singer which serves the role of both reducing as well as stabilizing agent. UV-vis spectroscopy showed maximum absorbance at 407 nm due to surface plasmon resonance. High resolution transmission electron microscopy (HRTEM) exhibited that the average diameter of the nanoparticles was 2.78±1.47 nm. The XRD analysis revealed face-centered cubic (fcc) geometry of AgNPs. Antibacterial activity of the AgNPs-PS conjugate was tested against multiple antibiotics resistant (MAR) *Escherichia coli* strain MREC33 and found that the killing was due to generation of reactive oxygen species (ROS). Internalization of AgNPs-PS conjugate along with its DNA degradation capability was demonstrated using Flow cytometry. AgNPs-PS conjugates showed negligible toxicity to human RBCs. This LD_{50} dosage of AgNPs-PS conjugates in combination with each of the four antibiotics (ampicillin, azithromycin, kanamycin and netilmicin) to which *E. coli* MREC33 was resistant, showed synergistic effect to inhibit complete bacterial growth.



MACRO 407

A Study on Acid and Enzymatic Hydrolysis of Millet Bran, Strain Screening and Effect of Neutralizing Agents on Fermentative Production of D-Lactic Acid

Rengesh Balakrishnan[a], Subbi Rami Reddy Taddi[b], Senthilkumar Sivaprakasam[b*], Shyam Kumar Rajaram[a*]

[a] *Department of Biotechnology, Kamaraj College of Engineering and Technology, Virudhunagar, Tamil Nadu - 626001, India.*
[b] *BioPAT Laboratory, Department of Biosciences and Bioengineering, Indian Institute of Technology Guwahati, Assam – 781039, India.*

* Corresponding authors: [a]*- kingshyam2003@gmail.com & [b]* - senthilkumar@iitg.ernet.in

Fig 4: Enzyme Hydrolysis – FCCD, RSM

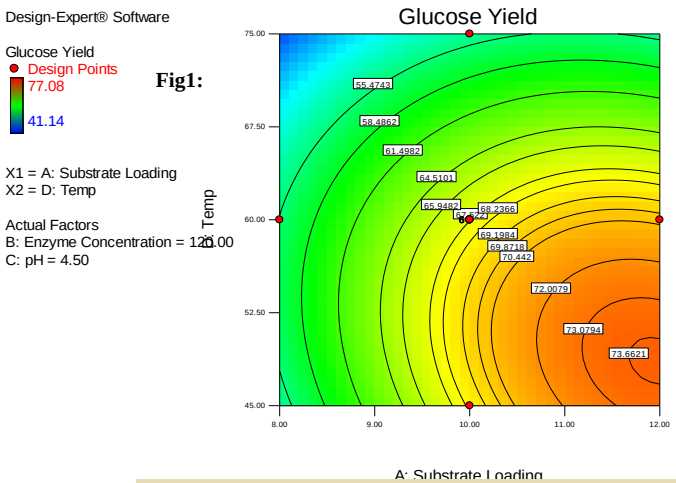
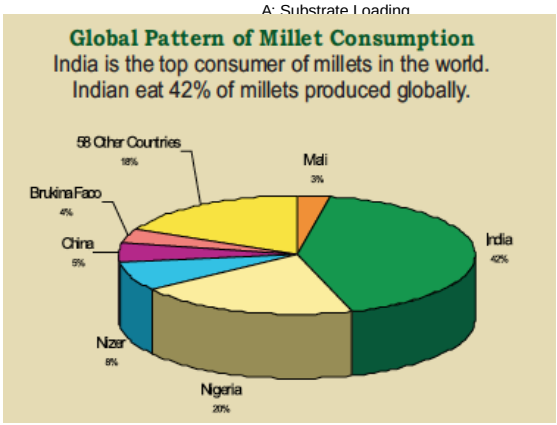


Fig1:

The exhaustive usage of fossil resources and earnest environmental threats as represented by global warming, has made an impact in search alternative viable biomass for sustenance of bioprocessing industries. Lactic Acid (LA) is an important multifaceted chemical that can be produced from biomass. It has applications in food, pharmaceuticals, packaging, leather and textile sectors. Two racemic mixtures of LA and its optical purity is a pivotal to the physical properties of PLA. There is a huge demand for the polymeric form of D-LA, a low valued isomer than its better-half especially for its thermostable biodegradable property. Many commercial producers worldwide have claimed to produce PLA through chemical or fermentative route utilizing agricultural residues. Some alternative feedstock that could overcome some disadvantages like more water consumption for its growth, economic, availability throughout the year for the production of D-Lactic Acid (DLA) is by the usage of millets. Millets are drought resistant xerophiles and may grow well in semi arid regions. They are pest resistant and thermophilic plants. This is the first study ever to report biorefinery potential of millet. In the present study we employed the use of bran of millet *Paspalum scrobiculatum*, as a nutrient source for the production of DLA. Bran of millet which accounts for nearly 20-25% of waste generated in millets processing industries was collected from a local industry in Tamil Nadu, India.

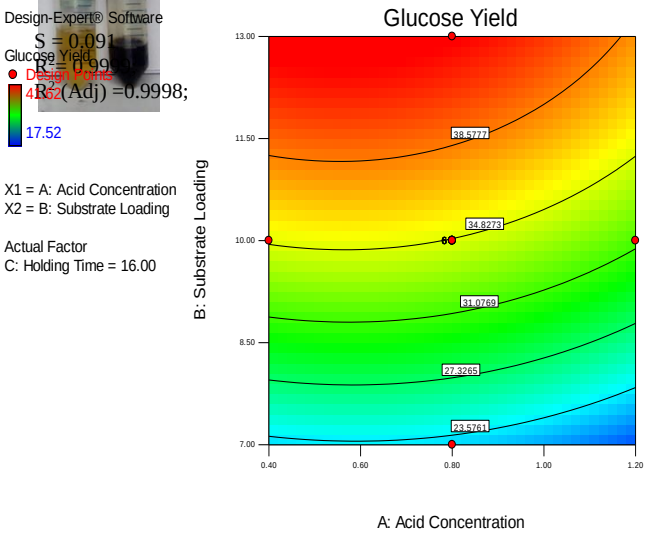




The bran powder was shade dried and sieved to size < 300 µm. This starch rich nutrient residue was characterised and further assessed statistically for its potential to produce reducing sugars through acid and enzymatic hydrolysis by FCCD, RSM procedures. Based on the results of the preliminary experiments HCl was chosen for acid hydrolysis. Three factors namely acid concentration (0.4 and 1.2 M), substrate loading (8 and 12 % (w/v)) and holding time (8 and 24 mins) was varied in three levels. While enzymatic saccharification step was optimized using four factors namely enzyme concentration (80 and 160 U/g), substrate loading (8 and 12 % (w/v)), pH (3.5 and 5.5) and Temperature (45 and 75ºC). Nearly 44 and 77 g/l of glucose was produced which was in accordance with the results of global optima predicted either of the above methods respectively.



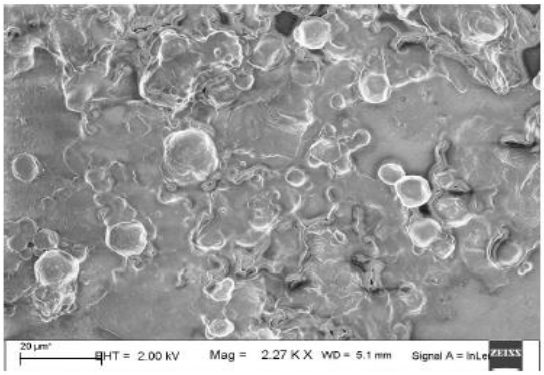
Fig 3: Acid Hydrolysis – FCCD, RSM

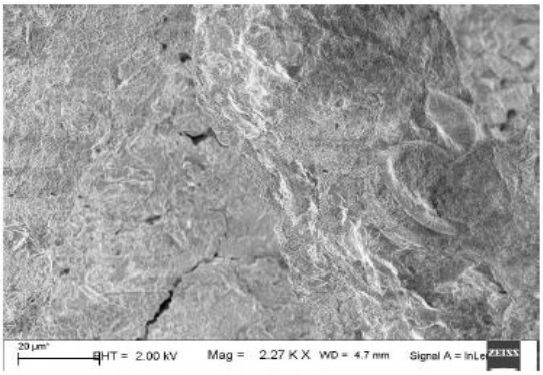


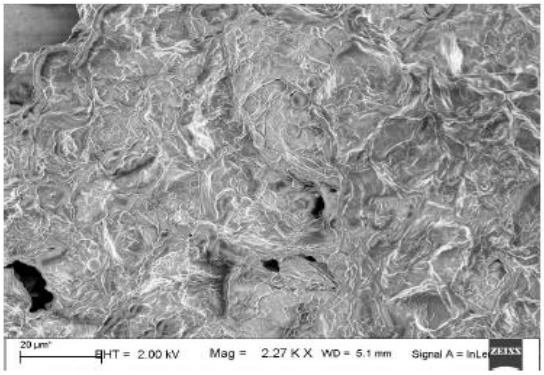
S=3.63
R^2= 93.59
R^2 (Adj) =87.62

Further analysis using SEM, FTIR confirmed the accessibility of glucose in the hydrolysate residue. Shake flask studies for strain screening was carried out using modified MRS media employing the hydrolysates. Bioreactor study was to done to investigate the effect of various

neutralizing agents for the high yielding optically pure DLA producer.







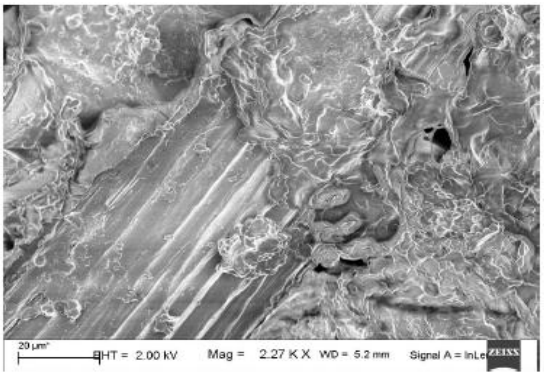


Fig 6. Bran of millet - Untreated

Fig 7. Acid Treated (HCl)

References

[54] Reddy Tadi, Subbi Rami, Arun EVR, Anil Mukund Limaye, and Senthilkumar Sivaprakasam. Enhanced production of optically pure d (–) lactic acid from nutritionally rich Borassus flabellifer sugar and whey protein hydrolysate based–fermentation medium. *Biotechnology and Applied Biochemistry* (2016) Just Accepted.

[55] Cingadi, Satish, Katla Srikanth, E. V. R. Arun, and Senthilkumar Sivaprakasam. Statistical optimization of cassava fibrous waste hydrolysis by response surface methodology and use of hydrolysate based media for the production of optically pure d-lactic acid. *Biochemical Engineering Journal* 102 (2015) 82-90.

[56] Yen, Hong-Wei, Tsia-Ju Chen, Wei-Chin Pan, and Hsien-Jen Wu. Effects of neutralizing agents on lactic acid production by Rhizopus oryzae using sweet potato starch. *World Journal of Microbiology and Biotechnology*. 26.3 (2010) 437-441.

MACRO 416

Osteogenic Drug–Layered Magnesiosilicate Complex and its Composite Scaffold for Bone Tissue Engineering Applications

S. Megha, [a] Bindu P. Nair, [a] Prabha D.Nair [b]

[a]*Department of Chemistry,Mahatma Gandhi College,Thiruvananthapuram-695022, India*

[b]*SreeChitraTirunal Institute for Medical Sciences and Technology,*

Thiruvananthapuram 695012, Kerala, India

** e-mail id: bindumelekkutu@gmail.com*

Abstract

We attempted to overcome the drawbacks of the oral and systemic administration of the drug for osteoporosis- strontium ranelate (SRA), by complexing it with an osteoinductive layered magnesiosilicate laponite and making its polymer composite scaffold. Laponite-SRA complex with electrostatic interaction between the drug and the clay was obtained through an aqueous phase reaction. Structural evaluation verified the complexation of the bulky SRA molecules with the negatively charged clay tactoid surfaces. The laponite-SRA complex was explored for bone tissue engineering by making its composite scaffold with polycaprolactone. The composite scaffolds with varying laponite-SRA complex content of 3-12 wt% were evaluated *in vitro* using human osteosarcoma cells. It was confirmed that an optimum composition of the scaffold with 3 wt% laponite-SRA complex loading would be ideal for obtaining enhanced ALP activity, by maintaining cell viability.

Keywords: *Clay; laponite; bone tissue engineering; strontium ranelate; osteoporosis*

Introduction

Osteoporosis is a very common disease condition among post-menopausal women. The bone cells osteoclasts and osteoblasts fail to create a balance between bone resorption and formation, which leads to a disruption of bone microstructure, leaving it porous and prone to fracture.

The positive effect of strontium, an alkaline earth metal on bone homeostasis has recently been explored for improving bone regeneration.[1] Utilizing the mechanism of action of strontium on bone regeneration, SRA has been used as an oral drug for the treatment and prevention of osteoporosis.[2] However, the disadvantages of SRA as a drug for the oral and systemic treatment of osteoporosis are the occurrence of adverse effects such as the increased risk of venous thrombosis, diarrhoea, nausea, headache and cutaneous hypersensitivity.[3] In the present study, the use of SRA for localized delivery in tissue engineering applications has been explored by combining it with an osteoinductive layered magnesiosilicate laponite, with a view to overcome the above drawbacks.

Laponite is a synthetic hectorite, consisting of relatively uniform disc-shaped particles of 25 nm diameter and 1 nm thickness and has an empirical formula of $Na^{+}_{0.7}[(Si_8Mg_{5.5}Li_{0.3})O_{20}(OH)_4]^{-}_{0.7}$ (Figure 1).[4] Studies have proven that laponite can induce bone formation even in the absence of any osteoinductive factors.[5] In the present study, a complex of strontium ranelate with laponite is attempted for the first time for bone tissue engineering, with a view to release the drug in a localized and controlled manner at the required site.[6] The complex was made into a composite scaffold with polycaprolactone (PCL). *In vitro* evaluation of the scaffold consisting of laponite and strontium ranelate, using human osteosarcoma cells is also presented in the article.

Experimental

Materials

Strontium ranelate and PCL (Aldrich, Mw = 70000- 90000 g/mol) were purchased from Sigma, India. The clay used was a synthetic hectorite Laponite RD from Bayville Chemical Supply Company Inc., USA. 1,4 Dioxane was purchased from Merck Specialties Pvt. Ltd., India. Dulbecco's Modified Eagles Medium, High Glucose (DMEM-HG), phosphate buffered saline (PBS), penicillin-streptomycin and fetal bovine serum (FBS) were purchased from Gibco (USA). Human Osteosarcoma (HOS) cell line was sub-cultured from a stock culture obtained from National Centre for Cell Sciences, India.

Methods

Preparation of Laponite-SRA Complex

SRA was complexed with laponite (LAP) by treating aqueous laponite suspension (2.2 wt %) with an aqueous solution of SRA and the solution was stirred at ambient conditions for 2 h. The turbid and the viscous solution obtained was slow-dried at ambient conditions at 37^{o}C in an air oven and the thin film-like material obtained was powdered using a mortar and pestle and used for further characterization.

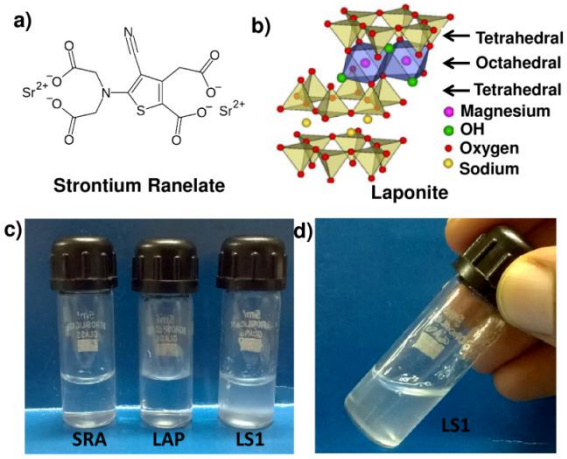
Fabrication of PCL-LS 3D scaffolds

PCL-LS composite scaffolds were prepared through solution blending method. PCL was dissolved in 1,4 dioxane to obtain a 7 wt% solution to which the required amount of LS1 complex was added (3, 6 and 12 wt% of PCL) and the mixture was blended manually. The PCL-LS blend obtained was lyophilized to obtain a three dimensional porous scaffold. The resulting composite scaffolds were denoted respectively, as PLS3, PLS6 and PLS12.

The LS complexes were characterized using X-ray diffraction (XRD), Fourier-Transform Infrared spectroscopy (FT-IR), UV-Visible spectroscopy and transmission electron microscopy (TEM) for its structure and morphology. The PLS scaffolds were characterized using scanning electron microscopy, for its morphology. Release of SRA from the PLS scaffolds was studied in water using UV-visible spectrophotometer, by comparing the intensity of the peak at a wavelength of 318 nm.The swelling and degradation studies of the scaffolds were carried out in PBS.

In vitro Evaluation

HOS cells were seeded onto PCL and PLS scaffolds as a concentrated droplet at a density of 1000 cells/mm^3 of the scaffolds. The cells were allowed to adhere on the scaffolds by incubating for about 30 minutes and supplemented with 1mL DMEM-HG containing 10% FBS and 1% penicillin-streptomycin. The medium was changed every 2 days, and the cells on the scaffolds were cultured for up to 8 days. The cell-seeded scaffolds were fixed in paraformaldehyde solution (4% w/v) for 4 h, and the morphology of the cells was examined by E-SEM scanning electron microscope. The cell viability on the scaffolds was assessed using the Live/Dead staining kit and the procedure is reported.[7] The images were obtained on a confocal microscope. ALP activity was determined by colorimetric endpoint assay which measures the enzymatic conversion of p-nitrophenyl phosphate (pNPP) to the yellowish product p-nitrophenol (pNP) in the presence of ALP and the procedure is reported elsewhere.[7]



Results and discussion

Figure 1.(a) Chemical structure of SRA molecule (b) schematic representation of laponite and (c) and (d) photographic images of aqueous 0.1% solution of SRA, 1.1% suspension of laponite and the LS1.

An aqueous solution of laponite was treated with SRA at two concentrations, one and two times equivalent to the cation exchange capacity of laponite. Upon mixing the laponite and the SRA solutions, turbidity and increase in viscosity of the solution become evident immediately, indicating the interaction of SRA with the laponite (Figure 1c and d). The laponite-SRA reaction products were retrieved by slow drying, powdered and analyzed using XRD. It was confirmed that the increase in the structural ordering of the laponite was occurring at the expense of the loss of crystallinity of the SRA. The FTIR peak at 1579 cm^{-1} for SRA was due to the characteristic C=O stretching vibrations for a carboxylate salt. It was evident that for both LS1 and LS2, this peak showed a shift to a lower value of 1522 cm^{-1} showing the complexation. It was confirmed from the UV-visible spectra that the electrostatic interaction of the SRA with the laponite does not lead to any structural change of the SRA. Based on the above findings, it is proposed that the bulky SRA molecules are unable to intercalate in the clay interlayer through the cation exchange mechanism. Rather, the SRA molecules when added to laponite at a concentration equivalent to the CEC will interact with the negatively charged surface of the clay tactoids, through electrostatic interaction. However, when the concentration of SRA was increased two equivalents to that of the CEC, a gradual decrease in the structural ordering was evident. This could be due to the excess of SRA molecules over that required to achieve structural ordering, which could disturb the extended ordering of clay tactoids.

Figure 2. SEM images of the horizontal cross-sections of the scaffolds (a) PCL (b) PLS3 (c) PLS6 and (d) PLS12.

Since LS1 or LS2 as such do not have the characteristics to form a scaffold for bone tissue engineering, and also a high dose of laponite or SRA can cause cytotoxic effects, the LS1 complex was made into a composite scaffold form, by blending it with the biodegradable polymer PCL using the solvent 1,4 dioxane and the technique of freeze drying. From the SEM images of the horizontal cross-sections of the scaffold (figure 2), the pore sizes of the scaffolds were found to vary between 30-150 µm.

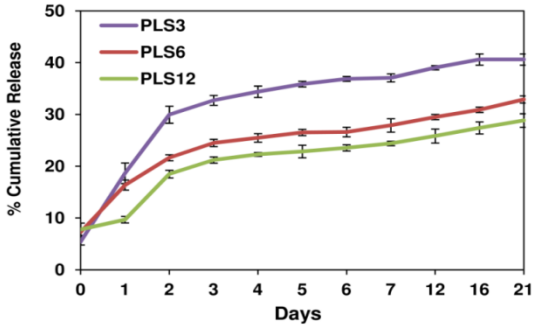
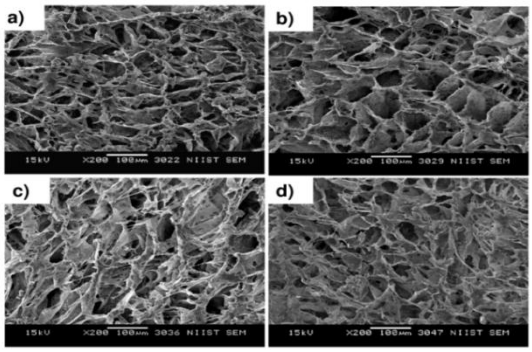


Figure 3. Release profile of the SRA from PLS3, PLS6 and PLS12.



Release of SRA from the PLS scaffolds was studied in water and it was confirmed that the cumulative release of the drug exhibited inverse relation with the loading of the LS1 complex in the PLS scaffolds. (figure 3) Percentage cumulative release from the PLS3 scaffolds was found to be the highest, by releasing a maximum of 40 % of the total drug loaded in 21 days.

The scaffolds were evaluated *in vitro* for its cytocompatibility by using HOS cells. From the confocal micrographs, the cells appeared mostly live on the control and all the PLS scaffolds (Figure 4). The cells on the PCL and the PLS3 scaffolds appeared to have spread morphology; whereas with increase in the LS content, cells appeared with round morphology. The cells were exposed to the released components from the scaffolds into the medium, which was found sufficient to exert a uniform effect on its physiological behaviour.

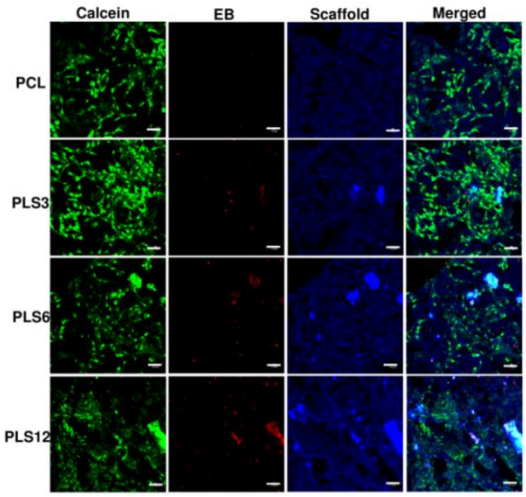


Figure 4. Confocal micrographs of the cell seeded scaffolds PCL, PLS3, PLS6 and PLS12 on day 8. Scale bar represents 50 µm.

As the scaffolds were cytocompatible, to elucidate which composition would be the best for bone tissue engineering, ALP activity of the cells on the scaffolds was measured (figure 5). Since differentiated osteosarcoma cells were used for the study, measurable ALP activity was expressed by the cells on all the scaffolds. However, when compared to the control PCL scaffold, the total ALP activity on the PLS scaffolds showed significant enhancement. Upon normalization of the total ALP activity with respect to the amount of the total protein, the significant enhancement in ALP activity was limited to the PLS3 and the PLS6 scaffolds. From the study, it is suggested that a 3wt% loading of the LS complex in PCL is sufficient to obtain enhanced ALP activity, which makes that composition ideal for bone tissue engineering.

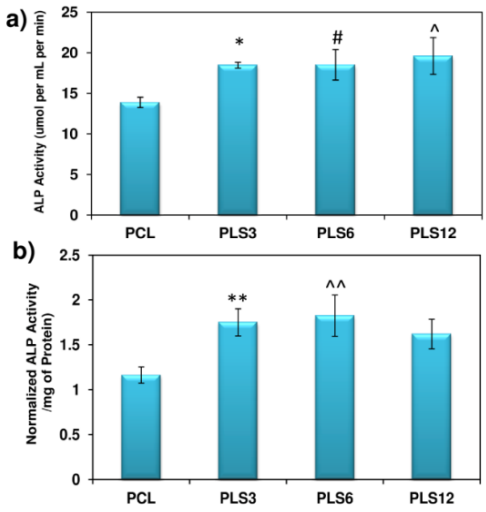


Figure 5. (a) Total and normalized ALP activity on day 8, Values is expressed as mean± standard deviation from three different replicates. The symbols *, #, and ∧ indicate $p < 0.01$, respectively for PCL vs. PLS3, PCL vs. PLS6 and PCL vs. PLS12; ** and ∧∧ indicate $p < 0.05$ for PCL vs. PLS3, PCL vs. PLS6.

Conclusions

In conclusion, a complex of strontium ranelate with the osteoinductive mineral laponite was attempted with a view to overcome the drawbacks of the oral and systemic administration of strontium ranelate. Strontium ranelate was complexed with laponite through electrostatic interaction between the negatively charged clay tactoid surfaces and the strontium cation. Polycaprolactone composite scaffolds containing varying amount of the laponite-strontium ranelate complexes were also fabricated. In vitro evaluation of the scaffolds using HOS cells verified that an optimum composition of 3 wt% loading would be sufficient to obtain enhanced ALP activity by maintaining cell viability.

Acknowledgements

This research was supported by DST-INSPIRE Faculty fellowship and research grant (IFA-11-CH-19) to BPN from Department of Science and Technology (DST), India.

References

20. E. Gentleman, Y. C. Fredholm, G. Jell, N. Lotfibakhshaiesh, M. D. O. Donnell, R. G. Hill, M. M. Stevens, *Biomaterials* 31,3949, 2010.
21. E. Bonnelye, A. Chabadel, F. Saltel, P. Jurdic, *Bone* 42, 129, 2008.
22. R. Rizzoli, J. Y. Reginster, *Expert Rev. Clin. Pharmacol.* 4, 593, 2011
23. W.K. Kegel,; H. N. W. Lekkerkerker, *Nat. Mater.10*, 5, 2011.
24. J. I. Dawson, R. O. C. Oreffo, *Adv. Mater.* 25, 4069, 2013.
25. B. P. Nair, S. Megha , P. D. Nair Colloids and Surfaces B: *Biointerfaces* 143 , 423, 2016.
26. B. P. Nair, D.Gangadharan, N. Mohan, B. Sumathi, P. D. Nair, *Mat. Sci. Eng. C*, *52*, 333, 2015

MACRO 419

Graphene Oxide immobilized Polyolefin membranes for Antibacterial surface properties

Mural, Prasanna Kumar S [a]*

[a] *Centre for Nano Science and Engineering, Indian Institute of Science, Bangalore-560012*

Prof. Giridhar Madras[b]

[b] *Department of Chemical Engineering, Indian Institute of Science, Bangalore-560012*

Dr. Suryasarathi Bose[c*]

[c] *Department of Materials Engineering, Indian Institute of Science, Bangalore-560012,*

** Corresponding E-mail address:sbose@materials.iisc.ernet.in*

Antibacterial membranes covalently bonded with graphene oxide (GO) were synthesized by chemical modification of polyolefins. Low Density Polyethylene (PE) was chemically modified with acid treatment followed by coupling it with GO. GO functionalization of PE membranes was confirmed by Fourier transform infrared spectroscope (FTIR), X-ray photoelectron spectroscopy (XPS), SEM and Raman mapping. The morphological studies by SEM were carried out and annealing revealed coarsening of uncompatibilized PE membranes and stabilized morphology for compatibilized PE membranes. Direct contact of bacteria with GO functionalized PE membranes resulted in 99 % bacterial inactivation after 6 h of contact time. The possible bacterial inactivation mechanism i.e. physical disruption of bacterial cell wall and reactive oxygen species (ROS) was discussed. The present study avails new avenue of covalent functionalizing GO sheets on inert PE membranes for effective antibacterial activity.

References

[57]Mural, P. K. S.; Jain, S.; Kumar, S.; Madras, G.; Bose, S.. *Nanoscale*, 8 (2016), 8048.
[58]Pendergast, M. M.; Hoek, E. M., *Energy & Environmental Science*, 4 (2011), 1946.

MACRO 423

Covalently Cross-linked Multifunctional Polycaprolactone / Graphene Composites for Bone Tissue Regeneration Applications

Padmavathy Nagarajan, L.R. Jaidev and Kaushik Chatterjee*

Department of Materials Engineering, Indian Institute of Science, Bangalore-560012

** kchatterjee@materials.iisc.ernet.in*

The present work demonstrates the importance of developing strong bio composites such as polycaprolactone (PCL) with high ductility by utilizing the potential of graphene oxide (GO) as a reinforcement filler. The abundant functional groups such as hydroxyl, carboxyl and epoxide groups were exploited as reactive sites (as co initiators) to grow PCL chains by in situ polymerization yielded GO-grafted PCL (GO-g-PCL) and amine

GO-grafted PCL (GO-NH_2-g-PCL) respectively. These covalently bonded fillers and non-covalently bonded fillers of these GO based particles (5 wt%) reinforced with PCL led to crosslinked composites and physically blended composites. Covalently grafted GO-PCL composites exhibited high ductility nearly identical to the neat PCL (elongation at break ~650%). Concurrently, grafted and blended amine GO composites displayed an enhanced strength and elastic modulus more than PCL and lesser than GO composites. A combination of improved yield strength (~ 27 MPa), elastic modulus (~ 450 MPa) and prominent ductility (~ 650 %) were remarked for covalently cross linked GO-PCL composites (GO-g-PCL+PCL). These observations pointed out that terminally hydroxylated / carboxylated PCL chains covalently grafted to GO surface prevented GO layers from re-stacking and agglomeration affording improved dispersion as well as stronger interfacial bonding between the matrix and GO. *In vitro* cell studies further supported in cell proliferation of human mesenchymal stem cells for the grafted composites of GO and amine GO. Taken together, GO-g-PCL+PCL and GO-NH_2 -g-PCL+PCL were demonstrated as more ductile, biocompatible composites as compared to their counterparts GO-PCL and GO- NH_2-PCL. This approach is expected to be helpful for developing strong and highly ductile biopolymers as load bearing biomaterial in orthopedic applications.

MACRO 431

Interpenetrating Photopolymers for Intraocular Lens Application

Shaik Syed Hussain, Shailaja Donempudi and Shekharam Tammisetti *

Polymers and Functional Materials Division, CSIR-Indian Institute of Chemical Technology

Hyderabad-500007, India.

**shekharam@iict.res.in*

Cataract is a very common eye ailment that affects millions of people around the world. Replacement of affected lens in the eye with a synthetic Intra Ocular Lens (IOL) is the preferred mode of treatment to restore clear vision to patients affected with cataract [1-2]. Interpenetrating photopolymer network materials suitable for Intraocular Lens (IOL) application are presented. Rapidly curable, transparent, hydrophobic material with appropriate optical and thermo-mechanical properties has been prepared from Benzyl acrylate and Benzyl methacrylate. To improve its biocompatibility and optimize surface-cell interactions, this material was modified to be either more hydrophobic or more hydrophilic by copolymerization with a fluoroacrylate or a PEG acrylate respectively. All materials were characterized for their optical and thermo-mechanical properties. Their biocompatibility and interaction with mouse fibroblast cells was also studied. More hydrophilic materials showed more advantageous cell interactions and may be better suited for IOL application [3].

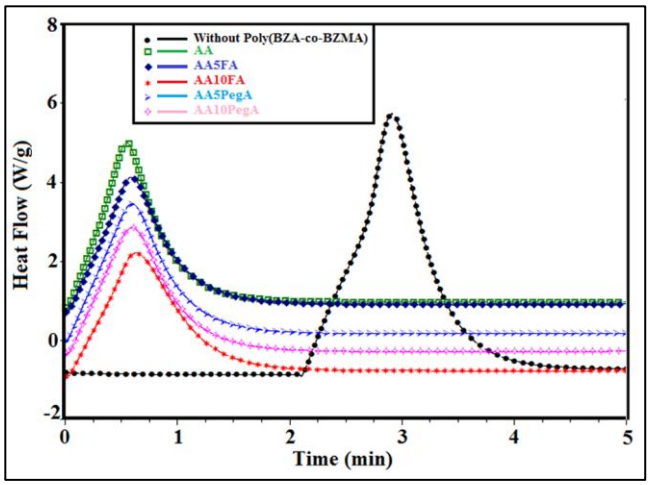


Figure: Photo DSC curing study of the modified resins.

References

[1] D, Bozukova; C, Pagnoulle; R, Jerome. *Materials Science and Engineering: R: Reports*, 69 (2010) 63.
[2] A W, Lloyd; R G, Faragher; S P, Denyer. *Biomaterials*, 22 (2001) 769.
[3] D, Bozukova; C, Pagnoulle; M C, De Pauw-Gillet; S, Desbief; R, Lazzaroni; N, Ruth; R, Jerome; C, Jerome. *Biomacromolecules*, 8 (2007) 2379.

MACRO 433

Copper Decorated Reduced Graphene Oxide nanoparticle Embedded Polycaprolactone Nanocomposite for Blood Vessel Tissue Engineering

L.R. Jaidev, Sachin Kumar, Sai Ramakrishna Meka and Kaushik Chatterjee*
Department of Materials Engineering, Indian Institute of Science, Bangalore-560012, India.

**Corresponding Author E-mail: kchatterjee@materials.iisc.ernet.in*

Abstract

Angiogenesis or Blood vessel formation is crucial for a successful regeneration of any organ in the body using tissue engineering methods. Here, we studied copper nanoparticle decorated reduced graphene oxide nanoparticles (RGO-Cu) and embedded with polycaprolactone (PCL) to develop a unique multifunctional nanocomposite (PCL-RGO-Cu) that promote angiogenesis and anti-bacterial activities. The RGO-Cu nanoparticles were characterized for the morphological properties using SEM and TEM. The TEM images showed the decoration of copper nanoparticles of average size 8 nm on the RGO. RGO-Cu blended PCL nanocomposite films were prepared by spin coating method. The cell proliferation and cell attachment abilities of the defect free nanocomposite films were studied by culturing SVEC (Smooth Vascular Endothelial Cells) for 7 days. The angiogenic potential of the scaffolds was studied in matrigel and assessed by tube formation assay. RT-PCR analysis for VEGF and ANG-2 genes showed increased fold expression which assesses the angiogenic potential of the scaffolds on SVEC cells. The antibacterial studies on Escherichia coli bacteria by PCL-RGO-Cu nanocomposite showed improved antibacterial activity. We observed that PCL-RGO-Cu

nanocomposite showed angiogenic and antibacterial properties. Hence it might be a suitable biomaterial for Blood vessel tissue engineering.

MACRO 448

Guar Gum Based Super Absorbent Hydrogels for Agricultural Applications

Thombare, Nandkishore*[a], Jha, Usha[b], Mishra, Sumit[b] and Siddiqui, MZ[a]

a. Processing and Product Development Division, ICAR-Indian Institute of Natural Resins and Gums, Namkum, Ranchi-834010, India.
b. Department of Chemistry, Birla Institute of Technology, Mesra, Ranchi-835215, India.

*Corresponding author: nandkishore.icar@gmail.com

Abstract:

In agriculture sector, use of synthetic polymers is more popular than natural polymers due to their stability towards environmental breakdown. But the non-biodegradability of these synthetic super absorbent polymers causes serious and long-term environmental issues. Also, SAPs derived from petrochemical sources may cause serious economic problems in future. Due to these growing environmental concerns attempts are being made to replace artificial SAPs by natural polymer based SAPs. Guar gum is considered as a potential natural candidate as starting material for modified polymers to be used in various applications [1]. Guar gum, when chemically blended with certain synthetic grafting and cross-linking agents, yields tailor-made products whose properties and biodegradability can be controlled. This property of guar gum and its easy availability at reasonable cost make it one of the best starting polymers for agricultural applications. Due to non-toxicity, biodegradability, varying solubility, film forming ability, drug release retarding property and susceptibility to microbial degradation, guar gum based polysaccharides can be used as an alternative material to the synthetic polymers.

Grafted and cross-linked hydrogels of guar gum have revealed tremendous potential to be exploited in pharmaceuticals, bioremediation, in agriculture as a matrix for sustained nutrient release, as soil conditioner and for many more uses. These hydrogels act as ‘miniature water reservoirs’ in soil, releasing water into the soil as per requirement of plant roots and also have the favorable alteration to the physical properties of soil [2,3].

In this study interpenetrating network of natural guar gum and polyacrylate was cross-linked to create complex web like structure, so as to absorb and hold maximum water in it. Reaction

conditions and reagent ratios were optimized for getting better desired properties for intended applications. The synthesized guar gum based hydrogels showed good water holding capacity, about 600-800 ml/g. Further these are being evaluated as soil conditioners as well as matrix for the controlled release of plant nutrients in soil and water.

References:

1. Thombare, N; Jha, U; Mishra, S; Siddiqui, MZ. *International journal of biological macromolecules*, 88 (2016) 361.
2. Taylor, KC; Halfacre, RG. *Horticulture Science*, 21 (1986) 1159.
3. Silberbush, M; Adar, E; De-Malach, Y. *Water Management*, 23 (1993) 303.

MACRO 453

Protein Induced Disassembly and Release of Guest Molecules from a Biodegradable Nanocontainer

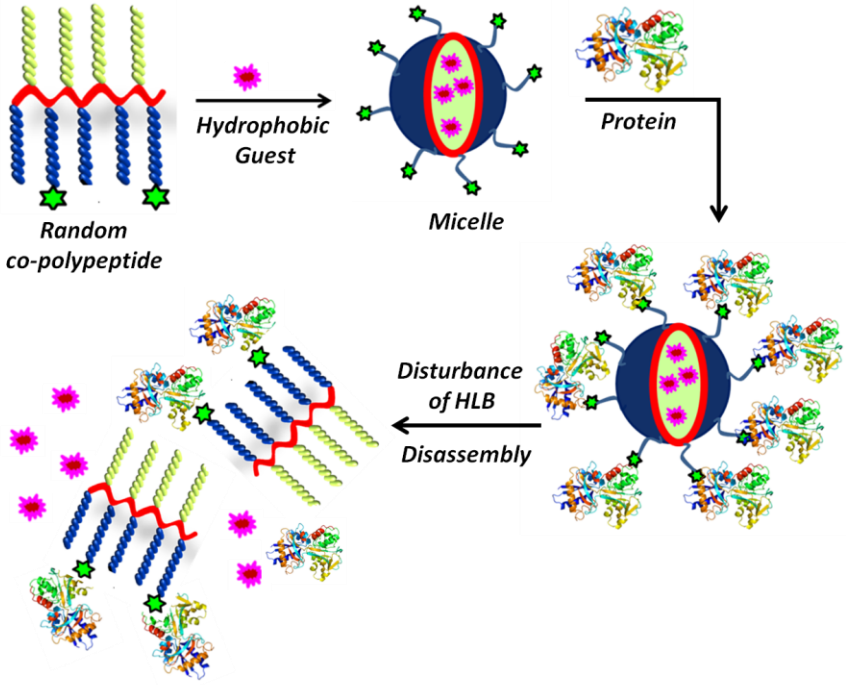
Molla, Mijanur[a] and Thayumanavan, S[b]*

[a]*Karlsruhe Institute of Technology, Karlsruhe, Germany-76344*
[b]*Department of chemistry, University of Massachusetts, Amherst, USA-01003*

** Corresponding author's Email: thai@chem.umass.edu*

Abstract: In the context of the delivery of drug and release to a specific location, stimuli responsive release of the drug has attracted great interest in recent years, because of controlled release, enhanced cell efficacy and less side effects. In general, commonly used stimuli are pH, temperature, redox potential and magnetic fields. To be precise, biological stimuli [1,2] like protein induced disassembly has become very much attractive because in most of the cases proteins are over expressed in the disease location and by utilizing this advantage delivery of the drug molecules to the specific location would be better. Polymeric micelle is more appealing because these assembly exhibit low critical aggregation concentration (CAC) and high stability relative to small molecular assembly. More specifically nanocontainer made of Amphiphilic polypeptide has become a promising candidate because of their biocompatibility and biodegradability.

In this context, we have designed a biodegragble amphiphilic polypeptide having pendant ligand 4-carboxy benzene sulphonamide which is inhibitor of protein named human carbonic anhydrase I (hCA1) (Scheme 1). We designed the system in such a way that after releasing the drug molecules, polymer will be degrading by the protease and esterase enzyme into small molecules which are GRAS (Gnerally Recognized As Safe) molecules. We synthesized the target polymer by the ring opening polymerization (ROP) of the NCA (N-Carboxy Anhydride) monomers of functionalized amino acid (glutamic acid) using propyl amine as an initiator. By varying the monomer and initiator ratio we can vary the molecular weight of the polymer according to the requirement. This amphiphilic polypeptide forms micelle in aqueous solvent and that can noncovalently sequester hydrophobic guest molecules and release these guest molecules in response to specific protein. Generally hydrophilic –lipophilic balance (HLB) is playing a crucial role for the formation of the miceller assembly. Our proposed



Scheme1: Schematic presentation of polypeptide self-assembly and release of guest molecule

mechanism behind the release of the drug molecules is ligand present on the surface of the micelle interacts with the specific protein which causes disturbance of the HLB and eventually micelle disassemble and release the guest molecules.

Synthesis and detail spectroscopic studies [3] in support of drug encapsulation and release will be the topic of this presentation.

References:

[1] Azagarsamy, M. A.; Sokkalingam, P.; Thayumanavan. S. *J. Am. Chem. Soc.* **2009**, *131*, 14184.
[2] Raghupati, K. R.; Azagarsamy, M. A.; Thayumanavan. S. *Chem. Eur. J.* **2011**, *17*, 11752.
[3] Molla, Mijanur.; Prasad, P.; Thayumanavan, S. *J. Am. Chem. Soc.* **2015**, *137*, 7286.

MACRO 454

Development of polysaccharide derived carbon blocks for the removal of perchlorate from water

R. Radhika *, G. Rekha Krishnan, Deepthi L. Sivadas, Salu Jacob, R. Rajeev

Analytical and Spectroscopy Division, Analytical Spectroscopy and Ceramics Group,
Propallents Polymers Chemicals and Materials Entity,
Vikram Sarabhai Space Centre,
Thiruvananthapuram- 695 022, India
** e-mail id: r_radhika@vssc.gov.in*

Abstract
Many biomaterials are organised from nanoscale to macroscopic scale to give hierarchical materials that are sculpted with complex forms. Polysaccharides can be manipulated in the aqueous phase to generate highly mesoscopic structure which may be maintained in a final dried product. A significant amount of research has been performed to evaluate treatment for perchlorate remediation in drinking water. Development of a cost effective and a green sustainable material in the form of a block for the removal of perchlorate from water is discussed in this paper. Characterisation of the synthesised CBs was done by FTIR, Raman spectroscopy, XRD, FESEM and surface area of the CBs was measured by the adsorption of nitrogen (BET) method.

Keywords: *polysaccharides; perchlorate; FTIR; adsorption capacity; co-existing anions*

Introduction
Nature is adept at the self assembly of organic polymers such as polysaccharides in a wide range of structural and storage roles in higher plants. The nanostructured forms of Polysaccharide biomass can be manipulated to generate more stable porous carbonaceous forms which may be maintained in a final dried product for high value applications.[1-3] Porous carbon materials are ubiquitous with a wide range of technologically important applications, including heterogeneous catalyst supports, water purification filters as well as the developing future areas of energy generation and storage.
The fast urbanization, industrialization and agricultural activities in recent years, toxic materials such as heavy metals and organic and inorganic chemicals can enter into water bodies causing water pollution.[4,5] Perchlorate is considered as a potential environmental contaminant and it has been detected in soil, surface water as well as ground water. Perchlorate and its salts are widely used as oxidizer in solid rocket propellants, explosives, missiles and various commercial products. Perchlorate has received tremendous attention in the recent years, mainly due to the challenges faced by the drinking water industry regarding its treatment.[6] The main health concern is its ability to interfere with iodine uptake by the thyroid gland resulting in decreased production of the thyroid hormones.[7,8] Due to its adverse effects on human health, USEPA set an interim health advisory level of perchlorate at 15 ppb in 2009 and has declared a decision to regulate perchlorate under the Safe Drinking Water Act in 2011.
The biggest advantage of using activated carbon in the drinking water treatment industry is that it can be easy to retrofit to target perchlorate in the water. Activated carbons for these applications are typically derived from low cost renewable materials.[9,10] Activated carbon is a carbonaceous material with a large internal surface area and

highly developed porous structure resulting from the processing of raw materials under high temperature reactions. A substance with a high carbon and low ash content can be used as a raw material.[11,12] Activated carbon can be produced via two routes: physical activation and chemical activation. The most commonly used chemical activating agents are H_3PO_4, $ZnCl_2$, K_2CO_3 and KOH.[13]

Starch has a naturally, nano-channelled biopolymer structure which can be utilized as a template. Cooking starch in water opens its internal structure forming an accessible mesoporous network. This utilizes nature's ability to form nano-channelled biopolymer structures in the starch granules of plants. It was found that at low temperature, further treatment with acid and heating will then convert the expanded starch template into stable, nanostructured, mesoporous carbonaceous networks. This approach towards the generation of nanostructures and new types of carbon-based materials with controllable physico-chemical properties, can be used in a variety of applications.

The present work deals with the synthesis and characterisation of carbon blocks (CB) obtained by using starch as the raw material. Batch experiments have been carried out to evaluate the removal of perchlorate from water using Ion chromatograph. The effect of different activating agents and different adsorption parameters were also studied.

Experimental

1. Materials

The raw material used for the synthesis of CBs is starch powder obtained from Light food products. The following chemicals used for the study were procured from Merck and of ACS grade: ethanol, (purity >85%), acetone (purity 99%), paratoluene sulphonic acid (purity 99%), H_3PO_4 (purity >85–89%), HCl (purity >36.5-38%), $ZnCl_2$ (purity > 99%), $FeCl_3$ (purity > 98%), NaCl (purity 99.5%), KOH (purity 85%), NH_4ClO_4 (purity >99.9%) prepared inhouse. Deionized water with an electrical resistivity of ≥ 18.1 MΩ/cm^2 prepared by a Millipore MilliPack 40 system was used in all experiment.

1.1 Synthesis of CB

The production of CB comprises of three main steps. Rice powder is gelatinised by heating in water. The resulting viscous solution is cooled to yield a porous gel. Water in the gel is then exchanged with the lower surface tension solvent ethanol and oven dried to yield a mesoporous starch. In the final stage the mesoporous starch is doped with a catalytic amount of an organic acid (para toluene sulphonic acid), heated under vacuum and carbonised. The mesoporous starch was further activated using different activating agents viz., HCl, $ZnCl_2$, $FeCl_3$, NaCl, KOH and H_3PO_4 and carbonised at 750°C for 2 hours in inert atmosphere (N_2 or Ar) at a heating rate of 5˚C/min. The main advantage of this synthetic route is to obtain CBs without using any template and also the low carbonisation temperature. Hence it is a greener sustainable material and surface chemistry tuneability enables post-modification strategies. The resultant CBs were evaluated for its efficiency for perchlorate removal by batch method. The maximum adsorption capacity for perchlorate was obtained for CB activated with phosporic acid and hence further studies were conducted using CB-H_3PO_4-750.

1.2 Characterisation of the CBs

Characterisation of the CBs was done by FTIR, Raman spectroscopy, XRD, FE-SEM, thermal analysis and surface area of the CBs was measured by the adsorption of nitrogen (BET) method. The moisture content in the sample was estimated by drying in an air oven at 105°C and the difference in weight gave the moisture content. The measurement of the extent of the pore surface developed within the matrix of the CB was done by using Quantachrome NOVA 1200 surface area and pore size analyzer. The specific surface area was determined by nitrogen adsorption of the sample by utilizing BET approach. The sample was preheated at 150 °C in vacuum condition and nitrogen adsorption was performed at 77 K.

X-ray diffraction and Raman spectroscopy are non destructive techniques. X-ray diffraction yields the atomic structure of materials and is based on the elastic scattering of X-rays from the electron clouds of the individual atoms in the system. XRD measurements were carried out using a Bruker D8-Discover X-ray diffractometer operating with a Cu anode (40 KV, 40 mA). Diffractograms were recorded using a solid state detector, LynxEye from 10 to 90° at a step size 0.02° and time/step 0.5sec. Samples were placed on top of a zero background silicon cup and diffractograms were recorded.

Raman spectroscopy is based on the inelastic scattering of monochromatic light. The Raman shift provides information about vibrational and rotational energies of molecular bonds. Raman spectroscopic analysis of the samples were carried out using WITec alpha 300R-Confocal Raman Microscope. The samples were illuminated with an excitation wavelength of 532 nm. Spectrum was obtained by accumulating five spectra with an integration time of 1 sec.

The surface and morphological study of samples were carried out by using Carl Zeiss, Supra 55 model field emission scanning electron microscope equipped with an energy-dispersive X-ray spectrometer (EDX). Energy Dispersive X-ray Spectroscopy, EDX identifies the elemental composition of materials.

Infrared spectra of the samples were recorded using Nicolet iS50 FTIR spectrometer. Solid samples were pelletized with KBr and IR spectra were recorded in the range 4000-400 cm^{-1} with resolution 4 cm^{-1}.

1.3 Estimation of perchlorate using IC

A Dionex model ICS 2000 Ion Chromatograph (IC) equipped with AS16 column, AG16 Guard column, ASRS 300 Suppressor column and a conductivity detector was employed for the analysis of perchlorate using 35.0 mM NaOH as eluent with a flow rate of 1 mL/min. Chromeleon chromatographic software was used for the data analysis of chromatograms by peak area and peak height methods. Before running a sample, the ion chromatography system is calibrated using a standard solution. From the calibrations and data obtained from the sample, concentration of perchlorate in the sample is calculated.

1.4 Batch adsorption experiments

1.4.1 Effect of different activating agents

The effect of different activating agents like HCl, H_3PO_4, NaCl, $ZnCl_2$, $FeCl_3$ and KOH on the activity of CBs on perchlorate removal was investigated and compared with CBs without activation. The adsorption experiments were carried out by taking 0.1 g of adsorbent (CBs obtained after activation and before activation) and equilibrate with perchlorate (50 mg/L) solution. All the adsorption experiments were carried out at room temperature in a shaker at a constant shaking speed and then monitored the aqueous-phase perchlorate concentration using IC.

1.4.2 Effect of contact time

The contact time required for the maximum adsorption of perchlorate (50 mg/L) was carried out using 0.1 g of CB-H_3PO_4-750. The concentration of perchlorate in the solution was analyzed at different time intervals from 10, 20, 30 min. upto 150 min.

1.4.3 Effect of perchlorate concentration

In order to study the effect of initial perchlorate concentration, CB-H_3PO_4-750 (0.1 g) was shaken with perchlorate solution having different initial concentrations (ranging from 10 -1000 mg/L) for 1 hour. The concentration of perchlorate in the solution was analyzed and the maximum adsorption capacity was calculated.

1.4.4 Effect of phosphoric acid percentage

The CB-H_3PO_4-750 had the maximum adsorption of perchlorate compared to other activating agents studied. The effect of the variation in the concentration of the H_3PO_4 (10-60 Wt %) on the adsorption of perchlorate was studied. The adsorption experiments were carried out by taking 0.1 g of adsorbent, equilibrate with perchlorate (50 mg/L) and monitored the perchlorate concentration in the aqueous phase.

1.4.5 Effect of co-existing ions

Effect of co-existing ions was examined by using 200 mg/L of perchlorate solutions which contain different amounts (ranging from 0 – 200 mg/L) of other commonly observed ions (nitrate, chloride & sulphate). 0.1 g of sample was weighed accurately, shaken with the perchlorate solution containing other anions for 1 hour in a shaker at room temperature and perchlorate adsorption was compared.

Results and discussion

2. Characterization of CBs

The surface area, pH and moisture content of the CB@750 and CB-H_3PO_4-750 ar given in Table 1. Surface area is used as a primary indicator of the activity level, based on the principle that the greater the surface area, the higher the number of adsorptive sites available.

Table 1.Physical parameters of CBs

Parameters	CB@750	CB-H_3PO_4-750
Moisture (%)	0.5	0.23
Surface Area (m^2/g)	175	256
pH	6.8	2

XRD patterns of CB@750 and CB- H_3PO_4-750 are shown in Figure 1. The 2θ corresponding to the (002) and (100) diffraction planes of graphite structure respectively are observed in both the samples. In the XRD spectra of these samples showed no obvious change in the case of (100) plane, but the peak around 2θ = 23.9° in the case of CB@750 slightly increased to 2θ = 25.8° in the case of CB-H_3PO_4-750. From the Figure 1, it is evident that the d(002) value decreased from 0.372nm to 0.345nm for CB-H_3PO_4-750 compared to CB@750. This indicates more ordering of layers is taking place on activation with H_3PO_4. The formation of interlamellar pores can increase surface reactivity and adsorption performance of CB- H_3PO_4-750.

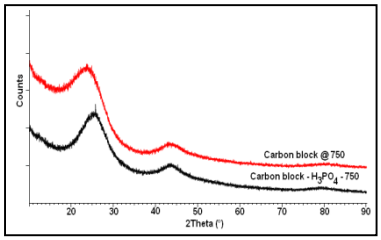


Figure 1, XRD pattern of CB @ 750 & CB - H_3PO_4- 750

Raman spectra of carbon materials show two broad bands, called D (disordered) and G (graphitic) bands at 1360 cm^{-1} and 1580 cm^{-1} respectively. The G band is obtained from the stretching vibrations of sp^2 carbon atoms in the carbon ring or long carbon chain in graphite, which is used to find the degree of symmetry and order of the

graphite structure. The D band is obtained due to the disordered arrangement and low symmetry of graphite lattice structure or defects in the crystalline nature of the carbon materials. The intensity ratio of D band to that of G band (ID/IG) and the average crystallite size La are used as parameters for graphitization. The average particle size La can be calculated from the relation La = 4.35*IG / ID.

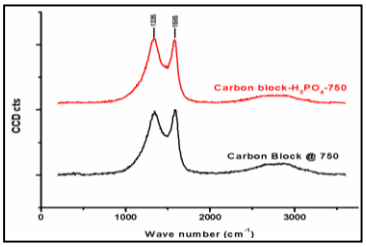


Figure 2, Raman spectrum of CB @750 & CB-H_3PO_4-750

The Raman spectra CB@750 and CB-H_3PO_4-750 are shown in Figure 2. The two peaks around 1335 cm^{-1} and 1585 cm^{-1} in CB@750 and CB-H_3PO_4-750 spectra correspond to the D band and G band that indicating the comparable amorphous carbon structure and graphite like structure of the samples. The La value of CB@750 and CB-H_3PO_4-750 are 4.43 and 4.26 nm respectively. The above result indicate that, the activation using phosphoric acid is beneficial for the formation of a more ordered structure which may further lead to an increase in the unsaturated carbon atoms in the surface of CB-H_3PO_4-750 and can increase the adsorption of perchlorate due to the active sample surface.

The CB@750 and CB-H_3PO_4-750 were examined by Field-Emission Scanning Electron Microscope (FE-SEM) to analyze the surface of the adsorbents. FE-SEM micrographs of CB@750 and CB-H_3PO_4-750 were represented in Figures 3 (a) & (b) respectively. In both the cases, well-developed porous surface (macro and meso) was observed at higher magnification. These pores are considered as channels to the microporous network. This may result in easy access of perchlorate through out the CB active centres.

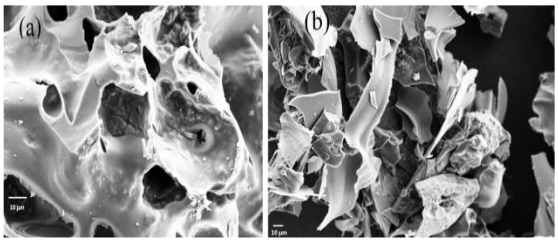


Figure 3, FE-SEM micrograph (a) CB @750,
(b) CB-H_3PO_4-750

FTIR spectra of the CB@750 and CB- H_3PO_4-750 are given in figure 4(a) and (b). The FTIR spectra of CB@750 and CB- H_3PO_4-750 are shown in Figures 4 (a) and (b) respectively. In both the cases, the broad band in the region from 3600-3000 cm^{-1} corresponds to the OH-stretching vibrations. The bands in the region between 1600-1400 cm^{-1} in both figures 4 (a) and (b) represents the C=C stretching vibrations. The C-O and C-C stretching contributes to the modes related to the band at 1200-1000 cm^{-1} in figure 4(a). In figure 4(b) the peaks seen in the regions 1100-1000 and 600-500 cm^{-1} corresponds to the stretching and bending vibraions of phosphate respectively.

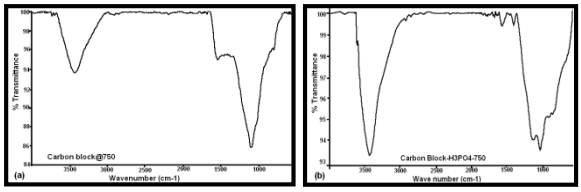


Figure 4, FTIR spectra of (a) CB@750 (b) CB-H_3PO_4-750

2.1 Effect of different activating agents The effect of different activating agent on the adsorption of perchlorate is given in Table 2 which indicates that the amount of perchlorate adsorbed on the CBs increased on activation. The maximum adsorption was obtained for the CB activated with H_3PO_4. The adsorption capacities of CB-750 and CB +HCl-750 were the same which indicates that HCl did not show any activating property.

An improvement in the adsorption capacities were observed in all other cases. The adsorption capacity for perchlorate varied in the order CB +NaCl-750 = CB +KOH-750 < CB +$ZnCl_2$ -750 < CB +$FeCl_3$ -750 < CB + H_3PO_4-750.

Table 2, Adsorption capacity for perchlorate

Material	Adsorption capacity, mg/g
CB -750	1.5
CB +HCl-750	1.5
CB +$ZnCl_2$ -750	5.0
CB +$FeCl_3$ -750	6.2
CB +NaCl-750	3.3
CB +H_3PO_4-750	14.7
CB +KOH-750	3.3

2.2 Contact time for adsorption equilibrium

Contact time between adsorbate and adsorbent is of considerable significance in the water treatment by adsorption. Fig.5 shows the effect of contact time on adsorption of perchlorate (50 mg/L) by CB- H_3PO_4-750 at the given experimental conditions. It is evident that the amount of perchlorate adsorbed on the CB- H_3PO_4-750 increased with increasing contact time and reached an equilibrium value beyond which no more perchlorate is further adsorbed from the solution. The equilibrium time was found to be 60 minutes.

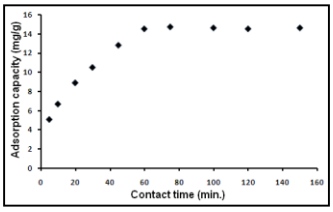


Figure 5, Effect of contact time

At this point, the amount of perchlorate desorbed from the CB- H_3PO_4-750 is in a state of dynamic equilibrium with the amount of perchlorate being adsorbed on the CB- H_3PO_4-750. The amount of perchlorate adsorbed at the equilibrium time reflects the maximum adsorption capacity of CB- H_3PO_4-750 under the operating conditions. The adsorption process is initially rapid and became slower near the equilibrium. This is because of the availability of increased number of active surface sites on CB- H_3PO_4-750 for adsorption and the increased concentration gradient between perchlorate in solution and in the adsorbent. Afterward, the remaining vacant sites are difficult to be occupied due to the repulsive forces between the perchlorate ions on the solid and solution phase.

2.3 Effect of phosphoric acid percentage

CBs were prepared by following simultaneous carbonisation and activation with varying percentage of phosphoric acid (ranging from 10-60 wt %). It can be seen from figure 6, that the as the percentage of H_3PO_4 increased there was an increase in the perchlorate adsorption on CB. This increase was observed upto 30 wt%

of H_3PO_4 activation and beyond that the adsorption was decreased. It was also observed that beyond 40 wt% the sample became sticky due to the presence of excess reagent.

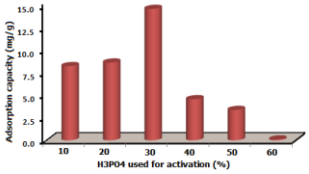


Figure 6, Variation in adorption capacity with weight % of phosphoric acid

2.4 Effect of perchlorate concentration

Effect of initial perchlorate concentration on adsorption was investigated at different concentrations ranging from 10 to 1000 mg/L (Table 3). It can be seen that the amount of perchlorate adsorbed on CB- H_3PO_4-750 at equilibrium increases with increase in initial concentration of perchlorate. As the initial concentration increased, the mass transfer driving force between solid and solution phases would become larger, hence resulting in higher adsorption of perchlorate. Also, the increased perchlorate concentration increases the interaction between perchlorate ions in the solution and adsorbent surface.

Table 3, Effect of perchlorate concentration

Initial concentration of perchlorate (mg/L)	Adsorption capacity(mg/g)
10	3.8
20	5.9
50	14.7
100	20.7
200	29.5
500	43.8
1000	55.0

2.5 Effect of co-existing ions

The effect of co-existing ions on adsorption of perchlorate was studied in the presence of anions viz., SO_4^{2-}, Cl^- and NO_3^- using CB- H_3PO_4-750 and results are shown in Fig.7. A reduction in the perchlorate removal was observed with the increase of the anion concentration. This is due to the competition among the anions for the adsorption sites on the CB-H_3PO_4-750 surface, which is decided by the concentration, charge and size of the anions. The perchlorate removal was adversely affected by ions in the order NO_3^-> SO_4^{2-} >Cl^-.

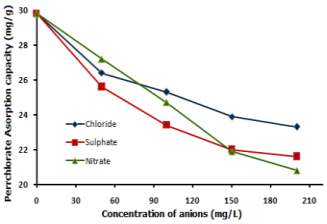


Figure 7, Effect of co-existing ions on adsorption of perchlorate

Conclusions

CBs with large internal surface area and highly developed porous structure was prepared by high temperature activation of biomass starch. Chemical activation was carried out using different materials. XRD, Raman and FESEM analysis revealed the ordering of layers on activation with phosphoric acid. Thus prepared CB were found to be an effective adsorbent for the removal of perchlorate from aqueous solution. Among the various

activating agents studied, CB treated with phosphoric acid (CB-H_3PO_4-750) gave the maximum adsorption capacity of 14.7 mg/g for perchlorate. The amount of perchlorate adsorbed on CB-H_3PO_4-750 increased with the contact time and concentration of perchlorate. The perchlorate removal was adversely affected by ions in the order NO_3^-> SO_4^{2-} >Cl^-. Removal of perchlorate by CB is a cheap, simple and safe method.

References

27. Vitaly Budarin, James H. Clark, Rafael Luque, Robin White, Starbons®: Cooking up Nanostructured Mesoporous Materials, *Material Matters* 2009, 4.1, 19.
28. Aik Chong Lua and Ting YangEffect of activation temperature on the textural and chemical properties of potassium hydroxide activated carbon prepared from pistachio-nut shell, *J. of Colloid and Interface Science* 2004, 274, 594–601
29. F. Rodriguez-Reinoso, M. Molina-Sabio, M.A. Munecas, Effect of microporosity and oxygen surface groups of activated carbon in the adsorption of molecules of different polarity. 96, 1992, 2707-2713
30. A.Castro-Muniz, F.Suarez-Garcia, A.Martinez-Alonso, J.M.D. Tascon, Activated carbon fibers with a high content of surface functional groups by phosphoric acid activation of PPTA. *J. of Colloid and Interface Science*, 361, 2011, 307-315
31. R.E. Franklin, Crystalline growth in graphitizing and non-graphitizing carbons. Proceedings of The Royal Society A, 209, 1951, 196-218
32. R. Srinivasan, G.A. Sorial, Treatment of perchlorate in drinking water: A critical review, Separation and Purification Technology 69 (2009) 7–21
33. E. T. Urbansky and M. R. Schock, Issues in managing the risks associated with perchlorate in drinking water, *J. of Environmental Management* (1999) 56,79–95
34. Burt, Michelle, Cooper, Michael, Hickey, Kevin, Kenyon Kevin, and St. Onge, Deanna. Clarkson University. Task 3: Perchlorate Treatment for Domestic Water Systems.

MACRO 458

Effect of Hydroxyapatite Loading on Polylactic acid/Hydroxyapatite Composites on its Mechanical, Thermal and Degradation Properties

Prasad Arbind[a], Sinha Aditya[b], Katiyar Vimal[c]*, Ravi Sankar M[a]

[a]*Department of Mechanical Engineering, IIT Guwahati,Assam,India-781039*
[b]*Department of Mechanical Engineering,NERIST,Nirjuli,Arunachal,India-791109*
[c]*Department of Chemical Engineering, IIT Guwahati,Assam,India-781039*

**Corresponding author's Email: vkatiyar@iitg.ernet.in*

This work focuses on the influence of bioactive biofiller, "Hydroxyapatite" (HAp) on the hydrolytic degradation behavior of poly (lactic acid) (PLA) biocomposites. Hydrolytic degradation studies were conducted in Phosphate buffer saline solution (PBS) in accordance with ASTM F1635-11. PLA was obtained from Nature Works LLC (Minnetonka, MN, USA). The selected grade (Ingeo 2003D, Mn = 88,500 g/ mol and Mw / Mn= 1.8) is recommended for extrusion. The polymer has a density of 1.24g/cm^3, while it is MFI is 6 g/10 min at 210°C at 2.16 kg load. HAp powders were fabricated through fish scales biowastes [1].The PLA/HAp composite was fabricated through melt blending technique using twin screw extruder machine [2]. The microstructure and morphologies of the blends were investigated through optical microscopy at various magnifications. The thermal studies of the composite before and after

degradation studies was done on differential scanning Calorimetry (DSC) and thermo gravimetric analysis. The degradation studies was done in PBS medium maintained pH equivalent to 7.4 at 37ºC. The initial and final mass loss were noted(figure 2).The mechanism proposed for degradation can be understood(figure 3).The surface wettability of the samples were also analyzed through contact angle measurement system in order to know its hydrophobicity character. The results demonstrated that incorporation of HAp improved the hydrophilicity, degradation behavior and its thermal stability towards its increase in HAp concentration increment. The hardness of the samples were also evaluated using the Shore-D apparatus, confirms increase in hardening of the biocomposites.

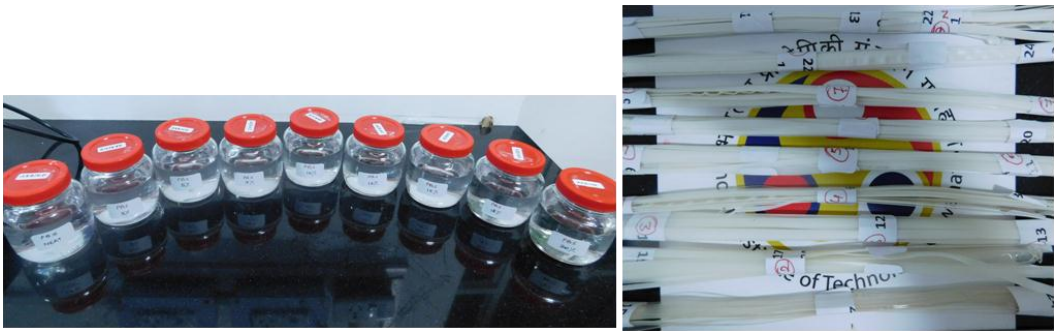


Figure 1.Degradation set up and samples of PLA/HAp composites

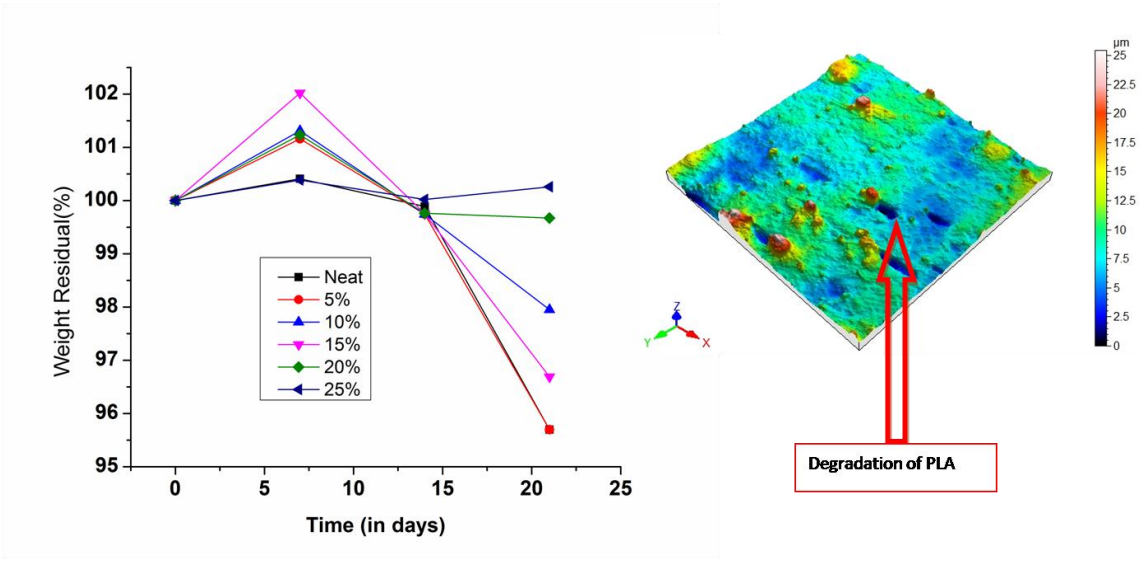


Figure 2.Degradation profile of PLA/HAp composite

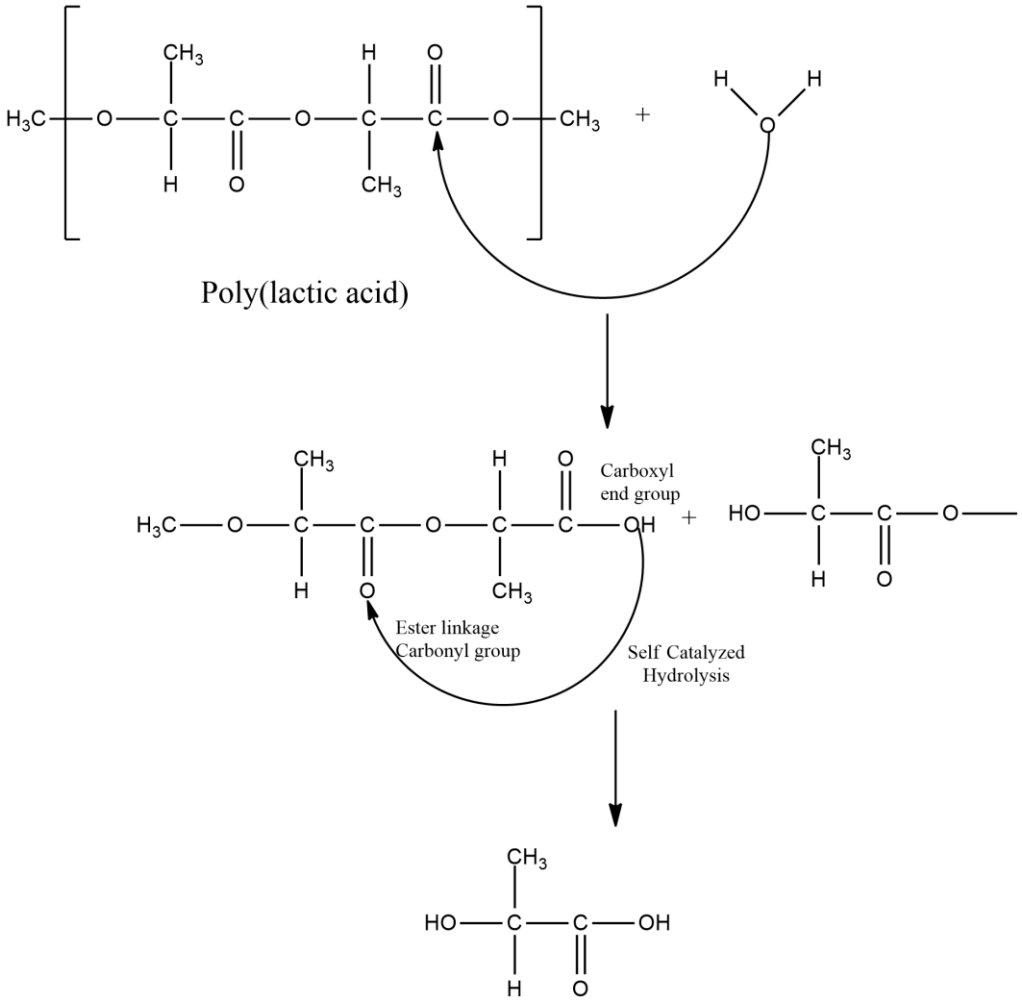


Figure 3.Degradation mechanism of PLA/HAp composites in PBS medium.

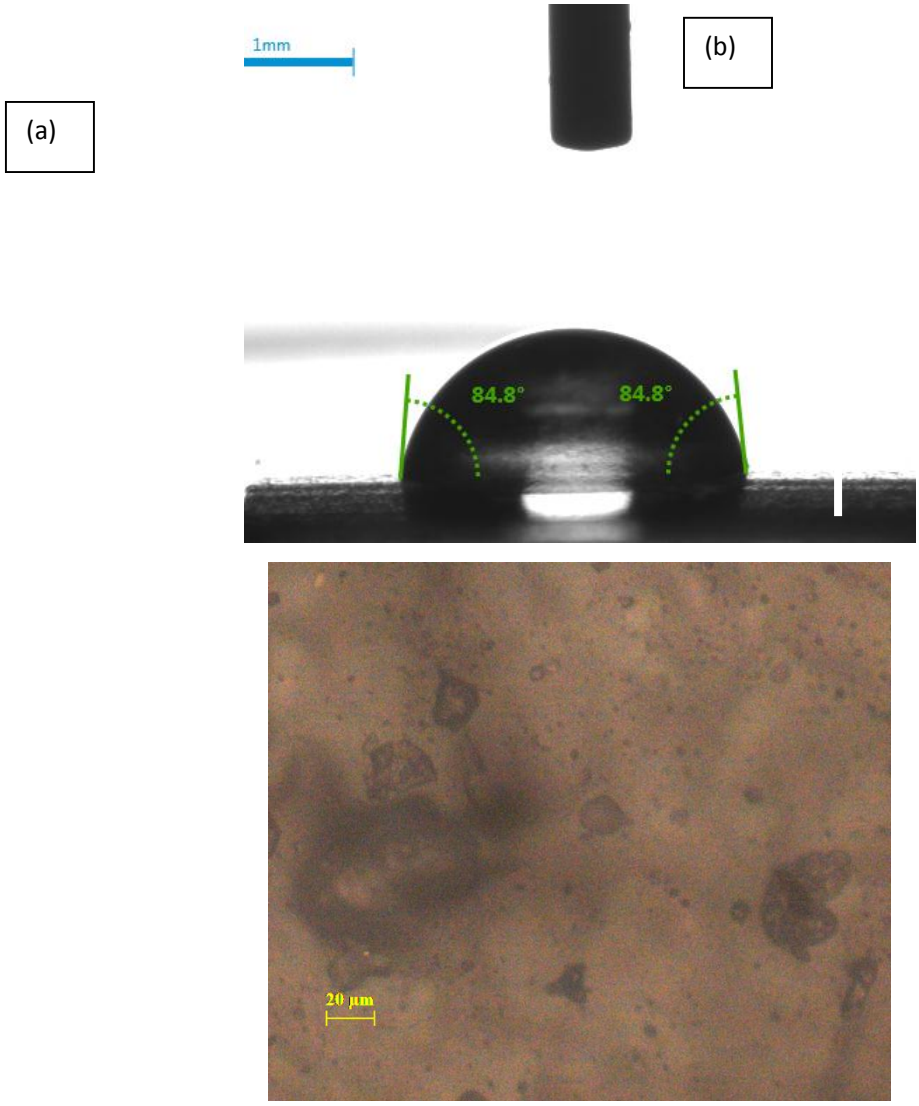


Figure 4. (a) Surface wetability of PLA/HAp composites. (b)Optical micrograph of degraded PLA/HAp composites.

References

[59]ASTM F1635-11. Standard Test Method for in vitro Degradation Testing of Hydrolytically Degradable Polymer Resins and Fabricated Forms for Surgical Implants. ASTM International. (2011).

[60]Prasad,Arbind; Devendar,B; Sankar,M R; Robi,P S. Mater. Today Proc. 2 (2015) 1216–1224.

MACRO 477

Self Cross-linkable Anionic waterborne polyurethane-silanol dispersions from Cottonseed oil-based phosphorylated polyol as ionic soft segment

Sashivinay kumar Gaddam, Aruna Palanisamy*

Polymers and Functional Materials Division, CSIR-Indian Institute of Chemical Technology, Tarnaka, Hyderabad, India, 500007

** e-mail id: aruna@iict.res.in*

Abstract

A series of phosphorylated polyols (Phospol-P5, P10, P15) have been synthesized by hydrolytic cleavage of epoxy groups of epoxy cottonseed oil (ECSO) in the presence of different concentration of *o*- phosphoric acid. Three phospols having different OH values ranging from 130 to 180, were used as internal emulsifiers in waterborne PUDs with IPDI and 3-aminopropyl triethoxysilane (APTES). All the three PU dispersions showed excellent storage stability (> 6 months) with a particle size, ranging between 30 to 68 dnm. The films of phospol-P5 based dispersion, exhibited better tensile properties, thermal stability, T_g value, contact angle and anticorrosive properties. All the experimental results reveal that both hydroxyl content of phospols and extent of siloxane crosslinking play an important role in deciding the thermo-mechanical properties, hydrophobic nature and anticorrosive properties of PUD films.

Keywords: Cottonseed oil, phosphorylated polyol, DMPA free, Self-Crosslinkable, waterborne polyurethane dispersion.

Introduction

In general, vegetable oil based anionic waterborne polyurethane dispersions (PUDs) have been synthesized by employing Dimethylol propanoic acid (DMPA) as an internal emulsifier.[1] This route have some disadvantages such as, increased film formation time,[2] and decrease in compatibility between hard and soft segments.[3] Introduction of vegetable oil based polyols as ionic soft segment, having both the hydroxyl and ionizble functionalities in their triglyceride backbone, is expected to be effective method for complete substitution of DMPA in PUD manufacturing.

Vegetable oil based phosphorylated polyols (phospols) have been synthesized by ring-opening hydrolysis of the epoxidized vegetable oils in the presence of Ortho phosphoric acid.[4] Most of these phosphorylated polyols were utilized in synthesis of polyurethane foams,[5] bioelastomers,[6] and also in corrosion resistant waterborne coatings.[7] Till date, waterborne polyurethane dispersion prepared with vegetable based phospols carrying both hydroxyl and ionizble phosphoryl groups have not been reported.

In this study, a series of phosphols have been synthesized from epoxy CSO and were employed as ionic soft segments to synthesize the DMPA free waterborne PUDs through a sol-gel process. The effect of phosphol functionality, as well as siloxane networks on the structure and functional properties of PUDs and their cured films have been investigated.

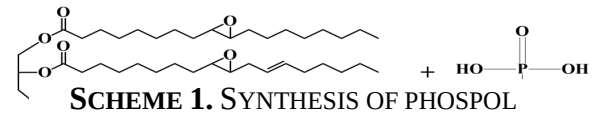
Experimental

Synthesis of phospol and their PU Dispersions

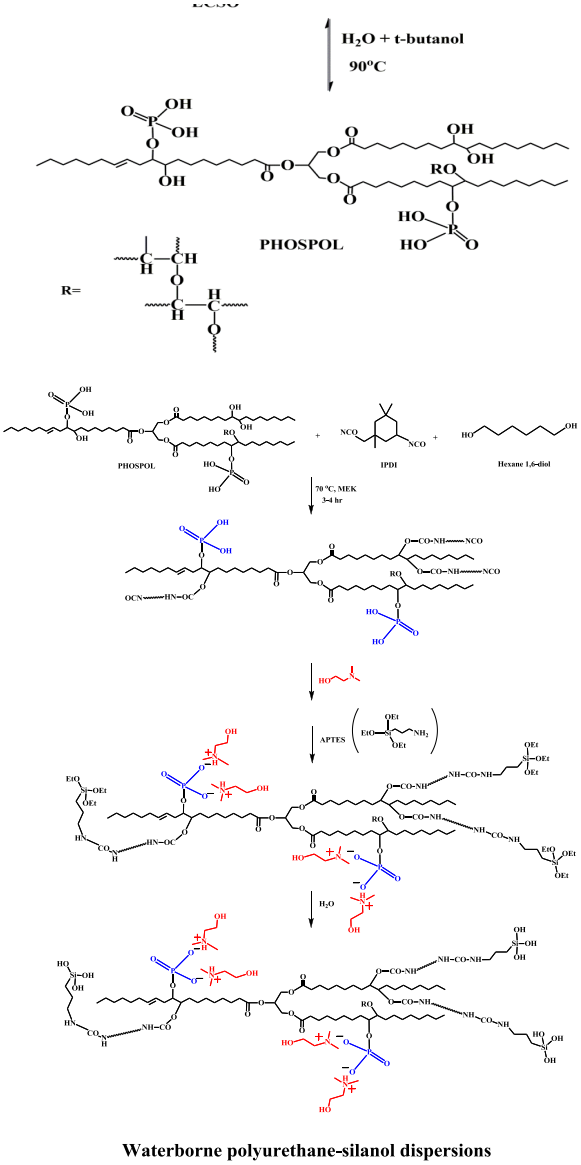
Phosphorylated polyols (Figure 1A), have been synthesized from epoxidised CSO by ring opening hydrolysis of epoxy groups in the presence of varying amount of ortho phosphoric acid (phospol-P5, P10, P15, the properties are shown in table 1) as shown in scheme 1. The characteristic properties of phospols are compiled in Table 1.

Table 1. Characteristics of Phospols

sample	Acid value mg KOH/g	OH value mg KOH/g	Molecular weight(*Mw*)
Phospol-P5	68	177	2889
Phospol-P10	82	161	3319
Phospol-P15	106	128	3028



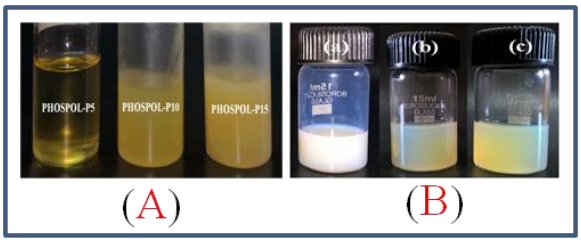
SCHEME 1. SYNTHESIS OF PHOSPOL



A prepolymer was prepared by reacting IPDI with phosphorylated polyol (of varying phosphate content) and HDO and then ionization of acid groups achieved by the addition of dimethyl ethanolamine (DMEA).

The NCO terminated ionized prepolymer was chain extended with APTES and then dispersed in water at high stirring speed to yield anionic PUDs (Figure 1B), with a solid content of about 30 wt% (scheme 2).

Scheme 2. Synthesis of phospol based anionic waterborne PUDs



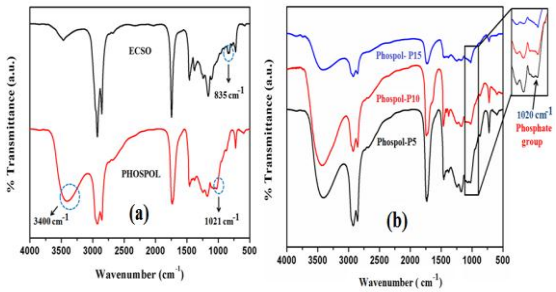


Fig. 1 Appearance of phospols (A) and PUDs [PUD-P5 (a); PUD-P10 (b); PUD-P15 (c)]

Results and Discussion

Properties of Phospols

In Figure 2 (a), the disappearance of absorption band at 835 cm^{-1} corresponding to epoxy groups, and the appearance of new peaks at 3400 cm^{-1} and 1020 cm^{-1} corresponding to -OH groups and phosphoryl groups, indicate the hydrolytic cleavage of epoxy groups initiated by phosphoric acid. In Figure 2 (b), three phospols with different phosphoryl content (P5, P10 and P15) exhibit peaks with increasing intensity at 1020 cm^{-1}, which is characteristic absorption of phosphoryl groups indicating the increasing degree of phosphorylation. H^1 NMR spectra of both ECSO and phospol also confirms the successful cleavage of epoxy ring by the disappearance of peaks between 2.8 and 3.2 ppm region corresponding to epoxy group (methylenic protons). New peaks between 3.4 to 4.4 ppm corresponding to methylenic protons of carbon bonded to phosphoryl groups in phospol appeared.

Figure 2. FT-IR spectra of (a) ECSO and Phospol ; (b) phospol-P5, P10, and P15.

Properties of PUDs

PUD-P5 was opaque and both PUD-P10 and P15 are bluish and translucent. All the three PUDs show very good shelf-life at room temperature (>6 months), due to narrow particle size distribution of PUDs. The pH varied between 7.8 and7.9. The particle size of the PUDs increased with an increase in the OH number of phosphols and the average particle sizes of P15,P10 and P-5 were approximately 32, 43 and 68 dnm After neutralization, PUD-P15 had high amount of phosphate counter ion and hence smaller particle size.

Properties of PUD films

In IR spectra (Figure 4A), the absorption band near 1040 to 1050 cm^{-1} is assigned to asymmetric stretching vibration of Si-O-Si bonds indicating the generation of siloxane crosslink networks and the absorption peak intensity gradually increased with the increase of silica (APTES) content. In ^{29}Si NMR spectra of PUD-P5 (Figure 4B), the peak at ─61ppm is assigned to the silicon bearing

unreacted hydroxyl group, and the strong peak on the right around ─72 ppm resulting from fully condensed silanol groups. The intensity of peaks indicate the formation of stronger Si-O-Si crosslink networks during the PUD film curing process.

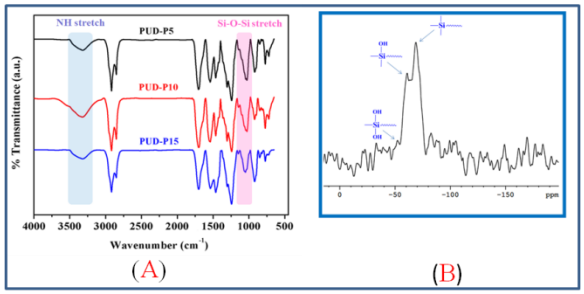


Figure 4. FT-IR (A), and ^{29}Si NMR (B) spectras of PUD films.

The storage modulus (*E'*) and T_g values of the phospol PUD films (Figure 5), increases as silica content increases due to the increasing siloxane crosslinking networks, which retard the relaxation of PU chains. Hence, the PUD-P5 film shows high storage modulus and T_g values compared to PUD-P10. The PUD films exhibited single tan δ peak indicating good phase compatibility between soft and hard segments.

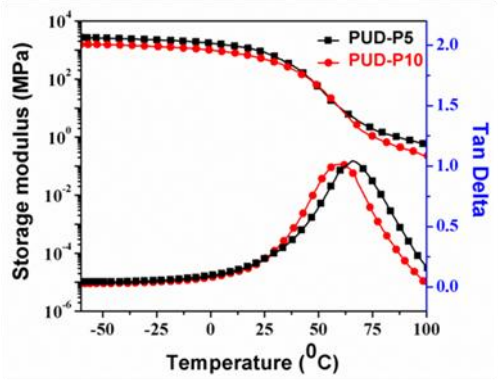


Figure 5. Temperature dependence of E' and tan δ of PUD films.

PUD-P5 had highest Young's modulus and tensile strength due to the high siolxane crosslink density resulting from the higher OH functionality of phospol-P5 (Table 2). On the other hand, the elongation at break values (139%) are lowest for PUD-P5 as expected.

Table 2. Tensile properties of Phospol PUD films

Sample	E(MPa)	σ(MPa)	ε(%)
PUD-P5	7.6±1.12	10.7±0.27	139±09
PUD-P10	4.8±0.53	6.8±0.69	194±19
PUD-P15	1.3±0.27	1.9±0.33	347±11

E = Young's modulus ; σ = tensile strengths ε = elongation at break

The water contact angles of the phospol PUD films (Figure 6), gradually increased with increasing siloxane crosslinking networks. In general, siloxane units possess high surface activity and migrate to the surface during the film formation stage, and these groups on surface reduce the surface energy leading to high degree of surface hydrophobicity.[8]

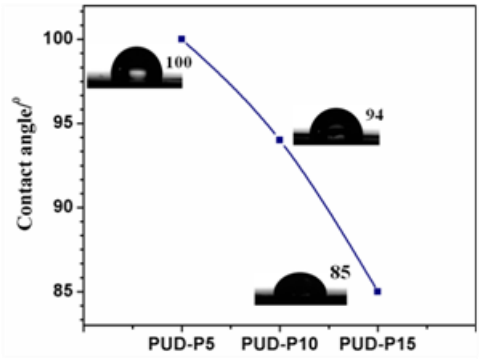


Figure 6. Contact angle of PUD films

Corrosion resistance studies- Potentiodynamic polarization studies

The effect of siloxane crosslink density on corrosion protection of phospol PUD films was evaluated by potentiodynamic polarization studies. From the results (Table 3), it was clear that the corrosion protection performance of the phospol PUDs increased with increasing siloxane crosslink density (Figure 7). The surface activity of siloxane units due to the lower surface energy, led to the increased surface roughness of metal substrate and acted as a physical barrier to restrict the penetration of corrosive species.[9,8]

Table 3. Tafel polarization data of coated and uncoated MS in 3.5% NaCl

Sample	Corrosion rate (mm/year)	Polarization resistance (MΩ)
Uncoated MS	1.75	340.62×10^{-6}
PUD-P5	2.02×10^{-5}	55.83
PUD-P10	3.11×10^{-5}	36.09
PUD-P15	3.22×10^{-5}	27.01

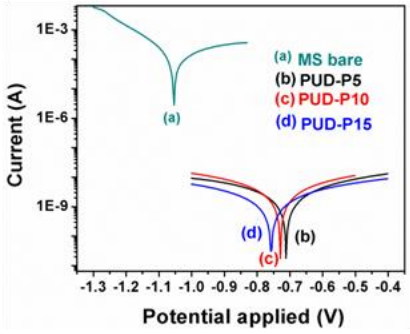


Figure 7. Tafel polarization of PUD films.

Conclusions

The phosphoryl functionalized polyols with different OH numbers have been synthesized via ring opening hydrolysis of epoxy cottonseed oil with different concentrations of *o*-phosphoric acid, and were charactarized by FTIR and H^1 NMR spectral analysis**.**. A series of waterborne PUDs were prepared from phosphorylated polyols, through a sol-gel process. The formation of siloxane networks was confirmed by solid state ^{29}Si NMR and ATR -FTIR spectral analysis of PUD films. The particle size of PUDs ranged from 32 to 68 dnm with increasing OH functionality of phospols. Siloxane crosslinking in PUDs improved their thermal and mechanical properties. The lower surface energy of siloxane networks imparted hydrophobic nature and corrosion resistance to phospol PUDs. Phosphorylated polyol induced hard-soft segment phase mixing in polyurethanes and was confirmed by appearance of single tan δ peak in DMA. Thus an effective and promising way to synthesize a new class of phosphorous containing waterborne PUDs for a wide range of industrial applications has been discussed in this work.

Acknowledgements

Sashivinay kumar Gaddam is indebted to Council of Scientific and Industrial Research (CSIR), India, for Senior Research Fellowship (SRF).

References

1. Gurunathan T, Mohanty S, Nayak SK. *RSC Adv.* **2015**, 5 (15), 11524-33.

2. Kim B, Yang J, Yoo S, Lee J. *Colloid Polym Sci.* **2003**, 281 (5), 461-8.

3. Yang CZ, Grasel TG, Bell JL. *J Polym Sci Pol Phys*. **1991,** 29 (5), 581-8.

4. Guo, Y., Hardesty, J. H., Mannari, V. *Journal of the American Oil Chemists' Society*. **2007**, *84*(10), 929-935.

5. Heinen, M., Gerbase, A. E., & Petzhold, C. L. *Polymer Degradation and Stability*. **2014**, *108*, 76-86.

6. Lubguban, A. A., Lozada, Z. R. *International Journal of Polymer Science*. **2011**.

7. Guo, Y., Mannari, V. M., Patel, P. *JCT research*. **2006**, *3*(4), 327-331.

8. Pathan, S., & Ahmad, S. *ACS Sustainable Chemistry & Engineering*. **2016**.

9. Ghosal, A., Rahman, O. U., & Ahmad, S. *Industrial & Engineering Chemistry Research*. **2015**, *54*(51), 12770-12787.

MACRO 478

Improved Haemocompatibility of Surface Modified Polycarbonate Urethane

Sudhin Thampi,[a,b] Vignesh Muthuvijayan,[a] P. Ramesh*[b]

[a] *Department of Biotechnology, Bhupat and Jyoti Mehta School of Biosciences, Indian Institute of Technology Madras, Chennai 600036, India*

[b] *Division of Polymeric Medical Devices, Biomedical Technology Wing, Sree Chitra Tirunal Institute for Medical Sciences and Technology, Thiruvananthapuram 695012, India*

** e-mail id: rameshp@sctimst.ac.in*

Abstract

Surface engineering of polymer surface to tackle issues with adhesion of platelets for better haemocompatibility is always a better method in comparison to synthesis of newer biomaterials. Surface engineering can considered an easier method if it chemical reactions can be avoided or if it can be minimized to a one step process. Focusing on these parameters we have designed a GO coating method to modulate the adhesion behavior of platelets over an electrospun PCU membrane. At the same time care was taken that %hemolysis stays within the acceptable limits. GOPCU the GO coated membrane was studied and owing to its hemocompatible nature could be a potentially suitable material to be used as an implantable material for cardiovascular applications.

Keywords: *Graphene Oxide; Raman mapping; Platelet adhesion; Surface engineering*

Introduction

Polyurethanes a widely accepted polymeric biomaterial for biomedical applications are mostly used for cardiovascular devices.[1] Haemocompatibility, is a crucial property for such materials to be used in blood contacting applications like, vascular grafts, so many researchers have explored to enhance the blood compatibility of biomaterials. In the development of novel hemocompatible polymeric biomaterials, surface treatment appears to be a suitable tool to reduce the thrombogenic characteristics of such biomaterials [2]. Surface treatment of medical devices and implants are one of the crucial steps before implantation.

For any blood contacting biomaterials, the most important part is to test their potential to prevent thrombus formation which in turn is initiated by platelet adhesion to its surface.[3] Since the first step in blood coagulation starts with adhesion of platelets,[4] anti-adhesion surface have an important role to play. Graphene based materials have found several application in biomedical arena.[5] These days nano-material based surface modifications are finding several applications due to their inherent characteristics. Biomimetic designs and nanosurfaced implants are capable of exhibiting several novel characteristics. Electrospun fibers with their ECM like structure hold lot of promise for biomedical implants. Herein, we've studied a GO-based coating over electrospun polycarbonate urethane (PCU) to reduce adhesion of platelets. Platelet adhesion study was carried out by exposing PCU to platelet rich plasma for 30 min under mild agitation. The modified surface GOPCU has shown to reduce both adhesion and aggregation of platelets as shown in ESEM micrograph.

Experimental

Materials

Carbothane manufactured by Lubrizol Corp. as PCU, was used in this study. 12% (w/v %) of PCU was dissolved in mixture of di-methyl formamide (DMF) and tetrahydrofuran (THF) (50/50 v/v) for electrospinning. Graphite flakes, was procured from Sigma-Aldrich, USA. DMF, THF, H_2SO_4, H_3PO_4, $KMnO_4$, HCl and 30% H_2O_2 were purchased from Merck, India.

Electrospinning of PCU

A syringe with PCU solution was loaded onto the electrospinning unit. The PCU solution was delivered to the charged spinneret by the syringe pump at a flow rate of 1 mL/h and electrospun at 8–10 kV potential.

GO synthesis and coating

GO was prepared according to the procedure reported elsewhere.[6] The GO was coated onto PCU membrane via electrospraying. The electrosprayed membranes were retrieved from the mandrel and air-dried to remove any residual solvent.

SEM /ESEM

Scanning electron microscopy (SEM) (Hitachi model S-2400) was used to study the morphology and topography of the membrane surface. Environmental scanning electron microscopy (ESEM) (FIE, Quanta 200) was used for observing platelet adhered membranes. Sample preparation was done by the sputtering of thin, flat sections of the materials with gold.

Raman spectra and Mapping

For Raman microscopic mapping, experiments were performed with the confocal Raman microscope (Witec Inc. alpha300R). Measurements were carried out with a frequency-doubled NdYAG laser: l = 532 nm. The distribution of chemical species on the sample was obtained in Raman spectral mapping mode. In this mapping mode a complete Raman spectrum was recorded (integration time of 0.025s) at every mapping point (100 x 100 points for 50 x 50 μm^2), leading to a 2D array of Raman spectra. Background subtraction, cosmic ray removal, averaging a certain region manually, and spectral de-mixing were performed on this 2D array of Raman spectra. Two distinct spectra for PCU and GOPCU were extracted using Cluster Analysis (CA) utilizing Witec Project plus software. Image J an open source image processing and analysis tool was further used to analyze the GO distribution, electrosprayed over PCU membrane.

***In- vitro* haemocompatibility evaluation**

The haemocompatibility of PCU and GOPCU membranes were evaluated using *in vitro* hemolysis assay and platelet adhesion study as per ISO 10993-4. These tests were done using human blood samples in accord to the ethical guidelines approved by the Institutional Ethics Committee of Sree Chitra Tirunal Institute for Medical Sciences and Technology(approval no.: SCT/IEC/594/2014 dated 21/04/2014).

The hemolytic character of the material was assessed by means of an *in vitro* hemolysis test. Total hemoglobin (Hb) was analyzed with a hematology analyzer (Sysmex-K4500). Disc shape test material of 6 mm diameter in triplicate was conditioned in PBS for 5 min before exposure to blood. The samples were kept in a polystyrene plate; 2 mL of blood was added to each well, and a well without any sample was treated as a reference. A volume of 1 mL of blood was taken immediately for initial analysis and the remaining 1 mL of blood was incubated with a sample for 30 min under agitation at 70±5 rpm at 35 ± 2° C.

The blood samples were centrifuged at 4000rpm for 15 min and platelet poor plasma was aspirated to prepare platelet poor plasma. The free hemoglobin (fHb) liberated into the plasma after exposure to samples was measured using UV spectrophotometer. Hemolysis was thus calculated and results were expressed as mean ± standard deviation (SD) (n=3).

A study for checking platelet adhesion was done by exposing the control and coated material to whole blood for 30 min. Study was concluded by analyzing reduction in platelet count before and after exposure to material. After that, the scaffolds were coated with gold for examination in ESEM. All results were the average of three parallel experiments.

Results and discussion

Surface morphology

SEM micrographs obtained reveals the surface topography of fabricated membranes (Fig. 1). Electrospun PCU membrane shows a fibrous architecture. However, over GOPCU, a very thin transparent film like layer with slight folds/wrinkles could be seen covering the fibrous architecture.

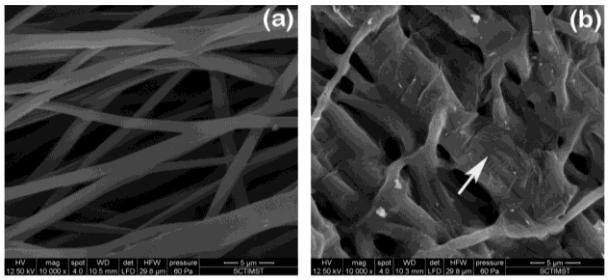


Figure1: SEM micrograph depicting topography of electrospun PCU (a) and GO sprayed GOPCU membrane (b) (Arrow) shows thin GO flakes, with visible architecture and outline of the electrospun fibers, through it.

These thin folded films appeared after electrospraying the electrospun PCU membrane with dispersed GO nanosheet solution. GO thin film morphology over electrospun PCU fibroporous membrane analyzed from their SEM micrograph presents GOPCU surface as the PCU membrane wrapped in a very thin blanket of GO nanosheets.

Raman spectral study and mapping

Raman spectral analysis was used to get spectral information of thin blanket like structures observed in SEM micrographs. It is an efficient characterization technique for graphene related materials and unlike other techniques detections can be made even for a single layer of material.[7] Spectral details of GO, PCU and GOPCU membranes are as shown in Fig.2 which shows distinct peaks of corresponding materials. GO has D band and G band peaks at 1339cm^{-1} and 1578 cm^{-1} respectively while for PCU peak at 1445 cm^{-1} can be assigned to the symmetric stretching mode of isocyanate (N=C=O) and the bending mode of CH_2 .[8]

Appearance of GO peaks can be observed in spectral details of GOPCU membrane surface also. The GO peaks show a blue shift on GOPCU membrane, wherein D band shifts to 1346 cm^{-1} and G band has shifted to 1596 cm^{-1} which may be due to decreased number of layers.[9] Thus confirming presence of thin layers of GO on GOPCU membrane.

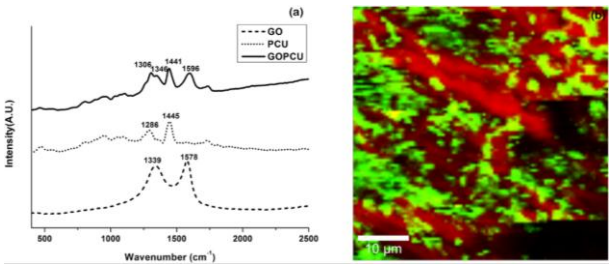


Figure 2: Raman spectra of (a): GO, PCU and GOPCU and (b): mapping of GO thin films (green) distribution over PCU (red) membrane.

Raman spectral mapping was done to map the distribution of GO over GOPCU surface (Fig.2). The colour red comprises spectral data of PCU and green colour presented that of GO. By analysing thus acquired image using ImageJ software, the colour distribution percentage was measured and coverage of GO was found to be ~ 75% on the PCU membrane surface.

Interaction of blood components with GOPCU surface

A slight increment in hemolysis percentage was indicated for GOPCU membrane but the concerned value is still less than 5% (Fig. 3). For any biomaterial to be acceptable as a blood contacting device it should have % hemolysis less than 5% as per ISO 10993-4. Hence GO coating has not brought any adverse change in blood contacting property of PCU.

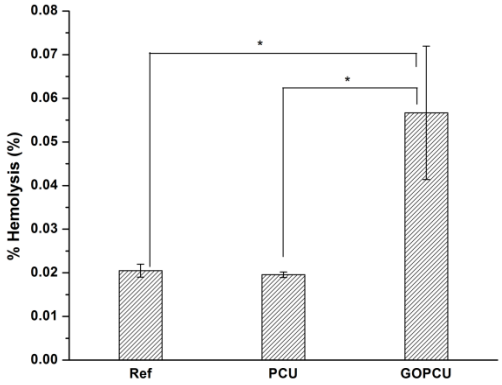


Figure 3: Percentage hemolysis study of PCU and GOPCU surfaces (n=3, P<0.05).

Platelet adhesion, activation and aggregation are also considered crucial for haemocompatibility of cardiovascular implants. PCU has been reported to have limited haemocompatibility, due to its inherent surface properties allowing adhesion and aggregation of platelets. While in GOPCU, the modified surface showed no aggregation of platelets as visible from ESEM micrograph after qualitative analysis of platelet adhesion using PRP (Fig.4).

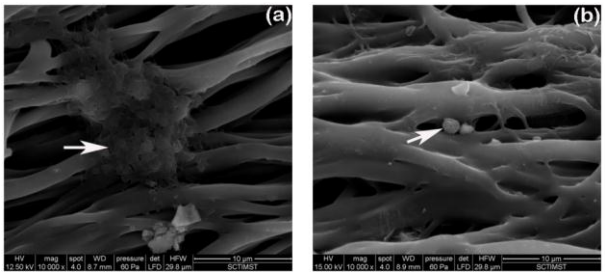


Figure 4: ESEM micrograph showing more platelet adhesion and aggregation on (a) PCU in comparison to (b) GOPCU, after exposing it to platelet rich plasma (PRP) for 30min. Arrow points to platelet adhered.

Henceforth, GOPCU promotes application of this surface engineering technique for improving hemocompatible properties of implants.

Conclusions

Herein GO was used as a surface engineering material and developed a simple electrospraying based technique to successfully coat GO thin films over a polymeric surface such as PCU. GO coating reduced the platelet adhesion and aggregation over PCU without causing any increase in %hemolysis. Thus GOPCU proves to be an ideal hemocompatible candidate for medical device development.

Acknowledgements

Author wishes to acknowledge assistance of Mr. Willi Paul at Central Analytic Facility, SCTIMST for acquiring Raman spectra and mapping. One of the authors S.T. acknowledges IITM for the fellowship and SCTIMST for providing essential facilities for completion of this work.

References

35. R. J. Zdrahala & I. J. Zdrahala. *Journal of biomaterials applications*, 14, 67-90, 1999.
36. C. Johanna, K. Gester; J. Roggenkamp, I. Mager; J. Maas; S. V. Jansen; U. Steinseifer. *Journal of Biomaterials Science, Polymer Edition* 25, 504-518, 2014.
37. B. Gao, Y. Feng, J. Lu, L. Zhang, M. Zhao, C. Shi & J. Guo. *Materials Science and Engineering: C*, 33, 2871-2878, 2013.
38. S. M. Fen, M. D. Shau, Cheng, C. Hsieh, J. Y. Cherng. *Molecules* 16, 8181-8197, 2011.
39. Z. Yin, T. R. Nayak, H. Hong, W. Cai. *Nanoscale* 4, 3833-3842, 2012.
40. D. C. Marcano; D. V. Kosynkin, J. M. Berlin, A. Sinitskii,; Z. Sun, A. Slesarev, L. B. Alemany, W. Lu, J. M. Tour. *ACS nano***,** 4, 4806-4814, 2010.
41. A. Ferrari, J. Meyer, V. Scardaci, C. Casiraghi, M. Lazzeri, F. Mauri, S. Piscanec, D. Jiang, K. Novoselov, S. Roth. *Physical review letters***,** 97, 187401, 2006.
42. B. Redondo-Foj, P. Ortiz-Serna, M. Carsí, M. J. Sanchis, M.Culebras, C. M. Gómez, A. Cantarero. *Polymer International***,** 64, 284-292, 2015.
43. A. Gupta, G. Chen, P. Joshi, S. Tadigadapa, P. Eklund. *Nano Letters***,** 6, 2667-2673, 2006.

MACRO 485

8-Hydroxypyrene-1,3,6-trisulfonic acid trisodium salt (HPTS) Based High Fluorescent Waterborne Polyurethane Dispersion Coating

Kumar Rajnish, Bhosale Rajesh, Yadav Ramkeval, Raju KVSN, Narayan Ramanuj*

Polymers & Functional Materials Division
CSIR-Indian Institute of Chemical Technology, Hyderabad, India

ramanuj@iict.res.in

Polyurethane dispersions (PUDs) (fine dispersed particles of polyurethanes in water) are a rapidly growing segment of the polyurethane coating industry due to environmental legislations such as the clean air act and also due to technological advances, that has made them an effective substitute for the solvent-based analogs. They are versatile and environmentally friendly coating materials that are available in a wide range of hardness and solid content. Their zero to low volatile organic content facilitate their formulation into a compliant coating for many different substrates. Their versatility and wide range of superior properties, such as abrasion resistance, impact strength and low temperature flexibility are the driving forces to their continuously expanding usage in many applications.

We have developed 8-Hydroxypyrene-1,3,6-trisulfonic acid trisodium salt (HPTS) and 1,3,6,8-Pyrenetetrasulfonic acid tetrasodium salt (PTTS) based waterborne fluorescent PUD coating and examine the effect of phenolic -OH group present in HPTS on fluorescence properties of these PUD films and come with an inference that HPTS based PUD Shows enhanced green fluorescence over PTTS based PUD film (figure). Further we characterised the film with Fourier transformed infrared spectroscopy (FTIR), X-Ray diffraction (XRD), Scanning electron microscopy (SEM), UV-vis absorption spectroscopy, Photoluminescence spectroscopy, Dynamic mechanical analysis(DMA), Thermogravimetric analysis (TGA), and Differential scanning calorimetry (DSC).

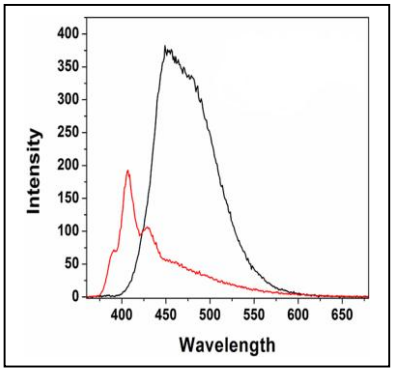


Figure: Photoluminescence spectra of HPTS (black line) and PTTS (red line) based PUD film

References

[61]Kim, B. K.; Colloid and Polymer Science, 274 (1996) 599.
[62]Madbouly, Samy A.; Otaigbe, Joshua U.; Progress in Polymer Science, 34 (2009) 1283.
[63]Wolfbeis, O. S.; Fürlinger, E.; Kroneis, H.; Marsoner, H.; Freseniu, Z.; Anal. Chem., 314 (1983) 119.
[64]Muller, B.; Hauser, P. C.; Analyst, 121 (1996) 339.

MACRO 487

Cellulose Nanomaterials: A Natural Biopolymer as Sustainable Material for Future

Chandravati, Saini Arun, Maji Pradip K.*

Department of Polymer and Process Engineering, Indian Institute of Technology Roorkee Saharanpur Campus, Saharanpur-247001, U.P., India.

**Corresponding author's email: pradip.fpt@iitr.ac.in*

In the present scenario, nanotechnology has engrossed the mind of researchers in almost all walks of our life, starting from physics to chemistry to biology and engineering. Nature surrounding us exemplifies the oldest supreme platform where the materialization of sophisticated nanotechnological products took place. Forest biomaterials are one of the natures' most abundant and renewable materials that has still concealed many astonishing materials in its lap with a potential of changing the entire lifestyle of humans [1,2]. Cellulose nanomaterials obtained from these forest materials has proven itself as one of the miracle material that has spread its feet in wide application areas starting as reinforcement phase for preparing high strength composite materials to extremely light weight aerogels and now in emerging areas of biomedical field [3,4].

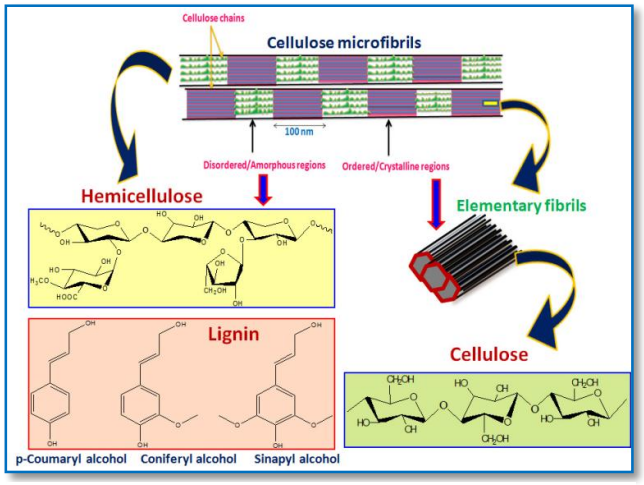


FIGURE 1. CELLULOSE MICROFIBRILS SHOWING AMORPHOUS DOMAINS (LIGNIN AND HEMICELLULOSE) AND CRYSTALLINE DOMAIN (CELLULOSE)

Cellulose, the basic building block of all trees and plants, is a long chain linear homo-polymer composed of repeating units of anhydrous-β-D-glucopyranose units linked together with β-(1→4) glycosidic linkage. In the native forms, individual cellulose chains do not occur in nature. Fundamentally, a hierarchical structure is observed within the cellulose structure where the long poly β-(1→4)-glucopyranose chains (elementary fibrils) are laterally stabilized and packed through strong inter- and intra- molecular hydrogen bonds as well as van der Walls forces forming fibrous long thread like bundles called microfibrils, which in turn plug together to form larger units called fibers. These microfibrils posses a lignin and hemicellulose **(Figure 1)** and contain both the crystalline and amorphous part. These crystalline regions are formed by the regular arrangement of individual cellulose nanofibrils of diameter 1.5-3.5 nm through H-bonding interaction and are reported to possess an elastic modulus of about 167.5 GPa as compared to e-glass fibre with an elastic modulus of 73 GPa. Hence, this hierarchical microstructure possessed by cellulose molecules allows the extraction of cellulosic nanomaterials, cellulose molecules with at least one dimension in nanometer range, which are basically termed as "Nanocellulose" [3-6].

Nanocellulose has been widely categorized as cellulose nanocrystals (CNCs), which possess rod or sphere like crystal structure, and the more flexible and longer cellulose nanofibres (CNFs). Its extraction either in the form of CNCs or CNFs has generated a momentous interest due to its extraordinary properties at nanoscale dimensions such as a very high surface-to-volume ratio, high aspect ratio, low axial thermal coefficient (10^{-7} K^{-1}) along with superior optical and mechanical

properties. Due to these remarkable characteristics endowed by CNFs, it is predicted to have many potential applications such as in aerogels, electronics, biocompatible materials, packaging, coatings and most importantly as reinforcing agent for fabricating nano-biocomposites.

Various procedures have been reported in literature for the extraction of nanocellulose including chemical, mechanical and enzymatic methods. The presented work is specifically directed towards the extraction of cellulosic nanomaterials as CNFs. First attempt to extract CNFs was reported by Herrick et al. and Turbak et al. (1983) by using a mechanical homogenizer which was based on a large pressure drop that facilitated microfibrillation. The product obtained was termed as MFC (microfibrillated cellulose). Numerous attempts has been made to extract CNFs based on mechanical treatments like grinding, high-pressure homogenization, cryocrushing, ultrasonication and high-speed blending. Chemical treatments like acid hydrolysis, biological treatments using enzymatic hydrolysis and TEMPO (2, 2, 6, 6 tetramethyl-1-piperidinyloxy)-mediated oxidation were also employed. The combination of these methods has also been used, resulting in CNFs with distinguishing features depending on the raw material as well as the isolation method used. Cellulose can be extracted from a variety of sources, including tunicates, bacterial and plants. However, extensive research has been focussed towards the extraction of CNFs from plant-based resources due to their low cost and easy availability. The diverse features (especially their dimensions) possess by CNFs is greatly dependent on the plant species used as they have varying proportions of crystalline and amorphous portions.

In the present work waste wood scraps obtained from furniture manufacturing industry has been used to extract CNFs by employing mild chemo-mechanical treatments. The decisive factor for choosing these waste materials was its abundant availability in the nearby furniture industry. A very mild chemical treatment of the raw fibres was carried out so as to remove the non-cellulosic amorphous components like lignin and hemicellulose. Most of the methods reporting the fabrication of CNFs by using chemo-mechanical treatments use acid hydrolysis as the final treatment step. The work demonstarted here exclusively deals with the acid free (strong acids like HCl and H_2SO_4) extraction of CNFs so as to ensure minimal destruction of obtained fibres. During harsh chemical treatments the transformation of cellulose I to cellulose II is possible. Besides, a well suited mechanical treatment, ultrasonication has been used to individualize the fibres in nano-dimensions. Ultrasonication has been reported to result in fibres with comparatively longer lengths. The process was carried out at an output power of 400 W which is much lower than that of most of the reported literature (700-1500 W) [7]. The hydrodynamic forces produced due to acoustic cavitations at low output power are found to be suitable for individualization of the fibres in nano-dimensions.

The detailed characterization of CNFs obtained by adopting a modified fabrication process was done using various characterization techniques. The FTIR (Fourier transform infrared spectroscopy) spectroscopy has been used for structural analysis while morphological analysis is carried out using FESEM (field emission scanning electron microscopy), AFM (atomic force microscopy) and XRD (X-Ray diffraction). Further Further TGA and DSC were used for thermal analysis of fibers. SLS has been used for the determination of weight average molecular weight. Other characterization techniques include contact angle measurement, fiber quality analysis, particle size analysis and zeta potential measurement.

The diameter of obtained fibres as investigated through FESEM analysis lies in the range of 10 to 80 nm and a diameter range of 2-15 nm was obtained through AFM analysis. The percent crystallinity as studied by XRD was found to increase after subsequent treatment steps. Two broad peaks were observed at 0.54 and 0.40 nm corresponding to (101) and (002) reflection of cellulose-Iβ with the finally obtained crystallinity of fibres as 75.67%. The dissappearnace of bands corresponding to amorphous parts i.e. lignin and hemicellulose in the FTIR analysis revealed the purity of cellulose fibres. The absence of these bands also supported the crystallinity increase of the fibres after various chemical and mechanical treatments.

The presented research effort is anticipated to maximize waste bio-resources utilization for fabricating high-performance materials, ultimately benefiting to construct greener products and thereby serving to reduce the environmental load to a certain extent. Interestingly, use of only mild chemical treatments in combination with ultrasonic processing at an output power of 400 W capitulate the formation of nano-dimension CNFs. The CNFs with high aspect ratio were obtained that can act as one

of the promising candidate for preparing green nanocomposites and can open up several opportunities in the field of bio-medical engineering attributing the strength and flexibility characteristics due, the foremost requirement of any biological appliance.

References:

[65]Invernizzi, N; Foladori G. *Nanotech Law & Bus.*, 2 **(2005)**, 101.

[66]Bhushan, B. *Philos. Trans. R. Soc. Lond. Ser. A*, 367 (**2009**), 1445.

[67]Klemm, D.; Kramer, K.; Moritz, S.; Lindström, T.; Ankerfors, M.; Gray, D.; Dorris, A. *Angew. Chem. Int. Ed.*, 50 (**2011**), 5438.

[68]Dufresne, A. *Mater. Today* 16 (**2013**), Number 6.

[69]Moon, R. J.; Martini, A.; Nairn, j.; Simonsen, J.; Youngblood, J. *Chem. Soc. Rev.*, 40 **(2011)**, 3941.

[70]Zhang, Y.; Nypelo, T.; Salas, C.; Arboleda, J.; Hoeger, I. C. Rojas, O. J. *J. Renew. Mater.*, 1**(2013),** 195.

[71]Xiao, S.; Gao, R.; Lu, Y.; Li, J.; Sun, Q. *Carbohydr. Polym.* 119(**2015)**, 202.

MARCO 490

Dual responsive alginate/poly(N-isopropyl acrylamide)/graphene oxide composite gels for controlled release studies of anti-cancer drug

K. Sudhakar[1], S.J.Moloi[1]

1.Department of Physics, University of South Africa, Private Bag X6, Florida 1710, South Africa.

Abstract:

In this work a controlled release behaviour of 5-FU as model cancer drug from Graphene oxide introduced by Sodium alginate and poly(N-isopropyl acrylamide) composite hydrogel beads has been studied. The composite hydrogel beads were prepared by emulsion crosslinking method and characterized by FTIR, TGA, XRD, and SEM techniques to investigate their formation, crystallinity and morphological properties. The encapsulation efficiency was found at around 94%. Furthermore, Invitro release studies were performed in both pH 1.2 followed by 7.4 phosphate buffer medium. The studies indicate the drug released from hydrogel networks to be more than 30 h. In general the results indicate these composite hydrogels can be potentially applied for controlled release carriers for other cancer drugs.

Key words: Composite, hydrogel, dual responsive, controlled release, cancer drug.

MACRO 491

Phosphorous and sulphur containing bio-based polyurethanes from non-edible renewable resource: Their thermal, mechanical and anti-corrosive properties

Somisetti Varaprasad, Ramanuj Narayan, K.V.S.N Raju*

Polymers and Functional Materials division, CSIR-Indian Institute of Chemical Technology, Hyderabad-500007, India.

** Corresponding author's email: kvsnraju@iict.res.in*

Over the last few decades there has been a continuous depletion of fossil fuels which are non-renewable natural resources and are being used for generating different kind of materials. So, the utilization of renewable feed-stocks for developing different sort of polymers and materials has gaining tremendous scope of interest, moreover, it meets the 7th principle of green chemistry. Cashew nut shell liquid (CNSL) is one of the promising chemicals in the generation of new polymeric materials, and is a non-edible renewable resource. CNSL contains chemicals such as linear unsaturated phenolic derivative, anacardic acid, cardanol, 2-methyl-cardol, and cardol. Cardanol was recovered from CNSL by vacuum distillation at 5-10 mm of Hg in the temperature range of 180-240^{o}C. In the present study, two different kinds of diols containing Phosphorus and Sulphur, and a bio-based epoxy resin by glycidating followed by epoxidation of double bonds of cardanol, have been prepared and further developed to bio-based polyols by common chemical transformations. The graphical representation has been given in Figure 1. All these were confirmed by FT-IR, H^1 and C^{13} NMR spectroscopic studies. Rheological studies for the bio based polyols also have been studied.

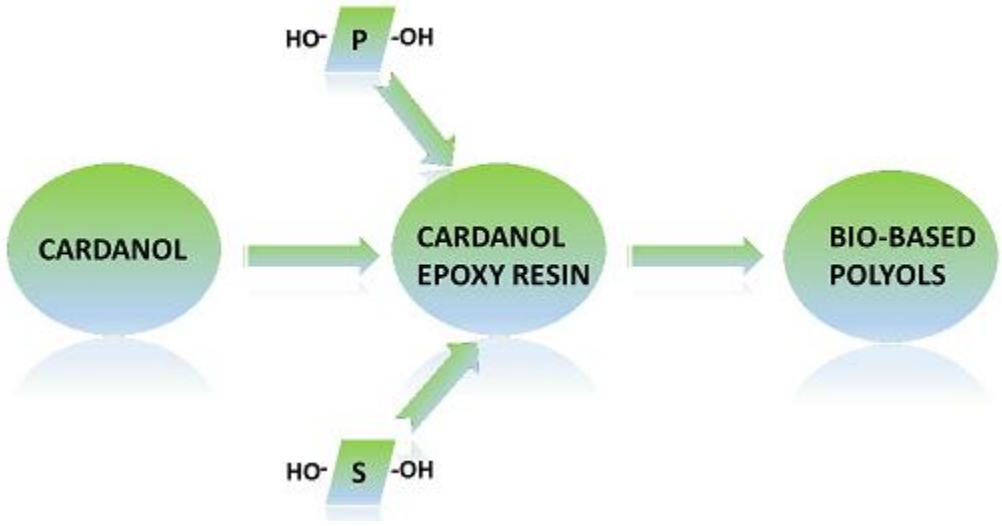


FIGURE 2: GRAPHICAL REPRESENTATION OF BIO BASED POLYOLS SYNTHESIS

Polyurethane coatings were generated by using polyisocyanate (MDI-VL) in 1.2:1 ratio of NCO:OH. These thermosets were casted on tin foil for obtaining free films and also on mild steel panels for electrochemical studies. The electrochemical study was done for coated samples and a bare mild steel

panel based on the polarization technique on an ACM electrochemical analyzer system (Gill AC) and analyzed by ACM software. Mechanical and thermal properties were studied by Thermogrametric Analysis, Dynamic Mechanical Analysis and Universal Testing Machine (UTM). The investigations showed that there has been an enhancement in anti-corrosion and mechanical properties by increasing the content of the phosphorous and sulfur content and synergic effect of both phosphorous and sulfur also increased the properties further.

References

[72] Bhunia, H.P.; Jana, R.N; Basak, A; Lenka, S.; Nando, G.B. *J Polym Sci part A: Polym Chem.*, 38 (1998) 391.
[73] Kumar, P. P.; Paramashivappa, R.; Vithayathil, P. J.; Subba Rao, P. V.; Srinivasa Rao, A. *J. Agric. Food Chem*., 50 (2002) 4705.
[74] Chen, J; Liu, Z; Jiang, J; Nie, X; Zhou, Y; Murray, R.E. *Rsc Advances, 5 (*2015) 56171.

MACRO 508

Silver and ZnO nanoparticles incorporated agar biodegradable composites for Antibacterial Applications

Rathore, Kalpana[a]; Verma, Vivek[a]*

[a]Department of Materials Science and Engineering, Indian Institute of Technology Kanpur, Kanpur 208016, India

**corresponding author: Email: vverma@iitk.ac.in*

Agar is derived from marine red algae and is extensively used as a gelling agent in food industries, pharmaceutical products, cosmetics and medicine. It is biocompatible, low in cost and biodegradable [1] but, lacks an inherent antibacterial activity to prevent bacterial infestation. To impart antibacterial activity, silver nanoparticles and zinc oxide nanoparticle were grown in the agar-based biopolymer films by serial imbibition [2] and sol-gel method [3] respectively.

The resultant agar nanocomposite films were characterized by X-ray diffraction (XRD), Fourier transform infrared (FTIR) spectroscopy, scanning electron microscopy (SEM) and energy-dispersive X-ray spectroscopy (EDS). XRD and FTIR peaks confirm the presence of metal oxide and silver particles in the polymer matrix. ZnO nano-flowers and spherical particles of silver were observed in the matrix using SEM

analysis and EDX studies reveal the presence of zinc and silver in the same. Biodegradability of the nanocomposite films was tested by soil burial method. These nanoparticle impregnated films show strong antibacterial activity against *Escherichia coli*, *Staphylococcus aureus*, *Pseudomonas aeruginosa*, and *Proteus vulgaris*. The antibacterial activity increased upon increasing the number of runs in the sol-gel method and increasing the concentration of silver nitrate. The application of this formulation can be used as packaging material, and increasing the shelf-life of some specific food products.

References

[1] Madera-Santana, T. J.; Freile-Pelegrín, Y.; & Azamar-Barrios, J. a. *International Journal of Biological Macromolecules*, *69*(2014), 176–184.

[2] Maneerung, Thawatchai; Tokura, Seiichi; Rujiravanit, Ratana. *Carbohydrate polymers*. 72(2008), 43-51.

[3] Gullapalli, Hemtej; Vemuru, Venkata S.M.; Kumar, Ashavani; Botello-Mendez, Andres; Vajtai, Robert; Terrones, Maurcio; Nagarajaiah, Satish; Ajayan, Pulickel M. *Small.* 6(2010) 15, 1641-1646.

MACRO 509

Click -Inspired Chemistry for (Bio) Conjugation in Macromolecular and Polymer Science

Mane, Shivshankar*, Delaittre, Guillaume, Barner-Kowollik, Christopher

Preparative Macromolecular Chemistry, Institute for Chemical Technology and Polymer Chemistry, Karlsruhe Institute of Technology (KIT), Engesserstr. 18, Geb. 11.23, Karlsruhe- 76131, Germany.
Email: shivshankar.mane@kit.edu

Click chemistry -a facile, fast and ambient-temperature avenue for providing a platform for technology; or synthesize a polymer with common reagents and subsequently employ this polymer with no further functionalization and efficiently carry out further conjugation without catalyst in biologically relevant media via click reaction.[1-3] As reported in literature, many reactive pairs of dienes and dienophiles potentially lead to conjugation through carbon−carbon or carbon−heteroatom bond formation so-called hetero-Diels−Alder (HDA).[4,5] HDA cycloadditions occur in water within a few hours at ambient temperature. Such an achievement would represent a major step forward in the field of polymer (bio) conjugation.

Here we introduced bio-conjugation of enzyme/protein to polymer via HDA approach. The polymer obtained by living/controlled reversible addition-fragmentation chain-transfer (RAFT) polymerization is demonstrated to react in water with diene-functionalized biomolecules without pre- or post-functionalization steps at ambient temperature. To demonstrate the possibility of RAFT-HDA cycloadditions in aqueous solution, water-soluble poly triethylene glycol methyl ether acrylate (PTEGA) was prepared by employing 2-cyanoprop-2-yl diethoxyphosphoryl dithioformate as chain-transfer agent. Addition of an excess diene to an aqueous solution of PTEGA resulted in an instantaneous discoloration indicating the consumption of the dithioester end-group. The quantitative conversions of HDA conjugations were monitored by SDS page. These results of RAFT-HDA

enzyme/protein conjugation open the avenue for enzyme/protein functionalization and could be useful for biological application.

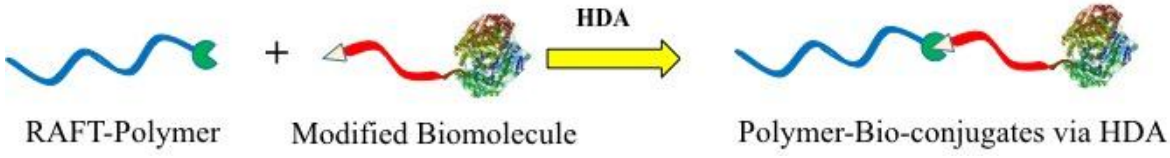


Figure 1. Schematic representation for polymer-Biomolecule conjugation via RAFT-HDA approach .

References

[75]Kolb, H. C.; Finn, M. G.; Sharpless, K. B. Angew. Chem., Int. Ed. 40, (2001) 2004.
[76]Delaittre, G.; Guimard, N.; Barner-Kowollik, C. *Acc. Chem. Res.* 48 (2015) 1296.
[77]Mane, S. R.; Sarkar, S.; Rao, N.; Sathyan, A.; Shunmugam, R. *RSC Adv.*, 5 (2015) 74159.
[78]Glassner, M.; Delaittre, G.; Kaupp, M.; Blinco, J. P.; Barner- Kowollik, C. *J. Am. Chem. Soc.* 134 (2012) 7274.
[79]Preuss, C. M.; Zieger, M. M.; Rodriguez-Emmenegger, C.; Zydziak, N.; Trouillet, V.; Goldmann, A. S.; Barner-Kowollik, C. *ACS Macro Lett.* 3 (2014) 1169.

MACRO 539

Synthesis and Characterization of Green Polyester Films

Sidhharth Sirohi[a], Krishna Dutt[a], Ratyakshi Nain[b], Naveen Yadav[a], Parth Bidaliya[a], Vinyak[b], Surbhi Singh[b], Ashwini K. Agrawal[c]

[a] *Department of Polymer Science, Bhaskaracharya College of Applied Sciences, D.U., India*
[b] *Department of Biomedical Sciences, Bhaskaracharya College of Applied Sciences, D.U., India*
[c] *Department of Textile Technology Indian Institute of Technology, Delhi, India*
* *e-mail id:* siddharth.sirohi@bcas.du.in

Abstract
The present work aims to synthesize thermoset bio-degradable lactic acid based polyester films as an alternative green approach.
The thermoset polyester resin was synthesized using poly(ethylene glycol), maleic anhydride, and lactic acid as monomers. Various ratios of the monomers were used to investigate the effect of each monomer on biodegradability. The obtained resin was characterized for its chemical and physical properties including acid value, hydroxyl value, viscosity, no. average molecular weight. The resin was used to prepare polyester films using thermal curing. Further, the biodegradation behaviour was analyzed for *Aspergillus (fungi), Bacillus (bacteria)*. The films were characterized using FE-SEM to analyse the microbial growth and morphology after microbial biodegradation. The weight loss in the films was observed for 15 days, 1 month and 2 months to study the biodegradation behaviour. It has been observed that the obtained green polyester films facilitate the microbial growth and hence have improved biodegradation behaviour.
Keywords: *polymer; biodegradable; thermoset; green composite*

Introduction

Synthetic polymers play an essential role in everyday life because of the broad range of properties they offer. They have important role in various industries including packaging[1], agriculture plastics[2], biomedical[3] etc. However, these synthetic polymers have undesirable influence on the environment related to the waste utilization and deposition[4]. The biodegradability of polymers is a major concern in this respect because of their long term existence in the environment[5]. The landfill[6] which is most common method of their disposition creates serious environmental hazards. As most of these polymers have resistance to chemical and physical degradation an alternate is to develop actively biodegradable polymer. Researchers have used biodegradable thermoplastic polyesters to resolve this problem[7]. However, limited literature is available for biodegradable thermoset polyesters[2].

Experimental

Materials and methods

Materials:

The chemicals used were Polyethylene glycol (Mw- 400, Fisher Scientific, 99.95%), maleic anhydride (CDH, 97%), lactic acid (MERCK, 88-92%), antimony trioxide (LOBA Chemie, 99%), styrene (*Otto*), Acetone (CDH / Fisher Scientific) and benzoyl peroxide (LOBA Chemie, 75%). All the chemicals were of analytical grade and were used as provided. Double deionized water was used in all the synthesis processes. All glassware was first rinsed with aqua regia and thoroughly with water followed by deionized water before use.

Synthesis of Polyester resin

The monomers for the polyesters were Polyethylene glycol (Mw = 400), Maleic anhydride (Mw = 98.06), Lactic acid (Mw = 90). Polyethylene glycol was used as saturated di-ol in order to provide

flexibility and maleic anhydride for curing sites, lactic acid for weak links to make it biodegradable. It was a two step reaction. In first step water drops were separate out at 120 °C and further in second step the temperature was increased up to 150 °C to increase the reactivity. Thermo-chemical curing of obtained polyester resin using styrene as monomer and benzoyl peroxide (BPO) as an initiator. The concentration of lactic acid was varied from 0.1-0.5 moles keeping the concentration of polyethylene glycol and maleic anhydride as 1.

The acid number and molecular weight were calculated by following equation:-

Acid number(C) = (56.1*V*N)/ m

Where, V is the volume of KOH consumed in titrating the sample

N is normality of KOH

m is the mass of sample taken

Molecular weight = F*100/ C

Where, F is the functionality of polyester

C is the Acid number

Biodegradation studies of Polyester films

Biodegradation studies of casted films using microbial degradation. The fungal and bacterial species used for the study were *Aspergillus sp. a*nd *Bacillus sp.* respectively. The 5 X 5 cm polyester films were placed for the degradation studies.

Results and discussion

Figure 1 and Figure 2 shows the effect of lactic acid concentration on the acid value and molecular weight of obtained resin respectively. It has been observed that increasing the concentration of lactic acid resulted in increased acid value and hence decreased molecular weight.

The obtained films were found to be flexible and non-porous. The surface was smooth and the films were off white in color as shown in Figure 3.

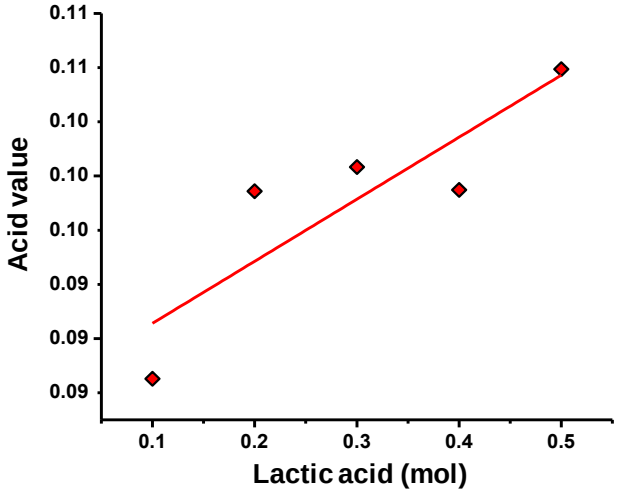


Figure 1. Effect of lactic acid concentration on acid value of the resin.

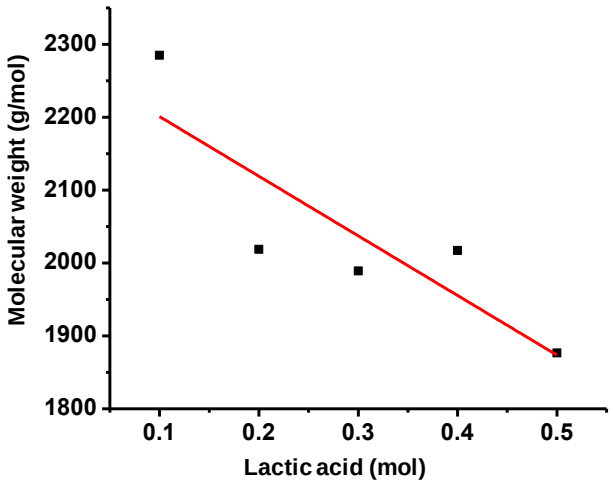


Figure 2. Effect of lactic acid concentration on the molecular weight of obtained resin.

The polyester films were characterized using FE-SEM (Field emission scanning electron microscope) to analyze the growth of bacteria on their surface. The bacteria were found to be adhered and the growth of bacillus was observed on the surface of polyester films (Figure 4).

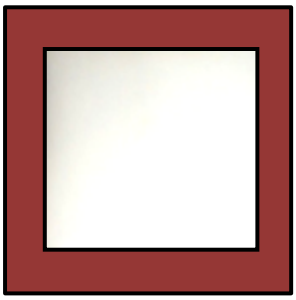


Figure 3. The polyester film obtained from the resin.

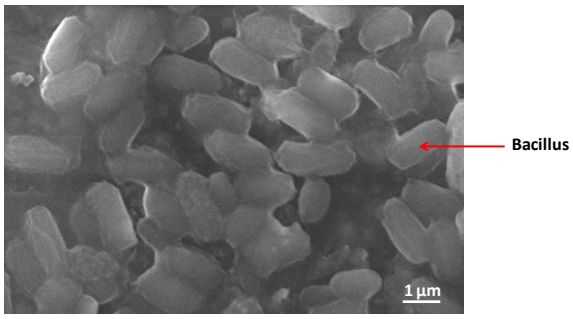


Figure 4. Growth of bacteria *(Bacillus)* on the surface of polyester film.

This clearly indicates that the polyester films facilitate the attachment of bacteria on the surface which is primary requirement for the biodegradation.

Conclusion

The polyester films, synthesized using poly(ethylene glycol), maleic anhydride, and lactic acid as monomers, were found to be smooth, flexible and non porous in nature. The increase in lactic acid concentration resulted in increase in the acid value and respectively decreases the molecular weight of the obtained films. The biodegradation studies confirmed that the films facilitate the attachment and hence growth of microbes. Further reduced weight of films after 1 month confirmed the biodegradable nature of the obtained polyester films. These films offer potential application in the area of packaging material because of their biodegradable nature.

Acknowledgements

Authors would like to thank Department of Polymer Science, Bhaskaracharya College of Applied Sciences for providing the lab facilities and University of Delhi for financial support.

References

44. Siracusa, V., Rocculi, P., Romani, S., & Dalla Rosa, M. (2008). Biodegradable polymers for food packaging: a review. *Trends in Food Science & Technology*, *19*(12), 634-643.
45. Sojka, R. E., Entry, J. A., Orts, W. J., Morishita, D. W., Ross, C. W., & Horne, D. J. (2005). Synthetic-and bio-polymer use for runoff water quality management in irrigated agriculture. *Water Science and Technology*, *51*(3-4), 107-115.
46. Gibas, I., & Janik, H. (2010). Review: synthetic polymer hydrogels for biomedical applications.
47. Moore, C. J. (2008). Synthetic polymers in the marine environment: a rapidly increasing,long-term threat. *Environmental research*, *108*(2), 131-139.
48. Thompson, R. C., Moore, C. J., Vom Saal, F. S., & Swan, S. H. (2009). Plastics, the environment and human health: current consensus and future trends. *Philosophical Transactions of the Royal Society B: Biological Sciences*, *364*(1526), 2153-2166.
49. Andrady, A. L. (1994). Assessment of environmental biodegradation of synthetic polymers. *Journal of Macromolecular Science, Part C: Polymer Reviews*, *34*(1), 25-76.
50. Mergaert, J., Ruffieux, K., Bourban, C., Storms, V., Wagemans, W., Wintermantel, E., & Swings, J. (2000). In vitro biodegradation of polyester-based plastic materials by selected bacterial cultures. *Journal of Polymers and the Environment*, *8*(1), 17-27.
51. Rösch, J., & Mülhaupt, R. (1993). Polymers from renewable resoureces: polyester resins and blends based upon anhydride-cured epoxidized soybean oil. *Polymer Bulletin*, *31*(6), 679-685.

MACRO 549

Thermally curable 2-Oxazoline coatings from bio-based building blocks

Roy, M.[a,b]; Wilsens, C.H.R.M.[a,b,*]; Noordzij, G.[a]; Rastogi, S[a,b].

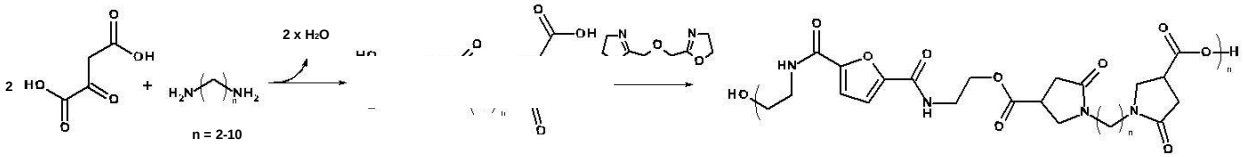
[a]*Department of biobased materials, Maastricht University, P.O. Box 616, 6200MD Maastricht, The Netherlands.*

[b]*Aachen-Maastricht Institute for BioBased Materials (AMIBM), Urmonderbaan 22, 6167 RD, Geleen, The Netherlands*

**corresponding author: karel.wilsens@maastrichtuniversity.nl*

Recently, our research group reported on the application of renewable bis(2-oxazoline) monomer based on 2,5-furandicarboxylic acid for application in thermally curable resins for coating applications [1]. In this follow up study, a range of flexible aliphatic dicarboxylic acids are used as reactive component in the developed resins. Fourier-Transform Infra-Red spectroscopy is used to monitor the chain-extension and cross-linking kinetics occurring during the polymerization (Figure 1), and a protocol is established to determine the reaction rates of both reactions that occur simultaneously. We demonstrate that both the chain-extension reaction and the branching/cross-linking reactions are second order reactions for all systems, thereby providing excellent control over the reaction times, temperatures, and the chemical composition of the cured materials. The obtained information is used to establish relations between the chemical structure of the materials and the thermal behavior of the ensuing polymers.

In the second part of this work, we report on the synthesis, isolation and characterization of various renewable dicarboxylic acids from itaconic acid and aliphatic diamines (Scheme 1). The ensuing dicarboxylic acids, made from both even and odd diamines, contain two lactam rings and are significantly more rigid than the aliphatic dicarboxylic acids explored in the initial part of this work. Thermal curing with furandicarboxylic acid based (2-oxazoline) yields rigid poly(ester-amide) materials with glass transition temperatures ranging from 80 °C for the linear chains up to 200 °C and higher for the cross-linked systems. Despite the high glass-transition temperatures of these poly(ester-amide)s, the presence of the numerous oxygen groups of the furan rings and amide groups result in significant water absorption, which supresses the glass transition temperatures and triggers water degradability. [2] The combined control over the reaction kinetics, thermal behaviour, and degradability makes these materials highly interesting for application where compostability, bio-degrability, or chemical recycling is desired.



Scheme 1. Schematic overview of the chain-extension reaction between bis-lactam based dicarboxylic acids and 2,5-furandicarboxylic acid based bis(2-oxazoline), yielding fully renewable poly(ester-amide)s. Please take note; providing an excess of bis(2-oxazoline) allows for cross-linking at the secondary amide positions, thereby yielding a thermoset polymer instead of the displayed linear polymer chains.

References

[1] Wilsens, C.H.R.M.; Wullems, N.J.M.; Gubbels, E.; Yao, Y.; Rastogi, S.; Noordover, B.A.J; *Polymer Chemistry*, 6, **2015**, 13280

[2] Qi, P.; Chen, H-L.; Nguyen, H.T.H.; Lin, C-C.; Miller, S.A; *Green Chemistry*, 18, **2016**, 4170

MACRO 550

Small scale screening of novel bio-based polyesters

Noordzij, G.[a,b]; Wilsens, C.H.R.M.[a,c,*]; Rastogi, S[a,c].

[a]*Department of biobased materials, Maastricht University, P.O. Box 616, 6200MD Maastricht, The Netherlands.*

[b]*Chemelot InSciTe, Urmonderbaan 20F, NL-6167 RD Geleen, The Netherlands*

[c]*Aachen-Maastricht Institute for BioBased Materials (AMIBM), Urmonderbaan 22, 6167 RD, Geleen, The Netherlands*

** corresponding author: karel.wilsens@maastrichtuniversity.nl*

There exists a clear paradox in the screening of new materials: Large volumes are required to accurately assess the material properties, but such large scale production is often expensive and tedious, without guaranteeing success of obtaining the desired material properties. To break this paradox, new tools are required that polymerize and characterize new bio-based building blocks on small scale, and in high throughput. In this work, we are evaluating various cyclo-aliphatic building blocks in small-scale polycondensation reactions in order to achieve high-molecular weight polymers, and to characterize their material properties and assess their suitability for up-scaling.

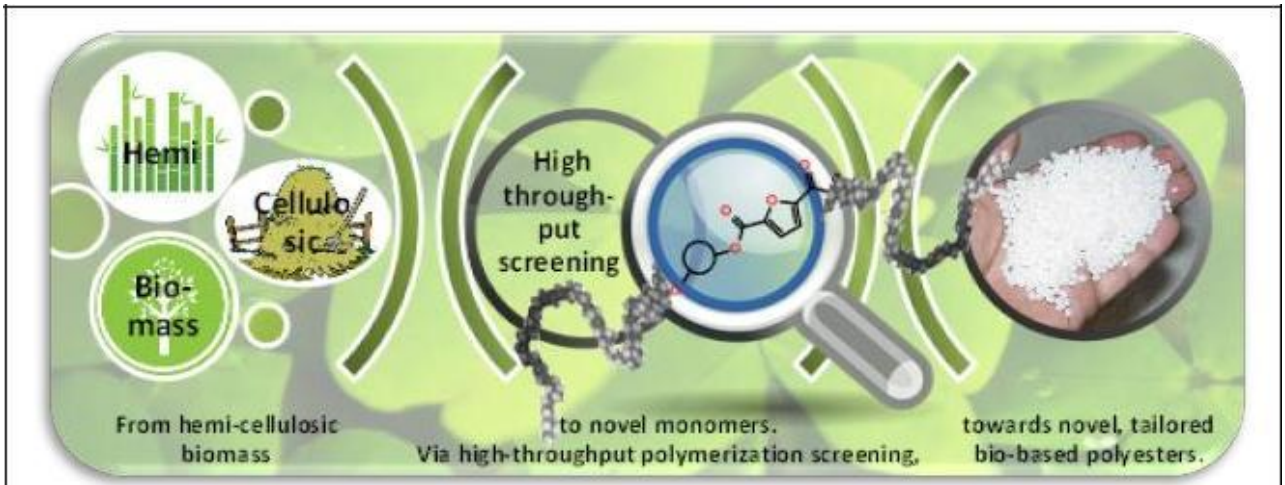


Figure 1. Schematic overview of the development of the small-scale screening technique for the evaluation of renewable polyesters

Via small-scale reactions (<10 mg) in TGA we perform polycondensation reactions at various reaction conditions, including time, temperature and catalyst requirement. In such reactions, the rate of polycondensation, evaporation and degradation are monitored as a function of weight loss. The optimized polymerization protocols, found from such TGA experiments are combined with characterization in DSC and GPC. The optimized conditions can be transferred to the high-throughput (57-parallel) reactor where high molecular weight polyesters can be made via thin-film polycondensation. We demonstrate that secondary cyclo-aliphatic diols are relatively inactive; hence catalysts to improve the rate of polycondensation are required. In this research, new polyesters have been prepared from various cyclo-aliphatic diols with rigid terephthalate (T), and flexible adipate (A) and sebacate (S) blocks. Generally, polymerization with terephthalic acid yields high melting semi-crystalline polymers, having a T_m close to the degradation temperatures. Furthermore, rapid crystallization during the polymerization limits the M_n (5 kg/mol) and M_w (10 kg/mol) build-up during polymerization. Since degradation occurs above the equilibrium melting temperature, further processing and characterization of these materials will prove to

be challenging.

In contrast, the polyesters containing flexible dicarboxylic acids have a drastically decreased Tg, generally below room temperature. Sufficiently high molecular weight, Mn (10-15 kg/mol) and Mw (25-50 kg/mol), has been obtained for the catalyzed polymerizations. Furthermore, depending on the selected dicarboxylic acid, these materials can be fully amorphous, or semi-crystalline with melting temperatures below 100 °C. Following the methods developed in this research, we envision novel co-polyesters having tailored physical properties.

MACRO 556

Engineering Protein Based Bio-polymer Coated Functional Nanomaterials for Bio-application

Chakrabortty, Sabyasachi;[a,] * Sison, Miguel;[b] Lasser, Theo;[b] Weil, Tanja[a,]*

[a]Department of Organic Chemistry III/Macromolecular Chemistry, Ulm University, Albert-Einstein-Allee 11, D-89081, Ulm, Germany.
[b]Laboratoire d'Optique Biomédicale, Ecole Polytechnique Fédérale de Lausanne (EPFL), Station 17, CH-1015 Lausanne, Switzerland

** Sabyasachi.chakrabortty@uni-ulm.de; tanja.weil@uni-ulm.de*

Chemical programming of protein based polymer structures to infuse a set of distinct chemical properties which are designed to behave in a precise and sequential manner, is a characteristic vision for creating next generation bio-hybrid.[1] They offer an attractive platform for the integration of complex chemical design into their backbone, providing accurate translation of chemical functionalities to biological activity. Coupling with the introduction of various site specific customization in native protein structures such as, amine, carboxylic acid and/or thiol functionalities, for attaching different molecules of interest, become very special. Those bio-hybrids can also be used to passivate colloidal nanomaterials such as luminescent quantum dots (QDs), metal clusters to study various interactions inside biological environments. Here, a facile synthetic approach of multifunctional peptide-polymer hybrids, based on blood plasma albumin protein and their subsequent encapsulation strategy towards QDs will be illustrated.[2] Moreover, significant pH responsiveness (e.g., an influence of the pH on the quantum yields of the peptide−polymer/QDs), which is attributed to conformational rearrangements of the peptide backbone will be demonstrated. Next, to provide deeper understanding of intracellular dynamics and vitality, this polypeptide platform is demonstrated as a carrier of various functionalities as well as nanoparticles to intracellular targeted organelles. Exploring these polypeptides passivated metal nanoparticles (e.g., Au) i) as NIR-emitting markers in confocal microscopy and ii) photo-thermal active probes in optical coherence microscopy, we will demonstrate their great potential for efficiently directing Au NP to

subcellular targets, i.e., mitochondria. Finally, it is envisioned that chemically reprogrammed smart proteins with careful designing of functional nanomaterials will bridge the vital link to overcome the limitations of synthetic and biological materials, providing a unique strategy for probing specific biological processes in live cells.

References

[80]Ng, D. Y. W.; Wu, Y.; Kuan, S. L.; Wei, T. *Acc. Chem. Res.* 47 (2014), 3471–3480.

[81]Wu, Y.; Chakrabortty, S.; Gropeanu, R. a; Wilhelmi, J.; Xu, Y.; Er, K. S.; Kuan, S. L.; Koynov, K.; Chan, Y.; Weil, T. *J. Am. Chem. Soc.* 14 (2010), 5012–5014.

MACRO 555

Synthesis and characterization of Flutamide loaded Carbopol/Poly(vinyl pyrrolidone) blend microspheres: *In-vitro* release studies

P. Kumara Babu[1], Y. Maruthi[1], A. Parandhama[1], C. Madhavi[1], M.C.S. Subha[2] and K. Chowdoji Rao[1]*

[1]Department of Polymer Science & Technology, Sri Krishnadevaraya University, Anantapuramu, Andhra Pradesh, India – 515 003.

[2]Department of Chemistry, Sri Krishnadevaraya University, Anantapuramu, Andhra Pradesh, India – 515 003.

Abstract

Carbopol/Poly(vinyl pyrrolidone) (CPL-PVP) blend microspheres were prepared by solvent evaporation technique using poly (Vinyl alcohol) as a stabilizer. Flutamide, an anti-cancer drug was successfully loaded into these microspheres. The effect of experimental variables such as ratio of Carbopol to Poly(vinyl pyrrolidone) on Flutamide encapsulation efficiency, release rate, size and morphology of the microspheres have been investigated. Flutamide loaded and unloaded microspheres were characterized using FTIR, DSC, X-RD and SEM techniques. Fourier transform infrared spectroscopy was used to explain the probable interactions between polymers, crosslinker and drug. Differential scanning calorimetry and X-RD techniques were used to investigate the crystalline nature of the drug after encapsulation in the blend microspheres and of the drug particlesin the blend microspheres. Scanning electron micrographs indicated the formation of

spherical microspheres with distinct size. Flutamide was successfully encapsulated up to 72% in these polymeric matrices. *In-vitro* dissolution experiments performed in pH 7.4 buffer medium indicated a controlled release of Flutamide from blend microspheres up to 16 hrs.

Key words: *carbopol, poly (vinylpyrrolidone), microspheres, Flutamide, In-vitro release*



FOCUS AREA

NANOSTRUCTURES, SELF-ASSEMBLY AND SUPRAMOLECULAR POLYMERS

MACRO 112

Supramolecular Approches Towards Novel Applications

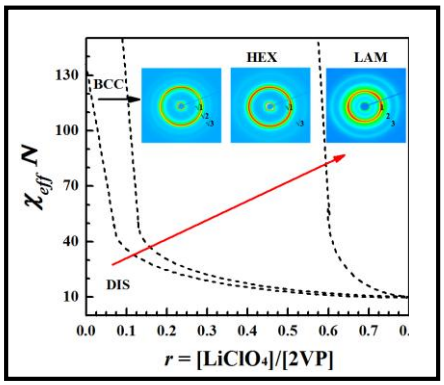
Tejas S Bhosale and Sudhakar Naidu Neppalli*

Polymer Science and Engineering Division, National Chemical Laboratory, Pune, Maharashtra, India

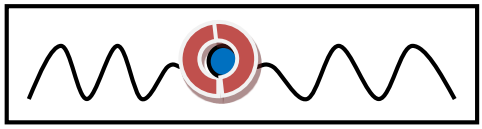
Contact E-mail: s.naidu@ncl.res.in

ABSTRACT: Block copolymers (BCP) are proving fascinating class of materials with unique advantage of self-assembly into miscellaneous ordered nanostructures in 10-100 nm length scale. Order-to-order transitions (OOT) and Order-to-disorder transitions (ODT) can also observe with the adjustment of experimental parameters such as degree of polymerization (N), volume fraction of the blocks (Φ), the Flory-Huggins interactions parameter (χ) and temperature. Tailored block copolymers, by introducing small molecules into one of the block component in block copolymer through non covalent interactions, can use advantageously in creating very well ordered nanostructures and that the concept can be applied for various applications.

Hence we covered the research that, the importance of non-covalent bonds in increasing the non-favourable segmental interactions of the blocks was well examined by attaching and detaching the bonds between the BCP and additive. And also studied, the phase transition of block copolymer and Floury-Huggins interaction parameter (χ) behavior in Li-doped polymers using *in-situ* small angle x-ray scattering (SAXS) and transmission electron microscopy (TEM). The effective interaction parameter (χ_{eff}) between two block components was evaluated using Leibler theory based on the incompressible random phase approximation (RPA) for ionized BCP in a disordered state. Furthermore, conductivity experiments demonstrate that the ionic conductivity in the samples quenched from the different structures is morphology-independent, while it increases with increasing ion salt concentration. Morphological transitions, interaction parameter and thermal stability also examined in quarternized block copolymer. D-spacing was used to estimate effective interaction parameter (χ_{eff}) of block components in weak and strong segregation regimes of ordered phase.



Metal-containing polymer has been the topic of great attention in recent years due to their wide range of potential application. Similarly, metal- ligand complex is used as a suparmolecular linker between the polymers giving rise to a 'Metallo-Supramolecule assembly. More precisely, functionalized polymer end capped with 2, 2':6', 2"- terpyridine ligand can be selectively complexed with wide range of transition metal ions and then subsequently attached to other terpyridine terminated polymer block. In compare to other supramolecular assembly, BCP involved metallo-supramolecule assembly offers vast applications such as optical activity, electrical conductivity, luminescence and photo refractivity.



References:

[1] Leibler, L. *Macromolecules* **1980,** 13, (6), 1602-1617
[2] Naidu, S.; Ahn, H.; Gong, J.; Kim, B.; Ryu, D. Y. *Macromolecules* **2011,** 44 (15), 6085-6093.
[3] Naidu, S.; Ahn, H.; Lee, H.; Jung Y.M.; Ryu, D. Y. *Macromolecules* **2010,** 43 (14), 6120-6126.
[4] Schmidt, K.; Schoberth, H. G.; Boker, A. *Nat Mater* **2008,** 7, (2), 142-145.
[5] Alexander A. Teran; Nitash P. Balsara *J. Phys. Chem. B* **2014**, 118, 4-17.

MACRO 120

Molecularly imprinted polymers

Kalsang Tharpa

SABIC Research & Technology Center, Off. Sarjapura - Attibele State Highway, Bangalore- 562125, Karnataka, India

kalsang.tharpa@sabic.com

Abstract

Molecularly Imprinted Polymer (MIP), also known as plastic anti-body is known for its high selectivity, equivalent to the property of biological antigen-antibody, towards a chosen molecule of interest [1]. The principle of MIP is based on polymerization of functional monomers and cross-linkers that are surrounded around a template molecule, and later the template molecules are removed creating a three dimensional selective recognition sites with shape, size and functionalities complementary to the template. The resultant MIP is being use in the field of separation, sensor, membrane, catalysis, regio-selective synthesis, drug delivery and drug discovery. This presentation is intended to compile comprehensively about MIP such as- its discovery, various synthesis routes, characterization techniques, applications, current trend and future perspective. More recent approach on alternative molecular imprinting on a cellulose acetate nano-fiber [2], leading to faster kinetic in contrast to conventional MIP beads will be discussed.

Keywords: *Imprinted polymer; synthesis; challenges & remedial*

Introduction

History

In the year 1931, Polyakvo published [3] a strange observation on the affinity of a silica gel. Based on his observation, when silica gel was cured under specific solvent the resultant gel showed specific affinity

towards the same solvent. Polyakyo continued to study on this strange phenomenon for some time, it was not until year 1949 when F.H Dickey with Linus Pauling [4] published a more concrete understanding of the phenomenon which has shaped into present day understanding of molecular imprinting.

After a steady flow of publications over a period of 15 years, the interest in imprinted silica experienced a temporary decline due to the limitations in stability and reproducibility of the imprinted silica materials. However, the popularity of molecular imprinting improved when in early 1970's group of Koltz and Wulff [4, 5] independently reported the first examples of molecular imprinting in synthetic organic polymers.

The principle of molecular imprinting [2] is based on the polymerization of functional monomers and cross-linkers that are surrounded around a template molecule, and later the template molecules are removed creating a three dimensional selective recognition sites with shape, size and functionalities complementary to the template molecule (Fig. 1).

Classification of molecularly imprinted polymers

There exist two way of classifying MIP- one is based on the nature of bond existing between the template molecule and the functional monomer which classifies MIP into covalent and non-covalent type, another is based on the synthetic procedure adopted wherein use of template, monomer and cross-linker for synthesis of MIP are called conventional MIP and the MIP synthesized through scaffolding of polymers is called alternative imprinting.

The first organic based MIP proposed by Wulff *et. al.*, [6] were covalent imprinting as shown in Fig. 2. This approach has advantage of creating stoichiometric amount of binding sites thereby decreasing the pore heterogeneity however it restricts the choice of functional monomer and often required long re-binding period. Therefore, a more versatile approach called non-covalent imprinting (Fig. 3) was proposed by Mosbach group [7]. Since the bond between the template molecule and functional monomer is universal the approach received wide spread applications. In comparison to covalent-MIP, the non-covalent MIP required less drastic synthesis procedure primarily due to weak Van der Waals force between template molecule and functional monomers. However, non-covalent MIP often give rise to pore heterogeneity and lesser selective functional sites.

A group of Whitecombe [8] proposed 'covalent sacrificial imprinting' (Fig. 4) which consider advantages of both covalent and non-covalent imprinting. The selective pores were created based on covalent imprinting thereby decreasing the pores heterogeneity and faster kinetic of template re-binding happens similar to non-covalent imprinting.

Although conventional MIP is now followed with much optimized procedure, the inherent challenge in it is imprinting of bigger biomolecules due to highly crosslinked network. Therefore, alternative imprinting procedure which is actively followed by group of Masakazu [7] have potential for imprinting of bigger template molecule since the process involve simple scaffolding of the polymerizable material around the template molecule.

Challenges & remedial so far

Ideally, as per the principle of MIPs it should perform in par with biological anti-body with additional qualities such as stability, re-generable and fabricate into different application needs which a usual polymer can offer. However, such a dream-state performance of MIP has encountered many practical challenges such as: non-uniform distribution of shape and size of polymer beads, loss of selective pores, slower kinetic of re-binding, and most importantly, difficulty in scaling up the process.

To achieve specific physical form of polymer for end application, many polymerization techniques were reported for synthesis of MIPs such as bulk, suspension, precipitation, multi-step swelling, and surface and *in-situ* polymerization.

The bulk polymerization is relatively easy which involved solution polymerization followed by mechanical grinding. However, mechanical grinding gives highly irregular size and shape polymers, which also result in loss of active sites. When use as column filling the efficiency of chromatographic separation decreases. To circumvent, advantages of bulk polymerization inside a column monolith were also reported.

To achieve spherically uniform sized polymer beads of the order down to 50 nm, a pre-polymerization mixture consisting of template and monomers were suspended in a large volume of inert solvent placed in a centrifuge and were polymerized under high RPM. The resulting MIP beads requires no additional work-up such as mechanical sieving which greatly limit the loss of active sites. Non-covalent based MIPs were performed in a tetrafluoro carbon solvent to avoid interference at building of hydrogen bonds between the template and functional monomer.

One of the most attractive solutions for slower kinetic of template re-binding, which were considered natural in MIP due to high amount of cross-linker hindering access to active sites, are approaches such as nano-beads MIP synthesis, encapsulation and surface imprinting. The faster kinetic of template re-binding approach of MIP when applied in the field of membrane called molecularly imprinted membrane (MIM) have shown considerable increase in both flux and perm-selectivity of the membrane [2]. The electrosprayed nanofiber membrane incorporated with the template molecule with the diameter of 100 nm was calculated to be approximately 40 m^2 g^{-1}, whereas the usual cast membrane gave a surface area of

approximately 0.2 m^2 g^{-1}. The surface area of the nanofiber membrane is 200 times greater than the usual membrane sheet. Additionally, the MIM shows a specific interaction toward one target molecule and not to others, the target molecule would be incorporated into the membrane selectively over the others. If the target molecule is in contact with two types of membrane, such as a usual cast membrane and a nanofiber membrane, the amount of the target molecule incorporated into the nanofiber one should be greater than that incorporated into the usual one. Assuming that the amount of substrate incorporated into a membrane is proportional to its surface area, the amount incorporated into a nanofiber membrane would be 200 times more than that for a usual membrane. If so, it can be expected that the solubility coefficient of the target molecule for a nanofiber membrane would become higher than that for a usual membrane.

Characterization

The evidence of molecular imprinting is broadly deduced from direct measurement of its physical/molecular form or indirectly through binding assay. Since the cavity created due to imprinting is at molecular level, it is difficult to directly correlate the physical appearances such as pore size or shape by techniques such as BET and SEM. However, recent report on use of positron annihilation spectroscopy which can probe cavity down to the atomic level have shown direct evidence of template size pore creation on MIPs. Two other direct evidence could be deduced from IR and solid state NMR (SS-NMR) techniques. The presence or absence of carbonyl frequency of usual methacyrlic acid monomer were largely use to prove formation of functional selective cavity. However, SS-NMR through study of long range coupling brings about more direct evidence of existence of selective cavity created by the template molecule except that the large amount of signal interferences makes this technique challenging.

More indirect study such as batch binding assay needs to be ultimately shown to prove presence of selective cavity. Ideally, batch binding assay using a mixture of template and template analogue molecule, preferably an enantiomer of the template molecule, would give much stronger evidence. Such a study would not only give binding capacity of the MIPs one can also calculate thermodynamically selective pores. These studies are done at infinite contact on a table shaker or dynamically in a MIP filled columns. The later have advantage of studying the effect of flow dynamics and binding saturation in case of continuous process.

Applications

MIPs received wide spread applications in areas such as purification of product from trace level impurities, sensor, drug discovery, drug delivery, stereo-selective synthesis, membrane separation and catalysis. Few interesting applications will be highlighted. A patent [10] on imprinted polymer for selective removal of gas phase nitrosoamine compound, a cancer causing agent, from the burning cigarette placed within a cellulose acetate usual filter attracts many such applications. In the field of drug discovery, MIP column

created by known anti-cancer molecule retains the most potent anti-cancer molecule when a crude extract of natural product where pass through it [11], opening a new frontier in rapid screening of leading drug molecules present in complex natural products. Although commercial application of MIP, largely by Sigma Aldrich, has been limited to its use as solid phase sample preparation, the more recent report such as the one [12] where MIP was use to remove precursor to bad body odor could open completely new market. Among the various application domains of MIP, the most serious persuasion could be found in the field of drug delivery. The MIP based sensor is an obvious application end if challenges such as selective layer to transducer communication is eased and research on more of ultrathin self-standing MIP are design.

Conclusions

There are many more to be do than done in the field of MIP. The scalable synthetic procedure, less heterogeneous pore distribution, self-standing imprinted membrane, nano or ultrathin imprinted material, ease of regeneration procedure, imprinting of large biomolecules, etc are some of the challenges that MIP research community can focus on. Practical challenges of large scale synthesis of conventional MIP could be overcome by alternative molecular imprinting therefore, research on self-assembly based imprinting and the optimization of parameters therein could bring more of MIP at the commercial front.

Acknowledgement

Author thank Dr. Arun Kumar for his encouragements to present an overview on molecular imprinting and authorities of SABIC for the permission and necessary approvals.

References

1. M. Yoshikawa; Kalsang Tharpa. Imprinting. Encyclopedia of Membranes, Eds. Enrico Drioli, Giorno Lidietta. ISBN 978-3-662-44324-8. Springer-Verlag Berlin Heidelberg (2016) 1-3.
2. M. Yoshikawa; Kalsang Tharpa. Application of membranes from cellulose acetate nanofibers. Handbook of Polymer Nanocomposites. Processing, Performance and Application. Volume C: Polymer Nanocomposites of Cellulose Nanoparticles. Eds Jitendra K. Pandey, Hitoshi Takagi, Antonio Norio Nakagaito, Hyun-Joong Kim, Berlin, Springer-Verlag. (2015) 355-367.
3. Polyakov MV (1931) Adsorption properties and structure of silica gel. Zhur Fiz Khim 2: 799–805.
4. F.H Dickey, The preparation of specific adsorbents, 1949, 35, 5,227-229.
5. I.M. Klotz and J.U. Harris. Biochemistry, 1971, 10, 923.
6. G.Wulff and A. Sarhan. Angew. Chem., 1972, 84, 364.
7. R. Arshady and K. Mosbach, Makromol. Chem,. 182, 687 (1981).
8. M.J. Whitecombe, M.E. Rodriquez, P. Villar, E.N Vulfson. J. Am.Chem. Soc., 117, 7105 (1995).

9. Masakazu Yoshikawa, Kalsang Tharpa, Ovidiu Dima. Chem. Rev., September 9, 2016. DOI: 10.1021/acs.chemrev.6b00098 (Article ASAP).
10. C.D.H Byrd, A.R Gerardi. US Patent. US 2012/0291793 A1.
11. XiaojieXu, Journal of Chromatography B, 804 (2004) 61–69.
12. S. Nestora, F. Merlier, S. Beyazit, E. Prost, L. Duma, B. Baril, A. Greaves, K. Haupt, B. Tse Sum Bui. Angew. Chem., Int. Ed., 55 (21) 2016, 6252-6256.

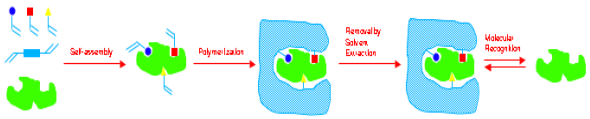


Fig. 1 Working principle of molecularly imprinted polymer

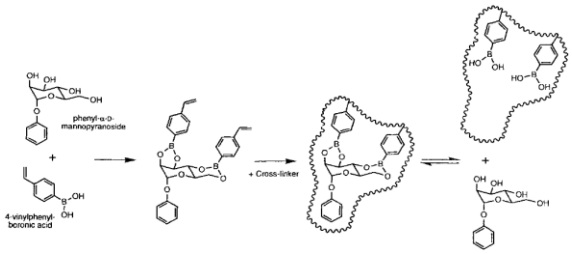


Fig. 2 Covalent imprinting using 4-vinylphenyl-boronic acid as functional monomer

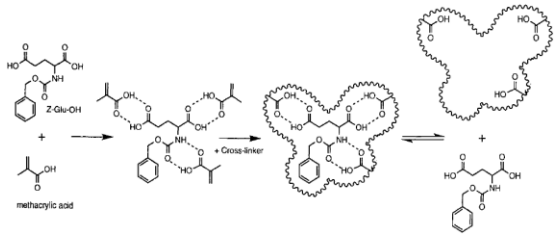


Fig. 3 Non-covalent imprinting using methacrylic acid as functional monomer

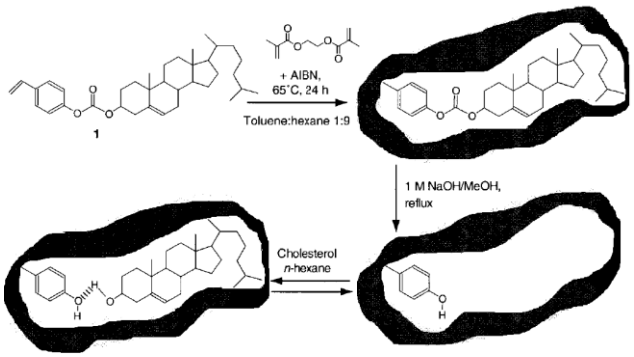


Fig. 4 Covalent sacrificial imprinting

MACRO 121

Amphiphilic and pH Responsive Functionalized Hyperbranched Copolymer: Self Assembling from Polymersomes to Aggregates and Waste Water Treatment through Host-Guest Applications

Das Tamalika[a]*, Sengupta Srijoni[a] and Bandyopadhyay Abhijit[a]

[a]Department of Polymer Science & Technology, University of Calcutta, 92 A.P.C Road, Kolkata 700009, West Bengal, INDIA

** Email id: psutd25@gmail.com*

Over the past few years, a lot of fundamental and technological advancement on the synthesis of hyperbranched polymers with random architecture (HBPs) prepared by free radical techniques (method named as "Strathclyde method") has occurred. HBPs find utilities in the areas where their structural uniqueness (high solubility in range of solvents, low solution/ melt viscosities, high degree of chain end functionality with air pockets for encapsulation of molecules) carries weight which includes delivery devices, biomedicine, waste water treatments, surface coatings, adhesives, additives, sensing, catalysis, construction, lithography, holography, cosmetics etc. Here we tried to induce amphiphilic and pH responsive properties in HBPs through combination strategy of "Strathclyde method" and post polymer functionalization which employed Cu (I) catalyzed click reaction [1]. In a typical process, a highly branched copolymer of poly (propargyl acrylate)-co-poly (divinyl benzene)-co-poly (acrylic acid); HBP1 was prepared in DMF in the presence of dodecane thiol and AIBN at 75°C for 24 hrs.

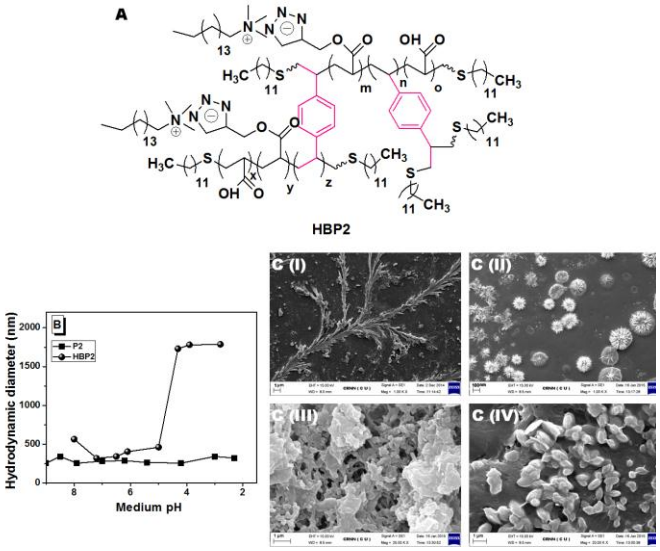


Figure 1. A) Chemical structure of HBP2, B) Sharp jump observed in hydrodynamic diameter of HBP2 (hyperbranched) and not in P2 (linear) at pK_a transition point, owing to self aggregation among HBP2 molecules, C) FESEM image of P2 & HBP2- I) & II) above pK_a, (III) & (IV) below pK_a of the polymers respectively

The choice of monomers was done in such a fashion that a marked difference in reactivity and polarity between the monomers with respect to the reaction medium enabled sequential radical polymerization (PDI< 1.5 but with high MW). In the following step HBP1 was further functionalized with cetyl trimethylammonium azide, a quaternary ammonium azide in the presence of Cu (II)/ NaAsc in t-BuOH: H_2O mixture at 60°C for 48 hrs. Introduction of long alkyl chains to HBP1 developed a new class of highly amphiphilic and pH responsive HBP; HBP2 was capable of self assembling from polymersomes to polymer aggregates at a particular medium pH which we considered as the pK_a of the polymers. An optimized extent of hyper branching and the presence of cetyltrimethyl ammonium triazole ion pairs as well as carboxyl groups played pivotal roles in the formation and subsequent stabilization of the two different macromolecular architectures in the two different ranges of medium pH (Fig. 1). HBP2 sequestered and retained hydrophobic molecules (pyrene), irrespective of medium pH (Fig. 2 A). HBP2 polymersomes (above pKa) encouraged encapsulation of both negatively charged (congo red; CR) and positively charged (methylene blue; MB) hydrophilic molecules (Fig. 2 B & C). HBP2 aggregates (below pKa) encapsulated, retained negatively charged molecules and repelled positively charged molecules (due to the absence of aqueous core & positive charges on carboxyl groups). Here again, extent of hyper branching, orientation of pendant cetyltrimethyl ammonium triazole ion pairs and charge of pendant carboxyl groups with the medium pH affected the encapsulation and the retention of different molecules by HBP2. Hence the new type of HBPs may be used as promising tools for the removal of organic wastes from water bodies without any pre-concentration and within reasonable time.

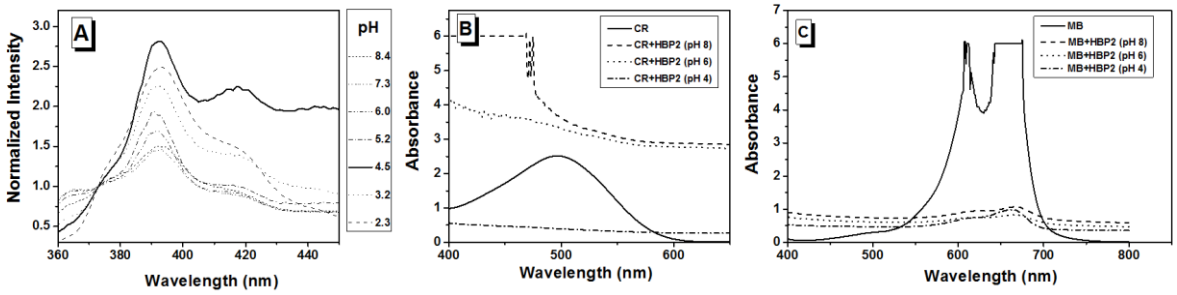


Figure 2. A) Normalized emission spectra of pyrene encapsulated in HBP2 in aqueous media with changing solution pH, UV-vis absorption spectra for the encapsulation of B) CR & C) MB by HBP2

References

[1] Das, T.; Sengupta, S.; Ghorai, U. K.; Dey, A.; Bandyopadhyay, A. *RSC Adv.*,124 (2015) 102932.

MACRO125

Synthesis and Characterization of HMDA-PCNSL Modified Kaolin (PBT-H) as a Reinforcing Filler in Rubber/Clay Nanocomposites

R. V Sreelekshmi,[a] Dr. J. D Sudha,[b] Dr. A. R. R Menon*,[a]

[a] *Material Science and Technology Division (MSTD),* [b] *Chemical Science and Technology Division (CSTD), CSIR-National Institute for Interdisciplinary Science & Technology (NIIST), TVM-695 019, India*

** e-mail id: drrarrmenon@gmail.com*

Abstract

Phosphorylated Cashew Nut Shell Liquid prepolymer (PCNSL), a derivative of CNSL (a low cost renewable natural resource) has been reported as a multifunctional additive for rubbers. The present work involves preparation and characterization of alkaline (hexamethylene diamine) derivative of PCNSL (PBT-H) modified kaolin. Processability characteristics and physico-mechanical properties of natural rubber (NR) compositions of different vulcanization systems containing 6 phr of PBT-H modified kaolin and unmodified kaolin have been studied in detail. Promising results show scope of PBT-H for design and development of cost effective industrial rubber products such as tread or sidewall of automobile tires.

Keywords: *Natural rubber; Kaolin, Hexamethylenediamine; Phosphorylated cashew nut shell liquid; Organomodifier*

Introduction

Rubber/Clay nanocomposites constitute a promising class of advanced materials. Exceptional improvements in many of the physico-mechanical properties

of rubber compositions have been reported at <10 phr (parts per hundred rubber) of organomodified clays.[1-7] Reports on the use of a comparatively less expensive grade of china clay (kaolin) and organomodifiers based on renewable natural resources or industrial by-products [rubber seed oil (RSO,[4,5] tea seed oil (TSO)[7] and cashew nut shell liquid (CNSL)[6]] are emerging.

Clay-rubber nanocomposites containing various aliphatic amines were reported to show faster cure rate and improved physico-mechanical properties. Kim et al. observed that d-spacing of MMT increased progressively with the increase in length of alkyl chain of modifier from C8 to C18.[1] Arroyo et al. have reported that mechanical properties of NR with 10 phr of ODA modified MMT are comparable to the compound with 40 phr of carbon black.[2] NR compositions containing 3 phr of bentonite modified with dodecyl amine, hexadecyl amine or didodecyl methyl amine have been studied by Li et al.[3]

In the present work we have used hexamethylenediamine (HMDA) modified PCNSL as the organomodifier for kaolin. The characteristics of the HMDA-PCNSL modified kaolin (PBT-H) and properties of NR compositions containing <10 phr of the same have been studied in different systems.

Experimental

Materials

Natural rubber (NR), grade-RSS5 and rubber chemicals of commercial grade were used. Kaolin (grade BCK) was obtained from M/s. English India Clays Ltd., Veli, Thiruvananthapuram. Phosphorylated Cashew Nut Shell Liquid (PCNSL) was synthesized by a patented process.[8]

Preparation of PBT-H :- 8ml of HMDA and 25g of kaolin were added to 7.5 wt. % PCNSL in toluene with constant stirring for 24 hours. The mixture was filtered out, dried and powdered. The HMDA-PCNSL modified kaolin was designated as PBT-H.

Methods

XRD, SEM, FTIR and TG measurements of PBT-H were carried out.[14]

Preparation of rubber mixes:-NR compositions were prepared on an open two roll mixing mill as given in Table 1. Test specimens were prepared by compression molding the mixes at 150°C for the respective optimum cure times as determined by a Moving Die Rheometer.

Mix code	CK6	CPH6	SEK6	SEPH 6	EK6	EPH6
MBT	1	1	2	2	2.5	2.5
Sulphur	2.5	2.5	2	2	1	1

*Base mix (phr):- NR 100; ZnO 5; Stearic acid 2; PBT-H 6

Table1. Composition of NR mixes containing unmodified kaolin and PBT-H

Processability characteristics of mixes:- Mooney viscosity and cure characteristics were measured as per ASTM standards. Cure Rate Index, CRI was calculated as, $\mathbf{CRI=[100/(t_{90}-t_{s2})]}$, where t_{90} is the optimum cure time and t_{s2} is the scorch time. Bound rubber content, BRC was determined using the relation, $\mathbf{BRC=[(M_B-M_F-M_D)/M_B]X100}$, where M_B is weight of uncured mix before immersion in toluene, M_F is weight of the filler in the uncured mix and M_D is weight of rubber dissolved in toluene.

Physico-mechanical properties of vulcanizates:-Hardness, tensile properties, tear strength, Abrasion loss, Heat build-up and Compression set of NR mixes were measured as per ASTM standards. Chemical crosslink density (CLD) index of the vulcanizates was measured as per the method reported by Yahaya et.al.[10]

Results and discussion

Characterisation of PBT-H clay

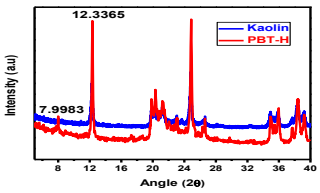
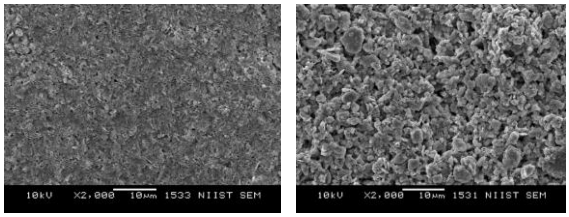


Fig.2.WAXD profiles of unmodified kaolin and HMDA- PCNSL modified kaolin (PBT-H)

The XRD profiles of unmodified kaolin and HMDA-PCNSL modified kaolin are shown in Figure 2. It shows an additional peak of small intensity at a lower 2θ=7.9983 (d-spacing around 11A°) which could be due to the presence of HMDA-PCNSL organic moiety between the platelets of kaolin.

The SEM images of unmodified kaolin and HMDA-PCNSL modified kaolin (Fig. 3a and 3b), show uniform sized particles of kaolin for both samples. It is expected that the surface modification / hydrophobization of kaolin with HMDA-Kaolin minimizes agglomeration of its particles that could enable better dispersion in a nonpolar matrix.



(a) (b)

Fig.3.SEM images of unmodified kaolin and HMDA-PCNSL modified kaolin (PBT-H)

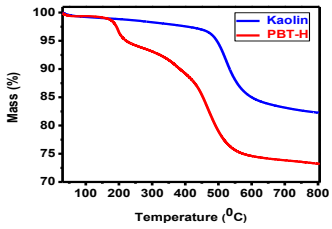


Fig.4. TGA traces of unmodified kaolin and HMDA- PCNSL modified kaolin (PBT-H)

The TGA profile of PBT-H modified kaolin shows a two stage decomposition with lower thermal stability as compared to that of unmodified kaolin (Fig.4). The initial high rate of decomposition for the former could be ascribed to the organic moiety of HMDA-PCNSL modified kaolin clay.

The chemical interactions of HMDA-PCNSL with kaolin are clearly evident from the FTIR spectra (Fig.5). The bands at 3618cm^{-1} and 3710cm^{-1} (inner hydroxyl and outer surface hydroxyl vibration respectively) of kaolin show reduction in intensity of absorption which indicates the interaction of the polar group of HMDA-PCNSL with the hydroxyl groups of kaolin.

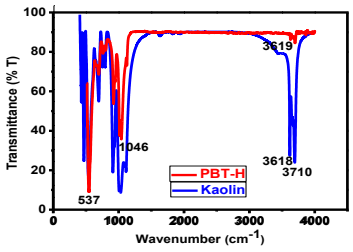


Fig. 5. FTIR spectra of unmodified kaolin and HMDA-PCNSL modified kaolin (PBT-H)

NR compositions containing PBT-H kaolin

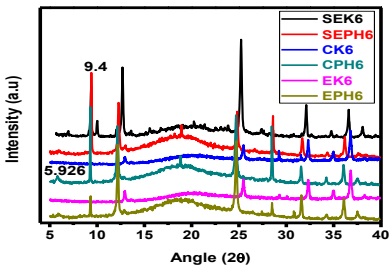
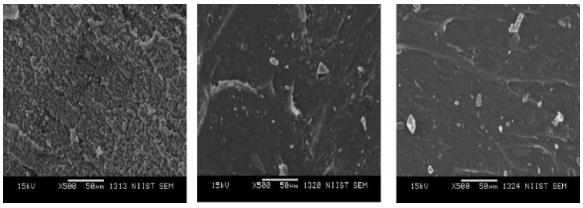


Fig. 6. XRD profiles of the NR vulcanizates

XRD profiles of the NR vulcanizates containing unmodified kaolin and PBT-H modified kaolin (Fig. 6) show a new small peak at a 2θ=9.4. This indicates possible intercalation of the organomodifier and rubber chains between the kaolin platelets, favoring filler –rubber interaction leading to the observed reinforcement effect.



(a) (b) (c)

Fig.7. SEM micrographs of NR mixes (a) SEPH6 (b) CPH6 and (c) EPH6.

The SEM micrographs (Fig. 7) show uniform dispersion of fine particles of the modified kaolin in the rubber matrix, contributing to the improved strength of the vulcanizates.

Thermogravimetric analysis

In the thermal decomposition profiles (Fig.8) notable increase in thermal stability (T_{50}) for the SEPH6 could be due to its higher degree of filler-rubber interaction (as indicated by its high BRC as given in Table 2) and higher state of cure, compared to the other vulcanizates. However, EPH6 shows a small decrease in T_{50} reflecting its relatively lower state of cure.

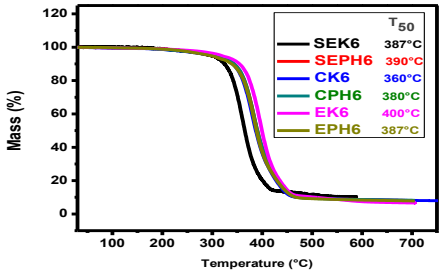


Fig.9. TGA profiles of NR mixes containing 6phr PBT-H modified kaolin of different vulcanization systems

Processability characteristics of mixes

Parameter	CK6	CPH6	SEK6	SEPH6	EK6	EPH6
Mooney viscosity	16.70	21.50	16.60	22.60	14.30	28.00
Minimum torque, M_L (dNm)	0.13	0.21	0.25	0.31	0.21	0.31
Maximum torque, M_H (dNm)	6.36	7.42	5.32	6.98	5.83	5.50
Scorch time.t_{s2} (s)	219	102	511	104	363	145
Optimum cure time, t_{90} (s)	568	307	1015	235	693	272
Cure Rate index, (s^{-1})	0.287	0.488	0.198	0.763	0.303	0.787
Bound Rubber Content (%)	25.75	53.01	41.10	78.75	31.05	69.76

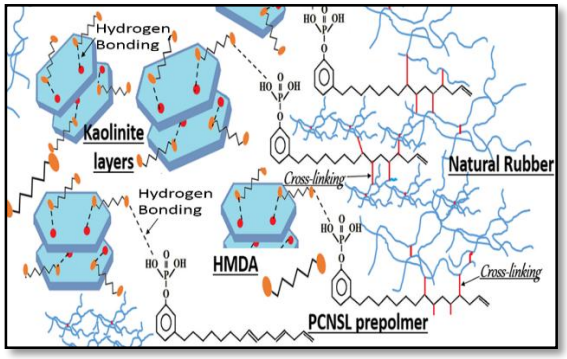
Table 2. Mooney viscosity, cure characteristics and bound rubber content of NR mixes containing unmodified kaolin and HMDA-PCNSL modified kaolin

Processability parameters of NR mixes (Table 2), show higher Mooney viscosity number, minimum torque (M_L) and BRC for SEPH6, CPH6 and EPH6 as

compared to that of unmodified kaolin. It is possible that the polar group of HMDA-PCNSL could interact with the polar groups of kaolin and the unsaturated hydrocarbon side-chain of PCNSL could interact with the isoprene chains of NR providing a higher extent of filler-rubber interaction.[11] The CRI of the mixes containing PBT-H modified kaolin are considerably higher than that containing unmodified kaolin. Thus, SEPH6 shows 76.8% reduction in the optimum cure time (t_{90}), compared to SEK6. Besides, the higher values of maximum torque (M_H) of NR mixes (SEPH6, EPH6 and CPH6) indicate a higher state of cure. [12]

Mechanical properties and CLD index

The results given in Table 3 show higher values of hardness, tensile and tear strength for SEPH6, EPH6 and CPH6 in comparison with unmodified. Also, SEPH6 shows 19.1% less abrasion loss compared to SEK6. CPH6 and SEPH6 show lower heat build-up and compression set compared to that of unmodified kaolin, due to the higher state of cure of the former. However, EPH6 shows higher heat build-up and compression set, presumably due to its lower state of cure. Table 3 shows a reduction in the CLD index for SEPH6, CPH6 and EPH6. The chemical CLD of NR vulcanizates containing PCNSL has been reported to be lower than that of unmodified NR vulcanizates.[13] This was considered to be due to the participation of the unsaturated side-chain of PCNSL in crosslinking reaction with that of NR.



Scheme 1

Based on the above results a schematic structure of NR mixes containing PBT-H modified kaolin (Scheme 1) may be proposed. HMDA-PCNSL may act as a coupling agent between kaolin and NR, with possible polar-polar interaction between kaolin and the modifier and crosslinking reaction between the unsaturated side chain of PCNSL and isoprene chains of NR, similar to our earlier observation.[14]

Parameters	CK6	CPH6	SEK6	SEPH6	EK6	EPH6
Hardness (Shore A)	29	35	30	36	28	30
Tensile modulus – 300% (MPa)	2.0	2.3	2.04	2.4	1.8	1.8
Tensile strength (MPa)	13.2	16.3	15.99	22.83	10	10.9
Elongation at break (%)	651	650	689	710	634	650
Tear strength (kN/m)	28.05	33.3	24.52	31.09	25.5	26.58
Abrasion loss (mm^3)	-	160.4	180	145.6	-	226.6
Heat build-up (°C)	11	5	16	6	9	12
Compression set (%)	35.8	34.4	33.4	28.2	33.2	37.8
CLD index, V_r	0.897	0.254	0.843	0.147	0.963	0.101

Table 3. Physico-mechanical properties of NR vulcanizates containing unmodified kaolin and HMDA-PCNSL modified kaolin

Conclusions

Characterization of PBT-H modified kaolin showed possibility for intercalation of the organomodifier between the kaolin platelets and polar-polar interaction between the organomodifier and kaolin. The improved processability parameters and physico-mechanical properties of PBT-H modified NR mixes indicate the reinforcing effect of PBT-H modified kaolin in NR at a dosage of 6phr.

Acknowledgements

Our sincere thanks are due to Director, NIIST-CSIR, for providing the necessary facilities for carrying out this work. We acknowledge RRII and SCTIMST for a part of the characterization. Research fellowship and financial assistance (CSC-0135) provided by CSIR is gratefully acknowledged.

References

1. Kim, J., Oh, T., Lee, D., Polym.Int., 52, 1058-1063, 2003.
2. M. Arroyo, M.A Lopez-Manchado, B. Herrero, *Polymer*, 44, 2447-2453, 2003.
3. P. Li, L. Wang, G. Song, L. Yin, F. Qi, L. Sun, J. Appl. Polym. Sci., 109(6), 3831-3838, 2008.
4. V.V. Raji, R. Surya, S. Rugmini, M. Brahmakumar, A.R.R. Menon, Polym. Int., 64(11), 1585-1593, 2015.
5. V. Raji Vijay, A.M. Anitha, A.R. Ravindranatha Menon, Polymer, 89, 135-142, 2016.
6. P. Roshin, V.V. Raji, R. Surya, S. Rugmini, A.R.R Menon, Appl Clay Sci., 105-106, 186-191, 2015.
7. S. Rugmini, A.R.R. Menon, J. Appl. Polym. Sci., 107, 3476-3483, 2008.
8. C.K.S. Pillai, J.D. Sudha, V.S. Prasad, A.R.R Menon, A.D. Damodaran, S. Alwan, S.K. Lakshmidasan, K.N. Govindaraman, Indian Patent 176069 to CSIR, 1988.
9. C. Sugata, S. Rajatendu, D. Saikat, M. Rabindra, B. Samar, J. Mangala, C.A. Suresh, Polym. Eng. Sci., 49, 1279-1290, 2009.
10. L.E. Yahaya, K.O. Adebowale, A.R.R. Menon, Appl. Clay Sci., 46, 283-288, 2009.
11. C. Shan, Z. Gu, L. Wang, P. Li, G. Song, Z. Gao, X. Yang, J. Appl. Polym. Sci., 119, 1185-1194, 2011.
12. M.A. Lopez-Manchado, B. Herrero, M. Arroyo, Polym. Int., 52, 1070-1077, 2003.
13. A.R.R. Menon, C.K.S. Pillai, G.B. Nando, J. Appl. Polym. Sci., 51(13), 2157-2164, 1994.
14. R.V. Sreelekshmi, J.D. Sudha, A.R. Ravindranatha Menon, Polym. Bull., DOI 10.1007/s00289-016-1745-9, 2016.

MACRO 128

Au@SiO$_2$@PSS Hybrid Nanostructures Prepared via Block Copolymer Template Approach: Catalytic Studies

Aruni Shajkumar,[a]* Bhanu Nandan,[b] Victoria Albrecht,[a] Myong-Hoon Lee,[c] Manfred Stamm[a,d] and Andriy Horechyy[1,]*

[a] *Leibniz-Institut für Polymerforschung Dresden e.V., Hohe Straße 6, Dresden D-01069, (Germany)*

[b] *Department of Textile Technology, Indian Institute of Technology Delhi, New Delhi 110016 (India)*

[c] *The Graduate School of Flexible and Printable Electronics, Center for Polymer Fusion Technology, Chonbuk National University, Jeonju, Chonbuk 561-756 (South Korea)*

[d] *Technische Universität Dresden, Physical Chemistry of Polymeric Materials, Dresden D-01062 (Germany)*

Email: shaj-kumar@ipfdd.de; horechyy@ipfdd.de

Metal nanoparticles have been widely used as efficient catalysts for various catalytic processes.[1] However, they tend to agglomerate, re-shape or sinter due to the changes in reaction environment, loss of capping agents, or at high temperature. To improve their stability, functionalized polymers, polyelectrolyte brushes, dendrimers, polymeric membranes, resins or metal oxides, have been used to coat, embed or support nanoparticles.[2,] Among supports of different structure and morphologies, hollow particles having reactant-permeable shell and nanocatalyst enclosed inside have been recognized superior as compared to other support types.[3] Such systems are often referred as yolk-shells or nanorattles. In yolk-shell catalytic systems catalytic reactions occur on the surface of the nanoparticle enclosed inside hollows cavity. Thus, the nanocatalyst is protected from agglomeration and mechanical leaching and accessible for reactants.

Here in, we demonstrate a simple and scalable method to produce catalytically active Au@SiO$_2$ yolk-shell particles embedded in a porous silica support (Au@SiO$_2$@PSS) and present results on evaluation of their catalytic activity. Au@SiO$_2$ yolk shells were prepared using block copolymer as a sacrificial template. The nanocatalyst-loaded block copolymer micelles are first coated with silica shell and then embedded into a porous silica network (one-pot process). The pyrolytic removal of block copolymer results in the formation of Au@SiO$_2$@PSS catalyst, and the porous nature of both the shell and the network provide an easy access for the reactants to the nanocatalyst surface located inside. The catalytic properties of Au@SiO$_2$@PSS have been studied

using a model reaction of catalytic reduction of 4-nitrophenol (4NP) and reductive degradation of different dyes. Kinetic studies show that Au@SiO_2@PSS catalyst possesses enhanced catalytic activity as compared to other analogous systems. Furthermore, catalytic experiments on reductive degradation of different dyes show that Au@SiO_2@PSS catalyst can be considered as a very promising candidate for waste water treatment.

References

[1] Astruc, D.; Lu, F.; Aranzaes, J. R., Nanoparticles as Recyclable Catalysts: The Frontier between Homogeneous and Heterogeneous Catalysis. *Angew. Chem. Int. Ed.* **2005,** *44*, 7852-7872.

[2] Li, G. L.; Tai, C. A.; Neoh, K. G.; Kang, E. T.; Yang, X. L., Hybrid Nanorattles of Metal Core and Stimuli-Responsive Polymer Shell for Confined Catalytic Reactions. *Polym. Chem.* **2011,** *2*, 1368-137.

[3] Li, G.; Tang, Z., Noble Metal Nanoparticle@Metal Oxide Core/Yolk-Shell Nanostructures as Catalysts: Recent Progress and Perspective. *Nanoscale* **2014,** *6*, 3995-4011.

MACRO 130

Environmentally Friendly Approaches to the Synthesis of Silver Nanoparticles (Ag-NPs) Using Polymeric Materials Extracted From Plants

Songca SP[1]*
Oluwafemi OS[2]

[1]*Department of Chemistry, Walter Sisulu University, Private bag X1, Mthatha, 5117, South Africa.*

[2]*Department of Applied Chemistry, University of Johannesburg, P.O. Box 17011, Doornfontein 2028, Johannesburg, South Africa.*

**Corresponding author email: oluwafemi.oluwatobi@gmail.com*

Several environmentally friendly approaches to the synthesis of silver nanoparticles (Ag-NPs) using polymeric materials extracted from plants have been reported. For example, the water hyacinth weed has been used as both reducing and capping agent in aqueous medium by varying the pH of the solution and reaction time [1]. The average particle mean diameters of the cellulose capped silver nanoparticles (C-Ag-NPs) were 5.69±5.89 nm, 4.53±1.36 nm and 2.68±0.69 nm nm at pH 4, 8 and 11 respectively. Plant extracts from Ocimum tenuiflorum, Solanum tricobatum, Syzygium cumini, Centella asiatica and Citrus sinensis were used for the synthesis of silver nanoparticles (Ag NPs) from silver nitrate solution. Ag NPs were 28 nm, 26.5 nm, 65 nm, 22.3 nm and 28.4 nm corresponding to O. tenuiflorum, S. cumini, C. sinensis, S. tricobatum and C. asiatica, respectively. Ag-NPs synthesized in these ways tend to exhibit more potent biological activity against micro-organisms. This paper discusses the various approaches that have been

employed for the Ag-NPs using polymeric materials extracted from plants, their characterization and potential applications in medicine. The paper describes the characteristics of Ag-NPs in terms of their maximum surface plasmon resonance (SPR) peaks, colour, transmission electron microscopy, the average particle mean diameters High resolution transmission electron microscopy to confirm crystallinity, and fourier transform infra-red spectroscopy to confirm the capping of the Ag-NPs with the polymeric materials extracted from plants.

References

[2] Mochochoko T, Oluwafemi OS, Jumbam DN and Songca SP. Green synthesis of silver nanoparticles using cellulose extracted from an aquatic weed; water hyacinth. Journal of carbohydrate polymers. 98 (2013) 290.
[3] Logeswari P, Silambarasan S, Abraham J. Synthesis of silver nanoparticles using plants extract and analysis of their antimicrobial property. Journal of Saudi Chemical Society. 19 (2015) 311

MACRO 133

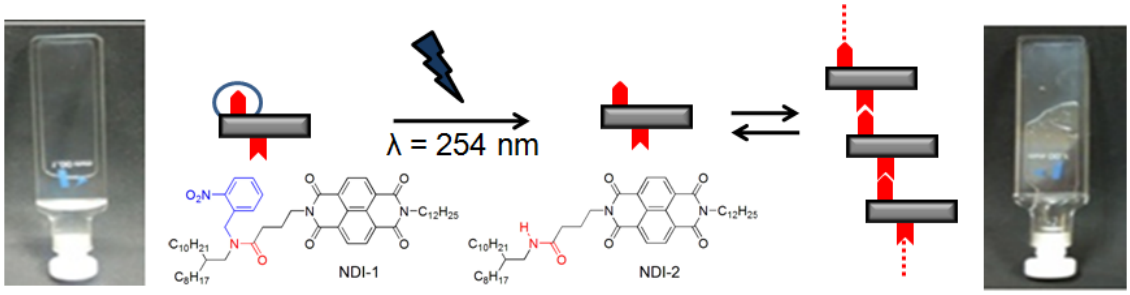
Triggered Supramolecular Polymerization

Pal, D. S.; Kar, H. and Ghosh, S*

Polymer Science Unit
Indian Association for the Cultivation of Science
Kolkata -700032
India

**Email: psusg2@iacs.res.in*

Spontaneous self assembly of abiotic systems often lack directionality and control resulting in structural irregularity. To tackle this issue, we envisioned it would be worth looking for a strategy that can induce control self-assembly. To achieve this, we have explored photo-triggered assembly of NDI-1 in which the amide group is protected by the ortho-nitrobenzyl (ONB) group and there is no possibility of H-bonding among the amides which is responsible for supramolecular polymerization. Upon UV light irradiation, NDI-1 generates NDI-2 (active monomer) that can self assemble, leading to 'photo-triggered' supramolecular polymerization and gelation after complete photo-deprotection of the ONB group in methyl-cyclohexane solvent. We have studied this supramolecular polymerization in detail which suggests linear growth as a function of photo-irradiation time. Interestingly the mode of self assembly of amide in the present case was quite different from their spontaneous assembly, of which we are ascertained from UV spectroscopy and DLS study. Morphology wise for spontaneous assembly we get entangled long fibrils whereas through photo-deprotection the same monomer yields spherulites-like morphology of the supramolecular polymer. The change in polymerization pathway was attributed to the dual role of the pro-monomer in producing the active monomer in controlled fashion and simultaneously acting as a chain-stopper established from viscosity measurements. The presentation will focus on elucidating pros and cons of this novel photo-triggered controlled supramolecular strategy and future implications.



Scheme 1: Schematic showing photo-triggered controlled supramolecular polymerization

MACRO 135

Fractionated Crystallization Behaviour of Semicrystalline Polymers Under Confinement in Electrospun Nanofibers of Polymer Blends

Samanta, Pratick[a] Srivastava, Rajiv[a], Nandan, Bhanu[*a] Chen, Hsin-Lung[b]

[a] *Department of Textile Technology, Indian Institute of Technology Delhi, Hauz Khas, New Delhi 110016 (India). E-mail: nandan@textile.iitd.ac.in*

[b] *Department of Chemical Engineering and Frontier Center of Fundamental and Applied Sciences of Matters, National Tsing-Hua University, Hsinchu 30013 (Taiwan)*

Abstract

We have studied the confined crystallization behaviour of poly (ethylene oxide) (PEO) in electrospun nanofibers which were prepared from immiscible polymer blend of polystyrene (PS) and PEO. The crystallization of PEO in the as-cast PS/PEO blends occurred exclusively through heterogeneous nucleation mechanism. However, in the blend nanofibers, when the weight fraction of PEO was ≤ 0.2, the crystallization of PEO predominantly occurred through homogeneous nucleation mechanism. Furthermore, the significant depression in the melting point of PEO in the nanofibers suggested that the small PEO volume combined with the confinement imposed by the glassy PS matrix restricted the growth of PEO crystals.

Keywords: *Crystallization; poly(ethylene oxide); nanofiber; confinement; blend*

Introduction

The electrospun nanofibers composed of the blend of an amorphous and a crystalline polymer, with the latter forming the dispersed phase in the fibers, offers interesting system for studying the effect of confinement on the crystallization behaviour[1-4]. In this case, the limited radial dimension of the nanofibers may restrict the length scale of phase separation between the immiscible constituents, so as to generate the domains in nanodimension. This type of confined system can

be fabricated easily and rapidly; however, compared to the other commonly studied systems, the size of the domains formed in the nanofibers is highly polydisperse, which may lead to a more complex crystallization behaviour. Polymer blends is far from clearly understood. In the present study, we systematically investigate the crystallization behaviour of PEO in PS/PEO blends in both cast-film and nanofiber, over a relatively wide range of PEO composition (10 – 40 wt%). It will be revealed for the first time that the crystallization underwent an abrupt transformation from heterogeneous nucleation-dominant mechanism to homogeneous nucleation-dominant process when PEO weight fraction in the blend nanofibers decreased slightly from 0.3 to 0.2. Attention will also be directed to the distinct difference in crystallization behaviour between the bulk film and the nanofiber to elucidate the degrees of confinement effect exerted by the phase-separated domains in these two sample forms.

Experimental

Materials. Poly(ethylene oxide) (Mv ~ 400,000 g/mol), polystyrene (Mw ~ 190,000 g/mol), and poly(4-vinylpyridine) (Mw ~ 160,000 g/mol), were procured from Sigma Aldrich, USA. The solvent used, dimethylformamide (DMF) was procured from Merck chemicals and used as it is.

Sample Preparation. The blends were prepared by co-dissolving the two polymers i.e. PS and PEO, at desired ratios, in DMF as the common solvent. The details are given in Table 1. The PS/PEO blends were prepared in 90/10, 80/20 and 70/30 (wt%/wt%) ratios and the respective blend compositions were coded as S9E1, S8E2 and S7E3. The bulk and nanofiber blend samples were differentiated by adding a prefix of C and N respectively to the blend composition codes.

Table: 1 Table 1. Samples code and process parameters during electrospinning

S. No	Sample name (Nanofibers)	Sample code	Process parameters			
			Conc. (wt.%)	Distance (cm)	Voltage (kV)	Flow rate (ml/hr)
1	PS/PEO(90/10)	N-S9E1	10	20	20	0.5
2	PS/PEO(80/20)	N-S8E2	8	20	20	0.5
3	PS/PEO(70/30)	N-S7E3	6	20	20	0.5

Characterizations Techniques

Differential Scanning Calorimetric (DSC). A TA Q 2000 DSC instrument was used to measure the crystallization and melting behaviour of PS/PEO blends. The non-isothermal crystallization studies of the blend samples were carried out by heating them from 30 to 90°C at the heating rate of 10°C/min and further holding for 4 min to destroy the previous thermal history. Subsequently, the samples were cooled to -50°C at the rate of 5°C/min and reheated upto 90°C again at the rate of 10°C/min

Scanning Electron Microscopy (SEM). Samples surface morphology was observed under scanning electron microscopy (SEM) ZEISS EVO 50. Before observation, samples were sputter

coated with thin layer of gold to avoid the accumulation of electrons on the samples surface. In order to develop contrast, the samples were washed either with water to etch out PEO.

Results and discussion

Figure 1 reveals that smooth and mostly bead-free nanofibers were produced under the optimized conditions. The diameter of the nanofibers were found to be 1.35, 1.26 and 0.76 μm for N-S9E1, N-S8E2 and N-S7E3, respectively (the sample code details are given in Table 1).

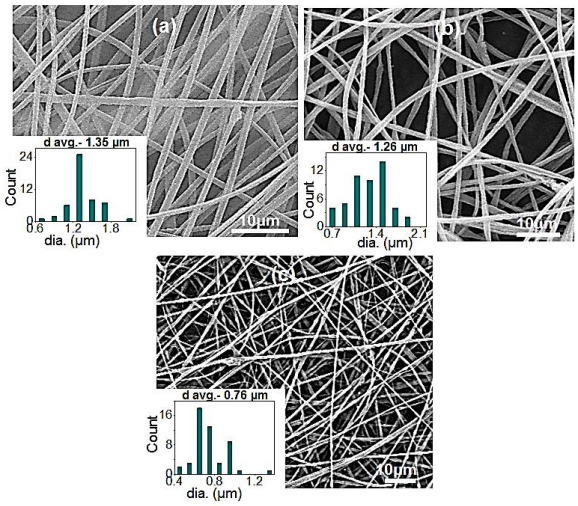


Figure 1. SEM micrographs of the electrospun PS/PEO blend nanofibers (a) N-S8E2; (b) N-S6E4; (c) N-S7E3. The inset in each figure shows the corresponding distribution of nanofibers diameter.

The smaller fiber diameter of the blend with higher PEO content was due to the lower solution concentration used for electrospinning. Furthermore, the polydispersity of the fiber diameter was higher in the blend with higher PEO content. Figure 2 shows the DSC curves collected in the cooling and subsequent heating cycles for recording the crystallization exotherms and melting endotherms, respectively, of PEO. Neat PEO film was found to crystallize with a peak crystallization temperature (Tc) of ca. 47°C upon cooling from melt (see Figure 2(a)). The crystallization at such a low supercooling is known to occur via heterogeneous nucleation mechanism which is prevalent for crystallization in the bulk. The PS/PEO blend films displayed almost the same Tc as that of neat PEO (see Figure 2(a)), The Tc's of the nanofibers containing 30wt% PEO content was only within 3°C difference from that of neat PEO nanofiber or the film, signaling that the crystallization in the PEO-rich domains developed in the nanofibers proceeded through heterogeneous nucleation mechanism.

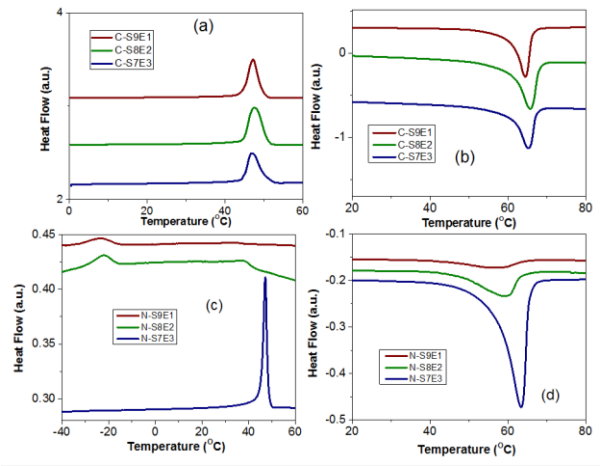


Figure 2. DSC cooling (a, c) and heating (b, d) curves of PS/PEO blends after first heating up to 90°C (a, b) cast film samples and (c, d) nanofiber samples

However, when the PEO content was further decreased to 20 wt% (i.e., for the N-S8E2 blend nanofiber), the cooling curve showed two crystallization peaks, as can be seen in the enlarged DSC profile displayed in the inset of Figure 2(c). The first peak centred at ~ 31°C was very broad, whereas the second peak observed at much higher supercooling (Tc ~ -23°C) was relatively sharp. For the N-S9E1 blend nanofibers containing only 10 wt% PEO, the DSC cooling curve exhibited only a single peak at high supercooling (Tc ~ -23°C). Furthermore, as shown in Figure 2(b), the melting points of the PEO in cast PS/PEO blend films were found to be almost the same as that of the neat PEO homopolymer. However, in the case of PS/PEO nanofibers, the PEO melting point gradually decreased with the decrease of PEO composition in the blend. In the case of N-S9E1 and N-S8E2, the Tm of PEO depressed by as much as 8 and 9°C, respectively, compared to that observed for neat PEO nanofiber. The reduction of melting point suggested that the crystalline lamellar thickness of PEO in the nanofibers, particularly at the lower weight fractions, was significantly thinner than that of bulk PEO.

The heat of fusion per unit weight of PEO, which is a measure of the degree of crystallinity, of PEO in the bulk films and nanofibers, are shown in Figure 3. It can be seen that, while in the films the crystallinity remained almost the same with respect to the change of PEO composition, the crystallinity in nanofibers dropped abruptly as the PEO composition was reduced to 20 wt%. As has already been indicated, PEO domains are expected to be small and well partitioned in the PS matrix at lower PEO weight fraction; hence, the suppression of crystallizability could be attributed to the restricted growth of the crystallites in the geometrically mismatched and nanoscopically confined PEO domains.

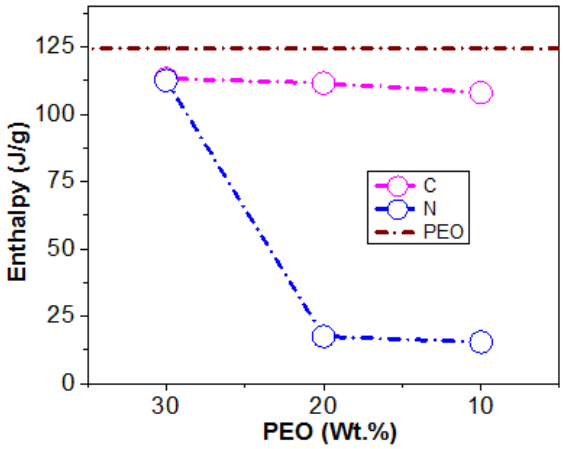


Figure 3. Variations of the thermal properties with PEO composition, as ascertained from DSC measurements, in as-casted and electrospunned PS/PEO blends (a) normalized heat of fusion. The respective values for neat PEO sample, in each case, has been represented with the dashed line

It is also noted that the sharp drop of ΔHm in the blend nanofibers occurred coincidently with the change of the nucleation mechanism from heterogeneous to predominately homogenous type. In the Figure 4 shows the SEM micrographs of the blend nanofiber after etching the PEO phase. For N-S8E2 and N-S7E3 nanofibers, short empty channels were observed on the surface. These channels were Our SEM results revealed that similar fibrillar domains of PEO were formed during the electrospinning of N-S8E2 and N-S7E3 blend nanofibers due to the extension of the phase-separated PEO droplets in the elongational flow field.

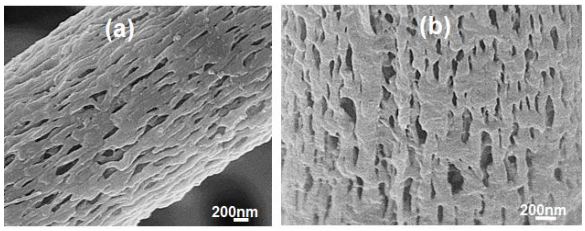


Figure 4. SEM micrographs showing the morphology of the electrospun PS/PEO blend nanofiber samples after selective etching of PEO phase with deionized water (a) N-S7E3 (b) N-S8E2

During the etching process, the PEO fibrils embedded in PS matrix were swollen and subsequently dissolved by perforating through the PS surface layer at several places along the fiber axis, which were visible as short channels in the SEM image.

Conclusions

The crystallization behaviour of PEO in the cast films and electrospun nanofibers of PS/PEO blends has been investigated in detail. The crystallization of PEO in the films was similar to that observed for bulk PEO which took place through heterogeneous nucleation mechanism. The nanofibers with low PEO weight fraction (≦ 0.2) crystallized predominantly through homogenous nucleation due to the small PEO domain size which excluded the presence of heterogeneities. An

abrupt transformation in the crystallization nucleation mechanism was observed when the weight fraction of PEO in the blend nanofibers was increased from 0.2 to 0.3, where the heterogeneous nucleation became dominant due to the presence of larger PEO domain size with spatial connectivity.

Acknowledgements

This work was supported by the Council for Scientific and Industrial Research (CSIR) under grant no. 22(0707)/15/EMR-II.

References

1. Samanta, P; Thangapandian, V; Singh, S; Srivastava, S; Nandan, B; Liu, L. C; and Hsin, Chen, L. C. *Soft Matter*, 12 (2016) 5110.
2. Zhong, G; Zhang, L; Su, R; Wang, K; Fong, H; Zhu, L. *Polymer*, 52 (2011) 2228.
3. Zhong, G; Su, R; Zhang, L; Wang, K; Fong, H; Zhu, L. *Polymer*, 53 (2012) 4472.
4. Zhong, G; Wang, K; Zhang, L; Li, M.-Z; Fong, H; Zhu, L. *Polymer*, 52 (2011) 5397.

MACRO 136

Chirality Issues in Supramolecular Polymerization using 1,3-Dihydroxyl Synthon

Ghosh G and Ghosh S*

Polymer Science Unit, Indian Association for the Cultivation of Science
2A and 2B Raja S. C. Mullick Road, Jadavpur, Kolkata-700032
* *Corresponding author's email: psusg2@iacs.res.in*

Inspired by nature chirality issues in abiotic systems have been studied with great interest over past two decades. With emerging reports in pathway complexity in supramolecular polymerization, chirality issues including chiral amplification, chirotopic switching, majority rule and others have found a renewed interest in the recent past. We have recently recognized a new supramolecular synthon in 1,3-dihydroxyl derivatives which by virtue of simultaneous intra- and intermolecular H-bonding generates supramolecular polymer in less polarizable solvents.[1] Currently we are investigating chirality issues in such newly discovered supramolecular systems by studying self-assembly of (*R*)-NDI and (*S*)-NDI (Figure 1). We find highly stable self-assembly with preferential helicity for both the pure isomers leading to the formation of helical fibers and gelation. Surprisingly 1:1 mixture of *R*- and *S*- isomers completely destroy the self-assembly suggesting strong influence of chirality on self-assembly. However with slight excess of one of the isomers, the majority rule applies and strong self-assembly is noticed. "Sergeant-and-Soldier" principle also works very efficiently in mixed assembly of the chiral synthon with structurally similar achiral synthon. Apart from elucidating chirality issues we also have studied thermodynamics, crystal structure and conductivity of these supramolecular polymers which will be the content of this presentation.

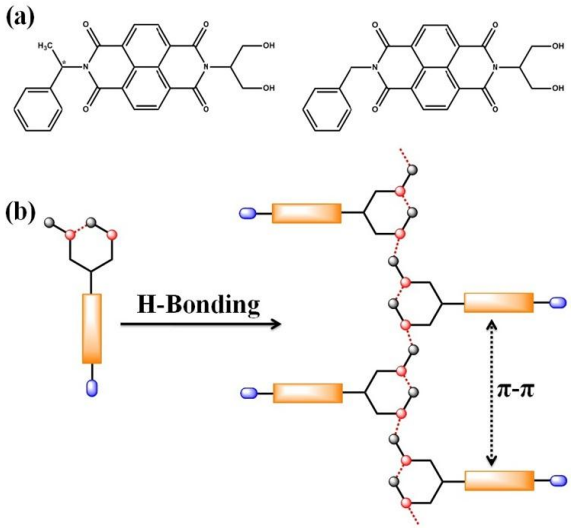


Figure 1. (a) Molecular structures of chiral and achiral NDI; (b) Proposed model for H-bonding induced π-stacking.

References

[1] Mondal, T; Basak, D; Ouahabi, A. A; Schmutz, M; Me´sini, P; Ghosh, S. *Chem. Commun.* 51 (2015) 5040.

MACRO 138

Functional Poly(disulfide)s: Synthesis, Aggregation and Triggered Disassembly

Raju Bej, Dipankar Basak, Suhrit Ghosh*

Polymer Science Unit, Indian Association for the Cultivation of Science

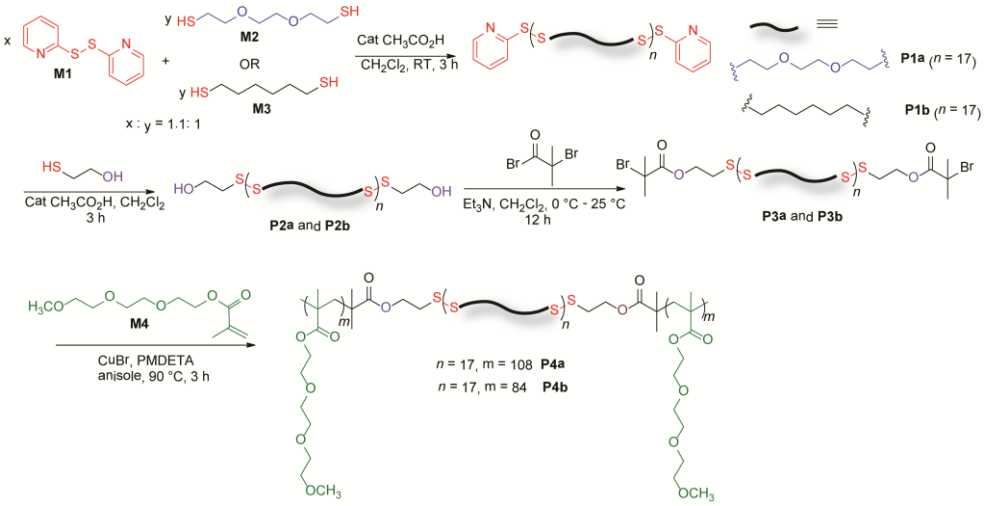
2A & 2B Raja S. C. Mullick Road, Kolkata, India-700032

e-mail id: psusg2@iacs.res.in

Abstract

Redox-responsive amphiphilic triblock copolymers based on poly(triethylene glycol monomethyl ether)methacrylate-b-poly(disulfide)-b-poly(triethylene glycol monomethyl ether)methacrylate (PTEGMA-b-PDS-b-PTEGMA) with different hydrophobicity of the PDS block were synthesized by step-growth followed by chain-growth polymerization. In aqueous medium, both the polymers form micellar aggregates with an average diameter of ~15 nm. To check the impact of structural

change of hydrophobic block on micellar disassembly and drug release kinetics, Nile Red (NR) was encapsulated as a hydrophobic probe at the interior of the micelles and glutathione (GSH)-induced disintegration of the backbone and consequently the release of the entrapped guest



Scheme 1 Synthesis of **P4a** and **P4b**

molecules were monitored. For micellar assembly with relatively more hydrophobic interior, slower disintegration of the backbone and dye-release kinetics were observed compared to the micelles with less hydrophobic character, owing to slow diffusion of the polar GSH toward more hydrophobic micellar core.

Keywords: *Amphiphilic poly(disulfide); Nile Red release; GSH responsive degradation.*

Introduction

Amphiphilic block copolymers containing disulfide functional group exhibit self-aggregation in water to variety of nanostructures[1] have been projected as potential delivery vehicles[2] for drug, gene, SiRNA and proteins owing to their cleavable nature to free thiol in a reducing environment. This is very relevant in the context of cancer therapy as an enhanced level of glutathione, capable of cleaving disulfide bond, is over expressed in tumor cell compared to that of normal cell. Furthermore emerging reports on enhanced cellular uptake[3] of poly(disulfide)s make them more attractive candidates for delivery application. Here utilizing our earlier developed mild methodology for functional poly(disulfide)[4], we have prepared telechelic poly(disulfide)s (Scheme 1) using di-thiols of different hydrophobicity and successfully modified the chain ends so that it could initiate polymerization of a hydrophilic monomer by atom transfer radical polymerization (ATRP) producing ABA type amphiphilic triblock copolymers. Here we report aggregation of these polymers in aqueous medium, glutathione (GSH) mediated disassembly and remarkable effect of hydrophobicity of the poly(disulfide) backbone on the rate of degradation impacting release kinetics of the entrapped guest molecules.

Experimental

Materials and Methods

Reagents and solvents were purchased from Sigma-Aldrich Chemical Co. and commercially available sources respectively. ^{1}H NMR spectra were recorded in Bruker DPX-500 MHz NMR, UV visible spectra were recorded in a Perkin Elmer Lambda 25 spectrometer. FT-IR spectra were obtained in Perkin Elmer Spectrum 100FT-IR spectrometer. TEM images were taken in JEOL-2010EX machine operating at an accelerating voltage of 200KV. Dynamic Light Scattering (DLS) measurements were carried out in Malvern instrument at a scattering angle of 173°. Fluorescence spectra were recorded in a FluoroMax-3 spectrophotometer, from Horiba Jobin Yvon. Number average molecular weight (Mn) and polydispersity index (PDI) of the polymers were measured by size exclusion chromatography at 30 ºC using a Waters GPC machine. MALDI-ToF mass spectrometry was performed on a Bruker Daltonics Flex-PC in positive reflectron mode, using Dithranol (DT) as matrix and sodium trifluoroacetate (NaTFA) as cationizing salt.

Sample preparation

Aqueous micellization of the polymers (P4a and P4b) was attempted by solvent-switch method.

DLS Study

Samples (c = 5x10-5 M) for DLS study were prepared as described above.

Transmission Electron Microscopy (TEM)

The aqueous solution of P4a (or P4b) prepared for DLS study (c = 5x10-5 M) was further used for TEM measurement. 10 µL of the respective aqueous solution was drop casted on copper grid coated with carbon and air dried for 24 h prior to imaging.

Nile Red Encapsulation and Release Studies

Nile Red was encapsulated in the polymer P4a (or P4b) by sonication method. Fluoroscence data were recorded time-to-time for these samples and % release of the dye was calculated using the following equation:

% release = $(I_0 - It)/Io \times 100$, where Io and It represent the emission intensities (λex = 530 nm, λem = 624 nm) at t = 0 (after GSH addition) and at any given time t, respectively.

Results and discussion

Synthesis and Characterization of the Polymers

Synthesis of the amphiphilic triblock copolymers **P4a** and **P4b** is depicted in Scheme 1. Firstly, **P1a** was synthesized using a condensation reaction between commercially available monomers 2, 2'- dithiodipyridine (**M1**) and 2,2'-(ethane-1,2-diylbis(oxy)diethanethiol (**M2**) with mole ratio of **M1** : **M2** = 1.1 : 1.0.

Pleasingly, the molecular weight obtained from ^{1}H NMR (Mn,NMR= 3200 g/mol) by end group analysis using the integration ratio of Hg and Hc (and terminal Hc' protons) (Fig.1) matches very well with GPC and theoretically estimated values (Table 1)

MALDI-ToF analysis of P1a indicates repeating peaks separated by 180.1 m/z unit, which corresponds to the predicted mass of the repeating unit, further confirming successful synthesis of the polymer. More importantly, each peak also indicates the presence of pyridyl sulfide groups at both chain terminals. Furthermore lack of any absorption peak at λ = 430-500 nm in the Ellman's assay[5] performed with P1a confirmed absence of any free sulfhydryl group at the terminals.

In similar fashion, polymer P1b was synthesized and characterized. Selective functionalization of

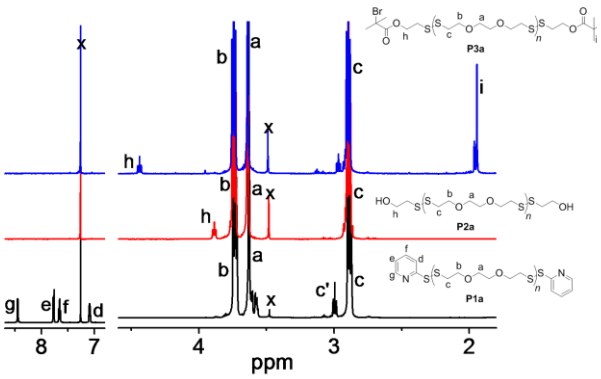


Fig. 1 ^{1}H NMR spectra of **P1a**-**P3a** in $CDCl_3$; X indicates peaks from residual solvents

the pyridyl disulfide groups of P1a (or P1b) was carried out using thiol-disulfide exchange reaction with 2-Mercaptoethanol producing P2a (or P2b) (Scheme 1), which are confirmed by ^{1}H NMR, UV/vis, FTIR and MALDI-ToF studies. Two terminal hydroxyl groups of P2a (or P2b) were reacted with α-bromoisobutyryl bromide in presence of triethylamine producing bifunctional ATRP macro-initiator P3a (or P3b) (Scheme 1), which was characterized by ^{1}H NMR, FT-IR and MALDI-ToF analysis. ATRP technique was employed for the chain extension of bi-functional macro-initiators P3a and P3b using 2-(2-(2-methoxyethoxy)ethoxy)ethyl methacrylate (M4) as hydrophilic monomer to produce the final triblock amphiphilic copolymers P4a and P4b, respectively and well characterized by GPC and ^{1}H NMR. **Self-assembly Study**

High-resolution transmission electron microscopy (HR-TEM) images reveal almost identical micellar particles with an average diameter of ~15 nm for both the polymers, which was further supported by DLS measurement. Critical aggregation concentration (CAC) of P4a was estimated from concentration dependent emission spectra using pyrene as a probe. Changes in the I_{373}/I_{384}

values were plotted as a function of polymer concentration and from the inflection point the CAC was estimated to be 10.0 µM. Likewise physical parameters for P4b were also estimated which interestingly indicate relatively low CAC, high encapsulation efficiency for less polar hydrophobic core.

Redox-responsive disassembly and guest release

Nile red (NR) was chosen as a hydrophobic probe and encapsulation was confirmed by blue shift of ca. 32 nm compared to the NR emission in water[6]. Emission intensity of the probe was monitored time to time in presence of 20 mM GSH which shows gradual decrease indicating release of the entrapped Nile red from micellar container. A plot of the emission intensity with time (Fig. 2a) reveals sustained release. It takes about ~ 80 h for release of the

entire amount of entrapped dye. To check the impact of GSH concentration on release rate,NR encapsulated P4a micelle was treated with various amounts of GSH. Upon increasing the GSH concentration NR release rate was accelerated (Fig 2b), while

Table1 Characterization of different polymers

Entry	Yield (%)	DP[a]	M_n[a]	M_n[b]	M_n[c]	PDI[c]
P1a	81	17	3200	3300	2900	1.42
P2a	78	17	2800	NA	3100	1.51
P3a	68	17	3500	NA	2200	1.44
P4a	52	17, 108[d]	28000	27600[e]	18400	1.35
P1b	76	17	2750	3300	3000	1.81
P2b	79	17	2700	NA	3100	1.77
P3b	67	17	3000	NA	2300	1.80
P4b	41	17, 84[d]	22500	22100[e]	17600	1.18

[a] DP and M_n were determined by end group analysis using ^{1}H NMR spectroscopy; [b] M_n were calculated according to the equation 1 [c] M_n and PDI were determined by GPC analysis relative to polystyrene standard. [d] DP of poly(triethylene glycol methacrylate)(PTEGMA) block determined from ^{1}H NMR spectra using integration ratio of H_d and H_c protons (Fig. 5b) of PTEGMA and poly(disulfides) blocks, respectively. [e] calculated by the equation: $M_{n,\,theory} = [M]/[MI] \times MW^{momoner} \times \alpha^{Monomer} + MW^{MI}$ where $[M]/[MI] = [TEGMA]/[macroinitiator] = 200$, $MW^{monomer} = 232.1$, $\alpha^{Monomer} =$

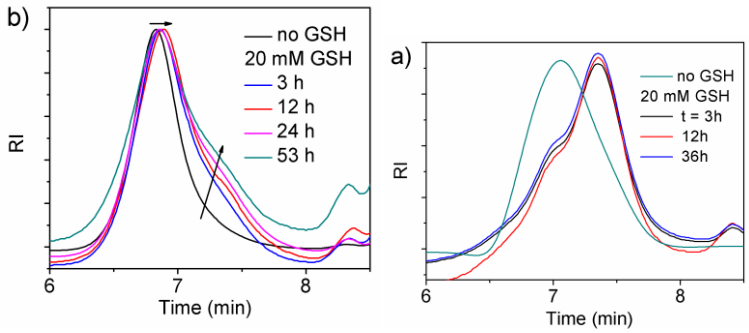


Fig.2 Degradation study (by GPC) of a) **P4a** and b) **P4b** in presence of GSH (20.0 mM)

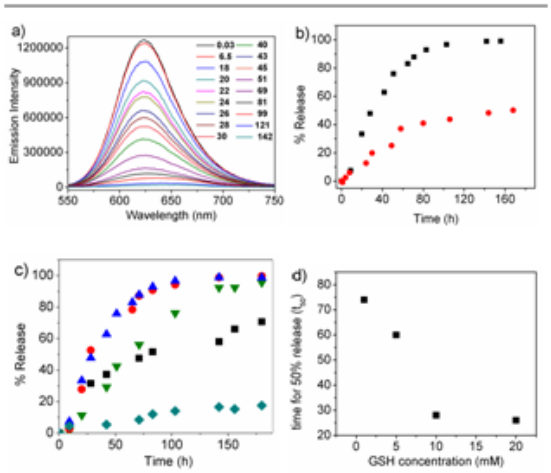


Fig. 2 a) Representative example of change in NR emission intensity over time (in h) in presence of 20.0 mM GSH for P4a (λ_{ex} = 530 nm); b) Comparative NR release profile of P4a (black) and P4b (red) upon treatment with 20.0 mM concentration; c) Comparative NR release profile of P4a upon treatment with different GSH concentrations: 20.0 mM (blue triangle), 10.0 mM (red circle), 5.0 mM (green triangle), 1.0 mM (black box), and 0.0 mM (cyan diamond); d) Plot showing time for 50% NR release (t_{50}) vs GSH concentration

control experiment shown excellent stability of the micellar aggregates in the present experimental conditions. To examine effect of difference in hydrophobicity of the micellar core on dye release profile, if any, fate of the NR encapsulated P4b micelle was tested in presence of 20.0 mM GSH. Interestingly in this case, the release rate was significantly slow compared to that obtained for P4a as evident from the data shown in Fig. 2b. This is attributed to the slow diffusion of the polar GSH towards the more hydrophobic micellar core of P4b than that of P4a. To correlate the differences

in dye release kinetics with redox-responsive structural disintegration of the polymer backbone, aqueous solution of P4a and P4b were separately treated with 20.0 mM GSH under identical experimental condition as the dye release experiments were studied previously. Aliquots were collected after certain time interval, freeze-dried, re-dissolved in THF and analyzed by GPC. The GPC trace of the aliquot taken after 3 h showed a shift to the higher retention time for P4a with a small but observable hump at the original peak position (Fig. 3a),while for P4b even after 53 h, the peak corresponding to the main polymer chain (t = 6.8 min) was predominantly present along with arrival of a new peak at higher retention time corresponding to the constituent hydrophilic block This study is in line with the different dye release kinetics observed for NR encapsulated P4a and P4b and attributed to polarity difference of the two different micellar cores depending on the structure of the poly(disulfide) block .

Conclusions

In conclusion, we have demonstrated a general synthetic strategy to produce thiol-responsive amphiphilic block copolymers with different hydrophobicity at the middle poly(disulfide) block by a combination of step-growth followed by chain-growth polymerization and investigated the impact of such subtle change at backbone hydrophobicity on final polymer assembly, guest encapsulation efficiency, glutathione-mediated structural disintegration and drug release kinetics. Despite their identical micellar assembly in water, more hydrophobic interior shows slower backbone disintegration and dye-release kinetics compared to the micelles with less hydrophobic character, indicating slow diffusion of the polar GSH toward more hydrophobic micellar core. Further structural variations of poly(disulfide)s and its implications in drug-release kinetics on biological samples is currently underway in our laboratory.

Acknowledgements

DB thanks SERB (project no: SB/FT/CS-098/2012) and RB thanks CSIR for research fellowship

References

1. (a) F. Ahmed and D. E. Discher, *J Control Release*, 96, 37, 2004. (b) F. Le. Devedec, A. Won, J. Oake, L. Houdaihed, C. Bohne, C. M. Yip, and C. Allen, *ACS Macro Lett*., 5, 128, 2016.(c) D. F. Evans and H. Wennerstrom, The Colloidal Domain, 2nd ed.; Wiley-VCH: New York, 1999.(d) Y. Mai and A. Eisenberg, Chem. Soc. Rev., 41, 5969, 2012.

2. (a) D. Roy, J. N. Cambre and B. S. Sumerlin, *Prog. Polym. Sci.*, 35, 278, 2010. (b) M. Elsabahy and K. L. Wooley, *Chem. Soc. Rev.*, 41, 2545, 2012.

3. E-K. Bang, M. Lista, G. Sforazzini, N. Sakai and S. Matile, *Chem. Sci.*, 3, 1752, 2012

4. D. Basak, R. Kumar and S. Ghosh, *Macromol. Rapid Commun*., 35, 1340, 2014

5. K. Velonia, A. E. Rowan and R. J. M. Nolte, *J. Am. Chem. Soc.*, 124, 4224, 2002

6. P. Greenspan and S. D. Fowler, *J. Lipid Res.*, 26, 781, 1985

J:\Macro\Word files\NSP\139 dr. garima agarwal.doc

MACRO 139

Multi-functional Microgels as Building Blocks for Nanostructured Materials

Agrawal, Garima[a,b]*, Pich, Andrij[b]

[a] *Department of Polymer and Process Engineering, Indian Institute of Technology Roorkee, Saharanpur Campus Paper Mill Road, Saharanpur- 247001, Uttar Pradesh, India*

[b] *Interactive Materials Research DWI an der RWTH Aachen e.V., RWTH Aachen University, Forckenbeckstrasse 50, D-52056 Aachen, Germany*

* *garimafpt@iitr.ac.in*

Aqueous, three dimensionally crosslinked, polymeric micro/nanogels exhibit tunable size and size distribution, chemical functionality, surface charge, and swelling degree. Additionally, their large surface area for multivalent bioconjugation, flexibility and softness, superior colloidal stability and stimuli responsive behavior enable them as a unique and versatile platform for various applications. Furthermore, the possibilities of post-modification reactions allow the incorporation of small organic molecules, synthetic polymers, bioactive molecules or inorganic nanoparticles into the porous polymeric network and thus leading to the formation of multifunctional colloids which can be used as building blocks for the preparation of well-defined nanostructured materials of different dimensions and complexity.

A mild, simple and reducing agent-free strategy will be presented for the synthesis of microgel/Au NPs hybrid nanostructures at ambient temperature. Poly(*N*-vinylcaprolactam) (PVCL) based microgels act as a "self-catalyzing"-soft polymeric template for Au NPs formation in water selectively confined to the core-region of the microgel with control over the loading. The resulting composite particles can be used as a hybrid catalyst exhibiting good catalytic activity towards the reduction of p-nitrophenol (4-NP) to p-aminophenol (4-AP) which is of great industrial importance.

Further, we have developed a simple route for the preparation of novel multi-sensitive PVCL microgel-based capsules. The variation of the microgel and polymer properties as well as their concentration provides a control over important capsule parameters such as size, morphology, wall thickness, mechanical strength and permeability etc. Synthetic approach for microcapsules formation along with their properties and release kinetics will be discussed in detail.

References

[4] Agrawal, G., Schuerings, M. P., Rijn, P. V., Pich, A. *J. Mater. Chem. A*, 1 (2013), 13244.
[5] Agrawal, G. Uelpenich, A. Zhu, X., Moeller, M., Pich, A. *Chem. Mater.*, 26 (2014), 5882.

[6] Birkholz, M.-N.† Agrawal, G.† Bergmann, C. Schroeder, R. Lechner, S. J. Pich, A. Fischer, H. *Biomedical Engineering/Biomedizinische Technik*, (2015), DOI: 10.1515/bmt-2014-0141.

J:\Macro\Word files\NSP\148.doc

MACRO 148

Antifouling Thin Film Composite Polyamide Nanofiltration Membranes for the Removal of Heavy Metals from Ground Water

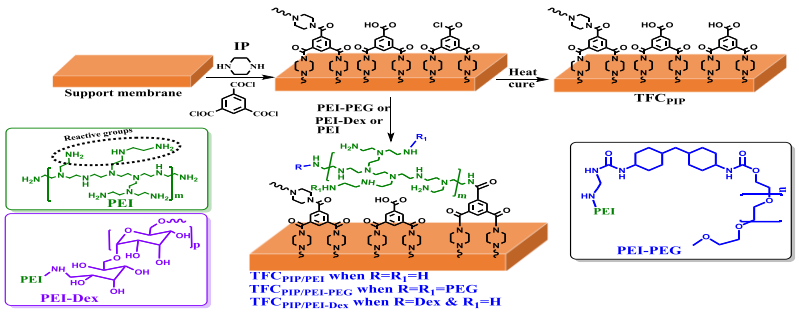
[a,b]Bera Anupam, [a]Bhalani Dixit, [a,b]Jewrajka Suresh Kumar*

[a]*Reverse Osmosis Membrane Division, CSIR-Central Salt and Marine Chemicals Research Institute, G. B. Marg, Bhavnagar-364002, Gujarat, India*

[b]*AcSIR, CSIR-Central Salt & Marine Chemicals Research Institute, G. B Marg, Bhavnagar-364002, Gujarat, India*

** Email: skjewrajka@csmcri.org*

Conventional poly(piperazineamide) [poly(PIP)] nanofiltration (NF) membrane, prepared through the interfacial polymerization (IP) between PIP and trimesoyl chloride (TMC), is extensively used for the desalination and purification of water [1-3]. Desalination of sea water through reverse osmosis (RO) membrane to make it suitable for domestic use demands some extensive pretreatment [4, 5]. In this context, NF of sea water is very useful for reducing the hardness for further desalination via RO process. In case of poly(PIP) membrane, trade-off rejection between multivalent action and anion arises due to high surface negative charge of the membrane which allow relatively faster passage of multivalent cation than that of anion. Furthermore, fouling of the membrane is very common problem during desalination process [6-9]. The intense surface charge together with adhesive surface nature cause fouling of membranes. [poly(PIP)] membrane is usually highly negatively charged (zeta potential, ζ is ca. -20 mV) at pH ca. 7 [10]. The poly(PIP) membrane shows ca. 93% rejection of divalent anionic salt (Na_2SO_4) and ca. 55% rejection of divalent cationic salt ($MgCl_2$) [10]. This membrane shows low rejection efficiency towards the heavy metal ion (containing divalent cation). Herein, we have used polyethyleneimine (PEI) or its conjugates namely PEI-polyethylene glycol (PEI-PEG) and PEI-Dextran (PEI-Dex) for the modification of poly(PIP) membrane surface for lowering the fouling problem and enhancing the rejection of divalent cation including heavy metal ions. (Scheme 1) [12].



Scheme 1. PEI, PEI-Dex and PEI-PEG used for post treatment of poly(PIP)

PEI or its conjugates was used on the membrane surface immediate after IP between PIP and TMC. During the IP, some –COCl groups remained unreacted. Therefore, the unreacted –COCl groups were allowed to react with the amine functionality of PEI of its conjugates (scheme 1) [12]. The trapping of hydrolysis step of –COCl groups resolves the high negative charge of the membrane surface. Moreover, the presence of some unreacted amine moieties of PEI of its conjugates on the membrane surface also helps to reduce the negative charge of the membrane surface. Therefore, the membrane surface charge (ζ values) lies close to the neutral at pH 7 (Table 1).

Table 1. Summary of the characteristic properties of TFC_{PIP}, $TFC_{PIP/PEI}$, $TFC_{PIP/PEI–Dex}$ and $TFC_{PIP/PEI–PEG}$ membranes and their rejection efficacy during the desalination of salt solution containing metal ions (feed 10 mg/L).

		TFC_{PIP}	$TFC_{PIP/PEI}$	$TFC_{PIP/PEI-Dex}$	$TFC_{PIP/PEI-PEG}$
ζ (mV) at pH 7		-20	+1	-4	+3
r_p (nm)		0.60	0.44	0.52	0.50
Rejection (%) of heavy metal ions	Pb^{2+}	$^{x}69$	$>^{x}98$	$^{x}97$	$^{x}97$
	Cd^{2+}	$^{x}56$; $^{y}62$	$^{x}92$; $^{y}96$	$^{x}88$; $^{y}91$	$^{x}90$; $^{y}95$
	Co^{2+}	$^{x}75$; $^{y}67$	$^{x}91$; $^{y}95$	$^{x}89$; $^{y}92$	$^{x}90$; $^{y}95$
	Cu^{2+}	$^{x}80$	$>^{x}98$	$^{x}94$	$^{x}96$

a-at pH 5; b-at pH 7.

Therefore, the charge effect during desalination of aqueous salt solution cannot influence the rejection of cationic salt. Moreover, after the reaction of amine groups of polymers and unreacted –COCl groups of the membrane surface, the pore radius (r_p) of the membranes reduced (Table 1). The lowering of pore size, also enhanced the rejection efficiency of the membranes. After the post treatment of nascent poly(PIP) membrane, the modified membranes became capable to separate heavy metal salts effectively (Table 1). In this regard, it should be noted that the TFC_{PIP} showed much lower separation efficacy to that of the modified membranes. The modified membranes exhibited much enhanced antifouling/antiscalling property compared to that of unmodified membrane [poly(PIP)]. This is due to the antifouling effect of PEG and Dex as well as low surface charge of modified membranes [13, 14]. The heavy metal ions removal in presence of other ionic salts will be the interesting tropic to investigate with these modified membranes which is our future work.

References

[1] Abuhabib, A A; Ghasemi, M; Mohammad, A W; Rahman, R A; El-Shafie, A H. *Arabian Journal for Science and Engineering*, 38 (2013) 2929.
[2] Mohsen, M S; Jaber, J O; Afonso, M D. *Desalination*, 157 (2003) 167.
[3] Lhassani, A; Rumeau, M; Benjelloun, D; Pontie, M. *Water Research*, 35 (2001) 3260.
[4] Pearce, G K. *Desalination*, 203 (2007) 286.
[5] Bruggen, B V d; Vandecasteele, C. *Desalination*, 143 (2002) 207.
[6] Chen, G-E; Liu, Y-J; Xu, Z-L; Tang, Y-J; Huang, H-H; Sun, L. *RSC Adv.*, 5 (2015) 40742.
[7] Li, L; Zhang, S; Zhang, X. *J. Membr. Sci.*, 335 (2009) 133.
[8] Wang, T; Yang, Y; Zheng, J; Zhang, Q; Zhang, S. *J. Membr. Sci.*, 448 (2013) 180.

[9] Lianchao, L; Baoguo, W; Huimin, T; Tianlu, C; Jiping, X. *J. Membr. Sci.*, 269 (2006) 84.
[10] Gol, R M; Bera, A; Banjo, S; Ganguly, B; Jewrajka, S K. *J. Membr. Sci.*, 472 (2014) 154.
[11] Yang, F; Zhang, S; Yang, D; Jian, X. *J. Membr. Sci.*, 301 (2007) 85.
[12] Bera, A; Jewrajka, S K. *RSC Adv.*, 6 (2016) 4521.
[13] Gupta, A S; Wang, S; Link, E; Anderson, E H; Hofmann, C; Lewandowski, J; Marchant, K K; Marchant, R E. *Biomaterials*, 27 (2006) 3084.
[14] Emilsson, G; Schoch, R L; Feuz, L; Höök, F; Lim, R Y H; Dahlin, A B. *ACS Appl. Mater. Interfaces*, 7 (2015) 7505.

MACRO 181

Preparation and properties of Hyperbranched polymides/MWCNT nanocomposites

M. Fathima Rigana and M. Sarojadevi*****

Department of Chemistry, Anna University, Chennai-25

E-mail : msrde2000@yahoo.com

A new triamine 1,3,5-tris(4-((4-(4-aminophenoxy)phenyl)sulfonyl)phenoxy)benzene (TAPOPSPOB) was synthesized using bisphenol-S, p-chloronitrobenzene and 1,3,5-trichlorobenzene. It was successfully polymerized into hyperbranched polyimides (HB PIs) with commercially available dianhydrides [3, 3', 4, 4'-benzophenonetetracarboxylic dianhydride (BTDA) and pyromellitic dianhydride (PMDA)] by A_2+B_3 method [1]. HBPI/MWCNT nanocomposites were prepared by the reaction of TAPOPSPOB, dianhydrides with amine functionalized multiwalled carbon nanotube using conventional method [2]. A series of HBPI/MWCNT composites were synthesized by varying the percentage of MWCNT (1, 5, and 10 wt %) [3,4]. The structure of the resulting hyperbranched polyimides were characterized by FT-IR, ^{1}H-NMR, and ^{13}C-NMR analysis. Glass transition temperature (T_g) and thermal stability were monitored by DSC and TGA analysis respectively. Dielctric constant and dielectric loss measurements were carried out with the help of impedence analyzer. The results from DSC and TGA show that the glass transition temperature (Tg) and the thermal stability of the HBPI/MWCNT composites was found to be higher when compared to pure HBPIs. The morphology of the HBPI/MWCNT nanocomposites is studied by Scanning electron microscopy and Trasmission electron microscopy [5].

Keywords:Hyperbranched polymer, poly(etherimides), multiwalled carbon nanotubes, nanocomposites.

References

[7] Fathima Rigana, M; Thirukumaran, P; Shanthi, K; Sarojadevi, M. *RSC Adv*, 6 (2016) 33249-33258.
[8] Govindaraj, B; Sarojadevi, M. *Polym. Compos*, (2015) DOI: 10.1002/pc.23426.
[9] Ali Takassia, M; Zadehnazaria, A; Farhadia, A; Mallakpour, S. *Prog. Org. Coat.*, 80 (2015) 142–149.
[10]Wu, G; Tang, Y; Weng, R; *Polym. Degrad. Stab.*, 95 (2010) 1449-1455.
[11]Thirukumaran, P; Shakila Parveen, A, Sarojadevi, M. *Polym. Compos*, 36 (2015) 1973–1982.

MACRO 193

POSS And Graphene Oxide Based Polymeric Nanocomposites For High Performance Applications

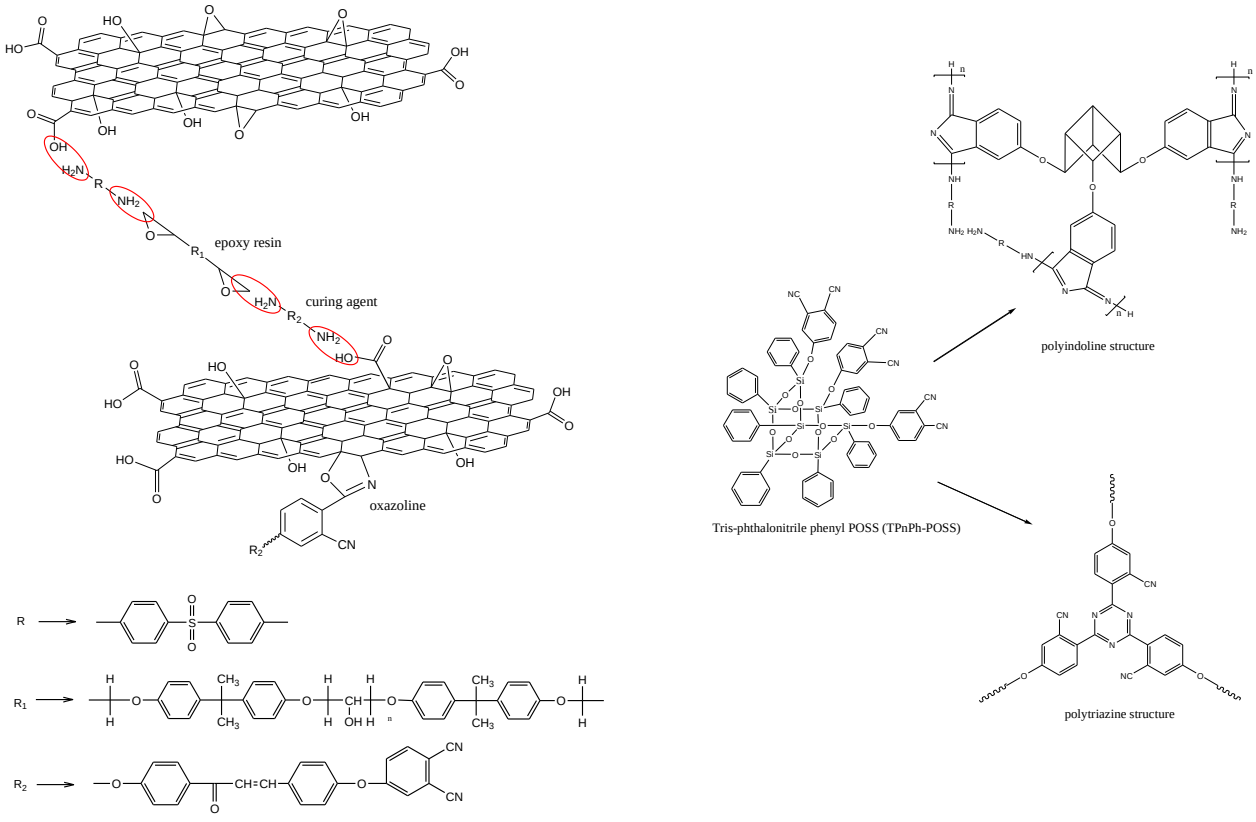
[a]M.Sarojadevi*, [a]K.Kumutha, [a]R.Balasubramanian, [a]P.Thirukumaran, [a]C.P.Sakthidaran, [a]S.Balaji and [b]P.R.Sundararajan

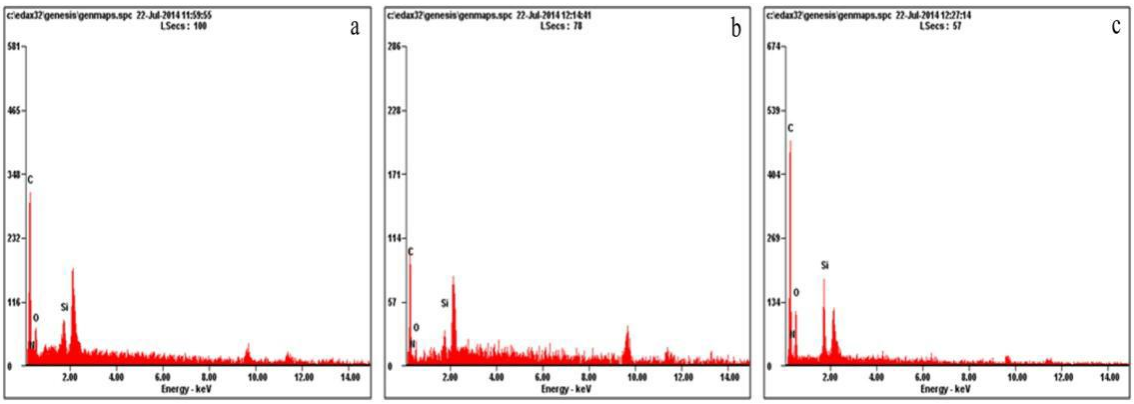
[a]Department of chemistry, College of Engineering, Anna University, Chennai – 600025
[b]Department of chemistry, Carleton University, Ottawa, Canada.
**E-Mail: msrde2000@yahoo.com*

The properties of polymers can be effectively enhanced by reinforcing with nanoparticles such as POSS, grapheme oxide, CNT etc. Nanocomposites belong to advanced materials family have gained significant attraction in research.

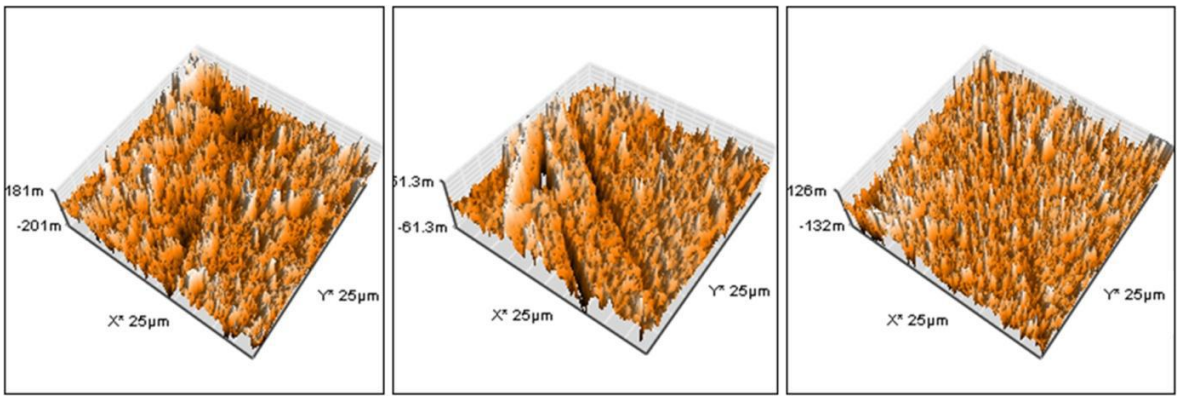
Polyhedral Oligomeric Silsesquioxanes (POSS) are well-defined, highly symmetric, Cage-like molecules with nanoscopic size, approximately 1.5 nm in diameter including the eight organic groups (methyl, isobutyl, cyclopentyl, cyclohexyl, phenyl, aniline, among others) which are tethered to its cage. POSS molecules are truly inorganic core/organic hybrid materials that are naturally compatible with the organic polymers. Substitution of one or more corner groups by functional groups such as cyanate ester, benzoxazine, amine, methacrylate, acrylate, styrene, norbornene, epoxy, alcohol, and phenol provide the possibility to incorporate POSS into a polymer chain or network through polymerization or grafting.

Graphene oxide sheets are widely utilized as reinforcements for polymer composites since it can be easily produced, cheaper and acts an effective toughening agent for polymers (Shivan Ismael Abdullah & Ansari 2014, Tianxi Liu et al 2014). Because of these remarkable properties, graphene oxide is identified as a very good alternative for carbon-nanotubes for making nanocomposites (Yan-Jun Wan et al 2014). There are plenty of functional groups such as hydroxyl, epoxy and carboxyl groups present on the surface or the edges of the graphene oxide sheets. Presence of these groups make them to interact with the polymer matrix, better dispersion is achieved thereby enhancing their properties.





EDX of POSS-Pbz nanocomposites



AFM images of the POSS-Pbz nanocomposites

POSS - epoxy/phthalonitrile , POSS- benzoxazine GO - epoxy/phthalonitrile, GO-polyimide GO/polytriazoleimide nanocomposites were prepared and characterised using FT-IR, 1H-NMR, 13C-NMR, SEM, TEM, AFM, DMA, TGA and DSC. The thermal, electrical and morphological properties will be discussed.

References

[12] Balaji Sadhasivam and Sarojadevi Muthusamy. *High Performance polymers*, 28 (2016) 547.
[13] Kumadha Kaliavaradhan and Sarojadevi Muthusamy. *High Performance polymers*,*28(2016)296.*
[14] Balasubramanian Rukmanikrishnan, Kumadha Kaliavaradhan and Sarojadevi Muthusamy, Polymer Bulletin, 73 (2016) 309.
[15] Thirukumaran Periyasamy, Shakila Parveen Asrafali and Sarojadevi Muthusamy, *New Journal of chemistry*, 39 (2015) 1691.
[16] Rakesh Samikannu, Sakthidharan Chettichipalayam, P., Sarojadev Muthusamy i, Sundarajan Pudupadi R., *European Polymer Journal*, 68 (2015) 161.
[17] Sahila S.and Jayakumari L.S., *Polymer Composites*, 36 (2015) 1.
[18] Sahila S., Anjali Chhonkar, Jayakumari L.S, *Advanced Composite Letters*, 24 (2015) 21.

MACRO 201

Dopant-Assisted Hierarchical Electrical Conducting Folic acid/Polyaniline/ silver-nanoparticles hydrogel with Enhancement of Photoresponse and Energy storage.

Das, Sujoy; Nandi, Arun K.*

Polymer Science Unit, Indian Association for the Cultivation of Science, Jadavpur, Kolkata-700032, India

** Corresponding author's email i.d: psuakn@iacs.res.in*

Electrical conductive hydrogels are an interesting class of materials that shows various energy and biomedical device applications. Tailoring the 3D porous structure within the xerogel is the key to those applications. We have synthesized a new macroporous conducting redox active hydrogel by *in situ* production of conducting PANI-silver nano (AgNPs) within non conducting folic acid gel matrix. The 3D nanoparticle ambedded PANI hydrogel exhibits macroporous hierarchical network with uniform dispersion of AgNPs. These gels are well characterised by morphology (SEM, TEM), spectroscopy (UV,FTIR,XPS), XRD and rheology. Here AgNPs incorporated hydrogel improved the electrical conductivity and electrical properties. FP2Ag hydrogel significantly improved the electrochemical properties, with specific capacitances up to 647 F/g and excellent cyclic stability with a retention ratio of 73.8% after 5000 cycles. FP2Ag shows larger photocurrent as well as photoresponse activities. Time-dependent photoresponse of FP2Ag confirm the current rise fast as well as decay fast within experimental timescales compared to FP2 gel.

References

[19] Pan, Lijia; Yu, Guihua; Zhai, Dongyuan; Lee, Hye Ryoung; Zhao, Wenting; Liu, Nian; Wang, Huiliang; Tee, Benjamin C.-K.; Shi, Yi; Cui, Yi; Bao, Zhenan; *PNAS*, 109 (2012) 9287.

[20] Chakraborty, Priyadarshi; Bairi, Partha; Roy, Bappaditya; Nandi, Arun. Kumar; *ACS Appl. Mater. Interfaces*, 6 (2014) 3615.

MACRO 203

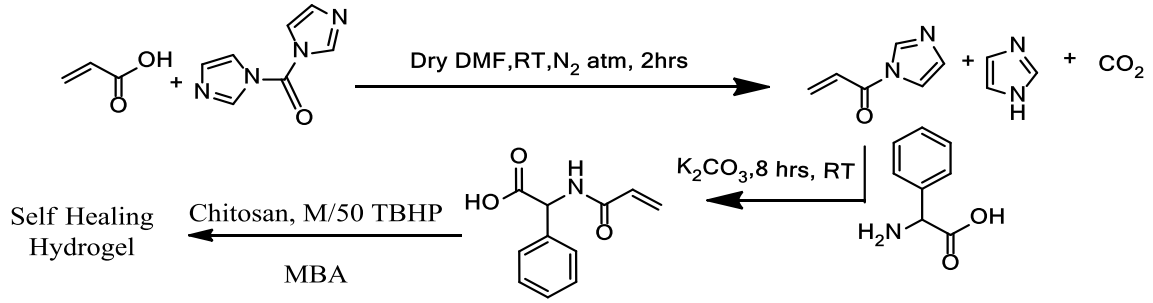
Synthesis and Characterization of pH responsive Self-healing Hydrogel

Swati Sharma, Deepak, Ashok Kumar, Sere Afgan, Rajesh Kumar*

Department of Chemistry, Centre of Advance Studies in Chemistry, institute of Science, Banaras Hindu University, Varanasi-221005, UP, India. E-mail: Rajesh Kumar* (rkr_bhu@yahoo.com), swativats92@gmail.com

Human skin, which can heal itself after being impaired, offers a good inspiration to study and design self-healing materials with enhanced properties of safety and durability, leading to their long-term use with stable functionality. Based on the healing mechanisms, self-healing materials can be grouped into extrinsic self-healing materials and intrinsic self-healing materials.[1] Extrinsic self-healing materials, including capsule based healing systems[2] and vascular healing systems, complete their self-healing process via releasing healing agents after crack propagation,[3] while intrinsic self-healing materials are based on either covalent interactions,[4] such as Diels–Alder (DA) and retro Diels–Alder (RDA) processes, or non-covalent interactions such as hydrogen bonds, ionic interactions, p–p interactions, host–guest interactions, metal–ligand coordination, and supramolecular interactions. In our present work, we designed a self-healing as well as pH responsive hydrogel which is composed of the chitosan backbone grafted with synthesized monomer (acryoyl phenylalanine) *via* free radical polymerization using tert-butylhydroperoxide as redox initiator. The amide groups on the hydrogel served as the self-healing motifs through the reversible hydrogen-bonding interaction. Based on this multiphase design, self-healing materials from chitosan and amino acid based monomer self-healing hydrogel were developed through free radical polymerization.

The self-healing hydrogel reported here is fast, occurring within 30 min of the insertion of a crack into the hydrogel of two separate hydrogel pieces. The healing is reversible, we also demonstrate various potential applications of such easy-to-synthesize, smart, self-healing hydrogels. The physicochemical properties of pH responsive hydrogels were investigated by using FT-IR, scanning electron microscope, atomic force microscope, rheology, and antibacterial study.



Scheme: Reaction condition of self-healing hydrogel

References

[1] M. D. Hager, P. Greil, C. Leyens, S. van der Zwaag and U. S. Schubert, Adv. Mater., 2010, 22, 5424–5430.
[2] D. Sun, J. An, G. Wu and J. Yang, J. Mater. Chem. A, 2015, 3, 4435–4444.
[3] D. Y. Wu, S. Meure and D. Solomon, Prog. Polym. Sci., 2008, 33, 479–522.
[4] P. Cordier, F. Tournilhac, C. Soulie´-Ziakovic and L. Leibler, Nature, 2008, 451, 977–980.
[5] Y. Amamoto, J. Kamada, H. Otsuka, A. Takahara and K. Matyjaszewski, Angew. Chem., Int. Ed., 2011, 123, 1698–1701.

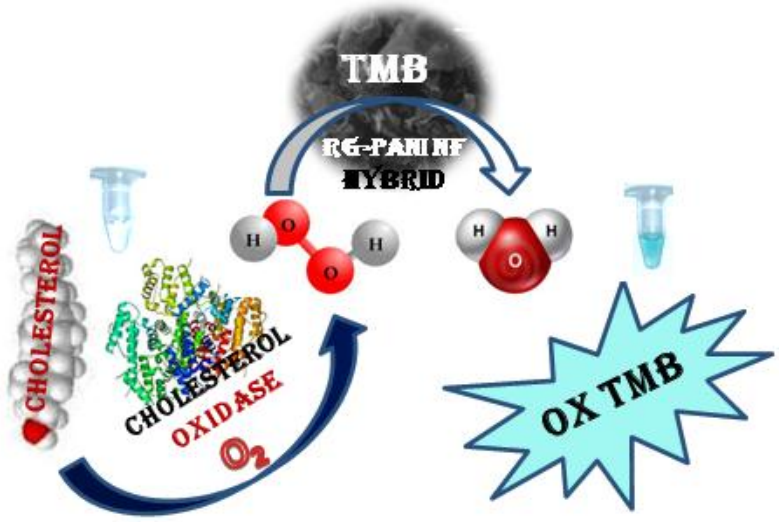
MACRO 211

Reduced Graphene-Polyaniline Nanofibres Hybrid as Peroxidase Mimetic Material: Exploited for H_2O_2 and Cholesterol Recognition

Singh Shikha[a], Gundampati Ravi K.[b], Mitra Kheyanath[a], Jagannadham Medicherla V.[b], Ray Biswajit[a]*

[a] *Department of Chemistry, Institute of Science, Banaras Hindu University, Varanasi – 221005, India*
[b]*Molecular Biology Unit, Institute of Medical Science, Banaras Hindu University, Varanasi–221005, India*

**Corresponding author email i.d.: biswajitray2003@yahoo.co.in*



Recently, much attention has been focused on the fabrication of "artificial enzymes" also called mimetic materials i.e. mimicking the natural one. Peroxidases are heme proteins containing Fe(III) protoporphyrin IX or ferriprotoporphyrin IX (four pyrrole rings are coordinated to Fe(III)) as the prosthetic group. These can be found in living organism and catalyzed many biological reactions in which peroxides such as hydrogen peroxides and alkyl peroxides are reduced, while a redox substrate acting as electron donor is oxidized. Graphene-based hybrid peroxidase mimetic materials attracted meticulous attention and extensively used for detecting many biological molecules such as H_2O_2, glucose, cholesterol, ascorbic acid, prostate specific antigen, interleukin etc. via colorimetry, voltametry, fluorescence and electrochemical methods.[1-5]

Herein, we have developed the novel use of reduced graphene-polyaniline nanofibre hybrid (RG-PANI NF) as very accomplished, low cost and eco friendly peroxidase mimetic material, for effective detection of cholesterol and beta sterosterol via colorimetric H_2O_2 detection in the presence of 3,3',5,5' tetramethylbenzidiamine (TMB) chromogen. Hybrid material has been well characterized by Raman, FT-IR, UV-Vis and X-Ray diffraction and TGA techniques. Zeta potential measurement has suggested its good dispersibilty in water. Morphology study has exposed its highly exfoliated nanostructure, which facilitated the diffusion of reactant, product and rapid electron transfer. pH, temperature, analyte and chromogen concentration dependent peroxidase activity of hybrid material has been studied. These results have revealed its proficient activity at lower pH and at 37 ^oC temperature. Further, the hybrid material has also been evolved as colorimetric sensor for the assay of cholesterol level in blood serum and for the detection hydrogen peroxides in waste water samples.

Reference

[21] Garg B.; Bisht T.; Ling Y-C. *Molecules*, *20 (*2015) 14155-14190;
[22] Nirala N. R.; Abraham S.; Kumar V.; Bansal A.; Srivastava A.; Saxena P. S. *Sensors and Actuators B*, 218 (2015) 42–50.
[23] Nipapan R.; Rangkupan R.; Rodthongkum N.; Chailapakul O. *Biosensors and Bioelectronics*, 52 (2014) 13–19.
[24] Ma Y.; Zhao M.; Cai B.; Wang W.; Ye Z.; Huang J. *Chem. Commun.*, 50 (2014) 11135—11138.
[25] Yang Z.; Qian J.; Yang X.; Jiang D.; Du X.; Wang K.; Mao H.; Wang K. *Biosensors and Bioelectronics*, 65 (2015) 39-46.

MACRO 218

Fluorescent Polymer Films of Carbon Dots-PMMA Nanocomposites

Suchithra C,[a]*Manjunatha Ganiga[b] and Jobin Cyriac[b]

[a]*ASD, ASCG/PCM, VSSC Thiruvananthapuram – 695022, Kerala*

[b]*Department of Chemistry, Indian Institute of Space Science and Technology*

Thiruvananthapuram – 695 547, Kerala

**Email: suchiniju@gmail.com*

Abstract

Fluorescent nanocomposites based on polymethyl methacrylate (PMMA) and carbon dots (CDs) were prepared by solution blending and *in situ* polymerisation methods. CDs impart fluorescent properties to the composites and the nanocomposite film exhibits solid state fluorescence. Materials characterization and the evaluations of optical properties of the nanocomposites have been performed. Nanocomposites prepared by solution blending route shows optimal photoluminescence (PL) intensity at 2.5 wt% of CDs addition. In the case of *in situ* polymerization approach, the best PL intensity was observed for 1.5 wt% loading of CDs.

***Key words**: Carbon dots (CDs), PMMA, polymer nanocomposites*

1. Introduction

Carbon dots (CDs) are a new class of fluorescent carbon materials with sizes less than 10 nm.Generally they are small carbon nanoparticles with various surface functionalisations (Figure 1). They can be amorphous or nanocrystalline in nature with sp^2 carbon clusters.[1] Though bulk carbon is a black material without any luminescence properties, CDs shows excellent fluorescent properties in addition to excellent solubility in water. Compared to luminescent semiconductor quantum dots (QDs) and metal nanoclusters, CDs are better choice in various aspects. CDs manifested superior properties such as chemical stability, excellent water solubility, resistant to photo bleaching, low cost, simple preparation route, etc.[2-5] Apart from sp^2 carbon core, presence of surface functional groups imparts excellent solubility in various aqueous solvents. To utilise CDs for various applications, it has to be supported by a matrix without losing CDs' photo-physical properties. Polymer matrices are one of the options. Applications of CDs-polymer nanocompsites have been demonstrated in various fields including photocatalysis, optoelectronics, biology, etc.[6,7]

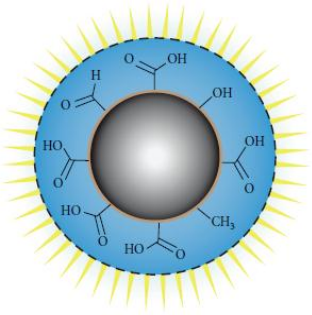


Figure 1. Representation of CDs

Here, we report a facile method for the preparation of CDs-polymethyl methacrylate (PMMA) composites by solution blending and in situ polymerization. Composites were casted as thin films and characterised using different microscopic and spectroscopic characterisation techniques. Photolumi-nescent (PL) properties of the composites were investigated in details. This simple technique enables the development of CDs-based composites for numerous applications.

2. Experimental

Materials: Phosphorus pentoxide (P_2O_5), methyl methacrylate (MMA) and glacial acetic (HOAc) were from Merk, India. PMMA (MW-120000)) was purchased from Sigma Aldrich, India. DMF (Spectrochem, India) was used as solvent without further purification.

Synthesis of carbon dots: HOAc was used as the carbon precursor for the synthesis of CDs. 1 mL of HOAc containing 80 µL of water was quickly added to 2.5 g of P_2O_5 to produce CDs. The prepared CDs were centrifuged and purified by dialysis sacks (2000 MWCO) for 24 hour[8].

2.1 Fabrication of composite film

(a) **Preparation of CDs-PMMA composite by blending:** DMF was used as the solvent because of the excellent solubility of both CDs and PMMA in DMF. In a typical experiment *0.01* g of purified CDs was added to 0.99 g PMMA and then dissolved in 10 mL of DMF. The solution was kept at 50 ^{0}C under vigorous stirring for ½ hour followed by sonication for 15 minutes. The solution is then poured into a Teflon mould (6 cm × 6 cm) and then dried at 60 ^{0}C for solvent evaporation. Films with different CDs composition were prepared by varying the wt% of CDs. Films were prepared with 0.5, 1.0, 1.5, 2.0, 2.5, 3.0 and 5.0 wt % of CDs**.**

(b) **Preparation of PMMA-CDs composite by in situ method:** For the preparation of the PMMA, monomer MMA was chosen. MMA undergoes free radical polymerisation in presence of benzoyl peroxide catalyst in inert atmosphere. Weighed amount of CDs was dispersed in monomer by ultra-sonication and polymerised using benzoyl peroxide as initiator at 80^{0}C in an oil bath. The viscous polymer formed is immediately casted on a Teflon mould and dried in vacuum at 50 ^{0}C to remove unreacted monomer. Different composition films were prepared by varying the amount of CDs.

2.2 Characterization

The nanocomposite films and the CDs were characterized by FT-IR spectrophotometry (Perkin Elmer spectrum 100FT-IR), UV-visible spectroscopy (Cary100 Bio-UV –Visible spectrophotometer) and fluorescence spectrofluorometry (Horiba, Fluoromax-4). All FT-IR measurements were done at Attenuated total reflectance (ATR) mode. The thermal stability was studied using thermogravimetric analysis (TGA) with a TA instrument TGA Q50 instrument. Structural morphology of the samples was studied using transmission electron microscope (TEM) (JEOL JEM-2100) and scanning electron microscopy (SEM) (NOVA NANOSEM 450).

3. Results and discussion

To understand the chemical interaction between CDs and PMMA in the composites, detailed FT-IR analyses have been performed (See **Figure 2**). The peaks at~1150 cm^{-1} (C-O-C_{str}), 1388 cm^{-1} and 754 cm^{-1} (α-CH_3), 1720 cm^{-1} (acrylate carboxyl group), 1444 cm^{-1} (–CH_{3bend}) and 2997 and 2941 cm^{-1} (C-H_{str}) are characteristic of PMMA. The CDs shows peaks at 3330 cm^{-1} (OH group), 1655 cm^{-1} (>C=O), 1050 cm^{-1} (C-O-C_{str}) and 1622 cm^{-1} (core C=C_{str}). In the composite prepared by solution blending, the broad band of CDs' observed at 3290 cm^{-1} is weakened because of interaction with PMMA. The 2941 cm^{-1} feature of PMMA was shifted to 2949 cm^{-1} and is ascribed to the increased restriction of C-H_{str} vibration due to the interaction of >CO (PMMA). The blue shift in >C=O stretching frequency to 1730 cm^{-1} might be due to the non-covalent interaction of >C=O group with -OH /COOH group of CDs. The composite prepared by in situ route shows a decrease in –OH features compared to solution blending route. Also, the C-H_{str} peak observed at 2960 cm^{-1} for pure polymer appeared 2923 cm^{-1} in the case of in situ composites. The peak at 1720 cm^{-1} changed to 1724 cm^{-1} in the composite. This may be due to the non covalent interaction of –COOH group of CDs with –C=O group of PMMA.

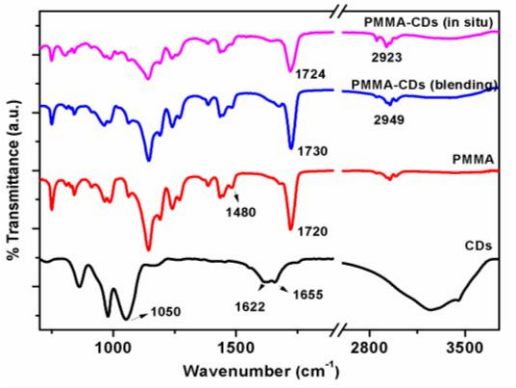


Figure 2. FTIR spectra of PMMA and PMMA-CDs (1.5 wt%) composites.

The peak at 1480 cm^{-1} in PMMA shifted to 1487 cm^{-1} in the composite. This is due to the fact that after incorporating CDs there is a restriction in the bending of C-H bond. In both type of nanocomposites, there is no shift for C=C_{str} frequency as it originates from the CDs' carbon core.

From the TEM images (**Figure 3**) it is clear that at low wt% loadings (0.5 – 1.5 wt%) there is almost homogeneous dispersion of CDs in the PMMA matrix (See Figure. 2). At higher loading (from 2.0 wt% onwards) considerable agglomerations take place, especially in the case of solution blending procedure. However, in the case of in situ route the extent of aggregation was minimum till a loading of 3.0 wt%. The selected area electron diffraction (SAED) pattern shows amorphous nature of both nanocomposites films via both routes. From the TEM images it is clear that CDs exhibits proper dispersion in the composites. Cross sectional area analysis performed using SEM shows that solution blending route results in solvent entrapment and consequent mesoporosity in the composite films.

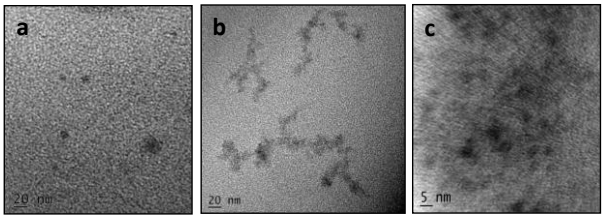


Figure 3.TEM images of (a) PMMA-CDs (0.5 wt%), (b) PMMA-CDs (2.5 wt%) solution blending and (c) PMMA-CDs (2.5 wt%) in situ method.

Thermal stability of the composites was investigated using TGA analysis. Similar to polymer degradation, the composites also showed three stage of degradation (**Figure 4**).TGA curves of PMMA and the composite prepared via solution mixing are showing similar thermal degradation curves. However, the composite prepared via in situ method shows thermal degradation at 200 ^{0}C. PMMA-CDs prepared via solution blending was thermally more stable compared to in situ method. In the case of solution blending composites decomposition completed at a temperature around 400 ^{0}C where as it is around 430^{0}C in the case of in situ composites.

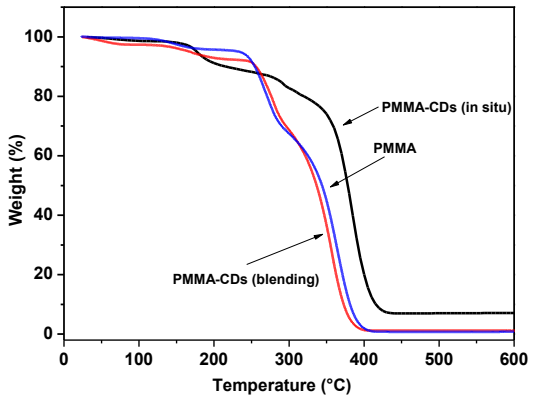


Figure 4. TGA of PMMA and CDs-PMMA composites

UV-visible absorption spectroscopy of the films revealed the optical transparency of the films. As expected, the composites show reduced optical transparency compared to PMMA film. The absorption in the UV–visible region is usual, and is due to the n→ π* as well as π→π* transition of the C=O bond. As a consequence CDs-PMMA films were less transparent in the wavelength region of 400-800 nm when compared with PMMA film (**Figure 5**).

Utilisation of photoluminescence (PL) properties of CDs in solid state was the prime objectives of the present study. A number of factors contributing to CDs luminescence are recombination of photo generated electron hole pairs taking place on the surface of the CDs, excitons of carbon, the presence of emissive traps, the quantum confinement effect, and so forth. Therefore, the selection of polymer is critical to retain the PL properties of CDs.

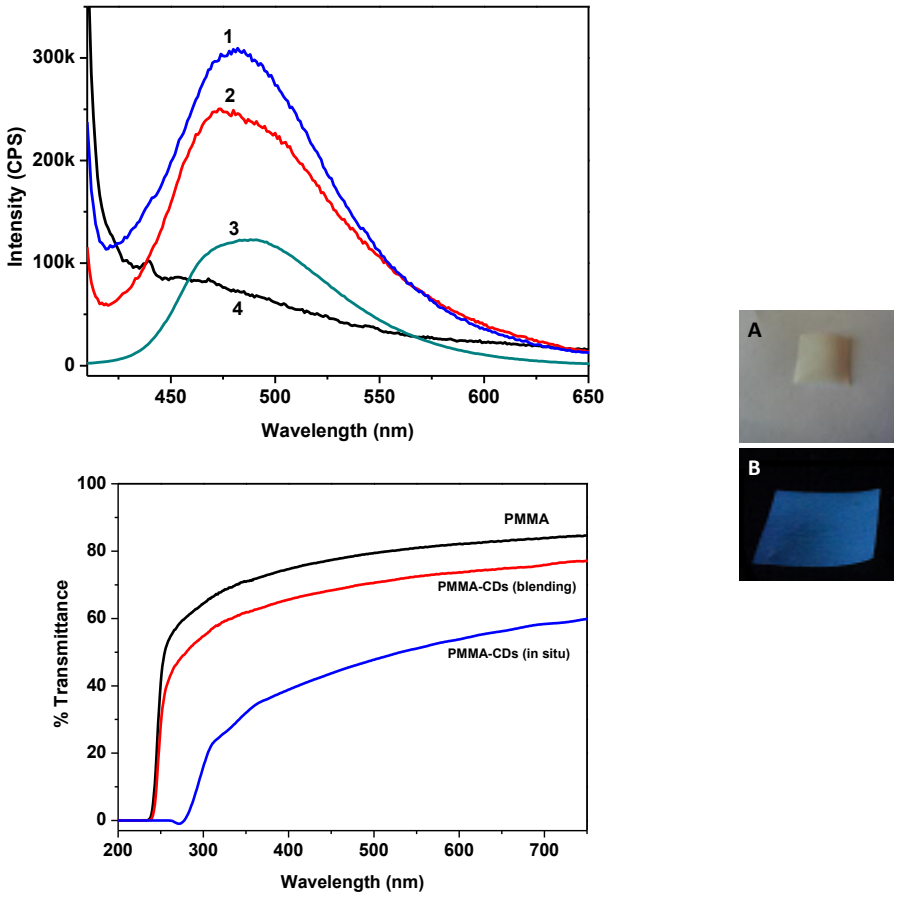


Figure 5. UV-visible spectra of PMMA and PMMA-CDs (1.5 wt%)composites

PL spectra of the prepared composite films in the solid state were measured. The PMMA film did not show any PL properties. The CDs-PMMA nanocomposite shows PL properties because of the presence of CDs **(Figure 6**). It indicates that in the composite the PL properties of CDs are retained. There was no apparent fluorescence quenching of CDs due to the presence of polymer matrix. A strong emission peak located at around 480 nm was observed upon excitation at 360 nm. These values are similar in the case of pure CDs as well.

The intensity of the PL spectra sharply increased with an increase in the loading of CDs. This is due to the fact that the PL intensity depends on the number of particles excited at a particular wavelength. As the number of particles increases with the CDs in the nanocomposites, the emission intensity also increases. The composite containing 2.5 wt% CDs exhibited a maximum PL intensity. Further loading of CDs leads to decrease in PL intensity mainly due to the

agglomeration of the CDs in the composites. This is visible in the TEM images. In the case of in situ composites the maximum PL intensity was observed for 1.5 wt% of CDs.

Figure 6. Fluorescence emission spectra of CDs and PMMA-CDs (1.5 wt%)composites. (1) *in situ*, (2) blending, (3) CDs and (4) PMMA. *Inset*: shows actual photographs of the nanocomposite film in (A) visible and (B) UV light.

4. Conclusions

The CDs-PMMA nanocomposites were prepared via solution blending and in situ polymerisation route. Materials characterisation and evaluations of the optical properties were performed. FT-IR spectroscopy shows that there is interaction between the functional groups of CDs and PMMA. Fluorescence analysis shows that the PL properties of CDs were retained in the polymer matrix. In the case of solution blending method, a maximum PL intensity was observed for 2.5 wt% loading of CDs in the PMMA matrix. But in the case of in situ procedure where polymerisation reaction was performed in the presence of CDs, the maximum PL was shown at 1.5 wt% of CDs loading. In both cases PL properties of CDs were retained in the composite though the extent of fluorescence of quenching was different. Hence, we have successfully prepared CDs-PMMA polymer nanocomposites without affecting the PL property of CDs. Also, it is found that in situ composites thermal stability was decreased. The solid state optical properties of the composites can be utilised for various applications. The range of applications includes optoelectronics, biosensing, catalytic and electromagnetic shielding.

Acknowledgements

Director, VSSC Thiruvananthapuram & Director, IIST Thiruvananthapuram.

5. References

1. Hussain, F., M. Hojjati, M. Okamoto, R. E. Gorga, *J. Compos. Mater.,* 40**,** 1511, 2006.
2. Xu, X., R. Ray, Y. Gu, H. J. Ploehn, L. Gearheart, K. Raker, W. A. Scrivens, *J. Am. Chem. Soc.,* 126**,** 12736, 2004.
3. Baker, S. N. & G. A. Baker, *Angew. Chemie. Int. Ed.,* 49**,** 6726, 2010.
4. Ray, S. C., A. Saha, N. R. Jana, R. Sarkar, *J. Phys. Chem. C,* 113, 18546, 2009.
5. Li, H., Z. Kang, Y. Liu, S.-T. Lee, *J. Mat. Chem.,* 22**,** 24230, 2012.
6. Zhu, S., Q. Meng, L. Wang, J. Zhang, Y. Song, H. Jin, K. Zhang, H. Sun, H. Wang, B. Yang, *Angew. Chemie Int. Ed.,* 52**,** 3953, 2013.
7. Zhou, L. Hea, B., Huanga, J., *Chem. Commun.*, 49, 8078, 2013.
8. Fang, Y., Guo, Y.S., Li, D. Zhu, C.Ren, W. Dong, S. and Wang,.*J. Am.Chem.Soc*.,6, 400–409,2012.

MACRO 221

Superhydrophobic and pH tolerant Silica Surface Decorated with Oligomers; Self-assembled Micro-flower Bunches and Nanofolds

Ramakrishna S., Dona Mathew, Santhosh Kumar K.S.*

Polymers and Special Chemicals Division, Vikram Sarabhai Space Centre, Thiruvananthapuram-22
**E-mail: santhoshkshankar@yahoo.com*

Studies toward superhydrophobic (SH) materials turn more attractive due to the wide range of potential applications like anti-wetting, anti-corrosion, anti-bacterial and self-cleaning [1, 2, 3]. In the present work, silica nanoparticles are grafted with oligomers containing short alkyl chains using a bifunctional diisocyanate molecule. The single step reaction results in superhydrophobic particles which are self-assembled into *micro-flower bunches* which are further ordered into *nanofolds* as seen in FESEM images in figure 1. The thin layer of particle coating displays static contact angle of 162 ± 2 ° in the pH ranging from 1 to 13 and rolled-off from the surface with sliding angle (SA) <10 °. The combination of ordered *micro-nano structure* is the rationale for superhydrophobicity and pH tolerance. A coating of SH particles based on polysiloxane exhibits Cassie-Baxter state of superhdyrophobicty (CA>150 °, SA<10°). Moreover, the surface can regain the SH properties even after the surface roughness is disrupted by strong mechanical forces.

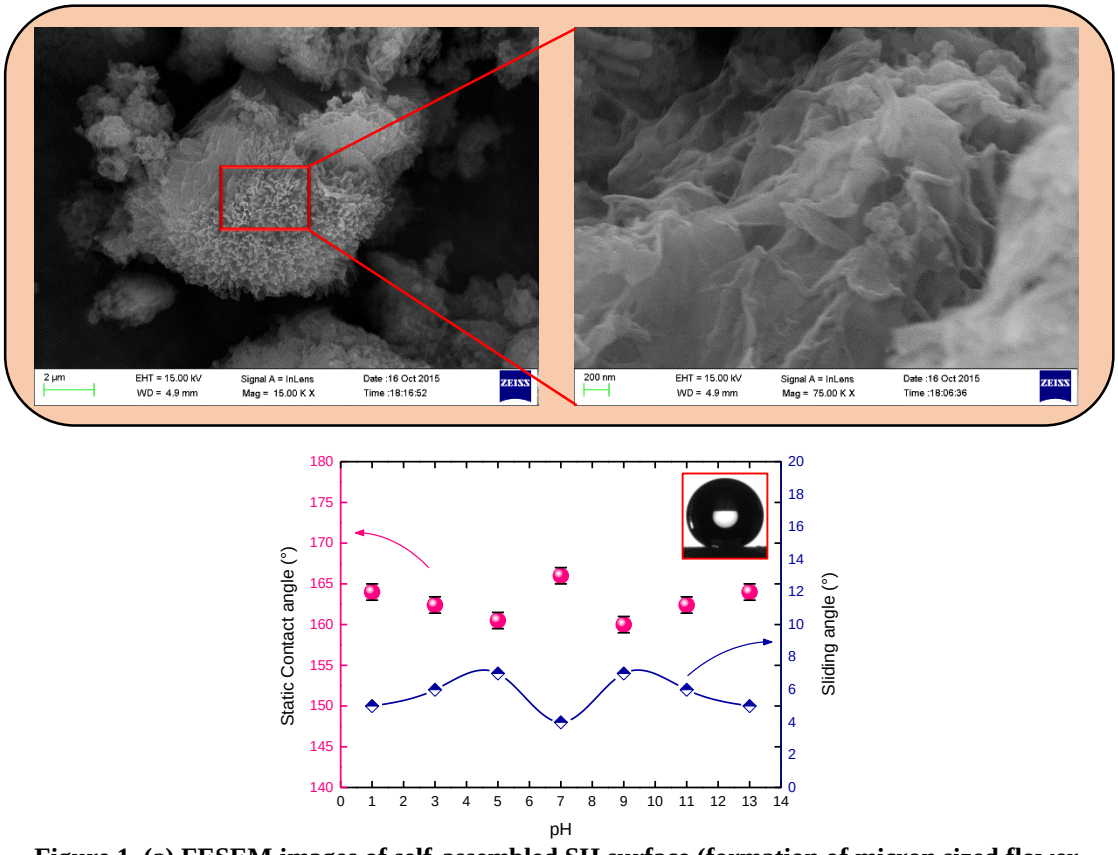


Figure 1. (a) FESEM images of self-assembled SH surface (formation of micron sized flower bunches and their re-ordering into nanofolds) (b) Cassie-Baxter state properties of SH particle coating (inset: Optical image of water droplet)

References

[1] Bhushan B, Jung YC. *Prog Mater Sci.* 56 (2011) 1.

[2] Ferrari M, Benedetti A. *Adv Colloid Interface Sci*. 222 (2015) 291.

[3] Ramakrishna S., Santhosh Kumar K. S., Mathew D. & Reghunadhan Nair C. P. *Journal of Materials Chemistry A* 3 (2015) 1465.

MACRO 225

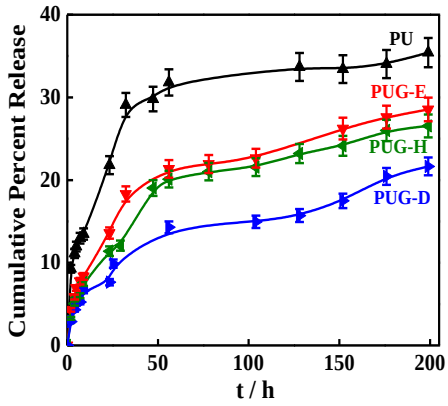
Influence of the diamine modified graphene on polyurethane properties and its biological applications

*Patel Dinesh and Maiti Pralay**

Email-id: dineshbhud10@gmail.com

School of Material Science and Technology, Indian Institute of Technology (Banaras Hindu University) Varanasi.

Functionalization of the graphene oxide with a series diamine moieties provides the better thermal, mechanical and biological response in nanohybrids as compared to the pure polyurethane. Functionalization of the graphene oxide with various diamine were verified through the FTIR and UV-visible spectroscopy. Nanohybrids of the polymer were prepared through the in-situ polymerization process. Interaction between the polymer chains and modified graphene was revealed through the FTIR and UV-visible spectroscopy. Morphological properties of nanohybrids are highly influence by the modified graphene and analyzed through the POM, AFM, SANS and XRD measurements. Enhancement in the thermal and mechanical properties was occurred in nanohybrids with respect to the pure polymer and it is measured through the TGA, DSC and UTM respectively. Biocompatible natures of nanohybrids were checked on human breast cancer cells MDA-MB-231 in term of cell viability, cell adhesion, fluorescence image, reactive oxygen species and mitochondrial tracker measurements. Control release of the dexamethasone an anticancerous loaded drug from the nanohybrids is given in figure indicates the prominent biomaterial for the drug carrier. Better biological response as well as the sustained drug release through the material indicates the developed material may have the potential to use as biomaterials.



MACRO 227

Size-Dependent Interaction between PIL Stabilized Silver Nanoparticles and DNA: A Spectroscopic Investigation

Kasina Manojkumar, Akella Sivaramakrishna, Kari Vijayakrishna*

Department of Chemistry, School of Advanced Sciences, VIT University,
Vellore-632014, Tamil Nadu, India

**Corresponding author: Kari Vijayakrishna e-mail: vijayakrishnakari@gmail.com*

Imidazolium-based polymeric ionic liquids (PILs) of the kind poly(1-vinyl-3-hexylimidaozlium bromide) of different DPs (degree of polymerization) such as 30, 50, and 100 were synthesized through conventional free-radical polymerization and used as stabilizing agents for the synthesis of silver nanoparticles (Ag NPs) [1]. The average-particle size of the synthesized silver nanoparticles decreased (43 > 36 > 26 nm) with increase in the molecular weight of PILs respectively (DP = 30 > 50 > 100) and were used to study their interaction with calf-thymus DNA. The experiments were performed in physiological conditions with constant DNA concentration and varying Ag NPs concentrations [2]. Different experiments such as UV-Visible absorption, fluorescence, and circular dichroism (CD) revealed the binding mode and binding constants of Ag NPs with DNA [3]. The effect of varying ionic strength on the binding between Ag NPs and DNA confirmed their interactions as mainly intercalative [4]. UV-Vis and fluorescence results showed an increase in Ag NPs binding constants with decrease in their average-particle size. Furthermore, CD results illustrated that the DNA has well retained the secondary structure (B-form) after binding with Ag NPs [5].

References

[26] Prabhu Charan, KT; Pothanagandhi, N; Vijayakrishna, K; Sivaramakrishna, A; Mecerreyes, D; Sreedhar, B. *Eur. Polym. J.*, 60 (2014) 114.
[27] Manojkumar, K; Prabhu Charan, KT; Sivaramakrishna, A; Jha, P C; Khedkar, VM; Siva, R; Jayaraman, G; Vijayakrishna, K. *Biomacromolecules*, 16 (2015) 894.
[28] Rahban, M; Divsalar, A; Saboury, AA; Golestani, A, *J. Phys. Chem. C*, 114 (2010) 5798.
[29] Misra, VK; Sharp, K A; Friedman, RA; Honig, B. *J. Mol. Biol.*, 238 (1994) 245−263.
[30] Kypr, J; Kejnovská, I; Renčiuk, D; Vorlíčková, M. *Nucleic Acids Res.*, 37 (2009) 1713.

MACRO 232

An Approach For Controlled Grafting of PANI Chains From Fluorescent Carbon Nano Dots

Ghosh, T.,[a]Basak, U.,[a]Majumder, S.,[b] Ball, R.,[c]Chatterjee, D.P.*,[a]

[a]*Department of Chemistry, Presidency University, Kolkata- 700073, India*

[b]*Department of Chemistry, Indian Institute of Technology*

Kharagpur- 721302, India

[c]*Department of Chemistry, Indian Institute of Technology Bombay, Powai, Mumbai-400076, India*

** e-mail id: dhruba.chem@presiuniv.ac.in*

Abstract

A novel synthetic approach for controlled grafting of conducting polyaniline (PANI) chains from the surface of aqueous soluble, fluorescent carbon nanoparticles (CNP) having sizes within (2-6) nm is presented. The CNP synthesis has been carried through some modification of literature reported methods[1] of CNP synthesis by oxidation of candle soot by aqueous nitric acid solution and the modification tremendously increased the CNP yield. The particles have shown high dispersion stability in aqueous medium (perfectly transparent dispersion even after 8 months with no precipitation at room temperature).

Synthesis of polyaniline (PANI) by oxidative polymerization using ammonium peroxodisulfate (APS) in acidic medium usually involves an induction period depending upon pH of the medium and temperature of reaction . This induction period ends after trimer and tetramer of aniline is formed. Oxidative polymerization of aniline in presence of APS follows auto-oxidation where emaraldine salts are oxidized to pernigrailine by APS , which auto-oxidises monomeric aniline and propagation of polymer chain occurs[2]. Polymerization of aniline in presence of N,N'-bis (4'-aminophenyl)-1,4-quinonenediimine which is a trimeric[3] form of aniline has shown complete disappearance of induction period during polymerization. The kinetics of aniline polymerization has shown increase in rate of polymerization with increasing amount of trimer added. Therefore, it may be assumed that this oligomeric form of aniline is behaving as 'seed' from which growth of polymer chains are taking place [4].

Our aim in this work has been the controlled grafting of PANI chains from carbon nano dot particles initiated from aniline trimers anchored on the surface of CNPs following a grafting from approach.

Keywords: *carbon nanoparticles;controlled grafting ; supercapacitor*

Introduction

With the ever growing need for energy in modern day applications and decaying stock of coal and fossil oils, the human civilization is moving rapidly towards acute shortage of energy in the near future. Therefore, development of new energy generation or energy storage systems involving lower cost and minimum environmental concern has become a real challenge to the scientific community. In this context super capacitors have emerged as a very important component in energy storage devices. Depending on the energy storage mechanisms, super capacitors are classified in two main categories 1) Electrochemical double layer capacitors (EDLC) and 2) pseudocapacitors.[1] Capacitance is originated in the first category due to accumulation of charges at the electrode-electrolyte interfaces and energy storage in pseudocapacitors originates from the reversible electron transfer between electrode and electrolyte due to redox reactions of the electrode material.

Graphene sheets, a 2 dimensional array of single atom thick hexagonally arranged sp^2 hybridized carbon atoms offer high electrical conductivity, tunable surface area, chemical stability and mechanical strength, have received significant attention as supercapacitor electrode material operating in EDLC mode. Similarly polyaniline (PANI) having the capability of reversible electron transfer is good candidate as pseudo capacitor. Now, relatively poor conductivity of pseudo capacitors restrict their performance as super capacitors. Theoretical specific capacitance of PANI is appreciably high but inaccessibility of the total surface area of the PANI chains only allows partial realization of their performance.[2] In addition to this, relatively poor mechanical strength and appreciable swelling and shrinkage during charge/discharge cycle results in rapid loss of specific capacitance value over repeated cycles of charging and discharging.

Therefore, the properties of graphene and PANI may complement each other well in their composites as super capacitor electrode material. Now covalent attachment of these two materials should ensure better synergy between them. Accordingly, there are already a few reports which have dealt with the oxidative polymerization of aniline by ammonium peroxodisulfate (APS) in acidic medium being initiated through anchored aniline moieties on the graphene oxide surface.[2,3] However, from the mechanism of oxidative polymerization of aniline,[4] the above systems should produce a composite consisting free PANI chains and GO-anchored PANI chains. Therefore, in this condition many of pseudocapacitor material chains are not getting the graphene support and therefore the properties obtained always should be inferior than expected.[2]

Here we report for the first time an approach for covalent grafting of PANI chains on spherical surface of CQD using oxidative polymerization of aniline in a 'grafting from' approach. In contrary to the previous cases where covalent grafting of PANI conducted on GO nano sheets, here PANI chains are grown from CQD surface having much larger surface area and very much distinct optical and electronic properties. Graphene surface operates as EDLC where the capacitor performance depends on the available surface area. Therefore nano structuring to increase the surface area in carbon quantum dots should improve capacitor performance than GO nano sheets.[5] Similarly much greater dispersibility of CQDs than relatively large sized GO nano sheets should make CQD-g-PANI more dispersible in water and hence better pseudo capacitor performance from PANI chains is expected due to better PANI-electrolyte interactions. Analysis of the PANI grafted CQD through electron microscopic techniques (SEM, TEM) have furnished strong evidences in favour of purely surface grafting of PANI chains. This protocol therefore results greater number of nucleation of the growing PANI chains and hence larger degree of interactions between the surfaces of graphene and PANI is expected. This should be helpful for getting better synergy between these two materials leading to the accomplishment of better electrochemical properties.

Experimental

p-phenelenediamine is purchased from Loba Chemicals and was used after recrystallization from water. Ammonium peroxydisulphate was purchased from Loba chemical. Dialysis tube was purchased from Sigma Aldrich. All other solvents were purchased from local chemical suppliers

and purified by distillation under reduced pressure. Double distilled water was used in different steps.

IR, XRD analysis done from IACS, Kolkata and TEM analysis were done from IIT Kharagpur .

Results and discussion

The synthesis of carbon nano particles(CNP) carried out using a reported method through nitric acid oxidation of candle soot.[6]The only exception is the supernatant after high speed centrifugation is taken instead of the residue. The isolated CNPs have shown (1-3) nm size range showing green fluorescence in neutral water when excited at 350 nm wavelength of radiation. **Figure 1**

shows the excitation dependent PL emission spectrum of aqueous dispersion of carbon nano particles. A gradual red shift of the PL emission with regular increase in excitation wavelength ensures formation of carbon quantum dots (CQDs). The exceptionally high solubility of the prepared CQDs(GOs) in water is explained by the presence of hydrophilic hydroxyl or carboxylic

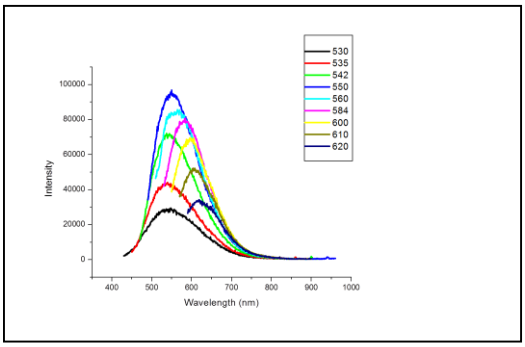
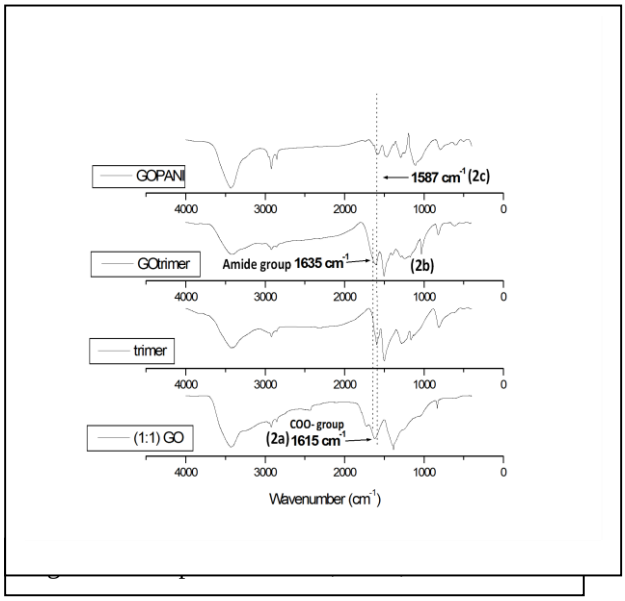


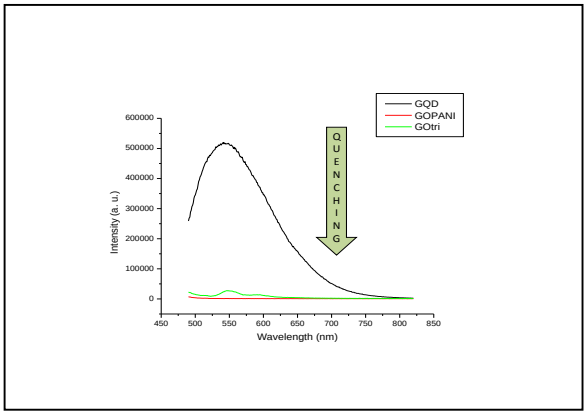
Figure 1 : Excitation Dependent PL emission spectra of CQD



acid groups on the CQD surface. In **Figure 2a,** the IR spectrum corresponding to CQD(GO) clearly shows the signals corresponding to

the carbonyl groups present in carboxylic acid and carboxylate ion moieties. Along with this the broad signal in 3500 cm^{-1} region indicates towards the presence of hydroxyl groups. In the subsequent step, N,N'-bis(4'-aminophenyl)-1,4 quinonenediimine, a trimer form of aniline synthesized following a reported methodology,[7] is tethered on CQD surface through coupling with carboxylic acid groups in a very much controlled way. The trimer anchored CQD so produced is named GOT. In the next step oxidative polymerization of aniline carried out in feebly aqueous acidic medium [0.02 (M) HCl] in presence of APS at 4^0C in presence of different amount of GOT to have composites with varied ratios of CQD and PANI. IR spectrum in **Figure 2b** ensures attachment of trimer moieties on the CQD surface by disappearance of carbonyl signals

at 1727 cm^{-1} and appearance of a new signal at 1635 cm^{-1} due to the anilide carbonyl group. **Figure 2c** shows signal at 1587cm^{-1} corresponding to the C-N-C stretching vibration of PANI. **Figure 3** shows that the PL emission intensity of CQD gets significantly quenched when trimer or PANI is anchored. This may be attributed to the significant (π-π) stacking between the conjugated domains of CQD and PANI indicating very much effective interactions between them. WAXS analysis shows absence of signals corresponding to CQDs after PANI grafting in **Figure 4**. This is also indicative of effective wrapping of PANI chains over CQD surface.



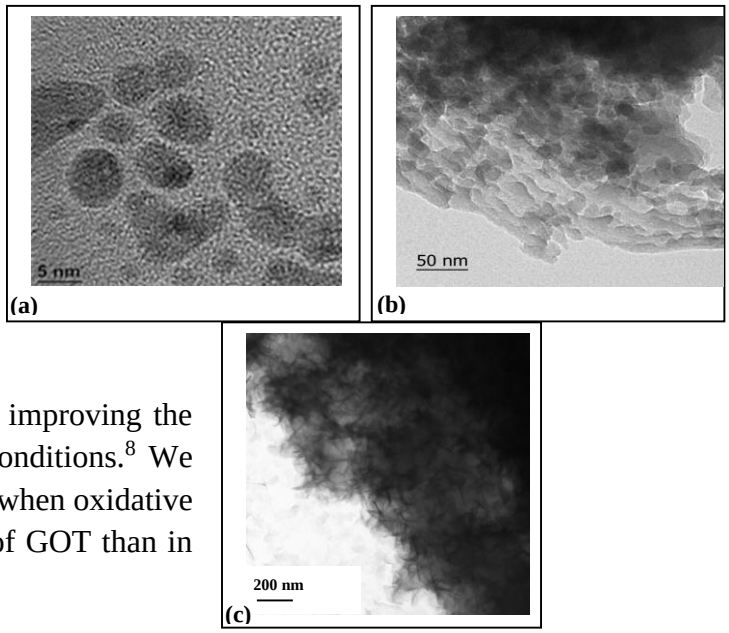
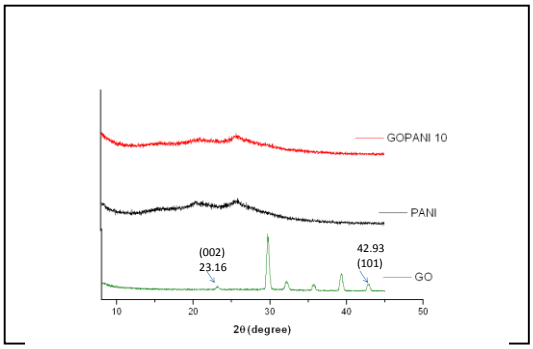


Figure 5 : TEM images of a) CQD, b) GOT-PANI, c) GOPANI

Aniline oligomers have been used previously for improving the rate of polymerization of aniline under the similar conditions.[8] We have also noted here significant rate enhancement when oxidative polymerization of aniline conducted in presence of GOT than in presence of CQD alone.



In the TEM micrograph **(Figure 5a)**, CQDs are observed as bright dots distributed randomly in every part of the grid, having a size range of (2-5) nm. However, upon grafting of PANI chains, similar spherical morphology is retained with increase in size in the range of (16-18) nm (**Figure 5b**). Therefore, this clearly indicates that growth of the PANI chains has [illegible] ace as targeted. Interestingly, polymerization in absence of GOT but in presence of equivalent amount of CQD shows a completely different

morphology having wrinkled PANI sheets (**Figure 5c**). Therefore, the TEM analysis ensures controlled grafting of PANI chains to occur only from the CQD surface.

Conclusions

The present work demonstrates for the first time an approach for covalently grafted CQD-PANI nano composite preparation from CQDs synthesized from readily available and cheap source like candle soot, for application as supercapacitor electrode material.CQDs showing a narrow size range (1-3) nm, which shows green fluorescence when excited at 350 nm wavelength, is synthesized at first through nitric acid oxidation of soot followed be size separation. The oxidative polymerization of aniline is then conducted in presence of aniline trimer anchored CQD surface which have shown significant development in the rate of aniline polymerization under a relatively low acidic and highly diluted reaction conditions. IR spectral analysis has proved the formation of aniline trimer anchored CQD or PANI grafted CQDs without any ambiguity. Subsequently, fluorescence spectroscopic analysis and WAXS analysis have provided strong evidences for wrapping of PANI chains on CQD surface. Finally TEM analysis has proved covalent grafting of PANI chains only from CQD surface without formation of any non-grafted PANI chain.

Acknowledgements

We thankfully acknowledge Presidency University for providing financial and infrastructural assistance and Department of Science and Technology (DST), Govt. of India, for the grant having the Sanction Order No and date: **SB/FT/CS-189/2011 dated 27.06.2014 under Fast Track Project Scheme for Young Scientists.** We also thank IACS, Kolkata, IIT Kharagpur and CRNN, the University of Calcutta for providing instrumental support.

References

1. K. Qingqing,W. John. *J.Materiomics 2*, 37, 2016.
2. L. Zhe-Fei, Z. Hangyu, L. Qi, L. Yadong, S. Lia, X. Jian. *Carbon 71*, 257, 2014.
3. A. K. Nanjundan, C. Hyun-Jung, S. Yeon Ran, C. Dong Wook, D. Liming, B. Jong-Beom. *ACS NANO 6(2)*, 1715, 2012.
4. J. Stejskal, , R.G. Gilbert *Pure Appl. Chem. 74(5)*, 857, 2002.
5. Y. Zenan, T. Laurene, Z. Lei, T. *Jayan Energy Environ.Sci. 8*, 702, 2015.
6. R., S.C., S. Arindam, J. Nikhil R., S. Rupa *J. Phys. Chem. C, 113(43)*, 18546, 2009.
7. W. Yen, Y. Chuncai, D. Tianzhong. *Tetrahedron Letters, 37(6)*, 731, 1996.
8. L. Wenguang, W. Hsing-Lin *J.AmChem.Soc. 126*, 2278, 2004.

MACRO 234

In situ Fabrication of Catalytic Platinum Nanoparticles Embedded Poly(Vinyl alcohol) and Fluorescent Gold Nanocluster Embedded Poly(methyl methacrylate) Films

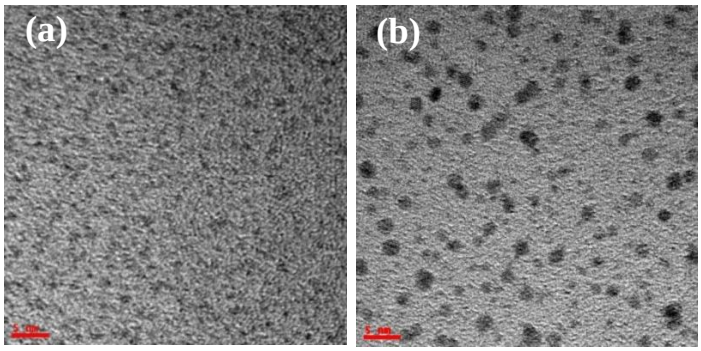
Madhuri, U. D and Radhakrishnan, T. P*

School of chemistry, University of Hyderabad, Hyderabad, India -500046

* *tpr@uohyd.ac.in*

Metal nanoparticles and nanoclusters are extremely interesting and useful because of their unique attributes that are different from than in their bulk state. Polymer metal nanocomposites possess unique properties due to synergistic effects between the properties of metal nanoparticles like electrical, optical, magnetic etc. and mechanical and thermal properties of the polymers. *In situ* fabrication in polymer thin films is a facile, efficient and environment friendly methodology for the synthesis of nanoparticles and their polymer composites [1]. Thin films of polymer metal nanocomposites are fabricated by spin coating a mixture of metal precursor and polymer solution on suitable substrate followed by thermal annealing at an optimal temperature [1]. Platinum nanoparticles embedded in poly(vinyl alcohol) (PVA) and gold nanoclusters embedded in Poly(methyl methacrylate) (PMMA) films are synthesized *in situ* following this general protocol.

Figure 1.TEM images (Scale bar – 5 nm) of Platinum nanoparticles embedded PVA films fabricated using metal precursor (a) H_2PtCl_6 (b) K_2PtCl_4



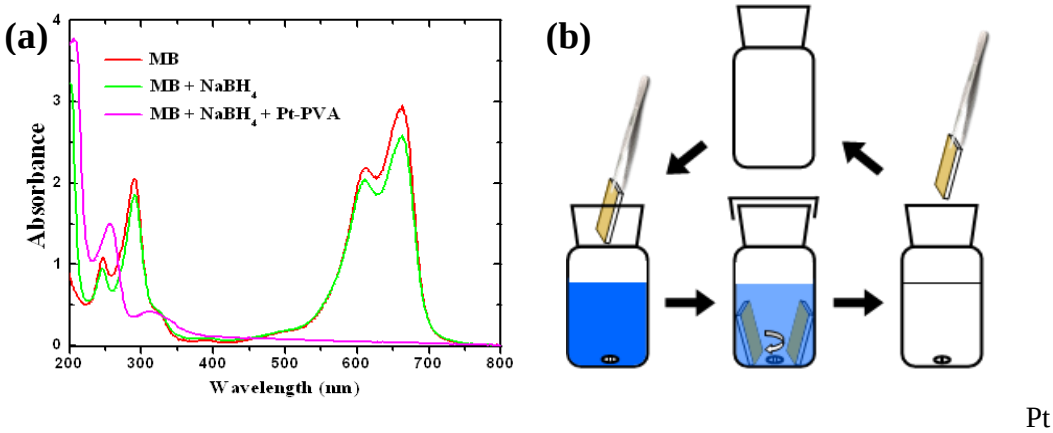


Figure 2. (a) Extinction spectra showing the reduction of MB (b) Schematic representation of the reuse of the Pt-PVA thin film 'dip catalyst' in the reduction of MB

nanoparticle embedded PVA (Pt-PVA) thin films were fabricated using two metal precursors H_2PtCl_6 and K_2PtCl_4 and PVA as the reducing as well as stabilizing agent. Films were characterized using various spectroscopy and microscopy techniques revealing the chemistry

behind the reduction. Platinum nanoparticles synthesized using H_2PtCl_6 and K_2PtCl_4 precursors are < 1 nm and ~ 1 – 2 nm respectively (Fig. 1). These films were used as dip catalysts [2] for reduction of the methylene blue (MB) using sodium borohydride (Fig.2a) and it was found that the films fabricated using K_2PtCl_4 are reusable at least for 10 cycles; higher TON, TOF than earlier reports were obtained [3]. The major advantage of using polymer nanocomposite thin film catalyst is its facile use and reuse (Fig.2b). It possesses the advantage of both homogeneous and heterogeneous catalysis. The swelling of PVA film allows the diffusion of reactants and products in the film facilitating the catalysis. The reaction yield, kinetics and rate, are consistent in the reuses of the same catalyst film (Fig. 3). Utility of Pt-PVA film as an efficient catalyst for

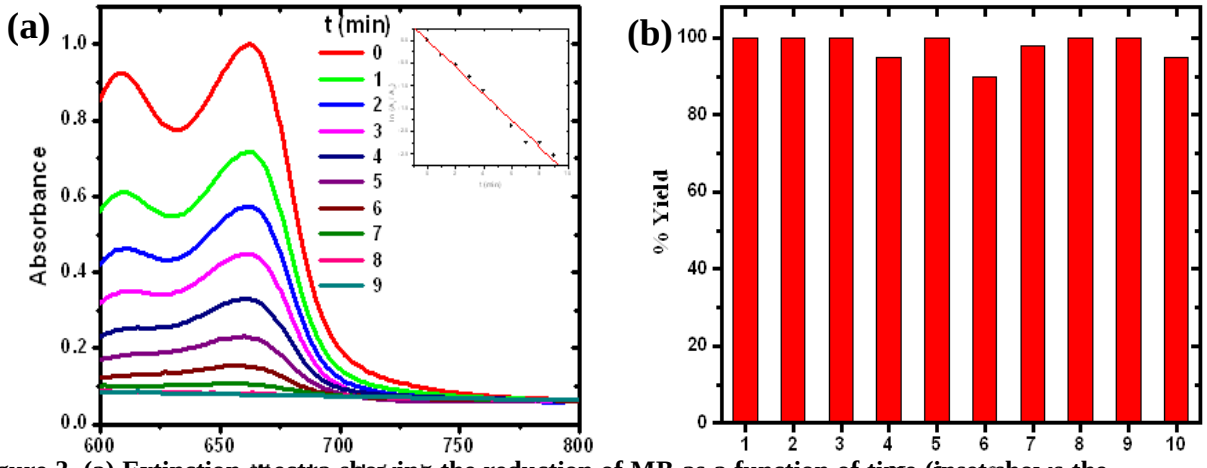


Figure 3. (a) Extinction spectra showing the reduction of MB as a function of time (inset shows the reaction to be first order) (b) percentage yield (at 12 min of reaction) in each use.

the industrially important 4-nitrophenol reduction and 4-nitrophenyl piperazine reduction reactions was also demonstrated showing the general potential of the catalyst (Fig. 3a,3b).

We have also fabricated recently, gold nanoclusters embedded in PMMA. The clusters exhibit fluorescence with a λ_{max} at 480 nm. The fluorescence of the Au cluster-PMMA films is found to be enhanced by the addition of polystyrene (PS) in the PMMA (Fig. 4a). Reason for this remains to be established. The clusters formed in the film appear to be Au_{10} as estimated from ESI mass spectrometry (Fig .4b). Computational modelling of the possible cluster geometry is under way.

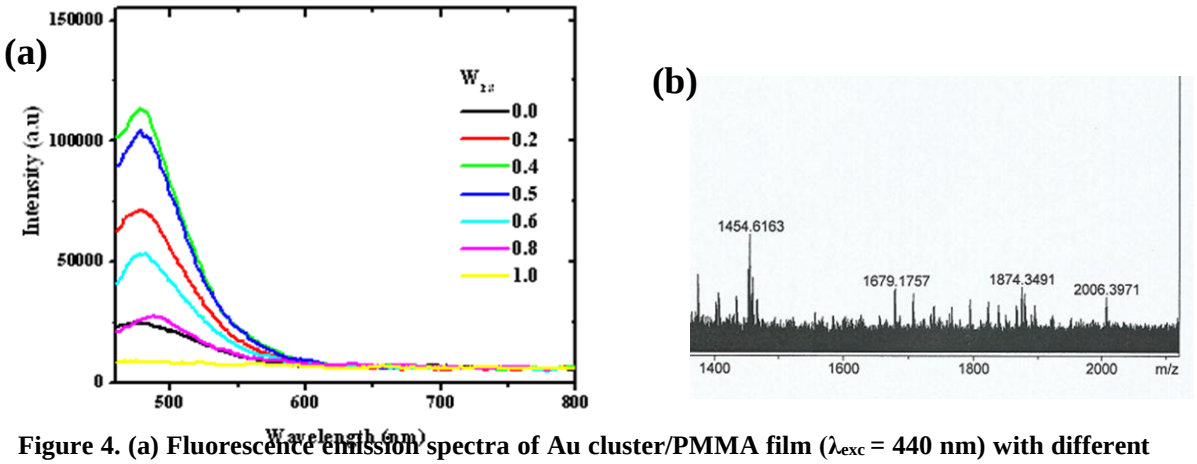


Figure 4. (a) Fluorescence emission spectra of Au cluster/PMMA film (λ_{exc} = 440 nm) with different weight % (W_{PS}) of PS; (b) ESI-Mass spectrum of Au cluster/PMMA film

Acknowledgments:

We thank the Department of Science and Technology, and the University Grants Commission (UPE and BSR program), New Delhi for financial support and the Central facility for Nanotechnology, University of Hyderabad for infrastructure support. UDM thanks the CSIR, New Delhi for a Junior Research Fellowship.

References

[1] Ramesh, G. V; Porel, S; Radhakrishnan, T. P. *Chem. Soc. Rev.* 38(2009)2646; Hariprasad, E; Radhakrishnan, T. P *Nanocomposites: In Situ Synthesis of Polymer-Embedded Nanostructures*, Eds. G. Carotenuto and L. Nicolais, New York: Wiley(2013)129.

[2] Hariprasad, E; Radhakrishnan, T. P. *Chem. Eur. J.*, 16(2010)14378.

[3] Madhuri, U. D; Rao, V. K; Hariprasad, E; Radhakrishnan, T. P. *Mater. Res. Exp.* 3(2016)045018.

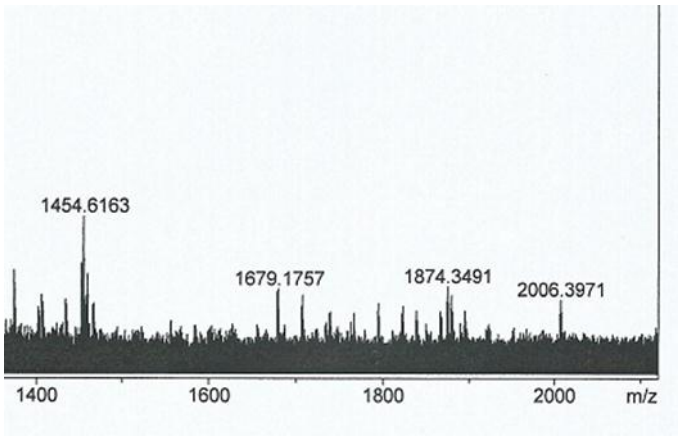
MACRO 237

Synthesis And Application of Carbon Quantum Dot Grafted Stimuli Responsive Polymer Systems.

Ball, R.; Majumdar, S.; Ghosh, T.; Basak, U.; Chatterjee, D.P.*

Department of Chemistry, Presidency University, Kolkata, India

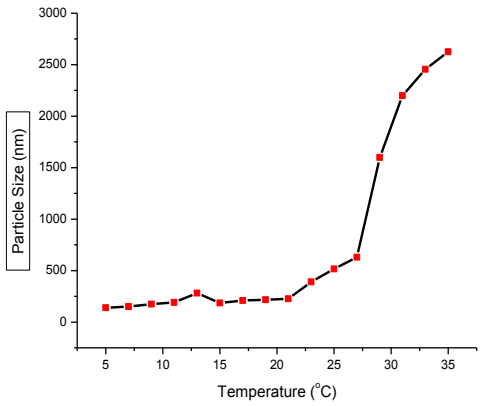
** dhruba.chem@presiuniv.ac.in*



Carbon quantum dot (CQD) has found its application in various areas like electronics, sensors, energy storage, drug delivery, bio-imaging etc. owing to its semi-conducting property, photoluminescent behaviour, large surface area, bio-compatibility and low cost of production. Carbon Nanoparticles(CNP)- Polymer composites have been extensively studied and their applications have been explored. Recent interest involves establishing method which would increase the consistency of such materials and also increase their efficiency. To do so, methods are being developed which involve covalent attachment of the polymeric chains with the CNP.

In this report we propose an economic method for the preparation of CQD from carbon soot and modification of CQD with stimuli responsive polymers[1]. The prepared CQD shows excellent dispersion stability in aqueous medium. Quantum dots having an average size of 3-5nm have been successfully prepared. The polymerisation has been carried out using the 'grafting from' approach implementing Atom transfer radical polymerisation (ATRP)[2] technique on modified CQD initiator. Such CQD-g-Stimuli responsive polymeric system shows variation in photoluminescent behaviour on application of external stimuli and can be used as molecular thermometer, pH detector or may have logic gate applications.

CQD has been prepared by nitric acid oxidation of carbon soot [3]. The prepared CQD has been modified with ethylene glycol followed by α-Bromobutanoyl bromide using simple coupling strategies to obtain the modified CQD-initiator. ATRP has been carried out with stimuli responsive polymers like Diethylene glycol methyl ether methacrylate (DEGMEM), dimethylaminoethyl methacrylate (DMAEMA) etc. using Cu^{I}/ Hexamethyltriethylenetetramine (HMTETA) and modified CQD-initiator. The crystalline nature of quantum dot has been verified from the TEM image. The covalent attachment of polymer on CQD has been confirmed by FT-IR and ^{1}H-NMR. The stimuli response of CQD-g-DEGMEM has been studied from DLS analysis and emission spectra.



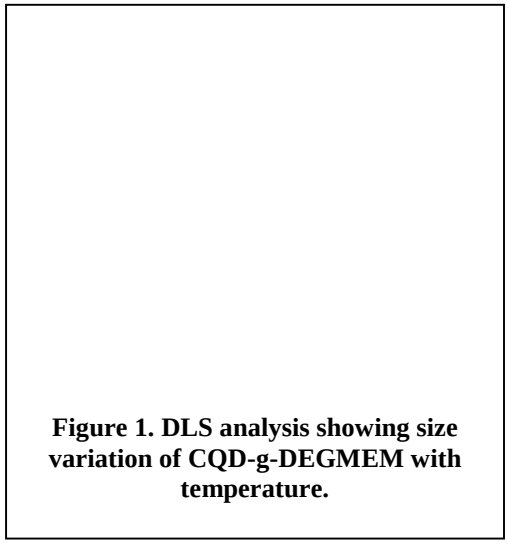


Figure 1. DLS analysis showing size variation of CQD-g-DEGMEM with temperature.

References
[1] Gibson, M.I.; O'Reilly, R.K. *Chemical Society Reviews,* 42 (2013) 7204
[2] Matyjaszewski, K.; Xia, J. *Chemical Reviews,* 101 (2001) 2921-2990.
[3] Liu, H.; Ye, T.; Mao, C. *Angew. Chem. Int. Ed.*, 46 (2007) 6473

MACRO 247

Formation of functional super-helical assemblies by constrained single heptad repeat

Sudipta Mondal[1], Lihi Adler-Abramovich[1,2], Ayala Lampel[1], Yaron Bram[1], Sophia Lipstman[3] & Ehud Gazit[1,4]

1 Department of Molecular Microbiology and Biotechnology, George S. Wise Faculty of Life Sciences, Tel Aviv University, Tel Aviv 69978, Israel.

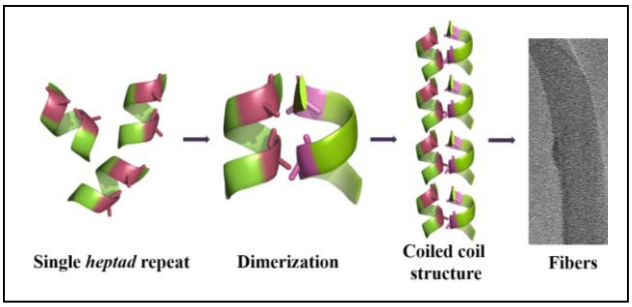
2 Department of Oral Biology, The Goldschleger School of Dental Medicine, Tel Aviv University, Tel Aviv 69978, Israel.

3 School of Chemistry, Sackler Faculty of Exact Sciences, Tel Aviv University, Tel Aviv 69978, Israel.

4 Department of Materials Science and Engineering, Iby and Aladar Fleischman Faculty of Engineering, Tel Aviv University, Tel Aviv 69978, Israel.

Abstract: Inspired by the key role of super-helical motifs in molecular self-organization, several tandem heptad repeat peptides were used as building blocks to form well-ordered supramolecular nano-assemblies. However, the need for stable helical structures limits the length of the smallest described units to three heptad repeats. Here we describe the first-ever self-assembling single heptad repeat module, based on the ability of the non-coded α-aminoisobutyric acid to stabilize very short peptides in helical conformation. A conformationally constrained peptide comprised of aromatic, but not aliphatic, residues, at the first and fourth positions formed

helical fibrillar assemblies. Single crystal X-ray analysis of the peptide demonstrates super-helical packing in which phenylalanine residues formed an 'aromatic zipper' arrangement at the molecular interface. The modification of the minimal building block with positively charged residues results in tight DNA binding ascribed to the combined factors of helicity, hydrophobicity and charge. The design of these peptides defines a new direction for assembly of super-helical nanostructures by minimal molecular elements.



References

[31] Mondal, S.; Adler-Abramovich, L.; Lampel, A.; Bram, Y.; Lipstman, S.; Gazit, E. Formation of Functional Super-Helical Assemblies by Constrained Single Heptad Repeat. Nat. Commun. 2015, 6.

MACRO 264

Fabrication of Anisotropic Self-assembled liquid Crystalline Poly (3, 3''' dialkylquarterthiophene) Films over Liquid Surface

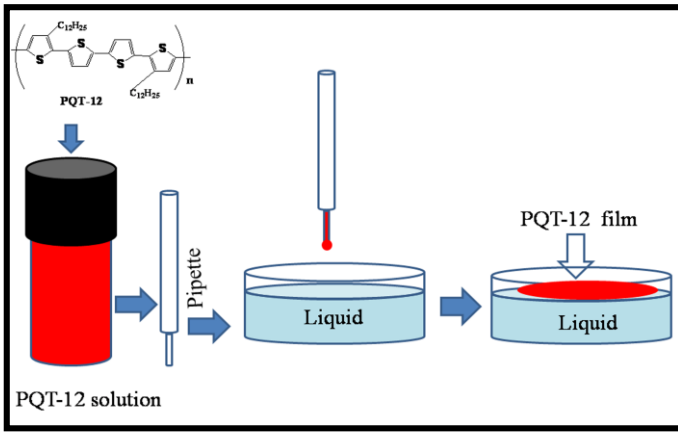
Pandey, R. K.; Mishra, R.; Prakash, R.*

School of Materials Science and Technology, Indian Institute of Technology (Banaras Hindu University), Varanasi-221005, India,
Email:richa.rs.mst14@itbhu.ac.in, rprakash.mst@iitbhu.ac.in
**Presenting author*

Abstract

Self-assembly is a process of autonomous organization of disordered components into ordered patterns and structures for high performance electronics devices. The ordered patterns and structures in π-conjugated polymer have great potential to improve the materials property significantly. Despite this, there is lack of thorough study about the dependency of self-assembly and ordered pattern on average molecular weight. Here we present the synthesis, liquid crystalline property and molecular weight dependent self-assembly property of poly (3, 3''' dialkylquarterthiophene) (PQT-12). The PQT-12 was synthesized via chemical route and different molecular weight polymers were isolated and extracted using different solvent Soxhlet extraction method [1]. Before formation of PQT-12 films, it was characterized using differential scanning

calorimetry (DSC) thermogram for investigation of thermal and liquid crystalline property [2]. The self-assembled film of PQT-12 was achieved using a facile and very new technique "floating film transfer method (FTM)" which provides air liquid interface [1]. The film properties were investigated by unpolarized and polarized light UV-Vis, AFM topography, phase imaging, Raman study and further transport property is investigated under sandwiched structure Al/PQT-12/ITO diode configuration. The polarized and unpolarized light UV-Vis. study of films reveals the dependency of spectra, its strong absorptions peak position and optical anisotropy on average molecular weight. The AFM and Raman study also reveals the dependency of morphology on average molecular weight. The average molecular weight dependent charge transport property of self-assembled PQT-12 was studied in sandwiched structure Al/PQT-12/ITO diode configuration which reveals the decrease in transport property with decrease in average molecular weight.



Schematic of Floating Film Transfer Method for PQT-12 film deposition.

References

[32] Pandey, R. K.; Takashima, W.; Nagamatsu, K.; Dauendorffer, A; Kaneto, K.; Prakash, R.; *J. Appl. Phys*. 114 (2013) 054309-1.

[33] Pandey, R. K.; Singh, A. K.; Prakash, R.; *J. Phys. Chem. C*.118 (2014) 22943.

MACRO 293

Change in Energy Transfer between Donor-Acceptor Molecules on Stimuli-Induced Disintegration/Transition of Nanostructured Assemblies Prepared from Amphiphilic Block Copolymers

Maiti, Chiranjit; Dhara, Dibakar*

Department of Chemistry
Indian Institute of Technology Kharagpur,
West Bengal 721302 India

** Email: dibakar@chem.iitkgp.ernet.in*

Stimuli-responsive amphiphilic block copolymers are attractive candidates to be investigated as delivery vehicles owing to their ability to spontaneous self-organization forming interesting micellar or vesicular nanostructures. The nanostructures can also undergo disintegration and/or transition to other structures in response to external stimuli. In this presentation, we demonstrate self-assembly of as synthesized block copolymer molecules in aqueous solution and also their disassembly or transition to other nanostructures induced by various stimuli such as temperature, pH, and reductive environment. RAFT polymerization technique was utilized for the synthesis of block copolymers with controlled molecular weight and narrow molecular weight distribution. The nanostructures of amphiphilic block copolymers were very useful for energy transfer because they provided opportunities for precise positioning of the donor and acceptor. When disintegration and/or transition of the nanostructures occurs in situ by a stimulus like temperature, reductive environment and pH, the energy transfer molecules get released and diffuse apart, reducing the energy transfer. By monitoring the energy transfer efficiency, the transition process like vesicles to micelles or micellar/vesicular swelling, and also dynamic release of the core-loaded probes to biological media can potentially be demonstrated.
In this presentation, we present the synthesis of different PEG containing temperature and pH-responsive block copolymers using RAFT technique, and also their stimuli- induced solution properties. PNIPA-*b*-PMAPTAC [1] copolymers self-assembled into vesicles in aqueous solution at physiological temperature (≥ 36 °C) as PNIPA block in the copolymer forms hydrophobic domains above the cloud point of poly(N-isopropylacrylamide) (PNIPA). These vesicles were disassembled to unimers by simply decreasing the temperature below the cloud point and thus were able to release encapsulated cargo. Fluorescence resonance energy transfer (FRET) studies between coumarin-153 (C-153, donor) and rhodamine 6G (R6G, acceptor) have been performed to probe the structural and dynamic heterogeneity of the vesicles. In another example, poly(L-Trp-HEA)-*b*-poly(PEGMA) [2] copolymer undergoes nanostructure morphological transitions in aqueous solution on changing the pH of the solution, with formation of vesicles at physiological pH and micelles at acidic pH (≤ 5.2). The vesicle-to-micelle transition resulted in selective triggered release of encapsulated hydrophilic guest molecules over hydrophobic ones. Further, these pH-responsive vesicles were successfully utilized to reduce $HAuCl_4$ and in situ synthesis of the gold nanoparticles, and this procedure was utilized to selectively stain the vesicles wall. The vesicle-to-micelle transition was followed by monitoring the energy transfer between gold nanoparticles (acceptor) and encapsulated rhodamine 6G (donor).

References

[34] Maiti, C.; Dey, D.; Mandal, S.; Dhara, D. J. Phys. Chem. B., 118 (2014) 2274.
[35] Maiti, C.; Banerjee, R.; Maiti, S.; Dhara, D. Langmuir, 31 (2015) 32.

MACRO 305

Polypeptide-Based Thermoresponsive Graft Copolymer and Their Self-Aggregation Behaviour in Solution

Bose Avijit, Jana Somdeb, Saha Anupam, Mandal Tarun Kumar*

Polymer Science unit, Indian Association for the Cultivation of Science, Jadavpur, Kolkata 700 032, India

Email : psutkm@iacs.res.in

In recent year, stimuli-responsive amphiphilic polymers have been attracted much attention because of their unique structural/conformational changes under different stimuli such as temperature, pH, light, ionic strength, redox reactions etc.[1] It is already established that graft copolymers can self-assemble into nanostructures in such solvents where solubility of its side-chains and backbone differ widely.[2] Herein, we envisage the synthesis of poly(2-ethyl-2-oxazoline)-*graft*-polytyrosine (PEtOx-*g*-PTyr) copolymer by ring-opening polymerization (ROP) of tyrosine-NCA followed by grafting of poly(2-ethyl-2-oxazoline) (prepared with cationic ROP) chains using 'click' reaction. The as-synthesized graft copolymer is well characterized by ^{1}HNMR, FTIR, MALDI-TOF MS and SEC analysis. PEtOx-*g*-PTyr shows concentration and chain length dependent lower critical solution temperature (LCST)-type reversible thermoresponsiveness in aqueous solution as shown in Fig. 1A.

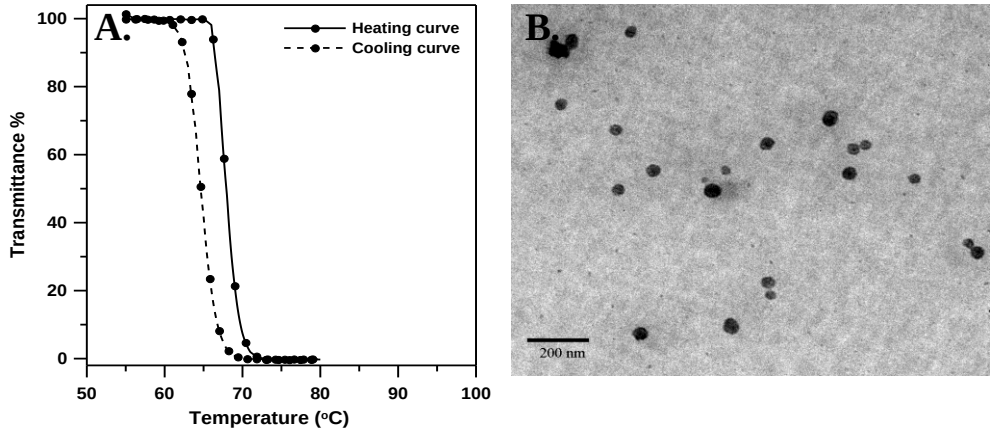


Figure. A. Turbidity measurement curve of 0.2 wt% aqueous solution of PEtOx-*g*-PTyr in UV-vis spectroscopy. **B.** TEM image of 0.2 wt% aqueous solution of PEtOx-*g*-PTyr.

Again, PEtOx-*g*-PTyr undergoes self-assembly into spherical micelles/micellar aggregates both in aqueous and in nonaqueous solution (Fig. 1B). Critical micellization concentration (CMC) of the graft copolymer in aqueous solution is determined by fluorescence technique using pyrene as probe. PEtOx-*g*-PTyr copolymer micelles undergo secondary aggregations with time and upon increasing solution temperature as examined through DLS. We encapsulate nile red into the hydrophobic core of the micelles/micellar aggregates, which remained stable even at a temperature above LCST cloud point of the copolymer. Furthermore, the extent of α-helicity conformation in PTyr backbone enhances upon grafting with PEtOx chains as analyzed by FTIR and CD spectroscopy.

Reference

[1] Huang, J.; Andreas, H.; *Chem. Soc. Rev.*, 42 (2013) 7373.

[2] Liu, C.; He, J.; Ruymbeke, E. v.; Keunings, R.; Bailly, C. *Polymer*, 47 (2006) 4461-4479.

MACRO 306

Preparation and Characterization of Shear Thickening Fluids with Surface Modified Silica Nanoparticles

Swarna[1], Pattanayek S.K[2] and Ghosh A.K[1*]

[1] Center of Polymer Science and Engineering, Indian Institute of Technology Delhi, New Delhi, India
[2] Department of Chemical Engineering, Indian Institute of Technology Delhi, New Delhi, India
Corresponding Email: anupkghosh@gmail.com

There has been an exponential growing interest in soft body armours due to increased demand for weight reduction with higher efficiency during combat [1]. Weight, flexibility, mobility, and comfort hence are prime importance to ensure its usability. The significant challenge is to provide protection under various levels of threats (stab, ballistic, fragment etc) and one such technique is to prepare soft body armours by impregnating shear thickening fluids (STF) into fabrics. STF in general consist of particles (spherical, monodisperse silica nanoparticles) suspended in a liquid medium [ethylene glycol, polyethylene glycol (PEG)] at high particle concentration [2-4]. It is a phenomenon in which the increase in shear rate/stress increases the viscosity after a threshold value. Figure 1 displays typical trend of two different STF behaviors with critical shear rate (γ_c).

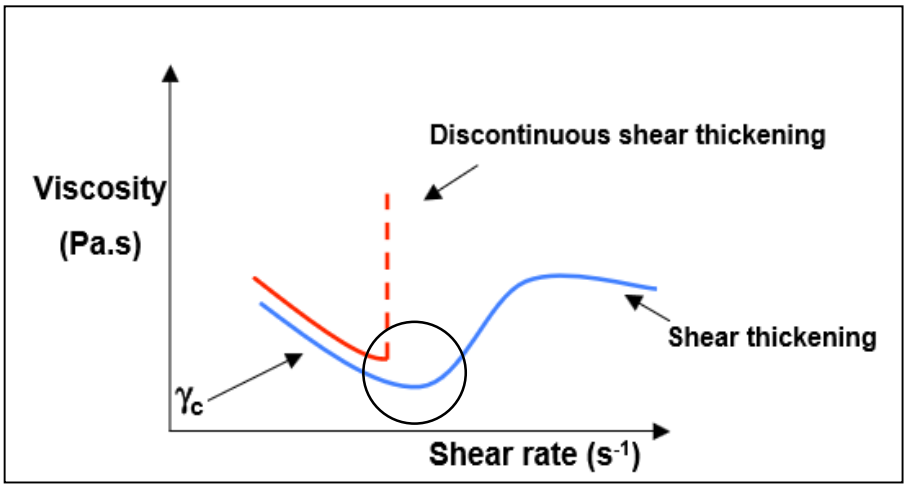


Figure 1: Viscosity vs shear rate graphs for suspension showing different types of shear thickening with critical shear rate

In the current work, we present the preparation and characterization of STF to alter the threshold value through modification of silica surface. Silica nanoparticles are surface modified with 5% of three different silanes viz.., 3-(Glycidoxypropyl)trimethoxysilane, (3-Aminopropyl)triethoxysilane (*APTES*) and trimethoxy(octyl)silane. To evaluate the extent of surface functionalization, the modified silica nanoparticles were characterized by FTIR and TGA. The STF was prepared with the hence modified silica nanoparticles in PEG 400 medium and correlated with unmodified silica. The rheological characterization (shear rate vs viscosity) exhibits a shift in the magnitude of critical shear rate for silane modified and unmodified particles. APTES based STF shifts to lower values of shear rate, but trimethoxy(octyl)silane shifts to higher values of shear rate. This is attributed to the back bonding of amine groups which in turn leads to dominant particle-particle attractions unlike the long octyl chain [5]. The dynamic rheology gives insight into the structural changes and viscoelastic behavior of STF. It provides an approximation on the stability of the suspension over a range of strain. The direct relation between the dielectric constant, capacitance and shear rate obtained by rheo-dielectric spectroscopy interpreters the structural behavior of

the suspension with respect to its stability. ESEM images show the morphology of STF indicative of the dispersive nature of silane modified and unmodified silica. Hence, the work provides a fundamental understanding on suspensions with alterations in particle-particle interactions by modifying the silica surface with different functional groups. These suspensions have a scope to be utilized in defence applications accordingly based on the rheological evaluation.

References:

1. Cavallaro P.V, "Soft body armour: An overview of materials, manufacturing, testing and ballistic impact dynamics", NUWC-NPT Technical Report 12,057, August (2011).
2. Lee Y.S, Wetzel E.D, Wagner N.J, "The ballistic impact characteristics of Kevlar woven fabrics impregnated with a colloidal shear thickening fluid" J Mater Sci 38:2825–2833 (2003).
3. Joselin R, Wilson J.W, "Investigation on Impact Strength Properties of Kevlar Fabric using Different Shear Thickening Fluid Composition," Defence Science Journal, Vol. 64, No. 3, May, pp. 236-243, (2014).
4. Egres R.G, Decker M.J, Halbach C.J, Lee Y.S, Kirkwood J.E, Kirkwood K.M, Wagner N.J, "Stab resistance of shear thickening fluid (stf)–kevlar composites for body armor applications" Proceedings for the Army Science Conference, (2005).
5. Rahul P. Bagwe, Lisa R. Hilliard, and Weihong Tan, "Surface Modification of Silica Nanoparticles to Reduce Aggregation and Nonspecific Binding" *Langmuir***,** *22,* 4357-4362,(2006).

MACRO 318

Preparation and characterization of PMMA/Cu-Cr LDH nanocomposites via melt intercalation method

Kumar Manish[a]*, Pradeep Upadhyaya [b], G. Pugazhenthi[a]

[a]*Department of Chemical Engineering, Indian Institute of Technology Guwahati, Guwahati-781039, Assam, India*

[b]*Central Institute of Plastics Engineering and Technology (CIPET), Ahmedabad 382 445, Gujarat, India*

**Manish Kumar manish.kamal@rediffmail.com*

Abstract: Layered double hydroxides (LDHs) commonly known as anionic clays, can be easily synthesized in the laboratory with high purity and tunable chemical compositions. LDHs exhibits potential advantage in flame retardant[1], capacitors[2] and medical science[3]. The aim of the current work is to investigate the influence of copper chromium (Cu-Cr) LDH on properties of PMMA nanocomposites. The Cu-Cr LDH was synthesized by co-precipitation method. PMMA nanocomposites containing LDHs content of 1-5 wt.% were fabricated by melt intercalation method using twin screw extruder. The morphological, thermal and mechanical properties of nanocomposites were evaluated by X-Ray diffraction (XRD), transmission electron microscope (TEM), thermogravimetric analysis (TGA), tensile and flexural test. The XRD results demonstrate the formation of exfoliated structure of PMMA nanocomposites. The exfoliated structure is further confirmed by TEM analysis (Figure 1). The TGA data demonstrate that the nanocomposites exhibit enhanced thermal stability with respect to pure PMMA. When 50%

weight is selected as a point of comparison, the decomposition temperature of PMMA/Cu-Cr 1%, PMMA/Cu-Cr 3%, PMMA/Cu-Cr 5% nanocomposites is found to be 26, 32 and 26 ^{o}C, respectively, higher than the neat PMMA. The PMMA/Cu-Cr 1% nanocomposites displays improved mechanical properties over compositions. The maximum improvement of tensile and flexural strength for the PMMA/Cu-Cr 1% nanocomposites over pure PMMA is estimated to be 18 and 22%, respectively.

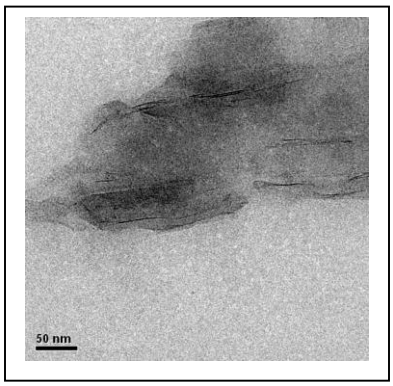


Figure 1. TEM image of PMMA/Cu-Cr 1% nanocomposites

References

[1] Hong N., Song L.; Wang B.; Stec A. A.; Hull T.R.; Zhan J.; Hu, Y. *Materials Research Bulletin*, 49 (2014) 657.

[2] Li M; Zhu J. E.; Zhang L.; Chen X.; Zhang H.; Zhang F.; Xu S.; Evans D.G. *Nanoscale*, 3 (2011) 4240.

[3]Wimalasiri Y.; Fan, R.; Zhao X. S.; Zou L.; *Electrochimica Acta*, 134 (2014) 127.

MACRO 321

Thermally Stable Poly(ether-ketone)/MWCNT Composites As An Efficient Electro-magnetic Shielding Material With Improved Mechanical Properties

Sampat Singh Chauhan,[a] Veena Choudhary [a*]

[a] Centre for Polymer Science & Engineering, Indian Institute of Technology Delhi, Hauzkhas New Delhi-110016, India

*Corresponding author email: veenac@polymers.iitd.ac.in, veenach@hotmail.com

Abstract

Poly(ether-ketone) [PEK]/multiwalled carbon nanotube [MWCNT] composites having varying amounts of MWCNTs were prepared via melt blending approach to investigate the capability of such composites as an

effective electromagnetic interference (EMI) shielding material in the frequency range of 26.5-40 GHz (K_a band). The composites were shown to exhibit up to -37 dB of shielding effectiveness (SE) at 3.2 vol% MWCNT loading. Mechanism of shielding was studied by resolving the total SE into absorption (SE_A) and reflection loss (SE_R). The correlation among complex permittivity, absorption loss, reflection loss and tan δ were also studied. The dc conductivity (σ) increased with increase in MWCNT loading with typical percolation behavior at 0.74 vol %. The effect of MWCNTs on thermal stability, mechanical properties has also been investigated. Incorporation of 3.2 vol % of MWCNTs led to enhancement in the tensile modulus (up to 5208 MPa) and tensile strength (upto 116 MPa), which were equivalent to 19% and 44% increment over neat PEK. This significant enhancement in strength and modulus attributed to reinforcement effect. Thermogravimetric analysis showed improvement in thermal stability of matrix by addition of MWCNTs. The overall mechanical, thermal and electrical performance and light weight of these versatile nanocomposites materials make them suitable for high strength, thermally stable EMI shielding application.

Key words: Absorption loss, Complex permittivity, Electrical conductivity, Electromagnetic interference, Mechanical properties

MACRO 325

Development of Methylcellulose Based Nanocomposites and their Application Possibilities

Pramanik, Dibyendu, Saha, Nayan Ranjan, Chattopadhyay, Dipankar*

Department of Polymer Sc. & Tech., University of Calcutta, 92, A.P.C. Road, Kolkata 700009, India
E mail: dipankar.chattopadhyay@gmail.com

In recent years, with increasing population and urbanization, the use of petroleum based non-biodegradable polymers have been drastically increased and coincidentally, it increases the percentage of non-biodegradable material in solid waste. Hence, polymer scientists are trying to replace non-biodegradable polymers with biodegradable polymers. Again, biodegradable polymers from renewable resources have some disadvantages over the non-biodegradable polymers in some properties like mechanical, water resistance, barrier and also in thermal properties. So, to replace the non-biodegradable polymers with biodegradable polymers, an improvement in properties is required. Researchers have proposed various routes in improving the properties of biodegradable polymers, including the blending of biodegradable polymers with synthetic or with natural polymers [1,2] or by incorporating nanofillers such as various types of layered silicate [3], mica flakes [4] and also by inter and intra molecular crosslinking [5].

Methylcellulose (MC)/Pectin (PEC) films were prepared with different ratios of MC and PEC where MC/PEC (90:10) (MP_{10}) gave the best results in terms of mechanical properties. Sodium momtmorillonite (MMT) (1, 3 & 5 wt %) was incorporated in the MP_{10} matrix. X-ray diffraction and transmission electron microscopy have been performed to characterize the films and it showed the nanocomposites were intercalated in nature. In mechanical studies, it is observed

that 3 wt% MMT loaded nanocomposite ($MP_{10}M_3$) gave best results in terms mechanical properties. Besides, thermo-gravimetric and dynamic mechanical analysis proved that decomposition and glass transition temperature is increased with increasing MMT concentration from 1 to 5 wt%. It was also observed that moisture absorption and water vapour permeability studies gave best results in the case of 3 wt% MMT. Optical clarity of the nanocomposite films was not much affected with loading of MMT. *In vitro* drug release studies showed that MC/PEC/MMT based films can be used for controlled transdermal drug delivery applications.

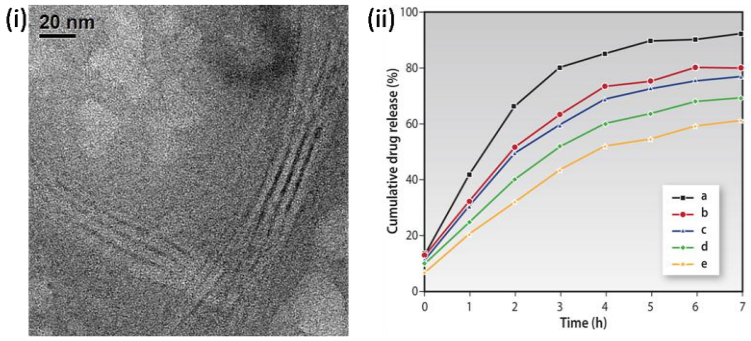


Figure 1. (i) TEM images of nanocomposites and (ii) cumulative drug release pattern of drug loaded film of (a) pure MC, (b) MP_{10}, (c) $MP_{10}M_1$, (d) $MP_{10}M_3$ & (e) $MP_{10}M_5$

References

[36] Arvanitoyannis, I., Biliaderis, C. G., Ogawa, H., & Kawasaki, N. *Carbohydrate Polymers*, 36(2) (1998) 89.
[37] Bhattacharya, M. *Journal of Materials Science*, 33(16) (1998) 4131.
[38] Tang, X., & Alavi, S. *Journal of Agricultural and Food Chemistry*, 60(8) (2012) 1954.
[39] Alves, V. D., Costa, N., & Coelhoso, I. M. *Carbohydrate Polymers*, 79(2) (2010) 269.
[40] Simkovic, I., Laszlo, J. A., & Thompson, A. R. *Carbohydrate Polymers*, 30(1) (1996)

MACRO 331

Polymer Supported Large Area Periodic Silver Nanostructures as an Efficient SERS Platform

V. Raji[a, b], RenyThankam Thomas[a], Nabeela Kallayi[a, b], Saju Pillai [a, b]*

[a]*CSIR-National Institute for Interdisciplinary Science and Technology (NIIST), Pappanamcode, Thiruvananthapuram, Kerala-695 019, India*

[b]*Academy of Scientific and Innovative Research (AcSIR), New Delhi-110 001, India*

pillai_saju@niist.res.in

Well-organized periodic array of noble metal nanoparticles over a large area have proved to be an excellent SERS substrate for sensing applications, which is based on electromagnetic field effects aroused due to localized surface plasmon resonance[1]. Herein, we presented the formation of ordered 2D porous polymer

films of different pore sizes over large area using breath figure (BF) method. Pore size and its distribution were controlled by optimizing various parameters like polymer concentration, humidity, substrate, solvent, etc. Later, silver nanoparticles (AgNPs) of different sizes and shapes were synthesized on patterned polymeric porous films. The morphology of Ag was tuned by controlling synthesis parameters such as time and reducing agents. AgNPs were synthesized by in-situ reduction of Ag^{+} on polymeric porous film. Further, shape-tuned AgNPs decorated periodic surfaces showed improved SERS signals. Our polymer template-directed synthetic approach is a facile and cost-effective method to prepare periodic AgNPs decorated surfaces over large area.

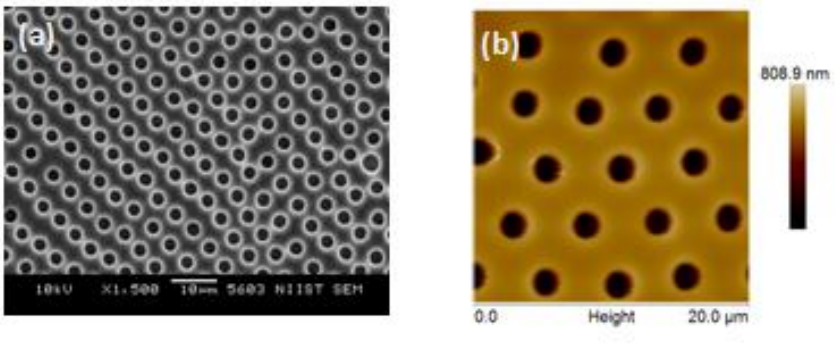


Fig (a) SEM micrograph and (b) AFM image of patterned polystyrene porous film.

References

[1] Nurmawati, M. H.; Ajikumar, P. K.; Renu, R.; Valiyaveettil, S. Adv. Funct. Mater, 18 (2008) 3213.

[2] Hernández-Guerrero, M ; Stenzel, M.H. *Polymer Chemistry*,3 (2012) 563.

MACRO 334

Supramolecular Synthons in Designing Gelators Derived from Multiple Drugs

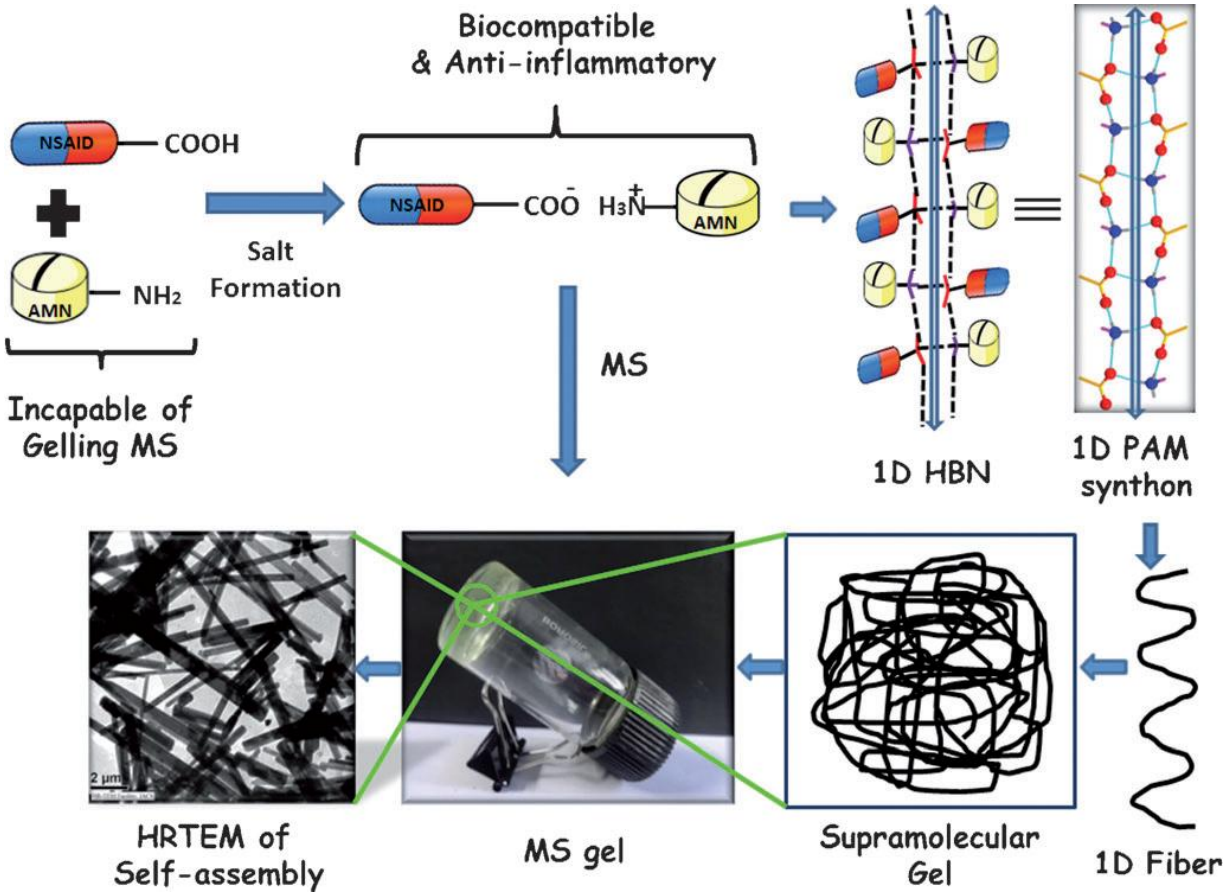
Roy, R.,[a] Deb, J.,[b] Jana, S. S.,[b]* Dastidar, P.[a]*

[a] *Department of Organic Chemistry, Indian Association for the Cultivation of Science (IACS), Kolkata*

[b] *Department of Organic Chemistry, Indian Association for the Cultivation of Science (IACS), Kolkata*

** ocpd@iacs.res.in*

Supramolecular gels formed by self-assembly of small molecules having a molecular weight of less than 3000 are generally known as Low Molecular Weight Gelators (LMWGs).[1] Gelator molecules self-assemble to form a 1D network that promotes growth of 1D fibers with high aspect ratio. These fibers were entangled to form self-assembled fibrillar networks (SAFiNs)[2] by various noncovalent interactions within which the solvent molecules are immobilized to form a gel. A simple strategy for



designing salt-based supramolecular gelators

Scheme 1: Schematic representation of the design of the salt-based supramolecular gel for plausible biomedical applications.

comprised of various non-steroidal anti-inflammatory drugs (NSAIDs) and amantadine (AMN) (an antiviral drug) has been demonstrated using a supramolecular synthon approach. Single-crystal and powder Xray diffraction proved the existence of the well-studied gel-forming 1D supramolecular synthon, namely, primary ammonium monocarboxylate (PAM) synthon in all the salts. Remarkably five out of six salts were found to be capable of gelling methyl salicylate which is an important ingredient in commercially available topical gels. One such selected biocompatible salt displayed an anti-inflammatory response in prostaglandin E2 (PGE2) assay, thereby indicating their plausible biomedical applications.[3]

References

[41] a) Weiss, R. G.; Terech, P. in Molecular Gels: Materials with Self-Assembled Fibrillar Networks, Springer, Dordrecht, **2006**; b) Steed, J. W. *Chem. Soc. Rev.* **2010**, *39*, 3686– 3699; c) Terech, P.; Weiss, R. G. *Chem. Rev.* **1997**, *97*, 3133 –3160.

[42] M. George, R. G. Weiss, *Acc. Chem. Res.* **2006**, *39*, 489– 497.

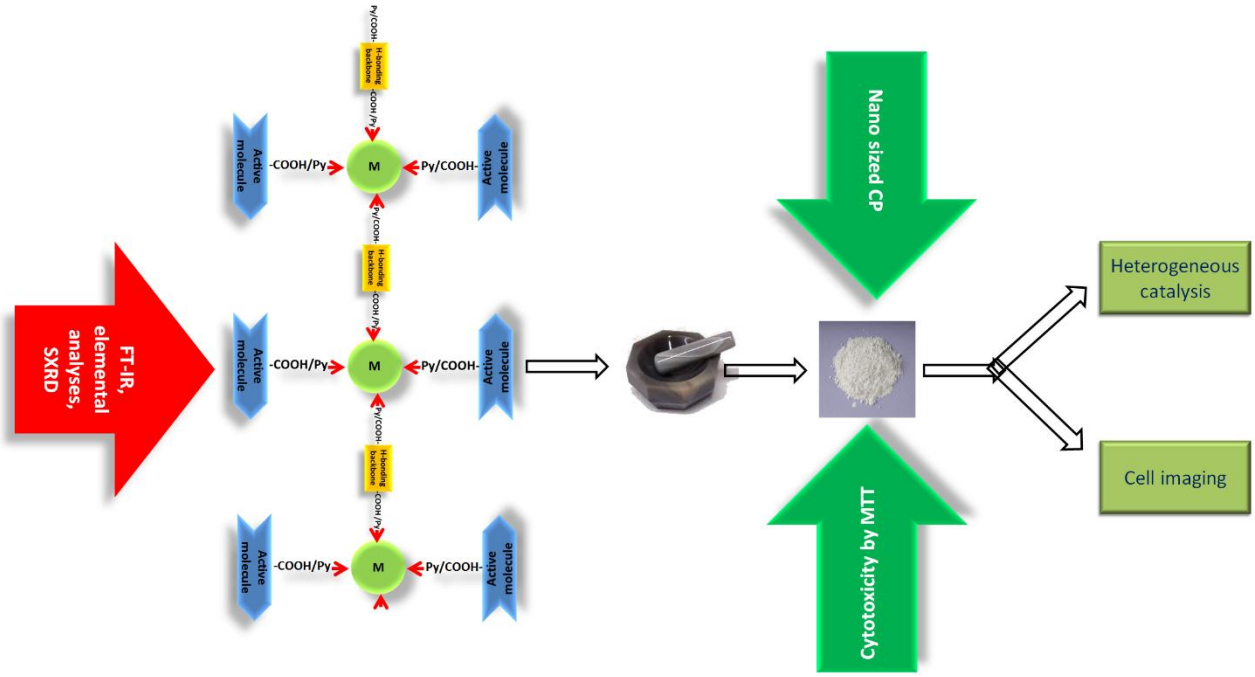
[43] Roy, R.; Deb, J.; Jana, S. S.; Dastidar, P. *Chem. Eur. J.* **2014**, *20*, 15320 – 15324.

MACRO 337

Nano-sized Coordination Polymers for Cell Imaging and Heterogeneous Catalysis

Sarkar, K.;[a] Dastidar, P.[a]*
[a] *Department of Organic Chemistry, Indian Association for the Cultivation of Science (IACS), Kolkata*
* *ocpd@iacs.res.in*

A series of Mn^{II} based coordination polymers[1] (CPs), namely, **CP1** $\{[Mn(\mu\text{-dpa})(\mu\text{-4,4′-bp})]\cdot MeOH\}_\alpha$, **CP2** $\{[Mn_3(\mu\text{-dpa})_3(2,2'\text{-bp})_2]\}_\alpha$, **CP3** $\{[Mn_3(\mu\text{-dpa})_3(1,10\text{-phen})_2]\cdot 2H_2O\}_\alpha$, **CP4** $\{[Mn(\mu\text{-dpa})(\mu\text{-4,4′-bpe})_{1.5}]\cdot H_2O\}_\alpha$, **CP5** $\{[Mn_2(\mu\text{-dpa})_2(\mu\text{-4,4′-bpe})_2]\cdot ½DEF\}_\alpha$ and **CP6** $\{[Mn(\mu\text{-dpa})(\mu\text{-4,4′-bpe})_{1.5}]\cdot ½DMA\}_\alpha$ have been synthesized and characterized by Single crystal X-ray diffraction (SXRD), FT-IR, elemental analysis, and thermogravimetry. Majority of the CPs exhibit a four connected sql-topology while **CP4** and **CP6** exhibit a two dimensional SnS network architecture, which further entangled in polycatenation mode. Two of the coordination polymers (namely, **CP2** and **CP4**) reported herein, are serendipitously chosen and scaled down to nanoregime for pursuing live cell imaging.[2] DLS, FEG-TEM analysis confirmed the nano dimensionality of these CPs. Remarkably, the nano sized CPs showed green fluorescene under fluorescence



Scheme 1: Synthesis of nano sized CPs for cell imaging and catalysis.

microscope when excited with blue light. MTT assay confirms the biocompatibility of these compounds. In vitro studies by using macrophage cell line (i.e., RAW 264.7) labeled with **CP2** and **CP4** revealed its potential applications as a biological fluorescent probe.**CP1** heterogenously catalyzes cyanosilylation reaction facilitated by an open channel in the structure.[3]

References

[44] a) Hoskins, B. F.; Robson, R. *J. Am. Chem. Soc.* **1989**, *111*, 5962−5964; b) Furukawa, H.; Ko, N.; Go, Y. B.; Aratani, N.; Choi, S. B.; Choi, E.; Yazaydin, A. O.; Snurr, R. Q.; O'Keeffe, M.; Kim, J.; Yaghi, O. M. *Science* **2010**, *329*, 424−428; c) Zhang, S.-Y.; Zhang, Z.; Zaworotko, M. J. *Chem. Commun.* **2013**, *49*, 9700–9703.

[45] Della Rocca, J.; Liu, D.; Lin, W. *Acc. Chem. Res.* **2011**, *44*, 957-968.

[46] Horike, S.; Dinca, M.; Tamaki, K.; Long, J. R. *J. Am. Chem. Soc.* **2008**, *130*, 5854–5855.

MACRO 342

Production of Multiwalled Carbon Nanotubes from PongamiaOil Using Chemical Vapour Deposition Method and Preparation of Polymer Nanocomposites By Using CNTs

Bagotia N.[a*], *Choudhary V.*[b], *Sharma D. K.* [a]

[a]*Centre for Energy Studies, Indian Institute of Technology Delhi, New Delhi, India.*
[b]*Centre for Polymer Science & Technology, Indian Institute of Technology Delhi, New Delhi, India.*

**nshnnl46@gmail.com*

Abstract

Carbon nanotubes has been synthesized by different methods and different precursors. Here, we synthesizedMultiwalled carbon nanotubes (MWCNT) are from pongamia seed oil (non-edible) by using chemical vapour deposition method. These MWCNTs are characterized by scanning electron microscopy, transmission electron microscopy, Raman spectra, X-ray diffraction and Energy-dispersive X-ray spectroscopy. Carbon nanotubes (CNTs) have attracted the attention of researchers in the field of polymer nanocomposites[1-3], since they were reported by Iijhima in 1991[4] due to their extra ordinary properties such as mechanical properties (elastic modulus ~ 1TPa), electrical conductivity (10_4 –10_6 S/cm) and thermal conductivity (3000–6000 W/mK)[9]. These synthesized MWCNTs used as nanofiller in production of polystyrene/MWCNT (PS/MWCNT) nanocomposites with different loading of MWCNTs. Nanocomposites are prepared by solution mixing. The nanocomposites were characterized by morphological studies, Raman spectra and X-ray diffraction. Electrical conductivity and EMI shielding of PS/MWCNT nanocomposites also studied. Better electrical and EMI shielding obtained at lower loading of MWCNTs in PS.

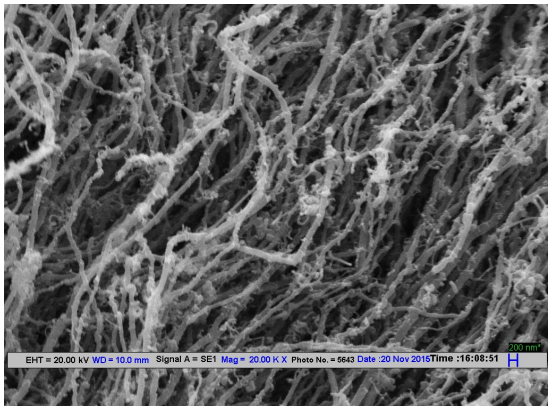


Fig. 4 SEM image of MWCNT from Pongamia seed oil

Reference:

[1] Moniruzzaman, M.; Winey, K. I. *Macromolecules*, 39 (2006) 5194-5205.

[2] Lu, X.; Zhang, W.; Wang, C.; Wen, T. C.; Wei, Y. *Progress in Polymer Science*, 36(2011) 671-712.

[3] Bilge, K.; Ozden-Yenigun, E.; Simsek, E.; Menceloglu, Y. Z.; Papila, M. *Composites Science and Technology*, 72 (2012) 1639-1645.

[4] Iijima, S.*nature*, 354(1991) 56-58.

MACRO 352

Mechanically Strong Self-healing Acrylic Copolymers

MirchandaniGirish[a,b]*, Singha Nikhil K.[a]

[a]Rubber Technology Centre, Indian Institute of Technology, Kharagpur, 721302, India

[b] Research & Technology Center, Asian Paints, Navi Mumbai, 400703, India

girish.mirchandani@asianpaints.com

The supramolecularroute to prepare self-healing polymers offers a facile approach towards achieving repeatable self-healing properties. A combination of supramolecular (ionic interactions, H bonding) and covalent bonding is used to prepare mechanically strong self-healing polymers.Functional acrylic copolymersprepared by random free radical polymerization are blended to prepare polymers which display repeatable healing. The effect of varying Tg, molecular weight and crosslinking density on the self-healing properties is studied. The polymers are characterized using FTIR, GPC, DSC and DMA. Rheological properties of the polymer blends have been studied. The repeatability of the healing is studied under

different conditions of temperature and humidity. A mechanically strong self healing polymer is obtained which can be recycled.

References

[1] F. Herbst, D. Döhler, P. Michael and W. H. Binder, *Macromol. Rapid Commun.*, 34 (2013) 203.

[2]P. Cordier, F. Tournilhac, C. Soulié-Ziakovic and L. Leibler, *Nature*, 451 (2008) 977.

[3] A. Das, A. Sallat, M. Suckow, D. Basu, B. Voit and G. Heinrich, *ACS Appl. Mater. Interfaces*, 7 (2015) 20623.

[4] M. A. Aboudzadeh, M. E. Muñoz, A. Santamaría, R. Marcilla and D. Mecerreyes, *Macromol. Rapid Commun.*, 33 (2012) 314.

[5] T. Aida, E. W. Meijer and S. I. Stupp, *Science*, 335 (2012) 813.

[6] D. Döhler, H. Peterlik and W. H. Binder, *Polymer*, 69 (2015) 264.

MACRO 354

Effect of Functionalised Graphene on Sulfonated poly(ether ether ketone) Membrane

Ghosh Priyanka[a], Ganguly Saibal[b], Banerjee Dipali[c], Kargupta Kajari[a*],

[a]*Chemical Engineering Department, Jadavpur University, Kolkata, India*

[b]*Chemical Engineering Department, BITS PILANI, Goa Campus, India*

[c]*Department of Physics, Indian Institute of Engineering Science and Technology (I.I.E.S.T), Shibpur, West Bengal, India*

* *e-mail id: karguptakajari2011@gmail.com*

Abstract

Sulfonated graphene (SG) nanocomposited Sulfonated poly(ether ether ketone (SPEEK) membrane is synthesized and characterized. The water uptake, acid uptake, proton conductivity are measured. The SG-SPEEK composite membrane gives better properties than the pristine SPEEK. The membrane runs well below 100^0C and it is a good candidate to serve well as proton exchange membrane for low temperature polymer electrolyte membrane fuel cell.

Keywords: *Sulfonated poly(ether ether ketone (SPEEK); Graphene; polymer electrolyte membrane fuel cells (PEMFC)*

Introduction

In recent days, polymer electrolyte membrane fuel cells (PEMFC) are one of the attractive and environment friendly alternative energy resources. The main part of a PEMFC is its membrane electrode assembly (MEA). Depending on the membrane's thermal stability it can be used for low temperature and high temperature range. A good membrane for PEMFC must possess good proton conductivity. For low temperature PEMFC ($<100^0$C), the most commercially used membrane till now is nafion. But it is very costly and shows very low proton conductivity, whereas, sulfonated poly(ether ether ketone) (SPEEK) is an inexpensive polymer electrolyte having very good mechanical property, thermal stability and chemical innernesss[1]. But low adsorption of water and acid limits its use upto low temperature range ($<100^0$C). Incorporation of the inorganic nanoparticles generally enhances the conductivity, chemical selectivity, thermal and mechanical stability, catalytic and optical activity of the organic polymer[2]. Generally, very small amount of inorganic nanoparticles are dispersed as fillers into the organic polymer matrices.

Graphene is a super material having sheet like 2-dimensional sp^2 networks of carbon. In addition to the high surface area and very light weight features, it has very good electrical conductivity, mechanical property, thermal stability and chemical selectivity[3]. It has immense potential to be used in different fields. Functionalisation extends the application of graphene. Sulfonation of graphene gives better property and wide range of applicability as inorganic fillers.



Figure 1. Image of SG-SPEEK membrane

Experimental

Graphene oxide is prepared by modified Hummers method[4] and reduced by hydrazine hydrate. Sulfonated graphene (SG) is synthesized by diazotising sulfanilic acid and by reacting it with reduced graphene. SPEEK is synthesized by sulfonating commercially available poly(ether ether ketone) (PEEK). The composite membrane is fabricated by simple conventional solution
casting method using N,N-dimethylacetamide (DMAc) as solvent.

Results and discussion

Sulfonated graphene (SG) is nanocomposited with SPEEK polymer. The membranes and SG are structurally confirmed by FTIR and Raman respectively. Membrane morphology is checked by SEM. The thermogravimetric analysis reveals enhancement of thermal stability of the SG-SPEEK membrane over the pristine SPEEK membrane. Several properties like water uptake, acid uptake, ion exchange, proton conductivities enhances with incorporation of SG into SPEEK.

Conclusions

SG-SPEEK nanocomposite membrane shows better properties than the pristine SPEEK membrane. The membrane works well below 100^0C, after that it starts to degrade. This low cost, easily producible SG-SPEEK can be a good alternative as electrolyte of the low temperature range PEMFC.

Acknowledgements

The financial assistance from Department Science & Technology (DST), India University Grants Commission (UGC), India and is gratefully acknowledged.

References

9. H. Wu, X. Shen, T. Xu, W. Hou, Z. Jiang. *J. Power Sources*, 213, 83–92, 2012.
10. A. Sacc`a, I. Gatto, A. Carbone, R. Pedicini, E. Passalacqua, *J. Power Sources*, 163, 47–51, 2006.
11. Wang L, Wang D, Zhang S, Tian H, *Catal. Sci. Technol*, 3, 1194, 2013.

4. W. S. Hummers Jr and R. E. Offeman, J. Am. Chem. Soc., 80, 1339, 1958.

MACRO 357

Ferrocene Functionalized HTPB based Segmented Polyurethanes through Supramolecular Interactions.

Billa Narasimha Rao and Tushar Jana*

School of Chemistry and ACRHEM, University of Hyderabad, Hyderabad, India.
Email: tusharjana@uohyd.ac.in

We studied non-chain extended, non-hydrogen bonding micro phase separation/segmentation in-to nano hard segment domains (HSDs) in the soft segment and their aggregation in case of ferrocene functionalized hydroxyl terminated polybutadiene diol (F-

HTPB). Electrostatic interactions, may be due to metal ion and/or π-interactions, playing vital role in microphase organization in the absence of hydrogen bonding. Ferrocene moiety was used as a key for tuning electrostatic forces which in turn alter the degree of phase separation (segmentation) and hence in tailor the properties. F-HTPB, was polymerized with isophorone diisocyanate and the resulting PUs were further cured at 70 °C for 5 days to prepare the free-standing elastic PU films. An in-depth small angle X-ray scattering study along with dynamic mechanical analysis (DMA) and field emission-scanning electronic microscopy (FE-SEM) revealed the strong microphase separation/segmentation into nano HSD and their aggregation. Thorough spectroscopic studies (FT-IR and ^{13}C CP-MAS NMR) of PU films confirmed that the hydrogen bonding interactions between urethane bonds in the PU matrix were disturbed by ferrocene substituents and the presence of favourable electrostatic interactions due to the presence of ferrocene moiety. All the properties like micro HSD size, tensile strength, aggregation induced emission (AIE) intensity and room temperature shape memory effect (SME) are proportional to the ferrocene (iron) content. This dependancy confirming that the ferrocene substituents are responsible for nano HSD aggregation into micro HSD. Another important part of the work is burning rate studies of these terminally ferrocene functionalized HTPB based propellants. We achieved 125% enhancement in burning rate compared to pristine HTPB propellant with lowest viscosity and high loading capacity (86% at RT).

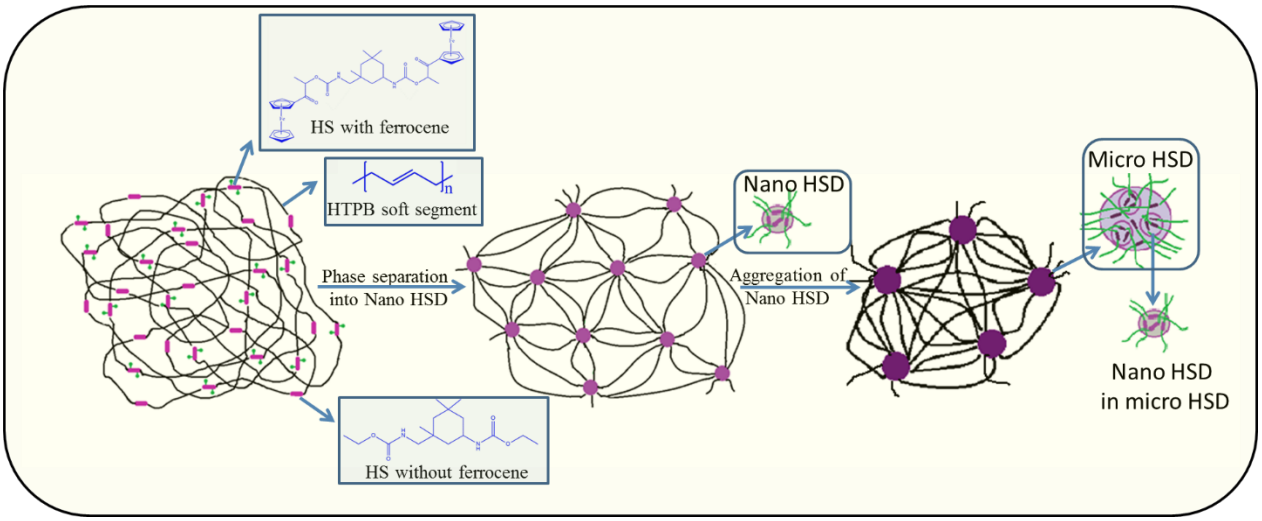


Figure 1. Graphical representation of micro phase separation/segmentation into Nano HSDs in the soft segment and their aggregation into micro HSD.

References

[47] Swanson, J. P.; Rozvadovsky, S.; Seppala, J. E.; Mackay, M. E.; Jensen, R. E.; Costanzo, P. J. *Macromolecules*, 43 (2010) 6135.

[48] Lu, Y.; Larock, R. C. *Biomacromolecules*, 9 (2008) 3332.

[49] Yilgor, I.; Yilgor, E. *Polymer Rev.* 47 (2007) 487.

[50] Kassaee, M. Z.; Heydari, H.; Hattami, M.; Fazli Nia A. *Macromolecules*, 36 (2003) 6773.

[51] Rao, B. N.; Yadav, P. J. P.; Malkappa, K.; Jana, T.; Sastry, P. U. *Polymer*, 77 (2015) 323.

[52] Rao, B. N.; Malkappa, K.; Jana, T.; Sastry, P. U.; Kumar, N.; Ramakrishna, P. A. *(Manuscript under preparation).*

MACRO 374

Surface Wettability Behaviour of Functionalized-Gum Arabic Dispersed Poly (lactic acid) Bionanocomposite Foams

Borkotoky, Shasanka Sekhar[a] and Katiyar, Vimal[a,*]

[a]*Department of Chemical Engineering, Indian Institute of Technology Guwahati, Guwahati, Assam, India 781039*

**E-mail: vkatiyar@iitg.ernet.in*

ABSTRACT

The detrimental effect in environment caused by the non-degraded petro-based polymeric foams, the study of biodegradable polymers now a major area in research. In the biodegradable foams, poly (lactic acid) foams has a promising potential to replace the conventional petro-based non-degradable foams like polystyrene foams. Poly (lactic acid) is a bio-based, bio-degradable and bio-compatible material which has a wide potential in bio-medical applications such as drug delivery, tissue engineering etc. Various properties of poly (lactic acids) can be tuned by the addition of nano bio-fillers to the desirable level and also to make it bio-medically viable [1].

In the current investigations, we have fabricated biodegradable PLA foams having unique surface characteristics for either of the surfaces and wettability and surface properties have been investigated in this report. One surface of the fabricated foam is having hydrophilic nature and the other side is having hydrophobic nature. This hydrophilicity is very much useful in applications where the surface needs to be in contact with the environment like in drug delivery, bio medical applications [2]. In this study, Gum Arabic (GA) bio fillers have been used to tune the surface properties at different loadings. Characterization techniques like differential scanning calorimeter (DSC) and thermo-gravimetric analysis (TGA) were used to find the thermal properties and stability of the fabricated foams in relation with dispersed GA. Density measurements were carried out to investigate the effect of bio fillers towards tuning of the foam density. Contact angle analysis and field emission scanning electron microscopy (FESEM) has been employed to understand the wettability behavior and morphological investigations of prepared foams. The results suggest that the loading of GA affects the surface

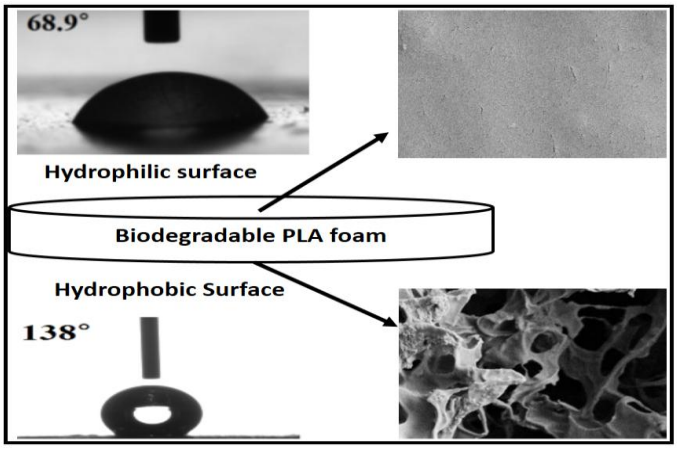


Figure 1. Graphical representation of the biodegradable foam

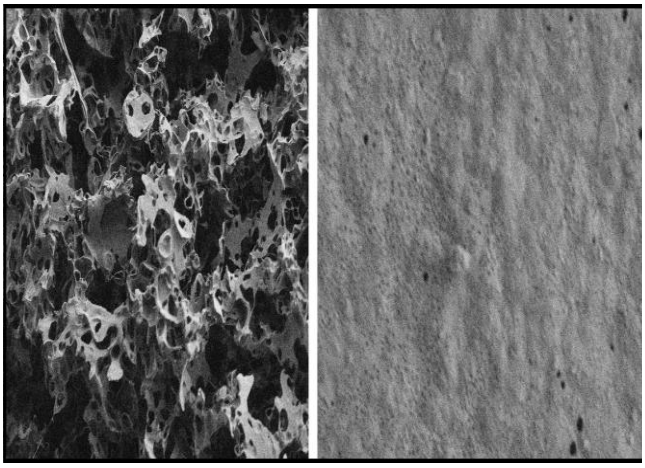


Figure 2. FESEM images of rough and smooth surface of the biodegradable PLA foam.

morphology and wettability of the fabricated foams. Figure 1-3 suggest the change in the wettability behavior of either side of the foamed surfaces. Detailed investigations will be discussed during presentation.

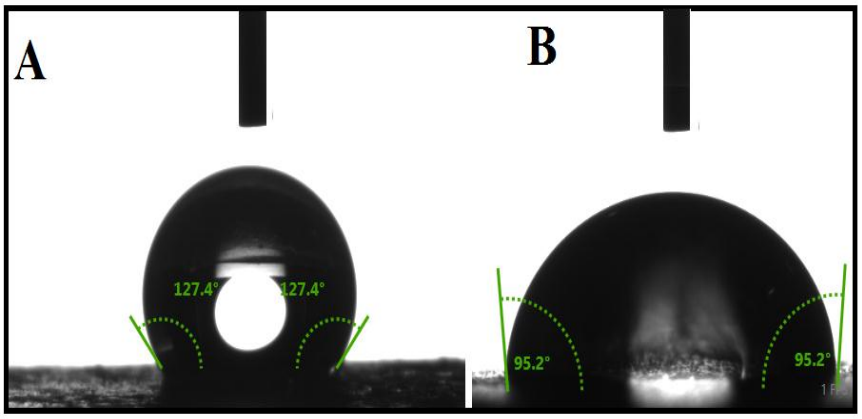


Figure 3. Contact angle of A) PLA/GA (1%) foam (rough) B) PLA/GA (1%) foam (smooth)

Acknowledgement

Authors are thankful to the Central Instrument Facility (CIF), IIT Guwahati for helping to perform FESEM analysis. Authors sincerely thank the Department of Chemicals & Petrochemicals, Ministry of Chemicals and Fertilizers, Government of India - funded Center of Excellence for Sustain-able Polymers at IIT Guwahati for research facilities to per-form this current research work. XRD used in this work was financially supported by a FIST grant (SR/FST/ETII-028/2010) from Department of Science and Technology (DST), Government of India.

References

[53] Dhar, P.; Tarafder, D.; Kumar, A.; Katiyar, V. *RSC Adv.*, 5(2015), 60426.
[54] Tripathi, N.; Katiyar, V. *J. Appl. Polym. Sci.* 133 (2016), 43458.

MACRO 377

PHBV Blends: Comparative Studies of Films and Nanofibers

Bhagyashri S. Thorat Gadgil and Dr. GVN Rathna[a]*

Polymer science and engineering division, CSIR- National chemical laboratory, Pune, 411008. INDIA.

*email- rv.gundloori@ncl.res.in

Nanotechnology emerges in the scientific field proving its advantages in many aspects like increased effectiveness, lower requirements, and tunable properties over the material in bulk. Nanomaterials showed some unimaginable changes in their properties of the same material on nanocscalelike different optical, mechanical, catalytic and biological activities mostly owing to its high surface area is to volume ratio.[1] In almost every area of science nanotechnology opens a new dimension, so as in polymer sciences. Polymeric materials in various nanoforms like nanoparticles, nanofibers, etc. are well studied. A new range of biopolymers, polyhydroxyalkanoates, are well known for their biocompatibility and biodegradability.[2] Polyhydroxybutyrate-co-valerate (PHBV) is a copolymer studied the most for its biological applications like tissue engineering, drug delivery vehicles, implant coating etc. PHBV showed good mechanical and permeability properties which is comparable to polyethylene and polypropylenes. But PHBV is highly hydrophobic and brittle therefore, hinders its unleashed use in bio-based applications.[3] To improve these properties PHBVs are blended with some other suitable polymers to get required level of hydrophilicity and elasticity.[4] Keeping its biological uses in mind we developed the blends of PHBV with PEO and PEGDA balancing its hydrophilicity and elasticity. These blends were fabricated in the form of films in various compositions as shown in Table 1 and evaluated their different properties. The same compositions was electrospun into nanofiber mats. The hydrophilicity of the implants were studied using contact angle measurements. Nonwoven electrospun nanofiber mat was comparatively studied against the films with respect to their mechanical and thermal properties using differential scanning calorimetry (DSC) and thermal gravimetric analysis (TGA). Thermal properties of blends were not changed in both film and nanofiber form. Unlike nanofibers, films were mechanically stronger but brittle retaining similar properties of its parent polymers. X ray Diffraction (XRD) studies showed no change in crystalline property of the material and furrier transform infrared spectroscopy (FTIR) studies proved the individual identity of polymers in blends for both film and nanofiber forms. The blends were used as coating material on PDMS implants to evaluate their biocompatibility. Wide range antibiotic metronidazole was incorporated in these blends to check its release profile and effectiveness. The cell viability and biocompatibility of the films were done using 3T3 fibroblast cells and macrophages respectively. Nanofibers were found more effective in release profile, cell viability, biocompatibility and antibacterial activity.

Table 1. Various compositions of blends in weight percent

PEGDA	PEO	PHBV
1	1	8
2	1	7
3	1	6
4	1	5

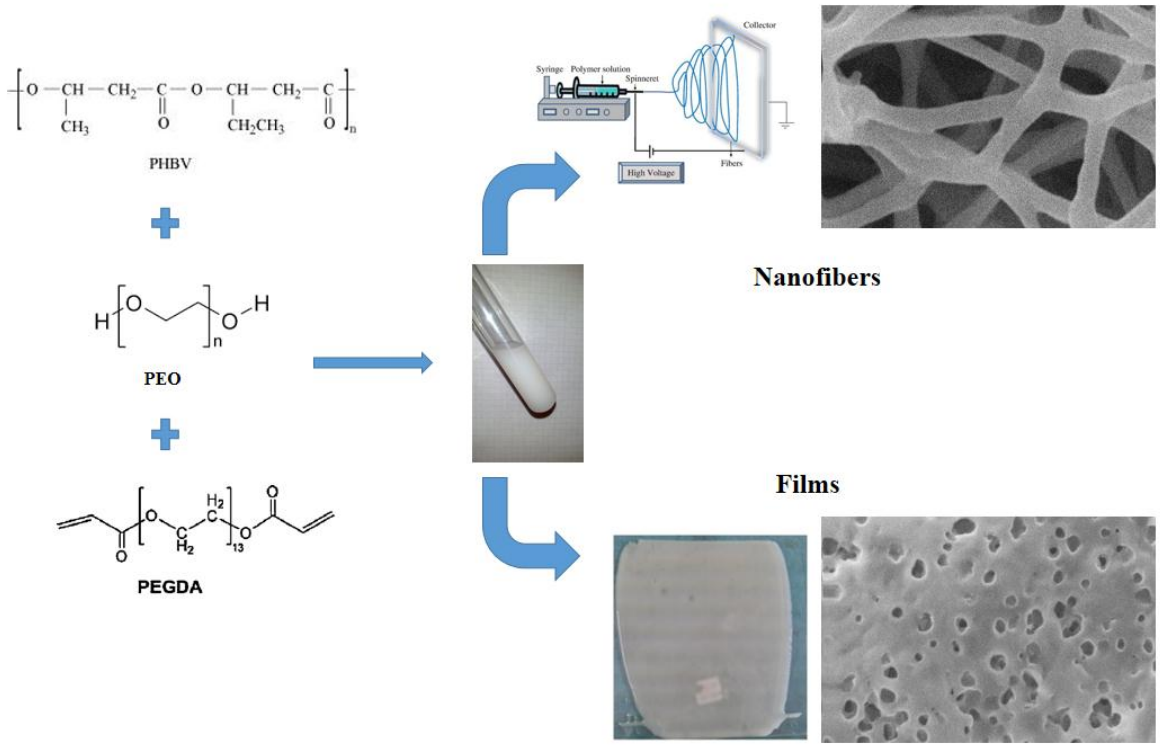


Figure 1. Schematic representation of the fabrication of films and nanofibers

References

[1]Heath, J. R.; Davis, M. E. *Annual Review of Medicine, 59* (1) (2008), 251-265.

[2]Manavitehrani, I.; Fathi, A.; Badr, H.; Daly, S.; NegahiShirazi, A.; Dehghani, F. *Polymers* (2016),*8* (1), 20.

[3]Wu, L.; Wang, L.; Weng, Y. *SuliaoKeji*, 40(2012)**,** 96-102.

[4] Siraj, S.; Sudhakar, P.; Mallikarjuna, B.; Chowdoji Rao, K.; Subha, M. C. S.*Int. J. Pharm. Sci. Rev. Res.* 25 (2014), 103-109, 7 pp.

MACRO 383

Electrospun Nanofibers of PLA composite with Silk Nanoparticles (SNP): Thermal, Mechanical and Wetting properties

S Narendren [a], Patwa Rahul [a] and katiyar Vimal [*]

[a] *Indian Institute of Technology Guwahati, Guwahati, Assam – 781039*
** Corresponding Author: Tel: + 91 361 2582278, email: vkatiyar@iitg.ernet.in*

Many studies have shown that new soft composite materials based on proteins and Biodegradable polymers are promising in biomedical applications. In this work Silk Nanoparticles (SNP) a novel material derived from silk, dispersed into Poly-lactic Acid (PLA) matrix and electrospun into nanofibers with different concentration of SNP (0.5% to 5%). The aligned bionanofibers composite were examined at room temperature for its change in storage modulus, young modulus and tensile strength of the nanofibers with increasing content of the SNP. The change in the fiber diameter and dispersion of SNP nanoparticles within the PLA matrix were examined under scanning electron microscopy. The variation in thermal stability and wetting properties of the novel PLA/SNP bionanofibers composite found to have enhanced properties.

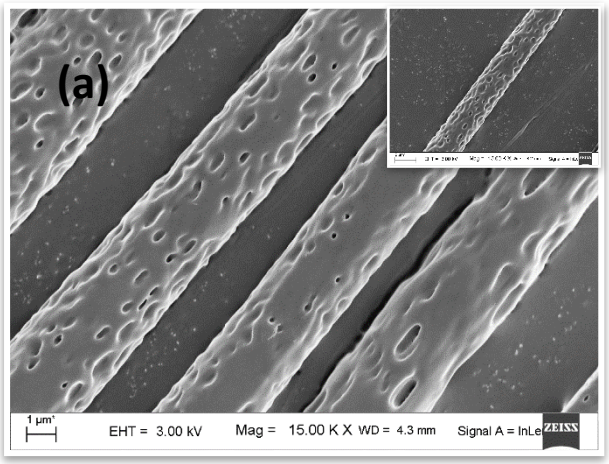
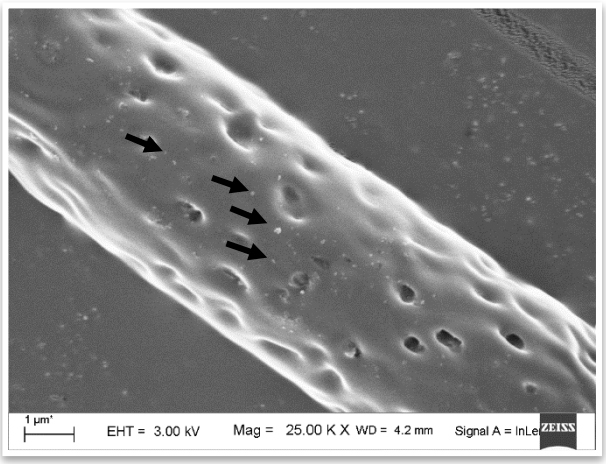


Figure 1(a) SEM Micrograph showing diameter of fibers



1(b) SEM Micrograph showing distribution of SNP in nanofiber

References

[55] Wei, K.; Kim, B.-S.; Kim, I.-S. *Membranes 2011, 1, 275-298.*

[56] Kowalczyk, M.; Piorkowska, E.; Kulpinski P.; Pracella, M. *Composites Part A: Applied Science and Manufacturing*, 42 (2011) 1509–1514.

MACRO 397

Salt-Induced Deposition of Thermoresponsive PNIPAM Coated Metal Nanoparticles on Solid Substrates

Maji, S.;[a] Zhang, Z.;[b] da Fonseca Antunes, A. B.;[b] De Rycke, R.;[c]
De Geest, B. G.;*[,b] Hoogenboom, R.*[,a]

[a]*Supramolecular Chemistry Group, Department of Organic and Macromolecular Chemistry, Ghent University, Krijgslaan 281-S4, 9000 Ghent, Belgium*
[b]*Department of Pharmaceutics, Ghent University, Ottergemsesteenweg 460, 9000 Ghent, Belgium*
[c]*Inflammation Research Centre, VIB, Ghent and Department of Biomedical Molecular Biology, Ghent University, 9052 Gent, Belgium*

** Br.DeGeest@UGent.be; Richard.Hoogenboom@UGent.be*

Thin films are used in wide range of applications including biotechnology, medicine, catalysis, microelectronics etc.[1-3] In contrast to bulk materials, for which the physicochemical properties are size independent, many nanoparticle properties strongly depend on particle size and shape.[4] Combining bulk materials with a thin coating offers the opportunity to engineer solid surfaces with very specific properties. The currently available toolbox for surface modification of solid materials comprises solvent casting, chemical vapor deposition and a wide variety of self-assembly approaches such as Langmuir–Blodgett, layer-by-layer self-assembly, and self-assembled monolayer formation.[1] In recent years, nature inspired compounds such as polyphenols and mussel-derived polydopamine that spontaneously deposit on solid substrates have fueled the interest for simple and straightforward surface coating techniques under all aqueous conditions.[1,5] However, there is a currently unmet need for easy and scalable methods that can deposit nanomaterials under benign all aqueous conditions.

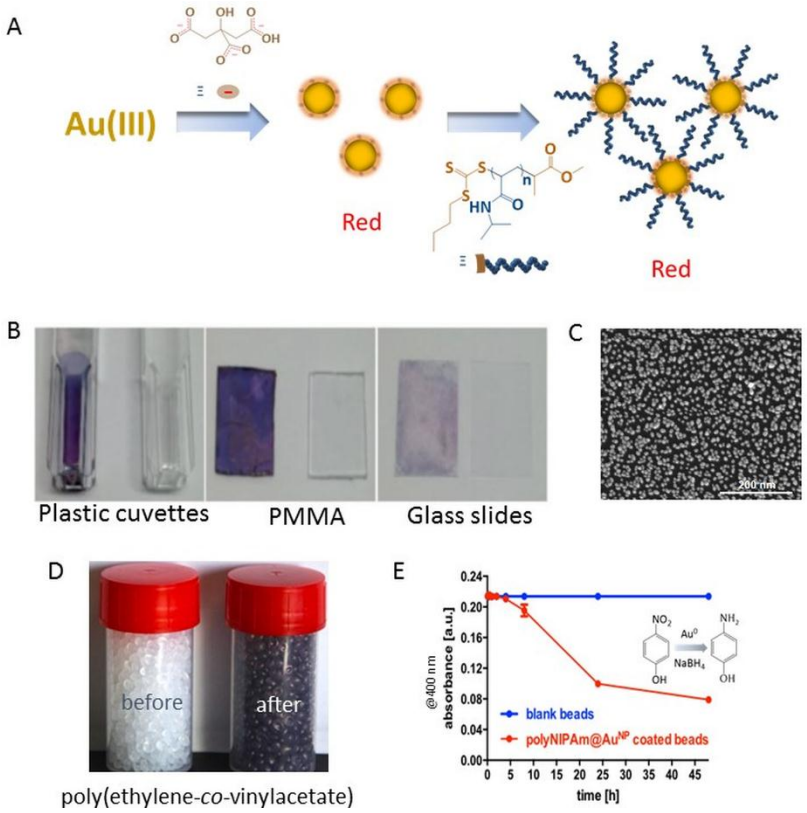


Figure 1. A) Preparation of citrate stabilized AuNPs and ligand exchange of citrate@AuNPs with trithiocarbonate containing PNIPAM; B) Photographs of plastic cuvettes, poly(methylmethacrylate) and glass slides immersed in a PNIPAM@AuNP solution in presence (left) or absence (right) of 0.1 M NaCl followed by extensive washing with deionized water; C) SEM image of PNIPAM@AuNP deposited onto silicon; D) Photograph of poly(ethylene-*co*-vinylacetate) beads before (left) and after (right) coating with PNIPAM@AuNP; E) Conversion of 4-nitrophenol to 4-aminophenol as function of time, monitored by UV-Vis absorbance at 400 nm.

In the present contribution, we report on a simple, generally applicable method for depositing metal nanoparticles on a wide variety of solid surfaces under all aqueous conditions. Noble metal nanoparticles (i.e. goldNP and silverNP) obtained by direct reduction of $HAuCl_4$

(Figure 1A) and $AgNO_3$ in aqueous medium in presence of sodium citrate, which acts both as reducing and stabilizing agent.[6-8] Subsequently, the nanoparticles were coated by ligand exchange with defined trithiocarbonate end-functionalized temperature-responsive polymer, poly(*N*-isopropylacrylamide) (PNIPAM), synthesized via reversible addition–fragmentation chain transfer (RAFT) polymerization. These PNIPAM coated NPs spontaneously form a monolayer-like structure on a wide variety of substrates in presence of salt whereas this phenomenon does not occur in salt free medium (Figure 1B). Earlier we reported that in water citrate-stabilized PNIPAM@AuNP only exhibit reversible temperature-triggered aggregation in presence of NaCl.[7] Atomic force microscopy (AFM) analysis revealed that the deposited film is composed of densely packed PNIPAM@AuNP that appear to form quasi monolayer-like structure.[1] Scanning electron microscopy (SEM) imaging data indicates the coating consist of a single nanoparticle layer (Figure 1C). Moreover, this approach is not limited to planar substrates only, but is capable of coating substrates with a complex morphology as demonstrated by coating of a rubber glove and poly(ethylene-*co*-vinylacetate) beads (Figure 1D). Even, when adsorbed onto the bead surface, the AuNP are still capable of catalyzing a chemical reaction (Figure 1E). Here we hypothesize that salt ion-induced screening of electrostatic charges on the nanoparticle surface entropically favors hydrophobic association between the polymer coated nanoparticles and a hydrophobic substrate. The attractiveness of our approach is that it allows for extremely easy engineering of bulk materials with ultrathin coatings specific properties (exemplified by plasmonic and catalytic functionality) under all aqueous conditions.

References

[57] Zhang, Z.; Maji, S.; da Fonseca Antunes, A. B.; De Rycke, R.; Hoogenboom, R.; De Geest, B. G. *Angew. Chem. Int. Ed.*, 55 (2016) 7086.
[58] Eda, G.; Fanchini, G.; Chhowalla, M. *Nat. Nanotechnol.*, 3 (2008) 270.
[59] Kishimoto, K.; Suzawa, T.; Yokota, T.; Mukai, T.; Ohno, H.; Kato, T. *J. Am. Chem. Soc.*, 127 (2005) 15618.
[60] Jin, R.; Cao, Y. C.; Hao, E.; Métraux, G. S.; Schatz, G. C.; Mirkin, C. A. *Nature*, 425 (2003) 487.
[61] Lee, H.; Dellatore, S. M.; Miller, W. M.; Messersmith, P. B. *Science*, 318 (2007) 426.
[62] Turkevich, J.; Stevenson, P. C.; Hillier, J. *Discuss. Faraday Soc.*, 11 (1951) 55.
[63] Maji, S.; Cesur, B.; Zhang, Z.; De Geest, B. G.; Hoogenboom, R.; *Polym. Chem.*, 7 (2016) 1705.
[64] Maji, S.; Zhang, Z.; Voorhaar, L.; Pieters, S.; Stubbe, B.; Van Vlierberghe, S.; Dubruel, P.; De Geest, B. G.; Hoogenboom, R. *RSC Adv.*, 5 (2015) 42388.

MACRO 401

Delaminated Layered Double Hydroxide Nanosheets as Multifunctional Nanofillers for Semicrystalline Polymers

Nagendra, Baku; Sijla Rosely, C.V and Bhoje Gowd, E*

Materials Science and Technology Division, CSIR-National Institute for Interdisciplinary Science and Technology, Trivandrum-695 019, Kerala, India.

**bhojegowd@niist.res.in*

Layered double hydroxides (LDH) are a class of layered materials with the flexibility in tuning the composition of both inorganic layers as well as balancing anions in the interlayer space. These materials can be used to modify the characteristics of polymers by incorporating them into the polymer matrices. The focus of the current investigation is to develop the novel methods to prepare the highly dispersed polymer nanocomposites and study the influence of different types of LDH on the flame retardancy, thermal stability, crystallization behavior, rheological and morphological properties of isotactic polypropylene. Recently, we have reported the preparation of highly dispersed isotactic polypropylene nanocomposites by the modified solvent mixing method using sonicated Mg-Al LDH nanoparticles. The sonication of LDH in a nonpolar solvent

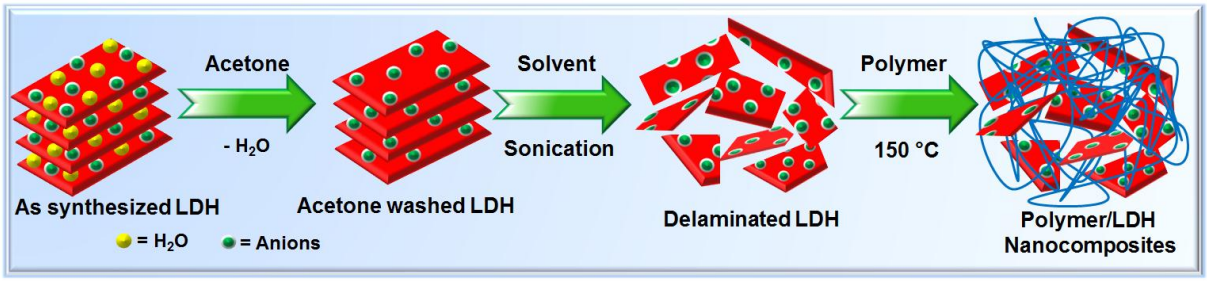


Figure 1. Schematic representation of the methodology used for the preparation of highly dispersed polymer nanocomposites.

(xylene) enables the modification of LDH surfaces to hydrophobic and simultaneously the LDH layers are broken into small fragments. The same procedure was adopted here for the synthesis of highly dispersed iPP nanocomposites with different types of LDH to understand the role of intralayer metal on the physical characteristics of iPP. In another work, we have prepared nano CoNiAl-LDH by coprecipitation method in the presence of hexamethylenetetramine (HMT) as base. The CoNiAl-LDH was utilized for preparation of biodegradable polymer/LDH nanocomposites by employing the binary solvents mixture (DMF+DCB). Physical characteristics of prepared nanocomposites were systematically examined by microscale combustion calorimetry (MCC), thermogravimetric analysis (TGA), differential scanning calorimetry (DSC), dynamic mechanical analysis (DMA) and wide and small-angle X-ray scattering (WAXS/SAXS).

References

[65] Chen, B.; Evans, J. R. G.; Greenwell, H. C.; Boulet, P.; Coveney, P. V.; Bowden, A. A.; Whiting, A. *Chem. Soc. Rev*., 37 (2008) 568.

[66] Nagendra, B.; Mohan, K.; Bhoje Gowd, E. *ACS Appl. Mater. Interfaces*, 7, (2015) 12399.

MACRO 402

Influence of Additives on the Formation of Block Copolymer-based Supramolecular Thin Films and their Microdomain Control

Deepthi Krishnan and E. Bhoje Gowd*

Materials Science and Technology Division

CSIR-National Institute for Interdisciplinary Science and Technology, Thiruvananthapuram, India

**bhojegowd@niist.res.in*

Periodic arrays of nanomaterials with narrow size distribution and ultrahigh density over a large area have attracted a great deal of research attention because they exhibit fascinating, size-dependent physical and chemical properties and their application ranging from biomedicine to electronics. In future, the increasing demands for electronic devices with smaller, faster, and denser systems require the development of advanced nanopatterning technology. Block copolymers received great attention in past two decades and seriously considered for nanotechnological applications including nanostructured membranes, photonic crystals, and high-density information storage media. The present work describes the formation of block copolymer supramolecular assembly (SMA) with different additives and the fabrication of bimetallic nanodots using the block copolymer supramolecular assembly approach. In addition, switching behavior of the cylindrical microdomains was investigated in the presence of various additives using solvent vapor annealing. It was found that the switching behavior of the cylindrical microdomains was dependent on the nature of the additive used for the SMA. A novel method to fabricate the bimetallic nanodots was demonstrated using the SMA approach.

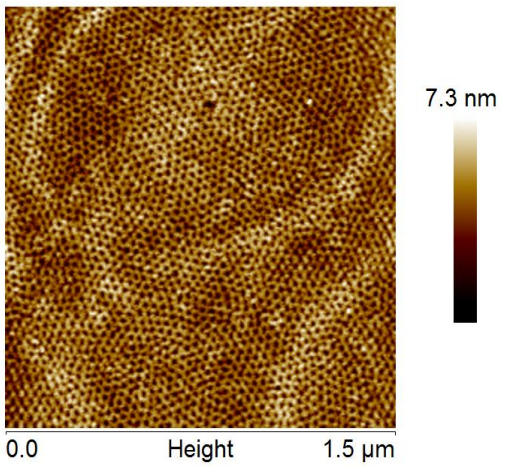


Figure 1: AFM image of PS-b-P4VP + additive SMA block copolymer thin film after surface reconstruction

References

[67] Kuila, B. K.; Gowd, E. B.; Stamm, M. *Macromolecule*, 43 (2010) 7713.

[68] Nandan, B.; Gowd, E.B.; Bigall, N.C.; Eychmuller, A.; Formanek, P.; Simon, P.; Stamm, M. *Adv. Funct. Mater*, 19 (2009) 2805.

[69] Gowd, E. B.; Nandan, B.; Bigall, N.C.; Eychmuller, A.; Formanek, P.; Stamm, M. *Polymer*, 51(2010) 2661.

MACRO 403

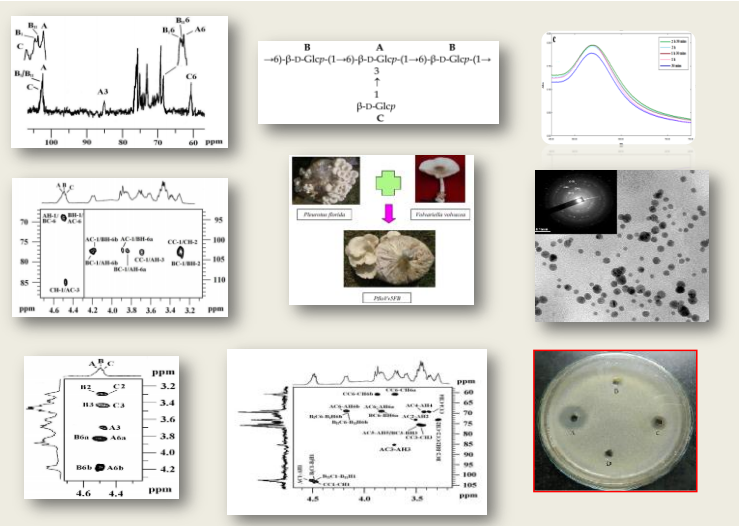
Water soluble polysaccharide from hybrid mushroom and its application in nanoparticle synthesis

Maity, Kankan Kumar* and Manna, Dilip Kumar
Department of Chemistry & Chemical Technology, Vidyasagar University, Midnapore, West Bengal, 721102.
* maity.kankankumar@gmail.com

Mushrooms have been extensively used for its medicinal value and high nutritional sources from the ancient times. Among the different types of mushrooms of the genus *Pleurotus*, namely, *Pleurotus ostreatus*, *P. sajor-kaju*, *P. florida*, *P. citrinopileatus* are reported as commonly available edible mushrooms. A water soluble polysaccharide isolated from the alkaline extract of the somatic hybrid mushroom (*PfloVv5FB*), obtained through protoplast fusion between *Pleurotus florida* and *Volvariella volvacea* strains was found to contain D-glucose only. Structural investigation was carried out using acid hydrolysis, methylation analysis; periodate oxidation, and NMR studies (^{1}H, ^{13}C, DEPT-135, TOCSY, DQF-COSY, NOESY, ROESY, HSQC, and HMBC). On the basis of the above mentioned experiments the structure of the repeating unit of the polysaccharide was established as:

→6)-β-D-Glc*p*-(1→6)-β-D-Glc*p*-(1→6)-β-D-Glc*p*-(1→
3
↑
1
β-D-Glc*p*

Synthesis of silver nanoparticles (NPs) was carried out using this water-soluble polysaccharide. The formation of NPs was monitored using UV-vis spectroscopy. The synthesized NPs were characterized by transmission electron microscopy technique for morphological studies. The obtained silver NPs exhibit enormous antibacterial and anticancerous activity.



MACRO 409

Nanostructured Semiconducting Polymer-Inorganic Composites for Opto-Electronic Applications

Sudha J. Devaki* and R. RAMAKRISHNAN

Chemical Science and Technology Division
CSIR-NIIST, Trivandrum-695019, Kerala, India.
** sudhajd2001@yahoo.co.in*

Hybrid Nano composites comprising of semiconducting polymers and inorganic materials offer favourable perspective for the development of high efficient opto-electronic devices through its tunable band gap, charge carrier mobility, increased charge carrier concentration in combination with an easy processability in large area, flexibility, light weight and low cost.

The synergistic properties arising from the designed structures expected to exhibit properties and functions hard to find the individual components. The incentive to co-assemble organic and inorganic semiconducting materials in the molecular level by tuning the interfacial interactions on the nanoscale can control the band gap and morphology for the formation of a highly efficient novel class of active materials for various electronic devices. The presence of conjugated polymer expected to enhance the solution processability, light weight, flexibility, low cost whereas the inorganic counter parts are endowed with unique opto-electronic, chemical and mechanical properties. The presentation will addresses on the nanostructured semiconducting polymer-inorganic composites, its fundamental aspects on the properties and applications such as photocatalysts, opto-electronic devices such as memory, thermoelectric, organic field effect transistors and dye sensitized solar cell and so forth.

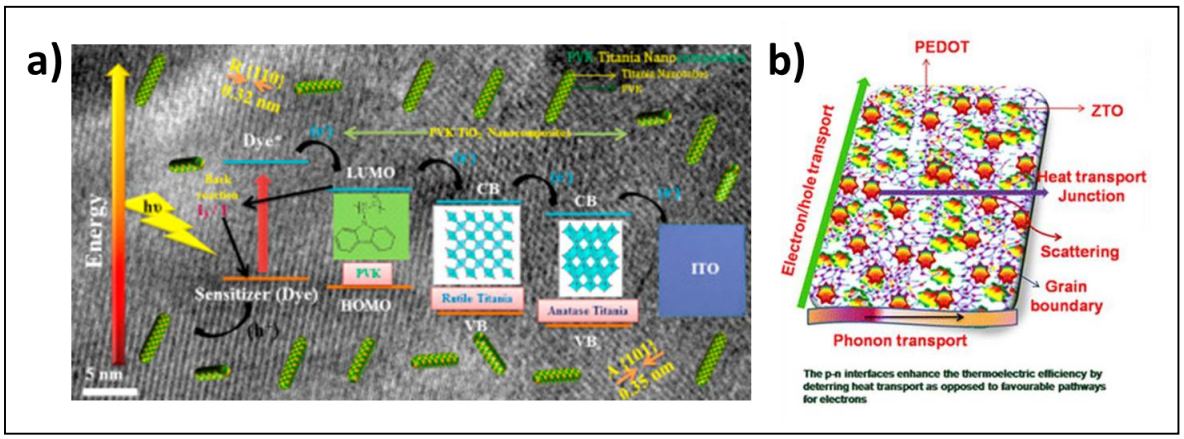


Figure 1. Application of conducting polymer inorganic hybrid composites in a) DSSC, and b) thermoelectric devices.

References

[70] Ramakrishnan, R.; Jinesh, K. B.; Sudha, J. D.; Varma, M. R. *Physica Status Solidi A*, Doi: 10.1002/PSSA.2016 000 58

[71] Aashish, A.; Ramakrishnan, R.; Sudha, J. D.; Sankaran, M.; Krishna Priya, G. *Solar Energy and Solar Materials*, 151 (2016), 169.

[72] Ramakrishnan, R.; Sudha, J. D.;Aashish, A.; Thomas, S.; Varma, M. R.; Najiya, K. P. P. *Journal of Physical Chemistry C*, 120 (2016), 4199.
[73] Neethu, K. S.; Sudha, J. D.; Rohini, K. N.; Molji, C. *ACS Appl. Mater. Interfaces*, 7*(*2015), 18028.
[74] Aashish, A.; Ramakrishnan, R.; Sudha, J. D.; Sankaran, M.; Krishna Priya, G. *Materials Chemistry and Physics*, 157(2015), 31.

MACRO 412

Carbon Nanoparticles Induced Shape-Recovery Behavior in a Hyperbranched Polymer Composite

Pilla Srinivasarao[a], Gaddam Rohit Ranganathan[b], Ramanuj Narayan[a*] and KVSN Raju[a*]
[a]*Polymers and Functional Materials Division, CSIR-Indian Institute of Chemical Technology Hyderabad 500007, India*
[b]*School of Chemical Engineering, The University of Queensland, St Lucia, Brisbane 4072 Australia*
** ramanuj@iict.res.in and * kvsnraju@iict.res.in*

Hyperbranched polymers (HBPs) have evolved as robust materials in coatings in the light of their globular architecture, high density of surface functional groups, simple surface engineering and low melt viscosity compared to their linear counter-parts. The present work demonstrates a robust method for the generation of Shape recoverable, corrosion resistant polyurethane-urea composite films using carbon nanoparticles (CPs) from coconut oil [1]. The CPs were modified with a piranha solution to obtain surface carboxylated (functionalized) carbon nanoparticles (*f*-CPs). The *f*-CPs was dispersed in different weight percentages into a hyperbranched polyester polyol. The HB polyester polyol was synthesized using Castor oil derived Sebacic acid and Triethanolamine. The presence of carboxyl groups in CPs aids in amide linkage formation which leads to a uniform dispersion of Cps in the polymer matrix. The prepared polyurethane composites posses exceptional physico-chemical and thermo-mechanical properties owing to the presence of nano-particulates. Interestingly, the resulting composite showed excellent shape recovery behavior and minimal corrosion rate. The shape recovery behavior of the obtained films was observed at 30^{o} C. The recovery of shape and corrosion resistance is found to increase with increase in CPs content [2-4]. The study presents an in-depth understanding of polymer behavior in the presence of nanomaterials.

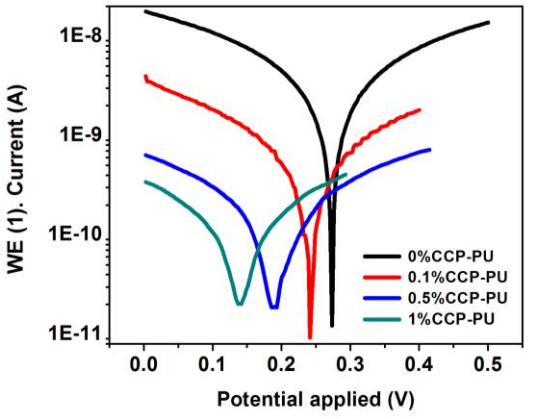


Figure: Polarization curves of different CCP-PU hybrid coatings: valuated using the Tafel method in a 3.5% NaCl solution

References

[1] R R,Gaddam; D, Yang; R, Narayan; K V S N, Raju; N A, Kumar; X S, Zhao. *Nano Energy*, 26 (2016) 346.
[2] M, Jikei; M. A, Kakimoto. *Progress in Polymer Science*, *26* (2001) 1233.
[3] B,Voit. *Journal of Polymer Science Part A: Polymer Chemistry*, *38* (2000) 2505.
[4] S, Pilla; R R, Gaddam; R, Narayan; C R, Rao; K V S N, Raju. *New Journal of Chemistry*, *39*(2015) 7219.

MACRO 420

Tailored Interface Resulting In Improvement In Mechanical Properties Of Epoxy Composites Containing Poly (ether ether ketone) Grafted Multiwall Carbon Nanotubes

Katti, Prajakta Prathamkumar [a]*

[a] Department of Materials Engineering, Indian Institute of Science Bangalore-560012,

Prof. S. Kumar [b]

[b] *Department of Materials Engineering, Indian Institute of Science Bangalore-560012,*

Dr. Suryasarathi Bose[c*]

[c] *Department of Materials Engineering, Indian Institute of Science, Bangalore-560012,*

** Corresponding E-mail address:sbose@materials.iisc.ernet.in*

In this work, hydroxylated HPEEK [poly (ether ether ketone)], which is miscible with the pre-polymer (epoxy), was covalently grafted on to carboxyl functionalized multiwall carbon nanotubes (a-MWNTs) to tailor the interface between MWNTs and the host resin (epoxy). The grafted MWNTs were systematically characterized using spectroscopic techniques. The epoxy composites with a-MWNTs and HPEEK grafted multiwall carbon nanotubes (HPEEK-g-MWNTs) were prepared using mechanical stirring coupled with a bath sonicator to improve the quality of dispersion of the nanoparticles and were subsequently cured at 80℃ and 180℃. With the addition of only a small amount (0.5 wt%) of HPEEK-g-MWNTs, an impressive 44% increase in the storage modulus, 22% increase in tensile strength, 26% increase in elongation to failure and 38% increase in fracture toughness was observed with respect to neat epoxy. In addition, the nanoindentation on the composites displayed significant enhancement in the hardness and diminution in the plasticity index. The resultant formulation also facilitated scratch healing ability and resulted in thermally stable coatings/formulations. Such simultaneous improvement in properties was attributed to the improved interface between HPEEK-MWNTs and epoxy matrix

MACRO 421

Fabrication and Tuning the Nanoporous Channel in Nanoporous Membranes derived using Crystallization Induced Phase Separation in Polymeric Blends

Bose Suryasarathi*
Department of materials engineering, Indian institute of Science, Bangalore, India-560012
** sbose@materials.iisc.ernet.in*

In this work, a unique strategy has been adopted to tune the pore size through crystallization induced phase separation in a model PVDF/PMMA (poly vinylidene fluoride/ poly methyl methacrylate) blend system. PVDF/PMMA blend is a well-known UCST (upper critical solution temperature) system which forms a miscible phase at higher temperature but phase separates upon cooling, either by liquid-liquid phase separation (LLPS) or by solid-liquid separation through crystallization of PVDF. There is always a competition between LLPS and crystalline-amorphous melt phase transition during cooling. The blending of PVDF with PMMA (≤ 40% concentration) leads to phase separation mainly driven by fast crystallization of PVDF and formation of three distinct regions: PVDF crystallites, crystalline amorphous interphase and liquid-like amorphous regions. During crystallization, the PMMA phase occupies the interlamellar and interspherulitic regions of PVDF and there exists a clear boundary between ordered crystalline region and liquid-like amorphous region. As PMMA resides in the interlamellar and/or interspherulitic regions of PVDF, depending on its composition in the blends, by selective etching of PMMA, nanoporous channels can be designed. The pore sizes of membranes were tuned by changing the concentration of PMMA in the blend. For instance, higher concentration of PMMA in the blend showed higher pore size as compare to lower concentrations. Scanning electron microscopy (SEM) studies revealed that the spherulites appeared more compact in 90/10 as compared to 70/30 and 60/40 PVDF/PMMA blends. As spherulites are more compact in 90/10 blends, the average pore size was minimum in these set of blends. In view of this unique fabrication method, the obtained flux was very high as compared to commercial available membranes. These membranes provide very high flux with exceptional antibiofouling properties which can open new avenues in the existing membrane industry.

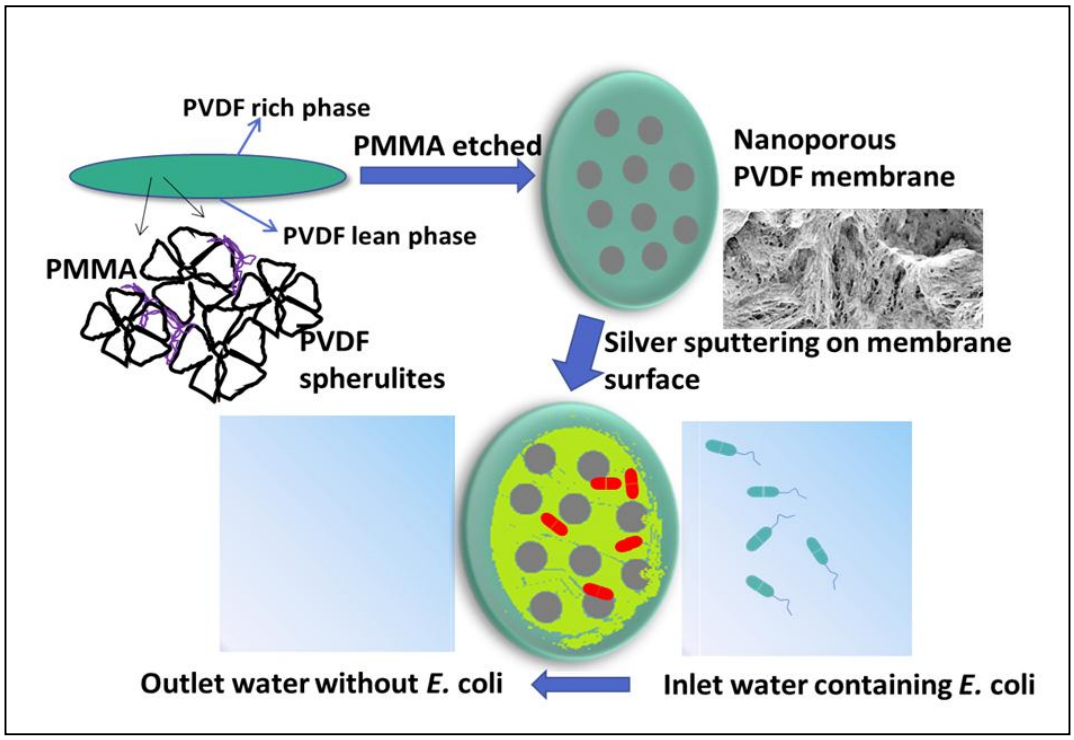


Figure 1: Cartoon illustrating the fabrication of antibacterial membranes derived using crystallization induced phase separation.

References

[75] M. Sharma, G. Madras and S. Bose, *Journal of Materials Chemistry A*, **3(**2015), 5991-6003.

MACRO 422

Layer-by-Layer Assembly of Engineering Nanostructured Polymer Blends to Screen Electromagnetic Radiation

Biswas Sourav[a,b], Panja Sujit[a]*, Bose Suryasarathi[b]* (Last/Surname, First name or initials)

[a] *Department of Chemistry, National Institute of Technology, Durgapur, WB, India-713209.*
[b] *Department of Materials Engineering, Indian Institute of Science, Bangalore, India 560012.*

** Author to whom all the correspondence should be addressed.*
Email: sbose@materials.iisc.ernet.in (SB); sujit.panja@gmail.com (SP)

Extensive use of electronic equipment brings with it the challenge of developing proper shielding materials for their proper functioning as the emitted electromagnetic (EM) radiation from nearby devices interferes with the functioning of adjacent ones [1-4]. Herein, a novel fluorophore-spacer-receptor has been designed with hydrazono methyl phenol as the receptor, anthracene as the fluorophore and imine (C=N) groups as spacer. This newly designed fluorophoric system has receptor that can bind with ferrites and a core

fluorophore that can conjugate non-covalently with multiwall carbon nanotubes (MWNTs) via π-π conjugation. The hybrid nanoparticles were thoroughly characterized using Raman, UV-vis and fluorescence spectroscopy. This unique hybrid is further explored as novel material to screen electromagnetic (EM) radiation. By precisely localizing these hybrids in a given phase of an immiscible co-continuous blend, unique microstructures can be constructed. Herein, blends of polyvinylidene fluoride (PVDF) and polycarbonate (PC) was chosen as model system. The hybrid nanoparticles were selectively localized in the PVDF phase owing to its higher polarity and were systematically characterized by electron microscopic and solution-dissolution techniques. The hybrid nanoparticles that were designed to fence the incident EM radiation resulted in >99.99% attenuation, dominated mostly by absorption. This non-covalent approach of conjugating MWNTs with the ferrites, aided by the fluorophoric system, was noted to be a more effective way to improve the properties (both bulk electrical conductivity and structural) than direct physical mixing/covalent conjugation approaches. In order to further enhance the shielding effectiveness (SE), a layer-by-layer architecture was constructed essentially with outer layers containing PC/PVDF blends with MWNT-ferrite hybrid and the inner layers consisting of PC/PVDF blends with only MWNTs. An ultra-thin shield of 0.90 mm showed >99.9999 % attenuation suggesting new pathways in designing lightweight, flexible EMI shielding materials.

References

[1] Al-Saleh, M. H.; Sundararaj, U., Electromagnetic interference shielding mechanisms of CNT/polymer composites. Carbon, 47 (2009) 1738-1746.

[2] Biswas, S.; Kar, G. P.; Bose, S., Engineering nanostructured polymer blends with controlled nanoparticle location for excellent microwave absorption: a compartmentalized approach. Nanoscale, 7 (2015) 11334-11351.

[3] Biswas, S.; Kar, G. P.; Bose, S., Tailor made distribution of nanoparticles in blend structure towards outstanding electromagnetic interference shielding. ACS Applied Materials & Interfaces, 7 (2015) 25448−25463.

[4] Biswas, S.; Kar, G. P.; Bose, S., Simultaneous Improvement in Structural Properties and Microwave Shielding of Polymer Blends with Carbon Nanotubes. ChemNanoMat, 2 (2016) 140-148.

MACRO 425

Janus Folded Structures Based on Alternating Periodically Grafted Polymers

Ramkrishna Sarkar and S. Ramakrishnan*

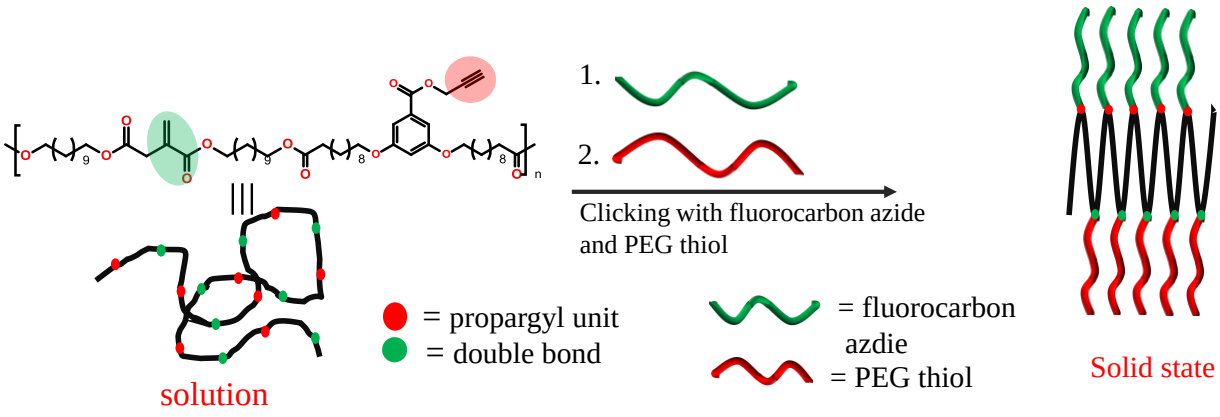
Inorganic and Physical Chemistry Department, Indian Institute of Science,

Bangalore - 560012, INDIA

E-mail: raman@ipc.iisc.ernet.in

Various interesting ordered nanoscale structures can be developed from block copolymers, which is driven by the immiscibility between the two blocks.[1] Recently, we demonstrated that immiscibility between the backbone and pendant graft segments in periodically graft copolymers can coerce the polymer to undergo self-segregation by folding in a zigzag manner leading to microphase separation at the nanoscale; crystallization of either backbone and/or pendant units often provides substantial stabilization to these sub-10 nm nanometer morphologies that are formed.[2-4]

Till date, the folded systems that have been studied are symmetrical, in other words the segments that lie above and below the zigzag folded chains are identical;[2-4] we explore here the possibility of designing periodically grafted copolymers wherein zigzag folding could generate unsymmetrical structures, which could be considered as Janus-type systems. In order to achieve this, we need to develop periodically grafted copolymers wherein alternated grafted segments are not only immiscible with the backbone but are also of
different types.



Schematic depiction of orthogonally clickable asymmetric polymeric system

To accomplish this, an orthogonally clickable polyester, bearing periodically clickable units (azide-yne and Michael acceptor), was prepared using a diacid chloride bearing the propargyl unit and a diol bearing the itaconate unit. Each of the monomers also carry long alkylene segments to promote the backbone crystallization once the collocation due to folding occurs; this is believed to be essential to stabilize the folded form. The two orthogonally clickable units were later used to quantitatively place polyethylene glycol (PEG) and fluorocarbon units at alternating locations. In such systems, we demonstrate for the first time that the anticipated folding permits the independent collocation and crystallization of all the three segments, namely the alkyl, perfluoroalkyl and PEG segments, as evident from DSC and SAXS studies. The design, synthesis and the structural and morphological features of these unique graft copolymers will be discussed in detail in the presentation.

References

[76] Mai, Y; Eisenberg A, *Chem. Soc. Rev.* **2012**, *41*, 5969.
[77] Roy, R. K.; Gowd, E. B.; Ramakrishnan, S. *Macromolecules* **2012**, *45*, 306.
[78] Mandal, J; Krishnaprasad, S; Shankar Rao, D. S; Ramakrishnan, S. *J. Am. Chem. Soc*. **2014**, *136*, 2538.
[79] Chanda, S; Ramakrishnan, S. *Macromolecules* **2016**, *49*, 3254.

MACRO 432

Effect of Cerium addition on Corrosion Characteristics of Smart Polystyrene MMT Clay Nano Composite coatings on Aluminum Alloys

Rajan, Ramya[a]., Ulaeto, Sarah Bill[a,b,c]., Jerin K Pancrecious[a,b]., T.P.D., Rajan[a]* and Pai, B. C.[a]
[a]*Material Science and Technology Division, CSIR-NIIST, Trivandrum, Kerala, India*
[b]*Academy of Scientific and Industrial Research(AcSIR), India*
[c]*Department of Chemical Sciences, Rhema University, Nigeria*
Email: tpdrajan@niist.res.in, ramyashylaja@gmail.com

Abstract

Corrosion protection of aluminium alloys has been performed by chromium conversion coatings. However the toxicity of chromium compounds led to the search for alternative corrosion resistant coatings. Polymeric coatings confer an impermeable barrier against corrosive species and a decorative appearance on metallic substrates. The present investigation is focused on the synthesis and evaluates the anticorrosion effects of cerium nitrate loaded polystyrene MMT clay nano composite coating. The nano composites were synthesized and coated on Al6061 alloy, which is one of the most widely used structural material for aerospace and naval applications. Varying quantity of cerium nitrate was loaded on organically modified MMT clay and polystyrene MMT clay nano composites were prepared by polymerization. The structure of coating formed by dip coating method have been characterized by SEM and AFM shows a uniform coated structure on the metal surface. The characterization of Polystyrene MMT clay composite have been done by XRD, TGA and FTIR spectroscopy. Hydrophobicity of the coatings were investigated by Contact angle measurements. Electrochemical impedance spectroscopy and potentiodynamic polarization studies were used to study the corrosion resistance of the coatings. Electrochemical Impedance data indicated that the cerium nitrate loaded Polystyrene MMT clay nano composite shows better corrosion resistance than the polystyrene coatings.

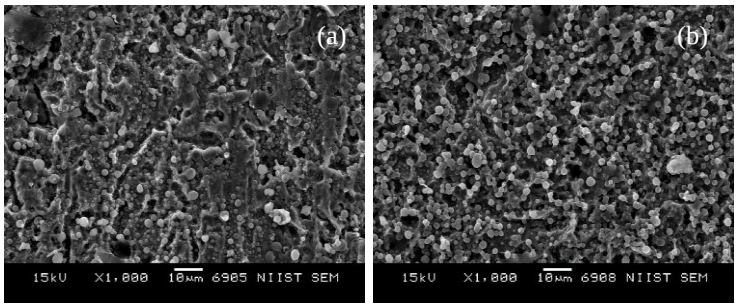


Figure 1. SEM images of the polystyrene and polystyrene MMT clay coated Al6061 strips

References

[1] Roohangiz Zandi Zand, Kim Verbeken, Annemie Adriaens, *Int. J. Electrochem. Sci*., 8, (2013) 548 - 563
[2] I. Danaee , E. Darmiani ,G. R. Rashed , D. Zaarei, *Iran Polym J*, 23, (2014), 891–898
[3] Lin Gu, Shuan Liu, Haichao Zhao, and Haibin Yu *ACS Appl. Mater. Interfaces* 7, (2015), 17641−17648
[4] Mitra Yoonessi, Bradley A. Lerch, John A. Peck, Richard B. Rogers, Francisco J. Solá-Lopez,and Michael A. Meador, *ACS Appl. Mater. Interfaces* 7, (2015), 16932−16937
[5] Min Wook Lee,Seongpil An, Hong Seok Jo, Sam S. Yoon, and Alexander L. Yarin, *ACS Appl. Mater. Interfaces* 7, (2015), 19546−19554

MACRO 440

Studies on polyurethane nanoclay composite as a barrier coating system

Srirangam Siripothu [a], S.K.Manu [b]*

[a , b] Propellant fuel complex, Vikram Sarabhai Space Centre, Trivandrum-695022, India

**e-mail id: srirangam45@gmail.com*

Abstract

A novel formulation based on nanoclay intercalated polyurethane system has been developed for engineering applications. Nanoclay intercalated PU resin was prepared with tailored formulation for use as barrier coating on suitable fabric material. By intercalation of nanoclay in the coating medium, significant reduction in permeability (50 to 60%) of the coated fabric could be achieved with a less number of coats. The extent of intercalation was verified by X-ray diffraction method and the impact of concentration of nanoclay on mechanical strength, areal density, thermal properties etc. was evaluated. A relatively small amount of nanoclay was found to cause significant improvement in many of the targeted parameters including the outgassing properties of the coated fabric.

Keywords: *polyurethane, nanoclay, permeability, barrier coating*

1. INTRODUCTION

Polymer-nano composites have been prepared and used for a wide variety of engineering applications [1]. Nanoclays of different types are used for improvement of properties of polymer composites where the polymeric resins such as silicones, epoxies, polyurethanes, etc forms the binder part [2, 3]. The platelet structure/morphology of nanoclay makes it an ideal choice for use as an additive in polymeric systems for improving permeability resistance.

The reasons for incorporating nano material into the PU resin as a coating system for use as barrier material include significant drop in permeability, improvement in interface properties of the PU coating over the untreated fabric, improved mechanical, out gassing, thermal properties and biocompatibility. Overall, a low content of nano material added leads to significant improvement in properties accompanied with reduction in areal density (grams per square meter). Nanoclay is dispersed in PU in the presence of solvent and during solvent evaporation, entropy gained by exit of solvent molecules from interlayer spacing allows polymer chains to diffuse between layers and form sandwich structure.

Nanoclay particles can play an important role in flame retardant textile (cotton or polyester) coating [3]. Recently, clays have become more important due to considerations linked with environmental concerns and remediation. it may have very little effect on the environment and human being [3]. The essential nanoclays are montmorillonite ($Na_{0.33}[(Al_{1.67}Mg_{0.33})Si_4O_{10}(OH)_2]H_2O$), which is a 2-to-1 layered smectite clay mineral with a platelet structure. Clays are known to have layered structure. The layers are built from tetrahedral sheets in which a silicon atom is surrounded by four oxygen atoms and octahedral sheets in which a metal like aluminium or magnesium is surrounded by eight oxygen atoms. The tetrahedral (T) and octahedral (O) sheets are fused together by sharing the oxygen atoms. Unshared oxygen atoms are present in hydroxyl form [1,4].

Individual platelet thicknesses are just one nanometer, but surface dimensions are generally in the range of 300 to 600 nanometers, resulting in an unusually high aspect ratio. Naturally occurring montmorillonite is hydrophilic. Dispersion of unmodified nanoclay in polymers is very great difficult [3]. Through clay surface modification, montmorillonite can be made organophilic and, therefore, compatible with conventional organic polymers. Organically modified nanoclays disperse readily in polymers. Lamellar nano-composites can be divided into two distinct classes, intercalated and exfoliated [3].

In exfoliated nano-composites the number of polymer chains between the layers is almost continuously variable and the layers stand >100 Å apart. The intercalated nano-composites are also more compound-like because of the fixed polymer/layer ratio, and they are interesting for their electronic and charge transport properties. On the other hand, exfoliated nano-composites are more interesting for their superior mechanical properties. Each nanoclay particle has a layered or leafy structure with each layer consisting of alumina-silicate. When mixed with a compatible material these layers separate and disperse evenly throughout and produce a stronger composite than the original.

The nanoclay selected for the present application is Cloisite 30B. Figure-1 shows three types of polymer nanocomposites [5].

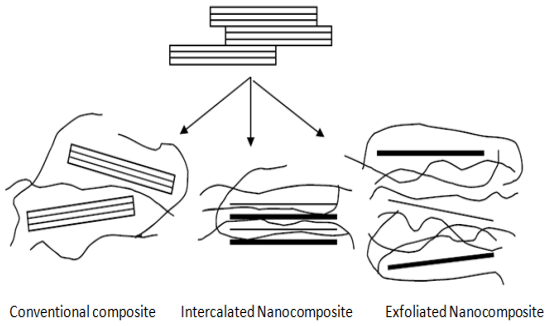


Figure-1: Three types of polymer nanocomposites

2. EXPERIMENTAL

2.1 Raw materials

Poly propylene glycol (PPG) (viscosity: 270 cps at 30 ^oC, OH value: 54 mg KOH/g, Mn.wt: 1900), 2,4-Toluene diisocyanate (TDI) (NCO content: 99.16%), 1,1,1 –trimethylol propane (TMP), glycerol and 4,4’ diphenyl methane diisocyante (MDI) along with some stabilizers.

2.2 Procedure

PU with urethane repeating units (R-NH-COO-CH-R^1)) is formed through chemical reaction between a di/poly isocyanate and a diol or polyol in presence of a chain extender, catalyst and/or other additives [6]. Figure-2 shows polyurethane reaction scheme.

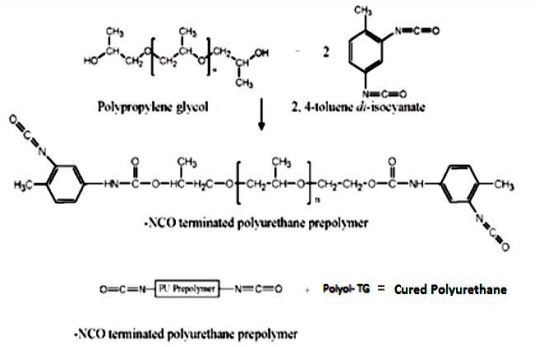


Figure-2: Polyurethane reaction mechanism

To 1000 g of vacuum dried polypropylene glycol, 1.25 g of n-propyl alcohol, 1.25 g of n-propyl iodide (stabilizer), 0.13 g of Pentaerythritol tetrakis(3-(3,5-di-tert-butyl-4-hydroxyphenyl)propionate) (antioxidant) and 0.13 g hydroxyphenyl benzotriazole (light stabilizer) were added and mixed thoroughly. Stoichiometric quantity of toluene diisocyanate was added to the contents and reaction was conducted for 4 hours at 70 ^{o}C under nitrogen atmosphere. The PU pre-polymer was stored in a tightly lidded container under nitrogen atmosphere

Nanoclay (0 - 2%) was dispersed in toluene AR using ultrasonication technique. Frequency was 20000 hz and the sonication time was fixed to 45 minutes at 25 ^{o}C. To the dispersion 100 g of PU pre-polymer was added and ultrasonicated under the previously mentioned conditions for 45 minutes. The solvent was evaporated off to obtain the nanoclay intercalated PU pre-polymer.

The nanoclay intercalated PU pre-polymer was admixed with stoichiometric quantity (3.71 g) of crosslinker comprised of 1,1,1 –trimethylol propane (TMP) and glycerol taken in the weight ratio 60:40 and 7 g of 4,4’ diphenyl methane diisocyante in toluene.

The formulated mixture was poured in a mold and kept for 48 hours for complete curing. Similarly same amount of mixture was prepared and coated over a nylon 6 6 fabric. The fabric was stretched and fixed on flat surface and the mixture was applied by doctors blade. Coating was done on both sides of fabric and after each coating, it is kept for partial curing for 24 hrs. Final coating was allowed for 48 hours of curing at ambient condition.

2.3 Mechanical property evaluation

Mechanical properties of the nanoclay - PU composite were determined by preparing slabs and specimens as per ASTM D-412. The specimens were tested using universal testing machine (UTM) at a strain rate of 10 mm/min at 30 ^{o}C. Five samples were tested for each composition and the graphs shown in figure are drawn for average values. The tensile properties were evaluated as bulk property [7-12].

2.4 Barrier property evaluation

One of the most considerable effects of clays in the polymer matrix properties is the dramatic improvement of barrier properties of polymers. Clay sheets are naturally impermeable. Clays increase the barriers properties of polymers by creating a maze or tortuous path that retards the diffusion of gas molecules through the polymer matrix [1, 13]. Helium gas permeability test of the PU and PU with nanoclay coated fabrics were carried out using PBI Dansensor; Lyssy line of permeability testers. The transport of gases (permeants) through a film is characterized by the permeant flow Q, which can, under the assumption that there is equilibrium, be calculated using Fick´s first law (Eqn 1):

$$Q = -D\,(dc/dx) \quad \text{----------} \qquad (1)$$

where D is the diffusion coefficient of the permeant and (dc/dx) is the concentration gradient. Testing was carried out as per ASTM D1434 Standard.

2.5 X-Ray diffraction evaluation

In the preparation of a polymer/clay nanocomposite it is important to know the degree of intercalation/exfoliation which effects on its properties. The common technique X-ray diffraction (XRD) analysis is widely used to characterize the micro structure of nanocomposite. Using the peak width at half maximum height and peak position (2θ) in the XRD spectra the inter layer space can be calculated utilizing Bragg's law (eq. 1).

$$\text{Sin}\theta = n\,\lambda / 2d \quad \text{----------} \quad (1)$$

Where λ is wave length of X-ray radiation used in the diffraction experiments, d is the space between layers in the clay lattice and θ is measured diffraction angle. [1]

Any change in the interlayer or d-spacing of a clay lattice by organic modification or polymer intercalation causes to change in position, broadness and intensity of the characteristic peak in XRD spectra. According to the Bragg law, increasing of d-spacing results to the broadening and shifting of related XRD peak toward lower diffraction angles (2θ).

2.6 Out gassing properties

Out gassing properties are much important for materials used for space application. Under this test total mass loss (TML), collected volatile condensable materials (CVCM) and water vapor regain (WVR) were tested. TML should be lesser than 1% and CVCM should be lesser than 0.1%.

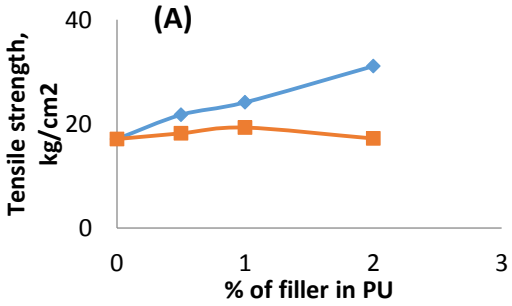
The test is under carefully controlled conditions, the changes in the mass of a test specimen on exposure under vacuum to a temperature of 125 °C for 24 hours and the mass of those products that leave the specimen and condense on a collector at a temperature of 25 °C. This test method covers a screening technique to determine volatile content of materials when exposed to a vacuum environment.

3. RESULTS

3.1 Mechanical properties

Mechanical properties were evaluated for 0-2% of nanoclay dispersed PU and 0-2% of MWNT dispersed PU. The results show that MWNT-PU was having better properties compared to nanoclay - PU. Figure-3 shows the mechanical properties.

The figure-3(A) shows that the tensile strength of MWNT-PU composite was increased by 80% for addition of 2% MWNT in PU. Whereas 12% increase for addition of 1% nanoclay in PU and there was not much noticeable increase by addition of 2% nanoclay. That means MWNT-PU has good tensile strength, it is due to the tubular structure of MWNT and high aspect ratio. Elongation of MWNT-PU and Nanoclay–PU shows that MWNT-PU is having better percentage of elongation.



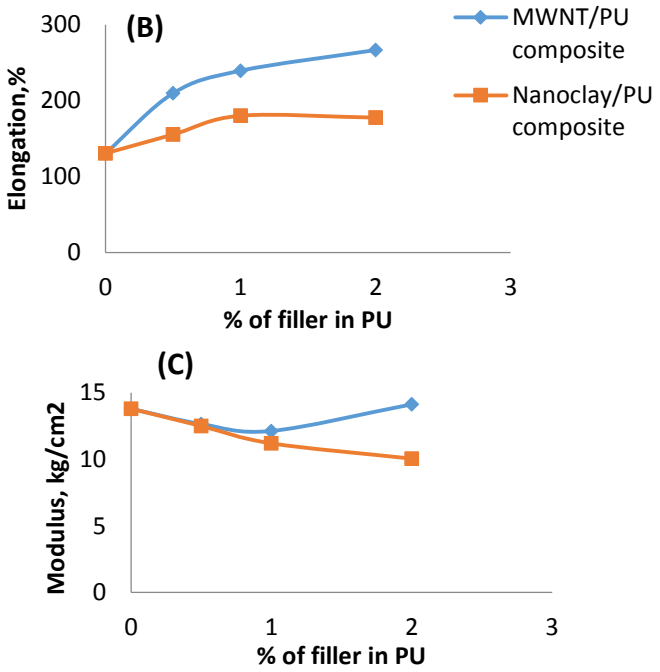


Figure-3: Mechanical properties

The figure-3(B) shows a drastic increase up to 1% of MWNT-PU composite and afterwards it increases gradually. But there is only a slight increase in the case of Nanoclay-PU composite. Modulus of MWNT-PU and Nanoclay-PU shows that MWNT-PU is having better modulus property. The figure-3(C) shows the modulus of MWNT-PU composite first gets decreased up to 1% of MWNT in PU composite since elongation increases and then it increased up to 2% of MWNT in PU. In case of Nanoclay-PU composite it decreased up to 1% Nanoclay in PU and further increase in concentration did not affect and compare to nanoclay – PU, MWNT – PU is having higher modulus for a particular concentration.

3.2 Barrier properties

Permeability of coated fabric came down by increasing the coating thickness over the nylon 66 fabric and to achieve 2600 ml/m^2/day permeability, 0.278 mm of coating thickness is required which corresponds to 270 g of resin per square meter of fabric. Figure -4 shows the permeability of neat PU coated nylon 66 fabric.

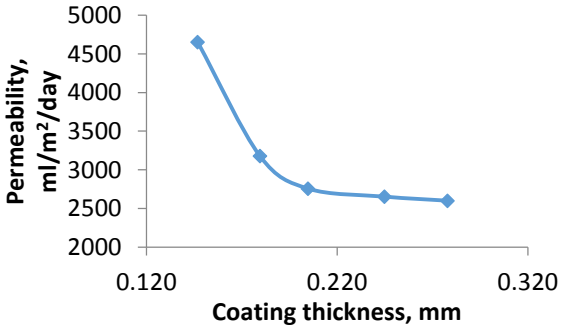


Figure-4: Permeability vs neat PU coating thickness

This higher thickness leads to increase in the weight and flexibility of coated fabric. By addition of small amount of nanoclay, the permeability was brought down significantly. Figure-5 shows the reduction in

permeability with concentration of nanoclay in PU formulation. The results show that presence of 0.5% nanoclay in PU could reduce the permeability to a magnitude of 2214 ml/m^2/day with a coating thickness of 0.130 mm correspond to 226 g of nanoclay – PU resin over the nylon 66 fabric whereas neat PU coated fabric having permeability of above 4500 ml/m^2/day.

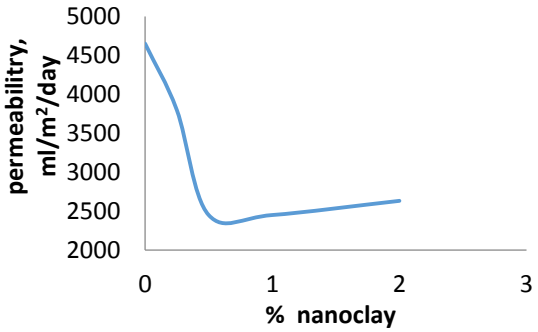


Figure-5: Permeability vs % of nanoclay in PU

A trial with multiwall carbon nanotube (MWNT) (ID: 12.5 nm, 38 nm) was also done for comparison. Figure-6 shows E-SEM morphology of neat PU, PU with 0.5% MWNT and PU with 0.5% Nanoclay.

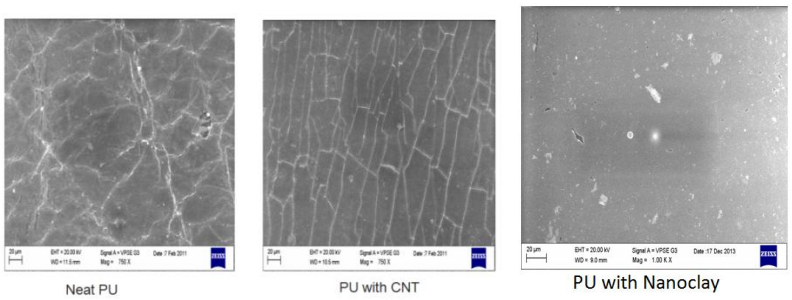


Figure – 6: E-SEM morphology

A comparison of the micrograph indicates the reinforcement of PU by MWNT and Nanoclay. The permeability of 0.5% MWNT dispersed PU coated fabric was evaluated and value obtained is 2500 ml/m^2/day but the coating thickness was 0.250 mm corresponds to 362 g of resin coating over the fabric. It shows that there no much significant effect on permeability which shows the advantage of platelet structure of nanoclay over tubular structure of MWNT for achieving low permeability.

3.3 X-Ray Diffraction analysis

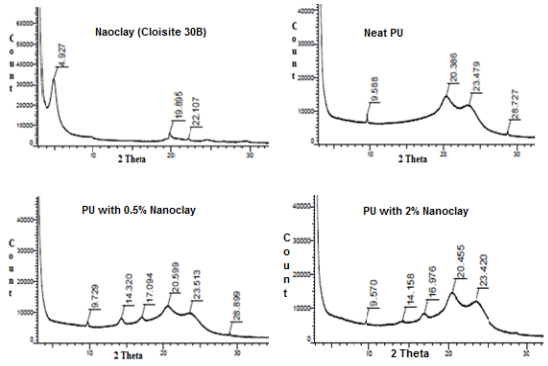


Figure-7: XRD of Nanoclay, PU and PU with 0.5% and 2% Nanoclay

From the figure -7 The XRD spectrums for nanoclay cloisite 30B shows that it has peak at 2theta of 4.927° angle, which corresponds to 18 – 19 Å. The peak is disappeared (shifted lower angle side below 3°, interlayer spacing higher than 30 Å) when the nanoclay dispersed in PU resin. The interlayer spacing between clay layers was increased and some extent of exfoliation may occur by diffusion of the PU into the clay galleries. When low concentration of nanoclay is dispersed in PU it is very difficult to identify the peak at lower angle side. The ultrasonication increases the interlayer spacing by delaminating the clay layers and gives intercalated to exfoliated dispersion morphologies [4, 14].The peaks at 2theta of 19.895° angle shifted to 17.094°, 16.976° and 22.107° angle shifted to 14.320° and 14.158° for 0.5% and 2% nanoclay respectively shows that good intercalation has occurred.

3.4 Out gassing properties

Under the out gassing properties, total mass loss (TML), collected volatile condensable materials (CVCM) and water vapor regain (WVR) were tested.

Table-1: Out gassing properties

SAMPLE	TML	CVCM	WVR
PU coated fabric	1.004	0.057	0.552
0.5%Nanoclay-PU coated fabric	0.881	0.045	0.482

The test results in table- 1 shows that by addition of 0.5% nanoclay in PU the TML was reduced by 12%, CVCM reduced by 21% and WVR was reduced by 13%.

4. CONCLUSIONS

The experiments have clearly shown that there is a significant change in properties for nanoclay dispersed system compared to neat PU.

The mechanical properties of nanoclay- PU and MWNT –PU was better than that of neat PU and the properties MWNT –PU were significantly increased compared nanoclay –PU. It is purely due to its tubular structure and high aspect ratio which effect directly on mechanical properties.

The permeability was reduced by 55 % by adding 0.5% nanoclay in PU and the thickness came down to 0.130 mm from 0.270 mm. It is purely due to platelet structure. XRD analysis data clearly indicates that intercalated to exfoliated dispersion of nanoclay in PU. Out gassing properties analysis shows that by addition of small amount of nanoclay in PU, the TML, CVCM and WVR can be reduced.

The study result shows that by incorporating small amount of nanoclay, significant property improvements could be achieved. It also shown that for mechanical property improvement, the MWNT is best suitable where as for barrier properties the nanoclay is best suitable.

5 REFERENCES:

1. Ali Olad. *Polymer/Clay Nanocomposites,* University of Tabriz, Iran. Chapter 07.

2. Nanotechnology, Wikipedia, the free encyclopedia

3. A. Ghosh. *Nano-clay particle as textile coating.* Daffodil international university, Dhaka, Bangladesh. International Journal of Engineering & Technology IJET-IJENS Vol: 11 No: 05

4. Ali Ahmed Abdel Hafiz. *Synthesis and Characterization of EVA-Cloisite Clay Nanocomposites,* A Thesis Submitted to The American University in Cairo School of Sciences and Engineering, (2013).

5. Igor V. Khudyakov, R. David Zopf and Nicholas J. Turro "*Polyurethane nanocomposites."* Designed Monomers and Polymers 12. (2009)279-290.

6. Eram Sharmin and Fahmina Zafar, *Polyurethane: An Introduction,* Chapter 01. http://dx.doi.org/10.5772/51663..

7. J. Abram, J. Bowman, J.C. Behiri, W. Bonfield, Plast. *Rubber Process. Appl*. 4 (1984) 261.

8. S. Wu, *Polymer* 26 (1985) 1855.

9. S. Wu, *Polym. Eng. Sci.* 30 (1990) 753.

10. Z.H. Liu, X.D. Zhang, Q. Zn, X.G. Zhu, R.X.Y. Li, F.S. Wang, C.L. Choy, *Polymer* 39 (1998) 5019.

11. Z. Bartczak, A.S. Argon, R.E. Cohen, M. Weinberg, *Polymer* 40 (1999) 2331.

12. A. Meddad, B. Fisa, J. *Appl. Polym. Sci*.

64 (1997) 653.

13. Pavlidou, S. & Papaspyrides, C.D. *A review on polymer-layered silicate nanocompopsites*. Prog. Polym. Sci., Vol. 32, (2008)1119-1198

14. M. Alex andre and P. Dubois. *Polymer-layered silicate nanocomposites: preparation, properties and uses of a new class of materials*. Materials Science and Engineering, 28 (2000)1–63.

MACRO 445

Formation of Shish-Kebab structure in poly(vinylidene fluoride)/ionic liquid modified clay nanocomposite

Eapen Thomas, S. Bhuvaneswari, C. Parvathy, B. Nisha, K. P. Vijayalakshmi*, Benny K. George

Analytical Spectroscopy and Ceramics Group, Propellants, Polymers, Chemicals and Materials Entity, Vikram Sarabhai Space Centre, Trivandrum-695022, India

** e-mail id: kp_vijayalakshmi@*vssc.gov.in

Abstract

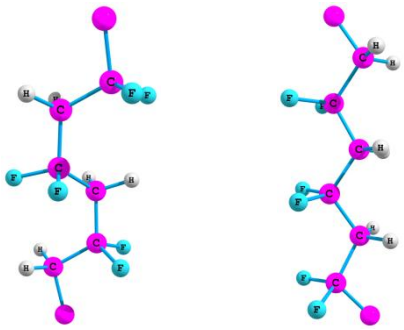
The interplay of phase changes and molecular orientation in PVDF-1-alkyl-3-methylimidazolium modified clay composite was studied. PVDF-1-butyl-3-methyl imidazolium clay composite (PVDF-C4) with equal ratio of α and β phase showed a shish-kebab structure while pristine PVDF and all other composites with either α or β phase in excess showed spherulite structures. Computational studies revealed an extended chain "α-phase" forms the shish, the back bone and

folded chain "β -phase" forms the 'kebab'. This was further supported by the superior mechanical and thermal properties for PVDF-C4 composite.

Keywords: *PVDF; ionic liquid; shish-kebab; thermal stability*

1. Introduction

Poly (vinylidene fluoride) (PVDF) is a semi-crystalline polymer known for its electrical properties.[1] PVDF exists mainly in the stable non-polar α-phase (TGTG' conformation) along with polar β-phase (TTT conformation) (Figure 1). β-phase is responsible for electrical properties and finds wide application in polymer sensors, actuators etc.[2-4]



(a) **(b)**

Figure 1. (a) α- phase and (b) β-phase with 3 repeating units in PVDF. The end atoms represent the head and tail atoms.

Nanofillers with stronger chain-particle interaction and retarding the relaxation of extended chains are known to form "shish kebab" structure.[5] Shish-kebab structures are important as it shows improved mechanical property and thermal stability. In this work, sodium montmorillonite (MMT-Na^+) modified with 1-alkyl-3-methyl imidazolium ionic liquids (ILs) were used for PVDF-clay nanocomposite preparation. The effect of alkyl chain length of IL cation on the crystallization morphology and orientation of PVDF structure was investigated.

2. Experimental

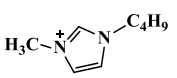
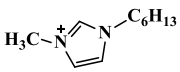
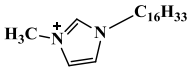
2.1 Materials

Sodium montmorillonite clay from Southern Clay Products, Inc., USA, 1-butyl-3-methyl imidazolium chloride from Ottochemie, India, 1-hexyl-3-methylimidazolium chloride and 1-hexadecyl-3-methyl imidazolium chloride synthesized in house were used for clay modification. PVDF from Alfa Aesar and HPLC grade N,N'-Dimethylacetamide (DMAc) from Spectrochem were used for the preparation of casting solution. Distilled water was used in coagulation bath as non solvent.

2.2 Functionalization of clay

Standard ion exchange procedures were used for the modification of MMT-Na^+ with ILs.[2] Table 1 shows the list of modified clays.

Table 1. List of clay modifiers, modified clays with d-spacing and PVDF-clay composites

Clay modifier	Clay	d-spacing	PVDF-clay composite
-	MMT-Na^+	12.09	PVDF-MMT
	C4-MMT	13.64	PVDF-C4
	C6-MMT	13.97	PVDF-C6
	C16-MMT	18.55	PVDF-C16

2.3 Nanocomposite preparation

PVDF-clay nanocomposite films were prepared by phase inversion method. Clay (2 wt % w.r.t PVDF) was dispersed in 50 mL DMAc by bath sonication (10 min.) and maintained at 50 °C using a water bath. 5 g PVDF powder was added to the clay dispersion, the mixture was stirred for 30 min. and the solution was kept at room temperature for 24 hours. PVDF–clay nanocomposite film was casted on a glass plate using doctor blade and the casted film on glass plate was immersed in water. Films peeled off from the glass plates were washed thoroughly with water to remove any solvent traces present and dried at 100 ^oC for 2 hour in an air oven.

2.4 Instrumental

PVDF films were characterized using Perkin Elmer Spectrum GX FTIR spectrometer in ATR mode in the wavelength region 4000-550 cm^{-1} with a spectral resolution of 4 cm^{-1}. For systems containing α and β–phases, the relative fraction of the β-phase, F(β), can be calculated from FTIR spectra by measuring the absorbance at 763 cm^{-1} (CF_2 bending and skeletal bending, A_α) and 840 cm^{-1} (CH_2 rocking mode, A_β) respectively using Eqn.1,[6]

$$F_{(\beta)} = \frac{A_\beta}{(1.26 \times A_\alpha) + A_\beta} \qquad \ldots(1)$$

where, A_α and A_β are the absorbance of the peaks corresponds to α and β respectively in the FTIR spectrum.

Thermal stability of PVDF-clay nanocomposite films were studied using TA Instruments SDT Q600 TGA from room temperature to 600 ^oC at a heating rate of 10 ^oC/min in nitrogen atmosphere. Molecular orientation was studied using AFM in contact mode using Agilent 5500 scanning probe microscope. Mechanical properties of PVDF-modified clay composites were measured using Universal Testing Machine INSTRON 5569 in tensile mode with testing speed of 50 mm/min. and gauge length of 80 mm.

2.5 Computational studies

PVDF was constructed using 'build polymer' tool in Materials Studio 4.0 (Accelrys Inc.) software with single chain of PVDF in α-phase or β-phase. Amorphous cell calculation was done using the polymer consistent force field (PCFF), Ewald electrostatic summation with accuracy = 0.0001 kcal/mol and temperature = 298 K with 20 monomer units.

3. Results and discussion

3.1 Phase changes

Organically modified clays facilitate the formation of β-phase in PVDF composites.[7] The characteristic IR absorption peaks of α-phase occur at 763, 974 and 1181 cm^{-1}. β-phase is associated with absorptions at 840 and 1275 cm^{-1}. In C16-MMT (Figure 2), the characteristic imidazolium ring absorption peak is at 1171 cm^{-1}. CF_2-CH_2 stretching vibration at 1181 cm^{-1} in pristine PVDF was shifted to 1171 cm^{-1} in PVDF-C16 (Figure 2), suggesting the specific interaction of PVDF chains with the imidazolium ring in the cation.

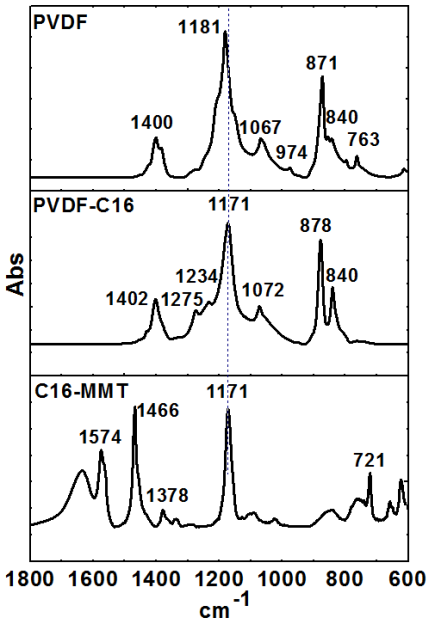


Figure 2. FTIR spectra of (a) pristine PVDF (b) PVDF-C16 and (c) C16-MMT.

The relative fraction of β-phase in pristine PVDF (0.43) was increased to 0.99 in PVDF-C16. PVDF-C4 showed equal proportion of both phases (α=0.49 and β=0.51). PVDF-MMT and PVDF-C6 showed 0.57 and 0.84 respectively. Higher conversion to β-phase in PVDF-C16 is attributed to the maximum d-spacing of C16-MMT (18.55 Å) which enhance the interaction of PVDF with imidazolium cation.

3.2 Molecular orientations

The change in molecular orientation was studied using AFM imaging (Figure 3). The texture aspect ratio (Str) of the surface was calculated from the image to find the structural orientation. AFM images of pristine PVDF, PVDF-C6 and β-phase rich PVDF-C16 films possessed spherulite morphology with isotropic nature (Str=0.77) and are devoid of oriented molecular structure. The spherulite morphology of PVDF was transformed to shish-kebab in PVDF-C4 due to stress induced during crystallinity change (Str=0.58). Stress induced in PVDF-C4 is evident from the equal proportion of α-phase (0.49) and β-phase (0.51) estimated from FTIR analysis. The Shish-kebab formation was further supported by computational studies and improved mechanical properties.

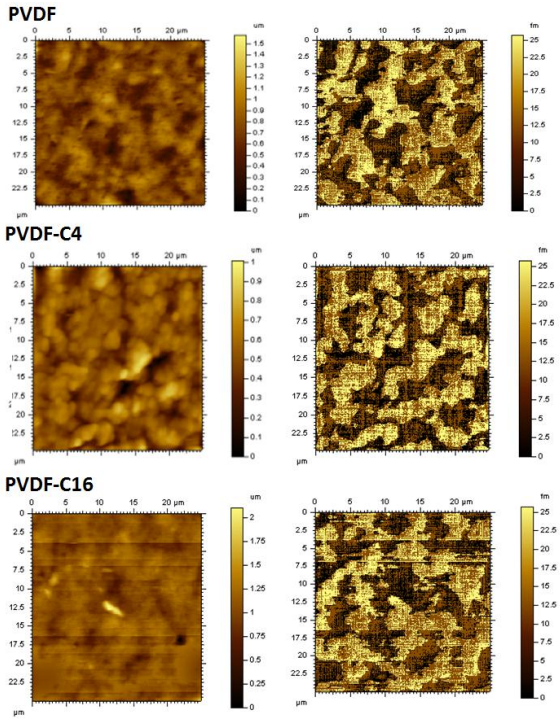
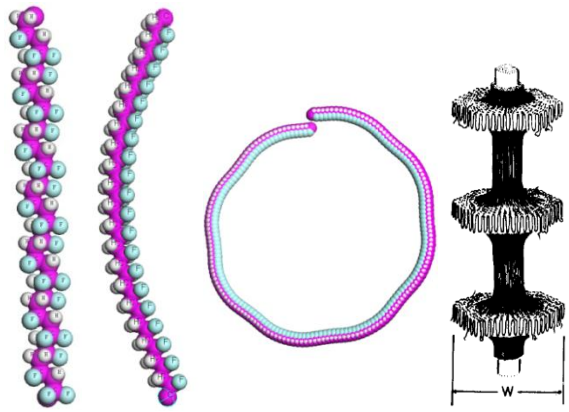


Figure 3. Topography images of pristine PVDF, PVDF-C4 and PVDF-C16 (left) with representation of repeating units (right).

3.2.1 Computational studies

The polymer chain was constructed with 20 repeating units initially and observed a linear structure for α-phase and a bent structure for β-phase as shown in Figure 4. The number of repeating VDF units in β-phase was increased and identified 160 repeating units for completing the folded chain to a circle (Fig.8c) whereas α-phase remained as linear molecule under similar condition.

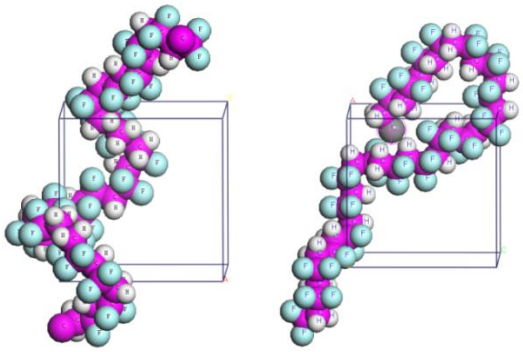


(a) **(b)** **(c)** **(d)**

Figure 4. Structure of PVDF (a) α-phase and (b) β-phase containing 20 repeating units, (c) β-phase containing 160 repeating units and (d) Penning's model for shish-kebab structure.

Equal ratio of α-chains and β-chains results in a symmetrical shish-kebab structure as explained by Penning's model. Alternatively, extended chain "α-phase" forms the shish, the back bone and folded chain "β -phase" forms the 'kebab'. Among the studied PVDF-clay composites, only PVDF-

C4 falls in this category and shows shish-kebab structure as evidenced in the AFM analysis. PVDF containing 20 monomer units of both α-phase and β-phase were used to construct the amorphous cell. The α-phase was lower in energy by 9.06 kJ/mol than β-phase. The higher stability of α-phase is evidenced from the energy of optimized structures (Figure 5).



(a) **(b)**

Figure 5. Optimized Structure of PVDF using amorphous cell with dimensions (Å) 12.9 x 12.9 x 12.9. (a) α-phase and (b) β-phase containing 20 monomer units.

3.2.2 Mechanical properties

The shish-kebab formation in polymers leads to improved mechanical properties, especially elongation as evident from the Penning's model. Mechanical properties of pristine PVDF and PVDF-clay composites are listed in Table 2. PVDF-C4 showed 8 % improvement in tensile strength, 77 % improvement in elongation and 17 % improvement in modulus than pristine PVDF film. This clearly supports the shish-kebab formation in PVDF-C4 nanocomposites. PVDF-modified clay composites except PVDF-C4 showed similar trends in mechanical properties. An increase in modulus and decrease in elongation, tensile strength and toughness were ob-served similar to reported PVDF-functionalized multiwalled carbon nanotube composite by Mandal et al.[8]

Table 2. Mechanical properties of pristine PVDF film and PVDF-modified clay composites

Film	Tensile Strength (MPa)	Elongation (%)	Modulus (MPa)
PVDF	2.21 ± 0.02	5.6 ± 0.6	108 ± 3
PVDF-MMT	1.66 ± 0.04	4.4 ± 0.5	109 ± 5
PVDF-C4	2.40 ± 0.06	9.9 ± 0.7	126 ± 6
PVDF-C6	1.50 ± 0.10	4.7 ± 0.5	113 ± 6
PVDF-C16	1.72 ± 0.10	5.2 ± 0.6	115 ± 5

3.2.3 Thermal properties

Thermal stability of PVDF decreased on addition of modified clay filler, an evidence for the phase conversion. The interaction of CH_2-CF_2 with the imidazolium ring leads to lower thermal stability.

Figure 6 shows the TG/DTG curves of pristine PVDF, PVDF-C4 and PVDF-C16. The maximum decomposition temperature (Ts) for pristine PVDF was 480 ^{o}C and PVDF-C16 showed the lowest thermal stability (457 ^{o}C) among the studied PVDF-clay nanocomposites. PVDF-C4 with Ts of 470 ^{o}C showed higher thermal stability than PVDF-MMT (Ts = 467 ^{o}C) and all other nanocomposites. The higher stability of PVDF-C4 is due to its oriented and self reinforced structural features.

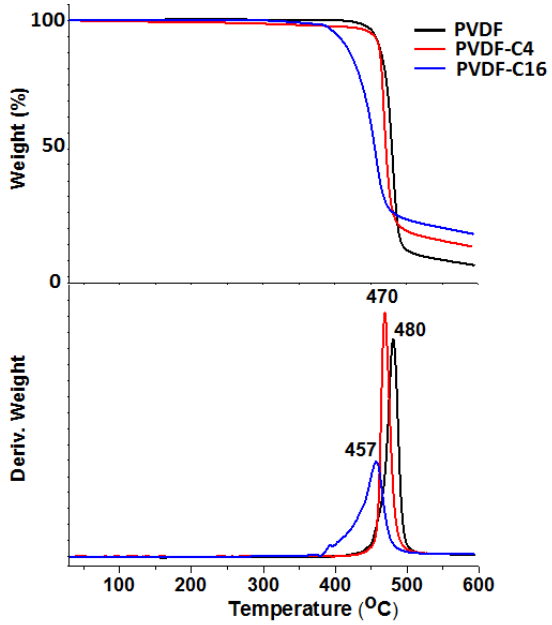


Figure 6. TG and DTG curves of pristine PVDF, PVDF-C4 and PVDF-C16.

4. Conclusions

The microstructural changes induced in PVDF by ionic liquid modified clay was investigated in the present study. Enhancement of electro active β-phase crystallization was observed with increased alkyl chain length of the organic modifier, 1-alkyl-3-methylimidazolium cations in the nanoclay. AFM analysis of PVDF-C4 composite showed a shish-kebab structure while pristine PVDF and all other composites showed spherulite structures. The PVDF-C4 composite showed superior mechanical properties and retained the thermal stability of pristine PVDF. The present study offers new avenues for studying different modifier cations in organoclay with varying chain length to produce self reinforced shish kebab structures in PVDF-clay composites.

Acknowledgements

The authors thank Director, VSSC for granting permission to publish this work. One of the authors (ET) thanks Indian Space Research Organisation for providing research fellowship.

References

12. H. Kawai, *Japan. J. Appl. Phys.*8, 975, 1969.

13. H. Zhu, M. Mitsuishi, T. Miyashita, *Macromolecules* 45, 9076, 2012.
14. C. S. Lee, J. Joo, S. Han, S. K. Koh, *Applied Physics Letters* 84, 1841, 2004.
15. P. K. Khanna, B. Hornbostel, R. Grimme, W. Schaefer, J. Dorner, *J. Mater. Chem. Phys.*87, 173, 2004.
16. N. Patil, L. Balzano, G. Portale, S. Rastogi, *Macromolecules* 43, 6749, 2010.
17. A. Salimi, A. A. Yousefi, *J. Polym. Sci. Part B: Polym. Phys.* 42, 3487, 2004.
18. Y. U. Patro, M. V. Mhalgi, D. V. Khakhar, A. Misra, *Polymer* 49, 3486, 2008.
19. A. Mandal, A. K. Nandi, *J. Mater. Chem.* 21, 15752, 2011.

MACRO 452

EFFECT OF COPOLYMER FUNCTIONALIZED GRAPHENE OXIDE AT LOW LOADING ON INTERFACIAL, THERMO-MECHANICAL AND WEAR PROPERTIES EPOXY NANOCOMPOSITES

Rohini Rani, K Lasitha, Bose Suryasarathi

Department of Materials Engineering, Indian Institute of Science,

Bangalore-560012, India

Abstract

In the present work, we have attempted to understand the effect of covalent functionalization of graphene oxide (GO) on epoxy nanocomposites, at a very low loading of filler (0.05 wt %) using different characterization technique at nanoscale level. Graphene oxide sheets were covalently functionalized with copolymer,styrene maleic anhydride (SMA). Functionalization of SMA on the GO sheets was confirmed using different characterization technique FTIR, Raman spectroscopy, Atomic force microscopy and X-ray diffraction, Thermogravimetric analysis. On functionalization of GO with SMA (S-f-GO), it was observed that GO was partly reduced. Further epoxy nanocomposites were fabricated withlow loadings (0.05 wt %) of modified and unmodified GO. Nanocomposites were cured in a Teflon coated mold. Molecular cooperativity of epoxy nanocomposites was studied using modulated differential scanning calorimetry (MDSC)

experiments. Dynamic mechanical analysiswas carried in the temperature range of 30-170 °C to understand effect of functionalization on viscoelastic behavior. Hardness, plasticity index and wear resistance were measured using Nanoindentation experiments.A thermal degradation study was carried out for epoxy nanocomposite, and it was found that epoxy nanocomposites were stable upto 350 °C. It was observed that even with low loading of SMA functionalized GO (S-f-GO), epoxy nanocomposites showed significant improvement in storage modulus and hardness. Adhesion performance was studied using single lap shear test.S-f-GO/epoxy nanocomposites can be employed as an adhesive in electronic circuit (PCB), as well as anti-corrosion coating in steel industry.

MACRO 470

Enhancement of β-crystal polymorph formation in poly(vinylidene fluoride)- zinc oxide nanocomposite films

Parvathy C, NishaBalachandran, Vijayalakshmi K P, Sadhana R, Rajeev R

Analytical and Spectroscopy Division, PCM Entity,

Vikram Sarabhai Space Centre, Thiruvananthapuram-695022

** e-mail id: c_parvathy@vssc.gov.in*

Abstract

This work describes tailoring of crystal behaviour of poly(vinylidene fluoride) **(**PVDF) by incorporating zinc oxide (ZnO) nanoparticles. PVDF mostly exists in non-polar α-phase, whereas the β-phase is polar in nature. Enhancement of polar crystal phases in PVDF could impart better dielectric properties making it a suitable candidate for variety of applications viz., sensors, transducers, actuators etc. Change in the crystalline nature of PVDF is studied as a function of method of preparation of nanocomposite films. ZnO filler is synthesised by surfactant assisted route and characterized by Fourier transform infrared spectroscopy (FTIR) and X-ray diffraction (XRD) techniques. PVDF-ZnO nanocomposites were prepared by phase inversion as well as solvent drying methods. The extent of α to β phase conversion as well as crystallinity of PVDF films prepared by the two methods were compared by techniques viz. FTIR, XRD and Differential Scanning Calorimetry (DSC).

Keywords: *PVDF, polymorph, zinc oxide, dielectric*

Introduction

Piezoelectric materials are having prime importance in diverse fields of applications viz., sensors, transducers, actuators etc. Flexible materials with high dielectric constant are preferred for such applications. Hence, nanocomposite films comprising of piezoelectric polymer and electroactive

fillers attracted many researchers as their properties can be easily tailored for different applications. The final properties of the piezoelectric nanocomposites depend on parameters such as filler properties, method of preparation of composites and dispersion of the filler particles in the polymer matrix [1].

PVDF is a semi-crystalline polymer and exist in four crystal polymorphs viz., α, β, γ and δ. PVDF mostly exists in α-phase, which is non-polar in nature, whereas the β, γ and δ phases are polar. PVDF in β-phase has the highest dipolar moment and hence exhibit excellent dielectric properties arising from the well organised highly polar C–F bonds of the polymer backbone [2]. Lot of research works have been reported on induction of β phase in PVDF by different methods. Incorporation of ZnO nanoparticles, which show high binding energy and also have interaction between PVDF matrix can modify its polymorphism and thereby can improve its dielectric properties [3].

In this work, the preparation of polymorphism controlled PVDF-ZnO films by phase inversion and solvent drying methods was investigated. ZnO nanoparticles were prepared by precipitation method. In order to control the size and crystal geometry surfactant assisted synthesis of ZnO was employed. ZnO particles synthesized were characterized using FTIR and XRD techniques. The extent of α to β phase conversion as well as crystallinity of PVDF films prepared by the above two methods were compared.

Experimental

Materials

Zinc nitrate heaxahydrate [$Zn(NO_3)_2$. $6H_2O$] and sodium hydroxide (NaOH) from Merck were used for synthesis of ZnO nano particles. The surfactant used was cetyltrimethylammonium bromide (CTAB) from Sigma Aldrich. PVDF from Alfa Aesar and HPLC grade N,N'-dimethylacetamide (DMAc) from Spectrochem were used for the preparation of casting solution. Distilled water was used in coagulation bath as non solvent.

Synthesis of ZnO nanoparticles

In this study, ZnO nanoparticles were synthesized from $Zn(NO_3)_2.6H_2O$ and NaOH by wet chemical method. 0.9 M aqueous solution of NaOH was added drop-wise (in 2 hours) to 0.3 M aqueous solution of $Zn(NO_3)_2.6H_2O$ containing the surfactant. After completion of reaction, the solution was kept overnight intact for settling of the precipitate. Next day, the supernatant solution was decanted and the precipitate was centrifuged, washed and dried in air oven set at 150°C. Characterisation of ZnO particles were carried out using FTIR and XRD.

Preparation of nanocomposite

PVDF films were prepared by phase inversion (PI) and solvent drying (SD) methods. PVDF powder was dried overnight at 100°C prior to processing. PVDF–ZnO nanocomposite films were prepared by adding 20 wt% of ZnO. PVDF film without addition of ZnO was also prepared for comparison. To ensure better dispersion, filler was added to DMAc (50 mL) and sonicated for 10 minutes. Casting solutions were prepared by dissolving PVDF (10 wt %) in the ZnO dispersion maintained at 50 °C using a water bath. The solutions were kept at room temperature for 24 hours. Composition of the casting solution is given in Table 1.

Table 1. Composition of the casting solutions

Film Name	Composition of the casting solutions			Method
	Wt. of PVDF (g)	Wt. of ZnO (g)	DMAc (mL)	
PVDF-1	5	--	50	PI
PVDF-ZnO-1	5	1.0	50	PI
PVDF-2	5	--	50	SD
PVDF-ZnO-2	5	1.0	50	SD

Next day the solutions were first sonicated and then casted on a glass plate using doctor blade (set at 35 rotations). In phase inversion method the casted films were immersed in the distilled water. The films peeled off from the glass plates were washed thoroughly with water to remove any solvent traces and then dried at room temperature. Whereas in solvent drying method the casted films were dried in air oven set at 80°C for 30 min. These films were characterized using FTIR, XRD and DSC.

Instrumentation techniques

FTIR spectroscopy

The prepared ZnO powders as well as the PVDF films were characterized using Nicolet iS50 FTIR spectrometer. FTIR spectra of ZnO powder were recorded in the wavelength range 4000-400 cm^{-1} by pelletising the sample with KBr powder. FTIR spectra of the PVDF films were taken in ATR mode in the wavelength region 4000-550 cm^{-1} with a spectral resolution of 4 cm^{-1}. For PVDF film containing α and β phases, the relative fraction of the β-phase, F(β), was calculated using Eq.1 [4].

$$F(\beta) = \frac{A\beta}{1.26\,A\alpha + A\beta} \quad \text{Eq. 1}$$

where A_α and A_β are the absorbance of the peaks corresponds to 763 cm^{-1} (assigned to α- phase) and 840 cm^{-1} (assigned to β-phase) respectively in the FTIR spectrum.

X-ray diffraction

XRD analyses of ZnO and PVDF nanocomposite films were carried out using Bruker D8 Discover diffractometer. Cu-K α radiation for X-ray of wavelength 1.549 Å at scan rate 4.8°/min was used. Two theta ranges between 10°–90° were used for the analysis. The average crystallite size of ZnO nanoparticles was calculated using Scherrer equation (Eq. 2) which is given below.

$$D = \frac{K\lambda}{\beta \cos\theta} \quad \text{Eq. 2}$$

where K is shape factor (0.89), λ is the x-ray wavelength, β is the peak broadening at half maximum and θ is the Bragg angle.

DSCanalysis

Percentage crystallinity of PVDF in the nanocomposite films was determined using TA DSC Q20. Melting of the samples was monitored by heating the sample (~2 mg) to 200°C at a ramp rate of

10°C/min in argon atmosphere. Percentage crystallinity, χ of PVDF was calculated from its enthalpy of melting (ΔH) using Eq. 3 [5].

$$\chi = \frac{\Delta H}{\Delta H\ (100\%\ \text{crystalline})} \times 100 \qquad \text{Eq. 3}$$

where, $\Delta H_{(100\%\ \text{crystalline})}$ is the enthalpy of melting of 100% pure crystalline polymer (104.6 J/g). Correction was made in ΔH due to the presence of ZnO in the system.

Results and discussion

Characterization ZnO

FTIR spectroscopy

FTIR spectrum of ZnO is shown in Fig. 1. The strong absorption bands around 500 cm^{-1} corresponds to Zn-O vibrational mode. Broad band at 3448 cm^{-1} is arising from stretching mode of -OH group contributed by moisture present in the powder. Also the peak at 1637 cm^{-1} may be due to deformation vibration of H_2O molecule.

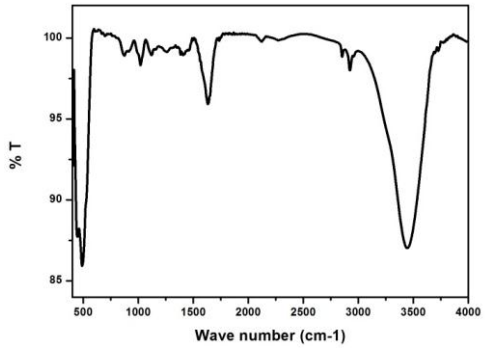


Fig. 1 FTIR spectrum of ZnO nanoparticles

XRD analysis

Fig. 2 illustrates the X-ray diffractogram of ZnO nanoparticles. The major diffraction peaks at 2θ values 31.8°, 34.5°, 36.3°, 47.6°, 56.7° and 62.9° can be assigned to diffraction from (100), (002), (101), (102), (110) and (103) planes of pure hexagonal wurtzite (zincite) phase of ZnO respectively (with lattice constants as a= 3.2 Å and c = 5.2 Å). The average crystallite size ofZnO particles was found to be 26 nm.

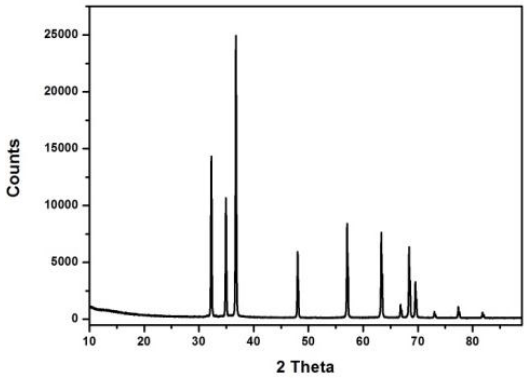


Fig. 2 X-ray diffractogram of ZnO nanoparticles

Characterization of PVDF films

FTIR spectroscopy

Overlaid FTIR spectra of the nanocomposite films, PVDF-ZnO-1 with pristine PVDF-1 prepared by phase inversion method is given Fig. 3. The vibrational bands at 763 cm^{-1} referred to α-phase, whereas peak at 840 cm^{-1} correspond to β-phase. In addition, peak at 1275 cm^{-1} also confirms the presence of β-phase. In PVDF-ZnO-1 nanocomposite films, intensity of β peak (840cm^{-1}) is higher as compared to the pristine PVDF. Relative fraction of β-phase in the films were calculated as 0.43 for PVDF-1 and 0.65 for PVDF-ZnO-1. In the case solvent dried films, complete removal of solvent traces were confirmed by FTIR spectroscopy. Fig. 4 shows the overlaid FTIR spectra of PVDF-ZnO-2 and pristine PVDF-2 prepared by solvent drying method. Both the spectra were almost similar with very small peak at 763 cm^{-1}, whereas a broad peak was observed around 840 cm^{-1}. For PVDF, the peak at 840 cm^{-1} is common for both β and γ phases. But it appears as broad peaks for γ phase as obtained in the case of solvent dried films. Moreover the diminishing peak at 1275 $cm^{-1}$and an additional peak at 1232 cm^{-1} verify γ phase formation in the films.

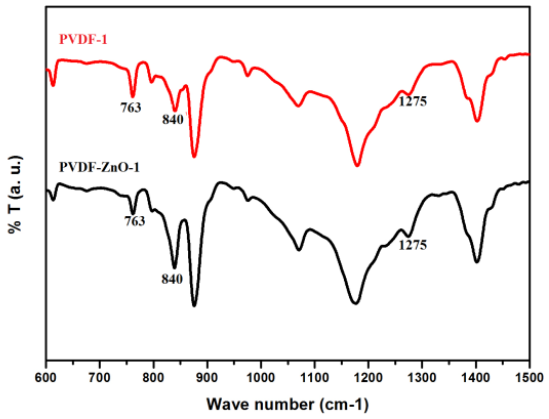


Fig. 3 Overlaid FTIR spectra of PVDF films (phase inversion)

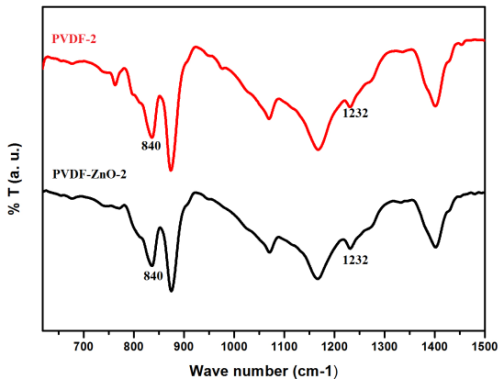


Fig. 4 Overlaid FTIR spectra of PVDF films (solvent drying)

XRD Analysis

For PVDF films, the peaks corresponding to the 2θ values of 17.7°, 18.3°, and 19.9° are described to the diffraction from (100), (020), and (201) planes, belong to α- phase. The peak at 20.3° refers

to the sum of the diffraction from the planes (110) and (200) planes, which is the characteristic of the β-phase. The γ phase exhibit a superposition of peaks at 18.5° and 19.2° from (020) and (002) planes respectively and a peak at 20.04° corresponding to the (110) crystalline plane. Overlaid XRD patterns of PVDF-1, PVDF-ZnO-1 and PVDF-ZnO-2 is given Fig. 5. Incorporation of ZnO in PVDF nanocomposite films (prepared by phase inversion) results in an increase in intensity of peak corresponding to β-phase. X-ray diffractogram of PVDF-2 is shown in Fig. 6. Solvent dried films exhibited γ phase formation. Results obtained are matching with FTIR analysis.

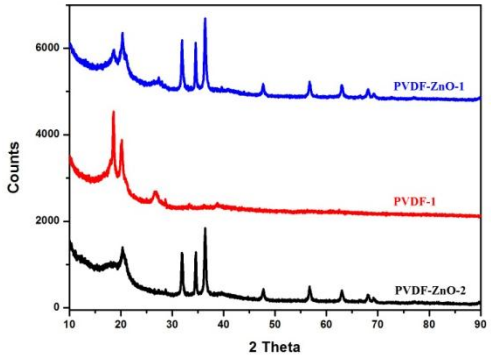


Fig. 5 Overlaid XRD pattern of PVDF films

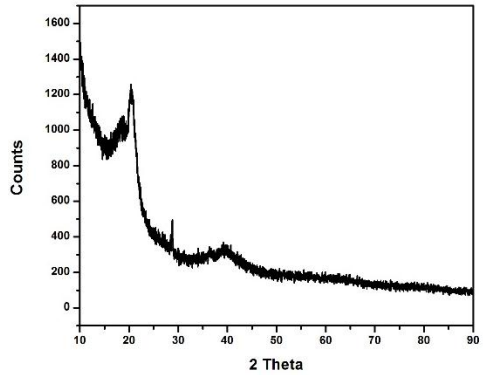


Fig. 6 XRD pattern of pristine PVDF film (solvent drying)

DSC analysis

Fig. 7 shows the overlaid DSC curve of PVDF-1, PVDF-ZnO-1 and PVDF-ZnO-2. Percentage crystallinity (χ) values are given in Table 2. In the case of films obtained by phase inversion method, it is observed that the addition of ZnO could improve the crystallinity of PVDF. The films prepared by solvent drying method showed almost similar crystallinity irrespective of the presence of ZnO. Also maximum crystallinity of 54.7% was obtained for PVDF-ZnO-1 film, which showed the highest β content. This may be attributed to favourable film formation at comparatively low temperature (room temperature) in phase inversion process as compared to the solvent drying

process (80°C), which allows the ZnO to act as nucleating agent to enhance crystallization to a greater extent. These results indicate a better dielectric property for the PVDF-ZnO-1 film.

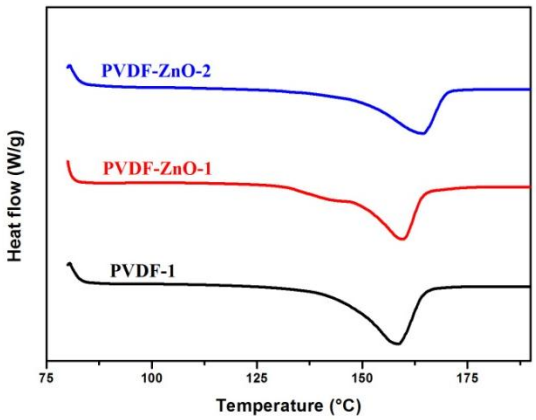


Fig. 7 Overlaid DSC curve of PVDF-ZnO-1 with pristine PVDF-1 film

Table 2. Percentage crystallinity of PVDF in nanocomposite films

Film	**χ(%)**
PVDF-1	43.1
PVDF-ZnO-1	54.7
PVDF-2	43.0
PVDF-ZnO-2	42.8

Conclusions

The polymorphism controlled PVDF films were prepared by incorporation of ZnO nanoparticles. Using Scherrer equation, the average crystallite size of ZnO nanoparticles were calculated as 26 nm. Nanocomposite films prepared via phase inversion method enhance β phase formation, whereas those prepared by solvent drying method improve γ phase formation. DSC results showed that the addition of ZnO improves the percentage crystallinity of PVDF in the films prepared via phase inversion method. The non-polar to polar phase conversion was confirmed using FTIR and XRD analyses. Relative β fraction of PVDF was quantified and found that it is maximum for PVDF-ZnO-1 nanocomposite film prepared by phase inversion method.

Acknowledgements

Deputy Director, VSSC (PCM) and Director, VSSC.

References

1. M. R. Gadinski, C. Chanthad, K. Han, L. Dong, Q. Wang, *Polymer Chemistry*, 5, 2014.
2. K. J. Loh, D. Chang, *Journal of Materials Science*, 46, 228, 2011.
3. J. S. Dodds, F. N. Meyers, K. J. Loh, *Smart Structures and Systems*, 12, 055, 2013.
4. P. Martins, A.C. Lopes, S. Lanceros-Mendeza, *Progress in Polymer Science*, 39, 683, 2014.
5. J. Liu, X. Lu, C. Wu, *Membranes, 3, 389*, 2013.

MACRO 476

Investigations on Thermoreversible Gelation of Self-assembling Amphiphilic Organogelators With PEG Core

M. Himabindu, Aruna Palanisamy*

Polymers and Functional Materials Division, CSIR- Indian Institute of Chemical Technology,
Hyderabad, Telangana, India 500007.

** Corresponding author's email: aruna@iict.res.in*

Amphiphilic gelators composed of functionalized hydrophilic polyethylene glycol core carrying hydrophobic chains (fatty acid chains of different length namely C_{14}, C_{16} and C_{18}) on either sides through highly polar linkages were synthesised. The molecular solutions of the amphiphiles formed stable three dimensional gel networks upon heating and cooling in polar aprotic solvents like DMSO, DMF, DMAc and NMP[1]. The gelation of each amphiphilic gelator in the polar aprotic solvents was tuned by sequentially increasing the hydrophobicity in the structure. The minimum gelation concentration was found to decrease drastically with increase in alkyl chain length for a fixed molecular weight of PEG unit (400 and 600). Depending on the molecular weight of PEG core, xerogels of these compounds showed flake like and fibre like morphology at the microscopic level as inferred from FE-SEM[2]. Rheological study exemplified the viscoelastic nature of the gels and showed that the mechanical strength of the gels increased with increase in concentration. Molecular packing and orientation of gelator molecules leading to self-assembly and hence a layered packing arrangement was confirmed by X-ray diffraction studies. It was observed that PEG_{600}-C_{18} was the most efficient organo gelator where the minimum gelation concentration was ~7mg/mL.

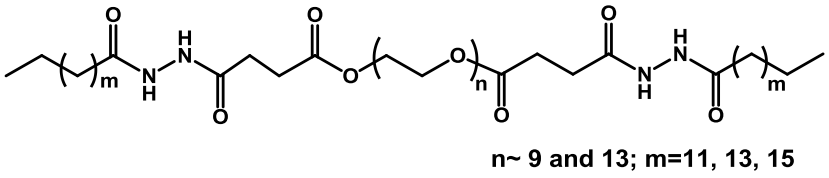


Figure 1. Chemical structure of PEG Amphiphiles with varying alkyl chain length.

References

[1] Das Mahapatra, R; Dey, J. Ultrasound-Induced Gelation of Organic Liquids by l-Cysteine-Derived Amphiphile Containing Poly (ethylene glycol) Tail. *Langmuir*, 31 (2015) 31.

. [2] Moniruzzaman, M; Sundararajan, P. R. Low molecular weight organogels based on long-chain Carbamates. *Langmuir*, 21 (2009) 9.

MACRO 486

Graphene Modified Polymeric Surfactant: Synthesis, Characterization and Application for Narrow Disperse Polystyrene Nanoparticles

Rajender Nutenki

Polymers & Functional Materials Division, CSIR-Indian Institute of Chemical Technology. Uppal Road, Hyderabad - 500007.

*Dr.K.I.Suresh** E-mail*: kisuresh@iict.res.in*

ABSTRACT:

Mono disperse polystyrene (PS) Nanoparticles are important for several industrial applications [1, 2]. The amphiphilic property of Graphene oxide and its derivatives are well documented and found useful in the preparation of Pickering emulsion nanoparticles of polystyrene. In the present work, we report the synthesis and characterization of a Graphene modified polymeric surfactant via surface initiated atom transfer radical polymerization (SI-ATRP). The prepared surfactant was characterised for structure and surface tension properties. It was used in the preparation of narrow disperse PS nanoparticles. The effect of Graphene surfactant on the synthesis, particle characterization and mechanical properties have been studied by using various techniques like IR, DLS, DSC, SEM, TGA. The Graphene surfactant was found to influence the film formation and film properties.

The synthesized polystyrene with Graphene based polymeric surfactant was characterized using techniques like FTIR, DSC, DLS, SEM and TGA. The Nano composites particles showed varying optical properties at different concentrations Graphene polymer Nano surfactant. This property can be used for the applications like coatings, optical applications and sensors [3].

Table.1 Composition and characteristics of nanocomposite emulsion prepared using GO-based polymeric surfactant.

Sample code	Surfactant[b] concentration (mg)	Styrene(gm)	Conversion[c] (%)	Particle diameter[d] (nm)
GO-PS-1	25	4.65	70	162
GO-PS-2	50	4.65	72	180
GO-PS-3	75	4.65	71	207
G0-PS-4	100	4.65	68	170

a= 1wt% of $K_2S_2O_8$ was used as the initiator in all cases. b= seed dispersions have a size 280±20 in all cases. c= determined by gravimetric method. d= determined from Malvern Nanosizer.

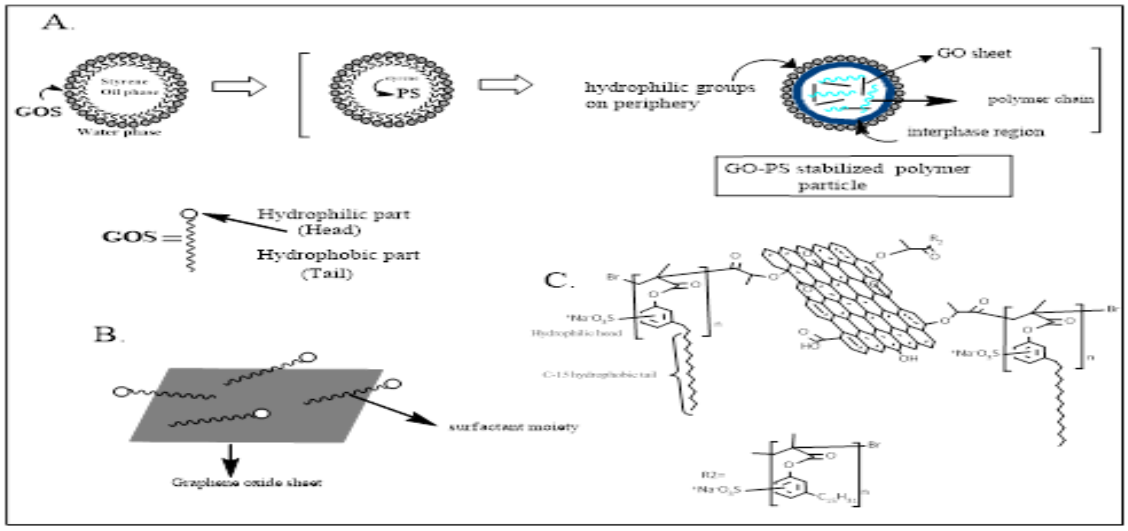


Figure.1. schematic representation of A. synthesis of GO-PS Pickering emulsion B. and C are GO-PDPMA surfactant via SI-ATRP.

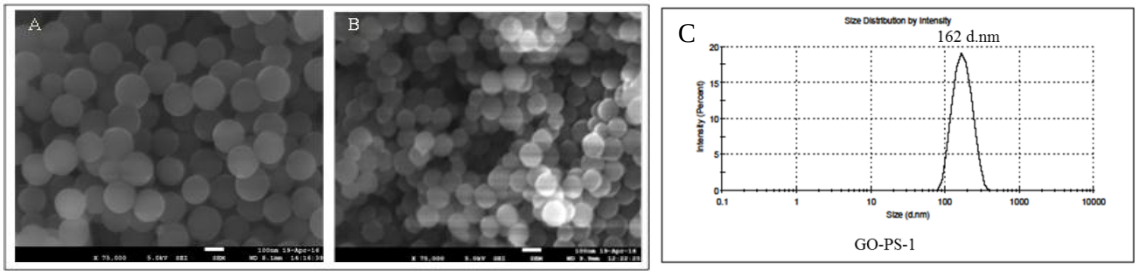


Figure.2. SEM images of A. GO-PS-1 and B. GO-PS-2 at 100nm scale and C. DLS size distribution image of GO-PS-1

References

[1] F, Iskandar; M, Abdullah; *Nano Lett. 1(5) (2001) 231.*

[2] A, Coll,; S, Bermejo; *Nanoscale Res Lett. 8 (2013) 26.*

[3] K, I, Suresh; K, Chidambaram et al. *Polym. Adv. Technol.* 26 (2015) 214–222

MACRO 494

TiO_2/Poly(thiourethane-urethane)-urea Nanocomposites Using Sulfur Rich Hyperbranched Polymers: as NIR reflective, High Refractive Index and Anticorrosion Materials

Ireni, Nagaraj Goud,[a,e] Karuppaiah, Murugan,[c,d] Basak, Pratyay,[b,e] Narayan, Ramanuj*[a,e] and Kothapalli, V. S. N. Raju,*[a,e]

[a] *Polymers and Functional Materials Division;*
[b] *Nanomaterials Laboratory, Inorganic & Physical Chemistry Division;*
[c] *Centre for Sol-Gel Coatings*
[d] *International Advanced Research Centre for Powder Metallurgy & New Materials (ARCI)*
[e] *CSIR-Indian Institute of Chemical Technology (CSIR-IICT)*
Hyderabad - 500 007, Telangana State, INDIA
Email: ramanuj@iict.res.in; kvsnraju@iict.res.in
Tel (O): +91-40-27191517; Fax: +9140-27193991

ABSTRACT

Herein, we are reporting the multifunctional Poly(thiourethane-urethane)-urea nanocomposites using functionalized TiO_2 nanoparticles and sulfur rich hyperbranched polymers (SHBPs). To the blend of a tetra functional thiol and SHBP, surface functionalized titania nanoparticles are added in different weight percentages (1, 2.5, and 5%) and reacted with a diisocyanate (NCO / OH+SH = 1.1) to achieve the targeted nanocomposite coatings. NMR, mid-FTIR, ESI-MS and GPC are used for structural characterization of aimed compounds and cured coating/films by TGA, DSC, DMTA, UTM, TEM/FE-SEM. The UV-vis-NIR spectrophotometer and ellipsometer, results revealed transparent coatings (%T >90%) with high refractive index (>1.6) at 550 nm in the region 400-800 nm and more than 85% reflectance in the NIR region indicating their great significance in the optoelectronics, solar cells and roof coatings, etc. Potentio dynamic measurements (Tafel plot) of the coatings showed the remarkable corrosion resistance (corrosion rate $>10^{-6}$ mm per year).

Key words Polythiourethane, polyurethane, high refractive index, NIR reflectance, corrosion resistance.

References

[80] Ireni, N. G ; Narayan, R ; Basak, P ; Raju, K. V. S. N. *Polymer*, 97 (2016) 370.
[81] Tao, P ; Li, Y ; Rungta, A ; Viswanath, A ; Gao, J ; Benicewicz, B. C ; Siegel, R .W; Schadler, L.S. *Journal of Materials Chemistry*, 21(2011),18623.

MACRO 502

Reversible Shape Switching Phenomena In Linear Thermoplastic Polyurethane Through Molecular Flipping: Potential Application As Smart Gripper

Arpan Biswas and Pralay Maiti*

School of Materials Science and Technology, Indian Institute of Technology (Banaras Hindu University), Varanasi 221 005, India.

E-mail: pmaiti.mst@itbhu.ac.in.

Abstract

Reversible shape Switching is developed in thermoplastic polyurethane by designing different components to enable molecular switching from actuator domain to self-assembled rigid hard domain and vice versa under a temperature cycle. Self-gripping is demonstrated revealing the novel mechanism of molecular flipping and temperature induced structural change along with molecular aggregation.

Keywords: *polyurethane, reversible shape switching, induced crystallization, molecular flipping*

Introduction

As an intelligent material**,** shape memory polymers (SMPs) are capable of being fixed into a temporary shape upon programming and subsequently able to recover their original shape under appropriate external stimuli such as heat[1], light[2], moisture[3,4], pH[5], electricity[6], or magnetic field[7,8]. SMPs have attracted great interest due to their scientific and technological applications.[9] However, one way characteristics of SMPs (*i.e.* not able to go back to their original shape under cooling)[10] restrict their applications. To circumvent this situation, a reversible shape switching effect on heating and cooling is highly desired for years. Recently, few groups have pioneered experimental studies enabling reversible shape memory effect[11] considering the strategies like persistent external mechanical forces,[12,13] chemically heterogeneous structure,[14] a broad melting transition,[15] and change in crystal structure[16] and it is important to reveal the molecular mechanism operates behind the reversible shape switching.

The actuating domains not only enable active movement from temporary shape to permanent shape by elastic recovery in one way SMPs, but also determine the geometry of the

shape change after shape giving.[17] The actuating domains of the polymer chains are oriented during a deformation above the transition temperature (generally above the melting point or glass transition temperature of the actuating domains) by the application of the external stress that results in a decreased state of entropy and on cooling to a temperature below the transition temperature causes the fixation of the temporary shape by crystallization or vitrification.[18] Polymers with multiple transition point are capable to memorise multiple shapes and they are generally called one way triple or multiple shape memory effect.[19,20,21] Polyurethane is well known for its distinct properties like easy preparation method, resistance to organic solvent and aqueous solution, tuneable elastic properties and possible biocompatibility. Polymeric self–assembly is responsible for its superior mechanical properties, better stability and obtaining metastable structure.[22-26] PCL based PUs has not only good biocompatibility and biodegradation but also good shape memory properties like relatively low shape recovery temperature and higher recovery ratio. Therefore, PCL based PU have attracted growing research interest in recent years.[27]

In this study, we report reversible shape switching effect in thermoplastic polyurethane capable of actuation between two different shapes under heating and cooling repetitively under stress free condition. Mainly three types of polyurethanes (PUs) (aliphatic-ester, aliphatic-ether and aromatic-ester based PU) have been synthesised to understand the effect of chemical changes leading to versatile shape memory material through structural alterations. A model has been proposed on the basis of experimental results and, thereby, correlates the macroscopic reversible shape changes under external stimuli like heating/cooling with the organized nanostructure originated by using various constituents of PUs. Developed reversible, bidirectional shape memory polyurethane (rbSMP) can be used as smart devices like self-sufficient smart grippers etc.

Experimental

Materials: Poly(tetramethylene glycol) (PTMG) (M_n= 2900), polycaprolactone diol (PCL-diol) (M_n=2000), 4,4'-methylenebis(phenylisocyanate) (Sigma-Aldrich), 1,6-hexamethylenediisocyanate (HMDI), and 1,4-butanediol (BD) (Meark, Germany) were used as received. The catalyst dibutyltindilaurate (DBTDL) and solvent, dimethyl formamide (DMF) were purchased from Himedia and Sigma-Aldrich, respectively.

Synthesis: Three different polyurethanes were synthesised in a three neck round bottom flask combining different diisocyanates (MDI, HMDI), polyol (PTMG, PCL-diol) and chain extender (BD) in two step condensation polymerization process, keeping the hard segment content (HSC) 30% and they are termed as HPL (HMDI + PCL-diol + BD), MPL (MDI + PCL-diol + BD), and HPT (HMDI + PTMG + BD). The 1st step is the prepolymerization process which was performed under nitrogen atmosphere for 3 hrs at 70 ^{o}C and it was followed by the addition of chain extender (butane diol) and catalyst (DBTDL: 0.1 ml of 1wt% toluene solution) in the second step. The second step was performed at constant temperature 70 ^{o}C for 24 hours to make sure that polymerization process was completed. The polymers were extracted by the non-solvent (distilled water) precipitation process and were dried under reduced pressure and constant temperature of 60 ^{o}C in a vacuum oven for 24 hours. The molecular weight was determined for all the polyurethanes using gel permeable chromatography (GPC) (***Supplementary table S1***).

Methods: The rbSM behaviour of thermoplastic PUs has been studied through two different procedures. For visual photographic procedure, standard polymeric strips (1mm thickness) were prepared by solution caste route and they were dried at 60 ^{o}C under reduced pressure. After that, a ring type shape was given at programming temperature (T_{prog} = 90 ^{o}C), the shape was fixed at a lower temperature (T_{fix} = 5 ^{o}C) and rbSM behaviour was studied at an intermediate temperature (T_{rev}= 50 ^{o}C). Quantitative shape memory properties were studied with standard samples of dimension (60×10×1) mm^{3}using Instron 3369 tensile tester and a temperature controller attached with it externally. The samples were uniaxially stretched to 100% with a strain rate 5 mm/min at programming temperature and equilibrated for 5 min. After cooling down to T_{fix} at constant strain, the condition was maintained for 10 min. Then, keeping the temperature fix, the stress was removed and at this condition shape fixicity was determined. Then, samples were reheated to T_{rev} under stress free condition. The reversible actuation cycles consist of cooling to T_{fix} and waiting for 5 min, then reheating to T_{rev} for another 5 min. The shape fixicity (R_F), shape recovery (R_R) were measured using equation (1) and (2) and the shape reversibility (R_r) was expressed in terms of reversible elongation which is the ratio between the difference in sample length of shapeB (l_1) and shape A(l_2) and the length of the sample in shape B.

$$\text{Shape Fixicity } (R_F) = [(L_2 - L_0) / L_0] \times 100 \qquad (1)$$

$$\text{Shape Recovery } (R_R) = [(L_1 - L_3) / L_0] \times 100 \qquad (2)$$

Shape Reversibility (R_r) = $[(l_1 – l_2) / l_1] \times 100$ (3)

where, $L_0$is the initial length of the strip, L_1 is the length after heating and stretching the strip, L_2 is the length after stress released; L_3 is the length of the strip after heating at programming temperature.

FT-IR Spectroscopy: Fourier transform infrared spectroscopy (FTIR) was performed using Thermo Nicolet 6700 of the thin solid films of the synthesized materials taking 100 scans with the resolution of 4 $cm^{-1}$to understand the role of interactions.

Morphological Investigation: Morphology of the synthesized polymers was investigated using polarizing optical microscope (POM), atomic force microscope (AFM), and transmission electron microscope (TEM). The morphology in the optical range of the thin films (prepared through solvent casting) of the synthesized polymers was examined using POM (Leitz). A NT-MDT multimode AFM, Russia, controlled by a Solver scanning probe microscope controller, was used to study the surface morphology of the synthesized polymeric samples. Semi contact mode was used with the tip mounted on 100 μm long single cantilever with resonant frequency in the range of 240-255 kHz and corresponding spring constant of 11.5 N/m.The bulk morphology was examined with TEM (FEI Technai 20) operating at a voltage of 200 kV.

Differential Scanning Calorimetry: The melting temperature, glass transition temperature of the samples were determined quenching the samples to -100 ^oC after melting at 200 ^oC at a heating rate of 10 ^oC / min using Mettler832 differential scanning calorimetry instrument. The degree of crystallinity and shape memory behaviour of the samples were determined over the temperature range of -30 ^oC to 70 ^oC for 1st heating and -30 to 200 ^oC for 2nd heating keeping the heating rate 10 ^oC. The cooling was done from 70 ^oC to -30 ^oC in 1st cooling and from 200 ^oC to -30 ^oC in 2nd cooling keeping the cooling rate 5 ^oC /min. The heat of fusion was calculated from the endotherms using a computer attached with the instrument. Calibration of the DSC was done using indium before use.

Mechanical response: The elongation at break, modulus and toughness of the samples were measured using an Instron 3369 tensile tester at a strain rate of 5 mm min^{-1} at room temperature. The samples were prepared through solvent cast methods keeping the thichness of the samples 1mm, width 10 mm and length 60 mm. several samples were examined to obtain good error estimates.

Thermal behaviour: The thermal behaviour of the synthesised samples was investigated through thermogravimetric analyser (TGA, Mettler-Toledo) in the temperature range from 40 to 600 ^{o}C keeping the heating rate 10 ^{o}C / min and maintaining the nitrogen atmosphere.

Small Angle Nutron Scattering (SANS): SANS experiment were done on the spectrometer at the Dhruva reactor at Bhabha atomic research centre, Mumbai, India. The data were collected in the scattering vector (q) range 017 $nm^{-1} \leq q \leq 3.5\ nm^{-1}$ at 30 ^{o}C, 60 ^{o}C and 100 ^{o}C. The lower scattering vector range was fitted with Debye – Bueche model. The characteristic length was calculated through the equation $\Lambda c = 2\pi/q_m$, where q_m is the scattering vector corresponding to the peak position in the scattering pattern.

X-ray Diffraction Study: X-ray diffraction of solvent cast thin films were performed with Rigaku Miniflex wide angle X-ray diffractometer using Cu Kα source with a wavelength of 0.154 nm and the voltage and current of the generator was kept 40 kV and 15 mA. The thin film samples was placed on quartz holder at 30 ^{o}C, 60 ^{o}C and 100 ^{o}C and were scanned at diffraction angle (2θ) 10^{o} to 40^{o} keeping scanning rate 3^{o} / min and 1^{o} to 10^{o} at 1^{o} / min.

Results and discussion

Chemistry of thermoplastic polyurethane has been altered by using aliphatic and aromatic diisocyanates and ether / ester polyols to understand the structure property relationship in a better way. Reaction scheme and designation of various PU have been mentioned in **Fig. 1a**. Urethane linkages undergo extensive hydrogen bonding as appeared from the FT-IR absorption band at 1680 cm^{-1} in HPL against the free carbonyl stretching frequency observed at ~1720 cm^{-1} in MPL and pure ester diol (**Fig. 1b**). Formation of hydrogen bond in MPL is not occurred due to the proximity of bulkier phenyl group attached with diisocyanate or in the urethane linkages while extensive hydrogen bonding occurs in HPT as evident from the strong peak at 1680 cm^{-1} with a small hump at ~1720 cm^{-1} (***supplementary Fig. S1***).[28] Similar trend has been observed for C–O–C of ester stretching frequency which decreases from 1106 cm^{-1} in PCL-diol and MPL to 1101 cm^{-1} in HPL and N–H stretching frequency was lowered from 3330 cm^{-1} in MPL to 3322 and 3318 cm^{-1} in HPL and HPT, respectively, suggesting strong interaction between urethane linkages in HPT vis-à-vis predominant interaction between ester carbonyl moiety and N–H group of urethane linkages in HPL. This is to mention that no shifting of peak positions occur in MPL due to lack of formation of hydrogen bond either between urethane linkages or ester-urethane interactions. Greater interactions, through hydrogen bonding, between the molecules lead to the formation of cluster of

size ~80 nm in HPL, as observed through bright field TEM image (**Fig. 1c**), against no such clustering noticed in aromatic based PU (MPL). Further, greater interaction has been revealed from the considerable lowering of melting temperature (37 ^{o}C) and heat of fusion (18 J.g^{-1}) in HPL as compared to the respective value of 42 ^{o}C and 22 J.g^{-1}in MPL (**Fig. 1d**) while pure PCL-diol exhibits a melting temperature at 51 ^{o}C (***supplementary Fig. S2)***. HPL shows a distinct melting peak at 151 ^{o}C arising from the crystallization of hard segment association against no melting peak noticed for MPL at that region clearly indicate the inability to form hard segment organization due to lack of hydrogen bonding in aromatic based PU. Ether diol based PU (HPT) exhibits melting of soft as well as hard segmented zone at 24 and 166 ^{o}C, respectively. Moreover, second order phase transitions are observed at -60, -30 and 0 ^{o}C for HPL, MPL and HPT, respectively, due to the glass transition relaxation (T_g) at sub-ambient temperature. Amongst the ester diol based PUs (HPL and MPL), higher T_g in MPL is due to the restriction in segmental mobility in presence of rigid aromatic ring. On the other hand, higher T_g for ether diol based PU (HPT) is explained from the extensive hydrogen bonding in hard segmented zone as compared to meagre hydrogen bonding in HPL (ester diol based PU) in hard segment zone and instead the formation of the association of hard segment with ester linkages in soft segment (*cf.* FTIR results). To understand the molecular interaction, simulation of energy minimized configuration has been performed through AM1 calculation, showing closest distance between ester carbonyl (>C=O) of soft segment and >N–H moiety of urethane linkage of neighbouring molecule is 2.07 Å in HPL against the value of 5.87 Å in MPL for similar bond pair (**Fig. 1e**). The minimum distance between two energy minimized molecules of HPT is found to be 2.049Å corresponding to the bond pair of carbonyl (>C=O) of hard segment with the >N–H moiety of urethane linkage of neighbouring molecule. Now, it is evident that good interaction between urethane linkage and soft segment occurs in HPL in addition to meagre hard segmented interaction while only hard segmented interaction takes place in HPT and very less interaction do happen in MPL because of their chemical constituents.

To visualize the effect of varying degree of association depending on the nature of diisocyanate/diol on the properties of PUs, stress strain curves have been shown in **Fig. 1f** indicating higher stiffness, slope of initial linear regime, of MPL and significantly higher toughness, measured from the area under stress-strain curve, in HPL (***inset of Fig. 1f***). The greater rigidity in MPL (47 MPa as compared to the value of 29 MPa for HPL) arises from the rigid benzene ring as the part of the main chain while the flexibility appear from the overall distribution

of hard segment in HPL (910 MJm^{-3}, four times higher than the value of MPL) (*cf.* FTIR and simulation studies) unlike HPT, where hard segments are assembled generating inhomogeinities causing very less elongation at break (~80%) against considerably higher elongation at break (200%) observed in HPL. Thus, chain sliding is facilitated in HPL because of typical interacting sites predominantly in soft segment and meagre in the hard segmented zone. Thermal stability appears to be low for hard segment as compared to soft segment and it is expected that greater assembly of hard segment should degrade at relatively lower temperature.[29] Higher order of hard segment assembly is further pronounced from the decreasing degradation temperature of 306, 282 and 275 ^oC for MPL, HPL and HPT, respectively (***supplementary Fig. S4***). Therefore, hard segment part of PU can be placed exclusively near soft segmented zone or hard segment of neighbouring molecules leading to the wide variation of nanostructure to control the crystallization directed properties like shape memory effect.

Figure 2a and demonstrate the reversible shape switching for HPL with shape giving (T_{prog}) and shape fixing (T_{fix}) temperature at 90 and 5 ^oC, respectively, and the strip of HPL was deformed/programmed at higher temperature (shape giving temperature) into a ring like shape which was fixed at lower temperature considering the crystallisable soft segment (T_m ~ 35 ^oC) to act as an actuator and hard segment as the geometry determining component. The reversible shape switching behaviour is observed at a reversible temperature (T_{rev} = 50 ^oC) where the ring opens up to some extent (Shape **A**; gap between the two ends of the strip becomes 1 cm) which goes back to the closed ring like shape (Shape **B**) upon cooling at 5 ^oC. The strip reversibly switches between these two shapes (ShapeA↔ ShapeB) on cyclic heating and cooling between T_{rev} and T_{fix}, as evident from the graph of distance vs. number of cycles (**Fig. 2a**) and prove its reproducibility of several repeating cycles. Further, the strip returns to its original shape upon heating to T_{prog} (90 ^oC) following its prearranged memory. On the other hand, MPL and HPT do not show reversible shape switching while they exhibit one way shape memory (owSM) behaviour with inappropriate shape fixing (***Supplementary Fig. S5(a,b)***). The reversible shape switching was further quantified with uniaxial tensile testing after deforming 100%, a huge deformation compared to others, shows reversible shape switching in polymers under stress free condition[14,30] showing better shape fixicity (R_F) and shape recovery (R_R) at 50 ^oC for HPL having both the values at 75% against the respective values of 71 and 68% for MPL (***Supplementary Fig. S6(a,b)***). Interestingly, only HPL exhibits considerable increment in length (shape B) upon cooling to T_{fix} while heating induced

contraction have been noticed both for MPL and HPL (shape A) at 50 ºC under stress free condition. Decrease in dimension of sheet upon cooling below T_m is expected from the elasticity phenomena[12] instead an increasing dimension on cooling indicate the crystallization of soft segments (actuator domain) in HPL which is responsible for the increment in length[14,31]. This is to mention that the shape switching phenomena is continued to repeat upon several heating and cooling cycles. Therefore, a reversible shape switching

effect has been observed in HPL alone which has potential to be considered as thermal actuation. Now, it is important to understand the cause of the reversible shape switching effect in polyurethanes and distinguish their shape memory behaviour based on structural alteration.

The melting temperatures during first heating are found to be 34 and 43 ºC, assigned for soft segment of HPL and MPL, respectively, for same PCL-diol as the soft segment for both the polymers and considerable lower melting of HPL indicates stronger interaction between the segments which is also supportive from the lower heat of fusion for HPL (10 J.gm^{-1}) as compared to MPL (20 J.gm^{-1}) (**Fig. 2b**). Further, crystallization is evident in HPL (T_c~3 ºC) during cooling against cold crystallization noticed in MPL during second heating and distinct hard segment melting is observed at 130 ºC for HPL vis-à-vis no hard segment melting and crystallization in MPL. This anomaly in crystallization behaviour reflects in their shape fixation/recovery where readily crystallisable HPL exhibit excellent SME against poor show by MPL due to its meagre crystallization tendency at similar temperature range. The higher degree of crystallization of the soft segment (actuating domain) of HPL is also confirmed through the study of morphological changes with temperature as observed using polarizing optical microscope where recrystallization of soft segment is evident after cooling from 60 ºC and recrystallization of hard segment after cooling from 200 ºC (**Fig. 2c** and ***supplementary Fig. S7***). Moreover, the separation of crystalline and amorphous domains is more clear at high magnification images, observed through AFM, where crystalline zones (black areas) are consisting of large number of smaller crystalline domains and white areas also have some tiny crystalline zone in HPL (**Fig. 2d**) as compared to clear absence of any crystalline zone noticed under white areas in MPL (***supplementary Fig. S8***). This morphological alteration indicates the distribution of hard segment throughout the polymer (even in amorphous zone) in HPL against the predominant agglomeration of hard segments in MPL. So, this higher degree of crystallization in HPL along with reformation and melting during cooling

and heating cycles make it able to switch between shape A and shape B reversibly. This is to mention that the morphology and changes in crystallization in HPT is not conducive enough to show reversible shape switching (***supplementary Fig. S9***).

Self-sufficient smart gripper is one of the appealing applications of reversible shape switching amongst wide range of important utilities of shape memory materials.[15] Grippers, created using two long strips, were arranged in a cross pattern and were programmed into a closed shape as shown in **Fig. 3a (top)**. Grippers take the complete close loop at T_{fix} ~5 ^{o}C for HPL, through T_{prog} ~90^{o}C, which again open up at T_{rev}~50 ^{o}C and exhibit its total reversibility at 5 ^{o}C. On the other hand, gripper made of MPL is unable to exhibit close loop at T_{fix} and do not show any reversibility. **Fig. 3a (bottom)** demonstrates the ability of HPL picking up a bolt at 5 - 25 ^{o}C automatically and releasing it at T_{rev} ~50 ^{o}C reversibly (by changing the temperature cycle as discussed above) showing the important function of a mini robot through reversible shape switching against the non-functioning of other polymers (MPL and HPT). To understand the temperature variant reversible shape switching of HPL, small angle neutron scattering has been performed at different stages of the change in shape (below, above the T_{rev} and at higher than T_m of soft segment but below the melting of hard segment). A peak appears at wavevector, q~0.49 nm^{-1} above the T_{rev} (~60 ^{o}C and higher temperature of 100 ^{o}C), clearly indicates the emergence of Bragg's type reflection due to the consolidation of hard segmented zone which is prominent in HPT (***supplementary Fig. S10***) below the T_{rev} at 30 ^{o}C, corresponding to the characteristic length ($\Lambda_c=\frac{2\pi}{q_m}$) of 13 nm similar to HPT, where, q_m is the wavevector associated to the peak position (**Fig. 3b**). In contrast, MPL do not show any peak at higher temperature indicating no change of structure or consolidation due to heating, rather a moderately steady decrease of intensity is noticed at higher wavevector. Interestingly, the correlation length, ξ, as calculated from the linear fit of initial wavevector using Debye-Buche fitting (*equation 4*), shows systematic diminish value of 1.8, 1.3 and 0.5 nm at 30, 60 and 100 ^{o}C for HPL indicating smaller correlation length at higher temperature (**inset figure of Fig. 3b**).

$$I(q)=\frac{I(o)}{(1+\xi^2 q^2)^2} \qquad (4)$$

This is to mention that correlation length indicates the size of blob and reduced dimension for HPL at higher temperature indicate the transfer of hard segment within the soft segment towards the

nearby organized hard segment against the unaltered values of MPL (2 nm), irrespective of temperature studied. The movement of hard segment is facilitated as the local environment become liquid and less interacted system at high temperature (T (60 ^{o}C) >T_m of soft segment (34^{o}C)). The local movement of the hard segment in molten soft segment has been shown in a schematic manner in **Fig. 3c** for HPL predominantly due to hydrogen bonded interactions between hard segments vis-à-vis no alteration observed in MPL due to initial consolidation.

Temperature induced structural change is evident in HPL as measured from the X-ray diffraction at below and above the T_{rev} and melting of soft segment exclusively (**Fig. 3d**). The crystal planes having the d_{110} spacing of 0.42 nm corresponds to the reflection at 2θ~21.24^{o} are presents both in HPL and MPL which arise due to the crystallization of soft segment of polyurethanes (shown by the vertical dotted lines). The peaks disappear upon heating above the melting of soft segment (*e.g.* at 60 ^{o}C and higher temperature) both for HPL and MPL while it reappears in HPL immediately upon cooling to room temperature but takes long time (approx. a day) for MPL. Ether based PU (HPT) does not exhibit this peak as the soft segment is in molten state at room temperature (***supplementary Fig. S11***). Interestingly, the relative intensity increases for (200) plane (d~0.41 nm; shown by the arrows) and the intensity of (010) plane (d~0.37 nm) gradually decrease with increasing temperature in HPL showing Brill transition from triclinic to pseudo hexagonal phase of hard segment crystal at high temperature.[32,33] Similar phase transition is observed in nylon system and more stable pseudohexagonal phase at higher temperature goes back to triclinic phase on cooling and, therefore, temperature induced structural change not only instigate the actuator domain (predominantly soft segment) but also determine the geometry of the shape provider domain (hard segment) in HPL which supports better stability to the shape A at T_{rev}.

Temperature variation *SANS* studies indicate the consolidation of hard segment at high temperature (peak at q~0.49 nm^{-1} above T_{rev}) made possible through the migration of hard segment closely associated with soft segment and this transfer of hard segment is feasible only when the soft segment is in liquid state (above its melting point). A model has been proposed based on the relative position of soft and hard segment for two different polymers (HPL and HPT) (**Fig. 3e**). HPT shows a strong peak at q~0.49 nm^{-1} due to organized hard segment while the absence of any peak for HPL at room temperature indicate its disordered/distributed structure as also evident from

the shifting of ester band at FTIR (**Fig. 1b**) unlike MPL and HPT, due to interaction between soft and hard segments. The presence of some hard segment around soft segment and move towards hard segment after the melting of soft segment leading to the molecular flipping which generate consolidation of hard segment and, thereby, shows a peak at q~0.49 nm^{-1} and those hard segments disperse during crystallization of soft segment at below T_{rev} justifying the absence of *SANS* peak again at room temperature. The disappearance of peak in XRD (d_{110} ~ 0.42 nm) at 60 ^{o}C and higher temperature and its reappearance at room temperature supports the melting and recrystallization of soft segment by changing the temperature cycle. Main reason behind this molecular flipping in HPL is better interactions between ester linkages in soft segment and hard segment together with entropically favoured state which is categorically absent in HPT (ether based PU) This is to mention that there is no shifting of >C–O FTIR peak either in HPT or MPL. The recrystallization kinetics of soft segment in MPL is very slow as evident of predominant amorphous nature just after cooling (**Figure 3d**) while it recrystallizes after one day. However, the combination of molecular flipping and recrystallization of soft segment in HPL allows it to exhibit reversible shape switching effect as compared to MPL or HPT and the presence of hard segment around soft segments help inducing recrystallization by providing the heterogeneous nucleation sites. Now, the soft segment lies between two tiny hard segments assembly and thereby act as a spring where some hard segments are distributed in HPL for showcasing the excellent shape memory effect. During heating at T_{rev}, soft segments coiled because of melting and the distributed hard segments get organised which make contraction in length dimension of the strip. Further, during cooling the organised hard segments get distributed in soft segments and induced the crystallization in soft segments resulting expansion of the strip to go back to the shape B. Therefore, molecular flipping, especially the hard segment, takes place during heating-cooling cycle along with the formation of stable pseudohexagonal phase at higher temperature which provide the stability of shape A (temporary shape) and subsequently make this system reversible shape switching material. On the other hand, no hard segment is distributed in soft segment in case of HPT and lack of recrystallization in MPL is responsible for imperfect SME.

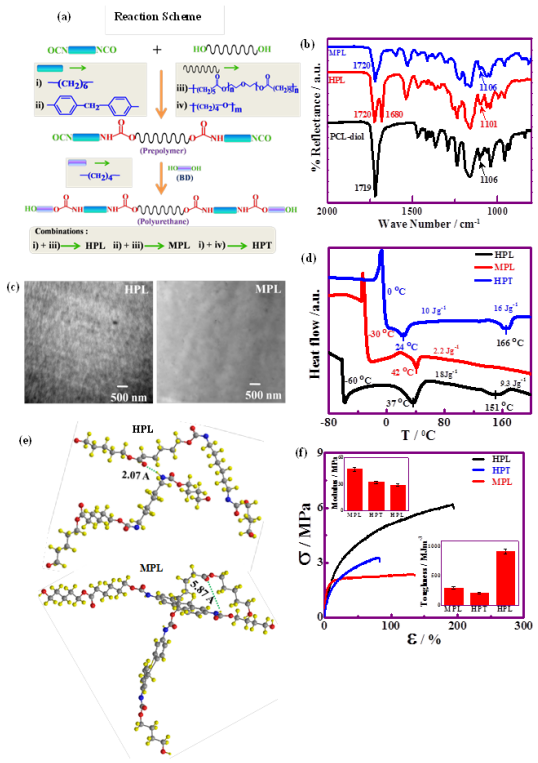


Figure 1: a) Schematic representation of polyurethane synthesis using different diisocyanates and polyols and keeping the chain extender same. They are designate as HPL (when hexamethylene diisocyanate and polycaprolactone diol are used), MPL (when 4, 4-Methylene bis (phenylisocyanate) and polycaprolactone diol are used), and HPT (when hexamethylene diisocyanate and polycaprolactone are used), **b)** Infrared spectrum shows the shifting in stretching frequency due to H-bonding in aromatic (MPL) and aliphatic (HPL) polyurethanes, **c)** Bright field transmission electron micrographs of indicated PU, **d)** DSC thermograms of different polyurethanes in the second run, **e)** Simulation of energy minimised configuration of two sheets of HPL and MPL considering one diisocyanate, one polyol and one chain extender unit through semiemperical AM1 method, as implicated in chem3D ultra 8.0. It shows that the minimum distance between ester carbonyl oxygen of one sheet and urethane NH hydrogen of another sheet is 2.07 Å for HPL and 5.87 Å for MPL, and, **f)** Mechanical behaviour of HPT, HPL and MPL. Inset shows the modulus and toughness of the indicated PUs

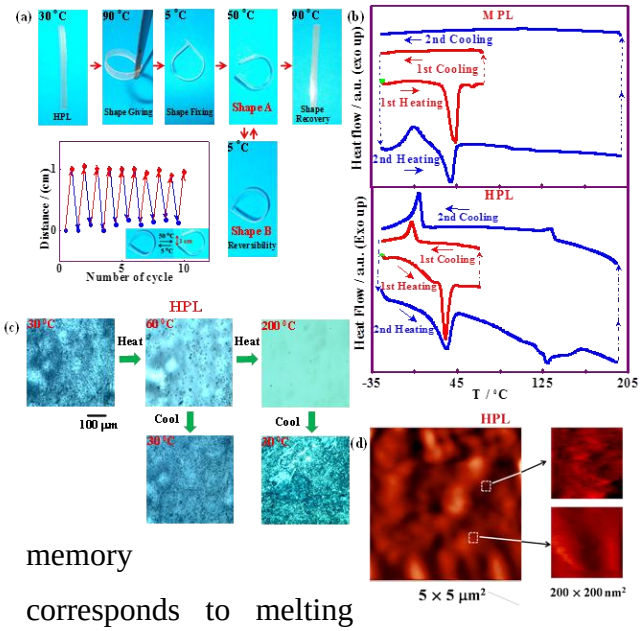


Figure 2: a) Photograph series demonstrating reversible shape switching of HPL and the plot shows 10 repeating cycles of reversible shape switching, **b)** DSC thermogramme of HPL and MPL showing the differences in crystallization behaviour and also the reversibility in shape memory behaviour for HPL. The 1st heating and cooling corresponds to melting and crystallization of soft segment (actuator domain) and 2nd heating and cooling corresponds to melting and crystallization of soft and hard segments. The heating and cooling rates are 10^{o}/ min and 5^{o} / min respectively, **c)** POM micrographs of HPL showing reversibly melting and crystallization of crystalline soft segment on heating above its T_m and cooling to room temperature and same thing for hard segment as well, and, d) AFM topographic images of HPL. The enlarge part shows further smaller crystallites in black region and some extent in white region also.

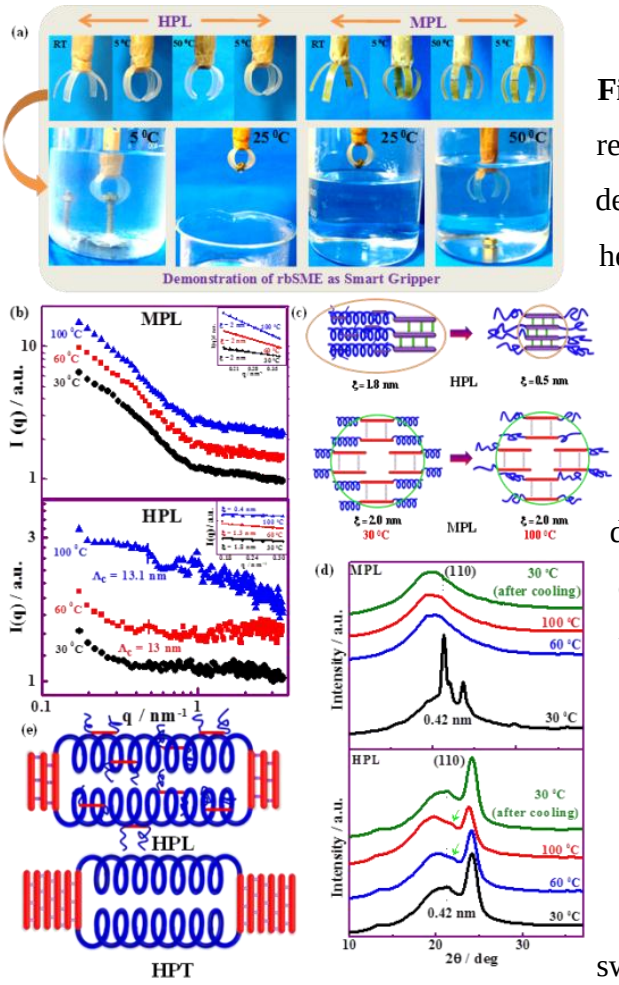


Figure 3: a) Demonstration device from HPL for reversible shape switching: A reversible gripper device reversible grips and releases a nut under heating and cooling cycle, **b)** Small angle neutron scattering study with temperature of MPL and HPL, **c)** Models showing change in cluster size with temperature, **d)** Study of change in crystal structure with temperature in wide angle X-ray diffraction, and, **e)** Proposed spring models to demonstrate reversible shape switching in HPL through molecular flipping.

Conclusions

Our strategy is to generate reversible shape switching phenomena in polyurethane and to assign two functions to two different structural domains which are connected to each other in an alternative manner at the molecular level. The soft segments of the polyurethane acts as actuator domains which expand during cooling to T_{fix} and collapse on heating at T_{rev} and the hard segments not only act as geometry determining domains which provide a skeleton at T_{rev} but also help to crystallize the actuator domains on cooling. The key point of the concept behind reversible shape switching is the flipping of the hard segment of polyurethane on heating and cooling in the actuating direction and the developed material has full potential to act as mini robot of future generation.

Acknowledgement: The authors acknowledge IIT (BHU) for supporting fellowship and Prof. B. Ray, Department of Chemistry, Institute of Science, Banaras Hindu University, Varanasi, India for GPC measurement.

References

(1) Xie, T. Tunable Polymer Multi-Shape Memory Effect. *Nature* **2010**, *464*, 267-270.

(2) Lendlein, A.; Jiang, H.; Jünger, O.; Langer, R. Light-Induced Shape-Memory Polymers. *Nature* **2005**, *434*, 879-882.

(3) Leng, J.; Lv, H.; Liu, Y.; Du, S. "Water-Driven Programable Polyurethane Shape Memory Polymer: Demonstration and Mechanism" *Appl. Phys. Lett.* **2005**, *86*, 114105.

(4) Mendez, J.; Annamalai, P.; Eichhorn, S.; Rusli, R.; Rowan, S.; Foster, E.; Weder, C. Bioinspired Mechanically Adaptive Polymer Nanocomposites With Water-Activated Shape-Memory Effect.*Macromolecules* **2011**, *44*, 6827-6835.

(5) Chen, H.; Li, Y.; Liu, Y.; Gong, T.; Wang, L.; Zhou, S. Highly Ph-Sensitive Polyurethane Exhibiting Shape Memory And Drug Release. *Polym. Chem.* **2014**, *5*, 5168.

(6) Jung, Y.; Yoo, H.; Kim, Y.; Cho, J.; Endo, M. Electroactive Shape Memory Performance Of Polyurethane Composite Having Homogeneously Dispersed And Covalently Crosslinked Carbon Nanotubes. *Carbon* **2010**, *48*, 1598-1603.

(7) Szabó, D.; Szeghy, G.; Zrínyi, M. Shape Transition Of Magnetic Field Sensitive Polymer Gels.*Macromolecules* **1998**, *31*, 6541-6548.

(9) Schmidt, A. Electromagnetic Activation Of Shape Memory Polymer Networks Containing Magnetic Nanoparticles. *Macromol. Rapid Commun.* **2006**, *27*, 1168-1172.

(10) Lendlein, A.; Kelch, S. Shape-Memory Polymers. *Angewandte Chemie International Edition* **2002**,*41*, 2034.

(11) Ohm, C.; Serra, C.; Zentel, R. A Continuous Flow Synthesis Of Micrometer-Sized Actuators From Liquid Crystalline Elastomers. *Adv. Mater.* **2009**, *21*, 4859-4862.

(12) Chung, T.; Romo-Uribe, A.; Mather, P. Two-Way Reversible Shape Memory In A Semicrystalline Network. *Macromolecules* **2008**, *41*, 184-192.

(13) Pandini, S.; Passera, S.; Messori, M.; Paderni, K.; Toselli, M.; Gianoncelli, A.; Bontempi, E.; Riccò, T. Two-Way Reversible Shape Memory Behaviour Of Crosslinked Poly(E-Caprolactone).*Polymer* **2012**, *53*, 1915-1924.

(14) Behl, M.; Kratz, K.; Zotzmann, J.; Nöchel, U.; Lendlein, A. Reversible Bidirectional Shape-Memory Polymers. *Adv. Mater.* **2013**, *25*, 4466-4469.

(15) Behl, M.; Kratz, K.; Noechel, U.; Sauter, T.; Lendlein, A. Temperature-Memory Polymer Actuators. *Proceedings of the National Academy of Sciences* **2013**, *110*, 12555-12559.

(16) I. Kolesov, O. Dolynchuk, D. Jehnichen, U. Reuter, M. Stamm, H. Radusch, Changes Of Crystal Structure And Morphology During Two-Way Shape-Memory Cycles In Cross-Linked Linear And Short-Chain Branched Polyethylenes.*Macromolecules* **2015**, *48*, 4438−4450.

(17) Osada, Y.; Matsuda, A. Shape Memory In Hydrogels. *Nature* **1995**, *376*, 219-219.

(18) Huang, W.; Zhao, Y.; Wang, C.; Ding, Z.; Purnawali, H.; Tang, C.; Zhang, J. Thermo/Chemo-Responsive Shape Memory Effect In Polymers: A Sketch Of Working Mechanisms, Fundamentals And Optimization. *Journal of Polymer Research* **2012**, *19*,9952.

(19) Ahn, S.; Deshmukh, P.; Kasi, R. Shape Memory Behavior Of Side-Chain Liquid Crystalline Polymer Networks Triggered By Dual Transition Temperatures. *Macromolecules* **2010**, *43*, 7330-7340.

(20) Ware, T.; Hearon, K.; Lonnecker, A.; Wooley, K.; Maitland, D.; Voit, W. Triple-Shape Memory Polymers Based On Self-Complementary Hydrogen Bonding. *Macromolecules* **2012**, *45*, 1062-1069.

(21) Li, J.; Liu, T.; Xia, S.; Pan, Y.; Zheng, Z.; Ding, X.; Peng, Y. A Versatile Approach To Achieve Quintuple-Shape Memory Effect By Semi-Interpenetrating Polymer Networks Containing Broadened Glass Transition And Crystalline Segments. *Journal of Materials Chemistry* **2011**, *21*, 12213.

(22) Riess, G. Micellization Of Block Copolymers. *Progress in Polymer Science* **2003**, *28*, 1107-1170.

(23) Discher, B. Polymersomes: Tough Vesicles Made From Diblock Copolymers. *Science* **1999**, *284*, 1143-1146.

(24) Mishra, A.; Purkayastha, B.; Roy, J.; Aswal, V.; Maiti, P. Tunable Properties Of Self-Assembled Polyurethane Using Two-Dimensional Nanoparticles: Potential Nano-Biohybrid. *Macromolecules* **2010**, *43*, 9928-9936.

(25) Mishra, A.; Das Purkayastha, B.; Roy, J.; Aswal, V.; Maiti, P. Nanoparticle Controlled Self-Assembly In Varying Chain Extended Polyurethanes As Potential Nanobiomaterials. *J. Phys. Chem. C* **2012**, *116*, 2260-2270.

(26) Mishra, A.; Singh, S.; Dash, D.; Aswal, V.; Maiti, B.; Misra, M.; Maiti, P. Self-Assembled Aliphatic Chain Extended Polyurethane Nanobiohybrids: Emerging Hemocompatible Biomaterials For Sustained Drug Delivery. *Acta Biomaterialia* **2014**, *10*, 2133-2146.

(27) Wei, Z.; Sandstrom, R.; Miyazaki, S. Shape memory materials and hybrid composites for smart systems: Part II Shape-memory hybrid composites *Journal of Materials Science* **1998,** *33*, 3763-3783**.**

(28) Patel, D.; Rana, D.; Aswal, V.; Srivastava, S.; Roy, P.; Maiti, P. Influence Of Graphene On Self-Assembly Of Polyurethane And Evaluation Of Its Biomedical Properties. *Polymer* **2015**, *65*, 183-192.

(29) Mishra, A.; Aswal, V.; Maiti, P. Nanostructure To Microstructure Self-Assembly Of Aliphatic Polyurethanes: The Effect On Mechanical Properties. *The Journal of Physical Chemistry B* **2010**,*114*, 5292-5300.

(30) Zhou, J.; Turner, S.; Brosnan, S.; Li, Q.; Carrillo, J.; Nykypanchuk, D.; Gang, O.; Ashby, V.; Dobrynin, A.; Sheiko, S. Shapeshifting: Reversible Shape Memory In Semicrystalline Elastomers.*Macromolecules* **2014**, *47*, 1768-1776.

(31) Hong, S.; Yu, W.; Youk, J. Two-Way Shape Memory Behavior Of Shape Memory Polyurethanes With A Bias Load. *Smart Mater. Struct.* **2010**, *19*, 035022

(32) McKiernan, R.; Heintz, A.; Hsu, S.; Atkins, E.; Penelle, J.; Gido, S. Influence Of Hydrogen Bonding On The Crystallization Behavior Of Semicrystalline Polyurethanes. *Macromolecules* **2002**, *35*, 6970-6974.

(33) Fernández, C.; Bermúdez, M.; Muñoz-Guerra, S.; León, S.; Versteegen, R.; Meijer, E. Crystal Structure And Morphology Of Linear Aliphatic N - Polyurethanes. *Macromolecules* **2010**, *43*, 4161-4171.

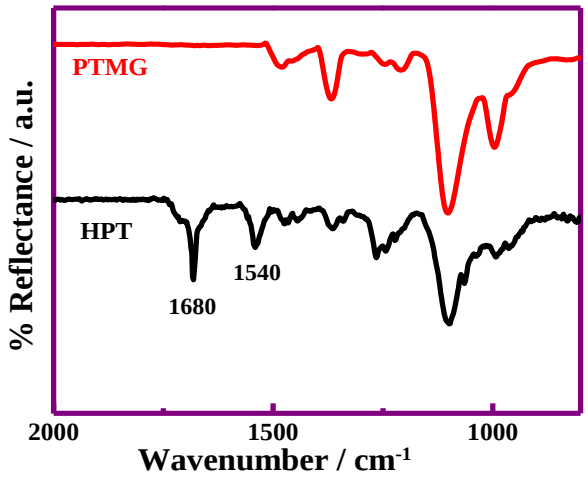
Supplementary Information

Reversible Shape Shifting Effect in Polyurethanes through Molecular Flipping: Roll of Induced Crystallizati

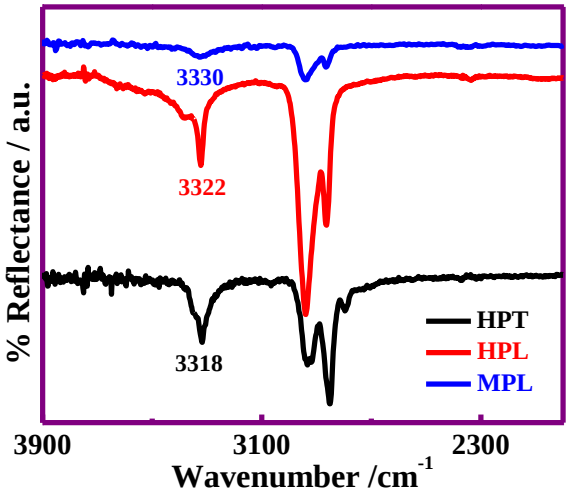
Arpan Biswas and Pralay Maiti[1]*

Table S1: Molecular weight of three synthesised polymer (HPL, MPL, HPT) were determined with GPC.

PU Samples	Mn	Mw	PDI
HPL	**35,680**	**64,000**	**1.79**
MPL	**24,600**	**43,100**	**1.75**
HPT	**34,168**	**1,08067**	**3.16**



a)



b)

Figure S1: a) FT-IR shows peaks at 1680 cm^{-1} and 1540 cm^{-1} in case of HPT which are the evidence of formation of urethane linkage and strong H-bonding, absent in PTMG. b) Here a continuous lowering in >NH stretching frequency from MPL, HPL, to HPT was observed, evidence of increase of extent of H-bonding respectively.

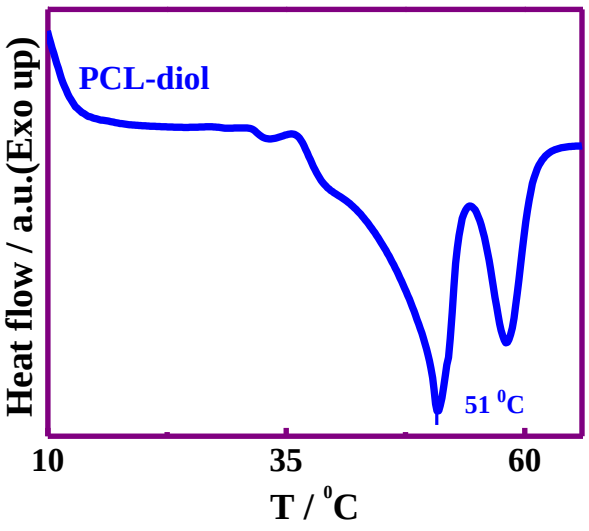


Figure S2: DSC thermogram of pure PCL – diol indicating melting of the crystalline part near around 51 ^{0}C and which shifts to lower temperature in the polymers.

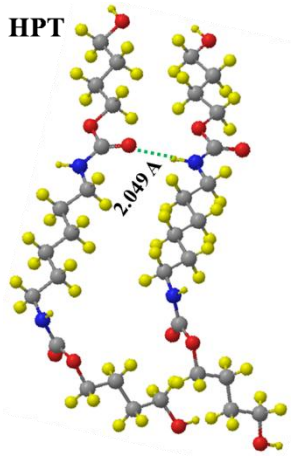
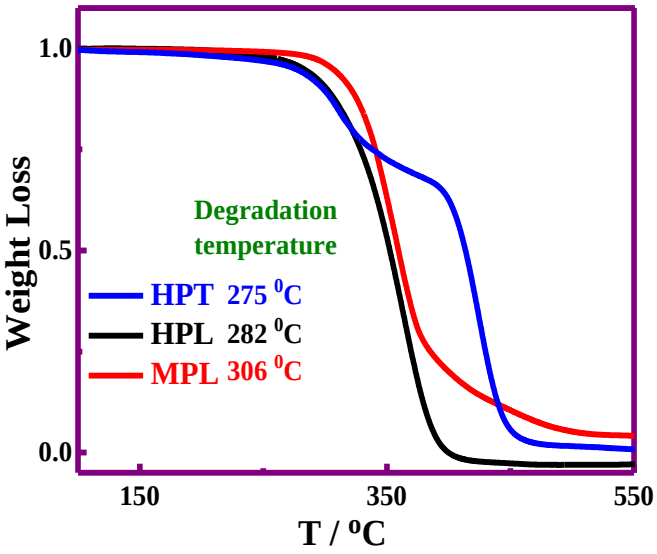


Figure S3: Simulation of energy minimised configuration of two sheets of HPT considering one diisocyanate, one polyol and one chain extender through semiemperical AM1 method, as implicated in chem3D ultra 8.0. It shows that the minimum distance between urethane carbonyl oxygen of one sheet and urethane NH hydrogen of another sheet is 2.049 Å.



a)

b)

Figure S4: TGA thermogramme of synthesised PUs. A two stage degradation was observed in case of HPT (HMDI – ether system) which is due to the microphase separation in presence of

strong H-bonding in urethane linkage only. On the otherhand, in spite of presence of strong interaction in HPL (HMDI – ester system) evident from FTIR, it does not show two stage degradation like HPT.

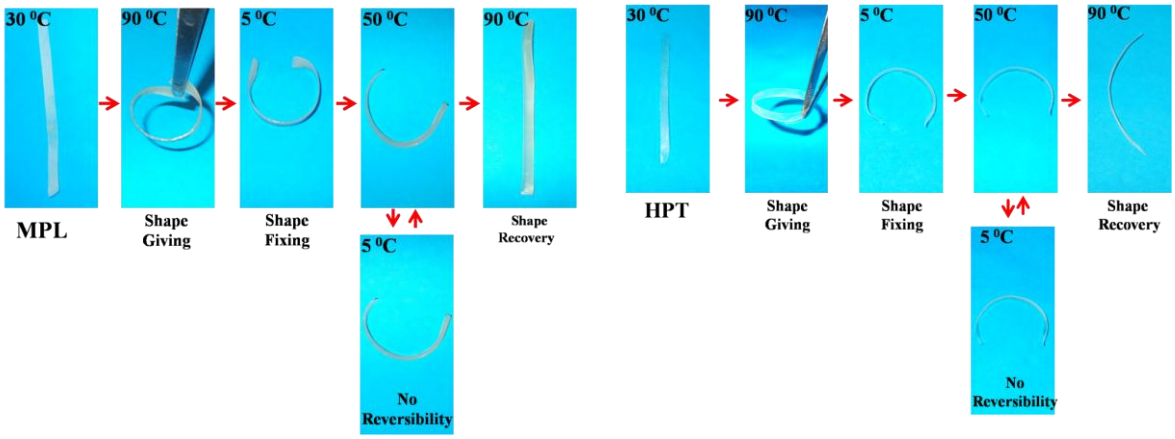


Figure S5: a) and b) are some photographic series that demonstrate one way shape memory behaviour of MPL and HPT respectively with poor shape fixicity and also the inability of them in reversible shape shifting upon heating and cooling under stress free condition.

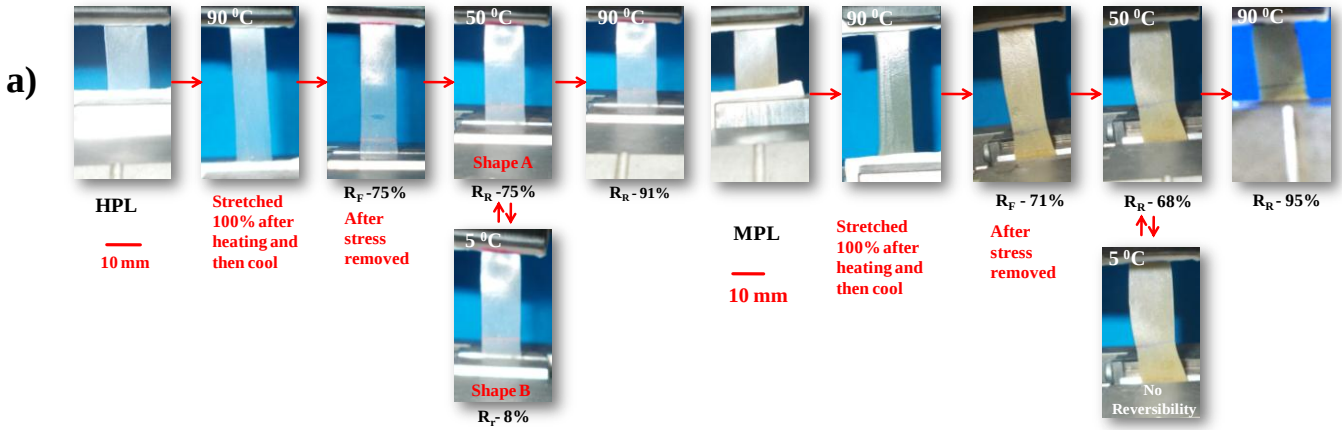


Figure S6: Quantitative measurement of the efficiency of shape fixation, shape recovery and reversible elongation (under stress free condition) of HPL (a) and MPL (b) were measured with uniaxial universal testing mechaine(UTM). Here HPL shows 8% (R_r) reversible elongation under cooling at 5 ^oC against no reversible shape shifting of MPL.

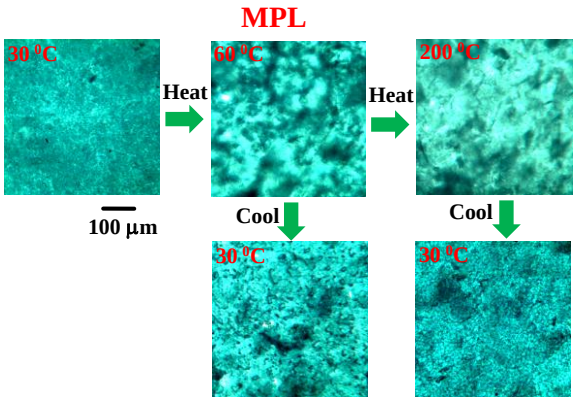


Figure S7: Morphological changes with temperature of MPL were observed with polarizing optical microscope (POM) in transmission mode. Crystalline parts which were disappeared above the T_m of soft segment, does not reappear upon cooling to room temperature. At 200 ^oC (above T_m of MPL) the black sports were due to the artefacts.

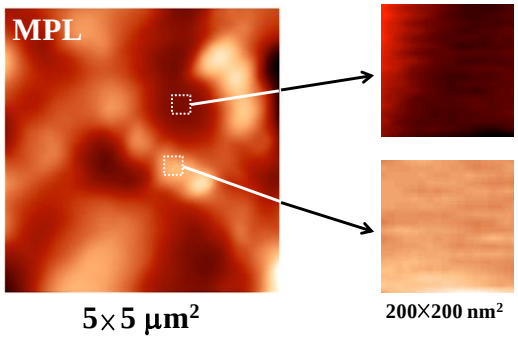
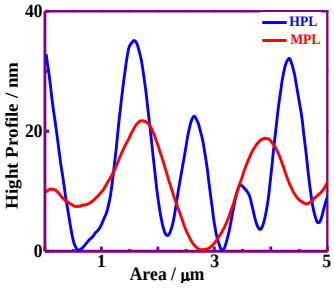
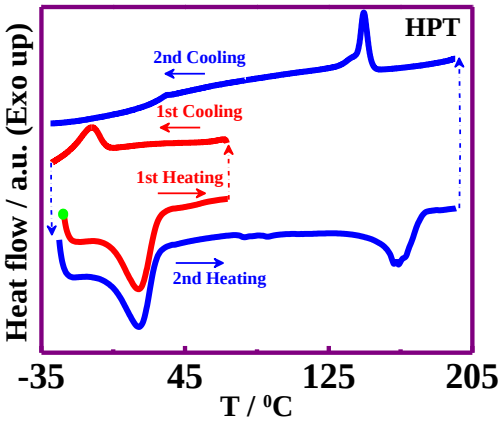


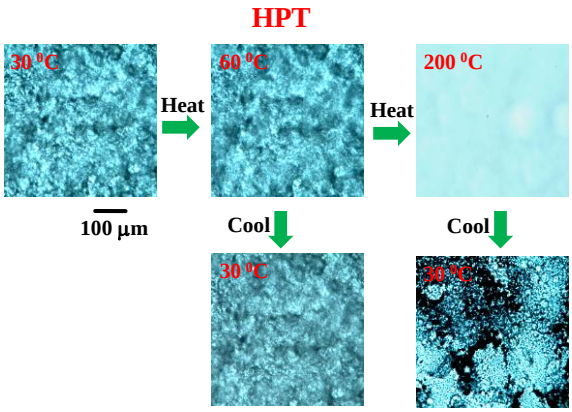
Figure S8: AFM topography of MPL contains some black and white clusters. Further scanning of black cluster reveals it contains some agglomerated hard segments on the otherhand white cluster is purely amorphous. Height profile support the distribution of hard segment throughout the polymer in HPL against the predominant agglomeration of hard segments in MPL.



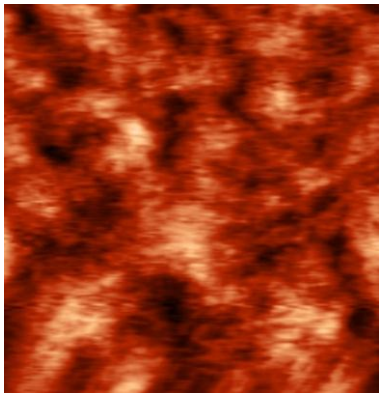
a)



b)



c)



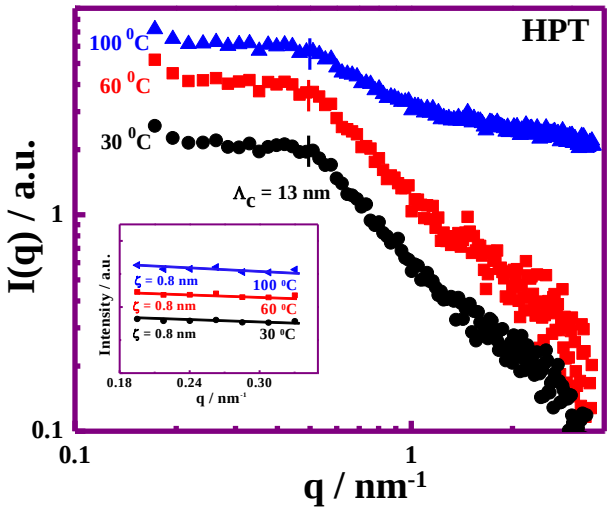


Figure S9: a) DSC thermogram of HPT was performed by maintaining the heating and cooling rate 10 degrees / min and 5 degrees / min respectively which reveals that soft segment melts at around 20 ^{o}C and crystallized at -7 ^{o}C, which is sufficiently low compare to crystallization of HPL (3 ^{o}C), during 1st heating and cooling respectively. On the otherhand during 2nd heating both soft

segment and hard segment melts at 20 ^{o}C and 163 ^{o}C respectively but surprisingly only hard segment get crystallized on cooling but soft segment fails to do so. Therefore rate of crystallization of HPT low enough compare to HPL and this dissimilarity in crystallization behaviour disable HPT to show rbSME b) Black and white domains were seen by cross nicol optical polarizing microscope in transmission mode. On increasing temperature from 30 ^{o}C to 60 ^{o}C no change in morphology has been observed but on further increases in temperature upto 200 ^{o}C the black domains (crystalline) fully disappear. These can be explained by the fact that at 30 ^{o}C the soft segment is in molten state (evident from DSC) therefore the morphological changes with temperature upto 60 ^{o}C which is observed in case of MPL and HPL, does not takes place in HPT but at 200 ^{o}C the black spots completely disappear because of melting of the crystalline hard segments at 163 ^{o}C but due to poor rate of crystallization it fails to recrystallize fully on cooling from 200 ^{o}C. c) AFM topograph of HPT consist black and white clusters in an alternative manner with an average size of black clusters 454 nm and this size decreases to 368 nm for HPL and to 196 nm for MPL. Clustering takes place due to extensive hydrogen bonding in hard segments (evident from FTIR). These small clusters further accumulate and become observable in cross nicol optical microscope. The domain size of crystallites observed in POM also follows the same decreasing order for HPT, HPL and MPL.

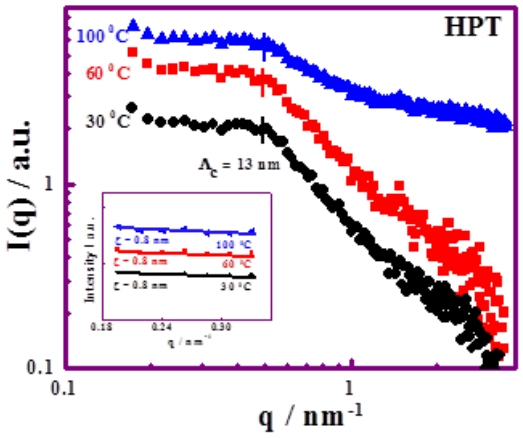


Figure S10: The development of the small angle neutron scattering (SANS) peaks at q ~ 0.49 nm^{-1} for HPT, corresponding to the characteristic length ($\Lambda_c = 2\pi / q_m$) ~ 13 nm, is an indication of ordered nanostructure within the cylindrical domain observed in AFM topographs. The corelation length (ξ= 0.8 nm) is obtained by fitting the initial wavevectors with Debye-Buche Equation (*equation 1*). There is no change in characteristic length and correlation length both with changing temperature. The extensive H-bonding (evident from FTIR) gives opportunity to molecular sheets to come closer. Now if the H-bonding takes place only one particular position then an orderings/assembly should present there and upto the temperature below the melting point the ordering/assembly should persist. The SANS, AFM and POM results of HPT confirms that the self-assembly takes place within the molecular sheets which results in extensive phase separated morphologies and the size of the crystalline phase (black) should increase with extent of self-assembly (evident from AFM). HPL also have extensive H-bonding (FTIR) and phase separated morphology in AFM and POM but it disable to show any peak in SANS at 30 ^oC although it shows peaks at higher temperature at q ~ 0.49, which is at the similar position which HPT have. Now, it is evident that good interaction between urethane linkage and soft segment occurs in HPL in addition to meagre hard segmented interaction (*cf. Simulation results*) and amorphous phase also content some tiny crystallites accompanied by crystallines phase. So, from this result we may conclude that the assembly also takes place in HPL system but it is distributed but at higher temperature when soft segment melts hard segments migrates and generates an ordered or assembled structure which produces a peak in SANS.

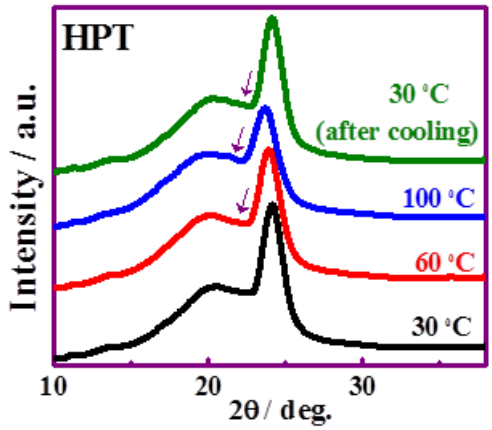


Figure S11: WAXS study also confirms that no structural changes take place due to soft segments when temperature is increased from 30 ºC to 60 ºC or 100 ºC. The structural changes which takes place at 60 ºC and 100 ºC is solely for hard segment. The relative intensity increases for (200) plane (d~0.41 nm; shown by the arrows) and the intensity of (010) plane (d~0.37 nm) gradually decrease with increasing temperature. Therfore, Brill transition takes place from triclinic(less ordered structure) to pseudohexagonal (more ordered structure).

MACRO 506

UV based Photocatalytic treatment of Methyl Tertiary-Butyl Ether (MTBE) contaminated water using TiO2–Reduced Graphene Oxide nanocomposites as a photocatalyst

Ojha Ankita[a] *, Singh P.K.[a]., Tiwary D.[a]and Mishra P.K.[b]

[a]*DepartmentofChemistry, Indian Institute of Technology, BHU, Varanasi, India*
[b]*DepartmentofChemical Engineering and Technology, Indian Institute of Technology, BHU, Varanasi, India*

ankitaojha1208@gmail.com

Methyl *tert*-Butyl Ether (MTBE), an oxygenate compound, is globally used as an anti-knocking fuel component in gasoline. The high water solubility and the pervasiveness of MTBE is the major reason behind its presence in groundwater aquifers and surface water bodies. It makes the water non potable by imparting a bad taste and is known to cause human ailments on constant exposure.

The present study focuses on the degradation of MTBE by using TiO_2– Reduced Graphene Oxide (RGO) nanocomposites as a photo catalyst. The catalysts were synthesized by a multi-stage process and its properties were characterized by XRD (X-Ray Diffraction), FT-IR (Fourier Transform Infrared Spectroscopy), SEM (Scanning Electron microscopy), EDX (Energy Dispersive X-Ray Spectroscopy), Raman Spectroscopy, UV Visible spectroscopy, XPS (X-Ray Photoelectron Spectroscopy) and TGA (Thermo gravimetric Analysis).

The photocatalytic efficiency of the catalysts was determined by degradation of MTBE in a photochemical reactor by UV irradiation under ambient conditions. It was observed that the degradation rate of hybrid catalysts was higher than that of bare TiO_2. The degradation was analyzed by using Gas chromatography. Effect of various parameters such as catalyst loading, pH levels and intensity of UV light exposure were also studied.

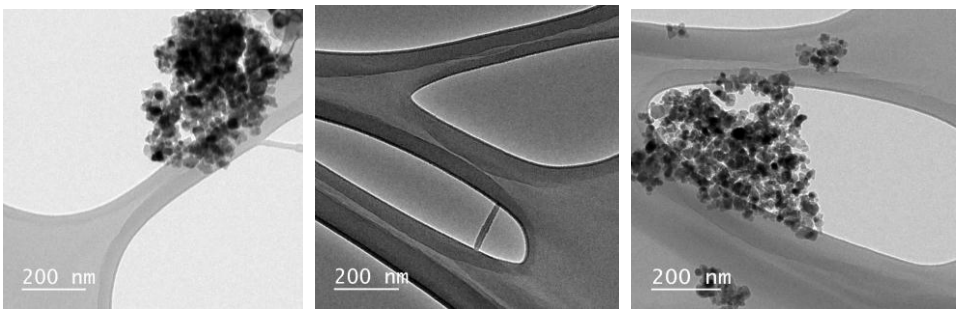


Fig: TEM images of the nanocomposites prepared

It is mandatory that the abstract should not exceed two pages. The font type, font sizes and margins given in this template shall be followed for the preparation of the abstract.

References

[82] Štengl V.; Bakardjieva S.; Grygar T.M., Bludská J.; Kormunda M. C*hemistry Central Journal* 7-41 (2013).

[83] Williams G.; Segerand B.; Kamat P.V.; *ACS Nano*,*2*(7) (2008) 1487–1491.

MACRO 512

Synergistic Effect of Nano Reinforcement and Cross-linking Towards Polyvinyl alcohol (PVA) Properties

Amit Kumar Sonker[a], Naveen Tiwari[a], Rajaram Krishna Nagarale[a], Vivek Verma[b*]

[a]*Department of Materials Science and Engineering, Indian Institute of Technology, Kanpur, India*

[b]*Electro Membrane Processes Division, CSIR-Central salt and marine chemicals research institute, Bhavnagar, India*

corresponding author's email - *vverma@iitk.ac.in*

Here, for the first time we are reporting far increase in tensile strength of the PVA composite material. The obtained best value of 122 MPa and 14.6% swelling shows the excellent synergistic effect of both cross-linker and reinforcement material. The composite films were prepared by

simple mechanical dispersion of reinforcement material, bacterial cellulose nano-whiskers (BCNW) into PVA solution followed by cross linking with diacids, succinic acid (SuA) and adipic acid (AdA). We have in detail evaluated the effect of aliphatic carbon chain length of cross-linker on thermal, mechanical and water uptake properties. Neat PVA had strength of 37.3 MPa. With 5% reinforced of BCNW i.e. without cross linking, it exhibited 97% increase i.e. 74.5 MPa. With cross-linking of 15 mmol of SuA and AdA PVA films for 2 hours had excellent thermal properties with swelling percentage of 19% and 26.6% and tensile strength of 103 MPa and 67 MPa, respectively. The best result obtained was for 5% BCNW-PVA films crosslinked with 15 mmol succinic acid. These results were explained on the basis of synergetic cross-linking and extended hydrogen bonding between PVA and reinforcement material. The BCNW-PVA cross-linked and cross-linked PVA films can be used as biological implants, bio-inspired materials, membrane for pervaporation and filtration systems etc.

Keywords: Bacterial cellulose nano-whiskers, cross-linker length, swelling properties, mechanical properties, thermal properties

Reference

[1] Sonker, A. K., Tiwari, N., Nagarale, R. K. and Verma, V. (2016), Synergistic effect of cellulose nanowhiskers reinforcement and dicarboxylic acids crosslinking towards polyvinyl alcohol properties. J. Polym. Sci. Part A: Polym. Chem., 54: 2515–2525. doi:10.1002/pola.28129

MACRO 513

Clay/Graphene nanohybrid incorporated Poly Vinyl Alcohol : An Efficient Flame Retardant

Stanly Sona, John Honey *

Dept .of Polymer Science and Rubber Technology, Cochin University of Science and Technology, Kerala-682022, India

** Corresponding author*honey@cusat.ac.in

Abstract

Recently, nano-composites have gained acceptance in improving the flame retardancy of polymer products. In this paper, we are reporting the synergistic effect of the nanohybrid based on organically modified MMT and reduced graphene (rGO) on the flame retardancy of PVA. Nano hybrid of rGO/MMT hybrids are prepared by in situ reduction of GO in the presence of O-MMT through three different methods viz chemical reduction, thermal reduction and hydrothermal

method. Flame retardant PVA nanocomposite films are prepared by simple ultra-sonication of nanohybrid in PVA solution containing cross linker. The nanohybrids and the composite is characterised using IR,TGA, XRD and TEM. Flammability studies are carried out using limiting oxygen index (LOI).

Keywords: *Clay-graphene hybrids; Flame retardant polymers; thermal stability, nanocomposites*

Introduction

During the past few decades the most promising solution to improve flame resistance of polymers is by using nano materials like CNT, silicates, graphene etc[1] because conventional flame retardants additives do not always functions as expected and is highly toxic.[2] Among the carbonaceous additives graphene attracted tremendous interest due to its high mechanical properties, thermal and electrical conductivity and gas barrier property but its flame retardancy is not so impressive because of its weak thermo oxidative stability. [3]The hybrid with clay, a 2D planar nano material with excellent barrier property and thermal stability will make graphene a good flame retardant material.[4]

In this research work, nano composite is developed using PVA as matrix, which is well known for its non-toxicity and biodegradability.[5]

Experimental

Materials

Graphite powder, particle size <20 μm, and montmorillonite clay (amino modified) were purchased from Sigma Aldrich. H_2SO_4 (98%), H_2O_2 (30%), DMSO, Gluteraldehydewere received from Merck, India.$KMnO_4$ obtained from Universal laboratories. PVA (98-100% hydrolyzed and mol.wt 60,000-1,25,000) purchased from Himedia , a 10% solution in distilled water used for composite preparation.

Synthesis of GO

Graphite Oxide synthesized from Graphite powder by an environmental friendly low temperature modified Hummers method.[6] The graphite powder (0.5 g) is stirred with 98% H_2SO_4 for 12 h at room temperature. The mixture is cooled below 10 ^oC and $KMnO_4$(2 g), the oxidizing agent is added gradually and stirred for 2.5 h. 25 ml of distilled water is added and continuously stirred for 1 h at room temperature. Finally the reaction is arrested by adding 5ml of 30% H_2O_2 and 76 ml of water. The GO obtained is washed with distilled water till free from acid , centrifuged and dried under vacuum for 12 h at 60 ^oC

Synthesis of rGO/MMT Hybrid

The hybrid is synthesized by three methods.

1. Thermal reduction: Properly dispersed GO/MMT (1:1 proportion) in DMSO was refluxed at 70 ^{o}C for 4h without any reducing agent and designated as B1.
2. Chemical reduction with Hydrazine hydrate: GO and MMT in 1:1 proportion was dispersed in DMSO via 2h ultra sonication. 100µl of hydrazine hydrate per mg of GO was added and refluxed for 4 h at 70 ^{o}C. The hybrid obtained was washed, centrifuged and dried and designated as B2
3. Hydro thermal reduction: GO/MMT dispersed in DMSO was taken in Teflon lined stainless steel autoclave and heated at 100 ^{o}C in an air over for 7 h. It was then cooled to room temperature and the product obtained was washed, centrifuged and dried. The material is designated as B3.

PVA Composite preparation

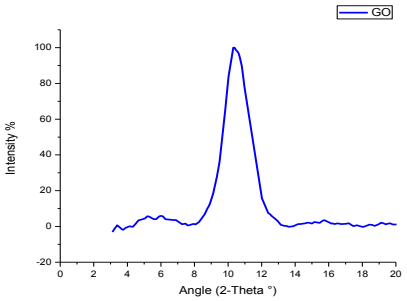
10% PVA solution was prepared by dissolving PVA in distilled water at 80 ^{o}C. The hybrid prepared [B3]was dispersed in 10 ml distilled water by ultra-sonication for 2 h and then mixed with 50 ml PVA solution. 400 µl of gluteraldehyde and 100 µl0.05 M H_2SO_4 were added and sonicated for 1 h. It was then casted on PTFE moulds.

Characterization methods

Fourier transform infrared spectroscopy (FTIR) characterization was done using Thermo Nicolet, Avatar 370 model IR spectrometer. The transmission electron microscopy (TEM) observations were made on a JOEL 3010 microscope. Thermo- gravimetric analysis (TGA) was carried out ranging from 30 ^{o}C to 800 ^{o}C at a heating rate of 10 ^{o}C/min with a TGA Q 50 Thermal Analyser (TA Instruments). X-ray diffraction (XRD) pattern of the samples performed using XRP-Bruker AXS D8 Advances. Limiting Oxygen index(LOI) done with oxygen index instrument Dynisco, Alpha Technologies, USA.

Results and discussion

Characterization of nanohybrid



(Figure 1)

The graphite oxide used in this study is synthesized from pristine graphite by modified Hummers method. From the XRD spectrum of GO(fig 1) it is clear that the 2θ peak of pristine graphite at 26.69 is shifted to 10.2 for graphite oxide.[7] The shift is due to the weakening of van der waals force between the layer because of the oxygen functional group.

TGA thermogram of graphite, GO and rGO is shown in figure 2. It can be seen that the graphite is highly stable upto700 ^{o}C. Graphite oxide shows slight mass decrease from room temperature to 150 °C and significant decrease from 150 °C to 370 °C. The mass of graphene oxide slowly further decreased up to 700°C.The major mass reduction at 150 °C to 370^{o}C is caused by pyrolysis of the oxygen-containing functional groups, generating CO, CO_2. On the other hand, reduced graphene shows an enhanced thermal stability due to the removal of oxygen-containing functional groups by reduction.

FTIR spectrum(fig-3) of GO shows a peak at 3425 cm^{-1} in the high frequency area corresponding to the stretching vibration of -OH groups. The presence of absorption peak at 1716cm^{-1} can be attributed to the stretching vibration of C=O carboxylic acid group and the peak at 1631 cm^{-1} to the unoxidiszed C=C stretching.

TEM images of GO and rGO Shown in figure 4 indicates the presence of wide and flat single- or few-layer of GO nano sheets, due to the presence of large amount of

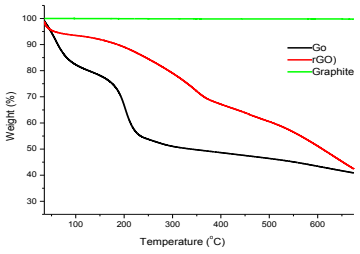


Figure 2

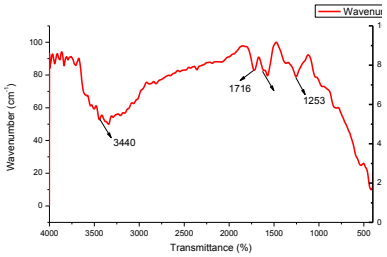
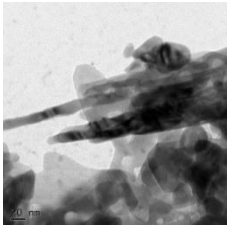
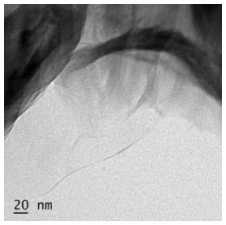


Figure 3





GO **Figure 4** **rGO**

oxygen-containing functional groups on the surface of GO nano sheets. The TEM picture also reveals that the graphene layers are exfoliated in reduced graphene oxide.

The FTIR spectrum of clay (fig-5) shows all the characteristic bands of MMT. Peak at 3629 cm^{-1} refers to the stretching vibrations of O-H in silicates and 3448 cm^{-1} corresponds to O-H stretching of water.

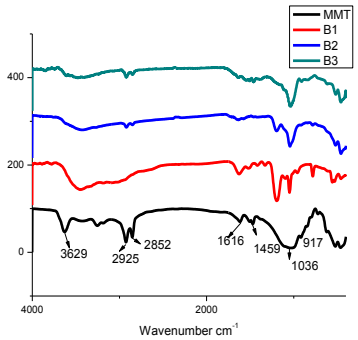


Figure 5

2925 cm^{-1}, 2852 cm^{-1} and 1459 cm^{-1} are C-H vibrations of methylene groups. 1616 assigned to O-H bending and 1036 cm^{-1} is representing Si-O-Si stretching in silicates. 917 cm^{-1} attributed to Al-O-Al deformation of aluminate.[4] FTIR spectrum of hybrids show all the characteristic peak of both clay and Reduced GO.

In the XRD pattern of hybrid(fig-6) , the characteristic peak of GO[$2\theta = 10^{o}$] is not observed which indicates the exfoliation of layered graphene sheet. It is also observed that in the case of

MMT in hybrid system shows a broader shape peak at 2θ value 6 indicating the increase of inter gallery distance when compared with the pristine MMT.[4]

TEM images [fig7] shows the exfoliated thin layers of rGO in all the hybrids. It is also clear from the images that the MMT layers are wrapped by graphene layers.

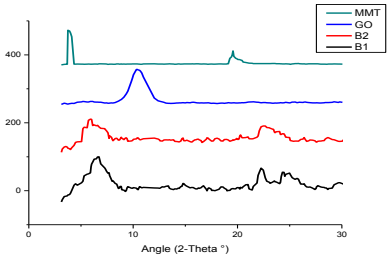
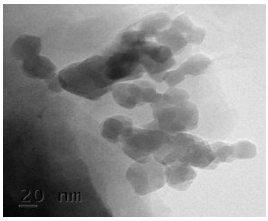
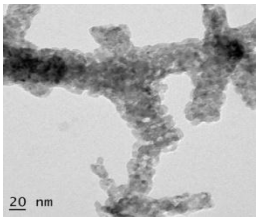


Figure-6

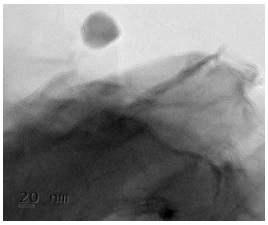
The TGA thermogram (fig-8) compares the



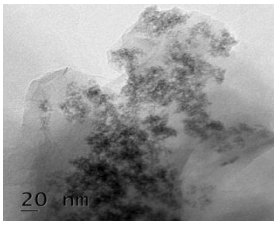
MMT



B1



B2



B3

Figure-7

thermal stability of GO, MMT/rGO hybrid with hydrazine reduction(B1) ,MMT/rGO hybrid with thermal reduction, B2 (i.e., without hydrazine hydrate) and MMT/rGO hybrid prepared by hydrothermal method (B3). For MMT/rGO hybrids, the decomposition temperature of GO is shifted to higher temperature [in GO majour weight loss started at 50 ^{o}C, in B1 it is 250, B2 it is about 300 and in B3 it is 350 ^{o}C] which indicates the higher thermal stability of the

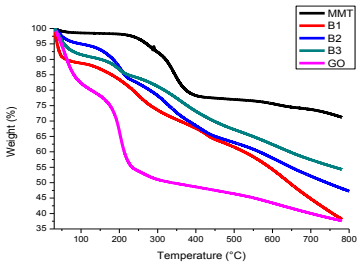


Figure 8

hybrid than GO. Among all hybrids, B3 shows a higher stability than that of the others. The final residue obtained for B1 is 38% , B2 is 45% and B3 is 54%. The thermal stability of the hybrids are enhanced due to the interaction of MMT.

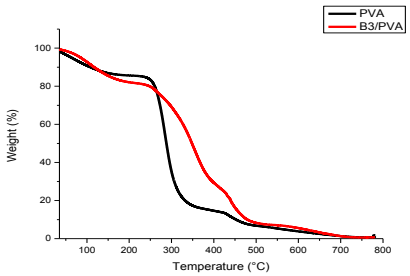


Figure-9

Characterization of PVA-MMT/rGO nanocomposites

Figure 9 shows the TGA thermogram of pure PVA and its composite with B3 hybrid (5mg/100ml of PVA). In pure PVA the first stage degradation below 200 ^{o}C is due to the moisture loss. The major weight loss [65%] due to the degradation of polymer is observed in the temperature range of 240 to 340 ^{o}C. The composite showing higher stability than the pure PVA. The major weight loss [70%] of the composite is observed in the temperature range of 250 to 500 ^{o}C.

Limiting Oxygen Index is measured using sheet material according to ASTM D2863 in an oxygen/ nitrogen atmosphere. Top of the sample is ignited and the minimum concentration of oxygen in an oxygen–nitrogen mixture required to sustain burning of a vertically mounted specimen is termed as LOI value of that material. The LOI values of pure PVA is found to be 19 which is in agreement with literature value [8] and the LOI value of PVA/hybrid composite is increased to 22 with very low percentage of hybrid (5 mg/100ml).

Conclusions

GO is synthesized by a low temperature modified hummers method and it is characterized by XRD, TGA and IR. MMT/rGO hybrid is prepared by three different methods. PVA rGO/MMT

nanocomposite shows higher thermal stability. LOI analysis confirms the improved flame retardancy for the hybrid compared to that of PVA .

References

1. D. K. Chattopadhyay and D. C. Webster, *Prog Polym Sci*, **34**, 1068, 2009.
2. G. Stieger, M. Scheringer, C. A. Ng and K. Hungerbühler, *Chemosphere*, **116**, 118, 2014.
3. R. Wang, D. Zhuo, Z. Weng, L. Wu, X. Cheng, Y. Zhou, J. Wang and B. Xuan, *J Mater Chem A*, **3**, 9826,2015.
4. P. Ming, Z. Song, S. Gong, Y. Zhang, J. Duan, Q. Zhang, L. Jiang and Q. Cheng, *J Mater Chem A Mater energy Sustain*, **3**, 21194,2015.
5. T. Wang, M. Turhan and S. Gunasekaran, *Polym Int*, **53**, 911,2004.
6. M.K Kavitha , S. C. Pilli, P. Gopinath, H. John. *J Env Chem Eng*, 5, 1194,2015.
7. N. F. Attia, N. S. Abd El-Aal and M. A. Hassan, *Polym Degrad Stab*, **126**, 65,2016.
8. J. S. Lin, Y. Liu, D. Y. Wang, Q. Qin and Y. Z. Wang, *Ind Eng Chem Res*, **50**, 9998, 2011.

MACRO 528

Polyethylenimine Grafted GO as a Novel Multi-functional Reinforcing Agent for Epoxy System

Raneesh Konnola and Kuruvilla Joseph*

Department of Chemistry, Indian Institute of Space Science and Technology, Thiruvananthapuram, Kerala-695 547, India

** kjoseph.iist@gmail.com*

Epoxy based composite materials are being increasingly used as structural components in aerospace and automobile industry due to their excellent mechanical properties, low-weight, and good chemical/corrosion-resistance. However, like other thermosetting resins, the crosslinking nature of epoxies pave way to a highly undesirable property of brittleness, leading to poor resistance to crack initiation and growth. The inherent brittle nature of epoxy resin necessitates toughening it for many structural applications [1]. Recently, many researchers showed that the incorporation of nano fillers in the epoxy matrix can improve the mechanical properties of the resultant composites. Epoxy composites reinforced with graphene oxide (GO) have exhibited significant improvements in the mechanical and other properties [2]. The larger surface area of GO increases the contact area with the polymer matrix maximizing the stress transfer from the polymer to the nanofiller. The major difficulty in optimizing composite properties with nano-reinforcing agent is achieving sufficient dispersion and interfacial interaction between filler and epoxy matrix. Chemical modification of graphene oxide has been a promising route to achieve good dispersion and better properties. By judiciously selecting the modifier and grafting with nano reinforcing agent, it is possible to improve both the mechanical strength and fracture

toughness of the composite. In this work, polyethylenimine (PEI) was used as a grafting agent to modify the surface of graphene oxide. Covalent modification of nanofiller is characterized by using FTIR, Raman, TGA, XRD and TEM analysis. GOPEI was used as reinforcing agent to prepare epoxy nanocomposite. Field emission scanning electron micrographs (FESEM) of fractured surfaces were examined to understand the toughening mechanism. The fracture toughness behavior of the system is carefully examined. The functionalization of the GO used in these composites resulted in stronger bonding interactions with the matrix material and promoted improved dispersion of the particles, both of which would contribute to improved mechanical performancename.

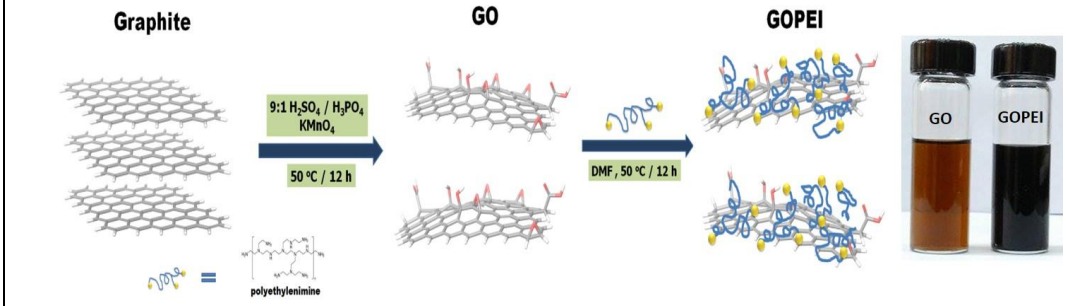


Figure 1: Schematic representation of preparation of GOPEI from graphite

References

[84] Swetha, Chandrasekaran; Narumichi, Sato; Folke, Tölle; Rolf, Mülhaupt; Bodo, Fiedler; Karl, Schulte. *Composite Science and Technology*, 97 (2014) 90.

[85] Manuela, Cano; Umar, Khan; Toby, Sainsbury; Arlene, O'Neill; Zhiming, Wang; Ignatius, T. McGovern; Wolfgang, Maser; Ana, Benito; Jonathan, Coleman. *Carbon*, 52 (2013) 363

MACRO 538

Graphene reinforced self-healing nanocomposites

S. Rana,* A. Mishra, J. K. Pandey*

Research and Development Department, University of Petroleum and Energy Studies (UPES), Dehradun 248007, India

** e-mail id: srana@ddn.upes.ac.in (S.Rana); jkpandey@ddn.upes.ac.in (J. K. Pandey)*

Abstract

"Click" triggered capsule based room temperature self-healing graphene nancomposites are reported, where the adverse effect of reduced tensile strength due to the embedded capsules is counter balanced by a graphene-based filler, the latter additionally acting as a catalyst for the self-healing reaction. The use of highly dispersible graphene immobilized Cu_2O demonstrates excellent catalytic performance with extraordinary reinforcement in tensile strength, resulting in 100% crack healing at 20 °C after 36 hours.

Keywords: *self-healing nanocomposites; graphene; mechanical properties*

Introduction

Graphene, a single layer of two-dimensional sp^2-hybridized carbon has attracted significant research interest due to its unique electrical and thermal conductivity, including exceptional mechanical, optical, and chemical properties.[1] The advantages of graphene in various fields of science reflect use of these materials in past decade for materializing various innovative and prolific scientific works around the globe, and the honey comb structure is considered to be even more promising than 1-dimentional nanotubes and 0-dimentional fullerenes.[2]

The improvement in the multifunctional composite materials by self-healing structures could lead to the creation of novel materials with strongly improved properties.[3] Among the several reported fast self-healing approaches, based on low temperature crosslinking, the Cu(I)-catalyzed alkyne-azide "click" reaction is highly applicable.[4] Graphene supported catalysts represent excellent characteristic properties, due to their high surface area, thermal stability, and porous surfaces, which act as a scaffold to prevent the agglomeration of the immobilized metal particles[5]. In the present study, we have immobilized Cu(I) catalysts onto the surface of graphene (GO)[6] to enhance the self-healing properties *via* click reaction of the resulting polymer composite materials. Furthermore, self-healing epoxy nanocomposites were prepared including the synthesized nano-catalysts and nano-capsules consisting of trivalent alkyne **(1)** and trivalent azide **(2)** based healing agents.

Experimental

The encapsulation of component **1** and **2** was achieved by following the established techniques (urea-formaldehyde capsules formation)[7] with slight modification, where 400 nm diameter capsules were obtained. To prepare the self-healing specimens a 15 wt% capsule concentration was selected including 5 mol% homogeneous catalyst ($Cu(PPh_3)_3F$, $Cu(PPh_3)_3Br$) per functional group of azide/alkyne), and, 2 mol% heterogeneous catalyst (TRGO-Cu_2O) per functional group of azide/alkyne.

Results and discussion

The mechanical performance of neat epoxy and the prepared composite specimens was characterized *via* tensile testing (Figure 1). We observed a decrease in both Young's modulus and ultimate strength after addition of capsules and commercial catalysts ($Cu(PPh_3)_3F$, $Cu(PPh_3)_3Br$). However, after incorporation of TRGO-Cu_2O, a dramatic increase in maximal strain-at-break and tensile strength was observed (Figure 1). Thus, TRGO-Cu_2O not only contributed to the strain-at-break, but also increased the Young's modulus of the specimens. Certainly, the tensile performance of the specimen with TRGO-Cu_2O also decreased with addition of capsules; however, it even demonstrated higher mechanical properties than the pristine epoxy specimen.

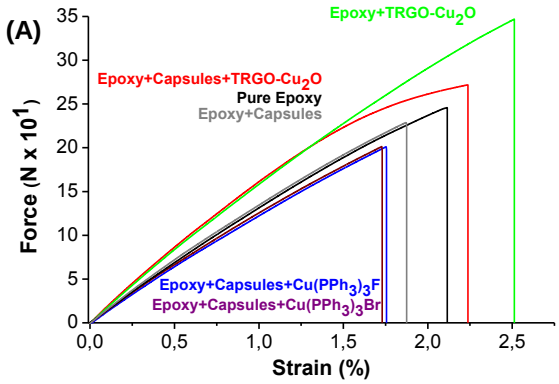


Figure 1. Tensile stress-strain curves of neat epoxy and the respective composite specimens.

The reinforcing mechanism of the composites containing TRGO-Cu_2O was attributed to the effective load transfer between epoxy and GO *via* interfacial adhesion, where the hydrophilic nature of GO can contribute to better disperse the TRGO-Cu_2O in the matrix, since a uniform nanofiller dispersion is known to enhance the mechanical performance of carbon-based nanocomposites.[8]

The self-healing performance of the prepared composites was evaluated through single-notch impact testing *via* dynamic mechanical analysis (DMA) of damaged and healed specimens (Figure 2). Therefore, the specimens were tested by applying a three-point bending mode, where DMA was conducted at low amplitude to check the tensile storage modulus (*E'*).

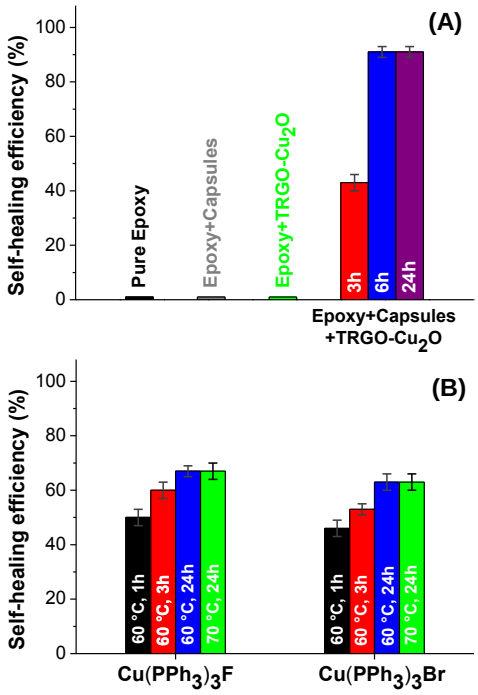


Figure 2. Bar graphs summarize the self-healing efficiency of epoxy specimens determined by tensile measurements

A sharp notch (V-shape, 1 mm depth, machined on one face) was created in the specimen. In order to propagate a crack along the notched plane an impulsive load of 7N was applied to the specimen *via* tensile force in three-dimensional bending mode, where the force-deformation curve signifies delamination in the specimen as a result of crack propagation. At this point, a sharp decrease of *E'* was observed by DMA, which further confirms the crack propagation in the specimen. After storage of the specimen for a period of 0-36 h at 25 °C, DMA was performed again to evaluate the self-healing response, where a sharp recovery in self-healing was observed, which was ascribed to the formation of a polymeric network *via* the azide/alkyne "click" crosslinking reaction of component **1** and **2**. In comparison, DMA of neat epoxy and a specimen with embedded capsules but without catalyst did not show any recovery of *E'*. However, the prepared specimens amid homogeneous catalysts also demonstrate lower in recovery compared to graphene based catalyst. Thus, the obtained results demonstrate a higher catalytic activity of TRGO-Cu_2O in comparison to homogeneous copper catalysts, related to the scaffold properties of the applied graphene sheets, which prevent the agglomeration of copper particles. Additionally, the unique interactions of metal particles with graphene including its ability for electron capture and transport, helpful to boost the catalytic activity of graphene supported metal particles. In contrast, an agglomeration of the homogeneous Cu(I)-catalysts in the epoxy matrix was observed,

which further emphasizes their limited self-healing performance compared to their heterogeneous counterpart.

Conclusions

In summary, we have realized a room temperature self-healing graphene -based epoxy nanocomposites with enhanced tensile performance. Therefore, a simple capsule-based self-healing concept was applied, resulting in network formation once the capsules get ruptured *via* the Cu(I)-catalyzed azide-alkyne crosslinking "click" reaction using homo- and heterogeneous copper catalysts. The addition of a highly dispersible graphene immobilized Cu_2O (TRGO-Cu_2O) based heterogeneous catalyst demonstrates a great combination of high catalytic performance for click based network formation (crack healing) at room temperature along with required reinforcement within the material, in turn allowing compensation of tensile strength reduction exerted by the embedded capsules.

Acknowledgements

Authors are thankful to Chancellor UPES for his strong support and guidance.

References

1. K. S. Novoselov, A. K. Geim, S. V. Morozov, D. Jiang, Y. Zhang, S. V. Dubonos, I. V. Grigorieva, A. A. Firsov, *Science* 306, 666-669, 2004.
2. C. N. R. Rao, A. K. Sood, K. S. Subrahmanyam, A. Govindaraj, *Angew. Chem. Inter. Ed. 48,* 7752-7777, 2009.
3. S. R. White, N. R. Sottos, P. H. Geubelle, J. S. Moore, M. R. Kessler, S. R. Sriram, E. N. Brown, S. Viswanathan, *Nature* 409, 794-797, 2001.
4. M. Schunack, M. Gragert, D. Döhler, P. Michael, W. H. Binder, *Macromol. Chem. Phys.* 213, 205-214, 2012.
5. Y. Li, H. Wang, L. Xie, Y. Liang, G. Hong, H. Dai, *J. Am. Chem. Soc.* 133, 7296-7299, 2011.
6. A. Shaygan Nia, S. Rana, D. Dohler, X. Noirfalise, A. Belfiore, W. H. Binder, *Chem. Comm.* 50, 15374-15377, 2014.
7. Y. Zhao, D. Döhler, L.-P. Lv, W. H. Binder, K. Landfester, D. Crespy, *Macromol. Chem. Phys.* **2014**, *215*, 198.
8. N. G. Sahoo, S. Rana, , J. W. Cho, L. Li and S. H. Chan, Prog. Polym. Sci. 35, 837-867, 2010.

MACRO 542

Development and rheological study of the polymer blended viscoelastic medium for finishing of microholes

Sachin Singh, Mamilla Ravi Sankar*

Department of Mechanical Engineering, IIT Guwahati, Assam, India-781039

* *E-mail id*: evmrs@iitg.ernet.in, Tel No: +91-361-258-2684

Abstract

Finishing operation is the final step in most of the manufacturing processes. This can cost as much as 15% of the total product manufacturing cost in the production cycle. As the requirement of surface finish increases, the cost of the product escalates exponentially. Abrasive flow finishing (AFF) is one of the advanced nano finishing technologies, which is specifically used to finish simple as well as complex surfaces. The finishing capabilities of the AFF process depends on the polymer based viscoelastic medium mixed with abrasive which is used a flexible tool for shearing the surface roughness peaks. In the current paper an attempt is made to develop an economic AFF medium. The rheological study of the medium is done on the MCR 301 rheometer. Later, to check the effectiveness of the developed medium AFF experiments for finishing of microholes are carried out.

Keywords: *polymer; rheology; abrasive flow finishing; surface roughness*

Introduction

With the advancement of technology the demand of products with micro/nano dimensions increased many fold in the last few decades. The main aim is to assemble and use these components to design a complicated system which is light weighted and covers as less space as possible. Few of the examples of the modern technologies are the modern cellphones and the computers which are more handy and useful as compared to their older generations. To finish macro components with complex features and difficult to finish materials many advanced finishing processes are developed such as are abrasive flow finishing (AFF) process, rotational-abrasive flow finishing (R-AFF) process, magnetic abrasive fining (MAF), magnetorheological abrasive flow finishing (MRAFF) process, rotational-magnetorheological abrasive flow finishing (R-MRAFF) process. Most of the advanced finishing processes employs magnetic field for finishing of the workpieces. Such process suffers the disadvantages of the decay of the finishing magnetorheological fluid over time, shielding effect of the magnetic field and the non-uniform finishing of the components with irregular shape due to the non-uniform magnetic field strength. To avoid such shortcomings, AFF process is mainly used for finishing. However to increase the efficiency of the AFF process many of its hybrid forms such as R-AFF and ultrasonic assisted-AFF are developed. Due to additional accessories the cost of hybrid set-up increases. In the present work the efficiency of the AFF process is increased by developing a polymer blended AFF medium that not only finishes microholes but also provides nano- surface roughness on its wall. Static and dynamic rheological study of the developed medium is done.

Literature review

AFF medium plays a vital role in finishing of workpiece. Medium mainly comprises of the base polymer which is viscoelastic in nature, additives (plasticizers, softeners) and abrasive particles. A good AFF medium possesses properties such as mechanically stable, chemically non-reactive, self-deformable, good fluidity and better abrading ability. Depending on the workpiece to be finished non-Newtonian base polymer is chosen which can be of nature such as shear thinning, shear thickening, bingham plastic etc. It is the rheology of the medium which determines pattern and aggressiveness of the abrasive action. Rhoades [1] developed a medium for abrading and deburring inaccessible openings of the workpieces. Rhoades [2] also developed an abrasive finishing set-up for finishing workpieces with large complex edges and surface as those of injection mold cavities, forging dies, gear wheels and like and accordingly to suit the functionality of the set-up media is developed which is rheopectic (increase in apparent viscosity with applied stress) in nature. McCarty [3] developed a semi-solid abrasive medium. The function of the medium is not only to carry the abrasive particles but to provide firm backing to the abrasive particles therefore increasing their cutting strength which is not possible while using liquid slurry. The rheological study of the commonly used polyborosiloxane as base polymer during AFF finishing operation was done by Hull et al. [4]. Abrasive polishing composition for finishing of complex workpieces produced by casting, forging, machining and like was developed by Gilmore [5]. Wang et al. [6] developed abrasive medium to finish complex chain holes. Commercially used carriers during AFF process are mainly silicon or polyborosiloxane rubber (PBS). Kar et al. [7] made an attempt to replace these costly carriers. Sankar et al. [8] developed an in-house AFF finishing media composed of styrene butadiene as base polymer and did the rheological study.

As found out from the literature review not much attention is made on developing an economic AFF medium. Also many of the researchers in the literature developed AFF medium and did its rheological study but didn't prove its efficiency by carrying out the actual AFF experiments. In the current paper, economic medium by blending various viscoelastic polymer is developed. Detailed rheological study of the medium is done. Also few of the finishing experiments on the microholes fabricated on surgical stainless steel (SS 316L) are carried out.

Experimentation

AFF process consists of main three parts viz. set-up, tooling and medium. Main components of the AFF set-up are upper-lower hydraulic cylinder, upper-lower medium cylinder, piston etc. (Fig. 1). The workpiece to be finished is paced between the upper medium cylinder and lower medium cylinder.

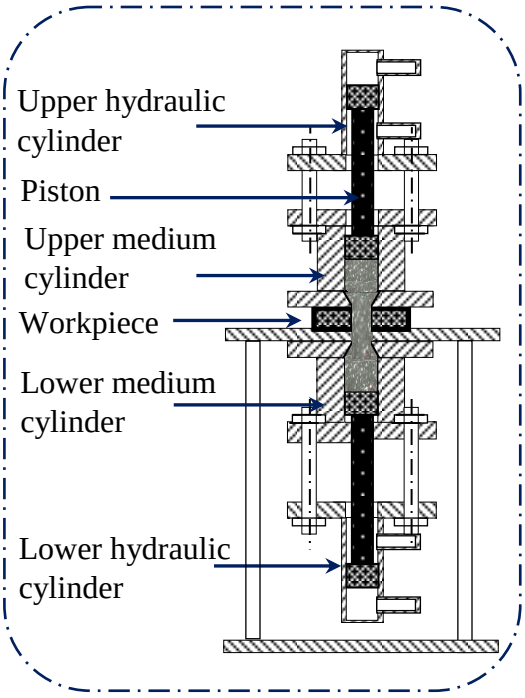


Fig. 1 Schematic diagram of the abrasive flow finishing set-up

Medium is extruded with the help of piston from one medium cylinder to other via workpiece passageway. This helps in shearing the surface roughness peaks on the workpiece surface by the abrasive particles mixed in the medium. Medium in the AFF process acts as the deforming tool taking the shape of the workpiece passageways from which it is extruded. It is this important feature of the medium due to which AFF process finds its importance in the field of finishing. Medium developed in the current paper is a mixture of soft styrene polymer blended with soft silicon polymer. Both the polymers are blended in suitable amount and are mixed with suitable quantity of plasticizers, softener and abrasive particles. Polymer acts as the base for proving the support and the finishing forces to the abrasive particles during the sharing of the roughness peaks.

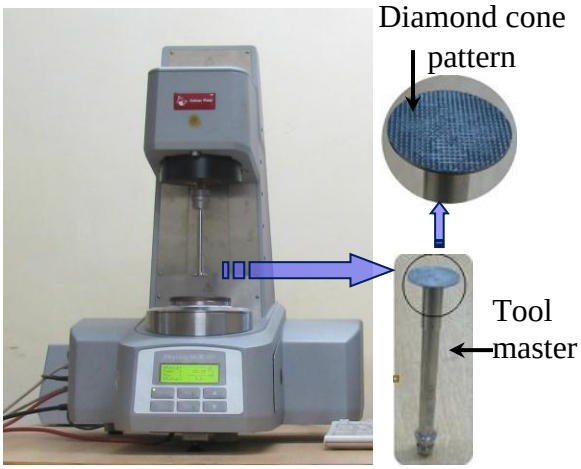


Fig. 2 Commercial rheometer used for measuring static and dynamic rheology (Anton Paar-MCR-301 series)

Complete static and dynamic rheological experiments are carried out using a commercially available parallel plate rheometer (Anton Paar MCR-301 series) (Fig.2). The top rotating plate (tool master) and bottom stationary plate (base plate) are provided with the diamond cone pattern in order to hold the semisolid medium samples.

Results and discussion

In the present section the results obtained by conducting static and dynamic rheological study of the developed medium on the rheometer are presented. Three different types of medium are prepared by changing the wt. % of the abrasive particles. Also the results obtained by using the developed medium during finishing of the microholes by the AFF process are presented.

1. Flow test

Flow test gives the idea of the viscosity of the medium at different shear rates. As shown in the Fig. 3 viscosity decreases with the increase in shear rate showing the shear thinning nature of the developed medium. Such medium when extruded through the microholes openings starts shearing and therefore, its viscosity decreases allowing it to flow through the fine microhole openings. As the wt. % of the abrasive particles in the medium increases the surface improvement efficiency of the medium increases. Surface obtained at higher wt. % of the abrasive in more fine finished as compared to the one obtained at low wt. % of the abrasives (Fig. 4). This is due to two reasons. Firstly, the number of abrasive particle shearing the roughness peaks increases with increase in wt. % of abrasives. Secondly, the viscosity of the medium with higher wt. % of the abrasive is more which not only provides strong backing support to the abrasive but also helps in effective transfer of finishing forces from the polymer chains to the abrasive particle during shearing of the roughness peaks by abrasive particles.

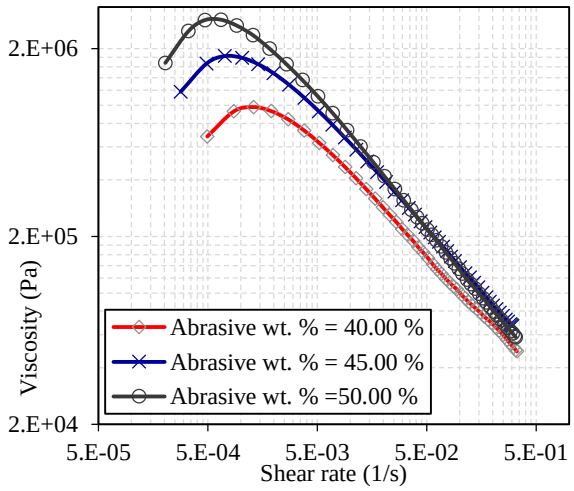


Fig. 3 Effect of shear rate on viscosity (Logarithmic scale on both X and Y axis)

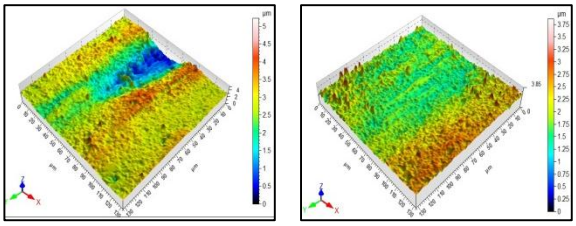


Fig. 4 Topographic of the workpiece surface at different wt. % of the abrasive particles in the medium **(a)** 40 % **(b)** 50 % (8 cycles, # 180, 4 MPa)

2. Amplitude sweep

Amplitude sweep test is carried out to know the linear viscoelastic range (LVE) of the polymer chains in which they are at their original state (without breakage). Medium with long LVE range is indicative of a well-dispersed and stable system. In LVE region storage modulus of the medium doesn't change with the change in % strain of the medium (Fig. 5).

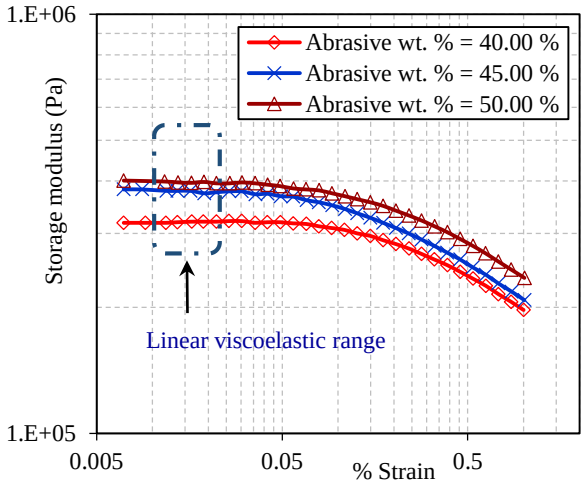


Fig. 5 Variation of storage modulus with percentage strain (Logarithmic scale on both X and Y axis)

Frequency sweep

Storage modulus is an indicator of the energy stored by the medium and loss modulus shows the energy dissipated by the medium under the influence of external forces. In frequency sweep test, as the frequency increases, the number of shearing oscillations per unit time increases.

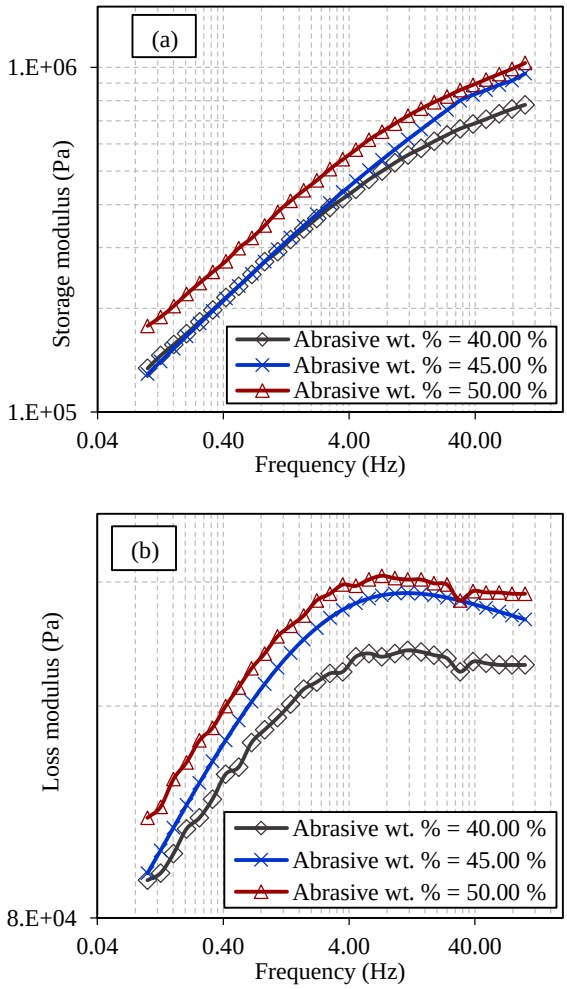


Fig. 6 Effect of frequency on **(a)** storage modulus and **(b)** loss modulus (Logarithmic scale on both X and Y axis)

As the frequency increases (shearing rate increases), the polymer chains stretch more and the more amount of energy is input to the polymer chains. Thus, the polymer chains try to retain more and more amount of energy and dissipate the amount of energy what they dissipate in natural way. Hence, the storage modulus increases (Fig. 6(a)) and loss modulus remains approximately same with an increase on frequency (Fig. 6(b)).

Similarly, during the AFF experiments as the extrusion pressure increases more amount of energy is stored by the medium which is then transferred to the abrasive particles for shearing the roughness peaks. Thus, finishing the microholes with AFF process at high value of extrusion pressure gives a microhole having low surface roughness as compared to the one at low extrusion pressure (Fig. 7)

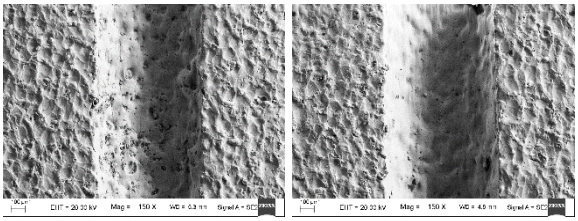


Fig. 7 Topography of the workpiece surface at different extrusion pressure **(a)** 3 MPa **(b)** 5 MPa (6 cycles, # 400, 35 wt. % abrasives)

Conclusion

In the current paper an economic AFF medium is developed. Static and dynamic rheological study of the medium is carried out. AFF experiments performed by using the developed medium confirm the effectives of the medium in finishing the microholes by the AFF process.

Acknowledgements

The authors are thankful for the financial support provided by Indian Institute of Technology Guwahati (Project Number: SG/ME/P/MRS/01), Board of Research in Nuclear Sciences (Project Number: ME/P/MRS/02), Department of Science and Technology for their Technology Systems Development Programme (DST/TSG/AMT /2015/619), Defence Research Development & Development Laboratory (CARS Project),

References

1. L.J. Rhoades, Medium for process of honing by extruding, United States Patent, 3,819,343, 1974.
2. L. J. Rhoades, Abrasive flow machining with an in situ viscous plastic medium, United States Patent, 5,125,191, 1992.
3. R. W. McCarty, Apparatus for abrading by extrusion and abrading medium, United States Patent, 3,634,973, 1972.
4. J. B. Hull, D. O' Sullivan, A. J. Fletcher, S. A. Trengove, J. Mackie, Rheology of carrier media used in abrasive flow machining, *Key Engineering Materials*, 1992, 72-24, 617-626.
5. J. R. Gilmore, L. J. Rhoades, Abrasive polishing composition, United States Patent, 6,918,937, 2005.
6. A. C. Wang, S. H. Weng, Developing the polymer abrasive gels in AFF process, *Journal of Material Processing Technology*, 2007, 192-193, 486-490.
7. K. K. Kar, N. L. Ravikumar, P. B. Tailor, J. Ramkumar, D.Sathiyamoorthy, Performance evaluation and rheological characterization of newly developed butyl rubber based media for abrasive flow machining process, *Journal of Material Processing Technology*, 2009, 209, 2212-2221.
8. M. R. Sankar, V. K. Jain, J. Ramkumar, Y. M. Joshi, Rheological characterization of styrene-butadiene based medium and its finishing performance using rotational abrasive flow finishing process, *International Journal of Machine Tools and Manufacture*, 2011, 51, 947-957.

MACRO 547

Cryo EM characterization of Self assembled Giant Bottlebrush Block Copolymer Surfactants

Marc Schmutz[a] *, Ryan Fenyves[b], Javid Razyed[b],

[a] *University of Strasbourg-CNRS- Institut Charles Sadron*
23 rue du Loess F 67084 STRASBOURG France
[b]*Department of Chemistry, University at Buffalo, The State University of New York,*
Buffalo, New York 14260-3000, United States

marc.schmutz@ics-cnrs.unistra.fr

Self assembled systems become more and more versatile for the preparation of new materials. Their structural characterization is an important step towards the designing of new materials. The ultrastructural characterization in their native state is important to preserve the highest resolution. Cryo electron microscopy (cryo EM) has been developed in the 80's for structural biology by J. Dubochet's group. Rapidly the power of this preparation technique has also been used for soft matter studies (Y. Talmon).

Programmed self-assembly of well-defined molecular building blocks enables the fabrication of precisely structured nanomaterials.

In this work, we explore a new class of giant polymeric surfactants (M_n = (0.7–4.4) × 10^6 g/mol) with bottlebrush architecture and show that their persistent molecular shape leads to the formation of uniform aggregates in a predictable manner. Amphiphilic block copolymers containing polylactide (PLA) and poly(ethylene oxide) (PEO) side chains (Figure 1) were synthesized by a grafting-from method. Cryo EM allowed to prove the structure of their assembly in their aqueous environment: for all the produced micelle structures we were able to visualize boasted rod-like hydrophilic PEO brushes protruding from the hydrophobic PLA cores normal to the interface. The interfacial curvature and core radii were varied by varying side chains lengths. Highly uniform spherical micelles with low dispersities were obtained from bottlebrush amphiphiles with packing parameters of ~0.3, estimated from the polymer structural data (Fig 1A). Long cylindrical micelles (Fig 1B). and other non spherical aggregates were observed for the first time for higher packing parameters (Fig 2). Shape-dependent assembly of bottlebrush surfactants allows for the rational fabrication of a range of micelle structures in narrow morphological windows.

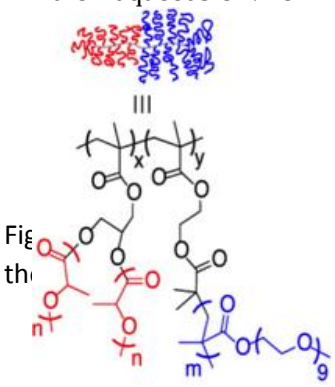


Fig
th

Table 1. Structural Characteristics of Amphiphilic PLA–PEO Bottlebrushes

Polymer	*n*(PLA)[c]	*m*(PEOMA)[c]	M_n[d] (kg/mol)	$Đ$[e]
LO-2[a]	24	14	970	1.05
LO-4[b]	86	8	1654	1.09
LO-5[b]	82	12	1790	1.09

a Prepared using poly(SM_{95}-*b*-$BIEM_{95}$) backbone.
b Prepared using poly(SM_{98}-*b*-$BIEM_{110}$) backbone.
c Number of repeat units per branch.
d Calculated by ^{1}H NMR analysis.
e Obtained from SEC using polystyrene calibration.

Table 2. Aqueous Self-Assembly Parameters of Amphiphilic PLA–PEO Bottlebrushes

polymer	$w_{sc,PEO}$ [a]	morphology [b]	R_{core} [c] (nm)	D_h [d] (nm)	p [e]
LO-2	0.66	S	19 ± 1	100	0.24
LO-4	0.24	B	-	-	1.50
LO-5	0.33	C	30 ± 3	-	0.91

a Weight fraction of PEO per side chain.
b Predominant morphology identified by cryo-TEM (S: spheres, C: cylinders, B: bilayers).
c The average core radius of spherical micelles (±standard deviation) measured from cryo-TEM images.
d Volume-averaged hydrodynamic diameters determined by dynamic light scattering.
e Packing parameter.

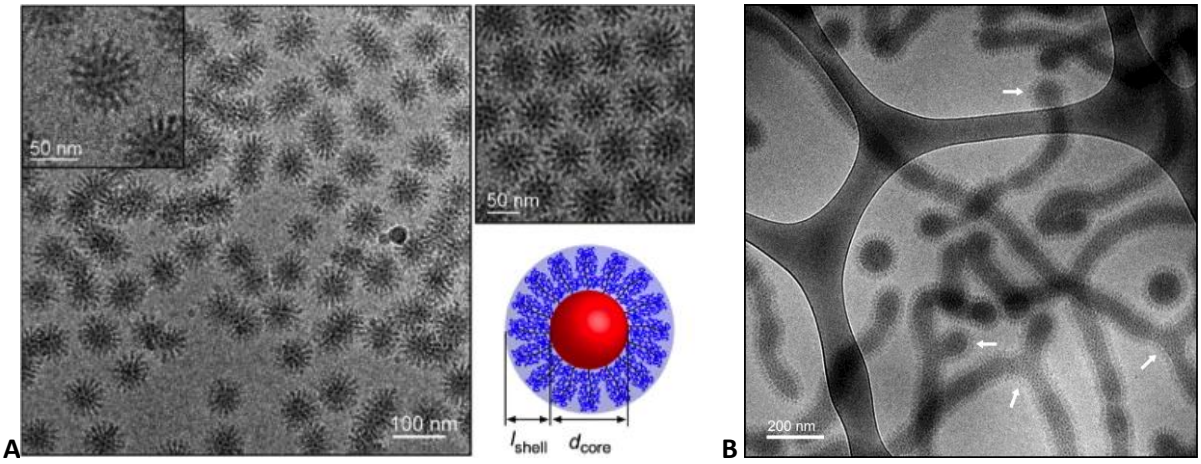


Figure 2: Cryo-TEM analysis of spherical micelles formed from polymer LO-2 (A) and LO-5 (B).

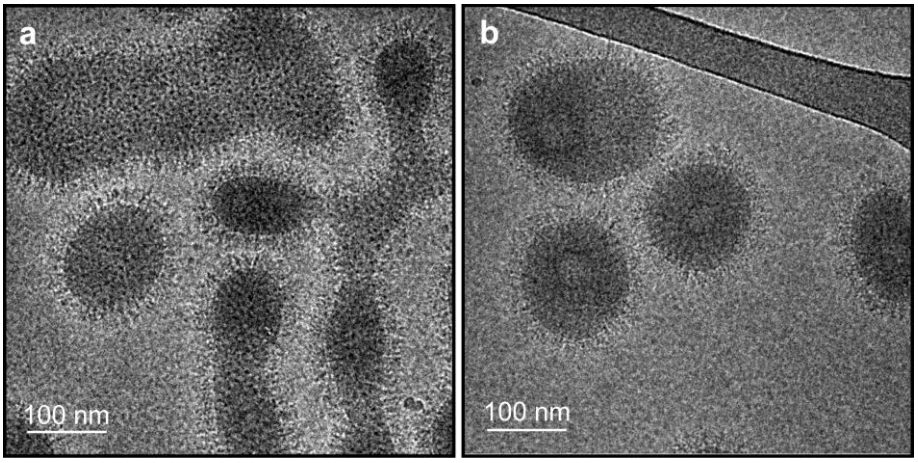


Figure 3: Cryo-TEM analysis of bilayer structures prepared from polymer LO-4.

References

[86] Dubochet J. ; *et al* Quarterly Review of Biophysics 21, 2 (1988), 129

[87] Wittemann A ; Drechsler M. ; Talmon Y ; and Ballauff M. *J. Am. Chem. Soc.* **2005**, 27, 9689.

[88] Fenyves R.; Schmutz M.; Horner I. J; Bright F. V.; Rzayev J.; *J. Am. Chem. Soc.* **2014,** 136, 7762.



FOCUS AREA

ELASTOMERS, POLYMER PHYSICS AND MODELING

MACRO 105

Molecular Dynamics simulations of hydrolyzed PVAc - PFO based anti-stain self-clean coatings

Sushanta K Sethi [a], Nityanshu Kumar[a], Shakeel Ehtisham[a], Krishnatri Devaspati[a], Gaurav Manik[a*]

[a] *Department of Polymer and Process Engineering, Indian Institute of TechnologyRoorkee, Saharanpur Campus, Saharanpur, India-247001*

First author e-mail id: kumar.nityanshu@gmail.com

Corresponding author e-mail id: manikfpt@iitr.ac.in, gauravmanik3m@gmail.com

Abstract

In this work we present a molecular simulation study on hydrolyzed polyvinyl acetate (PVAc)-perfluoroctane (PFO) systems as a potential anti-stain and self-clean coating materials. The PVAc content provides the film-forming property and the PFO contributes to the anti-stain property. The formulation could find potential wide-ranging applications as useful coatings for residential and industrial use. We have generated different equilibrated structures of the coatings with different weight % PFO content in 86% hydrolyzed PVAc. The relevant coating properties, such as surface free energy and contact angle with water, are estimated. The surface energy of the simulated surfaces are found to be significantly reducing with increasing fluorine based entities from 0–55.5 wt.%. Further, the water contact angle increases significantly with the increasing fluorine content from 0–55.5 wt.%. These results help us to screen and propose a potential useful coating formulation of 22.2 wt.% PFO in 86% hydrolyzed PVAc.

Keywords: 86% hydrolyzed PVAc, interaction energy, molecular dynamics, oleo-phobic coatings

Introduction

There is a tremendous interest for surfaces of specific wettability towards water and oil in academic sciences as well as in industrial technologies also [1-5]. The so called surfaces are well known as Omni-phobic surface and can be defined by having water as well oil contact angles higher than 900. In this approach, the water droplets sit mostly on the air and forms a shape of nearly spherical and therefore have a very small liquid-solid contact area, leading its easy-roll off from the surfaces. Recently, a number of research work has been devoted towards the preparation and theoretical modeling of hydrophobic surfaces as observed by the large number of publications and diverse approaches. A wide variety of strategies has been put forward for making hydrophobic coatings [6,7] from last two decades have been reported, such as phase separation [8], electrochemical deposition [9], template method [10,11], Emulsion [12], plasma method [13], crystallization control [14], chemical vapor deposition [15], wet chemical reaction [16], sol-gel processing [17-20], lithography [21], electrospinning [22], solution immersion [23] and so on [24-26]. Many of the preparation Techniques are inexpensive and simple; however, some of them involved multistep procedures and harsh conditions else require specialized reagents or equipments. Out of which a commonly used strategy is to coat the surfaces with a low surface energy material to obtain hydrophobic self-clean coatings. Interestingly many fluoropolymers, especially perfluoro polymers, have been found to reduce the surface wet ability towards water and oil [27, 28]. H. Zhou *et al.* and L.K. Gao *et al.* obtained highly durable super hydrophobic coatings by deposition of fluorinated and siloxane containing compounds [29, 30]. The presence of fluorine renders anti stain property because of its high electronegativity and high polarizability. Further, Parthab *et al.* [27] have shown the linear decrease in surface energy by

increasing fluorine content in the basic matrix. Lakshmi *et al.* [32] found that sol-gel nanocomposite coatings made with perfluoro alkyl methacrylic copolymer as an additive increased the lubricant oil contact angle from <10° to >113°.

This work presents the equilibrize structure of coatings with different PFO content in 86 %

Simulation Methodology

Molecular simulations have been performed using commercially available software, Material studio 7.0, purchased from Accelrys Inc [33]. The MM and MD simulations were carried out using the DISCOVER package employing the COMPASS force field [34, 35]. Then the energy minimization using a "Smart Minimizer" function of "Discover" module was performed using the methods of steepest descent followed by the conjugate gradient method. For dynamics, the pressure control developed by Berendsen *et al.* [36], and temperature control using the stochastic collision approach of Andersen [37] were used. The cut-offs [38] commonly encountered is atom-based and group-based approach with a cut-off distance of 9.50 Å. The group based approach is considered to be the best approach for the neutral fragments with dipoles as found earlier as well [27]. The Amorphous cell and forcite modules of Material Studio have been used to create the simulation cells and run atomistic MD.

Computation of density and solubility parameter

In order to construct the amorphous cells, chains of 86% hydrolyzed PVAc (of chain length, n= 26) with isotactic stereo chemical structure and molecules of PFO are generated and energy minimization was done separately using MM. the equilibration of the formed amorphous cells are carried out using the methodology mentioned by Kumar *et al.*[28]. The frames are stored after every 5000 steps in NPT dynamics simulation and the average density and solubility parameter of all saved equilibrated frames (around 60 frames) are taken and reported.

Computation of surface energy

The generated equilibrated PVAc-PFO cells mentioned in section 2.1 are elongated along one of the directions (z-axis) to a reasonable spacing of 100 Å so that the molecules of the simulation cells are found not to interact with their image along the elongated direction. Thin films are constructed according to the methodology used previously [39-41] for other polymeric systems. The surface energy, of the generated films is then calculated using the equation, Eq. 1., given below:

$$\gamma = \frac{\left(E_{\text{Thinfilm}} - E_{\text{Amorphous cell}}\right)}{2A}$$

Where, $E_{\text{Thin film}}$ represents the energy of the film, and $E_{\text{Amorphous cell}}$ the energy of equilibrated bulk amorphous cells, and 2*A* is the surface area of the two surfaces each of area A formed due to creation of film.

Computation of water contact angle

A surface having a contact angle of less than 90° to a liquid is considered as philic for that liquid, e.g., hydrophilic, and a surface having a contact angle exceeding 90° to a liquid is defined as phobic for that liquid, e.g., hydrophobic. A highly hydrophobic surface shows Dirt-repellency which is one of the most important properties of the coatings.

In the present work, calculation of hydrophobicity is confirmed by determining the concentration hydrolyzed PVAc in molecular simulation work-frame, and then evaluated their hydrophobicity and oleophobicity by using MD Simulations. The PVAc provides better film forming property and perfluouroctane lowers the surface energy and ultimately increases the hydrophobicity as well oleophobicity.

profile of water molecules, on the created coating surface. The choice of water (around 1000 molecules) has been made. The Forcite module of Material Studio 7.0 has been used for running MM and MD simulations of the two layered systems. The equilibrated cells of PVAc-PFO (with different wt% PFO) form one of the layers, *Layer-1* and separately equilibrated water molecules cell forms the *Layer-2* in the respective two layered systems. To quantify the hydrophobic nature of the simulated surfaces thin film amorphous cells of PVAc-PFO systems are used to build their respective super cells that have *x*- and *y*-dimensions as 4 times that of the respective amorphous cells and NVT dynamics simulation of 300ps has run on each individual system.

Results and discussion

Estimation of density and solubility parameter

The solubility parameter and cohesive energy density (CED) has been calculated by MM and MD. CED refers to the increase in energy per mole of polymer, E_{cohesive}, if all of its intermolecular forces are eliminated in a unit molar volume. Thus, if the molar volume of polymer is V_{molar}, then CED is given by Eq. 2.

$$CED = (E_{\text{cohesive}}/V_{\text{molar}}) \qquad (2)$$

Table 1: Simulated densities and solubility parameter values of 86% hydrolyzed PVAc PFO

PFO wt. % in 86%hyd. PVAc	PVAc: PFO	Density (in g/cc)	Solubility parameter $(MPa)^{1/2}$
0	6-0	1.0227 ± 0.0123	20.414
22.2	5-4	1.37 ± 0.0225	19.98 ±0.02
55.5	2-7	1.3 ± 0.0085	17.087 ±0.032

Estimation of surface energy

The surface energy, γ, estimated using Eq. (1) for different PVAc-PFO systems is reported in Table no 2.

Table 2: Simulated Surface energy values of 86% hydrolyzed PVAc- PFO systems

PFO wt. % in 86%hyd. PVAc	PVAc: PFO	Surface energy (k cal/mol /Å^2)
0	6-0	48.3
22.2	5-4	47.28
55.5	2-7	0.71

The MD simulated surface energies are found decreasing with increasing PFO content. There is noticeably decrease in Van der Walls with systematic increase in Columbic energy. The overall effect of the two opposite trends shows a decrease trend in surface energy with increasing fluorine content. This is due to a higher weightage of van der Walls component in overall surface energy, and also, a substantial higher decrease in the van der Walls energy than the increase in Columbic energy component.

Contact angle measurements

It is important to understand the fundamental science behind wetting and contact angle phenomena to the coating or thin film performance. Calculations based on measured contact angle values yield an important

parameter- the solid surface tension, which quantifies the wetting characteristics of a solid material. The results for the contact angles for water on simulated coating structures for different PFO systems are tabulated in Table 3 and the figures for different PVAc-PFO systems are shown in fig 1.

PFO wt. % in 86%hyd. PVAc	PVAc: PFO	Water Contact Angle
0	6-0	51.21°
22.2	5-4	105.72°
55.5	2-7	132.09°

Table 3: water contact angle values of 86% hydrolyzed PVAc- PFO systems

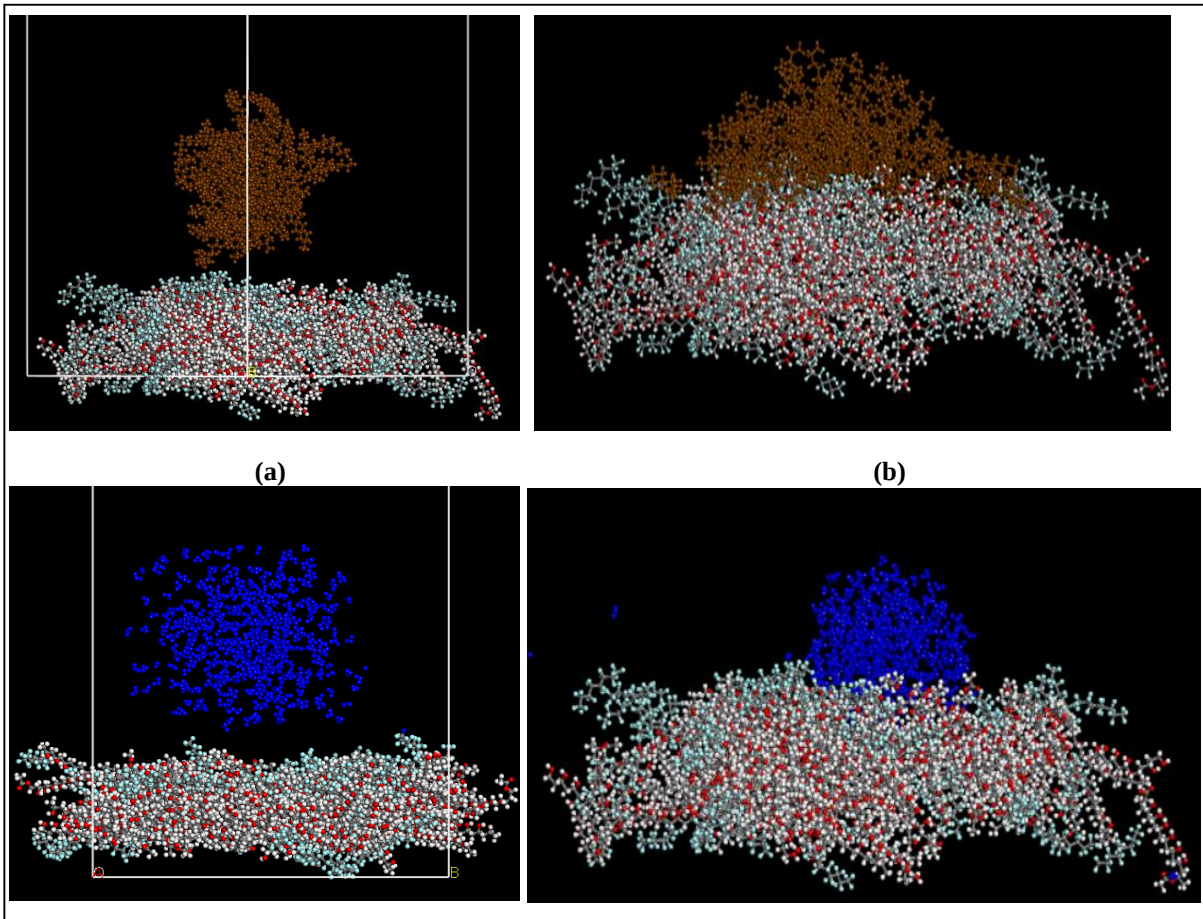


Figure 1 Illustration of the (a) *t* = 0 and (b) *t* = 300ps configuration of a drop mass of oil-like decane molecules (c) t = 0 and (d) t = 300ps configuration of a drop mass of water molecules on a 48.wt% PFO in PVAc simulated surface.

Summary and Conclusions

The surface energy and water contact angle of the simulated structures has been desirably found decreasing and increasing respectively, with increasing PFO content due to the surface aggregation observed with increasing PFO content. Thus, by showing increase water repellency by the decrease in surface free energy. Based on above sets of reasoning, we propose a formulation of 22.2 wt% PFO in 86% hydrolyzed PVAc for making a hydrophobic self-clean coating. The materials are robust and applicable by conventional wet coating techniques.

Acknowledgement

The corresponding author would like to sincerely acknowledge the grant (Grant Code: FIG-400136-DPT/13-14) provided by Indian Institute of Technology Roorkee, through its MHRD FIG initiative, for funding the work presented in this paper. The author gratefully acknowledges the financial support provided

References

[1] Ohkubo Y, Tsuji I, Onishi S, Ogawa K (2010) J Mater Sci 45:4963. doi:10.1007/s10853-010-4362-2

[2] Lee, H.J. & Owens, J.R. J Mater Sci (2011) 46: 69. doi:10.1007/s10853-010-4810-z

[3] Ryan A. Hayn • Jeffery R. Owens J Mater Sci (2011) 46:2503–2509 DOI 10.1007/s10853-010-5100-5

[4] Huang X, Fang X, Lu Z, Chen S (2009) J Mater Sci 44:4522. doi:10.1007/s10853-009-3660-z

[5] Lee H (2009) J Mater Sci 44:4645. doi:10.1007/s10853-009- 3711-5

[6] Y. Rahmawan, L.B. Xu, S. Yang, Self-assembly of nanostructures towards transparent, super hydrophobic surfaces, J. Mater. Chem. A 1 (2013) 2955–2969.

[7] X.M. Li, D. Reinhoudt, M. Crego-Calama, What do we need for a super hydrophobic surface? A review on the recent progress in the preparation of super hydrophobic surfaces, Chem. Soc. Rev. 36 (2007) 1350–1368.

[8] J. T. Han, X. R. Xu and K. W. Cho, "Diverse Access to Artificial Super hydrophobic Surfaces Using Block Copolymers," Langmuir, Vol. 21, No. 15, 2005, pp. 6662- 6665.

[9] N. J. Shirtcliffe, G. McHale, M. I. Newton, G. Chabrol and C. C. Perry, "Dual-Scale Roughness Produces Unusually Water-Repellent Surfaces," Advanced Materials, Vol. 16, No. 21, 2004, pp. 1929-1932.

[10] H. S. Hwang, S. B. Lee and I. Park, "Fabrication of Raspberry-Like Super hydrophobic Hollow Silica Particles," Materials Letters, Vol. 64, No. 20, 2010, pp. 2159-2162.

[11] Y. H. Huang, J. T. Wu and S. Y. Yang, "Direct Fabricating Patterns Using Stamping Transfer Process with PDMS Mold of Hydrophobic Nanostructures on Surface of Micro-Cavity," Microelectronic Engineering, Vol. 88, No. 6.

[12] T. Yang, H. Tian and Y. Chen, "Preparation of Super hydrophobic Silica Films with Honeycomb-Like Structure by Emulsion Method," Journal of Sol-Gel Science and Technology, Vol. 49, No. 2, 2009, pp. 243-246.

[13] H. Kinoshita, A. Ogasahara, Y. Fukuda and N. Ohmae, "Super hydrophobic/Super hydrophilic Micropatterning on a Carbon Nanotube Film Using a Laser Plasma-Type Hyperthermal Atom Beam Facility," Carbon, Vol. 48, No.15, 2010, pp. 4403-4408.

[14] Z. G. Guo, J. Fang, J. C. Hao, Y. M. Liang and W. M. Liu, "A Novel Approach to Stable Superhydrophobic Surfaces," ChemPhysChem, Vol. 7, No. 8, 2006, pp. 1674- 1677.

[15] K. K. Lau, J. Bico, K. B. K. Teo, M. Chhowalla, G. A. J. Amaratung, W. I. Milne, G. H. McKinley and K. K. Gleason, "Superhydrophobic Carbon Nanotube Forests," Nano Letters, Vol. 3, No. 12, 2003, pp. 1701-1705.

[16] F. Mumm, A. T. J. van Helvoort and P. Sikoski, "An Easy Route to Super hydrophobic Copper Based Droplet Microfluidic Systems," ACS Nano, Vol. 3, No. 9, 2009, pp. 2647-2652

[17] S. S. Latthe, H. Imai, V. Ganesan and A. V. Rao, "Super hydrophobic Silica Films by Sol-Gel Co-Precursor Method," Applied Surface Science, Vol. 256, No. 1, 2009, pp. 217-222.

[18] V. V. Ganbavle, U. K. H. Bangi, S. S. Latthe, S. A. Mahadik and A. V. Rao, "Self-Cleaning Silica Coatings on Glass by Single Step Sol-Gel Route," Surface and Coatings Technology, Vol. 205, No. 23-24, 2011, pp. 5338- 5344.

[19] S. S. Latthe, H. Hirashima and A. V. Rao, "TEOS Based Water Repellent Silica Films Obtained by a Co-Precursor Sol-Gel Method," Smart Materials & Structures, Vol. 18, No. 9, 2009, p. 095017.

[20] A. V. Rao, S. S. Latthe, C. Kappenstein, V. Ganesan, M. C. Rath and S. N. Sawant, "Wetting Behavior of High Energy Electron Irradiated Porous Superhydrophobic Silica Films," Applied Surface Science, Vol. 257, No. 7, 2011, pp. 3027-3032.

[21] R. Furstner, W. Barthlott, C. Neinhuis and P. Walzel, "Wetting and Self-Cleaning Properties of Artificial Super hydrophobic Surfaces," Langmuir, Vol. 21, No. 3, 2005, pp. 956-961.

[22] M. Ma, Y. Mao, M. Gupta, K. K. Gleason and G. C. Rutledge, "Superhydrophobic Fabrics Produced by Electrospinning and Chemical Vapor Deposition," Macromolecules, Vol. 38, No. 23, 2005, pp. 9742-9748.

[23] X. Zhang, Y. Guo, P. Zhang, Z. Wu and Z. Zhang, "Superhydrophobic CuO@Cu2S Nanoplate Vertical Arrays on Copper Surfaces," Materials Letters, Vol. 64, No. 10, 2010, pp. 1200-1203.

[24] H. Liu, L. Feng, J. Zhai, L. Jiang and D. B. Zhu, "Reversible Wettability of a Chemical Vapor Deposition Prepared ZnO Film between Superhydrophobicity and Superhydrophilicity," Langmuir, Vol. 20, No. 14, 2004, pp. 5659-5661.

[25] L. Huang, S. P. Lau, H. Y. Yang, E. S. P. Leong, S. F. Yu and S. Prawer, "Stable Super hydrophobic Surface via Carbon Nanotubes Coated with a ZnO Thin Film," The Journal of Physical Chemistry B, Vol. 109, No. 16, 2005, pp. 7746-7748.

[26] L. B. Zhu, Y. H. Xiu, J. W. Xu, P. A. Tamirisa, D. W. Hess and C. P. Wong, "Superhydrophobicity on Two-Tier Rough Surfaces Fabricated by Controlled Growth of Aligned Carbon Nanotube Arrays Coated with Fluorocarbon," Langmuir, Vol. 21, No. 24, 2005, pp. 11208- 11212.

[27] Prathab, B., et al., Molecular modeling and atomistic simulation strategies to determine surface properties of perfluorinated homopolymers and their random copolymers. Polymer, 2006. 47(19): p. 6914-6924.

[28]Nityanshu Kumar, Gaurav Manik., Molecular dynamics simulations of polyvinyl acetate-perfluorooctane based anti-stain coatings. Polymer, 2016

[29] H. Zhou, H.X. Wang, H.T. Niu, A. Gestos, X.G. Wang, T. Lin, Fluoroalkyl silane modi- fied silicone rubber/nanoparticle composite: a super durable, robust superhydrophobic fabric coating, Adv. Mater. 24 (2012) 2409–2412.

[30] L.K. Gao, Y. Lu, X.X. Zhan, J. Li, Q.F. Sun, A robust, anti-acid, and high-temperaturehumidity-resistant superhydrophobic surface of wood based on a modified TiO2 film by fluoroalkyl silane, Surf. Coat. Technol. 262 (2015) 33–39.

[31] Prathab, B., V. Subramanian, and T.M. Aminabhavi, Computation of surface energy and surface segregation phenomena of perfluorinated copolymers and blends – A molecular modeling approach. Polymer, 2007. 48(1): p. 417-424.

[32] Lakshmi, R.V., et al., Fabrication of superhydrophobic and oleophobic sol–gel nanocomposite coating. Surface and Coatings Technology, 2012. 206(19–20): p. 3888-3894.

[33] Material StudioTM, by Dassault Systèmes BIOVIA, UK (Accelrys®), http://accelrys.com/products/materials-studio/, License purchased by IIT Roorkee.

[34] Sun, H., COMPASS: An ab Initio Force-Field Optimized for Condensed-Phase ApplicationsOverview with Details on Alkane and Benzene Compounds. The Journal of Physical Chemistry B, 1998. 102(38): p. 7338-7364.

[35] Rigby, D., H. Sun, and B.E. Eichinger, Computer simulations of poly(ethylene oxide): force field, pvt diagram and cyclization behaviour. Polymer International, 1997. 44(3): p. 311-330.

[36]BerendsenHJC,PostmaJPM,vanGunsterenWF,DiNolaA, Haak JR (1984) J Chem Phys 81:3684
[37] AndersenHC(1980)JChemPhys72:2384.

[38] Brooks CL III, Montgomery Pettitt B, Karplus MJ (1985) Chem Phys 83:5897

[39] Misra, S., P.D. Fleming, and W.L. Mattice, Structure and energy of thin films of poly-(1,4-cis- butadiene): A new atomistic approach. Journal of Computer-Aided Materials Design, 1995. 2(2): p. 101-112.

[40] Natarajan, U., G. Tanaka, and W.L. Mattice, Atomistic simulations of the surfaces of thin films of random copolymers. Journal of Computer-Aided Materials Design, 1998. 4(3): p. 193-205.

[41] He, D., D.H. Reneker, and W.L. Mattice, Fully atomistic models of the surface of amorphous polyethylene. Computational and Theoretical Polymer Science, 1997. 7(1): p. 19-24.

MACRO 117

Influence of Long Chain Branching on Necking Behaviour in Melt Extruded Cast Polyethylene Films

Rokade, Dhammaraj; Mulay, Apoorv; Lele, Ashish; Pol, Harshawardhan*

CSIR-National Chemical Laboratory, Polymer Sci. &Engg. Div., Pashan, Pune - 411008

** hv.pol@ncl.res.in*

Extrusion film casting (EFC) is an important polymer processing technique that is used to produce several thousand tons of polymer films/coatings on an industrial scale. In the past[1-4] and also in the present research we are interested in understanding quantitatively how macromolecular chain architecture (for example long-chain branching or LCB) influences the necking behavior of viscoelastic melts in the EFC process. We have used three commercial polyethylene (PE) resins (of similar melt flow indices or MFI) of long chain branched molecular architecture to produce extrusion cast films under controlled experimental conditions. All the resins were characterized for their macromolecular properties such as moments of molecular weights, long-chain branching frequency (see Table 1), etc. Additionally, the resins were also extensively characterized rheologically under both steady and dynamic conditions wherein transient extensional and shearing properties (see Fig. 1) were measured. The necking profiles of the films were imaged and the velocity profiles during casting were monitored using particle tracking velocimetry (PTV) techniques. We present results that demonstrate that the extent of necking of the PE

films varies as a function of both the draw ratio (a process parameter) as well as the amount of long-chain branching (a molecular parameter).

Table 1. High-temperature GPC data for various LCB containing LDPE resins.

Resins	M_n (g/mol)	M_w (g/mol)	MWD	No. of LCB's per molecule
T-LDPE-D	25995	199737	7.7	10.1
A-LDPE-R	38526	379647	9.8	14.1
T-LDPE-R	18923	168007	8.8	19.1

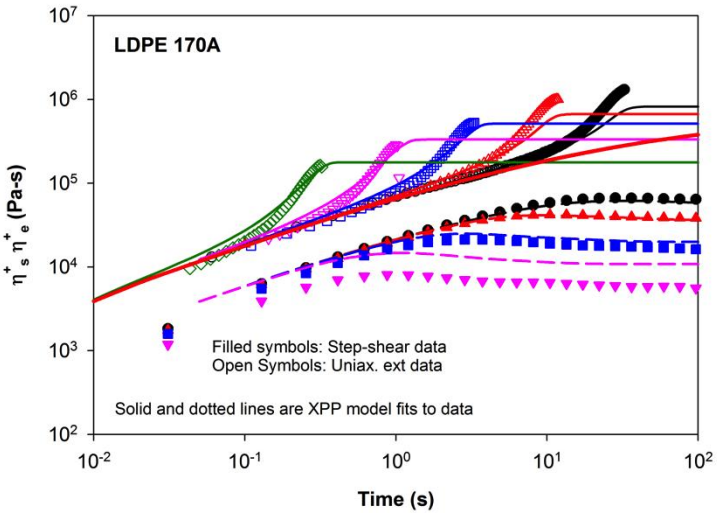


Figure 1. Transient Uniaxial Extensional and Shear Start-up Rheology of a Long-Chain Branched Low-density Polyethylene.

References

[1] Pol, H; Thete, S; Doshi, P; Lele, A. *J. Rheol.*, 57 (2013) 559.
[2] Pol, H; Banik, S; Azad, L; Thete, S; Doshi, P; Lele, A. *Rheol. Acta*, 53 (2014) 85.
[3] Chikhalikar et al., *Polym. Eng. Sci.*, 55 (2015), 1977.
[4] Thete, S; Doshi, P; Pol, H, *J. Plas. Film Sheeting*, appeared online (2016).

MACRO 119

Large Scale Production of Nylon Nanofibers through Electrospinning and their use in Structural Composites

Anand, Anoop*; Kumar, Narendhara;Harshe, Rahul; Joshi,Makarand

Composites Research Center, Research and Development Establishment (Engineers),

Defense Research and Development Organization - Ministry of Defense,

Alandi Road, Pune - 411 015, India

*aanand@rde.drdo.in

Electrospun polymer nanofibers have impelled considerable research attention owing to their extensive applications. A large number of polymers have been electrospun into nanofibersand their applications range from the making of scaffolds for tissue engineering to polymer nanocomposites.In the present investigation, an attempt has been made to evaluate the effect of electrospun nylon 6/6 nanofibers on the mechanical properties of fiber reinforced composites, for load-bearing applications. Nylon 6/6 has been selected for its good mechanical properties, dissolution characteristics in a solvent appropriate for electrospinning, and high melting temperature (250 - 260°C) which allows the nanofibers to maintain their morphology and integrity during the subsequent composite manufacturing.

The FRP composites are made of continuous, E-glass fabric reinforcement and epoxy resin matrix. Compared to their in-plane properties, relatively weak compression and interlaminar properties of the laminated composites remain as major challenges. Attempts have been made in the past to hybridize these composites with nanoparticles, for improving their matrix dominated mechanical properties [1,2]. The concept of hybridizing structural composites with polymer nanofibers can also benefit from the complimentary nanoscale reinforcement offered by the interleaved nanofibers. Nanofibers of diameter 80-100 nm were electrospun from formic acid solution of nylon 6/6 at optimized conditions, directly onto the fabric. Modified fabrics were used to realize composites through resin film infusion.



Figure 1.A close view of the scaled up

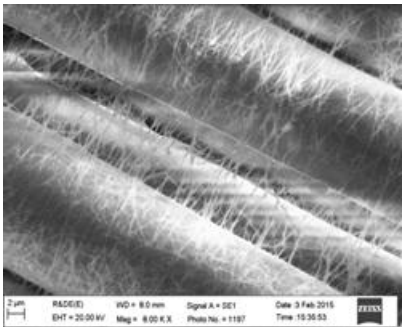


Figure 2.SEM image of electrospun nylon

A customized electrospinning machine has been used to prepare the nanofibers. A close view of the unit is given in Figure 1. This equipment has a motorized syringe pump that provides a constant flow of the polymer solution through the nozzles of a dozen syringe needles. The syringe needles are the positive terminal for the electrospinning process. The machine has a high voltage power supply with an output voltage range of 0 - 30 kV with a current capacity of 0.5 mA.

Polymer solution was taken in each of the 12 syringes and was supplied through 13 mm long stainless steel needles of diameter 0.45 mm using the programmable syringe pump. Solution concentration was restricted to 5% wt/wt. The conductive needles were electrically connected to a variable, positive polarity high voltage

power supply. High voltage power supply target rod made of stainless steel was electrically connected to the ground potential and the working distance from needle tip to target was varied from 10 cm to 30 cm. At each tip-target distance, the applied voltage was varied from 5 kV to 25 kV. Process parameters for the production of nylon 6/6 nanofibers of diameter 80-100 nm were optimized to SEM image of the resultant material is given in Figure 2.

Considering the concentration of solution, flow rate from 12 syringes and the movement of underlying fabric (500 mm wide fabric that conveys forward at a speed of 1 mm/sec), density of nanofibers deposited is approximated to be 0.1 gsm. Considering the areal density of glass fabric (830 gsm), weight fraction of the electrospun nanofibers is negligible, and they are interleaved in between the laminae of conventional fiber reinforced composites. Composite laminates were fabricated through resin film infusion; methodology involved has been reported elsewhere [3]. Composites of bidirectional E-glass/epoxy interleaved with nylon 6/6 nanofibers were made after drying the fabric under vacuum to ensure complete solvent removal from the electrospun material. Properties of laminates with various thicknesses of the nanofiber mats have been evaluated in comparison to a control composite specimen prepared without nanofibers. Compressive strength measurements were carried out as per ASTM D 3410. Interlaminar shear strength of composites was determined using standard short beam shear (SBS) specimens as per ASTM D 2344. Specimens for low velocity impact were made from balanced and symmetric laminates as per ASTM D 7136. Residual compressive strength of the impacted specimens was measured as per ASTM D 7137.

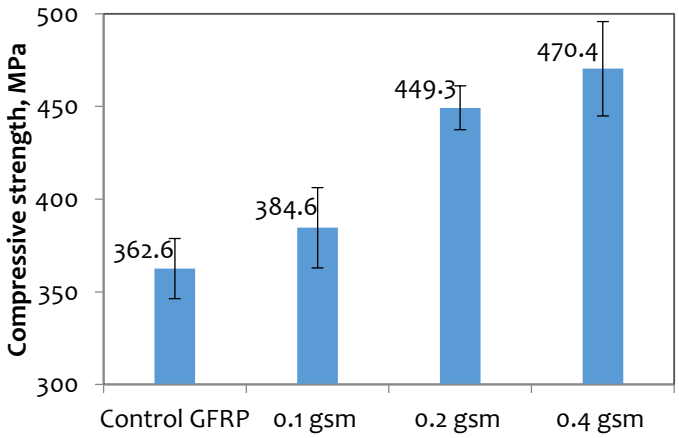


Figure 3. Effect of interleaved nanofibers on compressive strength of BD E-glass/epoxy composites

Effect of interleaved nylon 6/6 nanofibers on the compressive strength of continuous bidirectional (BD) E-glass/epoxy composites manufactured through resin film infusion, is depicted in Figure 3. It is evident that the compressive strength of composites with interleaved nanofibers improved considerably with respect to that of the control glass/epoxy composites. With an increase in the gsm of deposited nanofibers there is a gradual increase in the compressive strength of composites, 30% improvement has been achieved at 0.4 gsm of nanofiber deposition.

In compression, the fiber-matrix interface plays an important role in providing lateral support to the fiber. A combination of traditional glass fibers with a very thin deposit of electrospun nylon 6/6 nanofibers led to improved fiber polymer interfacial load transfer, which primarily affects the compressive strength of the composite [4]. Under compressive load, failure of composite laminates is initiated by fibermicrobuckling and subsequent plastic kinking of the material [5,6]. Nanofibers interleaved between the laminae delays fibermicrobuckling, and gives better resistance to crack initiation and propagation. As a result, this improves the overall matrix-dominated properties of composites such as compressive strength.

On further increasing the gsm of nanofibers, however, the laminates were predominantly dry. Hence it is inferred that there is an optimal loading for nanofibers and at their higher densities, flow of epoxy resin is hindered resulting in laminates with dry areas. Interlaminar shear strength of the laminates has also found to have improved by 17%.There was also a promising increase of 15-20%, in the residual compressive strength of composites after a low velocity impact event.

Our attempts have proved that interleaving electrospun nylon 6/6 nanofiber mats of 0.4 gsm in continuous bidirectional E-glass/ epoxy composites results in improved compressive, interlaminar shear strength and residual compressive strength after low velocity impact, of the composites. This technology can be an effective method to reinforce regions that have localized stress concentrations, without affecting the processing of composites and with no weight penalty for the final product.

References

[1] Anand,Anoop;Harshe, Rahul: Joshi,Makarand. *Journal of Composite Materials* 47 (2013) 2966.
[2] Panse, Prachi; Anand, Anoop; Murkute, Vinod; Ecka, Avinash; Harshe, Rahul: Joshi, Makarand. *Polymer Composites* 37 (2016) 1216.
[3] Anand,Anoop;Harshe, Rahul: Joshi,Makarand. *Journal of Applied Polymer Science* 129 (2013) 1618.
[4] Thostenson, E T; Li, W Z; Wang, D Z; Ren; Z F; Chou, T W.*Journal of Applied Physics* 91 (2002) 6034.
[5] Jumahat, A;Soutis, C; Jones, FR;Hodzic, A. *Composites Structures* 92 (2010) 295.
[6] Jumahat, A;Soutis, C; Jones, FR;Hodzic, A. *Journal of Materials Science* 45 (2010) 5973.

MACRO 129

Dynamic Viscoelasticity and Thermo-Mechanical Characteristics of TPV Composites: Theoretical and Morphological Approaches

Dey, P*[a,b]; Dash, B[a]; Gilbert, R[a]; Unnikrishnan, G; Nair, S. S[a]; Thomas, T. K[a]; Naskar, K[b]; Nando, G. B[b]

[a]*CEAT Limited, Chandrapura, Halol 389350, Panchmahal, Gujarat, India*

[b]*Rubber Technology Centre, Indian Institute of Technology Kharagpur, Kharagpur 721302, India*

* *pranab.dey@ceat.in*

Rubber elasticity and dynamic viscoelasticity of the TPV composites based on natural rubber, ethylene octene copolymer and carbon black (NR/EOC/CB) have been evaluated through dynamic mechanical analyzer (DMA). The elasticity of the rubber networks has been estimated through rubber index, which is a function of temperature and entropy. On the other hand, the measurement of dynamic viscoelasticity has been accomplished by adopting the concept of a classical damage parameter, obtained from initial tangent modulus through cyclic stress softening i.e. Mullins effect. Moreover, the mechanism of morphology evolution has been evaluated through thermodynamic calculations, which includes the measurement of thread break-up time, as obtained from the capillary number expression and morphological observations. The uneven dispersion of filler particles has resulted in reduced elasticity in the rubber networks, which is due to the reduced interconnectivity between the rubber domains, as evident from the experimental results as well as atomic force micrographs. This study has thus revealed an alternative aspect of dynamic mechanical analyzer in order to characterize the rubber-like materials.

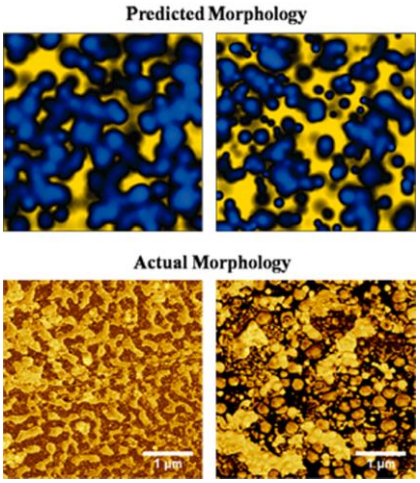


Figure 1. Predicted and actual morphologies of NR/EOC TPV composites containing different proportion of filler particles.

References

[1] Vennemann, N; Bökamp, K; Bröker, D. *Macromolecular Symposia*, 245 (2006) 641.
[2] Mirzadeh, A; Lafleur, P. G; Kamal, M. R; Dubois, C. *Rubber Chem. Technol.*, 86 (2013) 521.
[3] Wu, H; Tian, M; Zhang, L; Tian, H; Wu, Y; Ning, N; Chan, T. W. *ACS Sustain. Chem. Eng.*, 3 (2014) 26.
[4] Dey, P; Naskar, K; Dash, B; Nair, S; Unnikrishnan, G; Nando, G. B. *RSC Adv.*, 5 (2015) 31886.

MACRO 149

Segmental motions in PDLLA at the Glass transition temperature, probed using Solid-state NMR

Kavalakal Mathai Eldho ,[†] P.R. Rajamohanan, [†] Poorvi Purohith, [‡] Neelima Bulakh, [‡] Ashish Lele,[*‡] and T.G. Ajithkumar,[*†]

[†]Central NMR Facility, Physical Chemistry Division, [‡] Polymer Science and Engineering Division, National Chemical Laboratory, Pune 411 008, India.

Correspondence to: T. G. Ajithkumar, Central NMR Facility, National Chemical Laboratory, Dr. Homi Bhabha Road, Pune - 411008, Maharashtra, India; tg.ajithkumar@ncl.res.in (email) 91-20-2590-2569 (phone), (fax) and Ashish Lele, Polymer Science and Engineering, National Chemical Laboratory, Dr. Homi Bhabha Road, Pune – 411008, Maharashtra, India; a.lele@ncl.res.in (email)

[†]Central NMR Facility, Physical Chemistry Division, National Chemical Laboratory

[‡]Polymer Science and Engineering Division, National Chemical Laboratory

ABSTRACT: The aim of this study is to investigate the structural changes taking place in a 6% Poly-DL-Lactide (PDLLA) film, when annealed at slightly above it's glass transition temperature (Tg). Annealing of PDLLA film was carried out at 65ºC in an air circulatory oven. DSC and CODEX NMR experiments were carried out to establish a correlation between the macroscopic properties and the molecular level

segmental mobility in the amorphous region of the polymer film. At 65ºC, which is slightly above the glass transition temperature of PDLA film, the CODEX NMR experiments were used to measure the segmental mobility at the molecular level taking place inside the PDLA film and it was observed that there was a slowing down of segmental mobility with themal aging and it is attributed to the crystallinity which induced in PDLLA film after it was annealed for 15 days at 65ºC.

INTRODUCTION

Over the past few decades, several biodegradable polymers have been investigated as green alternatives to non-degradable polymers. Poly lactic acid (PLA) is a chief contender to be a commercial success among biodegradable plastics. It is a thermoplastic aliphatic polyester derived entirely from renewable resources, by fermentation of agricultural products such as corn starch, tapioca, maize, sugar, and wheat [1, 2]. Since PLA has very low or no toxicity, it is used as structural scaffolds in human body for reconstruction of damaged organs, sutures for wound closure, drug delivery applications, orthopeadic devices for surgical applications etc [2-5].

PLA is synthesized from lactic acid. The ring opening polymerization or condensation polymerization of lactic acid gives high molecular weight poly-lactic-acid. Homo polymer Poly lactic acid has a glass transition temperature of 55-60ºC (α transition) and melting temperature of 180ºC [1]. According to the monomer used for the preparation, there are three kinds of poly lactic acids, poly D lactic acid (PDLA), poly L lactic acid (PLLA) and poly D-L lactic acid (PDLLA). Enantiomerically pure poly lactic acid is semicrystalline in nature and always gives a high percentage of crystallinity to the material while PDLA and PLLA together form recemic or meso poly lactic acid. PDLLA is amorphous and transparent in physical appearance. The mechanical properties of semicrystalline PLA are better compared to the amorphous PLA. The PLLA has a good mechanical property to due to a high molecular mass of the polymer chain, the crystallinity and high entanglement density [6]. In the semicrystalline PLA the polymer chains are more entangled compared to amorphous state and results in cross linking between the chains. This result in

high molecular weight polymers and the tensile strength of the polymer increases. It is observed that a PLLA with relatively small amount of D isomer having 65% crystallanity is reported to have the highest impact strength. Recemization decrease the melting temperature of poly lactic acid by 20-30^{0}C, while it has the advantage of high mechanical processibility. Poly lactic acid is being used in variety of applications including interior parts of vehicles, electric appliances, bio-absorbable bone fixation devices etc [7, 8]. However, the low heat resistance and poor toughness of PDLLA limit its wider applicability.

Poly lactic acid is used in many biomedical applications, structural implantation, wound closure etc, there is particular interest in understanding the dynamics behavior of poly lactic acid. Different techniques such as DSC, DMA, DES, Thermally stimulated recovery (TSR) are used to obtain information about the dynamics in the polymer. Mijovic *et al.* studied the effect of crystalline region on chain dynamics of PLLA amorphous region using dielectric relaxation spectroscopy(DES) [9]. They observed that the amorphous phase in PLLA undergoes cooperative chain motions with motional lengths that are shorter than the distance between the crystalline lamellae. Kanchanasopa *et al.* proposed the existence of a rigid amorphous phase in PLLA along with amorphous and crystalline phases and interpreted that the crystallinity induction along with the microcrystalline structure influence the α process [10]. Mano has studied the glass transition dynamics in PLLA using DMA and TSR techniques and found that at the glass transition temperature, the polymer chains are undergoing cooperative chain mobility [11]. Majority of the studies on the dynamics of poly lactic acid is performed using DMA, DES and TSR and hence give only a macroscopic information.

To understand the mechanical behavior of polymers, it is very important to understand the contribution of the segmental and functional group motions. Theoretically, the random arrangement of coils results in motions at the molecular level. If the molecular scale of motions can be probed by solid-state NMR, and a correlation to the macroscopic behavior can be found, then probably more insight into the molecular origin for the mechanical property in poly lactic acid can be addressed. The aim of this study is

to understand the thermo-mechanical behavior of PDLLA as a function of thermal ageing and correlate these with segmental and functional group dynamics.

METHOD

Slow segmental Motions in the polymer can be measured using the CODEX experiment. The pulse sequence for CODEX is shown in figure 1[12, 13] . CODEX is an exchange experiment which uses two rotor synchronized CSA re-coupling sequences with a mixing time in between them, during which motion is expected to happen. The z filter time at the end of sequence is usually chosen in such a way that there is no possibility of motion happening during that period. In the CODEX experiment, re-coupling of chemical shift anisotropy is achieved by a series of rotor synchronized 180^o pulses separated by half rotor periods. The magnetization acquires a phase ϕ_1 before the mixing time and a phase ϕ_2 before the z filter due to the re-coupling of the chemical shift anisotropy afterthe 180^o pulse trains. If there is no motion during mixing time, (τ_m) the phase acquired during ϕ_1 and ϕ_2 will be same and there will be no de-phasing in the CODEX spectrum. On the other hand if there is motion present during the mixing time, τ_m then ϕ_1 is not equal to ϕ_2 and it will be reflected in the CODEX spectrum as a decrease in the signal intensity. The decrease in the CODEX signal obtained during mixing times (τ_m) and re-coupling times ($N\tau_r$) are not simple functions of motion alone but is affected by transverse relaxation (T_1) and longitudinal relaxation (T_2) also. The longitudinal relaxation time of spectrum is removed by normalising the CODEX spectrum with a REFERENCE spectrum, which is obtained by interchanging the mixing and z filter times with each other. The τ_m dependence measurement gives the correlation time of motion, obtained by varying the mixing time with a constant $N\tau_r$ period. An $N\tau_r$ dependence experiment is carried out to determine the $N\tau_r$ at which dephasing reaches a plateau and this is used for τ_m dependence experiment . The normalization of CODEX with respect to REFERENCE spectrum for fixed $N\tau_r$ at different mixing time gives the de-phasing due to the segmental motion in the polymer chain. Thus, the dephasing curve obtained

is fitted with Kolhrash's William Watt (KWW) function to obtain the correlation time of motion as given by

$$\left(\frac{S}{S_0}\right)_{motion} = (1 - M) + M * exp(-(\frac{\tau_m}{\tau_c})^{\beta}) \quad (1)$$

where τ_c indicated the correlation time obtained, M is the fraction of components which participating in the motion and β is the distribution in correlation time.

SAMPLE PREPARATION

The amorphous PDLLA used for the SSNMR study was prepared by compression molding. The crystalline sample of PDLLA (6% D-L Lactic Acid), having a molecular weight of 256000 g/mol, was first heated to 200ºC, kept for 2 minutes in the compression die and then compressed to a narrow thin film. The thin film formed inside the die was then quickly put into cold water for quenching. The sample obtained after the process was hard and transparent in physical appearance. To check the nature of the sample, Differential Scanning Calorimetry (DSC) was carried out.

The DSC graph of a fresh PDLLA is shown in figure 2. As the temperature rises, the curve goes linearly until 55ºC. In the region between 55ºC and 60ºC, the graph shows a dip indicating its glass transition (T_g). After the T_g the DSC curve is linear until 200ºC. The melting temperature of PDLLA is expected to be around 150ºC-160ºC, if there is a crystalline component present. Since no peak is observed in this region, it can be confirmed that the sample is purely amorphous.

EXPERIMENTAL

Differential Scanning Calorimetry (DSC)

All the DSC measurements have been carried out on a Q-100 differential scanning calorimeter from TA instruments. The DSC cell was first calibrated with 99.99% pure indium. About 3-7 mg of sample was

placed in an aluminum pan and used for the measurement. The thermal behavior of the sample was scanned from 0ºC to 200ºC with the rate of temperature increment at 10ºC/min. The percentage of crystallinity of the sample is determined by the comparison of melting temperature peak areas of amorphous PLA and 100% pure crystalline PLA sample. It is given by the equation

$$\%\ crystallinity = 100 * {}^{\Delta H}/_{93} \quad (2)$$

where 93 J/g is the heat of fusion of an infinitely large crystal of poly lactic acid.

Solid-state NMR

The NMR measurements were carried out on Bruker Avance 300MHz spectrometer in a 4 mm triple resonance probe which is used in the double resonance mode. The processed PDLLA films were cut into small pieces and perfectly packed in 4 mm rotor. All the experiments were carried out at a spinning frequency of 3 kHz. The RF frequencies of the ^{1}H and ^{13}C channels were 85 kHz and 67.5 kHz respectively. A mixing time of 2.5 $msec$ was used during the cross polarization. The TPPM-15 decoupling sequence with an RF power of 85 kHz was used during the acquisiton. ^{1}H longitudinal relaxation time (T_1) was measured using the saturation recovery experiment and a recycle delay of five times T_1 was used for all the NMR experiments. The probe temperature was calibrated using Methanol and $PbNO_3$ for the spinning rate of 3 kHz [14, 15]. The CODEX mixing time (τ_m) dependence experiment was carried out by varying the mixing time from 1 $msec$ to 2048 $msec$ in a logarithmic scale with 12 data points in between. Each experiment was carried out with 1152 transients.

The samples which were thermally aged for 9 and 15 days were prepared by heating the sample in a vacuum oven at 65ºC which is ~5ºC above the glass transition temperature. One portion of the sample was used for the CODEX experiments and the other portion for the DSC measurements. All the CODEX experiments were carried out at 60ºC, at the glass transition temperature of poly lactic acid.

RESULTS AND DISCUSSION

The chemical structure of PDLLA is shown in figure 3. PDLLA contain three chemically distinct carbons: CO, CH and CH_3. The CPMAS spectrum of PDLLA at 23ºC is shown in figure 3 and the chemical shift observed at 170.0, 69.5 and 16.9 ppm is assigned to the CO, CH and CH_3 environments respectively. The CPMAS spectra clearly indicates that the centre band do not overlap with the spinning sidebands at a spinning speed of 3 kHz.

The CODEX $N\tau_r$ dependence experiments were carried out with a mixing time of 100 $msec$. The CODEX $N\tau_r$ dephasing curve attains a plateau when $N\tau_r$ is equal to 3.33 $msec$ and therefore, all the CODEX τ_m dependence experiments were carried out with this $N\tau_r$. The results of the CODEX τ_m dependence experiments are discussed below. The CODEX τ_m dependence experiments were analyzed for the CH and CH_3 moiety, while the CO moiety was not analyzed due to poor signal to noise ratio.

It was observed that from 23ºC to 50ºC, the CODEX τ_m dependence curve does not show much dephasing in the difference signal, indicating that slow segmental motions are either absent or very slow. But as the temperature approaches 60ºC, the CODEX τ_m dependence curve shows dephasing indicating the onset of slow segmental and cooperative motions in the main chain. The CODEX difference spectrum obtained for the fresh PDLLA at 60ºC with mixing times of 1, 8, 64 and 1024 $msec$ are shown in the figure 4. A gradual change in the intensity of the CODEX difference spectrum indicates the presence of slow segmental motions at 60ºC.

The results of CODEX τ_m dependence experiments obtained for the CH_3 and CH environments in PDLLA are shown in figures 5a and 5b respectively. The CODEX τ_m dependence experiments were carried out on fresh, 9 days and 15 days thermally aged samples. The normalized signal intensity (S/S_0) is fitted using the KWW function (Equation 1) to extract the correlation time of motion. It is observed that the CODEX dephasing curves for both the CH_3 and CH environment show an upward shift with an increase in the annealing time.

The fitting of CODEX de-phasing intensity against mixing time gave the correlation time, degree of distribution in correlation time and the fraction of segments available for motion and the values obtained for the CH_3 and CH moieties in PDLLA are tabulated in table 1. The CH_3 moiety of freshly prepared sample have a correlation time of 85.4 $msec$. This indicates that slow segmental motions are present in PDLLA at 60°C. For the 9 days thermally aged sample a correlation time of 140.4 $msec$ was observed which indicates that there is a slowing down in segmental motion with respect to annealing. A correlation time of 205 $msec$ was obtained for the 15 days aged sample which confirms the slowing down of chain motion in the polymer with respect to thermal aging. The value of M indicates that the amount of segments available for motion increase with an increase in thermal aging. A similar trend is observed for the CH group also, where the correlation time increases from 150.9 $msec$ to 203.5 $msec$, as the annealing time increases. The correlation time of both the CH and CH_3 group increases with annealing time, indicating that the rate of motions decreases as annealing time increases.

DSC measurements were also carried out on all the samples to determine the percentage of crystallinity accumulated (Figure 6). It is seen that for the fresh sample the percentage of crystallinity is zero and it reaches 4% and 5% for the 9 and 15 days annealed samples.

CONCLUSION

The influence of thermal aging on the segmental and cooperative motion in poly lactic acid was studied using the CODEX experiment. Different thermally aged samples were prepared and the CODEX and DSC experiments were carried out on them. The CODEX experiments show that there are no slow motions in the polymer at low temperatures (23°C to 50°C). However, slow motions were observed as the temperatures approaches the glass transition temperature, 60°C. Slow motions in the range of 1-10 Hz were detected through the CH and CH_3 moieties of the polymer and the rate of motions decreases with the aging of the sample. The DSC measurements show that there is an increase in crystallinity with annealing

time. Therefore, it is concluded that the increase in crystallinity in polymer chain decreases the rate of slow segmental motions in poly D-L lactic acid.

REFERENCES

(1) Garlotta, D. *J. Polym. Environ.* **2001,** 9, (2), 63-84.

(2) Sodergard, A.; Stolt, M. *Prog. Polym. Sci.* **2002,** 27, (6), 1123-1163.

(3) van de Witte, P.; Esselbrugge, H.; Peters, A. M. P.; Dijkstra, P. J.; Feijen, J.; Groenewegen, R. J. J.; Smid, J.; Olijslager, J.; Schakenraad, J. M.; Eenink, M. J. D.; Sam, A. P. *J. Controlled Release* **1993,** 24, (1â€“3), 61-78.

(4) Schakenraad, J. M.; Oosterbaan, J. A.; Nieuwenhuis, P.; Molenaar, I.; Olijslager, J.; Potman, W.; Eenink, M. J. D.; Feijen, J. *Biomaterials* **1988,** 9, (1), 116-120.

(5) Middleton, J. C.; Tipton, A. J. *Biomaterials* **2000,** 21, (23), 2335-2346.

(6) Grijpma, D. W.; Pennings, A. J. *Macromol. Chem. Phys.* **1994,** 195, (5), 1649-1663.

(7) Maeda, H.; Kasuga, T.; Nogami, M.; Ueda, M. *Science and Technology of Advanced Materials* **2005,** 6, (1), 48-53.

(8) Park, S. D.; Todo, M.; Arakawa, K.; Koganemaru, M. *Polymer* **2006,** 47, (4), 1357-1363.

(9) Mijovic, J.; Sy, J.-W. *Macromolecules* **2002,** 35, (16), 6370-6376.

(10) Kanchanasopa, M.; Runt, J. *Macromolecules* **2004,** 37, (3), 863-871.

(11) Mano, J. F. *Macromolecular Bioscience* **2005,** 5, (4), 337-343.

(12) deAzevedo, E. R.; Hu, W. G.; Bonagamba, T. J.; Schmidt-Rohr, K. *J. Am. Chem. Soc.* **1999,** 121, (36), 8411-8412.

(13) deAzevedo, E. R.; Hu, W. G.; Bonagamba, T. J.; Schmidt-Rohr, K. *J. Chem. Phys.* **2000,** 112, (20), 8988-9001.

(14) Geet, A. L. V. *Anal. Chem.* **1968,** 40, 2227-2229.

(15) Bielecki, A.; Burum, D. P. *J. Magn. Reson., Ser A* **1995,** 116, (2), 215-220.

Figures

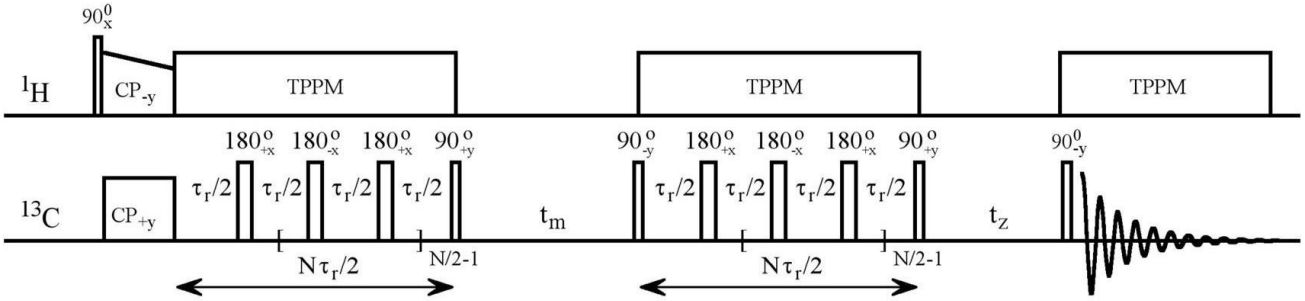


Figure 1: The pulse sequence used for CODEX experiment. It contains two rotor synchronized 180° pulse trains separated by a mixing time. At the end of the second 180° pulse train a z filter is present followed by signal detection. The REFERENCE spectrum is obtained by interchanging the mxing time and z filter time with each other.

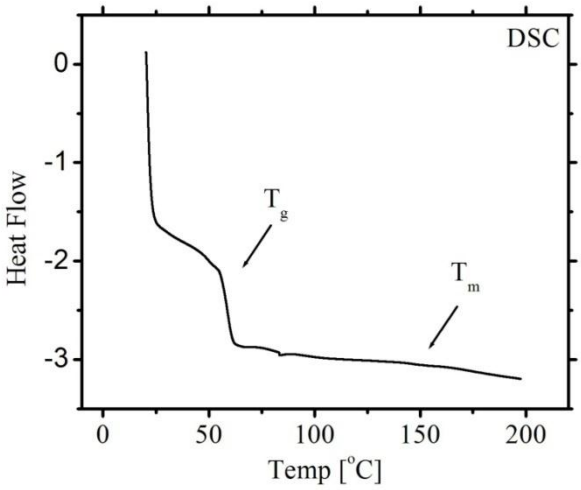


Figure 2: DSC curve of a freshly prepared poly DL lactic acid obtained from Q-100 TA instrument. Its shows a T_g around 55-60°C, while the melting temperature (T_m) peak expected at 150°C-160°C range is completely absent.

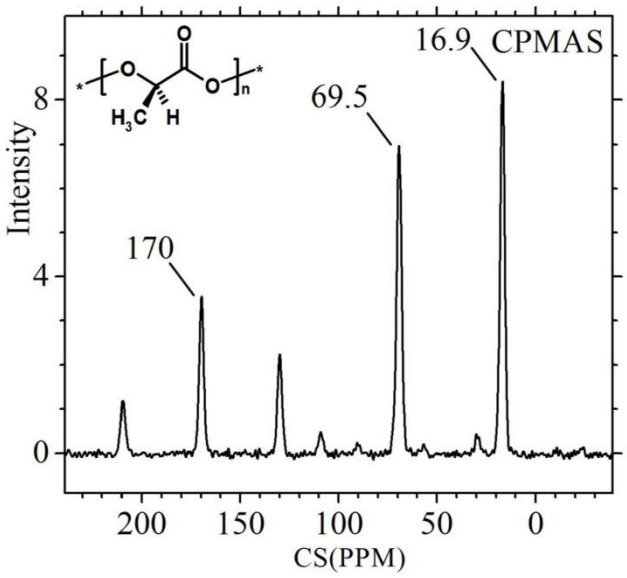


Figure 3: The CPMAS spectrum of poly D-L lactic acid at 60°C. The peak at 16.9 ppm, 69.5 ppm, and 170 ppm corresponds to CH_3, CH and CO environments respectively. The structure of polylacticacid is shown in the inset.

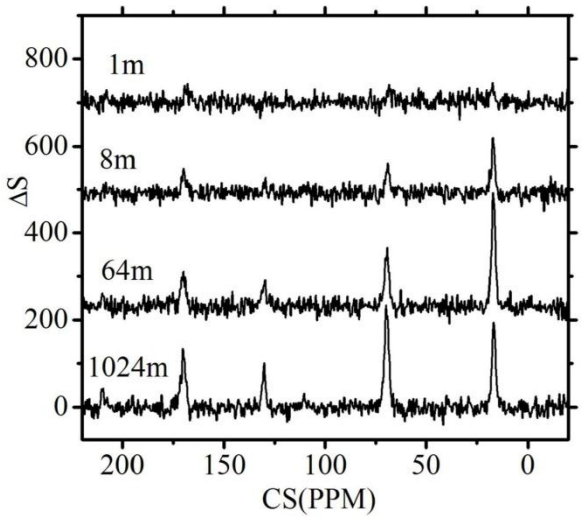


Figure 4: The CODEX difference spectrum obtained for a fresh PDLLA sample at mixing times of 1 $msec$, 8 $msec$, 64 $msec$ and 1024 $msec$. The spectra show a gradual increase in the dephasing signal with an increase in the mixing time.

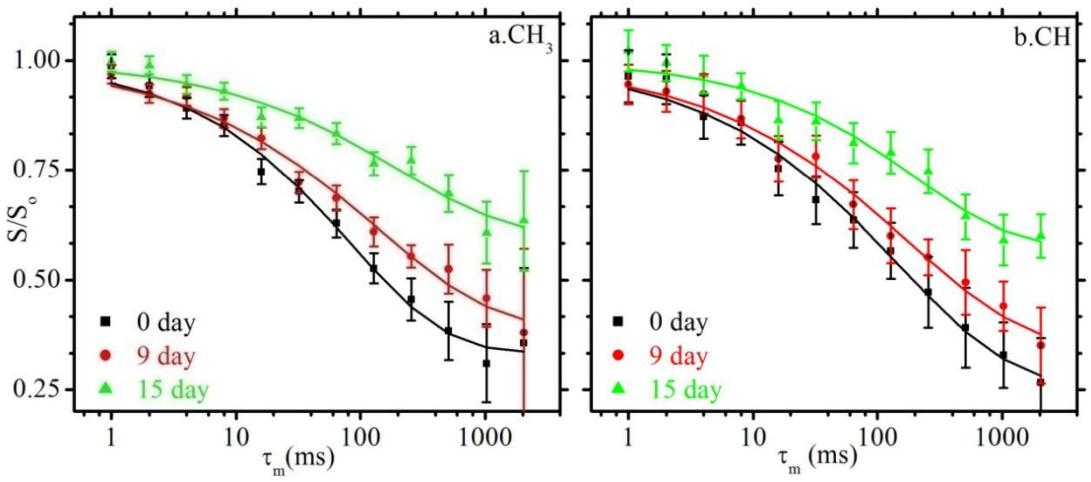


Figure 5: The results of the CODEX τ_m dependence experiments of a) CH_3 b)CH moieties in the PDLLA samples. The experiments were carried out on a fresh sample, 9 and 15 days thermally aged sample. It can be confirmed that at 60°C the chains possess slow segmental motions and the CODEX curve show an upward shift with annealing time. The CODEX signal intensity obtained was fitted with the KWW function to obtain the correlation time.

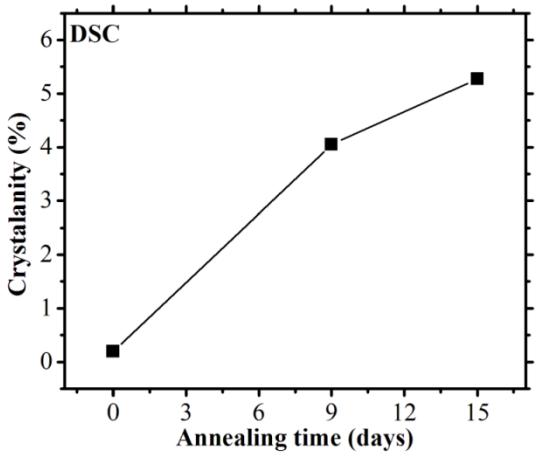


Figure 6: The crystallinity obtained from the DSC measurements for different annealing times. The crystallinity increases with increase in the annealing time.

	CH_3	CH

Aging (days)	M	$\tau_m\ (msec)$	β	M	$\tau_m\ (msec)$	β
0	0.67±0.02	85.4±12.9	0.57±0.04	0.74±0.03	150.9±37.5	0.48±0.03
9	0.60±0.03	140.4±40.3	0.47±0.04	0.66±0.04	180.8±59.9	0.45±0.04
15	0.40±0.04	210.7±103.5	0.50±0.08	0.42±0.04	203.5±79.9	0.56±0.08

Table 1: The correlation time τ_m of CH_3 and CH groups for different thermally aged samples along with the fraction of sample undergoing the dynamics (M) and the distribution in the correlation time (β).

MACRO 151

Effect Of Increasing Soft Segments On Properties Of Polyurea for blast mitigating applications

Iqbal Nahid[a,b], Mitra Arnab[c], Kumar Devendra[b], Roy Prasun Kumar[a]

[a]*Centre for Fire, Explosive and Environment Safety, DRDO, Timarpur, Delhi 110054, India.*
[b]*Department of Applied Chemistry and Polymer Technology, Delhi Technological University, Delhi 110042, India.*
[c]*Department of chemical Engineering, Birla Institute of Technology and Science, Pilani-333031*
** E-mail addresses:pk_roy2000@yahoo.com*

Abstract
Polyurea, an elastomer with repeating urea (-NH-CO-NH-) linkages, has been identified as an excellent protective coating. Polyurea is prepared by the spontaneous reaction of a diisocyanate and diamine possess hard domains dispersed randomly within the soft domains, with each domain exhibiting its own characteristic glass transition temperature. It is the unique microstructure of polyurea, which bestow them with their exceptional blast mitigating and ballistic protection capabilities. In this paper we have prepared polyurea formulations using a series of amines with an aim to study the effect of increasing soft segment: hard segment ratio on the properties of prepared specimen. The structural changes occurring during the preparation of polyurea was followed by FT-IR spectroscopy. Differential Scanning Calorimetric (DSC) studies were performed to quantify the characteristic thermal parameters. The changes in the mechanical properties of polyurea as a result of increasing hard segment was quantified in terms of tensile strength and elongation.
Keywords: *Polyurea; Blast mitigation; microstructure*

Introduction
Polyurea, belong to a class of segmented block (alternate hard and soft segments) polymer formed in situ by the rapid reaction of diisocyanate with diamine[ ]. The rigid isocyanate domains (hard phase) is embedded within the matrix of flexible chains (soft phase) [ ]. The hard phase formed as a result of strong hydrogen bonding between the urea linkages leads to the formation of nanometer-sized ribbon shaped hard segment [ ], which are relatively

ordered and exhibit T_g higher than ambient temperature. The soft domains present in polyurea are formed from long chain amines, which exhibit a glass transition temperature (T_g) much below the ambient temperature, and are responsible for imparting flexibility to the polymer. Thermodynamic incompatibility between the hard and soft segments result in phase separation which lead to the formation of a two phase morphology. This class of multi block elastomers can be tailored to exhibit a wide range of mechanical properties ranging from soft rubber to hard plastic by varying the chemical structure and molecular weight of the components. Similarly, the methodology adopted for preparation of polyurea, i.e. spray coating or solvent casting, also affects the morphology as well as properties of the resulting polymer appreciably.[1] It is well established, that the chain extenders are incorporated to lengthen the hard segment in order to obtain microphase separation in segmented copolymers with useful structural properties. Segmented non chain extended polyureas have been least investigated in the past. However, Yilgor et al. as well as Tyagi et al. were first to synthesize and investigate the structure- property behavior of non chain extended, segmented polyureas.

In the present study, the effect of soft segment molecular weight with increasing hard segment content (23-73%) was studied in detail.

Copolymers with Poly(propy1eneoxide) (PPO) based amines of different molecular weights JEFFAMINE®D-230, JEFFAMINE®D-400 and JEFFAMINE®D-2000 were studied. The hard segment of these Polyurea were based on the commercial MDI prepolymer (Suprasec 2054) The reaction of isocyanate with amine was followed using FTIR spectroscopy. The effect o soft segment molecular weight effect on the structure property relationship for all the segmented non chain extended polyureas was studied using UTM, DSC and TGA.

Experimental

Materials

$$m_{iso}.n_{eq,iso} = [m_{amine}.n_{eq,amine}]i_{NCO}$$

Commercial MDI prepolymer, especially designed for polyurea spray elastomers applications, Suprasec 2054 with a NCO = 15 %, viscosity of 775 mPas at 25 ºC, was purchased from Huntsman. Poly(propy1eneoxide) (PPO) based diamines of different molecular weights JEFFAMINE®D-230, JEFFAMINE®D-400 and JEFFAMINE®D-2000 were procured from Huntsman. The suffix 'D' refers to 'difunctionality' and the subsequent number refers to the approximate molecular weight of each species. CH_2Cl_2 (CDH) was used without further purification. Double distilled water was used throughout the course of this work.

Characterization methods

Calorimetric studies were performed using Differential Scanning Calorimetry (TA instruments, Q 20 module) under inert atmosphere. The thermal degradation behavior of samples was investigated using Perkin Elmer Diamond STG-DTA-DSC under N_2 atmosphere over the temperature range of 50-800 °C. Quasi-static mechanical properties were determined according to ASTM D638 using a Universal Testing System (International equipments) at ambient temperature. The samples were subjected to a cross head speed of 50 mm min^{-1}. Samples were tested in triplicate and the average values have been reported.

Results and Discussion

Polyurea films were prepared using solvent casting method and the effect of increasing hard segment on thermal and mechanical properties of polyurea was established.

Polymerization was performed by the rearrangement reaction of isocyanate with amine at room temperature in dichloromethane solvent (15-20% solid content). The diamine was aded dropwise into the diisocyanate solution under strong agitation. The amount of amine was calculated according to the following formula.

where m_{iso} and m_{amine} refer to the mass of isocyanate and diamine respectively and $n_{eq,iso}$ and $n_{eq,amine}$ are the equivalent number of isocyanate (3.57 mmol/g), and amine. The isocyanate index (i_{NCO}) was maintained at 1.1 for the entire set of experiments[19]. The hard segment (%) was calculated as per the following equation.

$$\text{Hard Segment (\%)} = \frac{m_{iso}}{m_{iso}+m_{amine}} \times 100$$

It is expected that the % hard segment in polyurea will decrease with increasing m. mass of the amine. The % hard segment of PU 230, PU 400 and PU 2000 was estimated to be , , and respectively. Films of requisite thickness (0.5-0.7 mm) were obtained by pouring the polymer solution into Teflon molds. The molds were covered with glass petridish to prevent rapid solvent evaporation with an aim to prevent bubble formation during the solidification stage. Post-solvent evaporation, the molds were placed in a vacuum oven at 60 ºC to ensure complete drying, the process being monitored gravimetrically. The resulting films were stored under vacuum for subsequent analysis. The polyurea films were designated as PU followed by a numerical suffix indicating the molecular weight of diamine from which it is derived. For example, PU 230 refers to the polyurea films obtained by the reaction of isocyanate with amine of molecular weight 230.

The reaction of isocyanate with amine was followed by FTIR spectroscopy. Figure 1 shows the spectra of samples removed at predetermined time durations for a representative case of PU 230. As expected the absorption associated with the NCO stretching (2170 cm^{-1}) decreases in intensity with time as a result of reaction with the amine, leading to the formation of urea linkages. The extent of reaction was quantified in terms of the ratio of absorbance at 2170 cm^{-1} (NCO stretch) to 1600 cm^{-1} (benzene). It can be seen that the said ratio decreases significantly within the first few minutes of the reaction, which is a result of the rapid rate of the reaction. Complete curing was confirmed by the absence of the peak due to NCO stretching at ~100 mins.

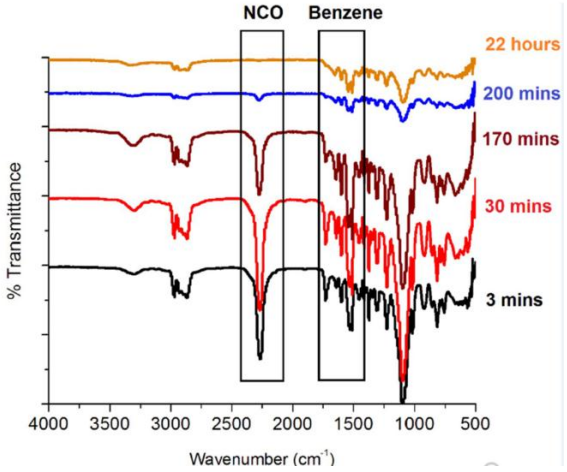


Figure 1: Changes in the FTIR spectra and NCO index as a function of reaction time a) 2 min, b) 6 min and c) 10 min.

Differential scanning calorimetry

The DSC traces of the polyurea films are presented in Figure 2. Polyurea possess a nano-segregated microstructure, with each domain exhibiting its own characteristic glass transition temperature. Hydrogen bonding between the urea linkages leads to the formation of nanometre-sized ribbon-shaped hard segments[33] which exhibit a super-ambient glass-transition temperature and are relatively ordered or crystallized. The soft domain on the other hand is of an amorphous nature and possess sub- ambient glass transition temperature, usually less than -30 °C [33]. As expected polyureas prepared using amines with higher molar mass, i.e. possessing lower % hard segment, were found to exhibit lower glass transition temperatures. The characteristic thermal parameters are presented in Table 1.

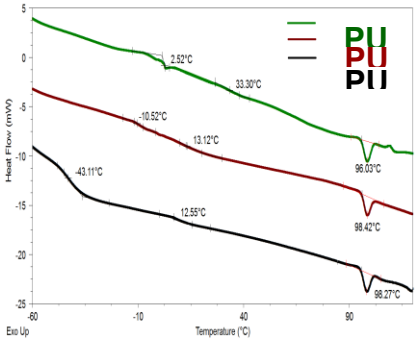


Figure 3: DSC curing profile

Table1: Effect of increasing hard segment on characteristic thermal parameters

	Hard segment%	T_{g1} (°C)	T_{g2} (°C)	T_m (°C)
PU230		**2.5**	**33.3**	**96.0**
PU400		**-10.5**	**13.1**	**98.4**
PU2000		**-43.1**	**12.5**	**98.3**

3.4. Mechanical properties: Effect of hard segment

The mechanical behaviour of polyurea films (under tensile loadings) was studied with an aim to establish the effect of increasing hard segment (%) on characteristic mechanical properties i.e. tensile strength and elongation at break, and the results are presented in Fig 4. Upon being subjected to uniaxial stretching, polyurea formulations possessing higher hard segment displayed the higher tensile strength and lower percentage elongation.

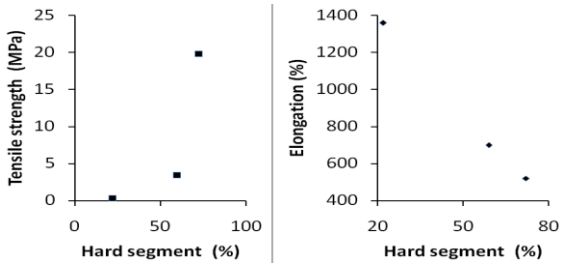


Fig 3: Effect of increasing hard segment on mechanical properties of Polyurea

Figure 3 illustrate the effect of soft segment molecular weight on the tensile hysteretic response of PU 230 and PU 400. In the deformation cycle shown, the polyurea samples were subjected to an elongation of 400% strain followed by an almost immediate withdrawal of the applied load. The hysteretic behavior was quantified in terms of the area under the curve, which was calculated to be 28.5 MPa for PU 230 and 1.6 MPa for PU 400. The difference may be attributed to the fact that the percolated hard segments break up with larger value of hysteresis for the system possessing higher percentage hard segment.

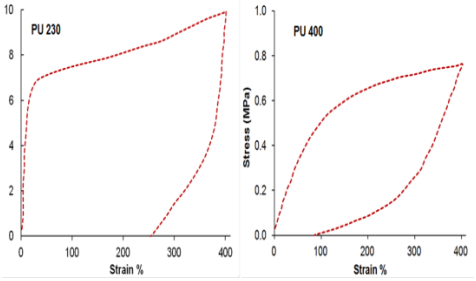
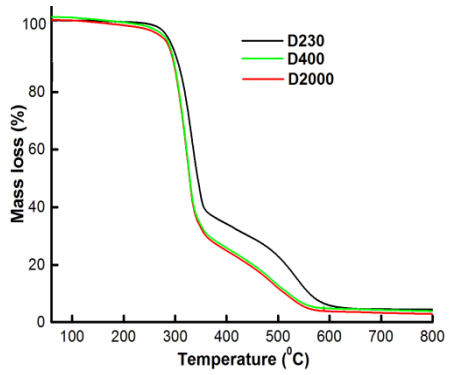


Fig 4: Tensile hysteretic behaviour of PU 230 and PU 400.

The TG-DTG traces of the polyurea samples are presented in Figure 5**.** The thermal degradation behaviour of the polyurea was found to remain practically unaffected due to increase in chain length of the amine used for its preparation. Polyurea degradation profile shows two steps, with a char content of ~ 6%. The first mass loss is attributed to the degradation of hard segment, because of the relatively low thermal stability of urea linkages. The subsequent second mass loss occurs due to decomposition of the soft segments.



Conclusions

Polyurea with varying hard segment (%) were prepared using solvent evaporation technique. All the samples were found to exhibit two glass transition temperatures. Polyureas prepared using amines with higher molar mass, i.e. possessing lower % hard segment, were found to exhibit lower glass transition temperatures. Polyurea formulations with higher hard segment displayed the higher tensile strength and lower elongation. The thermal degradation profile of the polyurea was found to remain practically unaffected due to increase in chain length of the amine used for its preparation.

Acknowledgements

Acknowledgements can be mentioned here.

References

1. A. Name, B. Name, C. Name, *J.Am.Chem.Soc.* 3, 1465, 2015.
2. A. Name, B. Name, C. Name, US Patent, Patent number**,** 1997.
3. A. Name, B. Name, C. Name, Conference title, Conference location, 2016.
4. A. Name, B. Name, C. Name, Editor Name, Elsevier, London,1-3, 1987.

MACRO 165

A Kinetics Study of Light-Induced E−Z Isomerization in Sol, Gel, Xerogel, and Powder States of an Anthracene-Based Organogelator: Fiber to Crystal Transformation

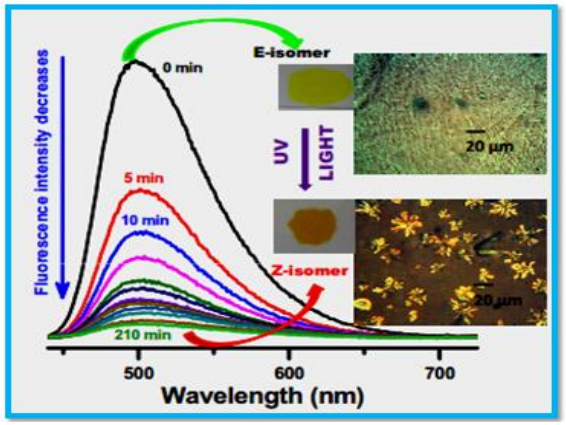
Mondal Sanjoy, Chakraborty Priyadarshi, and Nandi Arun K*

Polymer Science Unit, Indian Association for the Cultivation of Science,

Jadavpur, Kolkata-700 032, India

psuakn@iacs.res.in

The organogel of (E)-N′-(anthracene-10-ylmethylene)-3,4,5-tris- (dodecyloxy)benzohydrazide (**I**) in methyl cyclohexane having a fibrillar network structure exhibits excellent fluorescence, which decreases sharply with time upon photoirradiation at λ = 365 nm. It has been attributed to the transformation of the E isomer of **I** to the Z isomer, and the kinetics of E−Z isomerization are compared for the sol, gel, xerogel, and powder states. The rate constants at different temperatures are measured from Avrami plots and its increase with an increase in temperature, indicating temperature acts as a promoter for photoirradiated E−Z isomeization along the imine (C=N) bond. In the powder form, the rate constant values are the lowest compared to those of other states for all temperatures and the xerogels exhibit the highest rate of E−Z isomerization. The rate constants of sol and gel states mostly lie between the two. The wide-angle X-ray scattering pattern changes after ultraviolet (UV) irradiation with the generation of new sharp peaks whose intensities increase with an increase in irradiation time. A polarized optical microscopic study indicates formation of small crystalline dots on the fibers in the gels, dendritic morphology on the xerogel fibers, and large needlelike morphology at the surface boundary of the solid. The dried **I** gel exhibits a melting peak at 96.7 °C, but upon irradiation, two peaks are observed at 98.5 and 152.7 °C; the latter has been attributed to the melting of crystals of Z isomers. Similar higher melting peaks are observed both for the xerogel and for powders after UV irradiation; the powders exhibit the highest meting peak at 159.4 °C. Possible reasons for the variation of rate constant values in the four different states and the difference in morphology and melting points of crystals of Z isomers of **I** are discussed.



References

[1] Mondal, S; Chakraborty, P; Das, S; Bairi, P; Nandi, A. K; *Langmuir*, 32 (2016) 5373.
[2] Huang, X; Terech, P; Raghavan, S. R; Weiss, R. G; *J. Am. Chem. Soc.*, 127 (2005) 4336.

MACRO 171

Development of New Thermoplastic Elastomeric Polyamide Blends by Electron-Induced Reactive Processing

Shib Shankar Banerjee*, Uwe Gohs and Gert Heinrich

Leibniz-Institut für Polymerforschung Dresden e.V., D-01069 Dresden, Germany

**Corresponding author: E-mail: banerjee-shibshankar@ipfdd.de, shib.pst@gmail.com (Shib Shankar Banerjee).*

Electron-induced reactive processing (EIReP) is meanwhile a state-of-the-art technology to modify and develop several kinds of polymer materials during their melt mixing by high energy electrons [1]. EIReP uses the spatial and temporal tunable energy input by high energy electrons during melt mixing process in order to precisely control the desired chemical reactions and processability.

In the present report, thermoplastic elastomeric polyamide blends (polyamide/fluoroelastomer and polyamide/fluorosilicone rubber) with 50/50 blend ratio (w/w) have been developed by EIReP. Guided by

established relationships between raw materials characteristics, process parameters, morphology and final properties of ethylene propylene diene rubber /natural rubber based blends [1] we selected the material (viscosity) and EIReP process properties (non reactive mixing time, dose per revolution, electron energy) for our new systems. The polyamide/fluoroelastomer [2] and polyamide/fluorosilicone rubber blends are vulcanized by EIReP using a range of absorbed electron doses (100, 140, 200 kGy) while keeping constant values of electron energy (1.5 MeV), dose per revolution (90 kGy per revolution), temperature (230 °C) and rotor speed (60 rpm). In contrast to polypropylene, polyamide tends to crosslinking a 230 °C. The raw material-process-structure-property relationships of the prepared thermoplastic elastomeric blends are investigated using various methods such as mechanical, dynamic mechanical, rheological, morphological, thermal and swelling analysis. The results suggest that EIReP offers a novel route to prepare high-temperature and high-performance thermoplastic elastomeric compositions for various industrial applications without any classical curing agents and additives.

References:

[1] Naskar, K; Gohs, U; Heinrich, G. Polymer 91 (2016)203.

[2] Banerjee, S. S.; Bhowmick, A. K. Polymer 54 (2013), 6561.

MACRO 194

Nylon: Past, Present and Future Perspectives

Anuj Mittal and Suchetana K Shetty

Engineering Plastics Business, SRF Limited, Manali Industrial Area, Manali, Chennai 600076.

SRF Limited: Innovating tomorrow's solutions to fulfil the growing needs of our customers is the focus area that SRF serve at Engineering Plastics Business (EPB). Established in 1979, the EPB of SRF enjoys the status of being the first company in India to start polymer the polymer compounding. TUFNYL®, TUFBET®, TUFPC®, ENGOPET® are some of its engineered polymer brands that caters to automotive and electrical applications.

ABSTRACT

Polyamides (Nylon) comprise the largest family of engineering plastics (by volume) with a very wide range of applications. Nylon polymers have found significant applications in fibres (apparel, flooring and rubber reinforcement), in shapes (molded parts for cars, electrical equipment, etc.), and in films (mostly for food packaging). Production efficiency of nylon has drastically improved with advances in manufacturing technology (reactor design, utilities, RMs cost and availability) along with mordern analytical tools. Polyamide fibres ranks among the first type of synthetic fibers. The global demand of nylon resins and compounds was approximately US$20.5 billion in 2013. The market is expected to reach US$36 billion by 2020 by following an average annual growth of 5.5%. The fundamental research in the Nylons has become mature enough, except few academicians putting efforts in developing newer methods of nylon copolymer

synthesis, therefore compounding of Nylon with other additives is major focus of industrial players into automobile and electrical segments. Thus, the challenge lies in getting better margins meeting the customer demands. The article summarizes the past, present and future perspectives of Nylon. Focus on the recent research from academia and industry is also highlighted.

Keywords: Nylon, Polyamide, Markets, Production, Reactor, Adipic Acid, Caprolactam, Amine.

MACRO 209

Oriented Crystallization Templated in Aligned Multi-walled Carbon Nanotubes Arrays

Das, N. C[*a], Das, Poushali[b], Ganguly, Sayan[b], Banerjee S[c]

[a] *Rubber Technology Centre, Indian Institute of Technology, Kharagpur-721302, India*

[b] *School of Nanoscience and Technology, Indian Institute of Technology, Kharagpur-72130, India*

[c] *Materials Science Centre, Indian Institute of Technology, Kharagpur-721302, India*

** e-mail id: ncdas@rtc.iitkgp.ernet.in*

Abstract

The surface induced oriented crystallization of polyethylene (PE) on vertically aligned multiwalled carbon nanotube (MWCNT) arrays was investigated using small angle and wide angle (SAXs & WAXS) scattering techniques. Scanning electron microscopy (SEM) was also used to predict the growing of PE crystals on MWCNT surfaces. Polyethylene is infiltrated through melting into 6 mm long nanotube arrays under vacuum and then PE is allowed to crystallize under controlled conditions. Periodic PE lamellae crystals grow perpendicularly to the aligned nanotubes and completely fill the intertube spacing, forming oriented crystal structure.

Keywords: *Aligned carbon nanotubes; Polymer crystallization; small angle X-ray scattering*

Introduction

Considerable attention on intense research activities of carbon nanotubes based polymer nanocomposites has been generated because of their special feature like high aspect ratios, outstanding strength and stiffness, high thermal and air stability, and extraordinary electronic and thermal properties [1-8]. The aligned carbon nanotube arrays possess identical tube length, uniform orientation and extra high purity. Those characteristic features of carbon nanotube arrays were encountered into their outstanding electrical, thermal and mechanical properties and consequently, they become attractive to fabricate field emission devices, anistropic conductive materials, multi-functional membrances, photovoltaic devices, sensors and biocatalytic films [9,10]. Therefore, the quality of the CNT-polymer guided into the practical applications. Several theoretical simulation and experimental studies confirm the strong interfacial strength between CNTs and polymer. Those interfacial strength will be either chemical bonding or physical bonding between CNTs surface and polymers [11-13]. However, forming composites with polymer is one way to stabilize CNT arrays for applications. If the matrix is

a crystalline polymer, CNTs can affect polymer crystallization [14,15]. An ordered crystal layer of polymer form on the CNT surface through molecular chains orientation along the CNT axis and polymer confined on the CNT surfaces. CNTs-induced polymer crystallization has been studied in many polymeric systems such as polypropylene (PP), polyethylene (PE) and poly(vinyl alcohol) (PVA), etc.[14-22]. Epitaxial growth of PE on CNTs to form periodic crystal decoration has been observed in solutions [18].

Several researchers are tried to CNT synthesis to centimeter long aligned CNT arrays [23-26][23-26]. These ultra-long aligned CNT arrays are used to fabricate polymer nanocomposites with superior properties. Those continuous aligned nanotubes alos reinforced the polymers. Polymer/CNTs arrays composites can be prepared through in-situ polymerization. Alternatively, composites can also be prepared through infiltration of melt polymer or polymer solution, followed by solidification or solevent evaporation into long CNTs arras can be infiltrated into the CNTs array [27-29]. However, only few works has been reported on polymer crystallization in a confined system like aligned carbon nanotubes arrays through melting technique. Recently, the small angle X-ray scattering (SAXS) and neutron scattering (SANS) were successfully utilized to investigate alignment and order parameter of vertically aligned CNTs (VACNTs) arrays [30-32]. In this work, we report crystallization behavior of polyethylene in 6-mm long CNT-array with a CNT loading up to 75 wt.-% and illustrated template crystal growth among VACNT arrays in bulk, where crystals orientation varies with the height from the substrate, following the alignment order of VACNTs.

Experimental

VACNT arrays were grown on a Si (100) wafer by chemical vapor deposition. Two metal catalyst layers of 10 nm Al and 1 nm Fe were used. The acetylene and thermally evaporated ferrocene, $Fe(C_5H_5)_2$ were used as a feedstock for the MCNTs growth. Ferrocene enhanced the efficiency of the catalyst. These ferrocene also reduce the chance of the growth termination. Hence, CNTs were produced at higher growth rates and thicker CNT films [33]. An average diameter of 30nm and length of 6 mm of the CNTs was obtained in this method. Polyethylene (PE) with weight average molecular mass of 2100 g/mol and polydispersity ~1.15 was melted under vacuum at 140 ^oC on VACNT block for 20 min to allow infiltration of PE into the VACNT arrays and filling the voids. The obtained VACNT/PE composite was then quenched to 110^0C for PE to crystallize. After crystallization, the CNT arrays were rinsed with ethanol.

Scanning electron microscopy (SEM) images of net VACNT and PE-VACNT were obtained with a Zeiss 55 field-emission high resolution microscope operated at an accelerating voltage of 5 kV. Simultaneous SAXS/WAXS measurements were performed on the composite slab at the room temperature with a CuKα radiation (λ = 1.542 Å) from a 1.2 kW rotating anode x-ray generator of RUH3R (Rigaku Denki Co. Ltd, Japan X-ray system). The SAXS patterns were recorded with the sample-to-detector distance of 1571 mm to cover the scattering q range of 0.006 to 0.11 $Å^{-1}$ ($q = 4\pi/\lambda \sin(\theta/2)$, where λ is the x-ray wavelength and θ is the scattering angle) using a two-dimensional multi-wired detector. Silver Behanate with the first order scattering vector q = 0.1076 $Å^{-1}$ was used to calibrate the q values for the SAXS data. SAXS patterns were collected at different sample height positions from the substrate for both VACNTs and VACNT/PE composite.

Results and discussion

The two-dimensional (2D) SAXS patterns and SEM image of VACNTs at three different locations on the samples with the height, h =0.5, 2, 3.5, 5.0 and 6 mm from the substrate are shown in Figure 1(a)-(d), respectively. The SAXS patterns show anisotropic, distinct higher cloud along y direction indicates vertical alignment of CNTs. Apparent evolutions in morphology by 2D SAXS pattern are shown in Figures 1(a)-(d). The pattern anisotropy of the 2D spectra increment and intensifies along the y-axis indicates the alignment improvement with increasing height of the CNTs from the substrate. Scanning electron microscopy images illustrating the local

morphologies are shown in Figures 1(f)-(j). Aligned nanotubes arrays show the helical and zigzag morphology near the substrate as shown in Figure 1f with existence of few straight tubes at the same height. The coexisting the two morphologies of tubes, like straight as well as zigzag or helical path was observed (Figure 1g). The interplay of these two coexistence morphologies is reflected to the broadening of the scattering patterns shown in Figures 1(a)-1(d).

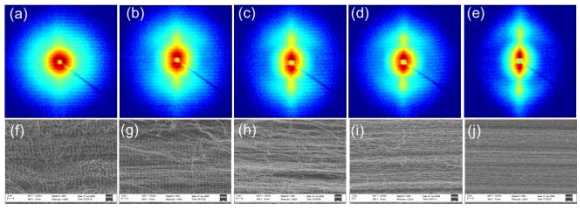


Fig. 1(a-e): 2D SAXS scattering spectra of the aligned CNTs at 0.5, 2.0, 3.5, 5.0 and 6.0 mm from the substrate, 1(f-j) SEM images of CNTs morphology at 0.5, 2.0, 3.5, 5.0 and 6.0 mm from the substrate.

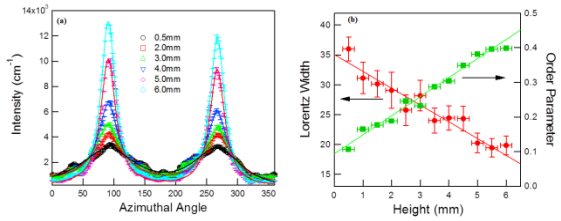


Fig. 2 (a) Azimuthal scans obtained from 2-D patterns at varying distances from the substrate at q =0.01 Å^{-1}. Sharp peaks at ø = 90^0 and 270^0 indicate preferential alignment of the nanotube bundles. (**b)** Hermans orientation parameter (green symbol) and Lorentz width (red symbol) as a function of distance from the substrate.

The azimuthal scan of 2-D SAXS patterns obtained from VACNT are shown in Figure 2a. The presence of peaks at ø = 90^0 and 270^0 corresponds to vertical alignment of the CNTs. The uneven change in intensity values between the regions near ø = 40^0, 170^0 and 330^0 close to the substrate may be due to the presence of the catalyst substrate, which is disappears with increasing *h*. Two superimposed peaks near the substrate, with a narrow peak corresponding to straight tubes and a broad peak remains corresponding to the helical tubes are observed. The peaks become narrower with increasing *h*, indicating enhancement of alignments of CNTs. The angular profiles are fitted with a two-peak model with a Lorentzian function for the narrow peak and a Gaussian for the broad peak. The solid lines through symbols are the best fit. The decrease in Lorentz with increase *h* indicates enhancement of alignment of the CNTs from the substrate in Figure 2b. The degree of alignment is quantitatively estimated by examining Hermans orientation parameter, which can be defined for axially oriented systems as [34-36].

$$f = \frac{1}{2}\left(3\left\langle \cos^2\phi \right\rangle - 1\right) \qquad (1)$$

The factor in broken brackets represents the mean-square consine of the azimuthal angle, calculated from the following equation:

$$\left\langle \cos^2\phi \right\rangle = \frac{\int_0^{2\pi} I(\phi)\cos^2\phi\, d\phi}{\int_0^{2\pi} I(\phi)\sin\phi\, d\phi} \qquad (2)$$

The limiting value for *f* =0, -1/2 and 1 correspond to perfect horizontal alignment, random orientation and perfect vertical alignment, respectively. Figure 2b shows that the order parameter (rectangular symbol) increases linearly with *h*. The increase in alignment from the substrate to the top is in good correspondence with the SEM micrograph of Figures. 1(e)-(h).

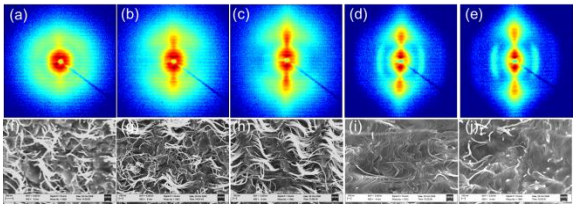


Fig. 3(a-e): 2D SAXS scattering patterns of the aligned CNTs/PE at 0.5, 2.0, 3.5, 5.0 and 6.0 mm from the substrate, **3(f-j)** SEM images of CNTs morphology at 0.5, 2.0, 3.5, 5.0 and 6.0 mm from the substrate.

The VACNT/PE composites at different locations on the sample with the height, h =0.5, 2.0, 3.5, 5.0 and 6.0 mm from the substrate are shown in Figure 3(a)-(e). The corresponding SEM micrographs of the VACNT/PE are shown in Figure 3(f)-(j). New feature appeared at h= 5.0 mm indicates oriented PE crystal (Figure 3d). The broader peaks in Azimuthal scan (Figure 4) for the VACNT/PE composite compared with that for VACNTs (Figure 3a) imply possibly both the effect of crystallization-induced distortion to the tube alignment and variation of

scattering contrast because of the heterogeneous nature of polymer crystals. The PE scattering peak on the meridian direction for the top location on VACNT/PE composite (Figure 5d) indicates that alignment of CNTs does affect PE crystallization orientation.

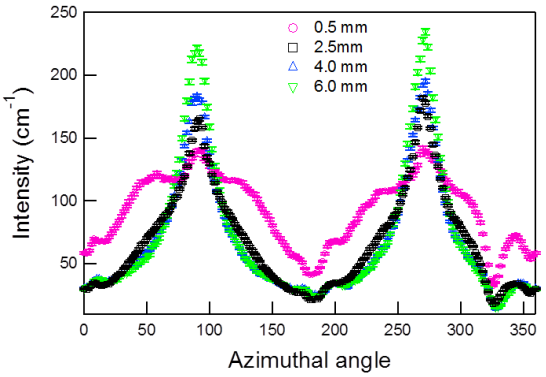


Fig. 4 Azimuthal scans obtained from 2-D patterns at varying distances from the substrate at q =0.01 Å^{-1} for PE/VACNT composites. Sharp peaks at ø = 90^0 and 270^0 indicate preferential alignment of the nanotube

Figures 5(a)-(b) show Azimuthally (circularly) integrated SAXS intensity as a function of scattering vector extracted for VANCT VACNT from the 2-D SAXS patterns over ± 5^0 conical slices around ø = 90^0 (a) and 180^0 (b) in the x-y plane of detector at different distance of CNTs from the substrate. The peak lies near q ≈ 0.04 (1/Å) indicates outer diameter of CNTs. The peak shifts to higher scattering angles with increase *h* implies that the object responsible for the scattering decrease in size with distance from the substrate. The difference in intensity between these two angles in Figures 5(a) and 5(b) further confirm preferential orientation of the CNTs. Furthermore, the shoulder become more resolved with increasing *h* further confirms preferential orientation of the CNTs from the substrate. Similarly, the circularly integrated SAXS intensity as a function of scattering extracted for VANCT VACNT/PE over ± 5^0 conical slices around ø = 90^0 (a) and 180^0 (b) in the x-y plane of detector at different distance of CNTs from the substrate are shown in Figure 5(c)-(d). New scattering peaks in Figure 5d VACNT/PE composite indicates that the oriented PE crystal. Well-aligned carbon nanotubes act as heterogeneous nucleating agents for PE crystallization. In these CNT arrays,the PE crystals are grow perpendicularly of the CNT axis. The well-aligned dense nuclei restrict crystal growth to normal to the CNT axis, resulting in oriented crystalline layers. CNTs are rather random near the substrate, which hinders the formation of anisotropic PE crystals.

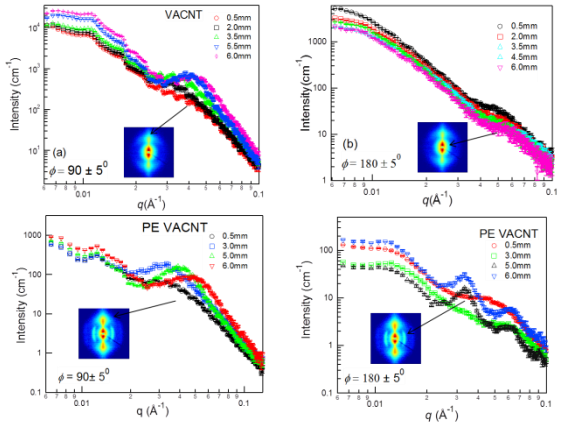


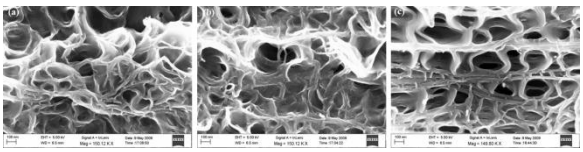
Fig. 5 Azimuthally (circularly) integrated SAXS intensity as a function of scattering vector extracted for VANCT VACNT from the 2-D SAXS patterns over ± 5^0 conical slices around ø = 90^0 (a) and 180^0 (b) in the x-y plane of detector at different distance of CNTs from the substrate.

The VACNT/PE composites at different locations on the sample with the height, h =0.5, 2.0, 3.5, 5.0 and 6.0 mm from the substrate are shown in Figure 3(a)-(e). The corresponding SEM micrographs of the VACNT/PE are shown in Figure 4(f)-(j). New feature appeared at h= 5.0 mm indicates oriented PE crystal (Figure 3d). The broader peaks in Azimuthal scan (Figure 4) for the VACNT/PE composite compared with that for VACNTs (Figure 3a) imply possibly both the effect of crystallization-induced distortion to the tube alignment and variation of scattering contrast because of the heterogeneous nature of polymer crystals. The PE scattering peak on the meridian direction for the top location on VACNT/PE composite (Figure 5d) indicates that alignment of CNTs does affect PE crystallization orientation.

Figures 5(a)-(b) show Azimuthally (circularly) integrated SAXS intensity as a function of scattering vector extracted for VANCT VACNT from the 2-D SAXS patterns over ± 5^0 conical slices around ø = 90^0 (a) and 180^0 (b) in the x-y plane of detector at different distance of CNTs from the substrate. The peak lies near q ≈ 0.04 (1/Å) indicates outer diameter of CNTs. The peak shifts to higher scattering angles with increase *h* implies that the object responsible for the scattering decrease in size with distance from the substrate. The difference in

intensity between these two angles in Figures 5(a) and 5(b) further confirm preferential orientation of the CNTs. Furthermore, the shoulder become more resolved with increasing *h* further confirms preferential orientation of the CNTs from the substrate. Similarly, the circularly integrated SAXS intensity as a function of scattering extracted for VANCT VACNT/PE over $\pm 5^0$ conical slices around $ø = 90^0$ (a) and 180^0 (b) in the x-y plane of detector at different distance of CNTs from the substrate are shown in Figure 5(c)-(d). New scattering peaks in Figure 5d VACNT/PE composite indicates that the oriented PE crystal. Well-aligned carbon nanotubes act as heterogeneous nucleating agents for PE crystallization. In these CNT arrays,the PE crystals are grow perpendicularly of the CNT axis. The well-aligned dense nuclei restrict crystal growth to normal to the CNT axis, resulting in oriented crystalline layers. CNTs are rather random near the substrate, which hinders the formation of anisotropic PE crystals. PE crystals in the CNTs physically lock the alignment of CNTs arrays. This interlocking phenomena enhance the load transferring efficiency from the PE crystals to the individual CNTs during stretching.

The skin of the composites was remove to ensure crystals growth and investigate the internal morphology of the PE crystals in the CNT arrays. Crystal morphology of the composites after peel off the skin are shown in Figure 6(a)-(c). PE crystal nanostructures were formed in the CNT array. Moreover, the crystals size are smaller inside the CNT arrays then on the surface of the CNT due to limited space under confined geometry. Therefore the degree of interlocking of the supramolecular structures are suppressed which affect the mechanical properties of the nanocomposites.



Figures 6(a)-(c) SEM images of PE/CNTs morphology at 0.5, 3.5 and 5.5 from the substrate.

Conclusions

Oriented polyethylene crystal was observed within 6 mm long carbon nanotubes under control crystallization conduction. We have successfully investigated the oriented polyethylene crystal in aligned carbon nanotubes arrays using small angle and wide angle X-ray scattering and SEM. Carbon nanotubes act as a nucleating agent for oriented polyethylene crystals formation in the carbon nanotubes arrays. Nucleation occurs at the surface of the aligned carbon nanotube, which provides template for aligned lamellar stacking normal to the tube axis.

Acknowledgements

Authors thank the Kalpana Chawla Space Technology Cell (IIT Kharagpur) (KCSTC-002/2015), ISRO, Thiruvananthapuram, Govt. of India for financial support.

References

1. Baughman, R.H., A.A. Zakhidov, and W.A. de Heer, Science, **297**(5582), 787, 2002.
2. Ajayan, P.M. and J.M. Tour, Nature, **447**(7148), 1066, 2007.
3. Coleman, J.N., U. Khan, and Y.K. Gun'ko, Advanced Materials, 2006. **18**(6), 689, 2006.
4. Liu, L., et al., Advanced Functional Materials, **15**(6), 975, 2005.
5. Schmidt, R.H., et al., Langmuir,. **23**(10), 5707, 2007.
6. Rahatekar, S., et al., Journal of Rheology (1978-present), **50**(5), 599, 2006.
7. Du, F., J.E. Fischer, and K.I. Winey, Physical Review B, **72**(12),121404, 2005.
8. Grossiord, N., et al., Advanced Functional Materials, **18**(20), 3226, 2008.
9. Kymakis, E. and G. Amaratunga, Applied Physics Letters, **80**(1), 112, 2002.
10. Rege, K., et al., Nano Letters, **3**(6), 829, 2003.
11. Liao, K. and S. Li, Applied Physics Letters, **79**(25), 4225, 2001.
12. Wagner, H.D., Chemical Physics Letters, **361**(1), 57, 2002.
13. Schadler, L., S. Giannaris, and P. Ajayan, Applied Physics Letters, **73**(26), p. 3842, 1998.
14. Quan, H., et al., Composites Science and Technology, **65**(7), 999, 2005.
15. Haggenmueller, R., J.E. Fischer, and K.I. Winey, Macromolecules, **39**(8), 2964, 2006.

16. Sandler, J., et al., Journal of Macromolecular Science, Part B, **42**(3-4), 479, 2003.
17. Bhattacharyya, A.R., et al., Polymer, **44**(8), 2373, 2003.
18. Li, L., C.Y. Li, and C. Ni, Journal of the American Chemical Society, **128**(5), 1692, 2006.
19. Zhang, S., et al., Polymer, **49**(5), 1356, 2008.
20. Minus, M.L., H.G. Chae, and S. Kumar, Polymer, **47**(11), 3705, 2006.
21. Li, C.Y., et al., Advanced Materials, **17**(9), 1198, 2005.
22. Zhang, S., et al., Macromolecular Chemistry and Physics, **211**(9), 1003, 2010.
23. Futaba, D.N., et al., Nature Materials, 2006. **5**(12), 987, 2006.
24. Yamada, T., et al., Nature Nanotechnology, 2006. **1**(2), 131, 2006.
25. Zhu, L., et al., Carbon, **45**(2), 344, 2007.
26. Zhang, S., et al., Journal of Materials Science, **43**(13), 4356, 2008.
27. Raravikar, N.R., et al., Chemistry of Materials, 2005. **17**(5), 974, 2005.
28. Zhang, M., K.R. Atkinson, and R.H. Baughman, Science, 2004. **306**(5700), 1358, 2004.
29. Lin, W., K.S. Moon, and C. Wong, Advanced Materials, **21**(23), 2421, 2009.
30. Mu, B., T. Wang, and P. Liu, Industrial & Engineering Chemistry Research, **46**(10), 3069, 2007.
31. Wang, H., Z. Xu, and G. Eres, Applied physics letters, **88**(21), 213111, 2006.
32. Ch Das, N., et al., Journal of Nanoscience and Nanotechnology, **11**(6), 4995, 2011.
33. Eres, G., et al., Applied Physics Letters, **84**(10), 1759, 2004.
34. Wang, B.N., et al., The Journal of Physical Chemistry C, 2007. **111**(16), 5859, 2007.
35. Alexander, L.E., *X-ray diffraction methods in polymer science*. 1969.
36. Hermans, J., et al., Recueil des Travaux Chimiques des Pays-Bas, **65**(6), 427, 1946.

MACRO 252

Reversible Shape Switching Phenomena In Linear Thermoplastic Polyurethane Through Molecular Flipping: Potential Application As Smart Gripper

Arpan Biswas and Pralay Maiti*

School of Materials Science and Technology, Indian Institute of Technology (Banaras Hindu University), Varanasi 221 005, India.

E-mail: pmaiti.mst@itbhu.ac.in.

Thermoplastic Polyurethanes have been synthesised by using aromatic and aliphatic diisocyanates and ester/ether diols to understand the structure property relation in a better way. Stepwise self assembly has been observed from nano to microstructure through WAXS, SANS, AFM and POM of aliphatic polyurethane in comparison to aromatic polyurethane. A reversible shape switching phenomena has been observed in aliphatic PU under heating-cooling cycle against no such type of phenomena in conventional aromatic PU. Temperature

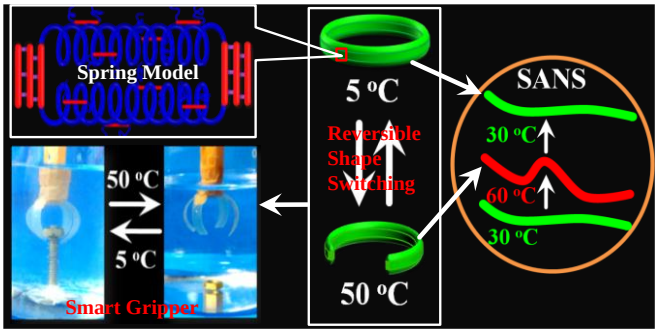


Figure1: Graphical representation of reversible shape switching phenomena, proposed spring model and its application in Smart Gripping .

dependence structure property relationship has been worked out using POM and DSC showing direct connectivity between the reversible shape switching and structural development in PU of varying constituents. The morphological study at different temperature with polarising optical microscope (POM) and differential scanning calorimetric (DSC) study reveal that the rate of crystallisation in aromatic polyurethane is much slower than aliphatic polyurethane. Temperature dependent SANS studies reveals that some consolidation of the hard segments takes place at temperature above the melting temperature (transition temperature) of the soft segments of aliphatic PU. A change in crystal structure from less stable triclinic to more stable pseudo hexagonal has been also observed at above the melting of the soft segment. Now, based on the above experimental results a "spring model" has been proposed to explain the reversible shape switching behaviour of novel polyurethanes. In spring model the soft segment (actuating domain) acts as a spring which is sandwich between chemically attached hard segments and some of the hard segment is also distributed in soft segments. Now, according to temperature dependent SANS and XRD studies we proposed a flipping mechanism of the hard segment. According to this mechanism on heating distributed hard segment switches into consolidated hard segment and again on cooling get distributed and induced the crystallization behaviour of the soft segments. Due to the presence of this reversible shape switching property under stress free condition, aliphatic PU has full potential to act like mini robot in smart gripping application. We demonstrate how the mini robot can grip some material at temperature below the transition temperature and can release it the above the transition temperature.

References

[1] Biswas, A., Aswal, V., Sastry P. U., Rana, D., and Maiti, P *Macromolecules,* DOI: 10.1021/acs.macromol.6b00536.

[2] Mishra, A.; Purkayastha, B.; Roy, J.; Aswal, V.; Maiti, P *Macromolecules,* 43 (2010), 9928−9936.

[3] Behl, M.; Kratz, K.; Zotzmann, J.; Nöchel, U.; Lendlein, A. *Adv. Mater*. 25 (2013), 4466−4469.

MACRO 254

Crystallization Kinetics, Fold Surface Free Energy in Immiscible Polymer Blend PVDF/ABS in Presence of Functionalized Multiwall Carbon Nanotubes

Goutam Prasanna Kar;* Suryasarathi Bose

[a]*Department of Materials Engineering, Indian Institute of Science,*

Bangalore 560012, India

** email i.d.: goutamchem06@gmail.com*

Abstract

Structure, evolution of morphology and crystallization kinetics of immiscible polymer blends (90/10 (wt/wt) PVDF/ABS with 5 wt% SAN) has been presented in the context of altered location of multiwalled carbon nanotubes (MWNTs). Matrix-droplet morphologies were obtained in the range of 90/10 composition. Homogeneity and stability of the morphologies were assessed by quiescent annealing at processing temperature of the blends. SAN, a miscible polymer with ABS were chemically grafted onto MWNTs to tune blend properties. Thermodynamically preferred location of MWNTs was altered with SAN-*g*-MWNTs. The immediate effect in crystallization kinetics was analyzed by isothermal crystallization method adopting Avrami model. The rate of nucleation and growth is largely modulated by location of MWNTs in PVDF phase, whereas SAN-*g*-MWNTs influences moderately. The fold surface free energy calculated to be less of the blend filled with SAN-*g*-MWNTs than with MWNTs. Our study reveals structures and steps of crystallization kinetics in semi-crystalline/amorphous blends with functionalized MWNTs.

Keywords: PVDF/ABS, MWNTs, SAN, ternary blends, fold surface free energy

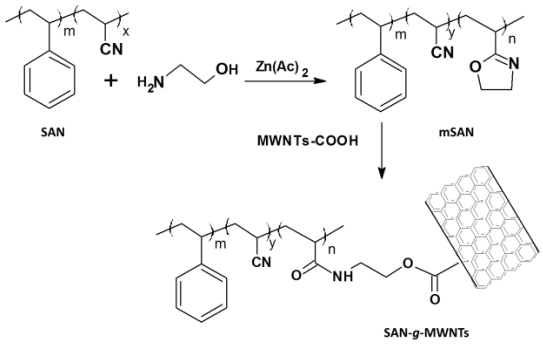
Introduction

Melt blending of immiscible polymers is an economical and efficient way to fabricate functional materials than synthesizing new polymers.[1] Morphology and structure determine the properties and performance of polymer blends.[2, 3] Depending upon the chemical properties of polymers, their interactions and processing condition diverse range of morphologies are yielded such as droplet, fiber, lamella and co-continuous.[4, 5] Droplet-matrix morphologies have attracted much attention recently because of its increasing use in membrane fabrication[6] and constructing tissue scaffold.[7] However, the structure of polymer blend is not in equilibrium, as little deviation during processing can alter the morphology.[8] Hence, stabilization of blend morphology is crucial for optimal performance.[9] Moreover, immiscible polymer blend consisting binary phase yield poor mechanical properties because of inefficient stress transfer across phase boundary.[10]

Clear understanding of energetics of crystallization process requires the knowledge of fold surface free energy (σ_e) and lateral free energy of surface (σ).[11] According to the secondary nucleation theory, proposed by Hoffman et al., σ_e and σ are the key parameters which control the whole process of nucleation and growth mechanism.[12]

Herein, we have investigated structure, morphology and mechanical properties of PVDF/ABS/SAN ternary blend to formulate a structure-property relationship in immiscible polymer blends. PVDF is an important engineering polymer with impressive ferroelectric properties and ABS is a high impact polymer with excellent chemical resistance. SAN is another thermoplastic with great thermal and chemical resistance, as well as miscible with the ABS phase. For tuning the localization, SAN were grafted onto MWNTs. Taking the advantage of high mechanical strength of MWNTs, tensile properties we improved for the ternary blends. Overall, a detailed structure, kinetics mechanism is revealed by studying morphology and isothermal crystallization kinetics.

Experimental section



Scheme 1: Steps of synthesis of SAN-*g*-MWNTs.

Results and discussion

Figure 1 shows the FT-IR spectra of functionalized polymers. SAN and modified SAN shows the characteristics C=C vibration at 1600 cm^{-1} attributed to the phenyl ring of styrene moieties. C≡N appears at 2237 cm^{-1}.[13] A new peak at 1664 cm^{-1} appears for mSAN which correspond to the vibration of oxazoline groups which confirms the reaction took place with SAN and AE. With the reaction of MWNTs-COOH this peaks disappears indicating the coupling between carboxylic functional groups and oxazoline after melt blending at high temperature.[13]

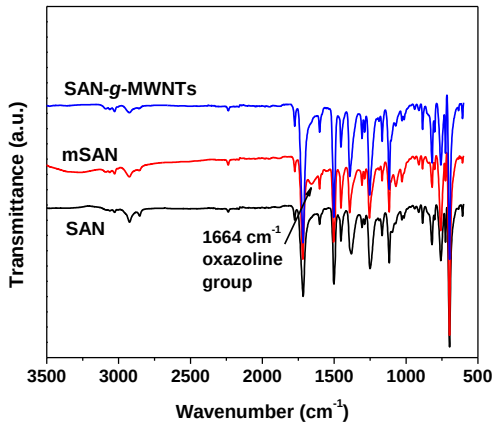


Figure 1: FT-IR spectrum of SAN, mSAN and SAN-*g*-MWNTs

Morphology

Figure 2 shows the SEM morphology of binary PVDF/ABS and ternary PVDF/ABS/SAN blends.

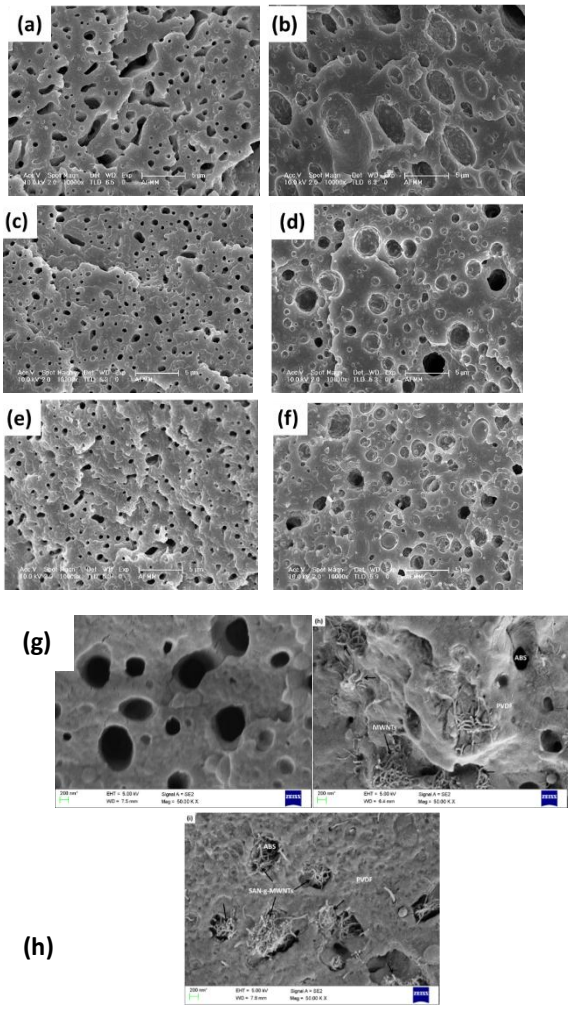


Figure 2: SEM morphology of (a) 90/10 PVDF/ABS, (b) 90/10 PVDF/ABS after annealing, (c) 90/10/5 PVDF/ABS/SAN, (d) 90/10/5 PVDF/ABS/SAN after annealing, (e) 90/10/5 PVDF/ABS/SAN-*g*-MWNTs and (f) 90/10/5 (i) [illegible]/ABS/SAN-*g*-MWNTs after annealing, (g) high resolution SEM image of 90/10 (h) high resolution SEM image of 90/10/5 PVDF/ABS/SAN with MWNTs showing localization of MWNTs in PVDF (i) high resolution SEM image of 90/10/5 PVDF/ABS/SAN-g-MWNTs showing localization of SAN-*g*-MWNTs in ABS phase which was partially etched by $CHCl_3$.

Spherulite growth and fold surface free energy

Turnbull-Fisher equation was adjusted by Lauritzen and Hoffman for homopolymer crystallization at large degree of supercooling. To keep the compatibility of Turnbull-Fisher equation with

homopolyer crystallization at large degree of supercooling, Lauritzen and Hoffman adjusted Lauritzen–Hoffman equation as,[14]

$$G = G_0 \exp\left[-\frac{U^*}{R(T_c - T_\infty)}\right] \exp\left[-\frac{K_g}{T_c \Delta T f}\right]$$

To gain more insight on the chain folding energy, q, can be calculated from σ_e, by using following equation,[14]

$$\sigma_e = \sigma_e^0 + \frac{q}{2a_0 b_0}$$

where, σ_e^0 is the value of σ_e if no work is required for chain folding and q signifies the amount of energy required for bending polymer chains. As, σ_e^0 is very small compared to $q/2a_0b_0$, can be ignored from the equation, and hence,

$$q = 2a_0 b_0 \sigma_e$$

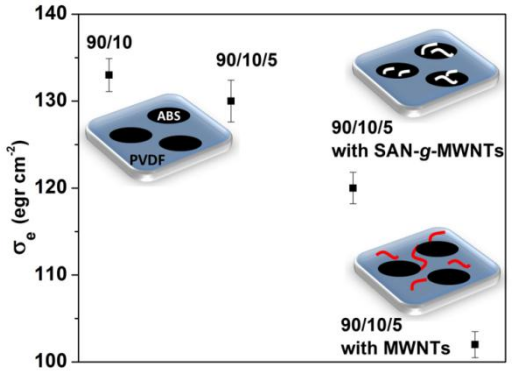


Figure 3: Interfacial energy of chain-folded surface (σ_e) for different blends.

Conclusions

Structure, mechanical properties and crystallization kinetics of ternary polymer blends wpere studied in details with unevenly localized MWNTs. Preferred location of MWNTs in 90/10 PVDF/ABS blends predicted by thermodynamic calculation can be altered by surface functionalization of MWNTs. With this aim, MWNTs were treated with concentrated acid to introduce carboxylic groups and SAN was modified with AE and $Zn(Ac)_2$ to impart oxazoline functional groups. With the conjugation of oxazoline functional groups and carboxylic groups SAN-*g*-MWNTs were made and thoroughly characterized by FT-IR. A peak at 1664 cm^{-1} which indicate the formation of oxazoline group disappears with the reaction of carboxylic groups of MWNTs. Moreover, the increase in diameter of MWNTs indicates the layer of SAN onto MWNTs. Morphology of 90/10 PVDF/ABS is more homogeneous with 5 wt% SAN and gain further stability in presence of SAN-*g*-MWNTs. However, the location of MWNTs is altered with SAN functionalization. As evident in high resolution SEM micrograph, MWNTs localizes in PVDF phase in 90/10/5 PVDF/ABS/SAN whereas SAN-*g*-MWNTs in SAN phase. This has a profound effect in growth kinetics of PVDF. Unlike SAN-*g*-MWNTs, MWNTs act as hetero-nucleating agent of PVDF crystallization and increase crystallization temperature to 140 °C, half-life is also decreased indicating the enhancement of crystallization growth. Fold surface free energy (σ_e) was calculated following Lauritzen–Hoffman theory. MWNTs greatly reduces σ_e, enhancing the ease of PVDF chain folding, whereas, SAN-g-MWNTs falls in the similar rages of neat blends. Hence, our study reveals an important relationship with structure, morphology and growth kinetics of ternary polymer blend with tailored MWNTs locations.

Acknowledgement

The authors would like to thanks DST and INSA for financial supports and AFMM, CeNSE in IISc for SEM facility.

References

1. P. Van Puyvelde, A. Vananroye, R. Cardinaels and P. Moldenaers, *Polymer*, 2008, 49, 5363-5372.
2. P. Van Puyvelde, S. Velankar and P. Moldenaers, *Current Opinion in Colloid & Interface Science*, 2001, 6, 457-463.
3. G. P. Kar, S. Biswas and S. Bose, *Phys. Chem. Chem. Phys.*, 2015, 17, 14856-14865.
4. L. Elias, F. Fenouillot, J. C. Majeste and P. Cassagnau, *Polymer*, 2007, 48, 6029-6040.
5. F. Fenouillot, P. Cassagnau and J. C. Majesté, *Polymer*, 2009, 50, 1333-1350.

6. D.-J. Lin, C.-L. Lin and S.-Y. Guo, *Macromolecules*, 2012, 45, 8824-8832.

7. F. Khan, M. Tanaka and S. R. Ahmad, *Journal of Materials Chemistry B*, 2015, 3, 8224-8249.

8. A. Pyun, J. R. Bell, K. H. Won, B. M. Weon, S. K. Seol, J. H. Je and C. W. Macosko, *Macromolecules*, 2007, 40, 2029-2035.

9. J. A. Galloway, H. K. Jeon, J. R. Bell and C. W. Macosko, *Polymer*, 2005, 46, 183-191.

10. G. P. Kar, S. Biswas and S. Bose, *Phys. Chem. Chem. Phys.*, 2015, 17, 1811-1821.

11. I. Stolte, R. Androsch and M. L. Di Lorenzo, *Colloid and Polymer Science*, 2014, 292, 1479-1485.

12. P.-D. Hong, W.-T. Chung and C.-F. Hsu, *Polymer*, 2002, 43, 3335-3343.

13. J.-H. Shi, B.-X. Yang and S. H. Goh, *European Polymer Journal*, 2009, 45, 1002-1008.

14. J. Song, C. Lu, D. Xu, Y. Ni, Y. Liu, Z. Xu and J. Liu, *Polymer International*, 2010, 59, 954-960.

MACRO 262

Electro-spinning of Non-ionic Cellulose Ethers and Characterization by Atomic Force Microscopy, Scanning Electron Microscopy and Contact Angle Measurements

A. C. Wali [a] Y. Zhang [b], Y. Higaki [b], A. Takahara [b], M. V. Badiger [a]*

[a]*Polymer Science and Engineering Division, CSIR-National Chemical Laboratory, Dr.Homi Bhabha Road, Pune 411008, India*

[b]*Institute of Material Chemistry and Engineering (IMCE), Kyushu University, 744 Motooka Nishi-ku, Fukuoka 819-0395, Japan*

**e-mail id: mv.badiger@ncl.res.in*

Abstract

The morphology of non-ionic cellulose ethers namely, ethyl hydroxyl ethyl cellulose (EHEC) and hydrophobically modified ethyl hydroxyl ethyl cellulose (HM-EHEC) and their blends with poly vinyl alcohol (PVA) was studied by spin coating and electro-spinning techniques. The surface thickness and roughness of spin coated EHEC were measured at different rpm (revolutions per minute). These polysaccharides upon blending with PVA exhibited smooth surface which was evidenced by Atomic Force Microscopy (AFM). The possibility of electro-spinning of these polysaccharides and heir blends with PVA was demonstrated. The addition of THF into the aqueous solution of EHEC/HM-EHEC improved the spinnability due to reduction in the surface tension. Comparison of the contact angles (CA) of spin coated and electro-spun fibers were made. The oriented fibers could be obtained using disc collector in electro-spinning process.

Keywords: *polysaccharides; AFM; SEM; contact angle; spin coating; electrospinning*

Introduction

Superfine nanofibers are produced by a simple and a novel technique known as Electro-spinning. Nanofibers exhibit special properties mainly due to extremely high surface to weight ratio compared to conventional fibers. These special properties make them suitable for a wide range of applications from medical to consumer products and industrial to high-

tech applications. Biopolymer-based fibers are advantageous due to their inherent nature of biodegradability and biocompatibility[1]. Due to their diversity and abundant availability, polysaccharides provide a range of possibilities for fiber production from cellulose, chitosan, hyaluronic acid, dextran, pullulan and starch. The biomedical application of nanofiber include tissue engineering, controlled drug release, dressings for wound healing, medical implants, nanocomposites for dental applications, molecular separation, biosensors and preservation of bioactive agents[2]. In the present work, we have performed the spin-coating of aqueous solutions of EHEC and HM-EHEC polymers at different speeds and also performed electro-spinning of these into nanofibers. The surface morphology of these spin coated and electro-spun fibers were characterized by Atomic Force Microscopy (AFM), Scanning Electron Microscopy (SEM) and Contact Angle (CA) measurements. There are no reports available on the electro-spinning of these polymers into nanofibers.

Experimental

EHEC and HM-EHEC polymers were obtained from Akzo-Nobel Functional Chemicals AB, Sweden with the trade names of Bermocoll E411 FQ and EHM-500 respectively. Their molecular weight (MW) was ~ 1200 Kg/mole with about 7000 anhydro glucose units (AGU). In the HM-EHEC, the hydrophobic modification (0.6 % of glucose units) was performed with nonyl phenol groups. Poly(vinyl alcohol) was obtained from Kurary Co., Ltd., Japan with the trade name of PVA-117. The MW and degree of saponification were 120 Kg/mole and 97-98% respectively.

Spin-coating

The spin-coating of aqueous solutions (1.0 wt-%) of EHEC, HM-EHEC and blends of EHEC/HM EHEC-PVA (50:50 wt-%) was performed on Silicon wafer of 1cm x 1cm square. 80 µL solution was used and spin-coating was carried out for 90 seconds at a spinning speed of 4500 rpm. The coated wafers were dried at 45 ^{o}C under vacuum for 1 day before taking them for CA and AFM measurements.

Electro-spinning

Electro-spinning of solutions of EHEC, HM- EHEC and their blends with PVA in water and tetrahydrofuran mixture (1:2 by v/v) at the polymer concentration of 1.0-1.5 wt-% was carried using a NANON-01A (MECC Co., Ltd., Japan) electro-spinning device. Both plate collector (static) and disc collector (rotating at 1000 rpm) were used to collect the fibers. The polymer solution was loaded into a syringe and discharged from the spinneret (0.5mm dia) at a flow rate of 0.2 ml/hr. The applied voltage was 27 kV and the distance between the spinneret and the plate collector was 150 mm. All the electro-spinning experiments were performed at ambient temperature.

Contact Angle measurements (CA)

The static contact angles with water droplet of 1.0 µL on the coated silicon wafers were measured using KSV Instrument, CAM-200.

Atomic Force Microscopy (AFM)

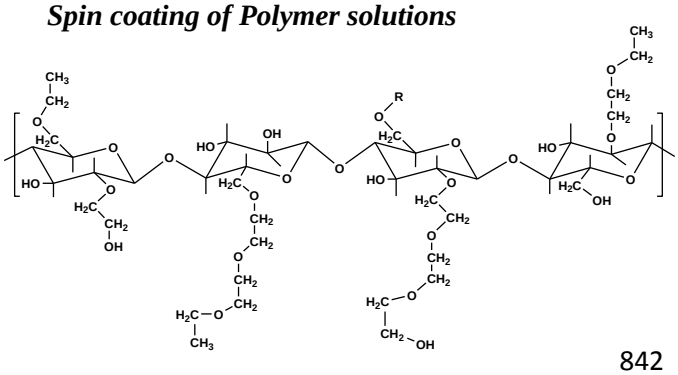
AFM images were obtained in the intermittent tapping mode. A silicon tip of f_o = 100-350 kHz was used. The scanning rate of 1.0 Hz with the scan range of 20 µm x 20 µm was used to obtain the images.

Scanning Electron Microscopy (SEM)

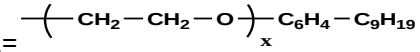
The SEM images of the electro-spun fibers were obtained using a Real surface View VE 7800 (Keyence Co., Ltd., Osaka, Japan) with an applied voltage of 5 kV. A small piece of aluminium foil on which the electro-spun fibers were collected was cut and mounted on a SEM sample holder. It was then coated with a thin osmium layer using HPC-1SW Hollow cathode Plasma CVD (Shinkun Device Co., Ltd., Mito, Japan) to prevent sample from charging.

Results and Discussion

Spin coating of Polymer solutions



EHEC : R=H

HM EHEC : R= 

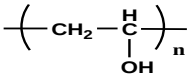
Polyvinyl alcohol 

Figure 1. Chemical structures of EHEC, HM-EHEC and PVA

The spin-coating of EHEC, HM-EHEC and EHEC/HM-EHEC-PVA solutions (1.0–1.5 wt-%) in THF:water mixture (2:1v/v) was done on silicon wafers at 3-different speeds. The surface thickness (nm) and surface roughness (nm) were measured as a function of spinning speeds (at 1500, 3000 and 4500 rpm) using AFM. The results are shown in **Table 1**. It can be seen from the results that although there is not much change in the surface thickness with different speeds, the surface roughness decreased with the increasing speed of the spinning. The smooth surface was obtained at 4500 rpm speed.

Table 1. Surface thickness and surface roughness of EHEC spin-coated sample

Parameters	EHEC in water (1.0 wt%)		
	Spinning speed (rpm)		
	1500	**3000**	**4500**
Surface thickness (nm)	83	103	75
Surface roughness (nm)	3.6	2.8	1.7

The AFM height and phase images are shown below. The ratio of EHEC/HM- EHEC: PVA in the blends is 50:50 wt-%.

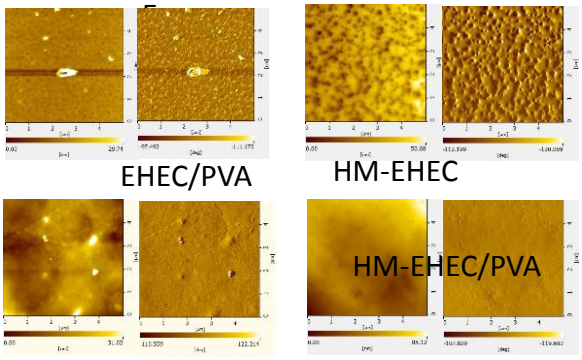


Figure 2. AFM images of Spin-coated EHEC, HMEHEC, EHEC-PVA and HM- EHEC-PVA

It is observed that the surface morphology of EHEC and HM-EHEC are slightly different. It could be attributed to the fact that the small hydrophobic modification of EHEC has resulted into a more hydrophobic nature of the polymer and gives rise to higher viscous solutions at the same polymer concentrations. Further, the presence of nonyl phenol hydrophobic groups in HM-EHEC can self-associate and give different microstructure to the polymer which can influence the surface morphology of the polymer. It can be readily seen from the figure that, the surface roughness of HM- EHEC is higher than that of EHEC. However, upon blending with PVA the surface has become smoother in both the cases.

Contact Angle (CA)

The wettability of spin-coated EHEC, HM- EHEC, EHEC-PVA and HM-EHEC-PVA samples were examined by static water droplet contact angle angle measurements. In **Figure 3**, side view of water droplets on spin-coated silicon wafers is shown.

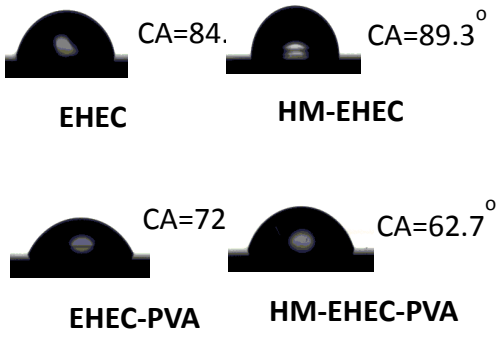


Figure 3. Contact angles of spin-coated EHEC, HM EHEC, EHEC-PVA and HM-EHEC-PVA

It is observed that the CA of HM-EHEC is slightly higher than the EHEC. This is expected due to the more hydrophobic nature of HM EHEC as a result of the nonyl phenol groups. However, upon blending with PVA, the hydrophilicity of the films increased significantly which was manifested in the decrease of CAs. It is known that surface roughness plays a very important role in wettability[3]. The relationship between surface roughness and contact angle for slightly hydrophobic material and hydrophilic material are described by Wenzel equation. $\cos\theta_r = r\cos\theta$. Where, r is the roughness factor. This equation indicates that when θ is smaller than 90°, θ_r decreases with increase in the surface roughness. If θ is higher than 90°, θ_r will increase with the increase in roughness. That is, a rough surface made by material with intrinsic water CA higher than 90° should be more hydrophobic or super-hydrophobic, whereas, a rough surface made by material with water CA lower than 90° should be more hydrophilic or super-hydrophilic[3]. Therefore, it is interesting to note that, the CA of HM-EHEC-PVA is lower as compared to EHEC-PVA indicating more hydrophilic character of HM EHEC-PVA film.

Electro-spinning

It is known that electro-spinning of polymer solutions strongly depends on the concentration, viscosity, conductivity and the surface tension of the polymer solution. Further, the operational conditions such as, electric field strength, flow rate and the distance between the tip and the collector have to be carefully adjusted to get good spinning. For our polymer solutions, we used the mixture of THF: water (ratio 2:1 v/v) to reduce the surface tension of the polymer solution and from several trial runs, suitable operating conditions were obtained.

In **Figure 4**, it can be realized that all the polymers showed the spinnability into fibers.

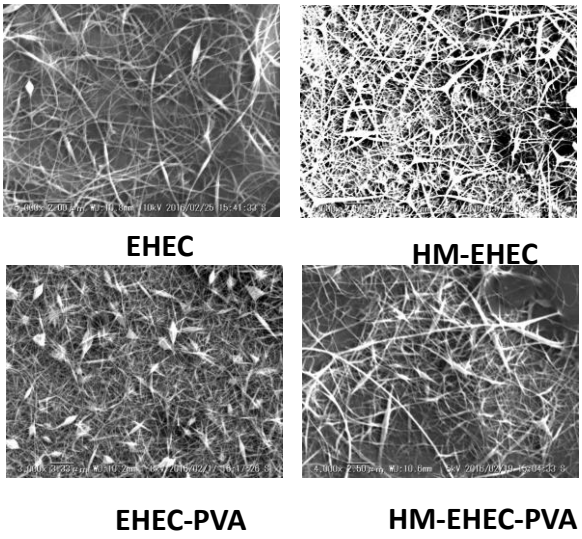


Figure 4. Electro-spun fibers of EHEC, HM-EHEC, EHEC-PVA and HM EHEC-PVA

EHEC showed long, uniform fibers with a thickness in the range of 0.5-1.0 µm. Whereas HM-EHEC gave short, interconnected fibers with a small amount of beads in the fibers. HM-EHEC polymer solution also required a slightly higher voltage and lower feed rate in the electr-spinning process. Upon blending EHEC/HM-EHEC with PVA the spinnability improved with a more dense fiber network. However, more bead formation was observed in the case of EHEC-PVA fibers. The fibers obtained from all the polymers were further examined by AFM. In **Figure 5**, the AFM height and phase images of various fibers obtained from the electro-spinning process are shown.

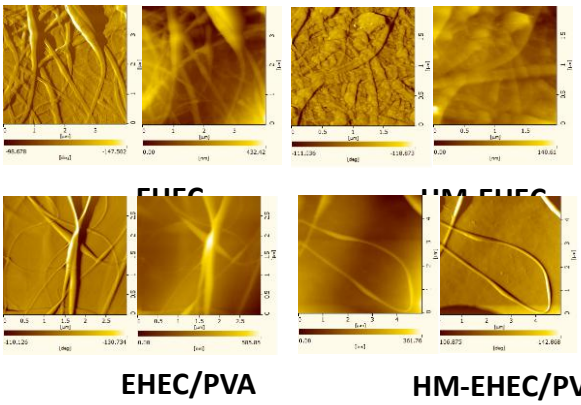


Figure 5. AFM images of EHEC, HM EHEC, EHEC-PVA and HM EHEC-PVA fibers

All the AFM images showed the formation of the fibers from the electro-spinning process. Compared

to the spin-coated samples, the surface microstructures of the electro-spun fibers showed significant difference. The EHEC gives smooth fibers, which is also evidenced by the SEM. The HM-EHEC exhibited a wrinkled surface on the fibers with an uneven texture. However, upon blending EHEC/HM-EHEC with PVA the spinnability improved. This could be due to the fact that PVA has better spinning ability and blending could improve the spinnability of non-ionic cellulose ethers.

Comparison of CAs of spin-coated and electro-spun samples

In **Figure 6**, water droplets on spin-coated and elctro-spun fibers are shown. It can be seen from the figure that the CAs of spin-coated EHEC and HM-EHEC samples are slightly higher than the respective electro-spun fiber samples indicating slightly more hydrophobic character of the spin coated samples.

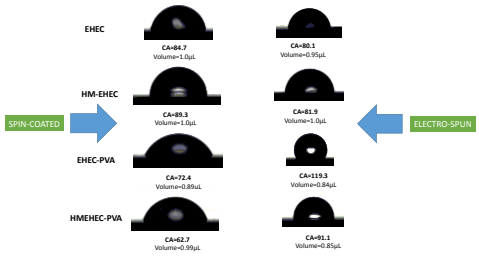


Figure 6. Contact Angles (CAs) of spin-coated and electro-spun samples of EHEC,HM -EHEC, EHEC-PVA and HM EHEC-PVA

Electro-spinning of EHEC solution (1.0 wt-%) in THF:water mixture (2:1 v/v) using rotating disc was performed . In **Figure 7**, the SEM images of electro-spun fibers obtained using static plate collector and rotating disc collector are shown. The oriented fibers could be obtained using disc collector.

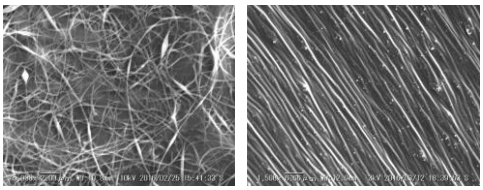


Figure 7. Oriented fibers of EHEC

Conclusions

The surface morphology of EHEC and HM-EHEC polymers and their blends with PVA was studied by Atomic Force Microscopy (AFM), Scanning Electron Microscopy (SEM) and Contact Angle (CA) measurements. The spin coating at 4500 rpm gave minimum surface roughness and moderate thickness. Also from the AFM images it was observed that the surface roughness of HM-EHEC is higher than the EHEC, and upon blending PVA with both EHEC and HM-EHEC, the surface became much smoother and finer. The contact angles for the spin coated EHEC and HM-EHEC samples were higher than electro-spun fibers. Upon blending of these polymers by PVA the electro-spun fibers showed significantly higher contact angles compared to spin coated samples. Electro-spinning of EHEC solution of 1 % (wt) in THF:water (2:1v/v) gave fine oriented fibers by using the disc collector. All the above studies reveal that these polymers could be electro-spun into nanofibers and can have a potential use in drug delivery and tissue engineering applications.

References

1. R. Rathinamoorthy; *Pakistan textile Journal. 2012.*

2. Tabata, Y; Ikada ,Y. *Advanced Drug Delivery Reviews*, 31, 287.*1998.*

3. M. Ying; C. Xinyu; F. Xinjian; M. Yongmei; Z. Hong; *Polymer*. 48, 7455, 2007

MACRO 263

Effect of Sepiolite on Non-isothermal Crystallization Kinetics of Polypropylene

Bindu Manchanda[1], K.K. Vimal [2], G. S. Kapur[2], Shashikant[2], Veena Choudhary[1,*]

[1]Centre for Polymer Science and Engineering, Indian Institute of Technology, Hauz Khas, New Delhi 110016

[2]Indian Oil Corporation Ltd., Research & Development Centre, Sector 13, Faridabad, Haryana, 121007

ABSTRACT:

The purpose of this paper is to study the non-isothermal crystallization kinetics of polypropylene (PP)/Sepiolite nanocomposites in the absence/presence of compatibilizer [maleic anhydride grafted-polypropylene (PP-g-MA)] using differential scanning calorimetry. Crystallization exotherms were recorded at four different cooling rates i.e. 5, 10, 15 and 20°C/min. Crystallization parameters were analyzed by Ozawa, Avrami, Jeziorny and Liu's models. Nucleation ability of Sepiolite was evaluated by employing Dobreva and Gutzowa models. The activation energy of non-isothermal crystallization kinetics process was estimated by using three isokinetic models (Augis–Bennet, Kissinger and Takhore). DSC exotherms scans of PP and PP/Sepiolite nanocomposites show that in the presence of Sepiolite, the crystallization onset, T_0 and peak temperatures, T_p increased. However, T_p decreased with increasing amount of PP-g-MA in PP/Sepiolite nanocomposites. The values of F (T), K_A and half time showed the rate of crystallization of PP was faster in presence of Sepiolite at a given cooling rate The $t_{1/2}$ values also decreased slightly for compatibilized PP/Sepiolite nanocomposites. The values of exponent 'n' determined using Avrami analysis indicated that nonisothermal kinetic crystallization

corresponded to three dimensional growths with heterogeneous nucleation in all samples. Sepiolite shows its better nucleating effect in the presence of PP-g-MA as investigated by Dobreva and Gutzowa method. Activation energy of crystallization was proportional to Sepiolite concentration but decreased on adding compatibilizer. Incorporation of Sepiolite in presence of compatibilizer, PP-g-MA in optimized ratio results in accelerating the overall non-isothermal crystallization process of PP/Sepiolite nanocomposites.

Keywords: PP, Sepiolite, PP-g-MA, crystallization, nucleation activity.

MACRO 269

Novel Super TPV: A New Generation Thermoplastic Elastomer

Kinsuk Naskar

Rubber Technology Centre, IIT Kharagpur, Pin- 721302, West Bengal, India

Thermoplastic vulcanisates (TPVs) are a special class of thermoplastic elastomers, produced by simultaneously mixing and cross-linking a rubber with a thermoplastic at elevated temperature. As a result a typical morphology is formed, where the cross-linked rubber particles are generally finely dispersed in a continuous matrix of thermoplastic. High performance TPVs or super TPVs are a new class of TPVs which exhibit high heat resistance as well as excellent oil resistance properties suitable for automotive under-the-hood applications. In the present work, a new super TPV based on carboxylated acrylonitrile butadiene rubber (XNBR) and polyamide (PA12) has been developed. TPVs of three different blend ratios (50:50, 60:40, 70:30) of (XNBR:PA12) have been prepared at an elevated temperature in an internal mixer by using a fixed concentration of Trigonox 311, which is a novel cyclic mono-functional cross-linking peroxide. The final morphology of the TPVs varies from a co-continuous to a dispersed one depending on the blend ratio. TPV of 50:50 XNBR-PA12 shows the best mechanical properties and the superior thermal stability amongst all TPVs. Detailed thermal characterisation through DSC and DMA and rheological characterisation have been performed. The lowest tanδ of the TPV with a 50:50 blend ratio of XNBR-PA12 indicates the highest degree of crosslinking and this is also well supported by the overall crosslink density

value of that TPV. Heat ageing and oil resistance studies have also been carried out to demonstrate the performance of these TPVs.

Keywords: **TPV, XNBR rubber, Polyamide 12, dynamic cross-linking, peroxide, morphology**

* Corresponding author and speaker: tel: 0091 3222 281748; fax: 0091 3222 282292; email: knaskar@rtc.iitkgp.ernet.in

MACRO 280

Mechanical & Electrical Properties of sPS/P3HT Composites

Samanta, Ketaki; Malik, Sudip*

Polymer Science Unit, Indian Association for the Cultivation of Science, Jadavpur, Kolkata-700032, India

** Corresponding author's email i.d: psusm2@iacs.res.in*

Syndiotactic polystyrene (sPS) is familiar to form co-crystal/ clathrate/ intercalate with series of solvents ranging from liquid to solid and there is also formation of δ-form of sPS in matrix.[1-2] During the formation of δ-form, there is formation of nano cavities in which solvent molecules reside as guest. Herein we want to grow nanocrystal of poly (3-hexyl thiophene) which is one of the most studying conducting polymers within the nano cavities of sPS. The formation of nano-crystal inside the sPS cavity have been investigated by UV spectroscopy, X-ray diffraction, Differential scanning calorimetry (DSC) and Thermogravimetric analysis (TGA), SEM and TEM. After the formation of P3HT nano-crystal there is an increase in average diameter of sPS fiber compared to pure sPS fiber as the P3HT fiber is encapsulated by sPS. P3HT induces an improvement of mechanical properties: increase of storage modulus and % strain in the composite gel compared to pure sPS gel. The presence of P3HT nano crystals have significantly improved the electrical conductivity.

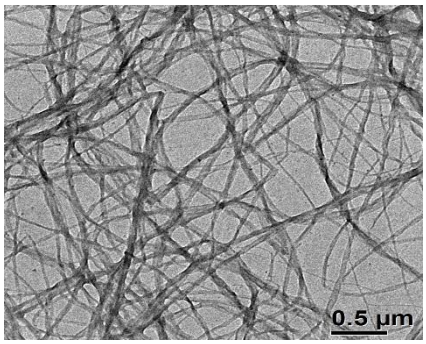


Figure: HRTEM image of sPS / P3HT composite prepared from p-xylene solution.

References:
[5] Malik, Sudip; Rochas, Cyrille; Schmutz, Marc; and Guenet, Jean Michel; *Macromolecules,* 38 (2005) 6024.
[6] Daniel, Christophe; Giudice, Simona; and Guerra, Gaetano; *Chem. Mater.*, 21 (2009) 1028.

MACRO 297

Biomimetic crystallization of polylactide and the development of polymeric brick-and-mortar semi-crystalline microstructure

S. Sabapathy, [a] C.B Park [b], A.K Ghosh [a]*

[a] [1]*Centre for Polymer Science and Engineering, Indian Institute of Technology Delhi, New Delhi, India.*

[b] [2]*Department of Mechanical and Industrial Engineering, University of Toronto, Toronto, Canada.*

** Corresponding e-mail id: anupkghosh@gmail.com*

Abstract

Can we learn from biomineralization process of natural materials to fabricate a three-dimensional (3-D) thick laminate microstructure by stacking of two-dimensional (2-D) crystalline structure? We find that instead of building a multi-layered morphology layer-by-layer, the lamellar microstructures can be built in one step by using self-organization principle of CO_2 induced 2-D crystallization (figure 1). The biopolymer PLA is compression molded and the molded samples are crystallized by using supercritical CO_2 (sc-CO_2) in a high pressure vessel. The CO_2-induced crystallization has a unique diffusion-controlled crystallization mechanism, which tends to produce a disc-shape spherultic structure. From microscopy analysis, we observe that these 2-D spherulites are self-organizing in nature and form 3-D thick laminate. This is the first time that a biopolymer has been crystallized two dimensionally in a way similar to the biomineralization process which produces a hierarchical crystalline microstructure morphologically similar to nacre biomaterials.

Keywords: *PLA, Self-templating; Nacreous microstructure.*

Introduction

Bio-mineralization is the crystallization and self-organization processes used by the living organisms to build a number of bio-structures with different hierarchical architectures in bone, teeth and nacre etc.[1] Nature develops such hierarchically organized crystalline structure by, exploiting the surface of 2D crystalline structures as a template and it is termed as self-templating assembly process. Imbuing this self-organizing principle in polymers, to give rise to stacks of two-dimensional crystallites, is the scope of this paper.

CO_2-induced crystallization process

CO_2-induced crystallization is an innovative approach that is used in polymer crystallization. It is faster than any other technique. And its accelerating crystallization kinetics and complex crystallization mechanism are widely known. The polymers' crystal growth mechanism in the

presence of CO_2 is quite different from the classical crystallization mechanism.[2] This is mainly due to the instantaneous exclusion of the CO_2 during the crystallization process. Park et al. studied the effects of dissolved CO_2 on the isothermal and non-isothermal crystallization behaviors of PLA melts at different CO_2 pressures and cooling rates by using high-pressure differential scanning calorimetry (HP-DSC).[3,4] It was found that the Avrami exponent's (n) value decreased with increased gas pressure (that is, up to 45 bar). This indicated that the crystallization growth mechanism had changed from a 3-D to a 2-D growth mechanism.

The present work focuses on a novel method of developing 2-D spherulites of poly-D-lactide (PDLA) by using CO_2. Compression molded PLA samples are gas saturated by using CO_2 which are thereafter allowed to crystallize two-dimensionally with the gas exclusion process to subsequently produce the disc-shape spherulitic structures. In addition, self-organization of 2-D spherulitic structures into a discontinuous laminate microstructure has been systematically investigated in molded PLA sample. The staggered arrangement of 2-D semi-crystalline microstructure with the interpenetrating amorphous phase is compared with "stack of coins" micro-structure and thus the biomimetic principle of self-organization is reported (figure 1).

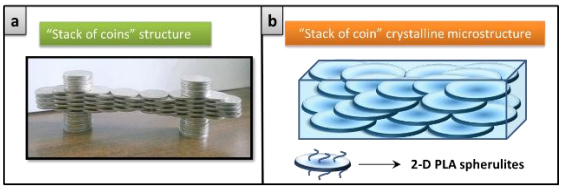


Figure 1: Bottom-up approach versus biomimetic crystallization approach: a) "Stack of coins" structure, b) "Stack of coins" crystalline microstructure made of 2-D spherulites.[5]

Material

PLA (PDLLA 8032D) was procured from Nature Works LLC, USA with the D-lactide molar contents (4.5 - 4.6 mol %). It was a foaming grade semi-crystalline PLA with a T_g of 60 ◦C, T_c of 120 ^oC and T_m of 155 ^oC.

Experimental

The CO_2-induced crystallization of compression molded samples is a two-step process, which uses CO_2 to saturate and crystallize PLA samples as shown in figure 2. The samples were saturated with CO_2 at a sub-crystallization temperature. Afterwards, they were preferentially crystallized with CO_2 under non-isothermal and isothermal conditions to yield PLA-CC1 and PLA-CC2 samples respectively. The PLA-CC1 and PLA-CC2 samples were investigated for the crystalline morphologies and their morphological results were correlated with toughening mechanisms.

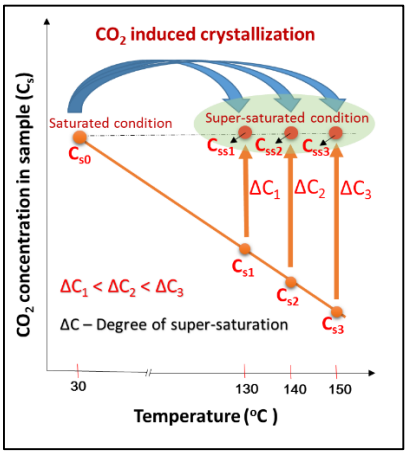


Figure 2: CO_2 induced crystallization of PLA samples.

Results and discussion

Crystalline morphology analysis

Our morphological investigations through various microscopic techniques showed that the 2D spherulitic structures of PLA were well integrated to each other to develop "stack of coins" crystalline microstructures (figure 3).

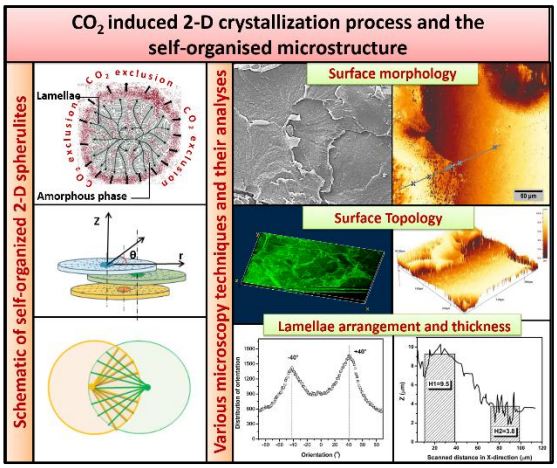


Figure 3: The various morphological investigations of 2-D spherulites morphology.

Impact strength of PLA-CCs

Notched impact test samples (63.5×12.7×3.2 mm) were saturated with CO_2 and were 2D crystallized at non-isothermal (PLA-CC1) and isothermal conditions (PLA-CC2) to yield stack of 2D spherulitic structures with two distinct inter-spherulitic amorphous regions. The lateral plane of CO_2 induced crystallized impact test samples with 2D spherulitic structures were characterized by SEM and the distinct difference in the cryo-fractured surface morphology of 2D spherulites were presented in figure 4.

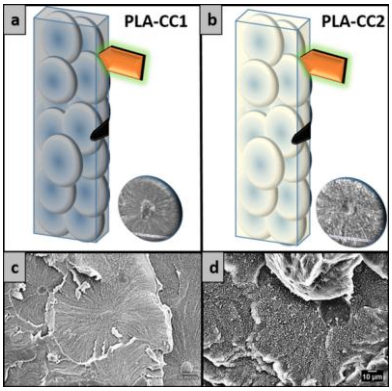


Figure 4: CO2 induced crystallized impact test samples and their spherulites morphologies: a) CO2 induced 2D crystallized impact test samples of PLA at non-isothermal crystallization process (PLA-CC1), b) CO_2 induced 2D crystallized impact test samples of PLA.

CO_2 induced crystallized impact test samples made up of stack of 2D spherulites encapsulated with unfoamed amorphous region (PLA-CC1) and nanoporous amorphous region (PLA-CC2) were tested for notched impact strength as per ASTM D-256 test method and the impact strength value of corresponding test samples is presented in the figure 5.

It is shown that 2D spherulites with unfoamed inter-spherulitc amorphous phase exhibits very low impact strength and this is due to the weak amorphous interface which fails before transferring the load to the stacked 2D spherulites as evident from the figure 5b. Whereas, the self-stacked 2D spherulites with nanoporous amorphous phase (PLA-CC2) exhibits impact strength of 60 J/m which is 3 time higher than PLA-CC1. The impact fracture of PLA-CC2 with tightly ingenerated layered crystalline structure confirms the prominence of strong nanoporous amorphous phase over weak amorphous phase in transferring the load to the stacked 2D spherulites (figure 5c).

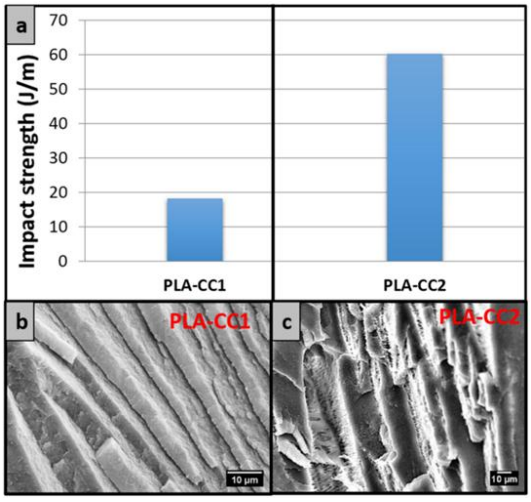


Figure 5: Impact strength of CO2 induced 2D crystallized PLA samples: a) Impact strength of CO2 induced crystallized PLA samples, b) Impact fracture surface of PLA-CC1, c) Impact fracture surface of PLA-CC2.

Conclusions

By using the CO_2-induced crystallization process, we demonstrated that it is possible to develop 2-D PLA spherulites without using 2-D templates. We successfully established the self-organizing principle of 2-D crystallization by developing the highly layered crystalline microstructure in bulk PLA samples.

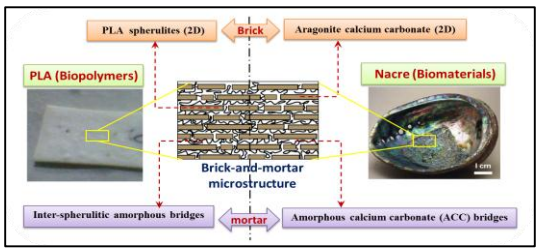


Figure 6: Biomimetic crystallization of PLA and the development of a polymeric nacreous crystalline microstructure.

It was shown that the self-organizing tendency of the 2-D PLA spherulites most likely resembles the biomineralization process of the nature biomaterials that produces a polymeric nacreous microstructure (figure 6).

References

1 J. Aizenberg, *Adv. Mater.*, 2004, **16**, 1295–1302.

2 M. Takada, S. Hasegawa and M. Ohshima, *Polym. Eng. Sci.*, 2004, **44**, 186–196.

3 M. Nofar, A. Tabatabaei, A. Ameli and C. B. Park, *Polymer.*, 2013, **54**, 6471–6478.

4 M. Nofar, A. Tabatabaei and C. Park, *Polymer.*, 2013, **54**, 2382–2391.

5 S. Sankarpandi, C. B. Park and A. K. Ghosh, *Polym. Eng. Sci.*, 2016.

MACRO 298

Effect of Chain Length on Properties Predicted by Molecular Dynamics Simulations

Nityanshu Kumar[a], Sushanta Kumar Sethi[a], Gaurav Manik [a,*]

[a] *Department of Polymer and Process Engineering, Indian Institute of TechnologyRoorkee, Saharanpur Campus, Saharanpur, India-247001*

First author e-mail id: kumar.nityanshu@gmail.com

Corresponding author e-mail id: manikfpt@iitr.ac.in, gauravmanik3m@gmail.com

Abstract

This work attempts to use molecular simulations to create equilibrated structures of a range of different polymers. Generated equilibrated structures for polyvinyl acetate (isotactic), polyvinyl alcohol (atactic), polystyrene, polytetrafluoroethylene,

polyproypelene and polycarbonate (bisphenol-A) are employed to estimate the correct chain length that will correctly predict the chain parameters and properties. Further, the library so built would reveal the underlying correlations between the molecular structure and the properties.

The simulated densities for polyvinyl acetate, polyvinyl alcohol, polystyrene, polypropylene and polycarbonate are 1.15 g/cm^3, 1.125 g/cm^3, 1.02 g/cm^3, 0.84 g/cm^3 and 1.223 g/cm^3 respectively are found to be in good agreement with the available literature estimates. Also, the critical repeating units or the degree of polymerisation after which the solubility shows saturation are 15, 20, 25, 10 and 20 respectively. These results help us to screen and propose a useful library which may be used by the research groups in estimating the polymer properties using the molecular simulations of chains with the predicted critical lengths. The library shall help to obviate the need for researchers to spend efforts in finding the critical chain length needed for simulating the mentioned polymer properties.

Keywords: molecular dynamics; polymer properties; density; solubility parameter

Introduction

Molecular Dynamics (MD) Simulations have been used in the past by many research groups for the prediction of different polymer chain properties. It have been used extensively in predicting the interfacial properties, surface properties, mechanical properties, electrical properties, phase diagrams and interaction parameters for liquid-liquid, polymer-polymer, and polymer-additive mixtures and many more. Polymeric materials, possess different properties, which are mainly distinguished on the basis of type of atoms, chain length, degree of branching, % crystallization, etc. % crystallization affects density, stiffness, strength, and ductility. Likewise the type of atoms, chain length, end groups of chain contribute to the free volume. Many research groups have put in a lot of efforts in determining the exact chain length and degree of branching that should be taken in estimating molecular properties that may have a better agreement with the experimental findings.

Sun *et al.* [1] used the NPT approach to predict the density of polysiloxanes using consistent force field (CFF) [1, 2] method. Later, Fried *et al.* [3] and B. Prathab *et al.* [4] attempted using condensed-phase optimized molecular potentials for atomistic simulation studies (COMPASS) force field [5, 6] and to compute densities of polyphosphazenes and found a good agreement with experimental observations. The different force-field's in MD uses different sets of empirical formulas so as to mimic the interatomic interactions in an average fashion [7, 8]. The force fields are widely used for predicting the structure based on the algorithms

Fan *et al*. [9] found that 21 repeating units of polycarbonate (PC) are enough for performing simulations to match experimental estimates. In contrast to this Deng *et al.* [10] used 17 repeat unit of PC throughout the study. Zhang *et al.* [11] on the other hand took 23 repeat units in a PC chain. This is a matter of concern to the research groups working in the field of MD simulations and none of them worked in the direction to solve this dispute. There is a need to bring standardization in the MD simulation protocols. The objective of this study is to standardize the protocol for selection of chain length, hence obtaining simulated values of density and solubility parameter to be in accordance with the experimental once.

As part of the molecular simulation strategy, COMPASS has been used as the

force-field as it enables accurate and simultaneous prediction of gas-phase properties (structural, conformational, vibrational, etc.) and condensed-phase properties (equation of state, cohesive energy, etc.) for a broad range of molecules. Molecular simulations have been performed using the commercially available software, Material Studio^{TM} 7.0, purchased from Accelrys Inc. The list of polymers taken for this study include polyethylene (linear), polypropylene (isotactic), polystyrene, polytetrafluoroethylene and polycarbonate.

Simulation Methodology

Molecular mechanics (MM) and Molecular dynamics (MD) simulations have been performed using commercially available software, Material Studio 7.0, purchased from Accelrys Inc. [12]. Interactions among the various atoms are calculated using COMPASS (condensed-phase optimized molecular potentials for atomistic simulation studies) force-field. COMPASS enables accurate and simultaneous prediction of gas-phase properties (structural, conformational, vibrational, etc.) and condensed-phase properties (equation of state, cohesive energy, etc.) for a broad range of molecules. Simutioanl methodology is depicted by Fig. 1.

Generation of equilibrated bulk structures

Chains of polyvinyl acetate (isotactic), polyvinyl alcohol (atactic), polystyrene, polyproypelene and polycarbonate (bisphenol-A) with a range of 3-40 repeating units are created and energy minimized separately using MM. The energy minimized chains of different polymers are used for the construction of different amorphous cells. Amorphous Cell module of Material Studio has been used to construct initial realistic 3D periodic structures. The equilibration of the formed amorphous cells are carried out using the methodology mentioned by Kumar *et al.* [13].

The amorphous cells obtained from the procedure are equilibrated cells and have been used for all further property estimations. The amorphous cells model of the generated structure has been shown in Fig. 2. NPT MD simulations are further performed on the equilibrated cells at 298 K and 0.0001 GPa (1 atm) for 30 ps to equilibrate the density. The frames are stored after every 0.1 ps. Then average of the densities of all the saved equilibrated frames for all the polymers for different chain lengths are averaged and reported.

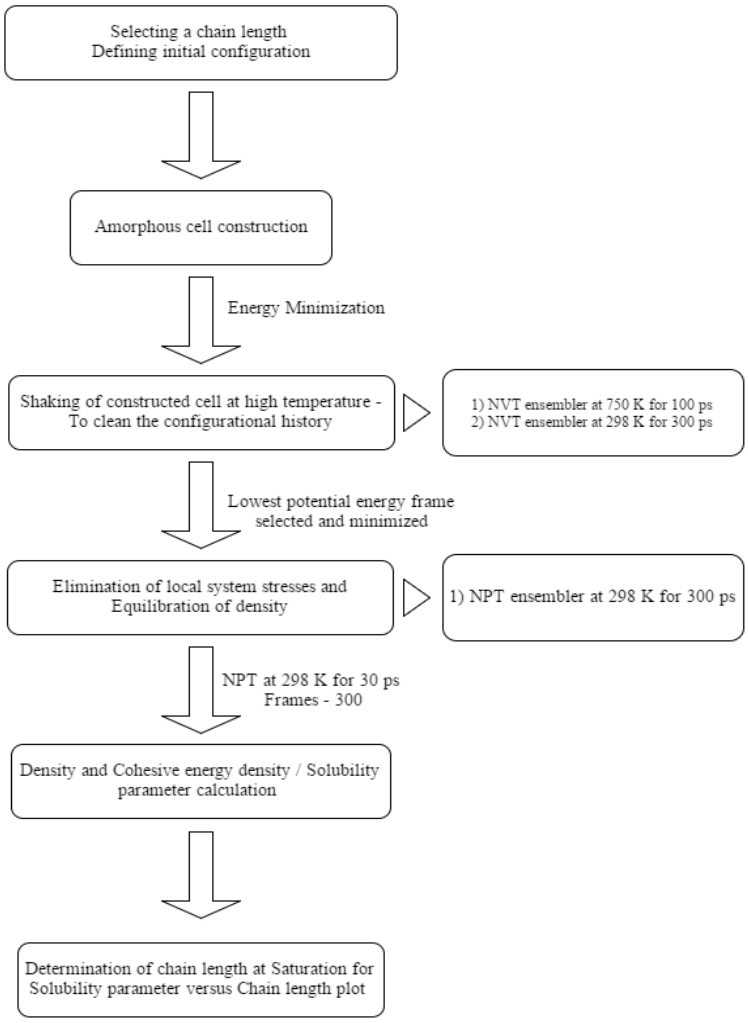
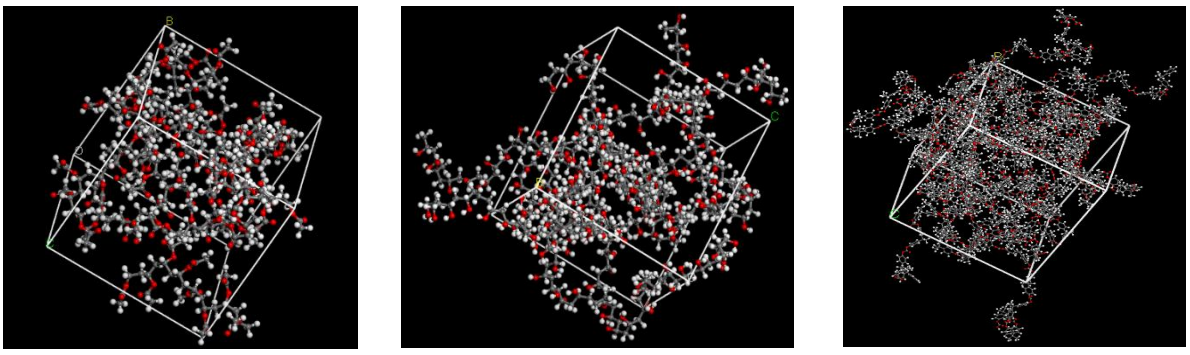


Fig. 1. Flow chart of the simulation strategy to estimate chain length for saturation of properties, especially solubility parameter.



(a) **(b)** **(c)**

Figure 2. Equilibrated amorphous cells made from a) Polyvinyl Acetate, b) Polyvinyl Alcohol and c) Polycarbonate

Results and Discussion

Estimation of solubility parameter

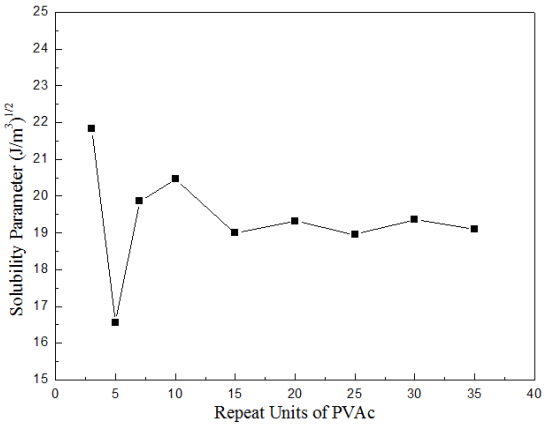
The solubility parameters have been calculated after estimating the cohesive energy density CED values. CED refers to the increase in energy per mole of polymer, $E_{cohesive}$, if all of its intermolecular forces are eliminated in a unit molar volume. Thus, if the molar volume of polymer is V_{molar}, then CED is given by Eq. (1):

$$CED = (E_{\text{cohesive}}/V_{\text{molar}}) \quad (1)$$

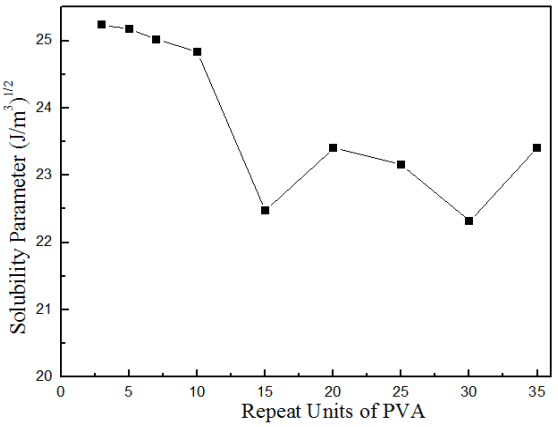
The Hildebrand solubility parameter (δ) is related to CED by the equation:

$$\delta = CED^{1/2} = (E_{\text{cohesive}}/V_{\text{Molar}})^{1/2} \quad (2)$$

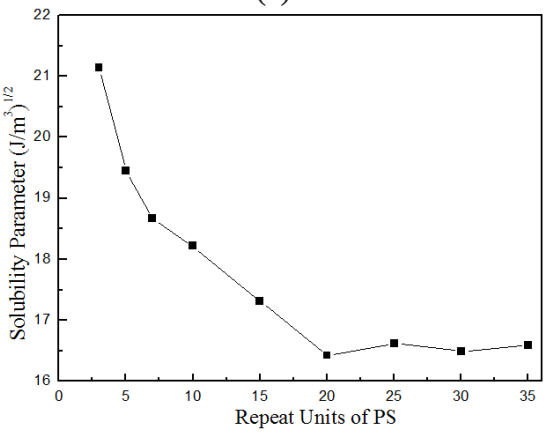
The simulated δ values, of polyvinyl acetate (PVAc), polyvinyl alcohol (PVA), polystyrene (PS), polyproypelene (PP) and polycarbonate (PC), are plotted versus the repeat units and presented in Fig. 3. and compared with the literature estimates. The comparison shows that the simulated values closely match with the reported values, thereby, validating the simulation protocol and results.



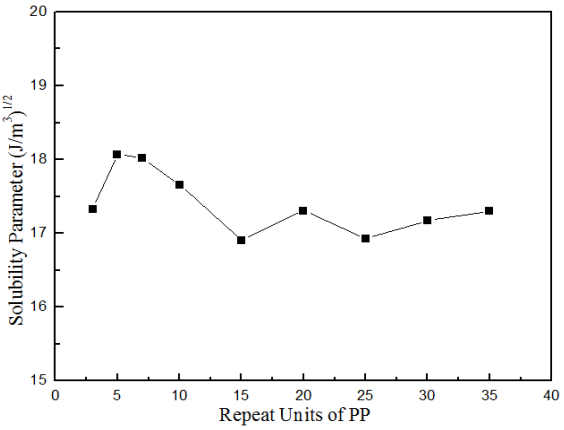
(a)



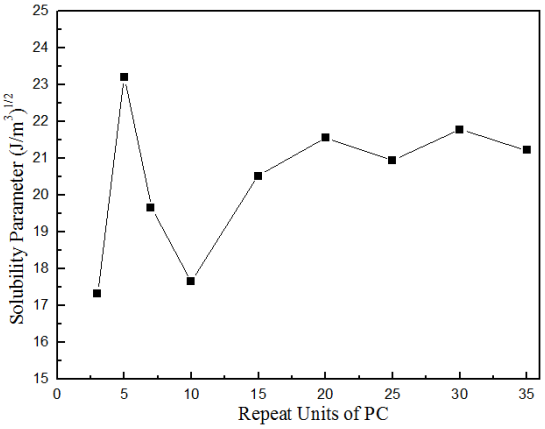
(b)



(c)



(d)



(e)

Fig. 3. Variation of solubility parameter with repeat units for polyvinyl acetate (PVAc), polyvinyl alcohol (PVA), polystyrene (PS), polyproypelene (PP) and polycarbonate (PC).

In Table 1, densities of equilibrated system made using critical length for polymers under consideration are reported with their standard deviations. The deviations in the reported densities are found to lie within 1.3% of average values indicating a good density equilibration. The simulated densities of the equilibrated structures are compared with the experimental values. The simulated densities are found to be in close vicinity to the experimental ones, thereby, validating the simulation protocol.

Table 1: Estimation of solubility parameter for different polymers and hence proposing the minimum number of repeat units required for molecular dynamics of respective polymers

Polymer	Critical repeating units required	Density (gm/cc)	Solubilty Parameter (δ) $(J/cm^3)^{1/2}$	Experimental (δ) $(J/cm^3)^{1/2}$
Polyvinyl Acetate (Isotatic)	≥15	1.154±0.009	19.005±0.024	18.61 [14], 19.33[15], 19.55[16]
Polyvinyl Alcohol (Atatic)	≥20	1.125±0.010	23.251±0.032	23-27[17]
Polystyrene	≥25	1.108±0.004	16.617±0.016	18.6[18]
Polyproypelene	≥10	0.831±0.007	17.655±0.043	17.3[18]
Polycarbonate (bisphenol-A)	≥20	1.223±0.024	21.56±0.022	20.04[19]

Summary and Conclusion

We propose a molecular simulation model for selecting the optimum chain length or the repeat units of monomer after which the solubility parameter or the cohesive energy density shows saturation. The chain length obtained can be used for further determination of properties through molecular simulations. NVT ensemble first shakes the cell at high temperature to remove the configurational history and then bring the amorphous cell to the lowest potential energy. The frame so obtained is minimized

and simulated till the density saturates using NPT ensemble.

The present molecular simulation study employs a strategy to estimate behavior of solubility parameter with chain lengths for different polymers, namely polyvinyl acetate, polyvinyl alcohol, polystyrene, polyproypelene and polycarbonate. The values of solubility parameter, for the listed polymers, obtained at the critical chain length are ~19.0, 23.2, 16.6, 17.6 and 21.5 $(J/cm^3)^{1/2}$ respectively, which are in great accordance with the available experimental values. The work paves the way for development and standardization of the properties and the chain lengths for all the available standard polymers.

Acknowledgement

The corresponding author would like to sincerely acknowledge the grant (Grant Code: FIG-400136-DPT/13-14) provided by Indian Institute of Technology Roorkee, through its MHRD FIG initiative, for funding the work presented in this paper. The author gratefully acknowledges the financial support provided.

References

1. Sun, H. and D. Rigby, *Polysiloxanes: ab initio force field and structural, conformational and thermophysical properties.* Spectrochimica Acta Part A: Molecular and Biomolecular Spectroscopy, 1997. **53**(8): p. 1301-1323.
2. Sun, H., *Ab initio calculations and force field development for computer simulation of polysilanes.* Macromolecules, 1995. **28**(3): p. 701-712.
3. Fried, J. and P. Ren, *Molecular simulation of the glass transition of polyphosphazenes.* Computational and Theoretical Polymer Science, 1999. **9**(2): p. 111-116.
4. Prathab, B., et al., *Computation of density of perfluoroalkyl methacrylates: a molecular modeling approach.* Theoretical Chemistry Accounts, 2007. **117**(1): p. 167-169.
5. Rigby, D., H. Sun, and B. Eichinger, *Computer simulations of poly (ethylene oxide): force field, pvt diagram and cyclization behaviour.* Polymer International, 1997. **44**(3): p. 311-330.
6. Sun, H., *COMPASS: an ab initio force-field optimized for condensed-phase applications overview with details on alkane and benzene compounds.* The Journal of Physical Chemistry B, 1998. **102**(38): p. 7338-7364.
7. Burkert, U. and N.L. Allinger, *Molecular mechanics*. Vol. 177. 1982: American Chemical Society Washington, DC.
8. Lifson, S. and A. Warshel, *Consistent Force Field for Calculations of Conformations, Vibrational Spectra, and Enthalpies of Cycloalkane and n-Alkane Molecules.* The Journal of Chemical Physics, 1968. **49**(11): p. 5116-5129.
9. Fan, C.F., et al., *Molecular modeling of polycarbonate. 1. Force field, static structure, and mechanical properties.* Macromolecules, 1994. **27**(9): p. 2383-2391.
10. Deng, M., V.B.C. Tan, and T.E. Tay, *Atomistic modeling: interfacial diffusion and adhesion of polycarbonate and silanes.* Polymer, 2004. **45**(18): p. 6399-6407.
11. Zhang, M., P. Choi, and U. Sundararaj, *Molecular dynamics and thermal analysis study of anomalous thermodynamic behavior of poly (ether imide)/polycarbonate blends.* Polymer, 2003. **44**(6): p. 1979-1986.
12. Material Studio™, b.D.S.e.B., UK (Accelrys®), *http://accelrys.com/products/materials-studio/, (License purchased by IIT Roorkee).*
13. Kumar, N. and G. Manik, *Molecular dynamics simulations of polyvinyl acetate-perfluorooctane based anti-stain coatings.* Polymer, 2016. **100**: p. 194-205.
14. Nelson, R., D. Mazey, and R. Barnes, *The thermal equilibrium shape and size of holes in solids.* Philosophical Magazine, 1965. **11**(109): p. 91-111.
15. Daoust, H. and M. Rinfret, *Solubility of polymethyl methacrylate and polyvinyl*

acetate. Journal of colloid science, 1952. **7**(1): p. 11-19.
16. Small, P., *Some factors affecting the solubility of polymers.* Journal of Applied Chemistry, 1953. **3**(2): p. 71-80.
17. Barton, A.F., *CRC handbook of solubility parameters and other cohesion parameters*. 1991: CRC press.
18. Miranda, J. and S. Sablotsky, *Solubility parameter based drug delivery system and method for altering drug saturation concentration*. 1997, Google Patents.
19. Kambour, R., C. Gruner, and E. Romagosa, *Biphenol-A polycarbonate immersed in organic media. Swelling and response to stress.* Macromolecules, 1974. **7**(2): p. 248-253.

MACRO 307

Rheology and Foamability of Styrene-Ethylene/Butylene-Styrene (SEBS)/ Polystyrene Blends

Ritima Banerjee,[a] Suprakas Sinha Ray ,[b] Anup K. Ghosh*,[a]

[a] *Centre for Polymer Science & Engineering, IIT Delhi, New Delhi-110016*

[b] DST/CSIR Nanotechnology Innovation Centre, National Centre for Nanostructured Materials, Council for Scientific and Industrial Research, Pretoria-0001, South Africa

** e-mail id: anupkghosh@gmail.com*

Abstract

Styrene-Ethylene-Butylene-Styrene (SEBS) and its blends containing 10%, 20%, 30% and 50% by weight polystyrene (PS) were prepared in a microcompounder. Blends with higher PS content were found to possess higher values of tensile modulus, storage modulus and complex viscosity. Batch foaming of the blends was carried out using carbon dioxide. At higher foaming temperatures (close to the the glass transition temperature of the PS phase), complex viscosity (η*) and storage modulus (E') determined the volume expansion ratio (VE) and the shrinkage of foams. Blends with 30% and 50% PS content produced stable foams having higher VE. At a much lower foaming temperature (35 ^{0}C), PS had a nucleating effect. However, irrespective of rheological properties, all foams shrank. A higher PS content resulted in a lower VE and more prominent shrinkage, due to the selective foaming of the elastomeric phase, impeded by the stiff PS aggregates.

.***Keywords:*** SEBS; polymer blends; batch foaming; rheology; foam shrinkage

Introduction

Foaming of thermoplastic elastomers (TPEs) is an area of immense interest, but having limited

understanding. The replacement of any solid polymer with its foamed counterparts leads to reduced material and fuel consumption, and also expands the possibility of property modification for new applications. In the present world of increased environmental awareness, TPEs are a much sought after class of materials that possess the properties of thermoset rubbers, yet can be processed like thermoplastics. Amongst the TPEs, styrene-butadiene-styrene (SBS) and its hydrogenated form styrene-ethylene/butylenes-styrene (SEBS) are of great commercial importance. In spite of its advantages over vulcanized rubbers, SEBS is seldom used as a neat polymer, because if inferior mechanical properties as comapred to thermoset rubbers. One of the methods of enhancing the mechanical properties of SEBS is by blending it with homopolymers. [1]

The limited understanding of the foaming behaviour of TPEs arises out of their complex microstructure. TPEs comprise of two phases, the thermoplastic phase and the rubber phase, the phases having widely different viscoelasticities. It is probably because of this reason, that there is there is scanty literature on the foaming of SEBS/ PS blends.

The dynamic rheological properties of a polymeric material have a profound influence on its foaming behaviour. The importance of complex viscosity and storage modulus in the foamability of various polymeric materials has been discussed by different research groups. [2–5] The presence of heterogeneous nucleating agents results in increased cell density and hence improvement of foaming behaviour. The efficiency of heterogeneous nucleation in blends and filled polymers depends on the quality of dispersion.

This study presents a systematic analysis of the foamability of SEBS/PS blends with respect to their rheological properties. An attempt has been made to relate rheological and mechanical properties to the morphology of the blends. Focus is on the study of foam shrinkage, so as to produce stable foams with appreciable volume expansion. This study is expected to provide guidelines in the production of TPE base materials with superior mechanical properties and foamability.

Experimental

SEBS (Kraton G1643 M) of Kraton Polymers India and PS (SC202EF) of Supreme Petrochemicals India were used in this study.

Blends containing 10%, 20%, 30% and 50% by weight PS, and designated as SEBS-10PS, SEBS-20PS, SEBS-30PS and SEBS-50PS were prepared in a microcompounder. The blends were subjected to subsequent studies on DMA, mechanical properties, morphology and foaming.

In DMA studies, temperature sweep was carried out in the range – 60 ^{0}C to 120 ^{0}C at a frequency of 1 Hz.

Pressure quench batch foaming of the moulded specimens of SEBS and the blends was carried out at higher foaming temperatures (close to Tg of PS phase), as well as at 35 °C. The shrinkage of the foams was measured by determining the decrease in volume expansion ratio with time.

Tensile testing of SEBS and the blends was carried out using a cross-head speed of 500 mm/min.

SEM studies of the blends and foams were carried out using back-scattered imaging technique. Morphological analysis of the blends was carried out after selective staining of the PS phase.

Results and discussion

SEM Studies of Blends

SEM studies revealed that a portion of the added PS increased the domain size of the styrene

domains of SEBS, while the remaining portion got phase separated forming micrometer sized aggregates. Increase in PS content of blend resulted in an increase in the number of micrometer sized aggregates, as seen in earlier studies. [1,5]

DMA Studies

SEBS-10PS was found to possess lower values of E' at temperatures lower than 97 °C. This may be attributed to the larger domain size. [5] Further increase in PS content resulted in increase in E' over the entire range of temperature used for study. This was possibly due to the over-riding effect of the phase separated stiff PS aggregates.

Mechanical Properties

SEBS-10PS was found to have a slightly lower value of modulus at 30% strain (E_{30}) as compared to SEBS, which may be again attributed to increase in domain size. Further increase in PS content was found to result in increase E_{30} values (Figure 1), due to predominance of phase separated PS aggregates.

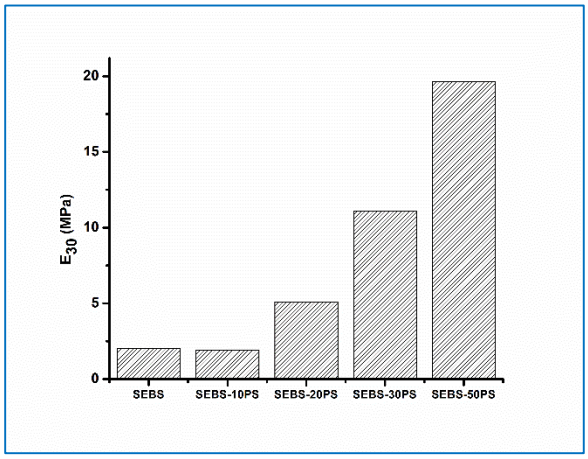


Figure 1. Tensile modulus values

Foamability of Blends

At higher foaming temperatures, foaming behavior was found to be controlled by rheological properties. SEBS-30PS and SEBS-50PS, which had significantly higher E' values than the other compositions, produced stable foams. Foams of SEBS, SEBS-10PS and SEBS-20PS shrank. The lower the E'value, the longer was the time over which shrinkage was observed.

A higher η* resulted in a higher value of VE. At a foaming temperature of 110 °C, SEBS-50PS which had the highest η*, produced a foam having almost double the VE of SEBS foam produced at the same temperature. Also, for a given composition, optimal VE was achieved at a foaming temperature close to the T_g of the PS phase of that composition, indicating the presence of a

complex viscosity window suitable for the foaming process. When two compositions were foamed within their respective complex viscosity windows, the one with a higher value of η* exhibited a higher VE.

At 35 °C, irrespective of rheological properties all foams shrank. Greater the PS content, lower was the volume expansion ratio and more prominent was the shrinkage. This may be attributed to the selective foaming of the elastomeric phase, impeded by the stiff PS aggregages, which were much below their T_g.

Image J analysis of the SEM micrographs of foams produced at 35 °C revealed that upto 30 weight % PS loading, an increase in PS content led to an increase in cell density, a smaller cell size and a narrower cell size distribution (Figure 2). This may be attributed to the nucleating effect of PS. An increase in PS content resulted in a greater number of phase separated aggregates and hence enhanced nucleating effect. A further increase in PS content resulted in a larger cell size and a broader cell size distribution. This was possibly due to selective foaming of the elastomeric phase in a co-continuous morphology.

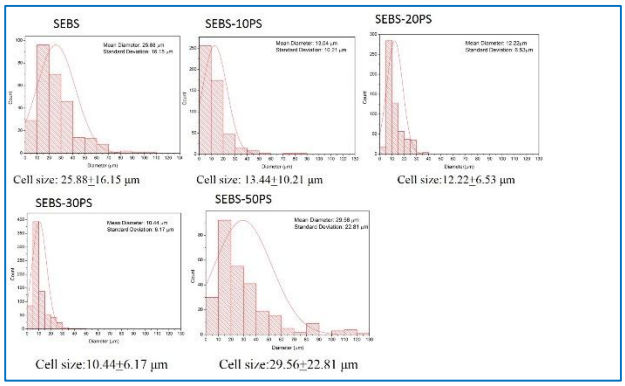


Figure 2. Cell size distribution of foams produced at 35 °C [6]

All foams produced at higher foaming temperatures were found to possess large, irregularly shaped cells. This may be attributed to lower melt strength at elevated temperatures.

Conclusions

❖ When PS is compounded with SEBS, a portion of the added PS increases the domain size of the copolymer, while the remaining forms phase separated aggregates. The phase separated aggregates cause enhancement of tensile modulus and storage modulus.

❖ The foamability of SEBS/PS blends depends on material characteristics and foaming temperature:

➢ At higher foaming temperatures foamability is ruled by rheological characteristics. Higher values of complex viscosity in suitable complex viscosity window, and higher storage modulus lead to foams having higher volume expansion and lower shrinkage.

➢ At foaming temperatures below the T_g of the PS phase but higher than that of the EB phase, the EB phase is selectively foamed with the PS phase exhibiting nucleating effect. Irrespective of rheological properties all foams shrink. A higher PS content results in lower values of volume expansion and a more prominent shrinkage.

References

[1] S. Raha, N. Kao, and S.N. Bhattacharya, Polym. Eng. Sci. **52**, 2559 (2012).

[2] Y. Zhang, M. Kontopoulou, C.B. Park, and

X. Ye, 8th World Congr. Chem. Eng. (2009).

[3] R. Gendron and C. Vachon, J. Cell. Plast. **39**, 71 (2003).

[4] F. Gunkel, A. Sporrer, G. Lim, D. Bangarusampath, and V. Alstadt, J. Cell. Plast. **44**, 307 (2008).

[5] R. Sharudin and M. Ohshima, J. Appl. Polym. Sci **128**, 2245 (2013).

[6] R. Banerjee, S. Sinha Ray, and A.K. Ghosh, J. Cell. Plast. 0021955X16652108 (2016).

MACRO 317

Effect of Compatibiliser on Morphology and Melt Extensional Properties of Halloysite Nanotubes -Filled High Density Polyethylene

V. P. Singh[1], K.K. Vimal[2] and G. S. Kapur[2], Shashikant, Veena Choudhary*[1]

[1]Centre for Polymer Science and Engineering, Indian Institute of Technology New Delhi, India 110016
[2]Indian Oil Corporation Ltd. Research & Development Centre Sector 13, Faridabad, Haryana, India 121007
**E-mail: veenach@hotmail.com*

Abstract

In the present study, high density polyethylene (HDPE)-based composites containing different amounts of Halloysite nanotubes (HNT) [1-10 wt %] and varying amounts ranging from 5-15% w/w of MA-g-HDPE as compatibiliser were prepared by melt compounding in a co-rotating twin screw extruder. The melt-extensional properties such as extensional viscosity melt strength and drawability were investigate by using Rheotens set up and extensional viscosity was examined by using two different methods i.e. Rheotens set up and capillary Rheometer. High shear viscosity and melt fracture analysis were also carried out using Capillary rheometer.

It was found that the melt strength and extensional viscosity of the HDPE/HNT composites were increased slightly with HNT concentrations up to 5wt%. Further increase in HNT concentration led to a severe reduction of melt strength as well as extensional viscosity. While the drawability of the HDPE/HNT melts was found to be independent of HNT concentration up to 10wt%. The tensile force as well as drawability increased significantly with the addition of compatibiliser to the HD/HNT composites. Extensional viscosity calculated from Wagner's master curve using Rheotens data as well as calculated by modified Cogswell method using convergent flow analysis from capillary data exhibited good agreement. High shear viscosity increased upon increasing filler

content with slight decrease in onset of melt fracture at 10% HNT loading. On the other hand, incorporation of compatibiliser up to 15wt% did not affect the shear viscosity with slight increase in the onset of melt fracture.

Keywords*: HDPE, HNT, Rheotens test, Extensional properties, Melt fracture*

MACRO 320

Design and Development of acrylonitrile (AN) and methylmethacrylate (MMA) copolymers for improving the scratch and mar properties of Polymethylmethacrylate (PMMA)

Rai, Roopali[a]*; Sikder, Arun [a]; Nandi, Sangita [a]; Tanwar Akhilesh [a]; Khatokar, Rukmini [a]; Pask, Stephen D. [b]; and Mitra, Susanta [a]

[a] SABIC, Bangalore-562125, India

[b] SABIC, Riyadh, Kingdom of Saudi Arabia

*Corresponding author: Roopali Rai, Email: roopali.rai@sabic.com

Abstract

Scratch and Mar resistance is one of the desirable surface properties for exterior applications as scratches reduce the life cycle and durability of a product, simultaneously affecting its aesthetics. PMMA based materials often finds its extensive use in such applications owing to its excellent optical transmission, weather resistance, hardness and an ability to get processed into various shapes.However, scratching & abrasion of surfaces causes a loss of optical and tribological performance, significantly affecting aesthetics and desired functions, which affects actual application. In this work, we have designed and developed copolymers of methyl methacrylate (MMA) and acrylonitrile (AN) [poly (acrylonitrile-co-methyl methacrylate), p(AN-co-MMA)]. The chosen co-polymer compositions were suggested by predictions of molecular modelling of copolymer system using Synthia model, which is based on quantitative structure-property relationship (QSPR). Tests revealed an increase in surface hardness of the films (0.32 GPa in copolymer with ~80 wt% AN vis-à-vis 0.22 GPa PMMA) with increasing acrylonitrile content.

Keywords: *Poly methyl methacrylate, hardness, Elastic modulus, Mar resistance*

Introduction

Poly methyl methacrylate (PMMA) is a transparent thermoplastic, often used in sheet

form as a lightweight or shatter resistant alternative to glass. It exhibits excellent optical transmission, weather resistance, hardness, and an ability to be processed into various shapes and colours giving it attractive design flexibility.[1] Due to these favourable attributes, PMMA finds extensive use in exterior applications for electronic displays, over-the-hood automobile components - windshield and lighting components, medical as well as in architectural and construction applications.[2] However, scratching and abrasion of surfaces causes a drastic loss of optical and tribological performance, which results in a reduction in the durability of products,[3-10] thereby limiting the widespread applicability of such materials.

The correlation between scratch resistance and the bulk material properties such as tensile modulus, yield stress, and elastic recovery as well as the coefficient of friction have been studied in detail by several reserachers.[4,5] Recent strategies for improving the scratch resistance of PMMA have largely involved blending with organo-modified layered aluminophosphates,[11] organoclays,[12] zirconia,[13] as well as their blends[14], to form nano-composites. Little focus has been given to the intrinsic scratch resistant behaviour of PMMA.[15]

Copolymerizing AN with MMA should increase the hardness[16] and thus the scratch resistance of PMMA but the melt blending of Polyacrylonitrile (PAN) and PMMA is not possible as PAN degrades before melting.[17] This paper presents the improvement of the scratch and mar resistance of PMMA by statistically copolymerizing MMA with AN. The p(AN-co-MMA) copolymers were synthesized as described elsewhere.[18] Copolymers of AN and MMA have been reported for various applications but mainly as PAN precursors for carbon fibre production.[19] As far as it is known, these polymers have not been explored for their improved surface properties.

Nano-indentation tests were performed on compression-moulded films of the prepared copolymers and the results were correlated with the E-moduli obtained from predictive study.

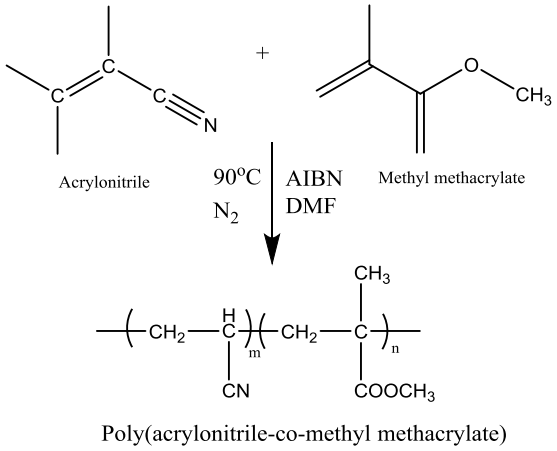
Experimental

(i) Materials: All solvents and reagents were purchased from Sigma-Aldrich unless stated otherwise. Acrylonitrile (≥99%) contains 35-45 ppm monomethyl ether hydroquinone as inhibitor, Methyl methacrylate (MMA ≥98.5%) used as co-monomer,2,2′-Azobis(2-methyl propionitrile) (AIBN, Spectrochem (98%)) was used as the initiator. Dimethyl formamide (DMF, anhydrous, 99.8%) was used as the solvent for the polymerizations.

(ii) Molecular Modelling Study: The elastic modulus and shear yield stress were calculated at 298K using the Synthia module in Accelrys Materials Studio 6.1.[20] Synthia employs quantitative structure-property relationships (QSPR) using information about the topology for the calculation of polymer properties. The properties are expressed in terms of connectivity indices (derived from graph theory) combined with geometrical variables and other structural descriptors.

(iii) Synthesis and Characterization of Copolymers: The copolymers of MMA and AN were synthesized as described and this synthesis is represented in scheme 1[18]. The prepared copolymers were characterized

using NMR, FTIR, DSC and TGA. Table 1 shows the final compositions of homo- and co-polymers synthesized, as calculated from the ^{1}H NMR spectra.



Scheme 1 Scheme representing synthesis of p(AN-co-MMA) Copolymer

Sample	Compositions of p(AN-MMA) (AN/MMA) (wt.%)
A	82/18
B	75/25
C	35/65
D	100 MMA
E	100 AN

Table 1 Compositions of synthesized co-polymers analysed by ^{1}H NMR

(iv) Preparation of Copolymer Films by Compression Moulding: The p(AN-co-MMA) copolymers synthesized by solution polymerization techniques were isolated as powders. The polymer powders were compression moulded into films at 220 °C

(v) Nano-Indentation: Nano-indentation experiments were conducted using the Nano-Indenter® XP (Keysight Technologies, Inc., Santa Rosa, CA) with depth control method at fixed depth of 1000 nm. The load and displacement data obtained in the nano-indentation tests were analyzed according to the model developed by Oliver and Pharr.[21]

(v) **Mar resistance measurement:** Mar testing was done with manually driven Atlas Crockmeter, Model CM-1 AATCC. For this Crockmeter, a 9N force is constantly applied to the protruding 16 mm acrylic finger which is covered with an abrading fabric held in place with a metal ring. A 50mm x 50mm piece of felt (Test Fabric Inc.) is placed between the acrylic finger and the abrading fabric in order to maintain equal pressure.

3. Results and Discussion

(i) Molecular modelling: It is generally accepted that bulk material properties such as tensile modulus, shear yield stress, elastic recovery as well as surface hardness and the coefficient of friction affect the scratch behaviour of polymers. In polymers, which show shear dominated deformation, an approximate linear correlation between hardness and yield stress is observed.[22] Shear yield stress is also roughly proportional to elastic modulus.[20] Therefore, as an initial approach, some of these properties were predicted using the Synthia software as mentioned above for various compositions of copolymers of AN and MMA. The AN moiety is expected to introduce hardness in the copolymers[15]. Figure 2 shows the calculated E-moduli and shear yield stresses

of p(AN-co-MMA) copolymers .Both the modulus and the shear yield stress increase as AN content in the copolymer system increases. This suggests that the hardness of PMMA can be improved by incorporation of AN into the MMA backbone.

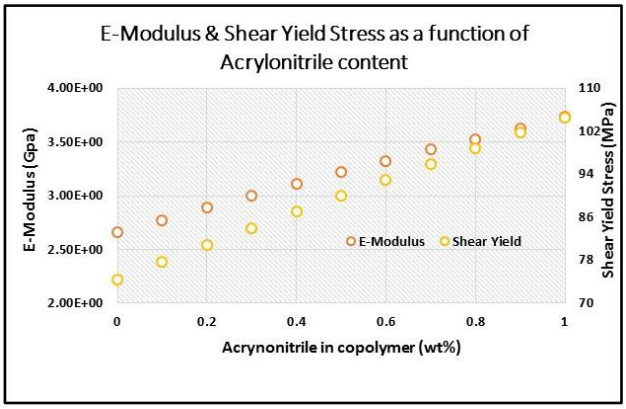


Figure 1: E-Modulus and Shear Yield Stress *vs* the AN content in the Copolymer (From Molecular Modelling Study.)

(i) **Nano-Indentation:** Nano-indentation is a commonly used technique to evaluate the surface-mechanical properties of polymer systems.[23] The test yields load-displacement curves, surface hardness and E-modulus data for the samples tested.

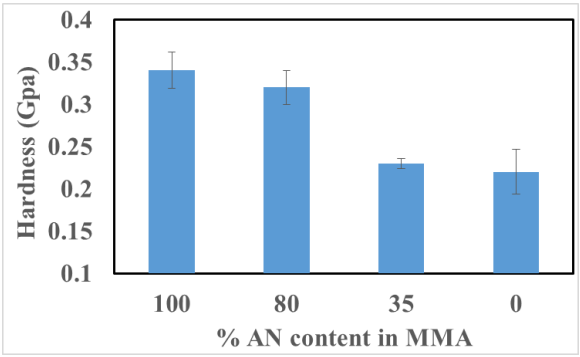


Figure 2: Surface hardness as a function of Acrylonitrile (Wt-%) in Copolymer

Figure 2 shows the surface hardness values for both the samples with different %AN content in the copolymer.

Surface hardness gives a good indication of the rigidity of materials and hence has been widely adopted to predict relative scratch resistance of the materials. Therefore, an increasing hardness with increased AN content indicates that the copolymers may have better scratch resistance than neat PMMA.

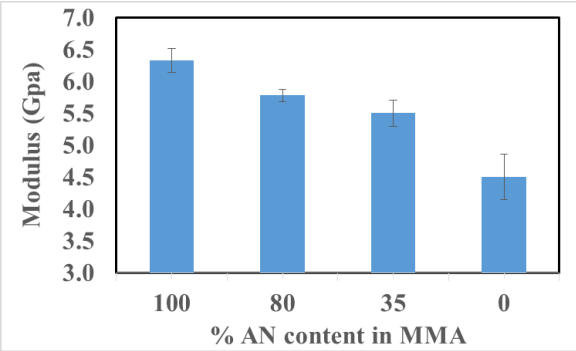


Figure 3: E-Modulus Vs the Acrylonitrile (Wt-%) Content of the Copolymer

Figure 3 shows the trend of the E-moduli as a function of AN content obtained from nano-indentation tests. The E-modulus also plays an important role in the scratch process, especially during the indentation stage. An increase in the modulus decreases the radius of the contact zone of the indenter tip on the testing surface and hence reduces the scratch depth.[4,5] It can be seen that as the amount of AN in the copolymer is increased, the E-modulus also increases from 4.5 GPa (neat PMMA) to 5.8 GPa (with ~82 wt% AN content). This is in agreement with the predictive molecular modelling study as discussed earlier (cf. Figure 1). Scratch tests

performed with these copolymers showed that scratch resistance improves with increasing AN content in the copolymers and these results will be published elsewhere.

Furthermore, Mar measurements on compression molded films (Figure 4) shows that copolymer surface seems to be better showing less visible mar on the surface.

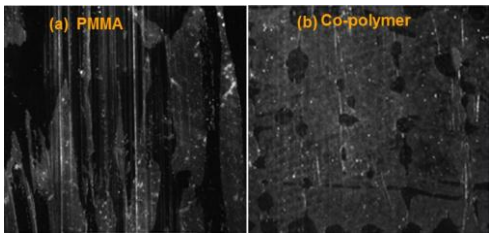


Figure 4: Pictures of (a) PMMA (b) co-polymer of AN & MMA with visible mar on the surface.

4. Conclusion

The present study demonstrates that the Synthia molecular modelling (Bicerano model), can usefully predict the properties, such as E-modulus and shear yield stress, of p(AN-co-MMA) as a function of AN content. Furthermore, these predictions were validated experimentally for p(AN-co-MMA) copolymers using nano-indentation and rheological stress relaxation studies. Nano-indentation studies revealed >20% increase in E-modulus and >30% increase in surface hardness with high AN content in the copolymers with respect to neat PMMA. As E-modulus, surface hardness and shear yield stress can be considered as critical properties for predicting the scratch resistance of a polymer, the observed trends suggest that higher AN content should improve the scratch performance of p(AN-co-MMA) copolymers. Thus, this systematic study presents a useful approach to improve the scratch resistance of polymeric materials which are intended for use as coatings and/or molded articles on or in electronic displays, automotive, decorative home-appliances as well as building and construction.

5. Acknowledgements

We extend our sincere thanks to Dr. Gurram Kishan and Dr A. Dhanabalan from SABIC Bangalore AN for their continuous encouragement and support. The authors would also like to thank Dr. Arup Ghosh, Dr. Debasish Banerjee, Dr. S. Yogesha and Mr. N. Satish from SABIC Bangalore for characterization and valuable discussions.

Notes and references

1. (a) A. D. Alobaidani, D. Furniss, A. S. Johnson, A. Endruweit and A. B. Seddon, *Opt. Laser Eng.*, 2010**, 48,** 575; (b) L. W. Mckeen, *Effect of UV light and weather on Plastics and Elastomers*, *3rd Edition*, Elsevier, Oxford U.K., 2013;
2. (a) Market Report on PMMA, *Grand View Research*, 2014; M. Younis, V. Darcos, C. Paniagua, P. Ronjat, L. Lemaire, B. Nottelet, X. Garric, Y. Bakkour, J. H. E. Nakat and J. Coudane, *RSC Adv.*, 2016, **6**, 5754.
3. B. J. Briscoe, P. D. Evans, E. Pellilo and S. K. Sinha. *Wear*, 1996, **200**, 137.
4. C. Xiang, H.-J. Sue, J. Chu and B. Coleman. *J. Polym. Sci. Part B: Polym. Phys.*, 2001**, 39**, 47.

5. K. Friedrich, H. J.Sue, P. Liu, A. A. Almajid, *Tribol. Int.*, 2011, **44,** 1032.
6. M. Bonne, B. J. Briscoe, C. J. Lawrence, S. Manimaaran, D. Parsonage and A. Allan. *Tribol. Lett.*, 2005,**18**, 125.
7. M. Manshaa; C. Gauthier; P. Gerardb; R. Schirrer. *Wear*, 2011, **271**, 671.
8. V. Jardret and P. Morel, *Prog. Org. Coat.*, 2003, **48**, 322.
9. a) M. Ö. Bora, *Tribol. Int.*, 2014, **78,** 75;
10. H. Jiang, R. Browning, H.-J. Sue, *Polymer*, 2009, **50,** 4056.
11. S. Jiang, G. Chen, Y. Hu, Z. Gui and Z. Hu, *Ind. Eng. Chem. Res.*, 2015, **54**, 4737.
12. S. J. Nikkhah, H. Hojati, and M. R. Moghbeli, *Polym. Plast. Technol. Eng*., 2014, **53**, 268.
13. Y. Hu, S. Zhou and L. Wu, *Polymer*, 2009, **50**, 3609.
14. J. An, B-H. Kang, B-H. Choi and H-J. Kim, *Tribol. Int.*, 2014, **77**, 32.
15. S. Y. An, D. Arunbabu, S. M. Noh, Y. K. Song and J. K. Oh, *Chem. Commun*., 2015, **51**, 13058.
16. R. Browning, H-J. Sue and P. Charoensirisomboon, *Polym. Eng. Sci.*, 2011, **51**, 2282.
17. (a) J. Udakhe, *J. Tex. Asso.,* 2011, **71**, 233; (c) N. C. Abeykoon, J. S. Bonso and J. P. Ferraris, *RSC Adv.*, 2015, **5**, 19865.
18. (a) M. S. M. Eldin, M. R. Elaassar, A. A. Elzatahry and M. M. B. Al-Sabah, *Arabian J. Chem.*, 2014, doi:10.1016/j.arabjc.2014.10.037; (d) A. V. Korobeinyk, R. L. D. Whitby and S. V. Mikhalovsky, *Eur. Polym. J.*, 2012, **48,** 97., N. Gupta, R. Rai, A. Sikder, S. Nandi, A. Tanwar, R. Khatokar, S. D. Pask and S. Mitra, *RSC Adv.*, 2016, **6**, 37933.
19. (a) P. Bajaj and A. K. Roopanwala, *J. Macromol.. Sci., Part C: Polym. Rev.*, 1997, **37**, 97; (b) X. Li, X. Ji. A. Qin and C. He, *RSC Adv.*, 2015, **5**, 52226;
20. **(a)** J. Bicerano, *Prediction of polymer properties*, Marcel Dekker, Inc., New York, 2002**; (b)** J. Bicerano, *Prediction of Polymer Properties*, Marcel Dekker Inc.: New York, 1993; (c) Material Studio 6.1 software, BIOVIA, USA.
21. W. C. Oliver and G.M. Pharr, *J. Mater. Res.* 1992, **7**, 1564.
22. (a) Z. Wang, P. Gu, H. Zhang, Z. Zhang and X. Wu, *Mech. Adv. Mat. Str*., 2016, **23**, 291; (b) H. Chakraborty, A. Sinha, N. Mukherjee, D. Ray and P. P. Chattopadhyay, *Polym. Compos.*, 2014, **35**, 948.
23. J. Chu, C. Xiang, H. –J. Sue and R. D. Hollis, *Pol. Eng. Sci*., 2000, **40**, 944.

MACRO 330

Synergistic Effect of Nucleation / Stereocomplexation with Plasticizer on Crystallization of Poly(lactic acid)

Susheela B. Idage*, Megha D. Deokar, Bhaskar B. Idage

Polymer Science & Engineering Division, CSIR-National Chemical Laboratory,
Dr. Homi Bhabha Road, Pune - 411 008, INDIA
**E-mail : sb.idage@ncl.res.in*

Abstract

Poly(L-lactic acid) (PLLA) crystallization is strongly dependant on the presence of D-lactic acid content and is hindered by increasing the D-lactic acid content. It also suffers from low crystallization rate unless it is subject to high orientation. The enhancement of crystallization rate is promising to improve its thermal resistance. The efforts have been made to improve the toughness of PLA by different techniques namely, plasticization, copolymerization and compounding with other materials. PLA can also be reinforced with inorganic fillers accompanied by deterioration in toughness and transparency. Hence, there is strong interest to prepare fully bio-based and biodegradable PLA material with improved and balanced performance. In the present work, PLA material was prepared *via* solution blending with and without Millad Gel using Poly(D-lactic acid) (PDLA) (10 wt.%). PLLA and PDLA were prepared from the respective lactides by ring opening polymerization using tin octoate catalyst. The effect of enhanced stereocomplex crystallites as nucleating agent was studied on the isothermal crystallization of PLLA.

Keywords: *L-lactide, D-lactide, PLLA, PDLA, tin octoate, Millad gel, ring opening polymerization, stereocomplex, thermal crystallization.*

Introduction

Poly(L-lactic acid) (PLLA) derived from bio-renewable resource materials has received considerable attention in the past decade due to environmental concern and sustainability issues as compared with the conventional petroleum based polymers. PLLA is thermoplastic polymer with good processability and mechanical properties. However, it suffers from brittleness, low T_g, low heat distortion temperature (HDT) and crystallinity. It is widely used in biomedical and commodity applications as a substitute to conventional petroleum based polymers. Hence, crystallization of PLA is a subject of great interest in the past decade. PLLA and its enantiomer PDLA can form a stereocomplex (*Sc*) upon mixing in equimolar quantities. The *Sc*PLA possess superior physico-chemical properties such as melting point which is 50^{o}C higher than PLA homopolymer[1]. Although, much attention has been paid to stereocomplexation of symmetric PLLA/PDLA (50/50) blend, it is still challenging in practice to achieve the high *Sc* content. This may be useful due to kinetic reasons and the degradation of PLA chains at a temperature higher than *Sc*-PLA. The drawing of PLA stereocomplex material is very expensive due to high cost of PDLA. The *Sc* crystallite network has been detected in blend with 2 to 10 wt.% of PDLA and *Sc*-PLA enhance the crystallization of PLLA matrix. However, the effect of *Sc* crystallite network on the properties of asymmetric PLLA/PDLA blend is still a subject matter of study.

A *Sc* crystal network was detected in asymmetric PLLA/PDLA blends with 2 to 5 wt.% of PDLA and *Sc*-PLA speeded up the crystallization of PLLA matrix[2,3]. However, the effect of *Sc* crystallite network on the properties of asymmetric PLLA/ PDLA blends is not clear. Brochu *et al*[3] showed that the stereocomplexation occurs with minimum 10 wt.% of PDLA.

Schmidt and Hillmyer[4] also reported the crystallization behavior in asymmetric blends of PLLA and low mol. wt. PDLA. They have showed the role of stereocomplex as a nucleating agent for PLLA.

Commercial PLA polymer made from the polymerization of L-isomer is very brittle material and toughness in it a raw state is inadequate to withstand a high level of impact strength. The inherent low HDT property also restricts the particular applications of PLA in long term commercial use such as in automotive and electronics. The poor thermal and mechanical stability of PLA limits its wide use in applications that require plastic deformation at high stress level, such as screws and fracture fixation plates. Therefore, there are still many challenges for market acceptance in utilization neat PLA as engineering material.

PLLA and PDLA were prepared from the respective lactides by ROP using tin octoate catalyst. The main objective of the present work is to prepare the PLA material with superior and balanced properties such as stereocomplexation and thermal in the asymmetric blends and to study the crystallization behavior of in house synthesized PLLA with 6 wt.% of D-lactide with mol. wt. 1 Lakh with and without preformed Millad gel along with 10 wt.% PDLA in PLLA (90/10) asymmetric blends.

PLA material was prepared *via* solution blending with and w/o Millad Gel using PDLA (10 wt.%). We report the enhanced formation of stereocomplex crystallites as nucleating agent with Millad Gel for the crystallization of PLA. Millad gel was prepared from Poly(ethylene glycol) dimethyl ether (PEGDME) (Mol. wt. 500). The addition of Millad Gel to PLA has improved the formation of stereocomplex crystallites which are useful to enhance the rate of thermal crystallization of PLA.

Experimental

Materials

D-Lactide and L-Lactide (Purac, USA) was purified by recrystallization from dry ethyl acetate. Tin (II) - ethylhexanoate [$Sn(Oct)_2$] (Sigma-Aldrich, USA), Millad 3988 [Milliken,1,3:2,4-bis(3,4-dimetyldibenzylid- ene)] Sorbitol (DMDBS), Poly(ethylene glycol) dimethyl ether (PEGDME, 500) (Aldrich, USA) were used as received.

Polymerization

PLLA (6 wt% D-lactide) and PDLA were prepared from the corresponding L-lactide and D-lactide by the ring opening polymerization method.

A typical ring opening polymerization (ROP) procedure is given below:

To a 50 mL thick glass ampoule added 2 g of purified lactide was added. To it was added 0.05 wt% of tin octoate and 0.01 wt% of 1,10-decane diol. The content in the glass ampoule were dried at 55^{o}C under reduced pressure for 3 h and the tube was sealed. The polymerization was carried out at 180^{o}C for 1 h. The polymer obtained was cooled to room temperature and dissolved in chloroform. The residual catalyst was quenched by adding aq. HCl (1 wt.%),

precipitated using petroleum ether and separated by filtration. The polymer was dried at 45^{o}C in a vacuum oven under reduced pressure.

Synthesis of Millad gel

To a 50 ml three necked R.B. flask equipped with nitrogen gas inlet and reflux condenser were added 0.15 g of Millad and 0.85g of PEGDME and heated at 230^{o}C under nitrogen atmosphere with continuous stirring (500 RPM) for 1h. The reaction mixture was cooled to room temperature. The gel formed was dried under reduced pressure.

The films of PLLA/PDLA blend with and without Millad gel (5 and 10 wt.%) in methylene chloride were prepared by solution casting technique. The films prepared were dried at 45^{o}C in a vacuum oven under reduced pressure.

Characterization

The molecular weights of PLLA and PDLA were determined by solution viscosity using Ubbelhode viscometer at 30^{o}C in chloroform and Waters Gel Permeation Chromatography (GPC) in Chloroform using RI detector and Polystyrene standards. The molecular weights of PLLA and PDLA used for this study possess Mn = 61500 g/mol, Mw = 116000 g/mol, PDI = 1.88 and Mn = 52800 g/mol, Mw = 86500 g/mol, PDI = 1.64 respectively.

The thermal properties of PLLA and PDLA were studied using differential scanning calorimetry (DSC Q10) (TA instruments, USA) with a heating rate of 10^{o}C/min. The first heating DSC thermogram of PLLA used in this study showed the T_m of 152^{o}C with the heat of fusion (ΔH_f) of 16 J/g when the sample was heated at 10^{o}C/min However, T_c was not observed in cooling cycle when the sample was cooled at the rate of 10^{o}C/min. The second heating cycle showed the T_g at 58^{o}C, T_c and T_m at 130^{o}C and 150^{o}C with ΔH of 6 J/g showing the amorphous nature of sample.

Results and discussion

The rate of thermal crystallization of PLA decreases by increasing the D-lactide content and hence its wide application is hindered. Hence, in the present study, a new thermal crystallization method has been proposed that accelerates the enhanced formation of stereocomplex crtstallites that will be useful to accelerate the rate of thermal crystallization of PLA.

A high degree of stereocomplexation between two PLA enantiomers is much more promising and effective to enhance the thermal stability of PLA. Although much attention has been paid to stereocomplex- ation of symmetric PLLA/ PDLA (50:50) blends, it is still challenging in practice to achieve high *Sc* content because of kinetic reasons and the degradation of PLA chains at temperature higher than melting point of *Sc*PLA. As a consequence, solution mixing was preferably used in fundamental research. The stereocomplex crystallites remain unmelted at 190^{o}C and embedded in the PLLA molten matrix.

The polymer film was made by solution mixing of PLLA and PDLA in chloroform without and with different composition of Millad gel. The self nucleation of PLA with

small crystallites of stereocomplex has been reported by blending up to 15 wt.% of PDLA with PLA[5].

The main objective of the present study is to accelerate the rate of nucleation of PLA by the addition of Millad gel which acts as a nucleating agent. It was observed that the DMDBS nanofibrils formed in the gel, which could supply active nucleating sites for PLA when the gel is added to PLA. The gel needs to be prepared separately because DMDBS molecules are difficult to self-assemble directly to form nanofibrils in the PLA matrix. It is homogeneously dispersed in the PLA matrix, then on cooling forms a thermo reversible nanofibrillar network within the polymer, resulting in faster and more organized crystal growth of the PLA matrix, hence leading to the desired properties. On the other hand, PEG in the gel acts as a plasticizer, enhance the chain mobility of PLA and introduces additional interactions between PLA molecules and DMDBS nanofibrils that help to make the nucleation easier and faster than linear PLA.

Figure 1 shows the DSC thermograms of (a) PLLA neat, (b) PLLA/PDLA (90:10) blend sample showed the formation of *Sc* crystallites having the T_m at 210°C and the heat of fusion (ΔH_f) of 8 J/g after isothermal heating along with a bi-modular T_m peak at 154°C with the ΔH_f of 25 J/g.

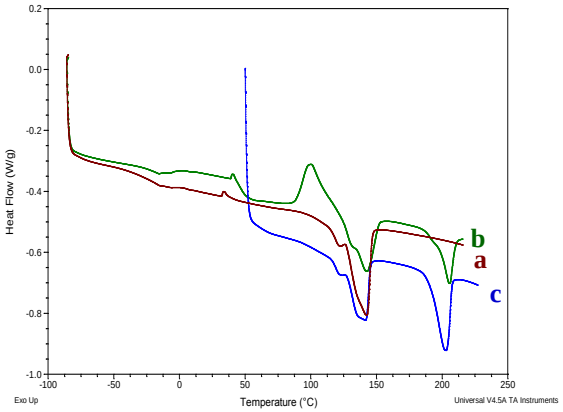


Fig. 1: DSC thermograms of a) PLLA, b) PLLA/PDLA without Millad gel and c) PLLA/PDLA with Millad gel by heating rate of 10°C/ min.

Figure 1 (c) shows the DSC thermogram of PLLA/PDLA (90:10) blend in the presence of Millad gel sample. It shows the formation of *Sc* crystallites with T_m of 207°C with the heat of fusion (ΔH_f) of 13 J/g along with a bimodular T_m peak at 147°C with the heat of fusion (ΔH_f) of 20 J/g after isothermal heating. The addition of Millad gel enhances crystallinity of PLA due to faster stereocomplexation and plasticization effect. The T_g decreases from 58 to 50°C in case of 5% gel and 45°C with 10% gel. In the presence of Millad gel, chain mobility of PLLA enhances with additional interactions between PLLA molecules and DMDBS nanofibrils that help to make the nucleation easier and faster for *Sc* crystallites than linear PLLA.

Figure 2 shows the DSC thermograms of a) PLLA, b) PLLA/PDLA (90:10) without Millad gel and c) PLLA/PDLA (90:10) with Millad gel by cooling rate of 10°C/ min.

Figure 3 shows the isothermal crystallization kinetics with the synergistic effect of Millad gel on the *Sc* crystallite formation. The crystallization half time ($t_{1/2}$) was decreased from 25 to 9 min at 100°C when the isothermal crystallization kinetics was studied from 90 to 120°C respectively.

The network of *Sc*-crystals formed by PLLA and PDLA confined the mobility of PLLA chain segments, thus decreasing the crystal growth rate, which influence the crystallinity of PLLA. The possible reason may be a part of PLLA cannot participate in a crystal, as it has been co-crystallized with PDLA as *Sc*-crystals[6].

The higher T_m of *Sc* crystallites also delayed thermal degradation of PLLA as observed from TGA analysis. The formation of *Sc* crystallites in PLA improves resistance to hydrolysis as compared with the hydrolysis of pure PLLA and PDLA.

More importantly, the presence of DMDBS (or DBS derivatives) in PLA shortens the processing time, improves mechanical properties and reduces the 'haze' in of the material.

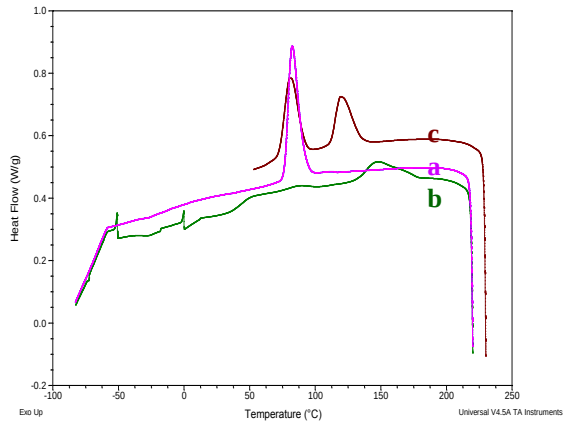


Fig. 2 : DSC thermograms of a) PLLA, b) PLLA/PDLA (90:10) without Millad gel and c) PLLA/PDLA (90:10) with Millad gel by cooling rate of 10°C/ min.

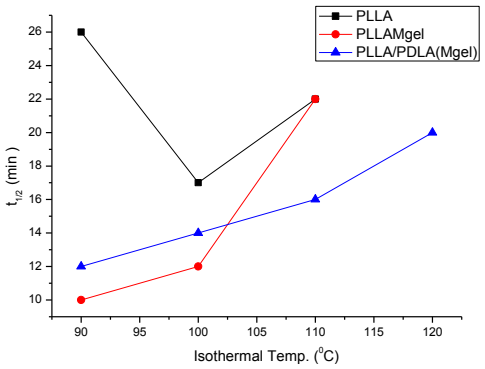


Fig. 3 : Isothermal crystallization kinetics of PLLA and PLLA/PDLA with Millad gel.

Conclusions

The decrease in T_g of PLLA from 58 to 45°C by the addition of Millad gel may be due to the plasticization effect which accelerates more number of stereocomplex crystallite formations. The crystallization half time ($t_{1/2}$) was decreased from 17 to 9 min at 100°C when the isothermal crystallization kinetics was studied from 90 to 120°C respectively. The crystallinity was increased 1.5 times due to the addition of Millad gel. The *Sc* crystallites formed and homogeneously dispersed in PLLA matrix as network of stereocomplex crystallites may be used as a nucleating agent for the further crystallization of PLLA.

Acknowledgements

The financial support received from Dr. S. Sivaram (Prof. S.S. Bhatnagar fellowship) is highly acknowledged.

References

1. Y. Ikada, K. Jamshidi, H. Tsuji, S.H. Hyon, *Macromolecules* 20, 904, 1987.

2. H. Tsuji, L. Bouapao, *Polym. Int.* 61, 442, 2012.
3. Brochu. S, Prud`home, R.; Barakat,I.and Jerome, R. *Macromolecules* 28, 5230 1995.
4. S.C. Schmidt, M.A. Hillmyer, *J. Polym. Sci. Part B: Polym. Phys.* 39, 300, 2001.
5. Y. Srithep, D. Pholharn, L. Turng, O. Veangin, J. Morris, *J. Polym. Engg.* 0357, 2015.
6. Wei-Chi Lai, *J. Phys. Chem. B*, 115, 11029, 2011.

MACRO 345

Processing and nanoclay induced piezoelectricity in poly(vinylidene fluoride-*co*-hexafluoro propylene) nanohybrid for device application

Anupama Gaur[1], Rahul Shukla[2], Kumar Brajesh[3], Sandeep Chatterji[4], Rajeev Ranjan[3] and Pralay Maiti[1,*]

[1]School of Materials Science and Technology, Indian Institute of Technology (Banaras Hindu University), Varanasi, 221005, India.
[2]Indus Synchrotrons Utilization Division, Raja Ramanna Centre for Advanced Technology, Indore,452013, India.
[3]Department of Materials Engineering, Indian Institute of Science, Bangalore, 560012, India.
[4]Department of Physics, Indian Institute of Technology (Banaras Hindu University), Varanasi, 221005, India.

Abstract:

Process and nanoparticle induced piezoelectric super toughened poly(vinylidene fluoride-co-hexafluoro propylene) (HFP) nanohybrids have been developed for device application. The nanohybrids have been prepared by incorporating organically modified nanoclay through solution route. The nanohybrids show improvement in toughness and modulus along with piezoelectric phase as compared to pure HFP. Piezoelectric phase has further enhanced to 75% in nanohybrid after uniaxial stretching of the thin film at moderately high temperature as compared to meager 18% β-phase before stretching. The structural changes including quantitative measurements have been confirmed through X-ray diffraction. The structural and morphological origins of super toughening phenomena have been worked out. The piezoelectric and pyroelectric coefficients (d_{33} and p) exhibit significant increase after stretching and the relative improvements are more in nanohybrid than that of pure HFP, arising from the presence of greater amount of β-phase in nanohybrid. Finally, fabrication of the unimorph has been performed using the high piezoelectric coefficient materials. The greater voltage generation under

impulse load is demonstrated for nanohybrid along with longer time response vis-à-vis pure HFP clearly indicating the superior piezoelectric device made using nanohybrid where the extent of piezoelectric phase is considerably higher.

Key words: Fluoropolymer; nanohybrid; structure; piezo- and pyroelectricity; device

INTRODUCTION:

Fluoropolymers like poly(vinylidene fluoride) (PVDF) and its copolymers with hexafluoropropylene (P(VDF-co-HFP)) are of technological importance because of their capability to crystallize in different forms, especially few of them are piezoelectric in nature. These polymers have applications in several fields such as sensors and actuators [1,2], having high abrasion, piezo- and pyroelectric behavior in addition to their uses in medical arena [3]. The crystalline structure of P(VDF-co-HFP) copolymer is similar to that of PVDF [4,5] while its flexibility and chemical resistance are considerably higher [5,6] due to lesser degree of crystallinity. Depending upon trans (T) and gauche (G) geometric chain configurations, it exists in several crystalline forms α, β, γ, δ and ε phases [7]. The α-phase ($TGT\bar{G}$) is inactive with respect to piezo- and pyroelectric properties, but the β-form (all trans, TTTT) shows ferroelectric properties which is suitable for electroacoustic transducer applications [8]. The β-form can be obtained from melt crystallization at high pressure [9,10], poling at high voltage [11,12], recrystallization of carbon coated oriented ultrathin film [13] and molecular epitaxy on the surface of potassium bromide [14]. Addition of nanoclay in PVDF shows the growth of the β-form and has been extensively utilized to enhance the mechanical, physical and thermal properties of polymer matrix [15-18]. This is one of the convenient ways to produce a polymeric piezoelectric material in bulk.

Two-dimensional nanoclay has greater advantage for structural amendment in presence of layered heterogeneity over the zero-dimensional fillers like silica and titania [19] where no change of structure is observed, or one-dimensional filler like CNT/nanorod [20] where there is a meager amount of β-phase on template due to dimensional constraints. Two-dimensional graphene sheets cause crystallization of primarily α-phase with a very less β-phase content as evident from the distinct spherulites in the hybrid [21]. It is apparent that the requirements of better compatibility and interaction of the filler and the matrix polymer is essential to generate the electroactive form in a polymer. Polar β-phase is the main factor for controlling the electronic properties and piezoelectric coefficient, d_{33} is a measure of the device performance. Stretching of the film is considered as one of the suitable methods to induce β-phase in polymer matrix, but the extent of the electronic phase restricts because of the brittleness of pure PVDF. A maximum of 74% β-phase is reported by deconvolution of FTIR peaks for pure PVDF [22]. Improvement in toughness in hybrid in presence of filler may help more piezoelectric β-phase to induce in fluoropolymers. Piezoelectric coefficients of PVDF, its copolymers and hybrids with CNT are reported, which depend on the copolymer composition, filler concentration and also on poling conditions [23]. Piezoelectric coefficient of PVDF in presence of nanoclay is also reported, where attempt of alteration of electronic structure is done by stretching at fixed draw ratio [24]. There is no report of the effect on piezoelectric coefficient of HFP copolymer in presence of nanoclay under uniaxial

stretching at different temperatures and device performances thereof.

In the present work, nanoparticles and process induced super toughening phenomena has been revealed. The nanohybrids of poly(vinylidene fluoride-co-hexafluoro propylene) with layered silicate is prepared through solution route. The morphology, nanostructures, crystalline structure, thermal and mechanical properties of the nanohybrids have been demonstrated in comparison to pure polymer. The extent of piezoelectric β-phase of nanohybrid has been enhanced to a significant amount under uniaxial elongation at different temperatures. Polarization under electric field has been measured to understand the extent of dipoles created through processing techniques and using nanoparticles. A device has been fabricated using the developed nanohybrid and its performance was evaluated and compared with pure polymer under similar processing condition.

EXPERIMENTAL SECTION:

Materials: A commercial SOLEF, 11008 copolymer of vinylidene fluoride and hexafluoropropylene, was used for the study, supplied by Ausimont, Italy. Henceforth, the copolymer will be termed as *HFP*. An organically modified clay, Cloisite 30B (bis-(hydroxyethyl) methyl tallow ammonium ion-exchanged montmorillonite), purchased from Southern Clay Inc., USA, was used as the nanofiller, whose density was 1.98 g/cc.

Preparation of nanohybrid: To prepare the HFP-nanoclay hybrid, dimethyl formamide (DMF) was used as solvent. Separate solution of HFP and dispersion of nanoclay (4wt% with respect to polymer) in DMF was mixed by stirring at 60 ºC for 1 hr. followed by sonication for 30 min to make homogeneous solution. The evaporation of the solvent in a Petri dish produced the nanohybrid which was kept at 60 ºC for one day under reduced pressure to remove trace amount of solvent from the nanohybrid. The nanohybrid will be termed as *NH*.

Sample preparation for characterization: The Compression molding technique was used to prepare the specimens. Thin sheet of samples (40 × 15 × 0.3 mm^3) for stretching in universal testing machine (UTM) at high temperature were prepared using a hot press compression molding machine (S.D.Instruments, India). Special care has been taken to produce air bubble free samples before stretching.

RESULTS AND DISCUSSION:

Influence of nanoparticle on structure and nanostructure:

Nanoclay embedded in polymer matrix has strong influence on the structure of polymer attached and nanostructure of the nanoparticle. The clay platelets are well dispersed in HFP matrix showing discrete layers of nanoclay as well as some tactoids as observed through bright field TEM image (**Figure 1a**). The intercalation of polymer molecules is primarily due to good interaction between nanoclay and HFP molecules as evident from the shifting of absorption peak at 252 nm of pristine nanoclay to 242 nm observed in nanohybrid (**Figure 1b**). The blue shift observed in nanohybrid arises from the constraint conformation caused by the insertion of polymer molecule inside the galleries. This is to mention that absorption peak of

pristine nanoclay

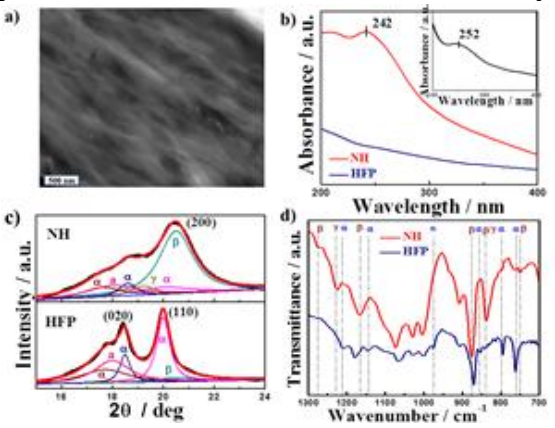


Figure 1: Structure and nanostructure a) Bright field transmission electron micrograph of HFP nanohybrid, b) UV-vis absorption spectra of HFP and nanohybrid. c) XRD deconvoluted diffractograms of HFP and nanohybrid and, d) FTIR spectra of pure HFP and nanohybrid.

appears from the olefinic double bond present in the organic modifier of the nanoclay while pure HFP does not show any absorption band in the energy range studied.

Apart from good dispersion, nanoclay induces piezoelectric smaller crystallite of β-phase as observed through deconvoluted XRD peaks (**Figure 1c**) [17]. HFP crystallizes in β form in presence of nanoclay as clear from the peak at 2θ~20.6^o (200/110 planes) against only α-form of pure HFP. Shifting of deconvoluted peaks towards higher 2θ at 18.08° (110), 18.6° (020) and 20.0° (110) peak in nanohybrid in comparison to 17.9° (100), 18.5° (020) and 19.9°(110) peak position of α-phase in pure HFP and the appearance of a new peak at 2θ~19.0^o in nanohybrid clearly indicates the formation of a metastable phase (distorted β or γ-conformation) in presence of nanoclay [25]. The crystallization of β-phase occurs on top and bottom of the silicate layers of nanoclay arising from the good interaction as mentioned earlier as revealed from the XRD peak position at 2θ~6.3^o corresponding to the inter planar distance of two crystallized zone below and above the individual silicate layer (*supplementary Figure S1*) [26]. The amount of β-phase content is estimated to be 18% in nanohybrid against the meager 0.1% in pure HFP, as calculated from the deconvoluted area fraction (**Figure 1c**). However, considerable amount of α- and amorphous phases are present in nanohybrid as evident from the deconvoluted XRD peaks. Pure HFP shows FTIR absorption bands of α-phase at 760, 797, 857, 975, 1144 and 1210 cm^{-1} which disappear in nanohybrid and instead the peaks at 749, 840, 878, 1165 and 1276 cm^{-1} appear, assigned for either β- or γ-phase including their distorted conformations (**Figure 1d**) [27,28]. Among these peaks, 840 cm^{-1} peak is due to both β- and γ-phase while the peak at 1227 cm^{-1} confirms the presence of γ phase in nanohybrid. However, the appearances of FTIR absorption bands at 749, 878, 1165 and 1276 cm^{-1} corresponds to pure β-phase occur in nanohybrid vis-à-vis pure HFP.

Processing induced phenomena:

Nanoclay induces the piezoelectric β-phase in HFP matrix but the extent is not sufficient (18%) for device application. Uniaxial stretching has been performed to induce more β-phase in presence of nanoparticle. Stretching condition has been optimized and 90 ^{o}C was found to be the optimum temperature for best elongation at break and highest toughness. Stress-strain curves for pure HFP and its nanohybrid at 90 ^{o}C are presented in **Figure 2a** showing higher stiffness and toughness of nanohybrid as compared to pure HFP. The toughness, area under the stress-strain curve, increases from 7 to 9.2 kJ/m^3 in nanohybrid as compared to pure HFP along with considerable increase in stiffness in

nanohybrid (1.06 to 1.59 MPa). This is worthy to mention that toughness values of pure HFP and its nanohybrid are 0.2 and 0.7 kJ/m^3, respectively, much less (more than one order in magnitude) than the values measured at 90 ^{o}C. The significant higher values of toughness in nanohybrid at higher temperature (90 ^{o}C) arise from the greater elongation at break (95 to 640%) at higher temperature predominantly due to ease of deformation at lower viscosity. However, the extension has very much increased (~6 folds) under uniaxial elongation at high temperature which helps improving the alignment of polymer chains in the direction of force field. Hence, it is expected that β-phase content should increase after uniaxial stretching at high temperature. **Figure 2b** compares the FTIR spectra of stretched samples vis-à-vis unstretched pure HFP and nanohybrid showing occurrences of distinct β-phase peaks at 749, 840, 880, 1168 and 1275 cm^{-1} in stretched samples against α-phase peaks at 759, 797, 854, 975, 1143 and 1211 cm^{-1} of unstretched HFP. This is to mention that the β-phase was present in unstretched nanohybrid while their intensities increase significantly after elongation and subsequently the peaks corresponding to the α-phase either disappear or diminished considerably.

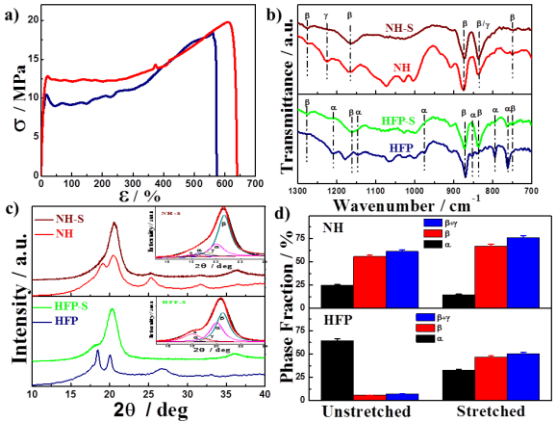


Figure 2: Effect of stretching a) Stress-strain curves for pure HFP and nanohybrid showing increase in elongation at break, b) FTIR spectra of pure HFP and nanohybrid stretched samples, c) wide angle X-ray diffraction pattern of pure HFP and nanohybrid stretched samples at 90 ^{o}C. d) Phase fraction of unstretched and stretched samples.

Structural change over after stretching at high temperature is also endorsed through XRD measurements. A change of structure from α to β is evident from the appearance of peak at 20.6^o due to (200/110) plane against 17.6^o (110), 18.6^o (020) and 20^o (110) of α-phase before stretching of pure HFP (**Figure 2c**). Intensity corresponding to β-peak in nanohybrid has significantly been enhanced after stretching with the suppression of α-phase peaks. The peaks are deconvoluted (**inset of Fig. 2c**) and the β-phase fractions have been calculated from the ratio of the peak areas. It is clear that major α-phase in unstretched HFP has been converted into β- and γ-phase in nanohybrid while the extent of piezoelectric phase has significantly been increased after stretching (**Figure 2d**). The formation of γ-phase is considerably low as compared to β-phase after stretching both for HFP and NH.

Now, it is pertinent to correlate the structural development with uniaxial stretching. Higher elongation at break or greater draw ratio [24] increases the molecular chain alignment in the direction of force field and greater alignment helps the HFP chain to crystallize in micro fibrillar all-trans planar zigzag conformation of β-phase. The conversion of amorphous phase into β-phase due to stretching is evident from the fact that considerable reduction of amorphous phase content after elongation both in HFP and nanohybrid (35→20% in HFP against 25→12% in nanohybrid stretched at 90 ^{o}C) (**Figure 2d**). Amorphous to β-phase conversion due to stretching is apparent

from the whitening of the film during elongation and increase of overall crystalline phase both for HFP and NH after stretching. Further, the formation of necking is considered as a starting point of the transformation from spherulitic pattern to needle like morphology, responsible for β-phase conversion from the α-phase [29,30]. However, higher β-phase is evident after stretching while the extent is significantly higher in nanohybrid and expects greater ferroelectric responses in nanohybrid in presence of nanoclay, nucleating agent of β-phase. Moreover, total 75% piezoelectric phase is observed in nanohybrid as opposed to only 50% noticed in pure HFP after controlled stretching at optimized conditions. Elongation temperature has a significant role towards β-phase transformation and much higher temperature (120 ^{o}C) increase the chain mobility causing crystallization of thermodynamically feasible α-phase [23,29]. Thus, an optimized temperature window has been found to generate maximum transformation to β-phase for possible device applications.

Piezoelectric responses and device fabrication:

Up to now, we have shown that the developed material is highly piezoelectric and pyroelectric especially in nanohybrid in presence of nanoclay and the piezoelectric phase has been increased considerably through processing of the nanohybrid. The piezoelectric coefficient, d_{33} is an important parameter for piezoelectric materials and values are reported in **Figure 3a**. The unstretched

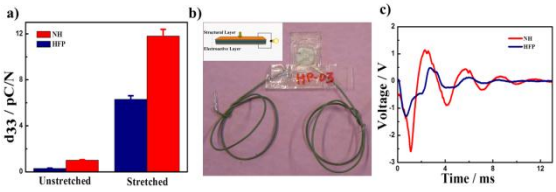


Figure 3: a)Piezoelectric coefficient for pure HFP and nanohybrid before and after stretching b) Representation of assembly of device, c) Image of a fabricated unimorph, and, d) Output voltage response as a function of time.

samples show very low d_{33} values of 0.3 and 1 pC/N for pure HFP and nanohybrid, respectively, while the corresponding values increase considerably to 6.8 and 12 pC/N after stretching (poled at 450 kV/cm) indicating improvement in piezoelectricity due to induction of β-phase in presence of nanoclay and induced through uniaxial elongation. However, it is pertinent to mention that higher β-phase content samples, either in presence of nanoclay or induced through processing, show greater d_{33} values which are suitable for piezoelectric devices.

We have fabricated the unimorph using the high piezoelectric coefficient materials NH and HFP following the technique as mentioned in the experimental section. **Figure 3b,c** shows the assembly of device and image of the unimorph. The voltage responses under impulse load are compared for HFP and nanohybrid as a function of time (**Figure 3d**). It is clear that nanohybrid shows the greater voltage generation along with longer time response vis-à-vis HFP. The unimorphs clearly demonstrate the superior piezoelectric device made using nanohybrid where the extent of piezoelectric phase is considerably higher. In brief, novel piezo- and pyroelectric polymer nanohybrid has been developed using two dimensional nanoparticle and thereby applying special processing technique with greater coefficients which shows considerably greater piezoelectric device performance. Moreover, the novel piezoelectric and ferroelectric properties of developed

nanohtybrid are of greater values for future applications.

CONCLUSIONS

The nanohybrid of HFP copolymer with organically modified nanoclay has been prepared through solution route. Finer dispersion of nanoclay in polymer matrix along with blue shift in UV absorption indicates the good interaction between the components. Nanoclay induces the piezoelectric β-phase in polymer which is further enhanced through processing technique by uniaxial stretching at moderately high temperature. Improvement in mechanical properties, both stiffness and toughness, of nanohybrid has been reported as compared to pure HFP. The maximum value of all-trans planar zigzag conformation of β-phase (75%) was obtained at 90 ^{o}C under stretching. The structural change over and its quantitative measurement has been confirmed through XRD, FTIR studies. The enhancement of piezoelectric β-phase in nanohybrid has been reflected in higher piezoelectric coefficient than that of pure HFP. The unimorphs are made using higher coefficient of HFP and its nanohybrid samples. The voltage response under impulse load is much higher in nanohybrid as compared pure HFP along with the longer response time indicating much better piezoelectric device performance using nanohybrid.

Acknowledgments:

AG acknowledges the Institute for her teaching assistantship and RS thankfully acknowledges the support of Laser Materials and Device Development Division for d_{33} measurements of polymer films.

References:

1. Lee, C. S.; Joo, J.; Han, S.; Koh, S. K. *Appl. Phy. Lett.* **2004**, 85, 1841.
2. Khanna, P. K.; Hornbostel, B.; Grimme, R.; Schäfer, W.; Dorner, J. *J. Mater. Chem. Phy.* **2004**, 87, 173–178.
3. Valentinia, R.F.; Vargob, T. G.; Gardellac, J. A.; Aebischerd, P. *J. Biomater. Sci. Polym. Ed.***1994**, 5(1-2), 43-36.
4. Huan, Y.; Liu, Y.; Yang, Y. *Polym. Eng. Sci.* **2007**, *7*(10), 1630.
5. He, X.; Yao, K.; Gan, B. K. *J. Appl. Phys. Volume,* **2005**, 97(8), 084101-6.
6. Moggi, G.; Bonardelli, P.; Bart, C. J. *Polym. Bull.* **1982**, *7*, 115-122.
7. Adema, E.; Rickards, J.; Burillo, G.; Avalos-Borja, M. *Radiat. Phy. Chem.* **1999**, 54, 637-641.
8. Tashiro, K.; Tadokoro, H.; Kobayashi, M. *Ferroelectrics* **1981**, *32*,167.
9. McGrath, J. C.; Ward, I. M. *Polymer*, **1980**, 21(8), 855–857.
10. Tamura, M.; Ogasawara, K.; Ono, N.; Hagiwara, S. *J. Appl. Phy* **1974**, 45, 3768.
11. Scheinbeim, J.; Nakafuku, C.; Newman, B. A.; Pae, K. D. *J. Appl. Phy.***1979**, 50, 4399.
12. Newman, B. A.; Yoon, C. H.; Pae, K. D.; Scheinbeim, J. I. *J. Appl. Phy.***1979**, 50, 6095.
13. Wang, J.; Li, H.; Liu, J.; Duan, Y.; Jiang, S; Yan, S. *J. Am. Chem. Soc.*, **2003**, 125, 1496-1497.
14. Lovinger, A. J. *Polymer*, **1981**, 22(3), 412-413
15. PRIYA, L.; JOG, J. P. *Journal of Polym. Sci., Part B: Polym. Phy.* **2002**, 40, 1682–1689.
16. PRIYA, L.; JOG, J.P. *Journal of Polym. Sci., Part B: Polym. Phy.* **2003**, 41, 31–38.
17. Shah, D.; Maiti, P.; Gunn, E.; Schmidt, D. F.; Jiang, D. D.; Batt,C. A.; Giannelis, E. P. *AdV.Mater*, **2004**, *16* (14), 1173-1177.
18. Shah, D.; Maiti, P.; Jiang, D. D.; Batt, C. A.; Giannelis, E. P. *AdV.Mater*, **2005**, 17(5), 525-528.

19. Li, J.; Seok, S.; Chu, B.; Dogan, F.; Zhang, Q; Wang, Q. *Adv. Mater*. **2009**, 21, 217–221.
20. Manna, S.; Nandi, A. K. *J. Phys. Chem. C*, **2007**, *111*, 14670-14680.
21. Yu, J.; Jiang, P.; Wu, C.; Wang, L.; Wu, X. *Polym. Compos.***2011**, 32, 1483-1491.
22. Liu, Y. L.; Li, Y.; Xu, J. T.; Fan, Z. Q. *ACS Appl. Mater. Interfaces.***2010**, 2(6), 1759-1768.
23. Salimi, A.; Yousefi, A. A. *Polym. Test.* **2003**, 22, 699-704.
24. Tiwari, V. K.; Prasad, A. K.; Singh, V.; Jana, K. K.; Misra, M.; Prasad, C. D.; Maiti, P. *Macromolecules*, **2013**, 46, 5595-5603.
25. Lopes, A. C.; Costa, C. M.; Tavares, C. J.; Neves, I. C.; Mendez, S. L. *J. Phys. Chem. C* **2011**, 115, 18076-18082.
26. Tiwari, V. K.; Shripathi, T; Lalla, N. P.; Maiti, P. *Nanoscale*, **2012**, 4, 167-175.
27. Layek, R. K.; Samanta, S.; Chatterjee, D. P.; Nandi, A. K. *Polymer*, **2010**, 51, 5846-5856.
28. Manna, S.; Nandi, A.K. *J. Phys. Chem. B* **2011**, 115, 12325-12326.
29. Gregorio, R.; Ueno, E. M. *J. Mater. Sci.***1999**, 34, 4489 -4500.
30. Matsushige, K.; Nagata, K.; Imada, S.; Takemur, T. *Polymer* **1980**, 21(12), 1391-1397.

MACRO 346

Optimization of PMMA Microcapsules using Taguchi Approach to Improve Self-Healing Performance of Polymer Composites

Sharma, Shilpi*; Choudhary, Veena; and Nibhani, Leena

Centre for Polymer Science & Engineering, Indian Institute of Technology Delhi, New Delhi (India)
Shilpi.16.sharma@gmail.com

Abstract

The present study is aimed to optimize the process parameters for the synthesis of epoxy loaded poly-(methylmethacrylate) microcapsules for the application of polymeric self healing (SH) composites. Effect of surfactant concentration (SC), core to shell ratio (CSR), temperature (T), agitation speed (AS) were considered as the influencing parameters which affects the encapsulation efficiency (EE) and core content (CC) % of the synthesized microcapsules. Various studies have been suggested that CC% plays the vital role in SH of composites. In this paper CC% of microcapsules was considered as the characteristic property and used for all analysis. PMMA polymer was used as a shell wall material and diglycidyl ether of bisphenol-A (DGEBA) was used as a core material for the synthesis of microcapsules. These microcapsules were prepared by water-in-oil solvent emulsion and evaporation method. Taguchi orthogonal array (OA) with L_{25} design for a four parameter five level design was used to optimize the reaction parameters, which reduces number of experiments from 625 cases to 25 cases and the signal-to-noise (S\N) ratio analysis were used to identify the optimum levels of parameters based on the highest CC%. Subsequently, analysis of variance (ANOVA) is performed to determine the significance of various parameters. MINITAB-17 software was used for all analysis. Free flowing, white colour and odourless microcapsules were obtained by solvent evaporation method. (S\N) ratio analysis identifies the optimum levels of various parameters. Taguchi analysis predict that at (10wt% SC, 1:3 CSR, 40 T and 300 AS) optimization conditions synthesized microcapsules can give 66.36 CC% and ANOVA analysis indicate that the SC is the most significant parameter compare to CSR, T, and AS in the improvement of CC% of the synthesized microcapsules. Confirmation experiments were performed to validate the Taguchi result on the predicted optimum process parameters and levels which gave the microcapsules with 63 CC%. The optimized microcapsules were characterized structurally (FTIR & ^{1}H-NMR), morphologically (OM and SEM) and thermally (TGA).The result indicates that the Taguchi method can predict the response satisfactorily.

Keywords: Microcapsule, Epoxy resins, Poly - (methylmethacrylate)

References

[1] Brown, E.N; Kessler, M.R; Sottos, N.R and White, S.R. Journal of microencapsulation, 20 (2003) 719-730.

[2] Q.Li; Siddaramaiah; Kim, N.H; Hui, D and Lee, J. H. Composites Part B: Engineering, 55 (2013) 79-85.

MACRO 348

Solvent-Free, Photocurable Mussel-Inspired Polyester Adhesive from Renewable Resources for Underwater Adhesion

Amal Narayanan[a], Qianhui Liu, Ying Xu, Abraham Joy*

[a] *Department of Polymer Science, The University of Akron, Akron, Ohio 44325, United States*

**abraham@uakron.edu*

Mytilus edulis (mussel) is known for its ability to adhere to a wide range of substrates under water. The adhesion and cohesion are brought about by the post-translationally modified amino acid sequences in the mussel foot proteins, such as L-*3,4*-dihydroxy phenylalanine and *o*-phospho-L-serine. Inspired by mussel adhesion, we have developed a three component, solvent-free underwater copolyester adhesive. The adhesive was designed to flow at room temperature such that it can be dispensed without the addition of any solvent. This feature was achieved by the design of a monomer with amide substituted hydrophobic aliphatic chains derived from soybean oil. The aliphatic chains also provide a hydrophobic environment which does not allow water infiltration. A second diol was designed with catechol units to provide adhesive interactions with the substrate. A third diol with coumarin pendant groups provided temporal control of polymer chain-crosslinking, leading to an increase of cohesive interactions in the adhesive.

In lap-shear strength measurements, 20.0 mg of polymer spread onto oxidized glass slides and exposed to 5 min UV irradiation ($\lambda \sim 350$ nm, power on substrate = 0.5 W/cm^2) on a lap-joint (area = 6.45 cm^2) displayed lap-shear strength of 0.90 MPa. The underwater spreading and immersion of the lap-joint underwater for 24 h did not decrease the lap-shear strength of the adhesive. Additionally, the lapshear strength of polymer when applied underwater on lap-joints of glass and various substrates (aluminum, stainless steel, polyethylene, poly(methylmethacrylate), porcine skin) showed that the above adhesive could be used as underwater adhesives on various substrates.

References

1. Waite, J. H. *Int. J. Adhes. Adhes.*, *7* (1987) 9−14.
2. Seo, S.; Das, S.; Zalicki, P. J.; Mirshafian, R.; Eisenbach, C. D.; Israelachvili, J. N.; Waite, J. H.; Kollbe Ahn, B. *J. Am. Chem. Soc.*, *137* (2015) 9214−9217.
3. Wei, W.; Petrone, L.; Tan, Y. P.; Cai, H.; Israelachvili, J. N.; Miserez, A.; Waite, J. H. *Adv. Funct. Mater*, *26* (2016) 3496-3507.
4. Gokhale, S.; Xu, Y.; Joy, A. *Biomacromolecules*, *14* (2013) 2489-2492.

MACRO 349

Novel Polysiloxanes with Inherent Flame Retardancy: Synthesis and characterisation

K. Indulekha [a*], Deepthi Thomas[b], R.S. Rajeev[a] , Gouri Cheruvally[c]

[a]*Polymers and Special Chemicals Division,*

[b]*Analytical and Spectroscopy Division,*

[c]*Polymers and Special Chemicals Group,*

Vikram Sarabhai Space Centre, Thiruvananthapuram 695 022, Kerala, India

**Corresponding author: k_indulekha@vssc.gov.in*

Abstract

Novel, unfilled and hyperbranched silicone polymers with inherently high flame retardancy are reported for the first time in this paper. A series of hyper branched $^{Me}D^{Ph}D^{Vi}T$ resins were synthesized by the acid catalysed copolymerization of dimethyldiethoxysilane (DMDES), diphenyldimethoxysilane (DPDES) and vinyltriethoxysilane (VTES). The polymers were characterized by Fourier transform Infrared Spectroscopy (FTIR) and Nuclear Magnetic Resonance Spectroscopy (NMR) (1H, 29Si nuclei). All the copolymers with VTES showed an onset temperature of decomposition above 250°C with char yields greater than 50% at 900°C, attributed to the retardation of depolymerisation by T-unit. The limiting oxygen index (LOI) of the copolymers bore a direct relation with VTES content and increased from 26% to 37% with increase in VTES content in the feed.

***Key words**: siloxane, hyper branched, T-resins, flame retardancy, char yield*

Introduction

Thermal degradation of conventional flame retardant polymeric formulations leads to evolution of toxic and corrosive gases such as halogens, raising serious environmental concerns. Industries including aerospace, construction, electrical, electronics and transportation demand halogen- free flame retardant systems for minimizing the environmental pollution [1-5]. These new materials require properties such as good thermo-oxidative stability, inherently low flammability and retention of material strength at elevated temperatures, low corrosion and better fatigue resistance, lower tooling costs and relative ease of fabrication.

Almost all resins do not have suitable flame retardancy and flame retardancy is achieved through the incorporation of flame retardant additives. There is a great demand for new polymers with inherent flame retardancy, devoid of halogen in the polymer structure and which do not require halogenated additives for achieving flame resistance.

Among many halogen free flame retardants, those based on siloxane systems play a pivotal role with a surface protective mechanism. Though reports are available where the thermal stability and flame retardancy of silicone polymers are improved by the incorporation of fillers, only few reports are available where silicones are rendered inherently flame retardant by means of modification of the polymer structure.

Recently, hyperbranched siloxane polymers have attracted considerable attention due to their remarkable properties owing to the large number of reactive end-groups within a molecule compared to their

linear analogues [6-9]. Multiple numbers of reactive end-groups enable further tailoring of the molecules.

In the present study, poly(dimethyl-co-diphenyl)siloxane linear chain is modified with vinyl triethoxysilane branching units to form thermally stable, flame retardant polymers. To the best of our knowledge, this is the first time reporting of an unfilled siloxane polymer devoid of hetero atoms in the backbone exhibiting high limiting oxygen index resulting in a halogen free and environment friendly polymer with inherent flame retardancy.

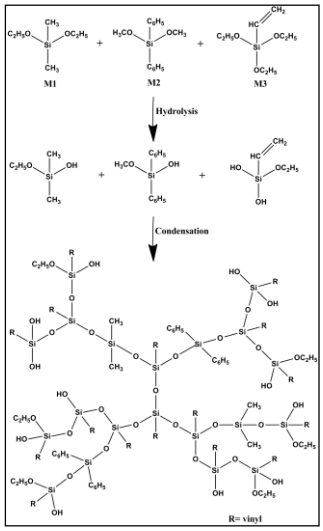
Experimental

Materials

Monomers, M1 (Dimethyl diethoxysilane (DMDES)) and M2 components, methyltris(methylethylketoxime) silane (MOS) and Dibutyltindilaurate (DBTDL) were obtained from M/s. Arima & Co. Meghalaya and Aldrich respectively. 6M aqueous solution of HCl was used as the polymerization catalyst.

Synthesis of $^{Me}D^{Ph}D^{Vi}T$ resins

Vinyl triethoxy silane (ViT) modified poly(dimethyl-co-diphenyl) siloxane polymers (MeDPhDViT resins), with varying MeD/ViT ratios (P1 to P6) were synthesized, as shown in Scheme 1. Details of the processed compositions are given in Table 1. (diphenyldimethoxysilane (DPDMS)) were obtained from Aldrich. Vinyltriethoxy silane (VTES) [M3] was procured from Alfa-Aesar. The curing under ambient conditions. The mechanism of cure involves hydrolysis of MOS to result with trisilanol(I) which further condenses



Scheme1.Synthesis of $^{Me}D^{Ph}D^{Vi}T$ resins

Curing of the polymers

The above obtained copolymers (Part A) were cured to corresponding elastomers by tin assisted polycondensation mechanism. Curing agent (Part B) was prepared by mixing MOS and DBTDL in the ratio 100:5 by volume. Curing initiates on admixing 10g of Part A with 0.8 ml of Part B and the blend got completely cured on keeping for 48 hrs

with hydroxyl groups in the polymer to form cross-linked structure through Si-O-Si linkages

Table 1. Formulations for the preparation ofvarious polymers

Reference of Polymer	M1 (DMe, mole%)	M2 (DPh, mole %)	M3 (^{Vi}T, mole %)	^{Me}D/ViT	Viscosity (cP)
P1	90	10	-	-	35
P2	75	10	15	5	115
P3	60	10	30	2	250
P4	45	10	45	1	440
P5	30	10	60	0.5	5750
P6	15	10	75	0.2	-

Results and Discussion

Synthesis and characterization of hyperbranched polymers

Copolymerization of the monomers, M1, M2 and M3 was carried out by H^+ assisted polycondensation by keeping mole percentage of M2 constant (10%) while M1 and M3 mole percentages were varied to get P2 to P6. The composition details are provided in Table 1. A mixture of dimethyl, diphenyl and vinyl silanols was polymerised to result in copolysiloxanes of varying branching unit contents. Terminal SiOH moieties underwent condensation in the presence of acid catalyst as shown in Scheme 1. The ^{1}H NMR spectra of different resins were recorded to confirm their structure. As typical example, ^{1}H NMR spectra of P5 is given in Fig.1. Chemical shift between 0.05 and 0.30 ppm (S1) was due to Si–CH_3 [10]. The multiplet appearing between 7.4 and 7.8 ppm is attributed to the phenyl groups which are present in all the systems. Chemical shift between 5.6 and 6.2 ppm is assigned to Si–CH=CH2. Signals appearing at 1.0-1.2 ppm and 3.7-4.0 ppm are attributed to β and α hydrogens of –OCH_2CH_3 groups respectively and those at 2.5-2.8ppm are attributed to hydroxyl groups on Si atom.

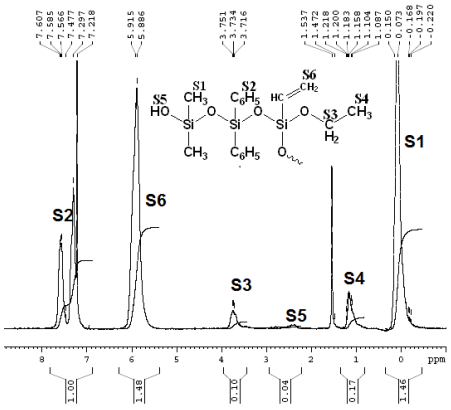


Fig. 1. ^{1}H NMR spectrum of P5

The infrared absorption spectra corresponding to the copolymers with different vinyl content are shown in Fig. 2. A strong absorption band at 1130 cm^{-1} to 1000 cm^{-1} is attributed to the Si–O–Si asymmetric stretching vibration [26]. Absorptions at 2963

cm^{-1} and 2905 cm^{-1} were assigned to the C–H stretching in $–CH_3$ which are more intense in the case of P1 when compared to others.

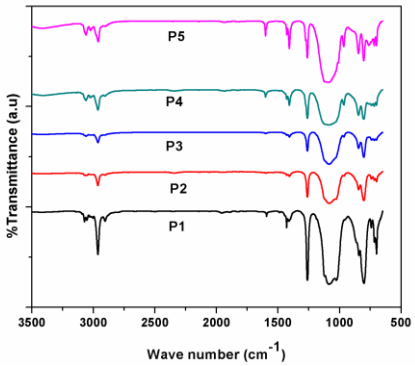


Fig. 2. FT-IR spectra of copolymers

Thermal stability

TGA was done to assess the high temperature performance of the crosslinked polymers and the thermograms are shown in Fig. 3. As can be seen, polymers P2 to P5 showed high char yields under nitrogen. On moving from P1 to P5, char yield at 900°C increases from 17% to 85%. The decomposition temperatures at 5% weight loss (Td5) for all the copolymers were above 250°C and a positive shift in onset decomposition temperature is observed with increase in VTES content, and it reached 543°C in P5, where branching sites are maximum.

Flammability studies: Since char yield increased with increasing vinyl content, it is interesting to inspect the flame resistance characteristics of these polymers. A systematic improvement in LOI is observed with increase in the vinyl content and it reached upto 37% in the case of P5 which is quite high for an unfilled silicone system. Fig. 4 depicts the relation between char yield and LOI on vinyl content in the copolymer.

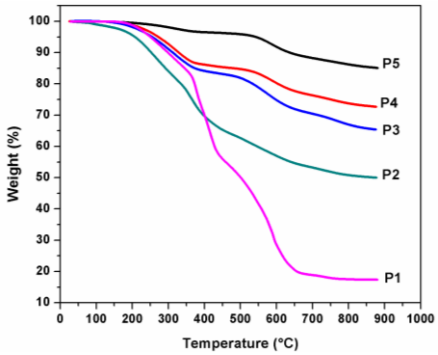


Fig.3. Thermograms of different copolymers

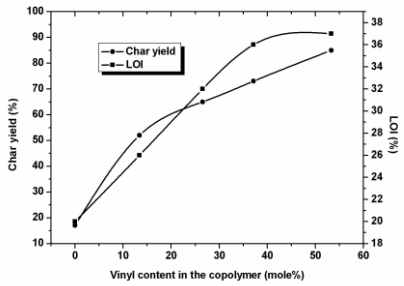


Fig. 4. Char yield & LOI vs vinyl content in the copolymer

Conclusions

A series of $^{Me}D^{Ph}D^{Vi}T$ resins with varying vinyl content were synthesised via acid-catalysed condensation of alkoxy silanes and characterised. All the polymers yielded high char residue at 900^0C in nitrogen atmosphere. The incorporation of the vinylated T- unit suppressed the depolymerisation reactions leading to the formation of cyclic siloxanes. The silicone resin systems exhibited high LOI when compared to conventional linear systems and

it reached upto 37% in the case of resin system with 53.3 mole% vinyl T-unit, which is unique for the present system. Thus the synthesised resin systems are promising flame retardants without requiring the incorporation of any hetero atom or flame retardant additives.

References

1. Y.L. Liu, S.H. Lee, Macromol Rapid Commun. 25 (2004) 1392.
2. H. Huang, M. Tian, L. Liu, Z. He, Z. Chen, L. Zhang, J. Appl. Polym. Sci. 99 (2006) 3203.
3. D. Zhuo, A. Gu, G. Liang, J. Hu, L. Yuan, X. Chen, J. Mater. Chem. 21 (2011) 6584.
4. R. Mosurkal, R. Kirby, W.S. Muller, J.W. Soares, J. Kumar, Green Chem. 13 (2011) 659.
5. S. Ravichandran, S. Nagarajan, B.C. Ku, B. Coughlin, T. Emrick, J. Kumar, R. Nagarajan, Green Chem. 14 (2012) 819.
6. L. Ji, A. Gu, G. Liang, L.Yuan, J. Mater. Sci. 45 (2010)1859.
7. A. Asif, W.F. Shi, X.F. Shen, K.M. Nie, Polymer 46 (2005)11066.
8. Z. Dongxian, G. Aijuan, L. Guozheng, H. Jiang-tao, C. Lei, Y. Li, Polym Degrad Stab 96 (2011) 505.
9. Y.H. Chia, C.S. Wen, S.W. Chuan, K. L. Liang, Y.H. Keh, L. L. Ying, Polymer 54 (2013) 2945.
10. A.L.Smith, JohnWiley & Sons, Inc. (1974).

MACRO 350

Dual Functional HQ-Resins: Promising One Shot Tool for both Reinforcement and Crosslinking in Transparent Silicone Polymers

P.S. Drishya[a], K. Indulekha[b]*, R.S. Rajeev[b]

[a]S.N, College, Kollam

[b]Polymers and Special Chemicals Division,

Vikram Sarabhai Space Centre, Thiruvananthapuram-695 022

**Corresponding author: k_indulekha@vssc.gov.in*

Abstract

Herein, we report the synthesis of MQ silicone resins with hydride functionality (HQ resins) by using tetraethoxysilane and 1,1,3,3,-tetramethyldisiloxane by sol-gel route. Resins weresynthesised by altering the catalyst concentration and characterized by FT-IR, ^{1}H NMR, and ^{29}Si NMR. The resin thus synthesised is reactive blended to vinyl functional PDMS in different proportions in

presence of Pt catalyst and the effect of incorporation of HQ resins on optical properties of the co-cured polymers are investigated. It is found that RI of PDMS is unaltered on incorporating HQ resin (up to 100phr). Further, we investigated the adhesive properties of the co-cured systems and found that with increasing concentration of HQ in the system, interface properties improved without affecting optical transparency. Thus the potential of HQ resins as both reinforcing filler and

crosslinking agent for optically transparent siloxane system is proven.

Keywords: *silicone, optical transparency, HQ-resins, adhesive*

Introduction

Silicone resins consist of highly branched polymer structures. Considered in detail, they are networks of irregular, mainly tri- or tetrafunctional structural units. Because they can be combined with many organic polymers, it is possible to tailor the numerous properties of silicone resins, e.g. their curing behaviour, flexibility, adhesion properties or weathering resistance. The outstanding heat resistance of silicone resins is particularly striking. They can sustain high temperatures of 200 to 250 °C in continuous service, and even up to 600 °C for brief periods. Their dielectric behaviour is ideal. Moreover, silicone resins' excellent oxidation resistance and superior mechanical properties make them particularly durable and economic materials.

Silicone resins' excellent heat resistance and outstanding range of properties are also very much in demand for electrical applications, such as binders for fiberglass laminates and cements for incandescent lamp bases, or impregnates for electrical windings. In addition, they are useful as water repellents in masonry protection or as binders in silicone resin facade paints.

Silicone resins are a type of silicone material which is formed by branched, cage-like oligosiloxanes with the general formula of $R_nSiX_mO_y$, where R is a non reactive substituent, usually Methyl (Me) or Phenyl (Ph), and X is a functional group Hydrogen (H), Hydroxyl group (OH), Chlorine (Cl) or Alkoxy group (OR). These groups are further condensed in many applications, to give highly crosslinked, insoluble polysiloxane networks[1].

MQ silicone resins representa broad range of hydrolytic condensation products of monofunctionalsilane (M) and tetrafunctionalsilane (Q) and they find application such as pressure sensitive adhesives, rubbers, coatings and additives [2,3]. MQ silicone resins of molecular weight in the range of 1000-10000 are very useful in using as pressure sensitive adhesives, silicone rubbers, coatings, additives and so on. MQ silicone resins are mainly synthesized from water glass, therefore, when ethyl silicate is used as starting material, the structure of MQ resins can be controlled easily and gel formation can be avoided effectively[4]. However, ethyl silicates are expensive,

resulting in limitations to its wide application in preparing MQ silicone resins. In contrast water glass is cheap and readily available. More recently, water glass and hexamethyldisiloxane (HMD) have been used as starting materials for the synthesis of MQ silicone resins[5]. The MQ silicone resins can be used as fillers for silicone adhesives.

Herein, we report the synthesis of MQ silicone resins with hydride functionality (HQ resins) by using tetraethoxysilane (TMDS) and 1,1,3,3,-tetramethyldisiloxane by appropriate synthetic strategies. This novel material find place as cross-linker for addition curable silicone matrix as well as filler material in siloxane matrix to improve the strength while retaining transparency.

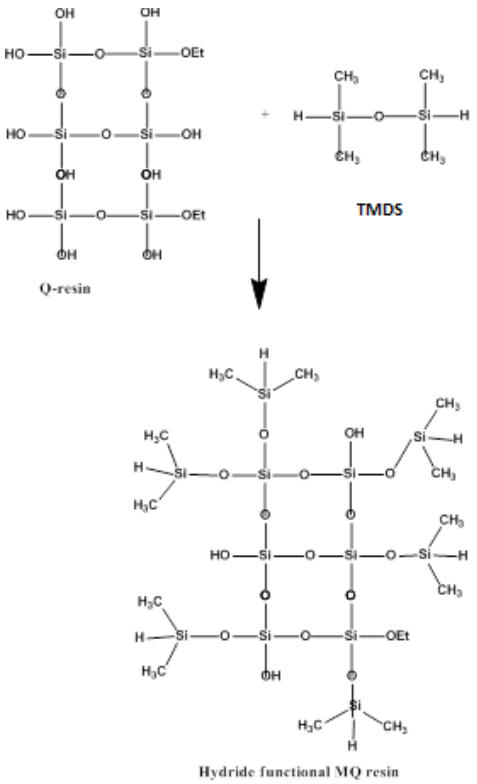
EXPERIMENTAL

Materials

Monomers, Tetraethoxysilane (TEOS) and 1,1,3,3-tetramethyldisiloxane (TMDS) and Pt catalyst, Pt(0)1,3-divinyl-1,1,3,3 tetramethyldisiloxane complex in vinyl terminated PDMS were obtained from Sigma Aldrich. All these chemicals were used as received. HCl was used as the polymerization catalyst. Toluene procured from Qualigens was used as received.

Synthesis of HQ resins

Synthesized HQ silicone resin by the tetra-ethoxysilane (TEOS) and TMDS reactionas per Scheme 1. In a typical case, to a three necked flask equipped with a stirrer and thermometer, 30ml ethanol is added with stirring followed by the addition of 15ml TEOS. After vigorous stirring, measured volume of HCl is added dropwise followed by addition of 30ml water. After 4 hours, 20ml 1,1,3,3-tetramethyldisiloxane is added and stirred for half an hour. During the entire process, temperature was kept as 50°C.



Scheme 1. Synthesis of HQresin

Characterization techniques

FT-IR Spectra of the synthesized polymers were taken using a Perkin Elmer Spectrum GX A FTIR spectrometer. 1H NMR and 29Si NMR spectra were recorded using a 300 MHz BRUKER Nuclear Magnetic Resonance spectrometer (Bruker, Germany), using CDCl3 as the solvent. Chemical shifts (δ) are expressed in ppm, downfield using tetramethylsilane (TMS) as

an internal standard. The thermal decomposition behavior of the cross-linked polymeric systems was studied using TA instruments SDT Q-600 simultaneous thermogravimetric–differential scanning calorimetric analyzer.

Results and Discussion

TEOS was the source of the Q unit and the TMDS was the source of the M unit. H-functional Q-resins (HQ resins) are synthesised by the condensation of TEOS in presence of HCl followed by capping with TMDS. Here, we have synthesised HQ resins by using 1 ml of HCl as catalyst.

Fig.1 shows the ^{1}H NMR spectra of HQ resinwhere the signalcentered at 0.2 ppm is the resonance of the methyl proton, and that at 1.2 ppm and 3.8 ppm representsethoxygroup.The signal appeared at 4.6 ppm corresponds to Si-H group. Presence of equal intensity signals correspong to methyl proptons and Si-H protons confirms the inclusion of H-containing M unit to the Q-resin.Further, the residual ethoxy group is very low in this resin which implies complete condensation of TEOS and effective capping with H-containing M-unit.

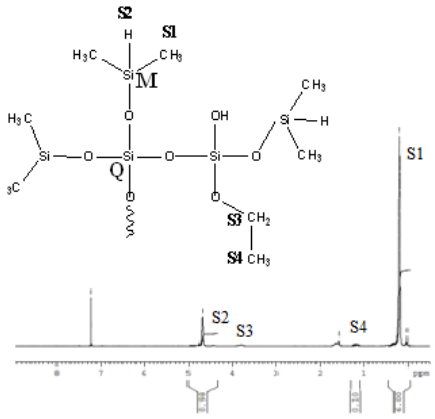


Fig.1^{1}H NMR spectrum of H-functional Q-resin

Further, the structure of HQ resin was examined by FT-IR and the spectrum is given as Fig.2. The broad absorption at 3100-3500 cm^{-1} was attributed to O-H stretching vibration of Si-OH. The peak at 2148 cm^{-1} is the characteristic absorption ofSi-H group. The sharp peak at 2962 and 2902cm-1 was because of the symmetric -CH3 and asymmetric C-H hydrocarbon portion of the resin. The strong peak at 1082 cm^{-1} belongs to Si-O-Si groups. The characteristic absorption of M unit were 2963, 756, 842, and 1257 cm^{-1}. Additionally, the appearance of the wide peak at 3100–3500 cm^{-1} expressed an indication of hydrolysis of the ethoxy group of the TEOS, as well as the peak at 1082 cm^{-1} and an indication of condensation of the hydroxyl groups of the TEOS and TMDS.

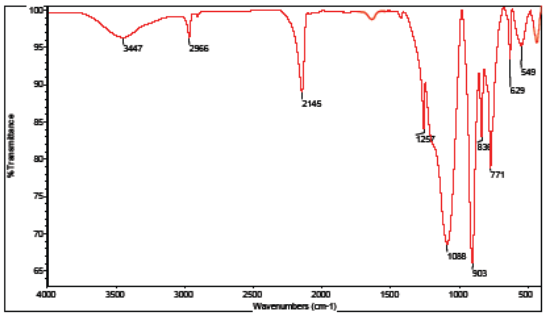


Fig.2 FT-IR spectrum of H-functional Q-resin

Figure 3 shows the ^{29}Si NMR spectrum of HQ-resin. The sharp signals at 12 ppm belongs to M unit and the signals at -100 ppm is due to Q-unit.

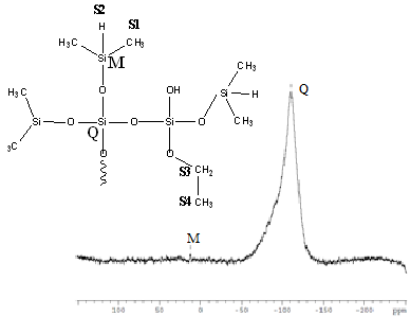
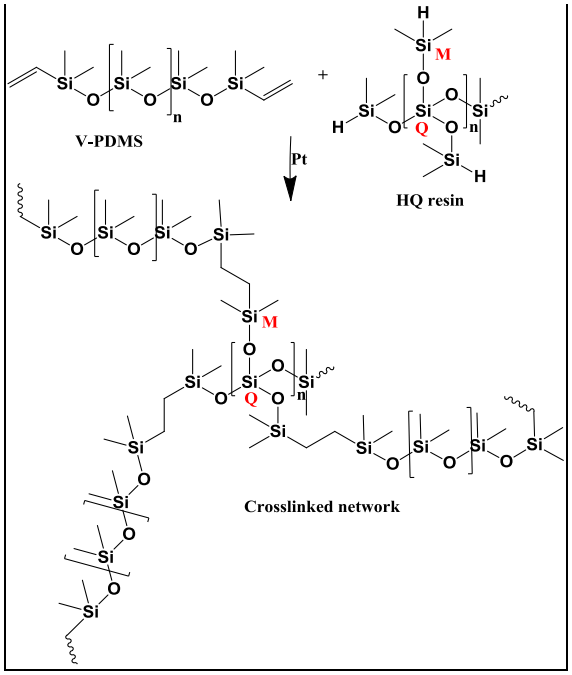


Fig.3 ^{29}Si NMR spectrum of Q-resin

Since we found HQ resins are having active hydride functionality, further we explored its possibility as both filler and curing agent in V-PDMS matrix. For that, we have incorporated different weight loadings of Q-resin to V-PDMS and the systems are cured by means of Pt assisted hydrosilylation, as depicted by Scheme 2.



Scheme 2. Curing mechanism of HQ resin filled V-PDMS

To evaluate the adhesive strength of these systems, LSS were done on Aluminum substrates and Table 1summarises the different results obtained.

Table 1: LSS of HQ resin filled V-PDMS

System	Average LSS (ksc)
V-PDMS	**1.73**
V-PDMS+20 phr HQ	**5.06**
V-PDMS+40 phr HQ	**5.15**
V-PDMS+ 60 phr HQ	**3.73**
V-PDMS+ 80 phr HQ	**3.86**
V-PDMS+100 phrHQ	**4.7**

There is significant improvement in the LSS on V-PDMS with the incorporation of HQ resins. System with 40 phr HQ resin loaded system exhibit maximum interface properties. Hence, HQ resin is identified as a

novel material to impart cohesive strength as well as cross-linking in addition curable silicone systems, which finds potential applications as transparent silicone adhesives for space applications.

REFRACTIVE INDEX

Since refractive index is a measure of optical transparency of the system, we have investigated the RI of various batches of resin in vinyl PDMS at about 30^0C temperature. Different weight loadings of HQ-resin to V-PDMS are made and the refractive index of HQ loaded system are summarized in Table 2

Table 2. RI of HQ loaded systems

System	Refractive index
V-PDMS	1.4034
V-PDMS+HQ-20wt%	1.4045
V-PDMS+HQ-40wt%	1.4046
V-PDMS+HQ-60wt%	1.4046
V-PDMS+HQ-80wt%	1.4048
V-PDMS+HQ-100wt%	1.4050

There is no significant changes in the RI of the HQ loaded system. It was found that they all have an approximately same value and thus possess optical transparency.

Conclusions

MQ resin with hydride functionality (HQ resins) is synthesized and characterized. Since HQ resins are having active hydride functionality, it has the possibility to act as both filler and curing agent in V-PDMS matrix. Different weight loadings of HQ to V-PDMS are done and the systems are cured by means of Pt assisted hydrosilylation. There is significant improvement in the LSS on V-PDMS with the incorporation of HQ resins. HQ resins are identified as novel materials to impart cohesive strength as well as cross-linking in addition curable silicone systems, which finds potential applications as transparent silicone adhesives for space applications.

References

1. S.J. Clarson, J.A. Semlyen, Prentice Hall, New Jersey (1993).
2. F.S. Kipping (1904). Proc.Chem.Soc. 2015
3. J. E. Mark; H. R. Allcock; R. West (2005). p. 155.
4. F. Sun, Y. Hu, H.G. Du *J. App.Polym. Sci*., 125, 3532, 2012
5. C.Feng, J.Kuo, J.B. Chen, C.Y. Shih, C.Y. Huang J. App.Polym. Sci., 40317, 2014.

MACRO 356

Dielectric Evaluation of Polymer Matrix Composites for Stealth Applications

Jayalakshmi C. G*, Narendhara Kumar, Vishal Madhukar Gavande

Composites Research Center, Research and Development Establishment (Engrs) (DRDO),

Kalas Road, Dighi, Pune, Maharashtra -411015 (INDIA)

*Corresponding author: Jayalakshmi C G; jayalakshmicg7@gmail.com

Abstract

Stealth technology is a sub-discipline of military tactics and passive electronic countermeasures, which cover a range of techniques used with personnel, aircraft, ships, submarines and missiles, in order to make them less visible (ideally invisible) to radar, infrared, sonar and other detection methods. Radar absorption is the basic and most critical requirements for aero stealth applications. Detect-ability reduction of military vehicles, often expressed as radar cross section (RCS) [1], affects not only mission success rates but also survival rate in the hostile territory. RCS reduction can be achieved by shaping of target, usage of Radar Absorbing Materials (RAM) and Radar Absorbing Structures (RAS). In this paper we highlighted the fabrication of Polymer Matrix Composite (PMC) radar absorbing structures using various filler materials such as Carbon fiber hybrid mats,

Carbon black, Mesoporous silica, and graphene etc. These radar absorbing materials were characterized for its dielectric properties such as real (ε') and imaginary permittivity (ε") and loss tangent (tan δ) in X band frequency region to explore the possibility for being used as lossy fillers for developing RAS. The composites fabrication methodology adopted was Resin Film Infusion (RFI), and the dielectric evaluation was carried out using free space measurement system.

Keywords: *Stealth, PMC's, Radar Absorbing Structures (RAS), Radar Cross Section (RCS).*

Introduction

Polymer matrix composites were conceived through efforts in the aerospace community during World War II to produce materials with specific strength and stiffness values that were significantly higher than existing structural materials [2]. PMC's comprise of a variety of short or continuous fibres bound together by an organic polymer matrix. These are having many advantages over conventional metal systems meeting the basic requirements of radar absorption for stealth applications. The high strength to weight ratio of a composite as a structural component results in improved capabilities, such as increased payload, higher top speed, greater range, and reduced fuel usage in

aerospace application. Being a layered material, composites are light and tailorable. In addition, multi functionalization can be incorporated with ease on composites as compared to any other materials. The Radar Absorbing Structures (RAS) satisfies both structural as well as radar absorbing property requirements [3]. The electromagnetic wave properties of the RAS can be tailored by controlling the content and type of Radar Absorbing Filler Materials (RAM) or lossy materials in each layer while fabricating RAS. The composite fabrication method adopted is Resin Film Infusion (RFI). This process involves resin formulation that is cast in form of a film. The resin films are then sandwiched between fiber layers, laid on the tool and component manufactured by vacuum bagging technique under ambient pressure and high temperature [4]. It has been observed that products made using RFI have mechanical properties comparable to prepreg autoclave cured products with near zero void content and improved drapability. Incorporation of functional filler materials and nano materials for up gradation of composite properties can also been done with relative ease. Hence RFI has been chosen as the process to manufacture composites for EM applications.

Loss Mechanism in composite (multilayered) structures

The characteristic that enables the PMC's to perform radar absorbing functions completely depend on its response towards electromagnetic waves used in radars. The electronic properties of PMC's mainly depends on the relative permittivity or di-electric constant (Dk) of both reinforcement and matrix. Di-electric constant is the property of a material that determines the relative speed that an electrical signal will travel in the material. Signal speed is inversely proportional to the square root of the di-electric constant. A low di-electric constant will result in a high signal propagation speed and vice-versa.

In di-electric materials, the absorption of microwaves is related to the material's relative complex permittivity ε_r (Eq. 1).

$$\varepsilon_r = (\varepsilon' - j\varepsilon'') \quad \text{.....Eq 1}$$

where, ε' and ε" are the real and imaginary parts of relative di-electric constant of the material.

When radar waves (microwaves) penetrate and propagate through a di-electric material, the internal field generated within the effected volume induces translational motions of free bound charges (electrons or ions) and rotates charge complexes such as dipoles. The elastic and frictional forces resist these induced motions and cause losses. These loss mechanisms are combined together for convenience to define di-electric loss parameter ε". The loss tangent is commonly used to describe these losses, which is defined as (Eq. 2)

$$\tan\delta = \frac{\varepsilon''}{\varepsilon'} = \frac{\sigma}{2\pi f \varepsilon_0 \varepsilon'} \qquad \ldots\text{Eq 2,}$$

where, σ is total effective conductivity caused by ionic conduction and displacement currents, f is the frequency. High tan δ implies very high attenuation of electromagnetic waves and thus it helps for reduction of RCS. Hence efforts are made to fabricate radar absorbing composite structures using radar absorbing filler materials such as carbon fiber hybrid mats, Carbon black, Mesoporous silica, and graphene for getting maxium loss tangent values.

Experimental

The matrix system used in composites of the present study consists of a proprietary epoxy resin formulation developed in-house. This resin system consists of diglycidyl ether of bisphenol-A (DGEBA)-based solid and liquid epoxy components, the ratio of which has been optimized to result in sufficient tackiness in order for the resin films to stick to the dry fabric during the composite manufacturing, in addition to appropriate rheological, thermal, and mechanical properties. This formulation has a shelf life of 2 years when stored at sub-zero temperatures. The fabric reinforcement used was E glass fabric 295 gsm satin weave style 7781.

Composites with stealth characteristics were developed with the best combination of dielectric, conducting, semiconducting and magnetic fillers. The fillers used were MCM-41 type mesoporous silica (bulk density of 0.34 g/cm^3; a specific surface area of 1000 m^2/g (BET) and the pore size is between 2.1 to 2.7 nm), conducting carbon black (Vulcan XC 72), Graphene (bulk density 1.8 g/cm^3) and carbon hybrid mat etc. These fillers will act as the sites for scattering, conducting and di-electric/magnetic losses which results electromagnetic attenuation.

Dispersing filler materials in Epoxy

Weighed amount of filler materials (conducting carbon black, mesoporous silica and graphene) were taken separately and mixed with acetone and ultrasonicated with a mechanical probe sonicator (13 mm, Vibra Cell Processor VCX 750, operating at 40% of the maximum power 750 W) over an ice bath. Ultrasonication for 15 min dispersed fillers well in solutions which were then mixed with liquid component of the epoxy resin formulation using a thorough mechanical mixing followed by subsequent removal of solvent. Further, this was mixed with the rest of the ingredients in a planetary mixer (3 kg capacity, three blades counter rotating at 10 rpm). A proper uniform mix is facilitated by a reduced viscosity of the resin being mixed at 120 °C prior to the addition of accelerator and hardener, followed by mixing at 60 °C for 2 h of the final formulation under vacuum. A control formulation containing no filler materials was also prepared for making laminates with carbon hybrid mat as well as E glass fabrics. The epoxy resin formulations are made into films using a casting machine and subsequently used for RFI process.

Composite fabrication

The composite laminates were fabricated through RFI; the methodology involved is as follows. Cast epoxy resin film is cut to the desired dimension and transferred to a fabric layer (placed over a metallic mould plate) ensuring that the film just sticks to the fabric. The process is repeated to yield sandwiches of resin films with two fabric layers on both sides. Such sandwiches are placed on one another to build desired thickness. The sandwich stack over the mould is then cured by vacuum bagging technique inside an oven. A thermocouple is placed on top of the job to continuously monitor the temperature. Vacuum is applied to the job and measured via digital sensor. The job is heated at 2 °C/min up to 80 °C, held at this temperature for 30 min while the resin films melt and infuse amidst the fabric plies. Curing process takes place with subsequent heating to 120 °C and holding for 60 min. After completing the heating cycle, oven is switched off and the job is allowed to cool slowly to room temperature before de-molding.

Composites of E-glass/epoxy containing different fillers were made and its dielectric properties were evaluated using Free Space Measurement system.

Electro magnetic Characterization

The frequency of operation of radars ranges from 3 MHz to 300 GHz. The major bands for long range surveillance, military, aircrafts and aerospace applications include L (1 - 2 GHz), S (2 -4 GHz), C (4 - 8 GHz), X (8 -12 GHz), Ku (12-18 GHz), K (18-24 GHz), Ka (24 – 40 GHz) bands. Majority of aviation and marine radars can be considered as specifically operating over 1 – 18 GHz frequency bands which encompasses the bulk of modern Air Defense (AD) radars, military and civil, Air Traffic Control (ATC) terminal approach and Primary Surveillance Radars (PSR) and marine navigation radars associated with larger vessels [6],[7]. Composites of 150 x 150 mm dimension of 2 mm thickness were evaluated for its electro magnetic properties using Free Space Measurement system (5.6-40 GHz Agilent make: N5222A, MY 51421600)

Results and Discussion

The composites made of filler materials such as carbon fiber hybrid mat, conducting carbon black, mesoporous silica, graphene and plain laminate (with no fillers) were characterized for its dielectric properties such as real (ε') and imaginary permittivity (ε") and loss tangent (tan δ) in X band frequency (8.2 to 12.4 GHz) microwave region. The results are demonstrated in Figure (1), Figure (2) and Figure (3) respectively.

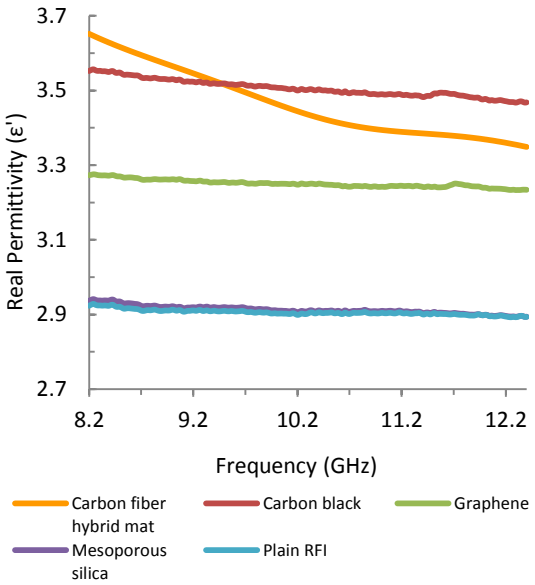


Figure (1): Real permittivity (ε') of 2 mm thick laminates.

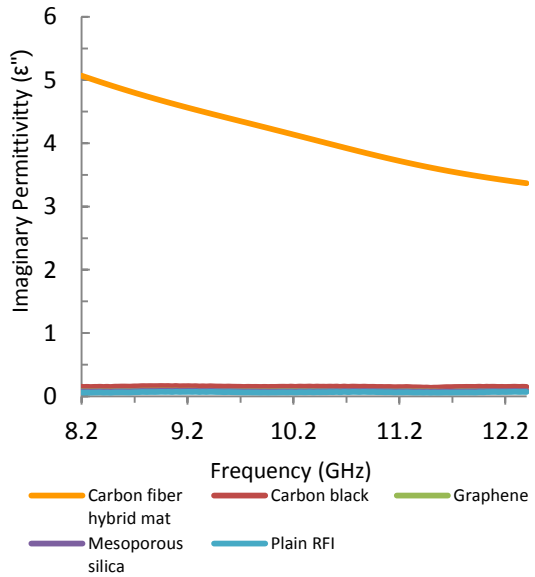


Figure (2): Imaginary permittivity (ε") of 2 mm thick laminates.

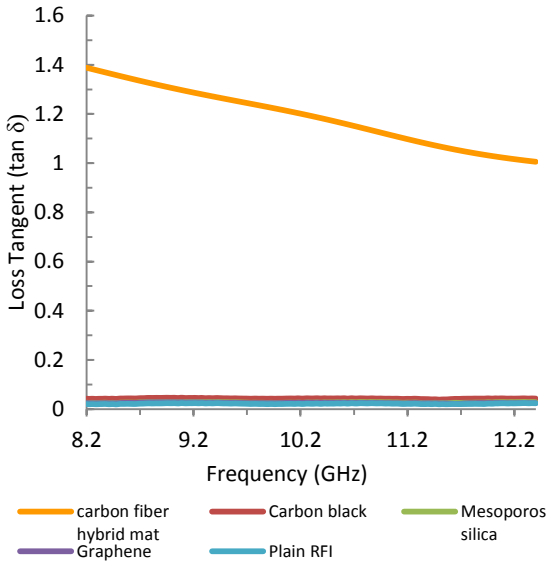


Figure (3): Loss tangent (tan δ) of 2 mm thick laminates.

Conclusions

Radar absorbing composite structures of E-glass and epoxy with different lossy filler materials were fabricated through RFI. Dielectric evaluations using Free Space Measurement system of composites fabricated using carbon fiber hybrid mats showed that the real permittivity (ε') lies between 3.4 – 3.6, imaginary permittivity (ε") between 3.5 – 5.0 and loss tangent (tan δ) values between 1.1 – 1.4 in X-band, rendering carbon fiber hybrid mats the best candidate for fabricating light weight Radar Absorbing Structures. The order of loss tangent values for other filler materials is as follows: carbon black > mesoporous silica > grapheme > plain laminate (no fillers).

Acknowledgements

The authors are thankful to Altaf Ali & Vipin (UCE Thodupuzha), Vishnu, Anjali, Pooja (CUSAT), for sample preparations and Abraham (DIAT), Rudresh Kumar (DMSRDE) for their support for evaluation of electromagnetic properties of composites.

References

1. Eugene F. Knott, John F. Shaeffer, Michael T. Tuley, "Radar cross section". SciTech Publishing, Copyright 2004.
2. Fiber reinforced composite Materials, Manufacturing and Design by P.K. Mallick, Department of Mechanical Engineering, University of Michigan-Dearborn, Michigan.
3. Vinoy K. J., Jha R. M., "Radar absorbing materials from theory to design and characterization". Boston Klwer Academic Publishers; 1996.
4. Anoop Anand, Rahul Harshe, Makarand Joshi "Resin Film Infusion: Toward Structural Composites with Nanofillers" J. Appl. Polym. Sic. 2013, DOI: 10.1002/APP.38855.
5. E. F. Knott, et al, 'Radar Cross-Section (Boston: Artech House) 1993.

6. R. Buderi, The invention that changed the world: the story of radar from war to peace, New York: Simon & Schuster, 1996.
7. Oh JH, Oh KS, Kim CG, Hong CS (2004), Design of radar absorbing structures using Glass/epoxy composite containing carbon black in X-band frequency ranges, Compos Part B, Vol. 35, 49–56.

MACRO 359

Investigation on Toughening of Epoxy Resin with addition curable PEEK

*Leena K, Temina Mary Robert and Dona Mathew

Polymers and Special Chemicals Division,

Vikram Sarabhai Space Centre,

Thiruvananthapuram

Kerala, India-695022

**Corresponding author e-mail:*

leenakarthi@yahoo.co.in

Abstract

Polyether ether ketone containing telechelic propargyl functions (PEEKPR) were synthesized from hydroxyl terminated PEEK (PEEKTOH) and was characterized by spectral, chemical and thermal techniques. Thermal polymerisation of PEEKPR initiated at around 180°C, as monitored by DSC analysis. PEEKPR was melt blended with bisphenol A- based epoxy-diamino diphenyl sulfone(DDS) system in varying proportions and cured at 180°C. Evaluation of mechanical properties of the cured networks showed that, the tensile strength got improved by 8 to 17% up to 10phr loading of PEEKPR. Fracture toughness also was improved by 22 to 33%. Properties of the blends were correlated with composition and morphology of the cured networks.

Introduction: Epoxy resins are widely used as adhesives, coatings and matrix resins in aerospace and electronic industries[1]. However, their high performance applications are severely hampered due to the inherent brittleness and poor resistance to crack propagation. The most popular technique of toughening epoxy resins include, blending with thermoplastic polymers, rubber particles, flexible/hyper branched aliphatic epoxy modifiers etc. Generally employed thermoplastic polymer toughening agents include functionalized Poly (EtherSulfone)[2], Poly(Ether Imide)[3], Poly Ether Ether Ketone(PEEK)[4] etc. PEEK constitutes a class of high performance thermoplastics characterized by outstanding thermal, chemical, and mechanical properties. Commercially available high molecular weight PEEK polymers are difficult to blend with epoxy resins as they are immiscible. Miscibility with epoxy resins and processability of the blends can be improved by functionalizing the PEEK polymers with appropriate functional groups and tuning the molecular weights. Incorporation of terminal functional groups onto the thermoplastic backbone and selection of appropriate molecular weights imparts these desirable features to the blend. Limited literature is available on the toughening of epoxy resins using functionalized PEEK[5-10] and studies on propargyl functionalized PEEK, which is capable of curing at the same temperature regime as that of the epoxy resin system is not reported. Present study focuses on the synthesis and characterization of a novel, heat-curable, propargyl terminated PEEK polymer (PEEKPR), its blends with diglycidylether of Bisphenol A-diamino diphenyl sulfone system and investigations

on the thermal and mechanical properties of the blends.

Experimental

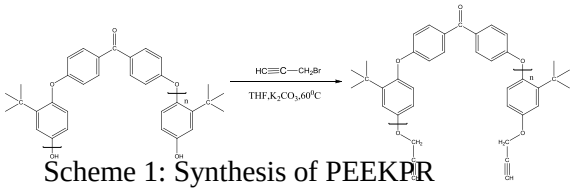
Materials: Hydroxyl terminated PEEK (PEEKTOH), bearing pendent tertiary butyl groups having a number average molecular weight around 2500 were synthesized as per the reported procedure[5]. Benzyl triethyl ammonium chloride (Sigma-Aldrich), Propargyl bromide (Sigma-Aldrich), Epoxy resin (diglycidyl ether of Bisphenol A) (M/s. Huntsman India pvt.ltd), DDS (M/s.Merck Indiapvt.ltd), Tetra hydrofuran (SRL, Mumbai) were used as such. Potassium carbonate (SRL, Mumbai), was dried at 150 °C for 4 h prior to use.

Synthesis of PEEKPR: PEEKTOH (15g, 6mmol) was dissolved in 250ml tetrahydrofuran in a three necked round bottomed flask equipped with a condenser for 1h at room temperature. Added freshly dried potassium carbonate (13g, 93mmol) and benzyl triethyl ammonium chloride (0.15g, 0.65mmol).Temperature was raised to 65° C and Propargyl bromide solution (13.75ml, 92mmol) was added drop wise from a pressure equalizing funnel over a period of 1h under agitation. Stirring was continued for 35h at 60°C. The product was isolated by filtering the reaction mixture followed by repeated precipitation of the filtrate in cold distilled water. The PEEKPR thus synthesised was dried under vacuum at 80 °C for 24hrs.

Preparation of Epoxy-PEEKPR –DDS blends(LY-PEEKPR): PEEKPR incorporated epoxy -DDS blends were processed by melt blending. PEEKPR oligomers were soluble in epoxy resin at around 100-110°C. Epoxy–DDS blends containing 5, 10 and 15phr of PEEKPR were processed as follows. Calculated amount of PEEKPR was blended with the epoxy resin by mechanical stirring for 30minutes at 100°C. Temperature was then raised to 180 °C and stoichiometric quantity of DDS was added to this blend and mixed for five minutes. The reaction mixture was then cured at 180°C for 3hrs followed by post curing at 200°C for 3 hrs.

Characterization: FTIR spectrum was recorded on a Perkin Elmer Spectrum GXA FTIR spectrometer. ^{13}C NMR spectrum was recorded using BRUKER AVANCE FTNMR spectrometer. DSC analysis was done using TA Instruments model 2920. TGA were determined using TA Instruments SDT Q-600 equipment. Fracture toughness and tensile properties were determined as per ASTM 5045 and ASTM D638 respectively. Scanning electron microscopy of the blends was imaged using a Jeol JSM-35CF scanning electron microscope operating at 20 kV.

Results and discussion: PEEKPR was synthesized as per the scheme 1.



Scheme 1: Synthesis of PEEKPR

FTIR spectrum of PEEKPR and PEEKTOH are shown in Fig.1. Characteristic absorption peaks corresponding to ≡C-H bond of propargyl groups were observed at 3295 cm^{-1} and that due to C≡C appeared at 2341 cm^{-1}. However, presence of a peak at 3450 cm^{-1} indicates residual –OH groups.

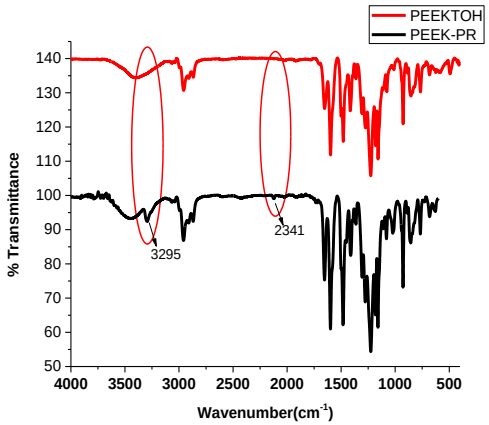


Fig.1 FTIR spectra of PEEKTOH and PEEKPR

Figure 2 depicts the ^{13}C NMR spectrum of PEEPR, where, two characteristic signals at 74ppm and 78ppm correspond to the -C≡C- atoms of propargyl group. Chemical shift at 55 ppm is attributed to $–CH_2$- moiety in the propargyl groups. Molecular weight determined using GPC (with polystyrene standards) shows that, Mn increased from 2520 to 2740 upon conversion of PEEKTOH to PEEKPR, as expected.

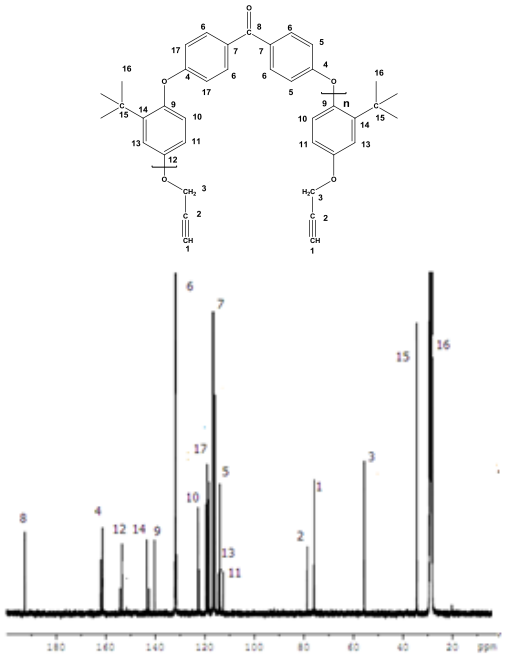


Fig. 2 ^{13}C NMR spectrum of PEEKPR

Curing of PEEKPR was monitored using DSC thermogram as shown in Fig3.

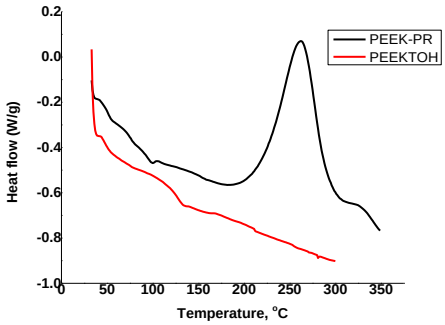


Fig.3 DSC curves of PEEKTOH and PEEKPR

An exothermic peak which initiates at 184°C and ends at 313°C with an enthalpy of reaction around 190J/g is observed in the case of PEEKPR. Phenyl propargyl ethers are well known for the Claisen type sigmatropic rearrangement to 2H-chromenes. The un-catalysed rearrangement is normally effected at higher temperature and is nearly always accompanied by thermal polymerization of the formed chromene to polybis-chromenes. PEEKTOH does not undergo any curing, except for the softening at around 145°C, as evident in the thermogram in Figure 3. Table 1 shows a systematic increase in the heat of reaction during curing of the blends, with increasing proportion of PEEKPR. This is attributed to the additional heat liberated during the polymerization of PEEKPR, in the epoxy amine blend which exhibits a cure enthalpy of around 190J/g.

Completion of the cure reaction was confirmed by FTIR and DSC. Vanishing of Peak at 915cm^{-1}after curing, indicating complete consumption of the epoxy groups. Fig 4 depicts the FTIR spectra of the typical uncured and cured blends. It is also evident

Table 1: Cure characteristics of LY-PEEKPR blends				
System	**T_{ini} (°C)**	**T_{peak} (°C)**	**T_{end} (°C)**	**ΔH, J/g**
LY PEEKPR(0)	148	229	333	379
LY-PEEKPR(5)	147	228	332	382
LY-PEEKPR(10)	137	230	335	391
LY-PEEKPR(15)	135	235	335	409

that the absorption due to propargyl groups was completely disappeared in the cured blends.

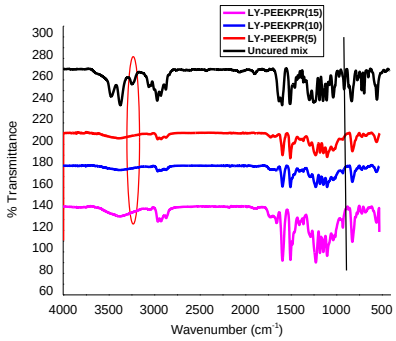


Fig. 4 FTIR spectra of cured and uncured blend

Absence of residual cure in the DSC of the cured blend also infers the completion of curing. Overlay of DSC thermograms of an uncured and cured blend is represented in Fig 5. Absence of any exothermic peak over the entire scanned range confirms the complete curing of the blends.

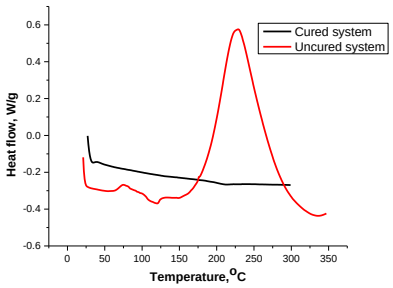


Fig 5. DSC curves of uncured and cured blend, LY-PEEKPR (10)

Glass transition temperature, Tg of the cured blends were obtained from DSC and are tabulated in Table 2. It may be noted that, addition of PEEKPR has resulted in a slight decline in the Tg of the blends. This is attributed to the toughness imparted by the thermoplastic additive

Table 2.Tg of epoxy blend formulations		
System	**Tg(°C)**	**Char yield at 900°C (wt %)**
LY-PEEKPR(0)	215	15
LY-PEEKPR(5)	202	16
LY-PEEKPR(10)	202	20
LY-PEEKPR(15)	204	18

which in turn has conferred flexibility to the network. Thermal stability of the epoxy-DDS blends obtained from TGA thermograms (Fig. 6) was not impaired by PEEKPR. Marginal increase in char yield has been observed for blends containing 10 and 15 phr PEEKPR, compared to the neat system.

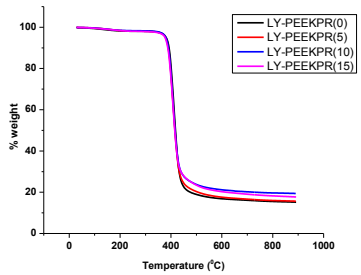


Fig. 6.TGA of epoxy blend formulations

Effect of PEEKPR incorporation on the mechanical properties (tensile strength and % elongation) of the blends is shown in

Fig7. Tensile strength increases from 67 MPa (for neat system) to 79MPa(LY-PEEKPR (10)) and declines thereafter. Toughness imparted by the PEEKPR has contributed to the tensile strength of the blend, up to a loading of 10 phr. However, at still higher loading of PEEKPR, the strength declined drastically. The elongation at break also increased by 31% with increase in PEEKPR concentration up to 10 phr and thereafter decreased. This may be attributed to the excessive phase separation and consequent weakening of interface at higher content of thermoplastic particles. Tensile modulus of all formulations was in the range of 2.8-3.0 GPa.

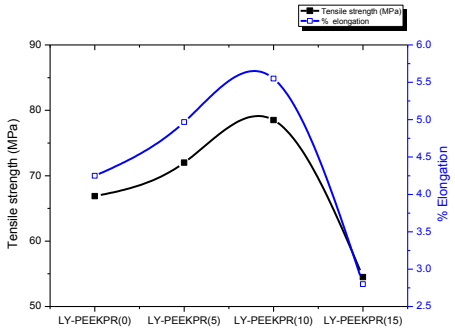


Fig. 7 Tensile properties of LY-PEEKPR formulations

The plot of stress intensity factor **K_{IC}**(Fracture toughness) versus PEEKPR content in the blend is represented in Fig 8.

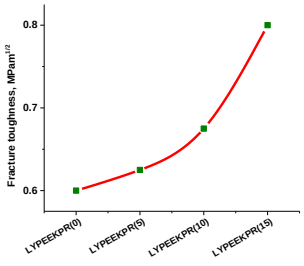
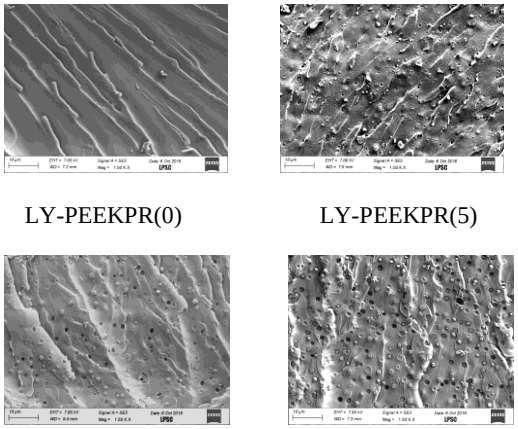


Fig.8 Fracture toughness of LY-PEEKPR blends

Fracture toughness of the blends increased from 22 to 33% with increase in the PEEKPR content from 5-15phr. The PEEKPR toughened matrix resins exhibited uneven fracture modes and crack branching that require additional energy for fracture. This eventually led to increased fracture toughness. In the present study, the LY-PEEKPR blends which were homogeneous before curing underwent reaction- induced phase separation upon curing. This is evident in the SEM micrographs (Fig.9). Thus, uninterrupted cracks in the neat system show a typical brittle fracture whereas the blends exhibited rough and ridgy surfaces which indicate a ductile failure.



LY-PEEKPR(0) LY-PEEKPR(5)

LY-PEEKPR(10) LY-PEEKPR(15)

Fig 9.Morphology of the cured resins

A phase separated heterogeneous morphology and the major toughening mechanism such as crack pinning, crack path deflection; crack arresting, particle de-bonding etc. are clearly visible in the case of blends, contributing to the increased toughness.

Conclusion: Propargyl terminated PEEK was synthesized from hydroxyl terminated PEEK and its curing was established by

DSC analysis. It was used as a toughening agent for epoxy resins. The blend was cured with DDS curing agent at 180°C. Glass transition temperature of the blends is slightly declined due to PEEKPR incorporation whereas the thermal stability was unaffected. Evaluation of mechanical properties of the cured networks showed that, the tensile strength got improved by 17% up to 10phr loading of PEEKPR. Fracture toughness was also improved by 22 to33%. Properties of the blends were correlated with composition and morphology of the cured networks.

Acknowledgements: The authors thank Director, VSSC for giving permission to present the paper in MACRO 2017. Thanks are due to Analytical and Spectroscopy Division /VSSC, Materials Group, LPSC (V) for the analytical support.

References

1. JKFink, William Andrew Reactive polymers fundamentals and applications, 2nd edn., New York,95–153, 2013
2. Brooker, R. D., Kinloch, A. J., & Taylor, A. C. *J. Adhesion*, 86, 726, 2010
3. Hourston, D. J. & Lane, J. M. *Polymer*, 33, 1379, 1992.
4. B Francis, S thomas, R. Sadhana, N Thuaud,R. Ramaswamy, S Jose, V. L Rao, *J, Poly. Sci: Part B*: *Poly. Phy.*, 45, 2481, 2007
5. B Francis, R. Ramaswamy, V. L Rao& S Thomas, *Int. J. Poly. Mat.*, 55,681, 2007.
6. T Iijima, T Tochimoto and M Tom, *J. of App. Poly. Sci.*, 43, 1685, 1991
7. X Song, S Zheng, J Huang, P Zhu, Q Guo, *J. App. Poly. Sci*, 79, 598, 2001
8. Bennett, R. J. Farris and S. A. Thompsont, *Polymer*, 32, 9, 1633, 1991.
9. Y Luo, M Zhang, G Dang, Y Li, X An, C Chen, X Yi, *J. of App. Poly. Sci.* 122, 1758, 2011
10 .Rao U, Balasubrahmanian KK. *Tetrahed.Lett*. 24, 5023, 1983.

MACRO 360

Space Durable Siloxane Based Thermal Control Coatings With Tailored Optical Properties For Spacecraft Structures

Archana T.S[1], *Ann Mathew[2], R.S.Rajeev[2]

[1]*S.N. College, Kollam*
[2]*Polymers and Special Chemicals Division, Vikram Sarabhai Space Centre, Trivandrum*

**Corresponding author: k_annmathew@vssc.gov.in*

Radiation-protection and thermal control are two fundamental assurances for the spacecraft's on-orbit operation. These are achieved by means of passive thermal control coatings with fixed thermal radiation characteristics. Thermal control coatings (TCC) are designed to have specific radiative properties that are tailored for each mission, depending on the objectives [1-2]. The function of TCC is to reduce external heat absorption and/or to regulate radiant heat exchange between on-board equipment on spacecraft. Silicones are specially designed systems that resist the hostile environment in space such as high vacuum, thermal cycling, solar radiation including high energy UV and X-ray, particulate radiation and atomic oxygen. The required optical, physico-chemical, thermo-physical and mechanical properties are

imparted to silicones by formulating the resinous polymer with suitable additives, fillers and reinforcing agents. Addition curable silicones are preferred for satellite applications due to their low outgassing properties.

Present work envisages the development of a siloxane based black thermal control coating with high solar absorptance and emissivity and low outgassing characteristics. Vinyl functionalised silicone polymers of varying molecular weights were synthesied and characterised by physical, thermal and spectroscopic techniques. The crosslinking of the polymers were optimised by hydrosilylation mechanism using platinum catalyst. Carbon fillers of varying morphological and dispersion features were selected for optimising the required optical properties.The vinyl functional polymers were compounded with various combinations of conducting carbon fillers including acetylene black, CNT and graphene and the influence of these fillers on the electrical, mechanical, optical and rheological characteristics were investigated. The molecular weight of the base polymer was tailored to achieve sprayable consistency. Using this matrix, the effect of type of carbon filler, structure and morphology, dispersion and extent of loading on the thermal and optical properties were investigated.The promising composition exhibited solar absorptance of 0.96, emissivity of 0.91 and surface resistivity of the order of $<10^3$ ohms/square using acetylene black as filler. The space durability of the developed coating was successfully established by subjecting the system to space environment simulation testings like thermo-vacuum cycling followed by evaluating the outgassing characteristics. Morphology of the coatings was examined by Scanning Electron Microscopy. Thus we have demonstrated the development of a black coating which is designed to have specific radiative properties that can be tailored for specific missions.

References

[1] J.I. Kleiman, Y.Gudimenko, Z.A, Iskanderova, D Edwards, M.Finkenor, *J. of Spacecraft and Rockets*, v 43, No.2, 2006, pp 443 – 450

[2] Zu-Po Yang, Lijie Ci, James A. Bur, Shawn-Yu Lin, Pulickel M.Ajayan, *Nano Lett*.2008 Feb 8(2):446-451

MACRO 362

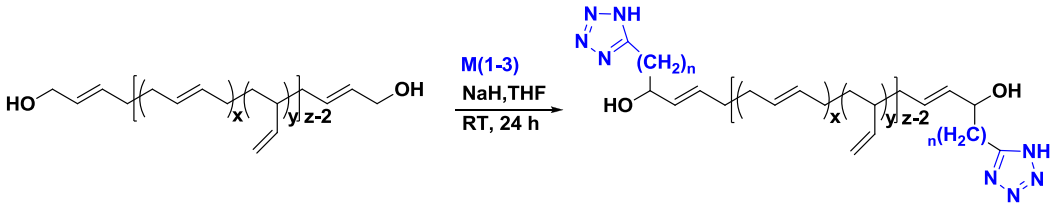
Tetrazole Functionalized Hydroxyl Terminated Polybutadiene polyurethane

Moumita Dhara, Bikash kumar Sikdar and Tushar Jana*

School of Chemistry, University of Hyderabad, Hyderabad-500046
E-mail: tusharjana@uohyd.ac.in

Hydroxyl-terminated polybutadiene (HTPB) has received much attention because it shows excellent properties such as hydrolytic stability, resistance to aqueous acids and bases, adhesion to a variety of substrates, high process ability with high solid loading (upto 90%), low temperature flexibility, and high elongation with good elastic recovery. Because of the above properties, HTPB has become the most potential candidate as a binder for oxidizers, metallic fuels and other additives in the composite propellant. The urethane network obtained by curing HTPB with a suitable diisocyanate (curative) not only provides dimensional stability to the composite but also imparts structural integrity and good mechanical properties. HTPB is an inert polymer which contributes nearly 10–15% mass of the propellant compositions and hence it is highly desirable to replace inert mass by energetic polymers. Generally; (1) To improve the ballistic performances of composite propellants, HTPB were modified by incorporating nitrogen rich molecules and; (2) To enhance the burn rate, molecules containing transition metals were grafted along the back bone of HTPB. Most of these modification demonstrated good energy output but lack in areas like post cure mechanical properties, process ability at higher solid loading and compatibility with other ingredients. In our lab we successfully attached various

commercially available nitrogen rich molecules at the terminal carbon of HTPB and now we have developed tetrazole modified HTPB which resulted simultaneous enhancement of stress and strain in the polyurethane obtained from HTPB. In the present presentation we will discuss the recent progress in these directions.



P0 Where P1 (n=1), P2 (n=2), P3 (n=3)

Figure 1. Synthesis of tetrazole terminated HTPB

References

[1] Gaur, B.; Lochab, B.; Choudhary, V.; Verma, I. K. J MacromolSci Polymer Rev 2003, 43, 505-545.

[2] Pant, C. S.; Santosh, M. S. S. N. M.; Banerjee, S.; Khanna, P. K. Propellants Explos. Pyrotech. 2013, 38, 748–753.

[3] K. Malkappa, T. Jana, *Ind. Eng. Chem. Res.* **2015**, *54*, 7423-7435.

[4] Rao, B. N.; P. Yadav, J. P.; Malkappa, K.; Jana, T.; Sastry, P. U. *Polymer* **2015**, 77, 323 - 333.

MACRO 363

MECHANICAL CHARACTERISATION AND SORPTION STUDIES OF AROMATIC SOLVENTS THROUGH ACRYLONITRILE-BUTADIENE RUBBER-CHITOSAN BIOCOMPOSITES

Meril Shelly, Sini K.S., Tania Francis*

Post Graduate and Research Department of Chemistry, St. Joseph's College Autonomous, Devagiri, Calicut -8

**Corresponding author: francistania76@gmail.com; +91-9895726068*

Abstract— Rubbers or elastomers constitute an important class of materials, like metals and ceramics, without which modern technology would be unthinkable. In this work acrylonitrile-butadiene rubber (NBR) is blended with chitosan (CS) biofiller to develop a novel biocomposite material of improved biodegradability. The fabrication of Acrylonitrile-butadiene rubber / Chitosan composites is followed by its mechanical and sorption characterization. The technique of two roll milling has been explored for the

development of the composite systems. The rheometric characteristics of the rubber mixes were determined using an oscillating disc rheometer. The cure characteristics and mechanical properties like tensile strength, modulus and elongation at break of NBR nanocomposites reinforced with different levels of chitosan were studied. The morphology of the composites was determined via FESEM. The diffusion of aromatic solvents through the prepared composites followed the order: Benzene > Toluene > Xylene which has been correlated with the size and solubility parameter values.

Keywords: Biocomposites, NBR, Chitosan, Tensile, Tear.

INTRODUCTION

Composites are multiphase systems that are produced by combining two or more components in such a way that the product is better suited for a particular application than either of the original components. They are mainly composed of matrix phase, which is generally continuous into which the other phase is embedded often called the reinforcement or dispersed phase. They combine each other and produce a multiphase system having new or better properties than the parents[1]. The use of natural biodegradable fillers can make the system biodegradable and biocompatible. To obtain a good composite, the perfect blending is necessary, *i.e.* the good dispersion of reinforcement phase is needed. Nitrile butadiene rubber is one of the elastomers of significant commercial and academic interest, widely employed for the manufacture of fuel hose, o-rings, seals, gaskets, gloves etc.[2] Environmentally friendly additives such as cellulose, rice husk, starch, chitosan etc are called bio fillers. It is known that the filler aggregates in the polymer matrix especially at high loading, leading to chain like filler structures or clusters. These are generally termed secondary structure or, in some cases filler network, even though the latter is not comparable to the continuous three-dimensional polymer network structure.[3] Chitosan is the second abundant natural polysaccharide, second only to cellulose. Chitosan can be obtained from chitin by the process called deacetylation. The deacetylation (DA), which is by definition the molar fraction of *N*-acetylated units, is a structural parameter influencing charge density, crystallinity and solubility, including the propensity to enzymatic degradation, with higher DAs leading to faster biodegradation rates.[4] Chitosan fiber is known to possess excellent physical and chemical properties and hence received much attention to be used as filler in various researches. The selection of chitosan, natural filler into polymer matrix offers the possibility to design new composite material with reduced environmental impact, better biodegradability and also cost reduction. İt has good film forming property, mechanical stability and flexibility.[5-7] The reinforcement of rubber with short fibers offers strength and stiffness compared to the soft and tough rubber matrix. Recently short fiber reinforced rubber has gained importance due to its advantages like design flexibility, anisotropy in technical properties, stiffness, damping and processing economy.

The study aims to prepare NBR- Chitosan biocomposite in which Chitosan biofiller is dispersed in NBR matrix using sulphur as the crosslinker. This study focuses on the curing mechanical property studies and sorption characterisation of the developed biocomposite samples. The effect of addition of biofiller, chitosan on the mechanical properties are mainly studied by varying the chitosan content as 0, 2.5, 5, 7.5 and 10 phr in the respective samples.

MATERIALS AND METHODS

NBR containing 33% acrylonitrile content was obtained from Common Facility Service Centre (CFSC), Manjeri, Kerala. Chitosan powders of size less than 100μm were obtained from Indian Sea Foods Kochi, Kerala, India with degree of deacetylation approximately 90%. The compounding ingredients used in this work are, Sulphur as vulcanizing agent, ZnO and Stearic acid

as activators, MBTS - (2,2'- dithiobis (benzothiazole), TMTD - Tetramethyltriuram disulphide, as accelerators and TDQ - 2,2,4-Trimethyl-1,2-dihydroquinoline as antioxidant. All the reagents used were of laboratory grade (LR).

2.1 Preparation of NBCS Composites

Formulation employed for the preparation of NBR-CS composites are listed below in Table 1

Sample	NBR	Chitosan (phr)	Sulphur
NBCS0	100	0	1.5
NBCS1	100	2.5	1.5
NBCS2	100	5	1.5
NBCS3	100	7.5	1.5
NBCS4	100	10	1.5
NBCSa	100	5 (DA = 80)	1.5

(NB- Acrylonitrilebutadiene rubber; CS-Chitosan; (ZnO-(4.5phr); Stearic Acid -(1.5phr);TMTD-(0.25phr);MBTS-(1phr); TDQ-(1phr); Sulphur-(1.5phr)).

2.2. Cure characteristics

The cure characteristics such as the minimum torque (ML), maximum torque (MH), delta torque (ΔH), Cure rate index (CRI), the cure time (t_{90}) and scorch time (t_{S2}) were determined using a Monsanto Moving Die Rheometer (MDR 2000) according to ASTM method D 2084. Samples of about 6 gm of the respective compounds were tested at a vulcanization temperature of 150˚C. The cure rate index is a parameter which indicates the speed of curing reaction was determined from rheometric data. CRI is calculated using the following relation.

$$\mathbf{CRI} = \frac{\mathbf{100}}{\mathbf{Cure\ time - Scrotch\ time}}$$

2.2 Mechanical properties

Dumb-bell shaped specimens were cut from the sheets and tensile strength, elongation at break and modulus, were determined Universal Testing Machine - ASTM D 412-06a Tension with Extensometer. Three samples were tested and their average values were taken. Tear resistance was also carried out on a ASTM D 624-00(2007) Tear. The tear resistances of the samples were reported in N/mm. Hardness were studied by using Shore A Hardness Tester-Durometer.

2.3 Sorption Studies

The sorption properties of the composite films were studied by immersing each film (1.94 cm diameter) in aromatic solvents such as benzene, toluene and xylene. The samples were kept at 25 °C. The weights of the samples were recorded after periodically removing them from the swelling medium, carefully blotting them with absorbent tissue to remove surface water and weighing them. They were weighed immediately using an electronic balance (Sartorius BSA224S-CW) that measured reproducibly within ± 0.0001 g and replaced into the solvents. The process was repeated till equilibrium swelling was reached. The time for each weighing was kept to a minimum of 30 - 40 s in order to minimize the errors due to the escape of solvents from the samples. This technique has been successfully employed earlier for investigating solvent transport into elastomer samples. The results of sorption experiments have been represented by plotting the mol % uptake, Q_t, against the square root of time. The solvent uptake was calculated as,

The results of the sorption experiments have been expressed as moles of solvent sorbed by 0.1 kg of the sample, Qt (mol%), given as follows:

$$\boldsymbol{Qt = \left[\frac{Mt/Ms}{Mp}\right] \times 100}$$

where Mt is the mass of the solvent absorbed at a given time t, Ms is the molecular mass of the solvent, and Mp is

the mass of the polymer blend. The Qt values obtained were plotted against the square root of the total time of immersion of the samples in different liquids. The Qt values so obtained have been plotted as a function of square root of time, to construct the sorption curves.

2.4 Morphological Analysis

Morphological analysis of the prepared composites were done by using a JEOL Model JSM – 6390

RESULTS AND DISCUSSION

3.1. Cure Characteristics.

A significant decrease in the cure time on addition of chitosan filler was observed. The cure time was found to reduce by around 3-4 minutes on adding 10 phr of the chitosan filler. The unmodified vulcanisate was found to have the highest curing time of 10.95 min. This reduction in the cure time is an indication of the enhancement in the cure rate with increased filler loadings and also an increase in the crosslinking offered by the introduction of the filler during vulcanization. Decrease in scorch time also indicates an increase in the rate of the cure reaction. This increase may also be due to the generation of amines from the chitosan filler by degradation at the curing temperature.

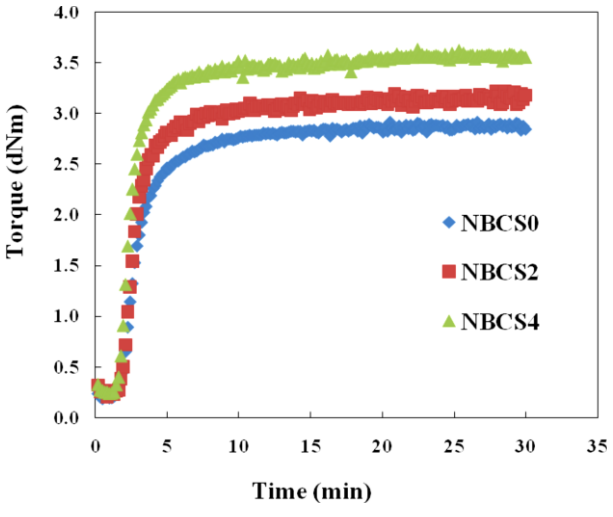


Fig.1 Typical rheograph of the tested samples indicate an increase in torque on addition of chitosan filler

The increase in torque values on addition of chitosan filler maybe attributed to the formation of hydrogen bonding interactions with the –OH and $–NH_2$ functional groups of the filler and –C=N functional group of the matrix. The (maximum-minimum) torque values increase from 0.295 N at 0 phr to 0.365 N in at 10 phr fiber, indicating a more restrained matrix in the case of composites.

Table 2. Cure characteristics of the developed NBR compounds

Cure characteristics	NBR Compounds		
	NBCS0 (A)	NBCS2 (B)	NBCS4 (C)
Cure time, t_{90} (min)	10.95	7.01	6.77
Scorch time (min)	1.97	1.93	1.78
Maximum torque (dNm)	2.95	3.295	3.648
M_H-M_L (dNm)	2.82	3.19	3.49
CRI	11.14	19.69	20.04

3.2. Mechanical Properties

3.2.1. Tensile and Tear Properties

The dilution effect on addition of filler at lower filler loadings is indicated by a decrease in tensile strength at lower filler loadings. The initial decrease may also be attributed to the fact that the filler concentration maybe insufficient to support the stress transferred from the rubber matrix. The tensile strength reaches an optimum value at 5 phr loading and thereafter decreases. The decrease has been attributed to the agglomeration of the filler added. The variation in tensile strength is seen in Fig.2.

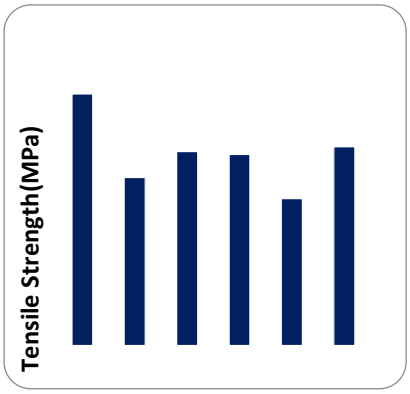


Fig.2.Variation of tensile strength in the developed composite

The overall decrease in tensile has been attributed to the dominant filler-filler interactions than matrix-filler interactions. Filler agglomeration is a possibility at filler loadings greater than 5 phr. Moreover, crosslinking diminishes the chain movement. The Young's Modulus was found to improve with addition of chitosan upto 5phr and then decreases as is seen in Fig.3.

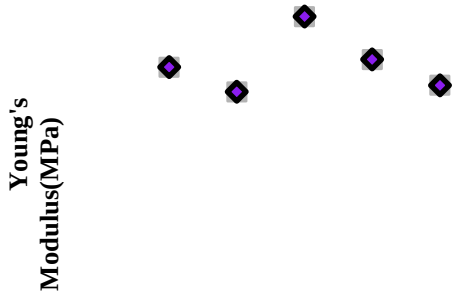


Fig.3. Improvement in Young's Modulus at 5 phr loading of chitosan filler

When the fibre concentration increases there is more hindrance to the propagating tear by the fibers and hence an improvement in tear strength has been observed. The tear strength values have been reported to be higher in the longitudinal direction at all fiber loadings. In the case of transversely oriented fibers, most of them being parallel to the propagating crack front, offers less resistance to propagating tear and hence the lower tear strength values. The observed values indicate that the chitosan short fibres have more of longitudinal orientation than in the case of transverse orientation as evidenced in the current study Fig. 4.

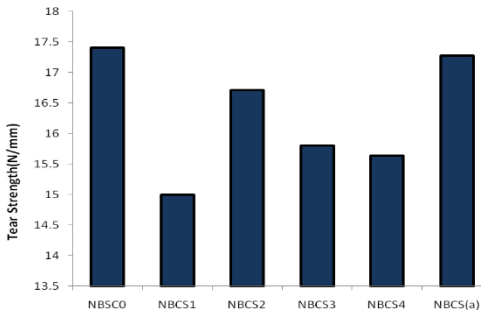


Fig. 4. Tear strength of the developed composites

The mechanical properties of the developed composites have been summarized in Table. 3

Table 3. The mechanical properties of the developed biocomposites

Sample ID	Tensile Strength (MPa)	Young's Modulus (MPa)	Tear strength (N/mm)
NBCS0	2.62	1.50	17.41
NBCS1	1.75	1.31	15.00
NBCS2	2.02	1.89	16.71
NBCS3	1.99	1.56	15.81
NBCS4	1.53	1.36	15.64
NBCSa	2.07	1.86	17.28

The result shows that the reinforcement of Chitosan fibers into the NBR matrix have more

effect on the mechanical properties like tensile strength, elongation at break etc. For NBR/ Chitosan composite the maximum property has been attained for 5 wt% loading.

3.2.2 Hardness

Hardness describes the combination of properties such as resistance to surface indentation, abrasion, and scratching. The hardness is found to increase linearly with the chitosan content because better interfacial interaction between filler and matrix might have occurred. The hardness was found to increase by around 20% of the unmodified vulcanisate.

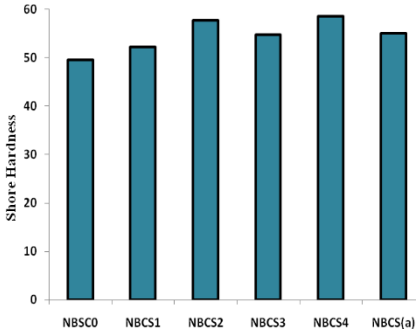


Fig.4. Shore A Hardness comparison o the developed biocomposites

3.3. Sorption Studies

The sorption of aromatic solvents such as benzene, toluene and xylene, through the NBR-CS biocomposites has been carried out to study the morphological distribution of the filler in the NBR matrix. Figure5 (a)–(c) shows the sorption behaviour of different NBR-CS composites at room temperature. It is clear from the figure that the solvent uptake tendency first increases and then decreases with increase in chitosan loading.

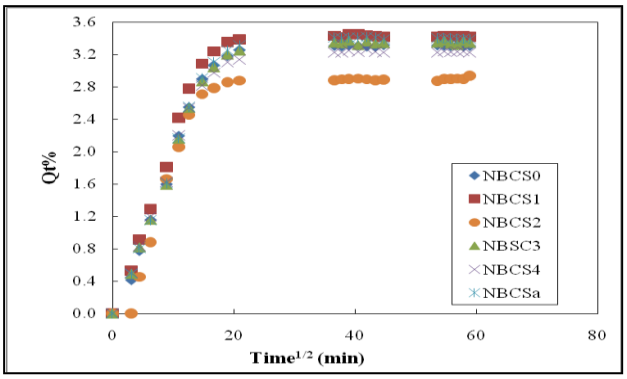


Fig.5(a). Diffusion Studies of Benzene

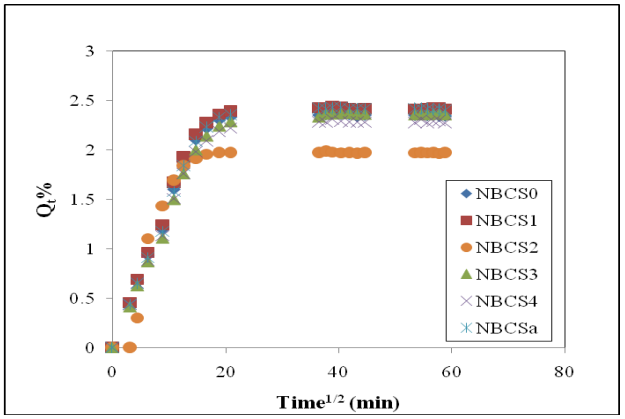


Fig.5(b). Diffusion Studies of Toluene

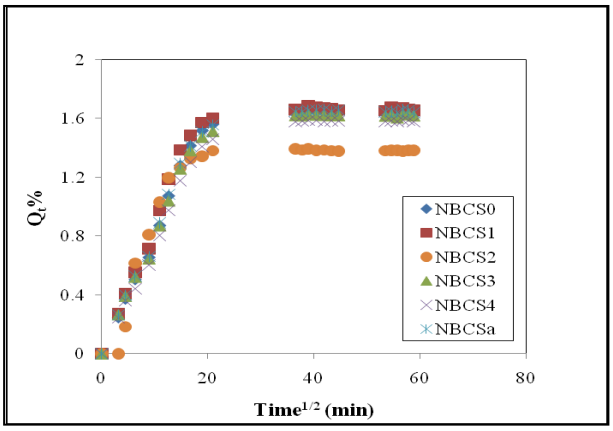


Fig.5(c). Diffusion Studies of Xylene

3.3.1 Effect of penetrants size and solubility parameter values

The effect of penetrant size on the sorption of three aromatic solvents through NBR-CS composites has been studied and the Q_t%

values are tabulated in Table 5. It can be seen from the table that as the size of the solvent molecule increases the Q_t % values decreases. According to solubility parameter values, xylene has more interaction with both the filler as well as the matrix. The lower Q_t value for xylene may also be attributed to steric factors as well.

The increase at higher filler loadings can be explained on the basis of solubility parameter (δ). The values of the solubility parameters of NBR and the solvents benzene, toluene and xylene are 8.9, 9.15, 8.91 and 8.85 respectively. These values have only very small difference. The interaction of the filler with the matrix is highest for NBCS2. Hence this mix shows lowest value. Due to higher filler – filler interaction in NBCS3 there is an increase in sorption values.

Table 5. Comparison of Q_∞ values

Sample	Benzene	Toluene	Xylene
NBCS0	3.31	2.36	1.65
NBCS1	3.45	2.44	1.69
NBCS2	2.90	1.99	1.39
NBCS3	3.37	2.37	1.63
NBCS4	3.26	2.32	1.59
NBCSa	3.42	2.43	1.66

3.3.2. Effect of degree of deacetylation of chitosan on solvent sorption

The sorption of benzene, toluene and xylene has been found to follow the same trend with the addition of Chitosan with 80% degree of deacetylation (DD). The Chitosan (90% DD) filled composite (NBCS2) however, showed lower sorption properties as compared to the other counterpart. This trend is attributed to the interaction of slightly more polar chitosan owing to the presence of higher degree of $–NH_2$ groups in the 90% deacetylated chitosan. This leads to lower chain relaxation and prevent the diffusion of penetrants through the developed composites.

As the amino group content in NBCS2 increases due to higher degree of deacetylation of CS used, the interaction of solvent with the filler also increases which is translated as a decrease in sorption values. Thus, from Fig.6., it is evident that NBCS2 shows lower sorption values as compared to NBCSa which employs CS of 80% degree of deacetylation.

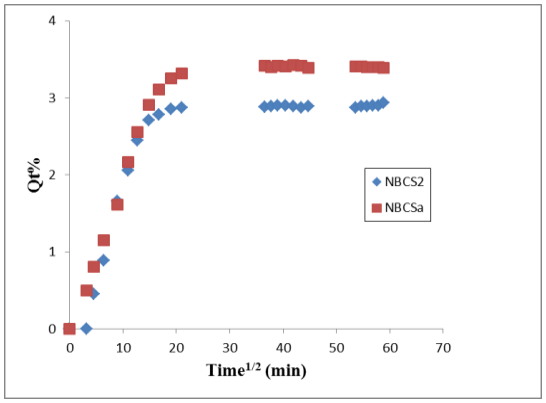


Fig.6.Comparison of degree of deacetylation of chitosan filler on solvent sorption

3.3.3. Mechanism of Transport

The mechanism of transport has been studied at 25 °C for the sorption of the various aromatic solvents through the developed composites using the following equation:

$$\log (Q_t/Q_\infty) = \log k + n \log t$$

The data up to 50% sorption from the sorption curves were used to compute the values of n and k, where k is a constant that depends on the structural characteristics of the polymer and gives information about the interaction between the polymer and

solvents. The value of *n* suggests the mode of transport. When *n* = 0.5, the mode of transport is of the normal Fickian type (Case I), where the rate of polymer chain relaxation is high compared to the diffusion rate of the penetrant. The value of *n* = 1 indicates that the transport approaches non-Fickian mode (Case II), where chain relaxation is slower than the liquid diffusion. If the value of *n* is between 0.5 and 1 it indicates anomalous transport behaviour.

Kinetic parameters

Diffusion coefficient

The diffusion coefficient D can be calculated using the equation

$$D = \pi \left(\frac{h\theta}{4Q\infty} \right)^2$$

where h is the sample thickness, θ is the slope of the linear portion of the sorption curves before attaining 50% of equilibrium, and Q_∞ is the mol% sorption at equilibrium. Eq. (A.3) holds for systems without appreciable swelling. For considerable swelling, a correction for the swelling of the polymer can be made by incorporating φ, the volume fraction of the polymer in the swollen mass, thus giving the intrinsic diffusion coefficient, D * as per the given Eq.

$$D^* = \frac{D}{\varphi^{7/3}}$$

The volume fraction of the polymer, φ, in the swollen mass was calculated using Eq. ,

$$\varphi = \frac{w1/\rho 1}{w1/\rho 1 + w2/\rho 2}$$

where w_1 and ρ_1 are the weight and density of the polymer sample, respectively; and w_2 and ρ_2 are the weight and density of the solvent.

Sorption coefficient

The sorption coefficient, that is related to the equilibrium sorption of the penetrant is calculated using Eq. (6)

$$S = \frac{W\infty}{Wp}$$

Where, W_∞ is the mass of the solvent at equilibrium swelling and W_p is the mass of the polymer sample.

Permeation coefficient.

The permeation process through any matrix is a combination of sorption and diffusion and hence it depends on the sorption and diffusion coefficients. The permeation coefficient, P, is calculated using Eq. (7)

P = D∗S (7)

where D * is the intrinsic diffusion

The values for n and k for the sorption of aromatic solvents benzene, toluene and xylene through the developed biocomposites have been tabulated in Table 6. The values indicate that 5phr CS loaded samples show better interaction between the polymer matrix and solvent as indicated by high *k* values. The biocomposes displayed normal Fickian mode of transport except in the case of NBCS2 where the transport behavior tends to non-Fickian mode indicated by a value very close to unity.

Table 6: Values of *n* and *k* for diffusion through NBR-CS Composites

Sample	*K*			*n*		
	Benzene	Toluene	Xylene	Benzene	Toluene	Xylene
NBCS0	1.7655	1.5913	1.6727	0.5684	0.4645	0.5145
NBCS1	1.6433	1.6290	1.6499	0.4967	0.4880	0.5007

NBCS 2	2.7684	8.0447	9.4309	1.0183	1.0886	1.2439
NBCS 3	1.6982	1.6195	1.6279	0.5296	0.4821	0.4873
NBCS 4	1.7110	1.6105	1.6446	0.5371	0.4766	0.4975
NBCS a	1.7432	1.5866	1.6352	0.5557	0.4616	0.4918

The diffusion and sorption co-efficient values for solvents benzene, toluene and xylene through the developed compounds have been calculated and are given in Table 7. The values indicate that the diffusion of the aromatic solvents followed the order benzene > toluene > xylene as has been correlated with the size as well as solubility parameter values.

The values are found to first increase slightly and then decreases, reaching a minimum in the case of NBCS2 indicating uniform mixing of the filler and the matrix. The mechanical studies show that NBCS2 has the best properties among the mixes prepared. As filler-filler interactions are higher at higher filler loadings the solvent diffusion increases owing to spaces in the matrix.

Table 7: Diffusion and Sorption coefficient values

Sample	Diffusion Coefficient $Dx10^{-2}$			Sorption Coefficient S		
	Benzene	**Toluene**	**Xylene**	**Benzene**	**Toluene**	**Xylene**
NBCS 0	19.94	6.90	1.32	2.58	2.17	1.74
NBCS 1	20.71	7.05	1.33	2.69	2.24	1.79
NBCS 2	8.38	4.83	3.57	2.26	1.83	1.48
NBCS 3	16.73	4.85	1.73	2.63	2.18	1.72
NBCS 4	10.26	6.13	1.62	2.54	2.13	1.68
NBCS a	15.48	7.87	1.87	2.66	2.26	1.76

3.5 Morphological Analysis

The work gives an insight into the mechanical properties of the NBR-CS biocomposite system. The SEM image shows a uniform mixing of the system.

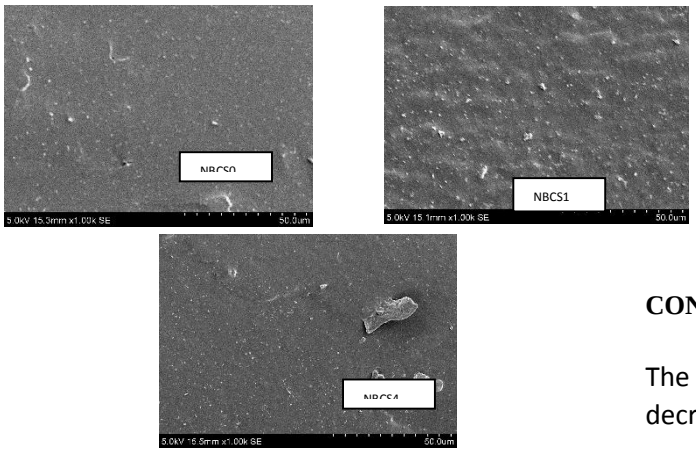


Fig.7 SEM micrographs of NB-CS composites

Hence, the current study helps us to conclude that addition of the filler CS to the NBR matrix does not affect adversely the solvent transport through the developed composites. Due to increased polarity of the filler the permeation of polar solvent is further reduced. Better interaction between filler and matrix also causes the improvement of aromatic solvent diffusion through the matrix. NBR is a commonly used packaging material in solvent transportation; the study proves to promise a potential compound for future applications. Further studies on degradation needs to be carried out for the study to be made industrially relevant.

CONCLUSIONS

The curing time of NBR-chitosan blends decreases on increasing the chitosan filler

content. This indicates that the incorporation of the filler improves the cure rate of the blend. From the cure data it is clear that the curing characteristics show an improved result for this new biocomposite.

Tensile strength and tear strength were maximum for the sample without filler, and shows a good and optimum value for the 5 phr filler. A decrease at high phr loadings was found to be due to the agglomeration of the filler at higher filler loadings. An increased Young's modulus for the blend of 5 phr shows a promising material for industrial application. Others showed values in the range of the pure sample. The hardness of the samples shows an increase up to NBCS2 and showed a decrease.

The study of sorption of aromatic solvents such as Benzene, Toluene, Xylene through NBR-CS biocomposite have decreased the solvent uptake tendency with increase in chitosan loading. The size and steric factor of the solvent molecule increases Q_t% values decrease. Xylene has more interaction with both the fillers and matrix due to the solubility parameter values. The diffusion of the aromatic solvents in the order Benzene > Toluene > Xylene has been correlated with the size and solubility parameter values. The FESEM analysis also confirmed the obtained results. The sorption of benzene, toluene and xylene shoes same trend with the addition of chitosan with 80% degree of deacetylation, but chitosan (90%DD) filled composite (NBCS2) shows lower sorption properties as compared with other matrix. This is due to the interaction of slightly more polar chitosan owing to the presence of higher degree of NH_2 group. From these data, NBCS2 sample i.e, the blend with 5 phr filler shows optimum values for all tests conducted. This is because of optimum interactions between the matrix and the filler. Thus the developed biocomposite may find application in the place of NBR applications which require higher solvent resistance and improved biodegradability.

Acknowledgements

Kerala State Council for Science, Technology and Engineering (KSCSTE) for SRS funding of the Junior Project Fellowship of Meril Shelly. Postgraduate and Research Department of Chemistry, St. Joseph's College (Autonomous), Devagiri, Calicut for infrastructural support.

REFERENCES

1. Z. Dan-Ying, T. Yong-Zhen, C. Yu-Bo, X. Wei-Lin, Polymer Bulletin, 62(5), 713-725, 2009.
2. M. Alneamah, M. Almaamori, *International Journal of Materials and Chemistry*, 5(1), 1-3,2015.
3. M. Hidetoshi, Y. Hiroshi, M. Minagawa, T. Akihiko, *Journal of Colloid and Interface Science*, 310(2), 678-681, 2007.
4. D.P. Chattopadhyay, M.S. Inamdar, *Research Journal of Engineering Sciences,* 1(4), 9-15, 2012.
5. J.K. Hwang, H.H. Shin*, Korea-Australia Rheology Journal,* 12(3),175-179,2000.
6. H. Ismail, S. M. Shaari, N. Othman, *Polymer Testing*, 30(7), 784–790,2011.
7. K. V. Harish Prashanth, R. N. Tharananthan, *Carbohydrate Research*, 341(1), 169-173, 2006.
8. T.D. Sreeja, S.K.N. Kutty*, *Journal of Elastomers and Plastics,* 34, 157, 2002.
9. 9. P.K. Nair, R. Joseph, *International Journal of Scientific & Engineering Research*, 3(3), 1-10, 2012
10. M N Radhakrishnan Nair, M R Gopinathan Nair:*Polymer Bulletin*, 56,619-631, 2006.

MACRO 367

Room temperature processable heat resistant epoxy-oxazolidone based syntactic foams

Soorya Nair [a], Temina Mary Robert[b], Sunitha K.[b], Dona Mathew[b] and C.P. Reghunadhan Nair [c]

[a] DB College, Sasthankotta, Kollam,
[b] Polymers and Special Chemicals Division, Vikram Sarabhai Space Centre, Thiruvananthapuram Kerala, India-695022
[c] Cochin University of Science and Technology
**Corresponding author e-mail: temirobert@gmail.com*

Abstract

Syntactic foams based on a urethane modified epoxy resin based using glass microballoons as reinforcing filler with varying densities were processed. The influence of various grades of glass microballoons, their concentration, and their mixtures in different proportions on the mechanical, thermal, thermo-mechanical, and flammability characteristics were investigated. Compressive strength increased with increase in density of the composites. The incorporation of mixture of micro balloons of varying shell thicknesses (at a given resin content), enhanced the compressive strength in comparison to a composition containing a single type of microballoon. By incorporating the microballoons, Tg of the syntactic foam increased from 90°C to 115°C. Thermal conductivity of the composites decreased from (0.064 to 0.056 W/(m.K)) in conjunction with decreasing resin: filler ratio. In the case of composites filled with K25 alone, creation of large voids due to less effective packing between the micro balloons, led to lower thermal conductivity. The specific heat of the different composites was in the range of 0.32-0.44cal/g/°C and the coefficient of thermal expansion (CTE) was in the range of 13.2 to 17.4x10^{-6} / ° C for all the systems. The foams exhibited limiting oxygen index in the range of 28-33%.

1.0 Introduction: Syntactic foams, a special type of particulate filled polymer composites possess superior specifc strength when compared to the conventional structural materials which enables them to be used in instances encountering moderately high stresses and low mass. The common matrices used in syntactic foam include polymers, metals or ceramics. The important thermosetting matrix resins used in such applications include epoxies, phenolics, cyanate, esters, bismaleimides, unsaturated polyesters, and polyurethanes. The properties of syntactic foams can be tailored by changing a wide variety of parameters: matrix and microballoon materials, type, size and size distribution and their wall thickness and volume fraction. [1, 2, 3] These variations affect the mechanical, dynamic mechanical, thermal and water-absorption properties of syntactic foams.

Syntactic foam-based lightweight polymer composites have been successfully used in thermal protection of atmospheric re-entry spacecrafts such as ARD (ESA), Apollo (NASA) and Shenzhou, China. Epoxy syntactic foams have been widely used in sandwich composites, thermal protection systems in rocket science to protect the sub structures.[4,5,6.] A ‘spray-on’ syntactic foam insulation that does not crack from repeated thermal cycling has been reported

for cryogenic applications. [7] Though a large variety of epoxy resin have been attempted as matrices, most of the case, the service temperature is limited due to its relatively low Tg of epoxy resins. Attempts to increase the Tg by structural modification are reported.[8] One such process is to incorporate cyanate ester modification of epoxy resin by reacting with isocyanates. This paper deals with the synthesis of such structurally modified epoxy resins and their use in syntactic foams. The impact of structural modification on the thermo mechanical properties of the resultant syntactic foams have particularly been investigated.

The present work focuses on the synthesis and characterization of a urethane modified epoxy resin and its syntactic foam composites using glass microballoons as filler. The influence of various grades of glass, their concentration, and their mixtures on the mechanical, thermal, thermo-mechanical, and flammability characteristics were investigated.

2.0 Experimental

Materials: Polytetra methylene oxide (PTMO, Sigma Aldrich, Mol. Wt 2000), 1, 4 butane dioldiglycidylether (Huntsman, epoxy value 8 eq./Kg), Tolylenediisocyanate(Sigma Aldrich, isocyanate content - 99%), Diglycidyl ether of Bisphenol A (Huntsman, epoxy value - 5-6 eq/Kg), Polypropylene glycol bis (2-aminopropyl ether)(Sigma Aldrich, amine value - 200-300mg KOH/g), Polyamido amine (Huntsman, nitrogen content -14-16%), 2,4,6 – tris (dimethyl aminomethyl) phenol (Huntsman, amine Value - 300-450) , Acetone(AR grade, Finar), Glass micro balloons K1 and K25 (3M Company, USA, True density - 0.125 g/cc and 0.25 g/cc respectively).

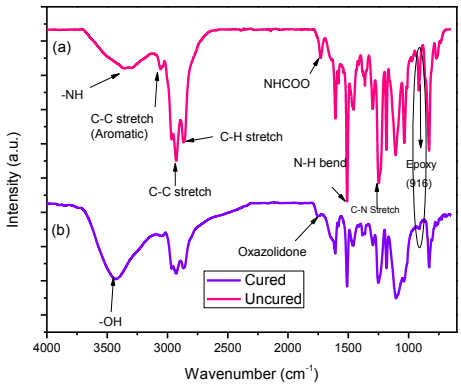
2.1. Synthesis of urethane modified epoxy resin: 450g of Diglycidyl ether of Bisphenol A, 75g of Polytetra methylene oxide and 50g of 1, 4 butanedioldiglycidyl ether were weighed into a three necked RB flask, equipped with a mechanical stirrer and N2 inlet. 20.1g of Tolylenediisocyanate (TDI) was added drop wise and the reaction was conducted at 150±5 °C for 3 h. After 3hrs, the temperature was raised to 190-200 °C for 2 h. the product was characterized by FTIR, NMR, GPC, Epoxy value and viscosity. The epoxy value was 4.6 eq/Kg and a bulk viscosity of 8810 cps was observed. Amine curative agent was processed by blending 90g of the polyamidoimidazoline, 90g of 2, 4, 6- tris (dimethyl aminomethyl) phenol and 24g poly propylene glycol bis (2- aminopropyl) ether at 80°C for 3hrs. Amine value was 360 mg KOH/g and a bulk viscosity of 360 cps.

2.2. Processing of Syntactic foam composites

Syntactic foams of the poly urethane modified epoxy resin syntactic foam was prepared by mixing the epoxy resin and amine curative in 1:1 mole ratio. Resin to microballoon ratios were varied from (25 to 60 wt. %) to achieve syntactic foam composites with densities of 0.15, 0.16,

0.2, 0.27 and 0.29 g/cc Table 1). The required quantity of the resin was weighed into a beaker and diluted with acetone. Calculated quantity of microballoon was added in small portions in to the resin solution and mixed well by hand mixing. The mixture of resin and micro balloon was then transferred carefully into the mould (151 x 151 x 58 mm) and allowed to cure for 24 h at touch pressure. Composites were also processed using mixture of microballons of different densities.

3.0 Characterisation: FTIR spectra were recorded (Perkin Elmer spectrum GXA spectrophotometer) using KBr pellets in the range of 4000-400 cm-1at a resolution of 4 cm-1. DSC was performed (TA instrument DSC Q-20) at a heating rate 10° C min-1 in nitrogen atmosphere and TGA (TA Instruments SDT Q-600 thermogravimetric analyzer) at a heating rate of 10°C min-1 in nitrogen atmosphere. Mechanical properties were determined using an INSTRON UTM 4202. Thermomechanical analyser was used to measure the Coefficient of thermal expansion using TA Instruments Q400, as per ASTM E831, at a ramp of 10 °C /min under N2 (50ml/min) up to 300 °C. The Limiting Oxygen Index (LOI) was determined as per ASTMD 2863.



4.0 Results and discussion: Urethane modification of the epoxy backbone was confirmed from the peaks at 3370, 1753, 1726, 1508, 1252, 916 cm^{-1} corresponding to the N-H stretch of amine curative, urethane, N-H bending, C-N stretch and epoxy groups respectively. The disappearance of the epoxy peak at 916 cm^{-1} in the cured resin indicates complete curing. A broad absorption band at 3455cm^{-1} corresponds to the O-H and N-H groups formed via the epoxy ring opening reaction with the amines

Figure1 FTIR spectra of the neat resin (a) cured and (b) uncured

Compressive strength of the various syntactic foams were characterized at 25°C, 200°C and -196 °C and the data are compiled in Table1.

Table 1. Variation of compressive strength at different temperatures

Ref	Density (g/cc)	Compressive Strength (Kg/cm^2)		
		-196°C	**30°C**	**200°C**
C1	0.150	21.6-26.7	11.5 – 15.8	6.5 – 8
C2	0.139	9.03-13.3	6.8-8.9	4.5-5.3
C3	0.151	11.0-13.7	6.9-9.8	5.7-7.0

The compressive strength was found to decrease with increasing micro-balloon loading since the amount of resin available is not sufficient enough to wet and hold the microballoons together and hence the entire load will be transferred to the microballoons, leading to early failure. In addition, the air space occupies a large volume of the composites, and this reduced the overall strength of the system. A crack will initiate in a porous composite at an oversized void when it is subjected to load and as the volume percentage of glass microballoons increases, the compressive strength and density

of the syntactic foams decreases. Thus between C1 and C2, C1 exhibits a higher compressive strength.

C5	0.230	18.8-20.0	21.7-28.8	8-10.5

4.1. Influence of nature of microballoon and composition

At the same resin content the incorporation of mixture of microballoons (C3) slightly enhanced the compressive strength in comparison to a composition containing K1 alone (C2). This may be attributed to the greater shell thickness of the K25 in comparison to K1 and also better packing achieved while using a mixture of microballoon fillers. The approach of changing the microballoon thickness while keeping the microballoon volume fraction constant is more effective than changing the microballoon volume fraction to change the syntactic foam density as this approach would considerably increases the specific strength. As expected, maximum mechanical properties are achieved for the system incorporating K25 owing to its superior strength compared to K1.

A similar trend is also observed for compressive strength at high temperature. Compressive strength is reduced almost to 50 % at 200 °C for C1, where the resin content is high. The higher compressive strength at low temperature is attributed to the enhanced rigidity of the molecular chains, therby increasing the capability to withstand higher loads.

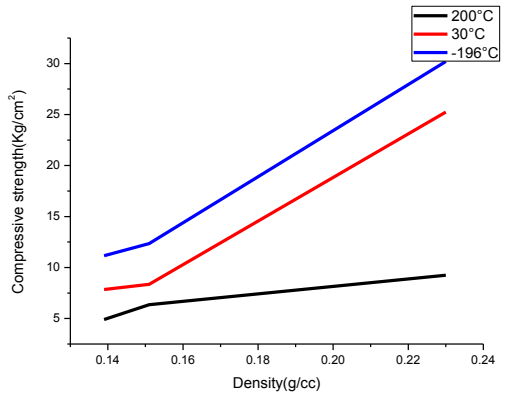


Fig 2. Average compressive strength with density at various temperatures

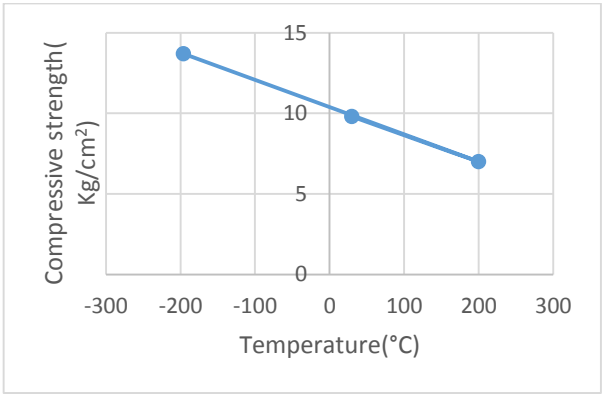


Figure 3 Effect of temperature on compressive strength of a typical composite (C3)

The effect of temperature on compressive strength for a particular composition is shown in Figure 6. It can be seen that the curve follows a linear fit enabling the predication of

compressive strength at any temperature between -196 to 200°C. Interestingly the LN2 properties showed an improvement in properties w.r.to the properties at RT, while the reduction in properties at high temperatures is not significant. Though the Tg of the system is 92°C, the significant property improvement at LN2 temperature is due to the sub Tg transition of the poly tetra methylene oxide group linked by oxazolidone moieties.

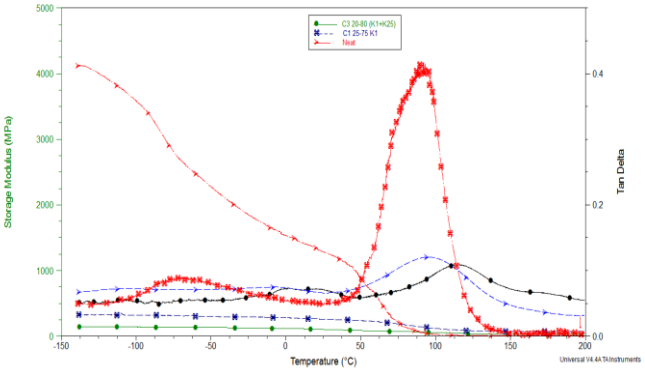
4.2. Transitions in the syntactic foam composites

For the syntactic foam composites, it can be seen that the transition temperatures are shifted to higher range in comparison to the unfilled system. This is due to the restricted movement of the bonds in the matrix by the microballoons. So more amount of energy is required for such sub Tg transitions. Hence with the incorporation of microballoons, the low temperature flexibility of the composites is reduced and the material becomes rigid. By incorporating K25 into the matrix along with K1, the Tg further shifted to 115°C.

Figure 4 Variation in storage modulus and tan delta

4.3. Thermo physical properties

The thermal conductivity and diffusivity of different composites at room temperature is tabulated in **Error! Reference source not found.**2. From the table it is evident that as the density of the composite increases thermal conductivity also increases. In the case of composites containing both K_1 and K_{25}, K_{25} having larger radius than K1, it cannot have an effective close packing since the void formed creates large gaps between the micro balloons, which are occupied by air, leading to lower thermal conductivity. In the case of composites containing K1 alone, the diameter is relatively smaller in comparison to K25 and hence can effectively be close packed and the voids formed will be smaller leading to higher thermal conductivity for its formulations at the same resin to filler ratio.



Between C3 and C4, owing to the higher resin content, thermal conductivity is higher for C4. In the case of mixture of microballoons, as in the case of C2 and C3, the thermal conductivity is marginally lower due to the lower packing efficiency.

Table 2 Thermal properties of various composites

The coefficient of thermal expansion of a composite gives its dimensional stability at predefined conditions of temperature. All the composites exhibited a CTE in the order of 10^{-6}/ ° C in the temperature range of -150 to 200°C. The specific heat was also found to increase with increasing microballoon content. The specific heat for the resin dominated composites were around 0.3-0.32 cal/g/°C while for the

Ref	Thermal Conductivity at RT(W/(m.K))	Thermal diffusivity (m2/s)	CTE x10^{-6} / ° C	Specific Heat cal/g/° C
C1	0.059	0.89394	15.1-16.0	0.44
C2	0.057	0.91127	14.8-15.9	0.45
C3	0.056	0.80622	13.2-15.6	0.46

microballoon dominated system, it was around 0.44cal/g/°C.

C4	0.064	1.02041	16.0-16.2	0.38

4.4. Thermal stability of the cured networks

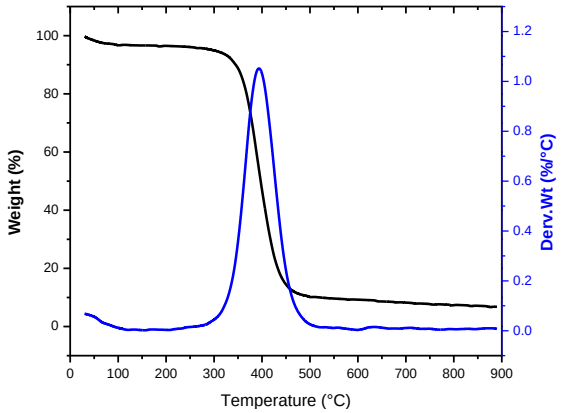


Figure 5 Thermogram of cured matrix resin

The thermogram of the neat resin (Fig 5) shows that it is stable up to 300 °C with peak decomposition at 395 °C and a char residue around 7% at 900 °C.

4.5.Flammability

LOI, often used to rate the relative flammability of the different composites, are compiled in the

Table 5. The LOI values were around 25-33% for all the five composites. In the case of C1 and C4 with higher resin content, the LOI was low and they caught fire immediately in air (atmospheric oxygen 20-22%). But as the microballoon content increases, LOI increased to 33%.

SI No	Reference	LOI (%)
1	C1	29
2	C2	32
3	C3	33
4	C4	25
5	C5	32

Table 3 Limiting Oxygen of different composites

SI No	Reference	LOI (%)
1	C1	29
2	C2	32
3	C3	33
4	C4	25
5	C5	32

5.0 Conclusions

Urethane modified epoxy resin was synthesized and characterized. The curing of the resin with amine based curing agent initiated at around 60°C with Tp at around 110 °C. Storage modulus increased rapidly beyond 100°C stagnated around 200°C, indicating the completion of the reaction. Mechanical and dynamic mechanical properties and thermal stability of the cured networks also were evaluated. From the TGA, the cured resin was found to be thermally stable up to around 300°. The cured network exhibited tensile strength of 47-50MPa with 3.6-5% elongation and modulus of 1.7-2.6GPa.

Syntactic foam composites of this system showed an increase in compressive strength with increasing density. The incorporation of mixture of micro balloons of varying shell thicknesses (at a given resin content, enhanced the compressive strength in comparison to a composition containing a single type of microballoon. At LN2 temperature, the compressive strength

increased significantly due to enhanced rigidity of the system while the reduction in properties at higher temperature is not significant. By incorporating the microballoons, Tg of the composites shifted from 90°C to 115°C. Thermal conductivity of the composites decreased with decreasing resin: filler ratio. In the case of composites containing K25, creation of large voids (due to less effective packing) between the micro balloons, led to lower thermal conductivity. The specific heat of the different composites was in the range of 0.32-0.44cal/g/°C and the coefficient of thermal expansion (CTE) was in the range of 10^{-6} / ° C for all the systems. The limiting oxygen index of the different the syntactic foam composites depended upon the resin content and were in the range of 23-33%.

References

1. P. Bunn and J. Mottram, *Composites*, 1993, **24**, 565-571.
2. N. Gupta, E. Woldesenbet and P. Mensah, *Composites Part A: Applied Science and Manufacturing*, 2004, **35**, 103-111.
3. N. Gupta and W. Ricci, *Materials Science and Engineering: A*, 2006, **427**, 331-342.
4. H. McIlroy and C. Smith, *CHARACTERIZATION OF AN EPOXY FOAM*, Bendix Corp., Kansas City, Mo., 1970.
5. A. Mansourighasri, N. Muhamad and A. Sulong, *Journal of Materials Processing Technology*, 2012, **212**, 83-89
6. T. Fine, H. Sautereau and V. Sauvant-Moynot, *Journal of Materials Science*, 2003, **38**, 2709-2716.
7. P. R. Marur, *Materials Letters*, 2005, **59**, 1954-1957.
8. J. J. Gebhardt and P. W. Juneau Jr, US Patents, 1984.
9. B. Song, W. Chen and D. J. Frew, *Journal of composite materials*, 2004, **38**, 915-936.
10. A. H. Landrock, *Handbook of plastic foams: types, properties, manufacture and applications*, Elsevier, 1995.

MACRO 378

Coconut Oil Plasticized Poly (lactic acid): Influence of Coconut Oil on Morphological, Rheological and Gas Barrier Properties

Bhasney Siddharth, Patwa Rahul, Kumar Amit* and Katiyar Vimal*

Department of Chemical Engineering, Indian Institute of Technology, Guwahati, Assam, India

e-mail: amitkumar@iitg.ernet.in, vkatiyar@iitg.ernet.in

In this work, blend of polylactic acid (PLA), biodegradable thermoplastic polyester, with coconut oil as plasticizer have been studied. PLA and coconut oil were blended in a twin screw extruder with the objective of obtaining flexible films with reduced water vapour permeability for food packaging application.

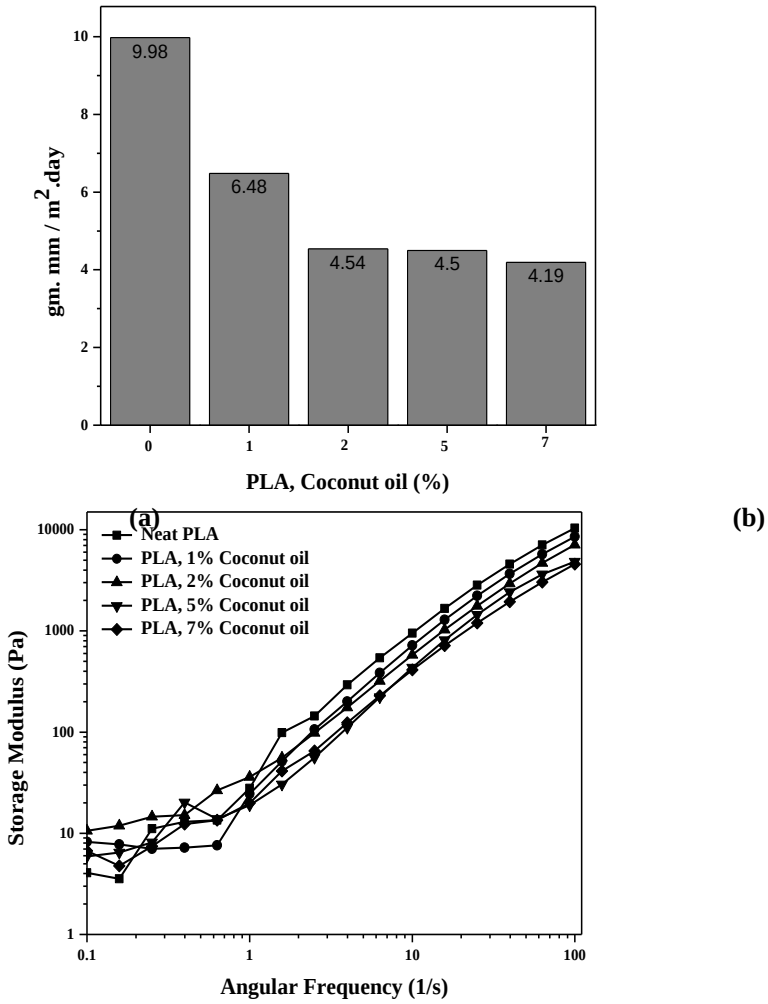


Figure (a): Water vapor permeability for PLA, Coconut oil blends films, (b): Frequency dependence of storage modulus (G') of PLA blends at 190°C

It is observed that while the addition of coconut oil, the glass transition temperature of PLA have been reduced upto 60.9°C therefore, confirms the improvement in chain mobility of PLA at a lower temperature. Further, the above effect enhances with the coconut oil loading. Single glass transition temperature confirms the compatibility of PLA with coconut oil. However, the decrease in the melting point with loading could be due to the formation of different crystallite size and shape. Interestingly, Incorporation of coconut oil into PLA led to a decrease in the water vapor permeability of processed film. It shows that dynamic storage modulus (G') of PLA/Coconut oil blends increased with angular frequency, but decreased with the increase of Coconut oil content in the blends. The use of plasticizers reduced the intermolecular force and increased the mobility of the polymeric chains, thereby improving the flexibility and extensibility of the plasticized as shown in Figure (a) & (b). Good compatibility was observed between the coconut oil and PLA. The flexibility and improved barrier properties make this blend suitable for biodegradable film manufacture for packaging application.

Acknowledgements

We sincerely acknowledge the Centre of Excellence for Sustainable Polymers (CoE-SusPol) at IIT Guwahati, for providing the research facilities. We also thank the Central Instrumental Facility, IIT Guwahati for providing characterization facilities.

References

[1] Hao, Y., Yang, H., Zhang, H., Zhang, G., Bai, Y., Gao, G., & Dong, L. Diethylene glycol monobutyl ether adipate as a novel plasticizer for biodegradable polylactide. *Polymer Bulletin*, (2016) 1-19.
[2] Qin, Y., Wang, Y., Wu, Y., Zhang, Y., Li, H., & Yuan, M. Effect of hexadecyl lactate as plasticizer on the properties of poly (l-lactide) films for food packaging applications. *Journal of Polymers and the Environment*, (2015) *23*(3), 374-38.
[3] Pal, A. K., & Katiyar, V. (2016). Nano-amphiphilic Chitosan Dispersed Poly (Lactic Acid) Bionanocomposite Films with Improved Thermal, Mechanical and Gas Barrier Properties. *Biomacromolecules*.

MACRO 382

Tuning base polymer molecular weight and filler composition for optimum cure, mechanical, rheological and dielectric properties of PDMS based one part RTV adhesive

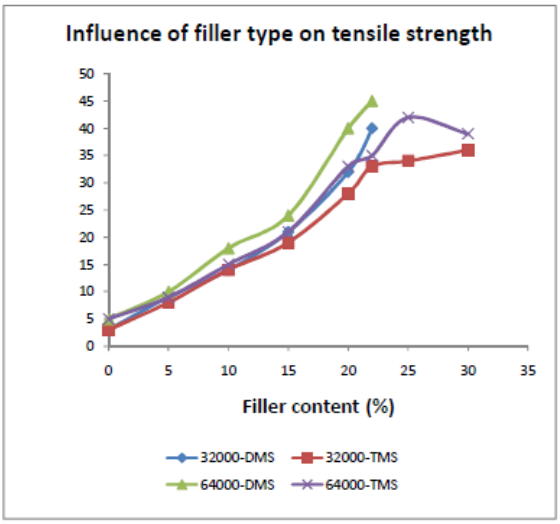
Smitha C Sukumaran*, Prasanta Kumar Behera, R. Pravin and R. S. Rajeev
Email: smithanimesh100@gmail.com
Polymers and Special Chemicals Division
Propellant, Polymers and Chemicals Entity
Vikram Sarabhai Space Centre
Thiruvananthapuram-695 022

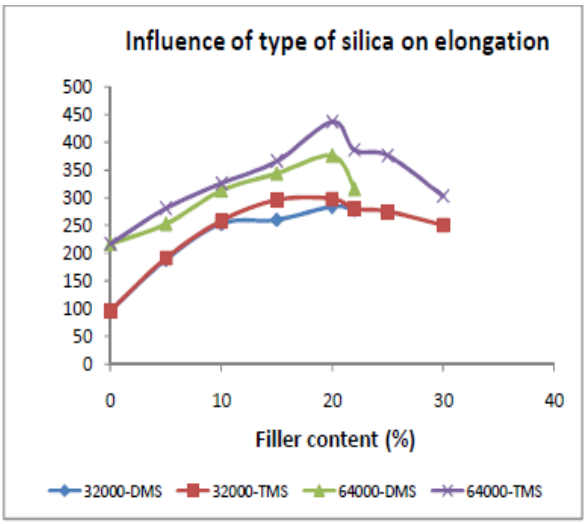
Abstract

Aerospace industry has traditionally been a pacemaker for development and introduction of new materials systems and technologies. The key driving forces for development of new materials are performance improvement, weight and cost reduction to bring significant impact on both economical and ecological issues. polymer- based materials are widely being used as composites, thermal control coatings, adhesives, tapes, potting compounds, toughening agents, seals, thin film substrate, etc. Among the different polymers available for an aerospace materials engineer, silicones1,2 stand out owing to their capability to withstand the temperature extremes that are experienced in space and. They also possess low outgassing properties and maintain good degree of flexibility at temperatures as low as -150°C where most of the other materials would stiffen and crack. Moreover the elastomeric properties effectively dampen the vibrations.

The present paper deals with developing a single part, room temperature vulcanizing silicone sealant having good mechanical, electrical and thermal properties and low outgassing characteristics. Systems having filler content varying from 0-25 wt% are prepared using OH- functional polydimethyl siloxanes of different molecular weights and combination of fillers consisting of titanium dioxide, carbon black and silica-blended in a definite proportion. Two grades of silica fillers (viz trimethylated silica (TMS) and dimethylated silica (DMS)) were used in the filler blend. Mechanical, electrical, thermal and outgassing properties of samples prepared were analyzed and the properties were correlated to the composition of the system and molecular weight of the base polymer. It is observed that trimethylated silica (TMS) loaded system exhibit better mechanical, electrical and thermal properties when compared to dimethylated silica (DMS) filled system. Figures1 (a) and 1(b) show the dependence of tensile strength and elongation at break of cured compounds on type and content of the Silica filler in PDMS matrices of two different molecular weights. From the figure it is clear that, tensile strength of samples increases with the filler content irrespective of the molecular weight of PDMS up to around 20% filler loading. Among the DMS and TMS- filled systems, dimethylated silica filled system has marginally

higher tensile strength compared to trimethylated silica filled system. At a given filler loading, the DMS- containing system exhibits higher interaction with the polymer, as implied by the increased viscosity of the compound. This led to difficulty in compounding more than 22wt% dimethylated silica filler in PDMS. Rheological, viscoelastic, dielectric and cure characteristics of the polymers of different molecular weights, loaded with different wt% of filler are also investigated and correlated to the nature of filler, composition and molecular weight of the base polymer.





References:

[1] [1].O. I. Hulai, O. I. Tselyukh, I. O. Nironovych, Ya. A. Serednyts'kyi." Effect of mineral fillerson the properties of silicone coatings"; Materials Science, Vol32, No 5,1996.

[2] [2].S.M. Kong1,M. Mariatti1⇓,J.J.C. Busfield2." Effects of types of fillers and filler loading onthe properties of silicone rubber composites" Journal of Reinforced Plastics and Composites, Vol26, No. 12,1999.

MACRO 385

Recyclable Polylactic Acid grafted Cellulose Nanocrystal Films through Reactive Extrusion Approach

Dhar Prodyut, Kumar Amit and Katiyar Vimal *

[a] *Department of Chemical Engineering, Indian Institute of Technology Guwahati, Guwahati, 781039, Assam, India.*

email: vkatiyar@iitg.ac.in

In this paper, we successfully demonstrate the grafting of polylactic acid onto cellulose nanocrystals (PLA-*g*-CNC) using dicumyl peroxide (DCP) as cross-linking agent via reactive extrusion process. PLA-*g*-CNC nanocomposite films showed improved compatibilization between the hydrophobic PLA and hydrophilic CNCs alongwith interesting property of recyclability. The maximum fraction of PLA chains grafted on CNC surface was found to be 66% with the highest grafting efficiency (~40.7 %) and gel yield (74.2%) achieved at 1 wt% CNC loadings. During the reactive extrusion process, it was found that the complex viscosities of PLA-g-CNC nanocomposites were higher (~50-70 Pa.s at various CNC loadings) in comparison to neat PLA (~40 Pa.s), probably due to the formation of branched and cross-linked structures [1].

NMR and FTIR spectroscopy studies showed that during reactive extrusion process, the radicals generated on CNCs surface instantaneously reacts with amorphous PLA chains thereby shielding the sulphate and hydroxyl groups of CNCs and forming a thin layer of PLA layers grafted on CNCs. Presence of such PLA encapsulated CNCs led to improved interfacial compatibility and dispersion within the PLA matrix and also prevented the thermal degradation during recycling. ^{1}H NMR spectroscopy analysis of PLA-g-CNC samples showed new characteristic peaks at 3.68 ppm and in the 4.1–4.5 ppm range which confirms the grafting. The new peak at 3.68 ppm corresponds to the methine protons formed in the PLA-*g*-CNC structure (marked as 'a' in the inset of Figure 1 (a). Both PLA-*g*-CNC (obtained through reactive extrusion) and rPLACNC (obtained after further recycling) are capable of forming transparent films with improved adhesion and dispersion of CNCs [1, 3].

Due to the chain extensions and formation of branched structures, the weight average (M_w) and number average (M_n) of PLA-*g*-CNCs increased significantly (by ~40 %) (Figure 1 (b)). Interestingly on the thermal recycling of the PLA-g-CNC gels (rPLACNC) at similar extrusion conditions, the M_w and M_n didn't showed any significant deterioration. Reactive extrusion of PLA with DCP in the presence of CNC (1–3 wt% range) shows an increase in both M_w and M_n by ~40 %. Such drastic increase in MWD is however absent during reactive extrusion of PLA in the presence of DCP alone. The PDI of the PLA-g-CNC did not changed significantly and was found to be ~ 2, which suggests that the chain length of branched PLA were formed with uniform distribution even at different CNC loadings. The GPC chromatograms for PLA-*g*-CNC were

broader compared to those for PLA and show the presence of two small distinct shoulders both at high and low molecular weight regions. This can be attributed to two possible phenomenon occurring during the reactive extrusion process: chain extension in the presence of DCP (leading to chromatogram shift to high MWD region) and chain scission in the presence of CNCs (leading to shift to low MWD region). GPC studies showed that recycling of the PLA-*g*-CNC gel led to decrease in Mw and Mn by ~18 and 15% only (at~3wt % loading), which is less compared to traditional PLA/CNC extrusion (~22 and 18% at 1wt. % CNC loadings during first time extrusion). The reactive extrusion based grafting approach effectively masks the interaction of sulfate and hydroxyl groups in CNCs with PLA, thereby preventing the drastic reduction in molecular weight. The PDI was found to be ~1.8 for recycled samples, which was lower than that of PLA-*g*-CNC probably due to chain scission of the long branched PLA chains during extrusion. However, after reprocessing the GPC chromatograms was found to be sharper, with a decrease in the shoulder area for high molecular weight peak and increase in number of peaks in the low molecular weight region. The area of the high molecular weight shoulder peak decreased from ~89 to 68% for 1 and 3 wt% CNC loadings respectively. Moreover, three low molecular weight peaks were found (at retention time ~16.5, 17.3 and 17.6 min), whose area increased with the higher CNC loadings (~8.46, 6.4 and 6.1% respectively at 3 wt% CNC loading). This is possibly due to lower grafting efficiencies at ~3 wt% CNC loadings, which enhances the thermal degradation of PLA due to presence of sulfate and hydroxyl groups. However, the decrease in MWD is not significant enough compared to the traditional approach of PLA/CNC processing and recycled polymers with Mw ~ 250 kDa finds potential engineering applications [2,3].

Due to formation of the C–C bonds with the CNCs, both the thermal stability and the mechanical properties of PLA-*g*-CNC nanocomposites improved significantly. The T_{onset} and $T_{1/2}$ of PLA-*g*-CNC was found to be improved by ~12ºC and ~5ºC respectively (at ~1wt. % loadings), compared to neat PLA. The percentage reduction in weight during the initial processing (upto ~300ºC) was also reduced significantly (only ~1.9 wt %) compared to traditional process. This is due to the formation of PLA encapsulated CNCs initially during reactive extrusion, which masks the sulfate and hydroxyl groups of CNCs, thereby delaying the degradation process. Also, the formation of C–C bond between the PLA and CNCs leads to enhanced thermal stability as higher activation energy is required to break such bridged linkages. Reprocessing the PLA-*g*-CNC nanocomposites led to the formation of low molecular weight fractions due to chain scission under thermal stress conditions. This led to a decrease in the T_{onset} and $T_{1/2}$ of reprocessed PLA-*g*-CNC, by 24ºC and 8ºC respectively (at ~1wt. % loadings), along with a reduction of ~5 % weight at 300ºC. Therefore, it can be concluded that the thermal properties of the PLA-g-CNC films do not alter significantly on reprocessing which is desirable for product fabrication.

The tensile strength and young's modulus improved by 41and 490% respectively, whereas the filler effectiveness coefficient (C_{FE}) values decreased, suggesting that the grafted CNCs act as an efficient reinforcing agent. The E' increased on incorporation of CNC (~2 wt %) in presence of DCP due to the formation of cross-linked structure and better interfacial adhesion with the polymer matrix. The tensile strength and modulus of the reprocessed PLA-*g*-CNC films decreased by ~28 and 56% respectively, probably due to degradation of bulk PLA chains (both branched and linear) takes place either during thermal reprocessing or due to the presence of sulfate groups on the agglomerated CNCs (at higher loadings), as confirmed by the MWD studies. Furthermore, XRD and DSC studies shows improvement in crystallinity, possibly due to grafting of the amorphous PLA chains onto the crystalline CNC segments which act as nucleating agent[4]. This novel, thermally stable, reactive extrusion-based strategy can be implemented for industrial scale fabrication of PLA-*g*-CNC recyclable biocomposite films for potential applications in packaging.

References

[4] Dhar, P., Tarafder, D., Kumar, A., & Katiyar, V. *Polymer*, 87(2016), 268.
[5] Dhar P., Tarafder D., Kumar A., Katiyar V., *RSC Adv.* 5 (2015) 60426.
[6] Furukawa T., Sato H., Murakami R., Zhang J., Duan Y.-X., Noda I., Ochiai S., Ozaki Y., *Macromolecules* 38 (2005) 6445.
[7] Zoppe J.O., Habibi Y., Rojas O.J., Venditti R.A., Johansson L.-S., Efimenko K., Österberg M., Laine J., *Biomacromolecules* 11 (2010) 2683.

Figure 1: (a) ^{1}H NMR spectra for the PLA-*g*-CNC sample (PLADCNC1) with the selected region (4.4-3.3 ppm being marked in black square) zoomed and shown as inset. The inset also shows the probable structure of PLA-g-CNC formed after reactive extrusion in presence of DCP and (b) Molecular weight distribution weight average (M_w) and mean average (M_n) of extruded PLA, reactively extruded PLA/CNC nanocomposites and reprocessed PLA-*g*-CNC gels respectively.

Acknowledgement

We acknowledge Centre for Excellence for Sustainable Polymers (CoE-SuSPol), Central Instrumentation Facility (CIF), and IIT Guwahati for the research facilities.

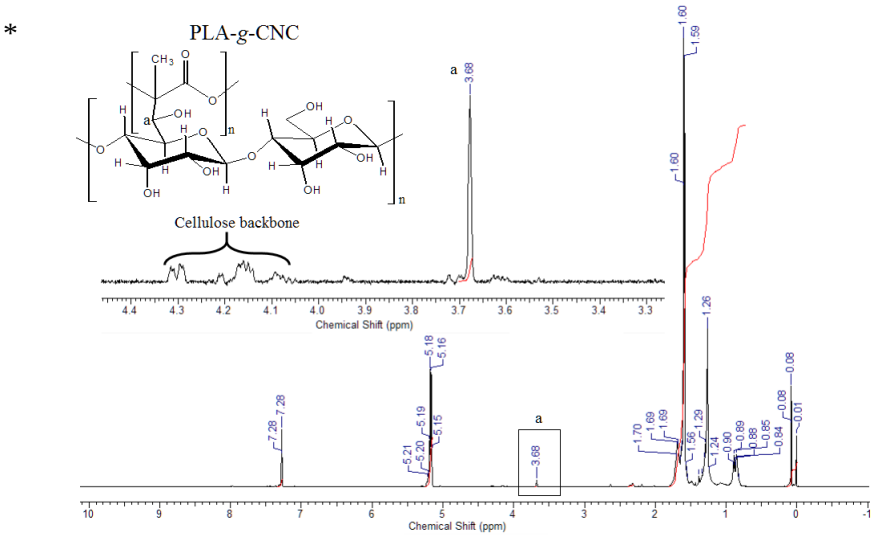
MACRO 386

Early prediction of polymer degradation due to weathering

A.K. Sikder*, Parthipan B and Chandrashekhar L

SABIC Research & Technology Pvt. Ltd, Sarjapura, Bangalore -562125, India

arun.sikder@sabic.com



Abstract

Weathering is a surface phenomenon and usually is monitored through change of aesthetics. Measurement of surface appearance often fails to predict bulk mechanical failure of polymer materials. In this study, surface sensitive nano-indentation technique was used with CSM (continuous stiffness measurement) to measure surface mechanical properties on molded samples after exposure at different time and extrapolate the obtained information to predict mechanical failure of the materials. In order to establish this concept, two samples, one thermoplastic (TP) and copolymer of the TP, were exposed to laboratory weathering conditions up to 4000h. Modulus and hardness measured though CSM method and found to be higher for copolymer compared to TP. It was found that rate of percent change of modulus was higher for TP compared to the copolymer, which indicates that TP degrades faster compared to the copolymer. Gloss retention and color shift with exposure time also indicates slight better performance of copolymer. Cross-sectional transmission electron microscopy shows that depth of degradation is higher for TP sample.

Keywords: *polymer; nano-indentation; weathering; degradation*

Introduction

Polymer degrades due to light, heat and moisture and hence have limited service life[1]. In order to understand this ageing behaviour of polymers, material suppliers usually conduct natural and laboratory accelerated weathering studies. Weathering is a long-term test, where natural weathering requires ~1-3 years and laboratory-accelerated testing methodology requires ~6-12 months to understand the materials performance[2].

When a material is exposed to weathering conditions, the degradation of a material starts from top layer at the initial stages and slowly propagates deeper as a function of time. This necessitates a detailed study in order to better understand the initial surface changes, which eventually lead to the failure of the product. Weathering is usually monitored through change of color, gloss and mechanical properties. However, change of mechanical properties at the early stage of exposure is difficult to capture through conventional mechanical testing (tensile, impact etc.). Hence, surface sensitive technique is required to capture early change of mechanical properties.

To evaluate the mechanical properties in a small scale, nano-indentation technique has been used extensively[3,4]. This is a depth sensing indentation at low loads and is a well-established technique for the investigation of localized mechanical behavior of materials. CSM (continuous stiffness measurement)[5] technique is used in this study to generate depth dependent hardness and modulus values.

In this study, nano-indentation technique along with optical and microscopic techniques were used to assess the change in properties on the top surface layers due to accelerated weathering. Methodology was used on a thermoplastic (TP) and its copolymer to compare their weathering behavior. Percent mechanical property changes were then correlated with the optical measurement and transmission electron microscopy.

Experimental

Samples selected for this study were a typical thermoplastic (TP) and its copolymer. Both the samples were in same level of gloss and color (black). Copolymer had a better weathering performance under same weathering conditions. Samples were lab scale formulations and do not match with any commercial grades. The 3mm thick color plaques were made using standard injection molding process.

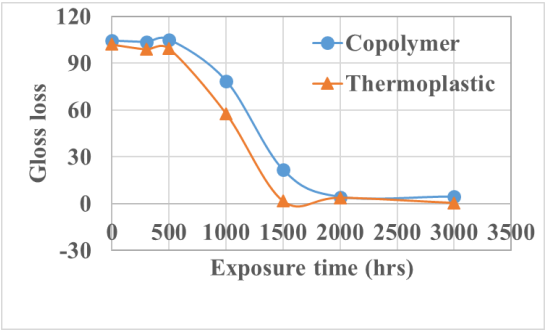
Weathering exposure was carried out in a Ci5000 weatherometer from Atlas Material Testing Groups. ISO 4892-2A; an exterior weathering test protocol was used for this study. This is a Xenon Arc weathering test standard for outdoor application. The test conditions were irradiation level of 0.51 W/m2 @340nm optical filter, BST (Black Standard Temperature) was 65°C and the RH (Relative Humidity) was 50%. Samples were exposed for 300, 500, 1000, 1500, 2000, 3000 and 4000h. Color was measured using the ColorEye 7000A spectrophotometer from GretagMacbeth following ASTM D2244 protocol. Gloss measurements were performed using BYK Gardner Tri-Glossmeter and the angle used was 60° [ASTM D523].

Indentation experiments were conducted using the Nano Indenter® XP (Keysight Technologies, CA). A three-sided Berkovich-shaped diamond indenter is used to indent the material surface. The load and displacement data obtained in the nano-indentation tests were analyzed according to the method proposed by Oliver and Pharr[3] using the software provided by vendor. CSM technique[5] was used for measuring absolute and depth dependent hardness and modulus values. Initially, software produces hardness and modulus vs. total displacement curves and the absolute values of hardness and modulus were calculated by specifying the range of indentation depth. Values were calculated by averaging a number of separate indentations at particular depth specifications.

Results and discussion

Material degradation was monitored through Color (Delta E) and gloss change before and after weathering and results are shown in Fig. 1 with respect to exposure time. Thermoplastic shows lower retention of gloss compared to copolymer up to 1500h. With respect to color shift,

both the polymer showed similar behavior up to 1500h. However, post 1500h, it was observed different transition for TP and copolymer, which may be because of surface erosion.



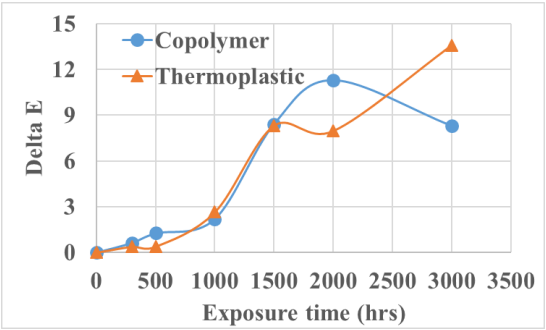


Figure 1: The gloss loss (at 60º) and color shift are plotted for TP and copolymer, measured at various interval of weathering exposure.

Depth sensing nano-indentation technique was used to assess the mechanical properties gradient created due to weathering on the molded surface. Figure 2 shows typical loading and unloading curves for TP and copolymer. Indentation depth was 3000nm. Higher load required for same penetration depth is indication of higher modulus and hardness for copolymer.

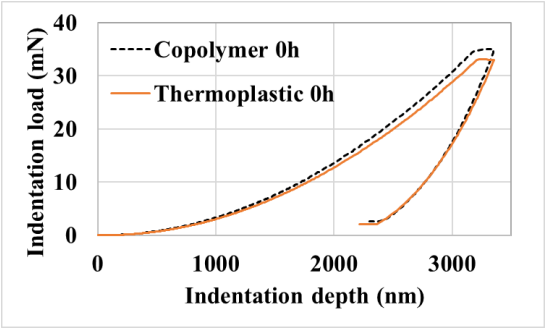


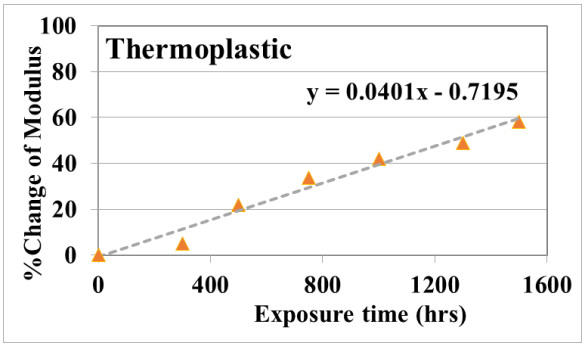
Figure 2: Typical loading and unloading curves for TP and copolymer before exposure.

The load and displacement data was obtained from CSM technique and analyzed for depth dependent hardness and modulus. Absolute values of hardness and modulus were calculated at ~500nm depth and compared between TP and copolymer exposed for different time.

It was found that with increasing exposure time, both hardness and modulus increased till 2000h for TP and till 4000h for copolymer, respectively. At exposure time of 2000h and above, loss of hardness and modulus near the surface was observed for TP. It was also interesting to note that as material surface is exposed for longer time, the hardness-modulus reached a critical point (H/E ratio normally gives the indication of brittleness) and then top surface will start disintegrating. At the same time underneath the brittle surface of exposed sample above 1500h showed increased hardness and modulus similar to the sample surface exposed at lower time. Therefore, it was shown that disintegration of material started from surface and it could be happening layer by layer. This depth sensing measurement of hardness and modulus indicates the thickness of degraded layer. Also depth-sensing measurement throws light on the gradient change of mechanical properties on the weathered surface.

Taking mechanical property data on unexposed sample surface as base line, %change of mechanical properties were calculated at each exposure hour. Figure 3 shows the plot of %change of modulus with respect to up to 1500h of exposure. It was found that rate of percent change of modulus was higher for TP compared to the copolymer. Higher slope for TP indicated faster degradation compared to the copolymer. At 1500h exposure there is 60 % change in modulus observed whereas copolymer shows only ~20% change.

(a)



(b)

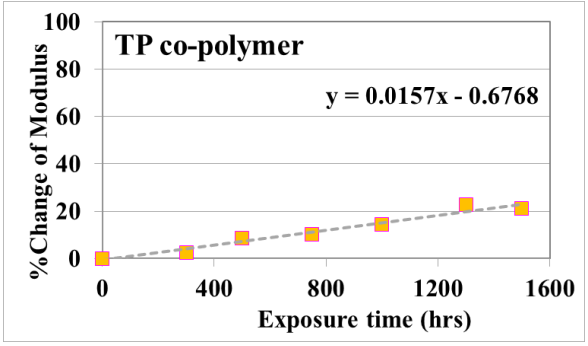


Figure 3: Percentage change of nano-indentation modulus measured at the surface for (a) Thermoplastic and (b)Thermoplastic co-polymer.

Upon extrapolating using the fitted equation (shown in Fig. 3a) it was found that in order to change 60% of modulus for copolymer it may take close to 4000h of exposure. In other word, copolymer retained more than double mechanical properties as compared to the TP at the same exposure time.

In order to analyze further hardness and modulus were also calculated at different depths of penetration using the CSM data (not shown here). It was found that at a given exposure time, change of modulus/ hardness were at higher depth for TP compared to copolymer. Higher degradation thickness for TP was also observed though TEM. Usually higher the degradation layer thickness chances of mechanical failure of a part increases.

Typical cross-sectional TEM images captured near the surface of TP and TP copolymer are shown in Fig. 4. Degraded layer on the very top surface clearly showed different contrast compared to good region. At exposure time 1000h, TP shows the degraded/transformed layer thickness to be >4 μm whereas copolymer showed it to be >1.5 μm. Higher degradation layer thickness makes the material more prone to bulk mechanical failure.

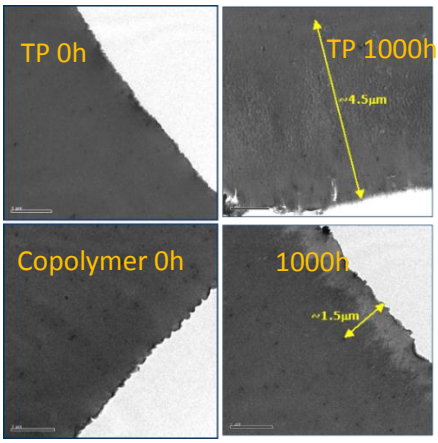


Figure 4: Cross-sectional TEM micrographs of Thermoplastic and copolymer showing the degradation layer thickness at 0h and after 1000h of exposure.

It was observed that near the surface, both TP and copolymer are initially getting hardened due to weathering and a decrease in modulus/hardness was observed due to surface degradation. But copolymer resin showed much lower change in modulus/hardness than TP with exposure up to 4000 hrs. At depths near 3 μm, hardness of TP showed complete degradation over 2000 h of exposure whereas copolymer was still in the phase of increasing the hardness even at 4000h of

exposure. This can be seen from typical load-unload curves shown in Fig. 5. At 4000h, TP showed decrease in load due to surface degradation, while for copolymer load continues to increase till 4000h. This again showed the superiority of copolymer over TP in weathering exposure.

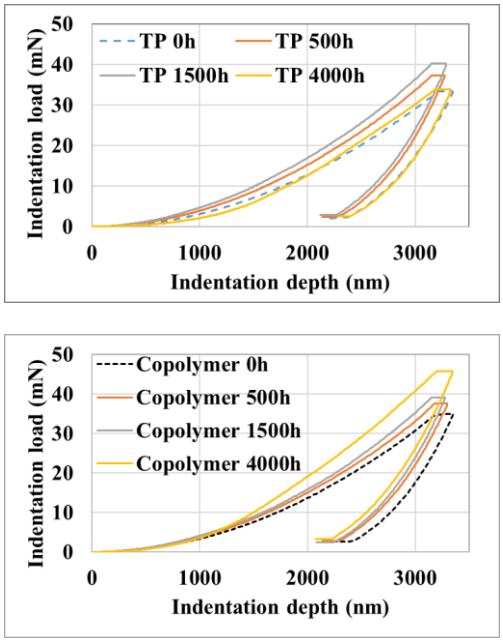


Figure 5: Typical load-unload curves for TP and copolymer at different exposure time.

Conclusions

In summary, in this study we have investigated the change of materials surface during weathering using advanced nano-indentation technique. Results showed the superiority of copolymer over standard Thermoplastic. It is shown that nano-indentation technique is a very sensitive tool to detect small changes in mechanical properties on the surface at the early stages of weathering and is also useful to assess the depth of change.

TEM studies show the evidence of degradation layer and complement the results of depth sensing indentation technique. The nano-indentation technique not only complements the surface appearance measurement but may also predict the mechanical failure early. Often change in gloss and color measurement on the surface fails to indicate true failure of underlying mechanical properties of materials. Present study established the nano-indentation technique to understand the polymer degradation at the early stages. This may enable to improve cycle time of materials development.

Acknowledgements

The authors would like to acknowledge SABIC management for their valuable comments and support to carry out this studies.

References

5. H. Zweifel, Stabilization of polymeric materials, Springer-Verlag; Berlin, Heidelberg: 1998.
6. J. R. White, A. Turnbull, J. Mater. Sci., 29, 584, 1994.
7. W. C. Oliver and G.M. Pharr, J. Mater. Res., 7, 1564, 1992.
8. G. M. Phar, Mat. Sci. Eng., A253, 151 (1998).
9. J. C. Hay and P. Padmanabhan, Mat. Res. Soc. Symp. Proc., 522, 317, 1998.

MACRO 390

Investigations On Low Density Insulation Materials For Solid Rocket Motors

Ajith kumar H,Shashi Bhushan Singh[*]*, Ratheesh.S, Bhatt Tushar Shiram, Muraleekrishnan R*
Elizabeth John
PCM Entiy, Vikram Sarabhai Space Centre,
Thiruvananthapuram 695 022 INDIA

[*]e-mail: singh.b.shashi@gmail.com

Abstract:
Our current investigation is related to the development of low density thermal insulators for all solid rocket motors. Short fibre reinforced rubber composites based on blends of EPDM and NBR as the matrix, silica and aramid fiber as reinforcement , sulphur based cure system along with other functional additives like tackifier and processing aids ,were evaluated to satisfy competing structural and thermal-ablative requirements desired of a solid rocket insulator.
The formulations so designed varied in terms of their blend ratios, filler content and extent of plasticisation which were subsequently studied for their characteristics for insulators.

Keywords: *EPDM; Thermal insulation: Interface properties*.

Introduction

The casing of a solid rocket motor need to be protected from the extreme hostile environment characterized by extremely high temperatures (3000 – 3500K), pressures (60 to 100bar) and turbulence
created of hot gas, molten slag and acidic fumes inside, once the rocket motor is ignited. Even the strongest and exotic alloys formed of metals cannot withstand these conditions and will lead to structural failures and explosion during motor firing. The requirement of a functionally acceptable insulation for the solid rocket motor case is generally addressed by an inner elastomeric insulation layer. This insulation layer also serves to hold the propellant grain intact under the thermal and mechanical strains

resulting from the motor processing operations and during storage. Thus the inert insulation mass in a solid motor, though does not contribute to the ballistics of the mission, is a functionally critical subsystem, as it protects the motor from catastrophic failures.

Elastomers are considered to be the most suitable material for rocket motor insulators due to its ablative nature, favorable thermal properties like thermal conductivity and specific heat, weight advantage, processibilty and resilient and flexible nature which helps to accommodate thermal strains experienced by the motors case. At present, a nitrile rubber (NBR) based insulation system is being used in the operational solid motors of ISRO. Disadvantages with nitrile rubber based insulation systems are its limited shelf life, higher density and inferior low temperature properties. Reduction in insulation mass can pay rich dividends in satellite launch vehicles in terms of increased payload capability and this is more prominent in the case of advanced launch vehicles like GSLV MkIII using two gargantuan solid boosters, where the insulation weighs about four tonnes. Even a marginal reduction in insulation density is highly advantageous in such cases. Being a material with a low specific gravity, high specific heat, very good thermal stability, good low temperature flexibility, good resistance to chemicals and low thermal conductivity compared to all other general-purpose synthetic elastomers, EPDM has emerged as a distinctive material for rocket motor insulation. However its induction calls for surmounting several issues related to its processibility, bonding characteristics with the adjacent surfaces etc. and continues to be a challenge if we are not to compromise on any of the properties of the nitrile rubber based insulation formulations.

Experimental

Materials & Methodology

An EPDM rubber is used as a binder resin for the insulation & sulphur is used as a curing agent to cure the rubber system due its better erosion rate characteristics compare to peroxide cure system. An EPDM rubber is chosen for the development of low density insulation system mainly due its low specific gravity &low thermal conductivity .The EPDM rubber consume a large amount of heat during the sacrificing combustion (ablation) due to its high heat capacity of adsorption. Although, EPDM have high heat of adsorption but produce no char on decomposition therefore, they must be reinforced with fillers to get thermal insulators for high temperature applications with better performance .Silica is used as a filler to impart mechanical & ablative properties to the insulation. Polyaramide fiber is used to arrest the erosion by converting into solid char when it is burned in a rocket motor. Tackifiers used in the design formulations to impart adhesion which plays a vital role in maintaining the integrity of the insulation systems. The Processing performance can be improved by the addition of processing aids (plasticiser) as these lower the viscosity of the batch, thus reducing the mixing energy and time & it also help in distribution of filler of rubber composites .The various accelerator systems used to accelerate the curing of the rubber sheets as sulphur alone has a low curing effect on EPDM rubber system due to lesser diene content in its backbone.

The rubber compound was mixed in a two-roll mill and calendared to sheets of 1 mm or 2 mm thickness. Normally, insulation is laid up in solid motors in sheets and the required thickness is built up layer by layer.

Characterization

The cure characteristics of the mixes were determined using MDR (Moving die rheometer) as per ASTM D 5289. Molding of

the rubber compounds was done in a hydraulic press at 145°C and at a pressure of 75ksc on the mold up to the optimum cure time as obtained from the moving die rheometer. Moldings were stored in a cold and dark place for 24 hours and were used for subsequent property measurements. The hot air autoclave was also used to cure the rubber sheets for subsequent physical/mechanical property measurement.

The stress-strain properties (tensile strength, elongation at break) of the cured samples were measured at room temperature according to ASTM D 412 specification using dumb-bell test pieces in Universal Testing Machine (UTM) at a crosshead speed of 500 mm/min. Hardness of the samples was determined using Shore A Durometer as per ASTM D2240-97. Interface properties were determined using samples prepared from integrated cartons. Peel strength determination was done using wheel pull method, a 180^0 peel test. The density of the vulacanisates was measured using the density meter based on "Archimedes' principle. Thermal conductivity and specific heat capacity values were determined using a thermal conductivity detector (Holomatrix Inc. USA) at 80°C and a Differential Scanning Calorimeter (Mettler). Erosion rate was determined using a test set. up (Plasma arc jet facility) in which high heat flux levels can be simulated. Cylindrical specimens of dia l0mm and length l00rnrn were used for erosion tests done at a heat flux of 300 W/cm^2 in air.

Results & Discussion

The rubber composites were made as per respective formulation. The rheographs and cure characteristics of respective EPDM rubber based composites are shown in fig.3.1.The graphs 1,2,3,4,& 5 symbolises LDI-C,LDI-E,LDI-D,LDI-A,& LDI-B mix respectively. The initial decline of torque is due to the softening of the rubber caused by heating. Then torque increases because of the formation of crosslinking bond.

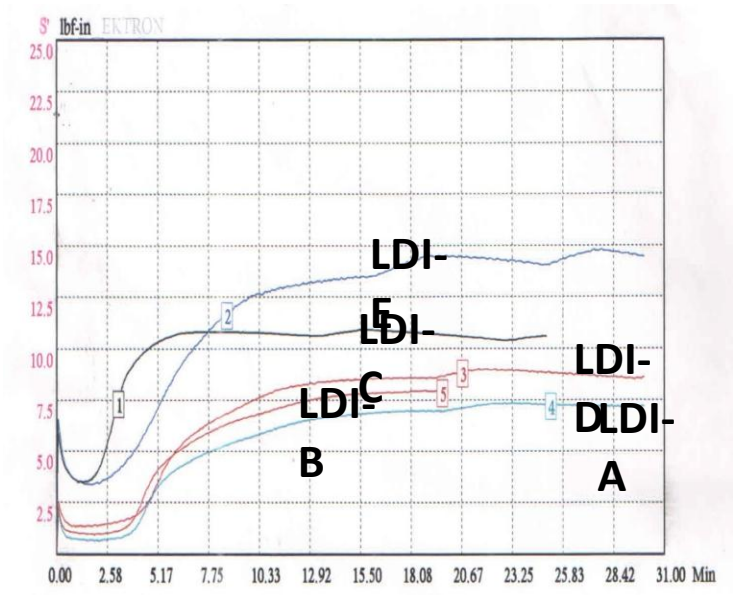


Figure 1: Rheograph of rubber composites

The data obtained from respective rheograph of EPDM rubber based composites were used to cure the rubber composites for further evaluation of the physical, mechanical,& thermal properties .

The comparative mechanical properties are tabulated in table 3.2..The comparative thermal & interface properties of rubber composites are tabulated in table 3.3 The rubber composites which showed high density were not subjected to thermal & interface properties measurement .

Table 1: comparative chart of mechanical properties of designed formulation w.r.t present insulation system

Mix	T.S. (ksc)	El.b (%)	Modulus (ksc)	Hardness (Shore-A)	Density (gm/cc)
LDI-A	73	714	32	74-78	1.04-1.06
LDI-B	68	1140	24	68-70	1.01-1.02
LDI-C	74	28	45	88-91	1.04-1.05
LDi-D	78	685	35	82-84	1.02-1.03
LDI-E	82	360	53	84-88	1.02

NBR-silica	**140**	**1000**	**-**	**60-65**	**1.17-1.21**

In the mix LDI-B, Hexamine & Resorcinol formaldehyde used to improve the adhesion between fiber & matrix.The tensile strength is not great in value as expected but %elongation is quite high attributed due to high loading of plasticiser in achieving the plastication of the composites which also resulted in low modulus and hardness of vulcanisates. The high loading of silica(60phr) in mix LDI-A does not contribute to increase in mechanical properties of the composites because at higher concentration silica formed aggregates which had negative effect on mechanical properties of the vulcanizates. The siloxane and silanol groups on the surface of silica make the filler acidic and moisture adsorbing. This causes loss of cross links density in sulfur-cured rubber .The siloxane and silanol groups and moisture content on the silica's surface enhance the filler-filler interaction and decreases the filler-rubber interactions, which results in formation of aggregates and decreases in mechanical properties at higher concentration of silica . That is why a significant increase in tensile strength at 60phr of silica was not observed. In mix ,LDI-D & E a compatibiliser Maleated EPDM used to bring the affinity between polar & non-polar constituents of the composites so that mechanical & interface properties could be improved, but it is not so evident. High hardness value in all mixes except mix LDI-B (high loading of plasticiser) are observed which is mainly due to loading of aramid fiber which is fibrous in nature brings rigidity in composites. Aramid fiber is more rigid than EPDM when they get into the rubber phase they replace parts of rubber with rigid parts and also reduced elasticity of the rubber chain, resulting in more rigid vulcanizates with more hardness. The density of mix LDI-A is high compare to other mixes due to high loading of silica filer. Since silica (specific gravity 2.1) is heavier than EPDM (specific gravity 0.86), which would ultimately increase the density of the vulcanizates.not only silica ,aramid fiber (specific gravity 1.46) which has higher density compare to EPDM contribute to the density of the composites.

Table 2: comparative chart of Thermal & Interface properties of designed formulation w.r.t present insulation system:

Mix	Specific heat (cal/g/0C)	Thermal conductivity (cal/cm/sec/ ^{0}c)	Erosion rate (mm/s)	Metal-rubber, peel, (ksc)	Propellant-rubber, peel, (ksc)
LDI-A	a	a	a	a	a
LDI-B	0.48	$4.32X10^{-4}$	0.12-0.15	1.5	a
LDI-C	a	a	a	a	a
LDI-D	0.5	$5.2x10^{-4}$	0.17	3.0	a
LDI-E	0.45	$4.9 x10^{-4}$	0.17	5.0	1.1
NBR-Silica	**0.39**	**$6.8x10^{-4}$**	**0.14**	**17**	**1.42**

a-The properties were not evaluated

It is evident from the table 2 that rubber composite with high loading of aramid fibre shown comparatively low erosion rate owing to its char forming nature. The high concentration of aramid fiber is not advisable due to its contribution in density of the composites. The specific heat & thermal conductivity of the insulation sheet are quite satisfactory which imparted by the matrix and reinforcing filler of the design formulation. The peel value of the composites mostly dependent upon the choice of adhesive system to evaluate the metal-rubber peel .In the mix, LDI-B proper adhesive systems were not used to evalaute the metal-insulation peel value which resulted in low peel value. In mix,LDI-D & LDI-E an advanced adhesive systems were used which resulted in improvement of metal-insulation peel value as compare to Mix, LDI-B. The insulation-propellant peel

values were not determined for mixes except LDI-E due to concern over the density of the composites

Conclusion

EPDM based thermal insulator formulation of density 1.02-1.03 was developed. An EPDM based thermal insulators formulations showed specific heat 0.45 cal/g, erosion rate value of 0.15-0.17 mm/sec at heat flux of 300 w/cm^2 with heat conductivity ~$4x10^{-4}$ ($cal/cm^2/s/^oC$) confirms it suitability to use as thermal insulation system in future solid rocket motors.

Though the thermal & rubber-propellant interface properties within the specification limit of current using insulation system based on nitrile rubber, the mechanical & metal-rubber interface properties are not up to the mark of current operational insulation system.

Acknoledgements

The authors are thankful to Dr. Benny K George, Mr. CR.Thomas & their teams for analysis & propellant processing support.

References

1. Tauzia, Jean-Michel. Thermal insulations, liners and inhibitors. *In Solid rocket propulsion technology*, edited by Alain Davenas. Pergamon
2. Muraleekrishnan, R.; Bhagawan, S.S.; Raghavan,A.J. & Rao, S.S. IRC. Rocket motor lowdensity insulation based on NBR. *In Proceedings of the 3rd International Conference*, 12-14, Dec.1997, Kharagpur
3. Blow, C.M, Raw polymeric materials. *In Rubber chemistry and technology*. Butterworths, London, 1971
4. Deuri A.S.; Bhowmick A.K., Degradation of rocket insulator at high temperature, *Journal of Thermal Analysis* Vol. 32, pp. 755-770, 1987

MACRO 399

Structural and Dielectric Properties of Syndiotactic Polystyrene in Bulk and Aerogels

Joseph A.M , Surendran K.P.*, Bhoje Gowd E *

Materials Science and Technology Division
CSIR-National Institute for Interdisciplinary Science and Technology,
Thiruvananthapuram, India

**bhojegowd@niist.res.in*

Syndiotactic polystyrene is a versatile engineering polymer which, due to its excellent physical and chemical properties, has been utilized for various automotive, electrical and electronic applications. This semicrystalline polymer crystallizes into different crystalline forms depending on the conditions of crystallization. sPS crystallizes into α and/or β forms in both pristine and composite with hybrid silica forms. However, the aerogels made out of sPS are in δ and δ_e forms. The morphology of the polymer changes to a fibrous network structure in the case of sPS aerogels obtained by the freeze drying of the polymer gels. As a result, the dielectric constant of the material also reduces drastically from 2.5 for the bulk to ~1.25 in the case of aerogel. This ultra-low dielectric constant is believed to be due to the presence of two types of porosity in the polymer aerogel, the nanoporosity emerging from the fibrous network structure and the porosity in the angstrom length scale originating from the cavities in the crystalline lattice of the nanoporous form (δ_e form).

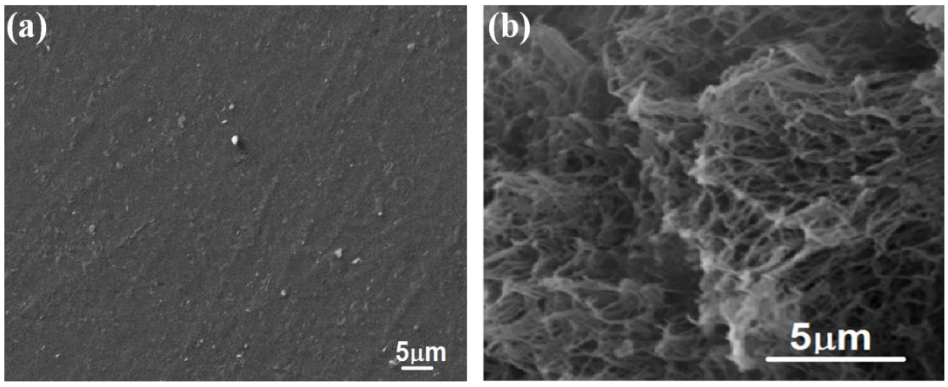


Fig 1. SEM images of sPS (a) in its bulk form and (b) aerogel form.

References

[1] Joseph, A.M; Nagendra, B; Surendran, K. P.; Bhoje Gowd, E. *ACS Appl. Mater. Interfaces*, 7 (2015) 19474

MACRO 400

Polymer-based Flexible Ferroelectric Nanocomposites

Anupriya Vijayakumari, Swapnil Aherrao, Aniket Gudadhe, Kadhiravan Shanmuganathan*

Polymer Science and Engineering Division
CSIR-National Chemical Laboratory, Dr. Homibhaba Road, Pune-4111008, India

** Corresponding author: k.shanmuganathan@ncl.res.in*

Piezoelectric and ferroelectric materials have been of tremendous interest in recent years owing to their potential applications as sensors and actuators, energy harvesting and storage devices, underwater transducers, impact detectors, medical probes, etc [1]. Ceramic materials having non-centrosymmetric crystals are notable inorganic ferroelectric materials including lead zirconate titanate (PZT), barium titanate and quartz. In the late 1960's, piezoelectric behavior of poly(vinylidene fluoride) (PVDF) was first documented and since then organic ferroelectric materials have gained increasing attention [2]. Inorganic ferroelectric materials have a much higher piezoelectric strain constant (d_{31}= 175 pC/N) than PVDF (d_{31}= 28 pC/N), and have been the material of choice for energy harvesting applications [1]. Nonetheless, polymer-based ferroelectric materials have many advantages [1]:

1. Piezoelectric stress constants (g31) of polymers are much higher than inorganic ferroelectrics, favouring their use in sensor applications.
2. Piezoelectric polymers exhibit a higher strain to fail as compared to ceramics.
3. Polymeric sensors and actuators are light weight and offer many advantages in terms of their processing flexibility, toughness, ability to be cut and molded into intricate shapes, high strength and impact resistance, low elastic stiffness, low dielectric constant, etc.
4. Acoustic impedance (proportional to the product of density and stiffness) of PVDF is much lower than ceramics making them highly desirable for medical and underwater applications.

Poly(vinylidene fluoride) (PVDF) is a well-known ferroelectric polymer exhibiting many crystal phases, of which the β phase is the most ferroelectric. Polymorphism (existence of different crystal phases such as α, β, γ, and δ) in PVDF has stimulated extensive research, particularly in establishing the conditions leading to different crystal phases [3,4]. The existence of different crystal phases and their transformation have a significant influence on the properties of the polymer. When melt-processed, PVDF typically crystallizes as nonpolar α phase. Strong ferroelectric behavior, however, is observed in the PVDF β phase. Since all the dipoles are aligned in the same direction normal to the chain axis, the all-trans β phase is highly polar. Other less polar phases such as γ, and δ are also possible under certain conditions. Some efforts have been made to promote β phase formation in PVDF by mechanical stretching [5], inclusion of additives [6], specific solvent processing conditions, confined crystallization and copolymerizing PVDF with other monomers. Though some copolymers of PVDF can readily crystallize into β phase, PVDF homopolymer has many advantages, such as, higher Curie temperature, larger intrinsic polarization, significantly lower cost, and ready availability. We report here our efforts to enhance the β phase formation in PVDF using biopolymers and bio-derived materials and a

systematic characterization of the crystalline microstructure of the nanocomposites at different processing conditions.

Cellulose nanocrystal fibres (CNF) were isolated from cotton (Whatman filter paper) using established procedures. Both phosphoric acid and hydrochloric acid were used and two types of cellulose nanocrystals were prepared. CNF's were blended into PVDF using two approaches. Lyophilized (freeze dried) CNF's were re-dispersed in dimethyl formamide and solution blended with PVDF. These solutions were casted into thin films in vacuum oven. In another approach solution blended PVDF and CNF's were precipitated in methanol and dried. These dry precipitates were further melt pressed at 180°C. Composite films with 2%, 5%, 10% and 20% CNF were prepared. The crystalline microstructure of the films was evaluated by X-ray diffraction and FTIR.

Solutions for electrospinning were made by dispersing CNF in dimethyl formamide and solution blended with PVDF. Pure PVDF and PVDF – CNF solutions were electrospun to make nanofibers. With both types of cellulose, nanofibers were made. Electrospinning was tried with different conditions. The morphology of fibers were characterized by scanning electron microscopy (SEM) and crystallinity studies by X-ray diffraction, FTIR and DSC

X-Ray diffraction and FTIR were used for investigating the crystalline microstructure of films. In the presence of CNF, there is shift in peak to beta phase. The alpha phase present in PVDF transformed to gamma phase. With higher concentrations of CNF (10 % w/w), the alpha content is reduced and beta phase crystallinity in PVDF is favoured [Fig(1)]. After melt pressing, some of the samples were annealed at 90°C for 5 hours. After annealing, pure PVDF also shows some beta phase. Differential scanning calorimetry (DSC) was done on annealed films, but overall crystallinity remained the same in the presence of cellulose and annealing. The morphology of electrospun fibers were characterized by SEM [Fig(2)]. Fibers formed by electrospinning shows beta phase crystallinity. Ferroelectric characterization of these materials is in progress to further understand the enhancement in performance.

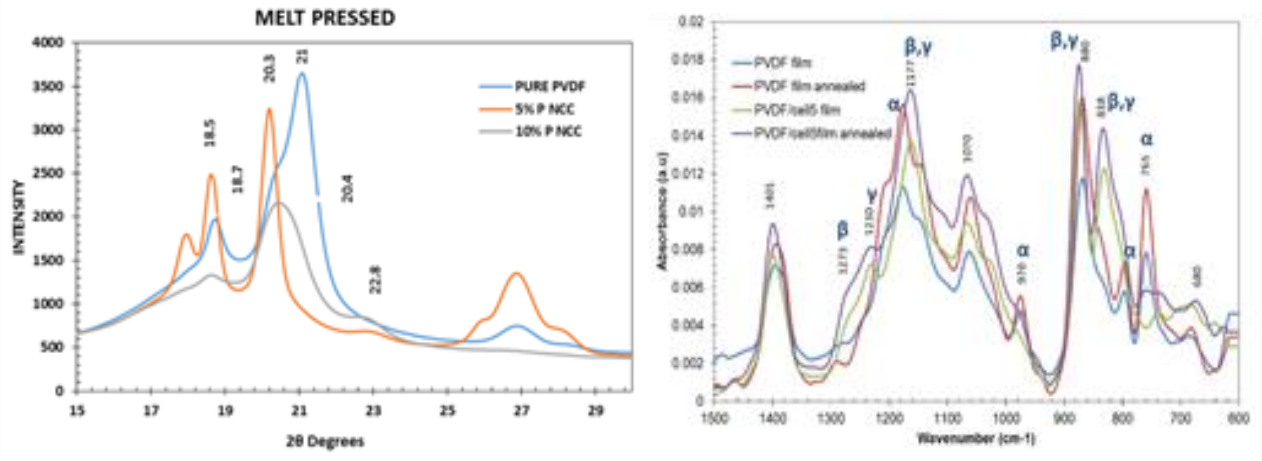


Figure 1. X-Ray diffraction (left) and FTIR (right) of PVDF and PVDF nanocomposite films.

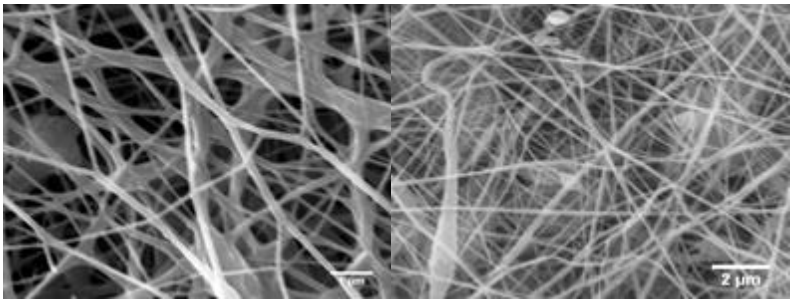


Figure 2. SEM images of PVDF (left) and PVDF nanocomposite fibres (right).

References

[8] Lovinger, A.; *Science*, 220 (1983), 1115.
[9] Ueberschlag, P.; Sensor Rev. 21 (2001), 118.
[10] Holstein, P.; Scheler, U.; Harris, R.K. *Polymer*, 39 (1998), 4937
[11] Zhang, M.; Zhang, A.; Zhu, B.; Du, C.; Xu, Y. *J. Membrane Sci*. 319 (2008), 169.
[12] Mohajir, B.; Heymans, N. *Polymer*, 42 (2001), 5661.
[13] Mendes, S. F.; Costa, C. M.; Caparros, C.; Sencadas, V.; Lanceros-Méndez, S. *J. Mater. Sci.*, 47 (2012),1378.

MACRO 406

Solvent-Induced Crystallization and Phase Transitions of Poly(L-lactide) (PLLA)

Shaiju, P and Bhoje Gowd, E*

[a]*Materials Science and Technology Division, CSIR-National Institute for Interdisciplinary Science and Technology(NIIST), Trivandrum 695 019, Kerala, India.*
[b]*Academy of Scientific and Innovative Research (AcSIR), New Delhi 110 001, India.*

**bhojegowd@niist.res.in*

The presence of solvents can significantly affect the crystallization process in polymers due to their plasticizing effect. The interaction of the solvent molecules with the polymer chains accelerates the segmental motion in the amorphous region. This results in the reduction of the glass transition temperature (T_g), which in turn facilitates the overall crystallization rate of the polymer. In the first part of the present work, we are mainly focussing on the solvent induced crystallization of Poly(L-lactide) (PLLA) in the presence of different solvents. The structural and morphological changes during the treatment with various solvents were followed by temperature-dependent wide- and small-angle X-ray scattering (WAXS/SAXS), scanning electron microscopy (SEM), UV-vis spectroscopy, dynamic mechanical analysis (DMA) and Fourier transform infrared spectroscopy (FTIR) measurements. SEM results revealed that the samples treated with different solvents showed major differences in their surface morphology. SAXS results proved that the lamellar structure is considerably influenced by changing the solvent. Moreover, the mechanical properties were also found to get affected by treating the polymer with different the solvents.

Apart from the solvent induced crystallization, the presence of solvents can also cause the formation of co-crystals depending on the experimental conditions used. In polymer cocrystals, the polymer acts as the host that accommodates the solvent molecules within its crystal lattice as the guest. In the second part of the work, we have prepared PLLA cocrystals (ε) that contain cyclopentanone (CPO) as the guest molecule and tried to understand the structural changes during heating, with the help of different characterization techniques. It was found that the ε cocrystal was transformed to the α form, which is the most stable crystalline form of PLLA, in a broad temperature range at ~ 50 °C. During this transition, all the solvent molecules were pushed out into the amorphous region. On further heating, CPO molecules, which are residing in the amorphous phase evaporates at its boiling temperature, which helps in improving the order of the α form.

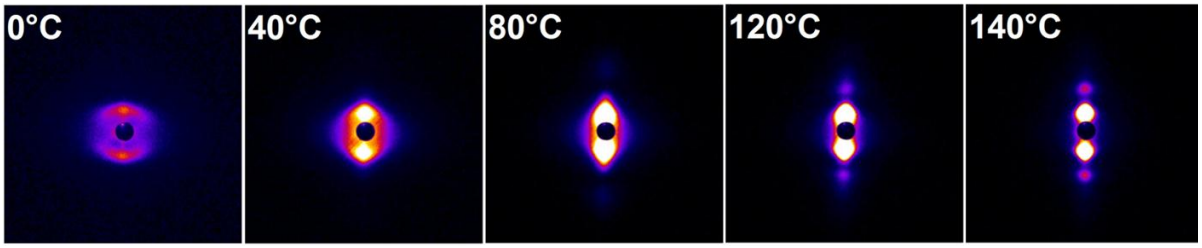


Figure 1. Two-dimensional SAXS patterns obtained at different temperatures during the heating process of uniaxially drawn PLLA/CPO co-crystal.

References

[14] Shaiju, P.; Murthy, N. S.; Gowd, E. B. *Macromolecules*, 49 (2016) 224.

[15] Marubayashi, H.; Asai, S.; Sumita, M. *Macromolecules*, 45 (2012) 1384.

MACRO 410

Fully "Face-on" *vs* Fully "Edge-on": Rational Functionalization of Thiophene Oligomers for Control over Film-State Packing

Ghosh, Tanwistha and *Nair, Vijayakumar**

Photosciences and Photonics Section, Chemical Sciences and Technology Division, CSIR-National Institute for Interdisciplinary Science and Technology (NIIST), Trivandrum 695 019, India.

* *E-mail: cvijayakumar@niist.res.in*

Film-state packing plays a crucial role on the optoelectronic properties and device performance of organic semiconducting materials. It was well established that "face-on" packing of oligomers/polymers is advantageous for photovoltaic device application as it would reduce the distance between the molecular backbone which in turn is beneficial for charge transport in the device,[1,2] whereas "edge-on" packing is more suitable for field-effect transistor application.[3,4] However, precise control over the supramolecular organization of organic semiconducting materials leading to such exclusive packing is still a challenging task. In the present work, we describe the fully "face-on" or fully "edge-on" packing of thiophene oligomers through rational designing.

In this context, we have carefully functionalized thiophene oligomers with dicyano containing *N*-ethyl rhodanine as acceptor end group (**OT1**) which results fully "face-on" packing, whereas functionalization with *N*-octyl chain containing rhodanine derivative (**OT2**) results in fully "edge-on" packing. Detailed studies including UV-vis film state absorption on different substrates, 2D-gracing angle X-ray diffraction (2D-GIXRD) and atomic force microscopy (AFM) were carried out to analyse the packing and resulting morphology in the film state. Details will be presented.

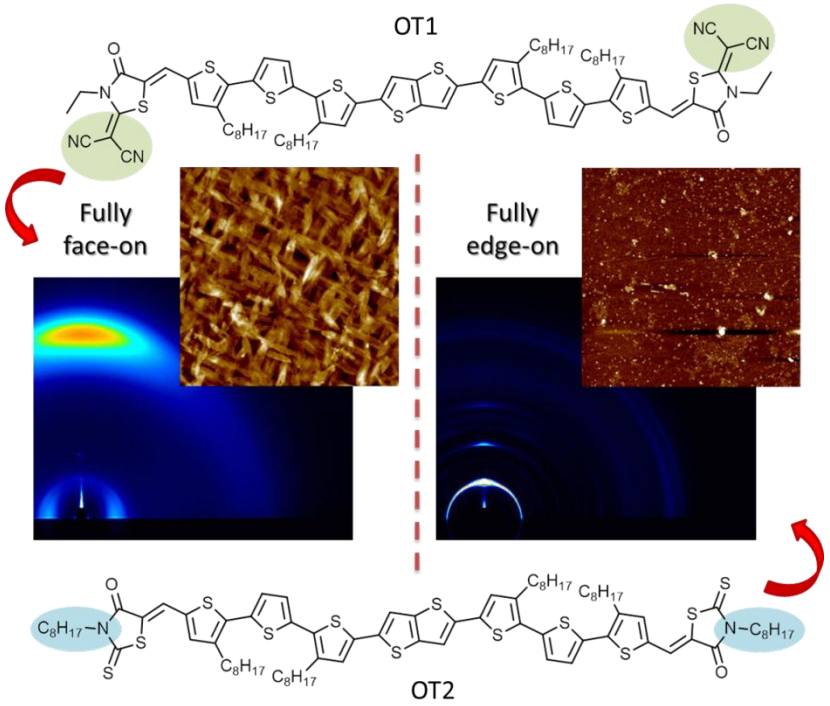


Figure 1. Structure of the oligomers **OT1** and **OT2**; Corresponding 2D-GIXRD and tapping mode AFM images of the oligomers.

References

[1] Piliego, C.; Holcombe, T. W.; Douglas, J. D.; Woo, C. H.; Beaujuge, P. M.; Fre, J. M. J. *J. Am. Chem. Soc.* 132 (2010), 7595.
[2] Ide, M.; Saeki, A.; Koizumi, Y.; Koganezawa, T.; Seki, S. *J. Mater. Chem. A*, 3 (2015), 21578.
[3] Botiz, I.; Stingelin, N. *Materials*, 7 (2014), 2273.
[4] Deng, Y.; Chen, Y.; Zhang, X.; Tian, H.; Bao, C.; Yan, D.; Geng, Y.; Wang, F. *Macromolecules* 45 (2012), 8621.

MACRO 414

Understanding the Interactions of Poly(propylene Glycol) with Thermoplastic Polymers

[a]Muthukrishnan. Sharmila* [a]Banerjee, Debasish and [b]Farhood-Al, Bander

[a]*SABIC Research & Technology Pvt. Ltd., Plot No. 81 to 85 Village, Chikkadunnasandra, Off. Sarjapura-Attibele State Highway, Bangaluru-562125*

[b] *SABIC STR, Al-Kharj High Road, Second Industrial City, P.O. Box:42503*

Riyadh 11551, Saudi Arabia

** e-mail id: sharmila.muthukrishnan@sabic.com*

Abstract

In this study, the interaction and compatibility of poly(propylene glycol) (PPG-2000) with a given thermoplastic or amorphous polymer containing carbonate groups prepared using melt mixing have been investigated using wide range of techniques. The objective is to understand the impact of the addition of PPG-2000 on to the physical, thermal and mechanical properties of the thermoplastic polymers/ amorphous polymers of interest.

Keywords: *Thermoplastic polymer; PPG;; thermal stability; melt mixing; HDT and amorphous polymer*

Introduction

A blend of two polymers can be characterized as miscible or immiscible, depending on whether the polymer chains of the two components form a homogeneous single phase or phase separate into individual domains of the two components. Further, the terminology "compatible" or "incompatible" is often used to describe how well the two components mix or as an assessment of their resultant properties. The term "compatible" has been used to describe blends that range from totally miscible (one phase) to interactions that are favorable and result in good physical properties. "Incompatible" usually refers to blends that have poor physical properties, delaminate upon impact, and often differ greatly in viscosity, polarity, or stability.

Lohith et al.[1] investigated the use of different compatbilizers for obtaining compatible blends of amorphous and crystalline blends. PEG-2000 was found to be the most effective one which induced the compatiblization through the hydrolytic degradation of the amorphous polymer resulting in an in-situ formation of the copolymer. Hence, in this study, the attempt has been made to understand the impact of the addition PPG 2000 on to the properties of the carbonate containing amorphous polymer and the degradation mechanism driving the same.

The addition of PPG 2000[2,3] does impact the optical, thermal and mechanical properties of the amorphous polymer of interest beyond a certain concentration. This study focuses on the impact of the addition of glycols to the polymers containing carbonate groups in the backbone and the mechanism driving the same.

Experimental

Amorphous polymer used in this study was made in house and dried for 6 hours at 80 °C. PPG 2000 was purchased from Sigma-Aldrich and used as such. Differential Scanning Calorimetry

(DSC) was carried out using DSC Q1000 TA, in the temperature range from 25 °C to 250 °C at a heating rate of 10 °C/min. Thermo Gravimetric Analysis (TGA) for PMMA and its blends were carried out using DSC Q5000 TA, in the temperature range from RT to 800 °C with a heating rate of 20 °C/min in N2 atmosphere. Heat Distortion Temperature (HDT) analysis was carried out on Zwick HDT instrument. HDT was carried out as per ISO 75-2 with 0.45 MPa Stress at flatwise direction and a temperature ramp of 120°C/hr. All the specimens with dimensions of 800 mm length, 10 mm width and 4 mm thickness were notched at the center with dimensions of the notch being 2mm depth and 0.25 mm radius. Samples were conditioned for a minimum of 24 hours after the notch cutting, before the actual testing. The test was done using CEAST make Impact Tester , which displays energy lost by the hammer while hitting the specimen. Hammer with 2 joules rating was used for the tests and the frictional loss of the hammer was determined before testing each formulation. Values reported are in kilojoules meter square.

The blends of the carbonate containing Amorphous Polymer (A) and PPG 2000 were obtained using the melt mixing at 260 °C using twin screw extruder at 250 rpm followed by injection molding of specimens as per the ISO/ASTM standards at 270 °C.

Results and discussion

The blends of carbonate containing Amorphous Polymer (A) and PPG 2000 were obtained using the melt mixing process. Up to 3% of PPG 2000 when added to the carbonate containing amorphous/thermoplastic polymer, the blends were transparent indicating that the optical properties were not affected and the blends were either partially or fully miscible at a molecular level.[4,5]

The thermal stability and the glass transition temperature (T_g) of the blends were evaluated using TGA and DSC measurements. As can be seen from Figure 1, the T_g of the Polymer A drops upon the addition of PPG 2000. This could be due to the fact that the chains become more flexible owing to the plasticizing effect upon the addition of PPG. This could also be attributed to the possible some interactions at the molecular level with the polymer matrix and PPG.

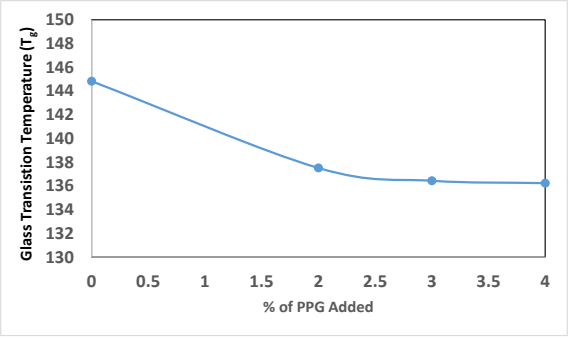


Figure 7*. Impact on the Glass Transition Temperature (Tg) upon the addition of PPG to the Amorphous Polymer (A)*

As can be seen from Table 1, the addition of PPG negatively impacts the thermal stability of the polymer of interest. Upon the addition of PPG, the onset of degradation shifts to the lower temperature as compared to the neat amorphous carbonate containing polymer and two peaks could be seen.

Table 1. *Thermogravimetric Analysis (TGA) of Amorphoous Polymer (A) and PPG Blends*

Compositions	Onset of Degradation (°C)	Remarks
Amorphous Polymer (A)	505.46	One Peak
(A)+2% PPG	382.30 and 500.21	Two Peaks
(A)+3% PPG	378.26 and 490.17	Two Peaks
(A)+4% PPG	375.26 and 492.10	Two Peaks

Heat Distortion Temperature (HDT) analysis (1.8 MPa) was also conducted to substantiate the results of the DSC and TGA analysis. As expected, there is a decrease in the HDT of the Amorphous Polymer upon the addition of PPG 2000. This clear indicates again that the chains are more flexible upon the addition of the glycols as compared to the parent polymer (Pls. refer to Figure 2) resulting in the deformation at a lower temperature than the parent Polymer.

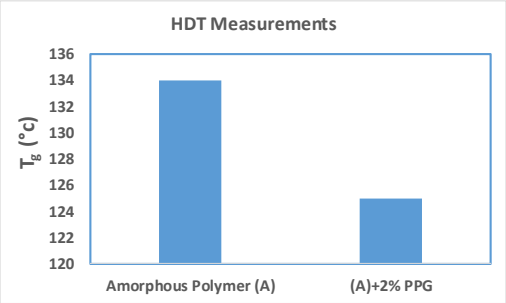


Figure 8. *HDT Measurements of the* Amorphous Polymer (A) and PPG Blends

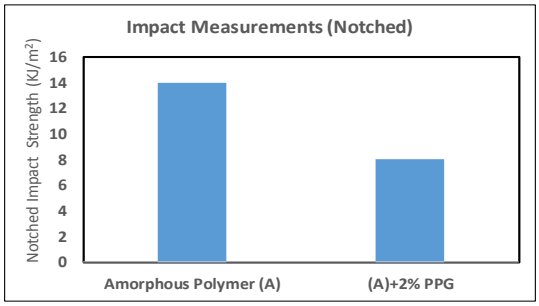


Figure 9. *Notched Impact Strength of Amorphous Polymer (A) and PPG Blends*

The impact strength data of the blends as shown in Figure 3 are lower than that of the parent Amorphous Polymer (A) which clearly indicates that PPG decreases the mechanical properties of the polymer. This could be attributed to the possible degradation of the parent polymer upon the

addition of PPG other than just the plasticizing affect. The rigidity of the blends drops considerably even upon the addition of 2 % of PPG 2000. This was further investigated by the GPC analysis (PS standards) to understand the impact of the addition of PPG on the molecular weights of the Amorphous Polymer as shown in Table 2.

Table 2. *GPC Results of the Amorphous Polymer (A) and Blends*

Compositions	**M_n**	**M_w**	**PDI**
Amorphous Polymer (A)	21370	46668	2.18
(A) + 2% PC	20975	45121	2.15
(A) + 3% PC	21719	46832	2.16
(A) + 4% PC	15951	23891	1.5

As can be seen from Table 2, the molecular weights of the blends decrease considerably upon the addition of 4% of PPG. The molecular weights of the blends almost remain constant upto 4% although the thermal and mechanical properties of the blends undergo significant changes even at 2 % of PPG levels in the blends. Hence, it can be concluded that the significant drop in the molecular weights upon the addition of 4 % of PPG indicates the chain scission or degradation of the parent polymer (A) under the melt conditions in the presence of PPG. At lower levels of PPG, 2 to 4%, there could be some plasticizing affect (not degradation) which results in the chain flexibility thereby reducing the T_g, HDT, thermal stability and mechanical properties.

Conclusions

The addition of PPG 2000 does impact the optical, thermal and mechanical properties of the amorphous polymer of interest beyond a certain concentration. The optical properties and molecular weights do not get impacted up to 3 % of PPG levels in the polymer matrix whereas the thermal and mechanical properties undergo significant changes (reduction) even at 2 % levels due to the possible plasticizing behavior of PPG. Beyond 3 % of PPG, the blends demonstrate lower molecular weights than the parent polymer owing to the possible degradation of the main chain apart from the plasticizing affect.

Acknowledgements

Authors would like to thank the analytical team at STCB for their timely and extensive support with the characterization of the materials developed within the scope of this project.

References

10. Manjunatha Nanjegowda, Lohith: Bommulu, Ramaraj; Juikar, Vishvajit and Hatna, Siddaramaiah *Ind. Eng. Chem. Res.*, 52 (2013) 5672.
11. Ruowen Zong*, Yuan Hu, Naian Liu, Shaofeng Wang and Guangxuan Liao. Polym. Adv. Technol., 16 (2005) 725.
12. Zhi Dai, Maria T Arévalo, Junwei Li, and Mingtao Zeng. Bioengineered. 5(1) (2014) 30.
13. Kinya Mizui, Yoshihisa Kiso, Tetsuo Hayashi, Masahide Tanaka. US 5387354 A
14. Heinrich Baer, Harold Ebneth, Karl Heinz Ott. US3450794 A

MACRO 424

Malachite Green based Photo-decross-linkable Systems

Orodepo Gabriel O. and S. Ramakrishnan*

Department of Inorganic and Physical Chemistry
Indian Institute of Science, Bangalore 560012, India.

* raman@ipc.iisc.ernet.in

Malachite green (MG) belongs to a triphenylmethane (TPM) class of dyes and has been widely used industrially in the dyeing of fabrics and as an effective fungicide in aquaculture. It has been demonstrated in the literature that when the chloride counter ion in MG is substituted with cyanide or hydroxyl ions, a colourless covalent adduct (MG-CN or MG-OH) is formed. These covalent adducts when irradiated with UV-light undergo photo-cleavage of MG-X bond thereby generating a highly coloured MG cation and a corresponding anion; this provides a strong visible and readily quantifiable signature of the photo-cleavage event. In the dark or upon heating the ions recombine to form covalent adduct [1, 2]. Intrigued by this interesting photochromic property, we decided to explore some fundamental aspects concerning the factors that govern the covalency of the MG-X adduct and further develop crosslinked polymeric systems wherein the crosslink density can be varied by shining light while simultaneously monitoring the extent of crosslinking using simple UV-visible spectroscopy. By a series of simple counter-ion exchange studies of MG with a variety of anions, we were able to demonstrate that there exists equilibrium between the covalent and ionic species, which is sensitive to both the solvent polarity and the pH of the solution. Acetates, methoxides, phenolates etc. provide significant covalency. Encouraged by these results we have designed some MG-based systems with polymerizable counter-ions so as to generate polymers and crosslinked systems that could be photoactively transformed; details of these and other studies will be presented in the poster.

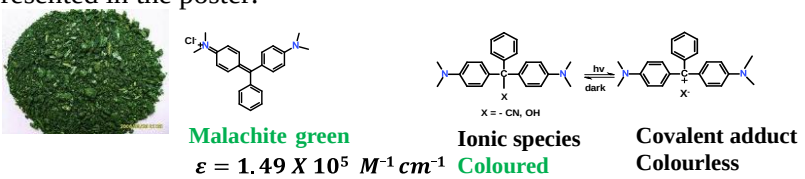


Figure 10: Illustration of photochromic property of malachite green leucoderivatives

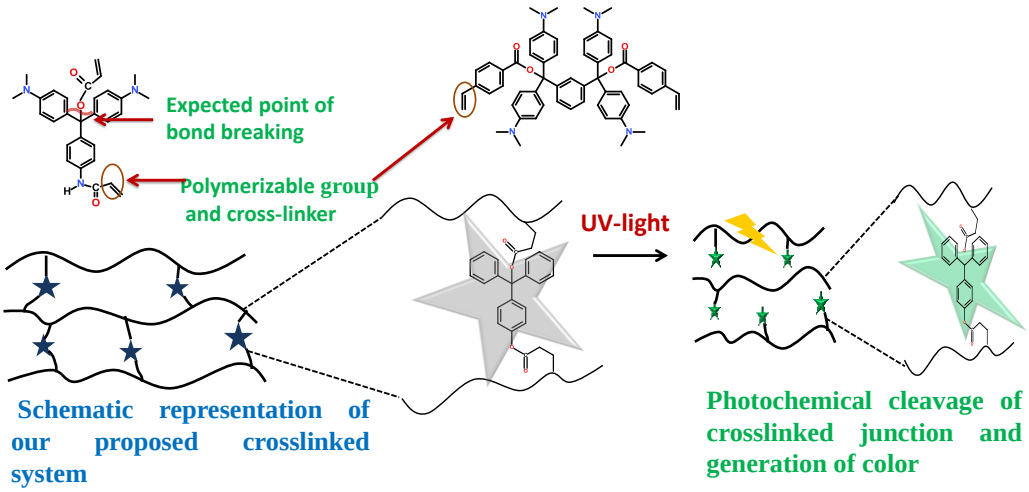


Figure 11 : Our designed MG-based photo-decrosslinkable systems

References

[16] Irie, M.; Kungwatchakun, D. *Makromol. Chem. Rapid Commun.* 5 (1985) 829.
[17] Irie, M.; Kungwatchakun, D. *Macromolecules* 19 (1986) 2476

MACRO 428

Studies on Novel Blend Membranes from Chemically Modified Natural Rubber Latex and Poly(vinyl alcohol)

Janisha Jayadevan[a]* Rosamma Alex[b], G.Unnikrishnan[a]

[a] *Polymers Science and Technology Laboratory, Department of Chemistry, National Institute of Technology Calicut, Kozhikode, Kerala, 673601, India*

[b]*Joint Director (Rt), Rubber Research Institute of India, Kottayam, Kerala, India*

** e-mail id: janishajayadevan@gmail.com*

Abstract

Chemical modification of *cis*- polyisoprene units in natural rubber is an emerging area of research. Grafting is one of the methods being used for this purpose. In this work, novel blend membranes were prepared from chemically modified natural rubber latex (NRL) and poly(vinyl alcohol) (PVA). Chemical modification of NRL was done by grafting (dimethylaminoethyl methacrylate) (DMAEMA) onto NR particles by using a redox initiator system viz; cumenehydroperoxide/tetraethylenepentamine (CHP/TEPA). The modified latex showed a significant increase in colloidal stability at low pH, which is attributed to grafted hydrophilic polymer acting as an electrosteric stabilizer. After removing the homopolymers, monomers and

initiators by dialysis, the modified latex was blended with PVA, a hydrophilic polymer and casted into membranes at 60± 2°. Moisture uptake, swelling ratio and contact angle of the membranes have been found to depend on the grafting and amount of PVA present in the membrane. Fourier transform infrared (FT-IR) spectroscopy, X-ray diffractometry (XRD) and thermogravimetry (TGA) were used to characterise the membranes.

Keywords: *NRL, PDMAEMA, redox initiated grafting, PVA, blend membranes*

Introduction

Natural rubber latex (NRL) is a polydispersed colloid in aqueous medium, in which cis-polyisoprene is the main chemical constituent [1]. It is a slight yellow milky liquid that undergoes coagulation by acids and electrolytes at room temperature [2, 3]. Average size of the polymer particles in NRL is 0.02-3μm. NRL is being used for a large number of applications because of its unique features [4, 5]. Irrespective of all its merits it has limitations such as sensitivity towards pH changes, low resistance to thermal degradation, poor resistance to ozone and organic solvents and biological incompatibility with the human body [6].

The chemical modification of natural rubber by grafting with hydrophilic vinyl monomers using various initiator systems has gained considerable importance by now [7]. The grafting process produces a novel copolymer structure in which the hydrophilic polymer chain extend into the aqueous phase from the surface of a hydrophobic polymer [8].This type of chemical modification results in an enhanced colloidal stability at a lower pH range, since the resultant hydrophilic shell can act as an electrosteric stabiliser. The enhanced colloidal stability makes latex resistant to any mechanical and chemical disturbances and improves its processability [9].

Polyvinyl alcohol (PVA) is a water soluble synthetic polymer. It is a macromolecule of great interest because of its desirable characteristics such as hydrophilicity, good film forming ability, resistance to oxidation and excellent mechanical properties [10]. It has also been employed for different pharmaceutical and biomedical applications [11,12]. PVA has by now been identified as an excellent partner for many macromolecular systems [13, 14].

The aim of the present work is to modify NRL physico-chemically, and to develop novel membranes out of it. The study initially focuses on the chemical modification of NRL with dimethylaminoethyl methacrylate (DMAEMA) by using a redox initiator system cummene hydroperoxide/ tetraethylene pentamine) (CHP/TEPA). The modified NRL has then been physically blended with PVA to form high quality membranes. The grafting has been monitored by DLS, FT-IR. The blended systems have been characterised by using FTIR, XRD and TGA.

Experimental

Materials

Natural rubber latex (34% DRC) used in this study was a commercial sample procured from a rubber plantation at Thekkumkutty, Calicut, Kerala, India. Dimethylaminoethyl methacrylate (DMAEMA) monomer and the tetraethylene pentamine (TEPA) co-initiator were purchased from Aldrich, Germany. Sodium dodecyl sulfate (SDS) and cumene hydroperoxide (CHP) were

procured from Alfa Aesar, Briton. PVA used for blending was purchased from Aldrich, USA with a molecular weight in the range 89,000 – 98,000 g/mol.

Dynamic light scattering

The change in NR particle size before and after grafting was examined using a Malvern ZS nano instrument at 25 ºC for 1 minute.

FT-IR

The grafted linkages and the compatibility of blended systems were examined by FTIR spectroscopy using a spectrometer (Thermo Nicolet 5700, USA) in the range of 4000 to 500 cm^{-1}. The grafted and blended systems were scanned as such in ATR (*Attenuated Total Reflectance)* mode.

X-ray diffractometry

The crystallinity examination was done by using a Rigaku miniflex 600 benchtop X-ray diffractometer. The X-ray source was Cu K∞ with a scanning range of 3-90º with a speed of 15º per minute.

Thermogravimetric analysis

Thermal stability of the grafted and blended membranes was monitored by using a thermogravimetric analyser TGA Q50 instrument. All the experiments were performed in the temperature range of 25-700 ºC under at a heating rate of 10 ºC min^{-1} in nitrogen atmosphere.

Water contact angle measurement

Static water contact angle measurements were made by placing the substrate at room temperature on the sample stage and recording the contact angle at RT using the instrument Digidrop GBX, France.

Results and discussion

The grafted systems with different phr of monomers are abbreviated as NR-g-2.5PDMAEMA [2.5PDNR], NR-g-5PDMAEMA [5PDNR], NR-g-10PDMAEMA [10PDNR], NR-g-15PDMAEMA [15PDNR] and NR-g-20PDMAEMA [20PDNR].

Dynamic light scattering

From the DLS studies (Table 1), the diameter of NR particles has been found to be increased after grafting initially with 2.5 phr of DMAEMA. It has also been seen that diameter regularly increases with an increase in the quantity of the monomer upto 15phr. The diameter enhancement is definitely due to the increase in the chain length of the graft on NRL surface, with increase in the concentration of DMAEMA. The increase in particle size is regular upto 15 phr of the monomer DMAEMA but decreases after it, typically for 20 phr of the monomer. This can be attributed to the possibility for the formation of more homopolymers than the graft.

The graft formation was further confirmed by ATR-FTIR analysis. Fig.1 shows the ATR- FTIR spectra of NR and 15PDNR scanned in the range of 4000 cm^{-1}to500cm^{-1}. The spectra show the characteristic peaks of saturated aliphatic sp^3C-H bond at 2847-2964 cm^{-1} for both NR and 15PDNR. The peak at 3293 cm^{-1} is due to the presence –OH group from the moisture absorbed by NR. This peak intensity has been found to be decreased in the case of 15PDNR. The peak at 1660cm^{-1}indicates C=C stretching in polyisoprene. A distinct peak at 1736 cm^{-1} for the 15PDNR sample, not seen for NR, due to C=O stretching of the ester group derived from PDMAEMA grafted onto NR confirms the grafting process.

The physical modification of the chemically modified NRL, with PVA in the ratios 15PDNR/2.5PVA, 15PDNR/5PVA and 15PDNR/10PVA resulted in transparent membranes.

FT-IR for blends

Fig.2. shows the FTIR spectra of PVA, 15PDNR and the blend membranes (15PDNR/2.5PVA, 15PDNR/5PVA and 15PDNR/10 PVA) scanned in the range of 1000 to 4000 cm^{-1}. In the FTIR spectra, 15PDNR shows distinct peaks at 2853-2962 cm^{-1} due to C-H stretching, 1659 cm^{-1} due to C=C stretching, 1370-1445 cm^{-1} due to C-H bending and 832 cm^{-1}due to C=CH wagging. However, it gives an additional peak at 1736 cm^{-1} corresponding to the C=O stretching of ester group derived from PDMAEMA grafted onto NR. The peak at 1639 cm^{-1} corresponds to the C-O stretching in PVA. The PVA gives a broader peak at 3316 cm^{-1}due to the stretching vibration of -OH group. The blend membranes produce a broader peak in the range of 3050-3500cm^{-1}. These are attributed to weaker hydrogen bonding interactions between the PVA and 15PDNR compared to the neat PVA. The major peaks of NRL, PVA and PDMAEMA are found in the grafted and blended membranes. No additional peaks apart from those of the basic materials are found for the polymer blends.

XRD

XRD patterns at 2θ = 5-90º for NR, 15PDNR,15PDNR/2.5PVA,15PDNR/5PV, 15PDNR/10PVA and NR/PVA are shown in Fig. 3. The NR, 15PDNR and NR/PVA do not show any peak indicating their amorphous nature. Pure PVA shows a 2θ peak at 19.51º due to the semicrystalline nature being emerged from strong inter and intramolecular hydrogen bonding between the polymer chains. In the blends, the peak intensity has been found to be increased as the PVA concentration is increased. The enhancement in crystallinity can be attributed to the intermolecular hydrogen bonding between PVA and 15PDNR after physical blending.

TGA

Thermograms of NR, 15PDNR and blended membranes are shown in Fig.4. NR shows a degradation peak at 347 ºC where as the modified NR shows the degradation at 364 ºC. After blending with PVA, there is a further improvement in the thermal stability of the membranes (366-371ºC). This can be correlated with the increased crystallinity of the blends as evident from the diffractograms (Fig.3). As discussed, the crystallinity is primarily due to the intermolecular hydrogen bonding between PVA and grafted PDMAEMA part on NR.

Water contact angle measurement

Water contact angle measurements were used to monitor the changes on the surfaces of the thin membranes and the enhancement in hydrophilicity. Contact angles of 73 ±2^o and 59±4^o were found for NR and 15PDNR respectively. NR membranes show the highest value of contact angle due to their higher hydrophobicity because of the isoprene hydrophobic part in the polymer, while a lower contact angle was seen for 15PDNR owing to the presence of the hydrophilic grafted part polydimethylaminoethyl methacrylate. Upon increasing the PVA content in the blends the contact angle has been found to be decreased from 54±4^o to 25 ±2^o as shown in Fig.5. This is definitely due to the higher hydrophilicity deriving from PVA.

Table 1

Particle sizes from DLS measurements

Composition	Particle size (nm)
NR	576.6
2.5PDNR	583.2
5PDNR	634.5
10PDNR	713.8
15PDNR	784.5
20PDNR	594.7

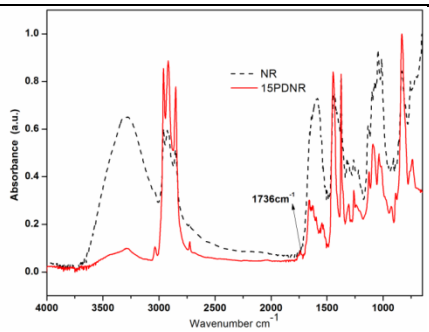


Fig.1. FT-IR spectra of NR and 15PDNR

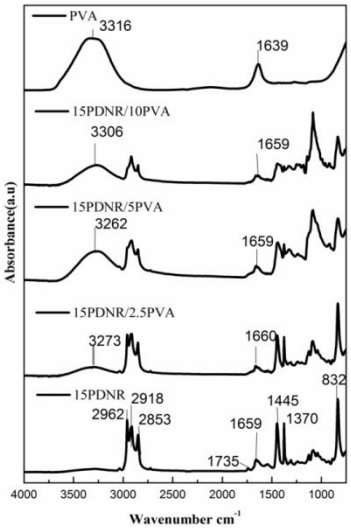


Fig.2. FTIR spectra of blends and PVA

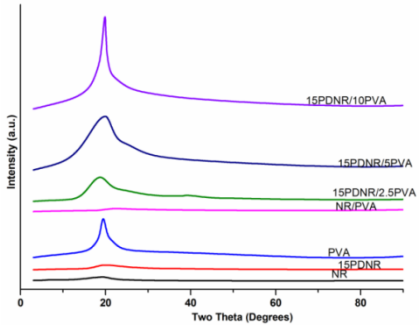


Fig.3. XRD diffractograms of NR, 15PDNR and their blends

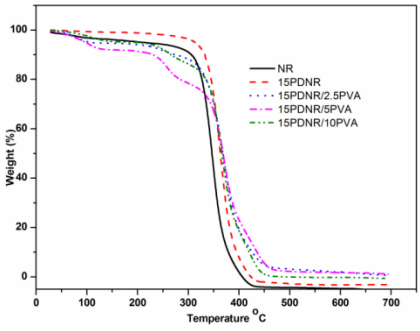


Fig.4.TGA and DTG plots of grafted and blended membranes

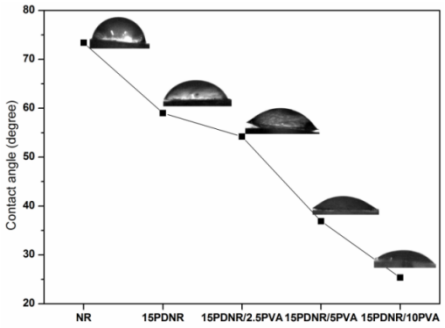


Fig.5. Water contact angle of the surface of the membranes

Conclusion

Natural rubber latex (NRL) has been functionally modified by grafting with DMAEMA followed by blending with PVA. Dynamic light scattering experiments indicated the enlargement of NRL dimension after grafting; which was subsequently confirmed by FT-IR spectroscopy investigation. Blending of the grafted NRL with PVA resulted in transparent membranes. These membranes were characterised by FT-IR, XRD, and TGA. In a separate experiment the blend membranes have been found to be ideal for the release of different commercial dyes.

References

15. A. Bogner, A. Guimarães, R. C. O. Guimarães, A. M. Santos, G. Thollet & P. H. Jouneau, C. Gauthier, Colloid Polym Sci 286, 1049–1059,2008.
16. A.D. Roberts, Oxford University Press, Oxford, U.K. 10-150,1998.
17. W. Pichayakorn,J. Suksaeree,P. Boonme,W. Taweepreda,G. C. Ritthidej, Ind.Eng.Chem.Res.51,13393-13404, 2012.
18. V.J. Tomazic-Jezic, D.H. Beezhold, H. Hashim, T. Palosuo, M. Raulf-Heimsoth, M. Swanson, R.G. Hamilton, J. Allergy Clin. Immunol. 113 S78, 2004.
19. E. Yip and P. Cacioli, J. Allergy Clin. Immunol. 110 S3-S14, 2002.
20. K.Simma, G.L. Rempel, P. Prasassarakich, Polym. Degrad.Stabil., 94 1914-1923, 2009.
21. Y. Promdum, P. Klinpituksa, J. Ruamcharoen, Songklanakarin J. Sci. Technol., 31 (4), 453-457, 2009.
22. D.J. Lamb, J.F. Anstey, C.M. Fellows, M.J. Monteiro, R.G. Gilbert, Biomacromolecules 2, 518-525, 2001.
23. W. Kangwansupamonkon, C.M. Fellows, D.J. Lamb, R.G. Gilbert, S. Kiatkamjornwong, Polymer 45 5775-5784, 2004.
24. A.M Mathur, S.K, Moorjani A.B Scranton, J. Macromol. Sci. Polym. Rev. 36, 405-430, 1996.
25. K.C.S. Figueiredo, T. L.M. Alves, C.P. Borges,J. Appl. Polym. Sci. 111(2009) 3074-3080.
26. B.Gupta, R. Agarwal, M. S. Alam, J.Appl.Polym.Sci.127 1301-1308, 2013.
27. J.M.Yang and H. C. Chiu, J. Memb. Sci.420, 65–71, 2012.
28. S. Liu, L. Wang, B. Zhang, B. Liu, J. Wang, Y. Song,J. Mater. Chem. A, 3, 2072-208, 2015.

MACRO 436

Electrochemical Behavior and Corrosion Inhibiting Effects of Green Nanosilver Modified Epoxy Coatings

Ulaeto, Sarah B.,[a,b,c] Rajan, Ramya,[a] Pancrecious, Jerin K.,[a,b] T.P.D. Rajan,*[a,b] Pai, B. C.[a]

[a]*Material Science and Technology Division, CSIR-NIIST, Trivandrum, Kerala, India*
[b]*Academy of Scientific and Innovative Research (AcSIR), New Delhi, India*
[c]*Department of Chemical Sciences, Rhema University, Aba, Abia State, Nigeria*
**Email: tpdrajan@niist.res.in; sarahbillmails@yahoo.com*

Epoxy resins the known reactive polymers can readily interact with other chemicals and result in numerous new ranges of materials. The major application of epoxy resins still remains for surfaces. The incorporation of modified materials by way of functionalization into epoxy resins offers environmentally friendly solutions to enhancing the integrity and durability of coatings. Being one of the most important matrices for structural composites applicability, the exploration of enhanced or novel blends based on epoxy chemistry is attracting more and more attention, and aims at maximizing the materials' compatibility [1-2]. These modifications of polymer matrices have been reported to give rise to coatings with desirable multifunctionalities [3-5].

Corrosion control is a collective effort of appropriate substrate surface treatments, inhibitors, and coatings etc. towards achieving the desired goal of protecting the metallic material from its aggressive environment. Nanotechnology has therefore provided the platform to explore the non-conventional composites of which polymer nanocomposites initiated from biomass is of interest in this work.

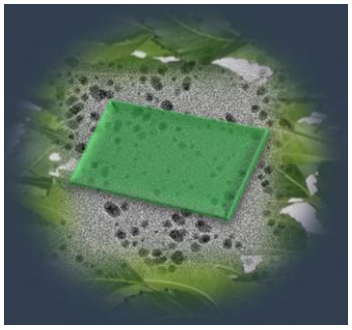


Figure 1. Schematic of modifying the epoxy coating.

Polymer nanocomposite coatings synthesized by loading modified silver nanoparticles within the epoxy network was investigated for corrosion inhibition purposes. The green-capped inorganic phase inside the organic matrix was meant to enhance coating properties by providing rigidity in the coating formulation. The presence of bio-reduced silver in solution via neem leaves extract was determined using UV-Visible spectroscopy. Crystallinity and Morphology of the silver nanoparticles were characterized using X-ray diffraction technique (XRD) and High resolution transmission electron microscope/energy dispersive x-ray analysis (HRTEM/EDX). The resultant hybrid organic-inorganic coating was further characterized using Fourier transform infrared spectroscopy (FTIR) and Differential scanning calorimetry (DSC). Corrosion inhibition effect of the investigated coatings was determined via the non-destructive electrochemical impedance spectroscopy (EIS) and DC potentiodynamic polarization (PP) techniques. Surface morphology of the modified coating was established with scanning electron microscopy (SEM). Results revealed superior anticorrosive properties in the

presence of the green additives in comparison to the unmodified epoxy coating for the protection of AA6061 alloys.

References

[1] Shi, X.; Nguyen, T.A.; Suo, Z.; Liu, Y.; Avci, R. *Surface and Coatings Technology*, 204 (2009) 237.
[2] Zhang H.; Yang J. *Smart Materials and Structures*, 23 (2014) 065003.
[3] Gonçalez, V.; Barcia, F. L.; Soares, B. G. *Journal of the Brazilian Chemical Society*, 17(2006) 1117.
[4] Zheludkevich, M.L.; Tedim, J.; Freire, C.S.R.; Fernandes, S.C.M.; Kallip, S.; Lisenkov, A.; Gandini, A.; Ferreira, M.G.S. *Journal of Materials Chemistry*, 21(2011) 4805.
[5] Ghazizadeh, A.; Haddadi, S. A.; Mahdavian, M. *RSC Advances*, 6(2016) 18996.

MACRO 438

Understanding the Dynamics of Multicomponent BTA Nanofibers in Aqueous Solutions

Bala. N. S. Thota, Xianwen Lou, René Lafleur, Anja Palmans and E. W. Meijer*

Institute for Complex Molecular Systems & Laboratory of Molecular Science and Technology
Department of Chemical Engineering and Chemistry, Eindhoven University of Technology, Eindhoven
The Netherlands

e.w.meijer@tue.nl

Supramolecular polymers are a best example to demonstrate the power of noncovalent synthesis and have been extensively investigated in recent times.[1,2] Although the mechanism of supramolecular polymerization has been well studied, the dynamics of the resulted nanostructures, which is an important factor in the design of supramolecular biomaterials, have not been well understood. In our group, we have been interested in the development of supramolecular biomaterials based on 1,3,5-benzenetricarboxamide derivatives (BTAs).[3] Supramolecular polymerization of water soluble BTA molecules results in nanofibers with high aspect ratio.[4] Recently, we have been interested in understanding the dynamics of BTA fibers in water. As a part of our interest, we investigated the BTA fiber dynamics using different analytical methods such as FRET, STORM.[5,6] However, all these methods involve labeling of the monomeric BTAs, which might influence the dynamics of BTA fibers. Very recently, we have evaluated HDX-MS as an alternative method to investigate the dynamics of BTA fibers without external labeling/probes. When an aqueous solution of nanofibers was diluted into deuterated water (D_2O), all the exchangeable protons on the surface of the nanofiber (OH groups) are replaced by deuterium immediately and the displacement of amide protons by deuterium provides the exchange rate of the monomer between the fiber and the solution. Now we would like to extend the application of this methodology to understand the dynamics of multicomponent nanofibers and thereby achieve a control over the dynamics of these supramolecular nanostructures through a rational design of individual components.

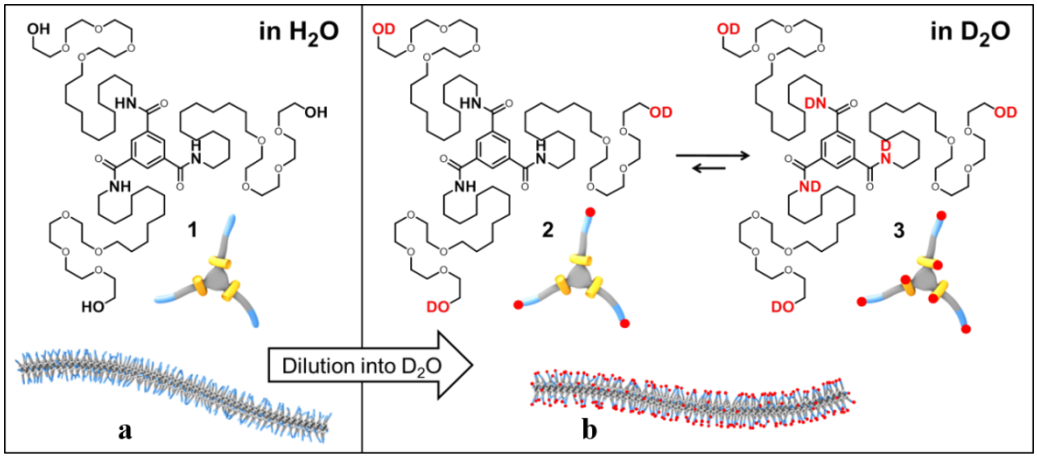


Figure 12. Schematic representation of BTA nanofibers in water (a) and in D_2O (b). The equilibrium between the two molecules representing the BTA nanofiber in D_2O is also shown (b).

Herein we studied mixtures of two BTA derivatives (nBTA and dBTA) that are quite different in their self-assembly to achieve multicomponent BTA nanofibers with tunable dynamics. More interestingly, in some cases, both the molecules attained better stability in mixtures compared to individual systems. Subsequently, we also studied two more BTA derivatives consisting of one and two dendritic wedges as hydrophilic entities, and compared the dynamics of nanofibers obtained from different molecules against the mixtures. Our investigations revealed that one could achieve a better control over the dynamics of nanofibers through multicomponent approach.

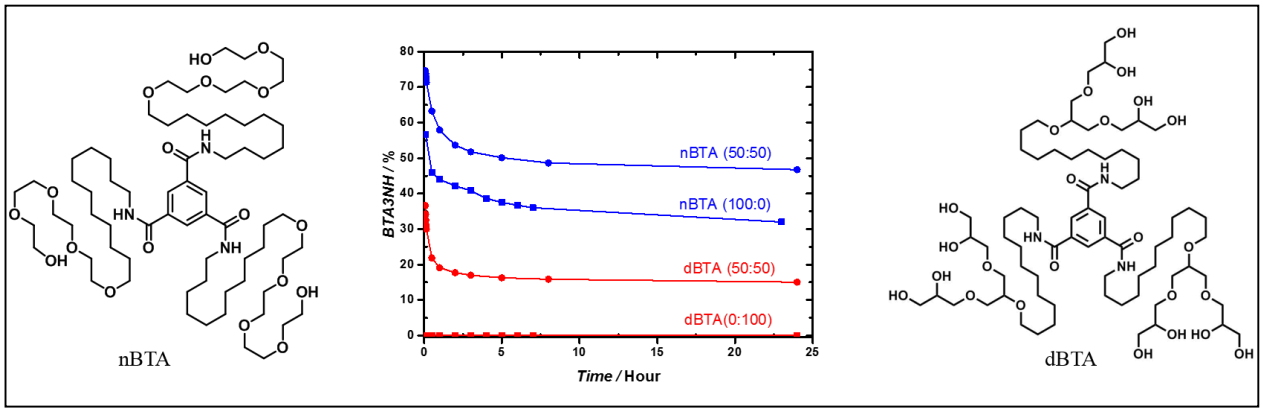


Figure 13. HDX experimental data of individual components and their mixture (1:1)

References

[18] Brunsveld, L.; Folmer, B. J. B.; Meijer, E. W.; Sijbesma, R. P. *Chem. Rev.*, 101 (2001) 4071.

[19] De Greef, T. F. A; Smulders, M. M. J.; Wolffs, M.; Schenning, A. P. H. J.; Sijbesma, R. P.; Meijer, E. W. *Chem. Rev.*, 109 (2009) 5687.
[20] Cantekin, S.; de Greef, T. F. A.; Palmans, A. R. A. *Chem. Soc. Rev.*, 41 (2012) 6125.
[21] Leenders, C. M. A.; Albertazzi, L.; Mes, T.; Koenigs, M. M. E.; Palmans, A. R. A.; Meijer, E. W. *Chem. Commun.*, 40 (2013) 1963.
[22] Albertazzi, L.; Martinez-Veracoechea, F. J.; Leenders, C. M. A; Voets, I. K.; Frenkel, D.; Meijer, E. W. *Proc. Natl. Acad. Sci. U.S.A.*, 110 (2013) 12203.
[23] Albertazzi, L.; van der Zwaag, D.; Leenders, C. M. A.; Fitzner, R.; van der Hofstad, R. W.; Meijer, E. W. *Science*, 344 (2014) 491.

MACRO 441

A Rheokinetic Approach to Cure Optimization of Polyurethane Binders in Composite Solid Propellant

G. Santhosh [a,*], S. Reshmi [a], Elizabeth John [a], C.P. Reghunadhan Nair [b]

[a] *Propellant Engineering Division, Polymers and Special Chemicals Group, Vikram Sarabhai Space Centre, Trivandrum 695 022, Kerala.*

[b] *Cochin University of Science and Technology, Cochin 682022, Kerala*
** e-mail id: g_santhosh@vssc.gov.in*

Abstract

The cure kinetics of a composite solid propellant based on ammonium perchlorate (AP) and hydroxyl terminated polybutadiene (HTPB) system was investigated using a rheometer. The cross-linking kinetics of HTPB resin in the presence of tolylenediisocyanate (TDI) in a propellant was studied under isothermal conditions in the temperature range of 60 – 70°C by rheometry. The kinetic parameters of curing reaction were calculated from the rheological measurements. The cure kinetics parameters were derived by a multiple regression analysis using a classical phenomenological model expanded by a diffusion factor derived empirically. The obtained kinetic parameters were used to generate a master equation capable of predicting the reaction profile at any given temperature. Excellent match between observed and predicted cure profiles in the entire temperature range validated the adequacy of the model.

Keywords: *polyurethane; composite propellant; rheokinetics; curing; HTPB; ammonium perchlorate;*

Introduction

Ammonium perchlorate (AP)-hydroxyl terminated polybutadiene (HTPB) based composite propellant is widely used by the propulsion community worldwide. The AP/HTPB system usually contains additives such as: 1) burn rate catalysts 2) anti-oxidants 3) plasticizers 3) cross-linking agent 4) metallic fuel etc., These highly filled systems containing HTPB binder are cured using a diisocyanate viz., tolylenediisocyanate (TDI).

The rheological properties of solid propellants, gel propellants and other energetic materials with a variety of binders were studied and reported in the literature [1-5]. Number of curing and rheological studies

involving the use of HTPB with other ingredients was also reported in the literature [6-13]. Though many reports deal with the chemical cure kinetics of the solid propellant systems, this one will not give any clear picture regarding the last phase of the reaction as the last phase of curing is associated with neither little change in chemical signals nor thermal changes and thus both spectral and thermal methods fail. The curing kinetics of epoxy-amine systems are the ones widely studied [14-21], and among the existing cure kinetics models, the most widely used one is the phenomenogical Kamal and Sourour model [14] which is extended by Fournier et al., [15] for diffusion effects to be taken into account. The cure kinetic parameters are temperature dependent as the curing involves changes in local temperature due to chemical crosslinking reaction and the heating schedule. A simple cure kinetics model applicable for the curing of HTPB-diisocyanate system may not adequately predict the cure kinetics of the propellant as it contains these additives. Therefore it is necessary to derive the cure kinetics of the propellant containing additives and to define the cure kinetics using an appropriate model.

In this study, the chemical crosslinking reaction of HTPB-diisocyanate in presence of AP and other additives was investigated by rheological measurements using a rheometer under isothermal conditions. An attempt was made to model the diffusion-control in the cure kinetics, and a new empirical model was developed and employed to study the cure kinetics and the kinetic parameters were derived based on this approach. A master equation was derived for the cure profile prediction and the time-conversion data was simulated for each isothermal temperature.

Experimental

Materials

AP-Coarse, AP-Fine, HTPB (binder), Dioctyladipate (plasticizer), Ambilink (cross linking agent), Aluminum (metal fuel), PBNA (anti-oxidant) and tolylenediisocyanate (TDI) were used for preparing the propellant mix.

Sample Preparation

Premix slurry was made from the above materials following the standard mixing procedure. A horizontal sigma blade mixer was employed for the mixing operations and the mixing temperature was kept at 43^{o}C. The propellant has a solid loading of 86% containing 68% AP (C:F=4:1) and 18% Aluminum. The premix slurry was then transferred and stored in air tight plastic carton under ambient conditionwith utmost care to avoid moisture ingression. 10g of premix slurry was weighed accurately in a small container and the required amount of TDI was then added to it and was thoroughly hand mixed using a glass rod.

Rheological Measurements

Rheological measurements were performed on a Bohlin Gemini 2 Rheometer (Malvern Instruments, UK). About 1g of the slurry was placed between the top and bottom plate (PP 40) of the rheometer adjusting the gap to 1000µ. Isothermal experiments were conducted in the temperature range of 60-70^{o}C and the time vs conversion data were obtained from the corresponding rheograms. The following conditions were used for each run for each temperature.

Geometry: Parallel plates (serrated) 40mm
Gap: 1000µ; *Frequency:* 1 Hz
Mode: Oscillation; *Strain:* 0.05%

Results and discussion

Isothermal cure analysis

The curing of the propellant was analyzed under isothermal conditions. The storage modulus (G') which is sensitive to the formation of network structure was used to monitor the crosslinking process.

The complex viscosity η*is related to the complex modulus G*as

$$\eta^* = \frac{G^*}{i\omega}$$

$$G^* = G' + i\,G''$$

Where, ω is the angular frequency, the storage modulus G' is a measure of the elastic (reversible) deformation energy stored by the material, the loss modulus G'' (viscous component) is a measure of the energy dissipated by the material.

Therefore, the extent of conversion can, *a priori*, be estimated using the formula given by equation. 1.

$$\alpha = \frac{G'(t) - G'(0)}{G'(\infty) - G'(0)} \qquad (1)$$

where G'(∞) is the final value of storage modulus, G'(t) is the value of G' at time t and G'(0) is the value of G' at the beginning of the crosslinking process.

Typical rheograms of the propellant obtained at three different temperatures are shown in figure 1.

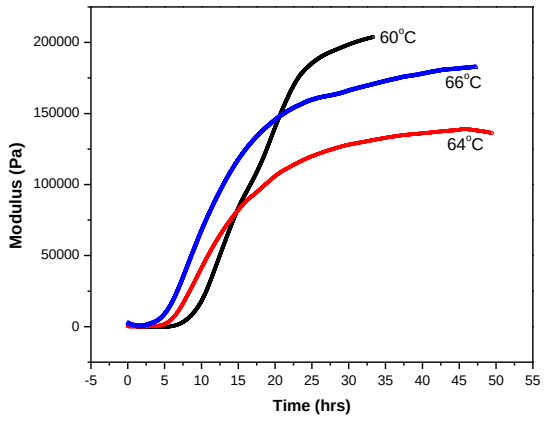


Figure 1: Experimental rheograms

It could be seen from figure 1, that the modulus builds up steadily and then proceeds at a slower rate after reaching around 20-25hrs. It is also noted that the appreciable modulus change can only be observed after a few hours from the start of the experiment. At an isothermal temperature of 60ºC, the modulus starts to build up at ~ 6.5hrs, while at 66ºC, the buildup starts at ~5 hrs. This happens as the initial chain extension processes does not impart adequate viscosity to the system to be sensed by the rheometer.

From the experimental rheograms, the gel times (t_{gel}) were also calculated. The gel time was taken as that corresponding to the change in slope of the two linear parts of the modulus curve.

Table 1: Gel times (t_{gel}) at different 'T'

Temperature, ºC	**t_{gel}, hrs**
60.0	6.74
62.5	6.35
64.0	5.81
65.0	5.89

66.0	5.13
67.5	4.53

The calculated gel times are tabulated in table 1. It is seen that the time of gelation decreases with increase in temperature.

The temperature dependency of the gel times are found as a function of temperature and alogarithmic relationship of ln(t_{gel}) vs 1/T can be obtained using equation 2, from which the apparent activation energy can be calculated from the slope of plots of ln (t_{gel}) vs 1/T.

$$\ln(t_{gel}) = \ln(c) - \frac{E_a}{RT} \qquad (2)$$

The linear fit of eqn.2 gave the expression **ln (t_{gel}) = -15.47 + 5803.72** from which the activation energy was found to be 48.25 kJ/mol. This activation energy tallies with the value reported in the literature.

Isothermal kinetic analysis

Cure kinetic models can be classified into two categories, phenomenological models and mechanistic models. However, mechanistic models are heavy to handle to identify the thermosetting chemical reactions such as HTPB-TDI. Hence phenomenological or semi-empirical models were considered for the cure kinetics modeling as they are easy to use. A lot of empirical models, have been suggested for cure kinetics. Nevertheless, it appears that the isothermal approach was based on an autocatalytic model which was first found by Horie et al.[16] and then extended by Kamal [17]. The Kamal and Sourour model [17] of cure kinetics seems to be the most widely used in the literature. This model shown in equation 3, accounts for an autocatalytic and non-autocatalytic reaction in which the initial rate is not zero.

$$\frac{d\alpha}{dt} = (k_1 + k_2.\alpha^m)(1-\alpha)^n \qquad (3)$$

where α is the degree of cure corresponding to the rate dα/dt and denotes the conversion at a given time t. k_1 is the rate constant of the reaction of partial order 'n' and k_2 is the rate constant of the autocatalytic reaction of partial order 'm'.

However, solving of cure kinetics in equation 3 mathematically tends to 100% of degree of curing. If the equation.3 is satisfying for the beginning of the degree of conversion, then this is not correct in comparison with final level of degree of curing obtained experimentally since it hardly tends to unity. As the curing process evolves, the cross linking reaction becomes diffusion controlled and must therefore be taken into account.

For the chemical cure kinetics a normal second order reaction (equation. 4) should be suitable.

$$\frac{d\alpha}{dt} = k\,(1-\alpha)^2 \qquad (4)$$

At the beginning of curing, the rate is dominated by the chemical reactivity of the –OH groups with –NCO before being controlled by a diffusion phenomenon. Various semi-empirical models were extended for equation 3 by introducing a diffusion factor, $f_d(\alpha)$ shown in equation 5.

$$\frac{d\alpha}{dt} = (k_1 + k_2.\alpha^m)(1-\alpha)^n f_d(\alpha) \qquad (5)$$

The isothermal conversion rate (dα/dt) was obtained from the differential plot of **α** versus **t** using a spacing of Δα = 0.005 and linear interpolation of the experimental data. The calculated dα/dt was then plotted as a function of conversion for each temperature. A typical plot showing the conversion rate vs conversion at 60°C is given in figure 2. Similar plots were generated for all other temperatures.

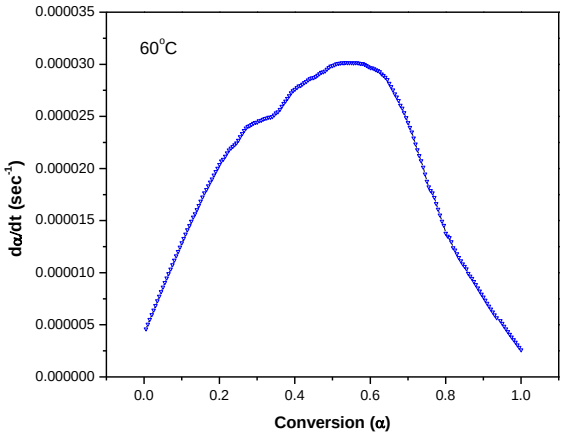


Figure 2: Dependency of conversion rate on conversion at 60°C

Description of the kinetic model and evaluation of kinetic parameters

The general autocatalytic model (given in equation 5) was modified by us to account for the diffusion phenomena by introducing a diffusion coefficient (d) as given in equation6.

$$\frac{d\alpha}{dt} = [k_1(1-\alpha)^n] + \frac{[k_2 * \alpha * (1-\alpha)^m]}{[1+(d*\alpha)]} \qquad (6)$$

In equation 6, the values for **m** and **n** denote the curing reaction order for the autocatalytic and catalytic parts of the chemical cure reaction respectively. From the first cut analyses of the data according to equation 6 gave the values of m and n as 0.8 and 1.2 respectively. In the present study, k_1 was calculated as the initial conversion rate of ln(dα/dt) versus α curve. The k_1 values are calculated from the linear plots of ln(dα/dt) vs α(*ln(1-α) = α*) for an initial conversion of up to 10%. The linear plots are verified and the fits with a good correlation coefficient was chosen for $0.1 \leq \alpha \leq 10$. The calculated k_1 values are summarized in Table 2.

Table 2: Values of 'k_1'calculated at different temperatures.

Temperature (°C)	k_1 (sec^{-1})	n
60.0	4.50645E-6	1.2
62.5	3.02077E-6	1.2
64.0	8.21129E-6	1.2
65.0	5.23575E-6	1.2
66.0	8.12959E-6	1.2
67.5	10.8970E-6	1.2

It is seen from table 2, that the rate constant values tend to show an increase with increase in temperature, however the trend is not prominent.

The other kinetic parameters, 'k_2'and 'd' were calculated by fitting the experimental data using non-linear curve fitting approach using ***Origin software*** for each isothermal temperature. Initial values of 'k_2', and 'd' were guessed and was fed into the program and iterated until the curve converges. Typical curve fitting plots for two different cases are shown in figure 3. The kinetic parameters (k_2, and d) obtained by this fitting method are summarized in table 3.

Table 3: Kinetic parameters a-priori derived from the non-linear curve fits

Temp	k_2 (sec^{-1})	m	d	R^2
60.0	1.171E-4	0.8	0.599	0.93719
62.5	1.596E-4	0.8	2.104	0.97724
64.0	1.700E-4	0.8	4.056	0.96048
65.0	1.828E-4	0.8	2.669	0.91598
66.0	1.893E-4	0.8	4.774	0.93782
67.5	2.364E-4	0.8	6.299	0.89388

It could be seen from table 3, that the k_2 values show an increasing trend with increase in temperature, similarly an increasing trend could also be observed for the values of 'd'. A reasonably good fit ($R^2 > 0.9$) shows overall adequacy of the current model.

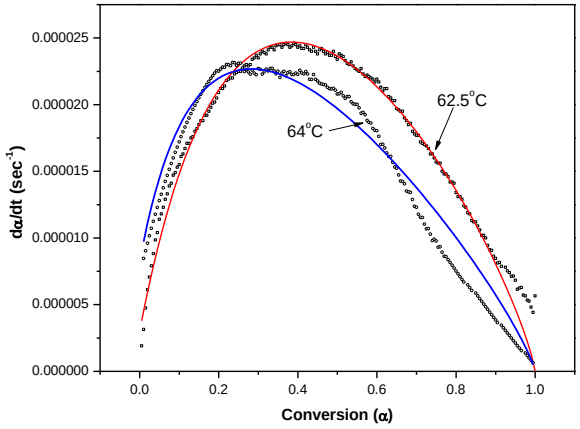


Figure 3: Plots of conversion rate as a function of conversion. Solid line is the fit of equation 6 using the calculated k_1 and m=0.8 and n=1.2.

It can be seen from figure 3, that the fitted curve closely matches with the experimental curve. Similar acceptable curve fits were obtained for all other cases. k_1 and k_2 are specific rate constants thus obtained, when plotted against the temperature follows the Arrhenius expression given by equation 7 which gave the expression as **$\ln k_1 = 22.79 - 11695/T$** and **$\ln k_2 = 20.94 - 9681.2/T$**.

$$k_{1=}A_1 \exp\left(-\frac{E_1}{RT}\right) \text{ and } k_{2=}A_2 \exp\left(-\frac{E_2}{RT}\right) \qquad (7)$$

The cure kinetic parameters obtained from equation 7 are listed in Table 4.

Table 4: Cure kinetic parameters obtained from equation 7.

E_1 (kJ/mol)	$\ln A_1$ (sec^{-1})	E_2 (kJ/mol)	$\ln A_2$ (sec^{-1})
97.2	22.79	80.5	11.8

It could be seen from table 4, that the first step of the curing reaction has an activation energy (E_1) of 97.2 kJ/mol, while the diffusion controlled reaction has a slightly lower activation energy (E_2) of 80.5 kJ/mol.

As the degree of conversion increases with curing, the diffusion parameter 'd' was found as a growing function of temperature, T and could be fitted to a linear function of temperature, which gave an expression **d=243.88-81074/T**.

Prediction of cure reaction profiles

The first cut kinetic data thus obtained were used for predicting the cure reaction profile at a given temperature. Using the kinetic parameters given in table 2 and 3, the numerical integration of the cure kinetics model defined by equation 6 was undertaken. The integration was done in small time intervals (Δt = 3sec) according to equation 8 and the corresponding conversion was calculated and the gel time was then added.

$$\alpha = \int_0^t [f(\alpha)\,]\,dt \qquad (8)$$

After establishing the time and temperature relationship of all variables, a master equation between conversion, time and temperature was established and expressed as given in equation 9. In all cases the t_{gel} values were added to the time scale.

$$d\alpha = \left[\left[\exp\left(22.79 - \frac{11695}{T}\right) * (1-\alpha)^{1.2}\right] + \frac{\left[\exp(11.8 - \frac{7027.7}{T}) * \alpha * (1-\alpha)^{(0.8)}\right]}{\left[1 + \left((243.88 - \frac{81074.81}{T}) * \alpha\right)\right]}\right] dt \qquad (9)$$

Typical comparison between the experimental and predicted reaction profile using the above master equation is shown in figure 4.

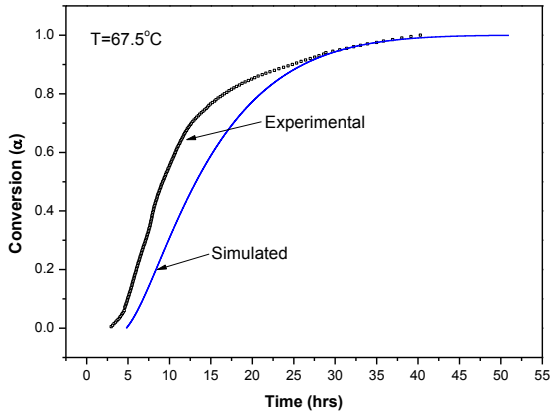


Figure 4: Experimental and predicted conversion versus time data (before refinement)

It is seen from figure 4, the predicted profiles for the isothermal curing at 67.5°C could not fit well with the experimental conversion data and only the end of the conversion data could fairly fit well. Similarly the comparison of the predicted conversion versus time data for the curing reaction at other temperatures also showed that a close fit could not be obtained for all the cases.

Refinement of model

As it is seen from figure 4, that the predicted profile does not seem to match well with the experimental data though the final conversion data have a close match. In order to obtain a reasonable good fit, the final iteration was done by refining the values of 'k_2'and 'm' marginally while keeping all other parameters intact, so that the experimental data fit well to the predicted. This was done for each temperature until the simulated curve matches closely with the experimental curve. The plot showing the experimental and predicted conversion vs time profiles after the refinement is shown in figure 5.

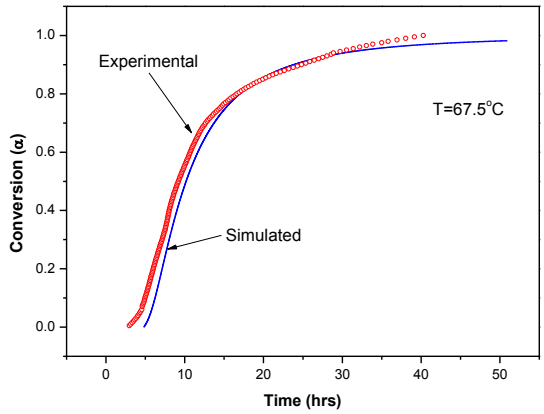


Figure 5: Experimental and predicted conversion versus time data (after refinement)

The comparison of predicted data with the experimental data led to satisfying results, as the predicted data after refinement fits well for all the isothermal curing temperatures employed. It is seen from figure 5, that the experimental and the predicted profiles of conversion vs time have a very close match. The refined values of 'k_2'and 'm' were thus re-estimated for all temperatures similarly and are given in table 5.The plot of ln(k_2) vs 1/T shown in figure 6 was made using the Arrhenius equation given in 7, which gave the expression as $\mathbf{\ln k_2 = 61.93 - 23782/T}$ and an activation energy (E_2) of 197.72 kJ/mol.

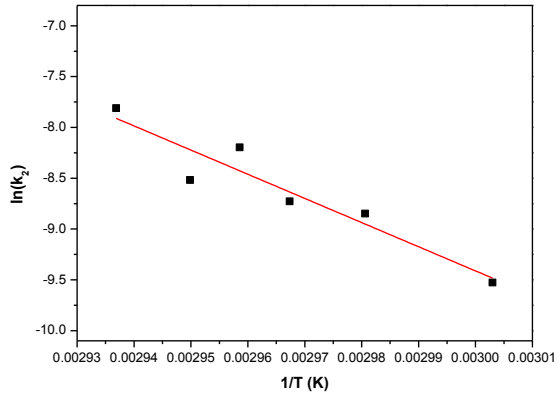


Figure 6: Plot of 1/T vs ln(k_2) for different temperatures

Table 5: Kinetic parameters derived after iterating of 'k_2' and the corresponding 'm' values for different temperatures

Temperature (°C)	k_2 (sec^{-1})	m
60.0	0.7290E-04	0.70
62.5	1.4354E-04	0.74
64.0	1.6196E-04	1.15
65.0	2.7571E-04	0.80
66.0	1.9990E-04	1.35
67.5	4.0507E-04	1.40

It is seen from table 5, the k_2 and m values showed a temperature dependence as the values increase with increase in temperature. Similarly the relationship for the 'm' values with temperature were established by plotting the temperature vs 'm', which could be fitted to a linear relationship given as **m=0.1106*T-36.209**.

After establishing the time and temperature relationship of all variables and the refinement of 'k_2' and 'm' values, a master equation between conversion, time and temperature was established. The model was thus changed and could be expressed by a master equation given in equation 10.

$$d\alpha = \left[\left[\exp\left(22.79 - \frac{11695}{T}\right) * (1-\alpha)^{1.2}\right] + \frac{\left[\exp(61.93 - \frac{23782}{T}) * \alpha * (1-\alpha)^{(-36.209+0.1106*T)}\right]}{\left[1 + \left((243.88 - \frac{81074.81}{T}) * \alpha\right)\right]}\right] dt \quad (10)$$

The conversion (α) at any given temperature (T) can now be made for an AP/HTPB based propellant by numerical integration of equation 10. For each temperature, the values of conversion (α) corresponding to overall conversion $0.001 \leq \alpha \leq 0.950$ in intervals of 0.001 were determined. This was done by calculating the small incrementsdα in very small time intervals of 2 to 3 secs and then numerically integrating by a ***FORTRAN*** program.

The values of T and α were then substituted in equation 10 to plot the effective time as a function of temperature and overall conversion. Typical simulated time versus conversion plots for three different temperatures are shown in figure 7.

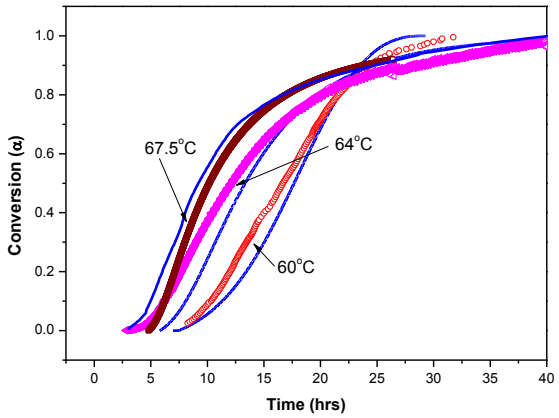


Figure 7: Comparison of simulated and experimental plots of conversion vs time (solid line represents the simulated curves)

It could be seen from figure 7, that the simulated curves fairly fit well with the experimental conversion curves. 3D plots were also generated for the dependence of time, temperature and conversion for isothermal temperatures of 60 – 70°C. The resulting plots are shown in figure 8.

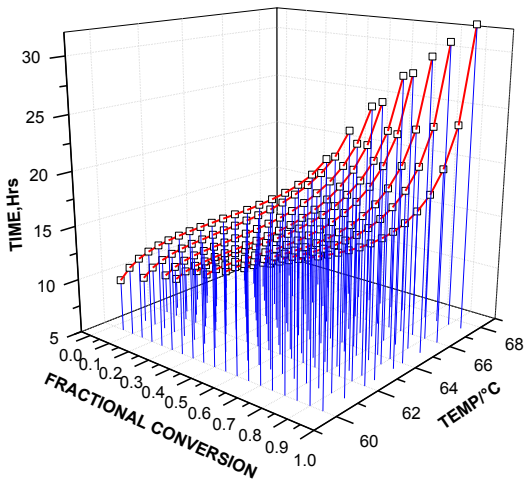


Figure 8: 3D plots of time as a function of (α) and (T) for the simulated process using equation 10.

It is seen from figure 8, the conversion increases with increase in temperature and it reaches a maximum at ~25-30hrs. The conversion rate is slow at 60°C than at other temperatures.

Conversion-Time-Temperature Correlation

The calculated times at different temperatures for different conversion are given in table 6 along with the corresponding gel times (t_{gel}). The comparison of data for different temperature conveys that on increasing the temperature, the conversion time reduces. However, because of the temperature dependency, the rheo-conversion nearly reaches 100%.

Table 6: Calculated time data for different conversions and temperatures along with gel times

Temperature	60°C	62.5°C	64°C	65°C	66°C	67.5°C
Time for 50% conversion, hrs	17.6	14.8	13.3	12.4	11.5	10.2
Time for 70% conversion, hrs	20.2	18.2	16.9	16.0	15.1	13.7
Time for 80% conversion, hrs	21.7	20.7	19.8	19.0	18.3	16.9
Time for 90% conversion, hrs	23.5	24.5	24.6	24.5	24.3	23.8
t_{gel}(hrs)	7.0	6.2	5.8	5.5	5.2	4.8

It is seen from table 6, that the time for conversion decreases with increase in temperatures. The computed t_{gel} values show a decreasing trend with temperature.

Real time cure data at 60°C

Rheokinetics predicts cure completion at a given temperature. A real time cure study was also carried out at 60°C for different periods of time (up to 120hrs) to understand the effect of post curing if any, on the mechanical properties of the propellant.

Table 7: Mechanical properties of the propellant cured for different times at 60°C

Time for curing (hrs)	Tensile strength (kgf/cm²)	Elongation (%)	Modulus (kgf/cm²)	Hardness (Shore A)
30	6.1±0.3	55±1.9	21.7±0.3	52.70-57.30
50	6.3±0.1	55±1.3	23.3±0.9	51.60-57.00
75	6.4±0.1	55±2.9	23.1±0.7	53.40-59.10
100	6.4±0.1	52±3.4	24.6±1.1	52.80-56.50
120	6.4±0.1	51±1.4	23.9±1.2	53.00-59.40

The results on the mechanical properties i.e. tensile strength, % elongation, modulus and hardness values are given in table 7.

Though rheokinetics predicts a cure completion at 30 hrs (at 60°C), the residual curing happens beyond this time. Thus the initial modulus increases by about 7% at 50 -75hrs of curing and it reaches a maximum at 100hrs. Tensile strength increases by 5% and elongation decreases to 5-7%. This means the "curing" process subtly goes beyond the "rheo-curing" time of 30 hrs. These changes in mechanical properties can be caused by the amount of (i) residual curing of the propellant (ii) crosslinking of the unsaturated double bonds.

Since the elongation goes down in a "pseudo continuous" form further even beyond 75 hrs, the real cause for these could be the crosslinking of the unsaturated double bonds of the binders. Hence the cure is predicted to be complete as per the rheogram. However to be on the safer side, the propellant can be cured as normal and given an additional cure for 30 hrs more. The data on the tensile strength, modulus and elongation (Table 7) show that the residual curing though not very significant needs about ~100hrs (4 days) of heating at 60°C.

Conclusions

The curing of a composite solid propellant was followed by a rheometer and an empirical model was established for conversion (α), temperature (T) and time (t). The prediction conforms to an autocatalytic model where the diffusion parameter has a major 'say' particularly at higher conversion. By establishing a time and temperature dependence of all the variables, a master equation was generated for the AP/HTPB solid propellant system which could adequately predict the conversion at any given time or temperature. Real time curing data showed the propellant needs about ~80 hrs of curing and beyond this time the change in the mechanical properties is attributed to aging and crosslinking of the unsaturated double bonds in the binders and not significantly due to post curing.

.

References

1. Shai Rahimi, Arie Peretz, *Prop. Expl. Pyro.*, 32(2), 165-174, 2007.
2. Botchu. V. S. Jyoti, Seung Wook Baek, *Prop.Expl. Pyro.*, 39, 866 – 873, 2014.
3. U. Teipel, U.F. Barth, *Prop. Expl. Pyro.*, 26, 268-272, 2001.
4. T. S. Reddy, J. K. Nair, R. S. Satpute, G. M. Gore, A. K. Sikder, *J. Appl.Polym. Sci.*,Vol. 118, 2365–2368, 2010.
5. Jong-Sung You, Si-Tae Noh, *Polym.Int.*,62: 158–164, 2013.
6. Makoto Kohga, Yutaka Hagihara, *Prop. Expl. Pyro.*, 25, 199-202, 2000.
7. A.K. Mahanta, Ila Dharmsaktu, P.K. Pattnayak, *Def. Sci. J.*, 57(4), 435-442, 2007.
8. B. M. Bandgar, V. N. Krishnamurthy, T. Mukundan, K. C. Sharma, *J.Appl. Polym. Sci.*, Vol. 85, 1002–1007, 2002.
9. Manohar Singh, B. K. Kanungo, T. K. Bansal, *J. Appl. Polym. Sci.*, Vol. 85, 842–846, 2002.
10. B. M. Bandgar, K. C. Sharma, T. Mukundan, V. N. Krishnamurthy, *J. Appl. Polym. Sci.*, Vol. 89, 1331–1335, 2003.
11. Abhay K. Mahanta, Monika Goyal andDevendra D. Pathak, *E-Journal of Chemistry*, 7(1), 171-179, 2010.
12. Rm. Muthiah, V. N. Krishnamurthy, B. R. Gupta, *Prop.Expl. Pyro.*,21, 186- 192, 1996.
13. Hai-Xing LI, Jing-Yu Wang, Chong-Wei AN, *Cent. Eur. J. Ener. Mat.*, 11(2), 237-255, 2014.
14. S. Sourour, M.R. Kamal, *Thermochim. Acta*, 14 (1–2), 41-59, 1976.
15. Jerome Fournier, Graham Williams, Christine Duch, George Anthony Aldridge, *Macromol.,29*, 7097-7107, 1996.
16. Horie, K., Hiura, H., Sawada, M., Mita, I. Kambe, H, *J. Polym. Sci. A-1 Polym. Chem.*, 8: 1357–1372, 1970
17. Kamal, M. R. Sourour, S., *Polym.Eng.Sci*, 13: 59–64, 1973.
18. K.C. Cole, J.J. Hechler, D. Noel, *Macromol.*, 24, 3098-3110, 1991.
19. G. Liang, K. Chandrashekhara, *J. Appl. Polym. Sci.*, 102(4), 3168-3180, 2006.
20. N. Rabearison, Ch. Jochum, J.C. Grandidier, , *J. Mater. Sci.*, 46(3), 787-796, 2011.
21. S.Corezzi, Daniele Fioretto, G. Santucci, Jose M. Kenny, *Polymer*, 51, 5833-5845, 2010.

MACRO 456

Studies on the Influence of Free Volume on Transport Properties of Millable Polyurethane/Natural Rubber Blends

Renu Jose [a], Lity Alen Varghese [b], G Unnikrishnan [a,*]

[a] *Department of Chemistry, National Institute of Technology, Calicut, Kerala-67360, India*
[b] *Department of Chemical Engineering, National Institute of Technology Calicut, Kerala-673601, India*
E-mail address: unnig@nitc.ac.in

Membrane technology is one of the most important separation methods due to lower energy consumption, higher performance and low cost requirements. Polymers in different applications are exposed to a variety of chemical environments during their lifetime. The presences of solvents in polymers or blends cause a reduction in the properties of polymer. Solvent sorption and diffusion change the mechanical properties and sometimes cause destruction in polymer structure, are the limiting factors of polymer in application purposes. For the effective application of these polymer membranes, it is necessary to understand their performance in various liquid environments [1, 2].

Two or more existing polymers can be blended together to achieve a material that has a combination of the properties of the constituents and can meet a specific set of requirements. Sometimes, this practice also helps in the creation of polymeric materials with novel properties [3].Millable polyurethane containing glycerol allyl ether as a chain extender (MPU) /natural rubber (NR) blend systems were developed using an accelerated sulphur vulcanisation strategy. The examination of the cure characteristics of MPU/NR blends showed that there was an increase in rheometric torque with increase in NR content; indicating a higher crosslink density for NR rich systems. The free volume content of MPU/NR blends were investigated using positron annihilation lifetime spectroscopy (PALS).The positron lifetime results showed a regular increase in free volume size (V_f) and free volume concentration (I_3) with an increase in content of NR in the blends. The mechanical properties of the blends have also been found to be increased with an increase in NR content.

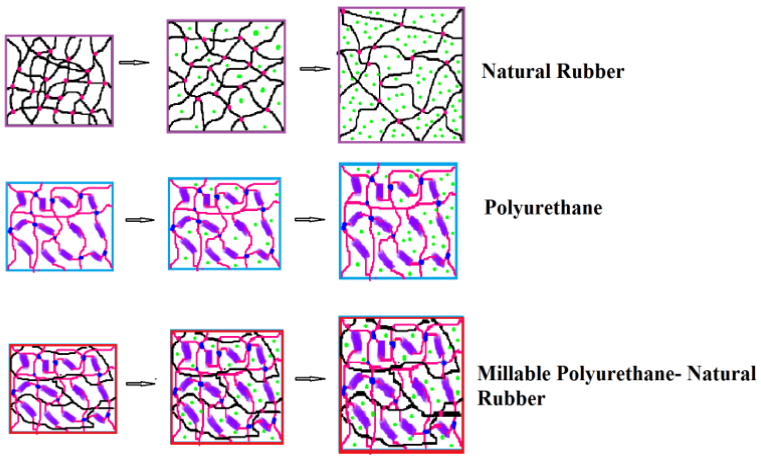


Fig. 1. Schematic representation of swelling behavior of MPU and NR blends

The degree of swelling in three hydrocarbons viz; petrol, diesel and kerosene have been studied. It is evident that NR alone possesses the highest degree of swelling followed by MPU/NR blends while MPU alone shows the lowest degree of swelling values. The swelling behavior of a given MPU/NR system in the penetrants follows the order Petrol>Kerosene>Diesel. A scheme showing the re-organisation of macromolecular chains under the influence of solvents is given in Fig.1

Table 1. Degree of swelling (%) values of different compositions of MPU/ NR blends

Samples	Diesel	Kerosene	Petrol
P 100/N0	27	34	165
P60/N40	85	110	270
P20/N80	183	212	292
P0/N100	212	224	296

The effect of blend ratio, free volume and penetrant size on the sorption properties of MPU/NR blends was studied. In the blends, the equilibrium solvent uptake decreases with an increase in concentration of MPU. The PALS results have been correlated with transport properties, which demonstrate that the transport properties possess a significant dependence on the free volumes of the blends [4,5].

References

[24] Minnath M A; Unnikrishnan G; Purushothaman E. *Journal of Membrane Science*, 379 (2011) 361.
[25] Goerge S C; Thomas S. *Prog.Polym.Sci.*26 (2001) 985.
[26] Fried J R. Text book of polymer science and technology. USA: Prentice-Hall(2000)
[27] Lu S J; Lee D T; Chen J Y; Chiu C H; Hu C C; Jean Y C; Lai J Y. *Journal of Membrane Science*, 325 (2008) 831.
[28] Maciel A V; Machado J C; Duarte Pasa V M. *Fuel*, 113 (2013) 679.

MACRO 457

Autonomic Healing of Polymers with Embedded Microcapsules

Rajasekaran Divya, Maji PK*

Department of Polymer and Process Engineering,, Indian Institute of Technology Roorkee, Saharanpur campus,, Saharanpur-247001(UP)
** e-mail id: div.feyo@gmail.com*

Abstract

Recent rise in technology has increased polymer usage in many important areas like structures, medical, space, automobile, defence etc. Proper and effective usage of these technological development gets accomplished only if the materials are 100% reliable, which do not undergo any damages in the upcoming years. A small wear induced tear or damage in these materials with continuous usage might have a huge toll. Therefore there is a huge need for durable materials which can withstand normal wear and tear. Any material manufactured may undergo minor damage over time or by accident. It is very difficult to track those minor imperfections and to fix them. These damages if left untracked might cause a small crack which will grow enormously. By the time the defect is detected and sealed off it might be too late. So many repair mechanisms are proposed in past like hot plate welding for fractured surface and resin injection for laminate composites [1]. These techniques are not found to be efficient in case of high engineering applications that require error free materials. Therefore it will be very ideal if the crack is sealed as and when it happens. The only way to achieve this is to generate a smart self-healing materials that glues itself back to original form if damaged.

Self-healing materials are in discussion for more than a decade but still they are yet to be 100% globally commercialized. The two most commonly preferred way of producing microencapsulated materials are either from raw sources or from prepolymer synthesis. S.R.White and Brown [2] developed a microencapsulation process based on insitu polymerisation which is adapted by many researchers and Yuan et al[3] synthesized self-healing polymers from prepolymer. Both the routes have insitu polymerization as primary reaction. The self-healing polymers produced by microencapsulation is actually a shell and core type material which have a reactive chemical as core and thermosetting polymers as shell because of better crosslinking ability. This concept of autonomic healing with microencapsulation shows healing ability by a basic logic which is illustrated in Fig.1. The microcapsule synthesized by shell and core concept is embedded into the matrix. The core is a reactive material commonly called as healing agent and curative is also embedded into the matrix in the form of wax proptected catalyst. In common applications, when a stress induced crack happens on surface, it propogrates throughout the material and eventually end up in failure.

In case of healing agent embedded matrix, when crack propogates it hits the surface of capsules and break them into pieces which will release the healing agent stored, thus they flow in crack plane and react with catalyst and gets polymerized on the crack region. Once they are polymerized the damage on the surface is overlayed with healed polymer and self healing occurs with human intervension[4].

Introduction:

Self-healing polymers are under discussion in scientific field for more than a decade while S.R White[1] is able to give a standard procedure with urea formaldehyde in 2001 which is followed worldwide. The healing ability can be achieved by various routes[2]. Microencapsulation was able to gain attention in recent years because they can act as a reservoir for healing agents until they are needed in action. Various materials are recommended for microencapsulation in recent years while work with melamine formaldehyde as shell material is limited[3]. Microencapsulation achieved by insitu polymerization have become most commonly used method[4] whereas microencapsulation by preparation of prepolymer is few in numbers[5]. Microcapsules containing healing agents have been used to prepare composites or coating systems which will result in self-healing material when a stress concentrated crack occurs on the surface of the material. The microcapsules act as a storage tank which encloses healing agents and protects it from external factors. For a well stabilized microcapsules which can withstand the healing agent without undergoing any damages are to be prepared for a better healing system which can always be counted on. For achieving it, number of parameters are to be monitored and controlled to achieve a uniform surfaced microcapsule which can hold healing agent.

In this paper we investigate the stabilization of microencapsulation of dicyclopentadiene with melamine formaldehyde process carried out by preparing two different mediums simultaneously followed by mixing chamber. The parameters that are responsible for betterment of microcapsules are also discussed with SEM images.

Materials:

Melamine, Formaldehyde, Sodium carbonate, Sodium Dodecyl benzene sulfonate (SDBS), octanol, Dicyclopentadiene (DCPD) are purchased from Himedia Laboratories are used without further purification.

Experimental part:

37 wt. % of formaldehyde was added to 20ml of distilled water after mixing the pH of the solution was changed to 8.5. Melamine was added to the obtained solution (mixture A), heated until prepolymer solution is obtained. The mole ratio of melamine to formaldehyde is taken as 1:3.5. On the other hand, 2 g of sodium dodecyl benzene sulfonate was added to 100ml of distilled water (mixture B) simultaneously. Both the mixtures are sent to a mixing unit where they were continuously agitated at 500 -600 rpm. 0.2g of resorcinol was added followed by 45ml of DCPD. The reaction mixture is allowed to stabilize for 30mins. After stabilization the agitator was started at the same rpm. In order to avoid air bubbles 1 drop of octanol was added. 20ml of PVA was added to form emulsion. The pH is adjusted to 4 by addition of Hcl. The temperature of the medium was increased to 65-75c and rpm was raised higher. After 3-4hrs microcapsules containing DCPD with melamine formaldehyde as shell was obtained. The obtained capsules are washed and filtered.

Characterization:

The molecular structure and respective functional groups are analysed using FTIR Spectrometer (Perkin Elmer, spectrum two). Sample (microcapsules) was prepared by crushing the microcapsules prepared along with potassium bromide. FTIR of melamine, formaldehyde and

DCPD were also taken for confirmation of peaks. The surface morphology of microcapsules were analysed by Fourier transform scanning electron microscopy (FESEM - TESCAN).

Discussion:

For synthesis of melamine formaldehyde microcapsules, the mole ratio of melamine to formaldehyde is taken into consideration because if stoichiometry is not maintained properly the reaction becomes unsteady. Analysing the molecular structure of melamine formaldehyde from reaction scheme incorporated in Fig.1. melamine contain three primary amine groups which have capability to react with formaldehyde and form trimethylolmelamine or hexamethylol melamine depending upon mole ratio.

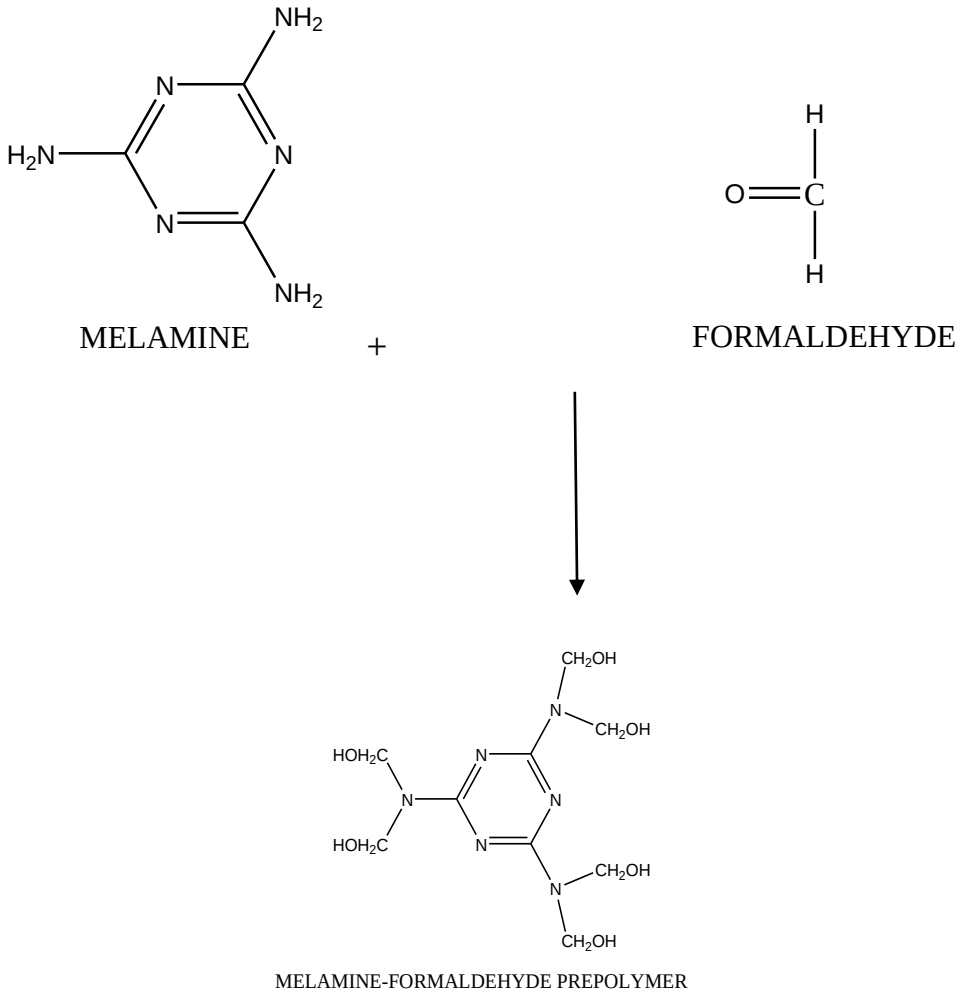


Fig:1 Melamine formaldehyde prepolymer scheme

One melamine react with three formaldehyde and result in melamine formaldehyde prepolymer. In this study the mole ratio of melamine to formaldehyde is 1:3.5, formaldehyde is taken 0.5 mole excess therefor maximum of methylol melamine species formed are trimethylol melamine which have good solubility in water hence a clear transparent prepolymer solution is obtained.

During preparation of prepolymer solution, 37wt % formaldehyde is added to water as first step and pH is changed. Melamine have very poor water solubility at room temperature, it is generally calculated as 0.12g melamine dissolve in 100g of water So for standardizing the microencapsulation procedure formaldehyde is first dissolved in water and later melamine is added to the solution. When melamine is added to the solution containing 37wt % formaldehyde in water and heated it leads to production of mixture of water soluble methylol melamines and prepolymer obtained was cooled later. Due to introduction of mixing unit in the scheme where both solution A and solution B are added at simultaneously with lower agitation rate, the dispersion of the mediums have increased and homogeneity of the system increases which results as an added advantage for better stabilization

Influence of pH on microcapsules:

In the process of preparing prepolymer solution, the solution formed is low in molecular weight. As the molecular weight increases it gets deposited at the interface becoming highly crosslinked structure and enables formation of microcapsules. During built up of three dimensional network, an insoluble resin no longer thermoformable is obtained. The hardening condition is achieved by lowering the ph of the medium. The ph is lowered to 4 by adding of hydrochloric acid. This acidic condition influence the condensation to restart and hardening of melamine formaldehyde resin occurs at lower pH. pH above 4 does not give necessary acidic nature and crosslinking is not efficient. Hence ph of reaction medium is maintained at 4 and is observed to be a stable level where microcapsules are more regular and easily separable. Below the ph of 3 the capsules starts losing its stability.

Influence of stirring rate on microcapsules:

Emulsion was produced by increasing the stirring rate slowly at regular interval of time. When reactions are carried out at varying stirring speed the microcapsules produced are observed to have lower average outer diameter which is included inTable.1. The reaction is generally carried out in a low shear mixture where rpm is increased after formation of emulsion and is maintained at the same level until the reaction gets over. As and when the rpm gets increased, the core material gets efficiently and uniformly dispersed into the mixture. Homogeneity of the medium is observed to be higher. With increasing rpm the molecules are segregated into individual particles and oil in water emulsion is stable and particles of lower diameter are observed in sem analysis. The plot inFig.2. depicts that with an increase in agitation rate the size of microcapsule decreases which also coincides with the concept of microcapsule formation[6].

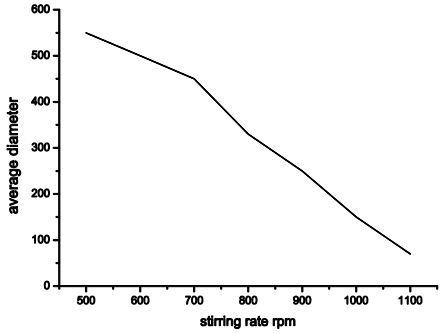


Fig:2 Diameter vs Stirring Rate

Table:1 Stirring rate and size of capsules

Sample no	Stirring rate	Average size
1	500-600	550
2	600-800	330
3	800-1000	150
4	900-1100	70

FTIR-SPECTRUM

The FTIR spectrum of DCPD and microcapsules synthesized are shown in Fig.3.

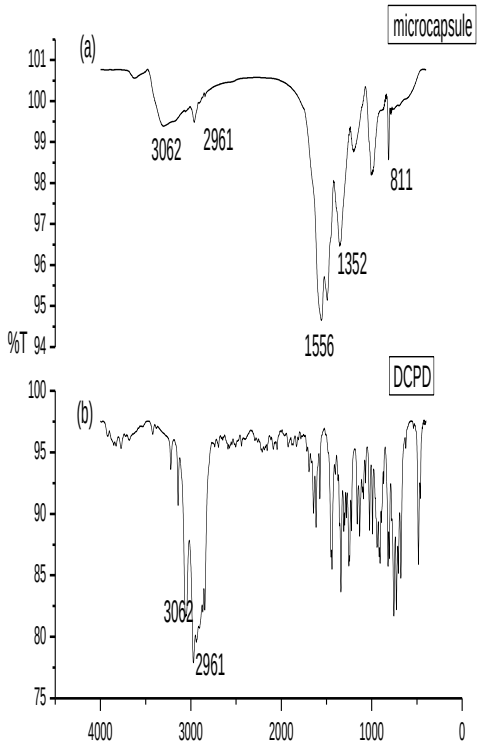


Fig:3 (a) melamine formaldehyde with dcpd core (b) dcpd

C=C stretching vibration peak at about 3062cm-1 and C-H stretching vibration peak at about 2961cm-1 are revealed in the spectrum of DCPD. N-H stretching vibration peak at 1556cm-1, 1352 cm-1 denotes the bending vibration of N-H, 811cm-1 peak signifies the triazine ring are melamine formaldehyde characteristics peaks along with characteristic peak of DCPD reveal the formation of melamine formaldehyde microcapsule with DCPD infilled.

FESEM

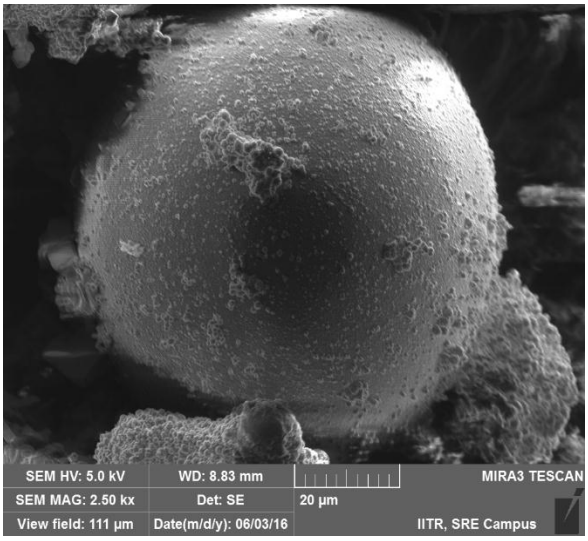

SEM HV: 5.0 kV
WD: 8.83 mm
MIRA3 TESCAN
SEM MAG: 2.50 kx
Det: SE
20 µm
View field: 111 µm
Date(m/d/y): 06/03/16
IITR, SRE Campus

Fig:4(a)


SEM HV: 5.0 kV
WD: 10.27 mm
MIRA3 TESCAN
SEM MAG: 560 x
Det: SE
100 µm
View field: 494 µm
Date(m/d/y): 07/06/16
IITR, SRE Campus

Fig:4(b)

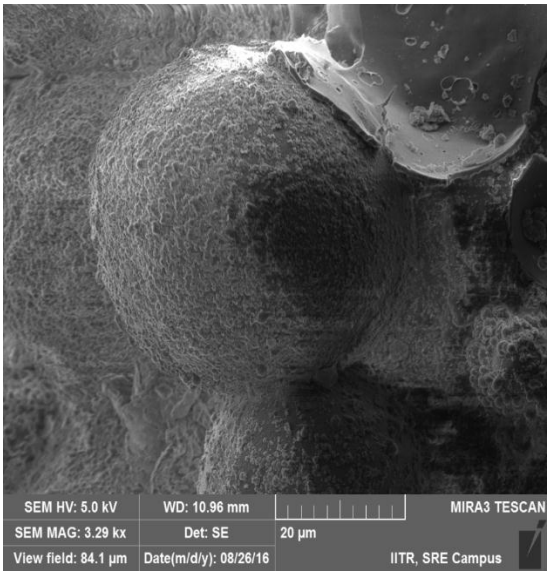


Fig:4©

The images of surface morphologies of melamine formaldehyde microencapsulated dicyclopentadiene prepared under agitation rate of 1100 rpm reveals a uniform outer surface, the capsules prepared will have smooth inner wall and rough exterior wall.Fig.4(a) shows irregular outer surface whileFig.4(c) shows a uniform regular spherical structure which is due to controlled pH, temperature, stirring rate and stabilized process.The Fig.4(b) is an image of a broken microcapsule from which it can be clearly seen that they have rough exterior wall with finer inner wall. The roughness of the surface can be modified by increasing the quantity of formaldehyde content[7] in the reaction medium

Conclusion:

The microcapsules with dicylopentadiene as core and melamine formaldehyde as shell material is prepared by altering various factors and routes inorder to achieve a uniform size and shape. Two solutions simultaneously prepared are dispersed with better homogeneity by mixing unit. By controlling the agitation rate, pH, incorporating a mixing unit the surface morphology and size distributions are said to be under control with improved uniformity. The microencapsulation of melamine formaldehyde with dicylopentadiene is successful which can be incorporated into polymer matrix composites for evaluating self-healing efficiency in future.

REFERENCES:

1. S. R. White, N. R. Sottos, P. H. Geubelle, J. S. Moore, M. R. Kessler, S. R. Sriram, E. N.Brown, S.Viswanathan: Autonomic healing of polymer composites, Nature 409, 794–797 (2001).

2. E.N.Brown,M.R.Kesslers,N.R Sottos,S.R White:In situ poly(urea-formaldehyde) microencapsulation of Dicyclopentadiene,J.Microencapsulation, vol 20, 719-730 (2003).
3. L.Yuan, G.Z. Liang, J. Q. Xie, S.B. He: Synthesis and characterization of microencapsulated dicyclopentadiene with melamine–formaldehyde resins,Colloid Polymer Science, 285,781–791 (2007)
4. S. Then, G.S. Neon, N. H. A .Kasim: Optimization of Microencapsulation Process for Self-Healing Polymeric Material, Sains Malaysiana, 40, 795–802 (2011)
5. B. Ali, U. ebenik, M. Krajnc: Microencapsulation of butyl stearate with melamineformaldehyde resin: Effect of decreasing the pH value on the composition and thermal stability of microcapsules, eXPRESS Polymer Letters, 6, 826–836(2012)
6. J. D. Rule, N. R. Sottos, S. R. White: Effect of microcapsule size on the performance of self-healing polymers, Polymer 48, 3520-3529 (2007)
7. B.Aissa, D.Therriault, E.Haddad, W.Jamroz:self healing materials systems: overview of major approaches and recent developed technologies, Advances in material science and engineering (2012)

MACRO 461

Rheological and Thermal Studies of Poly Lactic acid/Hydroxyapatite Composites

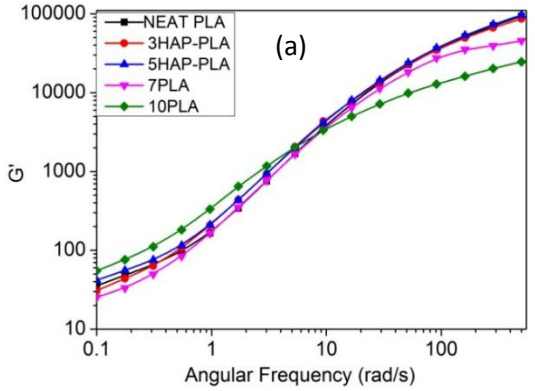
Prasad Arbind[a], Roy Kakoli[b], Katiyar Vimal[c]*, Ravi Sankar M[a]

[a]*Department of Mechanical Engineering, IIT Guwahati, Assam,India-781039*
[b]*Department of Mechanical Engineering, RSET, Guwahati Assam,India-781035*
[c]*Department of Chemical Engineering, IIT Guwahati, Assam,India-781039*

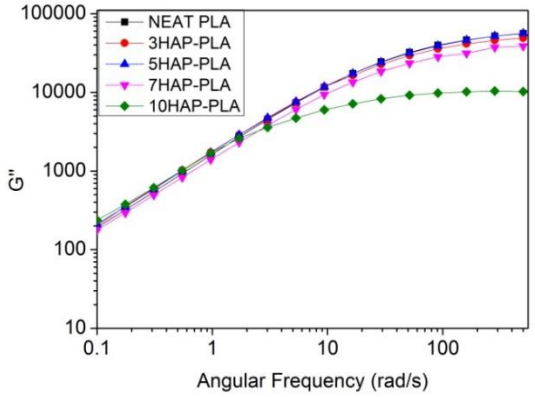
Corresponding author's Email: vkatiyar@iitg.ernet.in

In this work, fabrication of biodegradable Polylactic acid/Hydroxyapatite (PLA/HAp) composite has been done to target the wide application as bio implant for bone fracture fixation. Mostly the internal fixation devices which frequently used for fracture fixations are Pin, Screw, Plates, Staples and Rods. The manufacturing procedure to produce these implant devices are generally extrusion method, where materials gets extruded through injection moulding under certain environment and temperature. In this paper**,** rheological studies of various combination of PLA and HAp has been processed in order to know the optimum value of concentration of filler where molecular structure could not get distorted. PLA was

obtained from Nature Works LLC (Minnetonka, MN, USA). The selected grade (Ingeo 2003D, Mn = 88,500 g/ mol and Mw / Mn= 1.8) is recommended for extrusion. The polymer has a density of 1.24g/cm^3, while it is MFI is 6 g/10 min at 210°C at 2.16 kg load. HAp, an excellent bioactive biomaterial was fabricated from biowastes (fish scales). The PLA/HAp composite is fabricated through melt blending technique in twin screw extruder at 190°C. The recycle time was selected 1 min at 100 rpm. Rheological measurements of the blends were carried out on an Anton Paar Modular compact rheometer MCR 102 (figure 2).



(b)



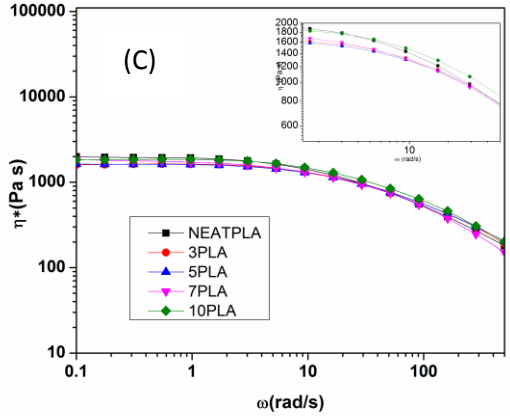


Figure 1.(a) Variation of storage modulus versus angular frequency for the PLA/HAp composites (b) Variation of loss modulus versus angular frequency for the PLA/HAp composites (C) Variation of complex viscosity versus angular frequency for the PLA/HAp composites.

Frequency sweep for the PLA/HAp samples was carried out using 50 mm parallel plate geometry. The gap maintained between the parallel plates was 0.55-0.7 mm for all the test. The test samples were about 1mm in thickness. A strain sweep test was initially conducted to determine the linear viscoelastic region of the materials. The strain amplitude was fixed at 5% to obtain reasonable signal intensities and to avoid the nonlinear response. The angular frequency range used during testing was 0.1-500 rad/s. Incorporation of HAp (3% to 9%wt) was attributed by significant improvements in the storage modulus (*G'*) of PLA/HAp blend due to intercalation at higher temperature (figure 1(a-c)[2]. The thermal studies were also conducted on thermo-gravimetric analysis from 30 to 700 ºC at the rate of 10ºC per min. The morphological properties of the composite were explored via optical microscope. From the thermal analysis (figure 3), it revealed that well dispersed HAp at the nanoscale level increased cold crystallization temperature and the addition of HAp enhanced the thermal stability of composite [3].The optical surface images is shown in figure 4 corresponding to Neat PLA and PLA/HAp composites.

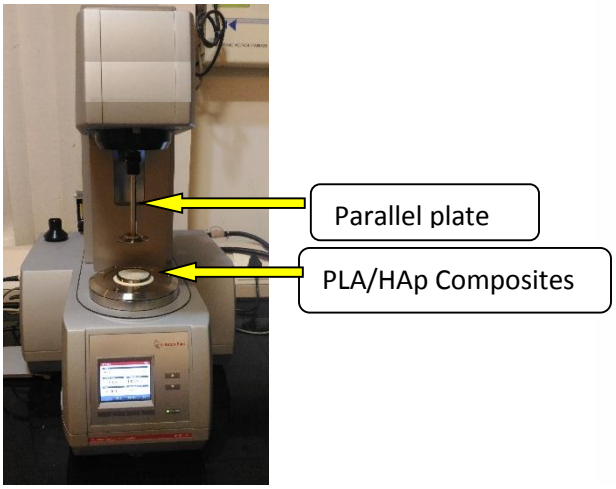


Figure 2.Experimental set up of Rheometer composites

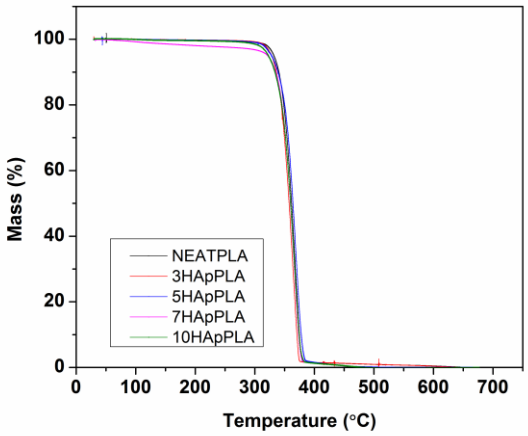
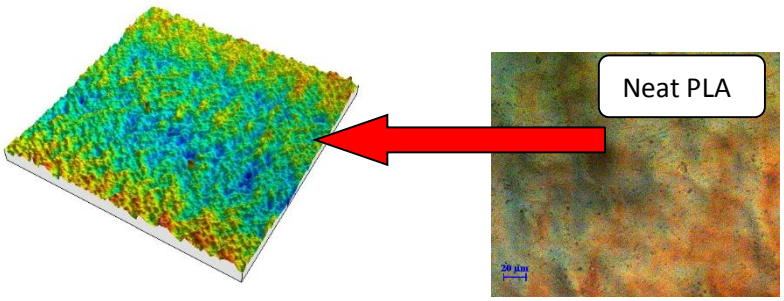


Figure 3. Thermogravimetric profile of PLA/HAp



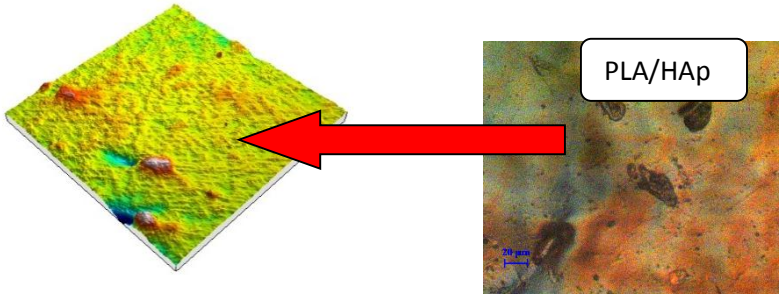


Figure 4.Optical micrograph (2D and 3D) of Neat PLA and PLA/HAp composites.

References

[1]Ahmed, J., Varshney, S. K., & Auras, R. Rheological and thermal properties of polylactide/silicate nanocomposites films. Journal of food science, 75(2), (2010), N17-N24.
[2]Gu, S. Y., Zou, C. Y., Zhou, K., & Ren, J. Structure-rheology responses of polylactide/calcium carbonate composites. Journal of applied polymer science, 114(3), (2009), 1648-1655.
[3]Chen, R. Y., Zou, W., Zhang, H. C., Zhang, G. Z., Yang, Z. T., Jin, G., & Qu, J. P. Thermal behavior, dynamic mechanical properties and rheological properties of poly (butylene succinate) composites filled with nanometer calcium carbonate. Polymer Testing, 42(2015), 160-167.

MACRO 462

Effect of Process Parameters and Cure Catalysis on the HTPB-IPDI Based Solid Propellant Behavior

CH Devi Vara Prasad*, SrinivasBabu N [a], P Kanaka Raju[b], Ranganathan V[c], K N Ninan[d]
*Scientist, Solid Propellant Plant, Satish Dhawan Space Center, Sriharikota, India
[a]Manager, Solid Propellant Plant, Satish Dhawan Space Center, Sriharikota, India
[b]DGM, Solid Propellant Plant, Satish Dhawan Space Center, Sriharikota, India
[c]Deputy Director, Solid Propellant Plant, Satish Dhawan Space Center, Sriharikota, India
[d]Former Emeritus Professor, IIST, Trivandrum, ISRO.
*Corresponding author e-mail ID : chdvprasad83@gmail.com

1. Abstract

Conventionally Toluene diisocyanate (TDI) and Isophorone diisocyanate (IPDI) are used as curatives for HTPB to form crosslinked urethane networks. Urethane formation is a fairly rapid reaction with TDI. Since this limits the useful pot life of the propellant, lesser reactive IPDI is more suitable in propellant formulations where a high pot life of the propellant paste is needed for processing big size grains. Lesser reactive IPDI is more suitable in propellant formulations where a high pot life of the propellant paste is needed for processing big size grains. The aliphatic nature of IPDI makes it slow reactive, thus yielding a longer pot-life and penetrometric pot life which are the favorable factors for processing large boosters [1-3]. IPDI is also less toxic and hence used by many manufacturers. One disadvantage is that its longer cure time. In this paper, a detailed study was made on the HTPB-IPDI propellant behaviour and also a comparative study was made with HTB-TDI propellant system to understand the viscous and mechanical behaviour of the propellant system by its process parameters and cure catalysis system for HTPB-IPDI system.

2. Keywords
IPDI propellant, cure catalyst, FeAA, TDI, cure time, final ix time, viscosity build-up, mechanical properties.

3. Introduction:

Extension of pot life for HTPB based propellant binder systems was attempted through employing a bi-curative system comprising of TDI and IPDI at various compositions [4]. Various parameters such as HTPB-IPDI stoichiometry, process temperature, pot-life, zero flow time, cure cycle, failure boundary and ageing characteristics were studied [5-8]. The activation energy for the cure reaction is found to be 27.1 kcal/mole for HTPB-IPDI system in comparison to 12.4 kcal/mole for HTPB-TDI system[9]. The ballistics are comparable for both HTPB-TDI and HTPB-IPDI propellants, however the pressure index is found to be lower for HTPB-IPDI propellant. The mechanical properties and failure envelope showing the margin of safety and the ageing characteristics of HTPB-IPDI propellant show an edge over HTPB-TDI system [10-11]. In the present investigation, the viscosity build-up after mixing, propellant slurry viscosity vs. final mix time was studied. Since sufficient pot life is available for IPDI based propellant slurry, it is possible to extend the mixing time to get the lower viscosity. Therefore the studies were carried out on the final mix time. Prolonged mixing of IPDI propellant slurry shows a thixotropic phenomenon since the viscosity decreases with final with time.

4. Materials:

HTPB resin used in the present study was produced at PFC, VSSC through H_2O_2 initiated free radical polymerization of butadiene in a mixed solvent system comprised of propan-2-ol and water. Hydroxyl content of HTPB was determined through acetylation method (34.8 mg KOH/g). TDI and IPDI were procured from M/s. A.G.Bayers and were used as such without further purification after ascertaining their purity. Estimation of NCO content in the isocyanate compound was undertaken by reacting the isocyanate with a known excess of n-butyl amine and back titrating the un-reacted amine. Assay of TDI and IPDI were found to be more than 99.0%. For all compositions, [NCO]/[OH] equivalent ratio (r value) was maintained at 0.95. The slurry was degassed under vacuum, poured into aluminum moulds and cured at 60°C for pre-specified period. The thickness of the cured slabs was maintained at 5 mm. The comparison of physical and chemical properties of IPDI and TDI used in the propellant system were tabulated in table.1.

Table.1 Physical and chemical properties of IPDI & TDI

	IPDI	TDI
Purity (%)	99.5	99.5
NCO Content %	37.5	48
Boiling Point,^{0}C	150	120
Viscosity, cps, 30^{0}C	10	3
Molecular weight, g/gmol	222	174
Refractive index ,30^{0}C	1.567	1.483
Specific gravity, 30^{0}C	1.218	1.059

5. Experimental Results and discussion

5.1 Viscosity build-up profile for TDI & IPDI propellant slurry: The hydroxyl functional groups of HTPB undergo stoichiometric urethane reaction with a variety of isocyanates to form the polyurethane network which imparts good mechanical properties to the propellant. HTPB-IPDI propellant system has got greater process ability and flexibility to meet any contingency especially during casting of large sized segments of propellant. IPDI has low volatility and hence low toxicity in comparison to TDI. Its boiling point is 150^{0}C against 120°C for TDI, both at 10 mm of Hg. pressure. This ensures higher human safety and less plant operational hazards during manufacture of the propellant. One disadvantage of HTPB-IPDI propellant system is that its longer cure time. The process temperature for TDI based propellant and IPDI based propellant was maintained at 40^{0}C and 60^{0}C respectively. IPDI is a slow reacting curative, hence it

can be processed at higher temperatures, however the usual process temperature is restricted to 60^0C because of hazards involved. The batch size was 4 kg and the final mix time was 40 minutes. All the propellant experimentations were done using standard HTPB formulation containing 86 % solid loading with 18% Al**.** Ammonium perchlorate prepared in house with a bimodal distribution was used as oxidizer. The results of an experiment are shown in the table 2.

Table. 2 Effect of curative on the viscosity build-up of propellant slurry

Time (hours)	Viscosity build-up (poise)	
	TDI (measured at 40^0C)	IPDI (measured at 60^0C)
0	8960	5120
1	9280	5760
2	10560	6080
3	12320	6620
4	14220	7120
5	16000	8400
6	-----	8900
7	----	9300
8	-----	10200

The rate of viscosity build-up was found to be lower for IPDI propellant slurry, despite a higher process temperature. IPDI cured HTPB based composite propellant system has considerably longer pot life because of relatively slower cure kinetics. The viscosity of the propellant slurry was measured at the respective process temperature.

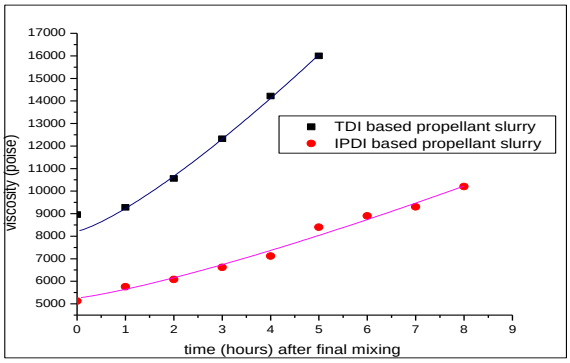


Fig.1 The viscosity build-up profile for propellant slurries using IPDI and TDI as curatives

The increase in viscosity for both the slurries, followed a power function with time, and in the form

$$\eta = m + n * t^{o}$$

where m, n and o are the empirical constants which depends upon the type of curative and 't' is the pot life in hours. From the equation, the pot life of the propellant slurry can be computed. The time to reach a viscosity of 15000 poise i.e. pot life, has been computed. From the eq., pot life of TDI propellant is 4.4 hours, whereas for IPDI propellant it is 13.8 hours.

3.1 **Influence of process parameters on mechanical properties of IPDI propellant:**

(i) Effect of mixing time on the mechanical properties of the propellant

Since TDI propellant slurry has a lower pot life, sufficient pot life is available for IPDI based propellant slurry, it is possible to extend the mixing time to get the lower viscosity. Therefore the studies were carried out on the final mix time. A 4 kg capacity horizontal sigma blade mixer was used for the experiments. Prolonged mixing shows thixotropic behavior. EOM viscosity is found to reduce with mixing time. Hence the final mix time varied from 20 to 120 minutes to study the viscous behaviour and mechanical properties. **A RVD II** model Brookfield viscometer was used to measure the viscosity of the propellant slurry during the cure reaction. From fig.1, EOM viscosity is found to reduce with mixing time. The viscosity, time data are fitted into a logarithmic function in the form $\eta = h_1 - h_2 * \ln (h_3 + t)$ where h_1, h_2, h_3 are empirical constants and "t" is the final mix time in minutes (fig.2). From the curve, the values of empirical constants are: h_1=21797; h_2=3856.6; h_3= -8.062. The optimum mechanical properties such as tensile strength, elongation and modulus are achieved by tuning the [NCO]/[OH] equivalent ratios and the optimum level of [NCO]/[OH] ratio for HTPB-IPDI propellant was found to be in the range of 0.95 to 0.98 for the HTPB hydroxyl content of 34.8 mg KOH/g. It is observed that the cure reaction was found to be slower for IPDI. IPDI propellant slurry shows a thixotropic phenomenon since the viscosity decreases with final with time and reaches a plateau at its optimum mixing time. Stress-strain data and the mechanical properties for the propellant slabs were evaluated with an Instron Universal Testing Machine (Model 4469) using dumbbell shaped specimens as per the ASTM-D412 test method. Tensile tests were performed at a cross-head speed of 50 mm/min. Initial modulus (Young's Modulus) was calculated from the slope of the initial linear portion of the stress-strain curves. At a final mix time of 20-40 minutes, higher viscosity rendered the propellant porous. The optimized time for IPDI propellant processing is around 80-100 minutes. From table 3, there is no systematic trend in mechanical properties with reference to mix time. The final mixing time is mostly decided by the viscosity and plant convenience.

Fig.2 Influence of final mix time on the viscosity of the HTPB- IPDI based propellant slurry.

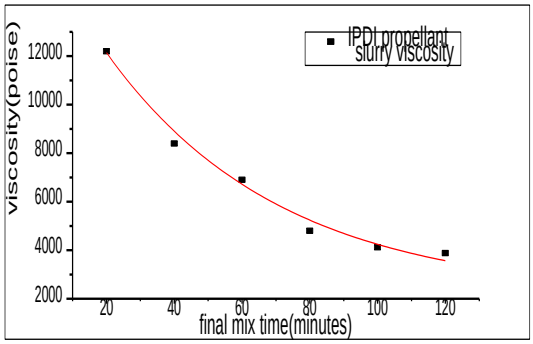


Table 3: Influence of final mix time on propellant mechanical properties

Propellant Property	Final mix time (minutes)					
	20	40	60	80	100	120
TS (kg/cm^2)	10.7	9.4	10.3	10.2	10	9.3
% E	37	38	34	39	43	40
Mod (kg/cm^2)	71	63	75	67	64	67
EOM viscosity(ps) X 1000	12.2	8.4	6.9	4.8	4.12	3.8

(ii) Influence of cure time on HTPB-IPDI propellant:

It is observed that the cure reaction was found to be slower for IPDI in comparison to TDI. The activation energy for cure reaction is found to be higher for HTPB-IPDI propellant and hence enhanced cure cycle is required for getting optimum mechanical properties. The cured propellant properties were leveled off only after 12 days whereas for HTPB-TDI propellant system it was only 4-5 days at 60^0C. The tensile

Toughness (kgf-cm/cm^3)	2.94	2.94	2.728	3.140	3.305	2.92

properties of the polyurethane elastomer are determined in the form of dog-bone test specimens under predetermined conditions. The cured samples are tested for their mechanical properties (tensile strength, elongation on break) at room temperature and with a cross-head speed of 50 mm/min using a conventional uniaxial testing system. The results are shown in table 4. Hence the cure cycle was optimized to 12 days @ 60^0C.

Table 4: Influence of cure time on mechanical properties of IPDI propellant.

Cure time	Tensile strength (kg/cm^2)	% elongation	Modulus (kg/cm^2)
8	5.1	70	14
12	8.1	55	32
16	7.9	52	35

(iii) Effect of sequence of addition on mechanical properties of IPDI and TDI based propellant:

Since coarse & fine ammonium perchlorate and aluminium are the major ingredients in propellant composition, studies were done to investigate the effect of the sequence of addition of these major ingredients on the rheological and mechanical behavior of the propellant. For all the addition sequences, first the weighed mass of HTPB and other minor ingredients were added into the mixer and mixed thoroughly for 10 minutes and thereafter the major solid ingredients were added in various following sequences of addition namely: (a) If the solids were added in the sequence of coarse AP in two lots followed by fine AP in two lots and then aluminium with an interval of 10 minutes after each addition is represented as 2C+2F+A. (b) If the solids were added in the sequence that half of the coarse AP followed by fine AP and then the remaining coarse AP and fine AP followed by aluminum in two lots with an interval of 10 minutes after each addition is represented as C+F+C+F+2A . From the table, the sequence 2C+2F+A has given higher fracture energy compared to other sequence of addition. Hence, the better sequence of addition could be opted from the fracture energy data. The results are tabulated in table 5.

Table 5: Effect of sequence of addition on mechanical properties for TDI and IPDI propellants.

Property	2C+2F+A for TDI propellant	2C+2F+A for IPDI propellant		C+F+C+F+2A for TDI propellant	C+F+C+F+2A for IPDI propellant
TS (kg/cm^2)	8.1(8.1)	7.9 (7.8-7.9)		8.3(8.0-8.5)	7.3 (7.2-7.3)
% elongation	51(51-52)	52(51-53)		46(44-48)	56(55-57)
Modulus (kg/cm^2)	37(36-37)	35 (34-36)		43(41-45)	26(25-26)

The Sequence 2C+2F+A is better than the sequence C+F+C+F+2A, in terms of mechanical properties. Hence the sequence 2C+2F+A

Cure time in days	**TS (kg/cm^2)**	**% elong**	**Modulus (kg/cm^2)**	**Shore A hardness**
3.5	6.8(6.8-6.9)	52(49-54)	37(36-38)	59-61
4.5	7.2(7.2-7.3)	49(46-49)	41(40-43)	61-63
5.5	7.6(7.5-7.7)	47(47)	44(43-44)	64-70
6.5	8.0(7.9-8.2)	50(49-51)	43(42-43)	60-64
7.5	8.1(8.0-8.3)	49(48-50)	44(43-44)	65-68
9	8.2(8.1-8.3)	48(47-49)	44(43-44)	66-68

Toughness kgf-cm/cm^3	2.931	3.058		2.778	2.928	10	8.4(8.3-8.4)	47(46-48)	46(46-47)	66-67
						12	8.3(8.2-8.4)	45(44-46)	51(50-51)	64-66
						14	8.5(8.5)	45(48)	55(55)	63-67

was employed for other experiments. The strain capability, toughness of IPDI propellant is marginally higher compared to TDI propellant.

5.2 **Influence of cure catalyst on mechanical properties of HTPB-IPDI propellant:**

IPDI cured HTPB based composite propellant system has considerably longer pot life because of relatively slower cure kinetics and also it takes longer time for curing. But when extra large size grains are the requirement for modern launch vehicle systems, an extended pot life becomes imperative with regards to achieving defect free propellant grains. The reaction between IPDI and HTPB, in the absence of a catalyst is extremely sluggish even at elevated temperatures. Hence, an attempt was made to add a cure catalyst which can enhance the cure kinetics. In the non-catalyzed IPDI system, propellant curing was done at 60°C for 12 to 15 days. FeAA (Ferric acetyl acetonate) was added as a cure catalyst for IPDI based propellant system to reduce the cure time. The rate constant of an un-catalyzed reaction is smaller than those obtained when a catalyst is employed. The propellant mixing was carried out in a 4 kg level mixer and the final mix time was 80 minutes. The propellant was cured at 60^{0}C. The mechanical properties were studied with cure time. It was evident from the Fig.3 that the required properties were achieved in shorter duration in comparison to the non-catalyzed system. The results are shown in table. The FE observed was lower for the catalyzed system (1.58 J/cm^2) when compared to the non-catalyzed system (1.72 J/cm^2).

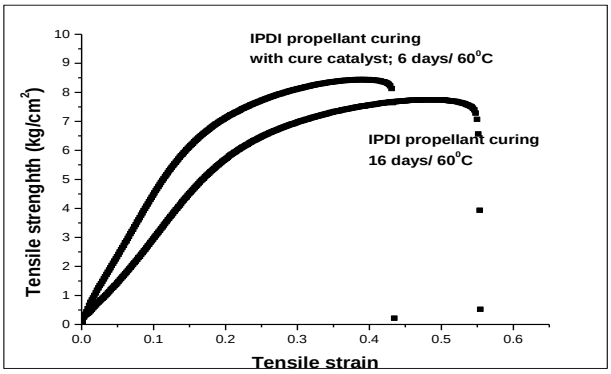


Fig.3 The stress-strain behaviour of non-catalyzed and catalysed HTPB-IPDI propellant

However, to reduce the time duration of propellant curing, the cure catalyst concentration is the deciding factor for slow-reacting curatives used for propellant processing. Initially a catalyst concentration of 0.5% w.r.t. binder was used. Then the paste was gelled during mixing. Then the concentration of catalyst was reduced to 0.05% w.r.t binder.

Table 6: Effect of cure time on the mechanical properties of FeAA catalysed IPDI propellant.

The concentration of catalyst could be optimized from the fracture toughness data and also by the pot life of the propellant slurry. From table 6, tensile strength increases with cure time and stabilizes at 8.4 kg/cm^2. Modulus also increases with cure time and stabilizes at 51 kg/cm^2. The elongation showed naturally a reverse trend, decreasing with cure time and stabilizes at 46 %. The properties of the catalyzed propellant were stabilized around 5-6 days of curing at 60^{0}C as against 12-16 days needed for the un-catalyzed propellant. Here the pot life of the slurry was only three hours when the catalyst concentration was 0.05% w.r.t. binder; therefore, it needs still lower concentrations of cure catalyst for the process able pot life for the casting of propellant slurry. Since the cure time is very slow, a cure catalyst can be used which can enhance the rate of curing. The reaction between IPDI and HTPB, in the absence of a catalyst is extremely sluggish even at elevated temperatures.

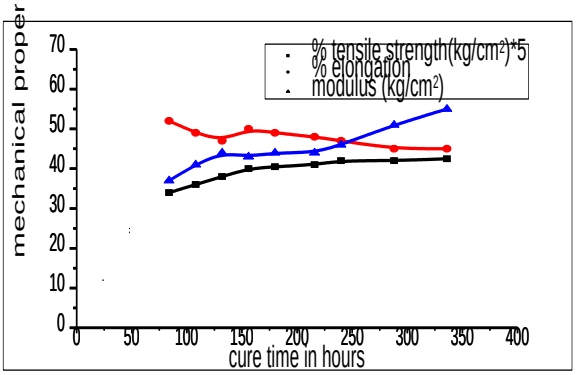


Fig.4 Effect of cure time on the mechanical properties of the propellant

6. Conclusion:

The alicyclic nature with combinations of primary-secondary isocyanate groups make IPDI slow reactive yielding longer pot-life and amenability for large scale processing. Introduction of IPDI slowed down the cure process, but at the same time, has not adversely affected the mechanical characteristics. In the absence of a catalyst, such as FeAA, the reaction between HTPB and IPDI is extremely sluggish resulting in tardy viscosity buildup during the propellant curing. The most immediate solution that can be the use of less reactive curatives, such as isophorone-di-isocyanate (IPDI) with cure catalyst like FeAA.

7. Acknowledgements

The authors would like to thank Director, SDSC/SHAR and also the propellant manufacturing/characterization team for their kind support in providing the data to publish this article.

8. References

[1]. Boyars, C.; Klager. K. (Eds). Propellants, manufacturing hazards and testing. American Chemical Society. Washington D.C., Publication No. 88, 1969. 88p.

[2]. Davenas A. Development of modern solid propellants. Journal of Propulsion and Power. (2003); Vol.19(6), pp.1108-1128.

[3]. The kinetics of the reaction of Isophorone di-isocyanate with mono-alcohols, Polymer (1985), Vol 26, pp. 301-306.

[4]. S.N. Jawalkar. Mchilal, R. Kurva, P.P. Singh, and R. Bhattacharya, "Influence of Bicurative on Processibility of Composite Propellant", Defence Science Journal, Vol. 57, No. 5, September 2007, pp. 669-675

[5]. HTPB-IPDI based solid propellants: Binder - liner interface characteristics., V.Sekkar, S.B.M. Guruvayurappan, C. Sreekumaran Nair and G.G. Bandhyopadhyay, HEMCE-2009, Pune, Dec. 7-9, 2009.

[6]. Serkan Burak Haska, Erdal Bayramli, Fikret Pekel,Saim Ozkar,. Mechanical Properties of HTPB–IPDI-Based Elastomers, J Appl Polym Sci **64: pp.** 2347–2354, 1997.

[7]. Development And Characterisation Of A New Generation High Pot-Life HTPB Propellant, T.L.Varghese, N. Prabhakaran**, Report No: PCM/PSCG/PED/TR-013/98.**

[8]. Studies on Interface Properties of HTPB-IPDI Based Case Bonded Composite Propellant and a Compatible Catalyzed Liner System, Ratheesh, R, Muraleekrishnan, Tushar S Bhatt, CPR Nair, KN Ninan.

[9]. D. Kincal and S. Ozkar, 'Kinetic Study of the Reaction Between Hydroxyl Terminated Polybutadiene and Isophorone Diisocyanate in Bulk by Quantitative FTIR Spectroscopy' J. Appl. Poly. Sci., 66 (1997) 1979-1983.

[10]. Performance evaluation of new generation IPDI cured HTPB propellant gem motors **Rm. Muthiah, ZE, Krishnan, T L. Varghese** , **A.J.** Raghavan & S. **Someswara** Rao, Internal report No: **PCM/PSCG/PED/TR-02/98.**

[11]. 'Pot Life Extension of PS-0, PS-I and PS-3 HTPB Propellant using IPDI', Report No. PCM/PSCG/PED/TR-13/96.

MACRO 468

Catalytic Action of CTAB/ KBr/ C_9OH Micellar Media on the Basic Hydrolysis of Crystal Violet

Karayil, Jasila [a] and Sreejith, Lisa [a]*

[a] *Soft Materials Laboratory, Department of Chemistry, NIT Calicut, Kerala, India,*

*[a] *Department of Chemistry, NIT Calicut, Kerala, India*

[a]*email i.d: jessekarayil@gmail.com*

Abstract

The kinetics of basic hydrolysis of crystal violet (CV) in CTAB/KBr/C_9OH micellar media was investigated under pseudo first order conditions. The reaction was monitored spectrophotometrically by measuring the decrease in absorbance of CV at 590 nm. It was observed that the pseudo first order rate constant increases with increase in C_0. The enhancement of reaction rate with C_0 is explained on the basis of dependence of reaction rate on micellar morphology. Further, the viscosity and DLS analysis supports nonanol induced morphological transitions. Fluoroscence spectroscopy has been used to understand dye-micelles interactions. The enhancement of fluorescence intensity of CV with C_0, suggests an increase in dye-micelles interaction with C_0. The concentration of surfactant and salt had a marked effect on reaction rate. The inhibition of reaction rate at high concentration of surfactant and salt is due to the ionic competition of OH^- and Br^-ions for the reaction center. The influence of [OH^-] on CV hydrolysis was also investigated. The results show that the pseudo first order rate constant, k', increases linearly with hydroxide ion concentration, indicating first-order dependence on [OH^-].

Keywords*:* Crystal violet, CTAB, nonanol, miceller morphology.

.

References

[29] Yesim, Talman; S, Gokturk; M, Tuncay *Colloids Surf*., A. 270 (2005) 77.
[30] I, Molinero; M, Sierr; M, Valiente; E, Rodenas *J .Chem. Soc., Faraday Trans*. 92 (1996) 59.
[31] M, Valiente; E, Rodenas, *Langmuir*. 6 (1990) 775.
[32] Sierra,M. L; Rodenas, *E J. Phys. Chem.,* 97 (1993) 12392.

MACRO 473

New Physical Insights into Shear History Dependent Polymorphism in Poly(vinylidene fluoride)

Amanuel Gebrekrstos,† Maya Sharma,‡ Giridhar Madras,† and Suryasarathi Bose,§*

†Department of Chemical Engineering, ‡Centre for Nanoscience and Engineering, §Department of Materials Engineering, Indian Institute of Science, Bangalore-560012, India

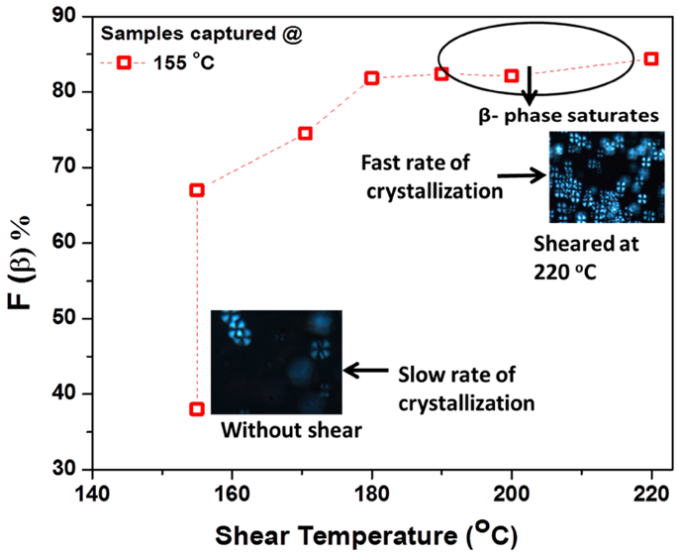
Abstract

Poly(vinylidene fluoride) (PVDF) is a semicrystalline polymer that exists in four crystalline phases (α, β, γ, δ). Among these, the β-phase has received tremendous techno-commercial importance due to its higher dipole moment as compared to the other phases, and thus many strategies have been explored in the recent past to obtain the β-polymorph of PVDF. In this study, the effect of shear history on crystalline morphology and behavior of PVDF has been investigated systematically by polarized optical microscopy coupled to a hot stage, Fourier transform infrared spectroscopy, differential thermal analysis, rheometry, and dielectric relaxation spectroscopy. Thin films of PVDF (120−150 μm) were sheared at different temperatures ranging from 155 to 220 °C and were allowed to isothermally crystallize at 155 °C. When the samples were isothermally crystallized at 155 °C, a remarkable increase in β-phase content was observed. More interestingly, this phenomenon was observed to be shear history dependent. For

instance, the samples which were sheared at high temperature (220 °C) reflected in higher β fraction as compared to samples which were sheared at lower temperature (155 °C). It is envisaged that the distance between T_{shear} (temperature at which the samples were sheared) and T_{cry} (crystallization temperature) significantly influences the

content of the β-phase in PVDF. This study clearly demonstrates the fact that both shear history and the depth from Tc influence the conformational changes in PVDF.

Keywords: Shear temperature; β-phase; Crystallinity; Morphology; Polarizing optical microscope.



Reference

[1] Zhang, C.; Wang, B.; Yang, J.; Ding, D.; Yan, X.; Zheng, G.; Dai, K.; Liu, C.; Guo, Z., Synergies among the self-assembled β-nucleating agent and the sheared isotactic polypropylene matrix. Polymer 2015, 60, 40-49.

[2] Pantani, R.; Coccorullo, I.; Volpe, V.; Titomanlio, G., Shear-Induced Nucleation and Growth in Isotactic Polypropylene. Macromolecules 2010, 43, 9030-9038.

[3] Huo, H.; Jiang, S.; An, L.; Feng, J., Influence of shear on crystallization behavior of the β phase in isotactic polypropylene with β-nucleating agent. Macromolecules 2004, 37, 2478-2483.

[4] Somani, R. H.; Hsiao, B. S.; Nogales, A.; Srinivas, S.; Tsou, A. H.; Sics, I.; Balta-Calleja, F. J.; Ezquerra, T. A., Structure development during shear flow-induced crystallization of i-PP: in-situ small-angle X-ray scattering study. Macromolecules 2000, 33, 9385-9394.

[5] Zhang, R.-C.; Xu, Y.; Lu, A.; Cheng, K.; Huang, Y.; Li, Z.-M., Shear-induced crystallization of poly(phenylene sulfide). Polymer 2008, 49, 2604-2613.Moro, T.; Takatori, Y.; Ishihara, K.; Konno, T.; Takigawa, Y.; Matsushita, T.; Chung, U.-i.; Nakamura, K.; Kawaguchi, H., *Nat. Mater.*(2004) 3.

MACRO 474

Translocation of polymer through nanopore under end pulling force

Bappa Ghosh,[a] Srabanti Chaudhury [a]*

[a] *Department of Chemistry, Indian Institute of Science Education and Research, Pune, Maharashtra-411008, India*

* *e-mail id: srabanti@iiserpune.ac.in*

Abstract

In this work, we study the translocation of a polymer pulled with a constant pulling force at one end through a narrow pore using extensive Langevin dynamics simulations. The drag or pulling force is strong enough so that the polymer does not get enough time to equilibrate. We study the time evolution of the translocation coordinate, the average translocation time, the monomer waiting time distribution as a function of the pulling force, and the movement of the drag force front with different magnitude of pulling force on the polymer.

Keywords: *polymer translocation, end pulling, tension propagation theory*

Introduction

Translocation of polymers through nanopores is of fundamental importance in many biological processes such as protein transport through membrane channels,[1] virus injection and so on. Translocation has applications in gene therapy, [2]drug delivery[3] and also in sequencing of DNA and RNA. Polymer translocation has been studied in details through experiments, theoretical models as well as computer simulations. In 1996, Kasianowicz *et. al* [4] demonstrated that the presence of an electric field could drive a single stranded DNA/ RNA through an alpha- haemolysin channel across a lipid bilayer membrane. It has been shown that the translocation time depends on the polynucleotide sequence of DNA/RNA threading through the channel. Theoretical and simulation studies have provided different scaling exponents of the translocation time as a function of polymer length, the amplitude of the driving force, nature of the driving force, pore width, etc. Polymer translocation has been studied extensively both in the presence and absence of external bias. From the theoretical point of view Sung and Park[5] and Muthukumar[6] modeled polymer translocation as a one-dimensional diffusion problem across a free energy barrier. 2D Monte Carlo simulations performed by Chuang et al[7] found out different scaling behaviors of the mean translocation times with respect to the chain length and the strength of the driving forces. Many other simulation studies, for example 3D MD simulations by Dubbledam *et. al*[8] suggested that translocation process is a case of anomalous diffusion. Different theoretical models have been proposed such as the fractional Fokker Planck method by Metzler and Klafter[9] and later by Dubbeldam[8] to study such anomalous nature of translocation dynamics and find agreement with simulation studies in both 2D and 3D.[10-11] All these studies confirmed that unlike unbiased translocation where the polymer can equilibrate given sufficient time and in certain limits, driven translocation is a non-equilibrium process due to the long relaxation time of polymer chains.[12-13] Over the last few years, Sakaue has developed a theory of forced translocation based on the concept of tension propagation (TP).[14-15] According to this TP theory, a tension force acts along the backbone of the polymer chain. This theory was given in the asymptotic limit for long chains and did not account for the finite chain polymers where polymer-pore interaction has significant contribution in altering the translocation dynamics. Ikonen *et. al* has generalized the tension propagation model by incorporating the finite chain length and polymer-pore interaction as an additional friction term in the tension propagation theory.[16] The TP model of pore driven polymer translocation was in good agreement with the molecular dynamic simulations.[17] Thus the Brownian dynamic tension propagation (BDTP) model was successful in presenting a coarse-grained minimal model of driven polymer translocation.

In this paper we study the translocation of a polymer pulled with a constant force at one end through the pore[18] from some equilibrium configuration using extensive Langevin dynamics simulations. Unlike previous studies, where every monomer within the pore experiences a force, in this study the force is exerted only on the first monomer bead as shown in Scheme 1. The drag or pulling force is

strong enough so that the polymer does not have enough time to equilibrate. This non-equilibrium pulling causes straightening of the polymer chain. We study the scaling of the translocation time, the monomer waiting time distribution as a function of the pulling force, and the movement of the drag force front as a function of time with pulling force acting on the first monomer bead of the polymer.

Model and Method

The polymer chain is modeled as Lennard Jones (LJ) particles interconnected by Finitely Extensible Nonlinear Elastic (FENE) springs. The beads experience excluded volume interaction, which is given by short range LJ potential –

$$U_{LJ}(r_{ij}) = 4\,\epsilon\left[\left(\frac{\sigma}{r_{ij}}\right)^{12} - \left(\frac{\sigma}{r_{ij}}\right)^{6}\right] \qquad (1)$$

where r_{ij} the distance between consecutive monomers, σ is the diameter of the monomer and ε is the depth of the LJ potential.

The expression of the FENE springs potential is given by -

$$U_{FENE}(r_{ij}) = -\frac{kR_0^2}{2}\,ln\left(1 - \frac{{r_{ij}}^2}{R_0^2}\right) \qquad (2)$$

k is the FENE spring constant and R_0 is the maximum allowed separation between consecutive monomers. In our simulations, $\sigma = 1$, $\varepsilon = 1$ and $k_BT = 1.2$. For the FENE potential, $R_0 = 1.5\sigma$, $k = 30$. For the purpose of simulations, a wall of LJ particles was created in yz-plane with a pore on the middle. The pore was created by removing the middle bead of the wall. The wall coordinates were frozen during the simulations and they interact with the polymer chain only via the LJ force. Each monomer is described by the Langevin equation of motion, which includes the conservational, frictional, and random forces, F_i^C, F_i^F and F_i^R respectively.

$$m\ddot{r}_i = F_i^C + F_i^F + F_i^R \qquad (3)$$

$$F_i^F = -\eta v_i$$

$$F_i^C = F_{LJ} + F_{FENE} + F_{Pulling}$$

where m is the mass of the monomer, η is the friction coefficient, v_i is the monomer velocity, and $F_{Pulling} = F\hat{x}$ with F being the strength of the force applied on the first monomer bead. The random force F_R satisfies the fluctuation-dissipation theorem. In order to get the initial uncorrelated configurations, the first bead is positional restrained at the pore. The chain was then allowed to relax to obtain the equilibrium configuration. To confirm the completion of equilibration, radius of gyration (R_g) was plotted with time until the average value becomes constant. The positional restrain on the first bead is removed at the pore and the whole chain is allowed to evolve according to Eq. 3 until the chain escapes to the trans side of the pore with pulling force acting on the first monomer bead. This corresponds to a successful translocation event. We average over roughly 1000 such successful translocation events. Here we have used Langevin dynamics (LD) to study the dynamics

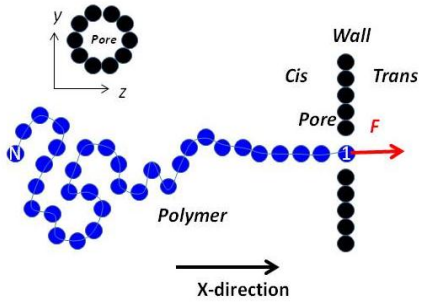
of polymer translocation using GROMACS simulation package with time step δt=0.005 ps at room temperature of 295 K.

Results and discussion

To begin with, we study the waiting time distribution as a function of individual monomers. Figure 1 shows the waiting time distribution $W(s)$ versus s for a polymer of length N= 50 with end pulling force F= 30. Here s refers to the translocation coordinate that corresponds to the number of monomers on the trans side of the pore. $W(s)$ is defined as the time that the each monomer spends inside the pore. The distribution is non- monotonic in nature and reveals two distinct physical translocation regimes: the initial increase in the waiting times describe the tension propagation stage and the final stage of decreasing waiting times corresponding to the tail retraction stage. The total area under this curve gives us the average translocation time. In Figure 2 we show the distribution of the translocation time for a polymer chain with 50 monomer beads (N=50) and two different magnitude of the pulling force (F= 30 and F= 10). In the low force regime F=10, the distribution is wide. With the increase in the end pulling force, the distribution becomes narrower. The MD data is averaged over 1000 successful translocation events. As the force is applied on the first monomer, the tension propagates along the chain with time. Because of the applied force, the polymer does not get enough time to equilibrate. As a result, the front end of the polymer becomes straightened. Hence, at a particular instant of time, the polymer is divided into two regions, one is straight and moving part and another is static and coiled. The junction of these two parts is called tension front. In Figure 1, the maxima of the waiting time distribution indicates the end of tension propagation, which means that at this time, the tension has propagated till the last bead of the polymer chain. Beyond this region, retraction occurs. In order to find out how the tension front propagates along the chain as a function of time, we obtain the velocity profile of the whole chain. Figure 3 shows the normalized velocity profile of the whole chain by running MD simulation at F= 30 for N= 50. The velocity is averaged over 1000 successful translocation events and a very small time window δt =2 ps. In Fig 3a the monomer velocity is plotted as a function of the number of monomers. The velocity curves at different time t collapse on to a single curve if the number of monomers is scaled by the monomer bead number where the tension front is located, i.e the monomer number where the average velocity goes to zero. In Figure 3b we plot the normalized velocity as a function of the perpendicular distance from the wall. The x- axis is normalized by the location of the tension front from the wall. Both the velocity profiles in Figure 3 have three distinct regions. Region I is the constant force regime, the region II shows a decrease in the velocity and finally region III where the velocity is zero. The onset of Region III denotes the location of the tension front. At the beginning of the translocation process, the polymer starts to move to the right side in the direction of the pulling force. After some time (4-10 ps), the polymer retracts towards the cis side. This is manifested by the negative velocity in Fig 3 in the 4-10 ps time scale. Finally as time progresses, the polymer translocates to the trans side of the pore.

Figures

Scheme1:



Scheme 1: Schematic representation of a polymer translocating through a nanopore with a pulling force *F* acting on the first monomer bead

Figure 1

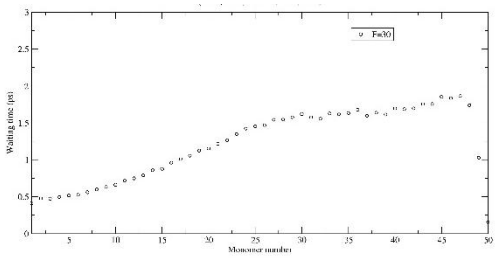


Figure 1: Waiting time distribution as function of the chain length at N=50 and end pulling force of strength F= 30. Other parameters are k_BT=1.2, η=0.7

Figure 2

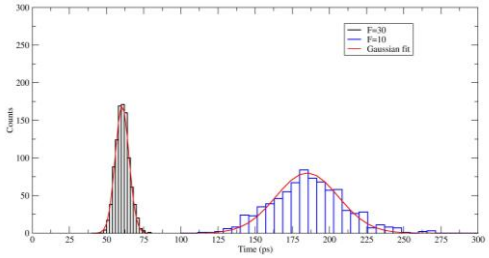
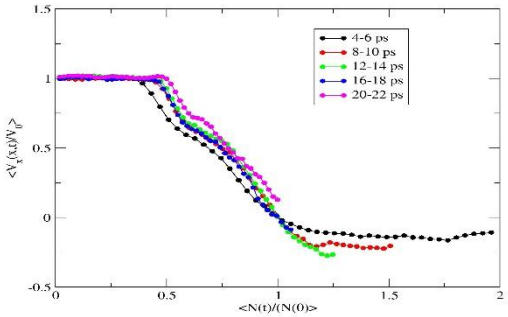


Figure 2: Translocation time distribution for a chain of length N=50 and end pulling force of strength F= 30 (black) and F=10(blue).Red lines are the Gaussian fits to the distributions. Other parameters are k_BT=1.2, η=0.7

Figure 3

(a)



(b)

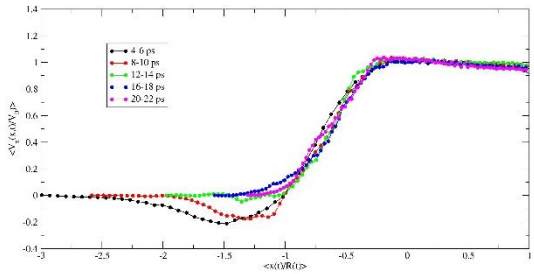


Figure 3: Normalized velocity for chain length N= 50 and F= 30 as function of (a) monomer number (b) perpendicular distance from the wall.

Conclusions

In this work, we employ Langevin dynamics simulations to examine the effect of a polymer chain pulled by a strong force applied on the first monomer bead. We study the effect of the end pulling force for a chain of length *N* and different pulling force. The waiting time distribution is non-monotonic, and its maximum occurs when the tension front has propagated till the last monomer bead. The translocation time distribution is narrower and more sharply peaked for higher value of end pulling forces. With increase in force, the mean translocation time increases. Finally we study the propagation of the tension front with time. Combining our simulation results with theoretical studies based on the Brownian dynamics tension propagation model is a future subject of study.

Acknowledgements

The authors acknowledge IISER Pune for funding. The authors thank Tapio Ala- Nissila and Jalal Sarabadani for discussions and valuable suggestions.

References

1. Driselkelmann, B., *Microbiol. Rev.* **1994**, *58*, 293.
2. Hanss, B.; Leal-Pinto, E.; Bruggeman, L. A.; Copland, T. D.; Klotman, P. E., *Proc. Natl. Acad. Sci. USA* **1998**, *95*, 1921.
3. Tseng, Y.; Liu, J.; Hong, K., *Molecular Pharm.* **2002**, *62*, 864.
4. Kasianowicz, J. J.; E., B.; Branton, D.; Deamer, D. P. N. A. S., USA 1996, 93, 13770, *Proc. Natl. Acad. Sci, USA* **1996**, *93*, 13770.
5. Sung, W.; Park, P. J., *Phys. Rev. Lett.* **1996**, *77*, 783.
6. Muthukumar, M. J., *J. Chem. Phys.* **1999**, *11*, 10371.

7. Chuang, J.; Kantor, Y.; Kardar, M., *Phys. Rev. E* **2001**, *65*, 011802.
8. Dubbeldam, J. L. A.; Milchev, A.Rostiashvili, V. G.; A., V. T., *Europhys. Lett.* **2007**, *79*, 18002.
9. Metzler, R.; Kafter, J., *Biophys. J.* **2003**, *85*, 2776.
10. Panja, D.; Barkema, G. T.; Ball, R. C., *J. Phys.: Condens. Matter* **2007**, *19*, 432202.
11. Vocks, H.; Panja, D.; Barkema, G. T.; Ball, R. C., *J. Phys. Condens. Matter* **2008**, *20*, 095224.
12. Bhattacharya, A.; Binder, K., *Phys. Rev. E* **2010**, *81*, 041804.
13. Luo, K.; Ala-Nissila, T.; Ying, S. C.; Metzler, R., *Europhys. Lett.* **2009**, *88*, 68006.
14. Sakaue, T., *Phys. Rev. E* **2007**, *76*, 021803.
15. Sakaue, T., *Phys. Rev. E* **2010**, *81*, 041808.
16. Ikonen, T.; Bhattacharya, A.; Ala-Nissila, T.; Sung, W., *J. Chem. Phys.* **2012**, *137*, 085101.
17. Ikonen, T.; Bhattacharya, A.; Ala-Nissila, T.; Sung, W., *Phys. Rev. E* **2012**, *85*, 051803.
18. Huopaniemi, I.; Luo, K.; Ala-Nissila, T.; Ying, S. C., *Phys. Reb .E* **2007**, *75*, 061912.

MACRO 497

ROLE OF SIZE OF FILLERS ON THE DEVELOPMENT OF AN ELECTRICALLY CONDUCTIVE RTV SILICONE SINGLE PART ADHESIVE FOR SPACE APPLICATIONS

Prasanta Kumar Behera, R. Pravin, Indulekha K and R. S. Rajeev
Email: pk_behera@vssc.gov.in
Polymers and Special Chemicals Division
Propellant, Polymers and Chemicals Entity
Vikram Sarabhai Space Centre
Thiruvananthapuram-695 022

Abstract

As microelectronic assemblies get more complex, there is an increased need for flexibility of design. Traditional systems are based upon attaching electronic components, e.g. capacitors, resistors, etc., to complete circuits, primarily by a solder based process (molten Sn/Pb alloy). Furthermore, the application of solder has become increasingly difficult in electronics due to the decreasing size and operational space of circuit boards. Due to component heat sensitivity, substrate flexibility, mismatched coefficients of thermal expansion and other design considerations, alternative approaches to attach component are needed. One approach gaining importance is use of an electrically conductive adhesive to "stick" the components onto a substrate, replacing the solder. Since the applications are envisaged to replace the metal with an adhesive of sufficient strength and conductivity. Properties are expected to remain relatively unchanged under environmental stress, e.g. thermal cycling and exposure to heat and humidity. Electrically conductive silicone adhesives possess good flexibility; low temperature Processability, easier assembly and environmentally benign nature promote its clear advantage over other systems.

In the present paper, an electrically conductive single part adhesive containing a mixture of metallic fillers dispersed in PDMS resin matrix is discussed. A room temperature vulcanizing single part silicone

adhesive is developed by embedding silver powder and aluminium powder in various proportions in PDMS system. Aluminium and silver powders of specific particle size in different ratios were

added to the system to study the role of filler combination on the electrical properties and arrived at the optimum ratio for the maximum electrical conductivity. Role of electrical conductivity on the particle size of the fillers were also studied. Cure chemistry of the system was modified suitably to make it single part room temperature curable adhesive giving lap shear strength of 12 to 18 ksc at RT on aluminium substrate. The outgassing property of the filled polymer was also found within the limit for space application. Thus we could successfully develop a space grade single part conducting adhesive for electronic packages in satellite components.

Keywords: electrically conductive adhesive, PDMS, silver powder, aluminium powder

1. INTRODUCTION

Electrically conductive adhesive consist of conductive particulate randomly dispersed in a polymeric adhesive matrix. Like solder, ECAs serve as electrical and mechanical linkages for component attachment. Also electrically conductive adhesive may be used for space applications and for bonding EMI gaskets and for providing EMI shielding and environmental protection.

Among the adhesive polymers for aerospace application, silicone stands out in view of its obvious advantages. Silicones are able to withstand the temperature extremes from -60°C to +200°C that are experienced in space and are able to maintain a good degree of flexibility at very low temperatures where other materials would stiffen and crack. Silicone adhesives possess good cohesive strength, moisture resistance, corrosion resistance, ageing resistance, ozone resistance and radiation resistance and can bond materials that have dissimilar coefficients of thermal expansion (CTE).

Silicone adhesives belong to two major types depending on whether they are formed at elevated temperatures or at room temperature. The mechanism of high temperature vulcanization is free radical in principle, based on the formation of the radical through decomposition of organic peroxides. Room temperature vulcanization (RTV) is based on hydrolysis of cross-linking components and further condensation with hydroxyl end groups of the siloxane polymer.

One-part moisture curable room temperature vulcanization silicones represent one of the largest volume and commercially most successful silicone technology. In one component vulcanization system, the reactive cross linker is mixed with the base resin into the dried rubber compound under anhydrous condition and the compound is filled into tubes or other closed containers. After extrusion from the tube, vulcanization takes place on exposure to atmospheric moisture. The problem of pot life and gelation does not take place as long as the adhesive is inside the tube.

This paper describes the methodology of processing a single component RTV silicone adhesive, the influence of fillers on their physical, thermal, mechanical and electrical conductivity properties.

2. EXPERIMENTAL

2.1 Materials

The polymer matrix used for the study is hydroxyl terminated polydimethylsiloxane (OH-PDMS) of viscosity 3000-7000 cps. Two different varieties of silver powder having average Particle size 1.6 µ (SP2) and 3.4 µ (SP1) and aluminium powder having average particle size 7.4 µ were used for the study. Cross

linking agent like methyl oximinosilane (MOS), adhesion promoter -aminopropyl triethoxy silane (APTES) and dibutyltindilaurate based catalyst were purchased from Sigma Aldrich and were used as such.

2.2 Process Methodology

The premix that contains PDMS resin and the fillers were processed in an automated mortar grinder followed by mixing in helicone mixer under vacuum and inert atmospheres at a motor speed of 1000 rpm. The processing of Single component RTV silicone adhesive was done in a helicone mixer (4 CV helicone mixer, DIT, USA), which provides efficient and thorough mixing with same degrees of mixing efficiency irrespective of the batch size within the mixing capacity range. The mixer contains twin opposing helical blade of conical helical configuration, which provides a constant blade to wall clearance with the bowl from top to bottom of the blade.

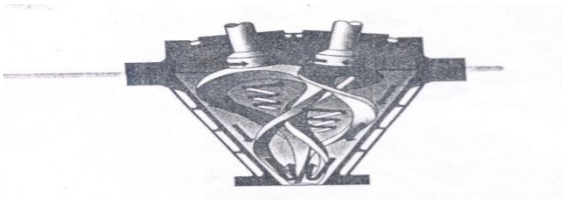


Figure 1: Schematic representation of helical blades of Helicone Mixer

A calculated quantity of the curing components were added into the mixer under inert atmosphere and the mixing continued under vacuum and inert atmosphere for a definite time. After mixing, the discharge valve was opened and the adhesive was pressurized through flexible polyurethane discharge tubes into the filling station where the adhesive was filled inside the squeeze tubes and sealed. The filling station temperature was maintained at 20±5ºC and relative humidity of 10± 5% by means of a desiccant type dehumidifier housed outside the building.

In these studies, two different grades of silver powder were used as conductive filler which are SP1and SP2 grades. The particle size of SP1 is bigger than SP2 and it is found that the grade SP1 imparts less volume resistivity compared to SP2. Also it is observed that with the grade SP2, the powder material has poor wetting in the polymer whereas the grade SP1 has good wetting and remains stable on the used substrate. Hence the grade SP1 is the filler selected for processing electrical conductive adhesive.

2.3 CHARACTERIZATION

Mechanical properties were evaluated using a computer-controlled Universal Testing Machine, Instron 4202, 10kg force transducer; 500mm/min cross-head speed according to ASTM D412. Dumbbell specimens were prepared as per ASTM D412. The lap shear strength of the specimen is determined as per ASTM D1002 (10mm/min-speed). Hardness measurement was done using shore A durometer, ASTM D 2240. Density was measured using D792. A minimum of four samples were evaluated for each mechanical property.

The investigation of thermal properties were performed by thermal conductivity [HOLOMETRIX Inc, Cambridge mass. USA Thermal Conductivity Tester(C-MATIC) at 100^0C as per ASTM C177-85(1993). The specific heat measurements were done using METTLER DSC 20, at a heating rate of 10°C/min at 100°C according to ASTM D 3947-86. TGA was done at a heating rate 50^o C per minutes under Nitrogen

using TA 3000 system in conjunction with TG50 thermo balance coupled with TC 10A TA processor. Viscosity was measured using a Brookfield synchro-electric HBT model.

3. RESULTS AND DISCUSSION

3.1 MECHANICAL PROPERTIES

TENSILE STRENGTH

Tensile strength of the samples prepared is measured using universal testing machine. The results are plotted against concentration of silver vs. tensile strength.

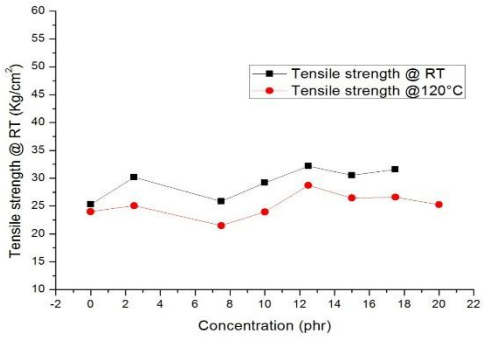


Fig 3.1: Effect of silver content on tensile strength of electrically conductive adhesive

From the above curve it is clear that as the increase in silver concentration increases the tensile strength slightly. This is same in the case for the test done at room temperature and at 120°C. This is because when filler loading increases the load applied to break the sample also increases. High tensile strength may be due to molecular entanglement resulting in superior intermolecular forces. From graph, it is clear that up to 12.50 phr, tensile strength is increasing drastically and a slight change after that.

ELONGATION

Elongation of filled PDMS systems with varying silver filler content is shown in figure 3.2..

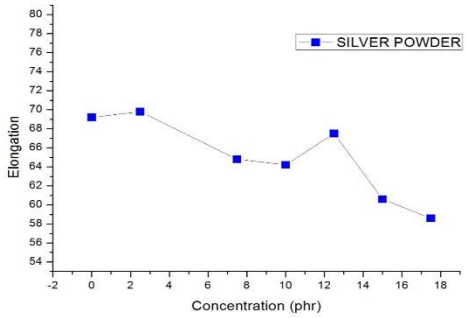


Fig 3.2 Effect of silver content on elongation at RT

From the graph it is clear that elongation decreases with filler concentration. This may be due to the reason that, as percentage of filler increases the crosslinking increases and uncoiling become difficult.

LAP SHEAR STRENGTH

Since the silicone electrically conductive adhesive has to provide mechanical connection between a component and substrate, adhesion strength is very important. Lap shear strength was used as a measure of adhesion strength.

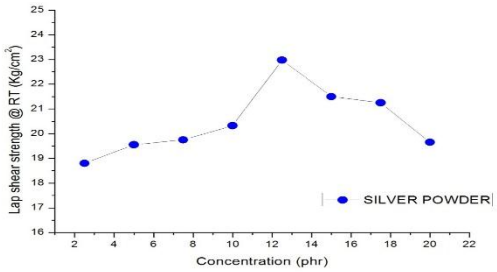


Fig. 3.3 Effect of silver content on Lap Shear Strength

From graph, lap shear strength is drastically increasing up to phr 12.50 phr and slightly decreases after that and it gives mixed adhesive and cohesive failure in all cases. Up to a 12.5 phr of silver loading, an adhesion property of ECA increases. After that, slight decrease in adhesion with increase in silver.

DENSITY

Density of filled PDMS systems with varying silver filler content is shown in figure 3.4

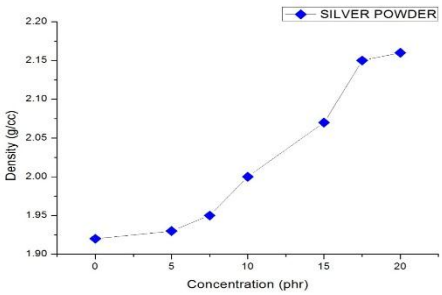


Fig. 3.4 Effect of silver content on Density

As filler loading increases the density increases as seen in Fig 3.4

3.2 THERMAL PROPERTIES

THERMAL CONDUCTIVITY

Thermal conductivity of the prepared samples are measured and the Fig 3.5 shows the effect of the silver concentration on thermal conductivity.

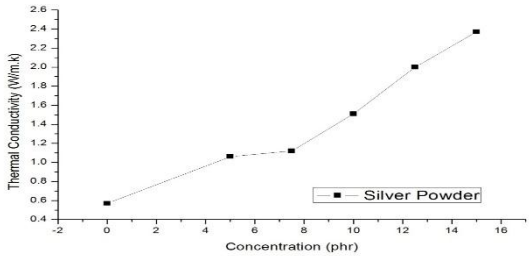


Fig. 3.5 Effect of silver content on Thermal conductivity

Figure 3.5 shows the dramatic increase in thermal conductivity with increased volume fraction of conductive fillers. Although it appears that the conductivity of the silver powder sample increases at a faster rate, however, it does show that the silver powder allows the heat to propagate through a continuous weave of strands, creating heat flow paths through the polymer, thus dramatically increasing the thermal conductivity of the adhesive**.** The filler particles conglomerate in a direction parallel to the heat flow allowing the heat to bypass the polymer**.**

SPECIFIC HEAT

Specific heat of filled PDMS with varying silver content is shown in figure 3.6. There is only a slight change in specific heat as silver content increases but the values are almost same in all cases. The filler content does not much affect the specific heat of the system.

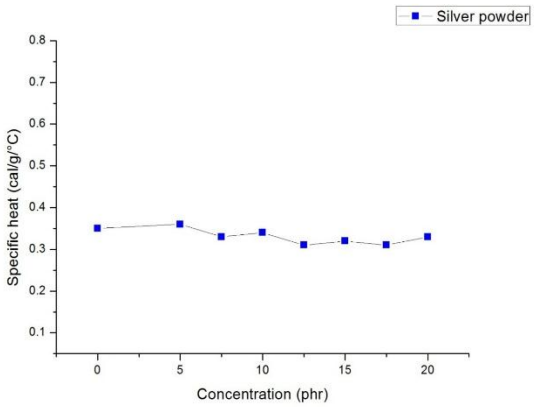


Fig.3.6 Effect of silver on specific heat

3.3 ELECTRICAL PROPERTIES

VOLUME RESISTIVITY

Volume resistivity of samples for a constant loading of aluminium with varying silver content in PDMS matrix resin is given in table 3.1

Silver content (Phr)	Aluminium content (Phr)	Volume resistivity (100V)

0	64.3	9.36x 10^{11}
2.5	64.3	3.75 x 10^{11}
5	64.3	2.58 x 10^{10}
7.5	64.3	1.22 x10^{10}
10	64.3	1.83 x10^{10}
12.5	64.3	< 10^{3}
15	64.3	< 10^{3}
17.5	64.3	< 10^{3}
20	64.3	< 10^{3}

Table 3.1. Effect of silver content on Volume resistivity

Volume resistivity of the prepared samples is noted. PDMS alone is an electrical insulator in a range of 10^{15}. When a percentage of aluminium powder is added to the matrix resistivity reduced to 9.36 x10^{11}. Silver is highly conductive filler so it is incorporated to the above compounds. Hence the volume resistivity gradually decreases. As silver content increases the volume resistivity decreases as shown in the table. As the percentage of silver increases above 12.5phr, the volume resistivity decreases drastically and the material is found as electrically conductive adhesive.

3.2 OUTGASSING PROPERTIES

Outgassing refers to the release of gas trapped within a solid Outgassing properties of prepared samples with varying silver content is illustrated in the table 3.2

Silver content (Phr)	Out gassing properties		
	TML (%)	**CVCM (%)**	**WVR (%)**
0	0.352	0.095	0.035
15	0.385	0.093	0.023
17.5	0.33	0.094	0.025

Table 3.2 Effect of silver content on outgassing properties

The outgassing properties are measured for neat PDMS system without silver and with silver content of 15 and 17.5 phr. The value of TML and CVCM of neat PDMS and filled systems does not vary much with increase in silver content.

4 Conclusion

Versatility of silicones offer the stress relief, excellent adhesion, and temperature stability that make silicones highly desirable in the electronics applications, they can be formulated in many ways to meet specific requirement. This is the case for the electrically conductive silicone adhesives, where a silicone adhesive is filled with a highly conductive filler to transform it from an insulator material to an electrically conductive product. These adhesives can be used in a wide variety of applications where electrical conductivity is needed. A silicone based room temperature vulcanizing electrically conductive single pat adhesive (ECA) was prepared. Several studies were carried out and the following conclusions were arrived:

For a given quantity of silver filler, higher particle size silver (Grade SP1) shows low volume resistivity compared to Lowe particle size silver filler (Grade SP2). The increase in the silver content increases the tensile strength of the adhesive both at ambient and high temperatures. The Elongation at break of the adhesive system decreases with increase in the silver content whereas the density increases with silver content. The lap shear strength of the adhesive increases with increase in silver content up to a particular concentration and then decreases on further silver loading. Specific heat does not show much change with silver content whereas a dramatic increase in thermal conductivity was found with increase in silver content. Volume resistivity of the adhesive decreases with increase in silver content and the outgassing properties does not change with filler content.

References

1. Paul F. Bruins, silicone Technology, Interscience Publishers (1970).
2. Walter Noll, chemistry and technology of silicones (1968)
3. E.J.Rochow, " An introduction to chemistry of silicones" , Chapman and Hall, ltd., London (1963)
4. http://www.tibtech.com/conductivity.php
5. Instant notes in Analytical Chemistry, David Kealey, P J Haines (2002)

MACRO 498

Effect of particle shape of BN in enhancing thermal conductivity of thermal interface materials

N.Neeraj*, K. Leena, R. Pravin, N. Supriya, R. Rajeev, K.G. Benny
Propellants Polymers Chemicals and Materials Entity, Vikram Sarabhai Space Centre
Thiruvananthapuram- 695022, India
** e-mail id: neerajnaithani@gmail.com*

Abstract

Miniaturization of electronic devices needs efficient thermal management for better and reliable performance. Thermal interface material (TIM), a silicone based material filled with thermally conductive but electrically insulating fillers like boron nitride, alumina and aluminium nitride are the better choice. Particle size and shape of fillers significantly influence the properties of filled polymeric materials. Thermal conductivity and mechanical properties of TIM with filler of different shape were investigated in this work. Significant improvement in the performance of TIM was observed with platelet shaped boron nitride. Thermal conductivity of 2.71 W/mK was obtained for the optimized composition of TIM with alumina and platelet shaped BN with good mechanical properties and thermal stability.

Keywords: *TIM, particle shape, platelet shaped BN, thermal conductivity*

Introduction

With the rapid growth of the electronics industry, heat dissipation become a critical problem for the electronic devices in terms of performance and reliability[1,2,3]. Heat produced during the operation of the device is generally dissipated by thermal conduction using heat sinks. Heat dissipation capacity of a heat sink decreases due to interfacial thermal resistance arising from the mismatch of surface roughness of both device and heat sink in the absence of a good thermal contact. In order to improve the performance of a heat sink, the remaining air gaps are filled with suitable thermal interface materials (TIMs), whose thermal conductivity must be greater than air. An ideal TIM must possess high thermal conductivity, low coefficient of thermal expansion (CTE) and low dielectric constant as well. Additionally, the material must be soft enough to be easily deformed by contact pressure to fill all the gaps between the mating surfaces[4]. Elastomeric thermal pads gain acceptance due to ease of handling and high compressibility. Elastomeric thermal pads are typically made of an elastomeric polymer, such as silicon rubber, and reinforced with thermally conductive but electrically insulating fillers, such as aluminum nitride (AlN), boron nitride (BN), silicon carbide (SiC), and alumina (Al_2O_3)[5]. Particle size and shape of fillers significantly influence the properties of filled polymeric materials[6,7]. In the present paper, effect of particle shape of the filler on the thermal properties of thermal interface material was studied.

Experimental

Material

Poly dimethyl siloxane from Anaobond, India was used as base resin, α-alumina, boron nitride (Polartherm PT110) and irregular shape boron nitride (HPLC 30535) were used as filler and oxyaminosilane based curator was used for curing.

Processing

Filler and resin in the required proportion were mixed using mortar and pestle. Mix was masticated in a three roll mill to ensure uniform dispersion. Finally curator was added and casted in the form of sheets and buttons.

Characterization

Fillers were characterized for the particle shape and size using Malvern Morphologi G3S, an optical image analysis based particle shape analyser. Since the fillers were free flowing, sample dispersion unit for dry dispersion was used. The analysis was done using standard operating procedure (SOP) which contains all the software and hardware variables. Circular equivalent diameter (CE diameter), circularity and intensity were measured for the particles.

Mechanical properties were evaluated using Instron 5569, universal testing machine.

Carl Zeiss field emission scanning electron microscope (FESEM) was used to observe the dispersion of the filler in the final composition.

Thermal conductivity of the samples were measured using HOTDISK TPS2500 thermal property analyzer. Thermal decomposition of the TIM was studied using TA instruments SDT Q 600 simultaneous thermogravimetric–differential scanning calorimetric analyser. About 10 ± 2 mg of sample was taken in an alumina crucible and loaded into the instrument. The TG analysis was carried out at 10°C/min from room temperature to 900°C in ultra-pure argon (99.99%) at a flow rate 100 ml/min.

The specific heat value of the system was determined using TA Instruments Q-20 Differential scanning calorimeter as per ASTM E 1269-11. A sample mass of 10±1 mg crimped in an aluminium sample pan was used for the analysis. Temperature program consisting of an initial isothermal segment at 30°C for 5 minutes, heating at 10°C/min up to 110°C, followed by a final isothermal segment for another 5 minutes was provided through the software. The same experimental conditions were given for blank and standard runs. The purge gas was ultra pure argon at the rate of 50 ml/min. Standard sapphire sample was used as the calibration standard.

Coefficient of thermal expansion was measured in TA Instruments Q-400 Thermo mechanical analyser. The 5x5x5 mm of the composite sample in contact with the TMA probe were heated from 30 to 150°C at 10°C/min under argon atmosphere at a purge rate of 100 ml/min.

Results and discussion

The objective of the study is to develop the thermal interface material with high thermal conductivity. At the same time the material should be soft enough to fill the gap due to surface roughness in electronic package and heat sink to provide better thermal management. The base material was chosen as PDMS since silicones are soft material and easily fill the gap on applying pressure, but the polymers are known to have poor heat conduction. It is because the heat conduction is through flow of phonon or through lattice vibrations[8] only. To increase thermal conductivity two possibilities are there, namely i) forming conductive networks through appropriate packing of fillers in the matrix and ii) decreasing the amount of thermally resistant junctions involving a polymer layer between adjacent filler units[8]. To form conductive networks, boron nitride, which is high conducting filler, was chosen.

The filler used in the study was characterized for its shape and size using Morphologi G3S particle shape analsyer. Irregular shape BN and platelet shaped BN were used in the preparation of TIM. The platelet shape of BN was ascertained by the particle shape analysis and electron microscopy. FESEM micrograph is given in Fig. 1. Fig.2(a). shows the images obtained from Morphologi G3S, 2(b) shows the circularity and 2(c) shows the intensity distribution of two types of BN used in the study. Volume weighted average particle size (D[4,3]) for both platelet shaped BN and irregular shape BN is 47µm, but CE diameter are 11 µm and 4 µm respectively.

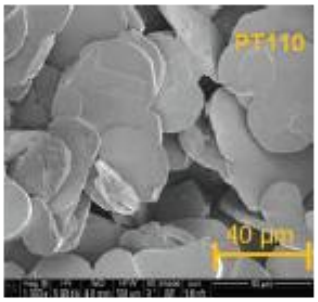


Figure 1. FESEM micrograph of platelet shape BN

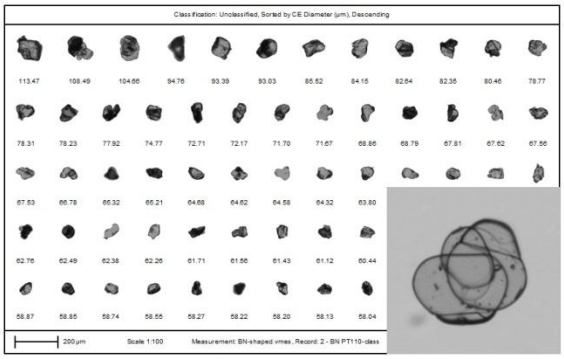


Figure 2(a) Particle shape of platelet BN using Morphologi G3S

The difference in the shape is ascertained by the CE diameter and circularity distribution curve, which clearly shows that both the particles are of different shape. Intensity mean distribution established that the particle in PT110 are flake type thin particles. FESEM micrograph confirms the platelet shape of the PT110 particles.

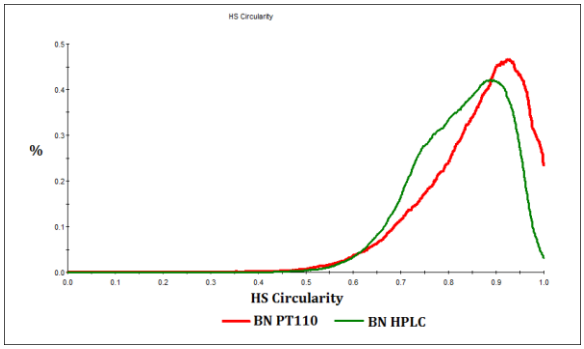


Figure 2(b) Circularity distribution of irregular shaped and platelet shaped boron nitride

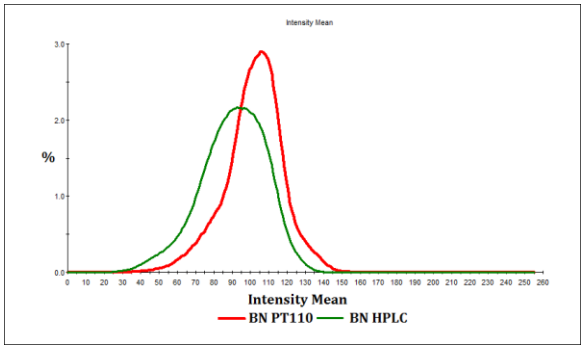


Figure 2(c) Intensity distribution of irregular shaped and platelet shaped boron nitride

Formulation at different phr (part per hundred of rubber) BN were made and thermal conductivity were measured (Table 1). Though thermal conductivity increased by increasing the filler loading, the increase was not linear. At 150 phr BN, thermal conductivity of 1.0 W/mK was obtained., Filler loading was not feasible beyond 150 phr.

Table 1. Thermal conductivity of different formulations with PDMS and irregular shape BN and with PT110 BN

Composition	Thermal conductivity (W/mK)
PDMS+10 phr BN	0.32
PDMS+ 50 phr BN	0.58
PDMS+100 phr BN	0.70
PDMS+150 phr BN	1.08
PDMS+150 phr PT110 BN	1.85

To further increase the conductivity, the amount of thermally resistant junctions involving a polymer layer between adjacent filler units need to be reduced. For that PT110 BN, a platelet shaped BN was used so that more contact will be ensured between the filler particles. At 150 phr thermal conductivity of 1.85 W/mK was obtained. Though higher thermal conductivity was attained, the processing of the mix was difficult. To aid processing of the mix and to increase the thermal conductivity further, alpha alumina was added. At optimum composition thermal conductivity of 2.43 W/mK was obtained.

FESEM analysis of PT110 BN formulation and the optimized formulation was done and micrographs are shown in Fig 3. The dispersion of the BN in matrix is confirmed in the FESEM micrograph. In the formulation containing BN alone, matrix is seen between the particles which is less conducting and thus having more thermally resistant junctions. In case of the composition

with alpha alumina mixed formulation, the matrix contains alumina which is conducting filler. The conducting filler added matrix is holding the BN particles giving the better thermal conduction.

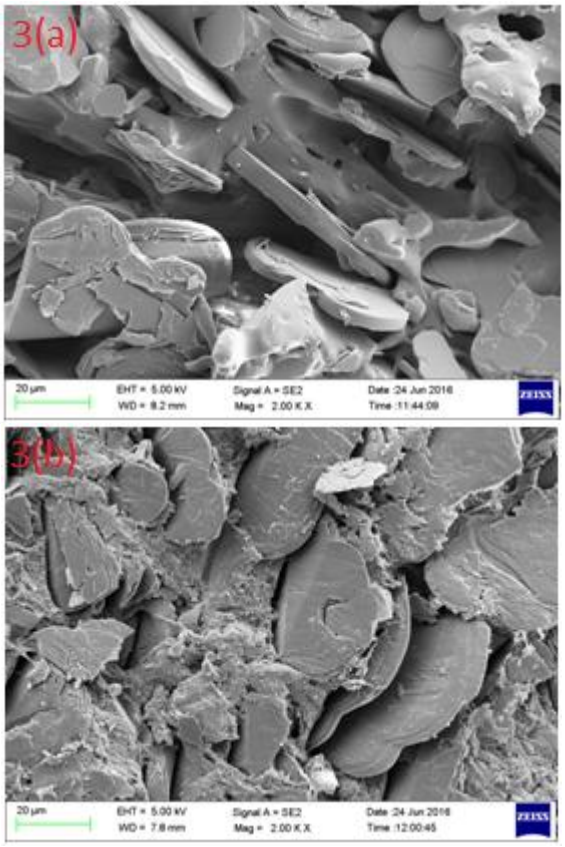


Figure 3. FESEM micrograph for the cured system a) with BN alone and b) with optimized composition

Thermal and mechanical properties of the optimized composition were evaluated and the results are summarized in table 2. Thermogram of the optimized composition is given in Fig.4.

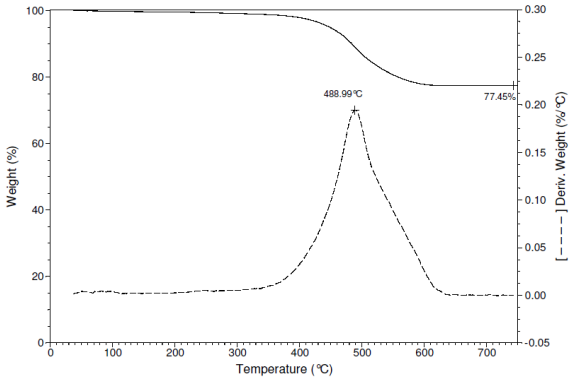


Figure 4. Thermogram of the optimized compostion of TIM

Table 2. Properties of TIM

Thermal conductivity	2.43 W/mK

Specific heat	0.27 cal/g °C
Filler content	77%
Coefficient of thermal expension	2.2 x 10^{-4}/°C
Tensile strength	22-24 ksc
Elongation	25-30%
Shore A hardness	70-75
Density	2.06 g/cc
Thermal stability	489°C

The composition with 77 % filler content has a low CTE of 2.2 x 10^{-4}/°C and high temperature resistance. The properties are ideal for thermal interface material. It has high thermal conductivity and good tensile strength to withstand the load while placing the sheet between the electronic component and heat sink. Since it is an elastomeric material, it can easily be deformed by small contact load to contact all the uneven areas of the mating surface, which help to improve heat dissipation efficiency of the heat sink.

Conclusions

Silicone rubber based thermal interface material was prepared with boron nitride of different shape. Platelet shaped BN has improved the thermal conductivity. Thermal pad with high thermal conductivity of 2.43 W/mK, with high thermal stability, low CTE and better mechanical properties were obtained. The newly developed material is ideal for better heat dissipation in miniaturized electronics.

Acknowledgements

Authors sincerely acknowledge Deputy Director, Propellants Polymers Chemicals and Materials Entity, VSSC and Director, Vikram Sarabhai Space Centre for their encouragement and permission to present the work.

References

29. Z. Liu, D.L.L. Chung, *ThermochimicaActa*366, 135, 2001.
30. W. Zhou, S.H. Qi, H.Z. Zhao, N.L. Liu, *Polymer Composites*28, 23, 2007.
31. W. Zhou, S. Qi, H. Li, S. Shao, *ThermochimicaActa* 452, 36, 2007.
32. W. Zhou, C. Wang, Q. An, H. Ou, *Journal of Composite Materials* 42, 173, 2008.
33. W. Zhou, S. Qi, C. Tu, H. Zhao, C. Wang, J. Kou, *Journal of Applied Polymer Science*104, 1312, 2007.
34. S.C. Das, S.R.V. Behara, D.A.V. Morton, I.Larson, P.Stewart*J. Powder Technology* 249, 297, 2013.

35. X. Fua, D. Huckb, L. Makeinb, B.Armstronga, U. Willenb, T. Freemana, *Particuology* 10, 203, 2012.
36. Y. Xu, D.D. Chung, C. Mroz *Composite A* 32, 1749, 2001

MACRO 499

Intermolecular Ene Reaction For High Temperature Curable Polybutadiene Systems

Gayathri S*, Reshmi S
Propellant Engineering Division, Vikram Sarabhai Space Centre
Thiruvananthapuram, India
gayathri_rajendran@vssc.gov.in

A wide variety of polymers are being used for space applications, for propellants as well as for structural applications. HTPB is one of the widely used hydroxyl terminated polymeric binder for different applications due to the flexible polybutadiene backbone and its peculiar microstructure which consists of different types of hydroxyl groups. The hydroxyl groups are cured using polyisocyanates forming polyurethane network. For urethane curing, there are more possibilities of side reactions which lead to the formation of voids or porosity in the cured networks which may lead to failure in the desired properties. A new curing methodology is attempted where the terminal hydroxyl groups of HTPB are modified and curing is made by Ene reaction. This system can be used for high temperature applications.

Allyloxy terminated polybutadiene was synthesized by functional modification of HTPB and characterized. The binder was synthesized by the reaction of sodium hydride on HTPB followed by reaction with allyl bromide at 60^0C for 48 hours. The conversion was ensured by the reduction in hydroxyl value of the binder (say 40.7 mgKOH/g reduced to 12 mg KOH/g). The absence of OH group in 3300cm^{-1} in FTIR spectrum confirmed the modification. The absorption at 993,966 and 911 cm^{-1} shows that the cis, trans and vinyl double bonds of HTPB remain intact. The peak at 1077 cm^{-1} shows absorption corresponding to due to ether group.

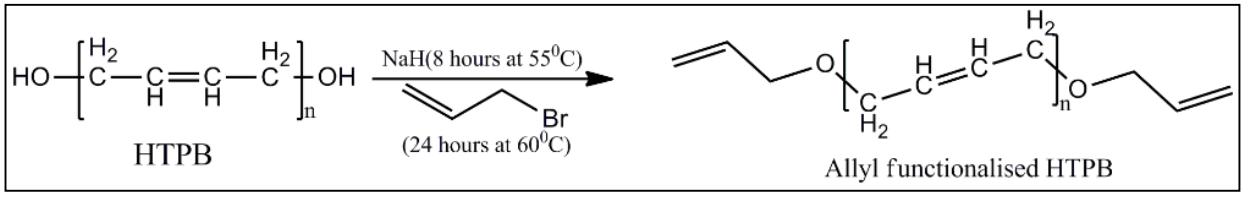


Fig 1. Synthesis of allyl functionalized HTPB

The curing of this system was studied using ENE reaction where the curing agent is maleic anhydride. The kinetics of curing by thermal as well as catalytic route using Boron based Lewis acid catalyst was studied using DSC. Thermal curing of the system was done at 100^0C for 24 hours whereas catalytic curing is possible at 50^0C for 24 hours.

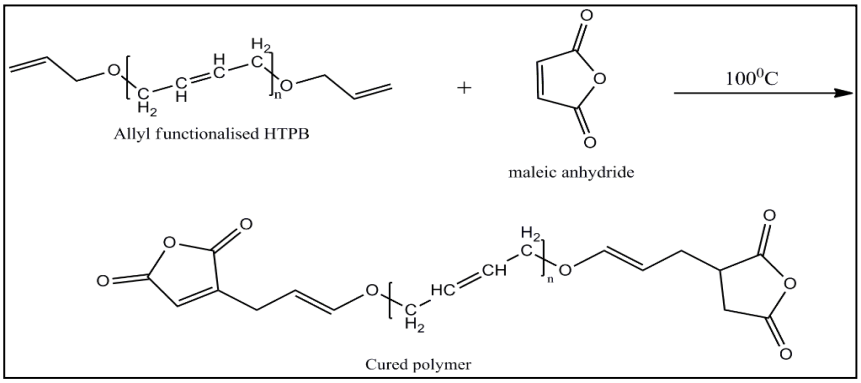


Fig 2.Cure reaction with maleic

The glass transition temperature of the system was evaluated and found to be -44^{0}C which shows the flexibility of the system.

This novel system can be used for structural applications for the launch vehicles due to their better thermal stability which is comparable to epoxy and bismaleimide systems but with advantages of better flexibility and low temperature applications. This system can also be used for adhesive systems where high temperature curing is being done similar to the epoxy based adhesives.

References

[1] V, Sekkar ; SS. Bhagawan; N,Prabhakaran; M, Rama Rao; KN, Ninan. Polymer, 41(2000), 6773–6786.

[2] Haoyu Tang; Wanwan Li; Xinghe Fan. Polymer, 50(2009), 1414–1422.

MACRO 505

Effect of maleic anhydride grafting on MA-g-ABS/EVA miscible blend for high impact strength materials

O. Manaf, A. Sujith*

[a] *Materials Research Laboratory,National Institute of Technology Calicut, Calicut-673601, India*

** e-mail id: sujith@nitc.ac.in*

Abstract

This work aims to study the effect of maleic anhydride (MA) grafting on poly-(acrylonitrile butadiene styrene) polymer (ABS) for the preparation of ABS/poly-(ethylene vinyl acetate) EVA miscible blend for high impact strength material. MA grafting reaction and blend preparation were performed using the internal mixer. All the samples were characterised by attenuated total reflection - infrared (ATR-IR) spectroscopy. MA grafting was confirmed by IR-spectra. The grafting degree was calculated using the peak area ratio (A_{1780}/A_{2237}) method. The miscibility of prepared blends was observed using DSC analysis. Thermal stability, mechanical properties include flexural and Izod impact strength of different samples was studied. The percentage of EVA was optimised by measuring the mechanical properties. Morphology of the cracked surface after impact test was observed suing SEM.

Keywords: *maleic anhydride; miscible blends; high impact strength material*

Introduction

Acrylonitrile butadiene styrene (ABS) is one of the most important engineering thermoplastic copolymer. It consists of an elastomeric segment of polybutadiene (PB) dispersed in a rigid plastic polystyrene acrylonitrile (SAN) matrix. The fascinating properties of ABS include high impact strength, excellent processability, very low conductivity and superior mechanical properties[1]. Owing to the ability of ABS to form the partially miscible blend with a broad range of thermoplastics as well as elastomers, it has commercial acceptance in automotive and electronic industries. Particular applications of ABS include electronic aids protective cases, keyboards, dashboard and bumper bar, etc. Even though ABS polymer has many advantages, there are some limitations such as poor thermal stability and low flame and chemical resistance. So the blending of ABS with required amount of other polymers can enhance the physicochemical properties of native ABS.

Physical blending of ABS ends up with the formation of immiscible or partial miscible blends. Recent decades researchers are trying to develop miscible blend which can perform better properties than immiscible blends. Recently grafting technique came up with producing reactive blends which can provide highly miscible blends. It can vanish the interfacial tension between two immiscible polymers. The reactive blends can be prepared either by grafting of parent polymer matrix with a functional monomer separately or addition of grafted polymer into the polymer mixture during the mixing time. Maleic anhydride (MA) is one of the promising functional monomers for improving the surface polarity and miscibility with a wide range of polymers and inorganic fillers.

There are many reports on MA grafted ABS polymer (MA-g-ABS) and its reactive blends and composites. The limitations associated with MA grafting on ABS have encouraged for modifying MA-g-ABS via simple mixing of an external modifying agent. Polyethylene vinyl acetate (EVA) is an elastomeric copolymer and can act as an excellent toughening agent[2]. Since both EVA and MA-g-ABS containing polar functional groups, they are highly compatible.

The main objective of the work is to modify MA-g-ABS matrix using EVA as an impact modifier and optimisation of EVA percentage by means of different mechanical testing such as tensile, flexural and impact tests.

Experimental

Industrial grade Poly-acrylonitrile butadiene-styrene (ABS) (Starex SD-0150) which is used in the typewriter, keyboard, etc. is obtained from Samsung SDI Co., Ltd. having M_n = 69000, M_w =135000, M_w / M_n = 1.96. Maleic anhydride (MA), 99% was supplied by Avra Synthesis Pvt. Ltd. Dicumyl peroxide (DCP) 99% was purchased from Himedia Laboratories Pvt. Ltd. India. Poly-ethylene vinyle acetate (EVA) with 40% vinyl acetate is purchased from K. N. Polymers Pvt. Ltd.

The different MA-g-ABS/EVA samples were prepared using mini internal mixer equipped with a mixing chamber volume of 40 cm^3. The mixing was done at 150 ^{0}C and screw rotation speed of 45 rpm. All the mixing components were added in 3 minutes time intervals in the order of ABS followed by MA, DCP and EVA respectively. The chemical compositions of different samples were given in Table. 1

Table.1 Composition of different samples

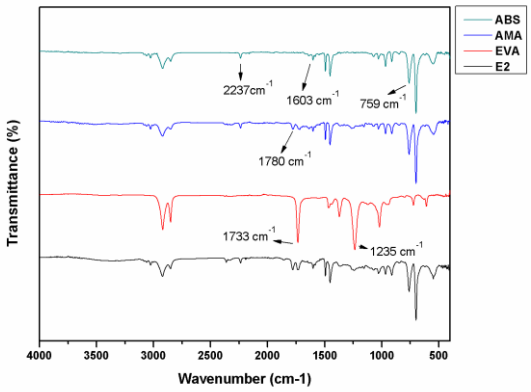
ATR-IR spectra of different samples were recorded using JASCO FTIR-4700 spectrometer in the range of 4000-400 cm-1. The grafting degree (GD) of AMA was calculated as peak area method[3]. The thermal behaviour of different samples was analysed using TGA Q-50 from TA instruments. The test was carried out in the nitrogen atmosphere at a flow rate of 60 mL/min and a scanning rate of 10 °C/min. The TGA gramme was obtained from 0 °C to 700 °C. DSC analysis was carried out on a TA instrument under the nitrogen atmosphere at heating and cooling rate of 10 °C/min. the specimens were scanned in the range of -50 to 100 °C. The flexural properties of samples were tested according to ASTM D790 in universal material testing machine Tinos Olsen, equipped with 10 KN connected with software. Izod impact strength of different samples was measured as per ASTM D256 using Resile impactor junior, CEAST technologies equipped with a 5.5 J pendulum. SEM images of samples after impact test were examined by field emission scanning electron microscope Shimadzu 6600. Prior to morphological observation all the specimens were gold sputtered using Hitachi E1010.

Results and discussion

Figure 1 presents the ATR-FTIR spectra of pure ABS and different samples (AMA, EVA and sample E3) prepared via melt mixing technique. In the FTIR spectrum of ABS, the peaks observed at 2237 cm^{-1}, 1603 cm^{-1} and 759 cm^{-1} attributed to the nitrile, butadiene and styrene components of ABS backbone. Except for these all peaks, sample AMA shows a new peak at 1780 cm^{-1}. The peak indicates the symmetric stretching vibration of MA in the grafted state. Similar observations are reported by various research groups[3, 4]. It shows the successful grafting of MA on ABS polymer. Sample AMA showed the GD of 1.6 wt%. The strong peak of EVA observed at 1733 cm^{-1} and 1235 cm^{-1} represent the C=O, and C-O stretching vibrations. Sample E3 shows all the peaks mentioned above. The variations in the peaks intensity are due to the variations in the concentrations.

Samples	Weight of components (g)			
	ABS	MA	DCP	EVA
ABS	20	0.0	0	0.00
AMA	20	1.0	0.2	0.00
AE1	20	1.0	0.2	0.43
AE2	20	1.0	0.2	0.88
AE3	20	1.0	0.2	1.34

Figure 1. IR spectra of different samples



The thermal stability of different samples is represented in Figure 2. The TGA curve of ABS display characteristic single step degradation behaviour in N_2 atmosphere and it shows 10 % degradation at 385 °C. The MA grafting slightly reduces the thermal stability of ABS and shows 10% degradation at 379 °C. While comparing the TGA of EVA with ABS, EVA shows comparably lower thermal stability and two-step degradation mechanism. It shows 10% degradation at 332 °C. Whereas, sample E3 show 10% degradation at 378 °C. It is similar to AMA. It indicates that addition of 6%EVA cannot reduce thermal stability of AMA.

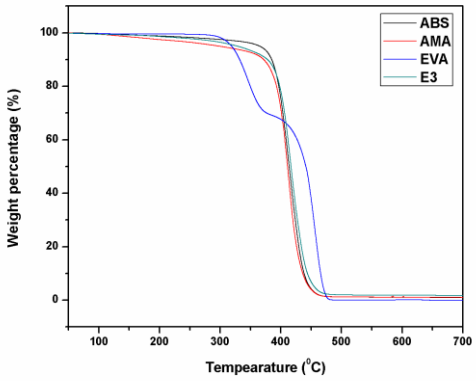


Figure 2. TGA thermogram of ABS, AMA, EVA and A3 at N_2 atmosphere

The glass transition temperature of different samples was given in Figure 3. The pristine ABS shows a transition point at 100 °C. The similar observation is reported by Biswal et al.[5] But the same time, AMA exhibit transition at 104 °C. So the MA grafting increases the Tg of ABS. while comparing the nature of the curve, AMA exhibits a sharp dip than ABS, it indicates the crystalline nature of AMA. The pure EVA shows a transition point at 7 °C. it is a rubbery material at room temperature and second and third transitions observed at 104 °C and 120 °C respectively. The physical blend of ABS with 6% EVA shows noticeable transitions at the same temperature mentioned above. While the sample E3 shows noticeable transition at a single point at 102 °C, it indicates high miscibility between AMA matrix and EVA polymer.

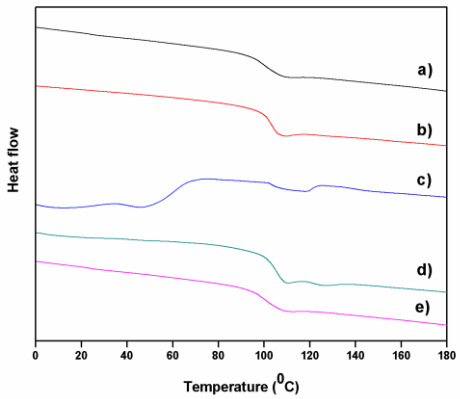


Figure 3. DSC analysis of a) ABS, b) AMA, c) EVA, d) 6%EVA/ABS physical blend and e) E3

The flexural strength and flexural modulus of different samples were calculated from the force-extension graph. The results obtained are plotted in Figure 4. The pristine ABS shows good flexural strength of 70 MPa. Similar to that of observations obtained from the tensile test, the flexural strength of AMA showed the maximum flexural strength of 76 MPa. That may because of the grafting of the bulkier group on the ABS polymer chain and it resist the segmental mobility under load is applied. There is a slight decrease in flexural strength when the EVA is added and reached a minimum strength of 66 MPa for sample E3. It is because of the incorporation of a flexible component to the rigid matrix of AMA. When looking into the flexural modulus, pristine ABS showed maximum flexural modulus of 1.85 GPa and the flexural modulus is decreasing when grafting occurs and showed flexural modulus of 1.51 GPa for sample AMA. It is because of the reduction in the flexibility due to the cross-linking and MA grafting on ABS polymer chain. There is no significant effect on the percentage of EVA up to 6%.

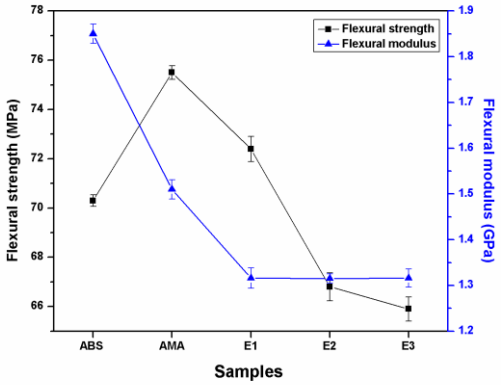


Figure 4. Flexural properties of ABS, AMA and different blends of EVA/AMA

The Izod impact strength of various samples has been shown in Figure 5. Pristine ABS shows considerable impact strength of 411 J/m and the impact strength is due to the rubbery phase of

butadiene component in ABS. the double bond of butadiene provides more entanglements in the polymer chain and act as a good shock absorbing site. There is a steep decrease in impact strength of ABS while grafting MA occurs. This is because of the reduction of rubbery nature in the matrix. The reduction in the double bond or rubbery nature can happen in two ways, either the cross-link reaction between adjacent ABS polymer chain due to the cumyl radicals as a free radical initiators or grafting of MA to the most feasible site of the double bond of butadiene segment in ABS backbone. When EVA is added, there is a considerable increase in impact strength of AMA and reached a maximum impact strength of 454 J/m for sample E2. It is much better than pristine ABS. Here the EVA could act as a good toughening agent for AMA. It may be because of the polar-polar interaction of carbonyl groups of EVA and MA.

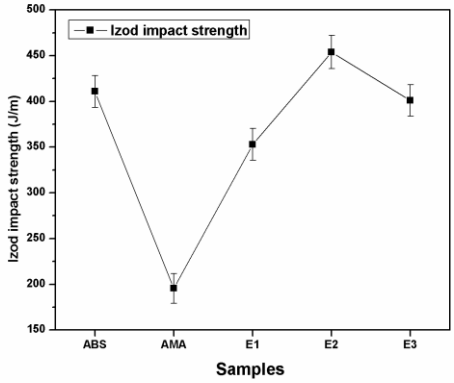
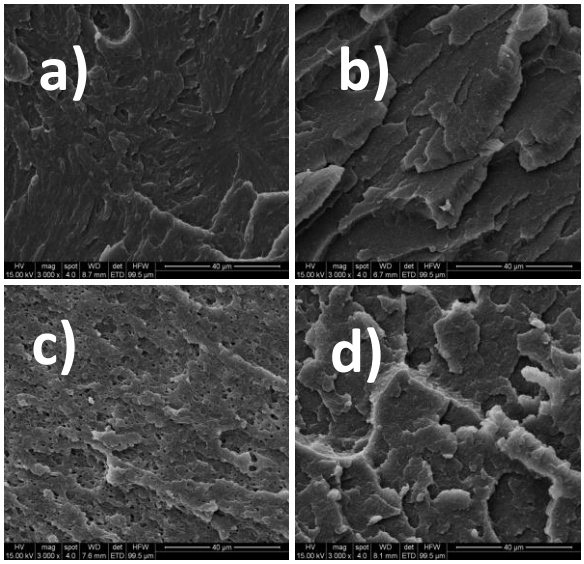


Figure 5. Impact strength of ABS, AMA and different blends of EVA/AMA

The cracked surface morphology of different samples after Izod impact test was studied using SEM images. The observed SEM images are given in Figure 6. The ABS show a white ductile lines appeared along with grains edges. It is because of the PB content. In the case of AMA, the



grains are sharp and appeared as a brittle fracture. It indicates that MA grafting reduces the ductility of ABS. Whereas physical blend of 6wt% EVA/ABS shows entirely different morphology. There was a formation of porous surface along with grains. It implies the poor miscibility of ABS and EVA phases. While 6 % EVA added to AMA, the sharpness of the grains reduces and the thickness of white ductile line increases. It shows the clear indication of the increment in the ductility. The SEM pictures support the results observed in impact tes.

Figure 6. SEM images of specimen cracked surface after Izod impact test a) ABS, b) AMA, c) 6%EVA/ABS physical blends and d) E3

Conclusions

The formation of a new peak in ATR-IR spectra at 1780 cm^{-1} has confirmed the grafting of maleic anhydride on ABS polymer with a considerable GD of 1.6 %. Even though MA grafting slightly reduce the thermal stability of ABS, addition of 6% EVA is not reduced thermal stability of AMA but slightly reduced flexural strength and modulus. MA grafting substantially reduces the impact strength of ABS, though it can be maintained by the addition of EVA. There are noticeable difference in broken surface morphology between ABS, AMA and E3.SEM images good agreement with impact test.

Acknowledgements

The authors are thankful to Mr. Ajay P. and Mr. Nishad K.V. for technical assistance.

References

37. M.D. Ana, D. Gasco, *ACS App. Mater. Interfaces*, 5, 12107-12119, 2013.
38. Siddaramaiah, P. Poomalai, B. Ramaraj, *J. Appl. Polym. Sci*, 104, 3145-3150, 2007.
39. A. K. Ghosh, S.C. Debnath, N. Naskar, D. K. Basu, *J. Polym. Sci,* 81, 831-836, 2001.
40. R. Qi, Z. Chen, C. Zhou, *Polymer,* 46, 4098-4104, 2005
41. M. Biswal, S. Mohanty, S. K. Nayak, *Int. Plast. Technol,* 17, 209-225, 2013

MACRO 507

Thermo-mechanical evaluation of organically modified clay filled Polymethylsilsesquioxane

Ancy Smitha Alex[a], R.S. Rajeev [b], Jamin Joy[a], Sreelekshmi K.R[a], Vijendra Kumar[a], Bandyopadhyay.G.G[a], Sekkar. V[a], Gouri. C[b]

[a]*Analytical Division, Chemical Systems Group, PCM, Entity, Vikram Sarabhai Space Centre, Thiruvanathapuram-695022, India*
[b]*Polymers and Special Chemicals Group, PCM, Entity, Vikram Sarabhai Space Centre, Thiruvanathapuram-695022, India*
**vsekkar@gmail.com*, *gouri.c.k@gmail.com*

Abstract

Polymethylsilsesquioxane (PMSQ) belongs to a class of organosilicone polymer and possesses distinguished properties such as high thermal stability, non-toxicity and chemical stability. However, its practical application is limited due to its brittle nature. In this study, an attempt was made to modify the properties of PMSQ by organically modified montmorillonite clay inclusion. The solution blending of clay and PMSQ in acetone was done prior to uni-axial pressing to obtain PMSQ-clay composite. Clay loading was varied up to 40% (by weight) to find out the tolerable limit of filler in PMSQ and to study the effect of clay content on its thermo mechanical properties. It is observed that clay inclusion of 20% resulted in good improvement in mechanical properties of the system. Thermogravimetric analysis conducted on PMSQ-clay composites showed good thermal stability but char residue was slightly decreased with increase in clay loading. Microstructure evaluation using XRD revealed exfoliated nature of PMSQ-clay composite.

Keywords: PMSQ*; clay; montmorillonite; thermal stability*

Introduction

Polymethylsilsesquioxane (PMSQ) with the empirical formula $(CH_3SiO_{3/2})_n$ is typically derived from methyl trialkoxy silanes and possesses unique properties due to the presence of hydrophobic methyl groups as well as hydrophilic silanol groups[1-3]. PMSQ has many interesting features such as good thermal stability, biocompatibility, non-toxicity and chemical stability. It has improved moisture resistance than silica, because PMSQ contains more hydrophobic methyl groups. When PMSQ is heated to 150 °C and above, structural rearrangements will occur and it will transform part of the PMSQ regular cage structure into an irregular network structure. However, these materials are brittle and their mechanical properties need to be improved.

Clays have been extensively used in polymer industry either as a reinforcing agent to improve the physico mechanical properties of the final polymer or as a filler to reduce the amount of polymer used in the shaped structures[4]. Particularly, smectite clays are used for such applications[5]. But its hydrophilic surface with high energy is incompatible with many polymers, whose low energetic surfaces are hydrophobic. But, proper modification of the clay surface through the use of organic ions (e.g., alkyl ammonium) renders the silicate organophilic and hydrophobic and lowers the surface energy of the platelets and increases the basal-plane or interlayer spacing (d-spacing) and this will facilitate the polymer to wet the surface of the clay and disperse the clay into the polymer[6]. Even after this modification, the clay layers still have the silanol groups on their edges, which can interact with silane compounds possessing silanol groups. In the present study, an attempt was made to improve the properties of PMSQ by organically modified montmorillonite clay inclusion and its effect on mechanical and thermal properties are discussed.

Experimental

YR 3370, a commercially available PMSQ (Momentive Performance Materials, Japan) with chemical composition $SiO_{1.78}$ $C_{1.22}$ $H_{3.67}$ was used as the matrix resin. Cloisite 30B (methyl tallow (bis-2-hydroxy ethyl) quaternary ammonium modified montmorillonite) supplied by Southern Clay Product, Mumbai, India was used as the filler material.1,4-Diazabicyclo[2.2.2]octane (DABCO) was used as the cure enhancer. Acetone from Merck India Ltd., Bangalore is used as solvent for processing the composites.

The organoclay was first suspended in acetone. The weight percentage of organo clay used with respect to PMSQ was 10:90, 20:80, 30:70, 40:60 (Clay: polymer) respectively. Then, PMSQ was dissolved in the solvent and added to the clay suspension and stirred for 30 minutes whereby it gets intercalated between the swollen clay layers. Finally, the solvent was removed by evaporation under vacuum to get PMSQ coated clay powder.1wt% of DABCO was added to the total mixture as a cure enhancer of PMSQ. The powder was uni-axially pressed at a pressure of 14 MPa at 85 °C for 1 h and at 150 °C for another 1 h to obtain clay reinforced PMSQ composites with a density of 1.2 g/cm^3.

Mechanical properties such as flexural, compressive and impact strength were determined using ASTM D 790, ASTM D 695, and ASTM D 256 respectively. Thermal decomposition of the nanocomposites was studied by TG/DTG from room temperature to 900 °C in nitrogen atmosphere at a flow rate of 100 ml/min. Morphological study on the fractured surface of the tested specimen was done using Low Vacuum Scanning Electron Microscope (LVSEM) CARL ZEISS-EVO 50 which is a high performance general purpose SEM operated up to 30 kV. XRD measurements of the nanocomposites were carried out using a Bruker D8-Discover X-ray diffractometer (XRD) operating with a Cu anode (40 kV, 40 mA).

Results and discussion

PMSQ-clay composite with varying clay contents (10 to 40 wt. %) were processed. Higher loading of clay was chosen tenaciously to find out the bearable limit of clay content required to reinforce the brittle PMSQ matrix. Normally, curing of PMSQ takes place at nearly 150 °C. But rapid heating of PMSQ–clay system to such high temperature will generate cracks in the composite. In order to avoid that DABCO (an amine catalyst) was added as the cure enhancer which will increase the deprotonated silanol concentration in PMSQ and it will help in silanol condensation and curing at a lower temperature. Organically modified clay was particularly selected as the filler since the high aspect ratio of the modified clay platelets can carry and transfer the load effectively, reducing the brittle nature, thus providing an effective reinforcement to PMSQ. Further, the -OH groups present in the clay system can effectively interact with the silanol groups present in the cage and ladder structure of PMSQ matrix.
The mechanical properties of polymer/clay composites largely depend on the degree of exfoliation of the clay layers as well as on the interaction between the clay layers and the polymer matrix. Microstructure evaluation of PMSQ–clay composite by XRD showed the exfoliated nature of the composite at all proportions. The diffraction peak of Cloisite 30B clay appears at $2\theta = 4.87°$ with an interlayer spacing (d_{001}) of 18.5 Å as calculated from Bragg's law. From the XRD spectrum (**Figure 1)** it is obvious that there is no perceptible diffraction peak at 2θ values from 3° to 10°. This indicates the exfoliated nature of the nanolayers of clay in the polymer matrix.

Morphological study of the fractured composite specimen was done by SEM. The SEM image of the composite with 20 % clay is shown in Figure 2 which showed good dispersion of clay platelets in the PMSQ matrix.

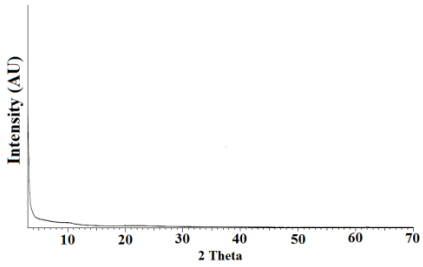


Figure 1. XRD profile of PMSQ-clay 20 composite

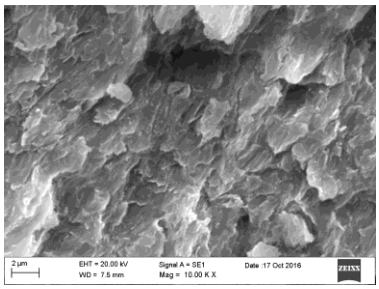
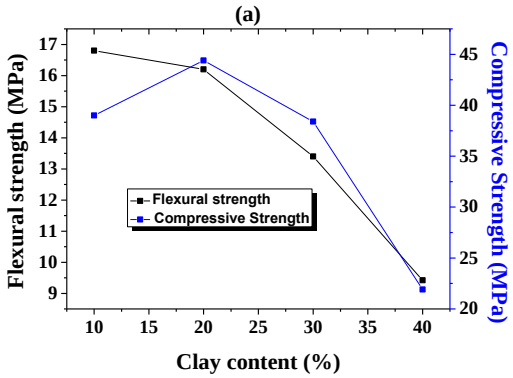


Figure 2. SEM image of PMSQ-clay 20 composite

Mechanical Properties

The mechanical properties such as compressive, flexural and impact strength of PMSQ-clay system were evaluated. The variation in properties with respect to clay content (10-40%) was systematically investigated and given in **Figure 3.** Pure PMSQ is too brittle to do the mechanical evaluation. Composites with lower clay content were also prepared. But their structural characteristics were so deflated to do the mechanical evaluation.

From Figure 3(a), it is clear that flexural strength showed comparable values (16 MPa) up to 20% clay inclusion and decreases on further addition of clay. Compressive strength increases with clay content up to 20% and decreases further. The increase in compressive strength is attributed to the better reinforcement and effective stress transfer by the organoclay platelets. But after 30% clay content interfacial adhesion between the clay and PMSQ got decreased causing deterioration in compressive strength.



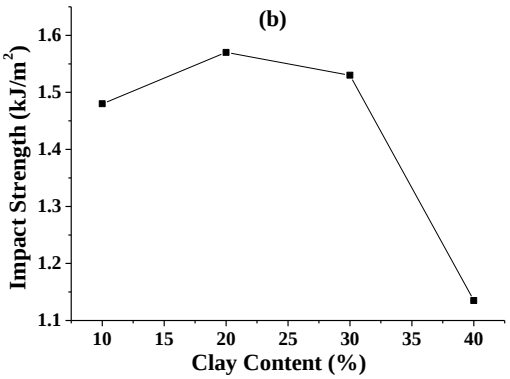


Figure 3. (a) Flexural and compressive strength (b) Impact strength

Impact strength also increased up to 20% and decreased with further addition of nanoclay. Impact strength is the resistance of a material to fracture under dynamic load. It is a complex characteristic which takes into account both the toughness and strength of a material and depends on many factors, such as the nature of the constituents, matrix/filler adhesion, construction and geometry of the composites, and test conditions. The trends in impact strength support the better interfacial adhesion up to a clay loading of 20%.

Compressive modulus, flexural modulus and toughness value is given in table 1.Toughness is a measure of the energy a sample can absorb before it breaks. It is observed that the toughness decreases consecutively with increase in clay content, whereas flexural modulus increases up to a clay loading of 30% and then decreased. Compressive modulus remains more or less same up to 30% and then decreased.

Table 1.Modulus and toughness values of PMSQ-clay composites

Clay Content (%)	Flexural Modulus (GPa)	Compressive Modulus (GPa)	Toughness ($kJ/m^{3)}$
10	1.55	0.84	1.09
20	1.86	0.83	0.68
30	2.35	0.86	0.56
40	1.77	0.78	0.20

Thermal Properties

Thermogravimetric analysis was employed to explore the thermal decomposition characteristics of the PMSQ-clay composites and the profile is given in Fig.4

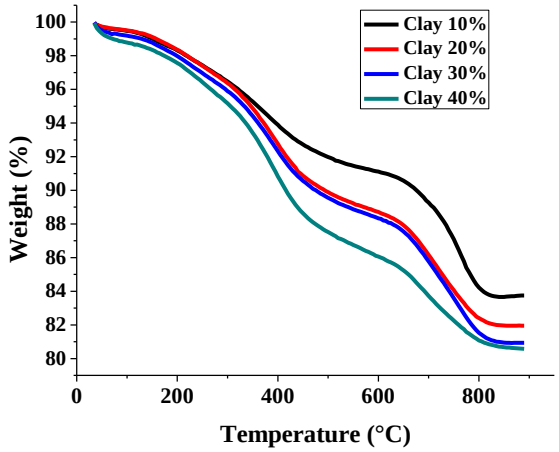


Figure 4. TGA profile of PMSQ-Clay composites

TGA curve of the pyrolyzed PMSQ-clay composites suggests that two major decompositions occur in the material as temperature is increased up to 900 °C. The data derived from the TGA and DTG curves for the composites are tabulated in Table 2. The first step weight loss begins almost immediately on heating continues to 100 °C. This is ascribed to the evolution of products due to the condensation of residual silanol and the reaction of methoxide groups. An overlapping weight loss is observed in the region at about 200 °C, which corresponds to the loss of low molecular weight cyclic PMSQ structures and due to the onset of degradation of organoclay at 180 °C. The loss of decomposition products of clay takes place in two steps i.e. at 270-297 °C and at 400° C. The T_{peak} of the first stage is around 390 °C due to the synergistic effect of aforementioned processes. The weight loss centered at 540–650°C is attributed to the evolution of CO, and that at 700-750° C is due to the evolution of CH_4. Above 800 ° C weight loss is limited and probably owing to the evolution of hydrogen from Si—CH_2—Si linkages which incorporate into the backbone by redistribution reactions. During the second stage decomposition, organic-ceramic conversion takes place by radical assisted mechanism. In PMSQ-clay composites as clay content increases the T_{peak} of the second decomposition is shifted to lower values indicating that the clay accelerates the organic to ceramic conversion.

Table 2. Thermal data of PMSQ-clay composites

Clay Content (%)	**10**	**20**	**30**	**40**
Temperature range for first step decomposition (°C)	40-500	40-500	40-500	40-500
T_{peak} for first step decomposition (°C)	390	390	390	390
Residue after first step decomposition (%)	91.2	88.9	88.5	86.3

Temperature range for second step decomposition (°C)	500-860	500-860	500-860	500-860
T_{peak} for second step decomposition (°C)	750	730	710	700
Char residue at 900 °C(%)	83.7	82.0	80.9	80.6

Conclusions

PMSQ-clay composites were prepared by powder compacting of PMSQ coated nanoclay. The clay content was varied from 10 to 40%. Morphological studies conducted by SEM revealed no visible agglomeration of clay platelets in the micro range and micro structural evaluation by XRD disclosed good exfoliation of clay platelets. It is observed that good mechanical properties are observed up to 20%. However toughness value calculated from stress-strain curve of flexural testing decrease with increase in clay content due to the increase in flexural modulus. TGA data reveals the acceleration of organic to ceramic conversion in PMSQ-clay composites with respect to increase in clay content.

Acknowledgements

Director, VSSC for granting permission to present the paper. Colleagues in ANLD, ASD and MCD, VSSC for analytical support.

References

42. J. Ma, L.H. Shi, Y.Y. Shi, S.U. Luo, J. Xu, J. Appl. Polym. Sci. 85 (2002) 1077.
43. H.S. Chae, S.J. Song, Y.H. Park, Mol. Cryst. Liq. Cryst. 492 (2008) 28.
44. H.J. Dong, M.A. Brook, J.D. Brennan, Chem. Mater. 17 (2005) 2807.
45. A.Lagashetty,A.Venkataraman,Resonance,(2005) 49-60
46. M.Yigit, T.Seckin, B. Yigit, S.Koytepe. Turkish J Chem. 37 (2013) 182
47. A B Morgany, R H Harris Jr, T Kashiwagi, L J Chyall, J W Gilman. Carbonaceous Char Formation Fire Mater. 26(2002) 247.

MACRO 511

Studies on Polysiloxane Derived Porous SiOC/ SiO_2 Ceramics *via* Sacrificial Filler Route

Shikha K.T, Jamin Joy, Ancy Smitha Alex, Nisha Hasmi K, Vijendra Kumar, Bandyopadhyay G.G, Sekkar V.

[a]*Analytical Division, Chemical Systems Group, PCM, Entity, Vikram Sarabhai Space Centre, Thiruvanathapuram-695022, India*

*vsekkar@gmail.com

Abstract

Fabrication of ceramic matrix composites by pyrolytic conversion of preceramic polymers has gained considerable attention in recent years due to their unique

combination of low temperature processing, applicability of versatile plastic shaping technologies and micro structural control capabilities. Moreover, polymer derived ceramics are additive-free ceramic materials possessing excellent oxidation and creep resistance up to high temperatures. To date, preceramic polymers are mostly used in the production of low density, highly porous products since loss of volatiles during pyrolysis leads to porosity and large shrinkage.

The present work explores the feasibility of formation of ceramic foams by pyrolytic conversion of preceramic polymer in combination with inert filler using sacrificial filler route. In the present work, highly porous Silicon Oxycarbide (SiOC) ceramics up to density of 0.5 g/cc were prepared from preceramic siloxane (PCS) using polymethyl methacrylate (PMMA) powder as sacrificial filler and short silica fiber as passive filler. The ceramic foam composites were processed by mixing silica fiber in definite proportion and PMMA powder in varying amount in the PCS matrix followed by pyrolysis at 1050°C in Argon atmosphere. It was found that pyrolysis of PCS under inert atmosphere leads to amorphous, oxidation resistant Silicon Oxycarbide (SiOC) ceramics with apparent porosity up to 75 % and low volume shrinkage (15 %) by varying the weight ratio of polymer and filler. The physical, mechanical and thermal properties of ceramic composites with varying amount of sacrificial filler composition and thus density were investigated and compared. The lowest dense ceramic foam (0.5 g/cc) exhibited a compressive strength of 2.5 MPa and flexural strength of 1.9 MPa and a resilience value of 0.30 kJ/m^2. The morphology and microstructure of the ceramic foams were investigated using SEM and XRD. SEM revealed the open pore structure of foam composite and XRD data proved its amorphous nature. Thermogravimetric analysis conducted on SiOC foam revealed high temperature stability of the porous ceramic.

Key words: *Preceramic polymers, Polysiloxane, Silicon Oxycarbide (SiOC), sacrificial filler, porous ceramic.*

Introduction

Polymer derived porous ceramics are cellular structures with growing importance in the field of catalysis, filters, membranes, thermal protection systems in aerospace industry, tissue engineering, thermo photovoltaic applications and scaffolds for cell growth. The pore size can be defined into three different dimensional ranges 1) micropores (<2 nm) 2) meso pores (2-50 nm) 3) macropores (> 50 nm). Microstructure and morphology of the porous ceramic structures precisely depend on the starting material and processing route. Fabrication of ceramic matrix composites from pyrolytic conversion of preceramic polymers has gained considerable attention in recent years due to their unique combination of low temperature processing, applicability of versatile plastic shaping technologies and microstructural control capabilities. Moreover, Polymer Derived Ceramics are additive-free ceramic materials possessing excellent oxidation and

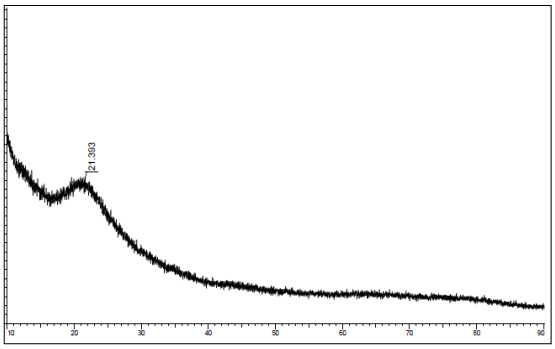
creep resistance up to high temperatures. To date, preceramic polymers are mostly used in the production of low density, highly porous products since loss of volatiles during pyrolysis leads to porosity and large shrinkage.[1,7]

Polysiloxanes represent surely the most studied class of preceramic polymers, their high thermo chemical stability, low price and easy synthetic route makes them the versatile, easy to handle precursor for the realization of silicon oxycarbide glasses with extremely interesting thermo-mechanical properties up to approximately 1200°C [5].The complete potential of polymer-derived porous ceramics can only be achieved when properties are tailored for a specific application, whereas proper control over the properties is highly dependent on the processing route. The strategic approaches are mainly classified into replica, sacrificial template and direct foaming [1,7]. In the present work, highly porous, low density Silicon Oxycarbide (SiOC) ceramics were prepared through sacrificial filler route using Polymethyl methacrylate (PMMA) beads and Silica short fibers as passive fillers in Argon atmosphere.

Experimental

Porous SiOC ceramic composites were prepared from a commercially available Polysiloxane (YR 3370, Momentive Corporation, Japan) which is a colourless, transparent solid in appearance and the analyzed chemical composition of the resin was $SiO_{1.78}C_{1.22}H_{3.67}$. [2] Polysiloxane (YR3370) material offers very good air stability and non-toxicity which enable easy storage and processing and consequently, cost reduction [3].The prepolymer was dissolved in acetone (Merck, Specialities, Private Ltd.) and thoroughly mixed with mechanically exfoliated silica short fibers (5 mm length) (Valeth Industries, chennai). The silica fiber content was maintained at 60 mass % of the molding mixture. Chopped silica fibers were used as passive filler in order to improve the mechanical properties of the pyrolyzed product. After drying, the mixture is powdered using a mixer-grinder and then sieved. PMMA micro beads (Kemphasol, Mumbai) was used as the sacrificial filler for preparing SiOC porous composites for this study, The composite monoliths were prepared from polymer , silica fiber and sacrificial filler (PMMA) in various ratios ranging from 10-50% of PMMA loading and mixed well using a ball mill. The sample Id and compositions are given in table 1. The molding mixture was placed in as MS mould measuring 80mm x 70mm x 30 mm, and uniaxially pressed using a hot press under 15 MPa at 200^{o}C for 2 hours. The compacts were cross-linked by heating to 500^{o}C for one hour [9]. This step will help to retain the generated pore morphology during high temperature pyrolysis. The cross-linked samples were pyrolyzed at 1050^{o}C for 1 hour at a heating rate of 1^{o}C/min in Argon.

The bulk density of the porous ceramics was calculated from the weight-to-volume ratio of the samples. The apparent porosity of the samples was determined using ASTM C 20(2015) method. The cell morphology was observed by scanning electron microscopy **(LVSEM, CARL ZEISS-EVO 50**). X-ray diffractometry (XRD) was performed on ground powders on a diffractometer (**D8 Discover, Bruker AXS**



GmbH, Germany).FTIR analysis were carried out using **Nicolet™ iS™ 50 FTIR spectrometer** and the chemical composition of the pyrolyzed samples were analysed by EDX using **Oxford Inka Energy Dispersive Spectroscope.** The Thermogravimetric characterization and Air oxidation resistance was analyzed using **Thermogravimetric analyzer SDT2960** instrument. For flexural strength (ASTM D750) and resilience measurements (ASTM D 256), bar-shaped samples were polished to a normal size of 3mm×10mm×55 mm and measured on an Instron machine (UTM 5569, Instron Co., Ltd., USA). The compressive strength was measured on 12.7mm×12.7mm×25.4mm-sized samples (ASTM C 1358).

Table 1. Sample Id and compositions

Sample Id	Weight % of YR3370-SiO_2 mixture	Weight % of PMMA loading
A	50	50
B	60	40
C	70	30
D	80	20
E	90	10
S1	100	0

Results and discussion

Generally, Polysiloxane under high temperature pyrolysis leads to the formation of amorphous SiOC matrix. XRD analysis showed that the resulting SiOC composite is completely amorphous with broad Bragg reflections between 15°and 30°range (2θ), Fig.1, which is typical of amorphous SiOC ceramics. [4]

The thermal conversion from organic siloxane network into the inorganic ceramic structure was also investigated using FTIR method. Fig.2 shows the infrared spectra of the samples E (pyrolyzed polysiloxane / Silica-PMMA (90/10), S_1 (polysiloxane / Silica (40:60)) and PMMA. The spectra give the vibration bands of 768 (assym. Si-CH3),

11 **Fig.1 XRD pattern of sample pyrolyzed at 1050°C under Ar atmosphere**

sa

complete removal of PMMA from the sample during pyrolysis.

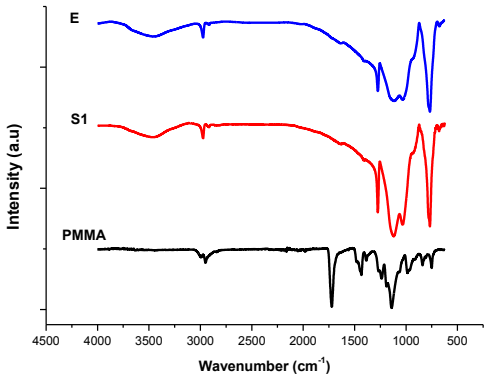


Fig.2 FTIR spectra of samples E, S1 and PMMA

Fig. 3 shows the typical fractured surface of the porous SiOC samples. All the ceramics showed an inhomogeneous morphology at the microscopic scale and surface cracks .The cracks occurred mostly due to the stresses originating from several

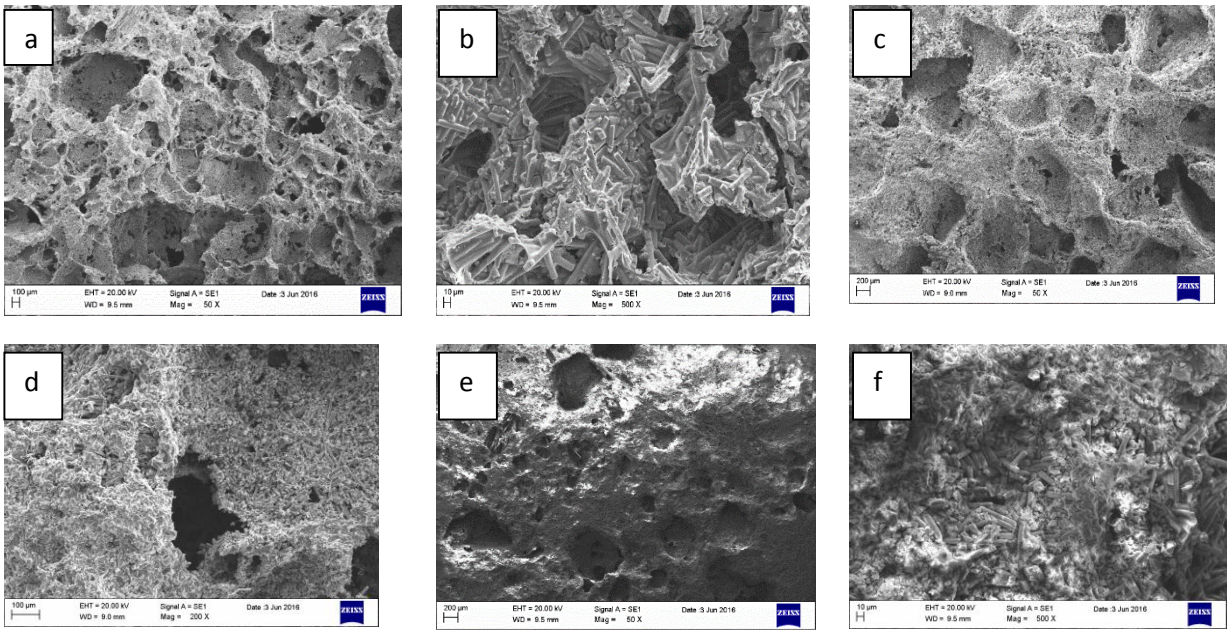
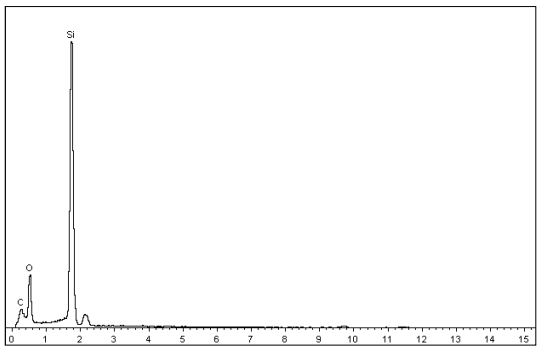


Fig.3. SEM images of (a& b) Sample A (50/50), (c & d) Sample C (70/30) and (e & f) Sample E (90/10)

fa[illegible]orphology of during pyrolysis because of the presence of large quantity of PMMA in the case of sample A, high volume shrinkage, and also because of inhomogeneous mixing of PMMA powder with YR 3370 polymer / silica fiber mixture. The fractured surface for the 90/10



mixture was quite smooth but the surfaces were progressively become rough with increasing the weight % of PMMA. All the ceramic samples illustrate that the residual porosity has a rather inhomogeneous dispersion in the bulk materials. The images show the presence of fine and well distributed open pores in the cellular structure of the primary pores was various shapes, but mostly roughly spherical shape, but the size of the most of the pores was quite different. As size of the PMMA particles were inhomogeneous and their shape was different, and also because of high volume shrinkage during ceramization process, therefore it can be expected that the pores it would produce in the ceramics would be inhomogeneous. The fractured surfaces became more heterogeneous with increasing weight% of PMMA and the heterogeneity is more evident the more PMMA was added.

EDX analysis was performed on the surface of sample C (70/30). The EDX analysis confirms the formation of the Si O C structure. However, the EDX spectra confirm that the fabricated porous ceramics are consist of Carbon, Silicone and Oxygen as their respective peaks are clearly visible in figure 4.. The chemical compositions of the porous ceramics made from 70/30 mixture on an average was Si = 42.32%, O = 33.05 %, and C = 24.63.The corresponding atomic ratio works out to be Si:O:C equal to 1:1.37:1.36. Higher Oxygen content shown may correspond to the presence of silica short fibres in the composite. Higher Carbon content may be due to some residue left by undecomposed PMMA.

Thermogravimetric analysis of sample Polymer/silica - PMMA mixture taken in 90/10 ratio, sample S1 in which polymer: silica in the ratio 40:60 (without PMMA) and PMMA were done. Fig.5. shows the combined TGA thermogram of Sample E (90/10), Sample S1 and PMMA.

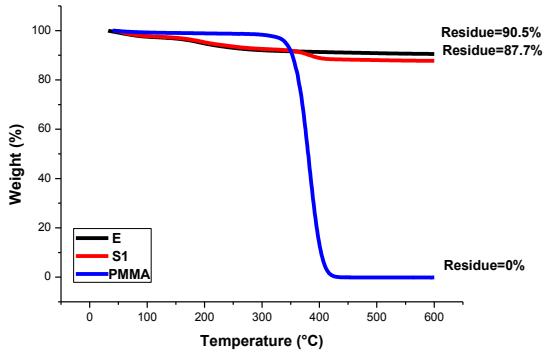


Fig.5. combined TGA spectrum of Sample E, Sample S1 and PMMA

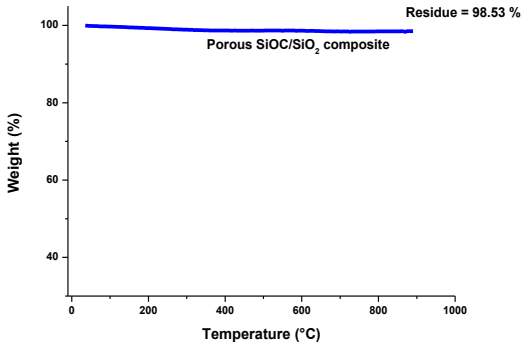


Fig6. TGA spectrum of porous SiOC ceramic.

Table 2. Mechanical properties, Bulk density, porosity and volume shrinkage results.

Sample	Density after ceramization (g/cc)	Compressive strength (MPa)	Flexural Strength (MPa)	Resilience (kJ/cm^2)	Water absorption %	Total Apparent porosity (%)	% Mass Loss	% Volume shrinkage
A (50/50)	0.5290	2.5	1.9	0.3	119	75	54.8	11.8
B (60/40)	0.6558	3.6	3.2	0.32	76	61	44.6	15.3
C (70/30)	0.7779	5.3	4.8	0.43	70	59	37.1	14.4
D (80/20)	0.8436	6.0	5.8	0.44	49	50	27.5	14.4
E (90/10)	0.9930	8.0	7.4	0.58	48	40	15.1	14.9

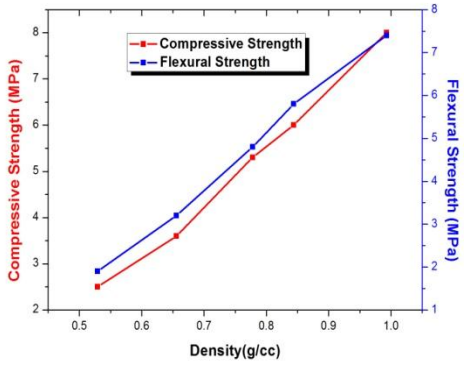
From the TGA analysis it is shown that the decomposition of PMMA occurs in the temperature range between 300°C and 420°C with a maximum decomposition rate at 381^{o}C (Fig. 5). From Fig.5 it is evident that the mass of sample E and S1 at 600^{o}C was nearly the same and the residue remained for Sample E at 600^{o}C is 90.5 % and to that of Sample S1 at the same temperature is 87.7 %.Which indicates that the sample E loses all the PMMA particles at a temperature 200 < T <500^{o}C and the final composition of Sample S1 and Sample E is nearly the same. FTIR analysis data also suggests the same. The high amount of residue remained at a temperature of 600^{o}C supports the high temperature stability of the porous ceramic and applicability as thermal protection system. The Air oxidation resistance of the porous SiOC sample was also determined by using TGA method. The sample showed excellent air oxidation resistance at high temperature of 900 ^{o}C, which is shown by Fig.6.

The bulk density for the porous samples was calculated by mass/volume measurements. Mechanical studies (compressive strength, Flexural strength and

Fig:7SiOC/Silica Porous composite; Plot of density vs compressive strength and density vs flexural strength.

Resilience) conducted for the porous SiOC samples are tabulated in the Table 2.

The plots of density vs compressive strength, density vs Flexural strength and density vs Impact strength are depicted in Figures 7 and 8. The properties of porous materials could be affected by factors, such as types of preceramic polymer, weight% of fillers, types of sacrificial filler, porosity, pore distribution, micro-cracks, and the cross-linking temperature of the pre-form fabrication stage [1].It is seen that these properties increase steadily with density. These porous materials have reasonably good strength. The compressive strength, flexural strength and resilience of low density porous sample A are found to be 2.5 MPa, 1.9 MPa and 0.3 kJ/m^2 respectively.



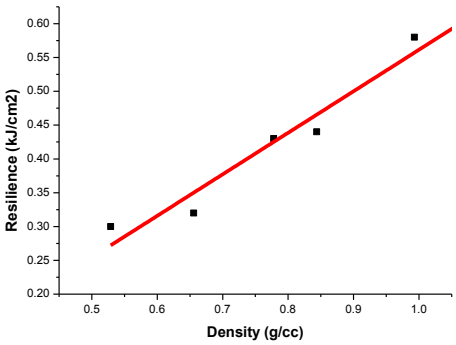


Fig:8. SiOC/Silica Porous composite; Plot of density vs Resilience

The apparent porosity and bulk density are also tabulated in table 2..The apparent porosity is found to be in the range 40-75 % and % water absorption is in the range 119-48 %.The % water absorption for sample A is found to above 100 % indicates a high open pore formation in the matrix. The values of porosity and % water absorption decreases with the decrease in PMMA loading as expected and evident from SEM images.

The mass loss and volume shrinkage of the samples after ceramization was calculated using the formula 1, 2. and tabulate in the table 2, where m_1 and m_2 are mass before and after pyrolysis and v_1 and v_2 are volumes before and after pyrolysis.

$$\% \text{ Mass Change} = \frac{(m1 - m2)}{m1} * 100 \qquad (1)$$

$$\% \text{ volume shrinkage} = \frac{(v1 - v2)}{v2} * 100 \qquad (2)$$

The mass loss and volume shrinkage for the pyrolyzed samples were observed about 55-15 % and 10-15 % respectively. The addition of Silica short fibers reduces the volume shrinkage. The mass loss is within the expected range.

Conclusions

Fabrication of novel ceramic materials from preceramic polymers in controlled atmosphere has been continuously investigated since the last two decades. In this regard, the oxide systems have potential interest in the high temperature application area for components working under harsh atmospheric conditions. In this study preceramic polysiloxane derived SiOC /SiO_2 porous ceramic matrix composite were fabricated using Polymethyl methacrylate powder as sacrificial filler and Silica short fibers as passive filler. The porous SiOC ceramics were exhibits a mass loss and volume shrinkage about 55-15 % and 10-15 % respectively. The addition of silica short fibers imparts mechanical integrity for the ceramic matrix composite and prevents high volume shrinkage during pyrolysis. The mass loss is within the expected range of 50-10 %.The FTIR and XRD analysis suggests the complete amorphous nature of resulted SiOC ceramics. The topology and chemical composition of resulted SiOC ceramic matrix is investigated through SEM-EDX analysis

and the pore morphology is clearly seen from the SEM images. The apparent porosity is found to be in the range 40-75 % and a high water absorption data indicates the nature of open pores in the matrix. The mechanical properties also studied. The porous SiOC ceramics exhibits reasonably good mechanical properties. TGA analysis shows the complete removal of PMMA powder and good thermal stability for the porous ceramics. The porous SiOC sample showed excellent air oxidation resistance upto 1000^{o}C .The good mechanical and thermal properties make porous SiOC ceramic a good candidate for components working under harsh atmospheric conditions such as in space applications.

Acknowledgements

The authors would like to thank the authorities of VSSC for granting the permission to present the work, co-workers of Analytical Division (ANLD) for their kind support, Analytical and Spectroscopy Division (ASD) for thermal and spectral analysis, and Materials Characterization Division (MCD) for SEM analysis.

References

1. B V Manoj Kumar and Young-Wook Kim "*Processing of polysiloxane-derived porousceramics: a review"* Sci. Technol. Adv. Mater. **11** (2010) 044303 (16pp)
2. Narisawa M, Sumimoto R, Kita K, Kado H, Mabuchi H and Kim YW 2009 *J. Appl. Polym. Sci.***114** 2600
3. *Material Safety Data Sheet (MSDS)for YR 3370*
4. Mohammad Mahbubul Hassan, Tatsuhiro Takahashi, Kyohito Koyama "*Preparation and characterisation of Si O C ceramics made from a preceramic polymer and rice bran"* Journal of the European Ceramic Society 33 (2013) 1207–1217
5. R. Riedel, G.Mera, R. Hauser, and A. Klonczynski, *''Silicon-Based Polymer- Derived Ceramics: Synthesis Properties and Applications—A review,''* J. Ceram Soc. Jpn., 114, 425–44 (2006).
6. Jones, R. G., Ando, W., and Chojnowski, J., eds*."Silicon-Containing Polymers: The Science and Technology of Their Synthesis and Applications"*, Kluwer Academic Publishers, Dordrecht, the Netherlands, 2000
7. Colombo, P., Mera, G., Riedel, R. &Soraru, G. D. *"Polymer-Derived Ceramics: 40 Years of Research and Innovation in Advanced Ceramics"*. Journal of the American Ceramic Society **93**, 1805-1837 (2010).
8. H. Zhang and C. Pantano. *"Synthesis and Characterization of SiloconOxycarbide Glasses".* J. of American Ceramic Soc., 73[4], pp. 958–963,1990.
9. Kim Y W, Jin Y J, Chun Y S, Song I H and Kim H D 2005 *Scr. Mater.*

MACRO 514

A Comparative Study on the Piezoelectric Generation in PANI/ZnO/rGO and PANI/ZnO/f-MWCNT Ternary Nanocomposites

[1]T.P.Nisha, [2]L.Ajai Raj, [3]KailasGautham, John Honey *

Dept. of Polymer Science and Rubber Technology, Cochin University of Science and Technology, Kerala-682022, India

** Corresponding author: honey@cusat.ac.in*
[1-3]All authors have contributed equally

Abstract

We report the synthesis, characterization and piezoelectric property evaluation of Pani/ZnO/graphene & Pani/ZnO/f-MWCNT ternary nanocomposites. Polyaniline, graphene and f-MWCNTs are used as conducting supplement fillers, and flexible piezoelectric nanogenerators (FPNG) is fabricated in PU matrix. From the comparative study, it is found that Pani/ZnO/graphene composite exhibits better piezoelectric energy harvesting capacity than Pani/ZnO/f-MWCNT.

Keywords: *Ternary Nanocomposites; Flexible Piezoelectric Nanogenerator, PANI/ZnO/graphene ternary hybrids.*

Introduction

Energy sources for human needs have evolved out from the years of industrial revolution as combustion of fossil fuels to a new modern era of clean technologies such as batteries, hydro and nuclear power plants. Several efforts were made to trap mechanical energy from different sources to power up portable electronic gadgets such as watches, calculators, smartphones, power bank etc. The outstanding mechano-electrical coupling process made nanodimensional scale of piezoelectric energy generation capable to meet the rising demand of energy in such tiny gadgets. It is reported that semiconductors with wurtzite structures like ZnS, ZnO, $BaTiO_3$, CdSe, GaN can replace the conventional way of piezoelectricity generation by electrical poling.As a typical II-VI wide band gap (3.37eV) compound, ZnO has been long studied as a piezoelectric material.[2] The wurtzite structure of ZnO exhibits excellent piezoelectric property along the [0001]-direction because of the noncentrosymmetricstructure[3] which possess three independent piezoelectric coefficients (e_{31}, e_{33}, and e_{15})[4] compared to its zinc blende structure which possess only a single independent piezoelectric coefficient (e_{14})[5]. It is reported that conducting supplement fillers (PANI or MWCNT) when used along with ZnO will enhance its piezoelectric property.[6] Recently Sulthana et al. demonstrated a PANI supplement ZnS Nanorods and PDMS-based flexible nanogenerator for powering up portable electronic devices that avoids electrical poling.[7]

In this work, we are reporting the synthesis, characterisation and piezoelectric property of polyaniline/Zinc oxide/ reduced graphene oxide [PANI/ZnO/rGO] & polyaniline/Zinc oxide/ functionalized multiwalled carbon nanotube [PANI/ZnO/f-MWNT].

Experimental

Chemicals.Zinc acetate dihydrate ($Zn(Ac)_2$. $2H_2O$), polyethylene glycol (PEG, mol. wt. 3,500 – 5,500) sodium hydroxide (NaOH), 98% sulfuric acid (H_2SO_4), 65% nitric acid (HNO_3) are purchased from Merck India. Aniline,30% hydrogen peroxide (H_2O_2), toluene sulphonic acid (TSA), ammonium peroxydisulphate (APS) was recieved from Spectrochem, India. Graphite powder (particle size < 20 μm) is obtained from Sigma Aldrich. Potassium permanganate ($KMnO_4$) from Universal Laboratories, India. MWCNT, Polyurethane (PU), from TCl Chemicals. All chemicals were used as received without further purification.

Synthesis. Wurtzite ZnO nanotops is prepared by a low temperature hydrothermal method by first stirring 0.216g Zinc acetate dehydrate with 100ml 0.05% PEG solution. After 24 h, NaOH solution is added in dropwise till pH of the solution reaches11. It is then transferred to a 100 ml Teflon-lined stainless steel Autoclave and kept in an oven at 100^{o}C for 7 h. The white precipitate obtained is filtered, washed and dried at 100^{o}C under vacuum. GO is prepared by modified Hummers method[8] from Graphite powder on treating with conc. H_2SO_4, $KMnO_4$ and finally with 30% H_2O_2 and water. The dispersion is washed several times with deionised water, centrifuged and dried under vacuum at 60^{o}C. MWCNT is functionalized by stirring 167 ml conc. HNO_3 with 2 g MWCNT for 6 h at 120^{o}C.

Pani/ZnO/rGO composite (in proportion 0.2:0.05:0.05) is prepared by the insitu polymerization of aniline in the presence of ZnO and rGO through chemical polyoxidation reaction. Aniline and APS is added after the complete dispersion of ZnO and GO in 40ml (1M) TSA solution, stirred for 9 h to form the ternary composite and named as PZR. The same procedure is followed for the preparation of Pani/ZnO/f-MWCNT composite, and named as PZC. In addition, to ensure the complete reduction of GO to rGO while polymerization, a small quantity of PZR is post-treated hydrothermally for 7 h, and named as PZRh. All precipitates were filtered, washed and dried in vacuum at 60^{o}C.

Fabrication of FPNG. Each of the prepared ternary composites is first made into a pellet(~0.5mm thickness and ~13mm diametre) and then stacked between Aluminium foils which serves as top and bottom electrodes. It is then connected with two copper wires and the entire system is encapsulated with thin PU layer. Schematics for the preparation of PZR-FPNG is shown in Fig. 1.

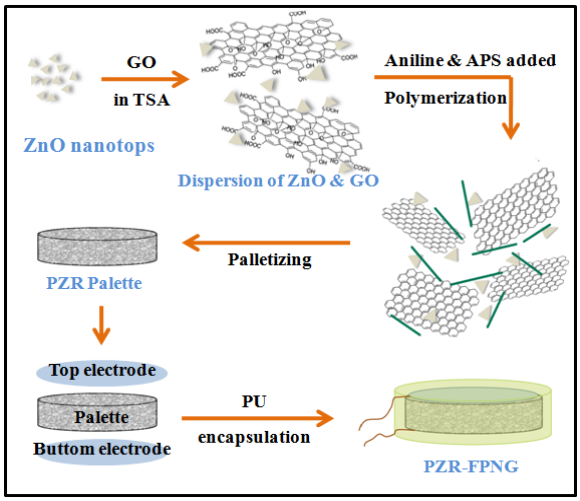


Figure 1. Schematics for synthesis of PZR ternary composite and fabrication of PZR-FPNG

Characterization. Crystallographicshape, structure and size of the prepared samples were investigated by X-ray diffraction (XRD, PANalytical X'Pert Pro) and transmission electron microscope (TEM, JEOL JEM-2100) images. Electrical property was studied using confocal micro Raman Spectrometer (Horiba Jobin Yvon Lab RAM HR), structural features of the samples using fourier transform infrared spectroscopy **(**FTIR) (JASCO FT/IR-4100), optical properties using UV-visible absorption (ThermoScientific Evolution 201), and thermal decomposition patterns using thermogravimetric analysis (TGA, TA Instruments Q50). Resistance of FPNG determined using KeithleyElectrometer/ High Resistance Meter 6517B.

Conductivity Measurements. A certain quantity of weight like 500mg, 700mg, etc. is kept on the FPNG and corresponding resistivity (ρ) is determined. Conductivity (σ) is calculated using the equation $\sigma = 1/\rho*(\ell/a)$ for the palette of thickness, ℓ and circumference, a.

Results and discussion

The XRD diffractogram of the as-synthesized ZnO nanotops are shown in Fig. 2a. All diffraction peaks correspond to the planes of hexagonal wurtzite structure (JCPDS file no. 36-1451). The average

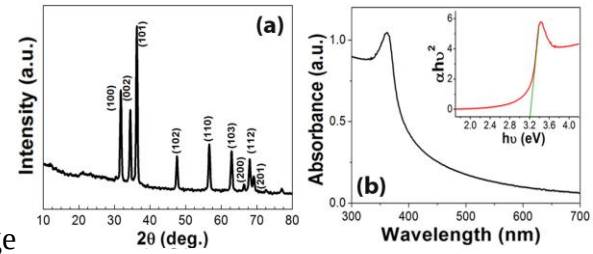


Figure 2. (a) XRD Spectra of as-prepared ZnOnanotops (b) UV-Vis Spectra of as-synthesized ZnOnanotops and inset shows the tauc plot

crystallite size of ZnO is calculated using Scherrer equation and is found to be 24nm. UV-Vis spectra of ZnO (Fig. 2b) shows a sharp absorption peak at 361 nm showing a blue shift relative to the bulk exciton absorption[9] (380 nm) as a result of the quantum size effect; and a band gap of 3.2 eV in the tauc plot (inset of Fig. 2b).

A typical non centrosymmetric wurtzite structure of ZnO is shown in Fig. 3a. As a result of Zn ion sitting slightly off-center inside the unit cell, an electrical polarity develops even in the unstressed condition, thereby turning the unit cell effectively into an electric dipole. A mechanical stress on the crystal further shifts the position of Znion, thus increasing the polarization strength of the crystal (Fig. 3b). Thus ZnO serving as the source of piezoelectric generation.[7]Hence we fabricated PZR, PZRh and PZC ternary nanocomposites of ZnO with the emeraldine salt of PANI and functional materials GO or f-MWCNT as conducting fillers.

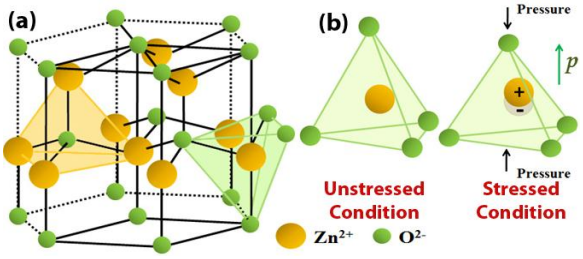


Figure 3. (a) Crystallographic structure of WurtziteZnO (b) Peizoelectric effect in a tetrahedron of ZnO is shown as when stress is applied a dipole moment is created due to the displacement of Zn^{2+} ion within the tetrahedron.

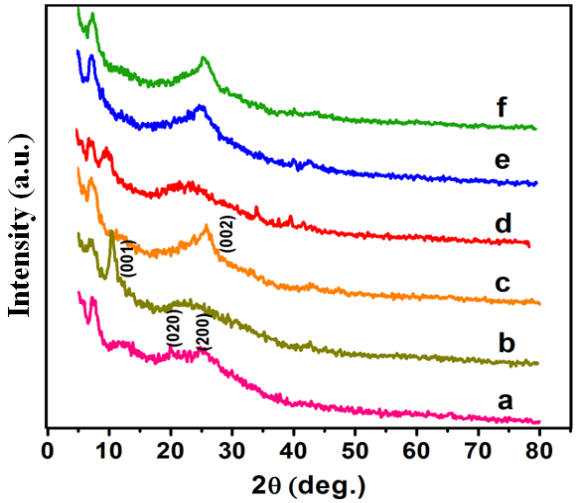


Figure 4. XRD diffractograms of PANI (a), GO (b), f-MWCNT (c), PZR (d), PZRh (e), and PZC (f).

The XRD diffractograms of the prepared samples(Fig. 4)showthat there is a characteristic peak shift of (001) plane from 2θ=10.54º to 25.2ºin PZRh which attributes to the complete reduction of GO to rGO by the hydrothermal treatment. Instead, in PZR there is a peak at 10.38º and at 25.1º corresponding to (001) plane of GO and rGO repectively, which means GO is not completely reduced in-situ by solution polymerization. The characteristic peak of f-MWCNTat 25.7ºforthe (002) plane is shown in Fig. 4e.

The morphology and crystal structures of the prepared samples are studied by TEM images. The TEM micrograph of PZR (Fig. 5a) shows PANI having rod-like structures

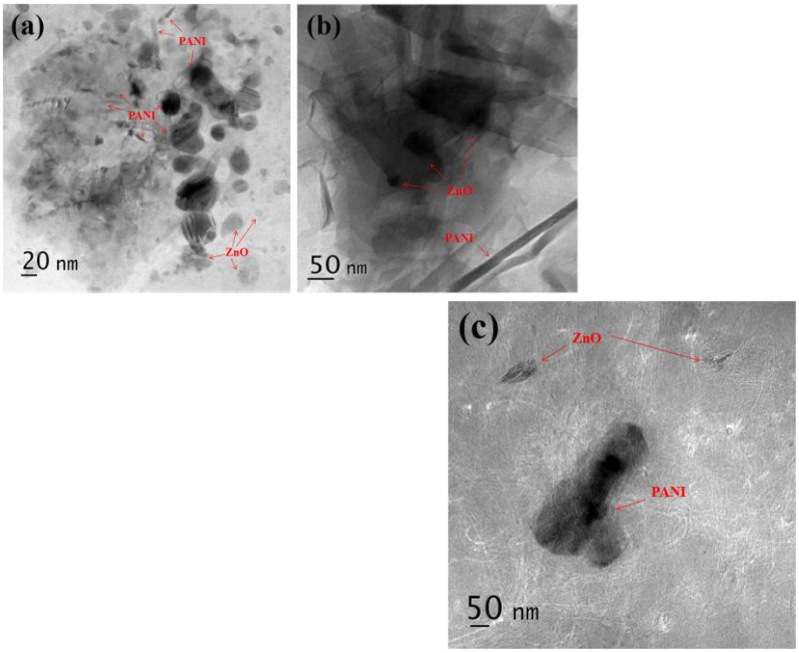


Figure 5.TEM micrographs of PZR (a), PZRh (b), and PZC (c).

and is almost uniformly distributed over the GO sheets along with ZnO. The as-prepared PZRh (Fig. 5b) shows ZnO particles embedded within the transparent sheets of graphene (GO is completely reduced by hydrothermal in-situ polymerization), and PANI is having a fine rod-like structure.The TEM image of PZC (Fig. 5c) shows a uniform distribution of f-MWCNTs along with ZnO and PANI.

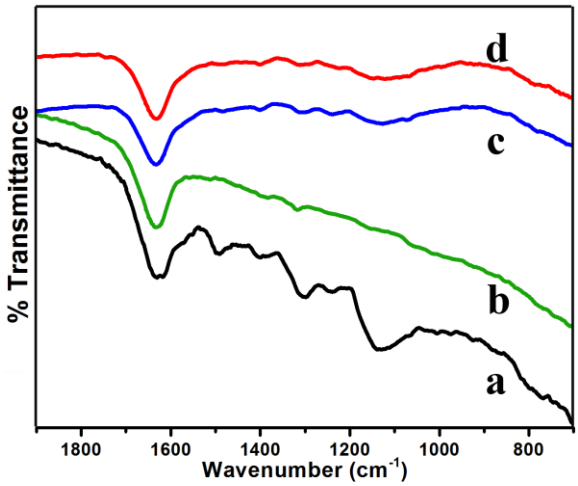


Figure 6.FTIR spectra of PANI (a), PZC (b), PZRh (c), and PZR (d).

Fig.6a shows all characteristicIR vibrations of PANI at 1630, 1484, 1305, 1140 and 571 cm^{-1} corresponding to C=C stretching of quinonoid rings, C=C stretching of benzenoid rings, C-N stretching, aromatic C-H in-plane bending, and C-H out-of-plane vibrations,respectively.[10] All

ternary nanocomposites show the characteristic peaks of polyaniline, but are shifted to higher wavenumber side due to the π-π interaction of polyaniline with the aromatic regions of GO or f-MWCNT. The peaks corresponding to GO & f-MWCNT are significantly reduced in the composite indicating the removal of functional groups of both GO & f-MWCNT during the composite formation.

The decomposition patterns of the samples are studied using thermogravimetric analysis. As shown in Fig. 7, PZC has greater thermal stability giving a residue of ~75.6%, than PZR or PZRh. The major weight loss of all samples is between 180 to 300°C which shows that the samples have maximum efficiency below this temperature range.

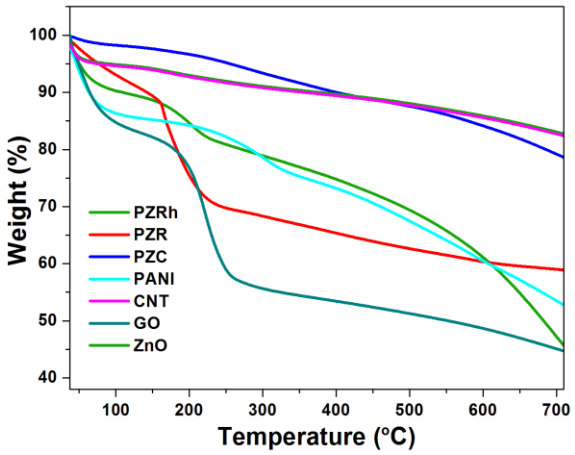


Figure 7. Thermographs of as-prepared samples

To test the piezoelectric property of as-prepared FPNGs, the DC conductivity is measured for different pressure impacts. Figure 8 shows the variation of conductivity on applied pressure. In the case of PZRh-FPNG and PZC-FPNG the conductivity is increased with increase in stress. It is clear that the conductivity in PZRh-FPNG (9.95 x 10^{-6} S/cm) is almost double than in PZC-FPNG (4.303 x 10^{-6} S/cm), for a pressure of 30.1Pa, corresponding to a weight of 1000 mg. The better response of PZRh-FPNG may be due to the better dispersion of ZnO within exfoliated graphene layers and the better interactions with. The response of PZR-FPNG is too low to report.

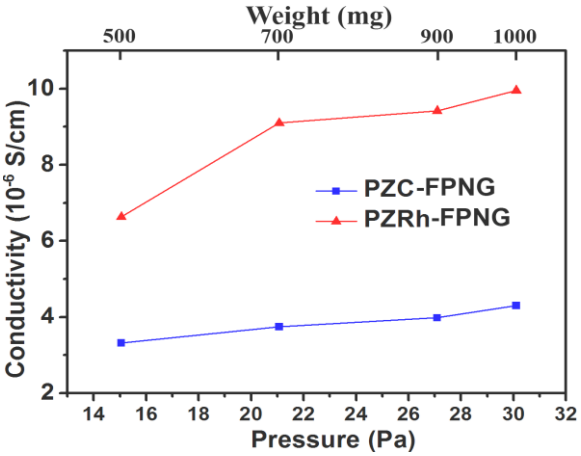


Figure 8. Dependence of conductivity on pressure corresponding to definite weights.

Conclusions

In summary, ZnOnanotops are synthesized via a low temperature hydrothermal method, and the flexible piezoelectric nanogenerators are fabricated with polyaniline/graphene and polyaniline/f-MWCNT, encapsulated in PU matrix. Conductivity in FPNGs increased with increase in stress. Both PZRh-FPNG and PZC-FPNG are expected to be potential tools in nanostructure based energy harvesting because of their excellent flexibility, robustness, durability and cost-effectiveness.

Acknowledgements

Authors are thankful to Prof. Dr. M. Jayaraj, for providing instrumental facilities in Advanced Materials Centre, Department of Physics, CUSAT.

References

[33] (a) J. M. Wu, C. C. Kao, *RSC Adv*., 4, 13882, 2014; (b) J. Song, J. Zhou, Z. L. Wang,*Nano Lett*., 6, 1656, 2006; (c) Z.-H. Lin et al, *J. Phys. Chem. Lett*., 3, 3599, 2012; (d) L. Dong, et al,*Adv. Mater*., 24, 5470, 2012 (e) L. Lin et al, *Nanotechnology*, 22, 475401, 2011.

[34] (a) Z. L. Wang, et al.; *Science* 312, 242, 2006; (b) Z. Fan et al,*J. Nanoscience& Nanotechnology*, 5, 1561, 2005; (c) S. R. Anton, H. A. Sodano,*Smart Materials and Structures*, 16, R1-21, 2007.

[35] Z. L. Wang, *J. Mater. Chem*., 15, 1021–1024, 2005.

[36] M. Catti, Y. Noel, R.Dovesi, *J. Phys. Chem. Solids*, 64, 2183−2190, 2003.

[37] D. Moore, Z. L. Wang, *J. Mater. Chem*., 16, 3898−3905, 2006.

[38] H. Sun et al, *Nanoscale*, 5, 6117–6123, 2013.

[39] A. Sulthana et al, *ACS Appl. Mater. Interfaces*, 7, 19091-19097, 2015.

[40] M. K. Kavitha, Suresh C. Pillai, PramodGopinath, Honey John, *J. Environ. Eng*., 3 1194, 2015.

[41] Z. Wang et al,*Langmuir* 20 (2004) 3441.

[42] T. Remyamol, J. Honey, G. Pramod, *Synthetic Metals*, 185-186, 38-44, 2013.

MACRO 517

Kinetics And Regioselectvity Of Phenol-Formaldehyde Reaction; New Insights

*Praveen Kumar Solasa[a], S.K.Manu[b], VijendraKumar[c], AncySmithaAlex[d], C.P ReghunadhanNair[e]

[a] *Scientist/Engineer, Propellant Fuel Complex, CSG, PCM Entity*

[b]*Deputy General Manager, Propellant Fuel Complex, CSG, PCM Entity*

[c]*Scientist/Engineer, Analytical Division, CSG, PCM Entity*

[d]*Scientific Assistant, Analytical Division, CSG, PCM Entity*

Vikram Sarabhai Space Centre, ISRO, Thiruvananthapuram-695 022

[e]*Visiting Professor, Cochin University of Science and Technology, Kochi – 682 022*

**e-mail id: pksvssc@gmail.com*

Abstract

In this study, we attempt to investigate the kinetics and reaction mechanism of formation of resole type phenolic resin using a base catalyst, at different temperatures. Experiments were carried out for a given molar ratio of phenol to formaldehyde at varying temperatures *viz*; 60, 70, 80 and 90^{o}C in a precisely temperature controlled sealed jacketed vessel. Samples were analyzed for free formaldehyde content, refractive index, moisture content and ortho para ratio by Nuclear Magnetic Resonance (NMR) spectroscopy. Reaction is continued till complete consumption of formaldehyde. Data were analyzed for the extent of the reaction as a function of concentration of formaldehyde. Rate constants (k) and activation energy for the reaction were evaluated. It was found that the order of the reaction with respect to the formalin was 1 and that w r t phenol is near zero. i.e the reaction followed a pseudo first order kinetics. Activation energy of the reaction was found to be 113.0 kJ/mole with respect to formaldehyde in this case. NMR data correlated reasonably well with kinetic data. Activation energy with respect to Ortho formation was found to be 78.0 kJ/mole.

Refractive index analysis to check the progress of the reaction beyond formation of methylol confirmed progress of chain extension reaction beyond methylolation reaction.

Key Words: *Phenolic resin, resole, kinetics, NMR*

1.0 Introduction

Silica and Phenolic composites are used as ablative liners for various rocket engine nozzles, heat shields, re-entry bodies and nozzle liners. Phenolic matrix composites provide superior ablative characteristics, high char yield, retention of strength, modulus and mechanical properties at elevated temperatures.[1,2,3,4] Silica phenolic composites for use in liquid engines have to withstand very high thermal resistance while retaining mechanical properties for long duration. To meet these requirements, a special grade resole type phenolic resin capable of high carbon yield and char strength coupled with remarkable thermal resistance was developed by VSSC in early 80's.

Phenolic matrix composites are the preferred thermo-structural materials for aerospace applications in view of their excellent processability, thermal and ablative characteristics. The phenolic polymers though known since very long, the resin chemistry is still not unambiguously established. The reactivity, product distribution, cure mechanism, properties, particularly the thermal characteristics all depend on polymerisation reaction.

A proper understanding of the relative reactivities of ortho para substituion during methylol formation is the first step.Though several studies have been devoted to this area, a comprehensive study addressing issues related to the region-selectivity of the reactants for the formation of resole is missing. This aspect is addressed here.

2.0 Experimental

2.1 Materials

Reactants used for conducting the experiments were Phenol (Purity > 99.0%) and Formalin (Concentration ~ 37%). Sodium Hydroxide (Purity > 98.0%) was used as base catalyst and Acetic Acid (Purity > 98.0%) was used for neutralization of base to a particular pH (7-8).

2.2 Experiment details

Experiments are carried out for a given molar ratio of phenol to formaldehyde (P:F = 1.12 : 1) at varying temperatures,*viz* 60, 70, 80 and 90 ^{o}C respectively in a precisely temperature controlled sealed jacketed vessel. Samples were withdrawn at various time intervals during the course of the reaction.

Samples were analyzed for free formaldehyde content, refractive index, moisture content and ortho para ratio by Nuclear Magnetic Resonance (NMR) spectroscopy. Reaction was ~~is~~ continued till complete consumption of formaldehyde. Data were analyzed for the extent of the reaction as a function of concentration of formaldehyde. Rate constants (k values) and activation energy for the reaction at the prescribed temperature were also evaluated.

2.3 Process

Approximately 750 g. of raw materials are charged as per the stoichiometry for a given molar ratio in a four necked round bottom flask (reaction vessel) of capacity 1000 ml. The temperature of the reaction mixture is controlled by placing the reaction vessel in a sealed jacketed vessel containing water and the jacketed vessel was connected with the refrigerant circulating bath to ensure precise temperature control. A condenser with water circulation was employed for vapour condensation during the reaction. To ensure homogeneity of the reaction mixture, stirrer was placed and maintained at 150 rpm. A digital thermometer was introduced to monitor the temperature of the reaction medium. Details of the reaction setup is shown in Figure1.

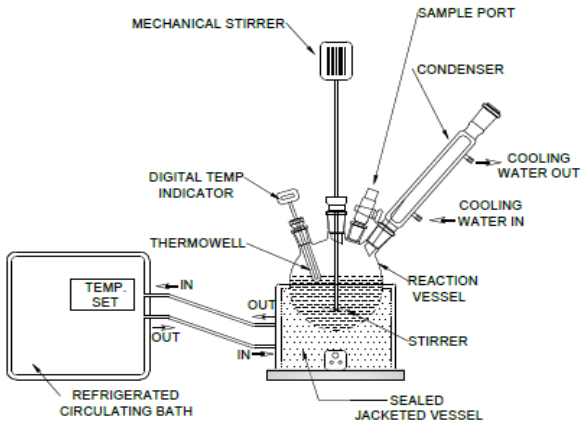


Figure 1: Experimental set up for Phenol Formaldehyde polymerisationreaction

2.4 Estimation of kinetic parameter

Samples for analysis of various parameters were collected from the reaction mixture throughout the experiment. During kinetic data estimation, correction factor in terms of the time required to reach the desired set temperature is also accounted. Hence, the time scales are proportionately adjusted to get the proper kinetic estimation. Generalized n^{th} order reaction is considered for kinetic data estimation. Equation is described as follows

$$-da/dt = k(1-a_f)^n(1-a_p)^m \quad \text{-------(1)}$$

Where;

a - overall monomer concentration

t - time

k - rate constant

a_f - concentration with respect to formaldehyde

a_p - concentration with respect to phenol.

n – order of the reaction with respect to formalin and m – order of the reaction with respect to phenol. Since, free phenol could not be estimated during progress of the reaction, equation of reaction progress with respect to the concentration of the formaldehyde is modified as follows.

$-da/dt = k (1-a)^n$ ---------(2)

Where, a – concentration with respect to formaldehyde

By taking the logarithm of the above equation,

$$- \ln (da/dt) = \ln k + n \ln (1-a)$$

By plotting ln(da/dt) against ln(1-a) , order of the reaction, n and rate constant, k of the reaction are determined. Rate constants are determined by the above procedure at four different temperatures. *Viz*;60, 70, 80 and 90 ^oC.

Estimation of the Activation Energy

The Arrhenius equation gives the quantitative basis of the relationship between the activation energy and the rate at which a reaction proceeds. The Arrhenius equation is expressed as

$$k = Ae^{-Ea/RT}$$

where*A* is the frequency factor for the reaction, *R* is the universal gas constant, *T* is the Temperature (in Kelvin), and *k* is the reaction rate coefficient. While this equation suggests that the activation energy (*Ea*) depends on the Temperature, in regimes in which the Arrhenius equation is valid. E_a can be evaluated from the reaction rate coefficient at any temperature (within the validity of the Arrhenius equation).

Logarithm of the above equation is

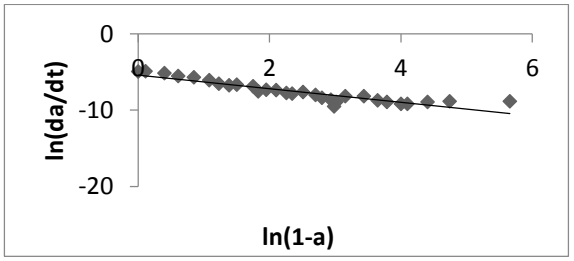
$$\ln (k) = \ln (A) + (-Ea/RT)$$ ---------(3)

From the Plot of ln (k) vs 1/T, activation energy is derived.

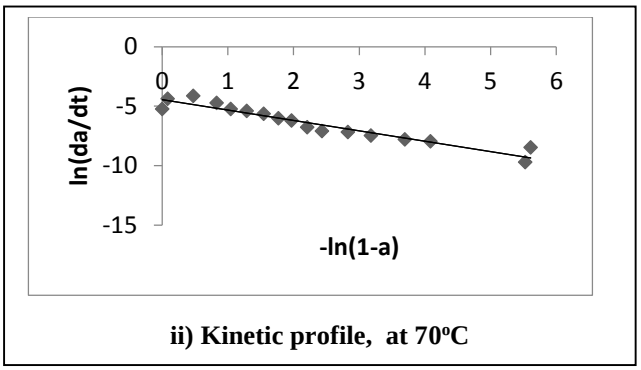
3.0 Results and Discussions

3.1 Kinetics with respect to Formaldehyde

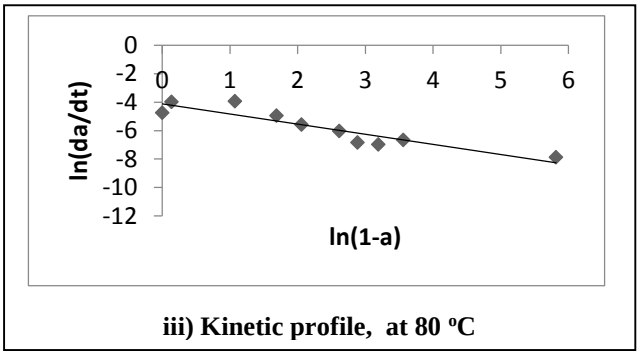
Kinetic profiles with respect to formaldehyde at different temperatures are given in the Figure 2. Order and rate constants obtained are given in the Table 1.



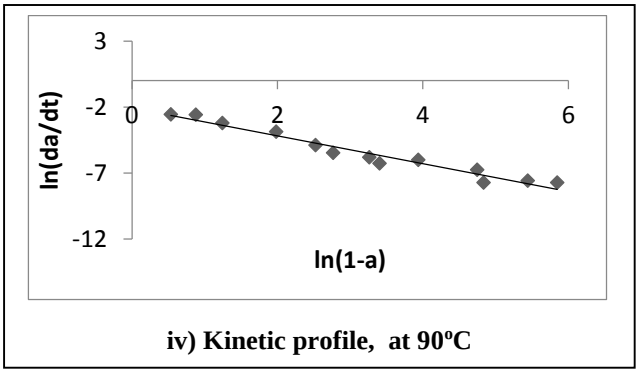
i) Kinetic profile, at 60^{o}C



ii) Kinetic profile, at 70ºC



iii) Kinetic profile, at 80 ºC



iv) Kinetic profile, at 90ºC

Figure 2: KineticProfiles with respect to extent of Formaldehyde consumed (a) at varying temperatures i) 60 ºC ii) 70 ºC iii) 80 ºC iv) 90 ºC

Table 1: Order and rate constants with respect to Formaldehyde

Temp (ºC)	n	ln k	k (min^{-1})
60	1.03	-5.12	5.98×10^{-3}
70	0.97	-4.28	13.84×10^{-3}
80	1.28	-2.68	68.56×10^{-3}
90	1.04	-2.14	117.65×10^{-3}

From the above table, it is inferred that the order of the reaction with respect to formalin is one at all temperatures. The rate of the reaction increases with increase in temperature, which is evident from the rate constant values varying from 5.98×10^{-3} to 117.65×10^{-3} min^{-1} for a Temperature increase by 30ºCi.e from 60ºC to 90ºC. The rate of reaction is increased by almost 20 times. Graph of 1/T vs ln k to determine the activation energy is given in the Figure 3.

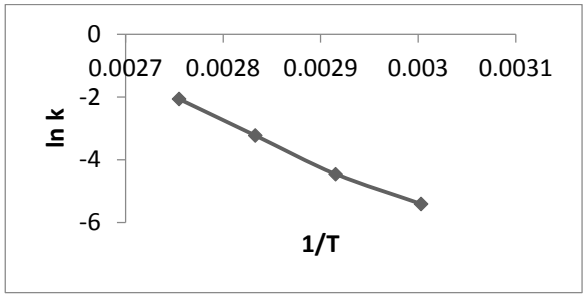


Figure 3: Plot of 1/T vs ln k with respect to Formalin

Activation energy with respect to the formaldehyde which is limiting reactant is found to be as 113.0 KJ/mole in this case.

3.2 Kinetics with respect to phenol

Calculations were done with an assumption that one mole of phenol reacts with three mole of formalin. Order and rate constants obtained are given in the Table 2. Activation energy is found to be 1.4 kJ/mole.

Table 2: Order and rate constants with respect to Phenol

Temp (°C)	n	ln k	k (min^{-1})
60	0.009	0.003	1.003
70	0.016	0.007	1.007
80	0.028	0.013	1.013
90	0.105	0.048	1.049

From the Table 2, it is inferred that the order of the reaction with respect to phenol (assumption) is not reasonable in lieu of reactions expected. Since phenol is present in large "effective" molar ratios, the order of the reaction w.r to phenol is zero order. In other words, the over all reaction is pseudo first order as the concentration of phenol is nearly buffered. Under these conditions the phenol molecules do not require special activation and the rate determining step is the addition of formaldehyde to phenol only. An important outcome of the study is that by following the rate of change in concentration of formaldehyde the whole of the kinetics for this particular formulation can be followed. The high pH promotes hydroxymethylation whereas lower pH condition promotes poly condensation of the formed methylols. As compared to mono hydroxymethylation all auxiliary reactions occur at higher rates, making the kinetics with respect to phenol more complex. The hydroxymethylation at ortho and para position of phenol play a key role in altering the product properties. Ortho product prefers to continue hydroxymethylation whereas para product takes part in poly condensation. Also, further reactions (substitution and condensation) of dihydroxydiphenyl methane proceeds at higher rate as compared to phenol.

3.3 Refractive Index

It is observed that the refractive index increases during the progress of the reaction. Moreover refractive index also increases with increase in temperature showing the reaction with respect to further condensation advancing with respect to time and temperature.

3.4 Estimationof methylol

Based on the water formed during the course of the reaction, extent of methylol condensed to form water was calculated. No definite trend is observed in the methylol condensation during the course of the reaction and at varying temperature. There is a possibility of separation of water layer from the polymer layer due to difference in the density and miscibility.

3.5 Estimation of Para and Ortho formation

Samples were analyzed for ortho and para fractions of the product formed during the course of the reaction at different temperature. Activation Energy with respect to the ortho product formed is 78.0 KJ/mol. Activation Energy with respect to the Para product formed could not be calculated precisely.

Reaction profile prediction

The conversion at any time t and temperature T can be represented by the equation

$d\alpha/dt = Ae^{-E/RT}(1-\alpha)$

Integration gives

$Ln(1- \alpha) = [Ae^{-E/RT}]_x t$

This equation helps us predict the reaction profile at a given temperature and time.

4.0 Conclusions

Kinetic parameters were estimated for resole type phenolic resin by conducting experiments at varying temperature. Order of the reaction with respect to the formalin was 1, irrespective of temperature. From the Kinetic parameter estimation, rate constant of the reaction is found to be 113.0 KJ/mole. The apparent order of the reaction w. r. to phenol is zero and the entire kinetics is driven by the concentration profile of formaldehyde. The reaction is pseudo first order. Refractive index analysis was done as supporting information to check the progress of the reaction beyond formation of methylol and it is observed that refractive index of the solution mixture increase with extent of reaction showing a progress in chain extension / polymerization reaction. The rate constant of ortho fraction k_{ortho} has been calculated with the data generated using NMR analysis and the activation energy with respect to the ortho product formed is 78.0 kJ/mol. No definite trend observed in the methylol condensation during the course of the reaction and at varying temperature. With the available data, it is possible to predict the reaction profile till exhaustion of the limiting reactant, formalin.

Acknowledgements:

Authors are sincerely thankful to Dr. S.C Sharma (DD, PCM) and Dr. S A Ilangovan (GD,CSG) for their support and encouragement.

References:

[1] Peer, H.G., The Reaction of Phenol with Formaldehyde, Rec.Trav.Chim., Vol. 78. Pp. 841-863, 1959

[2] Zavitsas, A.A., Base CatalyzedHydroxymethylation of Phenol by aqueous Formaldehyde. Kinetics and Mechanism, Journal of Polymer Science: Part A-1, Vol 6, pp. 2533-2559, 1968

[3] Atthajariyakul, S., Vanichseni, S., Development of A Kinetic Model for Resole Type Phenolic Resin Formation, Thammasat Int. J. Sc.Tech., Vol.6, No.3, 2001

[4] Marie, F.G.L., Stephane, L., Philippe, G., Jean, P.L., Didier, B., Phenolic Resins: 1. Mechanisms and kinetics of Phenol and of the first polycondensates towards formaldehyde in solution, Polymer, Vol. 35, No. 14, 1994

MACRO 518

ELECTROSPUN POLYURETHANE FIBRES REINFORCED RESORCINOL-FORMALDEHYDE COMPOSITES

S. Kiran,* N.R James

Department of Chemistry, Indian Institute of Space Science and Technology

Thiruvananthapuram – 695 547, Kerala, India

** e-mail id: kirans2779@gmail.com*

Abstract

The use of polyurethane electrospun nanofiber mats as reinforcement with synergistic effect in mechanical properties of resorcinol−formaldehyde (RF) resin is investigated in this work. Effect of wetting procedure for reinforcing the fiber mat by RF resin, on the morphology and mechanical properties of the composites is highlighted. The wetting of polyurethane fibers by passing through a solution of RF resin showed a core−shell morphology and a significant improvement in properties.

Keywords: *nanofibers. electrospinning; nanocomposites; mechanical properties.*

Introduction

Composites are one of the most fascinating and popular materials known to human. Among the different classes of composite materials, fiber reinforced polymer composites (FRP) play a crucial role in civil infrastructure and high-tech equipment for aerospace industry, military industry, civil engineering area and so on.[1,2] Reinforcing fibers for traditional fiber reinforced composites usually come from the natural, glass, carbon, aramid and nylon fibers, which often have big diameter in the range of tens to hundreds micrometers.[3,4] However, when the fiber diameter decreases from micrometers (10-100 μm) to submicrons or even nanometers (1000×10^{-3} - 1×10^{-3} μm), the fibers will present enhanced characteristics[5,6] and provide amazing properties forthe composites. It is readily obvious that the specific surface area increases dramatically as the fiber diameter approaches the nanometer scale.[7]This is a key factor in improving nanofiber-matrix interface adhesion and providing effective load-transfer from the matrix to the nanofibers. Furthermore the nanofiber has much higher aspect ratio (length to diameter, L/d) than that of microfiber. This is also one of the advantages in using nanofiber as reinforcement.

Recently, polymer nanofibers produced by electrospinning have been attracting more and more attention for the preparation of composites. The continuous long fibers produced by electrospinning do not exhibit fiber edges (ends) and therefore lack stress concentration points in composites. During the electrospinning, the polymer molecular chains tend to align along the fiber axis as the polymer jet is drawn up to 100000 times in less than 0.1 s. These highly oriented nanofibers can act as fillers for the preparation of fiber reinforced composites. Also, in most cases,

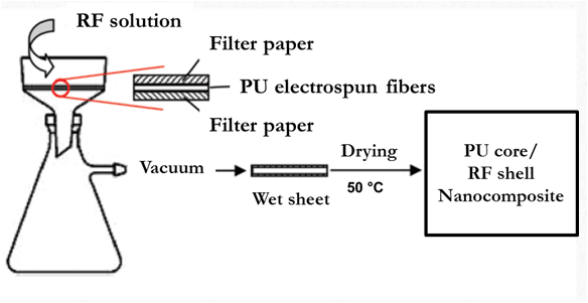
electrospunnanofibers are collected in the form of a random aligned nonwoven mat with high porosity and large specific surface area. Therefore, the nanomat can be impregnated effectively with the resin solution and could make a remarkable improvement regarding the fracture toughness compared to the bulk film counterpart.6 However, development of composites based on electrospun nanofibers as reinforcement is still in its infancy with just a few countable reports in the literature which involves the usage of Nylon-6 nanofibers produced by electrospinning. These nanofibers with excellent mechanical properties, such as toughness and high tensile strength, have been adopted to make composites with poly (methyl methacrylate),[8] poylaniline,[9] polycaprolactone,[10] andwith bis-glycidyl methacrylate/tetraglycidylmthacrylate. In this work, we highlight the use of PU nanofibers for preparing composites having improved thermal and mechanical properties with resorcinol-formaldehyde (RF) resin.

Experimental

Materials

PU, with the trade name of Carbothane manufactured by Lubrizol Corp., was used in this study. Resorcinol, formaldehyde, dimethylformamide (DMF), tetrahydrofuran (THF) and sodium hydroxide were supplied by Merck, Germany. All the materials were used as received without further purification.

Electrospinning and preparation of composite.



Polyurethane was dissolved in DMF/THF (50/50, w/w) to form an electrospinning solution with a concentration of 12 wt%. During electrospinning, 8 kV electrical potential was applied on the tip of the needle while the distance between the needle tip and the collector was20 cm. The polymer solution was delivered by a syringe pump at a feeding rate of 2 mL/h, and the polyurethane nano-fibers were collected on a cylinder, which rotated at 1000 rpm. The resulting nano-fiber was dried in a vacuum oven at 37 °C for 12 h. The dried nano-fiber mats were further used for the preparation of resorcinol−formaldehyde composites. RF solutions were passed through the fiber mats; i.e., a process similar to liquid filtration (Figure 1). The electrospunnano-mat is kept between two whatman qualitative filter papers (Grade 1, 11 μm) in a suction filtration flask, and RF solutions (solvent) of different concentrations (5,10,20 and 30% w/v) were passed under vacuum (about 20 bar). After wetting of the fibers, the sheets were dried at 50 °C for 12 h.

Results and discussion

Electrospinning is a fast and effective technology to prepare nanofibers with a diameter distribution from several to hundreds of nanometers.[11]In this work, polyurethane nanofibers were electrospun from 12wt% PU THF/DMF solutions. They comprised a smooth surface, a random alignment, and a centralized diameter distribution. As shown in Figure 2, the diameter of nanofibers is mainly distributed from 650 ±221 nm and no defects such as beads, pores, or ribbons were found.

Electrospun nanofiber reinforced composite was prepared by liquid filtration as shown in Figure 1. Polyurethane nanofiber mats were impregnated with different concentration of RF solution (5-30 %) to obtain PURF composites with varying RF concentration.

Figure 1. Schematic of the process for preparing PURF nanocomposites by passing a RF solution through the PU nanomat

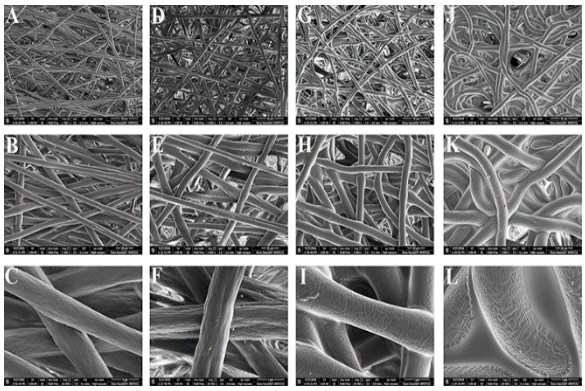


Figure 2. SEM images of (A,B and C) PU fibers, (D, E and F) RF/PU composites prepared by immersion into a RF solution of a concentration of 5 wt %, (G,H and I) RF/PU nanocomposite made by immersion into a RF solution of a concentration of 20 wt % and (J, K and L) PURF nanocomposite made by immersion into a RF solution of a concentration of 30 wt %.

SEM images of the nano-fibers and the composites are depicted in Figure 2.They exhibited quite different morphologies depending on the concentration of the RF solution used. SEM analysis revealed that coating by liquid filtration method led to deposition of RF resin on fibers and the whole PU mat was completely wetted without cracks and inhomogeneous wetting with respective diameter of about 650 ±221 nm for PU, 680±171 nm for PURF5, 688±108 for PURF10, 688±154μm for PURF20 and about 700±151 μm for PURF30. SEM pictures clearly showed the advantage of passing RF solution through PU mat by liquid filtration procedure. The RF solution provided complete coating of fibers and furthermore the shell of RF resin glued the fibers together and strengthened the interface between matrix (RF resin) and the reinforcing fiber (PU) in composites

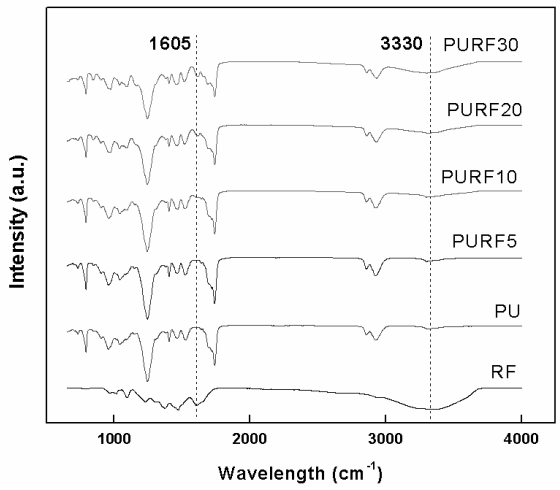


Figure 3. FT-IR spectra of composites with different concentration of RF concentration

The FT-IR spectra of the PU, RF and PURF (5-30) after filtration with different concentration of RF are presented in Figure 3. The broad absorption band at 3321–3541 cm^{-1} (bonded –OH str.) signifies the existence of phenolic –OH (due to resorcinol) groups in PURF. The absorption band at 1643– 1654 cm^{-1} (C–C str.) verifies the presence of aromatic ring in the samples
and confirms the presence of resorcinol-formaldehyde coating of the samples. Furthermore, some of the prominent peaks of PU can be seen at 1535 cm^{-1} due to N-H bending + C-N stretching,1242 cm^{-1}due to -C-O-C stretching and C-O-C stretching at 1102 cm^{-1}.

Table 1: Mechanical properties of fiber reinforced composites

Sample	Tensile Strength (MPa)	Modulus (MPa)	Elongation at break %
PU	8.2±1.2	3.2±0.4	368±28
PURF5	10.3±0.22	4.1±1.1	416±15
PURF10	12.8±1.4	4.9±0.8	400±22
PURF20	15.5±0.44	6.2±0.45	358±18
PURF30	11.3±0.66	6.8±1.2	265±26

The mechanical properties of PURF nanofiber composites coated with different amounts of RF made by above reported method were measured. The tensile properties are presented in Table 1. The pure electrospun PU nanomat (blank) exhibited a tensile strength of 8 MPa strength and elongation at break of around 368%. The PURF composite coated with 20 wt % of RF showed higher tensile strength of 15.5 MPa and elongation at break of about 358%. The reinforcement with PU nanofibers showed a synergistic effect regarding the tensile strength of the resulting composites with a value higher than those of PU nanofiber mats on RF resin. Further, a decrease in tensile strength and elongation at break on increasing the RF content in the composites was detected, but the tensile strength is always higher compared to that of pure PU nanofiber mats. The PU nanofibers were nonaligned and randomly distributed in the composites as shown in the Figure 2. During tensile testing, the stretching force was taken by reinforcing PU fibers and the friction between fibers helped in delaying composite failure and resulted in the overall improved mechanical property of resultant composites.

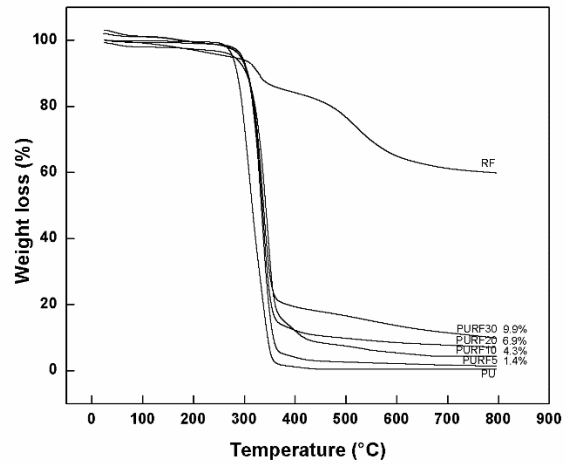


Figure 4. Thermal stabilities of pure RF resin, PU nanofiber sheets, and PURFnanocomposites with different concentration of RF

Thermal degradation studies of polymer composites are of supreme importance since they may come across elevated temperatures during processing and service. Thermal stability of the PU, RF and PURF composites were analyzed using TGA under a nitrogen atmosphere. Multistage weight loss was observed in the case of RF which involves evolution of water, unreacted oligomers and small groups at RT-350°C followed by the degradation of the resorcinol–formaldehyde from 350-550°C. An enhanced thermal stability was observed in the case of PURF composites which can be attributed to the presence of RF which is more thermally stable than PU. TGA analysis of PU revealed its thermal stability to be about 265°C. But the incorporation of RF has further improved the thermal stability of composite to about 297°C and significantly improved the char yield of the composite to about 9.9% on coating with 30% RF solution

Conclusions

PURF composites were prepared using electrospun PU mats as reinforcement. Filtration of RF solution through electrospun fibers provided complete coating of fibers and furthermore the shell of RFresin glued the fibers together and strengthened the interface between matrix (RF resin) and the reinforcing fiber. The reinforcement in mechanical properties of the RF resin could be seen using PU nanofiber mats. The fiber reinforced composites showed enhanced mechanical properties and thermal properties in comparison to those of pure PU nanomats and the RF resin.

Acknowledgements

The authors wish to thank Director, IIST for the laboratory facilities provided for this work.

References

48. C. Bakis, L.C. Bank, V. Brown, E. Cosenza, J. Davalos, J. Lesko. J Compos Constr. 6(2), 73, 2002
49. S. Chand, J. Mater. Sci. 35(6), 1303, 2000.
50. A. DiBenedetto, Mater Sci Eng A. 302(1), 74, 2001.

51. M. Jawaid, H. Abdul Khalil, Carbohyd Polym. 86(1), 1, 2011.
52. Z.M. Huang, Y.Z. Zhang, M. Kotaki, S. Ramakrishna, Compos. Sci. Technol. 63(15), 2223, 2003.
53. A.Zucchelli, M.L.Focarete, C.Gualandi, S.Ramakrishna, Polymer. Adv. Tech. 22(3), 339-349, 2011.
54. P. Gibson, H.Schreuder-Gibson, D. Rivin, Colloids Surf, A. 187, 469, 2001.
55. L.S. Chen, Z. M.Huang, G.H. Dong, C. L. He, L. Liu, Y. Hu. Polym. Compos. 30 (3), 239, 2009.
56. A. Romo-Uribe, L. Arizmendi, M.E. Romero-Guzman, S. Sepulveda-Guzman, Cruz-Silva. ACS Appl. Mater. Interfaces 1(11), 2502, 2009.
57. R. Neppalli, C. Marega, A. Marigo, M. P. Bajgai, H. Kim,V. Causin, Polymer 52 (18), 4054, 2011.
58. A. Greiner, J.H. Wendorff, Angew. Chem. Int. Ed. 46(30), 5670, 2007.

MACRO 520

A combined theoretical and experimental investigation on the effect of microphase separation on shape memory behavior of polyurethane

E. Swathi,[a,b] R. Rakesh,[a] S. Titus[a] and K.G. Sreejalekshmi[a]*

[a] *Department of Chemistry, Indian Institute of Space Science and Technology, Valiamala Post, Trivandrum-695547, India*

[b] *Department of Metallurgical and Materials Engineering, Indian Institute of Technology Madras, Chennai-600368, India*

** e-mail id: sreeja@iist.ac.in ; sreejalekshmi@gmail.com*

Abstract

Shape memory effect in physically crosslinked shape memory polymers are critically controlled by crystallisation of soft segments and H-bonding among hard segments. We investigated morphological importance and contribution of each segment towards shape memory properties of polyurethane (PU), both computationally and experimentally. Extent of phase separation and phase mixing among hard and soft segments were predicted from bond distances of H-bonded carbonyls [hard–hard segment H-bond (N–H···O=C)] and between N–H group and ether oxygen (N–H···O) [hard-soft segment] interactions. Frequency shifts were computed from vibrational frequencies and stability was determined using localized pseudospectral methods (PS-LMP2). Synthesis of PU combinatorially using polyethylene glycol (PEG), toluene diisocyanate, 4,4'-methylenebis(phenyl isocyanate) (MDI), butane-1,4-diol and ethylene diamine (EDA) led to property tuning and samples were characterized by IR, NMR, POM, XRD, DSC, DMA and AFM. An improvement in phase separation resulted by incorporating PEG6000 (high short segment length), MDI (increased symmetry) and EDA (enhanced H-bonding interactions). PEG6000_MDI_EDA showed elongation at break of 340%, tensile strength

11MPa, shape recovery ratio 96.4% and fixity ratio 51.4%. PU actuator was successfully demonstrated as circuit breaker in an electric circuit.

Keywords: *shape memory polymer; polyurethane; phase separation; computational*

Introduction

Microphase separation which leads to thermodynamic phase incompatibility and phase coarsing are the key factors in determining shape memory properties, especially shape recovery and shape fixity of a physically crosslinked block copolymer showing shape memory effect (SME).[1-5] Among various polymers, polyurethane (PU) whose transition temperature can be tailored over a wide range and properties be adjusted by modification of composition[6] could be an effective model to study the effect of phase separation on thermal, mechanical and shape memory properties.[1] In addition, flexible molecular design and network structure, pseudo-elastic behavior and thermal shape memory effect, better biocompatibility and processability and most importantly higher shape recoverability has led to extensive research in PU. In shape memory polyurethanes (SMPUs), better phase separation is achieved when the phase structure has discrete hard domains dispersed within a soft segment matrix. The possibility of optimal H-bonding between hard segments (HS) as well as crystallinity of soft segments[2,7] are the driving forces for phase separation since HSs aggregate via strong hydrogen bonding to form stable, dispersed domains, acting as physical crosslinks while soft segments are semi-crystalline or rubbery matrix responsible for shape-memory behavior.[2,8] Therefore, precise control of composition and structure of hard and soft segments, mainly soft segment length (SSL) and hard segment content (HSC) is a prerequisite to cater to the conditions demanded by various applications.[8-11] Majority of research to improve shape recovery of thermoplastic SMPUs mainly focused on achieving maximum crystallization of the HS, adding nano-fillers to strengthen the hard domains by physical interaction with HSs or incorporating mesogenic segments, ionic groups[7] and long alkyl chains to increase thermodynamic incompatibility thereby enforcing micro-phase separation.

Despite the relative importance of PUs, research that focus on understanding the contribution and criticality of soft and HSs i.e., the monomer type and ratios on the microphase separated structure of PU is scarce. Considering the present scenario of research on SMPU, and the wide range of commercially available synthetic building blocks, we planned for a systematic study to achieve effective phase separation by varying both SSL and HSC. Further, we noticed that albeit the huge potential for predicting critical interactions leading to phase separation/mixing in SMPs, very few computational studies are reported on H-bonding interactions of different diisocyanates based HSs in PU.[12-14] Here, we proposed to study the interactions among HSs including both diisocyanate and chain extender using computational tools with a view to provide a platform for detailed understanding of H-bonding mechanism in PU HSs. Such a study would facilitate developing models of PU based SMPs whereby appropriate choice of HSs would lead to tailoring of end user-specific shape memory properties. The present study envisages to develop SMPs based on PUs, perform computational studies to assess critical interactions between hard segments and finally the demonstration of shape memory property. Density Functional Theory (DFT) was used for predictions of H-bonding interactions among HSs followed by experimental evaluation of the effect of SSL by synthesizing

SMPU using polyethylene glycol (PEG) of different molecular weight (4000 and 6000g/mol) as polyol whereas both diisocyanates and chain extenders were tuned to study the influence of hard segments mainly between 2,4-toluene diisocyanate (TDI) and 4,4'-methylene diphenyl diisocyanate (MDI), butane-1,4-diol (BDO) and ethylene diamine (EDA). Finally, shape memory properties of SMPU were investigated followed by its demonstration as a circuit breaker in a simple electric circuit.

Experimental

Synthesis of shape memory PU

PEG, initially melt dried in a vacuum oven at 60°C overnight, was dissolved in DMF along with diisocyanate in a dry three-necked RB flask. The mixture was stirred under N_2 at 80°C for 2h to afford isocyanate terminated pre-polymer which on subsequent addition of chain extender was reacted further for 2h. The feed ratio (mole) for the PEG:isocyanate:chain extender was 1:2:1 based on the optimized mole ratio of [NCO]/[OH]PEG and was reacted in 25ml of DMF.

Computational calculations were performed using Jaguar module of Schrodinger suite. Geometry optimizations were carried out using B3LYP/6-31G** level of theory in gas phase and vibrational frequencies were calculated for optimized structures which were minimum in the potential energy surface. Binding energy of molecules of HSs interacting via H-bond was calculated using H-bond workflow in Jaguar[15] using correlation-consistent basis sets (cc-pVTZ(-f) and cc-pVQZ(-g)) and LMP2 theory, including corrections for basis set superposition error. The final correction to the binding energy ensured that they were accurate to within 0.5 kcal/mol when compared to the extrapolated CCSD(T) energies.

Results and discussion

Of the key factors influencing morphology, phase separation and shape memory properties in SMPUs, H-bonding plays a critical role. For example, H-bonding-enforced microphase separation of hard and soft domains in PUs endow the material with enhanced mechanical properties. We optimized the structures of different hard segment models of PU with H-bonding interactions (Fig.1) and their bond lengths (Table.1). Shorter bond distances R(NH..O) for -C=O hydrogen bonds suggested better hard segment-hard segment interactions leading to improved phase separation, whereas higher bond length for ester –O– H-bond suggested weaker interaction between hard and soft segments leading to poor phase mixing.

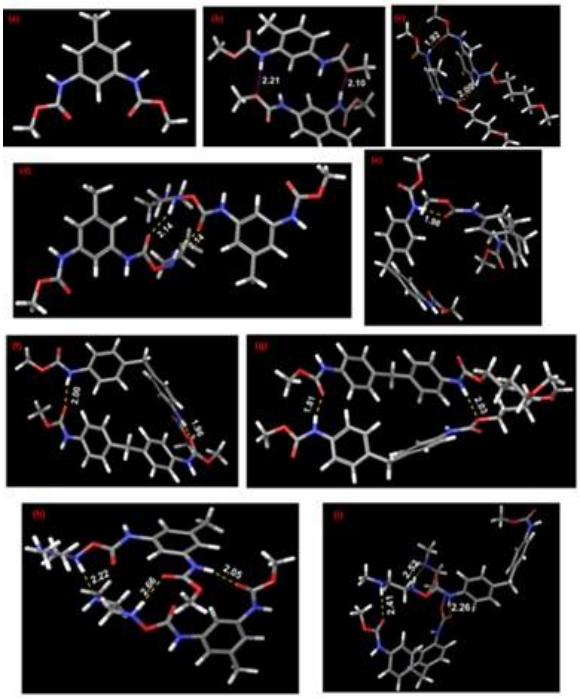


Figure 1. Optimised models of HSs of PU; (a) TDI based HS; (b) TDI-2H bond; (c) TDI_BDO-2H bond; (d) TDI_EDA-2H bond; (e) MDI-1H bond; (f) MDI-2H bond; (g) MDI_BDO-2H bond; (h) TDI_EDA-3H bond; (i) MDI_EDA-3H bond

Even though both MDI and TDI-based HSs showed almost similar inter segmental interactions irrespective of chain extender, MDI-based HS gave better phase separation due to its shorter bond length in comparison with that of TDI, hence predicting improved stability and properties for MDI-chain extender system. Remarkable change was observed with EDA chain extender in both MDI and TDI based systems which was attributed to an additional NH..NH interaction possible in the system. These results confirm DFT calculation as a powerful tool to study weak interactions, and indicate that H-bonds are indeed formed between carbonyl and N-H, or ester and N-H, the former being stronger.

HARD SEGMENT	NO. OF H-BONDS	NH···O=C (Å)	NH···O (Å)	NH···NH (Å)
TDI	**2**	**-**	**2.1, 2.2**	**-**
MDI	**1**	**1.98**	**-**	**-**
MDI	**2**	**1.96, 2.00**	**-**	**-**
TDI_BDO	**1**	**2.03**	**-**	**-**
TDI_BDO	**2**	**2.00, 1.92**	**-**	**-**
TDI_EDA	**3**	**2.05, 2.66**	**-**	**2.22**
TDI_EDA	**2**	**2.14, 2.14**	**-**	**-**
MDI_BDO	**2**	**1.81**	**2.0**	**-**
MDI_EDA	**1**	**1.96**	**-**	**-**
MDI_EDA	**3**	**2.41, 2.26**	**-**	**2.52**

Table 1. H-bond lengths in different PU models

One of the most useful methods of studying the type, extent and strength of competitive H-bonding in PUs has been the vibrational spectroscopy which mainly determines magnitude of frequency shifts in the peak positions of the (N–H) and (C=O) stretchings of urethane groups. Stretching vibrations of free -NH and -C=O in geometry optimized single TDI based HS model occurred at 3495 cm^{-1} and 1764 cm^{-1} respectively. On comparison with the remaining HS models

with expected H-bonding interactions, a reduction in frequencies was observed providing evidence for possibility of such interactions among hard segments. Decreasing trend of frequency consequent to chain extender addition and increasing number of H-bonds is attributed to the possibility of –C=O and –NH bonds getting more involved in the H-bondings (Table.2).

Models	**-NH (cm^{-1})**	**-C=O (cm^{-1})**
TDI based HS	3495	1764
TDI-2H bond	3418	1756
TDI_BDO-1H bond	3395	1739
TDI_BDO-2H bond	3324	1715
TDI_EDA-3H bond	3414,3332	1663
MDI_BDO-2H bond	3517	1632

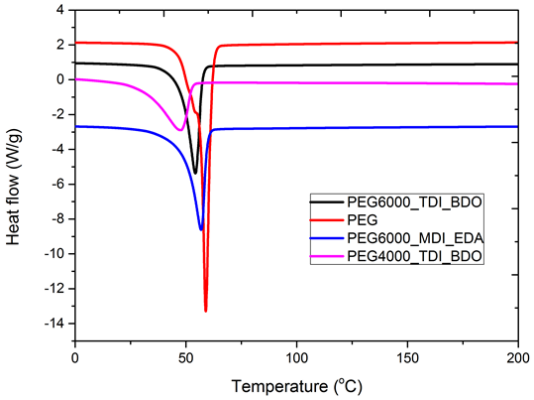
Table.2. Computed vibrational frequencies of HS models with possibility of H-bonding interactions

The strength of H-bonds between HSs of PU determine their stability along with critical analysis of phase separation/mixing. Localized pseudospectral methods (PS-LMP2) were used to calculate binding energies between the hard segments of PU. On comparing H-bond binding energy obtained for diisocyanate based hard segments with and without chain extender, better stability was estimated for the former which was found to increase with number of H-bonds.

The formation of SMPU was confirmed by IR and ^{1}H NMR spectroscopy. Synthesized PU exhibited absorption peaks near 2857cm^{-1} and 2923cm^{-1} due to asymmetric alkyl C–H stretching. The presence of urethane linkage was identified by peaks near 1635cm^{-1} and 3285 cm^{-1} due to (-NH-C=O) and -NH stretching respectively whereas disappearance of -NCO peak at 2265cm^{-1} confirmed complete consumption of TDI. A peak at 1701cm^{-1} was attributed to H-bonded –C=O found in HSs indicating phase separated microstructure. A shift in C=O stretching from 1708cm^{-1} for MDI_EDA based HS to 1697cm^{-1} for TDI_BDO system confirmed better phase separation for the former which well supports our theoretical predictions. ^{1}HNMR spectra also confirmed the product identity whereas thermogravimetric analysis suggested a 3-stage decomposition- initial one corresponding to the loss of entrapped water and solvents followed by steps starting at around 250°C and 350°C corresponding to decomposition of hard and soft segments respectively. First stage is a result of depolymerization of urethane groups while decomposition of PEG soft segments through radical breakdown is responsible for the latter.

DSC indicated the T_{trans} of PU to be less than that of pure PEG along with a broadening of melting endotherm mainly due to introduction of HS which suggested phase separation. A reduction in crystalline fractions of SMPU was noted mainly due to inhibition of crystallisation by hard segments. As compared to pure PEG, analyzed segmented PU samples showed an endotherm in the temperature range 47-57°C. An increase in T_{trans} was observed when higher molecular weight polyol was used which contributed to higher SSL. The observed difference of 7-9°C on comparing PEG6000_MDI_EDA and PEG4000_MDI_ EDA systems with similar hard segments led to the conclusion that an increase in T_{trans} accompany an increase in SSL and hence SSL can be used as a tunable parameter for tailoring T_{trans}.

Figure. 2. DSC analysis showing the effect of SS and HS on T_{trans}, crystallinity and specific heat of PU



Further, there was a decrease in T_{trans} with a broadening of melting temperature peak for both MDI and TDI based PU (Fig.2) with increase in HSC. T_g of PU with PEG6000 was found to be -28°C which was close to that of pure PEG (-22°C) which suggested better microphase separation. As SS molecular weight reduced, T_g broadened and rose to higher temperature.

Morphology analyses by Polarised Optical Microscopy (POM) indicated phase separated microstructure.

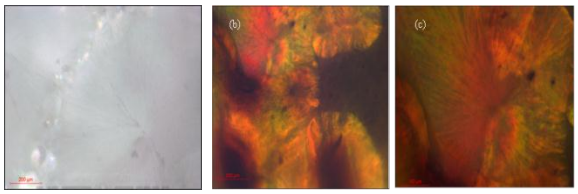


Figure. 3 POM images showing spherulite formation in (a) pure PEG; (b) PU under low magnification; and (c) PU under high magnification

Formation of spherulites gave a proof of crystallisation of the switching segments responsible for shape fixation which was studied using hot stage POM. Pure PEG and PU showed obvious cross-extinction patterns suggesting crystalline nature and were spherulites. Smaller and imperfect spherulites of PU (Fig.3(b)) as compared to pure PEG (Fig.3(a)) was due to the interference by hard segments on PEG crystalline behaviour.

From WXRD pattern, we concluded that higher SSL can lead to better crystallinity and hence improved phase separation. On varying HS components, more crystallinity was observed for MDI based system containing similar polyol and chain extender which also correlated with DSC results.

From mechanical testing using UTM, tensile strength and modulus of PU were found to increase while elongation at break decreased with increase in HSC due to much stronger interactions among HSs (Table.3). At equal molar concentrations of HSs, the polymers prepared with TDI exhibited lower strength properties, i.e., tensile stress and greater extensibilities than those with MDI which may be due to the increased molecular weight and higher degree of order in MDI because of their crystalline nature which was consistent with our theoretical predictions.

Sample	Yield Point (MPa)	Stress at break (MPa)	Strain at break (%)
PEG6000_TDI_BDO	0.47	1.24	469
PEG6000_TDI_EDA	1.4	6.45	448
PEG6000_MDI_BDO	5.4	8.34	175
PEG6000_MDI_EDA	4.9	11.06	340

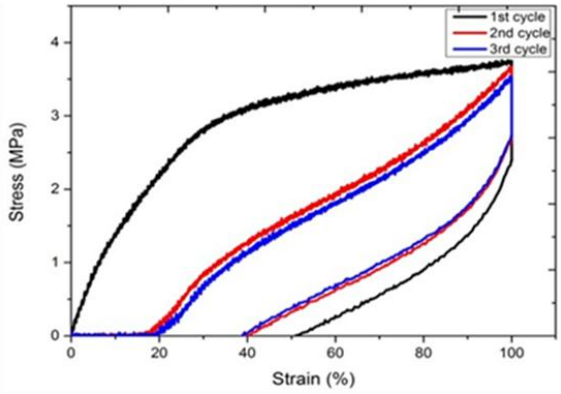
Table 3. Mechanical properties of PU with similar soft segment but different hard segments

A compromise between both tensile strength and elongation at break seemed to be necessary from a device perspective and hence the system containing MDI as diisocyanate and EDA as chain extender which gave an elongation at break of 340% and 11MPa tensile strength was chosen for further study of shape memory properties and demonstration of shape memory behavior. Accordingly, PEG6000_MDI_ EDA with better properties was further subjected to cyclic thermomechanical studies to obtain authentic and critical confirmation about the shape memory properties.

Figure 4. Thermomechanical cycle for PEG6000_MDI_EDA

PU samples had stable thermomechanical cyclic properties after two cycles. PU gave a recovery of almost 96.4% while the fixity ratio was only up to 51.4% at 100% maximum elongation mode where shape fixity mainly results from the crystallization of PEG SSs while the stable HSs played an important role in shape recovery. It can be concluded that the hard segment domain formed by MDI and EDA provides stable physical net-points to achieve good shape recovery (e.g. above 80%) because of its higher microphase separation but lesser shape fixity due to the increased hard segment content of more than 45 wt%.

Conclusions



In a combined theoretical and experimental approach, crystallisation of SSs and optimal H-bond formation between HSs in segmented PU were studied. The interactions among HSs were predicted by DFT using B3LYP method employing 6–31G** basis set by varying both diisocyanate and chain extender. Prediction of H-bonds and bond distances gave information regarding phase separation/mixing. Both TDI and MDI showed almost similar interactions irrespective of chain extender, but latter was found to be more stable as a diisocyanate based hard segment with chain extender. Among chain extenders, EDA containing systems showed increased number of H-bonds with better interactions mainly due to an additional NH..NH interaction which contribute to higher mechanical strength imparted by EDA. IR spectra were plotted using the vibrational frequencies and the type, extent and strength of competitive hydrogen bonding was estimated. Frequency was found to decrease with increase in number of H-bonds as well as with incorporation of chain extenders. H-bond binding energies were also determined using localized pseudospectral methods (PS-LMP2) providing accuracy to better than 0.5 kcal/mol.

SMPUs were synthesized in a combinatorial fashion and characterized using IR, TGA, DSC, POM, AFM, DMA and tensile testing. Effect of soft segments were studied from DSC and DMA where higher SSL led to better microphase separation due to the increased crystallinity. Tailoring of T_{trans} was made possible by varying both hard and soft segments. The effect of H-bonding critical for phase separated morphology was successfully investigated using IR, XRD, DSC and mechanical properties and finally correlated with conclusions drawn from computational studies. MDI_EDA system with 340% elongation at break and tensile strength of 11MPa was subjected to thermomechanical cyclic tensile testing and shape fixity and shape recovery was estimated to be 51.4% and 96.4% respectively. Our studies concluded that high molecular weight polyol contributes

to increased crystallinity (high SSL) and the use of MDI and EDA (optimum HSC), imparting increased interactions among hard segments leads to enhanced phase separation and hence improved shape memory properties.

Acknowledgements

We thank IIST for laboratory facilities. Acknowledgements are due to VSSC, NCESS and IISER Thiruvananthapuram for analytical support.

References

59. S. L. Cooper, A. V. Tobolsky, *J.Appl.Polym.Sci*. 10, 1837, 1966.
60. F. Li, J. Hou, W. Zhu, X. Zhang, M. Xu, X. Luo, D. Ma, B. K. Kim, *J.Appl.Polym.Sci*. 62, 631, 1996.
61. J. Hu, Advances in shape memory polymers, Elsevier, 2013.
62. M. R. Aguilar, J. Roman, Smart polymers and their applications, Elsevier, 2014.
63. C. P. Sung, C. Hu, C. Wu, *Macromolecules*, 13, 111, 1980.
64. B. K. Kim, S. Y. Lee, M. Xu, *Polymer*, 37, 5781, 1996.
65. Y. Zhu, J. Hu, K. Yeung, Y. Liu, H. Liem, *J.Appl.Polym.Sci*. 100, 4603, 2006.
66. K. Lem, J. Haw, S. Curran, S. Sund, C. Brumlik, G. Song, D. Lee, *Nanosci. and Nanoeng.* 1, 123, 2013.
67. Y. Camberlin, J. P. Pascault, *J.Polym,Sci: Polym.Chem.Ed.* 21, 415, 1983.
68. G. Senich, W. Mac Knight, Multiphase Polymers, 97, 1979.
69. C. Seefried, J. Koleske, F. Critchfield, *J.Appl.Polym.Sci*. 19, 3185, 1975.
70. P. Rodziewicz, J. Goclon, *J.Mol. Model.* 20, 1, 2014.
71. C. Zhang, J. Hu, S. Chen, F. Ji, *J.Mol.Model.* 16, 1391, 2010.
72. C. Zhang, J. Hu, X. Li, Y. Wu, J. Han, *J.Phy.Chem.A*, 118, 12241, 2014.
73. A. D. Bochevarov, E. Harder, T. F. Hughes, J. R. Greenwood, D. A. Braden, D. M. Philipp, D. Rinaldo, M. D. Halls, J. Zhang and R. A. Friesner, Int.J.Quantum Chem. 113, 2110, 2013.

MACRO 521

Influence of Catalyst and Alternate Polyamidoamine Hardener on the Chemical and Physical Properties of 4-Component Epoxy System Used in Solid Rocket Motor

Pradhan S K*[#], Sureshbabu K V[#], Rama Teja A S[#], Srikanth A[#], SrinivasBabu N[#], Kanakaraju P[#], Syed Hameed A[#]

[#]Solid Propellant Space Booster Plant (SPROB)
Satish Dhawan Space Centre, Sriharikota-524124

Abstract:

Case bonded solid propellant involves the casting of solid propellant to the case with insulated layer bonded to the case. During the solid propellant curing process the expansion and shrinkage of propellant grain is taken care by the unbonded insulation layer to motor case. This unbonded area termed as loose flap is later gets filled by 4 component epoxy systems which comprise of epoxy base, diluent, catalyst and curator. The two major factors in selecting epoxy base and

curator are its functionality and molecular structure which later determines the viscosity and potlife of the 4C system. This paper deals with a selection methodology involved for alternate curator source and comparing obtained parameters with the existing one.

Introduction:

Solid propellant motor segments are processed by casting propellant slurry into segment chamber under vacuum and cured at elevated temperature. To allow the expansion and shrinkage of propellant grain during curing, insulation layer is left un-bonded to the segment hardware. The unbounded layer of insulation shall be filled or closed to prevent entry of hot exhaust gases during combustion of motor. The entry of the hot gases may result in de-bond of insulation layer, exposure of motor hardware to the hot gases and thus may result in catastrophic failure of the motor.

The un-bonded insulation end is termed as loose flap. Inert compounds are filled into it to seal them. The necessary characteristics of filler compound are high temperature stability, chemical inertness, ease of synthesis and handling, no toxic or volatile by products and high hardness. Epoxy systems are ideal for such use[1-2].

Epoxy compounds can be cured in presence of amines at room temperature. Liquid epoxy mixed with amine curators show slow increase in viscosity with time and extent of reaction. The composition of epoxy resin and curator is chosen to allow the material to reach every corner. 4 Component (4C) epoxy system is used for filling loose flap in PSLV/ GSLV motors. The components of 4C Epoxy system are listed below.

1. **Epoxy Resin base:** Bisphenol A diglycidyl ether
2. **Reactive diluent:** 1,4 butanedioldiglycidyl ether
3. **Catalyst:** 2,4,6– tris(dimethylaminomethyl)phenol
4. **Curator:** Polyamidoamine

Commercial 4C Epoxy system from M/s Huntsman are used for loose flap filling of PSLV / GSLV solid propellant motor segments. Owing to commercial issues, the production of curator HY825 is stopped. Alternatives are explored to replace the curator.

The structure and functionality of epoxy base and polyamidoamine curator are crucial in obtaining end product with desired pot life, viscosity rise and mechanical properties.

Materials and Methodology:

GY257 (Epoxy Resin), DY026 (Reactive Diluent), HY960 (Catalyst), HY825 and AD125 (Curator) are obtained from M/s Huntsman and used as such. Chemical analysis is carried as per SDSC SHAR standards. INSTRON 4466 Universal Testing Machine is used for testing dumbbell as per ASTM D-0638. FTIR Spectrum is recorded on an ABB-MB 3000 Fourier transform infrared spectrometer by coating the sample on a KBr disc, GPC is recorded on Water 1525 with strylgel column,

Results:

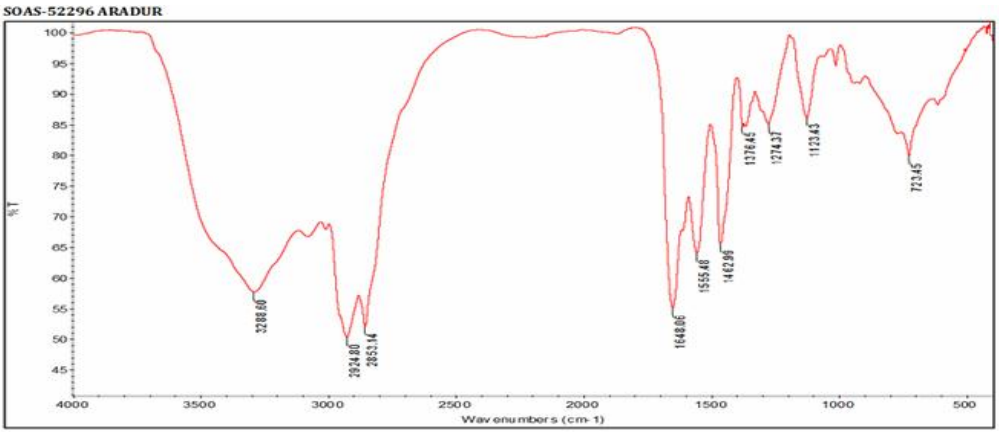
Chemical analysis is carried out to evaluate physical properties. The properties

are compared with Aradur AD-125, against reference HY 825.

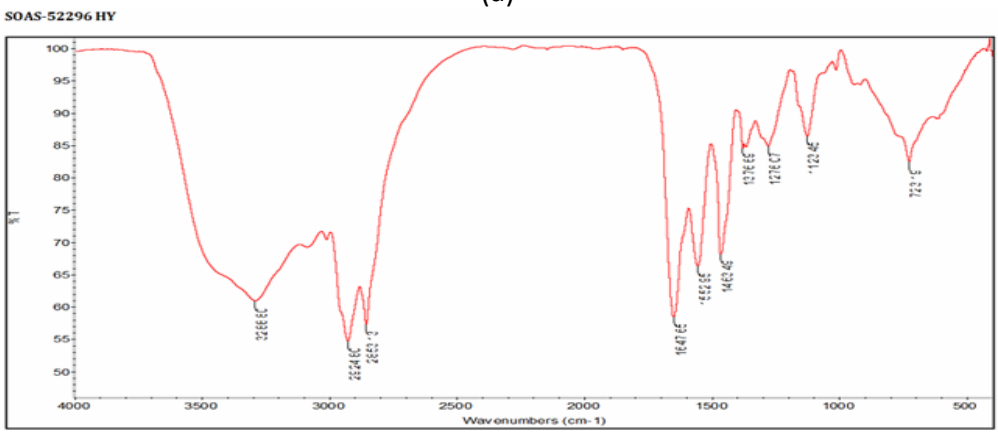
Parameter	ARADUR-125				Nominal values for HY-825
	Sample 1	Sample 2	Sample-3	Sample-4	
Amine value (mg KOH/g)	347	348	349	348	350
Sp. Gravity at 30°C	0.979	0.980	0.97	0.97	0.97
Viscosity at 30°C (cps)	27000*	28000*	20000	20000	21000

Table 1. Properties of Aradur AD-125 and HY-825

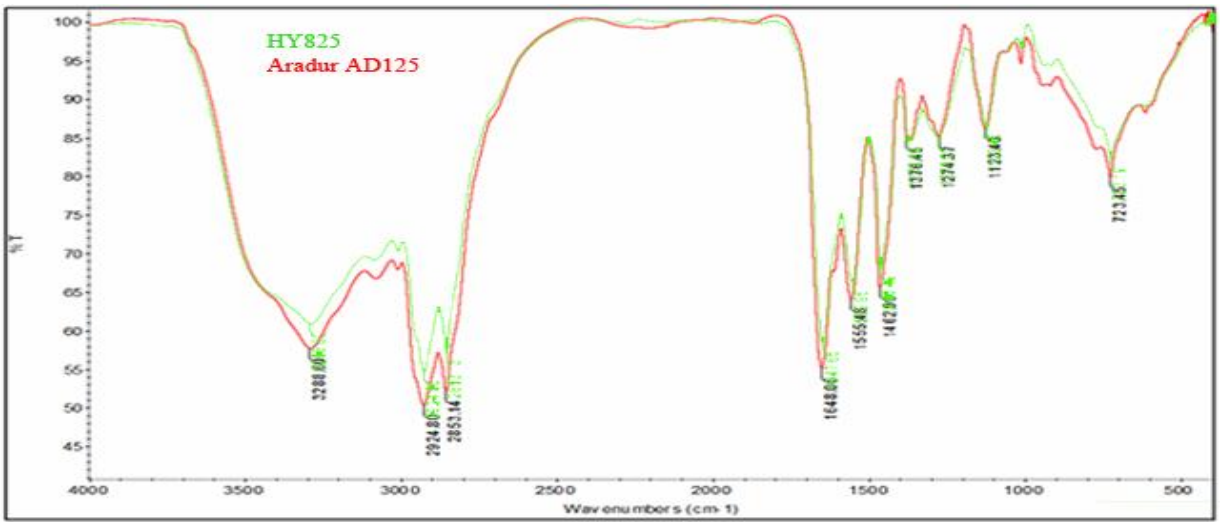
AD-125 is characterized by FTIR, NMR (^{1}H, ^{13}C) and GPC. The results are presented in Fig 1,2 and 3.



(a)

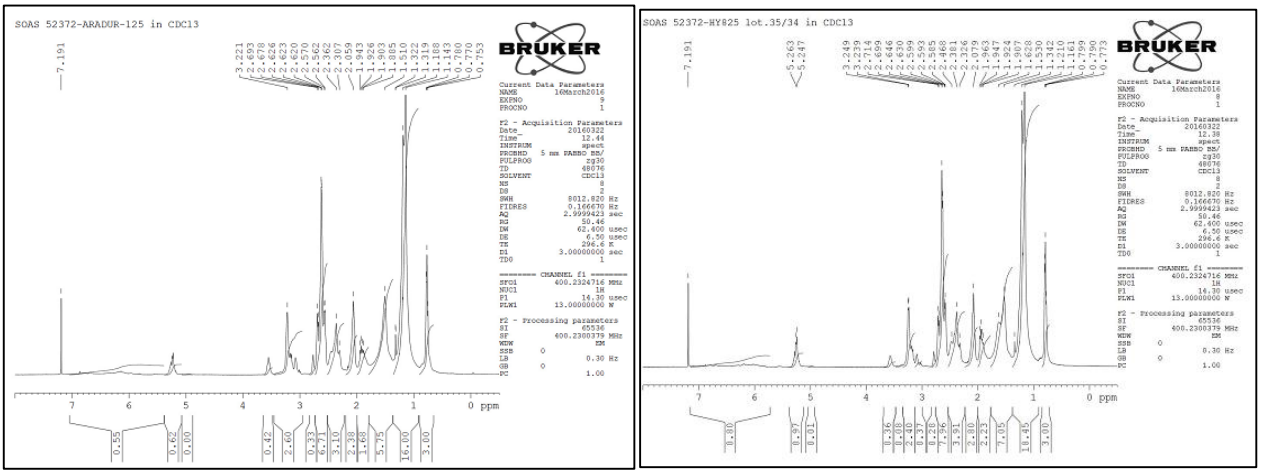


(b)

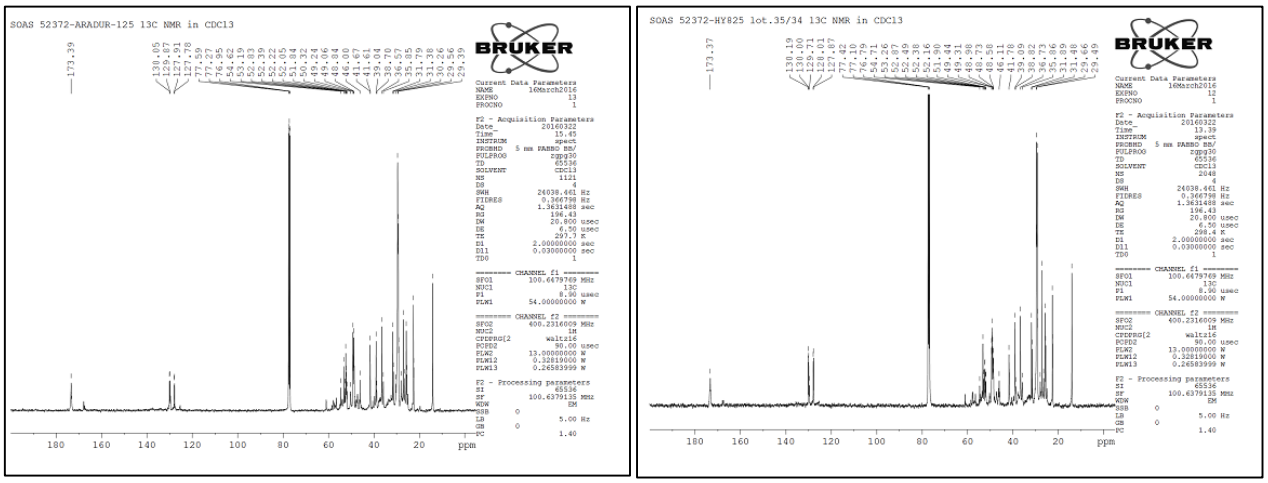


(c)

Fig 1. FTIR Spectrum of (a) AD-125, (b) HY825 and (c) Overlay



(a) (b)



(c) (d)

Fig 2. ^{1}H NMR Spectrum of (a) AD-125, (b) HY-825 and ^{13}C NMR Spectrum of (c) AD-125, (d) HY-825

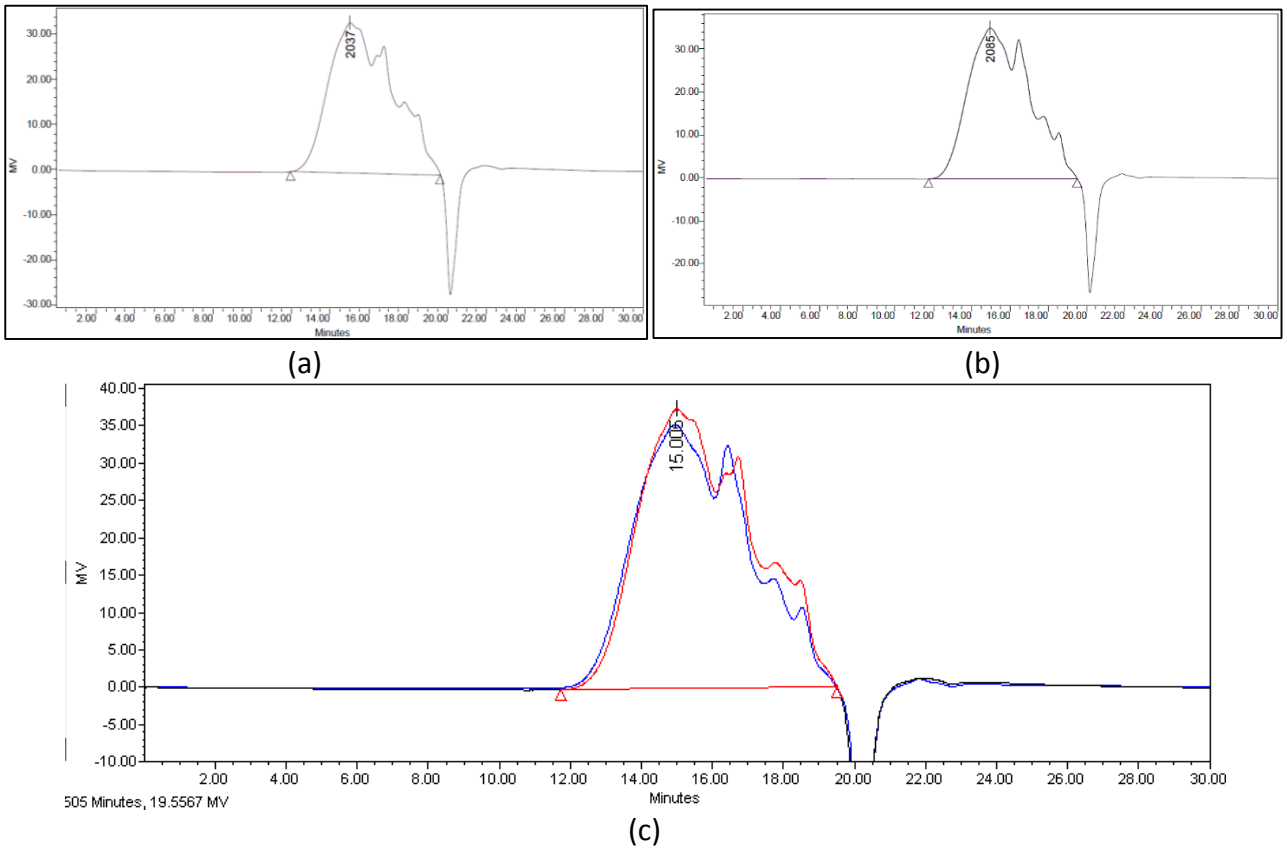


Fig 3. Gel Permeation Chromatogram of (a) AD-125 (M_n =1905), (b) HY-825 (M_n = 1948) and (c) Overlay

4 Component epoxy is made using AD-125 and HY-825 as curators. The pot life of mixture is evaluated and effect of relative concentration is also studied. The mixture is cured for 24 hours at room temperatures and mechanical properties of die cut dumbbells are evaluated.

Material	Sample ID	Pot Life (Minutes)	Accelerator (Parts)
HY-825	**HY825**	120	6.0
AD-125	AD1	90	6.0
	AD2	85	6.0
	AD3	110	5.5
	AD4	100	5.0
	AD5	133	5.0

Table2. Pot life Studies of 4C Epoxy system using AD-125 and HY-825 as curator

Parameter	HY-825	AD-125		
		AD1	AD2	AD3
Tensile Strength (ksc)	138	133	126	126.98
Elongation (%)	51.1	58.2	55.3	67.20

Hardness (Shore A)	80-85	90-94	92-96	90-92

Table 3. Mechanical Properties of 4C Cured slab dumbbells

Discussions:

The chemical analysis showed that the amine value for AD-125 varies from 347-349 and for HY-825 is 350. The viscosity at 30^{o}C showed that in the range of 20000-27000 for AD-125 and for HY-825 it is 21000. FTIR studies indicated that the peaks for AD-125 and HY-825 are observed at 3214, 2936, 2830, 16490, 15555, 14259, 13745, 12763 11274 and 723 cm^{-1}.

The pot life studies indicates the AD-125 showed 85-133 minutes and HY-825 showed 120 minutes with 6 parts of accelerator. The mechanical properties showed the tensile strength for AD-125 is 126-133 ksc and for HY-825 showed 138 ksc. % elongation varies from 55.3 – 67.2 for AD-125 and for HY-825 showed 51.1.

Conclusion:

The Chemical analysis, FTIR and NMR Spectroscopy and GPC chromatogram indicate similarities between AD-125 and HY-825. A marginal variation in viscosity and molecular weight is observed. The difference in pot life of 4C mixture and mechanical properties of cured slab dumbbells can be attributed to the variation in the molecular weight. The probable reason for slightly lower mechanical properties may be due to low mobility of AD-125 and hence lower crosslink density. Apart from the marginal variations the reactivity and end product performance of both compounds are comparable. Hence the AD-125 can be used as alternate to the HY-825 as 4 component epoxy system.

Acknowledgement:

Author express his gratitude to Dr. T V Ramana Reddy, Deputy General Manager, Chemical Testing Laboratory, SDSC SHAR and his team for their support in analysis.

References:

1. Ehsan Abbasi, Mohammad Vatankhah, Yaser Hosseini, Mohammad Amin Ariana, Moasoumeh Ayazi, “Synthesis, Structure and Mechanical Properties of Castor Oil-Based Polyamidoamines Toughened Epoxy Coatings”, *Journal of Applied Polymer science*, 2013, 4023 – 4030.
2. Henry Lee, Kris Neville, “Epoxy resins: their applications and technology”, 1957.

MACRO 522

Experiments on Filled and Unfilled HTPB based elastomeric materials for potential applications in solid rocket motors

Ravishankar.PM* , Venkat Ajay K, Himanshu Shukla, Venkateswara Rao V, Ranganathan V,

Solid Propellant Plant, Satish Dhawan Space Centre, Sriharikota-524124, India

** e-mail id: ravishankar.pm@shar.gov.in*

Abstract

Hydoxyl-terminated poly butadiene (HTPB) based elastomeric system is developed as a prospective candidate to replace castor oil - Asbestos based Inhibition resin [1] [2]. Inhibition resin forms a very important subsystem of a solid rocket motor. A predetermined Thrust-Time pattern is achieved by masking the undesired burn surface of propellant by Inhibition resin. The present work reported involves the development of a HTPB based elastomeric material with a novel clay material-sepiolite as filler. HTPB was cured with Toluene Di isocayante (TDI) and a cross linking agent. Experiments were carried out at the gumstock level to understand the effect of catalyst and plasticizer (Di-Octyl adipate) on the mechanical properties. 5% (w/w) Ferric acetylacetonate (FeAA) powder in Benzene solution is used as catalyst.

Introduction

Inhibition resin is used in the solid propellant rocket motors for controlling the burn surface area. It plays an important role in achieving pressure/thrust time pattern as per the mission requirement. The Inhibition resin currently used is a castor oil-TDI based polyurethane system with suspended inert filler (asbestos). The present filler asbestos is a proven carcinogen and castor oil, being a nature based product, is prone to batch inconsistencies. To alleviate these problems and to improve upon the existing inhibition system, experiments were conducted to identify a new polyurethane formulation with a novel filler.

After literature survey, Sepiolite (Magnesium Silicate) was selected to be the prospective filler because in addition to good thermal stability it exhibited high porosity, surface area and needle like morphology. The colloidal nature Sepiolite provides to its suspensions a pseudo plastic and thixotropic behavior which translates to better process ability. Sepiolite has surface area (BET, N_2) of 300 m^2/g which is the highest for all the clay minerals. The clay is hydrophobic due to high density of silanol groups (-SiOH). The small elongated sepiolite particles have an average length of 1µm to 2 µm, a width of 0.01 µm [3].

For the prospective Inhibition material, HTPB binder system is used. The main shortcomings of castor oil are

- Aging effect (depletion in properties).
- Natural material (Susceptible to batch inconsistencies)

A series of polyurethane compositions were formulated using HTPB as binder, TDI as curator and sepiolite as filler material. Hydroxyl terminated polybutadiene (HTPB) is the widely used polymer binder for solid composite propellant manufacture in the launch vehicle programs. The binder imparts Dimensional stability and structural integrity to the composite solid propellant grain. The hydroxyl functional group of HTPB undergo stoichiometric urethane reaction with Isocyanates to form a polyurethane network (Fig.1). Conventionally TDI is used as a curing agent for HTPB.

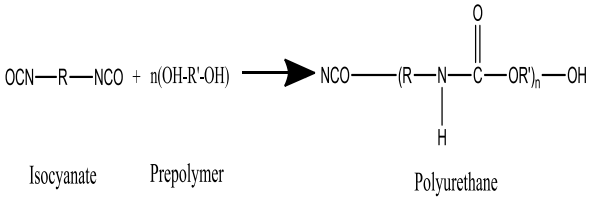


Fig 1 **Schematic Polyurethane reaction**

Since HTPB is being used as propellant binder, making Inhibition resin with the same will improve the interfacial property between them [4] [5]. Since, theoretically HTPB is only a di-functional pre-polymer and TDI is a Di-Isocayanate, cross-linking is intangible. To alleviate this problem a cross-linking agent (Ambilink) is introduced into the binder system. Ambilink is a mixture of 2:1 Buanediol (BDO) and Tri methylol propane (TMP). Di-Octyl adipate (DOA) is used as plasticizer.

Table 1**: Formulation**

S.No	Ingredients	Function	Phr (Parts per hundred of resin)
1.	HTPB	Resin/ Binder	100
2	DOA	Plasticizer	0-10
2.	TDI	Curing agent	16.9
3.	Ambilink	Cross-linking agent	2.22
4.	5% (w/w)FeAA in Benzene solution	Catalyst	0.2-0.5

Various binder to filler ratios were evaluated and also the plasticizer was added for ease in mixing (Table 1). The formulations were characterized for properties viz. viscosity, density, tensile strength & elongation.

Experimental

Materials:

HTPB: B.NO: ABB-44, with a OH value of 41.0 mg KOH/g and moisture content of 0.04% was used Ambilink of OH value 1235 and moisture content of 0.18% was used, TDI(Assay: >99.5%) was supplied form Bayer industries, Germany,

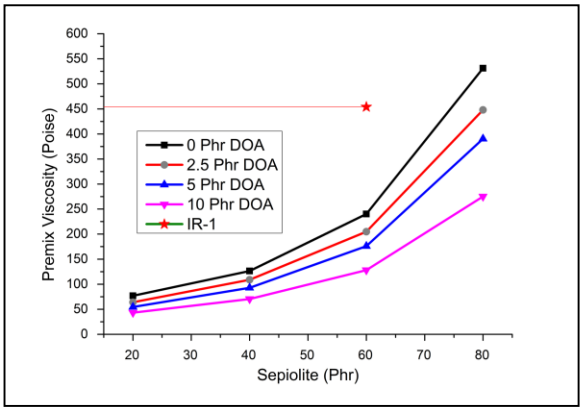
5.	Sepiolite	Filler	20 -80

Benzene (Assay: >99.5%) from Merck life sciences Pvt, Mumbai, FeAA (Assay: >99.5%) crystals from Merck, Germany was used.

1.1 Procedure:

Gumstock studies were carried out by taking 200 gm of HTPB, Cross-linking agent and plasticizer in a 1 liter Plastic container and a thorough premix is made by stirring the components for 10 minutes. Subsequently TDI corresponding to R-Value 1 was taken and the contents are stirred again followed by addition of catalyst and stirring.

After the container warms up sufficiently, the contents are transferred into a 200mm X 200mm X 5mm slab. The slab is allowed to cure overnight the samples are dispatched to laboratories for tensile property analysis. Tensile testing was carried out using INSTRON 3366, sample type ASTM D412 Type C.



Graph 1: Sepiolite concentration Vs premix viscosity

For composite level studies after addition of HTPB, cross-linking agent and plasticizer, a measured quantity of Sepiolite is added and the mixture is stirred continuously for 10 minutes until the mixture is homogeneous. Viscosity of the premix was measured using Brooke field viscometer HPT model with disc type spindle. To this premix resin, measured quantity of Curing agent and catalyst are added and mixed. Slabs of aforementioned dimensions are cast and sent for mechanical testing.

Results and discussion

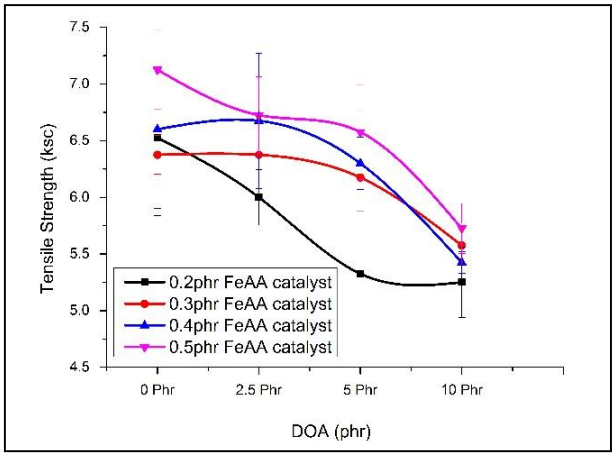
Viscosity of existing IR-1 is represented in the graph 1 to give a comparison between different resins. Lesser viscosity translates into ease of mixing since inhibition material is mixed with hand. Pr

ocessability is a very important parameter in preparing Inhibition resin.

The results are plotted in *graph 1*. With the increase in the filler percentage, viscosity increases and the effect is prominent after the filler above 60 phr. Similarly, as the plasticizer (DOA) phr increases there is a reduction in viscosity.

Gumstock studies

Gumstock level studies were carried out by varying the percentage of catalyst (FeAA) and the plasticizer (DOA). The result thus obtained is represented in the *graphs 2&3* below. The general trend observed is, with the increase in quantity of plasticizer a steep decrease in tensile strength is observed as a general trend. For 0.2 phr FeAA system it plateaus after 5phr of DOA, whereas for the resin system whose catalyst amount is above 0.2 phr, the mechanical property deceases further. Plasticizer, being the inert material, does not contribute in the chemical bonding and as such remains as an inert material thereby not contributing to the mechanical strength. This effect is considerably more prominent with the increase in amount of catalyst. This phenomenon may be due the variation in reaction rate for curing of the polymer. Elongation displays an interesting behavior when compared to tensile strength.

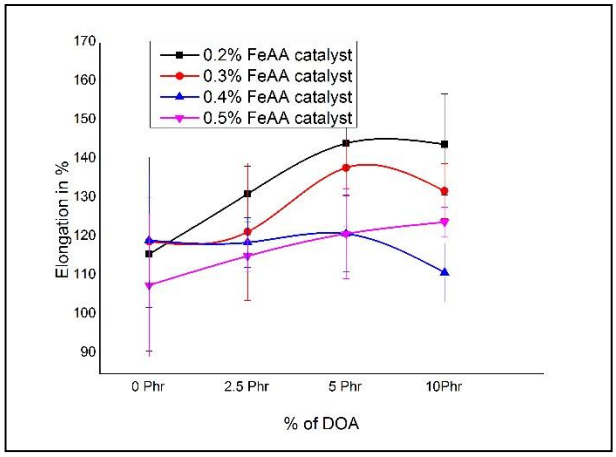


Graph 2: Tensile strength Vs DOA for various FeAA concentration

Elongation generally increases with the increase in amount of DOA and it decreases with the increase in the phr of FeAA catalyst. As the catalyst percent increases, reaction rate increases, thereby contributing to the cross-linking of the polymeric system. It can be inferred from the data that increase in catalyst percentage decreases the effect of plasticizer on system.

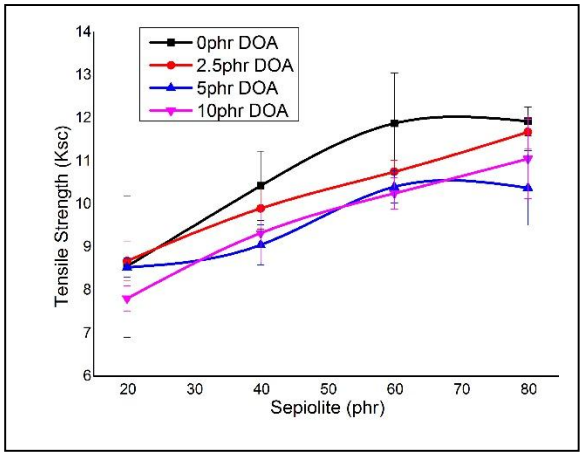
C

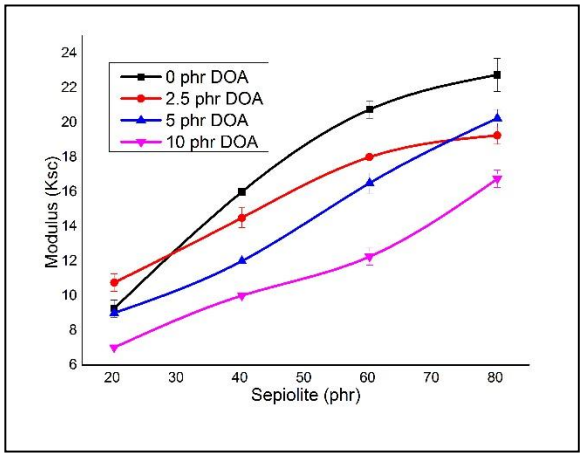
A nstock level it is noted that the maximum catalyst c hanical properties so it was decided to proceed with the same composition for the composite analysis with varying quantity of sepiolite and DOA.



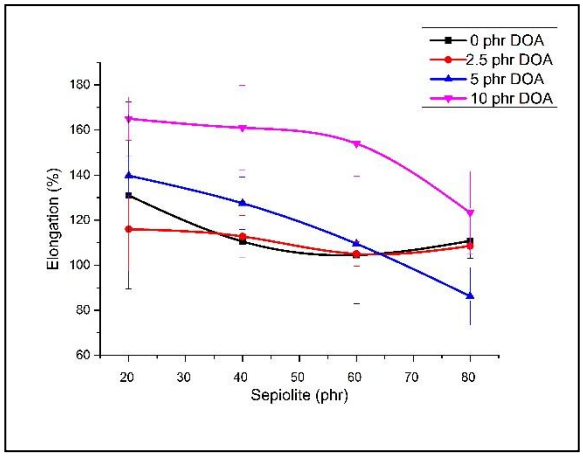
Graph 3: Elongation Vs DOA for various FeAA concentration

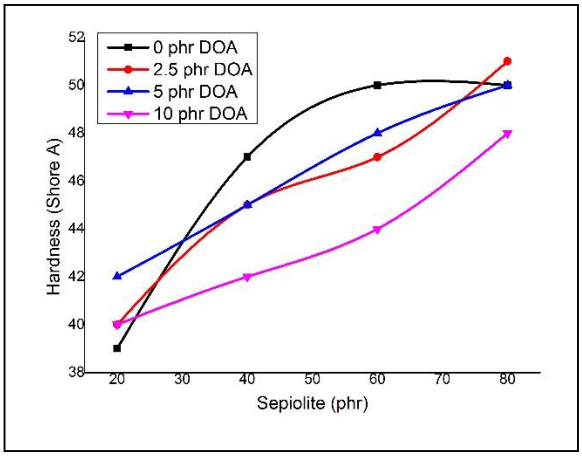
With the increase in sepiolite concentration the premix viscosity increased drastically for all quantity of DOA (*Graph 1*). For cured samples, tensile strength increased with the increase in quantity of sepiolite due to the reinforcing effect of the filler and the effect became less prominent with the increase in plasticizer content. The data is plotted in graphs 4 through 7. Elongation declines with the increase in sepiolite quantity and for lesser DOA concentration elongation stabilizes after 60 phr of sepiolite whereas for higher DOA c ses. Modulus and Hardness follows a general in cizer,





Graph 4: Tensile Strength Vs Phr of Sepiolite for various DOA concentration





Graph 5: Elongation Vs Phr of Sepiolite for various DOA concentration

hardness value saturated around 50 shore A after 60 phr of sepiolite and as the plasticizer percent increased the incremental trend of hardness continued.

Conclusions

Experiments were carried out to create a novel inhibition by replacing asbestos by sepiolite and by replacing castor oil by HTPB. Initial gum stock studies provided an insight into the role of plasticizer and catalyst in the final mechanical properties.Viscosity analysis of the premix revealed that the solid loading increased the viscosity drastically. Tensile strength increased by 40% for the composite system without plasticizer and for the system with maximum plasticizer (10phr DOA) it increased by 42% whereas elongation dropped by 18% and 34% respectively. Even though the newly developed resin shows excellent process ability and comparable mechanical property with

existing inhibition resin, some properties such as hardness are to be improved. Thermal property analysis will be carried out in the next phase to ascertain the ablative property of the system. With the aforementioned improvements, HTPB-Sepiolite based inhibitions can be a viable and practical replacement for existing Inhibition resin.

Acknowledgements

The Authors would like to acknowledge Director, SDSC-SHAR for his constant encouragement and support to pursue R&D activities.

References

[1] *P, R, Hima, A. J. Raghavan, S.S. Bhagawan, JohnDavid and S. S. Rao. "HTPB based Inhibition for Solid Rocket Motors". PED, VSSC.*

[2] *Sriniwas Panda*, M AuxilyVidhya, Imtiaz Ali Khan, Samir Kumar Das, S S Manna & C R Thomas "Development of Asbestos Free Inhibition Resin for Solid Propellant Rocket Motors", VSSC*

[3] *Galan, E. "Properties and applications of palygorskite-sepiolite clays." Clay Minerals 31.4 (1996): 443-454*

[4] *"Solid propellant grain with surface bonded burning inhibitor composition of hydroxy-terminated polybutadiene." U.S. Patent 3,433,158, issued March 18, 1969.*

[5] *Gupta, D. C., et al. "HTPB-based polyurethanes for inhibition of composite propellants." Journal of applied polymer science 55.8 (1995): 1151-1155.*

MACRO 523

Effect of Graphene Oxide (GO) on Properties of Thermoplastic Polymer Composites

*Shashikant Supare[1], Sachin Jain[2], Jayant Gadgil[3], Pramod Joshi[3], Deepti Marathe[1], Hemant Joshi[1] **

[1] Polymer Engineering Department, MIT, Pune
[2] DSM Engineering Plastics Ltd., Pune
[3] Polymer Consultant, Pune

** Corresponding author : hemant.joshi@mitpune.edu.in*

Abstract : Graphene is a one-atom thick layer of carbon atoms arranged in a honeycomb lattice. This special atomic arrangement gives graphene truly unique properties. The work aims at studying effect of graphene oxide (GO) on various properties, such as mechanical, thermal and electrical, etc., of composites based on thermoplastic polymer matrix. GO was synthesized from

graphite using modified Hummer's Method which was then melt compounded with Nylon-6 (PA6) using Banbury compounder [Brabender (Plastograph)]. The GO/PA6 compound has been characterized by FTIR, SEM and XRD for assessing modification graphite in terms of functional group and morphology. DSC and TGA studies were performed for studying effect on thermal stability. Nanocomposites were tested for mechanical properties such as tensile and impact strength, which showed a significant improvement as compared to Nylon-6 as well as Nylon-6 and graphite.

Keywords : *Graphene oxide, nanocomposites, Nylon-6*

Introduction:

Nanotechnology is a well-versed field for recent research and development activities in technical fields. It includes polymer blends, nanoelectronics, drug delivery, polymeric fuel cell electrode catalysts, polymer films manufactured by LBL self-assembly technique, electrospinning of nanofibers, polymeric nanocomposites, etc. The work in nanocomposites field constitutes studies related to reinforcements, permeability, flammability and so on. In last few years, there is a growing interest in polymeric nanocomposites due the promising results observed during the studies on carbon nanotubes and nanofibers, graphite/grapheme based systems, nanocrystalline metals and nanoscale inorganic filler [1-3].

Graphene is a honeycomb lattice arrangement of carbon atoms present with a layer of one-atom thickness which gives truly unique properties. Being one-atom thick it is the thinnest as well as perfectly flexible material. The electrical current flow is fastest amongst the known materials whereas faster heat flow is observed, thereby, making it the best thermal conductor. It is also the strongest material in the world. Compared to steel it is much stronger as well as lighter.

Graphite can be used as the source material to synthesize Graphene oxide (GO) using modified Hummer's method, which then can subsequently be modified to get functionalized GO. Synthesized GO can chemically be modified with various other organic functional groups via covalent bonding of functional groups with GO. Although the exact structure of GO is not yet clear, the predicted structure is expected to have higher concentration of hydroxyl and epoxy groups on the basal plane while carboxylic acid groups on the periphery of the sheets [6]. Because of water molecules intercalation, an increased interlayer spacing is observed with GO compared to graphite. Exfoliation of GO can be carried out most commonly using thermal shocking process [9] or by chemical reduction method [7, 10] having structural similarity to that of pristine graphene on a local scale.

In case of polymer nanocomposites, a substantial enhancement in properties even at lower filler content has been observed when compared polymer composites having micron sized filler particles. This results in reduction in filler weight alongwith simplification of processing operation [4]. Additionally, in case of nanocomposites, the possibility of multifunctional property enhancement opens up the window for variety of new applications [5].

In melt mixing, high shear rate is used to mix dry, powder form filler in polymer melt. This technique is more economical compared to solvent mixing as solvent is not required [11].

However, the dispersion level obtained with solvent mixing or in-situ polymerization methods is not achieved by this technique [8].

Experimental:
The desired GO was synthesized from graphite using Modified Hummers method. With the low temperature range method used for oxidation of graphite it was possible to get GO with good stability in a relatively simple and effective way. IR studies were carried out to assess various wavenumbers for confirming GO formation. SEM results show that the treatment of graphite results in increasingly more exfoliated GO.

It was possible to homogeneously disperse GO in PA6 using melt blending process. Compounded material has been characterized by various techniques such as SEM, DSC, TGA as well as these were tested for mechanical properties (tensile and impact strength). SEM data showed certain resemblance between surface morphology of GO with that reported in literature. In general, GO/PA6 nanocomposites showed a significant enhancement in mechanical properties compared to pure PA6. Even at lesser GO content, a slight improvement in the tensile strength was observed for nanocomposites. The improvement in strength revealed about effective transfer of the external load. The compatibility between PA6 and GO enhanced the glass transition temperature.

References:
1. Zhu Y., Murali S., Cai W., Li X., Suk J.W. and Potts J.R., Adv. Mater., 22:3906-24 (2010)
2. Geim A.K. and Novoselov K.S., Nat. Mater., 2007;6:183-91
3. Compton O.C. and Nguyen S.B.T., Small, 2010;6:711-23
4. Winey K.I. and Vaia R.A., MRS Bull., 2007;32:314-19
5. Ramanathan T., Abdala A.A., Stankovich S., Dikin D.A., Herrera-Alonso M. and Piner R.D., Nanotechnol., 2008;3:327-31
6. Dreyer D.R., Park S., Bielawski C.W. and Ruoff R.S., Chem. Soc. Rev., 2010;39:228-40
7. Park S. and Ruoff R.S., Nat. Nanotechnol., 2009;5:217-24
8. Kim H., Miura Y. and Macosko C.W., Chem. Mater., 2010;22:3441-50
9. Ruess V.G. and Vogt F., Monatsh Chem., 1948;78:222-42
10. Park S., An J.H., Jung I.W., Piner R.D., An S.J. and Li X.S., Nano. Lett., 2009;9:1593-7
11. Paul D.R. and Robeson L.M., Polymer, 2008;49:3187-204

MACRO 524

Kinetic studies of Phenol-Formaldehyde Resins using NMR spectroscopy

Srinivas Chinthalapalli*, Temina M. Robert, Praveen Kumar Solasa, Smitha Ancy Alex, Sadhana R., C. P. Reghunadhan Nair
Propellants, polymers, Chemicals and Materials Entity, Vikram Sarabhai Space Centre, Thiruvananthapuram, India-695022.

** srinivas_chinthalapalli@vssc.gov.in*

Phenol-formaldehyde (PF) resins, resol type are an important class of thermosetting resins which are formed under alkaline conditions. PF resins have a vital role from electronic appliances

and automobiles to space applications due to its highly favourable characteristics in terms of strength, heat resistance, long term reliability, cost and lightweight. Since from invention of these resins, many studies were done to understand its structure property relation. The studies include functional group analysis, IR, HPLC, NMR, XRD and MD simulations. Most of these studies use the disappearance of phenolic or formaldehyde content or formation of the products formed during the course of the reaction. NMR plays a vital role in understanding the structure and dynamics of various molecules. ^{1}H NMR and ^{13}C NMR studies were performed to analyse kinetic phenomena of PF reactions under different conditions such as temperature, stoichiometry, catalyst and p^{H} [1-5]. Still deeper insight is required to understand the influence of products formed in the prepolymerization reaction that lead to the end resin. Here we report the use of the major products formed during the reaction, i.e. ortho and para methylol phenol to assess the kinetics of the reaction using ^{1}H NMR as a function of temperature used during the synthesis which is further confirmed by the quantitative ^{13}C NMR.

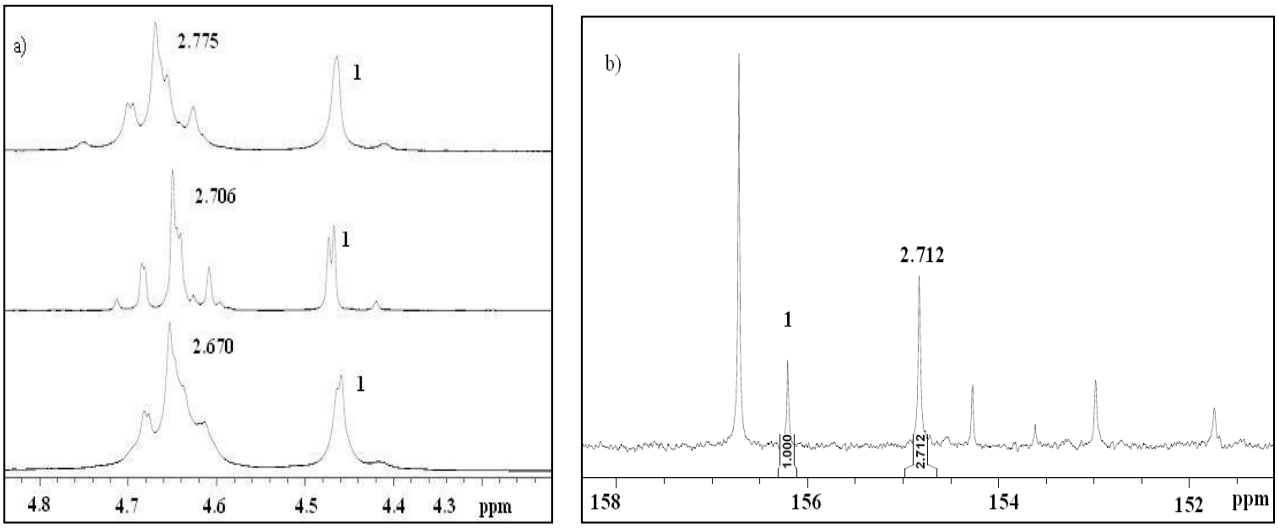


Figure 1. a) stacked plot of portion of ^{1}H NMR with arbitrary concentrations of PF end product (synthesised at 60°C) dissolved in Acetone-d6 showing ortho (4.55 to 4.8 ppm) and para fractions (4.35 to 4.55 ppm). b) portion of Quantitative ^{13}C NMR spectrum corresponding to ^{1}H NMR spectrum of Figure 1a (bottom).

PF prepolymeric resins were synthesised at four different temperatures (60, 70, 80 and 90^{0} C). Initially fraction of ortho and para methylol phenol of the PF end product of the prepolymerization reaction (Here, complete consumption of formaldehyde content) at these four different temperatures has been checked using area under the peak of respective forms in ^{1}H NMR which is further confirmed by quantitative ^{13}C NMR. As a function of temperature ortho fraction is increasing in proportional to temperature which is contradictory to the general argument where at high temperatures both the fractions are in equal proportions.

Table 1. Fractions of ortho and para forms of methylol phenol in the PF end product of prepolymerization reaction as a function of temperature

Temperature (in ^{0} C)	Ortho fraction (4.55 to 4.8 ppm)	Para fraction (4.35 to 4.55 ppm)

60	0.581	0.419
70	0.595	0.405
80	0.643	0.357
90	0.645	0.355

Kinetic studies of formation of ortho and para methylol phenol were done using ^{1}H NMR as a function of reaction time for all the temperature mentioned. Using the area of respective forms ortho and para content is calculated by multiplying with the amount of formaldehyde consumed which is determined by hydroxylamine hydrochloride reaction. The rate constants (k) for ortho fraction are obtained using n^{th} order differential equation by taking into consideration of disappearance of formaldehyde.

Table 2. Rate constants of ortho methylol phenol as a function of temperature

Temperature (in ^{0} C)	k_{ortho} (min^{-1})
60	$7.4*10^{-3}$
70	$23.7*10^{-3}$
80	$41.8*10^{-3}$
90	$67.9*10^{-3}$

Arrhenius equation is used to find the activation energy of ortho methylol phenol formation which is found to be 73 kJ/mol.

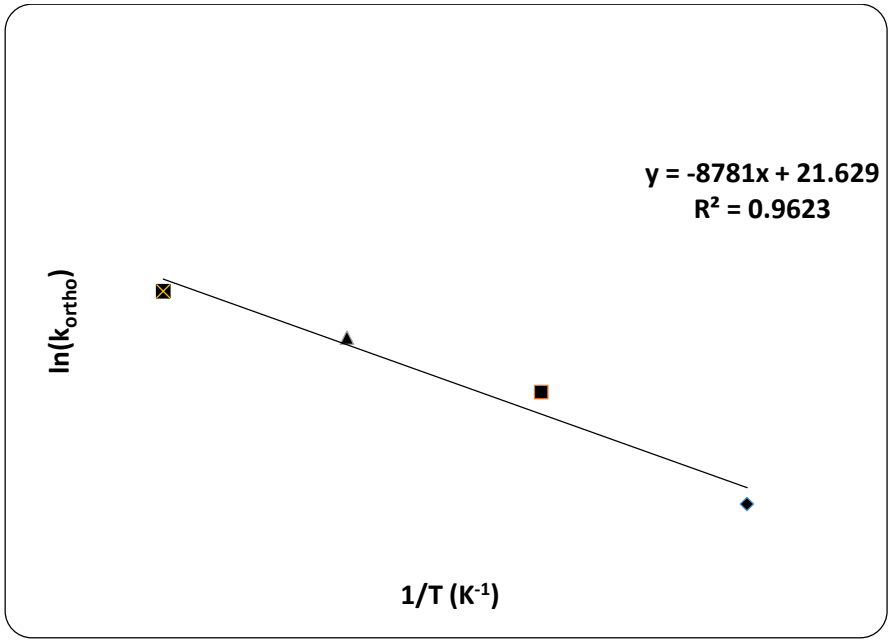


Figure 2. Rate constant of ortho methylol phenol as a function of temperature (Arrheneus equation)

References

[43] Hirano, K.; Asami, M. *Reactive & Functional Polymers*. 73 (2013) 256.
[44] Rego, R.; Adriaensens, P. J.; Carleer, R. A.; Gelan, J. M. *Polymers*. 45 (2004) 33.
[45] Loustalot, M. F. G.; Larroque, S.; Grenier, P. *Polymer*. 37 (1996) 939.

[46] Loustalot, M. F. G.; Larroque, S.; Grenier, P. *Polymer*. 35 (1994) 3046.
[47] Woodbrey, J. C.; Higginbottom, H. P.; Culbertson, H. M. *Journal of Polymer Science*. 3 (1965) 1079.

MACRO 525

Scale Up Of Processing Of Resole Type Phenolic Resin For Silica Phenolic Throat Inserts For Liquid Engines

*Praveen Kumar Solasa[a], Ambili K[b], N. Saravanan[c], K. Mohanakumar[d], S.K.Manu[e]

[a-d]*Scientist/Engineers, Propellant Fuel Complex, CSG, PCM Entity*

e, Deputy General Manager, Propellant Fuel Complex, CSG, PCM Entity

Vikram Sarabhai Space Centre, ISRO, Thiruvananthapuram-695022

**e-mail id: pksvssc@gmail.com*

Abstract

The liquid stages (VIKAS) of PSLV and GSLV use special type of Silica – Phenolic throat insert in the nozzle of the rocket engine. These throat inserts are made up of composite material consisting of a special grade resole type Phenolic resin (PF-108) as matrix and high strength silica cloth as reinforcement. Vikram Sarabhai space Centre had successfully developed the Silica – Phenolic throat insert using PF-108 produced at Propellant Fuel Complex.

Scale up of the processfor resole type phenolic resin froma batch size of 125 kg to 425 kg and further up to 600 kg was carried out by employing suitable scale-up strategy. Principles of similarity was employed after identifying the rate controlling step in the process. Reaction of this resole type phenolic resin follows condensation polymerization using a base catalyst, sodium hydroxide. A suitable reactor with process control was designed and commissioned for the scale up up work. The phenolic resin processed in the scaled up reactor was subjected to extensive qualification at resin and composite level. Excellent properties were achieved at composite level. Phenolic resin with consistent quality and reproducibility was processed and used successfully. The details of design and scale-up aspects of the reactor, processing, analysis, qualification studies carried for induction for flight use etc. are presented in the paper.

Key Words: *Phenolic resin, Scale-Up, Silica Phenolic Throat*

1.0 Introduction

Silica and Phenolic composites are used as ablative liners for various rocket engine nozzles, heat shields, re-entry bodies and nozzle liners. Phenolic matrix

composites provide superior ablative characteristics, high char yield, retention of strength, modulus and mechanical properties at elevated temperatures.[1,2,3,4] Silica Phenolic composites for use in liquid engines should have very high thermal resistance while retaining mechanical properties for long duration. To meet these requirements, a special grade resole type phenolic resin capable of high carbon yield and char strength coupled with remarkable thermal resistance was developed by VSSC in early 80's.

Phenol formaldehyde reactions are highly exothermic and probability of accident is higher than that for any other kind of chemical reaction. Once the reaction is initiated, exothermicityof the reaction increases the reaction rate and generates more heat, thus accelerating the reaction. According to the British Plastic Federation,[5]the heat of reaction is

ΔHR = - 17.2 kJ/mol of HCHO reacting to a $-CH_2OH$ methylol group

ΔHR = - 90.0 kJ/mol of HCHO reacting to a $-CH_2-$ methylene bridge.

Hence, control of reaction due to high exothermicity during polymerization plays a critical role in scale up of the process. In this paper, scale up of the process to produce phenolic resin at a batch size of 600 kg is discussed in detail.

2.0 Experimental

2.1 Materials

Reactants used for conducting the experiments were Phenol (Purity > 99.0%) and Formalin (Concentration ~ 37%). SodiumHydroxide (Purity > 98.0%) was used as base catalyst and Acetic Acid (Purity > 98.0%) was used for neutralization of base to a particular pH (7-8).

2.2 Procedure

Features of the reactors at different levels with important process parameters are given in the Table 1.

Table 1: Details of the reactors and process parameters

Sl. No	Details	Existing reactor	Augmented reactor	
1	Reactor capacity	250 litre	750 litre	750 litre
2	Mode of Control	Manual	Semi-auto	Semi-auto
3	P:F mole ratio	1.12 : 1	1.12 : 1	1.12 : 1
4	Reaction tempera-ture	Heating with steam up to 45°C and reaction control at 94±2°C till the end point test.	Heating with steam up to 45°C and reaction control at 94±2°C till the end point test.	Heating with steam up to 45°C and reaction control at 94±2°C till the end point test.
5	Separati-on time	24 hrs	24 hrs	24 hrs
6	Drying conditi-ons	Under pressure @ 50-200 mm Hg till the end point	Under pressure @ 50-200 mm Hg till the end point	Under pressure @ 50-200 mm Hg till the end point
7	Yield (in kg)	140 kg	420 kg	625 kg

Process was carried out as per the flow chart shown in figure 1 and 2.The production of Phenolic resin involves the following steps.

1. Melting of Phenol.
2. Charging of formalin and molten phenol into the reactor in the desired mole ratio.
3. Addition of catalyst.
4. Condensation polymerization of phenol and formalin.
5. Neutralization of reaction mixture with acetic acid to the desired pH.
6. Settling of reaction mixture.
7. Removal of water of reaction and sodium salt by decantation.
8. Vacuum drying of resin to remove the final traces of water and other volatiles.
9.

Process Block diagram is given in the Figure 1 and Process Flow Diagram is given in the Figure 2.

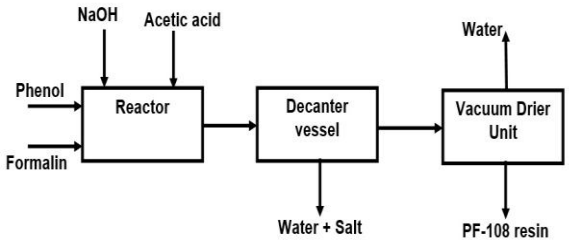


Fig 1: Process block diagram for Phenol formaldehyde reaction

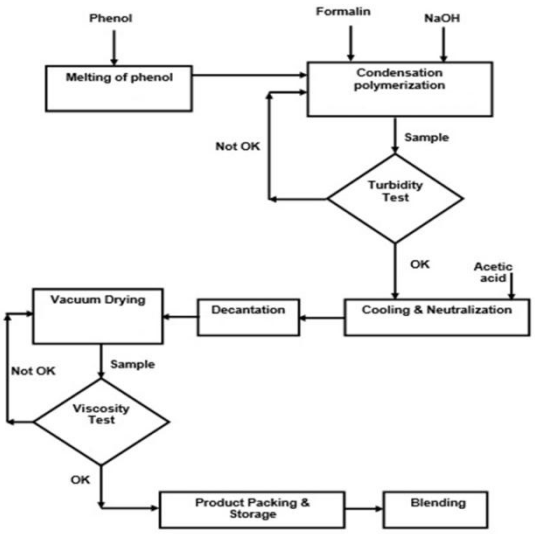


Fig 2: Process flow diagram for Phenol formaldehyde reaction

3.0 Scale up Details

The process of Phenol formaldehyde reaction is scaled up from a batch size of 140 kg (pilot) to 625 kg with 425 kg as an intermediate step. Principles of similarity was employed. The process was found to be in the thermal regime and thermal similarity consideration was found to be adequate for the scale up. Suitable scaled up reactor to process up to a batch size of 625 kg is designed by employing the scale up criteria such as a) L/D ratio and b) Heat transfer area per unit volume. Details of the scale up parameters estimated based on the input raw material in terms of heat load, heat transfer area from limpet coil and internal cooling coil for both the reactors is given in the Table 2. L/D ratio of 1.25 is maintained. It is ensured that the heat transfer area i.e heat transfer coefficient is maintained well above that of the 250 lit reactor in 750 lit reactor.

Table 2: Estimated Scale up parameters and comparison with that of 250 l and 750 l reactors.

Equipment	**Description**	**250 liter reactor**	**750 liter reactor**
L/D Ratio	**Length (mm)**	500	1100
	Diameter (mm)	400	900
	L/D	1.25	1.22

Heat Load Calculations			
Reactor	Amt of heat removed by coolant	50893 KW	151835 KW
Dryer	Heat supplied by steam	114250 KW	342750 KW
Heat Transfer Calculations			
Limpet coil	Inside Heat transfer Coefficient, $W/m^2.K$	185.57	369.10
	Outside Heat transfer Coefficient, $W/m^2.K$	292.83	292.83
	Over all heat transfer coefficient, $W/m^2.K$	56.52	66.61
	Heat transfer area, m^2	0.88	2.21
	Area per unit volume, m^{-1}	18.75	23.87
	Power per volume	1.26×10^{-9}	2.26×10^{-11}
Cooling coil	Inside Heat transfer Coefficient, $W/m^2.K$	357.24	675.21
	Outside Heat transfer Coefficient, $W/m^2.K$	747.32	747.32
	Over all heat transfer coefficient, $W/m^2.K$	70.57 W/m^2K	77.81 W/m^2K
	Heat transfer area, m^2	1.61	4.37m^2
	Area per unit volume, m^{-1}	117.58	174.40

4.0 Results and Discussions

Resin thus obtained is characterized for physical and chemical properties such as Viscosity, Refractive Index, Specific gravity, Free Phenol content, Free Formalin content, Total Solids content, Point of Trouble, Sodium and Ash content. Resin is also characterized for Chain initiation and saturation using Thermo gravimetric analysis, Molecular weight using Gel Permeation chromatograph and strcural aspects by Nuclear Magnetic Resonance spectroscopy. Comparison of the resin properties at various levels is given in the Table 3. The resin was subjected to qualification at composite level by processing silica phenolic composites. Composites processed as per the standardized procedure were characterized for by resin content, density, hardness, compressive strength along and across the ply and Inter Laminar Shear Strength (ILSS) at room temperature and elevated temperature. Details of the throats processed with resin batch identification no is given in the Table 4 and Throat properties in Table 5. Also, thermal properties were evaluated and resin storage studies for a period of 6 months are carried out by storing resin at a temperature of 5 to 8ºC.

Table 3: Resin properties of PF-108 resin processed at various batch sizes

Resin Properties			**MB-150**	**MB-151**	**MB-152**	**QB-01**	**QB-03**	**QB-04**	**SB-01**	**SB-02**	**SB-03**
1	Appearance	Specs	Yellowish brown to dark brown liquid								
2	Viscosity @ 30°C, cPS	400-600	480	440	510	470	490	480	480	440	420
3	Specific gravity @ 30°C	1.18 – 1.20	1.20	1.20	1.19	1.20	1.20	1.20	1.2	1.19	1.2
4	R.I @ 30°C	1.570-1.575	1.571	1.570	1.573	1.571	1.572	1.573	1.5739	1.5728	1.5719

Throat No.	Property	Density (g/cc)	Resin Conte (%)	Hardness (Barcol)	ILSS, MPa	CS (parallel),MPa	CS (Per'lar) MPa
					RT	RT	RT
	Spec	**1.70-1.74**	**28-34**	**52-60**	**19.61**	**73.5**	**225.5**
ST-116		1.713	30.85	56.2	27.96	96.303	310.21
ST-123		1.725	32.03	55.73	27.95	99.27	343.20
ST-124		1.712	33.86	56.63	25.93	92.71	274.34
ST-126		1.747	28.10	58.20	30.69	81.99	284.13
ST-132		1.734	29.51	59.00	22.12	90.87	281.49
ST-133		1.734	30.83	57.00	25.52	90.94	293.51

5	Total solid content at 170°C, %	72 - 75	73.3	73.5	73.8	74.4	74.2	74.3	74.8	74.8	74.4
6	Free phenol content, %	18 – 22	19.7	18.2	19.4	19.0	19.3	20.3	19.4	21	20
7	Free formalin content, %	0.5 Max.	0.5	0.3	0.3	0.5	0.4	0.3	0.3	0.5	0.4
8	Point of trouble at 0.863 Sp. Gravity, ml of water / 10 ml of resin	13 – 15.5	14.1	13.7	13.9	14.9	15.1	15.4	14.8	14.5	14.6
9	Water content, %	14.0 Max.	10.2	10.5	10.0	9.7	10.4	9.2	9.4	10.0	10.8
10	pH (5% aq. Solution)	7.3 – 7.8	7.4	7.4	7.4	7.6	7.4	7.5	7.6	7.5	7.5
11	Ash content, %	0.5 Max.	0.4	0.45	0.50	0.50	0.50	0.50	0.48	0.5	0.47
12	Sodium content, %	0.4 Max.	0.19	0.15	0.27	0.40	0.24	0.18	0.23	0.25	0.18
	Yield (Kg)		420	415	423	425	418	423	621	631	632

Table 4: Throat and resin batch details

Throat No	Resin Batch No	Batch Size	Remarks
ST-116	MB 146	420 Kg	Blend of 3 batches of 140 kg
ST-123	QB-01	425 Kg	Qualification batch -1 of 425 kg size
ST-124	QB-03	425 Kg	Qualification batch -2 of 425 kg size
ST-126	QB-04	425 Kg	Qualification batch -3 of 425 kg size
ST-132/ST-133	SB-01	625 Kg	First Qualification batch of 625 kg size.

Table 5: Properties of Silica Phenolic Throat Inserts

5.0 Conclusions:

Scale up of processing of resole type of phenolic resin from a pilot level of 140 kg batch size to 600 kg batch size was carried out by employing suitable scale up strategy. Thermal similarity was found to be the suitable scale up criteria for the process. Process parameters such as polymerization temperature and stoichiometry of the raw materials are maintained same as that of pilot batch size. A suitable reactor was designed and commissioned by incorporating the necessary provision for controlling the reaction in lieu of increased heat output and high exothermicity of the reaction at elevated temperatures. Basic scale up principles such as heat transfer area per unit volume, L/D ratio, Power number etc. are employed while designing the scaled up reactor. Additional safety features such as provision for chilled water etc. were also included to address the emergency situations. Process plant was automated suitably which can also be operated in semi-auto and manual modes also.

The phenolic resin thus processed was subjected to extensive qualification at resin and composite level. Resin is extensively characterized for physical and chemical properties. Also, spectral and thermogravimetric analysis were carried out. Ageing studies at a temperature 5 to 8 ^{o}C were also carriedfor a period of 6 months. Resin was evaluated by preparing composites for Pre-preglevel, Throat level and Thermal properties along the ply and across the ply were also evaluated. Properties are well within the specifications. Excellant properties were achieved at composite leveland well comparable with that of properties of pilot level of 140 kg batch size. Suitable shell and tube heat exchanger and cooling tower were designed and commissioned as part of thermal management of the process. Estimated values of Heat transfer for the Heat exchanger is 5.0 m^2 and that of cooling tower is 3.5 m^2 for a scaled up process batch of size 625 kg, i.e 750 liter capacity reactor.Thus, Scale up of processing of resole type resin capable of meeting the desired requirements at composite level with consistent quality and reproducibility was done successfully.

Acknowledgements:

Authors are sincerely thankful to Dr. S.C Sharma (DD, PCM) and Dr. S A Ilangovan (GD,CSG) for their valuable guidance, support and encouragement.

References:

1. D.O. Newling., E.J Walker, Proc. Intl. Conf. Carbon Fibres, London, p. 142, 1971
2. E. Fitzer., B. Tewiesch, Carbon, 10, p. 383, 1972
3. D.W. Meker., Carbon, 24, p 551, 1987
4. E. Fitzer., R. Gadoor, American Cer. Soc. Bulltin, 65, p 326, 1986
5. British Plastics Federation, (1979), “Thermosetting materials group, guidelines for the safe production of phenolic resins”. British Plastics Federation, London

MACRO 526

Development of High Performance In-Situ Polymer/Polymer Microfibrillar Composites Based on PP/Nylon 6 Blend System: Effect of Draw Ratio and Nano Fillers

Deeraj B.D.S, Konnala Raneesh and Joseph Kuruvilla*

[a]*Indian Institute of Space Science and Technology, Trivandrum, Kerala, India*

*kuruvilla.iist.ac.in**

Polymer/polymer in-situ microfibrillar reinforced composites (MFCs) based on two incompatible thermoplastics with different melting temperatures (Tm) are a new class of fiber reinforced composites. MFC system provides a way to develop commingled polymer composites in which both high temperature engineering plastics and low temperature general plastics co-exist and difficult to separate out. In this system, the high-melt-temperature component as the dispersed phase in situ deforms into microfibrils. The post processing temperature should be below the melting temperature of microfibrils in order to preserve the microfibrillar structure. The morphologies of MFCs, such as the shape of dispersed phase, size and its distributions of the microfibrils are mainly influenced by the concentration and draw ratio. In this work, the properties of MFCs prepared from polypropylene (PP) and Nylon 6 were analyzed. The effect of draw ratio on morphology, static and dynamic mechanical properties, thermal and rheological properties were studied. Due to the specific morphological structure, the rheology and crystallization behavior of MFCs show some interesting results. Finally, the conductive polymer composites (CPCs) based on the PP/Nylon 6 (70/30 w/w %) in-situ microfibrillar composites were prepared by adding conductive nano fillers, such as carbon nanotubes (MWCNT and SWCNT) at different loadings into microfibrils. The in-situ microfibrillar CPCs are tested for its static and dynamic mechanical, rheological properties. It is observed that in-situ microfibrillar CPCs have good conductivity and mechanical properties than the basic MFCs and the properties strongly depend on the filler loadings.

References

[48] Friedrich k; Evstatiev M; Fakirov S; Evstatiev O; Ishii M; Harrass M. *Composites Science and Technology*, 65 (2005) 107-116.

[49] Jayanarayanan K; Thomas Sabu; Joseph Kuruvilla. *Composites Part A: applied Science and Manufacturing*, 39 (2008) 164-175.

MACRO 527

Transparent and Electrically Conductive Polyimide Composites for Space Applications

KPP Najiya[a], K Raneesh[a], K.Joseph[a*], R.S.Rajeev[b], and Nalaperumaal[b]

[a]*Department of Chemistry, Indian Institute of Space science and Technology, Trivandrum, Kerala,*

India

[b]*Vikram Sarabhai Space Centre, Trivandrum, Kerala, India*

** kjoseph.iist@gmail.com*

Polyimides, due to their outstanding properties find wide applications in space when incorporated with carbon nanomaterials. Polymer nanocomposite based on CNTs have been used for improving mechanical, thermal, electrical properties of polymers because the CNTs possessing high flexibility, low mass density, and large aspect ratio[1]. In addition, the discovery of graphene with its combination of extraordinary physical properties (such as high electrical conductivity, mechanical strength and optical absorption properties) and ability to be dispersed in various polymer matrices has created a new class of polymer composite. The purpose of this work is to use a facile and green method to synthesize Gr-CNTs hybrid films, and use Gr-CNTs as a filler to synthesize Gr-CNTs/PI hybrid films. Assembly of graphene with carbon nanotubes (CNTs) can yield hybrid materials with new structural characteristics and different properties than the individual components. The main issue with CNT and graphenes is tendency to agglomerate and uniform dispersion of the CNT and graphenes are difficult to achieve. CNT/graphene nanohybrids exhibits good dispersion in the polymer matrix compared to CNT and graphenes alone. Compared with CNTs/PI, the electric conduction ability of this hybrid films can be improved more clearly by doping the lower content of Gr-CNTs in PI. And the conductivity of Gr-CNTs/PI hybrid films can be regulated by controlling over the content of Gr-CNTs nanocomposite in PI matrix. At the same time, the work used a novel and efficient route for the preparation of flexible and high conductivity Gr-CNTs/PI hybrid films. Gr-CNTs/PI hybrid film was prepared for different concentrations of the filler loadings. The presence of Gr-CNTs dramatically affects the films microstructure and the conductivity of Gr-CNTs/PI hybrid films. The Gr-CNTs/PI hybrid film exhibited a very sharp increase in the electrical conductance even for very low loading of the fillers. The prepared hybrid polyimide films also exhibited good optical transparency.

References

[1] Dan Chen, Hong Zhu, and Tianxi Liu, *ACS Applied Materials and Interfaces,*12(2010)3702

[2] Yaqin Chen, Baoping Lin, Hong Yang, Ying Sun, Xueqin Zhang. *Journal of Polymer Science*, 16 (2013) 3449.

MACRO 531

A theoretical investigation to evaluate structural and conformational effects of ligands in transition metal complexes useful for the preparation of ultra-high molecular weight poly(ethylene)s

K. Patel[a], K. Vanka[b], S. Chikkali[a*], S. Sivaram[c]

[a]*Polymer Science and Engineering Division, CSIR-National Chemical Laboratory, Dr. Homi Bhabha Road, Pune-411008. India*

[b]*Physical and Materials Chemistry Division, CSIR-National Chemical Laboratory, Dr. Homi Bhabha Road, Pune-411008. India*

[c]*Indian Institute of Science Education Dr. Homi Bhabha Road, Pune-411008. India*

** e-mail id: s.chikkali@ncl.res.in*

Abstract

One of the widely studied catalytic system for the synthesis of UHMWPE is phenoxy-imine group IV complex which is known to exist in five different isomeric forms. Our computational analysis reveals that the inter-conversion of isomers can be arrested by installing a suitable substituent on the imine-nitrogen. The phenoxyimine complex with bulky cyclohexyl substituent was found to be useful in reducing the fluxional behavior. This substitution showed conformationally restricted interaction between the hydrogen attached to the carbon β to the metal which is known to reduce the kinetic chain length of formed polymer via chain transfer.

Keywords: *UHMWPE; Computational chemistry; Bis(phenoxy-imine)grpoup IV metal complexes*

Introduction

Ultra-high molecular weight poly(ethylene)s (UHMW-PE) has elicited significant interest as an engineering material because of its outstanding mechanical properties, lightweight and biocompatibility. UHMW-PE is defined as linear polyethylenes[1] with molecular weight larger than ~2-3 million g/mol. They find applications in demanding areas, such as, bio-medical materials and materials for aerospace and defence industries [2]. For preparing ultrahigh molecular weight PE's one needs to, either, increase the rate of propagation (k_p) relative to rate of transfer (k_{tr}) or reduce the rate of transfer relative to the rate of propagation, or both. Greater fundamental understanding of factors that control chain growth and chain transfer will lead to strategies for a rational design of molecular catalyst for the preapration of UHMW-PE. The success of such

methodologies will significantly rely on the choice of ligands and the ability to manipulate electronic and steric environment around the active center.

A large number of homogeneous catalysts (group 4 metallocene catalysts,[3] constrained-geometry catalysts[4] (CGCs) and catalyst comprising of early transition metal with bidentate ligands (mainly bis (phenoxy imine) group 4 metal complexes[5,6] (Figure 1)) are employed in the polymerization of ethylene. Group 4 zirconium metallocene complexes show greater propensity for β-hydrogen transfer reactions due to favourable β-agostic effects. CGC catalysts possess an open ligand framework which also result in increased β-hydrogen transfer processes. Thus, these catalysts are generally not suitable for producing very high molecular weight PE's. In the post-metallocene family, bis(phenoxy-imine) ligands have attracted greater attention as it offers simple electronic and steric modifications in ligand framework to provide a diversified family of catalyst complexes leading to useful properties in polyolefins. However, bis(phenoxy-imine) complexes possess five possible structural isomers (Figure 1) which are in dynamic equilibrium and are distinguishable based on the nature of bonding in the axial and equatorial position. Of these isomers, only structure with a *cis* chlorine is believed to be catalytically active. Multiple catalyst structures with differing reactivities leads to multiple reaction rates apart from making the precise structure of the active site ambiguous.[5,6]

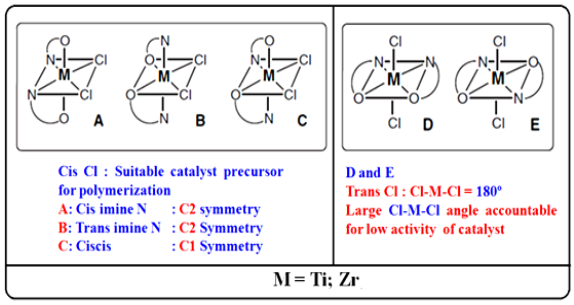


Figure 1. Five possible structural isomers in group 4 bis(phenoxyimine) complexes

One of the structural variant in this family of complexes has been reported to show a significant increase in molecular weight as function of increase in size[7] (cyclopropane to cyclohexane) of the substitution. However, the authors did not offer any rational explanation for this observation. It is , however, clear that a modification in ligand framework resulted in a significant increase in the rate of propagation. Guided by this precedence we decided to rationalize the behavior and provide a better understanding of the role of ligand structure on the properties of PE's. Further,

we aimed to create a variation in ligand framework by installing sterically bulky groups in order to reduce the fluxional behavior. To this end, we used computational and molecular modeling methods to estimate ground state energies, symmetry, geometry, electronic and steric effects of various types of substitutions in bis(phenoxy-imine) ligand framework and their corresponding metal complexes. Steric crowding in ligand framework was introduced by placing a substituent on the cyclohexyl ring in the ligand frame work of complexes (Figure 2).

Experimental

Computational Methods

To accomplish the goals we performed molecular modelling of various cyclohexyl substituted bis (phenoxy)imine ligands and their group IV metal complexes with various geometrical isomers (Figure 2). The geometry optimizations were conducted employing density functional theory (DFT) with the Turbomole 7.0 suite of programs.[8] The Perdew, Burke, and Ernzerhof (PBE)[9] function was used for the geometry optimization calculations. The triple-ζ basis set augmented by a polarization function (Turbomole basis set TZVP) was used for all the atoms. The resolution of identity (RI) along with the multipole accelerated resolution of identity (marij) approximations was employed for an accurate and efficient treatment of the electronic Coulomb term.

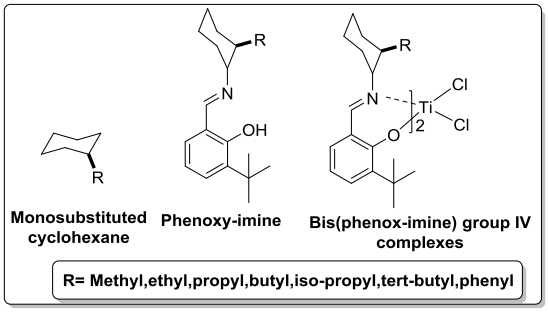


Figure 2. Substituted cyclohexane, phenoxy-imine ligands and their complexes used for modeling studies

Results and discussion

To better understand the fluxional behaviour of phenoxy-imine derived titanium complexes, we investigated the conformational effect and structural isomerism in a series of phenoxy-imine complexes with varying substitution on the cyclohexane ring. The minimized energy profiles are presented in Table 1.

Two chair conformers will exist due to presence of mono-substitution in cyclohexane ring: one with the substitution at axial and other with substitution at equatorial.

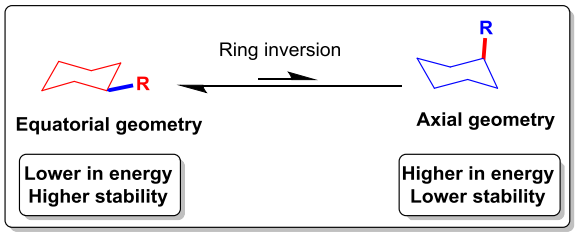


Figure 3. Ring inversion as function mono-substitution in cyclohexane

These two forms are in rapid equilibrium ; however, they do not have the same energy. In all cases (Table 1), the conformer with axial substitution possesses higher energy, suggesting a lower population of this conformer in equilibrium. This is due to 1,3-diaxial interaction between substituted group and respective hydrogen present at axial position. However, close inspection of structural parameters suggested that steric environment around the Cl-bound sites (i.e., potential polymerization sites) are fairly different among all the complexes. Namely, the distances between the Cl and its nearest C atom in the cycloalkyl group attached to the imine-N are presented in Figure 4.

Table 1. Energy difference in various substituted cyclohexanes in ligands and their complexes for the equatorially substituted conformer over the axially substituted

R_1	Cyclohexane	Ligand	Complexes
ΔE (kJmol^{-1}) = Energy difference between axial and equatorial conformers			
	0	0	0
Me	7.29	11.36	40.06
Et	7.78	8.99	37.60
Pr	8.12	10.05	39.65
i-Pr	10.19	6.99	94.41
Bu	8.59	7.52	57.15
t-Bu	23.98	26.42	377.40

Ph	10.62	16.06	69.07

All the bis(phenoxy–imine) Ti complexes

adopt an *Oh (Octahedral)* geometry around the metal centre with two imine nitrogen's, two phenolic oxygen's, and two chlorine atoms. These complexes exist as isomers (Figure 5) according to the position of ligands. Optimized energy profile (Table 2) suggested that the N,N-*cis*-O,O-trans isomers are energetically more favoured.

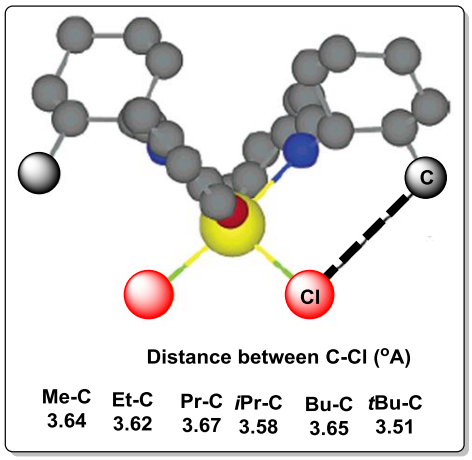


Figure 4. Distance between the Cl atom and substituted group on cyclohexane ring

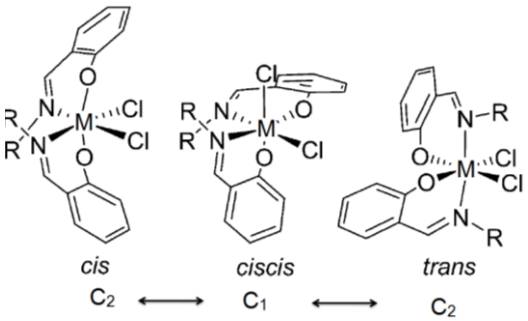


Figure 5. Isomeric forms of complexes

Table 2. Relative energies of the isomers of N-substituted bis(phenoxy-imine) group complexes, with respect to the most stable isomer, kJ/mol.

Complex	**Energy profile in**

	kJmol^{-1}		
Substitution on cyclohexane	C2 Cis	C1 Ciscis	C2 Trans
H	0	12	27
Me	0	9	34
Et	0	10	4
Pr	0	13	12
***i*-Pr**	0	11	1
Bu	0	10	5
***t*-Bu**	0	**	10
Ph	0	7	4

** Structure did not optimize

This approach is useful as it will restrict conformational changes in the time scale of polymerization (restricting chair-chair conformation) and provides sufficient steric crowding around the metal centre.

Conclusions

Using computational methods, we have demonstrated that the isomeric preferences in the bis(phenoxy-imine) group 4 complexes can be tuned by careful selection of the ligands. These preferences are determined solely by the nature of the substituent at the imine nitrogen atom and more particularly by its steric hindrance. The complexes with substitution at equatorial conformers display higher potential energy than that of axial conformer. Thus, a suitable substituent may potentially arrest one of the configurations at the time scale of polymerization. The steric crowding around metal center may further suppress β-hydride elimination from the growing polymer chain leading to UHMWPE. The molecular level understanding and theoretical approach presented here is a guide for validating the hypothesis by experimental design of appropriate bis(phenoxy-imine) metal complexes. Such phenoxy-imine derived transition metal complexes are being synthesized and currently investigated for the preparation of UHMWPE.

Acknowledgements

KP gratefully acknowledges financial support from CSIR Bhatnagar Fellowship and DST India Young Scientist Scheme.

References

74. S. M. Kurtz. The UHMWPE Handbook. pp 1-6. 1968

75. S. M. Kurtz, The UHMWPE Handbook. Ultra High Molecular Weight Polyethylene in Total Joint Replacement; Elsevier Academic Press: New York, 2004.

76. H. H. Brintzinger, D. Fischer, R. Mulhaupt, B. Rieger, R. M. Waymouth, *Angew. Chem. Int. Ed. Engl.* 34, 1143, 1995.

77. H. Braunschweig, F. M. Breitling., *Coord. Chem. Rev.* 250, 2691, 2006

78. H. Makio, T. Fujita., *Acc. Chem. Res.* 42, 1532, 2009.

79. H. Makio, H. Terao, A. Iwashita, T. Fujita., *Chem. Rev.* 111, 2363, 2011.

80. H. Terao, S. Ishii, J. Saito, S. Matsuura, M. Mitani, N. Nagai, H. Tanaka, T. Fujita., *Macromolecules.* 39, 8584, 2006.

81. R. Ahlrichs, M. Bar, M. Haser, H. Horn, C. Kolmel, *Chem. Phys. Lett.* 162, 165, 1989.

82. J. P. Perdew, K. Burke, M. Ernzerhof, *Phys. Rev. Lett.* 77, 3865, 1996.

MACRO 533

Studies on the effect of catalyst and reaction kinetics of Polyether Based PUIR Foam

*Remya Balakrishnan[a],Monisha K[a], Suresh Kumar[a], Vibhu Unnikrishnan[a], Vijayakumar V C[a]

Application Development Division, CSG, PCM entity

VSSC, ISRO, Thiruvananthapuram- 695022

**e-mail id:*remya_balakrishnan@vssc.gov.in

Abstract

Polyurethane modified isocyanurate (PUIR) foam finds extensive role in both space and non-space arena. In launch vehicles, PUIR foam acts as the major insulation of cryo tanks. However, optimization of density and foaming parameters is a major concern in the usage of PUIR foam for cryoinsulation. Density of PUIR foam has to be optimized without compromising thermo-mechanical properties. Similarly characteristic parameters such as cream time, rise time and tack

free time also needs to be optimised for the ease of application of foam over cryo tanks. Characteristic time and density of the foam can be optimised by altering the concentration of catalysts used. In the present work, effect of concentration of tin and variations in thermo-mechanical and physico- chemical properties such as thermal conductivity, specific heat, TGA and compressive strength are studied. The reaction kinetics of polyurethane foam formation was evaluated using Fourier transform infra-red spectroscopy.

Keywords: *PUIR foam; Cryogenic insulation; Reaction kinetics*

1. Introduction

Polyether based urethane modified isocyanurate (PUIR) is one of the commercially important class of polyurethanes. Polyurethanes are basically organic polymers made up of urethane linkages. Usually these polymers are obtained by the combination of a polyisocyanate with reactants which have functional hydroxyl groups e.g. polyethers, polyesters, castor oil etc. Polyurethanes stand for a wide range of plastics rather than being a single well defined polymer resin. The discovery of polyurethanes dates back to the year 1937, by Otto Bayer and his co-workers and first commercial production started in the year 1952 using TDI and polyester polyols. Today PU industry has grown significantly with PU products ranging from PU hybrids, PU composites and non-isocyanate PU with a wide scale of application in several fields, including both space and non-space arena. In launch vehicle scenario, PUIR foam has a major role in the insulation of cryo tankages and liquid stage tankages. Another variation of Polyurethane is flexible foam which acts as dampeners with good rebouncing properties. A wide range of products have been manufactured whose core ingredient is PU such as adhesives, paints, coatings, elastomers, flexible foams, rigid foams etc.
Rigid polyurethane foam was moulded according to the composition given in the following Table 1. Isocyanate index is defined as the ratio of isocyanate equivalent to hydroxyl equivalent and for the given experiment isocyanate index was maintained at 1.6.

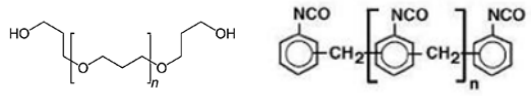
Table 1 Basic composition of Polyol Premix

Polyol	50 g
Amine catalyst	1.1-1.5 g
Tin catalyst	0.1-1.0 g
Potassium Octoate catalyst	0.7-0.8 g
Silicone surfactant	0.9-1.0 g
Distilled water	0.2-0.4 g
Blowing agent	10-20 g
Curing Agent	80-90 g

2. Experimental

2.1.Materials

Polyol with hydroxyl value 350- 550 mg KOH/g, viscosity in the range of 3000-4500 cP was provided by M/s Manali Petrochemicals, Chennai and was used as received. Amine catalyst with nitrogen content 5 - 7% and MDI with NCO content in the range of 29- 33% was obtained from M/s Surabhi Industries, Pune. Tin catalyst with tin content in the range of 18 - 18.6% was obtained from M/s Evonik, Germany. Blowing agent was procured from M/s Lab Chemie, Mumbai.



(a) **(b)**

Figure 1: Structure of (a) Polyether Polyol
(b) Polymeric MDI

2.2.Experiments – Effect of concentration of Tin catalyst

The thermo-mechanical properties and foaming properties need to be optimized for the application of PUIR foam on cryo tankages. Optimisation of properties is carried out by varying the concentration of tin catalyst. Polyol premix was prepared by mixing required quantity of polyol, catalyst, surfactants and distilled water as per the composition given in Table 1. In every polyol premix, concentration of tin catalyst was varied from 0.4 to 1 pbw of base polyol by keeping the concentration of other ingredients constant. Subsequent to that required quantity of blowing agent is added to the mixture and finally mixed with required quantity of curing agent. The foaming mixture was poured in an open mould to allow free rising of foam. The characteristics time was noted during foaming and the specimen was cured at room temperature for 24 hours.

2.3 Foam Specimen preparation

After complete curing, foam specimens of dimensions 50 mm x 50 mm x 50 mm and 140 mm x 80 mm x 20 mm were prepared from the cured block and characterised.

3. Results and discussion

3.1. Characteristics time

Variation in characteristics time like cream time, rise time and tack free time by varying the concentration of tin catalyst were studied. Characteristics time play a major role in determining the properties of the insulation especially when foam application was carried out by Spray on foam insulation technique (SOFI).In the present study, tin catalyst concentration of 0.5g gave the best results.

3.1. Foam Properties

Subsequently other thermo physical characterisation such as density, compressive strength, specific heat, thermal stability etc. were carried out by varying concentration of tin catalyst.

3.2. Density

Lowest density was obtained at 0.5 parts by weight tin catalyst and corresponding compressive strength was also within acceptable limits. Variation of density with change in concentration of tin catalyst is shown in below figure. From the figure it is clear that by increase in concentration of tin catalyst resulted in more closed cells formation thereby entrapment of more blowing agent. This result in decrease in density. After a particular limit, the gelation took place too fast so that effective blowing of all cells did not happen. This lead to an increase in density.

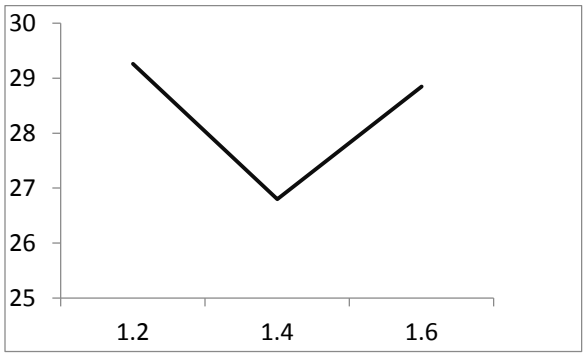


Figure 2: Variation of density with tin catalyst concentration

3.3. Compressive Strength

Externally applied stress deforms the cell structure, ultimately leading to cell collapse. For cryogenic insulation application minimum compressive strength required is 1.6ksc. From Fig.2, it is clear that the compressive strength is lower for low density foam i.e at 0.5g of tin catalyst. The main reason for this pattern is the fact that with increase in concentration of tin catalyst, the density of the foam decreases to a minimum value and then increases. Since compressive strength is directly proportional to density, the same trend is observed.

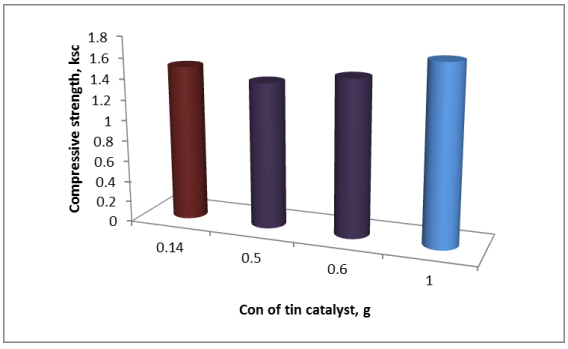


Figure 3: Variation in compressive strength w.r.t to concentration of tin catalyst

3.4. Specific Heat

Foam samples were analysed for specific heat and it was found that specific heat of PUIR foam was maximum at 0.5g tin catalyst. Since more closed cells with more enatrapped blowing agent are formed in lesser quanity of tin catalyst, the heat supplied will resulted in vapouristaion of blowing agnet inside the cells therby increasing the specific heat. As concnetartion of tin catlayst

is increased blowing agent inside the cells will be less. So heat supplied will be utilised for increasing the temaperture of the foam.

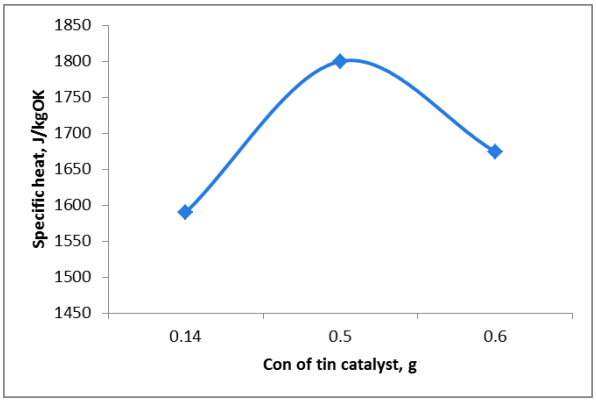


Figure 4: Variation of specific heat with change in catalyst concentration

3.5. Thermal stability

Thermal stability of PUIR foam was examined by TGA curves (weight loss versus temperature) are shown in Figure 4. Thermal degradation mechanism of polyurethanes is usually described as a very complex process that involves dissociation of the initial polyol and isocyanate components followed by thermal decomposition leading to the formation of amines, small transition components and carbon dioxide.

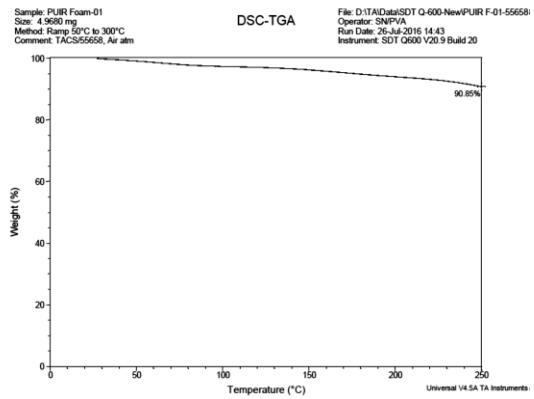


Figure 5: TGA curves of polyether based foam

TGA curves show that the polyether based polyurethane foam is stable up to 250 °C after that deformation occurs resulted in charring. Slight weight loss found is due to loss of volatile matter. The stability at these temperatures may be attributed to the complex cross-linked structure of PUIR foam.

3.6. Thermal conductivity

Thermal conductivity is an important property for insulating materials. For a good insulator, thermal conductivity should be very low. For PUIR foam used in cryoinsulation, thermal

conductivity at RT should be less than 0.035 W/mK. Thermal conductivity of PUIR foam is measured by hot wire method. It was found that thermal conductivity was not affected by varying tin catalyst concentration.

4. Kinetics of the reaction

4.1.Cure reaction by FTIR spectroscopy

In PU chemistry, reaction rate and extent of polyurethane formation is of great importance as it affects the mechanical and thermal properties of insulation. The kinetic study of the reaction between Polyol premix and MDI was carried out using FTIR spectroscopy. The spectra were recorded on a Nocole iS 50 FTIR spectrometer by spreading the sample between two KBr plates. The curing reaction between polyol and MDI was monitored using FTIR spectroscopy and the order of reaction was assumed to be second order due to the following equation:

R-OH + R'-NCO ⟶ R-NHCOO-R'--- (1)

The rate of reaction is given by the equation

$r = k[OH][NCO]$ ---------- (2)

where ;

OH stands for hydroxyl group in polyol; NCO stands for isocyanate group in MDI;

k stands for reaction rate constant.

4.2.Kinetic analysis

Polyol and MDI were mixed together with an isocyanate index of 1.6at room temperatures and FTIR spectra were recorded. The spectra were recorded at different time intervals and the disappearance of NCO (in MDI), which gets converted to form urethane (NHCO), was measured by monitoring the decrease in intensity of -NCO peak at 2269 cm^{-1}. The band at 2926cm^{-1} corresponding to C-H stretching, which remains unaffected during the cure reaction, was taken as the reference.

Isocyanate conversion was calculated as follows:

$$\alpha = 1 - \frac{(A_{NCO}/A_{ref})_t}{(A_{NCO}/A_{ref})_{t=0}} \text{----------(3)}$$

Where ;

A_{NCO} corresponds to absorption peak of NCO i.e peak at 2269cm^{-1}

A_{ref} corresponds to absorption of reference peak. i.e. peak at 2926cm^{-1}

The ratio A_{NCO}/A_{ref} was used to monitor the change in intensity at different time intervals quantitatively.

Isothermal kinetics is the conventional method for the evaluation of kinetic parameters, which are evaluated based on the following equation

$$\frac{d\alpha}{dt} = k(1-a)^n \text{ ------- (4)}$$

Where α is the fractional conversion of NCO to polyurethane, n is the order of the reaction and k is the reaction rate constant. A plot of ln(dα/dt) versus ln(1-a) will give a straight line with slope = n and intercept = k. However, as accuracy of differential determination is poor, integral approach is adopted for finding out the rate constant.
Rearranging and integrating the above equation we get;

g (α) = kt---------- (5)
where;
g(α) = 1- (1-α)^n / 1-n----------(6)

Plot of g(α) vs time give a straight line with slope = k. Here n=2 as the reaction follows second order.

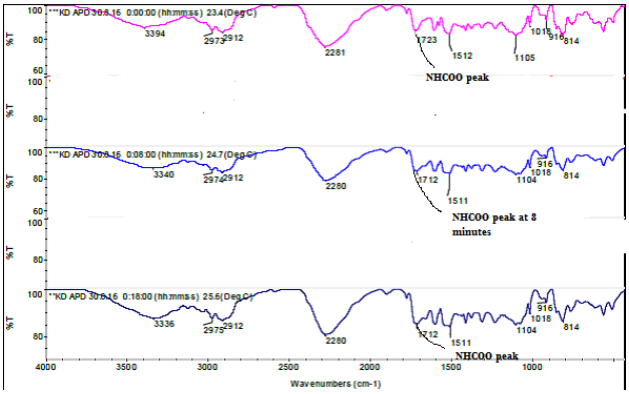


Figure 6. FTIR spectra of reactive sample recorded at different time intervals

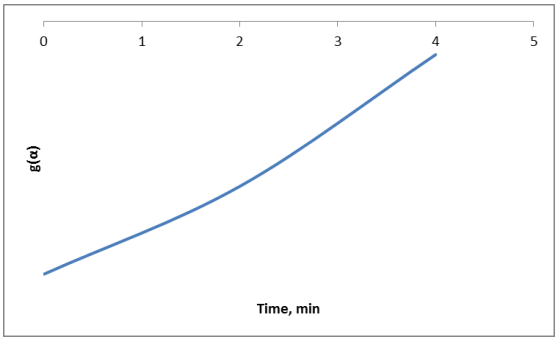


Figure:7. Plot of g (α) versus time

From the slope of the plot, rate constant was calculated as 4 x 10^{-5}.

Conclusions

The characteristics time, thermo-physical and mechanical properties of the polyether based polyurethane foam was evaluated as a function of varying concentration of tin catalyst. Density is seen to decrease up to a certain limit beyond which it was found to increase with increasing catalyst concentration. Specific heat was found to follow an opposite trend where the values increased up

to a certain point followed by a constant decline. The study of reaction kinetics of polyol and isocyanate is found to follow second order, as indicated by FTIR data.

Acknowledgements
Authors would like to thank ASD/VSSC and HTCSL/PRSO/VSSC for providing analytical support. Authors would like to express gratitude to Dr. Subal Chandra Bera, Former Head, APD/VSSC for giving proper guidance and his technical expertise. In addition authors would like to acknowledge Dr. S.C. Sharma, Deputy Director, PCM, VSSC and Dr.S.A.Ilangovan, Group Director, CSG, VSSC for their contributions to this paper.

References

83. Kinetics and thermodynamics studies of the formation of a polyurethane based 1,6-hexametheyle diisocyanate and poly(carbonate-coester)diol,B.FernandezArlas, L. Rueda, A.Eceiza.

84. Kinetics of HTPB based polyurethanes-An FTIR study, R. Sadhana, S.Reshmi, T.L.Varghese, K.G.Kannan and K.N. Ninan

85. Polyurethane Handbook, Chemistry- Raw materials - Processing- Application –Properties by Dr. Gunter Oertel.

MACRO 534

Flexible Polyurethane Elastomer bearing Ionic Liquid Crosslinks

Prasanta Kumar Behera, Nikhil K. Singha.

Rubber Technology Centre, Indian Institute of Technology Kharagpur, Kharagpur - 721302, West Bengal, India. E-mail: beheraprasanta68@gmail.com Tel: + 91-9475411594

Abstract: This investigation reports the influence of ionic liquid crosslinker on the properties of polyurethane (PU) elastomer. A novel ionic liquid (IL) crosslinked flexible polyurethane elastomer (PU-IL) was successfully synthesized by one pot polymerization method. The properties of this PU-IL were compared with PU prepared using conventional chain extender like butanediol (BDO). FT-IR spectroscopy shows that the hydrogen bonding interaction was significantly suppressed in the presence of ionic liquid crosslinker. Differential scanning calorimetry (DSC) analysis demonstrated the improved flexibility of PU-IL, as the glass transition temperature (T_g) of PUIL was lower than PU having BDO as chain extender. The

low T_g of PU-IL was also confirmed by DMA analysis. The flexible nature of PU-IL was also reflected in the mechanical properties. PUIL exhibited a significantly higher tensile strength as well as higher elongation at break than the conventional PU. Interestingly, PU-IL showed greater polarity as well as high-temperature oil resistance properties.

Keywords: Ionic liquid, Crosslink, Polyurethane, Elastomer, Thermal properties.

References:

1. H. Zhang, P. K. Behera, N. K. Singha, K. Hong and J. W. Mays, Polymerization in Ionic Liquids. *Encyclopedia of Polymer Science and Technology*, 2015.

2. S. R. Williams, W. Wang, K. I. Winey and T. E. Long, *Macromolecules*, 2008, **41**, 9072-9079.

3. M. Zhang, S. T. Hemp, M. Zhang, M. H. Allen, R. N. Carmean, R. B. Moore and T. E. Long, *Polym. Chem.*, 2014, **5**, 3795-3803.

MACRO 541

Role of sample preparation techniques for analysis of trace metals in polymers

A.D. Rosa ,[a] R. Ganeshan,[b]

[a] *Analytical Division, SABIC technology center, Bangalore562125, India*

[b] *Analytical Division, SABIC technology center, Bangalore-562125, India*

* *e-mail id: rosa.ad@sabic.com*

Abstract

Elemental analysis is one of the analytical techniques which gives information about the different types of metals present in a sample. Among the many techniques available for elemental analysis, ICP-OES/MS is one of the advanced techniques capable of estimating metals at trace levels accurately. However, it should be noted that however advanced the techniques may be, the key to obtaining accurate results also heavily depends on the accuracy of the sample preparation used for analysis. An understanding of the characteristics of the elements present in a particular matrix is absolutely necessary to generate the right results. This paper talks about one such study of metal analysis in a polymer which posed the challenge of subliming at high temperature. Additionally, it had a challenge of dealing with volatilization of the metal of interest itself i.e. Sb. The approaches used to address these challenges and obtaining accurate results for all metals including Sb are described in this paper.

Keywords: *polymer; ICP-OES/MS; Sulphated ashing; Microwave digestion; Validation; Antimony (Sb).*

Introduction

Polymers are formed by chemical reactions in which a large number of molecules called monomers are joined sequentially, forming a chain. In many polymers, only one monomer is used (homopolymer). In others, two or three different monomers may be combined (copolymer). Commercial polymers typically include a base polymer and a number of other components such as anti-oxidants, UV stabilisers, colour master batch, inorganic fillers, glass and carbon fibres, plasticisers, processing aids and cross-linking agents to name a few. Elemental analysis of polymers is important for establishing conformance to regulations such as WEEE and ROHS, investigating the cause of polymer degradation, identification of contamination, establishing if counterfeit materials have been used and for investigating interaction between polymers and metals.

The most common methods of sample preparations used for metal analyses in polymers are viz., (1) sulphated ashing method and (2) microwave digestion method [1, 2].

Experimental

In the current study, sample was first analysed by preparing the sample as per method – 1 i.e., sulphated ashing method. About 5g of sample was weighed in quartz crucibles and 1 mL of suprapure sulphuric acid was added and slowly ramped to 550° C and allowed to stay at that temperature for 6 hours. The ash obtained was dissolved using suprapure hydrochloric acid and made up to a known volume with water. During sample preparation, unexpectedly, lot of white deposits were seen on the walls of the fume hood and also on the vessels used in the sample preparation process. The deposited material was scraped from the walls of the vessels for further investigation and understanding. The ashed sample was analysed by ICP-MS after requisite dilutions in suprapure acids.

The results obtained from use of this approach was reviewed and based on the outcome, the sample was also taken up for digestion by microwave method (method – 2) wherein about 0.5 g of sample was digested in CEM Microwave Digester (Easyprep™) and the resulting sample was further processed for ICP-MS analysis. 2 mL of suprapure sulphuric acid and 6 mL of suprapure nitric acid was added to about 0.1g of polymer for microwave digestion. All analyses were done in triplicate for ensuring a good understanding of the precision of the method.

Agilent 7700 ICPMS [3] along with multi-element calibration standards from Merck Inc were used for study.

Results and discussion

The white deposits obtained during the study done as per method-1 were analysed by HPLC and the results showed that this was the monomer of the polymer used and was deposited on the wall due to degradation of the polymer due to heating, which was leading to sublimation of the resulting monomer. These results were also corroborated by the unexpectedly low levels of metal as per ICP analysis. It was concluded the sublimation of the monomer was aiding the loss of Sb present in the polymer, which itself was also volatizing during the heating/ashing process [4].

To confirm this understanding, the sample was re-prepared using method-2 wherein, the Sb content was close to expectation as shown in Figure 1. Additionally, spiking studies were carried out to confirm the accuracy of these results.

To accurately estimate the content of other metals, method-1 was modified in such a way, as to add double the normal amount of sulphuric acid than before (2 mL instead of 1 mL) to the wet the entire 5 grams

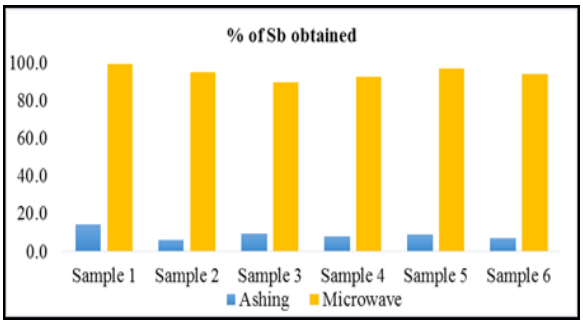


Figure 1. % of Sb obtained by ashing Vs microwave digestion methods

of polymer sample. This was done to ensure the coating of sulphuric acid will prevent the volatilization or undesirable loss of metals during the sublimation of the monomer resulting from the degradation of the polymer. The resulting ash was analysed by ICP-MS for all elements and showed good accuracy (1 ppm levels- 75 to 125 %), except Cr and Ti (Figure -2).

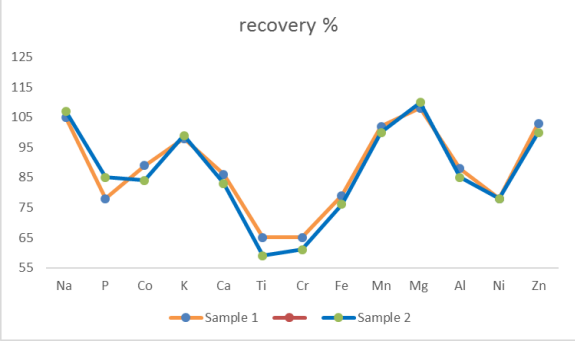


Figure 2. % recovery of metals from standard spiking study

Based on the literature survey, it was understood that this kind of observation or behaviour has been seen before by other researchers and has been addressed by dissolving the ash in aquaregia or by fusing the final ash with potassium bisulphate.

Conclusions

In this study the determination of complete elemental composition was accomplished by using a combination of two methods for sample preparation.

It may be concluded that sulphated ashing method is a preferred sample preparation technique for polymers that contain trace levels of metals. The advantage of this technique being, very low levels of metals i.e. as low as 1 ppm, can be quantified, as higher weight of sample can be taken for analysis depending on the crucible size. However, it is not suitable for elements that are volatile in nature such as Cd, Pb, As, Sb etc. as it is an open digestion method. However**, f**or samples containing volatile elements and metals above 5 ppm, microwave digestion is a preferred technique as it is a closed vessel digestion which prevents the loss of metals due to volatilization. The drawback of this technique is the limitation of the sample quantity that can be used for digestion i.e. 0.5 g for organic sample. This makes it difficult to quantify metals present in trace amounts (i.e. < 5 ppm).

Hence proper judgement is required in choosing the right sample preparation technique based on the concentration of the analyte and also the nature of the analyte.

References

1. T. R. Crompton, Polymer Reference Book. RAPRA Technology Limited, Shropshire, UK, (2006).
2. Z. Mester, R. Sturgeon, Sample preparation for trace element analysis, Ed: D. Barcelo, Amsterdam, Elsevier, 2003.
3. Robert. Thomas, Practical guide to ICP-MS, Taylor and Francis, FL, USA, 117-120, 2013.
4. N. A. Asryan, A. S. Alikhanyan, G. D. Nipan, Doklady, *Physical Chemistry*, 392, 221, 2003.

MACRO 544

A Promising approach to design and develop UV/ Thermal dual cure acrylate binder from renewable resources

Ozlem Kubra AKDOGAN and Vijayakumar Mannari
Eastern Michigan University, Ypsilanti, MI 48197, USA
oakdogan@emich.edu

Protection and decoration are inevitable needs of our lives. Coatings are one of the most important polymer-based products that improve performance and provide durability while attributing aesthetic appearance to the goods. Nevertheless, petroleum products are used as primary resources to produce raw materials in the coatings industry. We believe that, while creating such an extremely useful technology for industry, it is required to replace petrochemical-based raw materials with more sustainable alternative solutions.

Vegetable oil is fascinating bio-based resource that is used for myriads of chemical and specialty products including coatings and is at the center of my research. Bio-based chemicals have a very long history of being used in adhesive, sealant and coatings industry due to their versatility and nontoxic properties. Promoting bio-based chemicals in terms of design, formulation and synthesis are the key elements of my research. Rubber seed (1), linseed oil (2,3) soybean oil (4,5), cardanol oil (6,7) are used mainly due to their high-performance properties in coatings applications.

Epoxidized soybean oil (ESO) and acrylated soybean oil (ASO) are used to design and formulate sustainable building blocks for advanced UV-cure systems. Our research focuses on development of novel materials for UV-cure system that are not only bio-based and sustainable but also provide additional value proposition to some chronic industrial problems. Novel-dual cure systems that cures by both thermal as well as UV-cure mechanism are being designed and investigated for its performance, "green" character and suitability for practical application.

The research focuses on synthesis and characterization of polyester acrylate oligomers derived from epoxy resin (ER), itaconic acid (IA) (bio-based material), and glycdylmetharylate (GMA). This novel polyester acrylate is then be blended with Acrylated epoxidized soybean oil (AESO)

in varying proportions. This polymer blend containing both hard and soft materials, and containing both acrylate and hydroxyl groups has been used to formulate dual-cure coating systems. Dual-cure systems –that will cure by both radical polymerization (acrylate) and step-growth polymerization (-OH + -NCO) mechanism have been formulated by addition of varying amount of aliphatic polyisocyanate crosslinker. The wet films of the coatings were applied and cured under different conditions - only by thermal cure (step-growth), only by UV-cure and dual-cure. Cure study has been done using FT-IR spectroscopy (Peak area ratio method) to study the effect of cure type on properties of coatings. The

differential scanning calorimetric technique (DSC) is used to investigate their mechanical properties as a function of cure type. Effect of composition and cure type on various film properties such as adhesion, flexibility, pencil and pendulum hardness, and impact resistance, and solvent resistance has been studied.

This research will provide useful insight into the application of such high-bio-based content dual-cure coatings for commercial applications. This outcome of this research will demonstrate how principles of green chemistry can be applied for effective transition from petrochemical resources to greener bio-based materials for high performance advanced coatings, while reducing environmental impact.

References

A.I. Aigbodion, F. O. (2003). Rubber seed oil modified with maleic anhydride and fumaric acid and their alkyd resins as binders in water-reducible coatings. *J. Appl. Polym. Sci.*

D. Akram, E. S. (2009). Synthesis and characterization of boron incorporated polyester polyol from linseed oil: a sustainable material. *Macromol. Symp.*

D. Akram, E. S. (2010). Development and characterization of boron incorporated linseed oil polyurethanes. *J. Appl. Polym. Sci.*

M. Jalilian, H. Y. (2010). Preparation and characterization of polyurethane electrical insulating coatings derived from novel soybean oil-based polyol. *Polym. Adv. Technol.*

M.C. Brasil, A. G. (2007). Organic–inorganic hybrid films based on hydroxylated soybean oils. *J. Am. Oil Chem. Soc*.

Ren Liu, X. Z. (2015). UV-Curable Coatings from Multiarmed Cardanol-Based Acrylate Oligomers. *ACS Sustainable Chem.*

Eng.,.

Riya Srivastava, D. S. (2015). Mechanical, chemical, and curing characteristics of cardanol–furfural-based novolac resin for application in green coatings. *Journal of Coatings Technology and Research*.

MACRO 548

Fiber based poly(lactic acid) materials for self-reinforced composites

de Kort, G. W.[a,b]; Auhl, D*. [a,b]; Wilsens, C.H.R.M.[a,b]; Rastogi, S[a,b].

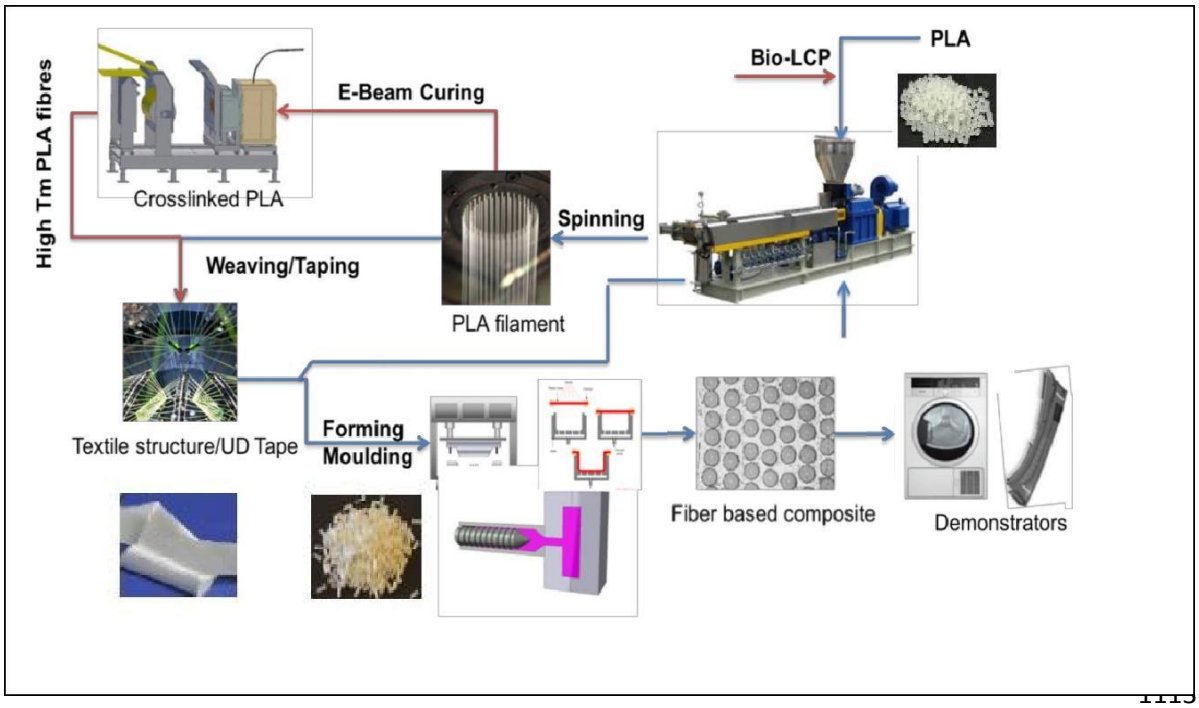
[a]*Department of biobased materials, Maastricht University, P.O. Box 616, 6200MD Maastricht, The Netherlands.*

[b]*Aachen-Maastricht Institute for BioBased Materials (AMIBM), Urmonderbaan 22, 6167 RD, Geleen, The Netherlands*

**corresponding author: dietmar.auhl@maastrichtuniversity.nl*

Poly(lactic acid) (PLA) is, from a scientific point of view, the most well known and most investigated bio-based thermoplastic polymer. It is an incredibly versatile material, with two distinct synthesis routes; a tendency to crystallise; and various properties that are readily tuneable by stereo-content or chain architecture. In spite of this incredible versatility and all available knowledge, the current industrial impact of PLA is fairly limited, as it is mainly used in packaging- and various medical applications. However, there might be more opportunities for large scale application of PLA, if the materials and processing conditions are carefully selected and modified. Therefore we are working towards bio-based self-reinforced composites (SRC).

In a self-reinforced composite both the matrix - and the reinforcing phase have the same chemical composition, which has great benefits in terms of recyclability, but imposes challenges in terms of the processing window.[1] The melting temperature of PLA can be tuned by the stereo-content, making it an excellent candidate for SRC-applications. We, and our partners in the BIO4SELF project, do not just want to achieve a self-reinforced PLA composite, but we also work to achieve additional reinforcement via the incorporation of a liquid crystalline polymer (LCP) in the reinforcing phase of the composite. LCP´s are highly effective in increasing the strength and modulus [2], and can be obtained from bio-based monomers [3]. In this way we are able to obtain bio-based composites with excellent mechanical properties, which are able to compete with oil-based materials.



Scheme 1. Schematic overview of the route towards highly functional self-reinforced PLA composites

References

[3] Mai, F.; Tu, W.; Bilotti, E.; Peijs, T.; *Composites: Part A journal*, 76, **2015**, 145
[4] Mandal, P.; Chakraborty, D.; *Journal of Applied Polymer Science*, 11, **2009**, 2346
[5] Wilsens, C.H.R.M.; Verhoeven, J.M.G.A.; Noordover, B.A.J.; Hansen, M.R.; Auhl, D.; Rastogi, S.; *Macromolecules*, 47, **2014**, 3306

MACRO 552

Cure Characteristics and Physico-Mechanical Properties of a Conventional Sulphur-Cured Natural Rubber with a Novel Anti-Reversion Agent

G.S Shibulal,* J.Y. Jung, K.U. Jeong, C. Nah

Haptic Polymer Composite Research Team & Department of Polymer-Nano Science and Technology, Chonbuk National University, 567 Baekje-daero, Jeonju 561-756, Republic of Korea

** e-mail id: gslal2009@gmail.com*

Abstract

Vulcanization of natural rubber (NR) with conventional accelerated sulphur (CV) system leads to vulcanizate with polysulfidic linkages in the network. These polysulfidic linkages are less stable at elevated temperature due to reversion, which reduces the mechanical properties and increases the compression set. Moreover, the high temperature vulcanization of NR is limited due to reversion. To solve these problems, 4, 4'-bis (maleimido) diphenylmethane (BMDM) was used as an anti-reversion agent. The cure behaviour of NR-CV system with 5 phr of BMDM exhibited excellent reversion stability even at high temperature without adversely affecting the scorch safety as well as the rate of vulcanization. The crosslink densities of NR-CV were greatly increased with the content of BMDM. This enabled us to reduce the compression set values of NR-CV from 38% to 18% at 70°C and from 68% to 38 % at 100°C with the use of 5 phr of BMDM.

Keywords: *natural rubber, bismaleimide, crosslink density, compression set*

Introduction

The reversion in natural rubber can take place both during vulcanization and after the vulcanization (during service). The reversion taking place during curing is an anaerobic thermal ageing process which is mainly due to the breaking of the polysulfidic crosslinks and the subsequent loss of network integrity in the vulcanizate. The physical manifestation of reversion during vulcanization is the reduction of the rheometric torque with time after it has achieved a maximum torque. The crosslink degradation from cure reversion reduces the mechanical performances such as stiffness (modulus), tear strength, tensile strength etc. From a practical point of view, the cure reversion greatly limits the cure time and temperature of especially thick rubber articles [1-7]

The primary objective of this study was to investigate the effect of 4, 4'-(bismaleimido) diphenyl methane (BMDM) as an anti-reversion agent on the curing behaviour of natural rubber (NR) with conventional vulcanization system. The vulcanization characteristics, physico-mechanical properties and the crosslink densities of the NR/CV vulcanizate were evaluated as a function of BMDM content. Based on the curing studies of neat NR with BMDM and N-phenyl maleimide (NPM: a monofunctional maleimide-bearing compound), the plausible reaction mechanism that is responsible for the enhanced the reversion resistance as well as the crosslinking densities in the vulcanizate of NR/CV with BMDM have been proposed.

Experimental

The natural rubber, STR 5CV60 (Mooney viscosity ML(1+4) at 100 °C: 55-65) was procured from Chalong Latex Industry Co., Ltd, Thailand. The bismaleimide [(4, 4'-bis (maleimido) diphenyl methane] with a purity of 99.2% procured from New Century Holding Group Co., Ltd. in China was used as the anti-reversion agent. Other ingredients such as sulphur, n-cyclohexyl-2-benzothiazole sulfenamide (CBS), stearic acid and zinc oxide (ZnO) were purchased from Sigma-Aldrich.

Preparation of rubber compounds

The formulations of the mixes are displayed in Table 1. The typical recipe for curing NR with CV system is designated as NR-CV. Similarly, the recipes taken for investigating the curing behavior of NR with CV in the presence of BMDM are designated as NR-CVB_1, NR-CVB_3 and NR-CVB_5 for 1phr, 3phr and 5phr BMDM content respectively. All the compounds were prepared using an internal mixer (Banbury-type mixer, Nam Yang Corporation, South Korea).

Characterization

The cure characteristics were determined using oscillating disk rheometer (ODR, Alpha Technologies, USA) at various vulcanization temperatures. . The degree of crosslinking was determined by equilibrium swelling method using toluene solvent. The tensile test was carried out using a LRX plus (Lloyd Instruments, UK) machine in accordance with the ASTM D-412 (ISO 37) at a cross-head speed of 500 mm/min at room temperature. The compression set of the vulcanized compounds were determined using cylindrical specimens (12.5 mm height and 29 mm diameter) by applying a 25% compression. FTIR analysis was carried out using NICOLET 6700 model, USA. The spectra was recorded at room temperature and collected over the range of 4000–400 cm^{-1}.

Results and discussion

Cure Characteristics

Depicted in Figure 1 are the cure profiles of natural rubber with CV system at three different temperatures for a period of 30 min. Their major cure characteristics are displayed in Table 2. As was expected, the maximum torque value gradually decreased due to reversion as the cure temperature increased. Moreover, the onset of reversion was shifted to a lower time scale with the increased vulcanization temperature. For instance, the delta torque value was reduced to about 20% as the vulcanization temperature is increased from 160°C to 180°C. This is very common in any CV cured diene elastomers particularly NR due to the breaking of the polysulfidic linkages established in the vulcanizate [1-2].

Figure 2 represents the vulcanization behaviour of NR-CV in the presence of different BMDM content at two different temperatures: 160 and 180 °C. For the sake of clarity, the cure behaviours obtained at 170°C are omitted. However, the cure characteristics obtained for all the three temperatures are listed in Table 2. It can be seen from the table that, incorporation of BMDM into NR-CV system greatly increased its induction period (scorch time) and also the time to optimum cure (t_{90}) particularly at a temperature of 160°C. However, both the NR-CV and NR-CV with BMDM exhibited almost comparable values of scorch time at the high vulcanization temperature (180°C). The increased induction period for the vulcanization of NR-CV in the presence of BMDM can be attributed to a slow rate of reaction between NR and BMDM compared to NR with CV system. However, at the high vulcanization temperature, the reaction between NR and BMDM may take place at a faster rate, consequently reducing the induction time.

Another interesting point is that as the BMDM content increased, the maximum torque (M_H) was also increased at all the vulcanization temperatures. For instance, at 160°C, the M_H for the NR-CV was raised to about 5% with 1 phr of BMDM and further raised to about 18%

with the addition of 5 phr of BMDM. This increase can be attributed to the formation of some additional crosslinks among NR chains by the action of BMDM. The plausible mechanisms between NR and BMDM will be discussed later. In addition to increasing the rheometric torque, the incorporation of BMDM greatly reduced the declination tendency of the rheometric torque (reversion) in the overcure region of NR-CV even at high temperature. For instance, the vulcanization of NR-CV at 160°C showed around 9% declination in the rheometric torque and further reduced to about 26% at 180°C from their respective M_H values at the end of the vulcanization process (30 min). On the other hand, under the same conditions, with the addition of 1 phr of BMDM (NR-CVB_1) showed only 3% and 16% declinations in the rheometric torques from their M_H values at 160°C and 180°C respectively. With the addition of 5 phr of BMI (NR-CVB_5), no declination in the rheometric torque was observed due to reversion at 160°C even up to a period of 1h. But, a negligible declination (< 4%) in the torque value was observed in the over cure region at 180°C for a period of 1h. These observations revealed that BMDM can be used as an efficient anti-reversion agent while curing NR with CV system. Moreover, it can also be concluded that with the presence of BMDM, the vulcanization of NR with CV can be done at high temperature without any severe reversion.

Proposed reaction mechanism between NR and BMDM

To explore the reaction mechanism of the reversion while curing NR with CV in the presence of BMDM, the cure profiles of neat NR with BMDM alone were analysed at two different temperatures: 160°C and 180°C as shown in Figure 3. Unlike the cure profiles for NR-CV, NR with BMDM alone exhibited a marching modulus curing profiles up to 1h. However, at 180°C, the reaction was relatively faster with a higher value of rheometric torque than that observed at 160°C.This means that BMDM alone can form crosslinks with NR and the density of such crosslinks being produced may be higher at a higher temperature. Since there are no other ingredients in the system other than NR and BMDM, one of the plausible mechanisms might be the reaction between the allylic hydrogen from NR with the ene-portion of BMDM via Alder-ene reaction as shown in Scheme I. In order to further confirm the possibility of this reaction, we have studied a comparative analysis of the curing behaviours of NR with N-phenyl maleimide (NPM) and BMDM. Depicted in Figure 4 are the cure profiles of NR with 5 phr of NPM and 5 phr of BMDM at a temperature of 160°C for 1h. It was expected that the monofunctional NPM cannot produce any torque due to crosslinking with NR. Surprisingly, the curing profile of NR with NPM indicated a considerable rise in the rheometric torque and achieved a maximum value in 10 min of curing and a plateau region thereafter. On the other hand, the reaction between NR and BMDM exhibited marching modulus cure behaviour with a 40% higher in the maximum rheometric torque over NR-NPM. This experimental result revealed that NPM can also react with NR via a similar mechanism shown in Scheme I. However, the reaction between NR and NPM cannot make crosslinks between the NR chains as did by the bifunctional BMDM, but can be attached onto the polymeric chains as grafted units. While grafting, the polymeric chain mobility may get restricted by the bulk aromatic units from NPM. This results in increased stiffness of the compound which naturally enhances the rheometric torque with time. Since NPM does not produce any crosslinks between

the NR chains other than grafting, the torque will be naturally lower than the torque produced by BMDM at the same condition.

It has been reported in the literature that the accelerated sulphur vulcanization of NR undergoes several structural modifications which include the formation of cyclic sulfide, conjugated diene and triene etc. in the rubber chains due to reversion [8-9]. Therefore, the observed healing of reversion during the vulcanization of NR-CV with BMDM seem to be ascribed to the scavenging of the *in-situ* formed conjugated dienes on the polymer chain by BMDM via Diels-Alder reaction as depicted in Scheme II. Because of this reaction, some additional non-sulphur thermally stable crosslinks in the form of BMDM bridges may be generated in the vulcanizate. This newly formed crosslinks may repair the loss of crosslinks in the network due to reversion and also prevent the vulcanizate from further reversion. In light of our experimental observations, we can say that both the reactions shown in Scheme I and in Scheme II are taking part in two different situations while curing NR-CV with BMDM. The reaction represented in Scheme I may be predominant during the initial stages of the vulcanization which may be responsible for the additional rise in rheometric torque. The reaction represented in Scheme II may be predominant only after the formation of conjugated diene at the point of reversion, which is responsible for the reversion resistance in the over curing region.

Crosslink density and set properties

Rubber products for sealing applications are usually used in contact with various fluids like hydraulic oils under compression. Vulcanized rubber with a high crosslink density is therefore very essential to resist swelling in an environmental situation involves deliberate or accidental contact with solvent/fluids. The crosslinking densities measured for the vulcanizate are displayed in Figure 5. It can be seen that the vulcanizate NR-CV shows the lowest crosslink density and its crosslink density gradually increased with the content of BMDM. As discussed above, the formation of stiff BMDM crosslinks between the polymeric chains in addition to the polysulfidic linkages is the primary reason for the higher crosslink density in the vulcanizate of NR-CV containing BMDM.

Compression set measures the ability of the cured rubber to recover its original shape after the deformation force is removed. It is well known that vulcanized NR with CV system has a detrimental effect on the compression set due to poor stability of the polysulfidic linkages under heat and pressure. The compression set values of the vulcanizates at two different temperatures: 70°C and 100°C are also displayed Figure 5. As expected, the set values of NR-CV were very high about 36% at 70°C and 66% at 100°C. Interestingly, the set values of NR-CV were greatly reduced from 36% to 18% at 70°C and 66% to 38% at 100°C with the addition of 5phr of BMDM. The reduced set values of NR-CV containing BMDM at elevated temperature can be attributed to the enhanced crosslink density due to the establishment of thermally stable BMDM bridges in the vulcanizates.

Conclusions

The problems associated with the reversion tendency of natural rubber with conventional accelerated sulphur vulcanization (CV) system could be greatly reduced with the use of 4,4'-bis (maleimido)diphenylmethane (BMDM) as an anti-reversion agent. With the use of a 5 phr of BMDM, it was possible to cure NR with CV system without any reversion even at 180°C for a period of 1h. The vulcanization kinetics studies revealed that the use of BMDM does not have an adverse impact on the original vulcanization characteristics of NR-CV system. Based on the curing analysis of neat NR with n-phenyl maleimide (NPM) and BMDM, two possible mechanisms have been proposed for the enhanced reversion resistance: one is the Alder-ene reaction between the active allyl hydrogen atom of NR with ene-portion of the bismaleimide and the other one is the Diels-Alder reaction between the in-situ generated conjugated diene in the main NR chains with the BMDM. The crosslink density values of the vulcanizate of NR with CV could be greatly enhanced with the use of BMDM. This enhanced crosslink density could help us to develope vulcanizate of NR-CV system with low compression set values at elevated temperature.

Acknowledgements

National Research Foundation of Korea (NRF) funded by the Ministry of Science, ICT and Future Planning.

References

86. W. Hofmann Rubber technology handbook. Hanser publisher, Munich,1989
87. H.W. Greensmith, A.A. Watson, J Rubb Res Inst Malaya 22, 120, 1969.
88. R.R. Babu, G.S. Shibulal, A.K. Chandra, K.Naskar, In: P.M. Visakh, S. Thomas, A.K. Chandra, A.P. Mathew (eds) Advances in Elastomers-I. Springer, Netherlands.
89. W.L. Cox, C.R. Parks, Rubber Chem.Technol.39,785,1966
90. Y.S.R. Yahya, A.R. Azura, Z. Ahmad, J.Phy.Sci. 22,1,2011.
91. N.R. Kumar, A.K. Chandra, R. Mukhopadhyay, J. mater.Sci. 32, 3717,1997.
92. R.L.Fan, V. Zhang, C. Huang, Y.X. Zhang, K.Sun, Y.Z. Fan, Polym. Test. 20, 925, 2001.
93. M. Akiba, A.S.Hashim, Prog.Polym.Sci, 22, 475, 1997.
94. A.M. Zaper, J.L. Koenig, Rubber Chem.Technol., 60, 252, 1987.

Table 1. Formulation of the mixes (unit: phr)

Table 2. Cure characteristics of the mixes

Ingredients	NR-CV	NR-CVB$_1$	NR-CVB$_3$	NR-CVB$_5$
NR	100	100	100	100
ZnO[a]	5	5	5	5
Stearic acid	2	2	2	2
Sulphur	2	2	2	2
CBS[b]	0.6	0.6	0.6	0.6
BMDM[c]	-	1	3	5

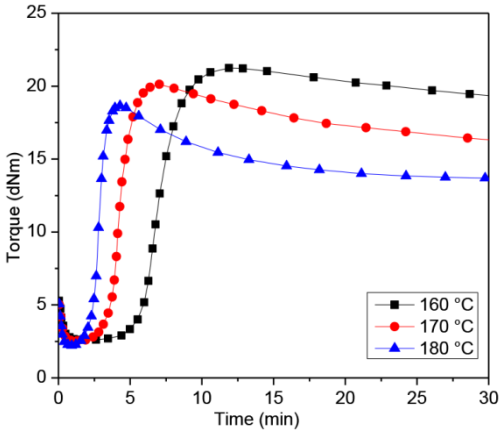


Fig. 1. Cure profiles of NR-CV at various vulcanization temperatures

Compounds	Temp (°C)	ΔM (dNm)	T_{S2} (min)	T_{90} (min)	CRI (min^{-1})
NR-CV	160	18.7	5.8	8.9	32.3
	170	17.7	3.5	5.4	52.6
	180	16.5	2.3	3.4	90.9
NR-CVB$_1$	160	19.1	7.3	12.8	18.2
	170	18.2	4.0	7.0	33.3
	180	17.2	2.4	4.2	55.5
NR-CVB$_3$	160	20.7	7.3	16.9	10.4
	170	19.7	4.1	8.8	21.3
	180	19.0	2.4	5.0	38.5
NR-CVB$_5$	160	22.9	6.8	22.4	6.4
	170	22.0	3.9	11.2	13.7
	180	22.0	2.4	5.7	30.3

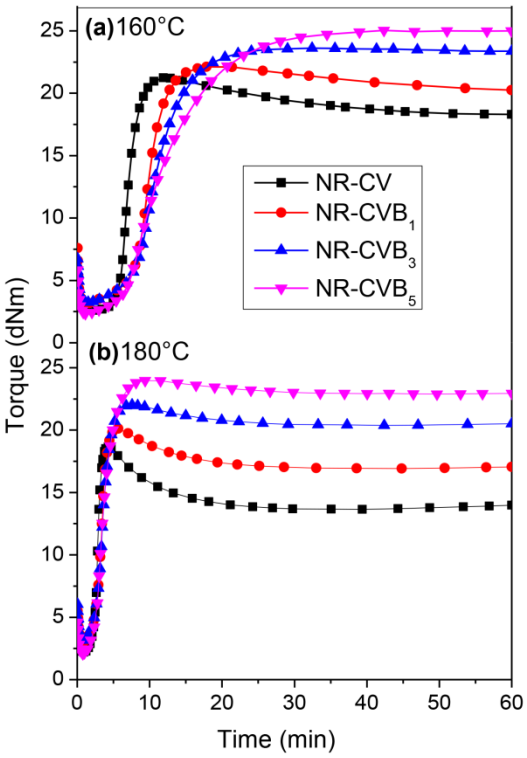


Fig. 2. Cure profiles of NR-CV with various BMDM content (a) at 160°C and (b) at 180°C

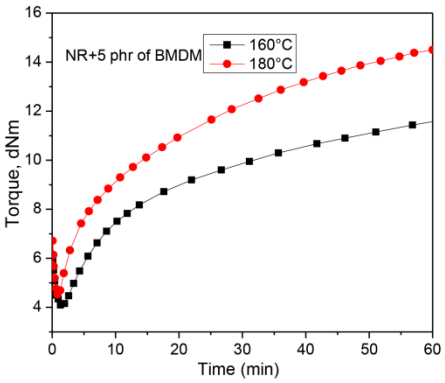


Fig. 3. Cure profiles of neat NR with 5 phr of BMDM at different temperatures

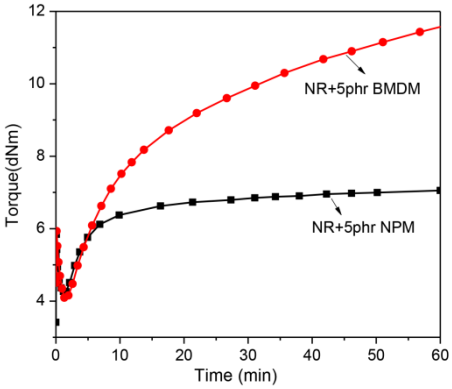


Fig. 4. Cure profiles of neat NR with 5 phr of NPM and 5 phr of BMDM at 160°C

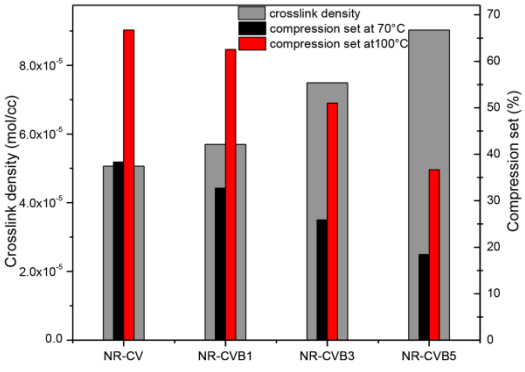
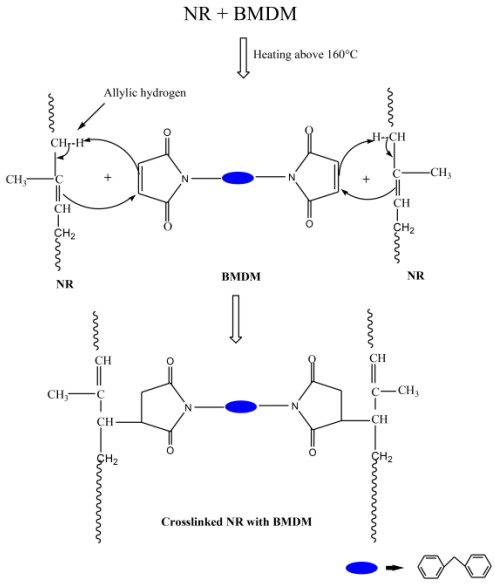
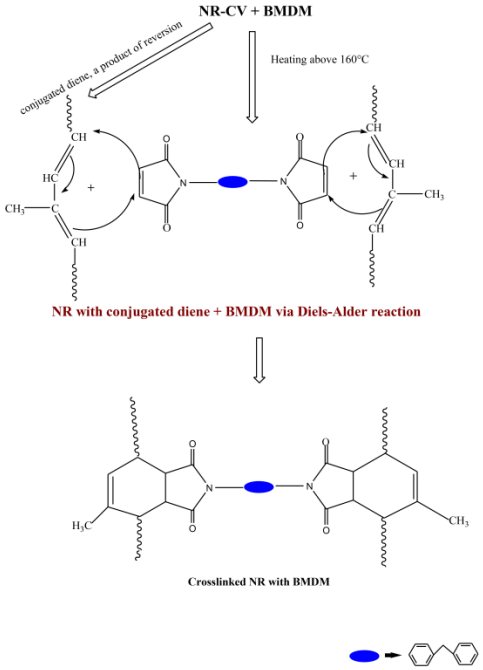


Fig. 5. Crosslinking densities of the vulcanizates and their compression values measured at 70°C and 100°C



Scheme I. Crosslinking of NR with BMDM via Alder-ene reaction



Scheme II. Crosslinking of NR with BMDM via Diels- Alder reaction

MACRO 554

Molecular design of high performing polymers for 3D FDM printing

Srinivas, V.[a,b]; Harings, J .[a]*; Van Hooy, T.[b] ; Dietmar, A. [a]; Rastogi, S[a]

[a]*Department of biobased materials, Maastricht University, P.O. Box 616, 6200MD Maastricht, The Netherlands.*

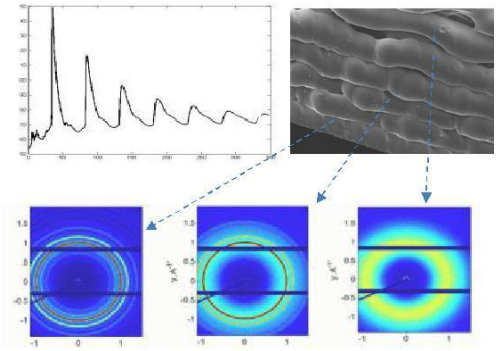
[b]*Zuyd University, Nieuw Eyckholt 300, 6419 DJ Heerlen, The Netherlands*

**corresponding author: Jules.Harings@maastrichtuniversity.nl*

Additive manufacturing, often simply referred to as 3D printing, is presently a rapid developing technology, whereby products are created by depositing material layer upon layer, rendering extraordinary dimensional flexibility and control in the realization of complex geometries. Consequently, via 3D printing technologies niche products of high added value are entering automotive, aerospace, defense, art and medical industries. However, from an economic perspective serious doubts are posed, which are often based on a mismatch between expectations and current product quality or processing speeds. This is particularly evident for macromolecules, especially of thermoplastic nature in fused deposition modelling (FDM).

FDM relies on the facile processability of thermoplastics, whereby material is extruded and shaped in liquid state, after which the new shape preserved upon solidification by lowering the temperature. However, thermoplastics differ from other construction materials classes such as ceramics and metals since covalent bonds and subsequent connectivity of elementary building blocks into large individual macromolecules can slow down the molecular mobility significantly. This has an impact on the final part quality (in terms of dimensional stability and mechanical performance).

Time [sec]



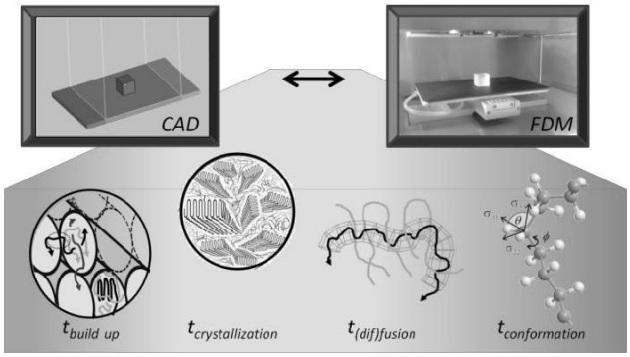

CAD
FDM
$t_{build\ up}$
$t_{crystallization}$
$t_{(dif)fusion}$
$t_{conformation}$

Figure 1: (a) Recording temperature of bottom layer upon a 7 layered object; (b) Gradients in decreasing dimensional stability; (c) WAXD pattern illustrating crystallinity variation across layers

Figure 2: Time scales in FDM with macromolecules solidification

In FDM as material is deposited layer by layer, it is important to consider that different layer experience different thermal trajectories (Figure 1 (a)). This typically leads to anisotropy in the final product, which can be seen in the form of inter layer adhesion, or molecular diffusion across interfaces (Figure 1 (b)). Additionally, the heating and cooling cycles affect the kinetics of molecular freezing and potential crystallization beyond or close to the glass transition temperature. This again can lead to varying degree of crystallinity across layers (Figure 1 (c)). An understanding of these effects, can help in tuning materials for several product functionalities.

In this work we aim to correlate macromolecular design i.e. stereo specificity and molar mass/distribution to macromolecular dynamics motions and kinetics of physical phenomena in FDM with the goal to define and tune thermoplastics and process design in managing product expectations. This requires consideration of the timescales of molecular chain diffusion across interfaces, timescale of crystallization, which needs to match the heat management and the timescale of product build up (Figure 2).

MACRO 557

FRACTURE MECHANICS OF NATURAL RUBBER AND BLENDS USING FINITE ELEMENT ANALYSIS

Anand Poomuthu[a], Santanu Chattopadhyay[a], Dipak Khastgir[a], Michael Kaliske[b], Arghya Deb[c],

Email: anandpoomuthu3@gmail.com, santanu@rtc.iitkgp.ernet.in, khasdi@rtc.iitkgp.ernet.in, michael.Kaliske@tu-dresden.de, arghya@civil.iitkgp.ernet.in

a – Rubber Technology Center, Indian Institute of Technology Kharagpur, India

b – Institute for Statics and Dynamics of Structures, Technische Universität Dresden, Germany

c – Department of civil Engineering, Indian Institute of Technology Kharagpur, India

Abstract

This contribution correlates determination of important fracture parameters for commercially important rubber blends by experimental and finite element modeling methods. NR/BR blends of various compositions have been tested under tensile loading and the behavior is utilized to determine the suitable hyperelastic material model. A model proposed by Yeoh has been found relevant to the test materials and has been used to represent them. To this end a single edge notched tensile sample is used for the analysis. The sample is tested for uniaxial Mode I fracture

(Tear), which is the commonly observed among the three modes of fracture. A finite element replica of the test specimen has been created using in-house codes, which uses an implicit mesh adaptive method to study the strain potential around the crack tip. The set of codes for each specimen is executed using commercially available third party software ANSYS Parametric Design Language (APDL). Stress-strain behavior from experimental and simulation responses were compared. The energy release rate otherwise known as tearing energy has been derived for both the studies. A new approach based on material force theory has been introduced as an alternate for the energy release rate method. Based on satisfactory results on comparison, material force approach is proposed as an efficient method to study fracture of rubber blends. Fatigue and fatigue crack growth (FCG) have been studied for the above material. An attempt has also been made to simulate the dynamic loading of samples and implement the proposed approach.

Keywords: Fracture – Simulation – Material Force – Qausi Static – Fatigue

References

1) Ghosh, P., Stocek, R., (2014) Investigation of fatigue crack growth characteristics of NR/BR blend based tyre tread compounds, Int. J. Fract, 188, p10-12.

2) Özenç, K., Kaliske, M. (2014). An implicit adaptive node-splitting algorithm to assess the failure mechanism of inelastic elastomeric continua, Int. J. Numer. Meth. Engng, 100, p669-670.

3) Nguyen, T.D., Govindjee, S. (2005). A material force method for inelastic fracture mechanics, J. Mech. Phys. Solids, 53, p93, p119.

MACRO 561

Effect of epoxy content and blend composition on the phase morphology and physico-mechanical properties of polyvinyl chloride/epoxidized liquid natural rubber (PVC/ELNR) blends

P. K. Biju*, M. R. Gopinathan Nair

School of Chemical Sciences, Mahatma Gandhi University, Priyadarshini Hills P.O., Kottayam, Kerala 686 560, India, E-mail : pkbijump@gmail.com

In this work, we prepared polyvinyl chloride/epoxidized liquid natural rubber (PVC/ELNR) blends and optimized their properties in terms of epoxy content and composition. The extent of epoxidation was quantitatively measured using FTIR and ^{1}H-NMR spectroscopic techniques and differential scanning calorimetry (DSC). The miscibility, phase behaviour and phase morphology of the blends were studied

using DSC and scanning electron microscopy (SEM). The mechanical, dynamic mechanical and thermal degradation properties of the blends were also investigated. It was found that the epoxidation of ELNR has remarkable influence on the molecular level compatibility of PVC and ELNR. The SEM micrographs showed that the blends exhibited two types of phase morphology viz., matrix/droplet and co-continuous morphologies. It was also observed that mol% epoxidation of ELNR and blend composition have great impact on the morphological parameters. Further, there was an intimate relationship between the morphology and mechanical properties of the blends. Moreover, the dynamic mechanical and thermal degradation properties were influenced by blend composition and rate of epoxidation.

MACRO 562

Novel High Temperature Resistant Materials Based on Polycyclic Silicones for Space Applications

Indulekha K[1]*, R.S.Rajeev[1], Dona Mathew[1],Gouri C[2], K.N. Ninan[3]

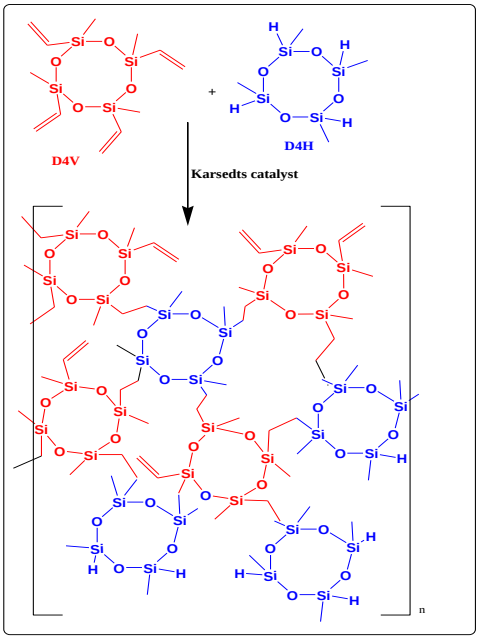
[1]Polymers and Special Chemicals Division,
[2]Polymers and Special Chemicals Group,
[3]IIST, Trivandrum
Vikram Sarabhai Space Centre, Thiruvananthapuram-695 022

*Corresponding author: k_indulekha@vssc.gov.in

Conventional silicone based polymers undergo debonding when exposed to temperature >300°C due to the depolymerisation of the polymer backbone. There are several approaches to arrest the depolymerisation of siloxane polymers by incorporating aromatic moieties or rigid structures to the backbone. Another approach is the realization of polycyclic silicones. Present work aims at synthesis of polycyclic siloxane with minimal amount of metallic catalyst and aromatic moieties and thereby arresting the depolymerisation observed in conventional silicones and to formulate the polycyclic silicone with suitable fillers to achieve a system capable of withstanding 500-600°C without deterioration in properties. Here, polycyclic siloxanes with ethyl bridges are synthesized from cyclic siloxanes through hydrosilylation reactions. Precursors selected were 2,4,6,8-tetramethyl-2,4,6,8-tetravinylcyclotetrasiloxane (D_4V) and 1,3,5,7-tetramethylcyclotetrasiloxane (D_4H) in varying proportions (as depicted in Scheme 1) and studied the composition-property relationhips. The system with 1:1 molar ratio of D4V and D4H resulted in polymer with onset decomposition temperature decomposition at 600°C. Further, this polymer was formulated to adhesive system by compounding with inorganic fillers and thermal and adhesive properties were evaluated. LSS at different temperatures were evaluated and found that system is retaining 50% of its strength at 460°C.

To the best of our knowledge this is the first time reporting of a polymeric silicone adhesive system capable of withstanding higher temperature regimes and is a suitable candidate for related applications in launch vehicles of ISRO space programmes.

Key words: *polycyclic, silicone, high temperature resistance, adhesive*



Scheme 1. Synthesis of polycyclic silicone

References:

1. Lorente, M.A. et al., *Macromolecules*, 1985, 18, 2663.
2. Dvomic PR, Lenz RW. In: Dvomic PR, Lenz RW, editors., New York: Huthig and Wepf Verlag Basel, 1990 (Chap 2).

Author index

A. Asif 364
A. C. Wali 841
A. K. Palai 211
A. Kalaiyarasi 259
A.D. Rosa 1107
A.Gopinath 24
A.K. Sikder 933
Adam Michalski 191
Adhikari 21
Agrawal, Garima 658
Ajith kumar H. 940
Amal Narayanan 886
Amanuel Gebrekrstos 1000
Amarnath Singam 494
Amin 109
Amit Kumar Sonker[a] 775
Anand Poomuthu 1125
Anand, Anoop 807
Ananya Deb 421
Ancy Smitha Alex 312
Ancy Smitha Alex 1028
Anirudhan T S 235
Anirudhan T S 389
Anirudhan T S 392
Anuj Mittal 830
Anupama Gaur 877
Anupriya Vijayakumar 946
Apparao Thota 132
Archana Samanta 380
Archana T. S. 909
Arindam Kumar Das 283
Arnab Shit 233
Arpan Biswas 749
Arpan Biswas 836
Arun Kumar Mahanta 470
Aruni Shajkumar 642
Asha Susan Chacko 543
Bagotia N. 699
Bajpai Rishab 51
Bala. N. S. Thota 965
Balakondareddy Sana 116
Ball, R. 684
Bandyopadhyay Sujoy 338
Bappa Ghosh 1001
Basak, U 54
Bavane Swapnil Ravindrakumar 354
Bera Anupam 659
Bera, Sharmita 526
Bhadja Vaibhavee 215
Bhagyashri S. 706
Bhasney Siddharth 927
Bhattacharjee Jayeeta 18
Bhavna Sharma 65
Billa Narasimha Rao 703
Bindu Manchanda 846
Bisoi 302
Biswas 94
Biswas Gargi 525
Biswas Sourav 719
Borkotoky 705
Borole Dinesh 1
Bose Avijit 689
Bose Suryasarathi 718
C Vibha 569
CH Devi Vara Prasad 992
Chakrabortty, Sabyasachi 624
Chandan Kumar 46
Chandel 386
Chandravati 611
Chatterjee 143
Chatterjee D. P 30
Chatterjee Uma 223
Chaurasia Siddhant 463
Chayanika Das 276
Das 43
Das Tamalika 634
Das, N. C. 831
Das, Sujoy 664
de Kort, G.W. 1112
Deepthi Krishnan 712
Deepthi L. Sivadas 288
Deeraj B.D.S. 1091
Deshmukh Satej S 41
Deshpande, Nilesh U. 531
Dey, P 810
Dhar Prodyut 931
Dhrubajyoti Das 45
Dr. Anirban Pradhan 23
Dr. Verma Savita 139
Dule 86
Dutta, Sujan 527
E. Murugan 145
E. Murugan 551
E. Swathi 1062
Eapen Thomas 730
G. Santhosh 967
G.S Shibulal 1114
Gahlout Pragati 287
Gaur, Surendra Singh 309
Gayathri S. 1021
Ghosh Radhakanta 264
Ghosh G 650
Ghosh Priyanka 701
Ghosh, T 676
Ghosh, Tanwistha 950
Gopi Chintada 339
Gourhari Chakraborty 568
Goutam Prasanna Kar 837

Author index

Hafeez Sumbul 135
Indulekha K. 1127
I.J. Induja 284
Iqbal Nahid 824
Ireni, Nagaraj Goud 748
Jana Somdeb 84
Janeni Natarjan 379
Janisha Jayadevan 957
Jayalakshmi C. G 896
Jeffrey Pyun 355
Jewrajka Suresh Kumar 225
Joseph A.M. 945
K Rambabu 308
K. Indulekha 886
K. Patel 1092
K. Sudhakar 613
K.A. Jisha 64
K.S.Dijith 317
Kalita, Kumar 556
Kalsang Tharpa 628
Kapil Dev Sayala 388
Karayil, Jasila 999
Kari Vijayakrishna 29
Karkare P 82
Kasina Manojkumar 675
Katti, Prajakta Prathamkumar 717
Kattimuttathu I 142
Kaur Banpreet 81
Kavalakal MathaiEldho 812
Khadeeja Sherin P. R. 341
Khandai Santripti 500
Khawas Koomkoom 95
Killi Naresh 527
Kinsuk Naskar 847
Kishor Pawar 61
Km Nikita 295
Komeri Remya 418
Korra, Praveen 533
Kousar Jahan 146
KPP Najiya 1091
Kranthikumar Tungala 553
Kuila Biplab K 104
Kuila, A 85
Kulkarni Bhagyashree 530
Kumar Ashok 447
Kumar Manish 692
Kumar Rajnish 610
L.R. Jaidev 582
Leena K 904
M. Fathima Rigana 661
M. Himabindu 745
M. Jakeer Hussain 144
M. Socka 195
M. Vintu 325
M.Sarojadevi 662
Madhuri, U. D 682
Maiti 73
Maiti, Chiranjit 688
Maity 237
Maity, Dipanwita 570
Maity, Kankan Kumar 714
Maji 97
Maji, S 709
Majumdar, S 37
Malhotra, Mehak 533
Malik Sudip 257
Mandal Debasish 241
Mane, Shivshankar 616
Mani Jayanthi 12
Manna, Dilip Kumar 571
Marc Schmutz 795
Meril Shelly 911
Mete 50
MettaLokanadham 535
Mili 117
MirchandaniGirish 700
Mitra Kheyanath 271
Mohammad Tahir Zafar 541
Mohanan A 422
Molla, Mijanur 584
Mondal Sanjoy 828
Monika 555
Moumita Dhara 910
Muthukrishnan. Sharmila 951
N.Neeraj 1014
N.S. Sumitha 303
Nagendra, Baku 711
Nalawade A. C 87
Neethu K. S. 320
Neha Tiwari 457
Nellepalli Pothanagandhi 36
Nikam, Shrikant B 240
Nisha Balachandran 332
Nityanshu Kumar 853
Noordzij, G. 623
O. Manaf 1022
Ojha Ankita 774
Orodepo Gabriel O. 956
Ozlem Kubra AKDOGAN 1111
P. A. Saeed 141
P. K. Biju 1126
P. Kumar 435
P. Kumara Babu 625
P. Rahul 561
P.S. Drishya 891
Padmavathy Nagarajan 580
Paik Pradip 377

Author index

Pal	137	Rajan, Ramya	722	Samanta Pratick	645
Pal, Akhilesh Kumar	558	Rajasekaran Divya	981	Samanta Ketaki	848
Pal, D. S.	644	Rajdeo Kishor	512	Samanta, Pousali	62
Pallavi Kumari	98	Rajdev, Priya	311	Sampat Singh Chauhan	693
Pandey Bhawana	511	Rajender Nutenki	203	Sandeep P.B	120
Pandey Swechchha	509	Rajender Nutenki	746	Sangam Naidu Karri	321
Pandey, R. K	687	Raju Bej	651	Sanoop B. Nair	428
Parekh Nimisha	519	Ramakrishna S	674	Sarabjot Kaur	258
Parthsarthy	214	Ramkrishna Sarkar	720	Sarkar, K	698
Parvathy C	738	Raneesh Konnola	783	Sashivinay kumar Gaddam	597
Patel Dinesh	675	Rathore, Kalpana	615	Satheesh Chandran M	128
Patel Pratikshkumar R	406	Ravishankar. P. M.	1075	Satheesh Kumar B	322
Patra D	446	Remya Balakrishnan	1099	Saumya Krishnan	251
Pattanayak	238	Rengesh Balakrishna	572	Saxena, Sonashree	529
Paul Anirban	212	Renjith Sasi	318	Sayantani Bhattacharya	409
Perala Suresh Kumar	129	Renu Jose	979	Selvam Mathi	296
Pilla Srinivasarao	716	Ritima Banerjee	860	Shaiju, P	949
Poorvi M. Purohit	423	Rohini Rani	737	Shaik Syed Hussain	581
Pousali chal	234	Rokade, Dhammaraj	805	Sharma Pratibha	371
Pradhan S. K.	1069	Roy Arkapal	285	Sharma Sandeep	239
Pramanik	694	Roy M.	622	Sharma, Shilpi	885
Prasad Arbind	989	Roy, R.	696	Shashikant Supare	1080
Prasad Arbind	593	S N Raju Kutcherlapati	74	Shete Abhijit	513
Prasad V S	552	S Narendren	708	Shib Shankar Banerjee	829
Prasanna Kumar S	580	S. Karpagam	310	Shikha K.T	1035
Prasanta Kumar Behera	1007	S. Kiran	1057	Shukla A	502
Prasanta Kumar Behera	1106	S. Megha	574	Shyambo Chatterjee	147
Praveen Kumar Solasa	1050	S. Mukherjee	441	Sidhharth Sirohi	617
Praveen Kumar Solasa	1085	S. Narayanan	66	Singh Asheesh	119
R. Radhika	586	S. Rana	784	Singh Saumya	282
R. V Sreelekshmi	636	S. Sabapathy	849	Singh Shikha	666
R.Aiswaryaa	340	Sachin S. Surwase	544	Siva Ponnupandian	160
R.R. Choudhury	210	Sachin Singh	788	Smitha C Sukumaran	929
Ragin Ramdas M	131	Saha Biswajit	415	Smitha George	8
Rai, Roopali	865	Saha, Sayantani	331	Somisetti Varaprasad	614
Rajan Kumar	242	Sahoo	63	Songca SP	643

Author index

Soorya Nair	921	Susheela B. Idage	870	Upadhyay Rahul	217
Sravan Baddi	342	Swapnil Shukla	357	Upadhyay Rahul	448
Srinivas, V.	1123	Swarna	691	V. P. Singh	864
SrinivasChinthalapalli	1082	Swati Sharma	665	V. Raji	695
Srirangam Siripothu	723	T. S. Anirudhan	399	V.D. Anumon	487
Stanly Sona	776	T.P.Nisha	1044	V.P. Ubale	160
Suchithra C	668	T.Vandana	227	Vikas Kumar	348
Sudha J. Devaki	715	Tapendu Samanta	247	Vineeth M Vijayan	416
Sudhin Thampi	604	Tarange Dattatray	136	Vinita	286
Sudipta Mondal	686	Tejas S Bhosale	627	Vishwakarma Sambhav	59
Sudipta Senapati	482	Tharakan Simi Annie	28	Wilsens, C.H.R.M	201
Sujoy Bej	133	Thombare, Nandkishore	583	X-Yu Cao	272
Sunitha K	127	Tiwari, P	294	Y. N. Marathe	450
Suresh Annam	265	Tushita Mukhopadhyay	324	Y. S. Patil	174
Sushanta K Sethi	799	Ulaeto, Sarah B.	964	Y.R. Nevare	153